Practical Design of Ships and Other Floating Structures

2001

PRADS

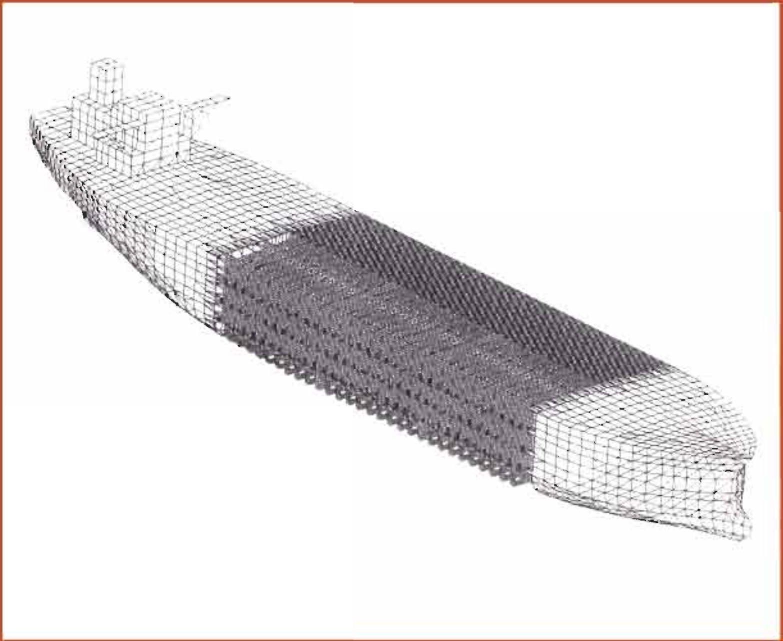

Volume I

Edited by
You-Sheng Wu, Wei-Cheng Cui
and Guo-Jun Zhou

ELSEVIER

Practical Design of Ships and Other Floating Structures

Elsevier Science Internet Homepage

http://www.elsevier.nl (Europe)
http://www.elsevier.com (America)
http://www.elsevier.co.jp (Asia)

Consult the Elsevier homepage for full catalogue information on all books, journals and electronic products and services

Elsevier Titles of Related Interest

BAI
Pipelines and Risers
ISBN: 008-043712-5

BJORHOVDE, COLSON & ZANDONINI
Connections in Steel Structures III.
ISBN: 008-042821-5

CHAN & TENG
ICASS '99, Advances in Steel Structures. (2 Volume Set).
ISBN: 008-043015-5

DUBINA
SDSS '99 – Stability and Ductility of Steel Structures.
ISBN: 008-043016-3

FRANGOPOL, COROTIS & RACKWITZ
Reliability and Optimization of Structural Systems.
ISBN: 008-042826-6

FUKUMOTO
Structural Stability Design.
ISBN: 008-042263-2

GODOY
Thin-Walled Structures with Structural Imperfections: Analysis and Behavior.
ISBN: 008-042266-7

GUEDES-SOARES
Advances in Safety and Reliability (3 Volume Set).
ISBN: 008-042835-5

MOAN & BERGE
13th Int Ship & Offshore Structures Congress (ISSC 1997).
ISBN: 008-042829-0

OHTSUBO & SUMI
Proceedings of the 14th International Ship and Offshore Structures Congress.
ISBN: 008-043602-1

OWENS
Steel in Construction (CD-ROM Proceedings with Printed Abstracts Volume, 268 papers).
ISBN: 008-042997-1

SRIVASTAVA
Structural Engineering World Wide 1998 (CD-ROM Proceedings with Printed Abstracts Volume 702 papers).
ISBN: 008-042845-2

USAMI & ITOH
Stability and Ductility of Steel Structures.
ISBN: 008-043320-0

VASSALOS
Contemporary Ideas on Ship Stability.
ISBN: 008-043652-8

VUGTS
BOSS '97 Behaviour of Offshore Structures (3 Volume Set).
ISBN: 008-042834-7

WATSON
Practical Ship Design.
ISBN: 008-042999-8

YOUNG
Wind Generated Ocean Waves.
ISBN: 008-043317-0

Related Journals

Free specimen copy gladly sent on request. Elsevier Science Ltd, The Boulevard, Langford Lane, Kidlington, Oxford, OX5 1GB, UK

Applied Ocean Research
Advances in Engineering Software
CAD
Coastal Engineering
Composite Structures
Computers and Structures
Construction and Building Materials
Engineering Failure Analysis
Engineering Fracture Mechanics
Engineering Structures
Finite Elements in Analysis and Design
International Journal of Solids and Structures
Journal of Constructional Steel Research
Marine Structures
NDT & E International
Ocean Engineering
Structural Safety
Thin-Walled Structures

To Contact the Publisher

Elsevier Science welcomes enquiries concerning publishing proposals: books, journal special issues, conference proceedings, etc. All formats and media can be considered. Should you have a publishing proposal you wish to discuss, please contact, without obligation, the publisher responsible for Elsevier's ocean engineering publishing programme:

Ian Salusbury
Senior Publishing Editor
Elsevier Science Ltd
The Boulevard, Langford Lane
Kidlington, Oxford
OX5 1GB, UK

Phone: +44 1865 843425
Fax: +44 1865 843920
E.mail: i.salusbury@elsevier.co.uk

General enquiries, including placing orders, should be directed to Elsevier's Regional Sales Offices – please access the Elsevier homepage for full contact details (homepage details at the top of this page).

Practical Design of Ships and Other Floating Structures

Proceedings of the Eighth International Symposium on Practical Design of Ships and Other Floating Structures

16 - 21 September 2001
Shanghai, China

Edited by

You-Sheng Wu
China Ship Scientific Research Center,
Wuxi, Jiangsu, China

Wei-Cheng Cui
School of Naval Architecture & Ocean Engineering,
Shanghai Jiao Tong University,
Shanghai, China

and

Guo-Jun Zhou
China Ship Scientific Research Center,
Wuxi, Jiangsu, China

Volume I

2001
ELSEVIER
AMSTERDAM – LONDON – NEW YORK – OXFORD – PARIS – SHANNON - TOKYO

ELSEVIER SCIENCE Ltd
The Boulevard, Langford Lane
Kidlington, Oxford OX5 1GB, UK

© 2001 Elsevier Science Ltd. All rights reserved.

This work is protected under copyright by Elsevier Science, and the following terms and conditions apply to its use:

Photocopying
Single photocopies of single chapters may be made for personal use as allowed by national copyright laws. Permission of the Publisher and payment of a fee is required for all other photocopying, including multiple or systematic copying, copying for advertising or promotional purposes, resale, and all forms of document delivery. Special rates are available for educational institutions that wish to make photocopies for non-profit educational classroom use.

Permissions may be sought directly from Elsevier Science Global Rights Department, PO Box 800, Oxford OX5 1DX, UK; phone: (+44) 1865 843830, fax: (+44) 1865 853333, e-mail: permissions@elsevier.co.uk. You may also contact Global Rights directly through Elsevier's home page (http://www.elsevier.nl), by selecting 'Obtaining Permissions'.

In the USA, users may clear permissions and make payments through the Copyright Clearance Center, Inc., 222 Rosewood Drive, Danvers, MA 01923, USA; phone: (+1) (978) 7508400, fax: (+1) (978) 7504744, and in the UK through the Copyright Licensing Agency Rapid Clearance Service (CLARCS), 90 Tottenham Court Road, London W1P 0LP, UK; phone: (+44) 207 631 5555; fax: (+44) 207 631 5500. Other countries may have a local reprographic rights agency for payments.

Derivative Works
Tables of contents may be reproduced for internal circulation, but permission of Elsevier Science is required for external resale or distribution of such material.
Permission of the Publisher is required for all other derivative works, including compilations and translations.

Electronic Storage or Usage
Permission of the Publisher is required to store or use electronically any material contained in this work, including any chapter or part of a chapter.

Except as outlined above, no part of this work may be reproduced, stored in a retrieval system or transmitted in any form or by any means, electronic, mechanical, photocopying, recording or otherwise, without prior written permission of the Publisher.
Address permissions requests to: Elsevier Science Global Rights Department, at the mail, fax and e-mail addresses noted above.

Notice
No responsibility is assumed by the Publisher for any injury and/or damage to persons or property as a matter of products liability, negligence or otherwise, or from any use or operation of any methods, products, instructions or ideas contained in the material herein. Because of rapid advances in the medical sciences, in particular, independent verification of diagnoses and drug dosages should be made.

First edition 2001

British Library Cataloguing in Publication Data
International Symposium on Practical Design of Ships and
other Floating Structures (8th : 2001 : Shanghai, China)
Practical design of ships and other floating structures :
proceedings of the Eighth International Symposium on
Practical Design of Ships and other Floating Structures
16-21 September 2001, Shanghai, China
1.Naval architecture - Congresses 2.Shipbuilding -
Congresses
I.Title II.Wu, You-Sheng III.Cui, Wei-Cheng IV.Zhou,
Guo-Jun
623.8

ISBN 0080439500

Library of Congress Cataloging in Publication Data
A catalog record from the Library of Congress has been applied for.

ISBN: 0-08-043950-0 (2 Volume set)

♾ The paper used in this publication meets the requirements of ANSI/NISO Z39.48-1992 (Permanence of Paper).
Printed in The Netherlands.

PREFACE

During the last century the science and technology of ships and marine structures experienced extremely great progress, and thus created the modern shipbuilding, shipping and ocean industries. The relevant achievements were a part of the driving sources, which changed the whole world and the society. Among the efforts towards these achievements was the creation of "The First International Symposium on Practical Design in Shipbuilding" in 1977 in Tokyo. Later on it became a series of symposia, PRADS as the abbreviation. Last century seven PRADS symposia were held in Tokyo ('77 and '83), Seoul ('83 and '95), Trondheim ('87), Varna ('89), Newcastle ('92) and The Hague ('98).

This proceedings contains the papers presented at "The 8th International Symposium on Practical Design of Ships and Other Floating Structures" held at Shanghai Everbright Convention & Exhibition Center, China on 16-21 September 2001. This is the first of the PRADS Symposia in the 21st century.

The overall aim of PRADS symposia is to advance the design of ships and other floating structures as a professional discipline and science by exchanging knowledge and promoting discussion of relevant topics in the fields of naval architecture and marine and offshore engineering. Inline with the aim, in welcoming the new era this Symposium is particularly for an increase in international cooperation and giving a momentum for the new development of design and production technology of ships and other floating structures for efficiency, economy, safety, and environmental production.

The main themes of this Symposium are Design Synthesis, Production, Hydrodynamics, Structures and Materials of Ships and Floating Systems. Proposals for over 270 papers from 26 countries and regions within the themes were received for PRADS'2001, and about 170 papers were accepted for presentation at the symposium. With the high quality of the proposed papers the Local Organizing Committee had a difficult task to make a balanced selection and to control the total number of papers for fitting into the allocated time schedule approved by the Standing Committee of PRADS.

Volume I of the proceedings covers the subjects about design synthesis, production and part of hydrodynamics. Volume II contains the subjects for the rest of hydrodynamics, structures and materials.

On behalf of the Standing Committee of PRADS and the Local Organizing Committee of PRADS'2001, we would like to thank all the participants for their great contributions to the successful symposium. The full support from the sponsors, Mechanical and Vehicle Engineering Division of Chinese Academy of Engineering, Chinese Society of Naval Architects and Marine Engineers, and Chinese Institute of Navigation are greatly acknowledged. Sincere gratitude is also extended to China Ship Scientific Research Center, Shanghai Jiao Tong University and other institutes and shipyards in China, who have helped the preparation of this Symposium.

You-Sheng Wu
Wei-Cheng Cui
Guo-Jun Zhou

These Proceedings of Volumes I and II contain papers presented at the 8th International Symposium on Practical Design of Ships and Other Floating Structures. The Symposium was held at the Shanghai Everbright Convention & Exhibition Center in Shanghai, China, on 16-21 September 2001, and organized by:

CAE	**Chinese Academy of Engineering, Mechanical and Vehicle Engineering Division**
CSNAME	**Chinese Society of Naval Architects and Marine Engineers**
CIN	**China Institution of Navigation**

These organizations are represented in the Local Organizing Committee.

The Local Organizing Committee organized the Symposium under supervision of the PRADS's Standing Committee. The Symposium gained the generous support of many sponsors. They are listed together with the membership of the committees in the following.

HONORARY ADVISORY COMMITTEE

Mr. Rong-Sheng Wang, *President, Chinese Society of Naval Architects and Marine Engineers*
Mr. Xiao-Jin Chen, *President, China State Shipbuilding Corporation*
Mr. Shan-Xiang Hong, *Vice Minister, Ministry of Communications*
Mr. Ping-Tao Huang, *President, China Shipbuilding Industrial Corporation*
Mr. Zai-Kuan Jin, *Vice President, China State Shipbuilding Corporation*
Mr. Ke-Jun Li, *President, China Classification Society*
Mr. Zu-Yi Lin, *President, China Institute of Navigation*
Prof. Dian-Zuo Wang, *Vice President, Chinese Academy of Engineering*
Mr. Hui Wang, *Vice President, China Shipbuilding Industrial Corporation*
Mr. Guang-Qin, Zhang, *Vice President of Commission of Science, Technology and Industry for National Defence*

PRADS STANDING COMMITTEE

Prof. S. Motora (Honorary Chairman), *Previously, Ship and Ocean Foundation, Japan*
Prof. You-Sheng Wu (Chairman), *China Ship Scientific Research Center, China*
Prof. T. Borzecki, *Technical University of Gdansk, Poland*
Dr. L.L. Buxton, *University of Newcastle, UK*
Prof. O.M. Faltinsen, *The Norwegian Institute of Technology, Norway*
Dr. R. Porcari, *Italian Ship Research Center, Italy*
Prof. J. J. Jensen, *Technical University of Denmark, Denmark*
Prof. H. Kim, *Seoul National University, Korea*
Dr. D. Liu, *American Bureau of Shipping, U.S.A.*
Prof. H. Ohtsubo, *University of Tokyo, Japan*
Dr. M.W.C. Osterveld (Ex-officio), *MARIN, The Netherlands*
Prof. H. Petershagen, *University of Hamburg, Germany*
Dr. S. G. Tan, *MARIN, The Netherlands*
Prof. Wei-Cheng, Cui (Secretary), *Shanghai Jiao Tong University, China*

PRADS LOCAL ORGANIZING COMMITTEE

Prof. You-Sheng Wu (Chairman), *China Ship Scientific Research Center*
Prof. Jian-Xun Lu (Co-Chairman), *China Ship Research and Development Academy*
Prof. Ze-Liang Chang, *Counselor's Office Shanghai Municipality*
Mr. Tian-Zu Cheng, *Chinese Society of Naval Architects and Marine Engineering*
Prof. Wei-Cheng Cui (Secretary), *Shanghai Jiao Tong University*
Prof. Shi-Tang Dong, *China Ship Scientific Research Center*
Prof. Xiao-Hong Gao, *Wuhan University of Technology*
Prof. Ri-Xiu Guo, *Naval Engineering University*
Prof. You-Sheng He, *Shanghai Jiao Tong University*
Prof. Bing-Han Hsu, *China Ship Scientific Research Center*
Mr. Ke-Yi Hu, *Shanghai Jiang Nan Shipyard*
Prof. Sheng Huang, *Harbin Engineering University*
Prof. Zhuo-Shang Ji, *Dalian University of Science and Technology*
Mr. Qi-Kang Liang, *Marine Design and Research Institute of China*
Mr. Zhi-Ping Lu, *Shanghai Merchant Ship Design and Research Institute*
Mr. Wen-Sun Shen, *Dalian New Shipyard*
Prof. Zi-Ying Sheng, *Shanghai Academy of Science*
Mr. Heng-Yuan Wang, *Shanghai Hu Dong Shipyard*
Prof. Xiu-Heng Wu, *Wuhan University of Technology*
Prof. Xue-Yan Xu, *Marine Design and Research Institute of China*
Mr. Heng-Yi Zeng, *China Ocean Petroleum Co.*
Prof. Bing-Yan Zhang, *Marine Design and Research Institute of China*
Prof. Sheng-Kun Zhang, *Shanghai Jiao Tong University*
Prof. Guo-Jun Zhou (Secretary), *China Ship Scientific Research Center*
Mr. Zhen-Bo Zhou, *Shanghai Corporation of Shipbuilding Industry*
Prof. Ying-Fu Zhu, *Wuhan Ship Design Institute*

PROGRAMME COMMITTEE

Prof. Ying-Qiu Chen, *China Classification Society*
Prof. Zhu-Shun Dong, *Naval Engineering University*
Prof. Yan-Liang Guo, *Marine Design and Research Institute of China*
Prof. Xiang-Lu Huang, *Shanghai Jiao Tong University*
Prof. Run-Pei Li, *Shanghai Jiao Tong University*
Prof. Guo-Ping Miao, *Shanghai Jiao Tong University*
Prof. Hong-Cui Shen, *China Ship Scientific Research Center*
Prof. Zhong-Kun Shi, *Hua Zhong University of Science and Technology*
Prof. Guo-Qiang Wang, *Shanghai Jiao Tong University*
Prof. Chang-Jian Weng, *Wuhan University of Technology*
Prof. Fei Xia, *Wuhan Ship Design Institute*
Prof. Zuo-Shui Xie, *Hua Dong Shipbuilding Institute*
Prof. Zao-Jian Zou, *Wuhan University of Technology*

SPONSORS

Chinese Academy of Engineering, Mechanical and Vehicle Engineering Division
Chinese Society of Naval Architects and Marine Engineers
China Institution of Navigation
Ship Mechanics Committee, CSNAME
China Ship Scientific Research Center
Shanghai Jiao Tong University
Marine Design and Research Institute of China
Wuhan University of Technology

STAFF MEMBERS OF THE SECRETARIAT

Prof. Guo-Jun Zhou, *China Ship Scientific Research Center*
Mr. Bo-Ling Kang, *China Ship Scientific Research Center*
Mr. Zhen-Ping Weng, *China Ship Scientific Research Center*
Mr. Ren-Han Li, *Chinese Academy of Engineering*
Ms. Wen-Ji Li, *China Ship Scientific Research Center*
Mr. Xue-Wen Yin, *China Ship Scientific Research Center*
Ms. Jie Xu, *China Ship Scientific Research Center*
Ms. Qi-Hua Li, *China Ship Scientific Research Center*
Ms. Jia-Yu Qian, *China Ship Scientific Research Center*
Mr. Zheng-Yu Song, *China Ship Scientific Research Center*

CONTENTS

VOLUME I

Preface v

PLENARY LECTURES

Maritime Safety Culture and Development of Ship and Offshore Installations Design Standards in the 21st Century 3
Ke-Jun Li

Structural Safety of Ships 13
D. Liu

Shipping Industry in the 21st Century 21
Jia-Fu Wei

1. DESIGN SYNTHESIS FOR SHIPS AND FLOATING SYSTEMS

LIFE CYCLE COST AND SHIPPING SYSTEM

A Consideration of Life Cycle Cost of a Ship 29
Yasushi Kumakura and Hiroshi Sasajima

The Experiment of River-Sea-Going Ore Barge Fleet and Renovation of Existing Integrated Barge 37
Shun-Huai Chen, Wei Zhang, Jun-Ming Li and Cheng-Fang Wang

DESIGN OPTIMISATION

Optimization of a Wave Cancellation Multihull Ship Using CFD Tools 43
C. Yang, R. Löhner and O. Soto

A Module-Oriented Optimization Tool 51
Ph. Rigo

The Fine Optimization of Ship Hull Lines in Resistance Performance by Using CFD Approach 59
L. Xu and Y.Y. Wang

HULL FORM DESIGN

Parametric Hull Form Design - A Step Towards One Week Ship Design 67
C. Abt, S.D. Bade, L. Birk and S. Harries

Mission Based Hydrodynamic Design of a Hydrographic Survey Vessel 75
S.L.Toxopeus, P.F. van Terwisga and C.H.Thill

Hull Form Design of a Passenger Catamaran for Operation in the Yellow Sea Region 83
Seung-Hee Lee, Young-Gill Lee and Jae Wook Lee

Hull Form Design of Cargo Ship in Shallow and Strong Current Waterways 91
Li-Zheng Wang and Long-Fei Xi

NOVEL SHIP CONCEPTS - HIGH SPEED VESSELS

The Impact Load of Wing-in-Ground-Effect Craft in Waves and Application of Hydro-Ski 97
Zu-Shun Dong, Xiao-Peng Gao and Wei Sun

Conceptual Design of Very Large-Size Super-High-Speed Foil Catamaran Containership 105
Keh-Sik Min, Seon-Hyung Kang and Oi-Hyun Kim

A Practical Application of Air Lubrication on a Small High Speed Boat 113
Jinho Jang, Il Jun Ahn, Jaesung Kim, Jung-Chun Suh, Hyochul Kim, Seung-Hee Lee and Museok Song

The Hybrid Hydrofoil Stepped Hull 119
B. Duffty and C.D. Barry

NOVEL SHIP CONCEPTS - TRIMARAN

The Design of Trimaran Ships: General Review and Practical Structural Analysis 127
T. Coppola and M. Mandarino

Calm Water Experimental Research on Geosims of High Speed Trimaran: Hydrodynamic Characteristics and Model-Ship Correlation 135
E. Begovic, C. Bertorello and P. Cassella

Trimaran Model Test Results and Comparison with Different High Speed Craft 143
C. Bertorello, D. Bruzzone, P. Cassella and I. Zotti

Hull Form Development and Powering Performance Characteristics for a 2,500 Ton Class Trimaran 151
Kuk-Jin Kang, Chun-Ju Lee and Do-Hyun Kim

FLOATING PRODUCTION SYSTEMS

Design Recommendations from the FPSO - Fatigue Capacity JIP 159
I. Lotsberg

Design of FPSOs Based on Maneuvering Stability 167
G.B. Matter, J.S. Sales Jr. and S.H. Sphaier

Extreme Response and Fatigue Damage of Ship-Shaped FPSO 175
Chun-Tian Zhao, Yong Bai and Yung Shin

VERY LARGE FLOATING STRUCTURES (I)

An Investigation into Wave Induced Drift Forces and Motions of Very Large Floating Structures 187
N. Ma, T. Hirayama and K. Ishikawa

A Study on the Horizontally Dynamic Behavior of a VLFS Supported with Dolphins 197
Hao Liu, Hiroo Okada, Takashi Tsubogo and Koji Masaoka

Experimental Study on the Hydroelastic Response Characteristics of a Pontoon Type Floating Structure 205
T.Y. Chung, J.H. Chung, S.Y. Hong and Y.J. Ji

VERY LARGE FLOATING STRUCTURES (II)

Simulation Study on Coastal Ecosystem Around a Very Large Floating Structure in Tokyo Bay 213
D. Kitazawa, M. Fujino and S. Tabeta

Effects of a Draft on Hydroelastic Responses of a Pontoon Type Very Large Floating Structure 221
H. Maeda, T. Ikoma, C.K. Rheem and M. Arita

A Study on Deck Wetness and Slamming of Very Large Floating Structures 229
Hyunkyoung Shin, Ho-Young Lee, Choon-Gyu Lim, Jeom-Moon Kang, Oi-Hyun Kim and Myung-Cheol Yoon

SAFETY ASSESSMENT

Probabilistic Analysis Tools for Surface Ships Under Seaway and Extreme Dynamic Loads 237
Y.J. Lua and P.E. Hess

Comprehensive Fuzzy Approach in Hazard Identification of Formal Safety Assessment (FSA) 245
Ying-Qiu Chen and Shao-Fen Lin

Estimating the Risk of Cargo Shifting in Waves – Methodology and Results 253
A. Ryrfeldt and T. Källstam

DESIGN PRINCIPLE AND CRITERIA

Ship Design Using Probabilistic Damage Stability Rules – A Sensitivity Study 261
P.H. Lauridsen, J.J. Jensen and J. Baatrup

Integration of First-Principle Approaches to Design for Damage Survivability 269
D. Konovessis and D. Vassalos

Rational Design Criteria and Their Application to Hull Form Optimisation of Floating Systems in Random Seas 275
L. Birk and G.F. Clauss

DESIGN METHODS

The Application of a Decomposition and Reuse Approach in Marine Design 285
K.G. Tan and P. Sen

Evaluating Design for Upgradeability: A Simulation Based Approach for Ships and Marine Products 293
I.L. Buxton and G.H. Stephenson

Model-Based Simulation for Container Loading / Unloading 301
Soon-Sup Lee, Jong-Kap Lee and Hong-Tae Kim

Research on 3D-Layout Design of Ship Compartment Based on CBR 309
Jun-Hua Li, Ying-Fu Zhu, Wen-Ye Ying and Jun Lu

Development of a Sophisticated Hull Form CAD System 'EzHULL' Based on a Non-Manifold Model and 'X-topology' 315
Kyu-Yeul Lee, Joong-Hyun Rhim, Sang-Uk Lee, Doo-Yeoun Cho and Young-Bok Choi

MARINE STRUCTURAL DESIGN

A Design Modification of VLCC with Wide Web Frame Space 323
Jae-Hyung Park, Chang-Hwan Jang and Joo-Ho Heo

Optimization of the Design of Ship Structures Using Response Surface Methodology 331
M. Arai and T. Shimizu

APPLICATION OF INFORMATION TECHNOLOGY

A Study on an Information System of Damages of Ship Structures 341
Y. Kawamura, T. Seki, T. Sakuragi and Y. Sumi

Bayesian and Neural Networks for Preliminary Ship Design 349
H.B. Clausen, M. Lützen, A. Friis-Hansen and N. Bjørneboe

2. PRODUCTION

DEVELOPMENT IN PRODUCTION TECHNOLOGY

Innovation in Ship Production: What Can We Expect ? 359
H. Wilckens

New Production System for Vessels of Composite Materials Using an Adjustable Mould 367
Jong Oh Kwon, Jaesung Kim, Jung Chun Suh, Hyochul Kim, Seung Hee Lee, Young Gill Lee, Kisung Kim, Jae Wook Lee, Jae Moon Lew, Sanghong Lee, Jae Kyu Lee, Dae Sun Kang and Duk Soo Chung

Mobile Agent Based Supply Chain Management in Shipbuilding Industry 373
Jing-Yun Cheng, Bei Lu and Sheng-Kun Zhang

Energy and Environment Dimension in Ship Manufacturing Processes 381
M.A. Shama

FABRICATION MECHANICS

Study on Heat Transfer Between Gas Flame and Plate During Line-Heating Process 389
Y. Tomita, N. Osawa, K. Hashimoto, N. Shinkai, J. Sawamura and K. Matsuoka

Study on the Process Technology of Line Heat Forming of Hull Fabrication 397
Yujun Liu, Zhuoshang Ji, Dong Wang and Yanping Deng

Numerical Simulation of Welding Distortions in Large Steel Structures 403
L.F. Andersen

3. HYDROMECHANICS

COMPUTATIONAL FLUID DYNAMICS - FLOW SIMULATION

Simulation of Viscous Flow of Modern Surface Ships Using the FINFLO RANS Solver 413
Ting-Qiu Li and J. Matusiak

Viscous Flow Around Rotating Ships 421
C. Levi and J.B.V. Wanderley

Numerical Simulation of Flows over Underwater Axisymmetric Bodies with Full Appendages 429
Zhen-Yu Huang and Lian-Di Zhou

Viscous Flow Calculations Used for Dredger Design 437
M. Hoekstra, A. de Jager and H.H. Valkhof

Fully Non-linear Wave Computations for Arbitrary Floating Bodies Using the DELTA Method 445
Tzung-Hang Lee and Chang-Lung Chen

COMPUTATIONAL FLUID DYNAMICS - ENVIRONMENT

Flow Behavior Around Tandem Oil Fences 451
Dong Gi Han, Choung M. Lee and Sang J. Lee

A CFD-Based Parametric Study on the Smoke Behaviour of a Typical Merchant Ship 459
Eunseok Jin, Jaedon Yoon and Yongsoo Kim

Application of CFD to Assessment and Design of the Air-Ventilation System in the Reefer Container Holds of Container Carriers 467
Bong Jun Chang

RESISTANCE

Wash and Wave Resistance of Ships in Finite Water Depth 475
Qinzheng Yang, O.M. Faltinsen and Rong Zhao

On Scale Effect of the Resistance Due to Stern Waves Including Forward-Oriented Wave Breaking Just Behind a Transom Stern 485
T. Yamano, Y. Kusunoki, F. Kuratani, T. Ikebuchi and I. Funeno

Numerical and Experimental Evaluation of the Hull Characteristics of Two-Semi-Displacement Fast Monohulls 493
C.M.P. Sampaio, K. Nishimoto, C.H. Miyagi, K. Hirata and I. Miwa

Empirical Prediction of Ship Resistance and Wetted Surface Area Using Artificial Neural Networks 501
K. Koushan

A New Method for Resistance and Propulsion Prediction of Ship Performance in Shallow Water 509
T. Jiang

Lower Frictional Resistance Characteristics of Foul Release Systems 517
M. Candries, M. Atlar, A. Guerrero and C.D. Anderson

PERFORMANCE

Evaluation and Computer Program on the Speed Trial Analysis Method of the Ongoing Work in ISO/TC8 525
Eun-Chan Kim, Hyun-Se Yoon, Sa-Young Hong and Yoon-Rak Choi

A Test Procedure and Evaluation Method for Seakeeping Trials with Address to Broaching-To 533
O. Lundbäck

Experimental Investigation of Bank Effects under Extreme Conditions 541
D.-Q. Li, M. Leer-Andersen, P. Ottosson and P. Trägårdh

SEAKEEPING AND RINGING

Effects of Different Three Dimensional Formulations on the Seakeeping Computations of High Speed Hulls 547
D. Bruzzone, P. Gualeni and L. Sebastiani

Measurement of Ship Motion During Model Tests and Full Scale Seakeeping Trials 555
Nan Xie, Guo-Liang Qian, Huan-Qiu Gao and Na-Xin Wei

Developing Seakeeping Performance Criteria for a Helicopter Pilot Training Vessel 563
P. Crossland and M.C. Johnson

Dynamic Behaviour of Rigid Mono- and Multi-Hulled Vessels in Waves, Incorporating Non-Linear Excitation 571
P.A. Bailey, E.J. Ballard and P. Temarel

Time-Domain Simulations and Measurements of Loads and Motions of Planning High-Speed Craft in Waves 579
K. Garme

Analysis of Ringing by Continuous Wavelet Transform 587
S.H. Kwon, H.S. Lee, J.S. Park, M.K. Ha and Y.J. Kim

DECK WETNESS AND IMPACT

Green Sea and Water Impact on FPSO in Steep Random Waves 593
C.T. Stansberg and S.I. Karlsen

Long Term Prediction Method of Shipping Water Load for Assessment of the Bow Height 603
Y. Ogawa, H. Taguchi, I. Watanabe and S. Ishida

A Practical Design Tool for Wave Impact on Bow and Deck Structures 611
Ø. Hellan, J.R. Hoff and C.T. Stansberg

SLAMMING AND SLOSHING

Wave Impact on Decks of Floating Platforms 621
R. Baarholm, O.M. Faltinsen and K. Herfjord

Impact Pressure Analysis on High-Speed Craft in Waves, through FE-Analysis on Full-Scale and Model Measurement Data 629
A. Rosén

Assessment of Sloshing Loads for Tankers 637
P.C. Sames and T.E. Schellin

MANOEUVRABILITY - COMPUTATION AND SIMULATION

Prediction of Hydrodynamic Forces Acting on Ship Hull in Oblique and Turning Motions by a Simple Surface Panel Method 645
K. Nakatake, T. Sekiguchi and J. Ando

A Numerical Study on Viscous Flow About a Ship in Manoeuvring Motion 651
Xie-Dong Zhang and Xiu-Heng Wu

Simulation of the Propulsion System Behaviour During Ship Standard Manoeuvres 657
G. Benvenuto, S. Brizzolara and M. Figari

MANOEUVRABILITY

Experimental Study on the Maneuverability for a Wide Beam New Suezmax Class Tanker 665
Heung-Won Seo, Tae-Il Lee and Seung-Myun Hwangbo

On Steady Horizontal Forces and Moment Due to Short Waves Acting on Ships in Manoeuvring Motion 671
M. Ueno, T. Nimura, H. Miyazaki and K. Nonaka

An Empirical Formula for Steering Gear Torque of Tankers with a Horn Rudder 679
D.I. Son, J.H. Ahn and K.P. Rhee

VOLUME II

Preface v

3. HYDROMECHANICS (*continued*)

PROPULSOR AND PROPULSION

Propeller Design and Analysis System Using an Object-Oriented Database in Windows Environment 685
Chang-Sup Lee and Chung-Ho Cho

A Propeller Design Method with New Blade Section for Improving Cavitation Inception Under Unsteady Condition 693
Wei-Xin Zhou, You-Hua Wu and Shi-Tang Dong

An Optimisation Method Based on Hilbert Space Theory for Design of Marine Propellers and Hull Form 699
T.S. Jang, T. Kinoshita and T. Hino

Numerical Analysis of Cavitating Propellers Including Viscous Flow Effects 705
F. Salvatore and P.G. Esposito

Propeller Design Based on Surface Panel Method by Prescribed Pressure Distribution 713
Ting-Shou Tan

CFD-Based Optimization of Tanker Stern Form – Minimization of Delivered Horsepower Using Self-Propulsion Simulator 719
Y. Tahara, J. Ando and Y. Himeno

Numerical and Experimental Studies of Ducted Propeller 725
R. Zhao

Design of Cavitating Propellers by Lifting Surface Theory 733
Guo-Qiang Wang and Chen-Jun Yang

Prediction of Transient Loading on a Propeller from an Approaching Ice Block 741
P. Liu, B. Colbourne and Chin Shin

PODDED DRIVES

Investigations of Podded Drives in a Large Cavitation Tunnel 749
J. Friesch

Triple Pod Propulsion in the World's Largest Ever Cruise Liner 757
R. Hämäläinen and J. van Heerd

Hydrodynamic Trends in Hull Lines of Podded Driven Large Cruise Vessels 767
R. Lepeix

HULL-PROPULSOR-APPENDAGES INTERACTION

Simulating the Self-Propulsion Test by a Coupled Viscous/Potential Flow Computation 777
S.K. Chou, C.Y. Hsin, S.W. Chau and W.C. Chen

Numerical Computation of Ship's Effective Wake and Its Validation in Large Cavitation Tunnel 785
J.W. Park, J.J. Kim, D.S. Kong and J.M. Lew

Wake Fields Prediction on the Propeller Plane by Neural Network 791
H.J. Shin and S.M. Hwangbo

Effect of Vertical Pre-Swirl Stator Vanes on the Propulsion Performance of a 300K Class VLCC 799
Jiman Yang, Kihyun Park, Kwang Kim, Jungchun Suh, Hyochul Kim, Seunghee Lee, Jungjoong Kim and Hyoungtae Kim

Development and Experimental Study of a Novel Submarine Guide Vane Propeller System 807
Hui-Zhi Yao and Hong-Cui Shen

EXPERIMENTAL TECHNIQUES

Development and Application of a High Speed Video System in HSVA's Large Cavitation Tunnel HYKAT 815
C. Johannsen

Uncertainty Analysis of Towing Test 823
Mo-Qin He, Hong-Cui Shen and Shu-Long He

Transient Flooding in a Damaged Ferry 831
J.M. Riola and J. Valle

4. STRUCTURES AND MATERIALS

WAVE INDUCED LOADS AND RESPONSES

Prediction of Wave-Induced Rolling Responses by a Time-domain Strip Theory 839
Zhao-Hui Wang, J.J. Jensen and Jin-Zhu Xia

Methods to Reduce the Effects of Irregular Frequencies in Hydrodynamic Analysis of Vessels with Forward Speed 847
S.X. Du, D.A. Hudson, W.G. Price and P. Temarel

The Effects of Forward Speed on Hydrodynamic Pressure and Structural Response of Ships in Waves 857
Chih-Chung Fang, Hua-Tung Wu, Hoi-Sang Chan and Chung-Yung Lu

Ship Motions and Sea Loads by a 3D Rankin Panel Method 865
Li Xu, Wei-Xing Zhang, Chen-Bi Zhao, Fa-Yan Xu and You-Fang Chen

EXTREME WAVE LOADS

Experiment on Extreme Wave Loads of a Flexible Ship Model 871
Rui-Zhang Chen, Shuang-Xing Du, You-Sheng Wu, Ji-Ru Lin, Jia-Jun Hu and Ya-Lin Yue

Estimation of Nonlinear Long-Term Extremes of the Vertical Bending Moments in Ships 879
G.S. Baarholm and T. Moan

A Direct Calculation Approach of Determining Extreme Combined Bending Moments for Fast Fine Form Ships 887
Xue-Kang Gu and Jin-Wei Shen

HYDROELASTICITY

Flutter of Hydrofoil in Viscous Field 895
Can Sima, Xiao-Ci Zhang and You-Sheng Wu

Symmetric and Antisymmetric Hydroelastic Analysis of a Bulker in Waves 903
S.E. Hirdaris, W.G. Price and P. Temarel

Hydroelastic Model for Bottom Slamming 911
A. Bereznitski and V. Postnov

Hydrodynamic Impulsive Loads Acting on Ship-Hull Plates 919
Gang Wang

RELIABILITY

Risk Analysis Applied to Occurrence of Maximum Wave Bending Moment 925
E.A. Dahle, D. Myrhaug and H.T. Wist

Fuzzy Reliability Analysis of a Ship Longitudinal Strength 931
J.M. Yang and J.Y. Huang

Reliability-Based Requalification of Existing Offshore Platforms 939
T. Moan and O.T. Vårdal

Deterministic and Probabilistic Assessment of FPSO Hull Girder Strength 947
A. Incecik and Y. Pu

Consistent Code Formulation for Ship Structural Design 955
A.E. Mansour, J.S. Spencer, P.H. Wirsching, J.E. McGovney and D.D.Tarman

Reliability of Stiffened Ship Decks 965
K. Rajagopalan

ULTIMATE STRENGTH - SENSITIVITY

Total Analysis System for Ship Structural Strength 971
T. Yoneya, H. Kobayashi, M. Abdul Rahim, Y. Sasaki and M. Irisawa

Uncertainty and Sensitivity Analyses in the Predicted Critical Buckling Strength of a Longitudinally Stiffened Sub-Panel 979
Wei-Cheng Cui, Li-Juan Shi and Jin-Fei Zhang

Sensitivity Analysis on Ultimate Hull Bending Moment 987
Ph. Rigo, C. Toderan and T. Yao

ULTIMATE STRENGTH - HULL GIRDER

Assessment of Ultimate Longitudinal Strength of Aged Tankers 997
A. Ikeda, T. Yao, O. Kitamura, N. Yamamoto, M. Yoneda and H. Ohtsubo

Ultimate Strength and Reliability Assessment for the Ship Hull Girders Used in ISSC-2000 Benchmark Study 1005
Hai-Hong Sun and Yong Bai

An Assessment of the Ultimate Plastic Strength of the Ship's Aged Hulls 1013
G.V. Egorov and V.V. Kozlyakov

ULTIMATE STRENGTH - STIFFENED PLATES AND SHELLS

A New Design Model for Ultimate and Buckling Strength Assessment of Stiffened Plates 1021
E. Steen, T.K. Østvold and S. Valsgård

Ultimate Strength of Longitudinally Stiffened Panels: Multi-Criteria Comparative Analysis 1029
J.Y. Pradillon, T. Quesnel, C. Toderan and Ph. Rigo

Ultimate Strength of Submersible Structures 1037
I.P. Pasqualino and S.F. Estefen

FATIGUE ASSESSMENT AND DESIGN

A Report on Fatigue Failure of a Highly Skewed Fixed Pitch Propeller 1045
Hochung Kim, Keunjae Kim, Sungpyo Kim and Moonchan Kim

Fatigue Analysis of Aluminium Box-Stiffener Lap Joints by Nominal, Structural and Notch Stress Range Approaches 1053
Naiquan Ye, T. Moan and B.W. Tveiten

Fatigue Strength Assessment of Cruciform Joints 1061
W. Fricke and R. Wernicke

Fatigue Strength Assessment of Hull Details for an FPSO 1071
S. Berge, A. Johansen and L.G. Bjørheim

Evaluation of Simplified Prediction Method of Stress Response Function From the Viewpoint of Fatigue Strength Analysis of a Ship 1081
T. Fukasawa, K. Hashimoto and Y. Tomita

Combination of Fatigue Damages Produced by Several Wave-Induced Loads Based on Correlation Coefficient Method 1089
H. Kawabe and K. Shibazaki

Fatigue Analysis of an Aged Jack-up Platform Structure Refitted to Cantilever-Beam Type 1097
Wu Nie, Yu-Wu Sun and Li-Ping Sun

FATIGUE STRENGTH - VARIOUS FACTORS

Analysis of Three-Dimensional Cracks in Ship Structures Subjected to an Arbitrary Loading by Numerical Weight Function Method 1105
Y. Sumi

Effect of Mean Stress Changes on the Fatigue Strength of Spectrum Loaded Welds 1113
G.B. Marquis and T.P.J. Mikkola

A New Look at the Effect of Bandwidth and Non-Normality on Fatigue Damage 1121
Lei Yu, P.K. Das and N.D.P. Barltrop

FATIGUE TESTS

An Experimental Investigation on Fatigue Behavior of Inverted Angle and T-Type Side Longitudinals in Tankers 1129
Jinsoo Park, Kuk Bin Kim, Wha Soo Kim and Doe Hyun Kim

Fatigue Behaviour of Different Bracket Connections 1137
H. Paetzold, O. Doerk and H. Kierkegaard

Fatigue Tests on Large Scale Knuckle Specimens 1145
O.D. Dijkstra, G.T.M. Janssen and J.W.L. Ludolphy

FATIGUE CONTROL

The Pre-Fabricated Hull Details for Application in Design and Repair 1153
S.V. Petinov

Fatigue Strength of Load-Carrying Box Fillet Weldment in Ship Structure 1161
Wha Soo Kim, Doe Hyun Kim, Sang Gab Lee and Yoon Ki Lee

VIBRATION AND NOISE

A VBAR Model to Identify the Dynamic Characteristics of Marine Structures 1169
C.F. Hung, Y.T. Peng and W.J. Ko

Vibration Analysis Method of Ship Structures in the Medium Frequency Domain 1177
F. Besnier, G. Bechepay, Y. Mavrakakis and M. Ferry

A New Method for Determining Acoustic Added Mass and Damping Coefficients of Fluid-Structure Interaction 1185
Q. Zhou, W. Zhang and P.F. Joseph

Vibration Prediction of Rectangular Tank Structures 1197
Y. Takeda

Influence of Journal Bearing Modelling Method on Shaft Line Alignment and Whirling Vibrations 1205
L. Murawski

VIBRATION CONTROL

Experimental Studies on Resistance Reduction and Vibration Reduction by Bubbly Layer 1213
Wen-Cai Dong, Fan Wu, Yun-Xiang Zhu and Ri-Xiu Guo

Application of Higher Order Balancer to Control the Superstructure Vibration of a Container Ship 1221
Soo-Mok Lee, Won-Hyun Kim and Kyoon-Yang Chung

NON-LINEAR DYNAMICS

Nonlinear Dynamics of Towed Underwater Vehicles – Numerical Modelling and Experimental Validation 1227
G.F. Clauss and M. Vannahme

Vortex-Induced Vibration of Two Dimensional Wing-Spring Coupled System 1237
Zhi-Xing Yu, Ying-Zhong Liu and Guo-Ping Miao

FIRE AND BLAST

Fire Risk Analysis and Its Application to Ships 1243
M. Dogliani and A. Vergine

The Characteristic Analysis of Marine Fire Spread Phenomena with Multi-Equations System for Fire Safety Design 1253
Nobuyoshi Fukuchi and Changhong Hu

Application of Computational Fluid Dynamics in the Fire Safety Design of Marine Systems 1261
Changhong Hu and Nobuyoshi Fukuchi

An Examination of Some Structural Limit States for Hydrocarbon Explosions 1269
P.A. Frieze, R.B. Corr, R.O. Snell and V.H.Y. Tam

COLLISION AND GROUNDING

Design Against Minor Impacts 1277
M. Lützen and P.T. Pedersen

Experimental Study on the Buffer Bow Structures 1285
H. Endo, Y. Yamada and O. Kitamura

Calculation of Collisions with the Aid of Linear FE Models 1293
E. Lehmann, E.D. Egge, M. Scharrer and L. Zhang

COLLISION AND EXPLOSION

A Simplified Internal and External Mechanics Model for Ships' Collision 1301
K. Suzuki, H. Ohtsubo and K.S. Sajit

Numerical Simulation of Ship-Submarine Collisions 1309
R. Donner, F. Besnier and H. Le Sourne

Fluid Mesh Modeling on Surface Ship Shock Response Under Underwater Explosion 1315
Sang-Gab Lee, Jeong-Il Kwon and Jung-Hoon Chung

APPLICATION OF COMPOSITE MATERIALS

Weight Reduction in Sandwich Structures by Use of Curved Panels 1323
C. Berggreen and B.C. Simonsen

Use of Large-Deflection Theories for Design of FRP Panels 1331
B. Hayman, M.J. Larsen, D. McGeorge and P. Noury

Design of Tee Connections in FRP Ships Using an Analytical Approach 1339
R.A. Shenoi and W. Wang

MISCELLANEOUS

History of PRADS 1345
M. Mano

AUTHOR INDEX I1

KEYWORD INDEX I7

PLENARY LECTURES

Practical Design of Ships and Other Floating Structures
You-Sheng Wu, Wei-Cheng Cui and Guo-Jun Zhou (Eds)
© 2001 Elsevier Science Ltd. All rights reserved

MARITIME SAFETY CULTURE AND DEVELOPMENT OF SHIP AND OFFSHORE INSTALLATIONS DESIGN STANDARDS IN THE 21ST CENTURY

Ke-Jun Li

China Classification Society (CCS)
40 Dong Huang Cheng Gen Nan Jie, Beijing 100006, China

ABSTRACT

This paper presents the development of safety culture and ship & offshore installation design standards. It is based on the demand of the development of ship, offshore engineering technology in 21st century and introduces a new design concept – safety, environmental protection and economy. It also briefly introduces what China Classification Society has achieved in this respect.

KEYWORDS

Maritime Safety Culture, Design Standards, Ship & Offshore installation

1 INTRODUCTION

Since mid seventeenth century when class came into existence, classification societies have been making every effort to prevent safety at sea and marine environmental protection. With the development of scientific technology and ship & offshore installations design standards, new technologies have been woven into class rules.

For the past half century, conventional technology has been challenged by information technology. Rule-making and survey which are carried out by class has changed radically. The challenges becomes even greater with ships becoming bigger, transportation becoming specialized.

With all these developments, design technology has undergone great change. In order for shipbuilders to obtain greater profit, systematic and standardized ship & equipment design has become increasingly important. In addition to safety requirement, there are increasing demand from shipping companies for operability and economy, which poses challenge to design technology.

The International Association of Classification Societies (IACS) has been working hard in this respect and set up new standards regarding ro/ro ships, bulk carriers, tankers and materials application. IACS is playing a significant role in reducing maritime disasters. Some of its technical standards have been incorporated into the mandatory requirements of the International Maritime Organizations(IMO).

In 1999, IMO decided, as part of its safety objective for the new millenium (W. O'neil, 1999), to take effective measures to identify at an early stage the factors affecting maritime safety, which is one of the most far-reaching policies ever established since mid 90s in 20th century. This means that Formal Safety Assessment (FSA) will be adopted as a methodology to assess rule-making process in the areas to which IMO attaches great importance. The key of FSA is to carry out risk assessment and management to human element, ship type, especially passenger ships including high –speed crafts, bulk carriers and tankers. IMO is endeavoring to increase the awareness of safety culture and environmental protection, not to make new rules but improve the implementation of the existing rules.

IMO's endeavor has been firmly supported among shipping industries. An effective way towards better implementation is to have dialogue with the experts from classification societies. The focus of discussions is as follows :

- How to define substandard ship
- How to reduce maritime accidents arising from the fact that new construction of bulk carriers engaged in unrestricted navigation areas is slowing down and existing bulk carriers that cannot be alternated are in poor condition.
- Shipbuilders adopt class rules as minimum construction standards to reduce costs while cost will increase once ship owners raise the standards.
- Absence of unified loading manual.
- Upon delivery of vessels, the scope of application such as sea condition restrictions, corrosive environment, is not in line with the requirements of ship owners
- Absence of powerful computer software designed for loading/unloading operations
- Whether and how can class be involved in the safety guarantee and conditions of delivered vessels provided by shipbuilders.
- How to solve the inconsistency between corrosion margin and reduction of structural scantlings resulting from direct calculation.
- How to solve the decrease of structural fatigue strength as a result of new design approach.
- Ballast exchange and induced cracks

Insurers are also concerned when facing such serious situation (M. Marshell, 1999). The International Underwriting Association (IUA) put forward its definition of substandard ships. "Substandard" cannot be defined by degree of compliance with rules and regulations. "Substandard" is the status of the ship that poses threat to safety. To be specific, it includes the following implications:

- the events leading to accidents or vessels failing to survive harsh environment such as heavy seas.
- the events deteriorating accidents if happens.

Substandard is a comprehensive concept. Some even propose a four "M" definition:

- **Metal**: improper design leading to poor working environment such as improper use of high tensile steel, which result in vibration and noise.
- **Machinery**: technical status of main engine and shafting
- **Men**: technical competence, training and health (including mental health) of seafarers
- **Management**: all parties involved in maritime safety, including shipping companies, ships.

Therefore, substandard is not only applicable to ships, but also to flags, port states, class, shipping companies, seafarers and technical factors including ship type, age, and economic elements. Today, it is not justifiable to blame one single party for an accident.

All the above-mentioned organizations, together with insurers, P&I(Premium&Indemnity), shipbuilders, cargo owners, charterers, maritime courts, maritime arbitration organizations, banks, training institutes, link up the maritime safety chain. All the interrelating partners must fulfil their share in maritime safety.

Maritime safety culture replaces the traditional safety concept. Today maritime safety and environmental protection are associated with ship's quality, shipping quality, the condition of waters, maritime biology, resource recycling, risk (assessment) management and investment, and associated with the responsibilities of everybody involved. The concept of safety culture has been incorporated into design standards of ships and offshore installations.

This paper will further illustrate the interrelationships between maritime safety culture and development of ship and offshore installations design standards.

2 ACCIDENT AND CASUALTIES – THE DRIVING FORCE TO IMPROVE SAFETY AND ENVIRONMENT PROTECTION STANDARDS

In shipping history, people had not paid much attention to maritime safety for centuries until Titanic disaster.

Today, great changes have taken place in maritime world. The international maritime industry does not tolerate loss of vessels, offshore installations, loss of life and damage to the marine environment. In the past ten years, a large number of international conventions, regulations have come into force after all the accidents. There are too many conventions and IMO has decided to shift its focus from making new rules to implementation of existing rules.

Lesson has been learnt from the loss of over 100 bulk carriers and 500 seafarers in 1990's. Improper design, irregular loading, untimely maintenance and pursuit of nothing but commercial interests will lead to accidents.

Lessons have been learnt from the loss of Estonia in Baltic sea in 1995 that aside from improving bow and stern door structure, great attention should be paid to the monitoring and management system of a vessel.

Lessons have been learnt from the losses of Leader L and Erika in recent years that ships under poor maintenance will pose great threat to safety at sea and marine environmental protection.

Statistics show that 80% of marine accidents are caused by human elements, which has been widely accepted among the maritime world.

Maritime safety chain provides a sound base for prevention of marine accidents. To ensure chain is working well, efforts must be make in all associated areas, such as ship and offshore installation design standard, quality assurance audit, management of maritime administrations and recognized organizations, training and examination of seafarers. Regional PSC MOU (Port State Control Memorandum) has also played an active role in promoting maritime safety and environmental protection.

Ship age is another key element leading to marine accidents. Therefore, safety control of ships within her life span is put on the top of the agenda. There is detailed analysis of the age of the world fleet as follows.

The youngest fleet is container fleet, 50% of which are under 5 years of age. Bulk carrier fleet is older, 30% of which are under 5 years and the average age is below that of the total world fleet. General cargo ship fleet comes last, 7% of which are under 10 years of age and only 2% under 5 years. This implies that general cargo fleet is shrinking and will be gradually replaced by containers including semi-containerships and multi-purpose vessels. The same thing happens to refrigerator ships. More seriously, world passenger ships are aging rapidly, 44.3% of which are above 25 years. Although there have been new constructions in the near decade, however the situation can not be changed quickly.

To solve the above problems, actions must be taken in two aspects. One is that new construction standards should be reviewed and improved, such as requirements for tanker to have double hull, and requirements regarding longitudinal strength, local strength including transverse bulkhead and double bottom, bow/stern door of ro/ro ships. The other is to review the technical status of existing ships including survey scheme and inspection method. Due to the implementation of IMO resolutions concerning transverse bulkhead between No.1 and No2 holds and new strength requirements for double bottom of No. 1 hold of bulk carriers, bulk carrier losses have been drastically reduced. Requirements for longitudinal strength and fatigue strength of tankers are under review. Enhanced Survey Program (ESP) of bulk carriers and tanker as well as Condition Assessment Scheme (CSA) to tankers will come into force shortly. The revised 13G of MARPOL will lead to the fact that a large number of tankers will be phased out.

It is true that any accidents will bring about the improvement of ship and offshore installation safety standards, design standards and management. Accidents are the driving force of better safety and environmental protection standards.

3 SAFETY CULTURE AND DEVELOPMENT OF SHIP AND OFFSHORE INSTALLATIONS DESIGN STANDARDS

3.1 Maritime safety culture

As I have mentioned previously, safety chain promotes safety culture. Maritime safety culture can be defined as spirit of safety at sea and the associated systems, behaviors. The spirit of safety at sea means the objective of safeguarding of safety at sea and prevention of marine pollution. To pursue such an objective, all the partners involved in the safety chain take their own responsibilities in the context of safety culture.

3.2 Extension of implication of maritime safety culture

Safety culture is evolving. Half of centuries ago, safety at sea was regarded as the responsibility of shipping companies and ships. Share of responsibility was not clear and not many parties were involved. Safety chain was not in place due to lack of insight and low level of scientific technology. Conventions and regulations did not have substantial content and class rules and regulations were far from mature. For one hundred years, class rules had relies on experience or a combination of experience and theory.

Today, it is changing. With the rapid progress of technology, globalization, development of information technology, ship and offshore engineering technology has developed into a systematic science. The rapid progress of ship and offshore engineering technology has promoted the development of shipbuilding industry, shipping industry and seaborne transportation. Safety chain has involved more and more parties in the areas of shipowning, administration, maritime economics, management, ideology, media and many others (See Fig.1). A well-functioning safety chain has greatly enriched the maritime safety culture (Li Kejun, 2001).

The discussions about substandard ships has gone more extensively and extensively and brought about the discussions on quality shipping, which is beyond technical considerations. Quality shipping is an extended concept. In addition to the four "Ms", it includes the concept of quality control. All partners are part of the quality system. In IACS, some members have acquired ISO9000 certificates aside from IACS QSCS certificate. Some shipping companies are working towards ISO/14000 and ISO/18000 in addition to ISO/9000. Quality shipping is also a part of safety culture.

One of the characteristics of modern society is associated with risk and risk-assessment. Classification societies have introduced the methodology of risk assessment to its rule-making process. Risk management has become a major part of safety culture.

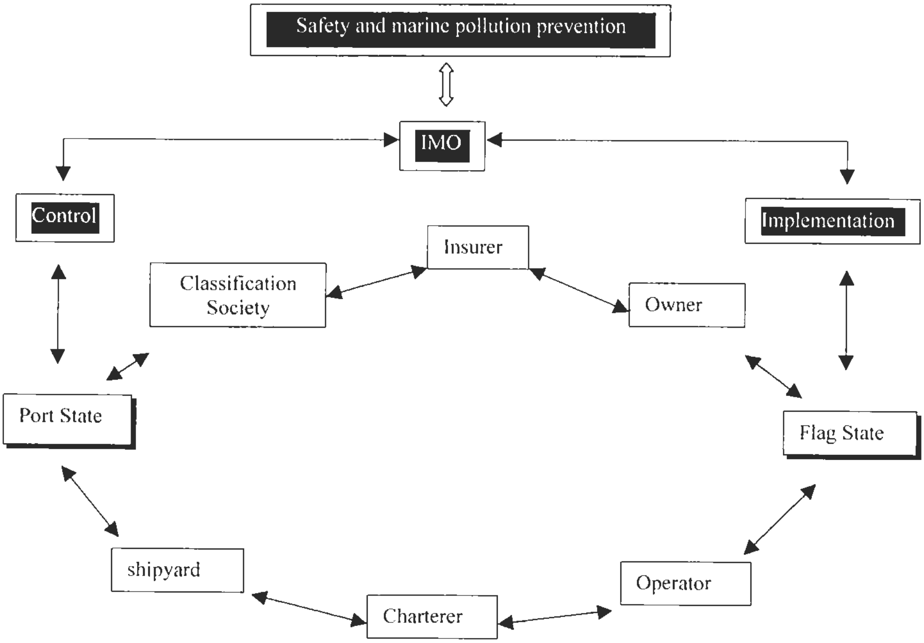
Safety and marine pollution prevention
IMO
Control
Implementation
Insurer
Classification Society
Owner
Port State
Flag State
shipyard
Operator
Charterer

Fig.1

3.3 Classification society – a major role in safety culture

Class has been working towards safety at sea and environmental protection for many years. For half a century, class has been widely recognized by the international maritime world for being internationalized, impartial and authoritative. Class nowadays is providing service for the maritime industry with its technical expertise in the following aspects:

Continuously improving rules and regulations in response to the development of ship & offshore installation design. Class rules reflect the most advanced technologies and researches. For the recent ten years, direct calculation and software adopted by class has contributed to solving the problem of increasing ship size, which is recognized by the International Ship and Offshore Structures Congress (ISSC). Class is also making efforts to increase transparency in its technical services.

Class has started to incorporate its services into risk management recently and become a technology producer rather than a mere technology verifier. Awareness of service provider has been enhanced. Through IMO ISM Code audit and certification, class is playing a significant role in promoting the safety system of shipping companies and ensuring their safety system to be in compliance with international standards. Under IMO Resolution A. 739 (18) and A. 789 (19), class is carrying out survey authorized by flag administrations and consequently taking its share of risk.

Self-discipline and continuously improving its survey and assessment method should comply with quality shipping requirements. QSCS (Quality System Certification Scheme) is one of the major step forward taken by IACS in this respect, including establishing Code of Ethics, Vertical Contract Audit, Enhanced Survey Program, Transfer of Class Agreement, and recently contributing to Condition Assessment Scheme. Some of the above are made mandatory by IMO.

3.4 Development of ship and offshore installations design standards in 21st century

As mentioned above, the international maritime world has come to know the fact that safety culture is taking form. Maritime safety culture and standard making are complimentary. Maritime safety culture has affected the development of ship and offshore installations design standards in the following aspects.

Risk management has been introduced into design standards, which indicates that a completely technical standard is not sufficient, while comprehensive, economics-wise standards in compliance with basic safety standard are needed. FSA is applied as one of the major methodologies regarding risk management, which has a significant influence on rules and regulations. Now, FSA is applied to areas of explosion prevention, fire protection, collision and grounding prevention.

The information technology (IT) and database developments have led to changes in design standards for ships and offshore structures. The following research areas with IT development have achieved substantial progress.

- design within the ships' life, such as
  fatigue design,
  crack extension design,
  ultimate strength design;
- application of new materials including consideration for geometry non-linearity, material non-linearity;
- wave-loading from 2D linear, 2D non-linear to 3D linear, 3D non-linear;
- transportation under high or low temperature for asphalt carrier, LPG and LNG;
- vessels of special purposes such as SWATH and WPC;
- direct calculation of vessels of large size, such as VLCC, ULCC, large sized bulk carriers and container vessels.

Great progress has been made in terms of techniques, such as application of high tensile steel, segmented and integrated construction, laser, equal-hydronium welding, cutting welding robots to the following areas (Wu Yousheng et. al., 1999):

- Moulding technics simulation;
- Precision control design;
- Disfigurement disciplinarian prediction;
- Improvement of fatigue strength at nodes by Titania Inertia Gas (TIG) and ultrasonic technology.

Today, ship & offshore engineering design have developed from singularity to complexity, from ambiguity to accuracy, from safety to safety economics. It is predictable that in the 21stst century, ship & offshore installation design standard as well as design technology will develop at a rapid speed.

3.5 Initiatives taken by classification societies with regard to services

To reduce the freight cost, it is inevitable to increase the size of the ships. VLCC, large-size container ships and bulk carriers are the main force of the international shipping. The development of building technology of such ships will remain the prevailing trend for a considerable period in the future. In my opinions, it is in such areas that classification societies should remain their advantages at the following aspects in order to provide better services. The objective of these initiatives is to:

- promote the scientific research and rules formation, so that classification societies are equipped with an ability in structural design and strength analysis of ships with added hi-tech and hi-value, and that the rules and guidelines affected can meet the present application on the one hand and are forward-looking on the other;
- train a contingent of well qualified bellwethers and followers in science and technology;
- search and conclude the new mode of operation in rules and research by focusing on the customer and market needs, its main contents being as follows:
- to integrate the updating requirements of IMO & IACS into the service plans, including:
  - longitudinal strength of bulk carriers;
  - bulkhead and double bottom strength of bulk carriers;
  - hatch cover strength of bulk carriers;
  - deck load of bulk carrier;
  - longitudinal strength of oil tankers;
  - fatigue strength of oil tankers;
  - IACS unified requirements concerning tanker structural scantlings;
  - effect of diminution allowance on structure strength;
- research on application of FSA;
- calculation methods and criteria for longitudinal strength and partial strength of large-size container ships;
- direct calculation software developed by classification societies;

Based on the above, we believe that new type of ships (embodying safety, environmental protection and cost-effectiveness) should be developed, which meet the following latest requirements:

- present international conventions;
- ship building rules in force;
- better cost-effectiveness as required by the using purpose (suitable main scantlings, energy-saving, excellent loading, etc.) ;
- structural type and corresponding standardization;

Appropriate class notations are to be assigned to the above ship type.

4 CONCLUSION

In conclusion of the above, maritime safety culture is taking shape on the basis of maritime safety chain, which is characteristic of the human advancement and will definitely create a deep influence on the development of the specifications for designing the ships and offshore installations in the 21stst century. The continuable marine production must be on the basis of maritime safety chain combined with consideration of economic influence in order to reach the objectives of both quality shipping and environment protection. CCS is determined to develop the maritime safety culture together with other partners on the same chain to make it the common fortune of the human beings and to create a safer and cleaner ocean in the 21stst century.

References

W. O'neil. (1999). The Presentation at Mare Forum '99, Amsterdam.

M. Marshell. (1999). Substandard Shipping – is there a problem and would greater transparency help? *Mare Forum '99*, Amsterdam, June

Li kejun . (2001). Safety Chain Theory is the Foundation of the of Maritime Safety Culture. *China Ship*. Survey, **2**

Wu Yousheng et. al. (1999). Ship Mechanics at the Beginning of the New Century. *Mechanics and Engineeing, Shanghai Jiao Tong University Press*, ShanghI, China (in Chinese).

Practical Design of Ships and Other Floating Structures
You-Sheng Wu, Wei-Cheng Cui and Guo-Jun Zhou (Eds)
© 2001 Elsevier Science Ltd. All rights reserved

STRUCTURAL SAFETY OF SHIPS

Donald Liu

Senior Vice President
American Bureau of Shipping
Houston, Texas, USA

ABSTRACT

The topic of this lecture is the Structural Safety of Ships. This is a very broad topic and this lecture will focus on tankers and bulk carriers, two ship types that have been the subject of structural safety in recent years. It is interesting to explore the motivating forces behind many of the technical developments that have affected structural design and safety of tankers and bulk carriers over the years by considering:

- What were the economic and regulatory forces driving technical change?
- How did the industry respond to these forces?
- Where do we stand today?
- And, what are the implications for the future?

KEYWORDS

Structural safety, Tankers, Bulk carriers, Human element, Casualties, Risk-based safety standards.

1 HISTORICAL PERSPECTIVE

I would first like to give a historical perspective on how the design and safety of tankers experienced the greatest changes during the last 40 years.

I will begin with the 1960's and 1970's, which were a time of incredible growth in the field of ship technology, particularly in tanker design. This growth was economically driven as it was a period of rapid developments in the economies of Europe, Japan and America.

In the decade of the 1960's oil consumption increasing at more than 7% annually. As a result tanker demand increased an annual average of more than 12%.
These economic driving forces promoted the most dramatic changes in tanker design that the marine industry has ever experienced. The 50,000 dwt super tanker became the 250,000 DWT VLCC and 500,000 DWT ULCC.

These changes, while initiated in the 1960's continued to influence tanker designs and tanker safety into the first half of the 1970's. However a single event in March 1967 began a shift from primarily economic driven change to primarily regulatory change.

That event was the grounding of the 119,000 DWT tanker, Torrey Canyon, off the southwest coast of England. For the first time the tanker industry and the public realized the unfortunate impact of a large tanker grounding on the marine environment. Also in a one week period in December 1969, three very large tankers experienced significant explosions while water washing crude oil tanks during the ballast voyage. One of the ships was severely damaged that it sunk, the other two were badly damaged. Studies later indicated that the large cargo tanks could actually have layers of hydrocarbon vapors, which were in the explosive range. It was also learned that water washing could build up charges of static electricity to cause such explosions to occur. A concerned industry would soon develop Inert Gas Systems as the solution to the explosion problem.
These events, the grounding of the Torrey Canyon and the VLCC explosions, changed the primary driving force for technical safety changes in tanker design from economic to regulatory.

2 TANKER DESIGN AND THE MARPOL CONVENTION

Following the grounding of the Torrey Canyon, public pressures began to build on governments to revise the standards for designing and operating oil tankers. As a result, the International Convention for the prevention of Pollution from Ships was held in London in 1973.

The resulting MARPOL 73 Convention and amendments established the need for segregated ballast tank capacity for new tankers over 73,000 deadweight tons, to be implemented in a phased manner by 1979. The amendments placed a limit on the size of cargo oil tanks, set limits on the oil outflow in the event of a collision or grounding, and set other operational requirements to minimize pollution.

In December 1976, the oil tanker ARGO MERCHANT ran aground off the East Coast of the United States. The vessel subsequently broke up releasing all of its cargo, which fortunately, did not pollute the U.S. shores. However, in the next three months there were 14 more tanker related incidents off the U.S. coast, of which eight were serious.

Following these incidents, the U.S. government threatened unilateral action to require double bottoms to reduce accidental oil outflow, if the international shipping community did not improve tanker regulations and pollution prevention measures. In response, the International Maritime Organization (IMO) scheduled the Tanker Safety and Pollution Prevention Conference for February 1978.

Shortly after the opening of that conference, the 250,000 ton AMOCO CADIZ grounded off the coast of Brittany, releasing its entire cargo into the English Channel and onto the beaches of France. This insured the decade of the 70's would be one of unprecedented regulatory change for the tanker industry.

The Convention on Tanker Safety and Pollution Prevention of 1978 dealt with a wide range of issues involving requirements for segregated ballast tanks, clean ballast tanks, crude oil washing and inert gas systems. These changes were directed at both new and existing tankers.

The outcome was a complex compromise that established protocols to both MARPOL 73 and SOLAS 74. Protective location of segregated ballast was accepted as a substitute for a double bottom requirement on new tankers, which was being proposed by the U.S. Inert gas systems and crude oil washing were also required for new tankers. Inert gas systems or crude oil washing were required to be retrofitted on existing crude oil tankers, and redundant steering gear facilities were required on all new and existing tankers.

With the new 1978 protocols to MARPOL and SOLAS, it was hoped that these new regulations would mark an end to regulatory driven changes. It was hoped that by tightening the standards on the design of the tanker structure, the seaways would be made safer and significantly less polluted. Fortunately it did for a while, lasting through most of the decade of the 80's

But that peace came to an end in March of 1989, when the oil tanker EXXON VALDEZ, which met the requirements of the 1978 protocols to MARPOL, ran aground in Prince William Sound, Alaska. The regulatory breather was over and the call for stricter regulations started over again.

3 THE U.S. OIL POLLUTION ACT OF 1990

As result of the VALDEZ oil spill, the U.S. Congress passed the Oil Pollution Act of 1990. OPA-90, as it is commonly referred, set double hull requirements for all new tankers operating in U.S. waters and mandated a phase out of existing single hull tankers. In its final impact, OPA-90 also prompted the 1992 amendments to MARPOL mandating double hull tankers or equivalent designs throughout the world.

Unfortunately the decade of the 90's had not seen much relief in regulatory pressures. There was the grounding of the oil tanker BRAER off the Shetland Islands, and the grounding of the oil tanker SEA EMPRESS off the coast of Wales.

4 NEW EMPHASIS ON THE HUMAN ELEMENT

Following OPA-90 and the requirement for double hull tankers, the regulatory pressure had shifted to a new emphasis on the human element in the marine safety equation. Within IMO, two initiatives were developed. One was the International Safety Management (ISM) Code, which defined a management system approach for the management and operation of all vessels. The other was major revisions to the Convention on Standards of Training, Certification and Watchkeeping (STCW) of Seafarers. While this has very little to do with technical design change in a direct sense, greater attention was being given to the human aspects of marine safety, since it is known that about 80% of accidents is due to human error.

5 RECENT CASUALTIES

Unfortunately tanker disasters resulting in oil pollution still make the news today. From December 1999 through January 1 2001 there were five major casualties that occurred in European waters. In December 1999, the 25 year old 37,000 dwt single hull tanker ERIKA broke in half and sank 40 miles off the coast of Brittany France, spilling over 10,000 tons of heavy fuel oil, resulting in the pollution of the coastline. Other recent tanker casualties were:

- IEVOLI SUN - an 11 year old chemical tanker that sunk due to internal flooding, likely due to structural failure.
- CASTOR - a 23 year old product carrier that had a 20 meter crack develop across its deck. Fortunately it did not sink.

- KRISTAL - a 27 year old product tanker that sunk due to cargo overloading.
- BALU - a 24 year old chemical tanker that sunk without a known cause.

Many of these recent casualties were old tankers, and there is now a renewed concern about the structural safety of aging tankers.

5.1 Aftermath – More Tanker Regulations?

With so many structural failures in older ships, the impact on the call for regulatory change is as great, if not greater, than that which occurred after the AMOCO CADIZ grounding in 1977. Now ten years after the passage of OPA-90 in the U.S., IMO is now considering accelerating the phase out scheme of single hull tankers to be more in line with OPA-90 in the U.S.

6 BULK CARRIER SAFETY

Whereas the tanker safety problems have been largely focused on the prevention of accidental oil pollution to the marine environment, the safety problems being experienced by bulk carriers has focused on the large number of seafarer lives being lost.

There have been numerous casualties in the late 1980's and continuing to the present. What the casualty statistics tell us is that bulk carriers are at higher risk as they get older. Single side skin bulk carriers carrying high density cargoes such as iron ore are at a higher risk than when carrying other lower density cargoes, and many of the casualties were related to flooding or structural failures in No. 1 hold.

During the period from 1983 to 1998, 48 bulk carriers were lost with many seafarer lives also lost. A possible loss scenario is that water enters a cargo hold as a result of fractures in the side shell, or loss of side shell plating in the forward hold in heavy weather. Seawater fills the hold causing the transverse bulkhead to fail with progressive flooding of an adjacent hold, resulting in the sinking of the ship. Under this scenario the bulk carrier losses can be attributed to an initial failure of the primary watertight barrier, such as shell plating or hatch cover - followed by failure of the secondary watertight barrier, such as a transverse bulkhead. A key issue regarding the bulk carrier casualties has been the effect of cargo hold flooding on the structural survivability of these ships, which has not been covered by existing rules and regulations.

Why many bulk carriers suffer damage to the side shell plating can be explained by considering the stiffness of its cross section. The lower portion of a bulk carrier's cross section consists of a double bottom and hopper tanks that are very rigid and stiff. The upper portion is also very stiff due to the upper wing ballast tanks. Both upper and lower portions are connected by the side frames, which are the weakest links in the structure. When carrying heavy iron ore, the bottom deflects causing the side frames to deform inboard. The external action of sea pressure and waves causes further deformation of the frames inboard. In addition if there is ballast water in the upper wing tanks, there is further bending and compressive loads on the frames. The upper and lower ends of the side frame attachments to the topside and hopper ballast tanks are therefore very critical areas affecting bulk carrier safety.

7 IACS AND SOLAS REQUIREMENTS

7.1 Existing Bulk Carriers

To reduce the risk of failure in older ships, IACS introduced new Unified Requirements to reduce the risk of progressive flooding in existing bulk carriers. To prevent progressive flooding due to sea water in No. 1 Hold, the corrugated transverse bulkhead between the first two cargo holds, and the double bottom in way of the first cargo hold had to comply with new strength requirements assuming that No. 1 cargo hold was flooded. A damage stability review had to be performed with No.1 Hold flooded, and more frequent and close-up surveys of critical areas such as side frames and side shell had to be made.

7.2 New Single Side Skin Bulk Carriers

The IACS requirements for new single side skin bulk carriers address the following structural areas:

- increased requirements for the strength of side frames
- longitudinal strength of vessel to withstand any hold being flooded
- transverse watertight corrugated bulkhead strengths of all cargo holds to withstand hold flooding
- double bottom strength to withstand hold flooding
- increased strength requirements for hatch covers in forward holds

7.3 SOLAS Regulations

At a SOLAS Conference held at IMO, in November 1997, a new Chapter XII on bulk carriers was added in SOLAS. The regulations/requirements are essentially similar to the IACS requirements. Compliance with IACS requirements is also required.

8 SAFETY IN CARGO HANDLING

Proper loading guidance is very important to safe cargo handling. The loading and discharging of cargo can be a very significant factor affecting the structural safety of bulk carriers. This is especially so in the case of dense cargoes such as iron ore.

How the ship is loaded and unloaded has not always been appreciated at the cargo terminals, where a 10-15 percent overload of a given hold has been known to occur. For a large bulk carrier such a discrepancy can amount to 5,000 tons of cargo in a hold. The magnitude of forces and stresses that can develop during cargo handling can be very significant, and marginal errors in loading can be catastrophic.

The importance of controlling the loading and discharging in the proper sequence so as not to accidentally overload the ship is extremely important. Bulk carriers have broken their backs due to improper cargo loading and discharging of holds. To increase the safety during cargo handling, loading Instruments are required for all bulk carriers of 150 meters and above. Existing single skin and new bulk carriers are to have a loading manual with typical loading and unloading sequences.

9 DOUBLE HULL BULK CARRIERS

Another approach to increasing the structural safety of bulk carriers is to consider the double hull bulk carrier. Some of the structural benefits of a double sided bulk carrier when compared to a single side skin bulk carrier are that the double side eliminates the exposed, damage-prone side frames and their end attachments. It also protects against corrosion and mechanical damage

The smooth tank surface provides a better quality surface preparation and coating application. The stiffer double side structure also eliminates the flexing or fatiguing of the side frames. Although the initial costs for a double hull bulk carrier will be higher than for a single side skin bulk carrier, the life cycle costs may be less bccause of lower maintenance and repair costs.

10 BALLAST WATER MANAGEMENT

Another area of loading and discharging aboard ships that can affect structural safety of both tankers and bulk carriers is the handling of ballast water. This concern has developed as a result of new regulations for ballast water management. The purpose of ballast water management is to prevent the spread of harmful aquatic species in ports. The regulations require ships to exchange ballast in open waters (away from ports) before entering a port. Some examples of harmful aquatic species are zebra mussels, which rapidly multiply and clog pipes and attach themselves to ships. In the U.S. it is estimated that the zebra mussel alone has caused more than US$5 billion in damage to water pipes, boat hulls and other surfaces in the Great Lakes region.

How did ballast water management come about? Beginning in 1989 governments started to institute regulations to protect local jurisdictions from introduction of unwanted marine organisms. IMO adopted guidelines for management of ship ballast water in 1997. There is now a growing list of countries imposing mandatory national and local requirements, including Canada ('89), Australia ('92), Great Lakes ('93), Israel ('94), Chile ('95), Alaska and Great Lakes (amended) ('96), New Zealand ('98). IMO is now progressing toward ever widening international regulations.

There are five approaches to minimizing unwanted organisms from ballast water:

(1) Retention of ballast on board - this is practically not feasible, as there is not sufficient ballast reception facilities in ports.
(2) Reducing organize taken on board - this can be done whenever practical by delaying the loading of ballast until the ship is in open ocean waters. Ballasting should be avoided in very shallow waters, in stagnant areas, in the vicinity of sewage outflows and dredging operations, in areas where organisms are present, etc
(3) Exchange of ballast at sea - these methods are about 95% effective in eliminating aquatic organisms.
(4) Shipboard ballast treatment - although ballast water treatments are currently being investigated, none has yet been shown to be practical or cost effective for general use by most ships (biocides, separators, ultraviolet light)
(5) On-shore ballast water treatment has advantages to shipboard treatment. However, many ships do not currently have the capability in their piping system to discharge water ashore.

Exchange of ballast at sea is presently the most practical approach. There are two methods used. One is the Sequential Empty and Refill Method wherein ballast tanks are completely emptied and refilled with open-ocean water. The other is the Flow Through (or Overflow) Method wherein open-ocean water is pumped into a full ballast tank, overflowing the tank to three times the tank capacity.

In the *sequential* method, emptying of certain tanks may lead to significantly reduced stability, higher stresses, high sloshing pressures, and/or reduced forward drafts. A secondary effect of reduced forward draft would be an increased probability of bow slamming.

The *flow through* method achieves 95% replacement. Applying the method does not alter the stability, stress, and ship attitude. Venting and overflow arrangements for each tank must be reviewed to insure that flow through is a practical alternative. It is also important to assess piping and overflow arrangements to insure tanks will not be over-pressurized. There are also safety concerns associated with the *flow through* method in that it may be necessary to remove manhole covers or butterworth openings to assure sufficient venting. This practice is labor intensive, and the overflow on deck is prone to icing in cold environments. The safety concerns associated with Ballast Water Exchange is representative of a case where regulations made to improve safety in one area - protection of the marine environment, can possibly adversely affect safety in another area - structural safety.

11 FUTURE DIRECTIONS IN STRUCTURAL SAFETY

Looking back at developments in ship structural safety, one can conclude that structural safety has been largely reactive, rather than pro-active. In some cases this is necessary because the types of problems encountered were new and unexpected, such as the fatigue problems in VLCCs. Once the causes of the problems were identified, appropriate changes were made to avoid those problems, thereby increasing structural safety. Factors not relating at all to structural safety, such as the sudden increase in size and number of tankers, led to an increase in the number of accidents and much larger oil spills when an accident occurred. That led to increased awareness of tanker safety and environmental protection that resulted in new regulations intended to reduce the **frequency** of accidents and reduce their **consequences**. Those changes also produced an improvement in structural safety.

11.1 Risk-Based Safety Standards

The definition of "risk" that is commonly used today is expressed mathematically as frequency (or probability of occurrence) times consequence. Thus efforts to reduce the frequency of accidents and reduce their consequence can be considered as efforts to reduce risk. Conversely, if safety is improved, one can assume that risk is reduced. Certainly, structural safety is not the only aspect of shipping which relates to risk, and in fact I believe it is a smaller part of the risk equation than many other factors such as human error and operational issues. However, the concept of risk assessment and risk management is something that enables us engineers to consider structural safety in the context of the whole safety equation. Classification societies, regulatory bodies, and ship owners are now attempting to place safety in the context of overall risk. This is a new way of looking at structural safety, and one which I am sure will be both challenging and rewarding. It will be a gradual evolution in which new technology, new methods and greater understanding of risk concepts, coupled with experience and knowledge, will be used to refine and improve future standards of safety.

Practical Design of Ships and Other Floating Structures
You-Sheng Wu, Wei-Cheng Cui and Guo-Jun Zhou (Eds)
© 2001 Elsevier Science Ltd. All rights reserved

SHIPPING INDUSTRY IN THE TWENTY-FIRST CENTURY

Jia-Fu Wei

China Ocean Shipping (Group) Company
Beijing 100031, China

ABSTRACT

In the present paper the trends of the development of international economy and trade at the beginning of the new Century are briefly analyzed. Seven major features of international shipping business are discussed in detail. It is also mentioned how a global shipping business operator, taking COSCO as an example, should act to meet the new challenges.

KEYWORDS

Twenty-first Century, Economic and Trade Development, International Shipping

1 TRENDS OF INTERNATIONAL ECONOMY AND TRADE AT THE TURN OF THE CENTURY

The overall picture of international economy and trade is quite rosy despite of the increasing uncertainties in world economy at present.

(1) Although the world economy is slowing down, the international economic outlook is quite healthy. With that several important economic regions keep growing, the development momentum will not be reversed.

Ever since 90's of the last century, the world economy was slowing down as a result of the regional turmoil in Southeast Asia. But this is a global cyclic economic recession. In fact, the key macro economic indicators showed at the opposite that the inflation and interest rates are relatively low worldwide, government deficits significantly reduced, and the environment of domestic demand and external sale quite relaxed. Thanks to institutional innovation, technological innovation and optimization of industrial structure, many economies have become more robust, with the IT-centered hi-tech industries constituting the major driving force behind. Those Asian countries, which bore the brunt of the financial crisis, still possess great potential for recovery because their economic basis remains relatively intact. Japanese economy will finally be brought back to normal when structural and institutional problems are solved, bringing new stamina to the world economy. Many experts predict that the world economy is heading for a third golden age after pre-WWI period and 1950-1973 period, with world average at around 4%.

(2) With major breakthrough in service trade liberalization, world trade will keep a steadfast development characterized by openness, fair competition and steady growth.

Openness: The three fundamental agreements of telecommunication, IT and financial services settled under WTO framework, which is distinguished by wide coverage and rapid opening up process, mark the penetration of world trade liberalization from cargo trade to service trade. Regional economic organizations have expedited the process of economic corporation. Special attention should be paid to Euro which embodies the voluntary delegation of national sovereignty of the member states, which is unprecedented in modern history. It will definitely cast profound influence on global and regional economic integration. Moreover, modern IT has already grew out of the traditional concepts of time and space. The interaction of technological advance and trade liberalization has enlarged the economic arena of many countries.

Competition: There is an intensified rivalry on market, assets and resources. The Southeast Asian financial crisis has triggered the reshuffle of world trade relations. And the competition among developing countries has become fiercer. The US' sustained attack on external trade has resulted in constant friction with Japan, Europe and new economies. Traditional trade protectionism, though still in low profile, will find its way in the WTO clauses. Raised technological and environmental standards have formed 'green barrier'. Those developing countries find their competitive edge blunted when low salary fails to bring about advantages. Things like policy, law and institutional system, which used to fall into the category of national sovereignty, have become the new focus for international trade.

The openness and fair competition will contribute to the steady development of world trade. The concepts of market, trade liberalization, and technological information, as well as cross border management of those multinational companies, cross border M&As and development of regional organizations have sped up the free flow of commodity, service, asset, technology, human resources and information in the world. The optimization of the allocation of resources, further classification of the jobs, and the expansion of market capacity will definitely push forward the steady development of world trade. It is estimated that world trade will grow at 6-7% on a year-on-year basis, 2-3 percentage higher than the growth rate of world economy. Service trade will grow 1-2 percentage faster than cargo trade.

2 FEATURES OF SHIPPING INDUSTRY AT THE TURN OF TWENTY-FIRST CENTURY

The development of the global shipping industry mainly depends on the development of the international trade, and the development of international trade is mainly based on the development of the international economy and politics. In a short time, the global shipping industry is usually effected by some bursting forth incidents in the international economy and politics. But in the long run, the development of the global shipping business mainly depends on the general trend of international economy and trade. We can see the features of shipping industry at the turn of the twenty-first century as below:

(1) The volume of the international trade will continue to grow steadily; the freight rate and quality of the transportation required will be increased constantly.

With the global economic technology developing quickly, the knowledge contained in merchandise and the value added in is increasing apparently. Therefore the volume in tons per unit in GDP is decreasing, which causes the increasing rate of the shipments in tons lower in a short time. But in a long term the volume of the international trade will continue growing steadily as a result of globalization, the freight rate will increase, and the quality of transportation increases as well. In the meantime the price of the raw commodity in the international trade will be decreasing. Accordingly, as a shipping company we should watch out the changes in the shipments' structure in the international trade, to adjust our transportation structure on time, to improve the method of transportation, and to obtain much higher freight rate, i. e., the high value-added commodities, to improve and assure the freight quality.

(2) The international transportation will enter into the era of comprehensive transportation, to accomplish the logistics system modernization.

With the development of international economy and trade, more and more transnational companies are requiring shipping companies to provide the global transport services. After the bulk carrier specialization and containerization, the international shipping is entering into the era of modern logistics. In the 21 century the new transport means will turn so many isolated transport methods into a whole system. In the future one shipping company should operate every method of the transportation. The carrier will not only transport the commodities from port to port, but also from door to door, from point to point.

Actually many large shipping groups have already made the modern logistics as their strategy. For instance, Maersk has announced that logistics will be their important business in the future. OOCL has planned to turn into a whole logistics provider in five years. NOL has changed their strategy to increase their logistics income ratio from 8% in 1998 to 30% in 5 years, and to decrease their owned-ship ratio as well. With the expansion of the value chain, those shipping companies who have developed the logistics services are lifting the competition platform from low level price-competition to the total logistics services value-competition. The shipping companies are facing more and more pressure from the lowering their cost and improving their services.

At the same time, the port is no longer the terminal of transportation, but only a part of the whole transport chain in international trade. As a result, for the time being the function of port will be changed completely and revolutionarily to comprehensive transportation center. The shipping companies are and will be increasing investment in port development.

(3) The international shipping market is becoming " the buyer's market". The competition in shipping industry is getting more and more intense. Shipping companies are providing the "mass customization" services, introducing larger and higher-speed ships, and pushing forward the development of middle-sized and small-sized ships in the meantime.

Currently the global shipping has already turned into the "buyer's market". With the development of the shipping industry, the "buyer's market" is furthering and the competition in shipping industry is getting heated. The shippers will require the carriers more and more specialized services, such as providing express services and calling fewer ports. On the other hand, the carriers will provide more and better services to satisfy the shippers' specialized services requirement. In order to provide the specialized services, and accomplish their own scale-economy as well, some shipping companies with foresight are ready to provide the "mass customization" services, which can satisfy both sides. To provide the service, the ships are getting larger and pushing forward with the middle-sized and small-sized ships' development in the meantime.

At the same time ship's speed is increasing. At the moment, the designed speeds of post-panamax containership are between 25-27 knots. According to some reports, many shipyards and shipping companies are designing the ships whose capacity is 8000~12000 TEU, and the speed is up to 30 knots. Norasia has already operated a 1400 TEU ship with 25 knots speed; Fastship has also planned to develop the 38 knots speed container ship in the transatlantic service. Their aim is not only to compete with other liners, but also to contend for the air freight market.

(4) Shipping companies are building a global information network shared by different companies all over the world.

As we all know, the New Economy is based on the information technology. It is the high-developed information technology that gives birth to the New Economy. The shipping companies should also harvest the benefit that IT brings. The shipping companies should attach more importance to the modernization of the information system, because a modernized information system will help shipping companies make better use of resources and become more competitive.

The Japan Maritime Research Institute recently conducted a general inquiry on the development of information system. About 20 liner companies responded to the inquiry. The result showed that 23% of the companies had built up the central information-process system, 31% had built up regional information system, and the remaining 46% had both systems. 85% companies provided booking and inquiring service via Internet. 31% had yield management system, other companies were developing such systems. So information technology has become a key measure for shipping companies to cut management cost, improve service quality, and get competitive edge.

(5) Trends of cooperation will be further developed from slot chartering to setting up alliance.

There have been tens of major mergers in international shipping industry recent years, such as P&O and NEDLLOYD in September of 1996, NYK and SHOWA in June of 1998, MOL and NAVIX in April of 1999. Some major acquisitions such as APL by NOL in April of 1997, and Sealand by Maersk in July of 1999.

(6) The role of liner conferences are gradually decreasing

The shipping policies of EU and US tend to be more and more liberalized, rendering a heavy blow to liner conferences. The emergence of Asian liner shipping carriers poses tremendous pressure on traditional liner conferences. And the fast development of global alliances also leaves liner conferences less active. You can see the changes in recent years from the evolution of liner conference organizations on the East-West trunk services.

The FEFC, based in London, was divided into 3 parts in 1992, namely MJEFC, WRA and EMA. In 1994, Mediterranean Westbound Liner Conference became independent, with JMFC of Japan/Mediterranean trade and AMRA of Asia/Mediterranean trade as parts of it. On the Far East/North America trade, liner conferences have lost their binding power as freight cartels as a result of the implementation of OSRA in May 1999, which allows ship owners to form service contract with shipper. Therefore, many freight conferences have decided to dissolve. Up to now, three conferences of ANERA, TWRA and Intra-America conference have stopped operation, and JUEFC has decided to stop setting price. TSA and WTSA nevertheless are still playing an active role.

(7) Shipping industry will be more and more liberalised, and the policy of free port will be pursued by quite a number of countries.

With the further development of world economic globalisation and trade liberalisation, international shipping will be further opened up, which in turn will prompt the adjustment of shipping policies. Traditional ways of protection have found their way in other forms, e.g., indirect hidden supporting measure vs. direct economic subsidy, and technical and environmental measures vs. administrative protection.

"Free port" is a highly efficient international trade policy aimed at promoting trade, developing regional economy and improving shipping services. It has a wider coverage than ordinary bonded warehouse, and is free of the custom supervision policy, which is quite common in the latter form. With the opening up of shipping industry and the reform of shipping policies, more and more countries will gradually phase in this free port policy.

3 COSCO GROUP IN THE TWENTY-FIRST CENTURY

COSCO Group was established in 1961. After 40 years of development, the group, who owns and operates some 500 vessels in different sizes and types with total carrying capacity of more than 20mdwt, has successfully developed itself into a large-scaled shipping conglomerate, offering services in over 1200 ports in more than 150 countries or regions. Here, I would like to express my sincere gratitude to all of you in the field of shipbuilding and shipping industries. Thank you for your consistent understanding and support for the development of our businesses in the past 40 years!

As a global ocean shipping operator, COSCO has already set the goals on how to develop itself in the new century. Under the new strategic plans, the group will continuously focus on ocean shipping as the core business by upgrading its competitive presence in the industry, further expand modern logistics business, embody itself to create outstanding capability against rivals through rationalizing, reorganizing and making full use of shipping resource as well as logistics resource. To split them into details, we intend to fix on these aspects as follows:

(1) To strengthen our core ocean shipping businesses

COSCO will continue to focus on developing container liner business while strengthening dry bulk sector and actively expanding tanker and specialized shipping businesses at the same time. What we need to do right now is to update and optimize the chain of shipping and value industries in such areas as fleet structure, voyage coverage, information technology, port service facilities, sales, marketing & canvassing system and so on. While keeping owned vessels operating profitably, we will manage to improve our financial performance by taking control of transportation demands, which are a bit more than what we actually can handle. We will adopt flexible policies of vessel-chartering tactic in accordance with the changes of market demand and supply, aiming at annually increasing the proportion of chartered vessels. As to the adjustment of voyage structure, more efforts will be made to the issues of network-planning and deployment of resources, sticking to the strategy of setting up transshipment hub around the world. Furthermore, much attention will be paid to obtaining long-term contracts and fundamental customs by providing with value-added and discrepancy of services in the field of sales & marketing sector. In short, COSCO will enable itself to meet the challenge of international merge and consolidation wave, gradually changing its position to a cooperative operator from an independent one, gradually improving the quality of our services. We are confident that we should have the capability of becoming one of the first-class shipping companies in the world.

(2) To expand modern logistics businesses

Being involved in logistics business has been identified as the inevitable choice to cater to the trend of the times and market competition. It is also regarded as the critical step for the realization of development strategy in the new century. COSCO's basic idea of dealing with modern logistics activity is based on the powerful shipping business at its core, making full use of the global abundant logistics resources, setting customer's satisfaction as our ultimate goals. The customer service portfolio begins with transportation. Then it will be expanded to such areas as storage, products-processing, cargo delivery before it finally goes through the most span of life of an product like production, circulation, distribution and consumption. COSCO will put emphasis on improving its capability of profitability and market competition by means of providing with value-added services, strengthening its presence as a global operator and gradually transiting itself to an international logistics provider. To serve this goal, the group will speed up its efforts to make out and conduct the strategy of modern logistics plan. Followed by the adjustment of structure, COSCO Logistics Group is about to set up with the support of transnational supply chain management companies, advanced information technology as well as global logistics B2B service platform, being designed to provide with products or services capable of resolving problems across the board and rapidly pushing forward the development of logistics business in the end.

(3) To optimize the land-based activity

COSCO will continue to adjust its business structure, targeting land-based activity as one of its important core of profits since this sector is now on the way of transiting from diversified pattern to a more concentrated one. Priority will be given to real estate, industry, finance and those which are more likely to gain heavy returns in profits. To set land-based business as example, COSCO will pay special attention to selecting project which should be independent or reverse to the fluctuation tendency of shipping industry with high potential of growth as well whenever we intend to get into a new game. These areas including information, environmental protection, energy-saving, new materials etc. are believed to have great complementary to ocean shipping business. In the short run, the expansion of information network turns out to be the main task in line with the requirement of company's strategic plan. In the course of running a new business, COSCO will gradually establish a set of systems which can assess risk of an investment project and help create a new profit channel.

(4) To reinforce the construction of network

The essence of the times of knowledge economy is a sort of the economy based on network. As a result, to reinforce the construction of network is sure to be not only the radical choice for COSCO positively facing up to the times of knowledge economy, but also the key to upgrading the presence as an international logistics provider. On the other hand, the task mentioned above is also the pressing matter at the moment in a move to carry out and push forward the strategy of technology innovation. COSCO is planning to optimize the layout of the current network, intensify the construction of COSCO Network on the internet basis, implement the integration of established network, aiming at building up a comprehensive network system capable of serving people both at home and aboard to take advantage of services for better distributing shipping and logistics resource worldwide.

Looking ahead to the new century, COSCO will continue to abide by the rules and regulations issued by International Maritime Organization (IMO) and SOLAS concerning the safety sailing and environment protection drive at sea around the world. In fact, some shipping arms of COSCO Group have already successfully achieved the certificates of International Safety Management Codes (ISM) and ISO9002 for quality service assurance, becoming one of the professional shipping companies with high levels of management.

1. DESIGN SYNTHESIS FOR SHIPS AND FLOATING SYSTEMS

Practical Design of Ships and Other Floating Structures
You-Sheng Wu, Wei-Cheng Cui and Guo-Jun Zhou (Eds)
© 2001 Elsevier Science Ltd. All rights reserved

A CONSIDERATION OF LIFE CYCLE COST OF A SHIP

Yasushi Kumakura[1] and Hiroshi Sasajima[2]

[1] Kinki University, Japan
[2] Ishikawajima-Harima Heavy Industries Co.,Ltd. , Japan

ABSTRACT

In order to look all phases of a product life and to analyze the cost effectiveness elements, life cycle cost of a product has been widely studied. In case of a ship, it consists of fabrication phase in shipyard, such as design and fabrication, and maintenance phase in service, such as inspection, repair and painting. So far life cycle cost of a ship has been calculated by the summation of fabrication cost and maintenance cost by the end of her life. Although it is desirable to be able to estimate the life cycle cost of a ship, when she is born in a shipyard, the estimation is very difficult due to the variety of levels of fabrication and the maintenance. In this paper main items of fabrication cost and maintenance cost of a VLCC are analyzed focusing in hull structure part, based on the actual data from shipyards and ship owners and the relations between these costs are studied.

KEYWORDS

Life cycle cost, Design, Fabrication cost, Higher tensile strength steel, Steel structure, Maintenance cost, Corrosion, Painting

1 INTRODUCTION

Ships are international commodities, which are freely sold and bought in the world. Ships are built in shipyards with the highest shipbuilding technology in the world and delivered to ship owners. Some ships are in service on the regular routes and others are in service on the irregular routes.

Transportation fees are decided in accordance with the laws of supply and demand of ships in the world markets. In consequence all the prices, including those for ship building, running, maintenance and selling to the other owners, are decided on these laws. With the participation of speculations these prices show big scale of amplitudes.

In the heavy storms of economic situation there have been many speculators who bought ships, when the prices of ships were at the bottom, made moderate maintenance on them and sold them to get big amount of profits, when their prices sharply rose. They regard the ships as the objects of speculation.

However, during these economic fluctuations the prices of building and maintenance of ships are kept rather in steady levels.

Big portions of fluctuation of prices are compulsorily absorbed by the profits of shipyards. The advanced technologies in the present days are surely applied to the new ship building and the reduced costs are shared by shipyards and ship owners.

The quality of ships at the delivery time is above the standard level, which is kept by the rules and the inspections of ship classification societies. After the delivery some ship owners intend to keep their ships for more than 20 years, the others are planning to sell their ships to get profit after using them for a few years. Then their attitudes for the inspections and maintenance of their ships are quite different. The former plan to increase the plate thickness above the rule scantlings and to raise the grade of painting specification at the construction stage, anticipating the wastage or crack initiation of hull structural members due to corrosion in service stage.

For ship owners the expenditures of ships are the summation of building cost and running costs, including inspection, maintenance cost, insurance, fuel and personal expenses of seamen. If the running costs are required much more than standard level on cheaper building cost, then life cycle cost will be increased. It should be emphasized that the importance of total summation of expenses, i.e., life cycle cost should be understood by the management of shipping companies.

On the other hand, the shipyards can not be released from the ships which they built. Fabricators have legally " Product Liability (PL)" on their products. Apart from this problem, shipyards must positively recognize the meaning of life cycle cost of ships in order to utilize the limited resources of the earth.

In this paper the life cycle cost of a VLCC is studied. To avoid the diffusion of the problem, steel structural members of VLCC are intentionally focussed and the life cycle cost is limited to the summation of building cost and maintenance cost of structural part of the hull. However the idea will be applicable to engine and outfitting parts of ships.

2 BUILDING COST

Building cost means total cost expended in a shipyard for building a ship. This is a part of life cycle cost and occupies a big amount. It is considered that building cost occupies about 2/3 of life cycle cost and maintenance cost occupies about 1/3. Table 1 shows the break down of the building cost of a VLCC with double hull.

TABLE 1

BULDING COST OF A VLCC WITH DOUBLE HULL

Items		Ratio(%)
Material	Steel	20
	Main engine	10
	Others	30
	Total	60
Fabrication		30
Design		5
Charge		5
Total		100

2.1 Material Cost

Material cost of a ship occupies a big amount and reaches to 50~60 % of the total building cost, as shown in Table 1. Among material costs, steel cost is the biggest one and occupies 35 %. For example, in a VLCC with double hull, thirty and some thousand tons of steel is used and 30~80 % of them is higher tensile strength steel.

The cost of main engine occupies about 15 % and those of other outfitting occupy about 50 %.

2.2 Fabrication Cost

Fabrication cost occupies more than 30 %. Among them hull structural part occupies about 50 % and outfitting part occupies about 15 %, depending on the features of ships.

2.3 Design Cost

It is said the ratio of design cost against the building cost of a ship is about 5 %. Design, although a simple word, continues from basic design through yard plans in shipyard, so it is a long duration before the completion. Design of ship is divided into two stages, basic design and detail design. It takes 2~3 months for basic design 6~8 months for detail design. Consequently design duration and costs vary in accordance with the features of ships.

2.3.1 Basic design

After the building contract is signed the basic characteristics of the ships are decided by basic design to satisfy the specifications attached to the contracts. Basic design consists of total design, hull structural design, outfitting design(hull part and machinery part) and electric design. The basic design cost is less than 10% of the total design cost. However by this basic design, 90 % of the total building costs of a ship is decided, so it is the most important division.

2.3.2 Detail design

This is the design for the actual building of ships and divided into functional design and fabrication design. Number of design plans of detail design exceeds some ten thousands sheets. The costs of detail design occupy 90 % of total design costs.

2.4 Influence of Application Ratio of Higher Tensile Strength Steel

The application ratio of higher tensile strength steel is between 30~ 80 % of total structural steel, depending on the requirements of ship owners. Figure 1 shows the results of the cost study on the application ratio.
(1) By increase of the application ratio of higher tensile strength steel from 23 % to 80 %, total steel weight decreases by about 6 % and material cost decreases by about 1 %.
(2) Fabrication cost decreases by about 1 % due to the change of the welding metal volumes and the reduction of the plate thickness.
(3) Design cost is not influenced by the application ratio of higher tensile strength steel.
(4) Finally the cost reduction by the application of higher tensile strength steel is about 1 %.

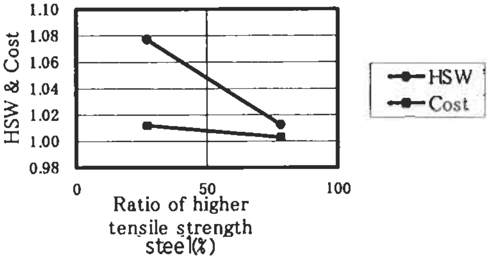

Figure 1: Influence of application of higher tensile strength steel

3 MAINTENANCE COST

Maintenance costs are influenced by the management policies of ship owners. Consequently the ship ages vary from 10 and several years to more than 20 years. Here age of 20 years is taken as standard life length.

3.1 Inspection

By IMO rules every ship classification society makes close up survey. In order to make this easier the inspection stages are installed in the double hull of VLCC, as shown in Figure 2. Using these stages close up survey is made in every part of structures.

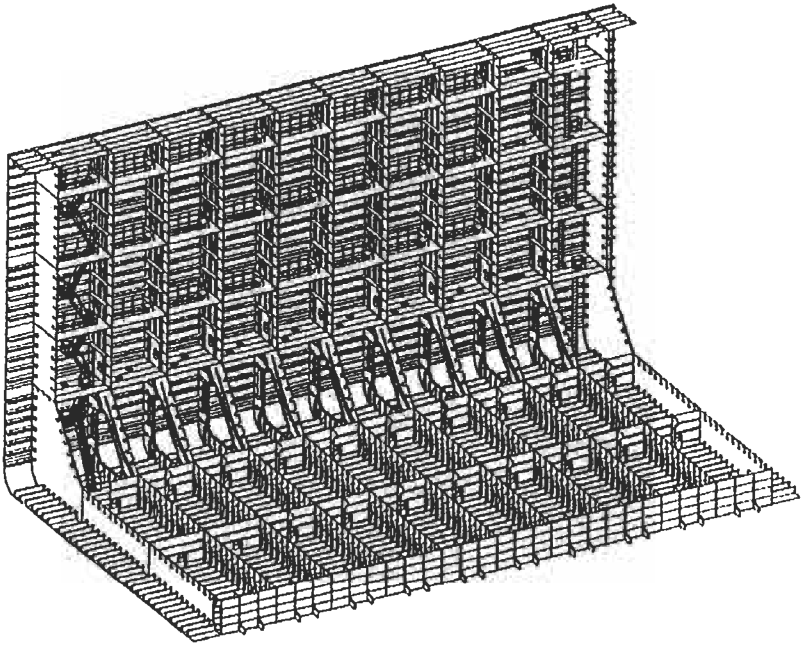

Figure 2: Maintenance stages in double hull of VLCC

Inspections are generally made at periodical survey and intermediate survey in accordance with ship classification rules. In some ships self inspections are made by ship owners and crews. By utilizing this information the scopes and costs of repairs are estimated. Also necessary materials and manpower can be previously prepared in ship yards.

It is almost impossible to make close up survey in all the holds and tanks at every inspection, so close up survey is divided into several times to concentrate on a few tanks. Maintenance costs include these inspections but comparatively small to the maintenance costs.

3.2 Repair

Repair cost is divided into general repair cost, which is periodical expenditure and special repair cost, which is required for a big failure at every few years.

In case of hull structural part, the number of failures suddenly increases after 10 years, as shown in Figure 3 (Nippon Kaiji Kyoukai, 1995). This is due to the influence of corrosion. Figure 4 indicates the same tendencies in general ships and VLCC but the average numbers of failures of VLCC are bigger than in general ships(Nippon Kaiji Kyoukai, 1995). Old aged ships have 10 failures per a year in average.

Consequently general repair cost is estimated to be 0.1 ~ 0.5 % of building cost per one repair. Special repair cost is not necessarily required for every ship but it rises to a big amount, once a big failure occurs.

Special repair cost is covered by insurance, if it is due to natural disaster.

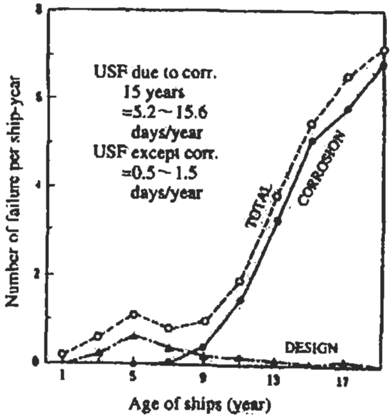

N.B:USF; unavailability due to structural defect.

Figure 3: Frequency of failure per ship-year v.s.ship's age(for all ships)

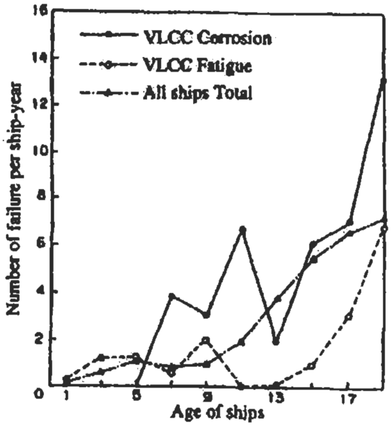

Figure 4: Frequency of failure due to fatigue and corrosion of VLCC per ship-year

3.3 Corrosion protection

Corrosion protection is very important. Paint films of ballast tanks are generally damaged after about 10 years and corrosion of steel structures starts. Plates are generally renewed one after another, if their thickness reduced 30 % by corrosion in accordance with the results of inspections.

The weight of renewed steel plates of a VLCC reaches a big amount per a year, if their painting films are not specially maintained in good condition.

4 TRADE OFF OF COST-RISK

It is a very difficult question how long the lives of ships are. They are influenced not only by technical matters, but also by political ones. Some ship owners invest enough money to building cost, expecting the less troubles in future and pay good attention for the maintenance of ships to keep their good conditions. The others repeat buy and sell of ships in short cycles to get profit from the market. It is difficult to judge their policies and to decide the best ships' lives.

Now let's compare which is a better way of maintenance from view point of life cycle costs of a VLCC at 10 years and 20 years, between by an ordinary painting or by heavy duty painting. Periodical survey is made once every 5 years and intermediate survey is made every 2 years.

The maintenance by an ordinary painting is based on the following assumptions,
(1) Number of average failures is 3 per a year until 10 years and 6 per a year after 10years.
(2) Steel weight of 20 tons is renewed at wasted structures due to corrosion every year after 10 years. It is equal to 0.25% of building cost.

From the above assumptions the life cycle cost, including building cost and maintenance costs are summarized in Table 2 for 10 years and 20 years.

If heavy duty painting is applied to this VLCC with the increase of painting cost of 20 %, which is equal to 1 % of building cost, it is estimated that the number of failures decreases by 50 % until 10 years and is kept 0 after 10 years.

The life cycle cost, including building cost and maintenance costs are summarized in Table 2 for 10 years and 20 years

TABLE 2
COMPARISON OF LIFE CYCLE COST OF A VLCC BETWEEN PAINTING METHODS

	Ordinary painting		Heavy duty painting	
	10years	20years	10years	20years
Building cost	100 %	100 %	100.50 %	100.50%
Period. surv.	0.50%	1.00%	0.50%	1.00%
Interm. surv.	0.63%	1.25%	0.63%	1.25%
Repair cost	0.38%	3.63%	0.19%	0.19%
	101.51%	105.88%	101.82%	102.94%

Then life cycle costs of both cases are shown in Figure 5. This figure shows that the life cycle cost of a VLCC with heavy duty painting is smaller than that of ordinarily painted VLCC by about 3 % at 20 years. Balancing point appears soon after 10 years. Of course there are many factors, which influence the life cycle cost, such as ratio of interest, chartering fee, oil price, etc., but it may be said that good painting will reduce life cycle cost in 20 years.

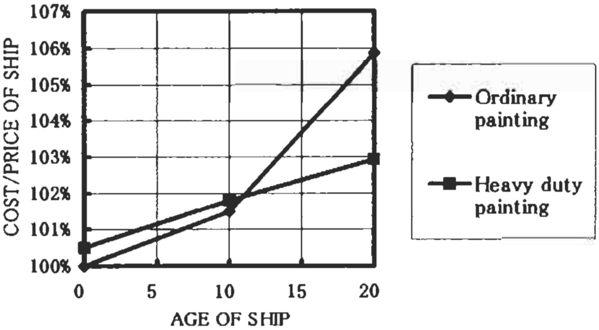

Figure 5: Comparison of life cycle cost by painting cost

5 CONCLUSIONS

In this paper main items of fabrication cost and maintenance cost of a ship are analyzed and studied, based on the actual data from shipyards and ship owners.

From these studies the following conclusions are obtained.
(1) Material cost occupies 60 % of building cost. Although basic design cost occupies 0.3 %, it decides 90 % of total building cost.
(2) By increasing the application ratio of higher tensile strength steel from 23 % to 80 % of hull structural steel, total steel weight is reduced by about 6 % and building cost is reduced by about 1 %.
(3) Life cycle cost should be taken into account in shipbuilding and ship management.
(4) For good maintenance of ships corrosion protection by painting is very important.
By applying heavy duty painting to VLCC at the building stage the life cycle cost will be reduced by about 3 %, compared with an ordinarily painted one.

Reference

KAIJI KYOKAI . (1995), *Guideline for Total Life Assessment of Ships and Offshore Structures*

Practical Design of Ships and Other Floating Structures
You-Sheng Wu, Wei-Cheng Cui and Guo-Jun Zhou (Eds)
© 2001 Elsevier Science Ltd. All rights reserved

THE EXPERIMENT OF RIVER-SEA-GOING ORE BARGE FLEET AND RENOVATION OF EXISTING INTEGRATED BARGE

Shun-Huai Chen [1], Wei Zhang [2], Jun-Ming Li [1] and Cheng-Fang Wang [1]

[1]Wuhan University of Technology,
Wuhan, Hubei, China
[2] China Changjiang Shipping Group
Wuhan, Hubei, China

ABSTRACT

Wuhan Steel Company (Group) is one of the biggest steel factories in china. Large amounts of raw material-iron ore used in this factory are imported from oversea. How to reduce the high producing cost is a key problem. A new kind of shipping system composed of river-sea-going ore barge fleet has been put forward to solving the problems such as high producing cost, environment pollution, etc. The key technology of the system is to develop a new kind of barge which can be used to form a large inland water pusher barge fleet and is suitable for navigating at sea. A typical pusher barge fleet at sea is selected to test on full scale by which the reforming has been taken to the barge. Then a model test has been carried out to check the reforming effects. In this paper, the conditions and results of tests are described. Some useful conclusions are given so that they can be applied in renovation of existing integrated barge.

KEYWORDS

Shipping system, River-sea-going ore barge, Full scale test, Model test, Renovation of existing integrated barge, Pusher-barge-line, Integrated fleet

1 INTRODUCTION

Wuhan Steel Company (Group) is one of the biggest steel factories in china. Large amounts of raw material-iron ore used in this factory are imported from oversea. The present shipping route includes three steps. The first step is from oversea mining place to the coastal harbor of China – BEILUN by 150000~300000DWT cargo ships. And then 20000~30000DWT cargo ships are used to transport iron ore from BEILUN to inland port like SHANGHAI port, NANTONG port, ZHENJIANG port. At last, the iron ore are transported from inland port to the destination by integrated barge fleet. It is not difficult to see from above that the steel producing cost is very high. It is a major problem that how to reduce the producing cost for WSC. For shipping unit, giving the best service to the users is certainly its duty. A detail tech-economic analysis has been taken to the transportation system of iron ore. Then a new kind of shipping system has been put forward to solving the problems such as high producing cost, environment pollution, etc. That is the river-sea-going ore barge fleet system. The key point of the system is to develop a new kind of barge which can be used to form a large inland water pusher barge fleet and is suitable for navigating at sea. A typical pusher barge fleet at sea is selected for full scale test to examine the possibility of using this barge fleet to consist a large freshwater pusher barge fleet. The reforming has been taken to the barge according to the full scale experiment and a model test has then been carried out to check the effects of the reforming. The research achievement has been applied to the renovations of existing integrated barge, and the operating of the system has proved its success.

2 FULL SCALE TEST AND ANALYSIS

The full scale test consisted of two parts. The first part was carried out on the sea, where the sea barge was pushed by the sea pusher. The second part was carried out on the river, where the sea barge was pushed as one of a part of large fleet by the river pusher. The ships concerned with test are listed in table 1. In order to test performance for different forms of fleet and reduce impact to the production plan, the form of fleet was altered in the test. The hybrid forms are listed in table 2.

The item of test includes fleet speed to the water, fleet speed to the bank, mooring force, manoeuvering test, operating test, etc. The equipment that used for the test includes KGP-912 navigating GPS, LS25-3 velocity-type flowmeter, marine radar,CK08 Sensor, UCOM-8L strain-gauge, C12 gyroscope, CKO6 rudder sensor, SC—16 oscillograph etc.

3 ANALYSIS OF TEST RESULTS

The river-sea-going barge in the test was typical barge for pusher-barge-line of marine route, where there is a large groove in the stern of the barge to install the pushing frame. That caused rough vortices behind stern of the barge. As we know, for large fleet, the formation of the barge is more important than the unit barge as velocity as concerned. The ideal formation for large fleet is so-called integrated tug-barge system. To pusher- barge fleet on the sea, the aft part of the barge and the fore part of the tug must transit smoothly so as to keep lower resistance. From resistance and propulsion point of view, the hybrid fleet on the river route is not ideal. Table 3 shows the working status of main engine on the river route.

TABLE 1
SHIP FOR FULL SCALE TEST

Ship name	F83002 F83005	21264	21075 21078 21198	41013	1006	22019
Ship type	Barge (sea)	Barge (river)	Barge (river)	Barge (river)	Pusher (sea)	Pusher (river)
Loa	79.2m	75m	75 m	67.5 m	32.56 m	46.2 m
Breadth	16 m	13.3 m	13 m	10.8 m	8.20 m	10 m
Depth	4.5 m	3.4 m	3.5 m	3.5 m	4.20 m	3.8 m
Draft	3.5 m	2.62 m	2.6 m	2.4 m	3.32 m	3.6 m
Deadweight	3134t	1500t	1500t	1000t		
Power	——	——	——	——	1227kW	1942kW

TABLE 2

RECORDS FOR TEST

Route & Date	Forms of fleet	Times	Anchoring times		Consuming fuel	Times for formation work
			Loading &unload	waiting		
PAOTAIWAN~BEILUN (11.28~11.29)	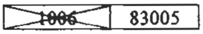	12.5h	1h	21h	2.25t	0.5h
BEILUN ~ PAOTAIWAN (11.29~11.30)	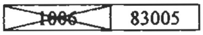	21h	0h	0h	3.25t	0.5h
PAOTAIWAN~NANTONG (11.30~12.2)	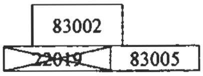 83002 22019 83005	14h	0h	10h	250kg/h	2.5h
NANTONG~MA'ANSHAN (12.2~12.4)	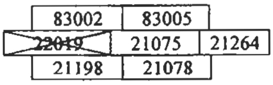 83002 83005 22019 21075 21264 21198 21078	40h	0h	11h	285kg/h	6h
MA'ANSHAN~TONGLING (12.4~12.5)	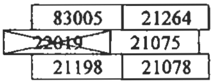 83005 21264 22019 21075 21198 21078	39.5h	0h	0h	279kg/h	1.5h
TONGLING~JIUJIANG (12.5~12.7)	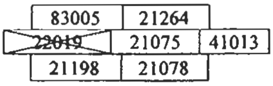 83005 21264 22019 21075 41013 21198 21078	23h	0h	0h	282kg/h	3.5h
JIUJIANG~HUANGSHI (12.7~12.8)	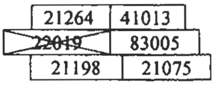 21264 41013 22019 83005 21198 21075	24h	0h	0h	255.3kg/h	4.5h
HUANGSHI~WUHAN (12.8~12.9)	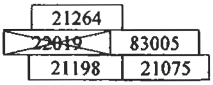 21264 22019 83005 21198 21075	21h	20h	0h	252kg/h	1.5h

TABLE 3

WORKING STATUS OF MAIN ENGINE ON RIVER ROUTE

Route	Relative fuel unit consumption	output power/specified power
PAOTAIWAN~NANTONG	1.0	54%
NANTONG~MA'ANSHAN	1.14	62%
MA'ANSHAN~TONGLING	1.116	60.7%
TONGLING~JIUJIANG	1.128	61.3%
JIUJING~HUANGSHI	1.021	55.5%
HUANGSHI~WUHAN	1.008	54.8%

The test result shows that the formation of the barge has great influence on the resistance and propulsion. In order to increase the efficiency of the transportation, the stern of river-sea-going barge

and the formation of the barges should be improved to reduce the resistance of the fleet.
The mooring force was measured when navigating on the route of NANTONG~PAOTAIWAN. When the test was carried out, the wind speed reached up 6~7 Beaufort scale. The maximum force was 31.2kN while rudder angle was 0 degree and 147.96kN while the angle was 25 degree, 274.4kN breaking force of mooring steel hawser was enough for the fleet under the test condition.

4 RENOVATION OF EXISTING INTEGRATED BARGE

Considering shipowner's assign condition and the restricting of the CHANGJIANG route, two kinds of 3000t and 5000t integrated barges are selected as investigation targets. As two kinds of barge were originally designed to navigate on the river route, the strength are unsuitable for the sea route. In order to navigate on the route of BEILUN to PAOTAIWAN(belonging to the shelter sea area), the shell and bottom structure of the 5000t barge must be replaced, that is too expensive for shipowner. For the 3000t barge, a few modifications such as reducing the cargo hatch opening and structural strengthening can make it suitable for the sea route. So the 3000t integrated barge was selected at last to renovate. The cross sections of 3000t barge are shown in figure 1.

According to the full scale test, the prototype of the sea barge is not ideal for the hybrid fleet on the river route. It is necessary to redesign the after bodyline. The simply cutting stern and the tunnel cutting stern were designed to contrast with the prototype. The abridged drawings are shown in figure 2.The main dimensions are listed in table 4.

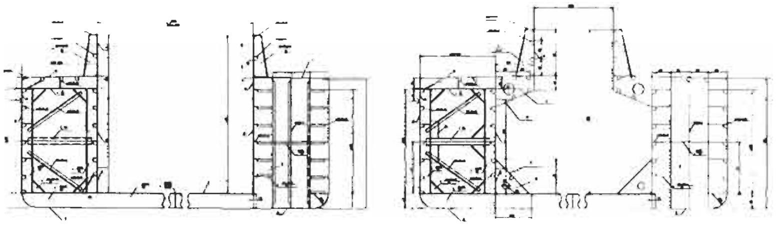

before changed after changed

Figure 1: The cross section structure

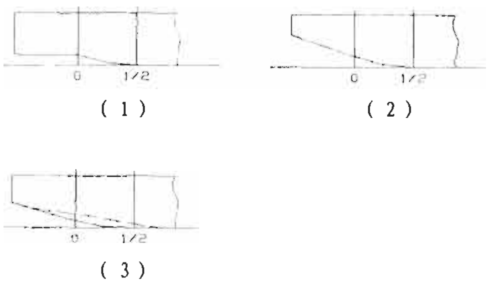

(1) prototype (2) simply cutting stern (3) tunnel cutting stern

Figure 2: Abridged drawing of stern

TABLE 4

MAIN DIMENSIONS OF THE PROTOTYPE AND RENOVATION

Type of barge	prototype	renovation
Length overall	75.00m	79.00m
Length on waterline	73.50m	77.50m
Breadth	16.00m	16.00m
Depth	4.50m	4.50m
Draught	3.80m	3.50m

The model test was carried out by three kinds of stern. The results are demonstrated in figure 3.
Some conclusions can be drawn from the test:

1) Comparing with the prototype, in the full scale, the resistance of the simply cutting stern reduce 15% at speed 10km/h.
2) The resistance of the tunnel cutting stern reduces 19.3% at speed 10km/h comparing with prototype.
3) In order to ensure the freeboard on the sea area route, the deadweight for the tunnel cutting stern barge has to reduce 130t. Under this condition, the resistance can be reduced 26.9% at 10km/h.

Considering the resistance and the cost for the rebuilding, the simply cutting stern was selected as the renovated barge's bodylines. The structure and other performance were designed based on the direct calculation or related regulations. The rebuilding barge was suitable for coasting line. The structure and the general arrangement are shown in figure 4.

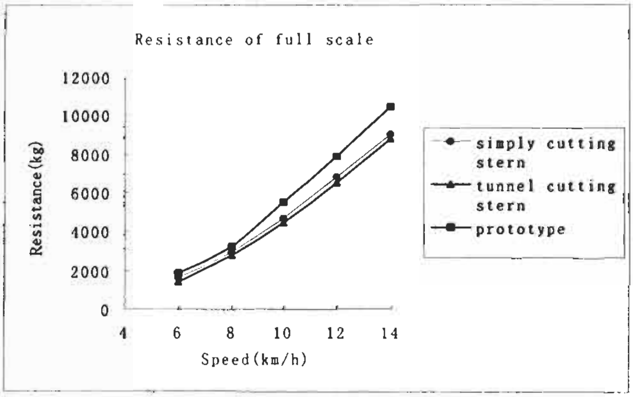

Figure 3: Test result

5 CONCLUSIONS

The pushing frame for the sea is reliable. It is convenience for the tug and barge to connect or separate. The frame makes the tug and barge linked rigidity as whole in the transverse direction while can roll in the longitudinal direction, which can ensure the safety of the fleet when navigating on the sea.

The current speed range measured in the test is from 3km/h to 13km/h. It is difficult for hybrid fleet to navigate counter-current flow in high flow speed. In order to navigate safely all the year, the design speed should be higher than 14km/h. But too high design speed is not suitable from economic point of

view. The design speed for the fleet must be considered carefully. A reasonable choice is to select a lower design speed, and by decreasing the barges of fleet or reducing cargo in high flow speed.
The typical barge bodylines for pusher-barge-line of marine route is not perfect for the large river pushing fleet. Renovating simply cutting stern is better, but it is still not perfect for the large river fleet. In order to invent ideal river-sea going fleet system, further researches must be taken on the new kind of pushing frame and ship form.

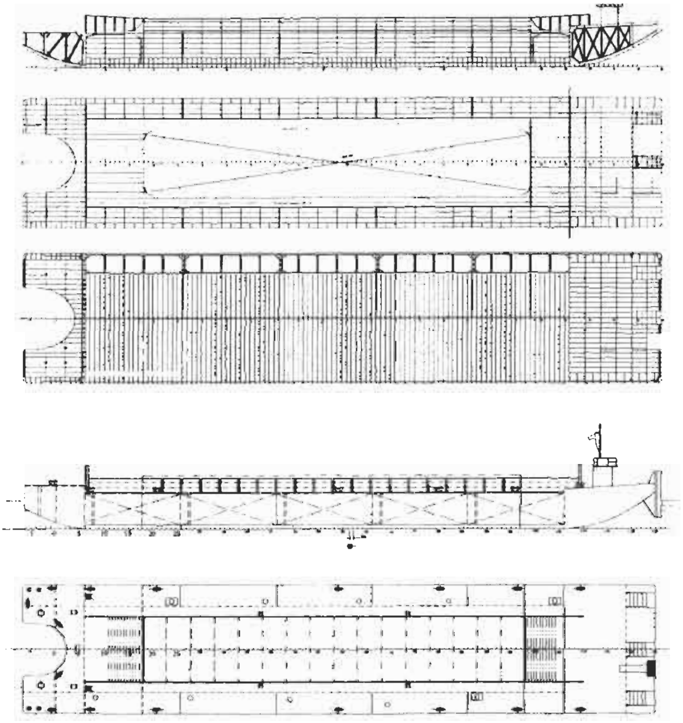

Figure 4: The structure and the general arrangement of the rebuilding barge

Practical Design of Ships and Other Floating Structures
You-Sheng Wu, Wei-Cheng Cui and Guo-Jun Zhou (Eds)
© 2001 Elsevier Science Ltd. All rights reserved

OPTIMIZATION OF A WAVE CANCELLATION MULTIHULL SHIP USING CFD TOOLS

C. Yang, R. Löhner and O. Soto

School of Computational Sciences, George Mason University
Fairfax VA 22030-4444, USA

ABSTRACT

A simple CFD tool, coupled to a discrete surface representation and a gradient-based optimization procedure, is applied to the design of optimal hull forms and optimal arrangement of hulls for a wave cancellation multihull ship. The CFD tool, which is used to estimate the wave drag, is based on the zeroth-order slender ship approximation. The hull surface is represented by a triangulation, and almost every grid point on the surface can be used as a design variable. A smooth surface is obtained via a simplified pseudo-shell problem. The optimal design process consists of two steps. The optimal center and outer hull forms are determined independently in the first step, where each hull keeps the same displacement as the original design while the wave drag is minimized. The optimal outer-hull arrangement is determined in the second step for the optimal center and outer hull forms obtained in the first step. Results indicate that the new design can achieve a large wave drag reduction in comparison to the original design configuration.

KEYWORDS

Hull form design, Hull form optimization, Wave cancellation multihull ship, Trimaran, Wave resistance, CFD tools, Slender ship approximation, Surface parameterization.

1 INTRODUCTION

A small-water-plane area, tri-hull ship, termed the wave cancellation multihull ship (or trimaran), offers the possibility of dramatic wave drag reduction due to wave cancellation. Experimental evidence, e.g. by Wilson et. al. (1993) indicates that indeed these gains are achievable. From a design point of view, an important question that requires attention is how to deal with these types of multihull ships inside a general design framework. For example: should one optimize hull position and shape at the same time, or first obtain an optimal placement of hulls, followed by an optimal hull shape? The answer is not obvious.

As a first attempt to solve such a general design problem, a two-step design process is employed in the present paper. The optimal center and outer hull forms are determined independently in the first step, where each hull keeps the same displacement as the original design while the wave drag is minimized.

The optimal outer-hull arrangement is determined in the second step for the optimal center and outer hull forms obtained in the first step. The present hull form optimization uses a gradient-based technique, which requires a field solution for each design variable. A very simple CFD tool based on the zeroth-order slender ship approximation is ideally suited for such an optimization technique because of its extreme simplicity and efficiency. It has been shown in Yang et. al. (2000) that this simple zeroth-order slender-ship theory, first given by Nobless (1983), is adequate for the purpose of determining the optimal hull arrangements for a wave cancellation multihull ship. This simple CFD tool has also been used with success for hull-form optimization in Letcher et. al. (1987) and Wyatt and Chang (1994).

The hull surface is represented by a triangulation. This triangulation can be used to evaluate the wave drag using present CFD tool. In order to obtain smooth hulls in the optimization process, the (very fast) pseudo-shell approach developed by Soto et. al. (2001) is employed. The surface of the hull is represented as a shell. The shell equations are solved using a stabilized finite element formulation with given boundary conditions to obtain the rotation and displacement fields. Almost every grid point on the hull surface can be chosen as design parameter, which leads to a very rich design space with minimum user input.

The optimal outer-hull arrangement for the optimal center and outer hulls is determined by searching the entire parameter space for each given Froude number for the purpose of minimizing the wave drag, that is evaluated very efficiently using the present simple CFD tool. Results indicate that the new design can achieve a fairly large wave drag reduction in comparison to the original design configuration.

2 OPTIMAL SHAPE DESIGN

Any CFD-based optimal shape design procedure consists of the following ingredients:

- A set of design variables that determine the shape to be optimized;
- A set of constraints for these variables in order to obtain sensible shapes;
- An objective function I to measure the quality of a design;
- A field solver to determine the parameters required by I (e.g. drag, lift, moment, etc.);
- An optimization algorithm to determine how to change the design parameters in a rational and expedient way.

The present hull form optimization uses a gradient-based technique. The gradients are obtained via finite differences. This implies that for each design parameter, a field solution has to be obtained, making the use of extremely fast solvers imperative. One optimization step may be summarized as follows:

- Evaluate the objective function I for the original geometry Σ_s.
- Evaluate the gradient of the objective function for each design variable $k = 1, N_d$:
  a) Perturb the coordinates of the *k-th* design variable in its deformation direction by a small ε; the rest of design parameters are not moved;
  b) Solving the pseudo-shell problem using given boundary condition; this yields a new perturbed geometry Σ_s';
  c) Evaluate the objective function I' for the perturbed geometry Σ_s';
  d) Obtain the gradient of the objective function with respect to the *k-th* design variable by finite differences as $(I - I')/\varepsilon$.
- Make a line search in the negative gradient direction to find a minimum.

The detailed discussion about this approach can be found in Soto et. al. (2001). In the sequel, we describe the objective function, the surface representation and the CFD solver used.

3 OBJECTIVE FUNCTION

From an engineering perspective, it is important to reduce the wave drag while still being able to achieve a given displacement. For this reason, the objective function used for hull shape optimization is given by:

$$I = \omega_1 \frac{C_W}{C_W^*} + \omega_2 \frac{|(V^* - V|}{V^*}$$

where C_W and C_W^* are the wave drag coefficient and its initial value, V and V^* the hull displacement and its initial value, and $0<\omega_1,\omega_2<1$ are relative weights. It was found to be very important to cast the optimization function in this non-dimensional form. Otherwise the weights $\omega_{1,2}$ have to be adjusted for different geometries.

4 SURFACE REPRESENTATION

There are many ways to represent surfaces. Analytical expressions given by B-Splines, NURBS or Coon's patches are common. Another possibility is to take a surface triangulation and then allow every point on the surface to move. This discrete surface representation can always be obtained from analytical surface descriptions, and, for sufficiently fine surface triangulations, provides a very rich design space with minimal user input. For this reason, this discrete surface description is used in the present work.

During optimization, the individual points on the surface may move in such a way that a non-smooth hull is produced. In order to obtain smooth hulls, the (very fast) pseudo-shell approach developed by Soto et. al. (2001) is employed. The surface of the hull is represented as a shell. The movement of points is recast as a forcing term for the movement of the shell. The shell equations are solved using a stabilized finite element formulation with given boundary conditions to obtain the rotation and displacement fields. The boundary conditions in a shape optimization problem are dictated by the design parameter displacement and the geometrical constrains. In the optimal design process, the user only needs to generate the original surface mesh and a few design variables. The rest of the design parameters and their respective deformation modes can be generated automatically by the method.

5 CFD SOLVER FOR WAVE DRAG REPRESENTATION

Consider a ship advancing along a straight path, with constant speed U, in calm water of effectively infinite depth and lateral extent. The x axis is taken along the path of the ship and points toward the ship bow, the z axis is vertical and points upward, and the mean free surface is the plane $z=0$. Non-dimensional coordinates (x, y, z) and velocities (u, v, w) are defined in terms of a characteristic length L (taken as the length of the center hull for a wave cancellation multihull ship) and the ship speed U. The wave drag C_W is evaluated using the Havelock formula

$$C_W = \frac{D_W}{\rho\ U^2 L^2} = \frac{\upsilon}{2\pi} \int_{-\infty}^{\infty} \frac{k\, d\beta}{k-\upsilon} \quad (S_r^2 + S_i^2) \tag{1a}$$

for the energy radiated by the far-field waves. D_W is the wave drag and ν is defined as

$$\upsilon = \frac{1}{2F^2} \qquad with \qquad F = \frac{U}{\sqrt{gL}} \tag{1b}$$

Furthermore the wavenumber k in Eqn. 1a is defined in terms of the Fourier variable β as

$$k(\beta\ ) = \upsilon + \sqrt{\upsilon^2 + \beta^2} \tag{1c}$$

S_r and S_i are the real and imaginary parts of the far-field spectrum function $S = S(\alpha, \beta)$ where α is defined in terms of the Fourier variable β as

$$\alpha\ (\beta\ ) = \sqrt{k(\beta\ )} \Big/ F \tag{1d}$$

This relation and expression Eqn. 1c follow from the dispersion relation $F^2\alpha^2 = k$.

The wave spectrum function $S = S_r + i\, S_i$ in the Havelock integral (Eqn. 1a) is approximated here by the zeroth-order slender ship approximation defined in Noblesse (1983) as

$$S = \int_{\Sigma} n^x e^{k\ z + i(\alpha\ x + \beta\ y)} dA + F^2 \int_{\Gamma} (n^x)^2 t^y e^{i(\alpha\ x + \beta\ y)} dL \tag{2}$$

Here, dA and dL stands for the differential elements of area and arc length of the mean wetted hull surface Σ and the mean waterline Γ, and n^x and t^y are the x and y components of the unit vectors, $\vec{n} = (n^x, n^y, n^z)$ and $\vec{t} = (t^x, t^y, 0)$, normal to the ship hull surface Σ and tangent to the ship waterline Γ; $\vec{n}$ points inside the flow domain (i.e. outside the ship) and $\vec{t}$ is oriented clockwise (looking down). Thus the wave spectrum function S in the Havelock formula for the wave drag is defined explicitly in terms of the ship speed and the hull form in the zeroth-order slender ship approximation.

The present wave cancellation multihull ship (see Wilson et. al. (1993) and Yang et. al. (2000)) consists of one main center hull centered at $(0, 0, 0)$ and two identical outer hulls centered at $(a, \pm b, 0)$. In the first step of the optimal design process, the wave drag for each individual hull is evaluated using Eqns. 1-2, and the center hull and the outer hull are optimized independently for the purpose of minimizing the wave drag of each hull.

In the second step of the optimal design process, the total wave drag C_W for the optimal center and outer hull forms obtained form the first step needs to be computed so that an optimal arrangement of the outer hull with respect to the center hull can be determined. The total wave drag C_W for such a wave cancellation multihull ship can be expressed as (see Yang et. al. (2000))

$$C_W = C_W^c + 2C_W^o + C_W^i \tag{3a}$$

where C_W^c and C_W^o are given by

$$C_W^c = \frac{\upsilon}{2\pi} \int_{-\infty}^{\infty} \frac{k\, d\beta}{k - \upsilon} \quad (S_r^{c2} + S_i^{c2}) \tag{3b}$$

$$C_W^o = \frac{\upsilon}{2\pi} \int_{-\infty}^{\infty} \frac{k\, d\beta}{k - \upsilon} \quad (S_r^{o2} + S_i^{o2}) \tag{3c}$$

and represent the wave drags of the center hull and of an outer hull, respectively. The spectrum functions $S^c = S_r^c + iS_i^c$ and $S^o = S_r^o + iS_i^o$ are defined by Eqn. 2 in which Σ, Γ are taken as Σ_c, Γ_c or Σ_o, Γ_o, i.e., the wetted surface and waterline of the center hull or the outer hull. The component C_W^i accounts for interference effects and is defined as

$$C_W^i = \frac{\upsilon}{2\pi} \int_{-\infty}^{\infty} \frac{k\, d\beta}{k - \upsilon} \quad \{\frac{A}{2}\cos(2b\beta\ ) + A^R \cos(a\alpha\ )\cos(b\beta\ ) + A^I \sin(a\alpha\ )\cos(b\beta\ )\} \tag{3d}$$

where A, A^R and A^I are defined as

$$\begin{Bmatrix} A \\ A^R \\ A^I \end{Bmatrix} = \begin{Bmatrix} (S_r^o)^2 + (S_i^o)^2 \\ S_r^c S_r^o + S_i^c S_i^o \\ S_i^c S_r^o - S_r^c S_i^o \end{Bmatrix} \tag{3e}$$

It is noted that the wave spectrum functions S^c and S^o are independent of the parameters a and b within the current approximation. Therefore, the wave spectrum functions S^c and S^o defined by Eqn.

2 and the related functions A, A^R and A^I given by Eqn. (3e) similarly need to be evaluated only once per Froude number.

6 NUMERICAL RESULTS AND CONCLUSIONS

The first design problem considered here is to determine the optimal hull arrangement for the original wave cancellation multihull ship for the purpose of minimizing the wave drag of the ship. Figure 1 depicts the experimental values of the residuary drag coefficient C_R given in Wilson et. al. (1993) and the corresponding predictions of the wave-drag coefficient C_W given by the present method for the four hull arrangements. These hull arrangements correspond to a=-0.128, -0.205, -0.256, -0.385 and b=0.136 for all four cases. In this figure, the C_R and the C_W are nondimensionalized in terms of the surface area of the wetted hull, in the usual fashion. In the rest of the figures, the C_W is defined by Eq. 1a. It can be seen that the C_W predicted by the present method is in fair agreement with the experimental C_R. In particular, the variation of C_R with respect to the Froude number F is well captured by the theory. The present method may therefore be used for the purpose of determining the optimal arrangements of the outer hulls.

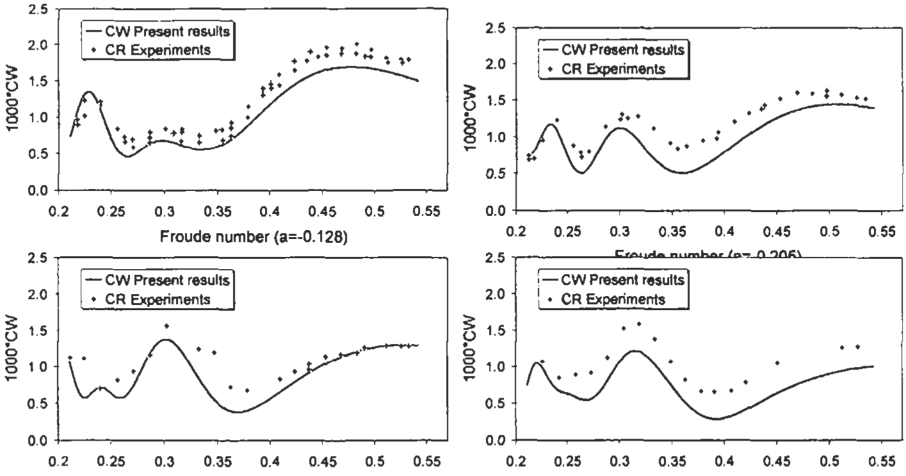

Figure 1: Calculated wave drag and experimental residuary drag

The hull arrangements within the range of $-0.75 \le a \le 0.75$ and $0.1 \le b \le 0.3$ with $\Delta a = 0.025$ and $\Delta b = 0.01$ are studied for 38 values of Froude numbers with $0.2147 = F_1 \le F_i \le F_{38} = 0.5426$. For a=0.75, the sterns of the outer hulls are aligned with the bow of the main center hull; similarly, the bows of the outer hulls are aligned with the stern of the center hull if a=-0.75. This study represents $61 \times 21 = 1281$ hull arrangements and $61 \times 21 \times 38 = 48678$ evaluations of C_W. The optimal hull arrangement for the speed range $F_1 \le F_i \le F_{38}$ approximately corresponds to a=0.55, b=0.11. Fig. 2 depicts the variations, with respect to the Froude number F, of the "no-interference wave-drag coefficient", $C_W^c + 2C_W^o$ and of the wave-drag coefficients C_W^{best} and C_W^{worst} associated with the best and worst hull arrangements found within the region. Fig. 2 also shows the wave drag-coefficient curve $C_W^{optml}(F)$ for the optimal hull arrangement (a=0.55, b=0.11). The wave-drag coefficient curve $C_W^{optml}(F)$ corresponds to a hull arrangement that remains fixed over the entire speed range, while the curves $C_W^{best}(F)$ and $C_W^{worst}(F)$ are associated with hull arrangements that vary with speed. The large differences between C_W^{best} and C_W^{worst} apparent in Fig. 2 demonstrate the importance of selecting favorable hull arrangements. Indeed, Fig. 2 shows that the ratio, C_W^{best}/C_W^{worst}, approximately varies between 2 and 6 within the speed range considered. Fig. 2 also shows that the wave-drag curve, $C_W^{optml}(F)$, is significantly lower than the curve $C_W^{worst}(F)$ corresponding to the worst hull arrangements, and even the curve corresponding to the no-interference wave drag $C_W^c + 2C_W^o$, over most of the speed range. In fact, the curve $C_W^{optml}(F)$ is remarkably close to the curve $C_W^{best}(F)$ corresponding to the best hull arrangement at every speed, over a broad speed range.

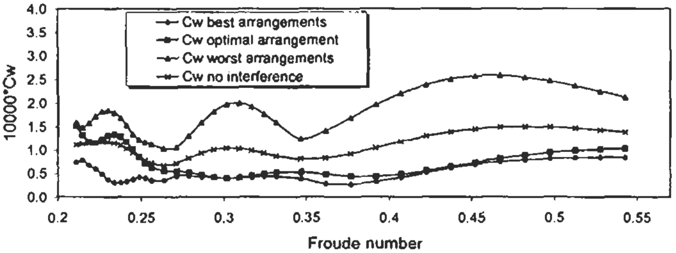

Figure 2: Wave drag coefficient for different hull arrangements

The second design problem considered here consists of two steps. The optimal center and outer hull forms are determined independently in the first step using present optimization technique. The center and outer hulls of the original wave cancellation multihull ship are used, respectively, as starting baseline hulls in the optimization cycles. During the optimization process, each hull keeps the same displacement as the original design while the wave drag is minimized. There are 76 design variables for the center hull and 64 for the outer hull. Four design cycles are required for each hull form optimization.

The optimal center hull (*A*) is obtained by minimizing $C_W^c(F)$ for one Froude number, *F*=0.5, and the optimal center hull (*B*) is obtained by minimizing $C_W^c(F)$ for five values of Froude number, *F*=0.3, 0,35, 0.4, 0.45, 0.5. Fig. 3a depicts the predicted wave-drag-coefficient curves corresponding to theoriginal center hull and two optimal center hulls. Fig. 3a indicates that the wave drag associated with the optimal center hull (*A*) is reduced tremendously in comparison to the original center hull when the Froude number is above 0.4. However, the wave drag is increased slightly at lower Froude numbers. Fig. 3a also indicates that the wave drag associated with the optimal center hull (*B*) is reduced over almost the entire speed range in comparison to the original center hull. As expected, the

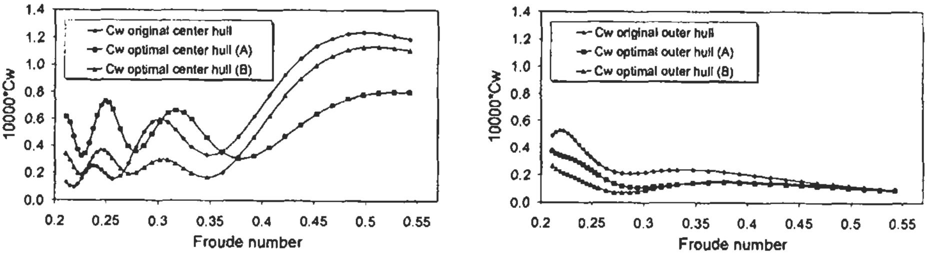

Figure 3: Wave drag coefficient for original and optimal hulls

wave drag reduction for the optimal center hull (B) at high Froude numbers is not as pronounced as that for the optimal center hull (A). Similarly, the optimal outer hull (A) is obtained by minimizing $C_W^o(F)$ for one Froude number, F=0.35, and the optimal center hull (B) is obtained by minimizing $C_W^o(F)$ for two values of Froude number, F=0.3, 0,35. Fig. 3b depicts the predicted wave-drag-coefficient curves corresponding to the original outer hull and two optimal outer hulls. Fig. 3b indicates that the optimal outer hull (B) has a larger wave drag reduction than that of the optimal outer hull (A) over almost the entire speed range in comparison to the original outer hull. Therefore, the optimal outer hull (B) and the optimal center hulls (A) and (B) will be used further on as two optimal hull design cases for determining the optimal hull arrangements. The optimal center and outer hulls are shown in Fig. 4.

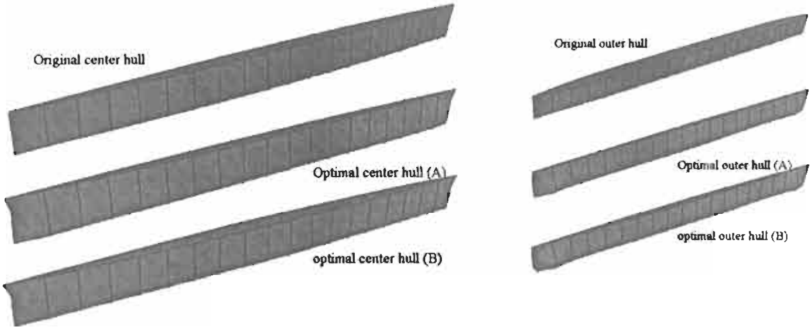

Figure 4: Original and optimal center and outer hulls

The optimal hull arrangement is determined in the second step of the design process using the hull forms obtained in the first step of this design problem. The same methodology and notations, described in the first example, are used hereafter for the combinations of two optimal center hulls and one optimal outer hull, i.e., optimal hull (A) (optimal center hull (A) and optimal outer hull (B)) and optimal hull (B) (optimal center hull (B) and optimal outer hull (B)), for the purpose of minimizing the wave drag of each new wave cancellation multihull ship. The optimal hull arrangements for the optimal hull (A) and (B) approximately correspond to a=0.65, b=0.11 and a=0.60, b=0.11, respectively. Fig. 5 depicts the variations, with respect to the Froude number F, of the computed wave-drag coefficients associated with the optimal hull arrangements obtained for the original hull (a=0.55, b=0.11) and optimal hull (A) (a=0.65, b=0.11) and optimal hull (B) (a=0.60, b=0.11), and the wave drag coefficients associated with the experimental arrangements for the original hull. Fig. 5 indicates that the optimal hull (A) can reach large wave drag reduction when the Froude number is above 0.4, and the optimal hull (B) can achieve noticeable drag reduction for almost the entire speed range. Fig. 5 also shows that the fourth experimental arrangement (a=-0.385, b=-0.136) are the best one for the purpose of minimizing the wave drag at higher Froude numbers in comparison to the other three experimental arrangements. Fig. 7 depicts the wave drag reduction for the optimal designs of the original hull, optimal hull (A) and optimal hull (B) with respect to the fourth experimental arrangement (a=-0.385, b=-0.136) of the original hull. This figure shows that these three designs can reduce drag for almost the entire speed range. The maximum wave drag reductions for these three designs are approximately 20%, 56% and 40% in high-speed range, and 71%, 76% and 87% in low- speed range.

In summary, the present simple CFD tool, coupled to a discrete surface representation and a gradient-based optimization procedure, can be used very effectively for the design of optimal hull forms and optimal arrangement of hulls for a wave cancellation multihull ship. Results indicate that the new design can achieve a fairly large wave drag reduction in comparison to the original design configuration. This optimization technique can be readily used in the routine single hull or multihull ship design to minimize the wave drag.

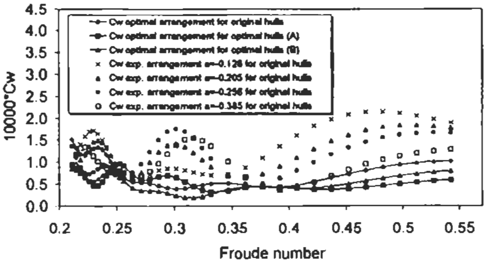

Figure 5: Wave drag coefficient for different hull forms and hull arrangements

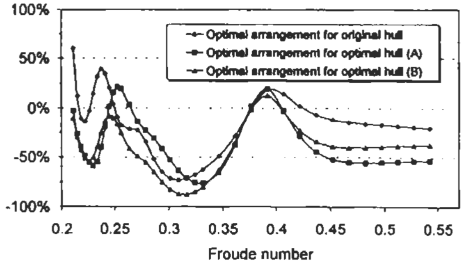

Figure 6: Wave drag reduction for different optimal hull arrangements

Acknowledgements

This work was partially funded by AFOSR (Dr. Leonidas Sakell technical monitor) and by NRL (Dr. William Sandberg technical monitor). All computer runs were performed on a 128-Processor R10000 SGI Origin 2000 at NRL.

References

Letcher, J.S. Jr., Marshall, J.K., Oliver, J.C. III and Salvesen, N. (1987) Stars & Stripes. *Scientific American*, **257**: 34-40.

Noblesse, F. (1983). A slender-ship theory of wave resistance. *Journal of Ship Research*, **27**: 13-33.

Wilson, M.B., Hsu, C.C. and Jenkins, D.S. (1993). Experiments and predictions of the resistance characteristics of a wave cancellation multihull ship concept, *23rd American Towing Tank Conf.*, 103-112.

Soto, O., Löhner, R. and Yang, C. (2001) A Stabilized pseudo-shell approach for surface parameterization in CFD design problems, submitted to *Comm. In Num. Method in Engineering*.

Wyatt, D.C. and Chang, P.A (1994). Development and assessment of a total resistance optimized bow for the AE 36. Marine Technology, **31**: 149-160.

Yang, C., Noblesse, F., Löhner, R., Hendrix, D. (2000). Practical CFD applications to design of a wave cancellation multihull ship. *23rd Symp. On Naval Hydrodynamics*, Val de Reuil, France.

Practical Design of Ships and Other Floating Structures
You-Sheng Wu, Wei-Cheng Cui and Guo-Jun Zhou (Eds)
© 2001 Elsevier Science Ltd. All rights reserved

A MODULE-ORIENTED OPTIMIZATION TOOL

Philippe Rigo

Deparment of Naval Architecture (ANAST) and NFSR*, University of Liege,
Chemin des Chevreuils n°1, B52/3, B-4000 Liege, Belgium
(*) National Fund for Scientific Research

ABSTRACT

The development of the LBR-5 "Stiffened Panels Software" is included in the development of a new design methodology to ease and to improve preliminary studies of naval structures and floating hydraulic structures. The ultimate target is to link standard design tools (steel structure CAD, hull form, hydrostatic curves, floating stability, weight estimation, etc.) with a rational optimization design module and a minimum construction cost objective function. This paper focuses on the "Module-Oriented Optimization" methodology and on the rational constraints. LBR-5 allows, as of the first draft, an optimization of the scantling of the structure's constituent elements. Relevant limit states of the structure are taken into account thanks to a 3D rational analysis of the structure. The optimization module is composed of 3 basic modules (OPTI, CONSTRAINT and COST).

KEYWORDS

Optimization, Preliminary design, Stiffened structure, Construction cost, Design methodology, Rational constraints, Structural constraints, Limit states.

1 INTRODUCTION

Floating structures are complex structures, generally composed of strongly stiffened plates, deck plates, bottom plates, and sometimes intermediate decks, frames, bulkheads, etc. Optimization of these complex structures is the purpose of this paper.

Structural design is always defined during the earliest phases of a project. It is thus not difficult to understand why a preliminary design stage optimization tool is attractive. This is precisely the way the LBR-5 optimization software for stiffened structures was conceptualised (Rigo 2001.a). "LBR-5" is the French acronym of "Stiffened Panels Software". Our target is to link standard design tools (steel structure CAD, hull form, hydrostatic curves, floating stability, weight estimation, etc.) with a rational optimization design module and a minimum construction cost/weight objective function. LBR-5 is this rational optimization module for structures composed of stiffened plates and stiffened cylindrical shells. It is an integrated model to analyze and optimize naval and hydraulic structures at their earliest stages: tendering and preliminary design. Initial scantling is not mandatory. Designers can start directly with an automatic search for optimum sizing (scantling). Design variables (plate thickness, stiffener dimensions and their spacing) are freely selected by the user.

LBR-5 (Figure 1) is composed of 3 basic modules (OPTI, CONSTRAINT and COST). The user selects the relevant constraints (geometrical and structural constraints) in external databases. Standard constraint sets are also proposed to users.

This paper describes briefly the rational optimization procedure, the innovative concept and methodology, and the way they are implemented. It focuses on the "Module-Oriented Optimization" concept and on the CONSTRAINT module. The LBR-5's major uniqueness is how the different modules interact.

A detailed application on the optimization of a floating storage offloading unit (FSO) and the relevant information on the mathematical algorithm of the OPTI module are available in Rigo (2001.b). Detailed information on the COST module is available in Rigo (2001.c).

As its advantages appear mainly at this level, application fields of LBR-5 include hydraulic structures and naval structures and concern the preliminary design stage. It is indeed during the first stages of the project that flexibility, modelling speed and ease of use provide precious help to designers. At this moment,few parameters/dimensions have been definitively fixed and a coarse modelling by standard finite elements is often unusable. For ships, the application domain is clearly the ship's central part (cylindrical and prismatic zone of cargo ships, passenger vessels, etc.). This zone is the most important in length for the big floating units.

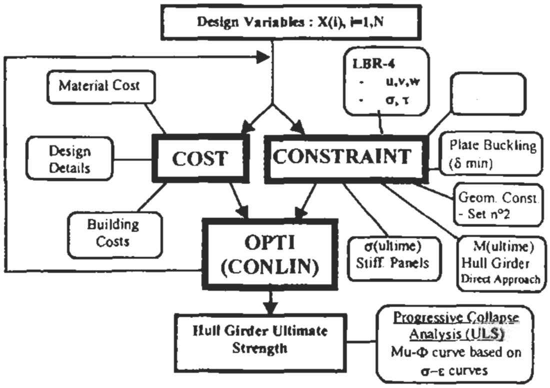
Design Variables : X(i), i=1,N
Material Cost
LBR-4
- u,v,w
- σ, τ
Design Details
COST
CONSTRAINT
Plate Buckling (δ min)
Geom. Const - Set n°2
Building Costs
OPTI (CONLIN)
σ(ultime) Stiff. Panels
M(ultime) Hull Girder Direct Approach
Hull Girder Ultimate Strength
Progressive Collapse Analysis (ULS)
Mu-Φ curve based on σ-ε curves

Figure 1: LBR-5 flow chart including some available sub-modules (constraints and cost data).

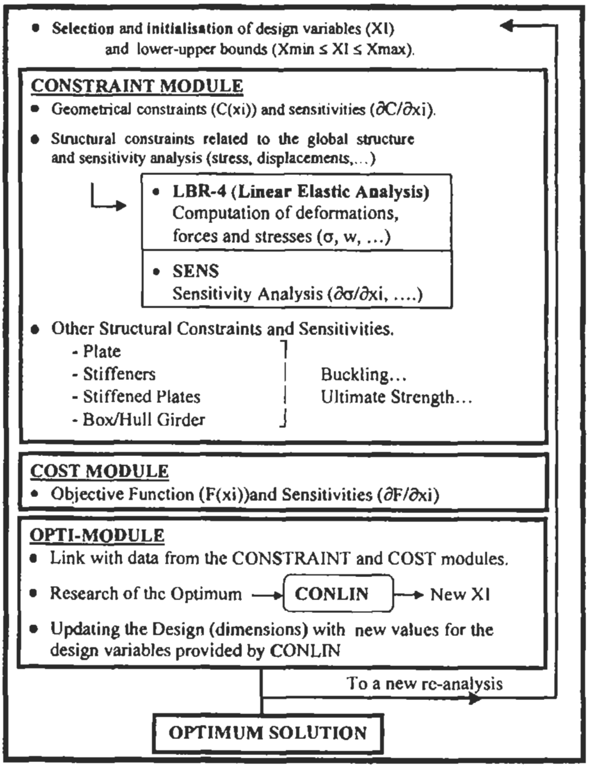

- **Selection and initialisation of design variables (XI) and lower-upper bounds (Xmin ≤ XI ≤ Xmax).**

CONSTRAINT MODULE

- Geometrical constraints (C(xi)) and sensitivities (∂C/∂xi).
- Structural constraints related to the global structure and sensitivity analysis (stress, displacements,...)

- **LBR-4 (Linear Elastic Analysis)** Computation of deformations, forces and stresses (σ, w, ...)
- **SENS** Sensitivity Analysis (∂σ/∂xi, ...)

- Other Structural Constraints and Sensitivities.
  - Plate
  - Stiffeners
  - Stiffened Plates
  - Box/Hull Girder

Buckling...
Ultimate Strength...

COST MODULE

- Objective Function (F(xi))and Sensitivities (∂F/∂xi)

OPTI-MODULE

- Link with data from the CONSTRAINT and COST modules.
- Research of the Optimum → CONLIN → New XI
- Updating the Design (dimensions) with new values for the design variables provided by CONLIN

To a new re-analysis

OPTIMUM SOLUTION

Figure 2: Chart of the LBR-5 model with CONSTRAINT, COST and OPTI modules.

For smaller units (sailboats, small craft, etc.), the cylindrical zone is smaller, or even non-existent. In this case, the LBR-5 model can be used to perform transverse cross-section optimization (midship section).

The module can also be used in the final stage of the project to perform a general verification or to refine the scantling. In addition, LBR5 can be advantageously used for education and training purposes, for instance to support lectures on 'Ship Design Methodology', 'Structure Analysis', 'Ship Optimization', etc. Many papers and books have been written on design philosophy and methodology, both present and future. The most well known methodology for the design of naval and marine structures is the "Design Spiral". Despite its age, it is still used. However the current tendency is to break with this design process and move towards "Concurrent Engineering". A comprehensive bibliography review related to design methodology is presented in Rigo (2001.c).

LBR-4 (Rigo 1992), the previous version of the "stiffened panel method" for elastic analysis of stiffened structures, was the starting point for the development of the LBR-5 optimization module presented in this paper. The role of LBR-4 is to provide a fast and reliable assessment of the stress pattern existing in the 3D stiffened structure.

The LBR-5 software is the result of the integration inside the same package of the LBR-4 (Rigo 1992) and CONLIN (Fleury 1988) software and constitutes a new tool to achieve scantling optimization of midship section. Methods similar to LBR-5 are proposed by, for instance, Hughes and al (1992) and Rahman and al (1995). LBR-5 is essentially preliminary design oriented. The structure modelling is simple and fast, but not over-simplified.

The optimized scantling can be obtained within a couple of hours (maximum 1 day for complex structures if starting from scratch). LBR-5 does not have the capability of a finite element analysis and is restricted to prismatic structures and linear 3D analysis. But, on the other hand, LBR-5 uses explicit exact first order sensitivities (derivatives of the constraint and objective functions by the hundreds of design variables). Heavy and time consuming numerical procedures are not required. Sensitivities are directly available as the method is based on an analytic solution of the differential equations of cylindrical stiffened plates using Fourier series expansions. So, sensitivity formulations are known analytically. In addition LBR-5 does not need to use the concept of local and global design variables. Due to the efficient CONLIN mathematical optimization algorithm (convex linearization and dual approach), optimization of the full structure can be performed with hundreds of design variables and constraints using less than 10~15 global structure re-analysis.

2 LBR-5 AND THE CONCEPT OF "MODULE-ORIENTED OPTIMIZATION"

A multi-purpose optimization model, open to users and compatible with different codes and regulations must contain various analysis methods for strength assessment that could be easily enriched and complemented by users. The user must be able to modify constraints and add complementary limitations/impositions according to the structure type studied (hydraulic, naval, offshore structures, etc), the code or the regulation in force and to his experience and ability in design analysis. The objective is to create a user-oriented optimization technique, in permanent evolution, i.e. that evolves with the user and his individual needs. We define this as "Module-Oriented Optimization".

The LBR-5 optimization model is based on this new concept and is composed of several modules. Neither the module number nor their type is imposed. At the start, the whole model is made up of 3 basic modules (Fig. 1) and forms the framework of the tool (COST, CONSTRAINT and OPTI).

Around the COST and CONSTRAINT modules there are a large number of sub-modules. Each of these sub-modules is specific to a type of constraint. In principle, it is necessary to have at least one sub-module for each constraint type. To date, only a limited number of modules are available (in general 1 or 2 for each constraint type). It is up to the user to complete, adapt and add new modules according to his specific requirements (type of structure, codes and regulations to be followed, technical and scientific level, available hardware, etc.). The objective is to enable the user himself to build the tool he needs.

Figures 1 and 2 show the basic configuration of the LBR-5 software with the 3 fundamental modules (COST, CONSTRAINT and OPTI) and the "DATABASES" in which the user can do his "shopping", i.e. chôose the relevant constraints and cost data. After selecting the geometrical and structural constraints and cost assessment tools in the databanks.

3 DESCRIPTION OF THE 3 BASIC MODULES: OPTI, CONSTRAINT AND COST

The problems to be solved can be summarised as follows:

▪ X_i	$i = 1, N,$	the N design variables,
▪ $F(X_i)$		the objective function to minimize,
▪ $C_j(X_i) \leq CM_j$	$j = 1,M$	the M structural and geometrical constraints,
▪ $X_{i\,min} \leq X_i \leq X_{i\,max}$		upper and lower bounds of the X_i design variables: technological bounds (also called *side constraints*).

The structure (Figure 3) is modelled with stiffened panels (plates and cylindrical shells). For each panel one can associate up to 9 design variables (X_i). These 9 design variables are respectively:

- Plate thickness (*1*),
- For longitudinal members (stiffeners, crossbars, longitudinals, girders, etc.):
  - web height and thickness (*2, 3*),
  - flange width (*4*),
  - spacing between 2 longitudinal members (*5*)
- For transverse members (frames, etc.):
  - web height and thickness(*6, 7*),
  - flange width (*8*),
  - spacing between 2 transverse frames (*9*).

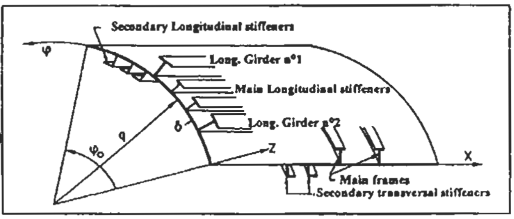
Secondary Longitudinal stiffeners
φ
Long. Girder n°1
Main Longitudinal stiffeners
δ
Long. Girder n°2
q
φ₀
Z
X
Main frames
Secondary transversal stiffeners

Figure 3: Basic stiffened panel (or basic element).

The **OPTI module** (Figure 2) contains the mathematical optimization algorithm (CONLIN) that allows solving non-linear constrained optimization problems. It is especially effective because it only requires a reduced number of iterations. In general, fewer than 15 iterations (including a structure re-analysis) are necessary, even in presence of several hundred design variables (X_i). CONLIN is based on a convex linearization of the non-linear functions (constraints and objective functions) and on a dual approach (Fleury 1989). This module uses as inputs the results/outputs of the two other basic modules, i.e. CONSTRAINT for the $C(X_i)$ constraints and COST for the $F(X_i)$ objective function. Due to the choice of a dual algorithm (CONLIN), the treatment of side constraints (X_i min and $X_{i\,max}$) is particularly easy. Thus we can dissociate them from other constraints (C_j (X_i) $\leq$ CM_j), which is particularly attractive.

The **COST module:** In 2001, even for a first draft, a least weight optimization process can no longer be justified and should be replaced by a least construction cost or, even better, by a minimum global cost (including operational costs). To link the objective function (Euro) to the design variables (X_i), the unit costs of raw materials (Euro/Kg), the productivity rates for welding, cutting, assembling, etc. (man-hours/unit of work = m-h/unit) and labour costs (Euro/m-h) must be specified by the user (Rigo 2001-c). These unit costs vary according to the type and the size of the structure, the manufacturing technology (manual welding, robots, etc.), the experience and facilities of the construction site, the country, etc. It is therefore obvious that the result of this optimization process (sizing optimization) will be valid only for the specific economic and production data under consideration. Sensitivity analysis of the economic data on the optimum scantling can also be performed, thus providing the manager with valuable information for improving the yard.

The **CONSTRAINT module** (see next section) helps the user to select relevant constraints within constraint groups at his disposal in a databank (Figure 1). In fact, the user remains responsible for his choice. However, in order to facilitate this selection, several coherent constraint sets are proposed to the user. These sets are based on national and international rules/codes (Eurocodes, ECCS Recommendations, Classification Societies, etc.). The user must first choose the types of constraints (yielding, buckling, deflection, etc.) then, for each type of constraint, select the method, the code or the rules to use and finally the points/areas/panels where these constraints will be applied.

4 STRUCTURAL AND GEOMETRICAL CONSTRAINTS

Constraints are linear or non-linear functions, either explicit or implicit of the design variables (X_i). These constraints are analytical "translations" of the limitations that the user wants to impose on the design variables themselves or to *parameters* like displacement, stress, ultimate strength, etc. Note that these *parameters* are functions of the design variables. So one can distinguish:

- Technological constraints (or side constraints) that provide the upper and lower bounds of the design variables (for example: $X_{imin} = 4mm \le X_i \le X_{imax} = 40$ mm).
- Geometrical constraints impose relationships between design variables in order to guarantee a functional, feasible, reliable structure. They are generally based on "good practice" rules to avoid local strength failures, or to guarantee welding quality and easy access to the welds. For instance, welding a plate of 30 mm thick with one that is 5 mm thick is not recommended.
- Structural constraints represent limit states in order to avoid yielding, buckling, cracks, etc. and to limit deflection, stress, etc. These constraints are based on solid-mechanics phenomena and modelled with rational equations. By rational equations, we mean a coherent and homogeneous group of analysis methods based on physics, solid mechanics, strength and stability treatises, etc. and that differ from empirical and parametric formulations.

The list of the structural constraints included in the LBR-5 model is intimately bound to the types of structures targeted by this research. Let's recall that these are mainly metallic, prismatic (box girders) and stiffened (orthotropic) structures used for hydraulic and marine structures. These structures are composed of stiffened panels that are either cylindrical or plane. The panels are joined one to another by generating lines (edges of the prismatic structure) and are stiffened longitudinally and transversely (Fig. 7).

- Stiffened longitudinally:
  - by stiffeners,

  and/or
  - by crossbars and girders, prompt elements of strong rigidity.
- Stiffened transversely:
  - by transverse bulkheads,

  and/or
  - by the main transverse framing,

  and/or
  - by secondary or local transverse stiffeners.

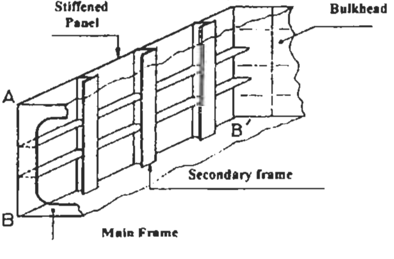

Figure 4: A stiffened panel.

When going from the "local" to the "general" (Figure 4), one differentiates three types of constraints: constraints on panels and components, constraints on frames and transversal stiffening, and constraints on the global structure.

- Constraints on stiffened panels (Figure 4).
  Panels are limited by their lateral edges (junctions with other panels, AA" and BB") either by watertight bulkheads or transverse frames. These panels are orthotropic plates and shells supported on their four sides, laterally loaded (bending) and submitted, at their extremities, to in-plane loads (compression/tensile and shearing).
  Global buckling of panels (including the local transverse frames) must also be considered.
  Panel supports, in particular those corresponding to the reinforced frames, are assumed infinitely rigid. This means that they can distort themselves significantly only after the stiffened panel collapse.
- Constraints on the transverse frames (Figure 4)
  The frames take the lateral loads (pressure, dead weight, etc.) and are therefore submitted to combined loads (large bending and compression). The rigidity of these frames must be assured in order to respect the hypotheses on panel boundary conditions (undeformable supports).
- Constraints on the global structure (box girder/hull girder).
  The ultimate strength of the global structure or a section (block) located between two rigid frames (or bulkheads) must be considered as well as the elastic bending moment of the hull girder (against yielding).

The limit states that will be considered are:

- A *service limit state* that corresponds to a situation where the structure can no longer assure the service for which it was conceived (examples: excessive deflection cracks).
- An *ultimate limit state* that corresponds to collapse/failure.

It is important to differentiate *service limit states* to *ultimate limit states* because safety factors associated to these two limit states are generally different.

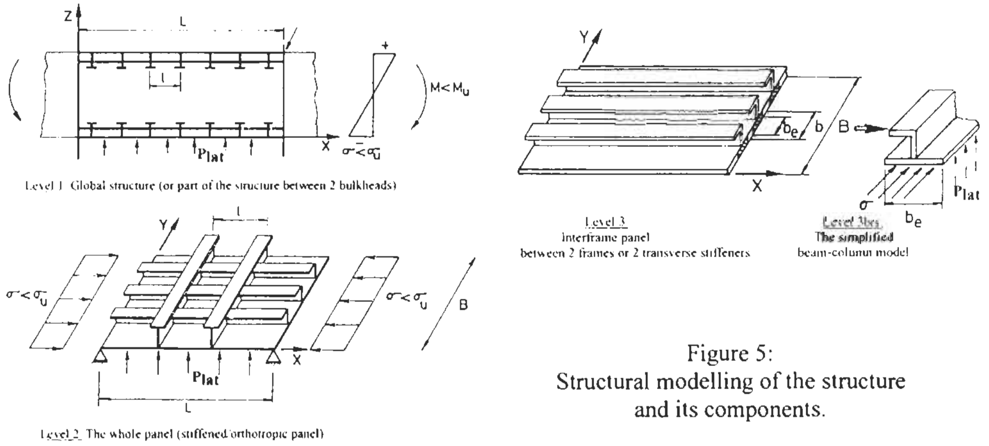

Level 1 Global structure (or part of the structure between 2 bulkheads)

Level 3
Interframe panel
between 2 frames or 2 transverse stiffeners

Level 3bis
The simplified
beam-column model

Level 2 The whole panel (stiffened/orthotropic panel)

Figure 5:
Structural modelling of the structure
and its components.

4.1 Ultimate Limit States

Figure 5 presents the different structure levels: the global structure or general structure (level 1), the orthotropic stiffened panel (level 2) and the interframe longitudinally stiffened panel and its simplified modelling: the beam-column (level 3 and 3bis). The relations between the different limit states and structure levels can be summarised as follows:

➡ Level 1: Ultimate bending moment of the global structure (hull girder): M_u

➡ Level 2: Ultimate strength of compressed orthotropic stiffened panels (σ_u).

$\sigma_u = \min [\sigma_u$ (mode i), i = a, b, c and d, the 4 considered failure modes]

➡ Level 3: Mode a: Global buckling.
Mode b: P_{ult} of interframe panels (beam-column or orthotropic models)
  - plate induced failure (buckling),
  - stiffener induced failure (buckling or yielding).
Mode c: Instability of stiffeners (local buckling, tripping, etc.).
Mode d: Yielding.

To avoid constraints related to the "a" mode, one generally imposes a minimal rigidity for the transverse frames so that an interframe panel collapse (mode b) always appears before global buckling (mode a).

In the LBR-5 model, all the available constraints are classified as follows:

1. Stiffened panels constraints:
   Service limit states
   1.1. Upper and lower bounds ($X_{min} \leq X \leq X_{max}$),
   1.2. Maximum allowable stresses against yielding.
   1.3. Panel deflection (local deflection).
   1.4. Buckling of unstiffened plates,
   1.5. Local buckling of longitudinal stiffeners (web and flange).
   Ultimate limit States
   1.6. General buckling of orthotropic panels (global stiffened panels).
   1.7. Ultimate strength of interframe longitudinally stiffened panel.
   1.8. Torsional-flexural buckling of stiffeners (tripping).
2. Frames constraints.
   Service limit states
   2.1. Upper and lower bounds ($X_{min} \leq X \leq X_{max}$)
   2.2. Minimal rigidity to guarantee rigid supports to the interframe panels.
   2.3. Allowable stresses under the combined loads,
   Ultimate limit states
   2.4. Frame buckling of the compressed members and local buckling (web, flange).
3. General constraints
   Service limit states
   3.1. Allowable stresses,
   3.2. Global structure deflection and relative deflections of components and panels.
   Ultimate limit states
   3.3. Global ultimate strength (of the hull girder/box girder) between 2 frames or bulkheads.

5 CONCLUSIONS AND FUTURE DEVELOPMENTS

Within the framework of the new "Module-Oriented Optimization" concept, the multi purpose LBR-5 optimization model is presented in this paper. The COST, CONSTRAINT and OPTI modules are the 3 basic modules. The global optimization process is presented including an emphasis on the CONSTRAINT module. Main characteristics of the LBR-5 are:

- Preliminary design oriented (easy and fast modelling, reduced amount of input data, etc.),
- Structure optimization at initial design (initial feasible scantling is not required, etc.),
- Least construction cost and least weight objective functions,
- Rational formulation of the constraints (technologic, geometric and structural constraints),
- User oriented (user constraints can be easily implemented),
- Efficient and reliable optimizer (only 10~15 iterations are necessary to get the optimum),

- Large structures can be studied (100 panels, 900 design variables and 5000 constraints to cover up to 10 loading cases).

A major aspect is how to integrate the LBR-5 module with existing tools (CAD, etc.). This work is now under completion with the collaboration of industrial partners. Using new interfaces, LBR-5 will be able to receive the geometric data (node co-ordinates, scantling, etc.) from, for instance, an AUTOCAD, FASTSHIP, MAXSURF file or even by a simple EXCEL or ASCII file.

References

- Fleury C. (1989). CONLIN, An Efficient Dual Optimizer Based on Convex Approximation Concepts. *Structural Optimization*. **1**, 81-89.
- Hughes O. F., Mc Natt T. R. (1992). Unified Structural Design Method for Standard and Non-Standard Design Requirements, PRADS'92, vol.2, Newcastle upon Tyne, UK, 860-872.
- Rahman M. K., Caldwell J. B. (1995). Ship Structures: Improvement by Rational Design Optimisation. *International Shipbuilding Progress*. **429**, 61-102.
- Rigo Ph. (1992). The Computation of Prismatic Structures, Applied to Naval Architecture. *Marine Structures*, Elsevier. **5:3**, 313-332.
- Rigo Ph. (2001.a). A Module-Oriented Tool for Optimum Design of Stiffened Structures, *Marine Structures*, Elsevier, (*accepted for publication*)
- Rigo Ph., Fleury C. (2001.b). Scantling Optimization based on Convex Linearization and a Dual Approach, *Marine Structures*, Elsevier, (*accepted for publication*)
- Rigo Ph. (2001.c). Least Cost Structural Optimization Oriented Preliminary Design, *Proc. Ship Production Symposium*, SNAME, Ypsilanti, Michigan, USA, 20p. (*accepted for publication*).

Practical Design of Ships and Other Floating Structures
You-Sheng Wu, Wei-Cheng Cui and Guo-Jun Zhou (Eds)

© 2001 Elsevier Science Ltd. All rights reserved

THE FINE OPTIMIZATION OF SHIP HULL LINES IN RESISTANCE PERFORMANCE BY USING CFD APPROACH

L. Xu and Y. Y. Wang

Department of Naval Architecture Dalian University of Technology
Dalian 116024, China

ABSTRACT

In order to complete the fine optimization of ship hull lines, a classified optimization procedure is developed in this paper. Altogether 5 levels are included in this procedure. *Level 0* is optimization of hull dimensions based on the method of experience or statistical formulae. *Levels 1*, *2* and *3* are optimizations of naked hull lines, local hull lines and appendage lines respectively. The method of Navier-Stokes equations is used with thick-layer approximation and integral numerical approach for *Level 1*, with thick-layer approximation and differential numerical approach for *Level 2*, and with partly-parabolic approximation and differential numerical approach for *Level 3*. *Level 4* is optimization of finalized hull lines by using model test with flow field measurements. The practical design of ship hull has shown that CFD code is applicable for optimization of ship hull lines in the view of hull resistance performance.

KEYWORDS

Hull resistance, Regressive analysis, Reynolds Average Navier-Stokes equations, Integral numerical approach. Differential numerical approach, Optimization procedure, Ship design.

1 INTRODUCTION

The optimization of ship form is a traditional approach in ship design and one of contents is the optimization of ship hull lines. It can be seen that the optimization technique is continuously improved along with the development of engineering science especially with the development of computer and numerical techniques.

So called optimization of ship hull lines may be regarded as lines fairing only, but this is not comprehensive both in theoretical category and in engineering practice. In fact optimization or fairing of ship hull lines can not be seen as pure mathematical or geometrical problem because it should satisfy so many engineering requirements, such as loading, general arrangement, hydrodynamic performance, and structure consideration. From this viewpoint it may be more suitable that the optimization approach is called the weighing design for ship hull lines.

Preliminary optimization approach of ship hull lines is based on design experience such as the method of parent ship, which can provide so much information not only in design but also in operation. Secondary optimization approach of ship hull lines is set on model tests such as the series tests of ship model, which can directly give the result of optimized lines. In above optimization approaches the main mathematical tool is the regressive analysis based on the least square method. Those approaches used to play an important role in ship design before 1960's as so many ships have been built with big batches which are based on the series model tests, such as well known Series 60, BSRA Series, SSPA Series and so on.

In recent 20 years one may find two important changes: the dimensions of newly built ocean-going ships were gradually increasing and the techniques of Computational Fluid Dynamics (CFD) were developing. The former led to the difficulties of applying the methods based on experiences and the latter gave a space to employ the theoretical methods to optimize ship hull lines. To compare with model test CFD is provided with excellence of economic aspects and celerity. And the predicted accuracy by using CFD in ship hydrodynamic performance depends on the level of CFD code. It should be pointed out that CFD can not always be substituted for model tests, but CFD can concentrate model test with the least scale. In the ship designing practice some of CFD codes have been successfully applied to alternate design of ship hull lines and the final result may be determined by Experimental Fluid Dynamics (EFD). The fine optimization of ship hull lines is aimed at traditional optimization method. The optimized objects may not only include dimensions and naked lines of hull but also include local lines and hulls with appendages.

In the present paper an optimization method of ship hull line design for improving resistance performance is presented computational example exhibits favorable results. Some of criteria used to distinguish the ship hull lines are discussed.

2 CLASSIFIED OPTIMIZATION

In the different design stages the optimization approach with different levels can be used for efficiently designing the ship hull lines.

2.1 Optimization of Hull Dimensions (Level 0)

So many regressive results can be applied to mathematical models when optimization of ship hull dimensions is made. Such as BSRA Series (Wang and Huang, 1993), Series 60 (Wang, 1980), Series of Fishing Boats (Wang and Huang, 1977), ships with homogeneous hull and high speed (Wang and Xu, 1996) and so on are frequently used at the preliminary design stage. The objective function is the total resistance (coefficient) or the residual resistance (coefficient) and the optimized objects include principal dimensions and coefficients of hull form.

2.2 Optimization of Naked Hull Lines (Level 1)

A calculation of thick dimensional boundary layer on ship hull with special velocity profiles and eddy viscosities (Wang and Long, 1989; Wang and Wan, 1989 and Wang and Long, 1992) and with the integral numerical method is employed to determine the viscous resistance. In addition, the Michell integral is used to predict the wave-making resistance. The objective functions are the viscous resistance (coefficient) and the wave-making resistance (coefficient) and the optimized object is naked hull lines.

2.3 Optimization of Local Hull Lines (Level 2)

Reynolds Average Navier-Stokes (RANS) equations with 2-turbulence model and linear free surface boundary condition, together with the differential numerical approach (Wang and Wan, 1991; Wang and Wang, 1994; Wang and Wang, 1995; and Wang and Wang, 1996) are applied to simulate flow around ship hull in time domain. The objective functions are the viscous resistance coefficient and the wave-making resistance coefficient, with the local hull lines being the optimization object.

2.4 Optimization of Appendage Lines (Level 3)

Partly-parabolic type of Navier-Stokes equations with 2-turbulence model by use of differential numerical approach with the pressure marching or the finite-volume method (Wang and Cai, 1998; Li, Lin and Wang, 1997; Li, Lin and Wang, 1998) is used to simulate flow considering the interaction between hull and propeller. The objective functions are the viscous resistance (coefficient) and the wake fraction and the optimized objects are local hull lines, appendage lines and propeller set.

2.5 Optimization of Finalizing Hull Lines (Level 4)

Model test is employed to confirm the optimization result. In fact the information both for the optimized model and for the modification of tested model can be obtained from the computations based on *Level 2* and *3*.

At present the relative accuracy of predicting resistance performance by using CFD code can be ensured, that means it could be used to make comparison with different models. But the final prediction of hull resistance should be determined by use of model test. Up to now the CFD code can predict the resistance performance of ship hull with model size ($\mathrm{Re} = 10^{6-7}$) and thus the model test can be carried out under the same scale of computational model. The prediction of resistance performance for a ship with full scale (generally $\mathrm{Re} = 10^{8-9}$) should consider the scale effects.

Ship designers hope that the resistance performance could be directly predicted by a suitable CFD code, and hence the requirement of model test could be minimized. However this objective may only be partly achieved for some of series ships and for ships that have support from big relative database. For new ship form developing the model test is necessary and all of CFD's results must be validated by model tests.

3 APPLICATION

DSMT tanker model as an example of optimization process is provided as follows. The optimization of *Level 2* has been made after *Level 0* and *1*.

3.1 Hull Lines Parameters

TABLE 1
THE PRINCIPAL PARAMETERS

L/B	B/T	∇/L^3	C_B
5.5	3	0.009	0.8158

The bow and stern have been modified based on the parent ship, and four hull lines schemes have been provided as follows:

Scheme 1: the parent ship of DSMT tanker

Scheme 2: the DSMT tanker with modified bow (raising the center of gravity of bulbous bow)

Scheme 3: the DSMT tanker with modified stern (increasing the value of a/b)

Scheme 4: the DSMT tanker with modified bow (raising the center of gravity of bulbous bow) and modified stern (increasing the value of a/b)

TABLE 2

PRINCIPAL DIMENSIONS OF BOW AND STERN FOR 4 SCHEMES

		Scheme 1	Scheme 2	Scheme 3	Scheme 4
Block Coefficient C_B		0.8158	0.8159	0.8159	0.8160
Parameter of Bow	l_b/l_{pp}	0.16	0.16	0.16	0.16
	h_b/T	0.489	0.485	0.489	0.485
	$b_{\max}/B$	0.1684	0.169	0.1684	0.169
	s_p/s	0.00607	0.00612	0.00607	0.00612
Parameter of Stern	a/b	0.412	0.412	0.538	0.538
	h_b/h_s	1.00	1.00	1.00	1.00

l_b/l_{pp} : the ratio of length of bulbous bow to length between perpendiculars.

h_b/T : the ratio of distance from draft to the position where bulbous bow is widest to design draft.

$b_{\max}/B$: the ratio of the maximum width of bulbous bow at zero station to molded breadth.

s_p/s : the ratio of the transection area of bulbous bow at zero station to the midship section area.

a/b : the ratio of the minimum width to the maximum width at the defined station of the bulb stern.

h_b/h_s : the ratio of the height of the bulb stern's center to that of the propeller's axis above the baseline.

3.2 Model Test and Calculation

The model test and calculation have been made under 15℃ freshwater. The results have been shown in Table 3.

TABLE 3

DATA FOR MODEL TEST AND CALCULATION

	Scheme 1		Scheme 2		Scheme 3		Scheme 4	
	Model Test	Calculation	Model Test	Calculation	Model Test	Calculation	Model Test	Calculation
$C_F \times 10^3$	3.334	3.230	3.334	3.229	3.334	3.228		3.227
$C_{PV} \times 10^3$		0.8278		0.8277		0.8344		0.8313
$C_W \times 10^3$		0.155		0.151		0.179		0.175
$1+k$		1.216		1.215		1.217		1.216
$C_T \times 10^3$	4.376	4.213	4.314	4.208	4.420	4.241		4.233
$1-w$	0.7343	0.498		0.498	0.605	0.485		0.485
η_h	1.1647				1.198			

3.3 Analysis

For Scheme 2, the pressure coefficient C_p (ratio of dynamic pressure to $0.5\rho v^2$) is lower than that of Scheme 1 at the same height around the bow (Figure 1). This is favorable to reduce the viscous pressure resistance. And the free surface elevation (FSE) at the same position is lower than that of Scheme 1 (Figure 2). This is favorable to reduce the wave-making resistance from the aspect of energy. So the resistance performance of Scheme 2 has been improved.

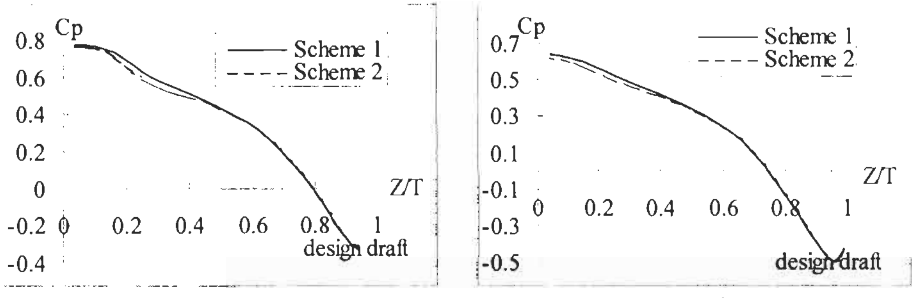

(a) (b)

Figure 1:Distribution of C_p along Z-axis at 19-station (a) and $19\,2/3$-station (b)

For Scheme 3, the gradient of pressure along X-axis at the same height is greater than that of Scheme 1 (Figure 3). In addition, the pressure coefficient C_p is lower than that of Scheme 1 at the same height around the stern (Figure 4). These are unfavorable to reduce the viscous pressure resistance. And the free surface elevation at $-1/2$-station has increased about two percent. This is unfavorable to reduce the wave-making resistance from the aspect of energy. Thus, the resistance performance of Scheme 3 has not been improved. But the results of model test show that the propulsive performance of Scheme 3 has been bettered.

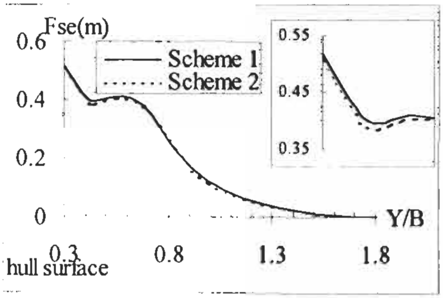

Figure 2: The free surface elevation (Fse) along Y-axis at $19\,1/4$-station

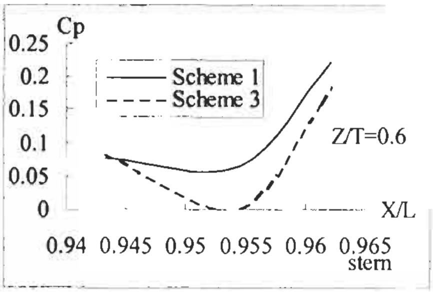

Figure 3: Distribution of C_p in the vicinity of 1-station

For Scheme 4, it synthesizes Scheme 2 and 3. Analyses have also been made based on the distribution of the pressure coefficient around the bow or stern and the free surface elevation. Results have shown that the resistance of Scheme 4 is increased, but not so much as Scheme 3 because of the different bulbous bow.

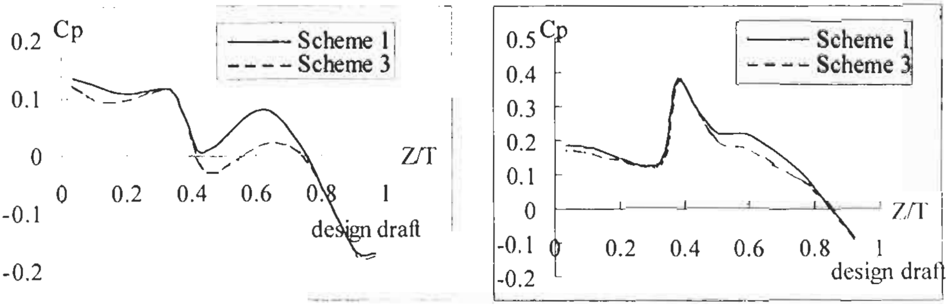

(a) (b)

Figure 4:Distribution of C_p along Z-axis at $3/4$-station (a) and 1-station (b)

4 CONCLUDING REMARKS

Based on above analyses and results of the example some conclusions about CFD approach in the view of hull resistance performance can be drawn as follows:

The resistance performance can be appraised by the calculated results such as the distribution of pressure coefficient and the information of free surface elevation at any position. The separation of flow$(d\theta/dx=0)$ can be determined by the calculated information about the momentum thickness (θ).

The results from model test and calculation have the same tendency for resistance and wake distribution. The calculated results can be obtained more easily and quickly, moreover the information from calculation is much richer. Thus, it is feasible that the CFD approach could be used to make the optimization of ship hull lines in the view of resistance performance.

Reference

Wang Y. Y. and Huang D. L. (1977). Experimental Report on Series of Fishing Boats. *Fishing Boat and Port* **2**, 19-25 (in Chinese).

Wang Y. Y. (1980). Regression Analysis of Ship Data. *Journal of Dalian University of Technology* **19:1**, 101-114.

WANG Y. Y. and LONG J. H. (1989). Analysis of Turbulent Boundary Layer Equations for Ship Viscous Flow. *Proceedings of the 18th Session of Scientific and Methodological Seminar on Ship Hydrodynamics* (SMSSH), 101—106. Varna, Bulgaria.

WANG Y. Y. and WAN D.C. (1989). A Discussion on Velocity Profiles and Eddy Viscosities for Three-Dimensional Boundary Layer around Ship After-Bodies. *Proceedings of the 4th International Symposium on Practical Design of Ships and Mobile Units* (PRADS), 251—259. Varna, Bulgaria.

WANG Y. Y. and WAN D.C. (1991). On Determination of Initial Values in Calculation of Tree-dimensional Boundary Layer around Ship Hulls. *Journal of Dalian University of Technology* **31:1**, 71—77(in Chinese).

WANG Y. Y. and LONG J. H. (1992). Calculation of Thick Dimensional Boundary Layer on Ship Hulls. *Journal of Dalian University of Technology* **32:3**, 310—320(in Chinese).

Wang Y. Y. and Huang D. L. (1993). Supplementary tests for the BSRA ship series forms with $C_B = 0.80 - 0.85$. *Shipbuilding of China* **122:3**, 54-57(in Chinese).

WANG Y. Y. and Cai S.H. (1993). Calculational Investigation of Propeller-Hull Interaction. *Journal of Hydrodynamics* **A8:Supplementary Issue**, 601—608.

WANG Y. Y. and WANG Q.X. (1994). Calculation of Boundary Layer considering Free-Surface Effect around Ship Hulls. *Proceedings of the 20th Symposium on Naval Hydrodynamics*(SNH), **4**, 51—56. Santa Barbara, USA.

WANG Y. Y. and WANG Q.X. (1995). Calculation of Ship Flow in Viscous Fluid with Free-Surface Effect. *Journal of Dalian University of Technology* **35:5**, 685—689(in Chinese).

WANG Y. Y. and Xu S.N. (1996). Prediction of Propulsive Power for Ships with Homogeneous Hull and High Speed. *Journal of Dalian University of Technology* **36:3**, 324—328(in Chinese).

WANG Y. Y. and WANG Q.X. (1996). Calculation of Boundary Layer Considering Free-Surface Effect for Ship Hulls, *NAVAL HYDRODYNAMICS*, 906—912, Published by National Research Council, Printed by National Academy Press, USA

Li T. L., WANG Y. Y. and Lin Y. (1997). Ship Wave-making Resistance Calculation by Panel Method and Numerical Flow Field Visualization. *Journal of Dalian University of Technology* **37:1**, 87—90(in Chinese).

LI T. L., LIN Y. and WANG Y. Y. (1997). A Finite-Volume Method for Three Dimensional Viscous Flow around Ship Stern. *Journal of Hydrodynamics* **A13:1**, 758—760.

LI T. L., LIN Y. and WANG Y. Y. (1998). Calculation of Free-Surface Wave Patterns by Steady Moving Ship. *Journal of Dalian University of Technology* **38:4**, 463—468(in Chinese).

Practical Design of Ships and Other Floating Structures
You-Sheng Wu, Wei-Cheng Cui and Guo-Jun Zhou (Eds)
© 2001 Elsevier Science Ltd. All rights reserved

PARAMETRIC HULL FORM DESIGN – A STEP TOWARDS ONE WEEK SHIP DESIGN

C. Abt, S.D. Bade, L. Birk, S. Harries

Institute of Land and Sea Transportation
Technical University of Berlin Germany

ABSTRACT

This paper presents a parametric modelling approach to the design of ship hull forms which allows to create and vary ship hulls quickly and efficiently. A design-oriented parametric definition language is introduced which features high-level descriptors of hull characteristics well-known in naval architecture. A modelling system is presented that produces a complete mathematical description of the hull via geometric optimisation, enabling effective shape variations by keeping selected parameters constant while adjusting others automatically. All curves and surfaces yield excellent fairness. Examples illustrate parametric shape design and variation. Thus, the parametric modelling approach provides the ideal basis to hydrodynamic optimisation and one week ship design.

KEYWORDS

Hull form design, Parametric modelling approach, Geometric optimisation, One week design

1 INTRODUCTION

In order to be competitive on the market, preliminary ship design has to be performed in continually decreasing time spans. Accurate estimation of weights, building cost and performance are essential for the success of a bid. Decision-taking at the early design stage fixes the major expenses while uncertainties about the upcoming costs have to be reduced as much as possible. A considerable number of design alternatives and their thorough evaluation increases the competitiveness of a shipyard. Selecting a design from a larger stock or being able to create designs of high quality on demand offers a huge advantage. The ultimate goal of advanced modelling systems for future developments is to provide a complete generic model for the entire ship which includes production as well as lifecycle costs. However, software tools applied in the preliminary design phase today generally feature a different view of ships than geometric modelling systems. Moreover, using state-of-the-art computer simulations, for instance CFD and FE methods, require a complete geometric representation of the ship – mostly in discretized form.

This paper therefore aims at introducing a new approach to hull form design based on a parametric, design-language-oriented definition. Different descriptors used by the various partners involved in the design process have been analysed and a top-down hierarchy of design elements has been identified. Within the novel approach the high-level descriptors used in the shipyard's daily optimisation process can be translated directly into a geometric definition. Physical properties of the hull shape are maintained automatically and the resulting curves and surfaces yield excellent fairness. The naval architect's craftsmanship of geometric modelling has become part of the internal generation process without compromising his or her freedom of creativity. The flexible set of parameters and the fully-automated adoption of patch arrangement makes the program a powerful tool. The designer can thus concentrate on the optimisation of the ship to improve its performance and thereby its value as well as the competitiveness of the designing yard.

In the sections to come a classification of design language is presented. Subsequently, the modelling approach and the hierarchical character of design parameters and their implementation in the generation process of complex hulls are outlined. Global variations induced by single parameter changes as well as local changes typically applied in the hydrodynamic optimisation process illustrate the applicability of the parametric design methodology.

2 DESIGN LANGUAGE

The geometric design of ship hull forms consists of several subsequent procedures based on a wide range of abstraction levels. The description of specific properties of a ship may vary from a global expression like *a post pan max container carrier with draft restriction* to a mathematical detail like *the weight of the second-to-last control point on that frame should be slightly decreased.* Both descriptions are needed to carry the necessary information from one partner to another without burdening the communication with excessive data.

The view on a ship, and therefore the language applied for its description, depends basically on the context which governs the particular situation. While at the global level of description the appearance of a ship dominates the vocabulary, at the stage of hydrodynamic optimisation the communication on the basis of functional descriptors, e.g. form parameters, is more useful. The CAD-system which is applied to model the ship shape again requires a completely different language since it is based on patch arrangements, vertex coordinates and weights defining the hull by means of a specific mathematical method.

The modelling process of a hull can be performed independently at any of these three levels. The selection of features used to describe the hull form at any of these levels has to follow a topological description. For a better distinction let us introduce three topology levels that we call

- *Topology of Appearance,*
- *Topology of Design and*
- *Topology of Representation.*

All three levels are applied within the design process in close relation, see Figure 1.

Applying state-of-the-art CFD-programs represents today's standard for performance evaluation of ships in the early design stage. Due to their reliable ranking, see e.g. (Harries and Schulze 97), they can be utilized in the optimisation process. Shape variation and decision-taking is generally performed on the basis of functional descriptors – at the level of topology of design, i.e., the second level in Figure 1. However, the numerical simulation programs (CFD) require a complete geometric description stemming from the lowest level, i.e., the third level in Figure 1. Even though the simulation expenses in terms of computing time play a significant role, the implementation of the desired shape variation is of even higher magnitude since it is usually brought about by hand. Consequently, the limited period of design refinement restricts the number of iterations possible and systematic variations cannot be performed in general.

The different languages applied to the description of ship characteristics represent a major bottleneck in hull form development. Design decisions are usually taken on a more abstract level and the lack of automated mapping of functional descriptors into a corresponding mathematical representation makes optimisation a time-consuming, highly interactive process. In most cases no comprehensive optimisation process is achieved. In order to improve this situation the new method of hull modelling is developed such that the design-oriented parameters are directly translated into a mathematical hull representation. New geometry generation procedures based on hierarchical rules ensure variability and applicability of the approach.

3 MODELLING APPROACH

Traditional CAD-based geometric modelling is characterized by employing mathematically defined curves and surfaces which are manipulated by means of a graphical user interface (GUI). The model generally consists of a considerable number of free variables which have to be modified in a highly concerted manner. The initial set-up of a feasible arrangement of entities requires knowledge about both the ships topology of appearance and the mathematics of its representation. Once the set-up is done for a specific hull form, global changes cannot be accomplished easily and modifications of functional parameters remain time-consuming tasks.

3.1 Requirements of the Mathematical Representation

For further utilization within the design process a complete geometric model – in the meaning of a computer internal representation (CIR) – is required. CAD-models based on B-spline technology are employed successfully in many marine-related software packages. The B-splines' advantageous characteristics with regard to local shape control, internal continuity and variability makes them a powerful element for all kind of shape representations.

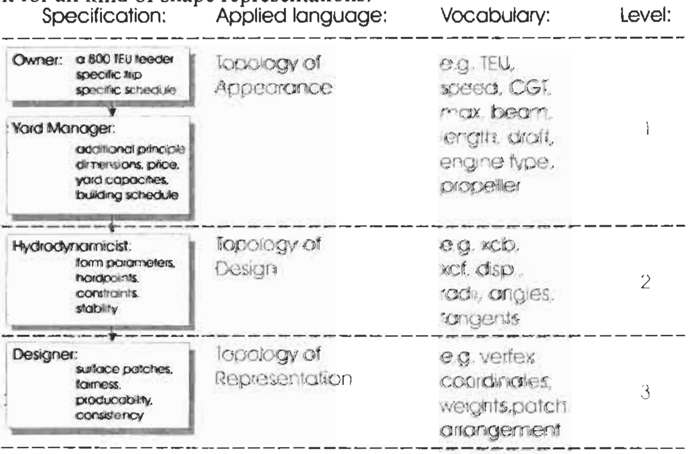

Specification:	Applied language:	Vocabulary:	Level:
Owner: a 800 TEU feeder specific trip specific schedule **Yard Manager:** additional principle dimensions, price, yard capacities, building schedule	Topology of Appearance	e.g. TEU, speed, CGT, max. beam, length, draft, engine type, propeller	1
Hydrodynamicist: form parameters, hardpoints, constraints, stability	Topology of Design	e.g. xcb, xcf, disp., radii, angles, tangents	2
Designer: surface patches, fairness, producability, consistency	Topology of Representation	e.g. vertex coordinates, weights,patch arrangement	3

Figure 1: Levels of topology

The arrangement of surface patches for a feasible representation of a given shape depends basically on shape characteristics which make up the general appearance of the hull, e.g. flat areas, knuckle lines, curved regions. Moreover, gaps and overlaps within the representation have to be avoided which possibly leads to a more complicated arrangement, depending on the complexity of the desired shape. The quadrilateral nature of standard B-spline surfaces may cause additional subdivisions to avoid discontinuities in unfavourable regions. An example surface patch arrangement for a fast RoRo-ferry is depicted in Figure 2. In addition to these formal requirements, the resulting surface has to display excellent fairness, which normally is realized interactively by the designer who creates the CAD-model. Manually, however, these requirements are typically non-trivial to fulfil. Naturally, any automated hull generation process has to accomplish a result which complies with these requirements, too.

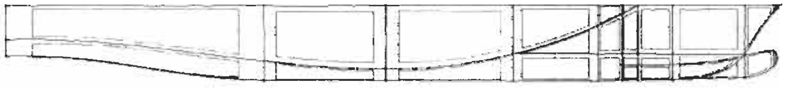

Figure 2: Example surface patch arrangement

3.2 Parametric Design Approach

The modelling technique presented in this paper is based on a parametric curve generation approach developed by Harries and Abt (1997) and has been successfully utilized for the generation and automated optimisation of bare hulls by Harries (1998). The method utilizes a parametric curve generation process where the vertices of all B-spline curves are computed from a geometric optimisation, employing fairness criteria as measures of merit and capturing global shape characteristics as equality constraints. Properties of the hull, such as the shape of the centerplane curve or the shape of the deck for instance, are represented as curves created from form parameters. Parametric curves – e.g. for the flare angle or the submerged sectional area – reflect the properties of the sectional shape of the ship at any longitudinal position. Once this set of so-called basic curves is created from the specified input, a numerical algorithm is applied to create a set of sections at selected locations and, subsequently, a skinning (Woodward 1988) is performed to create a surface definition from the skeleton of design sections. A suitable arrangement of design sections is determined automatically from an analysis of the basic curves.

The geometric modelling system developed by the authors – called FRIENDSHIP-Modeler – is based entirely on parametric principles. The parameterisation is implemented on the basis of a user-readable, marine design-oriented model-file. An excerpt of a model-file is depicted in Figure 3.

The model-file features a number of blocks representing elements from a very high modelling level, i.e., levels 1 and 2 of Figure 1. In the example principle dimensions and selected properties of the midship section and the design waterline are displayed. The entire model-file features between 30 and about 150 parameters, depending on the desired detail of specification. While some of the parameters are mandatory for the generation process many are optional. If a parameter is not specified, either its value is set to a default or, alternatively, a change in topology is performed, depending on the modelling context. An example for the creation and modification of a midship section is given in Figure 4 to Figure 7. The rule-based generation process is described in the following paragraphs.

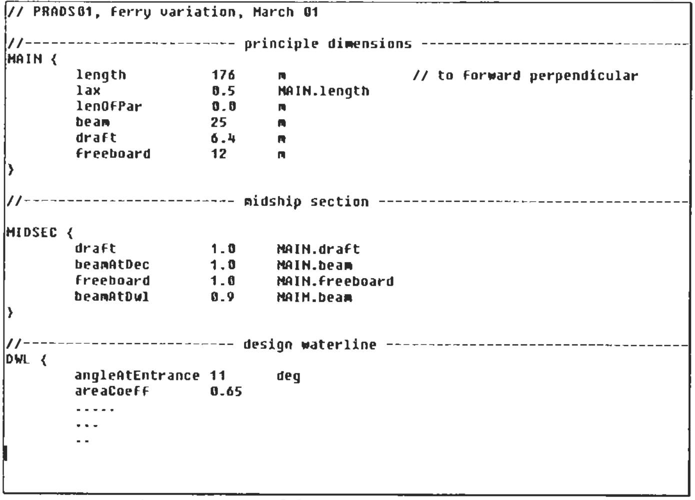

```
// PRADS01, ferry variation, March 01

//------------------------ principle dimensions -------------------------------
MAIN {
        length          176     m               // to forward perpendicular
        lax             0.5     MAIN.length
        lenOfPar        0.0     m
        beam            25      m
        draft           6.4     m
        freeboard       12      m
}

//------------------------ midship section ------------------------------------

MIDSEC {
        draft           1.0     MAIN.draft
        beamAtDec       1.0     MAIN.beam
        freeboard       1.0     MAIN.freeboard
        beamAtDwl       0.9     MAIN.beam
}

//------------------------ design waterline -----------------------------------
DWL {
        angleAtEntrance 11      deg
        areaCoeff       0.65
        .....
        ...
        ..
```

Figure 3: Part of the FRIENDSHIP model file

3.3 Rules of Creation

Instead of expecting a comprehensive specification of each element utilized to model the desired shape, an inverse procedure is applied to most features within the FRIENDSHIP-Modeler. A midship section for instance could be specified and set up with just a single information, namely the beam at the design waterline. Without any additional information, all necessary parameters would be derived from the principle dimensions, see Figure 3. The parameters *draft*, *beam* and *freeboard* have been included in the MIDSEC block in order to simplify the picture. Any additional information given by the user specializes the shape of this design feature and possibly induces changes in topology. Figure 4 shows the extract of the midship section's block complemented by a parameter called *deadrise*. Its default value is zero but here it has been modified to 4°. Figure 5 extends the specification by a straight part at its bottom. The corresponding shapes of the initial section and the modified ones are depicted in Figure 7.

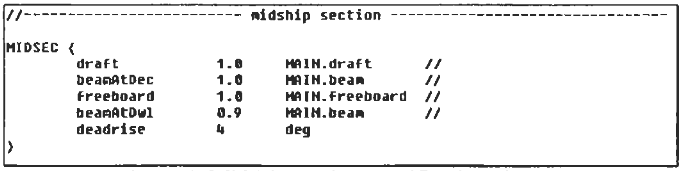

```
//------------------------ midship section -------------------------------

MIDSEC {
        draft           1.0      MAIN.draft       //
        beamAtDec       1.0      MAIN.beam        //
        freeboard       1.0      MAIN.freeboard   //
        beamAtDwl       0.9      MAIN.beam        //
        deadrise        4        deg
}
```

Figure 4: Midship section specification (Part 2)

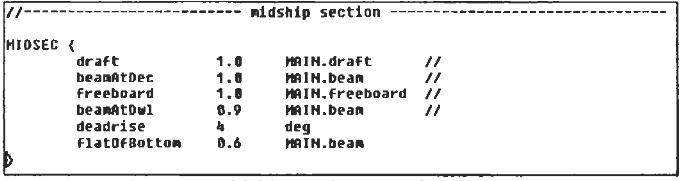

```
//------------------------ midship section -------------------------------

MIDSEC {
        draft           1.0      MAIN.draft       //
        beamAtDec       1.0      MAIN.beam        //
        freeboard       1.0      MAIN.freeboard   //
        beamAtDwl       0.9      MAIN.beam        //
        deadrise        4        deg
        flatOfBottom    0.6      MAIN.beam
}
```

Figure 5: Midship section specification (Part 3)

As stated above, the generation process follows a methodology which depends on the existence of specific parameters. According to the naval architects' language, a set of parameters has been introduced and chosen as the basis for a generation hierarchy. Figure 3 to Figure 5 depict the parameterisation of the midship section applying parameters located at a similar priority level. Other parameters exist at higher and lower levels, respectively. The parameter for the design waterline beam for example is located one level below since a combination of draft, a large deadrise angle combined with a straight part from the flat of bottom may cause a dependency. (For conventional merchant ships this case is not relevant.)

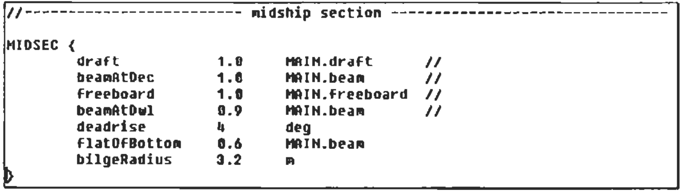

```
//------------------------ midship section -------------------------------

MIDSEC {
        draft           1.0      MAIN.draft       //
        beamAtDec       1.0      MAIN.beam        //
        freeboard       1.0      MAIN.freeboard   //
        beamAtDwl       0.9      MAIN.beam        //
        deadrise        4        deg
        flatOfBottom    0.6      MAIN.beam
        bilgeRadius     3.2      m
}
```

Figure 6: Midship section specification (Part 4)

In contrast to the set of coexisting parameters in the previous figures, an example of a higher level parameter is the bilge radius, see Figure 6. Stating a bilge radius dominates the generation process and causes the parameters for the flat of bottom and the beam at the design waterline to be overruled and, thus, ignored. In addition, a straight part for the flat of side is created which makes the section become a typical midship section.

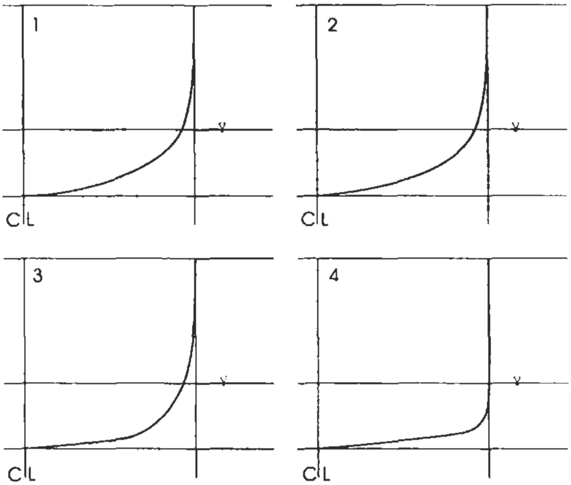

Figure 7: Shape modification of the midship section

The midship section has been selected to demonstrate the different levels of priority in the generation process of the hull shape. Every single parameter that is part of the vocabulary available in the model has to be related to a set of rules embedded in the generation process.

4 EXAMPLE

To demonstrate the performance of the entire modelling approach, two different shape variations – namely global and local modifications – are presented. The change of global parameters depicts the capabilities of shape generation in the early design phase. Local changes of hydrodynamic relevance have been selected to demonstrate the applicability of the modelling approach for automated shape variation without shape deformation.

4.1 Variation of principle dimensions

At the early stage of preliminary design the appearance of the ship is specified and some of the principle dimensions have to be initialised and, possibly, fixed. Typically, a subset of important parameters suffices to capture the requirements resulting from the transportation task. The freedom for shape variations is substantial and yet all desired geometric attributes are readily available in full detail. Once the model-file is created with a limited set of parameters, a complete geometric description can be created on demand. The values of parameters can be specified either in absolute terms or relative to others. Figure 8 shows three shape variations of a fast RoRo-ferry in side view. The picture shows (i) the ferry of 176 m in length without a parallel part, (ii) the hull after introducing a parallel midbody of 40 m in length, and subsequently, (iii) the geometry after a draft reduction from 8.4 m to 6.4 m. In the side view the relation of parameters can be seen: The aft end of the bulb fairing shifted upwards as the draft was reduced while the position of the bulb top was defined in absolute terms and, therefore, did not change in this example.

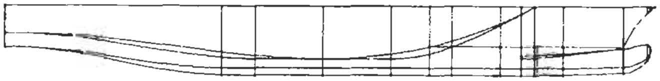

Figure 8: Global shape variation in side view

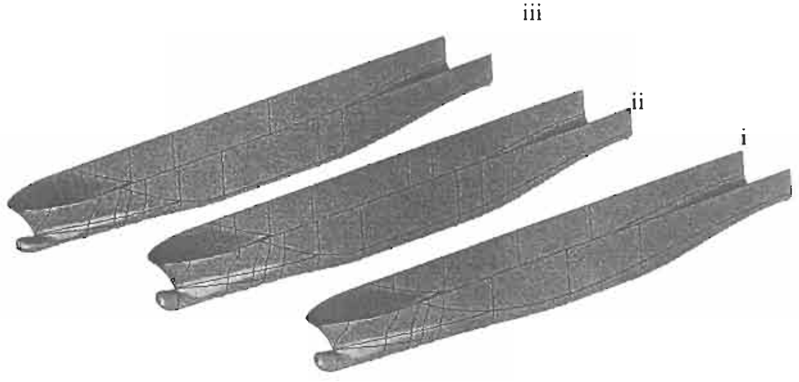

Figure 9: Global shape variation in perspective view

The rendered view depicted in Figure 9, shows the same hull variations as displayed in Figure 8. The automated adoption of the topology of representation is illustrated here clearly. The hull in the foreground, featuring no parallel midbody, consists of less surface patches than its two variations with a parallel part.

4.2 Bulbous Bow Variation

After several principle dimensions have been fixed as a result of economic and / or hydrodynamic optimisations, a subsequent improvement of the hydrodynamic performance is usually carried out to refine the design. Parameters typically used for the manipulation of wave resistance are related to the shape of the bulbous bow. Also, to increase the propulsive efficiency a stern gondola could be subject of changes. Figure 10 presents a variation of a single geometric parameter of the bulbous bow, namely the buttock angle of the bulb contour at the forward perpendicular. The parameterisation of the bulb is closely related to the parameters proposed by Kracht (1978). All of them have been implemented and can be applied in any suitable combination. In addition, the contour of the bulb can be defined by a number of parameters, defining the slope of the buttock, the location of the top of the bulb as well the length and height of the fairing into the bare hull. The bulb is regarded as a blister-type appendage and its volume is specified by means of a separate sectional area curve.

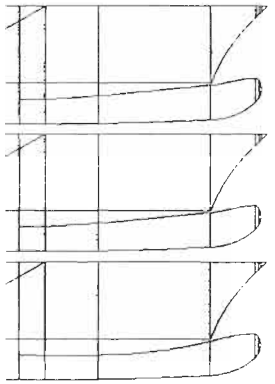

Figure 10: Local shape variation of the buttock angle at the FP

The variation depicted in Figure 10 features a variation of the buttock angle from 5° through 10° to 15° of buttock slope.

5 OUTLOOK

A new approach to parametric hull form design has been presented. Three prominent levels of topology have been introduced – Topology of Appearance, Topology of Design and Topology of Representation. These levels serve to characterize more clearly the various stages of specification, definition and realization typical of today's ship design process, comprising the complete spectrum from the abstract description to the mathematical detail. The new modelling approach is placed at the intermediate level of topology of design. Form parameters are utilized as the descriptors to express design ideas. They can be specified flexibly and problem-dependently. A hierarchical, context-related and rule-based system has been presented to support the naval architect, the hydrodynamicist and the designer in their mutual task to create, vary and optimise the hull geometry quickly and effectively. Examples are given to illustrate the design philosophy and to demonstrate the applicability of the method. The approach is well-suited for the integration into formal techniques of systematic optimisation.

Further work is needed to accommodate additional hull features like appendages, gondolas etc. Moreover, current and future applications focus on the automated optimisation of the hydrodynamic performance associated with the hull geometry, covering calm water resistance and propulsion as well as seakeeping.

Acknowledgement

Parts of this work are funded by the EC GROWTH programme, contract no. G3R D-CT2000-00096.

References

Harries S., Abt, C. (1997). *Parametric Curve Design Applying Fairness Criteria*, International Workshop on Creating Fair and Shape-Preserving Curves and Surfaces. Network Fairshape, Berlin/Potsdam; published at Teubner, 1998.

Harries S., Schulze D. (1997). Numerical Investigation of a Systematic Model Series for the Design of Fast Monohulls. *FAST97 – 4th International Conference on Fast Sea Transportation.* **1**, Sydney, Australia.

Harries S. (1998). Parametric Design and Hydrodynamic Optimization of Ship Hull Forms. *Ph.D. Thesis.* Institute of Naval Architecture and Ocean Engineering, Technische Universität Berlin; Mensch & Buch Verlag, Berlin.

Kracht A.M. (1978). Design of Bulbous Bows. *SNAME Transactions.* **86**.

Woodward C.D. (1988). Skinning Techniques for Interactive B-Spline Surface Interpolation. *Computer-Aided Design.* **20:8**.

Practical Design of Ships and Other Floating Structures
You-Sheng Wu, Wei-Cheng Cui and Guo-Jun Zhou (Eds)
© 2001 Elsevier Science Ltd. All rights reserved

MISSION BASED HYDRODYNAMIC DESIGN OF A HYDROGRAPHIC SURVEY VESSEL

S.L. Toxopeus[1], P.F. van Terwisga[2] and C.H. Thill[1]

[1]Maritime Research Institute Netherlands (MARIN)
Haagsteeg 2, Wageningen, The Netherlands
[2]Royal Netherlands Navy (RNLN)
V.d. Burchlaan 31, The Hague, The Netherlands

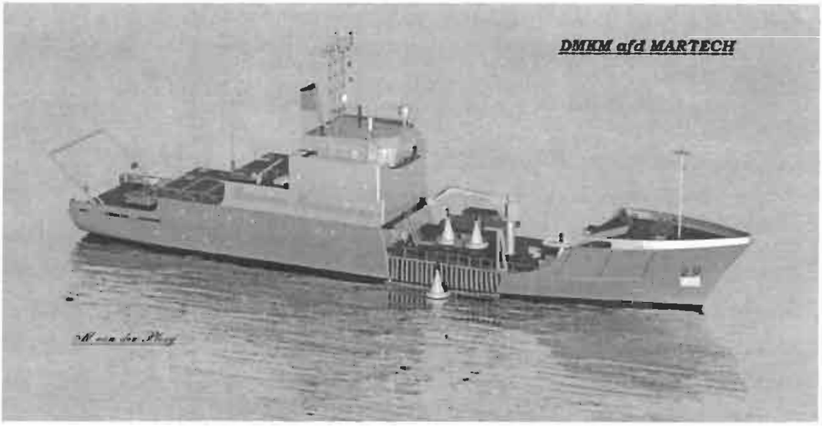

Artist impression of the new hydrographic survey vessel

ABSTRACT

This paper presents the requirements and design for a new hydrographic survey vessel for the Royal Netherlands Navy (RNLN). Based on the mission of the ship, a dedicated integrated hydrodynamic study was conducted at MARIN to verify compliance of the design with all requirements. Using this approach, an optimum balance between hydrodynamic, operational and economical requirements was found.

KEYWORDS

Hydrodynamics, Mission Based Design, Hull Form Optimisation, Manoeuvring, Seakeeping

1 INTRODUCTION

The operational and technical necessity to replace two existing North Sea hydrographic survey vessels (HSV) of the Royal Netherlands Navy initiated a materiel project for two new vessels. The primary mission of these vessels will be carrying out hydrographic surveys to comply with civil and NATO commitments. These tasks will in particular be carried out in the Netherlands part of the Continental Shelf and in the area of the Netherlands Antilles and Aruba. Secondary tasks consist of general military support tasks, assistance in calamities, and support in typical coast guard operations. The development of a more rational design method (see Wolff (2000)) as well as the operational experience within the hydrographic service of the RNLN have resulted in a clear and complete set of operational requirements regarding the hydrodynamic performance. The approach taken and described has lead to a balanced design between those hydrodynamic performance aspects and cost.

2 THE REQUIREMENTS

2.1 Propulsion

A) Cruising speed at least 13 kn in calm water with 6 months fouling allowance.
B) The ship should be able to sail for prolonged periods at low speeds, e.g. 1.5 to 2 knots and at intermediate speeds during surveying, i.e. between 4 and 9 knots.

2.2 Manoeuvrability

A) Good manoeuvrability and course stable in particular for typical surveying speeds (4 – 9 kn).
B) For 95% of the time within 5 m lateral distance deviation during trackkeeping for conditions up to Bf5, 2 kn current and sea state 4 (H_{sig} = 1.88 m, T_1 = 6 s).
C) During autopilot sailing, less than 5° heading deviation, in the same environmental conditions.
D) The ship should be able to turn 180° and change tracks that are 100 m apart within 5 minutes.
E) Unassisted berthing or unberthing should be possible in wind speeds corresponding to up to Bf7.
F) Buoy handling in winds up to Bf7 combined with up to 2 kn current, with less than 10 m positioning deviation relative to the sea floor.

2.3 Seakeeping

The ship has to be able to perform measurements during 128 days/year on the Netherlands part of the Continental Shelf (NCS). Given per year a total of 210 sailing days and 30 days transit to and from the measurement location, 10 days loss due to technical reasons and 16 days for secondary tasks, there is a number of 154 survey days available. This leads to the conclusion that the maximum allowable downtime due to ship motions on the NCS equals 17%. The seakeeping requirements for the new hydrographic vessel are much more stringent than for the current survey vessels. The ships to be replaced are on average capable of 103 measurement days/year corresponding to a downtime of 33%.

2.4 Sea Conditions

Looking at available wave statistics on the operational area, a probability of exceedance of 17% for the Netherlands coastal waters leads to a significant wave height of 2m. In the more northerly part of the NCS this probability leads to a significant wave height of 3 m, so the requirement of 128 hydrographic survey days can be met if the ship motion behaviour meets the criteria for seastates up to maximum sea state 4

2.5 Criteria

A) Significant vertical motion amplitude of the echosounder/sonar < 1.0 m for heave compensation
B) Allowable roll angle of echosounder/sonar and for launching and retrieving RIB < 5°
C) Criteria for security / operability of the crew
Significant pitch amplitude <3.5°
At the location of the RIB / sloop, measurement analysis work spaces, deck spaces for launch and retrieval of buoys and the bridge:
Significant amplitude vertical accelerations < 2 m/s^2
Significant amplitude of lateral accelerations <1.5 m/s^2 (on the bridge < 2 m/s^2)
D) General criteria:
Green water over the bow < 30 times/hour, on the aft deck < 1 time/hour
Slamming < 20 times/hour

3 DESK STUDY

Extensive desk studies have been conducted in the early phase of the project. The first analysis comprised a feasibility study of the application of an existing conventional, single-screw, single-rudder ship for the purpose. Compliance with the staff requirements was verified for this ship. The desk study showed that the existing ship could be adapted in such a way that all requirements were met.

The second, more elaborate, desk study was conducted to determine the operability of the ship and which propulsion and steering arrangements could be applied. Pods and thrusters prove to be promising for application to various ships and therefore the idea arose that those concepts might be advantageous. The propulsion and steering arrangements comprised the following concepts:

- Single-screw single-flap rudder
- Single pod
- Twin screw/twin rudders
- Twin pods
- Single propeller with wing thrusters arrangements.

3.1 Seakeeping

The main dimensions of the hull form resulted from operability requirements, the required deck width and stability requirements. Operability is defined here as the proportion of time the ship is able to successfully accomplish its missions for given combinations of sea area, speeds, and headings, see Lloyd (1989) and NATO STANAG 4154. The complement of operability is referred to as downtime.

For the above mentioned ship motion criteria and wave statistics the downtime in bow quartering and head waves is governed by the vertical motion limits of echosounder and sonar. For beam and stern quartering waves, the vertical motions continue to affect the downtime together with lateral acceleration limits. The limiting roll angle affects the downtime in stern quartering waves as well.

In a hull form variation study, length, displacement, C_p and the draught were varied to investigate their effects on operability. Also, a pram shaped aft hullform was evaluated and applied because of its beneficial effect on vertical motions (Blok and Beukelman (1984) and Kapsenberg and Brouwer (1998)). Finally, the study resulted in the following dimensions and coefficients for further model testing.

TABLE 1

MAIN PARTICULARS OF THE SHIP.

L_{pp}	75 m	Δ	1850 t	C_b	0.47
B	12.8 m	LCB	36.02 m	C_m	0.80
T	4 m			C_{wl}	0.80

The calculations also showed the importance of effective anti roll tanks (ART) for beam and stern quartering waves, which would therefore receive special attention in the seakeeping experimental program.

3.2 Hull form optimisation and propeller verification

The mission profile of this vessel was rather complicated. Good propulsive efficiency is required while at the same time the wake field of the ship has to allow for the design of a low noise signature propeller. Above all, excellent steering ability was demanded.

The concept with wing thrusters was believed promising, as the wing propulsors might be sufficient to achieve the survey speed, whereas the central propeller needs to deliver the thrust for normal transition speed. For full speed all three propulsors would be used, filling the gap between 9 and 13 knots by the thruster power enabling direct diesel drives for all shafts. Unfortunately, it was found that the power for the wing thrusters was too little to fill the gap. The single pod arrangement was dismissed because of the high associated costs and minimal advantage of applying a single pod over a single propeller-rudder configuration. Finally, the twin screw exposed shaft arrangement failed in efficiency compared to a single screw arrangement, so that the single screw concept was chosen. The shaft power demand of all the four concepts can be found in Figure 1 below.

As the cavitation inception speed of the design affects the noise signature to a large extent, special attention was paid to the wake field of the vessel. In this regard, a single screw design usually suffers from a wake peak in the top and bottom position. Aiming at a minimisation of this peak, an open shaft layout was designed. At MARIN, good experiences exist with such a design from former projects and therefore it was applied in this project.

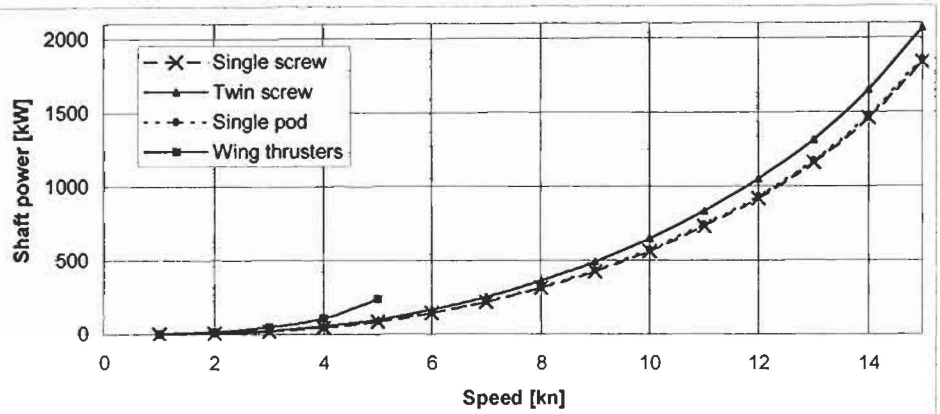

Figure 1: Shaft power of the four investigated concepts.

The lines of the ship were verified by applying MARIN's potential flow code RAPID. The wave patterns have been evaluated for design speed and survey speed. It appeared that further optimisation of the lines was not profitable.

3.3 Dynamic Tracking, Position Keeping and Manoeuvring

During the desk study, the following calculations were carried out to verify compliance with the requirements, for all steering arrangements:

- Standard zig-zag, turning circle and reversed spiral manoeuvres, to verify the directional stability and controllability of the ship.
- Track change ability simulations, to determine the time required sailing from one survey track to the next.
- Dynamic tracking manoeuvres, to verify the ability of the ship to follow a pre-defined track, in

wind, waves and current.

- Dynamic positioning simulations, to verify the ability of the ship to hold station in wind and current.

Based on the standard manoeuvres and the track change ability manoeuvres with the SurSim simulation program, it was concluded that all steering arrangements provided a controllable ship, with a slight preference to podded propulsion. The application of a sufficiently large centre line skeg however, proved to be necessary to ensure the directional stability of the ship.

Using dynamic tracking and positioning simulations, conducted with the MARIN program DPSIM, the deviations from the track and steering actions were compared for all steering arrangements. By applying the appropriate controller coefficients, the ship met the requirements, irrespective of the steering arrangement. The difference between the final results of the configurations was small and therefore no conclusions were drawn regarding the best arrangement.

Besides the above mentioned simulations, also calculations were conducted to determine the required bow thruster power in order to be able to berth or unberth without tug assistance up to BF7.

4 MODEL TESTS

Based on the desk study results, in combination with operational and economic requirements, the single-screw, single-rudder option was selected for the model test phase of the project. The complete model tests program was based on the results of the desk study, concentrating on risk areas and therefore minimising the number of tests.

4.1 Calm Water

A paint smear test was conducted in order to position the appendages such that least resistance and disturbance of the flow was achieved. The speed-power relation and propeller hull interaction was determined by means of resistance and propulsion tests. Finally, a wake survey was conducted to determine the essential wake distribution.

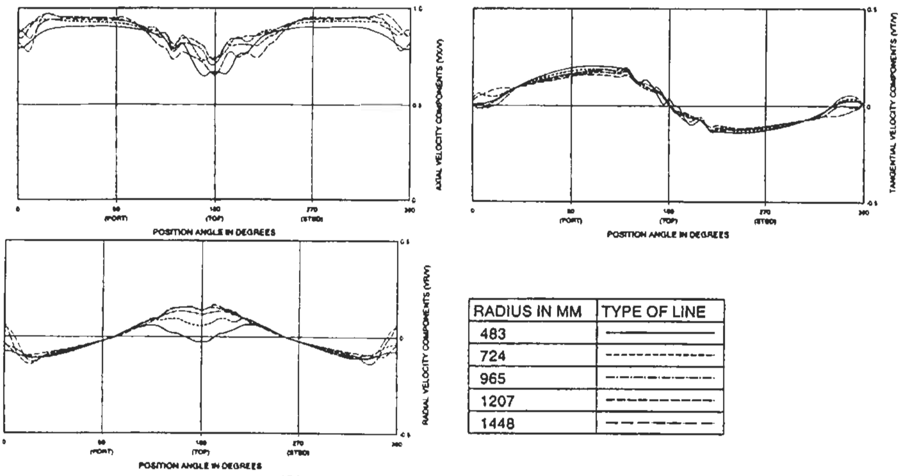

Figure 2: Result of the wake survey

The results presented in Figure 2 were found to be very favourable for a single screw vessel, showing that the solution of exposed shafts even for a single screw vessel is worthwhile, when cavitation inception is an item that needs to be considered.

4.2 Propeller design

Propeller performance calculations were conducted using MARIN's computer programs TIPVCI and DESPRO, together with knowledge from individually and systematically tested propellers, such as the B-series. Parameters that were varied were the diameter, blade area, blade number and pitch (distribution). When the inception speed of tip vortex cavitation was accepted as the determining criterion, a 7 bladed propeller with a pitch of about 1.3 was found to be favourable from cavitation point of view. It was found that a diameter of 2.75 m should be applied. Although the propeller tips touch the boundary layer of the hull, the lower rotation rate in this case is beneficial.

4.3 Manoeuvring and Dynamic Tracking

The manoeuvring tests were conducted to verify the conclusions drawn during the desk study and to obtain more accurate information regarding the manoeuvring characteristics. As was predicted in the preliminary analysis, the ship complied easily with all manoeuvring requirements. Although not applicable to this ship, the manoeuvring characteristics also complied with the draft IMO Resolution A.751(18) requirements (1993). During the model test phase, also dynamic tracking (DT) tests in wind and waves with correction for current were conducted, to verify compliance with the dynamic tracking requirements. After proper calibration of the DT control system, it was found that the requirement was met:

TABLE 2

FINAL RESULTS OF DYNAMIC TRACKING TESTS IN WIND, WAVES AND CURRENT

$\sigma_{\text{track deviation}}$	$\sigma_{\text{rudder angle}}$	Requirement exceeded
2.3 m	8°	3.1 % of the time

With the model tests uncertainties during the desk study were removed and the vessel demonstrated excellent manoeuvring and trackkeeping characteristics. It was found that with a single-screw/single-flap rudder arrangement, the dynamic tracking requirements were met, resulting in a cost-efficient solution.

4.4 Seakeeping

In the desk study phase of the design, two anti roll tanks were foreseen, each 2.4 m long. This was also the configuration tested. In a later stage it became apparent that it was impossible to maintain the lower ART in the general arrangement, a decision which was partly compensated for by lengthening the upper anti roll tank by 25%. The model test results on roll damping showed significantly lower roll damping characteristics than the initially predicted roll damping. Figure 3 shows the corrected final downtime analysis for the enlarged anti roll tank. The correction was made using the model test results. By a variation of the GM value in the operability calculations, the lower KG limit was derived from the criterion that at 45 and 60 degrees the 17% downtime should not be exceeded. The seakeeping test results in severe head seas also led to the decision to increase the bulwark and the addition of a breakwater on deck.

A comparison with the current survey vessels showed the desired increase in operability for the final design, for the greater part caused by the main dimensions, but also through the optimised hull form as it resulted from the variation study[1]. With the exception of beam waves, the operability requirement of 83% is met for all wave headings.

---

[1] The calculated downtime for the current survey vessels was verified with the experience of the hydrographic service, and confirmed for head and bow quartering wave headings

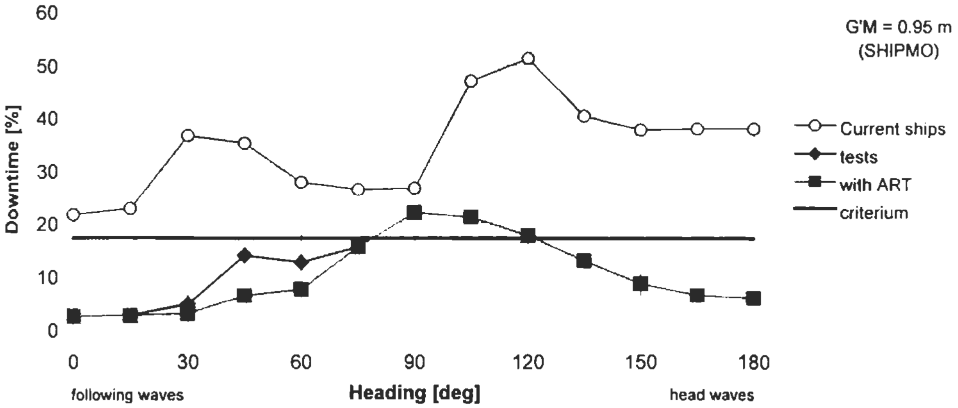

Figure 3: Downtime analysis for enlarged upper ART

5 CONCLUSIONS

Traditionally applicable only to propulsive performance, the hydrodynamic design based on clear definitions of operability requirements and mission criteria have made seakeeping and manoeuvring oriented design decisions easier through a quantitative description of performance throughout the design process. By utilising available knowledge, dedicated computational tools and verification by model tests, a balanced design that met all the numerous requirements was obtained.

Based on the desk studies, a single-screw single-rudder configuration with open shaft arrangement was chosen for the propulsion and steering of the ship. During the model tests, it was found that this steering arrangement could be used successfully to comply with the dynamic tracking requirements, resulting in a cost-effective solution. For further improvement of the operability an anti roll tank was installed.

References

Blok J.J. and Beukelman W. (1984). The High Speed Displacement Ship Systematic Series Hull Forms – Seakeeping Characteristics, *SNAME Transactions.*

IMO Resolution A.751(18). (1993). *Interim Standards for Ship Manoeuvrability.*

Kapsenberg G.K. and Brouwer R. (1998). Hydrodynamic Development for a Frigate for the 21st Century, *PRADS 1998 Proceedings Practical Design of Ships and Mobile Units*, Elsevier Science, NL.

Lloyd A.R.J.M. (1989). *Seakeeping: Ship Behaviour in Rough Weather*, Ellis Horwood Ltd., UK.

STANAG 4154 (1998, Edition 3), Common Procedures for Seakeeping in the Ship Design Process. *ATO Standardisation Agreement*. unclassified.

Wolff P.A. (2000). *Conceptual design of warships*. ISBN 9036514495.

Practical Design of Ships and Other Floating Structures
You-Sheng Wu, Wei-Cheng Cui and Guo-Jun Zhou (Eds)
© 2001 Elsevier Science Ltd. All rights reserved

HULL FORM DESIGN OF A PASSENGER CATAMARAN FOR OPERATION IN THE YELLOW SEA REGION

Seung-Hee Lee, Young-Gill Lee and Jae Wook Lee

Center for Transportation System of Yellow Sea, Inha University,
Incheon, 402-751, Korea

ABSTRACT

The Yellow Sea between Korean peninsula and northeast China possesses a strong hinterland composed of major industrial complexes and cities of the neighboring countries. With recent economic growths of the countries, trade volume in the Yellow sea region is rapidly increasing and hence necessitate an introduction of efficient and integrated logistics systems for the region.

Incheon Metropolitan City is a geopolitical center of the Yellow Sea region as well as the sea and air gateway to the Korean capital area. In the present paper, a passenger catamaran has been planned to meet economical and natural requirements for operation in the city. Hull forms of the catamaran and their resistance characteristics in both deep and shallow waters are studied through model experiments and numerical simulations to determine its practical applicability.

KEYWORDS

Hull form design, High speed, Catamaran, The Yellow Sea, Shallow water, Model test, Numerical simulation

1 INTRODUCTION

The Yellow Sea region, encompassed with Capital and major cities of Korea as well as the key cities and industrial complexes in northeast China, possesses a great economic power and a vast population. The region is expected to emerge soon as a major trade area in the world and it becomes more important for prosperities of both countries in the new century. Incheon Metropolitan City (hereafter Incheon) is located at the geopolitical center of the Yellow Sea region and has been served as a gateway from the sea to the central Korea where almost half of the total population inhabits. The role of the city becomes more important with recent opening of Incheon international airport (hereafter ICN) at Young-jong Island aiming a hub port of the Northeastern Asia.

In the present paper, hull forms of a passenger catamaran for operation in the sea routes inside and vicinities of Incheon have been studied. The routes between ICN ~ main Incheon, ICN ~ Kyung-In Canal ~ Seoul (Han River) and Duk-Jeok Island ~ main Incheon, among others, have been selected for the purpose. The water is relatively calm for the most part of the routes but is shallow with extreme tidal differences reaching almost 10meters in some places. The size of the canal gates and bridges across the Han River further restricts the size of the ships operable in the routes. With careful investigation on the natural condition of the routes and various economic aspects, principal dimensions of a catamaran carrying 300 passengers at relatively high-speed ranges have been selected. [Chun & Lee (1999)] Total of three hull forms of the catamaran have been studied and their resistance characteristics are investigated experimentally and numerically.

2 HULL FORM DEVELOPMENTS

2.1 CATA I & II

The initial hull form, CATA I has been derived from a project done by a group of undergraduate students. In the project, a 1/100th scale model of a 165m long wave-piercing catamaran with a center bow and for operation in 'ICN ~ main Incheon' route had been manufactured and tested by the group in the model basin of the Inha University. The ship may not be appropriate for the general use in Incheon area mainly because her draft is too large and too fast to operate in the river and the canal. But it can be a good starting point, however, especially in calibrating numerical and experimental tools and procedures for predicting catamaran performances operating in the shallow water. [Millward (1984)]

The model is assumed to be a 1/20th scale model of a 33m long catamaran running at 30 knots. The principal dimensions and body plan are shown in Table 1 and Figure 1, respectively. In the figure, L denotes the length between perpendiculars, B the breadth, T the draft, B_d the breadth of a demi-hull, S the distance between centerlines of demi-hulls, Δ the displacement and V the design speed of the catamaran.

TABLE 1

PRINCIPAL DIMENSIONS OF CATA I

$L\,(m)$	33.0
$B\,(m)$	12.0
$T\,(m)$	1.7
$B_d\,(m)$	2.0
L/B_d	16.5
S/L	0.3
$\Delta(tons)$	152.3
$V(kts)$	30.0

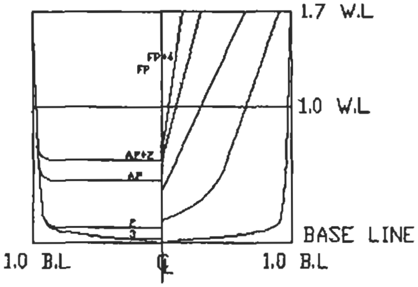

Figure1 : Body plan of a demihull of CATA I

Since it have been already known that CATA I has a profound fore shoulder and subjected to comparatively high resistance, the hull form has been modified for comparison purpose with aids of the numerical code, INHAWAVE, to have a better performances and named as "CATA II". In INHAWAVE, flows are assumed to be incompressible and inviscid and so three-dimensional Euler equations are used as the governing equations. A finite difference method based on a marker-and-cell in the variable rectangular mesh system is implemented in the numerical scheme. [Kim & Lee (2000)] The cross sectional area curves and body plans of the CATA I and II are compared in Figure 2 and 3, respectively, in which CATA II apparently has smoother distribution of cross sectional area.

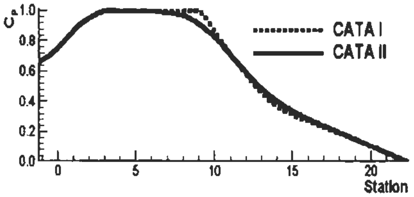

Figure 2: Comparison of cross sectional area distributions of CATA I & II

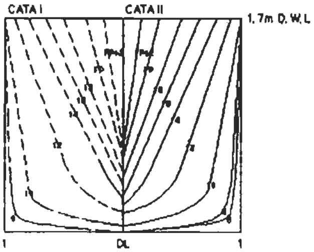

Figure 3: Comparison of Body plans of CATA I & II

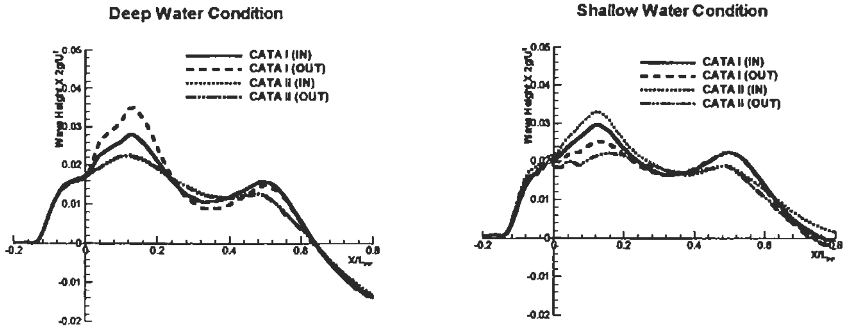
Deep Water Condition

Shallow Water Condition

Figure 4: Comparison of computed wave height profiles of CATA I and II for shallow and deep water conditions (*S*/*L*=0.26)

The computed wave profiles of CATA I and II for *S*/*L* = 0.26 indicate that bow and shoulder waves of CATA II are reduced with the modifications for both deep and shallow water conditions as shown in the Figure 4. Here, 'shallow' refers water depth of 8m, the mean water depth of the planned routes and which corresponds to the depth of 0.4m in model scale. A 1.65m long wooden model of CATA II is made and undergoes a series of tests in the towing tank of Inha University equipped with an adjustable false bottom. The results for CATA I and II are compared in the figures below. Figure 5 compares the residuary resistance coefficients C_R of CATA I and II for demi-hull spacing *S*/*L* of 0.17 and 0.26 and for various ship speeds *V*. The figure shows that CATA II experiences lower residuary resistance for both water depths in the whole speed ranges of the tests. The reductions in the residuary resistances reach almost 10% near the Froude number of 0.5 but it reduces to 1~3% near 0.8, the design speed of the catamarans. Figure 6 shows, however, the trim and sinkage of the models indicating that the hull attitudes are almost similar for the tested range. Effective horsepower of the two ships at the various speeds are given in the Figure 7 where CATA II shows about 3% gains over CATA I at the design speed of 30 knots.

2.2 CATA III

With successful application of experimental and numerical methods in predicting performances of the catamarans, CATA III, a new practical hull form for use mainly in the ICN ~ Kyung-In Canal ~ Seoul (Han River) route is designed. Principal dimensions and body plans of the CATA III are shown in the Table 2 and Figure 8, respectively where the length and draft of the ship has been reduced but the breadth increased than before to meet the limitations imposed by the canal and the river. The design speed also has been reduced to 25 knots but even the speed may not be reached at the Han River since the mean depth of the river decreases to 2m at some locations in dry seasons.

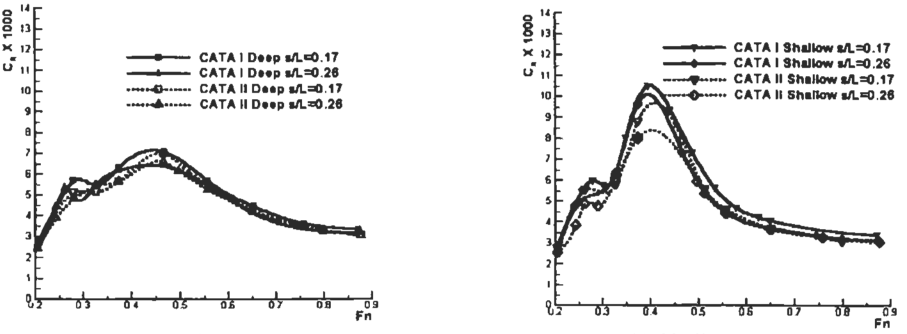

a) Deep water

b) Shallow water

Figure 5: Comparison of residuary resistances of CATA I and II (demi-hull spacing *S/L* = 0.17, 0.26)

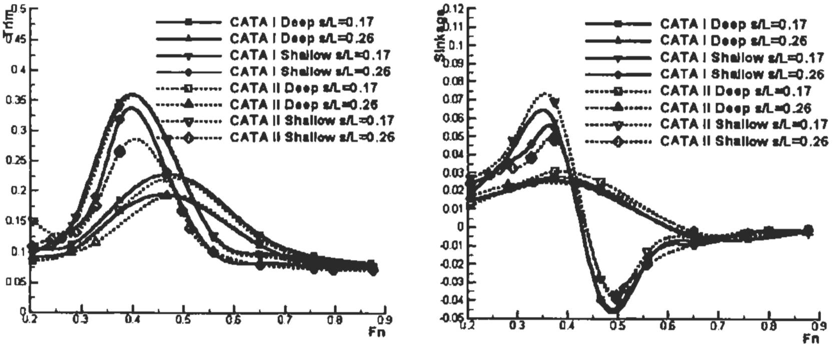

a) Trim curves

b) Sinkage curves

Figure 6: Comparison of hull attitudes of CATA I and II (demi-hull spacing *S/L* = 0.17, 0.26)

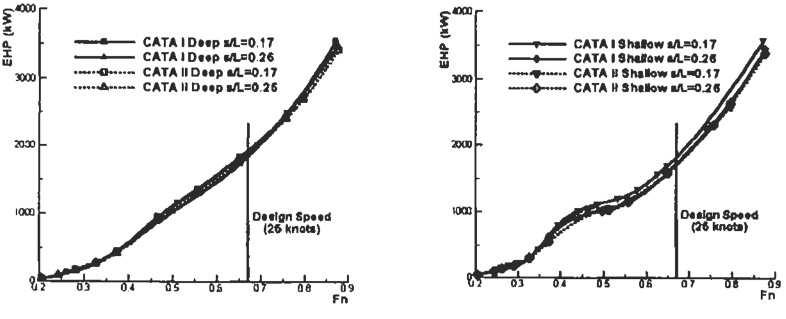

a) Deep water

b) Shallow water

Figure 7: Effective horsepower of CATA I and CATA II (demi-hull spacing *S/L* = 0.17, 0.26)

TABLE 2
PRINCIPAL DIMENSIONS OF CATA III

L (m)	30.00
B (m)	10.26
T (m)	1.00
B_d *(m)*	2.759
L/B_d	10.875
S/L	0.26
Δ(tons)	110.8
(kts)	25.0

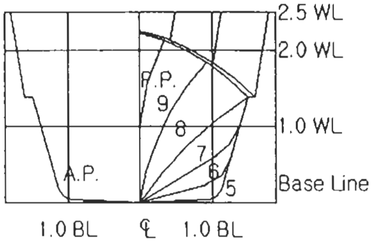

Figure8: Body plan of CATA III

In the initial stage of the CATA III design, numerical computations are done to simulate the flow fields around several hull forms running both in deep and shallow waters and those for the finally chosen hull form are shown in Figure 9.

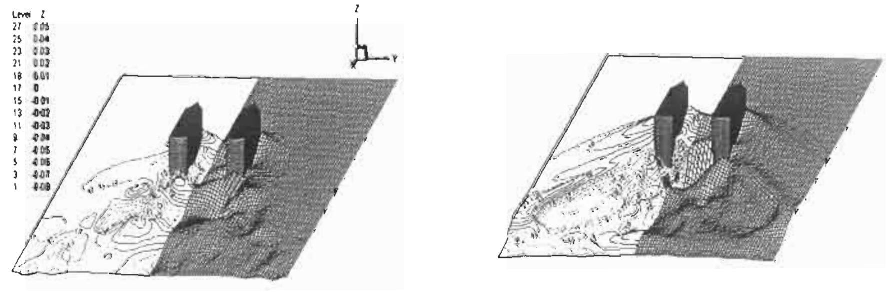

a) Deep water

b) Shallow water

Figure 9: Free surface deformation around CATA III at the design speed for shallow and deep water conditions (*S/L* = 0.26, *Fn* = 0.750)

A 2m long model of CATA III is made of wood and tested in the towing tank. Now, the depth of the shallow water is set to be 2m, the mean depth of the river and Figures 10 and 11 show the results. Figure 10 shows the residuary resistance and effective horsepower. The curves for shallow water at the high-speed range are obtained for comparison purposes only and it does not mean that the catamaran will run so fast in the river or canal. The rapid increase in C_R curve of the shallow water is evident around *Fn*=0.26, corresponding to the critical speed. The hump and hollow in the curve for deep water near *Fn*=0.4 is believed to be from the interaction between wave systems generated by each demi-hull. After that, residuary resistance coefficients decrease with increase of speed until those for the deep and shallow water become almost equal over the speed range exceeding the design speed *Fn*=0.75. Effective horsepower at the shallow water become lower than those at the deep water if *Fn* exceeds 0.4. The estimated EHP curve of the CATA III indicate that two 1500 kw water jet is enough for achieving design speed of 25 knots if η_D is assumed to be 0.49 and sea margin 10%.

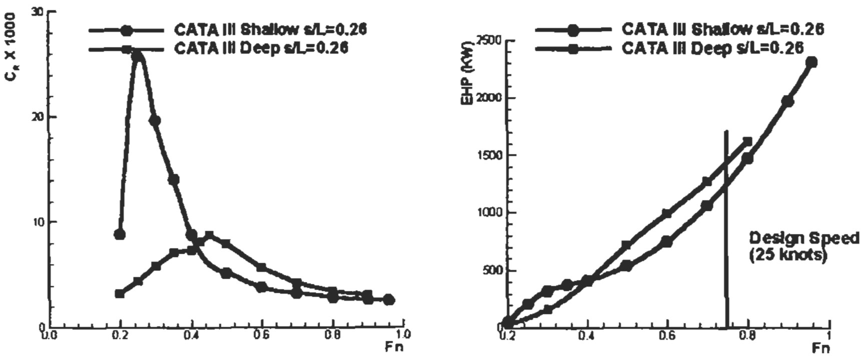

a) Coefficients of residuary resistance b) Effective horsepower

Figure 10: Coefficients of residuary resistance and effective horsepower of CATA III for shallow and deep water conditions($S/L = 0.26$)

Figures 11 shows trim and sinkage curves, respectively. It is seen that the trim and sinkage for the shallow water are rapidly varies near the critical speed and CATA III will be operate mostly in trim by stern condition

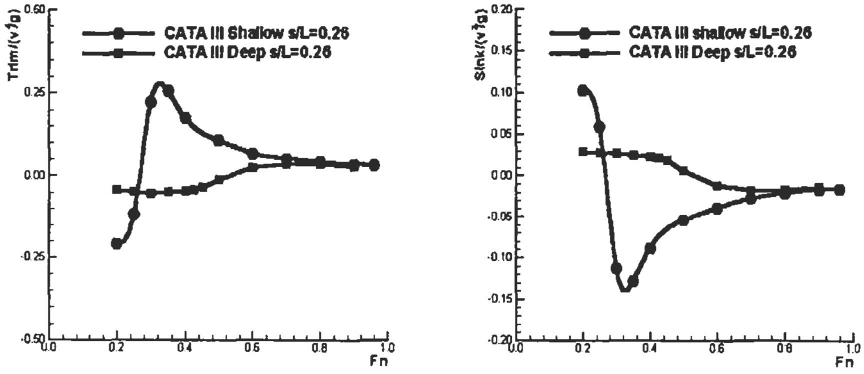

a) Trim curves b) Sinkage curves

Figure 11: Hull attitudes of CATA III for shallow and deep water ($S/L = 0.26$)

Figure 12 compares effective horsepower per unit displacement for CATA I, II and III. The power needed for CATAIII is apparently higher than those for CATA I and II as expected by considering the fact that L/B_d of CATAIII is less than two thirds of the values for CATA I and II. But comparing to a catamaran of similar size operating at the open sea and selected for the comparison purpose, CATIII requires similar power per unit displacement at the same design speed in spite of the fact that she is designed to operates in the restricted water.

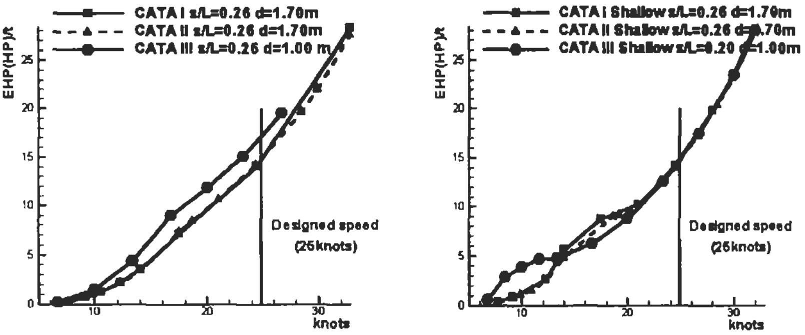

Figure 12: Comparison of Effective Horsepower per unit displacement

3 CONCLUSIONS

Hull form of a passenger catamaran has been derived to meet economical and natural requirements for operation in the planned routes. The hull forms and their hydrodynamic characteristics both in deep and shallow waters are investigated through model experiments and numerical simulations to determine its practical applicability. It is found that the approach in which numerical and experimental methods incorporating is beneficial in the initial design stage of a catamaran. The hull form of the catamaran obtained with the approach seems to show relatively good performances.

Acknowledgement

The present research has been supported by the Center for Transportation System in Yellow Sea founded by Korea Science and Engineering Foundation at the Inha University.

References

Chun J.-W. and Lee S.-H. (1999). A Feasibility Study on the Economic Aspect of Sea Transportation System between Incheon and Youngjong Island. *J. of Ocean Eng. and Tech* **13:4**, 234-244.

Kim H.-E. and Lee Y.-G. (2000). A Study on the Hull Form of a High-Speed Trimaran in the Yellow Sea (1). *Proc. of the Annual Autumn Meeting SNAK, Ulsan*, 9-10.

Millward A. (1984). The Effect of Hull Cross Section on the Theoretical Wave Resistance of a Fast Ship in Shallow Water. *International Shipbuilding Progress*, Delft University Press **31**, 28-33.

Practical Design of Ships and Other Floating Structures
You-Sheng Wu, Wei-Cheng Cui and Guo-Jun Zhou (Eds)
© 2001 Elsevier Science Ltd. All rights reserved

HULL FORM DESIGN OF CARGO SHIP IN SHALLOW AND STRONG CURRENT WATERWAYS

Li-Zheng Wang and Long-Fei Xi

Transportation Collage, Wuhan University of Technology Wuhan 430063, China

ABSTRACT

In China there are some rivers located in mountain area and its valley appears to be V or U type alternatively, where there are many beaches, quick and disorder waters, narrow course, curved channel, greater changes of depth in different seasons and so on. As far as the waterways with shallow and rapid current having characteristics described above is concerned , it is a key problem how to development new lines plan of cargo ship with high performance. In this paper a new afterbody of cargo ship in Wujiang, one of the typical rivers with shallow and rapid current , which is called tunneled combined with twin-stern is presented. By means of model test in tank., it is proved that in waterways with shallow and rapid current, the tunneled combined with twin-stern is one of the better ship types with high performance. It's synthetical index of speed performance is smaller than tunneled stern which was excellent ship types in Wujiang river in the past.

KEYWORDS

Waterways with shallow and strong current, High performance, Model test in tank, Hull form, Cargo ship

1 PREFACE

In China there are some rivers located in mountain area and its valley appears to be V or U type alternatively, where there are many beaches, quick and disorder waters, narrow breadth of course, curved channel, greater changes of depth in different seasons and so on. As far as the waterways with shallow and rapid current is concerned , it is a key problem how to development new lines plan of cargo ship with high performance. In this paper a new hull form of cargo ship in Wujiang which is a typical river having characteristics described above is presented by means of model test in tank.

2 DESIGN OF NEW AFTERBODY

2.1 The Assumption of New Afterbody

Wujiang is a tributary of Yangtse River. According to the shipping practices of many years it is proved that the afterbody with tunneled stern is better hull form of cargo ship in this River. The typical afterbody plan of "150t barges " is given in figure1 and it's main particulars is shown in table1. When this type of stern is applied in shallow waterway, the diameter of propeller can be increased so that the propulsive efficiency of ship is raised. Because enough water flow passing through propeller can be pledged by tunnel , ship still has steady propulsive efficiency and then it is adopted widely in rivers with shallow and rapid current. But along with the advance of technology and appearance of new ship types, the tunneled stern presents some defects such as higher resistance, lower propulsive factor, etc. So it is necessary to quickly develop new hull forms of cargo ship in Wujiang instead of tunneled stern.

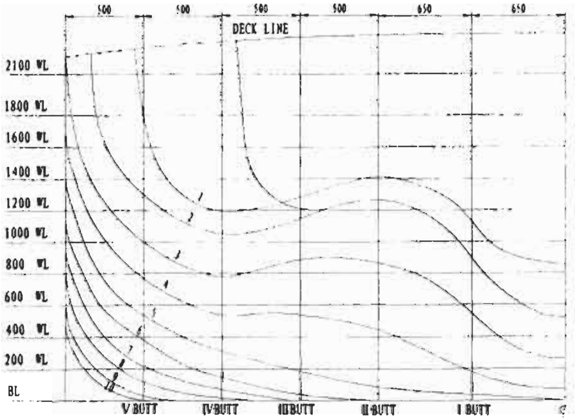

Figurc1: Afterbody plan of tunneled stern

TABLE1
SHIP'S MAIN PARTICULARS

Afterbody	Tunneled stern	Tunneled combined with twin-stern
Length overall (L_{OA})	35.70m	39.75m
Length on waterline(L_{WL})	34.50m	39.00m
Breadth moulded(B)	6.60m	7.00m
Depth(D)	2.10m	2.18m
Draught(T)	1.60m	1.40m
Displacement(Δ)	244.04t	235.50
Block coefficient(C_B)	0.67	0.62
Longitudinal prismatic coefficient (C_P)	0.677	0.623
Main Engine Type	6135ACaB	6134AZCaB
Power(BHP)	294.2kW	294.2KW

Since 1980, a new afterbody of twin-stern has been applied widely in cargo ship, passenger ship and so on in the middle and lower reaches of Yangtse River. By using twin-stern, propellers work in high wake region. So ship's quasi-propulsive coefficient(QPC) is higher. But in this afterbody ship's D/T is still smaller than 1, where D/T is the ratio of diameter of propeller to draught of ship. Because in waterways with shallow and rapid current, the power of main engine is higher in general to resist rapid current. In order to improve ship's propulsive performance, the diameter of propeller is usually greater than draught . While that is not contented by means of twin-stern.

As stated above, each afterbody has advantages and disadvantages. It is a key problem how to develop an afterbody that has merits of two types of stern above. From the point of view of higher wake and great diameter , We assume a new afterbody which is defined as tunneled combined with twin-stern.

2.2 The Determination of Main Parameters of New Ship Types

As a result of limitations of Wujiang waterways, length overall(L_{OA}) and breadth are not greater than 40m and 7m apart. While draught is ought to be alterable so as to fit the great changes of water depth from low water to flood all the year round and to enhance the transport benefit. As far as block coefficient(C_B) is concerned, it effects velocity and cargo capacity by a long way. Because waters is quick and disorder and depth of waterways alters consumedly in different seasons in Wujiang , the velocity in deep and calm water is required to be high and not lower than 19 km/h. So C_B must be selected to be smaller on condition that the capacity is enough to carry cargo. Longitudinal prismatic coefficient (C_P) is determined considering the appropriate matching with C_B and good resistance performance. Furthermore we must choose longitudinal buoyancy center (X_B) from layout and floating state of ship.

On the basis of above consideration, ship dimensions is optimized by tech-economic evaluation in order to ensure safety of shipping and improve ship's tech-economic performance. Then new lines plan having tunneled combined with twin-stern is drawn. The main particulars of ship is shown in table1 and the new afterbody plan is given in figure 2.

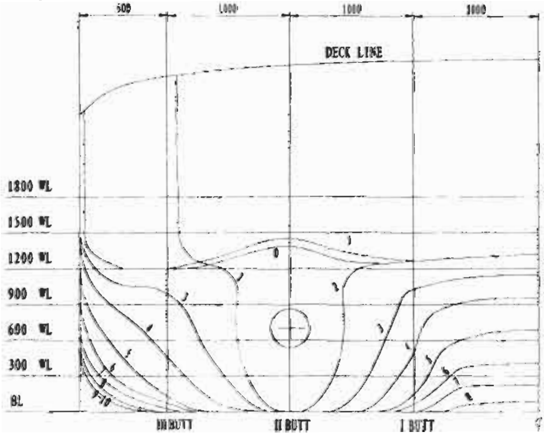

Figure2: Afterbody plan of tunneled combined with twin-stern

3 MODEL TEST AND ANALYSIS

In order to know if the performance of new afterbody is better than tunneled stern , model experiment is tested in tank. By self-propelled model test, the propulsion factor of actual ship with two afterbodys in deep water are listed in table 2 in which the propellers are outwards. At one time, their propulsion factor in shallow corresponding to different speed are shown in table 3, where the ratio of water depth to ship draft is 1.5.

From table1 we can see that the propulsive performance of tunneled combined with twin-stern is better than one of tunneled stern in deep water. While seeing table 3 shows that, two afterbodys have similar propulsive performance in shallow water.

By resistance test , the curves of R/D to Fn in deep and shallow water are given in fig.3 and fig. 4 respectively, where R/D is the resistance in kilogram over displacement in ton. and Fn is Froude number

It shows that the difference of resistance performance between tunneled combined with twin-stem and tunneled stem is small at same Fn.

TABLE 2
PROPULSION FACTOR OF TWO AFTERBODY IN DEEP WATER

Afterbody	Tunneled stem	Tunneled combined with twin-stem
Propeller type	B4-41	B4-55
Propeller diameter (D)	1.35m	1.40m
speed of actual ship (V)	19.60km/h	21.25km/h
Draft of actual ship (T)	1.60m	1.40m
Trust deduction fraction (t)	0.2546	0.2308
Wake fraction (ω)	0.2572	0.2635
Relative rotative efficiency (η_R)	1.0352	1.03780
Hull efficiency (η_H)	1.0036	1.0440
quasi-propulsive coefficient (QPC)	0.5438	0.6220

TABLE 3
PROPULSION FACTOR OF TWO AFTERBODY IN SHALLOW WATER (H/T=1.5)

V		8.1942km/h	9.2667km/h	10.3793km/h	11.4719km/h
Tunneled afterbody	t	0.2595	0.2878	0.2844	0.2831
	ω	0.2598	0.2725	0.2864	0.3675
	η_R	1.0017	1.0139	1.0222	1.0257
	η_H	1.000	0.9790	1.000	1.0467
	QPC	0.5600	0.5458	0.5315	0.5300
tunneled combined with twin-stem	t	0.2885	0.3183	0.3160	0.3200
	ω	0.3025	0.3220	0.3180	0.3170
	η_R	0.9860	1.0200	1.0350	1.0330
	η_H	1.0201	1.0055	1.0029	0.9956
	QPC	0.5600	0.5560	0.5400	0.5000

In order to compare their performance of speed further, a synthetical index noted k is introduced which is defined as:

$$K=P_D/(\Delta \times V)$$

Where P_D — delivered power at propeller in kW.

Δ — displacement in ton.

V — speed of ship in Km/hr

From the above expression we can see that the more smaller value of k is, the more higher performance of speed is. By calculation according to test results, the curves k~Fn are given in figure5. By comparing tunneled combined with twin-stem to tunneled stem , we can see that the synthetical index of speed performance (k) of the former is smaller than one of the latter. The new hull form of tunneled combined with twin-stem is one of high performance hull form in shallow and strong current indeed.

4 CONCLUSIONS

On the basis of above analysis stated over , It can concluded that

1. Along with the advance of technology and appearance of new ship types, the tunneled stern presents some defects such as lower propulsive factor, etc. So it isn't best cargo ship types again in Wujiang, a typical waterways with shallow and strong current.
2. Although ship types of twin stern is higher wake, it isn't fit to apply in shallow and strong current because of lower D/T.
3. In order to increase the diameter of propeller and improve propulsive performance, tunneled combined with twin-stern is a better ship types having high performance in shallow and strong current.

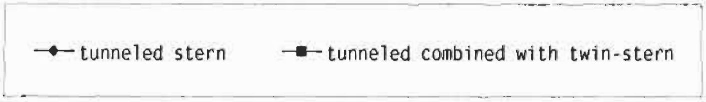

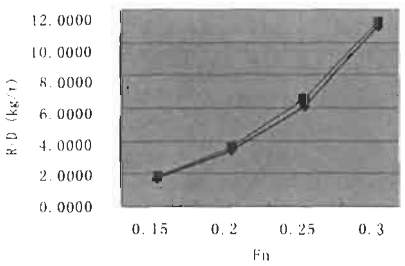

Figure 3: R/D ~Fn curves in deep water

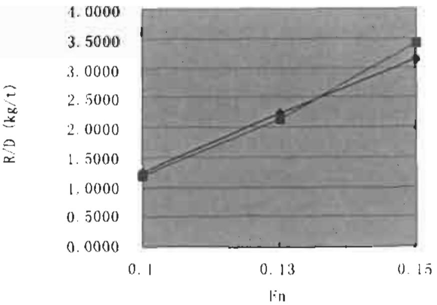

Figure4: R/D ~Fn curves in shallow water

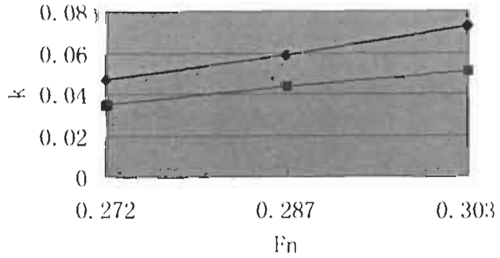

Figure5: k ~Fn curves of two afterbodys

References

1. Long Fanyi.(1989). Test Research of Twin-stern in Changjiang River. *Technology Intercourse of Ship Design* **1**, 9-15.
2. Li Shimo ,Wang Dexun and Chen qiuzhi(1991).Test Research of Speed Performance of New Motor Barges in Shallow and Rapid current. *Journal of Wuhan Transportation University* **20:4**, 211-217.
3. Wuhan Transportation University(1995) and Bureau of Inland Navigation in Guizhou Province. *The Reports of Ship Transportation Form and Development of New Ship Types*. 19-26.

Practical Design of Ships and Other Floating Structures
You-Sheng Wu, Wei-Cheng Cui and Guo-Jun Zhou (Eds)
© 2001 Elsevier Science Ltd. All rights reserved

THE IMPACT LOAD OF WING-IN-GROUND-EFFECT CRAFT IN WAVES AND APPLICATION OF HYDRO-SKI

Zu-Shun Dong, Xiao-Peng Gao and Wei Sun

NAVAL UNIVERSITY OF ENGINEERING
Wuhan, China

ABSTRACT

Wing-in-ground-effect craft (WIG) has been accepted by more and more countries because of its high speed like an airplane but low cost as a ship, and also because of its outstanding performance of safety and concealment. However, some technical problems must be solved to get a large and practical WIG, first of all is the prediction and reduction of hydrodynamic impact load in rough sea. An effective method has been proposed to calculate the impact load of WIG in waves. The theoretical research quite agrees with the result of model test. Furthermore it is effective for WIG to reduce its impact load in waves by using hydro-ski.

KEYWORDS

WIG, Impact, Impact load, Ski, Hydro-ski, Plat-ski, Ground effect

1 FOREWORD

Wing-in-ground-effect craft (WIG) has been accepted and attached importance to by more and more countries because of its high speed like an airplane but low cost as a ship, as well as its outstanding performance of safety and concealment. It has been regarded as a new kind of carrier-platform of 21 century with a good future for either military or for commercial purpose.

Now, many countries such as Russia, China, Japan and America are studying this new kind of ship, but only Russia has built out their applied large WIG of about 100 to 400 tons weight which has already been used in naval[1][2]. After all, some key technical problems such as impact load in waves, structure design rule, automatic pilot and aerodynamic layout with high efficiency must be solved to get a large WIG. Furthermore impact load in waves is one of the most important technical problem among them.

2 IMPACT LOAD IN WAVES

A WIG flies just over sea surface, impact load in waves during different phases like takeoff, landing and cruising should be considered. However research shows that the most serious impact happens when WIG land on rough sea. So it is the main problem to discuss in this paper.

3 THEORY FOR IMPACT LOAD IN WAVES

It's lucky that there are many research results of seaplane that is effective to be used as reference in WIG study. According to experience of seaplane, impact load is the most serious load that a WIG should sustain. Furthermore, it is the most serious situation when step of WIG hull impact on sea surface symmetrically. Von-Karman and Wagner's impact theory of wedge has been used in research of seaplane[3].

The main difference between WIG and seaplane is that WIG is required to sustain higher sea state in operation, including its landing. Furthermore, WIG always flies close over sea surface. It is more frequent to encounter waves during flight. This situation must be considered in the research. In this paper, correction about three aspects based on Wagner's theory is considered as follows:

(1) Wave effect on impact load must be considered accurately.
(2) Change of aerodynamic lift will affect impact load remarkably, so it must be considered in the research[4].
(3) At relative low speed, the effect of hull bilge immersion should be taken into account.

3.1 Basic Assumptions and Coordinate System

3.1.1 Basic assumptions

(1) WIG hull is regarded as a rigid body.
(2) Inertial force is governing while buoyancy and viscous can be neglected during landing course.
(3) Due to the time is short enough from the moment of beginning landing to the biggest overload reached, velocity parallel to keel can be regarded as a constant.
(4) Hull rotation, which doesn't affect impact load much, can be neglected in analysis when WIG landing, that is to say trim angle is regarded as a constant at that time[5].

3.1.2 Coordinate system

Oxy is a fixed coordinate system where ox is an axis settled on undisturbed free surface along the direction of velocity and oy is vertical downward. $o_1 s \zeta$ is moving coordinate where $o_1 s$ is parallel to keel with positive direction forward and $o_1 \zeta$ is an axis vertical to keel with positive direction upward, the origin o_1 is at stern.The coordinate systems are shown in figure1.

3.2 Motion Equations and Impact Load

3.2.1 Motion equations

Forces acted on WIG are shown in figure 2. Basal equations for landing are listed as follow:

$$-\frac{W}{g} y_{cg} = F_y + L - W \qquad (2\text{—}1)$$

$$I_{cg} \dot{\tau}_{cg} = M_{cg} \qquad (2\text{—}2)$$

$$\frac{W}{g} \dot{x}_{cg} = F_x \qquad (2\text{—}3)$$

where: W: landing weight of WIG(kg) L: aerodynamic lift (kg)

I_{cg} : longitudinal moment of inertia about CG （kg× m^2 ）

x_{cg} 、 $\ddot{y}_{cg}$:cceleration of CG （m/ s^2 ） τ_{cg} :angular acceleration （rad/ s^2 ）

F_x 、 F_y :component of impact force (Fn) along x and y axis （kg）

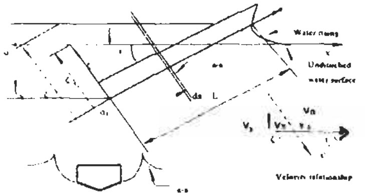

Figure 1: Coordinate system

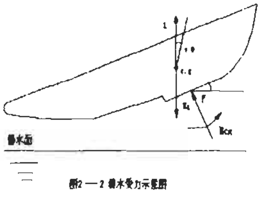

Figure 2: Forces acted on WIG

$x_{cg}=0$, $\tau_{cg}=0$, $L=pW$, $F_y=F_n\cos\tau$, because of mentioned assumption, then basal equations can be written :

$$-\frac{W}{g}\ddot{y}_{cg} = F_n\cos\tau+(p-1)W \qquad (2\text{—}4)$$

3.2.2 Fn

According to strip theory, immersed hull is cut into many elements (ds - length of strip piece) and every element is regarded as a two-dimensional wedge, then hydrodynamic force acted on whole body can be get:

$$F_n=\varphi(\lambda')\int_0^l dF_n \qquad (2\text{—}5)$$

$\varphi(\lambda')$ is a correction coefficient of three-dimension flow, dF_n is the hydrodynamic force acted on ds. Base on principle of momentum, there is:

$$F_n=\varphi(\lambda')\left(\int_0^l \dot{\zeta}\frac{\partial m_w}{\partial t}ds+\ddot{\zeta}\int_0^l m_w ds\right) \qquad (2\text{—}6)$$

(1) $\varphi(\lambda')$

Empirical formula for $\varphi(\lambda')$ according to Pabst's experimental research of plate [6] is:

$$\varphi(\lambda')=\left[\frac{1}{1+(\frac{1}{\lambda'})^2}\right]^{\frac{1}{2}}\left(1-\frac{0.425}{\lambda'+\frac{1}{\lambda'}}\right) \qquad (2\text{—}7)$$

$$\lambda'=\lambda[1+c\varphi(\frac{1}{\lambda})] \qquad (2\text{—}8)$$

where: λ'- efficient length-beam ration λ - average length-beam ration c=0.4

(2) Added mass for two-dimensional wedge

Hull's added mass (m_w) is different with or without bilge wetted, both of them are discussed here:

(a) m_w without bilge wetted

According to reference [7] and [8], m_w for two-dimensional wedge is:

$$m_w = \frac{\rho\pi}{2}\zeta^2[f(\beta)]^2 \qquad (2\text{—}9)$$

at the moment of bilge wetted:

$$m_{wc} = \frac{\rho\pi}{8}b^2[f(\beta)]^2\tan^2\beta \qquad (2\text{—}10)$$

(b) m_w with bilge wetted

m_w with bilge wetted which doesn't take free surface into account has been obtained according to Bobyleff's theory, while the one with consideration of free surface has not existed, it can be calculated by the sum of m_w and Δm_w, where m_w is added mass at the moment of bilge wetted and Δm_w is additional one which can be get with reference of Bobyleff's theory.

when a two-dimensional wedge is moving in fluid with a velocity of $\dot{\zeta}$, force acted on hull of unit length is :

$$f_n = B\frac{\rho}{2}(\dot{\zeta})^2 b \qquad (2\text{—}11)$$

B is a function about deadrise (β) [9], according to momentum theorem, there is:

$$m_w = m_w + \Delta m_w = \frac{\rho\pi}{8}b^2[f(\beta)\tan\beta]^2 + B\frac{\rho}{2}b^2(\frac{\zeta'}{b} - \frac{\tan\beta}{2}) \qquad (2\text{—}12)$$

(c) m_w for random section shape

m_w for random section shape before its bilge immersed is [10]:

$$m_w = \frac{m}{2C_\Delta\sin^2\tau\cos^2\tau}\int_0^{\frac{y}{b}} C_B d\frac{y}{b} \qquad (2\text{—}13)$$

C_B is planing lift coefficient in calm water [10], then:

$$F_n = \varphi(\lambda')\left(\int_0^{m_{ws}}\frac{\dot{\zeta}\dot{\zeta}'}{\tan\tau}dm_w + \dot{\zeta}\int_0^{\zeta'}\frac{m_w}{\tan\tau}d\zeta'\right) \qquad (2\text{—}14)$$

The change of surface rising is rather small when immerging depth is large enough, so it can be regarded as a constant, assume: $\dot{\zeta}' = \dot{\zeta}$, then:

$$-\frac{W}{g}\ddot{y} = \varphi(\lambda')\left[\frac{m_{ws}}{\tan\tau}(\dot{y}+\kappa\dot{y}_0)^2 + \ddot{y}\int_0^{\zeta'}\frac{m_w}{\tan\tau}d\zeta'\right] + (p-1)W \qquad (2\text{—}15)$$

3.2.3 Solution of motion equations

From Eqn.2-15, Eqn.2-16 can be get:

$$\frac{\ddot{y}}{(\dot{y}+\kappa\dot{y}_0)^2} + \frac{(p-1)g}{[1+\varphi(\lambda')\frac{g}{W}\int_0^{\zeta'}\frac{m_w}{\tan\tau}d\zeta'](\dot{y}+\kappa\dot{y}_0)^2]} = -\frac{g\varphi(\lambda')m_{ws}}{W\sin\tau + \varphi(\lambda')g\sin\tau\int_0^{\zeta'}\frac{m_w}{\tan\tau}d\zeta'} \qquad (2\text{-}16)$$

This formula can be solved by numerical integration, then the changing value of $\ddot{y}$, $\dot{y}$ and y about t is obtained finally.

3.3 Impact Load in Waves

WIG must operate on rough sea where the impact load is much bigger than the one on calm water. Motion parameters such as trim angle, track angle and downward velocity will change randomly because of random encountering waves, so lots of mathematics statistic must be done to predict impact load accurately. From viewpoint of engineering usage, the biggest load is the impact load corresponding to the largest slope angle, which is regarded as the most dangerous situation for structure. It is assumed that τ is initial trim angle, γ_0 is initial track angle, V_x is horizontal velocity, V_y is vertical velocity, θ is maximum wave slope, with consideration of waves, the corresponded effective initial parameters can be get:

effective trim angle: $\tau_e = \tau - \theta$ effective horizontal velocity: $V_{xe}=V_x+/-V_w$,
effective track angle: $\gamma_e = \theta + tg^{-1}(V_y/V_{xe})$ effective vertical velocity: $V_{ye}=V_y\cos\theta+(V_x+/-V_w)\sin\theta$
the largest wave slope: $\theta = tg^{-1}(\pi h/\lambda)$ wave velocity: $V_w \approx 1.25\lambda^{1/2}$

where 'h' is wave height and λ is wave length, so method for impact load in calm water can be used for that in waves with effective parameters mentioned above.

4 COMPARISION BETWEEN RESULTS OF THEORY STUDY AND MODEL TEST

TABLE 1

ACCELERATION EXTREME COMPARISION IN CALM WATER

No.	Trim angle (°)	Horizontal velocity (m/s)	Vertical Velocity (m/s)	Acceleration extreme of CG(g)		
				theoretical result	experimental result	Error (%)
1	0.728	13.84	0.979	1.569	1.516	5.3
2	1.56	13.79	0.848	1.371	1.327	4.4
3	1.46	12.70	0.870	1.579	1.630	-5.1
4	3.95	12.00	1.153	2.070	2.047	2.3
5	3.95	12.04	1.175	2.115	2.198	-3.8

Comparision between the result of theoretical research and model test is shown in table 1 and table 2. Main dimensions of calculated model is:

Length $L=0.8m$ Beam $b=0.28m$ Deadrise $\beta=15°$ Weight $\Delta=25kg$

TABLE 2

ACCELERATION EXTREME COMPARISION IN WAVES

No.	Trim angle (°)	Horizontal velocity (m/s)	Vertical velocity (m/s)	Slope angle (°)	Acceleration extreme of CG(g)		
					theoretical result	experimental result	Error (%)
1	4.16	14.36	1.63	3.44	6.90	6.88	0.3
2	5.41	14.71	1.36	4.38	5.89	6.56	11.4
3	6.66	14.63	1.60	4.38	7.20	6.79	5.7
4	7.28	14.96	1.04	5.15	5.08	5.10	0.3
5	7.90	15.08	1.10	4.38	6.75	5.73	15.1

(wave height h=210mm, wave length L=6.1m)

The theorctical result is quite agree with the test one. Error in waves is a little bit large than in calm water, the main reason of this is wave encounter phase being not accurate. So a conclusion can be drawn that the method provided here could reach the need of engineering usage.

5 SOME PARAMETERS' EFFECT ON IMPACT LOAD

5.1 Motion Parameters

a WIG model test with different motion parameters include V_x, γ_0, τ_0 has been conducted. According to the result of calculation, η_{max} (Maximum impact overload coefficient) increases rapidly along with increasing V_x and the relationship of them is almost in proportion to V_x^2. In fact, if γ_0 =const, the amount of V_x varies with the vertical velocity component directly ($V_y = V_x \, tg \, \gamma_0$), that is to say impact overload is proportional with vertical velocity square and this is just agree with the result of wedge impact theory. The η_{max} also rises rapidly along with the increasing γ_0. When V_x is fixed, the change of γ_0 actually means the change of vertical impact velocity, if γ_0 is small enough, as γ_0 increases, η_{max} will rise a little bit, when γ_0 increases not too large. But η_{max} will rise with γ_0 obviously when γ_0 is large. The η_{max} rises a little bit along with τ when γ_0 is fixed, so the influence of τ is rather small than that of γ_0.

5.2 *Effect of Hull's Main Parameters*

The important hull parameters are deadrise β and beam-loading coefficient C_b. If β increase, η_{max} will decrease, this phenomenon will be more evident with small β. Small C_b doesn't affect impact load evidently according to the result of calculation, only when C_b gets to a larger value, impact overload begins to decrease. Critical value of C_b which η_{max} begins to decrease notably is about 4.0. If there is C_b =18, the η_{max} decreases about 50%, so C_b >18 is an ideal situation, in this case, η_{max} can decrease more than 50%.

6 PRIMARY STUDY OF HYDRO-SKI

How to reduce impact load in waves is one of the most important problems which should be solved for large WIG in service. Besides theoretical prediction and influence rule research, hydro-ski is a kind of efficient method to reduce impact load. Theoretical and experimental research for plate-ski which has been used by Russia on its large WIG, or for strut-type-ski shows that hydro-ski is efficient for WIG to reduce impact load in waves.

6.1 Impact Load with Plate-ski

Model test about impact load with changing attachment of both plate-ski and strut-type-ski have been carried out and the results show that ski can reduce impact load efficiently like what we have imagined.

6.2 Planing Resistance during Takeoff with Plate-ski

Model test on resistance of ski has been carried out to study the effect of plate-ski on planing resistance, the result shows:

(1) Influence of plate-ski on planing resistance at low speed ($Vm \leq 2m/s$) is not evident.

(2) At relatively high speed ($Vm > 2m/s$) lift/drag ratio will increase and this will be more evident under the condition of rather small trim angle (τ). In general, the sum of τ and α which is the angle of ski installed is favorable at about 10 degrees.

(3) Ski which is installed near CG can make lift center moved slightly on planing surface when the trim angle changes, this is good for longitudinal stability during takeoff.

7 CONCLUSION AND RECOMMENDATION

(1) Theorical method proposed in this paper for predicting impact load in waves has been proved by model test to have enough precision for engineering application.

(2) Hull parameters' selection is one of efficient ways to reduce impact load of WIG.

(3) Controlling motion parameters reasonably can also reduce impact load.

(4) It is efficient for WIG to reduce impact load by installing plate-ski near CG, there is no harm to the performance of takeoff including resistance and longitudinal stability.

(5) It can be seen from the result of theoretical analysis that impact load reducing is limited because plate-ski's breath is rather large and the distance between ski and hull bottom is too close, so it's necessary to develop a new kind of ski with better performance of impact such as strut-type-ski.

Reference

[1] H.Wagner. (1932). Z.Ang.Mach.12,

[2] H.Wagner. (1934). Proceedings of the IVth Inter. Congr. For Applied Mech. Cambridge(England)

[3]R.J.Monahan M.A. and P.R.Crewe , M.A. (1949). Formulae for Estimating the Forces in Seaplane —Water Impacts without Rotation or Chine Immersion, NACA, **RN 2804,** January,

[4]Robert W.Miller, Theoretical Analysis of Hydrodynamic Impact of a Prismatic Float Having Freedom in Trim, NACA, **TN 2698**

[5]Joseph L.Sim and Emanuel Schnitzer. (1952).A Theoretical Investigation of the Effect of Partial Wing Lift on Hydrodynamic Landing Characteristics of V—Bottom Seaplane in Step Impacts, NACA **TN 2815**

[6]Pabst , Willelm. (1931). Landing Impact of Seaplanes, NACA, **TM 624**

[7]Steiner, Margaret F. (1948). Analysis of Planing Data for Use in Predicting Hydrodynamic Impact Loads, NACA, **TN 1694**

[8]Emanuel Schnitzer. (1952). Theory and Proceduer for Determing Loads and Motions in Chine—Immersed Hydrodynamic Impacts of Prismatic Bodies,NACA, **TN 2813,**

[9]Lamb, Horace. (1932). Hydrodynamics, sixth ed. Cambrridge Univ.

[10]Robert F.Smiley. (1952). The Application of Planing Characteristics to the Caculation of the Water —Landing Loads and Motions of Seaplanes of Arbitrary Constant Cross Section, NACA, **TN 2814**

Practical Design of Ships and Other Floating Structures
You-Sheng Wu, Wei-Cheng Cui and Guo-Jun Zhou (Eds)
© 2001 Elsevier Science Ltd. All rights reserved

CONCEPTUAL DESIGN OF VERY LARGE-SIZE SUPER-HIGH-SPEED FOIL CATAMARAN CONTAINERSHIP

Keh-Sik Min, Seon-Hyung Kang and Oi-Hyun Kim

Hyundai Heavy Industries Co., Ltd.
1, Cheon-Ha Dong, Dong-Ku, Ulsan, Korea

ABSTRACT

Following the established 3-stage R & D program of super-high-speed ships, a study on the conceptual design of a large-size super-high-speed foil catamaran containership has been performed as the 3rd(the final) stage work utilizing the accumulated experience and technology. In this paper, some main features in the conceptual design shall be briefly discussed together with the present technical problems in realizing actual ships.

KEYWORDS

Super-High-Speed Ships, Large-Size Foil Catamaran, Containership

1 INTRODUCTION

Hyundai Maritime Research Institute(HMRI) prepared a Three-Stage R and D Program for super-high-speed ships in 1990 and has actively carried out the research works following the established plan. As the largest single shipyard in the world, however, the ultimate goal of the research is in the development of large-size super-high-speed ships. In this respect, the first and the second stage studies for the development of small and medium size super-high-speed ships are regarded as the intermediate steps to achieve the above goal. Therefore, the decisions on ship type and main characteristics have been made considering the ultimate goal.

In order to increase ship speed significantly, it is necessary to prevent the rapid increase of resistance. This purpose could be achieved in different ways. One way is to utilize the dynamic or static lift effects. For dynamic or static effect ships, however, it is extremely difficult to increase the ship size beyond a certain limit, which is regarded as the fatal disadvantage of these types of ship.

On the other hand, the hull form of displacement-type catamaran ships could be made very fine so as to achieve the goal of high speed by preventing rapid increase of wave resistance. Among many practical advantages of catamaran ships, the most noticeable merit is in the fact that ship size could be easily increased without any limitations and without sacrificing any other characteristics.

The general advantages of catamaran ships could be still further improved by properly combining the hull itself supported by buoyancy and the hydrofoil system which produces dynamic lift. During normal sailing, desired part of the ship hull would be lifted up above free-surface by the dynamic lift. Therefore, hull resistance would be decreased and ship speed could be increased. Furthermore, the foil system significantly improves ship's seakeeping quality in heavy weather, since the system acts as the motion control device.

The 3-stage super-high-speed ship R & D Program has been completed successfully. Numerous research reports and papers have been prepared and presented[1 - 9]. This study is the third stage(the final stage) research work and deals with the conceptual design of □Large-Size Super-High-Speed Foil Catamaran Containership□. Actually, conceptual design works for 4 different ships have been carried out in the final stage study, that is, about 1,000 TEU - 60 knot ship and about 4,000 TEU - 50, 60 and 70 knot ships. Due to limited space, however, only the brief summary of the design features for 4,000 TEU - 60 knot foil-catamaran containership shall be presented and discussed in this paper.

2 SELECTION OF MAIN CHARACTERISTICS

Catamaran ships have many practical advantages such as large deck area, high stability, superior maneuverability, easy operation and maintenance, etc. Different from conventional mono hull ships, therefore, the container loading capacity(number of containers) for catamaran ships is not determined by deck area or stability, but by weight. The average weight of 7.5 tonnes per 20-foot container was selected in this study. To determine ship length and breadth, about 4,000 twenty-foot size containers were arranged on the deck. From this investigation, appropriate ranges of ship length(LPP) and breadth(BR) were obtained.

Hull weight was estimated iteratively. Higher tensile steel(AH32) was selected as hull material. Main engines were selected from the power estimation made from the results of the previous studies[9]. The amount of fuel was calculated with the selected engine and the estimated power. All the weight components were summed up to figure out the overall ship weight, that is, ship's displacement. The above procedure had to be repeated several times.

With the displacement and the initial ranges of dimensions obtained in the above process, the principal characteristics were determined utilizing the result of the “Study on the Optimum Dimension Selection and the Resistance Prediction of the Displacement Type Super-High-Speed Ships”[7], and are summarized in Table 1.

TABLE 1

SUMMARY OF PRINCIPAL CHARACTERISTICS

Length between perpendiculars (LPP)	240.0 m
Breadth (BR)	60.0 m
Demi-Hull Beam (B)	16.0 m
Draft (T)	10.0 m
Number of 20' Containers	about 4,000
Design Speed	60.0 knot
Cruising Range	8,000 NM

3 HULL FORM DESIGN AND BARE HULL RESISTANCE TESTS

Hull form design is one of the most important technologies in the shipbuilding industry. The authors, long engaged in this industry, have made much efforts to the research on the hull form design technology. As the result, several different theoretical methods have been prepared and published by the authors. As far as the authors' knowledge is concerned, no analytical optimum hull form design method practically exists in the world except the authors' works. Recently, the authors have developed a theoretical hull form design method for displacement type super-high-speed ships utilizing the "Minimum Resistance Theory" and "Sectionally-Varying Hull From Equation"[8]. This method quickly produces displacement type super-high-speed ship hull forms which not only possess superior resistance characteristics, but also require almost no correction or adjustment. The hull form design concept and the method have been presented several times and shall not be discussed in this paper.

To improve effectiveness of the study, it was decided to first carry out the study on the demi-hull forms and to design the catamaran ship hull form utilizing the result of the demi-hull form study. As discussed earlier, the ship type in this study is the type whose resistance is greatly decreased during normal sailing, since designated part of the ship hull is lifted up above the free-surface by the dynamic lift. Therefore, it does not have much meaning to optimize the hull form for the full load condition. The primary importance is to design the hull form to have the least resistance in the normal sailing condition when desired part of the ship hull is lifted up. In order to do that, the optimum ratio between buoyancy and lift should be known in advance. However, it is not known in the initial stage. From the previous experiences, therefore, the buoyancy/lift ratio has been tentatively selected as 40 : 60.

In principle, two optimized hull forms were designed first - one for the full load condition(upper hull form) and the other for the normal sailing condition(lower hull form), and the upper and the lower hull forms were combined to a single hull form. In this way, total 4 demi-hull forms were prepared. Model tests were carried out for 4 demi-hull forms, and the test results were compared. One best hull form was selected focusing the performance characteristics to the condition of desired buoyancy/lift ratio. The catamaran ship hull form was designed based on the selected demi-hull form, and is shown in Figure 1.

All the model tests were carried out in deep water towing tank of Hyundai Maritime Research Institute(HMRI). Since model tests for the demi-hull forms were regarded as qualitative ones, small models of 2.5m length were manufactured using wood and polyurethane. For the catamaran hull form tests, 6.0m long ship model (□=1/40) was manufactured using wood.

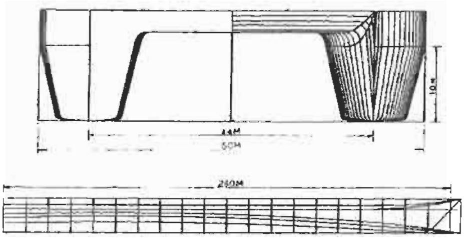

Figure 1: Catamaran Ship Hull Form

4 STUDY ON THE OPTIMUM BUOYANCY/LIFT RATIO

As the ship hull is lifted up above free-surface, the hull displacement is decreased, and hence, the hull resistance is also decreased. On the other hand, resistance of the hydrofoil system is increased as dynamic lift is increased. The sum of these two resistance components, that is, the sum of the hull resistance and the foil system resistance is the overall resistance for buoyancy/lift combination ships. The overall resistance varies according to the buoyancy/lift ratio. In general, therefore, the buoyancy/lift ratio exists at which the overall resistance for the given ship speed becomes minimum. This ratio is the optimum ratio. Figure 2 shows the concept of the optimum buoyancy/lift ratio. It is important to design the hydrofoil system to produce the lift as much as the amount designated by the optimum ratio.

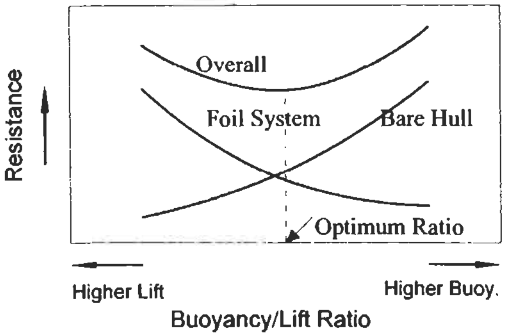

Figure 2: Concept of the Optimum Buoyancy/Lift Ratio

The general method to find out the optimum ratio is as follows :

- pre-select several buoyancy/lift ratios
- design several hydrofoil systems for each of ratios
- manufacture ship and foil system models
- conduct model tests for all the combinations of buoyancy/lift ratio and foil systems
- analyze the test results and determine the optimum ratio

The above procedure could possibly be carried out only by an expert who possesses the high level technologies on the buoyancy/lift combination ship and the foil system. Furthermore, it will take enormously long time and high cost to carry out the model tests for such numerous combinations. In practice, therefore, it is almost impossible to perform the above procedure.

In the way of long continuous studies on super-high-speed foil catamaran ships, however, the authors have developed a theoretical and empirical method that quickly determines the optimum buoyancy/lift ratio with sufficient practical accuracy. It is considered that the authors' method is the only method in the world which could determine the optimum buoyancy/lift ratio without model tests. This method is being actively utilized in actual designs.

In order to determine the optimum buoyancy/lift ratio, a number of ratios should be pre-selected systematically and resistance components for the following items should be calculated for each of pre-selected ratios :

- bare-hull resistance
- foil resistance
- side strut resistance
- center strut resistance (if any)
- blockage resistance at corners

The overall resistance is obtained by summing up the resistance components, and the buoyancy/lift ratio versus overall resistance curve could be prepared. The optimum ratio is the ratio where the overall resistance becomes minimum in the curve. The method of calculation or estimation for each of resistance components shall not be discussed in this paper due to limited space. In this study, the optimum buoyancy/lift ratio is found to be 45 : 55, which is very close to the initial estimation of 40 : 60.

5 HYDROFOIL SYSTEM DESIGN

Hydrofoil system for large-size foil catamaran ships are mainly consisted of forward foil, aft foil, side struts which connect foil to ship hull and one or two center struts. Basically, hydrofoil system should be designed to satisfy the following two conditions in normal sailing :

- the system should produce as much lift as the amount designated by the selected buoyancy/lift ratio
- forward and aft foils should properly share the lift to maintain the desired dynamic trim

In fact, it is very difficult to design the optimum hydrofoil system for foil catamaran ships. First of all, accurate estimation of the effect of free-surface on the hydrodynamic characteristics is very difficult. Interactions between ship hull and foil system, and between forward and aft foils are very complicated. Due to such complicated physical phenomena, no proper method has been practically existed to predict the performance characteristics or to determine characteristics of a foil system. Along the course of extended research works on the super-high-speed foil-catamaran ships, however, the authors have prepared a practically accurate method to predict the hydrodynamic characteristics or to determine main characteristics of a hydrofoil system operated in the vicinity of free-surface[10 - 12]. This method has been actively utilized in the actual design of various foil systems. In this study, the hydrofoil system has been designed to produce the lift equivalent to 55% of ship's design displacement and to maintain the even keel state during normal sailing from the stationary state of 0.5 degree trim by stem.

6 PREDICTION OF THE TRIAL PERFORMANCE

The final catamaran ship model with the designed foil system was manufactured and shown in Figure 3. Detail model tests were carried out with this final ship model. Figure 4 shows the catamaran ship model test in 60 knots with the hydrofoil system. It is clearly visible in Figure 4 that ship hull is properly lifted up above the free-surface with the desired dynamic trim.

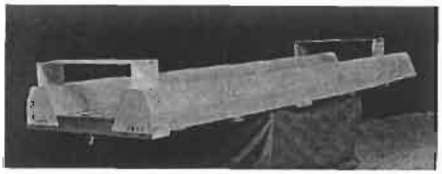

Figure 3: Catamaran Ship Model with Hydrofoil System

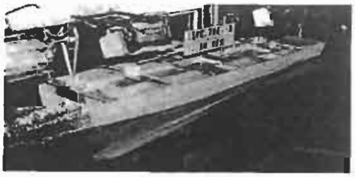

Figure 4: Catamaran Ship Model Test with Hydrofoil System

In order to predict the trial performance, the air resistance has been estimated and incorporated. Figure 5 shows the resistance prediction during sea trial. Figure 5 also shows the available thrust of very large capacity waterjet(KaMeWa 255S□ waterjet) for the fixed power. The trial ship speed is determined from the resistance and the thrust curves in Figure 5..

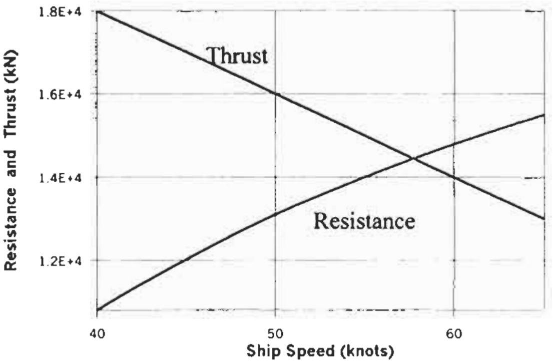

Figure 5: Trial Resistance and Available Thrust

7 CONCLUSIONS

In this paper, the study on the conceptual design of very large-size super-high-speed foil catamaran containership with about 4,000 TEU loading capacity and 60 knot ship speed has been very brief discussed. From the result of the study, the following conclusions could be made :

- If five large-capacity waterjets such as KaMeWa 255S□ type each coupled with 60,000 kW gas turbine such as GE LM6000 + type are installed in each of demi-hulls, the ship would achieve the speed of about 58 knots. This is rather conservative prediction.

- If the overall system is more carefully optimized utilizing the experiences in this study, the object ship is expected to achieve more than 60 knots of ship speed with the above propulsion system.

- The reduction in resistance from that of bare hull due to the hydrofoil system is about 10% for this object ship, which is considered to be very small compared with those for small size ships. The effectiveness of the hydrofoil system is reduced as the ship size is increased.

- For the object ship, the design speed of 50 knot may be more practical. It is estimated that eight 60,000 kW gas turbines and two 6,500 kW auxiliary diesel engines are required to achieve higher than 50 knots of ship speed.

- Through the execution of the 3-stage R & D program, a vast amount and high level experiences and technologies have been developed and accumulated for the design of buoyancy/lift combination type super-high-speed ships, that is, super-high-speed foil catamaran ships.

References

1. Min K-S.(1991). Long-Range High-Speed Catamaran Passenger Ship Design. *the Proceedings of the First International Conference on FAST Sea Transportation(FAST '91)*, Trondheim, Norway.

2. Min K-S.(1992). Design and Construction of Long-Range High-Speed Foil Catamaran Passenger Ship. *the Proceedings of the Nineteenth Symposium on Naval Hydrodynamics*, Seoul, Korea.

3. Min K-S., Kim O-H. and Park J-S.(1993). A Study on the Structural Design of the Hydrofoil System for High-Speed Foil Catamaran Ships. *the Proceedings of the Second International*

Conference on FAST Sea Transportation(FAST '93), Yokohama, Japan.

4. Yum D-J., Min K-S., Song K-J. and Lee H-Y.(1995). Theoretical Prediction of Seakeeping Performance and Comparison with Sea Trial Results for High-Speed Foil Catamaran Ship. *the Proceedings of the Third International Conference on Fast Sea Transportation(FAST '95)*, Lubeck-Travemunde, Germany.

5. Min K-S., Kim O-H., Kim J-H. and Kang S-H.(1997). Design and Construction of 300 Passenger Super High-Speed Foil Catamaran Ship. *the Proceedings of the Fourth International Conference on Fast Sea Transportation(FAST '97)*, Sydney, Australia.

6. Min K-S., Kim O-H. and Kang S-H.(1997). Design of Mid-Size Super High-Speed Foil Catamaran Ferry. *The Proceedings of the Spring Meeting*, 1997 of the Society of Naval Architects of Korea.

7. Min K-S. and Kang S-H.(1996). Systematic Study on the Hull Form Design and the Resistance Prediction of Displacement Type Super High-Speed Ships. *Journal of the Society of Naval Architects of Korea*, 33:4.

8. Min K-S. and Kang S-H.(1998). Systematic Study on the Hull Form Design and Resistance Prediction of Displacement-Type Super-High-Speed Ships. *Journal of Marine Science and Technology*, 3:2, The Society of Naval Architects of Japan.

9. Min K-S., Kang S-H. and Kim O-H.(2000). Conceptual Design of Large-Size Super-High-Speed Foil Catamaran Containership. *the Proceedings of the Seventh International Marine Design Conference(IMDC2000)*, May 21-24, 2000, Kyungju, Korea.

10. Min K-S. and Lee H-G.(1995). Systematic Studies on the Development and the Estimation of Hydrodynamic Characteristics of New Hydrofoil Sections Moving under the Free Surface. *Maritime Research Institute Report No. HMRI-95-06-S100*, Hyundai Heavy Industries Co., LTD.

11. Min K-S. and Lee H-G.(1996). Systematic Study on the Prediction of Hydrodynamic Characteristics for HMRI NP-Series 2-Dimensional Hydrofoils Operated under the Free-Surface. *Maritime Research Institute Report No. HMRI-96-04-S068*, Hyundai Heavy Industries Co., LTD.

12. Min K-S., Streckwall H. and Kang S-H.(1998)., Numerical and Experimental Studies for the Prediction of Hydrodynamic Characteristics of 2-Dimensional Hydrofoils Operating under the Free-Surface. *the Proceedings of the 22nd Symposium on Naval Hydrodynamics*, Washington, D. C., USA

Practical Design of Ships and Other Floating Structures
You-Sheng Wu, Wei-Cheng Cui and Guo-Jun Zhou (Eds)
© 2001 Elsevier Science Ltd. All rights reserved

A PRACTICAL APPLICATION OF AIR LUBRICATION ON A SMALL HIGH SPEED BOAT

Jinho Jang [1], Il Jun Ahn [1], Jaesung Kim [1], Jung-Chun Suh [1], Hyochul Kim [1],
Seung-Hee Lee [2] and Museok Song [3]

[1] Dept. of Naval Architecture & Ocean Eng., RIMSE, Seoul Nat. Univ., Seoul, Korea
[2] Dept. of Naval Architecture & Ocean Eng., Inha Univ., Inchon, Korea
[3] Dept. of Naval Architecture & Ocean Eng., Hongik Univ., Jochiwon, Korea

ABSTRACT

The reduction of resistance with lubrication of an air cavity and the similarity relations involved are investigated with a series of towing tank tests on geometrically similar models. Three geometrically similar models of different size are tested in the towing tank of Seoul National University. The results indicate that an introduction of air cavity by artificially supplying air beneath the bottom of a model ship with a backward-facing step is effective for reduction of the model resistance. The areas of air cavity and the required flow rates of air, both of which are directly related to the effective wetted surface area and the overall energy saving are found to be dominated by the Froude number scaling. Both the traditional two-dimensional method and Telfer's three-dimensional method seem to be applicable to the extension of the model resistances in the tested range if corrections are made to account the changes in the frictional resistance caused by the changes in the effective wetted surface area. Based on the findings obtained above, a small test boat of practical size is constructed and the effect of air cavity on the reduction of ship resistance is studied. The results will confirm the results found in the model tests and assure the practical applicability of the air cavity for the resistance reduction of a real ship.

KEYWORDS

Air lubrication, Frictional resistance, Drag reduction, Bottom Step, Geometrically similar models, Model experiment, Scale law

1 INTRODUCTION

The researches on drag reduction of displacement type ships have been focused mainly on reduction of wave resistance or form drag, and many valuable concepts are derived already and practically utilized to achieve the high energy efficiencies from the modern hull forms. On the contrary, however, little attempts have been made to reduce the frictional resistance in spite of the fact that the frictional resistance occupies a major portion of the total resistance of conventional ships. In these days, with increase in the understanding of the phenomena involved in the friction and the harsh request for energy efficiency from economical and environmental considerations necessitates more rigorous effort for reducing the frictional resistance.

Among several methods for frictional drag reduction, reducing the effective wetted surface area by covering some portion of the hull surface with air film is conceptually easy to understand [Bushnell & Hefner (1990)]. These air films can be generated through a natural intrusion of the air into the bottom of the ship, but frequently formed more effectively by an intentional introduction of the air near the step formed under the hull bottom. The wake of this step provides spatially fixed circulating flow region behind the step. If air is supplied inside of this circulating region, water is displaced gradually by air behind the step and eventually a single air cavity of nearly steady state can be formed [Knapp *et al.* (1970)]. When the size of this air cavity is large enough and sufficiently stable, a significant reduction in wetted surface area can be obtained. The reduction has been reported to reach up to 20% of the total resistance with a careful arrangement of the steps and an appropriate supply of air [Jang & Kim (1999)]. However, the application of same idea to the reduction of frictional resistance of a real ship requires more thorough understanding on the similarity relation.

In the present work, the effect of the step on the cavity formation is studied experimentally with the geometrically similar models equipped with air supplying devices and backward-facing steps on the bottom. In the first stage, the role of the key parameters, such as the step heights and the flow rates of air at various advancing speeds of the models are examined. And then, scaling laws governing the cavity area and the flow rate of air is sought. And then, the extrapolation procedure of the total resistance is studied with two-dimensional and three-dimensional estimation methods. In order to complete the study, a small test boat is constructed and the trials are underway.

2 RESISTANCE REDUCTION OF GEOMERICALLY SIMILAR MODEL SHIPS

2.1 Geometrically Similar Models

Three geometrically similar model ships have been manufactured to investigate the effects of air lubrication on the resistance reduction. Shells are made of transparent plastic to observe the shapes of the air cavity beneath the hull easily. As shown in Figure 1, the fore part of the model has a simple shape consisting of developable surfaces and the after part has a prismatic hull form. Two parts are manufactured separately to allow easy adjustment of the step height.

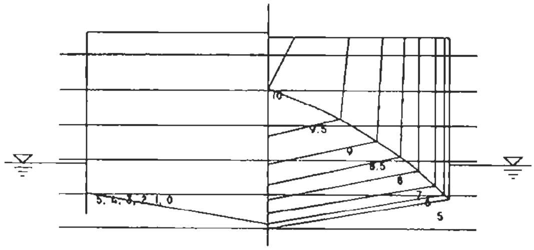

Figure 1: Body plan of geometrically similar model ships

Longitudinal strips are attached along the bilge of the after hull at the both sides to prevent air leakage and to minimize any three-dimensional effects occurring in the flow behind the step [Jang & Kim (1999)]. The three model ships are named as "L", "M" and "S" representing large, medium and small, respectively and the principal particulars are shown in Table 1.

TABLE 1

PRINCIPAL PARTICULARS OF GEOMETRICALLY SIMILAR MODEL SHIPS

Model Name	L	M	S
Scale Ratio, λ	1	1.33	2
LWL (m)	1.8	1.35	0.9
Breadth, B (m)	0.4	0.3	0.2
Dratf, T (m)	0.0756	0.0567	0.0378
Step Height, h (mm)	5	3.75	2.5
Deadrise, α (°)		10	

2.2 Air Cavity and Scale Law

From the previous experience, it is known that area of the air cavity formed behind a step usually increases with increase in flow rates of air but do not above a certain flow rate of air, *i.e.*, the critical flow rate of air. The amount of drag reduction also ceases to increase at the critical flow rate of air and so increase in flow rate of air beyond the limit is useless. The critical flow rates of air for each geometrically similar model ships have been measured over the range of the Froude number, $Fn \cong 0.35 \sim 0.6$. The flow rate of air, Q_{Air}, non-dimensionalized with V_M, the towing velocity of the model ship, B, the breadth of a model ship, and h, the step height as shown in Eqn. 1[Sato *et al.* (1997)] and the results are summarized in Figure 2.

$$C_{QV} = \frac{Q_{Air}}{V_M \cdot B \cdot h} \tag{1}$$

The area of air cavity, A_c at the critical flow rate of air is measured and also shown in Figure 2 in the form of the ratio A_c/S where S is the wetted surface area when air is not supplied. Both the figures(2a and 2b) show that scale effects are not dominant and the two variables C_{QV} and A_C/S have almost identical values for all three models at a given Froude number.

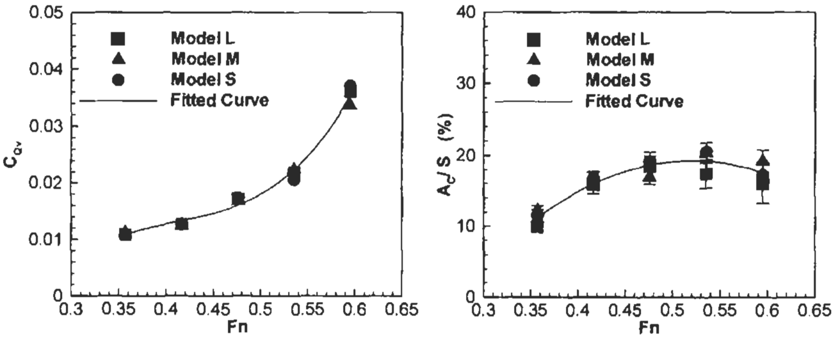

(a) Critical flow rate of air (b) Area of air cavity

Figure 2: Critical flow rate of air and area of air cavity dependent on Froude number

In Figure 3, observed shapes of air cavities formed under the bottoms of three models at the Froude number of 0.595 are shown when air is supplied at their critical rate. The length scales are non-dimensionalized by the step height in the figure and the shapes of the air cavities are almost same except the region near the stem where the air cavities are unstable and hard to measure the shapes exactly. Therefore, it is concluded again that the Froude number scaling rules the phenomena and viscosity and surface tension can be neglected at the critical flow rate of air.

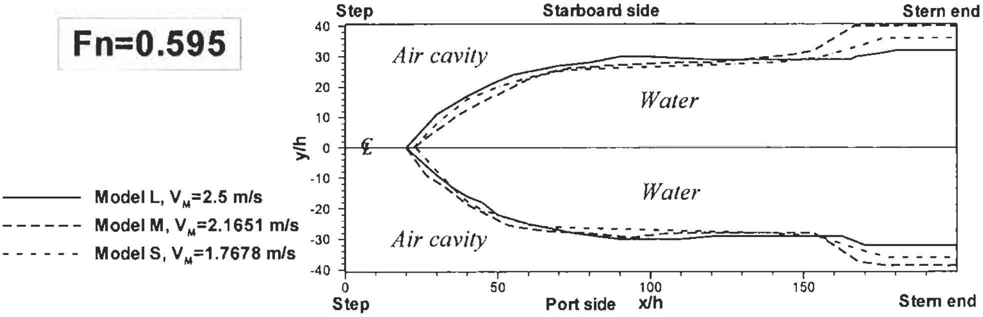

Figure 3: Air cavity shapes formed behind the step under the bottom of each model at $Fn = 0.595$

2.3 Estimation of Resistance for Larger Geometrically Similar Models from Smaller Ones

In two-dimensional approaches, resistance of a real ship can be estimated from the values obtained in model tests with the Froude's similarity law and model-ship correlation line [Lewis (1988)]. If the air cavity covering the hull surface is geometrically similar and hence the reduction in the wetted surface area is, the total resistance coefficient, C_T can be estimated by the two-dimensional method shown in Eqn. 2 in which C_F is the frictional resistance coefficient and C_R is the residuary resistance coefficient. In three-dimensional method, resistance of a real ship may be estimated with Eqn. 3. However, it is difficult to adopt the original Prohaska's method since the form factor k is difficult to define in this case since the effective hull shape due to the air cavity will become quite different if Froude number changes. The difficulty can be partly overcome if Telfer's approach is used since form factors are defined at each Froude number in there[Tanaka (1991)].

$$C_T = \frac{S - A_c}{S} C_F + C_R \tag{2}$$

$$C_T = \frac{S - A_c}{S} (1 + k) C_F + C_R \tag{3}$$

Based on the above discussions, accuracies of the two proposed methods(two-dimensional and Telfer's three-dimensional) are examined by predicting the resistance of different models. For the purpose, the resistance of the largest model "L" is predicted from the results obtained for the medium and small model "M" and "S", respectively by using the Eqn. 2 and 3. The ITTC 1957 curve has been used as the model-ship correlation line. The results are shown in Figure 4 where the resistance of model "L" without supply of air is also presented for comparison. It is seen that approximately 10% of the total resistance of the model "L" is reduced and both the two and three-dimensional method give reasonably good estimations. The results of the three-dimensional analysis indicate that a considerable amount of the resistance reduction comes from the non-frictional components. It is possible that the air cavity is playing a certain role in smoothing the flow behind the step but more careful study to identify the cause and to accommodate the effect of changes in the wetted surface area in the resistance prediction procedure will be necessary.

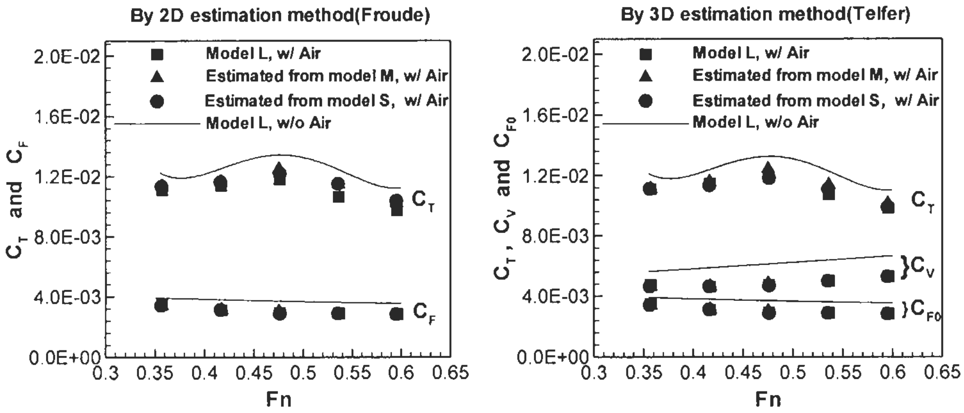

(a) Estimation by 2D method(Froude's method) (b) Estimation by 3D method(Telfer's method)

Figure 4: Resistance coefficients of model "L" estimated from the test results of model "M" & "S"

3 APPLICATIONS TO A TEST BOAT

A small test boat equipped with an outboard engine of 15 hp is built with fiber reinforced plastic to examine the practical applicability of the air lubrication method. The length of the test boat is 3.16 m and the breadth is 1.089 m. As shown in the body plan of Figure 5, a step is placed at the bottom in the vicinity of the midship and air is forced into the holes located at the step. The boat has a wedge shaped barriers at the both sides to prevent the air from leaking. The hull form also allows natural ventilation from the front of the step if possible. Figure 6 shows some pictures of the test running made so far and the trials are still underway.

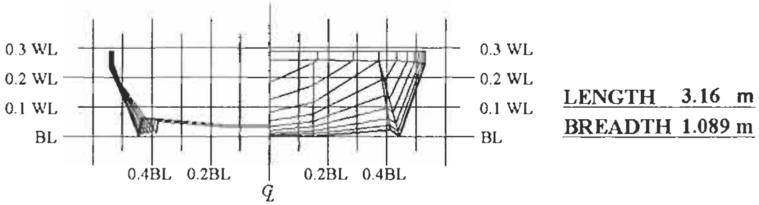

Figure 5: Body plan of the test boat for applications of air lubrication

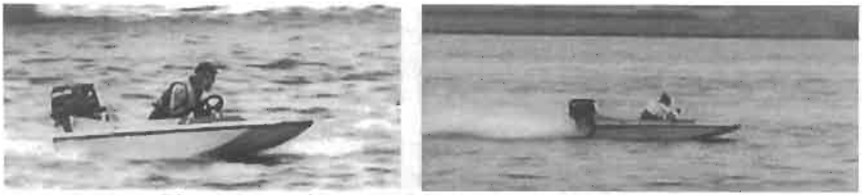

Figure 6: Running tests of the test boat in the Han River

3.1 Estimation of Air Flow Rates for the Test Boat

Tests for model "S" have been performed to estimate the flow rate of air adequate for the test boat. The scale ratio, λ between the model and the test boat has been selected by considering the speed limit of the towing carriage. Since the model "S" is not geometrically similar to the test boat and a small block is attached as shown in Figure 7 to make the bottom of the model "S", on which air cavity forms, similar to the shape of the test boat. The flow rate that provides the maximum cavity area is determined based on the procedure mentioned earlier and the results are summarized in Table 2.

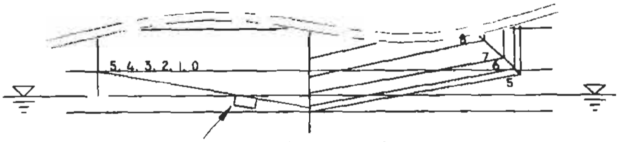

Figure 7: Body plan of the modified model "S" for estimating flow rates of air for the test boat

TABLE 2
ESTIMATION OF CRITICAL FLOW RATES OF AIR FOR THE TEST BOAT

Fn_h	$C_{QV,\ Critical}$	Model ($\lambda = 19.5$)		Test boat	
		V (m/s)	$Q_{Air,\ Critical}$ (l/min)	V (kts)	$Q_{Air,\ Critical}$ (l/min)
9.9814	Less than 0.0119	1.398	Less than 0.1	12	Less than 170
13.3085	Less than 0.0089	1.864	Less than 0.1	16	Less than 170
16.6356	0.0107~0.0143	2.330	0.15~0.2	20	250~340
19.9627	0.0119~0.0149	2.796	0.2~0.25	24	340~420
22.4581	0.0185~0.0212	3.145	0.35~0.4	27	590~670

4 CONCLUSIONS

Three geometrically similar models are made to investigate the scale law governing the air lubrication. Air is supplied behind a step placed on the bottom of the model and relations between flow rates of air and the shapes and areas of air cavity as well as the resistance reduction are observed.

It is found that there exist critical flow rates of air for each Froude number above which no significant changes in shape of cavity or reductions in the resistance occur. The critical rate and cavity area depend on the Froude number and scale effect is not dominant. If air is supplied above the critical rate, the shapes of air cavity generated on the geometrically similar models are also similar. If it is assumed that the wetted surface area decreases as much as air cavity area, conventional methods for resistance extrapolation may also be applied to the ship with air cavity.

A test boat of 3.16m long is constructed to examine the practical applicability of the air lubrication and trials are going underway. The results will help understanding of scale law for air lubrication.

References

Bushnell D.M. and Hefner J.N. (Edited by) (1990). *Viscous Drag Reduction in Boundary Layers,* The American Institute of Aeronautics, Inc., Washington, DC, USA

Jang J. and Kim H. (1999). On the Reduction of a Ship Resistance by Attaching an Air Cavity to Its Flat Bottom, *Journal of the Society of Naval Architects of Korea*, **36:2**, 1-8.

Knapp R.T., Daily J.W. and Hammitt F.G. (1970). *Cavitation*, McGraw-Hill, USA

Lewis E.V. (Edited by) (1988). *Principles of Naval Architecture Vol. II*, SNAME, USA

Sato T., Nakata T., Takeshita M., Tsuchiya Y. and Miyata H. (1997). Experimental Study on Friction Reduction of a Model Ship by Air Lubrication, *Journal of the Society of Naval Architects of Japan*, **182**, 121-128.

Tanaka H., Nakato M., Nakatake K., Ueda T. and Araki S. (1991). Cooperative Resistance Tests with Geosim Models of a High-Speed Semi-Displacement Craft, *Journal of the Society of Naval Architects of Japan*, **169**, 55-64.

Practical Design of Ships and Other Floating Structures
You-Sheng Wu, Wei-Cheng Cui and Guo-Jun Zhou (Eds)
© 2001 Elsevier Science Ltd. All rights reserved

THE HYBRID HYDROFOIL STEPPED HULL

Bryan Duffty and Christopher D. Barry

Fast Hulls, Inc., 3020 Daurine Ct, Gilroy, CA 95020 USA
USCG ELC-024, 2401 Hawkins Pt. Rd. Baltimore MD 21226 USA

ABSTRACT

Planing hybrid hydrofoils or partially hydrofoil supported planing boats are hydrofoils that intentionally operate in what would be the take off condition for normal hydrofoils. They offer a performance and cost that would be appropriate for some ferries, light cargo and recreational vessels.

The stepped hybrid hydrofoil configuration made its appearance in the high speed boat scene in the late nineteen thirties, but never was widely used. It is a solution to the problems of instability and inefficiency that has limited other type of hybrids. The purpose of this paper is to reintroduce this concept to the marine community while proposing what the authors believe address the problems that initially limited this concept.

KEYWORDS

Hydrofoil, Hybrid Hydrofoil, Partially Supported Hydrofoil, Stepped Hull

1 BACKGROUND

A hybrid hydrofoil is a vehicle combining the dynamic lift of hydrofoils with a significant amount of lift from some other source, generally planing lift. The attraction of hybrid hydrofoils is the desire to meld the advantages of two technologies in an attempt to gain a synthesis that is better than either one alone. Partially hydrofoil supported hulls mix hydrofoil support and planing lift. The most obvious version of this concept is a planing hull with a hydrofoil more or less under the center of gravity. Karafiath (1974) studied this concept with a conventional patrol boat model and a hydrofoil. His studies revealed many configurations were unstable in pitch. The subject of this paper is a particular configuration of partially hydrofoil supported planing hull that addresses the pitch instability issue.

The authors initially became involved with the hybrid concept when working on FMC's High Waterspeed Test Bed (HWSTB) for the US Marine Corps, which was a hybrid with an aft hydrofoil and a forward planing surface. The HWTB project is beyond the scope of this paper, but the concept worked. A half scale demonstrator representing a 66,000 lb. armored vehicle made 35 knots true speed. The authors independently developed the stepped hull concept from this system before discovering that it was previously developed and actually in service, but for some reason, never found a niche and has disappeared. This paper is intended to reintroduce the hybrid hydrofoil concept to the marine industry and to provide some inspiration to others. We believe that there were critical issues creating difficulties for the early steeped hull hybrids and that this is why they are not now common, despite their obvious potential. We also believe that we have solved them, and present our suggestions.

2 PITCH INSTABILITY

Pitch instability is the chief issue in a hybrid hydrofoil. Planing hybrid hydrofoils can exhibit a dynamic pitch instability similar to porpoising. This phenomenon can be best understood for a nominal configuration with a single hydrofoil beneath the center of gravity of a planing hull. If such a configuration is slightly disturbed bow up from an equilibrium position, the lift on both the foil and the hull will increase. The hull accelerates upwards and the intersection of the water surface and the keel moves aft. This develops a bow down moment, but at a relatively slow rate. By the time the bow drops enough to reduce the excess lift, the vessel is well above the equilibrium position, and the keel/waterline intersection is well aft. It falls back down toward the equilibrium position bow down, as if it had tripped on its stern. Then, it carries through equilibrium, takes a deep dive and springs up again. This cycle repeats, each time growing more severe. The only way that this motion can damped is if the hull provides enough damping to prevent the increasing overshoot. Note that this is a smooth water instability and occurs with only a nominal initial disturbance.

3 STEPPED HULL

The stepped hull concept is obvious from this discussion. The foil is at the extreme stern of the vehicle and a step is provided forward of the CG. The step confines the planing lift to the forward part of the hull so that the relative position of the center of gravity, the step and the foil control the proportioning of lift between hull and foil. Bow up pitch of the vehicle produces a strong bow down moment, directly proportional to pitch, that reduces the pitch much more rapidly than the movement of the center of planing lift. The step also means that the running attitude of the planing hull can be set at a trim producing optimum lift. (This is the whole point of a stepped planing hull.)

The authors developed a simple program, discussed in more detail in Barry and Duffty (1999), using a standard Blount and Fox (1976) approach to calculating planing forces combined with standard methods form DuCane (1974) and Hoerner (1958) for calculating foil forces. The input and output parameters are per figure 1. The coordinate system is fixed to the vehicle with the origin at the step/keel intersection.

The terms used in the figure are:

BX	Planing beam, the effective beam of the each hull, generally the beam at transom.
β	The deadrise at the station chosen for effective beam.
Stagger	Location of the foil fore and aft, negative if aft of the step or transom.
Gap	Location of the foil below the transom, negative if below.
Dekalage	The angle of the nominal foil midline to the coordinate system.
LCG	The longitudinal center of gravity, positive if forward of the step.
Lc	The length of the wetted chine, including wave rise.
Lk	The length of the wetted keel.
Drag	The angle of the keel with respect to the coordinate system.
τ	Trim of the coordinate system from the dynamic waterline, positive bow up.
Draft	Draft of the origin below the dynamic waterline.

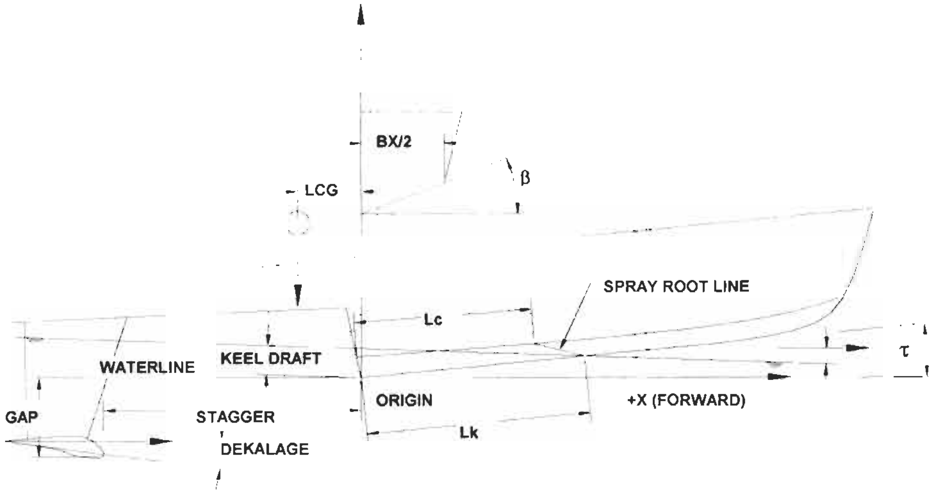
BX/2
LCG
β
SPRAY ROOT LINE
Lc
τ
WATERLINE
KEEL DRAFT
GAP
STAGGER
DEKALAGE
ORIGIN
+X (FORWARD)
Lk

Figure 1 - Nomenclature and Axes

Resistance results from this program are shown in figure 2 for a boat with characteristics as follows:

Length O.A	20 Ft
Weight	2,000 Lb.
LCG, forward of the extreme aft end of the boat	7 Ft.
Planing Beam	6 Ft.
Deadrise	15 Degrees

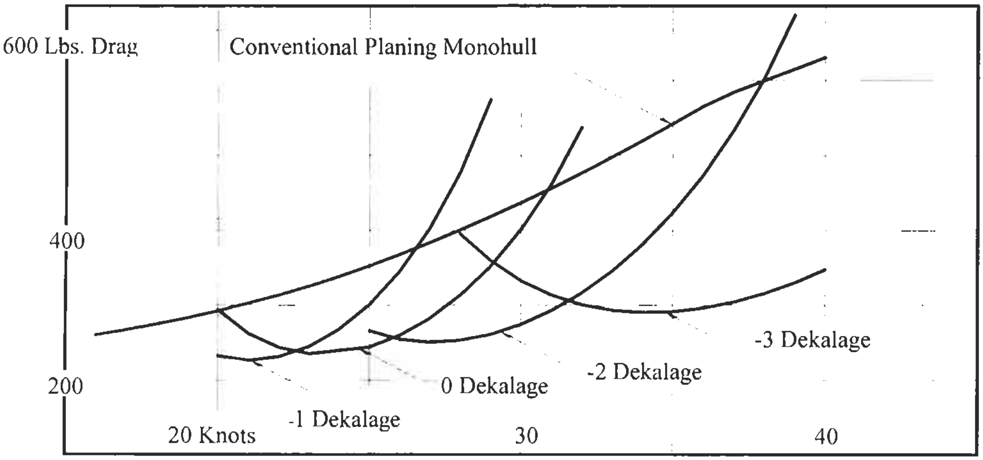

Figure 2 - Resistance results

The hybrid version has its step eight feet forward the extreme aft end of the boat and is equipped with a pair of two foot span by half foot chord foils at the extreme rear end one half foot below the baseline.

The foil section is the NASA GA(W)-1 section (McGhee and Beasley, 1973). The foil dekalage is set for several values. It is important to note that an incorrect dekalage angle results in larger drag than the comparable planing hull. In fact, further investigation of this configuration shows that the maximum proportion of foil lift is not associated with the minimum total drag. This is thus not an optimum configuration in some more fundamental way, though it is superior to the planing (only) hull. This shows the first lesson we have learned: The numerous parameters available in this concept allow many configurations, few of which are optimal and some of which are quite poor. Computer simulation is vital to optimizing a hybrid hydrofoil, even at the most basic level.

4 FOILS

The use of the NASA GA(W)-1 is worth discussing further as we believe the use of this type of foil is another issue critical to the success of the concept. This section is one of a class of supercritical sections that are designed by computer to achieve maximum lift coefficient (above 2.0) with minimum possibility of stall. They achieve this by reducing the peak suction near the tip and "filling in" the suction aft, so that the total area of high suction is increased without severe peak. This is achieved by retaining significant thickness aft, often terminated in a reflex curve, hence the term "barn roof" section. Since hybrids will operate at high angles of attack and low speed during take-off, foil stall is a significant problem and makes takeoff difficult (especially considering propulsion effects). Cavitation is also reduced, at least for the relatively low speeds that hybrids operate.

5 DYNAMIC STABILITY

Though it seems unlikely that a stepped hybrid will develop pitch dynamic instability, there is a definitive criteria. Martin (1978) developed the theoretical methods of determining stability for high speed planing boats, producing two equations, one in pitch moments and one in heave forces, each with various cross products wherein pitch and heave kinematics produces heave forces and vice versa. Extending these equations to the case of a hybrid hydrofoil only requires adding the foil dependent terms. These terms are available from standard ship control methods. For example, pitch moment due to pitch angle is simply the lift curve slope of the foil times the stagger and pitch moment due to pitch rate is lift curve slope times stagger squared. Such a set of equations has to be numerically solved, so no insight can be gained directly by examining an analytic solution. Instead, numerous systematic variations have to be examined. However, the two exemplar terms are the main damping effects, and they will be very large in any practical stepped hybrid, so smooth water stability is almost guaranteed.

6 SEAKEEPING

Many high speed craft are limited by motion in waves rather than power. Methods to analyze motions will be required to determine limiting conditions for crew and passengers, and structural loads. Martin (1978) demonstrated how this proceeds for pure planing craft by extension of the stability method. This can be extended in a similar fashion by adding the foil terms for forces and moments from waves, but is worth noting that the foil excitation due to waves is relatively small because the foil is effected only by the orbital velocity of the waves and very slightly by the elevation of the foil beneath the waves. The velocities are small compared to the vehicle speed and the effect of elevation is minimal if the foil is in submerged below a chord length. The particle velocity effects and wave height effect also are opposed, so the net force is even smaller. It is difficult to make general predictions about the seakeeping of stepped hybrid hydrofoils because this is profoundly affected by optimization, but there are two important points that suggest good seakeeping is possible:

First, let's examine what has become the norm for planing and semi-planing craft designed for good motions in waves. Motions in head seas dominate the problem of seakeeping for fast craft, because at high speeds, all seas are head seas. Offshore racing craft, and "wave-piercing", catamarans both approach the problem of reducing motions in head seas in the same way, by moving the sensitive load as far aft as possible and by reducing the rate of lift force with respect to immersion of the forward sections, usually by making them narrow, with high deadrise. To a certain extent then, seakeeping and planing efficiency must be traded off, paying for one with the other.

Also, if a planing hull strikes a wave, the force induced on the hull by the wave is still primarily at the intersection of the hull and the instantaneous water surface. As the hull travels, this intersection moves aft, and the force becomes larger as the hull gets wider and deeper and the hull both rotates backwards and heaves up, thereby producing large combined accelerations. In contrast, a stepped hybrid hull will initially rotate, but the rotation will increase the angle of attack of the aft foils, which lifts the vehicle bodily upwards from the rear and reduces pitch acceleration. The hull is therefore "anticipating" the oncoming wave and goes over it. This motion has to be carefully tuned to the anticipated wave environment for optimum performance, but it is clear that a properly designed stepped hybrid hydrofoil would have excellent motions. Since this behavior is enhanced by high lift in the foil, good seakeeping is associated with good lift efficiency, rather than degraded by it.

Second, with the wide range of parameters available to the designer, it is clear that there is considerable latitude to optimize for motions. A hull form with very high deadrise, low freeboard planing hulls forward and foil support aft could be developed with very good motions because the foil would bear the majority of the load and the hulls could be relatively inefficient, hence relatively soft riding. In a pure planing hull, the designer has to lose efficiency by accepting a high deadrise, soft riding hull. The cost of non-optimum lift production for the sake of seakeeping would be much less for a hybrid hydrofoil.

7 PROPULSION

A problem of hybrids is that of propulsion: Getting the force into the water often requires passing it through the struts which is costly in terms of money, appendage drag, complexity and efficiency. Hydrofoils use mechanical, electric and hydraulic drives to props on foil pods, jets taking suction through the foil, and shafts from the hull. Each of these methods has problems. There is some consolation that the struts of a hybrid are somewhat shorter, but this is only important for through-strut jet drives, and jet drives require higher flow rates for efficiency at the lower speeds of a hybrid.

However, unlike a pure hydrofoil, a hybrid can be propelled by hull mounted components. A jet drive could be mounted in the forward planing hull and discharge at the step. A prop shaft could penetrate through the step as well or surface piercing props could be mounted on or below the raised tail and dip down to the water. This gives some added versatility to the hybrid concept that a pure hydrofoil doesn't have. The choice of propulsion method is economic and operational and will be determined by the mission. The hybrid offers wider latitude for less costly methods than a pure hydrofoil, but requires an innovative approach to the issue.

8 EXPERIMENTS

The authors have had limited funds and time to explore this concept, but with the help of those acknowledged have been able to experiment with a few small unmanned and manned models. The latter experiments have produced two final significant insights. First, one manned model exhibited severe, uncontrollable broaching instability due to the combination of a narrow planing surface and forces similar to those reported by Blount and Codega (1992) originating in the curved bow sections forward. Based on this, the authors are convinced that the preferred hull form is in fact essentially a "three point catamaran" comprising two slender hulls forward and the foil aft between the extension of the centerline of the hulls. The other point should have been obvious upon retrospection, but became evident when some models either failed to lift or lifted only with great difficulty (their announcement of takeoff was accompanied by a radical change in the engine sound which was the clue): The propeller is very heavily loaded at the low takeoff speed as it is operating at much lower advance ratio than the propulsion system is optimized for. This can prevent the engine from achieving full power when it is most needed.

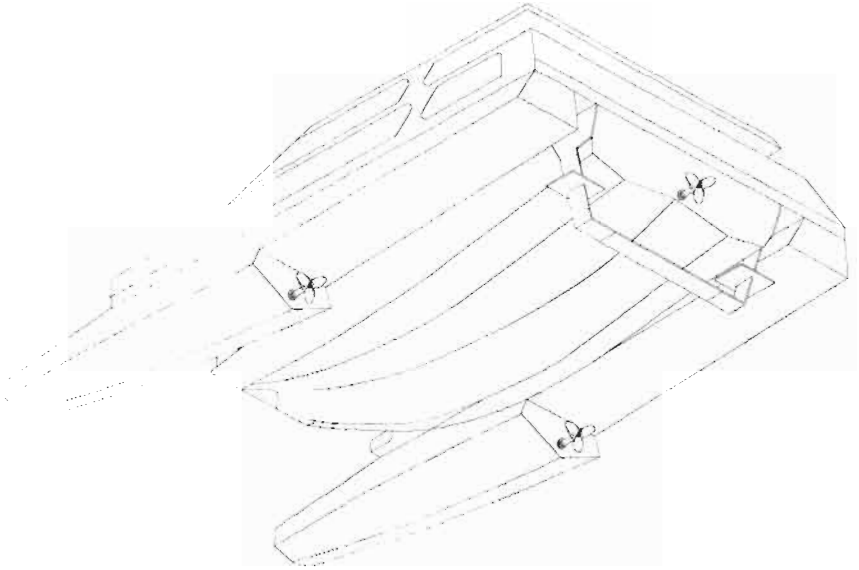

Figure 3 Stepped Hull Hybrid Hydrofoil Catamaran Ferry Concept

Any practical hybrid will have to have a propulsion system that will not overload the engine in the takeoff condition. This can be achieved by two speed gearboxes (which have recently become available), surface piercing drives forcibly ventilated by propulsion machinery exhaust or by use of jet drives, which have other advantages as well.

9 HYBRID HYDROFOIL FERRIES

A high speed ferry is one obvious applications for the hybrid hydrofoil stepped hull concept. A ferry is a single speed vehicle, and the hybrid concept is well suited for this. Most practical new ferry routes in require a speed on the order of thirty to forty knots to compete with automobiles provided the speed can be achieved at an acceptable level of cost and reliability. This appears to be the optimum range for this concept, so a stepped hybrid may be able to achieve a lower cost and better reliability at these speeds than hydrofoils, SES's, or planing boats. The stepped hybrid concept is much less dependent on size for speed and seakeeping than a conventional planing hull, so smaller, less expensive ferries are feasible. This allows either more ferries on a given run or use of ferries for runs with much less traffic. A number of high speed ferries are limited by wake damage to the shore. As a result, they can only run at speed for a small portion of the route. A hybrid should produce substantially less wake than a planing monohull or even an SES because the foils generate substantially smaller waves. Our concept of a passenger ferry for a typical San Francisco Bay Area route as described in Barry and Duffty (1999) is shown in figure 3 above.

10 CONCLUSIONS

The stepped hull hybrid hydrofoil has merits in reduced resistance compared to planing hulls at lower complexity than pure hydrofoils. It also has merits in seakeeping and other operation areas. Its current status may be due to being eclipsed by the pure hydrofoil or by problems in takeoff stall, roll instability or propulsion matching. But it should not be viewed as a partial step to the hydrofoil, and there are solutions to these other problems. It is a valid concept with its own special characteristics and capabilities and merits consideration. Hybrid hydrofoils especially merit consideration for high speed ferry service for partially sheltered runs where seakeeping is a consideration but not an overriding one, there are factors limiting size on a given run, such as traffic dispersion and moderately high speeds are required.

Acknowledgments

The authors would like to acknowledge FMC Corporation, the FMC Human Powered Vehicle project. George Thomas, Bruce Wade, the Cal Sailing Club, Paul Kamen, Kenneth Foster, Michelle Barry and Ramon S. Villareal for their support in many aspects of this project.

References

Barry C. and Duffty B. (1999). The Stepped Hull Hybrid Hydrofoil. *Fast '99.* Society of Naval Architects and Marine Engineers

Blount D. and Codega L. (1992). Dynamic Stability of Planing Boats. *Marine Technology.* Society of Naval Architects and Marine Engineers

DuCane. CDR P. M.(1974). *High Speed Craft*, David and Charles Ltd., Devon

Hoerner S. F. (1958). *Fluid Dynamic Drag.* (Published by the Author)

Karafiath G. (1974). An Investigation Into The Performance of NSRDC Model 5184 Configured as a Partial Hydrofoil Supported Planing Craft and a Comparison with a Powering Prediction *Technique. Report SPD-585-01.* NSRDC

McGhee R. J. and Beasley W. D. (1973). Low-Speed Aerodynamic Characteristics of a 17-Percent-Thick Airfoil Section Designed for General Aviation Applications. *TN D-7428, NASA.*

Martin, M. (1978). Theoretical Determination of Porpoising Instability of High-Speed Planing Boats. *Journal of Ship Researc.* Society of Naval Architects and Marine Engineers

Martin M. (1978). Theoretical Prediction of Motions of High-Speed Planing Boats in Waves. *Journal of Ship Research.* Society of Naval Architects and Marine Engineers

The views and opinions expressed are those of the authors and are not to be construed as official policy or reflecting the views of the U S Coast Guard or the Department of Transportation.

Practical Design of Ships and Other Floating Structures
You-Sheng Wu, Wei-Cheng Cui and Guo-Jun Zhou (Eds)
© 2001 Elsevier Science Ltd. All rights reserved

THE DESIGN OF TRIMARAN SHIPS: GENERAL REVIEW AND PRACTICAL STRUCTURAL ANALYSIS

T. Coppola, M. Mandarino

Dipartimento di Ingegneria Navale, University of Naples "FEDERICO II"
Via Claudio 21 80125 Naples Italy

ABSTRACT

In the last years, the applications of fast commercial transport at sea have aroused an increase of high-speed ships demand. More in particular mono-hull and catamaran passenger ships, in service on brief routs, are able to halve, respect to the conventional ships, the voyage times.

More of recent, the attention has been moved on multi-hull vehicles with function also of container ship in service on transoceanic routs.

In this respect, the trimaran configuration seems to be more encouraging to combine greater demands of space and high speeds.

The main characteristics of a trimaran can be so synthesized:

- The main-hull is more slender than the actual mono-hull (L/B would change among 12 and 18), with a consequent wave resistance reduction.
- Two lateral hulls with very small displacement than that one of the main hull; their fundamental function is that one of maintaining a sufficient stability of the ship and furnishing a bigger decks area.

The main objective of the paper is to validate the greater advantages offered from the trimaran ships, for commercial, tourist and naval fields: better available surface for decks; reduced interference of weapon systems; large flight deck area; possibility of realizing multifunctional naval ship (i.e. frigates with particular characteristics of air, surface and A.S. zone defense).

In this respect firstly, an investigation has been carried out, on the possible fields of applicability of the trimaran ships; then models of global maximum loads have been proposed.

A discussion has been carried out about the preliminary design of trimaran. Particularly the autonomy problem and the hull forms optimization problem have been treated. In addition, a method has been developed for the global load evaluation.

The numerical example show that the torsion stresses are negligible for trimaran; the shear and bending stresses are instead very relevant and decide for the transverse strength of trimaran.

KEYWORDS

Trimaran, Global Loads, Design, Structures, Main-Hull, Multi-hulls, Outriggers, Naval.

1 INTRODUCTION

It is well known that there is a greater demand of data and acceptable techniques for the preliminary design of fast ships. In the same time there is an increase of interest for trimaran ships design, due to the business that they offer for bigger spaces and higher speeds.

Actually intensive researches concern the minimization of the total resistance by the optimization of the main hull and outriggers form, of the longitudinal and transversal outrigger positions, of the ratio between the main hull and the outrigger displacement. The peculiarities of trimaran vessel furnish two main applications: the first one in the military field, like polyvalent frigates, and the second one in the commercial and tourist fields, like ferries or passengers ships in service on brief routs.

As far as the naval field is concerned, the presence of a great deck area consents to amplify, the active defense component, with all the advantages for efficiency and operational flexibility. It also allows, the installation of more efficient weapon systems of modular type and a better disposition of operational and life spaces (figure 1).

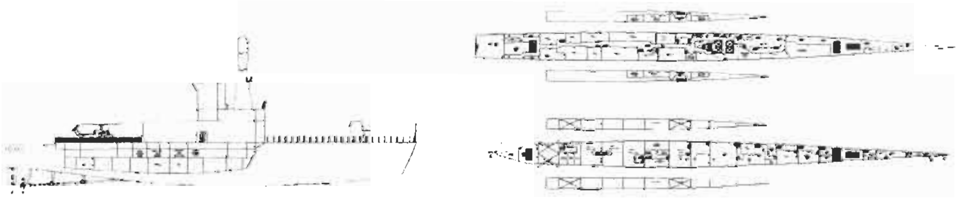

Figure 1: General Layouts of 160 m trimaran frigate

The conformation of the hull assures an elevated stability, a good seakeeping behavior and consequently a greater efficiency of the weapon systems. The lateral hulls also assure a protection of the main hull.

2 PRELIMINARY DESIGN OF TRIMARAN SHIP: AUTONOMY, GENERAL LAYOUT, FORMS AND GEOMETRY OF THE HULLS

According to a different comfort request and, consequently, a different voyage tolerable time on board of a fast ship, by a passenger and a driver, the following upper limits of autonomy can be assumed, for a transfer velocity of about 40 Knots:

- 250 nautical miles for the tourist application;
- 400 nautical miles, for commercial application.

As far as the naval field is concerned, elevated autonomy is required for carrying out long distance missions.

In the commercial and tourist fields, the following ranges can be estimated from the market trend: length between 85 m and 150 m; velocity between 36 to 45 knots and with medium load capacity of about 1000 passengers and 250 cars.

General layout study and preliminary choice of the arrangements for tourist and commercial application can be carried by the following criteria: -Minimum area available for each passenger; -Area of the car decks according to the load capacity; -Shipping from stern on the main deck garage; -Height of deck garage of 5m at least, for bus or T.I.R..

Starting from the following parameters ranges, allowable in literature: (when the m and o suffixes are adopted to denote the main hull and the outriggers respectively):

TABLE 1

MAIN AND SIDE HULL PROPORTION RANGE

	$V/\sqrt{gL}$	$(L/B)_m$	$(B/T)_m$	$(C_B)_m$	$(L/B)_o$	$(B/T)_o$	$(C_B)_o$
Min	0.25	12	1.3	0.35	12	0.4	0.35
Max	0.6	18	2.5	0.65	35	2	0.7

With: V= velocity; L= length of water line; T= Immersion; C_B = Block coefficient; g= gravity acceleration; and assuming the following resistance relation, for 64 hulls:

$$R_T = R_T\left(\Delta_m, C_{Bm}, \left(\frac{B}{T}\right)_m; \Delta_o, C_{Bo}, \left(\frac{B}{T}\right)_o, \frac{L_o}{L_m}\right) \tag{1}$$

A minimization procedure can be carried out, when the L_m and V values are known (and constants), and the interference resistance is neglected. The consequent results of a trimaran of 120 m in length and with velocity of 36 knots are shown in the table two.

TABLE 2

MAIN AND SIDE HULL RESULTS

	Δ(t)	L(m)	B	T	C_B	L/B	B/T
Main-hull	1662.2	120	10.4	2.6	0.50	11.54	4
Outrigger	43.75	41	2.04	1.02	0.45	20.1	2

With effective power of 11534 MW.

3 SOME CONSIDERATIONS ABOUT THE GLOBAL LOADS

The absence of structural experimental data for trimaran obliges to deduce the loads formulas from those ones obtained for the more tested catamarans, when an initial structural model has to be obtained and verified, in a first step of the structural design.

As far as the transverse global loads are concerned, it may be interesting to synthesize the principal concepts on which the register formulas for catamarans are based (A.B.S 1997).

- The sea loads are applied on the middle plane of each hull, with the same values. They are decomposed, as usual, in the buoyancy and hydrodynamic forces.
- The hydrodynamic forces can be considered as derived from the superposing of those ones generated by the heaving and the pitching or the rolling motions.
- The pitch and roll rotation axes are assumed coincident with the longitudinal and the transverse central axes, respectively.
- The pitch (res. roll) inertia forces are considered transversally (res. longitudinally) uniformly distributed, and longitudinally (res. transversally) linearly distributed.
- The transverse and longitudinal inertia moments are assumed according to the previous distributions of the inertia forces.
- The most significant conditions for the determination of the bending moment, the shear force and the torsion moment, are assumed generated by, respectively, the only heaving, the heaving coupled with rolling and the heaving coupled with rolling and pitching. In all these conditions, the heaving inertia loads and the gravitational ones are considered transversally uniformly distributed, the

buoyancy forces S are assumed as concentrated; in the only last case the hydrodynamic forces are regarded as uniformly distributed on the middle part of the impacting hull.

- The heaving hydrodynamic forces are always given by:

$$F_h = \frac{\Delta}{2g} a_{cg} g \tag{2}$$

with : $a_{cg} g$= vertical acceleration in the centre of gravity. The pitch and roll hydrodynamic forces are opposite and their moduli are assumed equal to F_h: $F_p = F_r = F_h$; the pitch and roll moments are then given by $\Delta\, a_{cg} \frac{b}{2}$ and $\Delta\, a_{cg} \frac{L}{4}$ respectively, where b and L are the distance between the centrelines of the two hulls, and the ship length.

The previous hypotheses imply the load distributions represented by Fig. 2,3and 4, and consequently the following expressions of the considered internal force and moments:

$$M(x) = \frac{\Delta}{2b}(1 + a_{cg})(bx - x^2) \tag{3}$$

$$T(x) = -\frac{\Delta x}{b} + \Delta\, a_{cg}\left(\frac{1}{2} - \frac{3x}{b}\right)\left(\frac{1}{2} + \frac{x}{b}\right) \tag{4}$$

$$M_t = \Delta\, a_{cg} \frac{L}{8} \tag{5}$$

where the last relation has to be applied to every section between the impact hull and the centre of the hull.

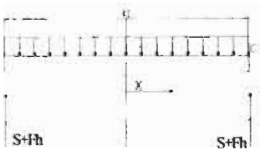

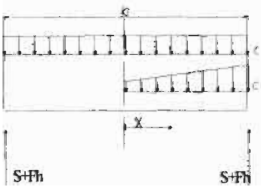

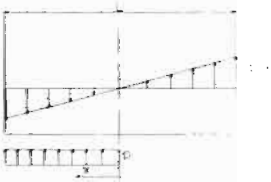

Figure 2: $c = \frac{\Delta(1 + a_{cG})}{b}$; $S = \frac{\Delta}{2}$

Figure 3: $c_i = \frac{\Delta}{bg} a(x)$; $c = \frac{\Delta}{b}$; $a(x) = g\, a_{cg}(1 + \frac{6x}{b})$

Figure 4: $c_p(x) = \frac{3}{2}\frac{\Delta}{L^2} a_{cg} x$ $p = \frac{2\Delta a_{CG}}{L}$

Staring from these catamaran formulations, their extension to the trimaran study requires some hypotheses, according to the substantially different configuration of the trimaran. They regard the barycentric acceleration, the distribution of the hydrodynamic forces between the main hull and the outriggers, the assumption of the critical load conditions, and can be summarized as it follows:

1. The maximum allowable value of the a_{cg} acceleration, is expressed, according to the rules for high speed crafts, by:

$$a_{cg} = S \frac{V}{L^{0.5}} \tag{6}$$

this relation can be applied separately to the main hull and the outriggers, but it falls when applied to the entire trimaran, because it doesn't consider the interaction between the hulls.

Assuming for the absolute values of the a_{cg} variations the same linear law as for a_{cg}, gives:

$$a_{cg}=a_{cgo}-\frac{a_{cgo}-a_{cgm}}{1+\sqrt{\frac{L_o}{L_m}}}=a_{cgm}+\frac{a_{cgo}-a_{cgm}}{1+\sqrt{\frac{L_m}{L_o}}} \tag{7}$$

2. The hydrodynamic forces are proportional to the displacements, as the buoyancy ones, what furnishes:

$$\begin{cases} F_{hm}=\dfrac{\Delta}{1+2\dfrac{\nabla_o}{\nabla_m}}a_{cg}=\gamma\nabla_m a_{cg} \\ \\ F_{ho}=\dfrac{\Delta}{2+\dfrac{\nabla_m}{\nabla_o}}a_{cg}=\gamma\nabla_o a_{cg} \end{cases} \tag{8}$$

with : γ= sea weight density ; $\Delta, \nabla_o, \nabla_m$ = trimaran displacement and displacement volumes of the outriggers and the main hull.

3. As far as the critic conditions individuation is concerned, two cases are considered for the shear force and the bending moment (res. the torsion moment):

I) the heaving and roll (res. heaving, roll and pitch) hydrodynamic forces acting on the raising outrigger, are opposite (as for the catamarans);

II) the roll (res. roll and pitch) hydrodynamic force acting on the impacting outriggers is equal to the sum of the buoyancy and heaving forces on the same outrigger.

As far as the transverse bending moment is concerned, it has to be considered in conjunction with the shear force: the effects of the roll inertia and hydrodynamic forces on the transverse bending moment are null only at the middle section, which isn't necessarily the most stressed section (as for the catamarans).

4. In both previous cases, the hydrodynamic forces are assumed uniformly distributed on the fore part (relatively to the centre of the trimaran) of the main hull and the impacting outrigger, when the torsion moment has to be calculated.
5. For the longitudinal and transversal inertia moments (respectively I and I_t), the following expression are utilized:

$$I=\frac{\Delta b^2}{12g} \tag{9}$$

$$I_t=\frac{\Delta}{12gL_m(\nabla_m+2\nabla_o)}\left[\nabla_m L_m{}^3+8\nabla_o\left(L_{fo}{}^3+L_{oo}{}^3\right)\right] \tag{10}$$

Where L_{fo} and L_{oo} are the length of the fore and aft parts of the outrigger (relatively to the centre of the trimaran). What implies the following expressions for the inertia loads intensity:

I. Transverse shear force and bending moment

$$c_i(x)=\frac{\Delta a_{cg}}{b}\left[1+\frac{12\ \nabla_o x}{b\left(\nabla_m+2\nabla_o\right)}\right]\ I\ case \tag{11}$$

$$c_i(x)=\frac{\Delta}{b}[\ a_{cg}+\frac{12\ \ 1+a_{cg}\ \ \nabla_o}{b\ \ \nabla_m+2\nabla_o}x\ \ ]\ II\ case \tag{12}$$

II. Transverse torsion moment

a) On the outrigger

$$c_{io}(x) = \frac{\Delta \nabla_o}{gL_m\left(\nabla_m + 2\nabla_o\right)} x \ddot{\vartheta} \tag{13}$$

b) On the main hull

$$c_{im}(x) = \frac{\Delta \nabla_m}{gL_m\left(\nabla_m + 2\nabla_o\right)} x \ddot{\vartheta} \tag{14}$$

With:

$$\ddot{\vartheta} = \begin{cases} 3a_{cg} g \left[\dfrac{\left(\nabla_m L_m{}^2 + 4\nabla_o L_m L_{fo}\right)}{\nabla_m L_m{}^3 + 8\nabla_o\left(L_{fo}{}^3 + L_{ao}{}^3\right)} \right] & \text{I case} \\ g \dfrac{3\nabla_m L_m{}^2 a_{cg} + 6\nabla_o L_m L_{fo}\left(1 + 2a_{cg}\right)}{\nabla_m L_m{}^3 + 8\nabla_o\left(L_{fo}{}^3 + L_{ao}{}^3\right)} & \text{II case} \end{cases} \tag{15}$$

Applying these hypotheses gives the following expressions for the internal force and moments:

- ◆ Transverse shear force and bending moment

I case

$$T(x) = \frac{\Delta}{b}\left(\frac{b}{2} - x\right)\left(1 + a_{cg}\right) + 6\Delta a_{cg} \frac{\left(\frac{b^2}{4} - x^2\right)\nabla_o}{b^2\left(\nabla_m + 2\nabla_o\right)} - \begin{cases} \dfrac{\Delta\nabla_o\left(1 + 2a_{cg}\right)}{\left(\nabla_m + 2\nabla_o\right)} & ;x \geq 0 \\ \dfrac{\Delta}{\left(\nabla_m + 2\nabla_o\right)}\left[\nabla_o\left(1 + 2a_{cg}\right) + \nabla_m\left(1 + a_{cg}\right)\right] & ;x < 0 \end{cases} \tag{16}$$

$$M(x) = \frac{\Delta}{2b}\left(1 + a_{cg}\right)\left(\frac{b}{2} - x\right)^2 + \frac{\Delta \nabla_o}{2b^2\left(\nabla_m + 2\nabla_o\right)} a_{cg}\left(b^3 - 3b^2 x + 4x^3\right) + \\ - \begin{cases} \dfrac{\Delta \nabla_o}{\left(\nabla_m + 2\nabla_o\right)}\left(1 + 2a_{cg}\right)\left(\dfrac{b}{2} - x\right) & ;x \geq 0 \\ \dfrac{\Delta \nabla_o}{\left(\nabla_m + 2\nabla_o\right)}\left(1 + 2a_{cg}\right)\left(\dfrac{b}{2} - x\right) - \dfrac{\Delta \nabla_m\left(1 + a_{cg}\right)}{\left(\nabla_m + 2\nabla_o\right)} x & ;x < 0 \end{cases} \tag{17}$$

II case

$$T(x) = \frac{\Delta}{b}\left(1 + a_{cg}\right)\left(\frac{b}{2} - x\right)\left[1 + \frac{6\nabla_o}{b\left(\nabla_m + 2\nabla_o\right)}\left(\frac{b}{2} + x\right)\right] - \begin{cases} 2\dfrac{\Delta\nabla_o\left(1 + a_{cg}\right)}{\left(\nabla_m + 2\nabla_o\right)}; & x \geq 0 \\ \Delta\left(1 + a_{cg}\right); & x < 0 \end{cases} \tag{18}$$

$$M(x) = \frac{\Delta}{2b}\left(1 + a_{cg}\right)\left(\frac{b}{2} - x\right)^2 + \frac{\Delta \nabla_o\left(1 + a_{cg}\right)}{2b^2\left(\nabla_m + 2\nabla_o\right)}\left(b^3 - 3b^2 x + 4x^3\right) + \\ - \begin{cases} 2\Delta\left(1 + a_{cg}\right)\dfrac{\nabla_o}{\left(\nabla_m + 2\nabla_o\right)}\left(\dfrac{b}{2} - x\right) & ;x \geq 0 \\ 2\Delta\left(1 + a_{cg}\right)\dfrac{\nabla_o}{\left(\nabla_m + 2\nabla_o\right)}\left(\dfrac{b}{2} - x\right) - \dfrac{\Delta \nabla_m}{\left(\nabla_m + 2\nabla_o\right)}\left(1 + a_{cg}\right)x & ;x < 0 \end{cases} \tag{19}$$

- Transverse torsion moment

The M_t values for a section between the impacting outrigger and the main hull, are given by :

I case

$$M_t = \frac{\Delta\nabla_o a_{cg}}{(\nabla_m + 2\nabla_o)}\left\{L_{fo} - \frac{(L^3{}_{fo} + L^3_{ao})(\nabla_m L^2{}_m + 4\nabla_o L_m Lfo)}{L_m\left[\nabla_m L^3_m + 8\nabla_o(L^3_{fo} + L^3_{ao})\right]}\right\} \tag{20}$$

II case

$$M_t = \frac{\Delta\nabla_o}{(\nabla_m + 2\nabla_o)}\left\{\frac{(1 + 2a_{cg})L_{fo}}{2} - \frac{(L^3_{fo} + L^3_{ao})}{3L_m}\left[\frac{3\nabla_m L^2_m a_{cg} + 6\nabla_o L_m L_{fo}(1 + 2a_{cg})}{\nabla_m L^3_m + 8\nabla_o(L^3_{fo} + L^3_{ao})}\right]\right\} \tag{21}$$

4 NUMERICAL EXAMPLE

In order to demonstrate the practical applicability of the 2-21 relations, a numerical example has been developed and applied to the trimaran frigate of the figure 1.
The results obtained are the following:

TABLE 3

FIRST CASE: TRANSVERSE SHEAR FORCE, BENDING MOMENT AND TORSION MOMENT

$x \geqslant 0$	4	5	6	7	8	9	10
T(x) (T)	2270.70	1983.03	1691.45	1396.0	1096.68	783.49	486.45
M(x)(T m)	7773.80	5646.60	3809.04	2264.99	1018.33	72.91	-567.38

$x \prec 0$	-4	-5	-6	-7	-8	-9	-10
T(x) (T)	-2079.90	-1827.0	-1577.98	-1332.81	-1091.52	-854.1	-620.54
M(x)(T m)	8702.18	6749.05	5046.87	3591.80	2379.95	1407.46	670.46

Mt(') = 2659.16 T m

TABLE 4

SECOND CASE: TRANSVERSE SHEAR FORCE, BENDING MOMENT AND TORSION MOMENT

$x \geqslant 0$	4	5	6	7	8	9	10
T(x) (T)	2374.57	2068.0	1753.0	1430.0	1099.0	760.53	413.5
M(x)(T m)	7268.70	5046.79	3135.57	1543.12	277.51	-653.17	-1240.85
$x \prec 0$	-4	-5	-6	-7	-8	-9	-10
T(x) (T)	-1976.0	-1742.12	-1516.25	-1298.44	-1088.7	-887.1	-693.54
M(x)(T m)	7268.70	5046.79	3135.57	1543.12	277.51	-653.17	-1240.85

Mt(') = 4967.01 T m

As far as the a_{cg} value is concerned, the following procedure has been carried out:

$$a_{cgm} = S_1 \frac{V}{\sqrt{L_m}} = 0.771\ g; a_{cgo} = S_1 \frac{V}{\sqrt{L_o}} = 1.137\ g \Rightarrow a_{cg} = 0.919\ g \tag{22}$$

with: $S_1 = 0.65[0.2 + (0.6/ {}^{V}\!/_{\sqrt{L_m}})] = 0.291$; $S_2 = 0.65[0.2 + (0.6/ {}^{V}\!/_{\sqrt{L_o}})] = 0.24$

what implies, according to the rules formulations: $S_1 = S_2 = 0.32$.

Starting from the previous values of T(x), M(x), Mt(') and a_{CG}, give the following ones for the maximal stresses:

Torsion stress: $\sigma_{id} = 0.4N/mm^2$; **Bending Stress:** $\sigma = 80.64N/mm^2$

$$\textbf{Shear Stress: } \tau = \begin{array}{l} 103.96N/mm^2 \text{ on the cross deck bottom;} \\ 141.19\ N/mm^2 \text{ on the neatral axis.} \end{array}$$

The Von-Mises stress for the bending- shear stress is given by:

$$\sigma_{id} = \begin{array}{l} 197.29N/mm^2 \text{ on the cross deck bottom} \\ 244.56N/mm^2 \text{ on the neutral axis.} \end{array}$$

The existence of the last stress implies the utilization of high stress steel.

Acknowledgements

The paper has been financially supported by MURST 60% and 40% founds.
A particular acknowledgement has to be given to the Naval officers P. Dafieno and A. Bignone for the utilization of data and plans of their graduation thesis.

References

1) A.B.S. (1997). Guide for building and classing high speed craft. *Rules.*
2) Alimento M. (1994). High speed craft: The impact of the new IMO code on the design, construction and management. *Nav '94.*
3) Cervetto D. et al. (1997). Application of the new Rina Rules to the Structural Design of High Speed Craft. *HSMV'97.*
4) Dafieno P., Bignone A. (2000). Progetto di massima di una fregata non convenzionale di tipo trimarano - Tutors: M. Mandarino and T.Coppola. *Graduation Thesis.*
5) Dr. Pattinson et al. (1994). Trimaran Ships. *R.I.N.A. Trans*, 143-161.
6) Dinsenbacher A.L. (1970). A Method for Estimating Loads on Catamaran Cross-Structure. *Marine Technology*, 477-489.

Practical Design of Ships and Other Floating Structures
You-Sheng Wu, Wei-Cheng Cui and Guo-Jun Zhou (Eds)
© 2001 Elsevier Science Ltd. All rights reserved

CALM WATER EXPERIMENTAL RESEARCH ON GEOSIMS OF HIGH SPEED TRIMARAN: HYDRODYNAMIC CHARACTERISTICS AND MODEL-SHIP CORRELATION

Ermina Begovic, Carlo Bertorello and Pasquale Cassella

Department of Naval Architecture and Marine Engineering University of Naples Federico II
via Claudio, 21-80125 Napoli, Italy

ABSTRACT

In this paper a trimaran ship equivalent to a typical high speed craft in service in the bay of Naples has been considered. Two vessels having different only outrigger hull forms have been designed on the basis of required lay-out, of the limits in the main dimensions and of the available data from existing design.

Calm water resistance model tests have been carried out for two main purposes:

Firstly, the investigation has been carried out on a large model in order to verify the influence of the main hull trim and of the outrigger hull form and position on the trimaran hydrodynamic resistance.

Secondly, the investigation has been carried out on two geosim models of a trimaran hull configuration with the goal to compare the ITTC'57 with the ITTC'78 model-ship correlations.

For this last purpose a form factor of the trimaran has been determined by different methods. The results show that the ITTC'57 could be preferable to ITTC'78 model-ship correlation, in the higher Froude number range.

KEYWORDS

Trimaran, Passenger ferry, HSC, Resistance test, Model-ship correlation

1 INTRODUCTION

The last years have seen a remarkable increase in the number of high speed craft operating all over the world. The current trend in high speed vessels, especially for coastal car-passenger ferries has led to the search for-hull forms with superior characteristics.

Several comparisons among multihull and the monohull ships, on the basis of equivalent service capabilities, have highlighted the advantages of each hullform; the catamaran is known to be very well adequate to the above mentioned service.

Furthermore, in recent years, interest about the trimaran ships has been growing because of the advantages due to their large deck area and to the increased stability under damaged conditions. In addition, by making the main hull very slender and optimising the wave drag by means of side-hull form and position, the total resistance could be the same or even smaller in comparison with the equivalent catamaran or monohull.

In this work the results of towing tank trimaran resistance tests performed at University of Naples are presented. The first part of the research programme has dealt with the modification of transverse and longitudinal position of outriggers in order to minimise the total hydrodynamic resistance through favourable wave interference among the hulls and favourable effect of the lift. The influence of the side hull form on the total resistance has been considered testing two different outrigger forms. Special attention has been focused on model ship correlation; resistance data of two trimaran geosim models have been analysed through the ITTC-57 and ITTC-78 correlation procedure.

TABLE 1

PRINCIPAL CHARACTERISTICS OF THE TRIMARAN IN FULL SCALE

	MAIN HULL (series 64 hullform)	SIDE HULL (series 64 derived hullform)	SIDE HULL (Wigley)	TRIMARAN (series 64 hullform)
Length over all (m)	47.700	23.850	23.47	47.700
Length waterline (m)	46.940	23.470	23.47	46.940
Draught (m)	1.668	0.463	0.463	1.668
Wetted surface (m^2)	194.8	25.2	29.4	245.2
Displacement (t)	120.489	4.259	5.300	129.007
Max speed (kn)				40
CB	0.45	0.35	0.43	
L/B	14.070	21.500	21.500	
B/T	2.000	2.356	2.356	
Fn	0.958	1.356	1.356	
Beam waterline (m)	3.336	1.092	1.092	

2 THE TRIMARAN MODEL CONFIGURATION

The resistance model tests were carried out on trimaran ship design whose main characteristics are reported in Table 1. A round bilge transom stern displacement hull with high length to beam ratio was selected from series 64 as the main hull. Two different side hull forms were selected: one was the well known Wigley mathematical form and the second one was derived by geometrical affinity from the series 64. Each outrigger hullform had length equal to one half of the main hull length and displacement equal to 4 % of the main hull. The trimaran hulls body plan is shown in Fig. 1.

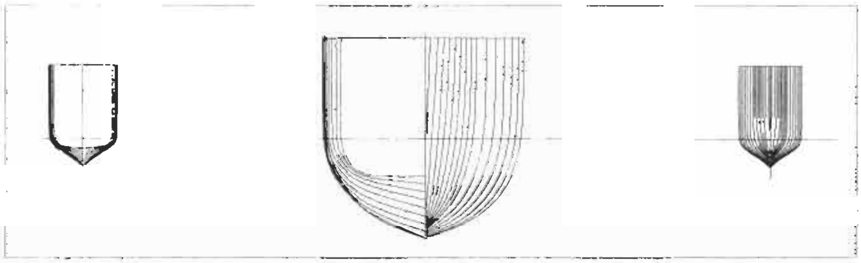

Figure 1: Trimaran hulls body plan

3 RESULTS AND DISCUSSION

3.1 Static Trim Optimisation

The first objective of the work was to test the influence of the main hull trim and of the side-hull position on the hydrodynamic resistance. Five trim positions of the main hull were tested (level trim 0°, aft trims + 0,5° and + 1°, forward trims – 0,5° and –1°). The minimum resistance for high values of the Froude number occurred at aft trim of + 1° so all trimaran configurations have been subsequently tested with this static trim.

3.2 Side Hull Positions

The tests on the optimisation of the trimaran side hull location were carried out with the outrigger hulls derived from series 64 considering three lateral positions (clearances) y/L = 0.10; 0.11; 0.12 for a given longitudinal position x/L = -0.0625 and four longitudinal positions (staggers) x/L = +0.25; 0; -0.0625; - 0.125 for a given clearance y/L = 0.10 (fig. 2).

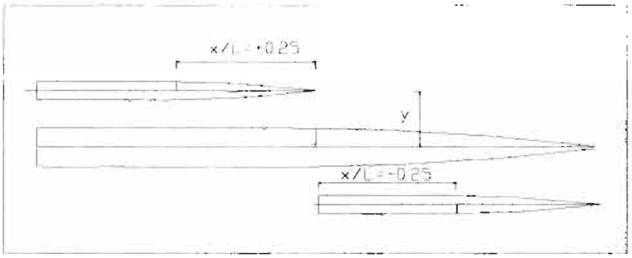

Figure 2: Trimaran configuration; staggers and clearances.

3.3 Resistance Test Results

The measured total resistance of the model was expressed in non-dimensional form as

$$C_T = R_T / 0.5\ \rho\ SV^2 \qquad (1)$$

Calculated C_T values for the tests carried out on trimaran model λ=10 for different configurations are shown in Fig. 3 and Fig.4.

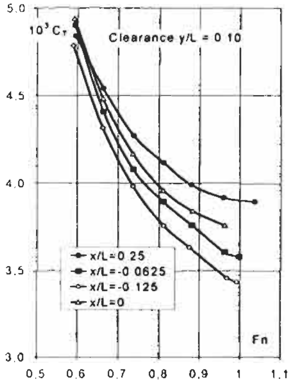

Figure 3: Resistance results for different staggers

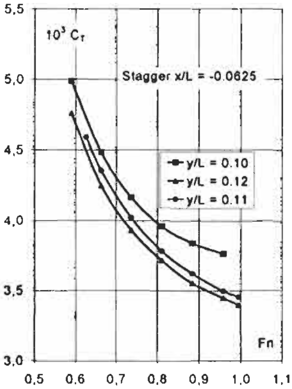

Figure 4: Resistance results for different clearances

The effect of the running trim on the resistance was also investigated and the trim was measured for all the tests. Figures 5 and 6 show the difference Δτ between the running trim and the trim at rest. There is an evident correlation between the running trim and the trimaran resistance; this last decreases as Δτ (positive when bow up) increases.

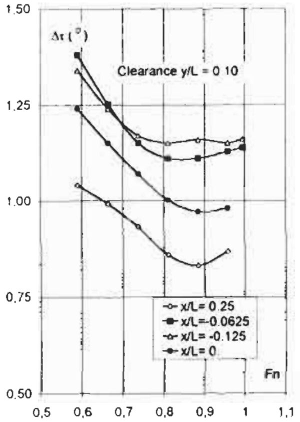

Figure 5: Running trims for different clearances

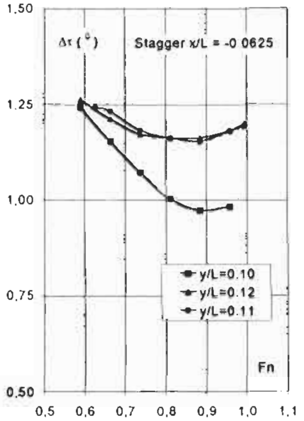

Figure 6: Running trims for different staggers

For the tested clearance 0.10 (Fig. 3) we have the minimum resistance for the stagger -0.125 in the Froude number range 0.70-1.00 probably due to a larger lift effect than in the other trimaran configurations. However, the lay out of the stagger -0.125 can be considered of hard realisation for a trimaran in the full scale. Therefore the following resistance model tests were carried out considering only two more realistic staggers 0 and -0.0625. Due to interference phenomenon the hydrodynamic resistance decreases when increasing clearance (Fig. 4).

In the trimaran with Wigley outriggers only one configuration has been considered (Clearance 0.10, stagger 0) and it has been tested in the Froude number range 0.60-0.80; its resistance is about 2.5 % lower in comparison with trimaran with the 64 derived outriggers (Fig. 7).

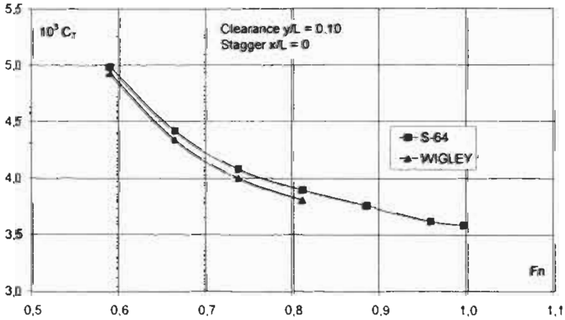

Figure 7: Comparison between the Wigley and Series 64 outriggers

Due to a large spray observed at Fn > 0,80, no other model tests were carried out on Wigley side hull trimaran. This phenomenon, the operating Froude number range of the trimaran ship (0.80-1.00), and design considerations suggested that the Wigley side hull is not realistic, so no further experiment on this hullform was carried out.

4 MODEL-SHIP CORRELATION

The main purpose of the investigation carried out testing two trimaran geosim models has been to have useful information on the model-ship correlation for this vessels at high speed.

In order to verify the validity of the ITTC'57 correlation methodology, the analysis of the geosim models results was performed using the residuary resistance coefficients C_R calculated by the expressions:

$$C_{R(T)}\,(Fn) = C_{T(T)}\,(Fn, Rn) - C_{F(T)}\,(Rn) \qquad (2)$$

$$C_{F(T)} = C_{F(M)} \cdot S_{(M)} / S_{(T)} + 2 \cdot C_{F(O)}\, S_{(O)} / S_{(T)} \qquad (3)$$

where the suffix code T, M, O are referred to trimaran configuration, main hull and outrigger respectively.

Because the side hulls are only 50% of the length of the main hull, the frictional resistance coefficient $C_{F(T)}$ of the trimaran has been determined by considering the $C_{F(M)}$ for the main hull and the $C_{F(O)}$ of the outriggers at the same speed multiplied by the ratio of their wetted surface areas.

The C_F values have been obtained from the ITTC 1957 correlation line.

In fig. 8 the results of the so obtained residual resistance coefficients for the model with scale ratio $\lambda = 10$ are compared with the results relative to the model $\lambda = 20$ tested in two different towing tanks. As can be seen in the figure there are significant differences of C_R between the two models for Fn<0.65, but very small differences in the range of Fn 0.70 – 1.00.

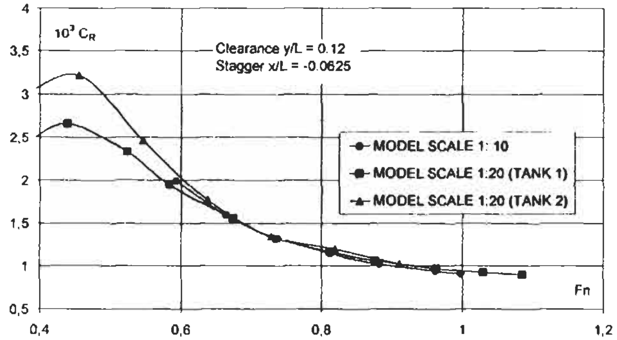

Figure 8: Comparison between geosims results – ITTC-57 correlation

The analysis of the geosim model results was also performed with ITTC '78 correlation methodology. For this purpose a form factor k was determined only for the model with scale ratio $\lambda=10$ by transom emerged model tests carried out at low speeds, with a wire fitted, as turbulence stimulator.

The analysis of the trimaran resistance model data was conducted using the expression

$$C_W(Fn) = C_T\,(Fn, Rn) - (1+k)\ C_F\,(Rn) \qquad (4)$$

where:

C_W wave resistance coefficient

C_F frictional resistance coefficient according to ITTC'57 correlation line

$1+k = 1.19$.

The value of the form coefficient has been obtained both by Prohaska method and by Hughes method (Fig. 9) enveloping the total resistance coefficient C_T versus Reynolds number. As shown in fig. 10, the differences between the wave resistance coefficients of the two geosims are significant in the

whole tested Fn range, and the wave resistance coefficients C_W relative to the model scale $\lambda = 10$ are about 10% larger than the coefficients C_W relative to model scale $\lambda = 20$.
Anyway as the wave resistance coefficient of the two models in scale $\lambda = 10$ and $\lambda = 20$, should be the same at equal Fn, the form coefficient 1+ k (Fn), function of Froude number, has been also determined by the relation

$$1+k(Fn) = (C_{T(20)}-C_{T(10)}) / (C_{F(20)}-C_{F(10)}) \quad (5)$$

So obtained values of 1+k (Fn) are very close to the value one in the Fn range 0.70 – 1.00; this could be considered as confirmation of the equality of the wave resistance with the residuary resistance coefficient for the tested trimaran configuration.

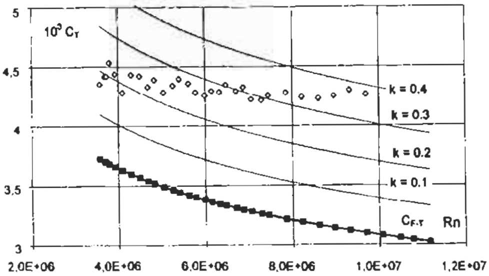

Figure 9: Trimaran form factor by Hughes method

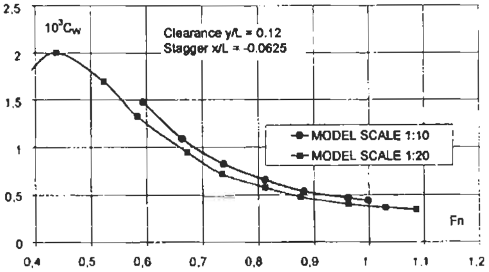

Figure 10: Comparison between geosims results – ITTC'78 correlation

5 CONCLUSIONS

Systematic resistance model tests have been carried out for a trimaran ship equivalent to operating high speed craft.
Different locations of side hulls were tested; the optimal position was identified as well as the correspondent running trim.
At the designed high Froude numbers of the considered trimaran, the Wigley side hull form seems not realistic. However, because of a lower total resistance this side hull form could be adopted at lower Froude numbers.
The investigation on the model ship correlation by the geosim model tests highlights that the ITTC'57 is preferable to ITTC '78 methodology in the range of Fn = 0.70 – 1.00; the opposite is true for Fn < 0.60.
The results of this research are valid only for the examined hull forms. Further research will show if the obtained results are applicable to other trimaran hull forms.

Acknowledgments

This work was supported by the Italian Ministry of University and Scientific Research in the frame of the 1999-2001 research plan.

References

Ackers B.B., Micheal T.J., Tredennick O.W., Landen H.C., Miller E.R., Sodowsky J.P., Hadler J.B. (1997). An investigation of the Resistance Characteristics. of Powered Trimaran Side-Hull. *SNAME Trans.* **105**, 349-380

Andrews, D., Zhang, J.W. (1995). Consideration in the design of a Trimaran Frigate. *Proc. of Int. Symposium on High Speed Vessels for Transport and Defence*, London, UK

Batiste D.; Danielli A.; Zotti I. (2000). Numerical and Experimental Investigations on Wave Resistance of Trimaran Configuration. *Proc. of IMAM 2000*. **1**, 56-63, Ischia, Italy

Begovic E., Migali A., Pensa C. (2000). Experimental Study on the Resistance of a Trimaran Hull Configuration. *Proc. of NAV 2000*. **1**, 2.6.1-2.6-10, Venice, Italy

Bertorello C. (2000). Trimaran Hull Performances for Fast Passenger Ferries. *Proc. of NAV 2000*. **1**, 2.4.1 –2.4.10, Venice, Italy

Brizzolara S., Bruzzone D., Cassella P., Scamardella A., Zotti, I. (1998). Wave Resistance and Wave Patterns for High Speed Crafts; Validation of Numerical results by Model-Test. *Proc. XXII Symposium on Naval Hydrodynamics*. 55-69, Washington, USA

Bruzzone D., Cassella P., Zotti, I. (2000). Resistance Components on a Wigley Trimaran: Experimental and Numerical Investigation. Proc. *ICHD 2000*. 115-120, Yokohama, Japan

Bruzzone D., Cassella P., Miranda S., Pensa C., Zotti I. (1996). Wave Patterns and Wave Resistance: Validation of a Numerical Method using Geosim Experimental Results. *Proc. of the 2nd Int. Conf. On Hydrodynamics*. **1**, 127-132, Hong Kong,

Cassella P., Coppola C., Lalli F., Pensa C., Scamardella A., Zotti I. (1998). Geosim Experimental Results of High Speed Catamaran: Cooperative Investigation on Resistance Model Tests Methodology and on Model-Ship Correlation. *Proc. PRADS 1998*. 447-452, The Hague, Netherlands

Doctors L.J. (1999). On The Great Trimaran-Catamaran Debate. *FAST 99*. 283-296, Seattle, USA

Grubisic I., Zanic V., Begovic E. (1997). Concept Design Model of An Outrigger Trimaran Ferry. *IMAM '97*. 5.1-17-5.1-26, Istanbul, Turkey

Larsson L., Janson C.E., Brun P. (1997). A Numerical Investigation of Trimaran Configuration. *FAST 97*. 537-544, Sydney, Australia

Mizine I., Thorpe R. (2000). High Speed Slender Monohull - Trimaran: Optimized Chain of Efficiency. *IMAM 2000*. **2**, 26-36, Ischia, Italy

Pattison D. R., Zhang J.W. (1994). Trimaran Ships. *RINA Spring M.*. 143-161, London, UK

Suzuki K., Nakata Y., Ikehata M., Kai H. (1997). Numerical Prediction on Wave Making Resistance of High Speed Trimaran. *FAST 97*. 611-620, Sydney, Australia

Suzuki K., Ikehata M. (1993). Fundamental Study on Optimum Position of Outrigger of Trimaran from view Point of Wave Making Resistance. *FAST 93*. 1219-1230, Yokohama, Japan

Tuck E.O., Lazauskas L. (1998). Optimum Hull Spacing of a Family of Multihulls. *Ship Technology Research*. **45**, 180-195

YEH, H.Y.H. (1965). Resistance Experiments on High Speed Displacement Forms. *Marine Technology*. 112-157

Practical Design of Ships and Other Floating Structures
You-Sheng Wu, Wei-Cheng Cui and Guo-Jun Zhou (Eds)
© 2001 Elsevier Science Ltd. All rights reserved

TRIMARAN MODEL TEST RESULTS AND COMPARISON WITH DIFFERENT HIGH SPEED CRAFT

C. Bertorello[1], D. Bruzzone [2], P. Cassella[1] and I. Zotti[3]

[1]Università di Napoli Federico II, Dipartimento di Ingegneria Navale
via Claudio, 21 - 80125 Napoli Italy
[2]Università di Genova, Dipartimento di Ingegneria Navale e Tecnologie Marine
via Montallegro, 1 - 16145 Genova Italy
[3]Università di Trieste, Dipartimento di Ingegneria Navale, del Mare e per l'Ambiente
via A. Valerio,10 - 34127 Trieste Italy

ABSTRACT

This paper summarises the results of a research program on high speed trimarans, jointly performed at Genoa, Naples and Trieste Universities. Two geosim models of a trimaran hull (scale ratio $\lambda = 10$ and $\lambda = 20$) equivalent to high speed vessels operating in the bay of Naples have been built. Resistance tests were carried out in order to assess the best trim and configuration as regard the hydrodynamic resistance. Wave pattern experimental research was also carried out for the main hull, for the outrigger and for the best obtained trimaran configuration. Besides, seakeeping tests have been executed in head regular waves on the main hull and on the trimaran configuration. Some of the obtained experimental results have been analysed and compared with corresponding data relating to catamaran and monohull with equivalent service capabilities.

KEYWORDS

Trimaran model tests, Resistance, Seakeeping, HSC comparison.

1 INTRODUCTION

Various hull forms have been proposed in recent years to satisfy the world trend for high speed maritime transportation, especially in the field of passenger/vehicle ferries. The demand for fast sea transportation has led to a significant growth of interest in multi-hulled ships. An interesting possibility seems to be the trimaran, for a more convenient accommodation layout and for the increased stability also under damaged conditions. Besides, a trimaran configuration with the optimum position of the side hulls can produce a beneficial wave interference at a given speed and could also offer powering benefits when compared to conventional monohull and catamarans.

In order to minimise the total hydrodynamic resistance, a theoretical and experimental research on the optimal position of the outriggers should be carried out with designed realistic hull forms and dimensions of the main hull and of the outriggers.

The wave making interaction between the main hull and the outriggers has been investigated by model tests. In addition, the wave pattern resistance of the isolated main hull, of the isolated side hull and of the whole trimaran configuration have been measured using capacitive probes and applying the longitudinal cut method, as proposed by Sharma (Eggers et al. 1967).

The seakeeping characteristics are also very important for the comparison among different ships, therefore seakeeping tests were conducted both on the main hull and on the trimaran configuration.

The aim of this paper is to provide some hydrodynamic characteristics and to compare the considered trimaran with equivalent monohull and catamaran ships.

2 RESISTANCE EXPERIMENTAL RESULTS

The resistance model tests were carried out on two geosims of a trimaran configuration which was developed on the basis of the requested layout, of the limits due to service considerations and of data available from existing designs. The principal dimensions for the larger model of the main hull and of the outrigger are reported in table 1.

TABLE 1

PRINCIPAL CHARACTERISTICS OF THE TRIMARAN MODEL (SCALE $\lambda=10$)

	MAIN HULL (series 64 hullform)	SIDE HULL (series 64 derived hullform)	TRIMARAN (series 64 hullform)
Length waterline (m)	4.694	2.347	4.694
Draught (m)	0.166	0.0463	0.166
Wetted surface (m^2)	1.948	0.252	2.245
Displacement (kg)	120.489	4.259	129.007
Beam waterline (m)	0.332	0.109	

At first, for the investigation of the total hydrodynamic resistance, tests were carried out only on the larger models for the following cases:

- several different static trim positions of the isolated main hull and of the outrigger to find the best trim for the trimaran;
- several trimaran configurations (three different clearances and four staggers for a given clearance) with the purpose to verify the influence of the side hull location on the hydrodynamic resistance.

All the experimental results of these model tests have been given in previous papers.(Bertorello et al. 2001). Then, the wave pattern tests were carried out on the geosims of the isolated main hull of the isolated outrigger and of the trimaran configuration relating to the best clearance (y/L = 0.12) and the best realistic stagger (x/L=-0.0625) as shown in fig. 1 and determined by previous tests.

Measurements of wave pattern resistance were performed at the towing tanks of Naples and Trieste Universities, by using four capacitive probes in different transverse positions. The wave pattern resistance was calculated using the longitudinal cut method.. The waves were measured at transverse distances y corresponding to ratios y/L ranging from 0.25 to 0.55; these values assure adequate wave pattern records far from the model boundary layer and sufficiently long to avoid an immediate wave reflection. The wave components were calculated up to wave propagation angles of about 85° to include the most of the energy content.

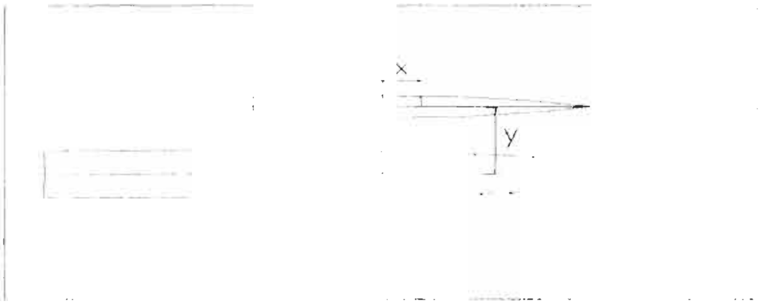

Figure1: Trimaran hull: staggers (x) and clearances (y)

Fig. 2,3,4 show the total resistance coefficient C_T obtained from tests carried out on larger models of the isolated main hull, isolated side hull and trimaran configuration respectively, in the velocity range of 4.00-6.75 m/s. In the same figures the comparison between the residuary resistance coefficient C_R, obtained using ITTC 57 friction line, and the wave pattern experimental resistance coefficient C_{WP}, determined from the wave pattern analysis, can be observed.

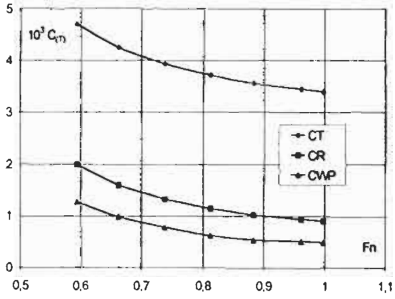

Figure 2: Trimaran hull: C_T , C_R , C_{WP} versus Fn

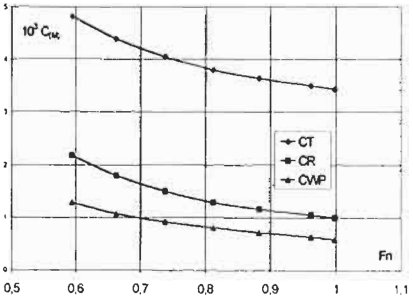

Figure 3: Main hull: C_T ,C_R ,C_{WP} versus Fn

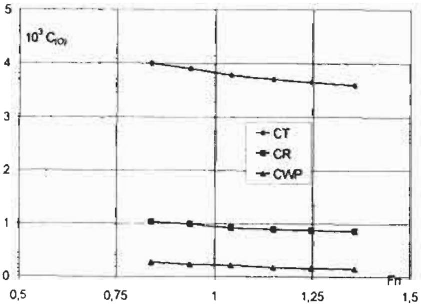

Figure 4: Outrigger; C_T , C_R , C_{WP} versus Fn

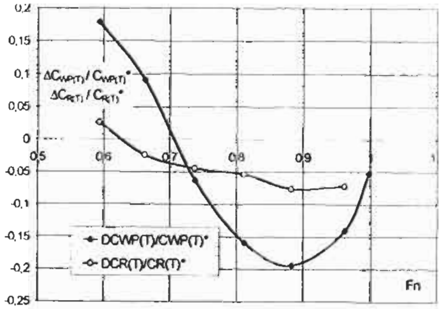

Figure 5: $\Delta C_{WP(T)}$ /$C^*_{WP(T)}$ and $\Delta C_{R(T)}$ /$C^*_{R(T)}$ versus Fn

By analysing the results given in these figures it can be observed that the trend of the residuary resistance and of the wave pattern resistance curves versus Fn agree well each other, the gap between the two curves could be considered nearly constant. The energy loss due to this part of resistance is a high percentage of the residuary resistance (50-80%). This percentage increases with Fn. Anyway the average percentage of the residuary resistance is about 25% of the total.

The interference phenomenon was also investigated for the optimised trimaran configuration. For this purpose the wave pattern and the residuary non interference resistance coefficients were determined by the expressions:

$$C^*_{WP(T)} = C_{WP(M)} \cdot S_{(M)}/S_{(T)} + 2\, C_{WP(O)} \cdot S_{(O)}/S_{(T} \tag{1}$$

$$C^*_{R(T)} = C_{R(M)} \cdot S_{(M)}/S_{(T)} + 2\, C_{R(O)} \cdot S_{(O)}/S_{(T)} \tag{2}$$

Were the suffix, codes T, M, O refer to trimaran, main hull and outrigger respectively.

The differences $\Delta C_{WP(T)} = C_{WP(T)} - C^*_{WP(T)}$ and $\Delta C_{R(T)} = C_{R(T)} - C^*_{R(T)}$ between the resistance coefficients of trimaran configuration and corresponding non interference resistance coefficients are due to interference phenomenon. Figure 5 shows the percentages $\Delta C_{WP(T)}/C^*_{WP(T)}$ and $\Delta C_{R(T)}/C^*_{R(T)}$ versus Fn. From the obtained results it can be seen that in the optimised configuration of the examined trimaran, the wave making interaction between the main hull and the outriggers reduces the wave resistance in the Fn range 0.70-1.00. The most beneficial interference results for Fn ~ 0.90, and this value could be a reference in the design procedure of an operating trimaran.

3 SEAKEEPING TESTS

The seakeeping tests have been carried out in the basin of the University of Trieste (50.00 m x 3.10 m x 1.50 m). The experiments were carried out in head regular waves generated by a plunger wave maker. Because of the small tank a light weight carriage was used and its acceleration and deceleration were controlled by a specific software. Heave, pitch and added resistance have been measured; the added resistance was calculated subtracting the resistance measured in calm water.

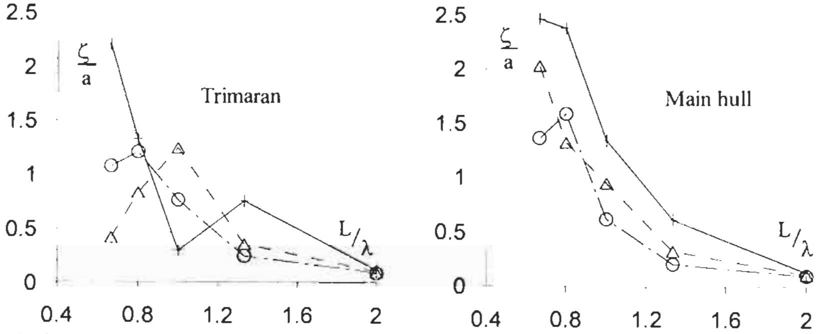

Figure 6: Heave response amplitude operators. Cross: Fn=0.45; triangle: Fn=0.63, circle: Fn=0.82

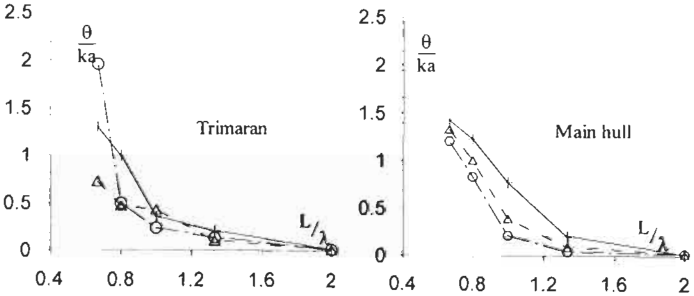

Figure 7: Pitch response amplitude operators. Cross:Fn=0.45; triangle: Fn=0.63, circle: Fn=0.82

The tests were carried out on the main hull and on the aforementioned optimised trimaran configuration for $\lambda/L=0.5-1.5$.The seakeeping experiments carried out so far are to be considered as preliminary, in fact only a trimaran configuration, the one optimised with respect to resistance has been considered. To have a first rough indication about the comparative behaviour of a trimaran ship in waves, with respect to a single hull, also the isolated main hull of the trimaran itself has been tested for the same wave lengths. First results of this experimental investigation are reported in fig. 6 and 7. In fig. 6 the heave response operators ζ/a and in fig. 7 the pitch response amplitude operators are shown (in non-dimensional form with respect to the wave amplitude a and the wave steepness ka respectively, as usual). From the reported results is hard to try any definite conclusion, but, in general the lower values resulting from the trimaran curves can be noted.

4 HIGH SPEED CRAFT COMPARISON

The trimaran model resistance results have been utilised for a comparison with the equivalent catamaran and monohull ships using the results obtained from previous model tests (Brizzolara et al. 1998; Cassella et al. 1998). Fig. 8 and fig. 9 show the residuary resistance to displacement ratios and the total full scale resistances respectively. Model data have been analised by ITTC'57 friction line. From the figures we can note the different trend for the curve relative to the monohull. It must be noted that this vessel presents an hard-chine hull whereas the catamaran and the trimaran have round bilge hull forms. It can be supposed that, at the higher Froude numbers the monohull is subjected to some hydrodynamic lift. From fig 8 a relevantly lower residuary resistance is highlighted for the trimaran, on the contrary the monohull definitely presents the higher resistance.

Due to the effects of different waterline lenghts and wetted surfaces, smaller differences among the values can be observed in fig. 9. However, the same ranking among the various types of hulls is generally evidenced, with the trimaran always presenting the lowest resistance up to $Fnv=v/(gV^{1/3})^{0.5} = 3$ while, for Fnv>3 the monohull ship seems to become the best performance.

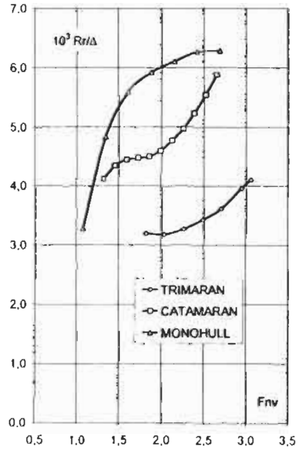

Figure 8: Residuary Resistances Values of Trimaran, Monohull and Catamaran

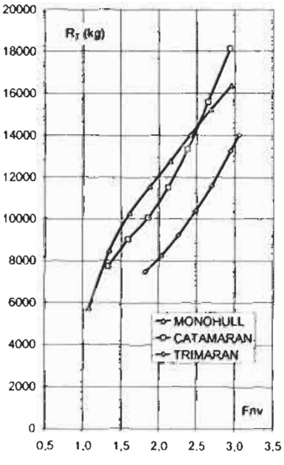

Figure 9: Total Resistances Values of Trimaran Monohull and Catamaran

5 CONCLUSIONS

Systematic model tests have been carried out on a trimaran hull equivalent to operating high speed catamaran and monohull ships. Resistance and wave pattern tests have been carried out separately on the main hull, on the outrigger and on the trimaran. Seakeeping tests have been also carried out on the main hull and on the trimaran for λ/L 0.5-1.5. The resistance results have been analysed by ITTC 57 model ship correlation.

From the results of this experimental research program the following consideration can be derived:

- due to very slender hulls the wave resistance of the considered trimaran is a low percentage of the total resistance;
- the wave interference phenomenon is generally beneficial:

from the comparison with monohull and catamaran, the trimaran seems preferable in the Fnv range - 1.8-3.0.Then for Fnv>3 the monohull ship seems to become the best hullform.

Preliminary seakeeping tests in regular waves show very significant differences of heave and pitch motions of the trimaran with respect to those of its main hull. The reported data seem to indicate a significant beneficial effect of the outriggers on the seakeeping performances. Further study is however necessary to confirm these results and to evaluate other configurations with different outrigger position so to have indications also for what seakeeping optmisation is concerned.

Acknowledgments

This work was supported by the Italian Ministry of University and Scientific Research in the frame of the 1999-2001 research plan.

References

Ackers B.B.; Micheal T.J, Tredennick O.W., Landen H.C., Miller E.R., Sodowsky J.P., Hadler J.B. (1997). An investigation of the Resistance Characteristics. of Powered Trimaran Side-Hull, *SNAME Trans.*, **105**, 349-380

Battistin D., Danielli A., Zotti I. (2000). Numerical and Experimental Investigations on Wave Resistance of Trimaran Configuration, *Proc. of IMAM* **1**, 56-63, Ischia, Italy

Begovic E., Migali A., Pensa C. (2000). Experimental Study on the Resistance of a Trimaran Hull Configuration, *Proc. of NAV 2000*, 2.6.1-2.6-10, Venice, Italy

Bertorello C. (2000). Trimaran Hull Performances for Fast Passenger Ferries *Proc. of NAV 2000*, 2.4.1 –2.4.10, Venice, Italy

Bertorello C., Bruzzone D., Cassella P., Zotti I. (2001). Experimental Performance Investigation on Different High Speed Crafts: Monohull Catamaran and Trimaran *Hiper 2001 May 2001* Hamburg, Germany

Brizzolara, S., Bruzzone, D., Cassella, P., Scamardella, A., Zotti, I. (1998). Wave Resistance and Wave Patterns for High Speed Crafts; Validation of Numerical results by Model-Test, *Proc. XXII Symposium on Naval Hydrodynamics*, 55-69, Washington, USA

Cassella, P., Coppola, C., Lalli, F., Pensa, C., Scamardella, A., Zotti, I. (1998). Geosim Experimental Results of High Speed Catamaran: Cooperative Investigation on Resistance Model Tests Methodology and on Model-Ship Correlation, *Proc. PRADS 1998*, 447-452, The Hague, Holland

Eggers K.W.H., Sharma, S. D., Ward, L.W. (1967). An Assessment of Some Experimental Methods for Determining the Wave making Characteristics of a Ship Form *Trans. SNAME*, **74**.

Larsson L., Janson C.E., Brun P. (1997). A Numerical Investigation of Trimaran Configuration, *FAST 97*, 537-544, Sydney, Australia

Suzuki K., Nakata Y., Ikehata M., Kai H. (1997). Numerical Prediction on Wave Making Resistance of High Speed Trimaran, *FAST 97*, 611-620, Sydney, Australia

Suzuki K., Ikehata M. (1993). Fundamental Study on Optimum Position of Outrigger of Trimaran from view Point of Wave Making Resistance, *Proc. of FAST 93*, 1219-1230, Yokohama

Tuck E.O., Lazauskas L. (1998). Optimum Hull Spacing of a Family of Multihulls, *Ship Technology Research* **45**, 180-195
Yeh, H.Y.H. (1965). Resistance Experiments on High Speed Displacement Forms, *Marine Technology*, 112-157

Practical Design of Ships and Other Floating Structures
You-Sheng Wu, Wei-Cheng Cui and Guo-Jun Zhou (Eds)
© 2001 Elsevier Science Ltd. All rights reserved

HULL FORM DEVELOPMENT AND POWERING PERFORMANCE CHARACTERISTICS FOR A 2,500TON CLASS TRIMARAN

Kuk-Jin Kang[1], Chun-Ju Lee[1], Do-Hyun Kim[1]

[1] Korea Research Institute of Ships and Ocean Engineering,
P. O. Box 23 Yusung, Taejon, 305-600, Korea

ABSTRACT

This paper presents the results of hull form design and powering performance for a 2,500ton class trimaran. A series of resistance tests and numerical calculations have been conducted to figure out the influence of side-hull forms, longitudinal and transverse locations on the resistance characteristics of the trimaran. And the propulsion test was conducted to investigate the propulsion efficiency of the trimaran, and the powering performance of the trimaran was compared with that of the similar mono-hull ships in full scale. From the research it was found that the longitudinal location of side-hull had a large influence on the resistance characteristics of the trimaran while the side-hull form and transverse location had a small influence on it. The trimaran showed favorable resistance performance when the side-hull was located near the stern, which was resulted from the fact that the side-hull stem was located near the primary wave hollow generated by the main hull. The powering performance of the trimaran was superior to that of the similar mono-hull ships above the middle speed range.

KEYWORDS

Trimaran, Side-hull, Optimum Location, Powering Performance, Resistance, Wave Interference

1 INTRODUCTION

The demand for high-speed ships has been increased in the car/passenger ferry market during last decade. Many different types of ship concept and hull forms have been considered to meet the demand. Among them, the trimaran, which consists of a slender main hull and two very fine side-hulls, is one of the most interesting hull form. The trimaran has several advantages over other hull forms, such as low resistance at high speeds, easy arrangement on wide deck, superior seakeeping performance in waves, high survivability in damaged condition and reduction of thermal signature and radar cross-section etc. On the other hand, the trimaran has several disadvantages, such as increase of hull weight, difficult handling in harbor etc. The feasibility studies and the application examples on the trimaran were introduced in recent FAST symposium and etc. In particular, many researches on the trimaran and the construction of "RV Triton" in U.K. is very encouraging the possibility for the future warship.

The present work is to develop a 2,500ton class trimaran and to quantify the powering performance of it. A series of resistance tests and numerical calculations were carried out to investigate the influences of side-hull form and the location of side-hull on the resistance characteristics of trimaran. Also, the propulsion test was conducted to investigate the propulsion efficiency of the trimaran, and the powering performance of it was compared with that of the similar mono-hull ships in full scale.

2 PRINCIPAL DIMENSIONS AND HULL FORM DESIGN

2.1 Principal Dimensions

Hull form should be designed to satisfy the whole hydrodynamic performance at design speed, where the resistance performance is very important. In particular the main hull and side-hull should be optimized at the same time to ensure the excellent resistance performance for the trimaran. The key parameters for trimaran design are main hull length to beam ratios, side hull length and location etc.
The principal particulars of the 2,500ton class trimaran are shown in table 1, which are decided from the concept design referring to the design requirement and the 'RV Triton'.

TABLE 1
PRINCIPAL PARTICULARS OF THE 2,500TON CLASS TRIMARAN

Item (unit)	Main Hull	Side-Hull	Trimaran
Displacement (ton)	2,324	176	2,500
Length between perpendiculars (m)	120.0	45.0	120.0
Breadth (m)	9.0	1.8	30.0
Depth (m)	12.0		12.0
Draft (m)	4.2	2.5	4.2
Block coefficient	0.50	0.423	
Water-plane area coefficient	0.7745	0.9	
Mid-ship section area coefficient	0.8468	0.5	
Longitudinal center of buoyancy (%)	-2.48	0.0	
Cruising speed	18 knots (Fn=0.27)		
Maximum speed	30 knots (Fn=0.45)		
Propulsion	Twin propellers, diameter = 3.0m		

2.2 Hull Form Design

The wave resistance of the main hull affects dominantly on the resistance performance of the trimaran. Therefore, it is very important to find out the hull form with excellent resistance performance for the design of main hull form at initial design stage. A displacement type hull, which was recently developed as a high-speed hull in KRISO, was selected as a parent ship of the main hull. Three kinds of side-hulls (inboard, symmetry and outboard type) with a wedge shape were designed referring to Ackers.(1997). Figures 1 & 2 show the graphic model of the trimaran and the definition of the side-hull location at each. Figure 3 shows drawings of main hull and three kinds of side-hull.

3 MODEL TEST AND NEMERICAL METHOD

The numerical and experimental studies were conducted to figure out the influences of side-hull form and location on the resistance characteristics of the trimaran. And the propulsion test was also conducted to investigate the propulsion efficiency of the trimaran.

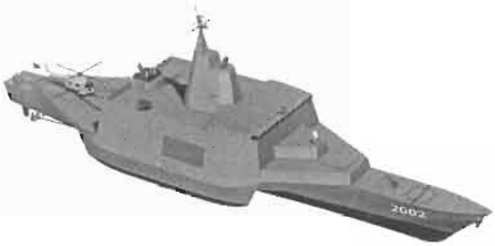

Figure 1: Graphic design model of trimaran

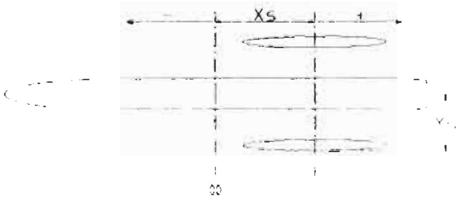

Figure 2: Definition of side-hull location

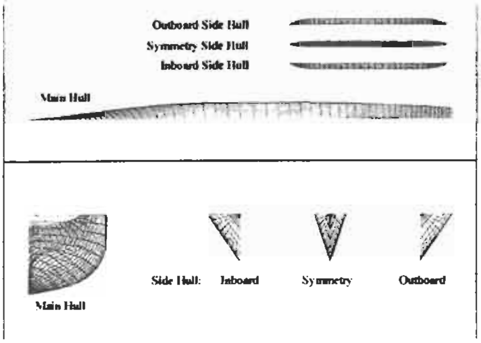

Figure 3: Drawing of a 2,500ton class trimaran (main hull and three side hull forms)

The 1/16.667 scale trimaran model was manufactured to carry out the resistance and propulsion tests. Based on the Froude's assumption and 1957 ITTC model-ship correlation line, the full-scale values were predicted from the resistance tests. The scale effect correction was carried out based on the 1978 ITTC Performance Prediction Method.

The numerical method to calculate the wave resistance was developed by Kim, et al. (1998). The method adopted the first order panel method, which was developed by Hess and Smith. For the free surface effects, the pioneering paper by Dawson demonstrated the promising results of the free-surface panel method. Furthermore, Xia, Raven and Kim extended and refined the method. The present method is based on the numerical schemes of the above-cited papers. For the free surface treatment basically the well-known Dawson's approach is adopted in the present method. To enforce the radiation condition the present method employs Dawson's 4-point upwind-difference operator in a longitudinal direction. For a transverse direction 3-point central-difference operator is used. Furthermore, the collocation points are shifted upstream in order to smooth out the source strengths and to prevent the upstream waves at high speeds. The shifted distance is usually about 10%~30% of panel length. To take into account the transom stern effect, the Cheng's method based on dry transom assumption is used in the present approach. Due to the transom stern of the main hull, the static pressure component of a main hull is included by somewhat adhoc fashion when calculating the wave resistance of a trimaran.

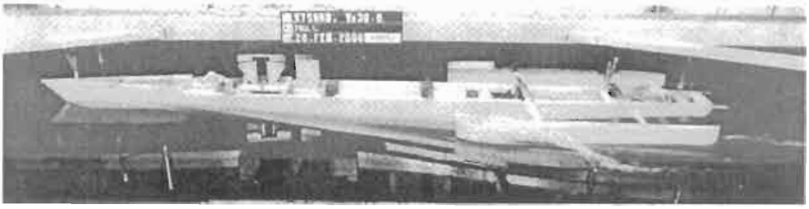

Figure 4: Running trimaran model with outboard type side-hull (30 knots, Ys/Lpp=0.125, Xs/Lpp=0.3)

4 RESULTS AND DISCUSSION

4.1 Effects of Side-hull Form

Three kinds of side-hull forms (inboard, symmetry and outboard type) were investigated to figure out the influence on the resistance performance of the trimaran. Model tests and numerical calculations were carried out at the side-hull location Xs/Lpp=0.3 in length and Ys/Lpp=0.125 in beam. Figure 4 shows the running trimaran model with outboard type side-hull at 30 knots. It was observed that the outboard and inboard type side-hull made the stem wave spray outward and inward at each. However, the symmetry type side-hull showed the moderate stem wave. Figure 5 shows the residuary resistance coefficient (C_R) curves obtained from model tests. Figure 6 shows the comparison of calculated wave patterns between the inboard and outboard type side hull at 30 knots, where was no significant difference in global wave system except local wave change. Figures 7 & 8 show the calculated wave resistance coefficient (C_W) curves together with C_R values at 18 knots and 30 knots at each, which show very good agreement in tendency. From the above results, it was found that the symmetry shape among the three side-hull forms has a favorable resistance characteristic comparatively though there were no big differences among them.

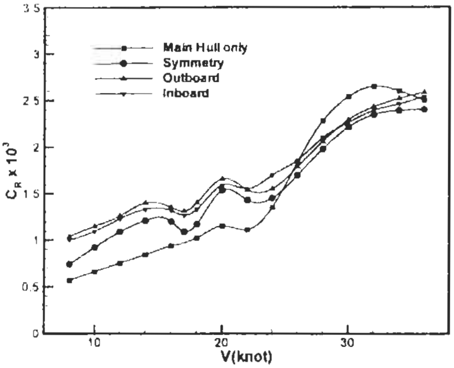

Figure 5: C_R curves for three side-hull forms

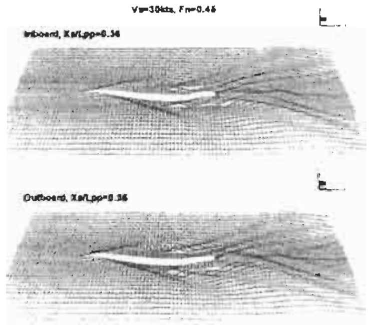

Figure 6: Comparison of wave patterns

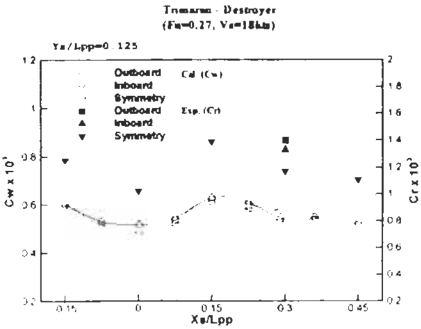

Figure 7: C_R & C_W at 18 knots (Fn=0.27)

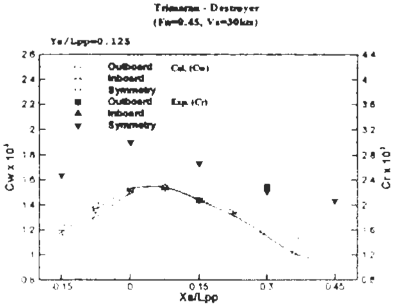

Figure 8: C_R & C_W at 30 knots (Fn=0.45)

4.2 Effects of Side-hull Location in Longitudinal Direction

Longitudinal location of side-hull was investigated to figure out the influence on the resistance performance of the trimaran. Model tests and numerical calculations were carried out for the side-hull location at Xs/Lpp=-0.15, 0.0, 0.15, 0.30 & 0.45 in length and Ys/Lpp=0.125 in beam. Figures 7 and 8 show very good agreement between the calculation and the experiment at 18 knots and 30 knots at each. It is almost possible to select the optimum longitudinal location by numerical calculation. Figure 9 shows the C_R curves obtained from model tests. The differences were caused by the wave interference according to the longitudinal locations of side-hull. Figure 10 shows the comparison of calculated wave patterns for the side-hull locations Xs/Lpp=0.36 and 0.075, which shows big difference in wave system. It can be found from the wave system that the former shows favorable wave interference but the latter shows nearly the worst case.

From the above results, it is found that the optimum longitudinal location is related with the ship's speed. And the trimaran shows a favorable resistance performance when the side-hull moves toward the stern of main hull at high speeds. However, it is supposed that the optimum longitudinal location is near Xs/Lpp=0.3 if the ship's constraint conditions etc. are considered.

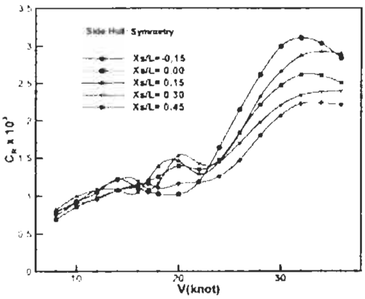

Figure 9: C_R curves for side-hull locations in length

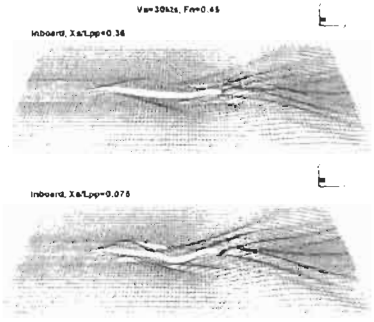

Figure 10: Comparison of wave patterns

4.3 Effects of Side-hull Location in Transverse Direction

Numerical calculations were carried out to investigate the effect of the side-hull's transverse location on the wave resistance characteristics of the trimaran. The trimaran with symmetry type side-hull was used for the calculation. Figure 11 shows the calculation results for the transverse locations Ys/Lpp=0.125~0.225 while the longitudinal location is fixed at Xs/Lpp=0.15 at 30 knots. Figure 12 shows the calculated wave height for the main hull only in transverse direction at main hull center Xs=0.0, which corresponds to the $0.1L_{side\text{-}hull}$ aft of side-hull. From these two figures it seems that the wave resistance is related with the wave height a little, which the side-hull stem encounters.

The maximum difference of the wave resistance coefficient C_W due to the transverse locations does not exceed 10% of that due to the longitudinal locations.

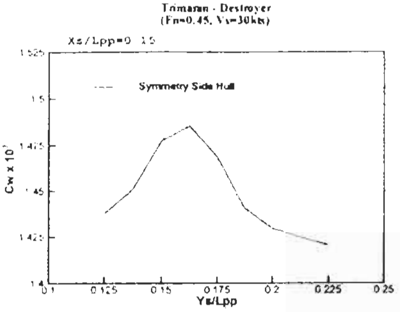

Figure 11: Calculated C_W curve according to the transverse locations of side-hull

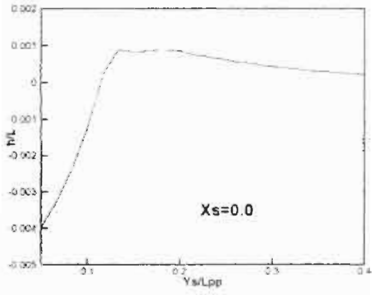

Figure 12: Wave height generated by main hull in transverse direction (30 knots)

4.4 Discussion on the Optimum Location of Side-hull

The present topic is to find out the easy way to predict the optimum location of side-hull at initial design stage. The resistance characteristics of trimaran are highly affected by the wave interference between the main hull and the side-hull. Therefore, the optimum location of side-hull is supposed to be the place where the waves generated by the main hull and the side-hull cancel out each other. Figure 13 shows the wave profile generated by main hull at 30 knots (Fn=0.45) and five locations of side-hull at the transverse location Ys/Lpp=0.125. This relative location seems to show a close relation with the wave resistance as shown in figure 8. Therefore, it can be said carefully that the trimaran has favorable resistance performance when the side-hull stem is located near the primary wave hollow generated by the main hull.

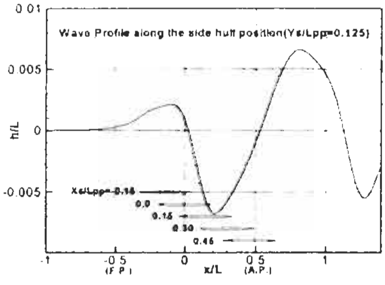

Figure 13: Relation between wave profile and side-hull location (30 knots)

4.5 Comparison of Powering Performance

Figure 14 & 15 show the comparison of C_R curves and Admiralty coefficients (Cadm) for the trimaran and the similar mono-hull ships, respectively. The propulsion efficiency of trimaran is almost same as the others. The trimaran shows good powering performance in most speed range though the wetted surface area is increased by 28% comparing to the others.

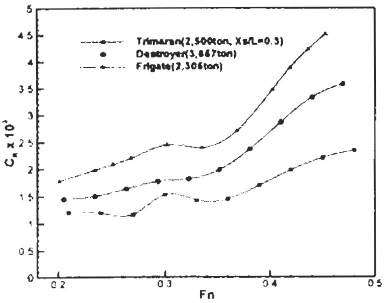

Figure 14: Comparison of C_R curves

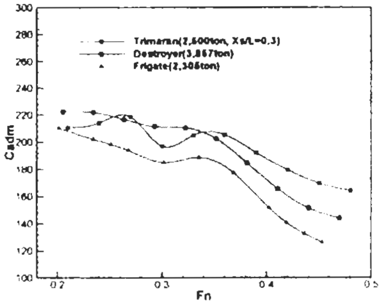

Figure 15: Comparison of Adimiralty coefficients

5 CONCLUDING REMARKS

The 2,500ton class trimaran was designed and the powering performance was investigated. The results obtained from the research can be summarized as follows.

- The longitudinal location of side-hull has a large influence on the wave resistance of the trimaran while the side-hull form and transverse location has a small influence on it.
- The symmetry side-hull shows comparatively good performance on wave resistance among three kinds of side-hull forms.
- The optimum location of side-hull is changed according to the ship's speed. Then the optimum location moves to the stem or stern part as the trimaran runs fast.
- The trimaran shows favorable resistance performance when the side-hull stem is located near the primary wave hollow generated by the main hull.
- The trimaran is superior to the similar mono-hull ships in powering performance except the low speed range though the wetted surface area is increased by 28% comparing to the latter.
- The optimization of principal dimensions and the hydrodynamic performance including seakeeping and maneuvering characteristics for the trimaran should be studied synthetically.

References

Benjamin B. Ackers et al. (1997). An Investigation on the Resistance Characteristics of Powered Trimaran Side-Hull Configurations. *SNAME Transactions* **105**, 349-373.
http://www. trimaran.dera.gov.uk/
Kang, K. J., et al. (2000). Development of the Core Technologies of Hydrodynamic Performance for Large High Speed Special Ship (4/4). *KRISO report UCE00918-2296*
Kim, D. H., et al. (1999). Estimation of the Optimum Position for the Side Hulls of a Trimaran by Panel Method. *4th J-K Joint Workshop on Ship & Marine Hydrodynamics*, Fukuoka, Japan
RINA (2000). RV 'TRITON':Trimaran Demonstrator Project. *International conference proceeding*

Practical Design of Ships and Other Floating Structures
You-Sheng Wu, Wei-Cheng Cui and Guo-Jun Zhou (Eds)
© 2001 Elsevier Science Ltd. All rights reserved

DESIGN RECOMMENDATIONS FROM THE FPSO – FATIGUE CAPACITY JIP

I. Lotsberg

Det Norske Veritas, Veritasveien 1, 1322 Høvik, Norway

ABSTRACT

A joint industry project on the Fatigue Capacity of FPSOs has been carried out with 19 participants from oil companies, designers, shipyards and classification companies in the period 1998 -2000. The main objective of the project was to reduce the risk for fatigue cracks and fracture in FPSOs. The project provides small scale and full scale S-N data on typical fatigue sensitive details in FPSOs and tankers. It also provides improved information on the important link between S-N data and finite element analyses for fatigue life assessment. Finally it provides data to assess more reliable the risk for unstable fracture of FPSOs when fatigue cracks are present in the structure. This paper provides links to other sources where a more detailed description of some of the main achievements have been presented.

KEYWORDS

Fatigue, FPSO, Fatigue testing, S-N data, Hot spot stress, Finite element analysis, Fracture.

1 INTRODUCTION

A joint industry project on the Fatigue Capacity of FPSOs has been carried out with 19 participants from oil companies, designers, shipyards and classification companies in the period 1998 - 2000. For background and a more detailed description of the scope of work for this project see Lotsberg (2000). For an overview of work performed see also Lotsberg (2001). (FPSO = Floating Production Storage and Offloading unit).

The main objective of this project was to reduce the risk for fatigue and fracture in FPSOs.

Finite element analysis (FEA) is becoming a design tool also for fatigue assessment of FPSOs. In order to have a reliable analysis procedure it is important that there is a proper link between the calculation of hot spot stress and the hot spot stress implicit the S-N curve that is used for assessment of fatigue damage. Therefore hot spot stress evaluation from FEA and corresponding S-N curves were important issues in this project. Also FEA of a number of FPSO details were performed to derive stress concentration factors that can be used for efficient fatigue design of FPSO structures. These items are described more in detail in this paper. Unstable fracture may initiate from fatigue cracks at welded connections with materials showing a low fracture toughness. This issue was also investigated in this project. Reference is made to Pisarski (2001) for further details.

2 DESIGN RECOMMENDATIONS

2.1 Hot Spot Stress Analysis

The hot spot stress in tubular joints has the last 25 years been derived by some extrapolation of the measured/calculated stress at the hot spot region back to the weld toe. The local stress effect due to the weld is accounted for in the S-N curve. Similar concepts were also investigated in the present project, ref. Fricke (2001). Three different methods for derivation of hot spot stress (geometric stress) were investigated:

- Linear extrapolation of stresses to the weld toe from stress at distances 0.4*t and t from the toe (t = plate thickness). This method is recommended by the International Institute of Welding (IIW).
- Linear extrapolation of stresses to the weld toe from stress at distances 0.5*t and 1.5*t from the toe. This method is used by some of the Classification Companies.
- Stress at a distances 0.5*t from the weld toe. (No extrapolation).

For analysis by shell elements the distance to the stress read out points is measured from the intersection lines as the weld is not normally included in the model. For analysis by solid elements the distance to the stress read out points is measured from the weld toe.

It should be noted that the finite element modelling might influence the calculated stress at the hot spot region. Parameters effecting this are:

- type of element used,
- size of elements at the hot spot region,
- how the stresses are derived from the analysis (Gaussian stress, nodal stress etc.).

See Fricke (2001) for recommendations on finite element modelling for derivation of hot spot stress at different positions shown in Figure 1.

2.2 S-N Data

Available S-N data from the The Welding Institute were reviewed in terms of hot spot stress S-N curves. In addition a number of typical ship details were fatigue tested by Hyundai Heavy Industries in Korea (HHI), (Kim et al., 2000, 2001). Five full scale test specimens as shown in Figure 2 were tested at DNV laboratories. (Lotsberg et al., 2001). The purpose of these tests was to achieve test data for calibration of the FEA and for verification of S-N data. Based on the present work the following main recommendations were drawn by Maddox (2001):

- An extensive database for transverse butt welded joints suggests FAT90 as a suitable hot-spot stress design curve for plate thicknesses up to 25 mm. This S-N curve corresponds to the D- curve in DNV (2000) and is approximately the same as the D curve in HSE (1995).
- This proved to be consistent with the HHI data and some published data for hot-spot types (a) and (c) in Figure 1 (i. e. weld end and toe on plate surface respectively) provided the hot-spot stress is obtained by one of the extrapolation methods.
- However, considering all the published data located, apart from those for doubler plate details, data for type (c) hot-spots strongly supported lower FAT 80. Further work is needed to resolve this apparent contradiction.
- Lower FAT80 is recommended if the hot-spot stress is assumed to be that 0.5t from the weld toe. This S-N curve corresponds to the E- curve in HSE (1995) and DNV (2000).
- Fillet welds that may fail in the throat should be assessed based on the FAT36 design curve when analysed using the standard method based on the ‘engineering shear stress’ on the weld throat. This S-N curve corresponds to the W’ curve in HSE (1995) and the W3- curve in DNV (2000).

The fatigue endurance to a 12 mm crack in the full scale tests are shown in Figure 3 for the same ballast loading. It is observed that the geometry with double bracket design (specimen 1) is favourable in terms of fatigue life. This comparison is based on sideways pressure. In the case of longitudinal loading, the conclusions are likely to be different. (Specimen no 2 was subjected to the loaded condition and the fatigue capacity is not presented in the same figure as for ballast loading).

2.3 Finite Element Analyses of Details

Different typical ship details were analysed that earlier were missing in design guidance documents to provide stress concentration factors. As mentioned in the introduction the procedure for derivation of stress concentration factors are linked to the hot spot S-N curve used. Thus the presented stress concentration factors are linked to the hot spot stress derivation method.

2.3.1 Cut outs and man holes

Different cut out geometries were analysed by Umoe:

- Circular cut-out with diameter = 600 mm
- Rectangular cut-out 600 x 800 mm with rounded corner R = 300 mm
- Rectangular cut-out 600 x 1200 mm with rounded corner R = 300 mm

A number of different stiffener arrangements around the cut out were analysed, see Figure 4. The analysis procedure and some selected results are presented by Chen and Landet (2001). The following main conclusions were drawn:

- ➢ To insert a plate at the cutout edge is an efficient measure to reduce the stress concentration at the plate edge.
- ➢ A single side reinforcement may not reduce the stress concentration in the plate around cutout edge due to extra local bending deformation.
- ➢ A double side reinforcement will reduce the stress concentration in the plate around cutout edge.

2.3.2 Longitudinal to web frame connections

Five different geometries of longitudinal to web frame connections similar to that of specimen 4 shown in Figure 2 were analysed by Aker Maritime/Maritime Trosvig. The analysis results are presented by Ulleland et al. (2001). It is shown that the local design of the lug plates is important for the calculated fatigue life.

2.3.3 Scallops

Different scallop geometries were analysed by Germanischer Lloyd (Säbel et al., 2000). A number of stress concentration factors were presented.

2.3.4 Topside supports

A number of different geometries (R and ϕ) of topside supports were analysed by Bluewater (2000), see Figure 5. The results were presented in terms of stress concentration factors. It is demonstrated that the radius and the angle are important parameters with respect to fatigue when considering the force range from the topside. However, it is of small influence considering the fatigue life due to the stress range in the deck plate.

2.3.5 Doubling plates

A number of different geometries of doubling plates on deck plates were analysed by Bluewater (2000). Stress concentration factors and stress intensity factor for some fatigue cracks at hot spots were derived. For a well defined stress direction a radius of the doubling plates in the order of the plate thickness is sufficient. A circular doubling plate leads to a larger stress concentration factor than a quadratic plate of similar size with rounded corners. The stress concentration factor increases with the size of the doubling plates.

2.3.6 Hopper knuckle

The effect of fabrication tolerances for a hopper knuckle was investigated in analyses performed by Lloyd's Register, see Figure 6. The analysis results are presented by Polezhaeva and Chung (2001). A load case with motion induced pressure acting inside the ballast tank was analysed. Based on this analyses it was found that a nominal eccentricity of 0.25 t would result in the lowest stress concentration factor and the longest fatigue life.

2.3.7 Experience from finite element analyses of the full scale tests

All the full scale test specimens were analysed by shell elements. (Bureau Veritas, Umoe and DNV performed these analyses). In general there is a very good correspondence between these analyses and the measured stress for specimens 3-5. There is less good correspondence for specimen 1. It is observed that it is difficult to model the connection between the bulb and the buckling stiffener including brackets properly by use of shell elements only. Specimen 4 was also analysed by three-dimensional finite elements and there is a very good correspondence with the measured stress, see Figure 7. Some selected analysis results are presented by Rucho et al. (2001).

3 EXTENSION OF THE PROJECT

A number of participants have shown interest in planning an extension of the project (Phase II).
An extension of the project is planned to contain:

- ➢ Further work to achieve a reliable link between calculated stress from FE analyses and S-N data for fatigue cracks initiating from weld toes and from the roots of fillet welds that is numerical accurate, robust and efficient to use by engineers.
- ➢ Further fatigue testing to achieve S-N data for other typical FPSO details that can be used for calibration of analysis technology.
- ➢ Verification of analysis procedure on full scale test specimens tested in Phase I.
- ➢ Methodology for fatigue assessment of the transverse structure of FPSOs. This includes determination of local pressure around the mean water level, linearised frequency analyses for wet and dry areas (non-linear problem), and fatigue testing of capacity of connections subjected to pressure loading.
- ➢ Procedure for inspection and repair of fatigue cracks in FPSOs on the field.

An extension is planned carried out in the time period 2001-2003.

References

Chen W. and Landet E. (2001). Stress Analysis of Cut-outs with and without Reinforcement. OMAE Rio deJaneiro.
Doc. No. FFC-S910-RP-0002/Rev. C SCFs for Topside Support Stools. Bluewater 2000.
DNV (2000) Recommended Practice RP – C203 Fatigue Strength Analysis of Offshore Structures.
Fricke W. (2001). Recommended Hot Spot Analysis Procedure for Structural Details of FPSO's and Ships Based on Round-Robin FE Analyses. ISOPE Stavanger.
Hobbacher A. (1996). Fatigue Design of Welded Joints and Components. IIW. XIII-1539-96/ XV-845-96.
HSE (1995). Guidance on Design, Construction and Certification.
Kim, W. S. (2000). Fatigue Test of Typical Weld Joints. Hyundai Heavy Industries Co., Ltd.

Kim W. S., Kim D. H., Lee S. G. and Lee Y. K. (2001). Fatigue Strength of Load-Carrying Box Fillet Weldment in Ship Structure. PRADS Shanghai.
Lotsberg I (2000). Background and Status of the FPSO Fatigue Capacity JIP, OTC Paper No 12144. Houston.
Lotsberg I. (2001). Overview of the FPSO – Fatigue Capacity JIP. OMAE Rio deJaneiro.
Lotsberg I., Askheim D. Ø., Haavi T. and Maddox S. (2001). Full Scale Fatigue Testing of Side Longitudinals in FPSOs. ISOPE Stavanger June.
Maddox S. (2001). Recommended Design S-N Curves for Fatigue Assessment of FPSOs. ISOPE Stavanger.
Pisarski H. (2001): Fracture Toughness Data for Crack Initiation and Crack Arrest in FPSOs. OMAE Rio deJaneiro.
Polezhaeva H. and Chung H. (2001): Effect of Misalignment on the Stress Concentration of a Welded Hopper Knuckle for a Typical FPSO. OMAE Rio deJaneiro.
Rucho P. Maherault S., Chen W., Berstad A. and Samnøy G. E. (2001). Comparison of Measurements and Finite Element Analysis of Side Longitudinals. ISOPE Stavanger.
Säbel A., von Selle H. and Fricke W. (2000). Parametric SCF-Calculation for Scallops using FEM. GL Report No FF99.188.C, July.
Ulleland T., Svensson M. and Landet E. (2001). Stress Concentration Factors in Side Shell Longitudinals Connected to Transverse Webframes. ISOPE Stavanger.

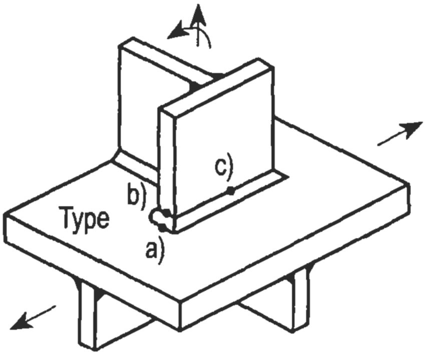

Figure 1: Types of Hot Spots in Welded Structures (From Fricke, 2001)

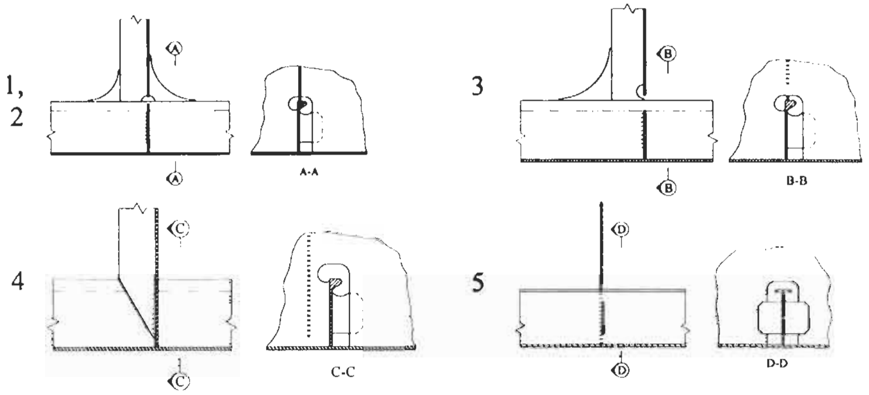
1,
2
A
A-A
3
B
B-B
4
C
C-C
5
D
D-D

Figure 2: Overview of full scale test specimens

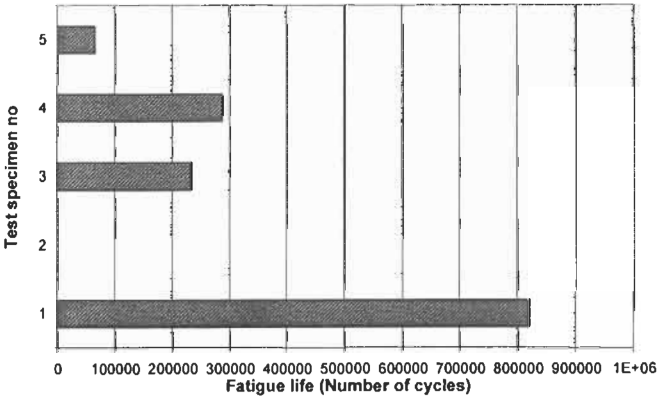

Figure 3: Fatigue lives in the ballast condition for the same load range

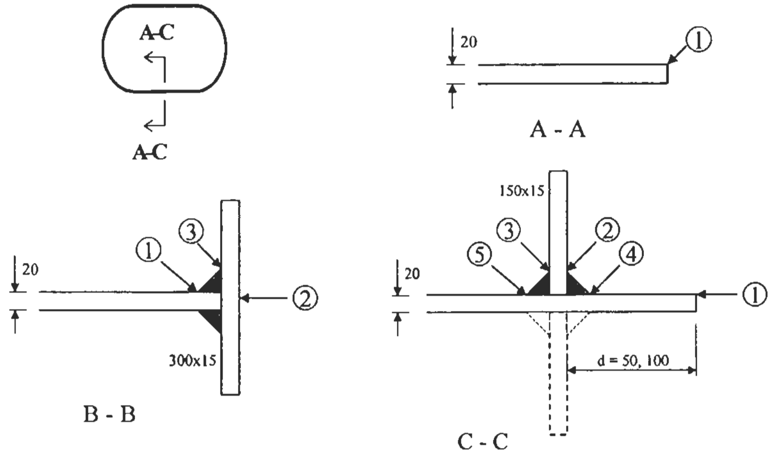
A-C
A-C
20
①
A - A
20
①
③
②
300x15
B - B
150x15
20
⑤
③
②
④
①
d = 50, 100
C - C

Figure 4: Different cut-out geometries

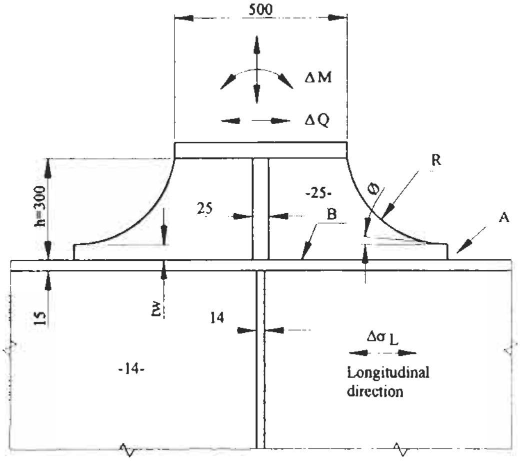
500
ΔM
ΔQ
R
A
h=300
25
-25-
B
Ø
15
tw
14
-14-
Δσ L
Longitudinal direction

Figure 5: Topside support geometry

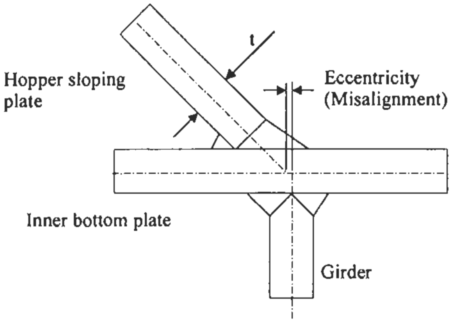
t
Hopper sloping plate
Eccentricity (Misalignment)
Inner bottom plate
Girder

Figure 6: Eccentricity of hopper plate connection

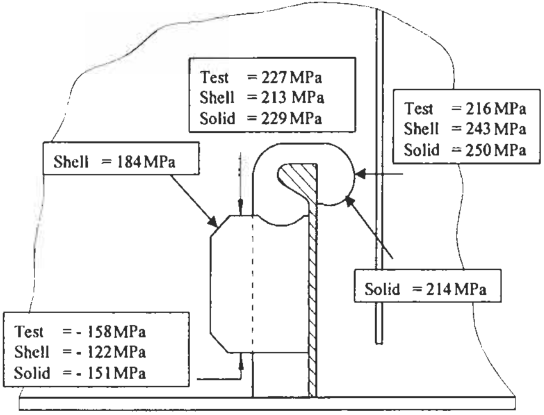
Test = 227MPa
Shell = 213 MPa
Solid = 229MPa
Test = 216MPa
Shell = 243MPa
Solid = 250MPa
Shell = 184MPa
Solid = 214MPa
Test = - 158MPa
Shell = - 122MPa
Solid = - 151MPa

Figure 7: Comparison of calculated hot spot stress with measured stress

Practical Design of Ships and Other Floating Structures
You-Sheng Wu, Wei-Cheng Cui and Guo-Jun Zhou (Eds)
© 2001 Elsevier Science Ltd. All rights reserved

DESIGN OF FPSO's BASED ON MANEUVERING STABILITY

G.B. Matter[1], J.S. Sales Jr.[1] and S.H. Sphaier[1]

[1] Department of Ocean Engineering, COPPE, Federal University
of Rio de Janeiro, Brazil

ABSTRACT

Ships have been used as floating units to store, process and transfer oil to shuttle ships. In currents their movements in the horizontal plane may present an unstable behavior. Based on linear stability analysis, a procedure is presented here to help the engineer to account for the phenomena in the design of new units and in the offloading operation. Three examples of application are presented.

KEYWORDS

Stability, Maneuvering, Offloading, FPSO, DICAS, Spread-mooring, Turret.

1 INTRODUCTION

An economic and practical solution to store and to process oil exploited in deep water is the use of large ships as stationary units, provided with large tanks and a processing plant. However, ships moored to a single point or connected to the sea floor by a mooring system in presence of a current may adopt an unstable behavior of the motion in the horizontal plane. This is not a new problem, once the unstable behavior of ships when towed or moving in a channel or even in open seas motivated many research for a long time (Abkowitz, 1964, 1967, Eda and Crane, 1965).

Bernitsas and Krekides (1985), Schellin, Jiang and Sharma (1987) and Papoulias and Bernitsas (1988) brought many concepts of the theory of dynamic systems to the analysis of the behavior of moored ship in currents. After that, many other substantive contributions appear in the literature. More recently Garza-Rios and Bernitsas (1996, 1998 and 1999) developed some analytical expressions to study the stability of floating systems based on the Routh-Hurwitz conditions.

Associated to the use of converted VLLC to operate as FPSOs in Brazil by Petrobras, Sphaier, Fernandes, Correa and Pontes (1996, 1997, 1998, 1999, 2000a, 2000b) developed a maneuvering model, based on experimental tests carried out in Brazil, and a time domain code to simulate the dynamics of floating systems. Further, a procedure to analyze the stability of those kind of systems were developed, consisting on the calculation and the analysis of the eigenvalues. Later on, Matter, Sales and Sphaier (2001) and Matter, et al (2001b) extended the procedure by developing analytical expressions for the eigenvalues and their derivatives for SPM (single point mooring), TMS (turret mooring system), SMS (spread mooring system) and DICAS systems (SMS with differentiated compliance). These expressions are here applied to problems involved in the design of new ships, in the conversion of a VLCC into a FPSO and in the offloading operation, with the objective of furnishing procedures for the engineers to avoid the undesirable unstable dynamics of a floating system.

2 EQUATIONS OF MOTION

To study the dynamics of a stationary floating body in the horizontal plane a system attached to the ship and an earth-fixed system are used (see figure 1). The ship is exposed to a current with constant intensity C and an angle of incidence α ($\alpha = 0^o$ means current coming from astern). The ship is moored to the sea floor by a schematic spread mooring system. Then, the external forces and moments acting on the ship are the hydrodynamic action due to the current and the reaction due to the mooring system. The hydrodynamic forces and moments are written as functions of the relative hull-current velocity and acceleration according to the quadratic maneuvering model developed by Sphaier, Fernandes, and Correa (1998, 1999, 2000a and 2000b) for stationary floating units. The mooring line forces are expressed as a function of the distance between the fairleads and the anchor points, calculated from a catenary's formulation and considering the drag forces on the mooring lines.

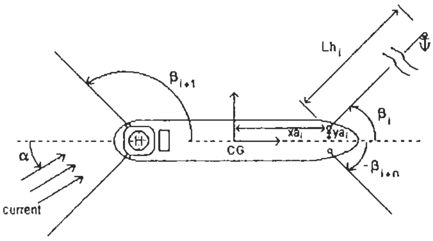

Figure 1: Geometric definition of the mooring system

Setting together the external forces and moments and the inertial terms according to Newton's second law, the equations of motion, expressed in the body-attached system, are given by:

$$(m - X_{\dot u})\dot u = X_{uu} u + m \cdot u \cdot r + X_{|vvv|u} |v^3| u + X_{|vvv|v} |v^3| v + X_{vr} v \cdot r + X_{rr} r^2 + T_u \tag{1}$$

$$(m - Y_{\dot v})\dot v - Y_{\dot r}\dot r + m \cdot u \cdot r = Y_v v + Y_{v|v|} v|v| + Y_r r + Y_{r|r|} r|r| + Y_{|r|v} |r| v + Y_{ur} u \cdot r + T_v \tag{2}$$

$$(I - N_{\dot r})\dot r - N_{\dot v}\dot v = N_v v + N_{v|v|} v|v| + N_r r + N_{r|r|} r|r| + N_{rvv} r \cdot v^2 + N_{rrv} r^2 v + N_{uv} u \cdot v + N_{ur} u \cdot r + T_n \tag{3}$$

where the parameters m and I are respectively the mass and the inertia of the ship. The components of the velocities in the longitudinal axis, in the transversal axis and the angular velocity are respectively u, v and r. The terms $X_{()}$, $Y_{()}$ and $N_{()}$ are the hydrodynamics derivatives related to $()$. The dots over the variables means time derivative and $r = d\psi/dt$, and ψ is the yaw angle. T_u, T_v and T_n are the reaction forces due to the mooring system and can be written as:

$$T_u = \sum_{i=1}^{n} T_i \cos(\psi - \beta_i) \tag{4}$$

$$T_v = -\sum_{i=1}^{n} T_i \cdot sin(\psi - \beta_i) \tag{5}$$

$$T_n = -\sum_{i=1}^{n} T_i \left[xa_i sin(\psi - \beta_i) + ya_i \cos(\psi - \beta_i) \right] \tag{6}$$

where n is the number of mooring lines, xa and ya are the longitudinal and the transversal points of the fairlead, T_i is the mooring line tension ($T_i = f(L_{hi})$). These expressions, developed for a single ship system, can be used for a multiple-ship system by considering the coupling of the ships due to the connection hawser in the terms T_u and T_v.

The velocities in both coordinate systems are related by the following expressions:

$$\dot{\xi} + C = u \cdot \cos(\psi) - v \cdot sin(\psi) \tag{7}$$

$$\dot{\eta} = u \cdot sin(\psi) + v \cdot \cos(\psi) \tag{8}$$

where ξ and η are the absolute displacement of the ship. The acceleration relation is obtained by the time derivative of eqns. 7 and 8. Introducing eqns. 7 and 8 in eqns. 1, 2 and 3, the equations of motion can be expressed as function of the absolute accelerations, velocities and displacements of the ship as:

$$\vec{F}(\xi, \dot{\xi}, \ddot{\xi}, \eta, \dot{\eta}, \ddot{\eta}, \psi, \dot{\psi}, \ddot{\psi}) = 0 \tag{9}$$

The final expression are extensive and are not included in the text, but can be obtained following the steps presented above (see Matter, Sales and Sphaier, 2001)

3 THE STABILITY ANALYSIS

The stability analysis consists on the observation of the ship movements around the many possible equilibria, the equilibrium positions of the system, for different incidence angles of the current. The equations of motions (Eqns. 1, 2 and 3) are expanded in a Taylor's series around the equilibria and linearized. The final expressions are similar to:

$$t_{11}\psi + t_{12}\dot{\xi} + t_{13}\dot{\psi} + t_{14}\dot{\eta} + t_{15}\ddot{\xi} + t_{16}\ddot{\eta} - Tu = 0 \tag{10}$$

$$t_{21}\psi + t_{22}\dot{\xi} + t_{23}\dot{\psi} + t_{24}\dot{\eta} + t_{25}\ddot{\xi} + t_{26}\ddot{\eta} - Tv = 0 \tag{11}$$

$$t_{31}\psi + t_{32}\dot{\xi} + t_{33}\dot{\psi} + t_{34}\dot{\eta} + t_{35}\ddot{\xi} + t_{36}\ddot{\psi} + t_{37}\ddot{\eta} - aTv = 0 \tag{12}$$

where the t_{ij}'s are the resultant terms of the linearization. These terms can be obtained analytically as shown in Matter et al (2001a). The linearized expressions (Eqns. 10, 11 and 12), can be written as:

$$\dot{x} = A \cdot x \tag{13}$$

where $x = \{q, z, w, \xi, \eta, \psi\}^T$ and q, z and w are respectively the time derivatives of ξ, η and ψ. This is the classical eigenvalue problem with $x = \Phi.e^{\lambda t}$. The eigenvalues λ are obtained from the solution of a polynomial like:

$$\sum_{k=0}^{n} a_n \cdot \lambda^n = 0 \tag{14}$$

The index n is equal to the number of ships times twice the number of degrees of freedom for a single ship. Sometimes, this polynomial can be solved analytically and then, it is possible to obtain the eigenvalue derivatives in relation to each parameter of the system and perform a more detailed study of the stability, including a bifurcation study. Extending the study to the offloading operation, the equations of motions have six degrees of freedom and a polynomial of the 12th degree is obtained to determine the eigenvalues, a very difficult task to be treated analytically. For a single ship in SPM or a FPSO provided with a turret, there are only three equations of motion and the longitudinal movement equation is independent of the others and is stable. This reduces the problem to the solution of a 4th degree polynomial. Even in this case a complex algebraic manipulation is necessary to obtain an analytical solution. However, the use of symbolic computation systems, avoiding the long algebraic manipulation, makes possible the analytical treatment of this problem. Although, the eigenvalues can be expressed as functions of the system parameters, the derived expressions arc cven too extensive (see Matter et al (2001b)).

In the next sections three cases studies concerning the use of the derived expressions in the selection of stabilizer device for a TMS, in the definition of the main dimensions of the floating unit in the preliminary design stage and in the analysis of the offloading operation of a DICAS mooring system.

4 STABILIZER DEVICE SELECTION

A very important factor in the design of a FPSO is the longitudinal position of the Turret. If it is located close to the ship's bow end, forward of the critical point, the equilibria can be stable in the horizontal plane, but the ship can be submitted to large vertical movements, which could affect seriously the structure. On the other hand a central turret makes the system unstable.

Here, the selection of a stabilizer device to be used in a FPSO, to operate in 1000 meters water depth is presented with the turret positioned at 0.2 L forward of the midship section (astern of the critical point). The Esso Osaka hull was used as the FPSO with the maneuvering derivatives obtained from Abkowitz (1980). The position of the critical point a_{crit} is expressed by (Sphaier, Fernandes and Correa, 2000a, 2000b):

$$a_{crit} = \frac{N_v + N_{uv}}{Y_v} \tag{15}$$

TABLE 1

Eigenvalue	Real Part	Imag. Part	Modified Eigenvalue	Real Part	Imag. Part
EV1	-1.656	9.2050	EV1	-1.402	-9.1470
EV2	-1.656	-9.2050	EV2	-1.402	9.1470
EV3	-0.2466	0.0000	EV3	-0.9677	0.0000
EV4	0.6554	0.0000	EV4	-0.1957	0.0000

The eigenvalues obtained from the stability analysis are presented in table 1, showing that the system is unstable for this configuration since the fourth eigenvalue is a positive real. The use of a stabilizer device modifies the hydrodynamic derivatives according to the following expressions (Fernandes, Sphaier and Correa, 1999):

$$Y_v = Y_v^{(0)} - \frac{\partial C_L}{\partial \alpha}(0) A_R'(1-\omega) \tag{16}$$

$$Y_r = Y_r^{(0)} + \frac{\partial C_L}{\partial \alpha}(0) s' A_R'(1-\omega) \tag{17}$$

$$N_v = N_v^{(0)} + \frac{\partial C_L}{\partial \alpha}(0) s' A_R'(1-\omega) \tag{18}$$

$$N_r = N_r^{(0)} - \frac{\partial C_L}{\partial \alpha}(0) s'^2 A_R'(1-\omega) \tag{19}$$

where s' is the distance between the stabilizer and the midship section, A'_R the non-dimensional stabilizer area, ω the wake coefficient (set as 0.25) and the derivative of the lifting coefficient with respect to the attack angle can be obtained from Thwaites (1987). The substitution of the Eqns. 16 and 18 in Eqn. 15 gives the area of the stabilizer necessary to change the position of the critical point:

$$A_R' = \frac{\left(a \cdot Y_v^{(0)} - N_v^{(0)} - N_{uv}^{(0)}\right)}{\frac{\partial C_L}{\partial \alpha}(0) \cdot (1-\omega) \cdot (a + s')} \tag{20}$$

To stabilize the system the new device must have a non-dimensional (A_r/L^2) area equal to 0.002935 with the aspect ratio equal to 2.4. This means that two rudders (see figure 2) should be used to stabilize the system, each one 27.0 meters high and 11.2 meters large. The eigenvalues for the modified system are also presented in table 1. All of them have negative real part confirming that the system is stable.

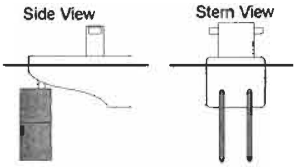

Figure 2: Two rudders Configuration

5 PRELIMINARY DESIGN

In the preliminary design stages, a sensibility analysis of the influence the main parameters of the ship (L, B, T and C_b) have on her stability can be performed. Such analysis goes through the estimation of the hydrodynamics derivatives of the ship from her main characteristics (Clarke et al (1982)).

Stability maps for a 300 kton VLCC, in TMS with the turret positioned at 0.25 L for three different drafts are presented in figure 3, where the length and the beam of the ship were varied. According to these figures, for a fixed beam, the range of possible length to have a stable ship, increase with the decrease of the draft, which means that the stability range increases for greater B/T ratios.

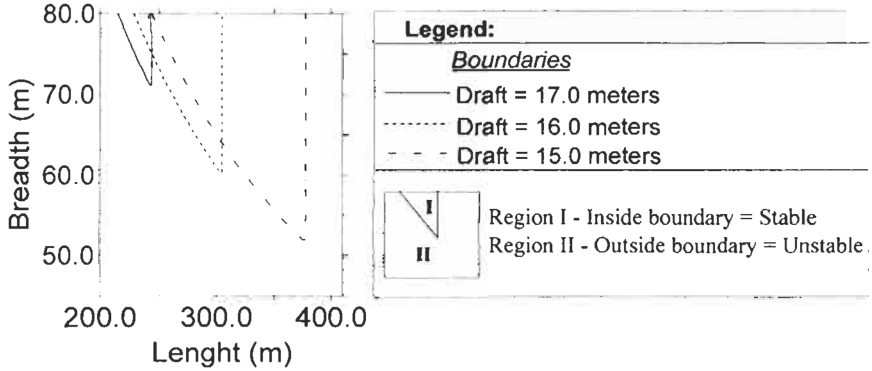

Figure 3: Stability map for three different drafts

This conclusion associated with the installation of stabilizer devices suggests the use of a ship form like a barge provided with skegs as stabilizer devices. Such configuration has already been used in the offshore industry and presents advantages in many aspects such as stability, cost and construction. The methodology used here can be improved by the use of expressions for the calculation of the hydrodynamic derivatives specifically developed for barge-ship forms, although, for the preliminary design stage analysis, the present results are very satisfactory.

6 STABILITY ANALYSIS IN THE OFFLOADING OPERATION

The stability analysis for the offloading operation with a FPSO (L = 320 m, B = 52 m, H = 21 m, Δ = 300 kton) , converted from a VLCC to operate in a water depth of 780 meters, connected to a 130 kton shuttle is performed for different incidence angles of the current with magnitude of 2.0 knots. The mooring system consists of ten lines in the forebody and eight lines in the aftbody with symmetry in relation to the longitudinal plane in a DICAS configuration. Figure 4a presents the real part of the twelve eigenvalues as functions of the incidence angle of the current. It can be observed that the real parts of the six eigenvalues associated to the FPSO are negative for most of the current incidence angles. The presence of the shuttle introduces an unstable behavior to the system. It should be emphasized that the shuttle has a stable behavior around the equilibria when connected to a single point mooring. In order to extend the stability analysis; a time domain simulation is carried out for the FPSO-Shuttle configuration with a current coming from astern. The results are presented in figures 4b.

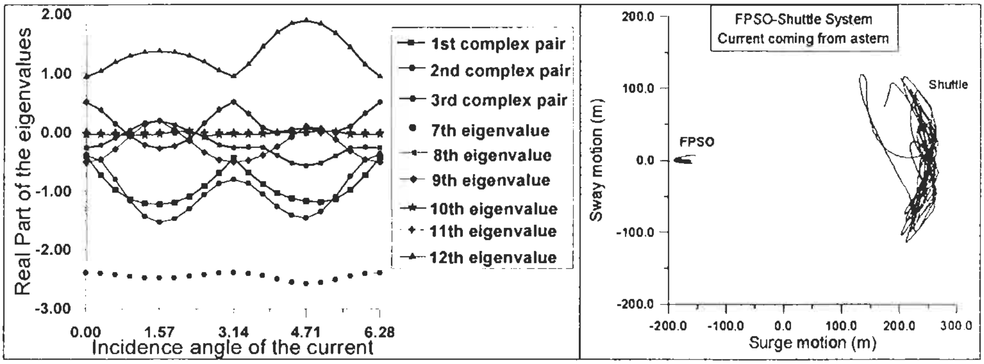

Figure 4: a) Eigenvalues of the system and b) Sway versus Surge motion

As observed in figure 4b, the system is unstable. The instability is more related to the shuttle, while the FPSO shows an almost stable behavior. These results are in agreement with the stability analysis. Although the FPSO execute small excursions, they are large enough to stimulate the unstable behavior of the shuttle.

In field operation it is common to use a tug to assist the offloading procedure. In this case the tug can be used as a stabilizer device. For the case simulated above a tension equal to 65 tonf was applied to a 200 meters long cable connected to the stern of the shuttle ship, provided by the tug. The stability analysis shows that the system is stable around the equilibria, since none of the eigenvalues have positive real part (real part of the eigenvalues: -0.4087, -0.4087, - 0.2463, -0.2463, -0.3535, -0.3535, -0.3691, -0.3691, -0.5025, -0.5025, -0.03024, 0.0). The time domain simulation also confirms this.

Acknowledgements

The authors thank ANP (Brazilian National Petroleum Agency) and CNPq (Brazilian National Agency for Research and Technological Development) for the support to this work.

References

Abkowitz, MA, (1964). Lectures on Ship Hydrodynamics Steering and Maneuverability, Report No. Hy-5, Hydro-og Aerodynamisk Laboratorium, Lyngby, Denmark.

Abkowitz, MA, (1967). Stability and Motion Control of Ocean Vehicles, MIT Press.
Abkowitz, MA, (1980). Mesurement of hydrodinâmic characteristics from ship maneuvering trials by system identification, *Transactions SNAME.* **89**, 283-318.

Clarke, D. Gedling, P and Hine, G, (1982). The Application of Manouvering Criteria in Hull Design Using Linear Theory, *Transactions of the Royal Institution of Naval Architects*, UK.

Eda, H and Crane Jr., CL, (1965). Steering Characteristics of Ships in Calm Water and Waves. *Transaction of SNAME.* **73**.

Fernandes, AC and Sphaier, SH (1997). Dynamic Analysis of a FPSO System. *ISOPE'97.* Hawaii, USA.

Fernandes, AC, Sphaier, SH and Correa, SHS (1999). The Feasibility of a Central Turret in FPSO Systems. *Journal of OMAE.*

Garza-Rios, L.O. and Bernitsas, M.M., (1996). Analytical Expressions of the Stability and Bifurcation Boundaries for General Spread Mooring Systems, *Journal of Ship Research.* **40:4**.

Garza-Rios, L.O. and Bernitsas, M.M. (1998). Analytical Expressions for Stability and Bifurcations of Turret Mooring Systems, *Journal of Ship Research.* **42:3**.

Garza-Rios, L.O. and Bernitsas, M.M. (1999). Slow motion dynamics of turret mooring and its approximation as single point mooring, *Applied Ocean Research.* **21**, 27-39.

Matter, GB, Sales Jr., JS and Sphaier, SH. (2001a). An Analytical Procedure to Analyze the Maneuvering Stability of FPSO's Systems in the Design Stage. *OMAE'2001.* Rio de Janeiro, Brazil.

Matter, GB, Sales Jr., JS, Sphaier, SH, Correa, SHS and Masetti, IQ. (2001b). Dynamic Analysis of the DICAS Mooring configuration for Floating Systems. *ISOPE'2001.* Stavanger, Norway.

Sphaier, SH., Fernandes, AC, Pontes, LGS and Correa, SHS. (1998). Waves and Current Influence in the FPSO Dynamics. *ISOPE'98.* Montreal, Canada.

Sphaier, SH., Fernandes, AC and Correa, SHS. (1999). The Unstable Offloading of a FPSO. *ISOPE'99.* Brest, France.

Sphaier, SH, Fernandes, AC and Correa, SHS. (2000a). Maneuvering Model for the FPSO Horizontal Plane Behavior. *ISOPE'2000.* Seattle, USA.

Sphaier, SH, Fernandes, AC and Correa, SHS. (2000b). Maneuvering Coefficients from Model Test for FPSO's Station Keeping Behavior. *OMAE'2000.* New Orleans, USA.

Thwaites, B. (1960). Incompressible Aerodynamics, Reprinted by Dover.

Practical Design of Ships and Other Floating Structures
You-Sheng Wu, Wei-Cheng Cui and Guo-Jun Zhou (Eds)
© 2001 Elsevier Science Ltd. All rights reserved

EXTREME RESPONSE AND FATIGUE DAMAGE OF SHIP-SHAPED FPSO

Chun-Tian Zhao, Yong Bai and Yung Shin

American Bureau of Shipping,
16855 Northchase Drive, Houston, TX 77060

ABSTRACT

In the design of ship-shaped Floating Production Storage Offloading (FPSO) systems, a rational strength assessment is required to ensure structural safety. This paper presents a systematic method to predict extreme response and conduct fatigue assessment, in which the site-specific wave conditions and the service history are accounted for. The extreme response is predicted using both short-term and long-term approaches, and the fatigue strength is assessed using a closed-form spectral fatigue method. The proposed approach may be applied to newly built or converted FPSOs.

KEY WORDS

FPSO, FPI, Extreme Response, Strength, Fatigue

1 INTRODUCTION

A FPSO is usually designed for a specific installation site. The site-specific wave environment has to be taken into account for each design. In addition, if the FPSO is a conversion from an oil tanker, the evaluation of past fatigue damage is required. This paper aims at developing a reliable and systematic method with consideration for the long-term wave conditions involved with assessing extreme structural response and fatigue damages.

To predict the extreme load or extreme structural response, various methods have been proposed (Ochi, 1981). In this paper, approaches based on both long-term and short-term (survival storm) wave data are recommended, depending on the conditions of application.

In the fatigue-damage, a simplified method is sometimes used, in which a Weibull distribution for the long-term responses is usually assumed, and Weibull parameters are determined in advance. Due to the excessive sensitivity of estimated fatigue damage to the Weibull parameters, this kind of method is basically not reliable if the Weibull parameters are not exactly known. Providing accurate values for the Weibull parameters in advance is very difficult because these values are environment and response dependent (Chen, 1988). In this paper, closed-form spectral fatigue integration is applied.

2 WAVE CONDITIONS

Wave conditions used in the strength and fatigue assessment should cover all operational modes, including normal operation, transition, and extreme-storm survival conditions. In the following discussion, both short-term and long-term descriptions of sea states are used.

The slowly varying local sea state can be reasonably assumed to be stationary in a 'short' time interval, for instance, in a three-hour duration. A sea state is usually described by a wave spectrum, which describes only a short-term sea state. The extreme value based on a short-term sea state is referred to as *short-term* extreme. In predicting extreme responses by the short-term method, an family of 'extreme' storm wave spectra based on long-term wave statistics is usually required as the short-term sea states.

Suitable wave spectra should be chosen to represent the waves for different geographical regions and wave development stages. For example, the Bretschneider wave spectrum is usually employed to describe tropical storm waves, such as those generated by hurricanes in the Gulf of Mexico or typhoons in the South China Sea. The JONSWAP wave spectrum is used to describe winter storm waves of the North Sea. Both Bretschneider and JONWASP ($\gamma = 3.3$) wave spectra are used in the following examples to investigate their effects on extreme values and fatigue damage.

To reflect the variation of sea states, long-term description is required. The Wave Scatter Diagram (WSD) provides a joint probability table of significant wave heights and characteristic periods for a local site. To obtain a WSD, various short-term wave data are statistically averaged, which have been accumulated over a long period of time (for example, 10 years or more) and cover all sea states defined by different combinations of pairs (H_S, T). Two WSDs are retrieved from ABSWAVE database for zones W156 and W391. Contours of these WSDs are compared in Figure 1. Obviously, the wave environment at site W156 is much more severe than that at W391. The extreme value based on the long-term description of sea states is referred to as *long-term* extreme. Wave directional probability corresponding to each WSD table should be provided also. Figure 2 shows the wave directional probability distributions at these two grid zones with 24 directional divisions (refer to Figure 4). The time length T_S for each short-term wave record in a WSD should be the same.

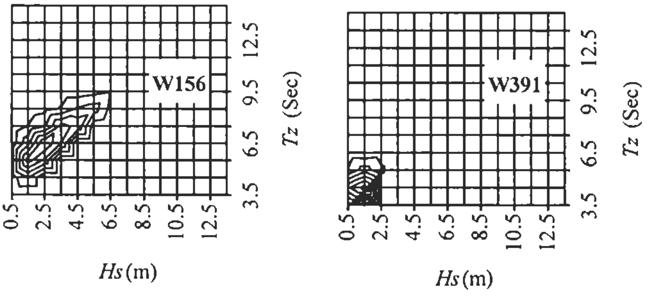

Figure 1: Graphic comparison of Wave Scatter Diagrams for two locations (W156: A site in the North Sea ; W391: A site in the Gulf of Mexico)

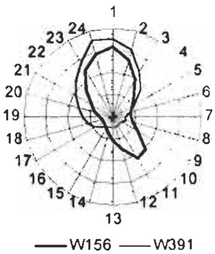

Figure 2: Wave directional probabilities for a FPSO

A WSD provides a long-term wave description for only one specific region. To assess the fatigue damage on past route services, additional wave information along the routes is necessary. For this purpose, a global wave database can be used, from which wave data for any wave zone on the service route can be retrieved.

ABSWAVE is a global wave database, covering the world's oceans with 1,103 wave grid zones. It is derived from a numerically predicted, 10-year averaged hindcast wave database, GSOWM. For each wave zone, a complete WSD is stored with its associated directional probability distribution of waves. Figure 3 shows the global wave grid of ABSWAVE and two example ship routes.

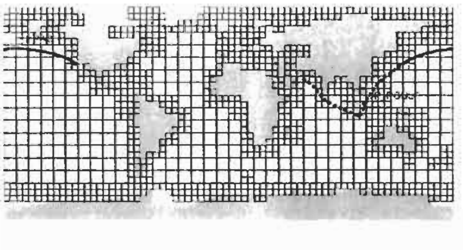

Figure 3: Wave grid of ABSWAVE database and two example service routes

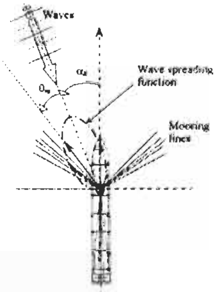

Figure 4: A FPSO system and coordinates for wave directionality and wave spreading

3 HYDRODYNAMIC LOADS AND STRUCTURAL RESPONSES

Determining the stress Frequency Response Function (FRF), $H(\omega; \alpha_k, \Lambda_l)$, is one of the major efforts in the strength assessment. The general procedure is

1. defining the major service profiles for a FPSO based on the operations that affect the local deck and storage tank loads and global motion responses significantly. Typical operations include normal operation, storm survival condition, loading condition and offloading condition.
2. determining a series of static deck and tank loading patterns Λ_l based on the major service profiles.
3. calculating the hydrodynamic forces on the FPSO and global motion responses under the action of the mooring system and hydrodynamic forces for each Λ_l,
4. loading the hull-girder structure under each Λ_l, wave frequency and wave heading. The following components should be included (Zhao, 1996; ABS, 1992):
   - i. static deck and internal tank loads
   - ii. static structural loads
   - iii. hydrostatic forces
   - iv. hydrodynamic forces
   - v. motion induced hydrostatic restoring forces
   - vi. motion induced structural inertial loads and internal tank sloshing loads
   - vii. mooring forces
   - viii. shear forces, bending moments and torsional moments as structural boundary conditions if the structural model contains middle holds only.

   Components i to iii are static and must be included in overall strength assessment. In this paper, only dynamic components are considered. For ocean-going vessels, ABS uses the Dynamic Loading Approach (DLA) (Liu *et al*, 1992) to calculate the wave and motion induced loads. Steps 1 through 4 of the above procedure may be used to extend the DLA to offshore structures.
5. performing structural analysis to calculate stress FRF $H(\omega; \alpha_{k,}\Lambda_l)$ for each wave frequency ω, wave heading α_k, and loading pattern Λ_l. Each combination of $(\omega;\alpha_k,\Lambda_l)$ forms a loading case in structural analysis. The Finite Element (FE) method or other simplified structural analysis can be applied,

depending on the level of analysis. For example, to check the strength of deck and bottom plating in the hull-girder strength level, calculations using vertical bending moment and sectional modulus can provide satisfactory results.

The hydrodynamic force components consist of incident wave forces, diffraction wave forces and motion-induced radiation forces (added mass and damping forces). The potential theory of fluid mechanics with boundary element method using source distribution can be applied to numerically calculate the hydrodynamic forces. Currently, hydrodynamic analysis software using a three-dimensional modeling (preferred) or two-dimensional strip method is widely applied. A detailed discussion of numerical techniques and other effects of loads (such as bow flare impacting, bottom slamming, green water, ice loads, and accident loads) on the extreme response and fatigue are beyond the scope of this paper, and will not be discussed further.

The wave heading α_k is defined with respect to a FPSO (see Figure 4). Depending on the mooring type, the wave probability at direction α_k needs to be converted into FPSO local coordinates. For example, if the turret-mooring system is adopted, the weathervaning should be considered, and some of the wave headings can be removed.

The stress FRFs of a deck plating at twenty-four incident wave directions are calculated by using the 2D strip method and cross-sectional modulus for the purposes of illustration (3D hydrodynamic and FE method can be used for general structural details). With the WSD and the FRF, the spectral density function $S_x^{ijkl}(\omega)$ of the responses x (stresses or loads) to a wave spectrum can be determined.

4 EXTREME RESPONSE

Strength analysis generally involves assessing the yielding strength, buckling strength, ultimate strength and fatigue strength. Details of structural strength and fatigue evaluation may be found in Bai (2001) and ABS (2000). The first three aspects of structural strength are directly related to the extreme values of stress responses, which will be discussed in this section. The fatigue strength assessment will be covered later.

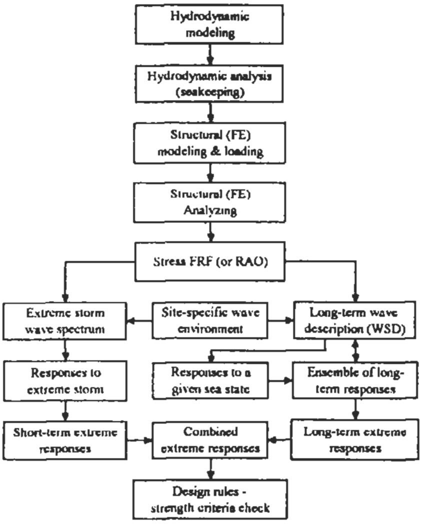
Hydrodynamic modeling
Hydrodynamic analysis (seakeeping)
Structural (FE) modeling & loading
Structural (FE) Analyzing
Stress FRF (or RAO)
Extreme storm wave spectrum
Site-specific wave environment
Long-term wave description (WSD)
Responses to extreme storm
Responses to a given sea state
Ensemble of long-term responses
Short-term extreme responses
Combined extreme responses
Long-term extreme responses
Design rules - strength criteria check

Figure 5: FPSO Strength assessment procedure

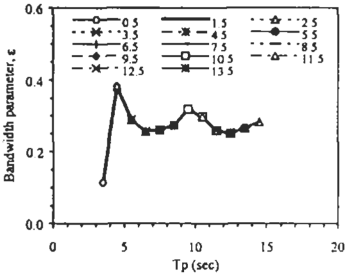

Figure 6: Variation of bandwidth parameters of stress responses vs. T_P and H_S (Wave spectrum used : JONSWAP; Wave: W156)

Figure 5 demonstrates the strength assessment procedure, which uses short-term and long-term approaches. Ochi (1978) showed that both long- and short- term approaches predict very close extreme values. Although their extreme values depend on the number of members of the derived spectral family in their examples, it seems that applying one approach is good enough. However, this is only true for ideal situations. As a matter of fact, using either approach cannot guarantee conservative design in practice because of the following reasons:

(a). It is difficult to exactly predict the extreme storm spectrum defined with (H_S, T). For example, in different wave development stages or regions of a storm, the characteristic wave period may be different even with the same H_S.

(b). Structural responses depend on both incident wave height and wave frequency. It is obvious that an extreme storm may not generate the largest structural response.

(c). The WSD currently used in the long-term extreme prediction may be incomplete to cover all severe storms (not enough data), while the long-term extreme value predicted is sensitive to those storms. Therefore, if possible, both short-term and long-term approaches should be used to achieve conservative design.

4.1 Short-term Extreme Approach

The short-term extreme values can be estimated based on a known initial probability distribution of maxima. For a response spectrum with $\varepsilon \le 0.9$, the probability density function of maxima (peak values) can be generally represented as

$$p(x) = \frac{2}{1+\sqrt{1-\varepsilon^2}}\left[\frac{\varepsilon}{\sqrt{2\pi m_0}}\exp(-\frac{x^2}{2\varepsilon^2 m_0}) + \sqrt{1-\varepsilon^2}\,\frac{x}{m_0}\exp(-\frac{x^2}{2m_0})\phi(\frac{\sqrt{1-\varepsilon^2}}{\varepsilon}\frac{x}{\sqrt{m_0}})\right] \quad (x \ge 0) \qquad (1)$$

in which $\phi(r) = \frac{1}{\sqrt{2\pi}}\int_{-\infty}^{r}\exp(-\frac{r^2}{2})dr$, $\varepsilon = \sqrt{1-\frac{m_2^2}{m_0 m_4}}$, where m_0, m_2, and m_4 are the moments of response spectral density functions of zero-th, second, and fourth order, respectively. The Probable

Extreme Value (PEV) at possibility level α (risk parameter) can be determined by (Bhattacharyya, 1978; Ochi, 1981)

$$x_{ext}\big|_{\alpha} = \sqrt{2\ln\left(\frac{2\sqrt{1-\varepsilon^2}}{1+\sqrt{1-\varepsilon^2}}\frac{N}{\alpha}\right)}\sqrt{m_0} = \sqrt{2\ln\left(\frac{(60)^2 T_S}{2\pi\alpha}\sqrt{\frac{m_2}{m_0}}\right)}\sqrt{m_0} \qquad \text{for } \varepsilon \le 0.9 \quad (2)$$

in which N is the number of observations (or cycles), $N = (60)^2 \frac{T_S}{4\pi} \cdot \frac{1+\sqrt{1-\varepsilon^2}}{\sqrt{1-\varepsilon^2}} \sqrt{\frac{m_2}{m_0}}$, and T_S is the time length of wave data, unit of time in hours. When α=1, $x_{PEV}=x_{ext}|_{\alpha=1}$ represents the value that may be exceeded once out of N observations. α (≤ 1) is chosen at the designer's discretion, depending on the condition of application. Figure 6 indicates the dependency of ε vs. spectral peak periods in a WSD. In this figure, the range of ε of the stress responses is mostly between 0.25 and 0.40. It is found that ε can easily be close to 0.4, and an error at the 5% to 10% level could be introduced for N if ε is ignored. So it is suggested that a correction for ε should always be used.

When the short-term approach is used, a design wave spectrum of the extreme storm condition is usually provided with a long-term extreme value of H_S and related T. Ochi's (1981) results indicate that the probability density function of (H_S, T) takes a bivariate log-normal distribution. A commonly used approach is to determine the long-term extreme of H_S first, and then the T is obtained with the conditional probability distribution $p(T|H_S)$ or a simple formula between H_S and T based on the wave steepness.

The long-term PEV of H_S with different return periods is listed in Table 1, in which H_S is calculated by applying the long-term extreme approach discussed in the next section. To determine the extreme wave environment (two parameter wave spectra in this example) used in the short-term approach, T_P is required. Table 2 lists the peak periods associated with H_S. The values of T_P are calculated by using $p(T|H_S)$ at confidence levels 0.5, 0.75, 0.85, and 0.95, separately (Ochi, 1978). Each H_S and the related T_P form a wave spectral family, which is used to determine the response spectrum, and finally the short-term extreme values.

Table 1 Extreme significant wave height

Wave	H_S (m) with Return period		
	20 years	50 years	100 years
W156	17.0	18.2	19.1
W391	10.2	11.6	12.6

Table 2 Wave spectral family with different H_S

	H_S (m)			Weighting factor
	17.0	18.2	19.1	
T_P (sec)	13.1	13.4	13.5	0.0500
	13.8	14.1	14.3	0.0500
	14.8	15.0	15.2	0.0875
	15.7	16.0	16.2	0.1875
	16.6	16.8	17.0	0.2500
	18.4	18.7	18.9	0.1875
	19.7	19.9	20.1	0.0875
	20.7	21.0	21.2	0.0500
	22.1	22.4	22.6	0.0500

Table 3 Short-term stress extreme values

Method	Wave	Spectrum	Stress (Kgf/cm^2)		
			20 year	50 year	100 year
I	W156	JONSWAP	2021.0	2135.4	2139.6
	W156	Bretschneider	1991.9	2121.4	2156.2
	W391	JONSWAP	1288.6	1446.9	1527.6
	W391	Bretschneider	1211.0	1372.7	1467.4
II	W156	JONSWAP	2304.1	2468.7	2565.7
	W156	Bretschneider	2081.3	2226.6	2334.0
	W391	JONSWAP	1381.3	1568.0	1714.7
	W391	Bretschneider	1248.9	1412.8	1547.2

Table 4 Long-term stress extreme values

Wave	Spectrum	Stress (Kgf/cm^2)			Cycles per hour
		20 year	50 year	100 year	
W156	JONSWAP	2476.9	2669.3	2818.2	509.2
W156	Bretschneider	2166.4	2328.0	2452.8	500.9
W391	JONSWAP	1751.6	1982.9	2169.9	694.0
W391	Bretschneider	1676.6	1899.1	2079.0	673.2

To apply Eq. 2, m_0 and m_2 need to be calculated properly. Table 3 compares the short-term stress extreme values of the deck plate obtained by two different methods. Method I uses the weighting factors listed in Table 2 to calculate the mean values of m_0 and m_2, while method II uses each member of the spectral family in Table 2, and takes the maximum. The extreme values provided by the latter are up to 16% larger than those by the former method. This is understandable because the sample size (or exposure time) for the latter is relatively larger. In this example, extreme values for H_S with risk parameter $\alpha = 1$ are directly applied. Obviously, the final extreme values of responses are dependent on the designer's discretion and choice of H_S.

4.2 Long-term Extreme Approach

To predict a long-term extreme value, a long-term initial cumulative probability distribution function $P(x)$ of responses is required. Although function $P(x)$ cannot be predicted explicitly due to the complications of the responses in various sea states, it can be built up approximately through accumulations of short-term statistical analyses. Generally, $P(x)$ can be assumed to be in the form of

$$P(x) = 1 - \exp[-q(x)] \qquad (q(x) \geq 0) \qquad (3)$$

In practice, a Weibull distribution or log-normal distribution is commonly used for $P(x)$. In this paper a generalized form suggested by Ochi (1981) is used to achieve higher accuracy in the curve fitting. *i.e.*, $q(x) = cx^m \exp(-\rho x^k)$, in which c, m, ρ, and k are four constant parameters to be determined by nonlinear least-squared fitting. Once the mathematical expression of $P(x)$ in Eq. 3 is obtained, the long-term PEV can be determined by

$$1 - P(x_{ext}|_\alpha) = \frac{\alpha}{N} \qquad (4)$$

Here α is the possibility level as in Eq. 2. Here N is the number of observations or cycles related to the return period. In the design of offshore structures, a return period of 100 years is widely used for estimating the long-term extreme values. When the WSD is applied, the $P(x)$ above can be obtained by using the definition of probability density function of maxima

$$p(x) = \frac{\sum\limits_{i,j,k,l} n_{ijkl} \Pr(w_{ij}) \Pr(\alpha_k) \Pr(\Lambda_l) p_{ijkl}(x)}{\sum\limits_{i,j,k,l} n_{ijkl} \Pr(w_{ij}) \Pr(\alpha_k) \Pr(\Lambda_l)} \qquad (5)$$

where

$Pr(w_{ij})$:	normalized joint wave probability of $(H_S(i),T(j))$ or cell w_{ij} in WSD, $\sum\limits_{i,j} \Pr(w_{ij}) = 1$.
$Pr(\alpha_k)$:	probability of wave in direction α_k, $\sum\limits_{k} \Pr(\alpha_k) = 1$.
$Pr(\Lambda_l)$:	probability (or percentage) of loading pattern Λ_l during service, $\sum\limits_{l} \Pr(\Lambda_l) = 1$.
n_{ijkl}:	average number of responses in T_S corresponding to cell w_{ij} of WSD, wave direction α_k and loading pattern Λ_l.
$p_{ijkl}(x)$:	the probability density function of short-term response maxima associated with n_{ijkl}.

Figure 7 displays the long-term $p(x)$ of stress responses to waves W156 and W391. It is obvious that the wave environment is the dominant factor affecting the long-term probability distribution; the effects of spectral shape are not significant.

After the mathematical formula of $q(x)$ in Eq. 3 has been determined by curve fitting, the extreme value can be calculated by Eq. 4. Figure 8 compares the long-term extreme values for wave zones W156 and W391 using the JONSWAP and Bretschneider spectra. The extreme values of stress dynamic components are listed in Table 4. By comparing the long-term extreme values to those short-term extreme values listed in Table 3, it is found that the extreme values provided by the long-term approach are larger up to 9%. Because the long-term approach uses the probability distribution of responses directly, it can avoid the uncertainty caused by the choice of extreme H_S and associated wave spectral family (a series of T_P). Based on this point of view, the long-term approach is more reliable than the short-term approach under the circumstances of same environmental information available.

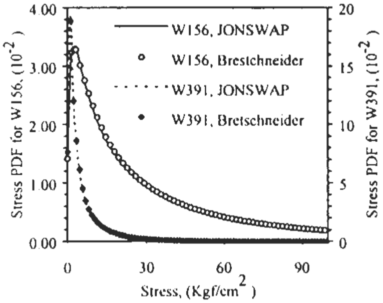

Figure 7: Long-term probability density function $p(x)$ of stress responses for deck plate

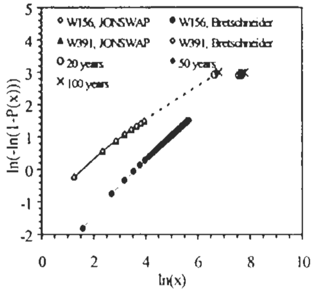

Figure 8: Long-term extremes of stress for deck plate with return period: 20, 50, 100 years

5 FATIGUE DAMAGE EVALUATION

The fatigue strength of welded joints and structural details in highly dynamically stressed areas need to be assessed to ensure structural integrity and to optimize the inspection plan. The analyses of fatigue strength should be based on the combined effects of loading, material properties, and flaw characteristics. At the global scantling design level, the fatigue strength check for hull-girder members can be conducted for screening purposes. At the final design level, analyses for structural notches, cutouts, bracket toes, and abrupt changes of structural sections need to be performed. In addition, deck facilities, pipelines, risers, mooring system and its interface structure with the FPSO hull also need to be designed with adequate fatigue strength.

Stress types commonly used by fatigue analysis based on the S-N curve include nominal stress, hot-spot stress, and notch stress. Each of these methods has specific applicable conditions. Although nominal stress is used in the examples, the analysis approach is not limited to any stress type.

5.1 Spectral Fatigue Analysis

Spectral Fatigue Analysis (SFA) based on the S-N curve and Palmgren-Miner's cumulative damage hypothesis has been widely applied in the fatigue damage assessment of offshore structures. However, choosing a proper method is important to avoid unnecessary numerical errors. Figure 9 shows the procedure for fatigue assessment, which applies the 'closed-form' integration to eliminate the error due to numerical integration.

Denote the stress range by s ($s = 2a$, where a is the amplitude), then the short-term probability density function $p_{ijkl}(s)$ can be approximated by the Rayleigh distribution as

$$p_{ijkl}(s) = \frac{s}{4\sigma_{ijkl}^2}\exp\{-\frac{1}{8}(\frac{s}{\sigma_{ijkl}})^2\} \tag{6}$$

where σ_{ijkl} is the variance of stress responses, *i.e.*, $\sigma_{ijkl}^2 = m_0^{ijkl}$. The total damage in T_D (unit in years) can be represented by

$$D = \frac{T'_D}{T_S}\sum_{i,j} D_{ij} = T'_D \sum_{i,j,k,l} f_{ijkl}\Pr(w_{ij})\Pr(\alpha_k)\Pr(\Lambda_l)\int_0^\infty \frac{s^m}{K} p_{ijkl}(s)ds \tag{7}$$

where T'_D (unit in hours) is the duration of service T_D, D_{ij} is the long-term based, average fatigue damage caused by cell w_{ij} of WSD in T_S ; f_{ijkl} is the average number of cycles per unit time of a short-term response corresponding to cell w_{ij} of WSD, wave direction α_k and loading pattern Λ_l, $f_{ijkl} = n_{ijkl}/T_S$ (unit in 1/hour). With Eq. 6, D can be further simplified. For a two-segment S-N curve as shown in Figure 10, the total damage in T_D (unit in years) can be represented by

$$D = \frac{T'_D}{K} 2^{\frac{m}{2}} \Gamma(\tfrac{m}{2}+1) \sum_{i,j,k,l} f_{ijkl} \lambda_{ijkl} \mu_{ijkl} \Pr(w_{ij}) \Pr(\alpha_k) \Pr(\Lambda_l) (2\sigma_{ijkl})^m \tag{8}$$

in which $\mu_{ijkl} = 1 - \dfrac{\gamma(\frac{m}{2}+1, \upsilon) - \frac{K}{K'} (\frac{s_q}{\sqrt{\upsilon}})^{\Delta m} \gamma(\frac{m+\Delta m}{2}+1, \upsilon)}{\Gamma(\frac{m}{2}+1)}$, integral $\gamma(\rho, x) = \int_0^x r^{\rho-1} \exp(-r) dr$ is the incomplete gamma function, and $\upsilon = \upsilon_{ijkl} = \frac{1}{2} (\frac{s_q}{2\sigma_{ijkl}})^2$. in which the rain flow correction $\lambda(m, \varepsilon_{ijkl}) = a(m) + \{1 - a(m)\}(1 - \varepsilon_{ijkl})^{b(m)}$ has been introduced to improve the counting of cycles of the stress fluctuation. λ can be determined by curve fitting (Wirsching, 1980) as $a(m) = 0.926 - 0.033m$ and $b(m) = 1.587m - 2.323$. The two-segment S-N curve consists of the first segment (K', m') for $0 \le s \le s_q$ and the second segment (K, m) for $s \ge s_q$, where $m' = m + \Delta m$. For a one-segment S-N curve, $\mu_{ijkl} = 1$.

From Eq. 7 or 8, the annualized fatigue damage $\overline{D}$ can be determined by letting T_D=1 year. When D = 1, T_D (T'_D) becomes the fatigue life T_L. Therefore, after considering the safety factor f_S, the fatigue life can be represented as

$$T_L = \frac{1}{f_S \overline{D}} \tag{9}$$

Table 5 lists the fatigue life and annualized fatigue damage with respect to the wave environments W156 and W391 using the JONSWAP and Bretschneider wave spectra, respectively. In this example, the S-N curve in Figure 10 is utilized. It is found that the fatigue life under a more severe environment (W156, in the North Sea) is much shorter than that under a more benign one (W391, in the Gulf of Mexico). Also, the choice of wave spectrum can have significant effects on the fatigue damage. The fatigue life predicted by using the JONSWAP spectrum is shorter (worse) than that predicted by using the Bretschneider spectrum in this example.

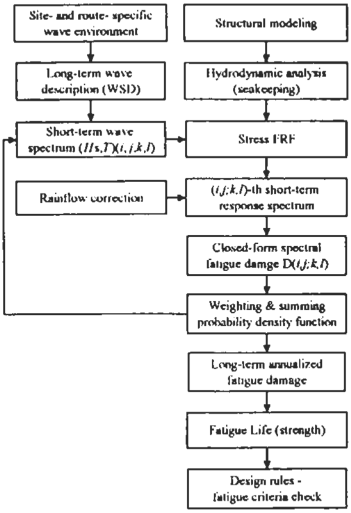
Site- and route- specific wave environment
Long-term wave description (WSD)
Short-term wave spectrum (Hs,T)(i,j,k,l)
Rainflow correction
Structural modeling
Hydrodynamic analysis (seakeeping)
Stress FRF
(i,j;k,l)-th short-term response spectrum
Closed-form spectral fatigue damge D(i,j;k,l)
Weighting & summing probability density function
Long-term annualized fatigue damage
Fatigue Life (strength)
Design rules - fatigue criteria check

Figure 9: Procedure of spectral fatigue analysis

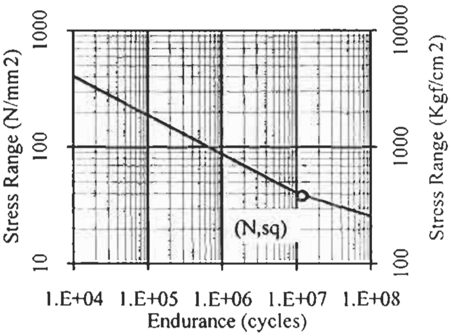

Figure 10: A typical two-segment S-N curve, $N = KS^{-m}$: (N,S_q) = $(10^7$, $39.8\text{N/mm}^2])$, (m',K')=$(5,9.975\times10^{14})$,(m, K)=$(3,0.315\times10^{11})$

Table 5 Fatigue analysis results

Wave	Spectrum	Fatigue Life	Annualized Fatigue Damage
W156	JONSWAP	15	6.615×10^{-2}
W156	Bretschneider	20	5.030×10^{-2}
W391	JONSWAP	795	1.258×10^{-3}
W391	Bretschneider	1100	9.093×10^{-4}

5.2 Fatigue Damage Assessment for Past Services

For a FPSO conversion, the fatigue damage D_H accumulated during its past route services can be calculated with theory similar to the above. The only difference is a new WSD should be derived based on the crossed wave zones in the global wave database and the percentage of time spent in each crossed wave zone. For an existing FPSO, past site services may have occurred. By adding the site-specific WSD to the derived WSD, the fatigue damage introduced in the site service is then covered. Finally, when the derived WSD is obtained, D_H can be calculated with Eq. 7 or 8, and the remaining fatigue strength D_R can be represented as

$$D_R = 1 - D_H \tag{10}$$

Similar to Eq. 9, the remaining fatigue life is

$$T_R = \frac{1 - D_H}{f_s \overline{D}} \tag{11}$$

6 CONCLUSIONS

A systematic method for FPSO analysis has been developed to predict extreme response and fatigue assessment under varying wave conditions. The results indicate that:

- FPSO design is highly wave condition dependent. Both extreme response and fatigue life can be significantly affected by site-specific wave environments. Collecting accurate wave data is an important part of the design.
- Wave spectral shapes have significant effects on fatigue life. Choosing the best suitable spectrum based on the associated fetch and duration is required.
- The bandwidth parameter ε of responses is dependent on spectral (peak) period only. The effects of H_S on ε can be ignored. The value of ε can easily approach 0.6 for waves, 0.4 for stress responses. In the calculation, ε should not be simply ignored; Otherwise, an additional error of 5% to 10% could be introduced.
- In predicting extreme responses, the long-term approach is preferred because it has less uncertainty. However, the authors recommend using the long-term approach together with the short-term approach for obtaining a conservative result.
- The short-term extreme approach depends on long-term prediction of extreme wave spectra and proper application of the derived wave spectral family. It is not necessarily simpler than the long-term approach.
- In the examples, probable extreme values predicted by long-term approach are larger than that by short-term approach up to 9% (when $\alpha=1$).
- The proposed method for extreme response and fatigue assessment is reliable and applicable to any type of FPSO, including FPSO conversions.

ACKNOWLEDGEMENTS

The authors wish to thank Dr. D. Liu, Senior Vice President, for his encouragement and support. The views expressed in this paper are those of the authors and are not necessarily those of ABS.

References

ABS (1992). Analysis Procedure Manual for the Dynamic Loading Approach (DLA) for Tankers. *American Bureau of Shipping.*

ABS (2000). Guide for Building and Classing Floating Production Installations. *American Bureau of Shipping.*

Bai, Y (2001). Marine Structural Design. *Elsevier Ocean Engineering Book Series*, to be published by Elsevier Science.

Bhattacharyya, R (1978). Dynamics of Marine Vehicles. John Wiley & Sons, Inc.

Chen, YN and Mavrakis, SA (1988). Closed-Form Spectral Fatigue Analysis for Compliant Offshore Structures. *Journal of Ship Research*, **32:4**, 297-304.

ISSC (2000). Specialist Committee V.4: Structural Design of Floating Production Systems. *14th International Ship and Offshore Structures Congress 2000.* Nagasaki, Japan, **2**.

Liu, D, Spencer, J, Itoh, T, Kawachi, S and Shigematsu, K (1992). Dynamic Load Approach in Tanker Design. *SNAME Transactions*, **100**, 143-172

Ochi, MK (1978). Wave Statistics for the Design of Ships and Ocean Structures. *SNAME Transactions*, **86**, 47-76.

Ochi, MK (1981). Principles of Extreme Value Statistics and their Application. *SNAME, Extreme Loads Responses Symposium, Arlington,* 15-30.

Wirsching, PH and Light, MC (1980). Fatigue under Wide Band Random Stresses. *J. Structural Div.*, 1593-1606.

Zhao, CT (1996). Theoretical Investigation of Springing-ringing Problems in Tension-Leg-Platforms. *Dissertation, Texas A&M University.*

Practical Design of Ships and Other Floating Structures
You-Sheng Wu, Wei-Cheng Cui and Guo-Jun Zhou (Eds)
© 2001 Elsevier Science Ltd. All rights reserved

AN INVESTIGATION INTO WAVE INDUCED DRIFT FORCES AND MOTIONS OF VERY LARGE FLOATING STRUCTURES

N. Ma[1], T. Hirayama[2] and K. Ishikawa[3]*

[1]National Research Institute of Fisheries Engineering
Ebidai, Hasaki, Kashima, Ibaraki, Japan
[2]Department of Naval Architecture and Ocean Engineering
Yokohama National University
Tokiwadai 79-5, Hodogaya-ku, Yokohama, Japan
[3]Sumitomo Heavy Industries, Ltd., Yokosuka, Japan

ABSTRACT

In this paper, the drift forces and motions of very large floating structures (VLFS) in head waves are investigated through numerical simulations and model experiments. Three dimensional numerical method based on direct integration of pressure is applied to estimate the steady wave drift forces taking the elastic modes into account. Numerical simulations and experiments are performed with respect to two different types of VLFS, pontoon unit type and semi-submersible unit type. Consequently, the different tendency of motion and wave drift force of these two types had been shown. The numerical results were verified by the corresponding model experiments using large elastic floating models. Based on the results, the authors conclude that the near field theory is applicable for predicting both hydro-elastic response and wave drift force of flexible floating structure with fair accuracy sufficiently, the elastic deformation of structure can be taken into account satisfactorily by using mode superposition method. Furthermore, the effects of bending rigidity on both motion and wave drift force are discussed.

KEYWORDS

Very large floating structure, Steady drift force, Hydro-elasticity, Deflection, Numerical simulation, Near field theory, Mode superposition

1 INTRODUCTION

Very large floating structures (VLFS) are expected to become feasible candidates for purpose of floating airports, agriculture bases, storage facilities and floating piers and so on, especially in areas where lack adequate land. Nowadays, the possibility of utilization of VLFS had been enhanced where lack adequate land. Nowadays, the possibility of utilization of VLFS had been enhanced gradually through recent researches and developments. A varieties of researches on response in waves can be found (for example, Mamidipudi & Webster (1994), Hirayama & Ma (1995a), Kashiwagi & Furukawa (1997), Ohkusu & Namba (1998)), however, most of concerns in these studies are paid on hydro-elastic response, which is considered to be induced by first order wave forces in general. On the other hand, as many other floating structures, wave drift forces and mooring problem is one of key points in design. Therefore, an adequate prediction method for the wave drift force is indispensable. However, for the reason of enormous structure size and complexity arose from the existence of elastic deformation modes, few studies both theoretically and experimentally are available (Maeda et al (1998)). Thus, the basic knowledge on wave drift forces as well as wind, current loads on VLFS are considered to be insufficient from the viewpoint of establishment of the design synthesis.

---

* Formerly Graduate School of Yokohama National University

In this paper, three dimensional numerical method based on direct integration of pressure was applied to estimate the steady wave drift forces. The results have been verified by the corresponding model experiments in wave basin using large elastic floating models, which are moored linear springs. Through the comparisons of numerical and experimental results, the availability of so-called "Near Field Theory" for predicting wave drift forces had been confirmed. It is shown that bending distortional modes, which dominate the deflection of structure, can be taken into account successfully using mode superposition approach. Furthermore, influence of flexibility on drift forces, which might be great interest of design, is discussed through numerical and experimental results.

The different tendencies of wave drift force of two typical VLFSs, i.e. semi-submersible unit and pontoon unit supported floating structure are discussed as well as their hydro-elastic responses. The important factors for design, such as shape of underwater floating unit, rigidity of structure are investigated consequently.

2 NUMERICAL PREDICTION

In order to predict the hydro-elastic response and drift force in regular waves, a widely used numerical method, three-dimensional source method was applied. The deformations of elastic structure were determined by modal analysis approach. By accomplishing these two analyses, hydro-elastic response can be obtained easily by superposing the necessary modes. As for steady wave drift force, a so-called "Near Field Theory", which integrates the pressure of second order on wetted surface, was applied. The fluid is assumed to be ideal fluid, the motion and wave amplitude are assumed to be small. For the sake of simplicity, we limit the analysis to heading wave condition here.

2.1 Hydro-elastic Response Analysis

As it is well known, fluid motion surrounding oscillating body in regular waves can be described in forms of velocity potentials expressed as follows.

$$\phi(x,y,z,t)=\left[\phi_0(x,y,z)+\phi_d(x,y,z)+\sum_{r=1}^{m}\phi_r(x,y,z)p_r\right]e^{i\omega t} \tag{1}$$

Where, ϕ_0, ϕ_d, ϕ_r represents incident, diffracted, radiated wave respectively, p is the principal coordinate of mode including elastic deformation, m is number of mode (m= 1-6: rigid motions, m>6: elastic mode). For an undisturbed free surface of incident wave, we can write its potential as follows.

$$\phi_o=-\frac{ig\varsigma}{\omega}\cdot\frac{\cosh k(z+d)}{\cosh kd}\cdot e^{ik(x\cos\chi+y\cos\chi)}\cdot e^{-i\omega t} \tag{2}$$

ω, ζ, χ denote angular frequency, amplitude and incident angle of wave respectively, d is water depth, k is wave number which satisfies $\omega^2 = kg\tanh kd$.

In general, diffraction and radiation velocity potentials can be determined by solving Laplace Equation and applying suitable boundary conditions on free surface, sea bottom and wetted body surface. For the case of VLFS, the elastic modes can be considered as the manner as in Ma & Hirayama, 1997. In addition, hydrodynamic force and wave exciting force are evaluated directly; the motions and deflections can be obtained without many difficulties. The detail formulations are given in our previous paper (Hirayama and Ma (1995a), (1995b))

In head wave condition, deflection of the structure is mainly caused by vertical bending deformation, thus, the structure can be treated as an elastic uniform beam with two free ends. Then, vertical displacement is expressed as following equation.

$$\rho A\ddot{z} + \frac{\eta EI}{\omega}\frac{\partial^4 \dot{z}}{\partial x^4} + EI\frac{\partial^4 z}{\partial x^4} + kz = q(x,t), \qquad (0 < x < L) \tag{3}$$

where ρ is the mass density, A is the sectional area, η is the structural damping coefficient, EI is the bending rigidity, k is spring coefficient of foundation. L is beam length. q(x, t) represents external load acting at x coordinate. Over-dots denote differentiation with respect to time (t).

According to the principle of mode superposition, the deflection z can be represented as an aggregation of the product of mode function Z_r and principal coordinate p_r as shown in Eqn. 2.

$$z(x,t) = \sum_{r=1}^{m} Z_r(x) \cdot p_r(t) \tag{4}$$

In this study, we applied the analytic mode functions of beam for Z_r. The motion equation of principal coordinate of mode p_r is un-coupled and could be expressed as following.

$$(a_{rk} + A_{rk})\ddot{p}_r + (b_{rk} + B_{rk})\dot{p}_r + (c_{rk} + C_{rk})p_r = F_r e^{i\omega t} \tag{5}$$

Where a_{rk}, b_{rk}, c_{rk} are the generalized mass, structural damping and stiffness of mode, A_{rk}, B_{rk} are the generalized hydrodynamic added mass and damping coefficient respectively. C_{rk} is the generalized hydrostatic restoring force coefficient. Finally, the displacement of beam can be obtained from Eqn. 4.

2.2 Steady Wave Drift Forces

The steady drift forces in regular waves are the time averaged mean force due to second order pressure, and the forces can be obtained from integration the pressure on wetted surface (near field method). On the other hand, far field method is also available which is based on momentum theory (Maruo (1960)). In that, the momentums of fluid motions in far field are considered in terms of Kochin functions. However, the near field method provides straightforward way in solving the drift forces and the force are resolved into each component. Thus, the near field method is applied in this study. By using the perturbation approach, the final expression of horizontal drift force is given in Eqn.6 (Pinkster (1980)). Here, the contribution of second order potentials and hydrostatic force due to second order displacement are ignored.

$$\overline{F}_d^{(2)} = -\int_{WL}\frac{1}{2}\rho g\zeta_r^{(1)2}\cdot\overline{n}dl - \iint_{S_0} -\frac{1}{2}\rho\left|\overline{\nabla}\phi^{(1)}\right|^2\cdot\overline{n}ds - \iint_{S_0} -\rho(\overline{X}^{(1)}\cdot\overline{\nabla}\phi_t^{(1)})\cdot\overline{n}ds + \overline{\alpha}^{(1)}\times(M\cdot\ddot{\overline{X}}_g^{(1)}) \tag{6}$$

In which, $\overline{n}$ is normal vector of the point on wetted surface S_0, ζ_r is relative wave elevation, $\overline{X}_g$ is the motion of CG in space-fixed coordinate system, ϕ_t is time differential of velocity potential. $\overline{X}^{(1)}, \overline{\alpha}^{(1)}$ are first order linear and rotational motion vectors respectively, which satisfied the following relation.

$$\overline{X}^{(1)} = \overline{X}_g^{(1)} + \overline{\alpha}^{(1)} \times \overline{x} \tag{7}$$

Where, $\overline{x}$ is position vector of the point on wetted surface.

Once the first order potentials and motions are determined, the drift force will be able to obtained according to Eqn.6. For very large floating structure, the deformation due to elastic mode should be included and the results of hydro-elasticity analysis fore-mentioned are utilized.

3 VLFS MODELS AND EXPERIMENTS

In order to validate numerical results and to clarify the trend of wave drift forces of VLFS, model experiments were carried out in the towing tank (100m length, 8m width, 3.5m depth) of Yokohama National University. Semi-submersible units and pontoon units supported elastic floating models were used in experiments. The models are shown in Figure 1. The measurements of motions and deflections are also shown in the figure. Each model consists of 36 removable units, 12 lengthwise and 3 widthwise. Semi-submersible type unit is compromised of 4 column footings arrayed squarely and pontoon type unit is square shaped box with shallow draft. The elasticity of structure is modeled by connecting the units with aluminum beams transversely and longitudinally at top of supporting unit.

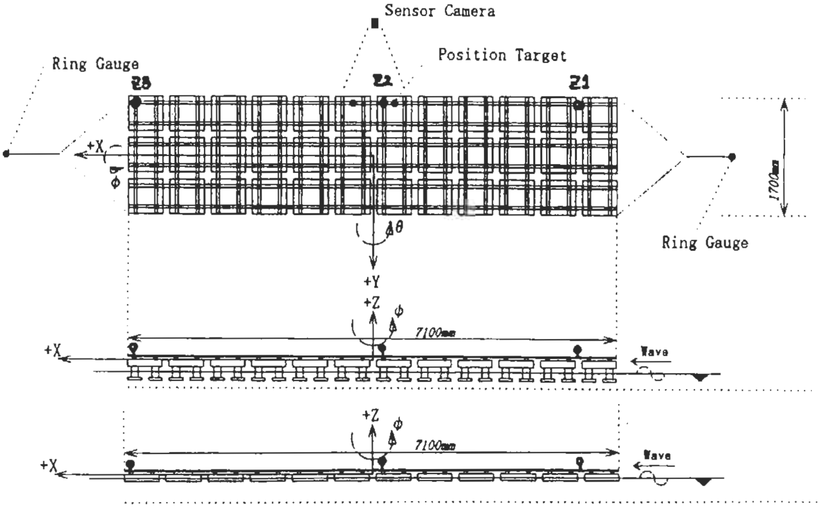

Figure 1: Very large floating models (upper: plan view, middle: side view of semi-sub, lower: side view of pontoon) moored by linear springs

The deflections were detected by using a non-touch type optical sensing system (Position Sensitive Detector cameras and LED). Two linear springs, pulleys and strings were used to moor the fore and aft end of the structure longitudinally. Thus, only surge drift motion was prevented by the mooring system. All experiments were executed in head wave condition. Prior to experiments in waves, free oscillations were conducted to determine the natural frequencies of rigid motion and elastic vibration modes. The principal dimensions of models and measured natural frequencies are shown in Table 1. It should be pointed out that two models are prepared to have same length, width and closed displacement, but the bending rigidity are considerably different each other, i.e. pontoon type model is more flexible than semi-submersible type (in air). This also made the free decay tests of vertical motion and vibration modes to be impossible.

In Figure 2, analytic models for hydrodynamic calculations are shown. The mean wetted surface of structure is discretized into 1152 panels for pontoon type model and 4608 panels for semi-submersible type model. Furthermore, a rigid structure, 1/4 part of semi-submersible type model composed from 3*3 units (square shape) is also used to investigate the effect of rigidity on wave drift force.

TABLE 1

PRINCIPAL DIMENSIONS AND NATURAL FREQUENCIES (MODEL SCALE: 1/256)

	Semi-submersible unit type		Pontoon unit type	
	Model	Prototype	Model	Prototype
Length (L)	7.1 m	1817.6 m	7.1 m	1817.6 m
Breadth (B)	1.7 m	435.2 m	1.7 m	435.2 m
Depth (D)	0.36 m	92.2 m	0.10 m	25.6 m
Draft (d)	0.132 m	33.8 m	0.034 m	8.6 m
Displacement	267.4 kg	4.49×10^{6} ton	301.5 kg	5.06×10^{6} ton
Rigidity (EI/B)	357.3kgfm	1.5×10^{12} kgfm	17.3 kgfm	7.4×10^{10} kgfm
KG	0.27m	68m	0.092m	23.7m
Natural Frequencies (rad/sec)				
Surge	0.40	0.025	0.47	0.029
Heave	3.47	0.22	-	-
Pitch	3.57	0.23	-	-
1st Bending	4.52	0.28	-	-
2nd Bending	8.89	0.56	-	-
3rd Bending	17.95	1.12	-	-

4. RESULTS AND DISCUSSIONS

4.1 Motions and Deflections in Regular Waves

Surge motion of pontoon type VLFS is shown in Figure 3 and the vertical displacements at three points (fore end, midship, aft end) of semi-submersible type VLFS are shown in Figure 4. The experimental results were obtained from tests in linear transient water waves, although the experimental results scatter at higher frequencies, the calculations for both rigid motion and deflections agree with experiments well on the whole. The disagreements in Z-displacement at fore end can be considered as the non-linear interaction effect of waves and structure, which are not included in calculations.

4.2 Steady Drift Forces in Regular Waves

Steady wave drift forces (non-dimensioned) in surge direction are shown in Figure 5 for pontoon type VLFS and in Figure 6 for semi-submersible type. On the whole, the correlations between calculation and experiment are found to be well in agreement. The discrepancies in semi-submersible type are associated with the accuracy in deflection prediction at fore end for the same reason as mentioned in previous section. However, different tendency in two type models has been observed. Drift force of pontoon type is negligibly small in relatively low frequencies (less than 5 rad/sec in model scale) and it increases from 5 rad/sec rapidly. On the contrary, drift force of semi-submersible changes its value considerably at relatively low frequencies when wave frequency changes. The frequency dependence becomes more complicated than pontoon type.

In Figure 6, drift force component corresponded to the terms on right hand side of Eqn.6 are shown. It can be confirmed that the contributions of relative wave elevation (term 1) and pressure drop due to velocity potentials (term 2) are dominant components for steady drift forces.

Drift forces of 9 units rigid semi-submersible model (1/4 of VLFS model) are shown in Figure 7. It can be stated that the agreement between the calculated and experimental results are comparatively well except frequencies from 5 to 7 rad/sec. For rigid semi-submersible model, the drift force varies its value with wave frequency remarkably and this could be explained as the effect of wave scattering phenomenon among columns, which is the well-known fact for first order wave force.

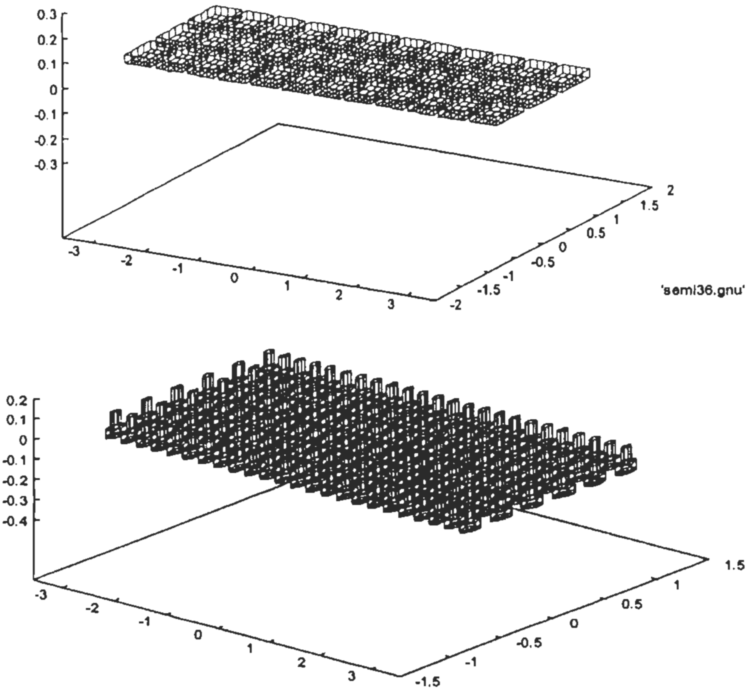
0.3
0.2
0.1
0
-0.1
-0.2
-0.3
-3
-2
-1
0
1
2
3
-2
-1.5
-1
-0.5
0
0.5
1
1.5
2
'semi36.gnu'
0.2
0.1
0
-0.1
-0.2
-0.3
-0.4
-3
-2
-1
0
1
2
3
-1.5
-1
-0.5
0
0.5
1
1.5

Figure 2: Discretization of models (upper: pontoon lower: semi-sub) for hydrodynamic analyses

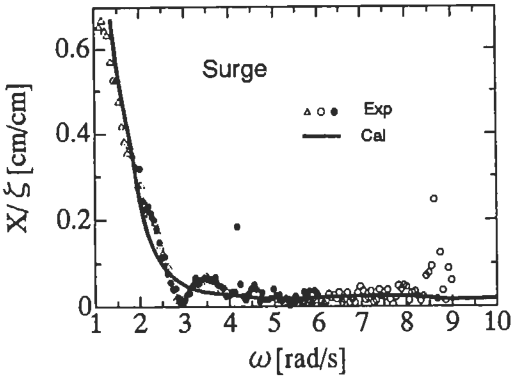

Figure 3: Amplitude of surge motion of pontoon type VLFS in regular waves

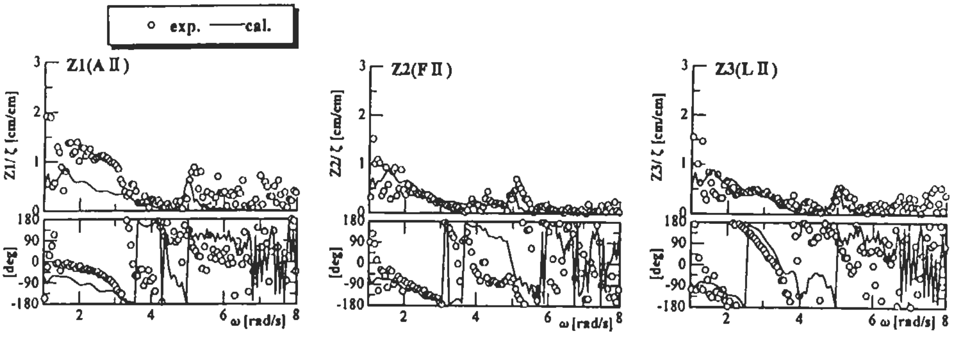

Figure 4: Z-displacements (Z1: fore, Z2:mid, Z3: aft) of semi-submersible type VLFS

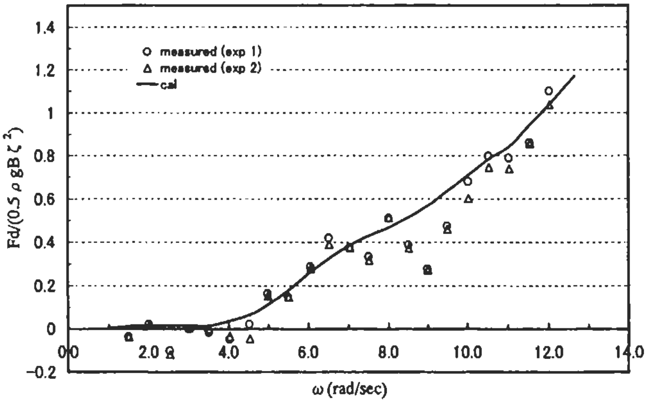

Figure 5: Wave drift force coefficients of pontoon type VLFS

Finally, the comparisons of experimental results of pontoon and semi-submersible type are plotted in Figure 8. It is obviously observed that semi-submersible type shows larger drift forces in long waves but it becomes superior than pontoon type in short waves. According to Table 1, the natural frequencies of lower bending modes correspond to those wavelengths and the large relative wave elevation due to the resonant vertical displacement contributes to wave drift forces considerably. However, we must consider that two structures have different rigidity, i.e. pontoon model is more flexible than semi-submersible model. As one can expect, the different tendency in elastic response (especially vertical displacement) affects its drift force, i.e. smaller deflection brings smaller drift force. Anyhow, this fact should be studied further through parametric calculations.

5 CONCLUSIONS

The steady drift forces and hydro-elastic response of two types of very large floating structures have been investigated through numerical simulations and model experiments. Based on the results obtained from the present work, following conclusions are derived.

(1) Near field theory can predict the steady drift forces on VLFS properly by accounting its elastic deformation modes. In that, three-dimensional source method is effective in calculation of hydrodynamic forces.
(2) The rigidity affects both deflection and drift forces considerably, however the flexibility brings conflicted effects toward deflection and drift force, thus, it is necessary to apply an optimizing technique from viewpoint of reduction of both hydro-elastic response and wave drift force.
(3) Semi-submersible type VLFS shows smaller drift forces at higher wave frequencies, but larger drift force at lower wave frequencies than the pontoon type and this depends on the rigidity, configurations of underwater body of the structures.
(4) The relative motion of structure affect the drift force dominantly for a beam like very large floating structure in head sea wave condition, thus, it is vitally important to move away the natural frequency of deflection from the frequency range of incident waves.

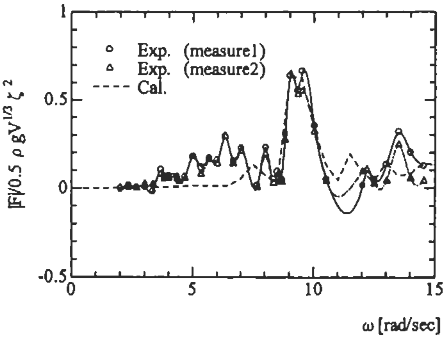

Figure 6: Wave drift force components of rigid semi-submersible type floating structure

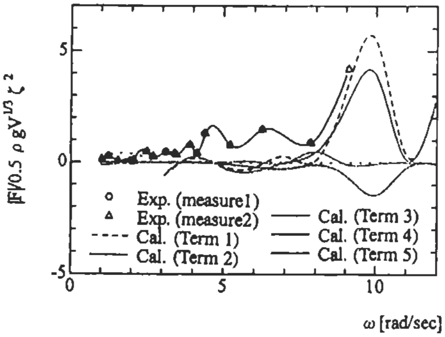

Figure 7: Wave drift force coefficients of semi-submersible type VLFS

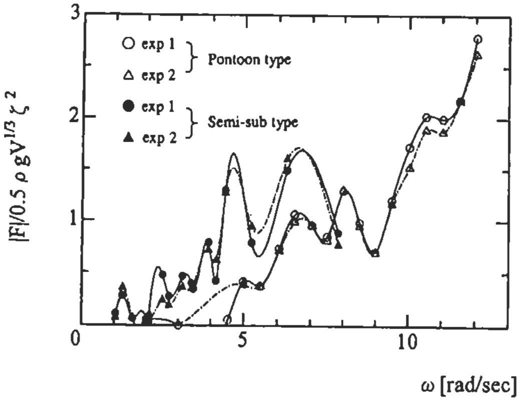

Figure 8: Comparison of measured drift forces of pontoon type and semi-submersible VLFS

Acknowledgement

The authors are grateful to Mr. K. Miyakawa and Mr. T. Takayama from Yokohama national University for their supports in the preparation of model and execution of experiments. Mr H. Abe and Mr. T. Ishikawa and other students of seakeeping laboratory of YNU are also acknowledged for their helps during experiments.

References

Hirayama T., and Ma N. (1995a). Response Characteristics of a Long Life Type Floating Airport in Waves (1st report). *Journal of the Society of Naval Architects of Japan* **177,** 219-230. (in Japanese)

Hirayama T., Ma N. and Nishio F.O. (1995b). Response Characteristics of a Long Life Type Floating Airport in Waves (2nd report). *J. of the Society of Naval Architects of Japan* **178,** 225-236. (in Japanese)

Kashiwagi M. and Furukawa C. (1997). A Mode Expansion Method for Predicting Hydroelastic Behavior of a Shallow-Draft VLFS. *16th Int'l Conf. on Offshore Mechanics and Arctic Eng* **VI,** 79-186.

Ma N. and Hirayama T. (1997). Hydroelastic Response of Two Types of Very Large Floating Structures. *16th Int'l Conf. on Offshore Mechanics and Arctic Engineering* **VI,** 211-218.

Maeda H., Ikoma T. and Masuda K. (1998). Wave Drift Forces of a Very Large Flexible Floating Structure. *7th International Symposium on Practical Design of Ships and Mobile Units,* 1037-1043

Mamidipudi, P. and Webster, W.C. (1994). The Motion Performance of a Mat-Like Floating Airport. *International Conference on Hydroelasticity in Marine Technology,* 363-375

Maruo H. (1960). The Drift of a Body Floating in Waves, *Journal of Ship Research* **4:3,** 1-10.

Ohkusu M. and Namba Y. (1998). Hydroelastic Behaviors of Floating Artificial Islands, *Journal of the Society of Naval Architects of Japan* **183,** 239-248

Pinkster J.A. (1980). Low-Frequency Second Order Wave Exciting Force on Floating Structures. *Report of Netherlands Ship Model Basin,* Publication No. **650.**

Practical Design of Ships and Other Floating Structures
You-Sheng Wu, Wei-Cheng Cui and Guo-Jun Zhou (Eds)
© 2001 Elsevier Science Ltd. All rights reserved

A STUDY ON THE HORIZONTALLY DYNAMIC BEHAVIOR OF A VLFS SUPPORTED WITH DOLPHINS

Hao Liu

Graduate Student, Osaka Prefecture University, Sakai, Osaka 599-8531, Japan

Hiroo Okada, Takashi Tsubogo and Koji Masaoka
School of Engineering, Osaka Prefecture University, Sakai, Osaka 599-8531, Japan

ABSTRACT

This paper deals with the horizontally elastic behavior of a very large floating structure (VLFS) supported with dolphins under dynamic loads. Eigen frequencies for vertical vibration of VLFS exist continuously in relatively high frequency zone due to the buoyancy effect. On the other hand, the lowest eigen frequency for horizontal vibration may appear in the lower frequency zone than the heave-mode frequency, because of no effect of buoyancy on the horizontal deflection behavior. Therefore, it is important to investigate the horizontally elastic behavior of VLFS under dynamic loads. At first, basic studies on the eigen frequency characteristics of a VLFS under trial design are carried out. The eigen frequency characteristics of a VLFS are investigated by using the combined model considering the shearing rigidity of the main structure and mooring effects. Effects of mooring characteristics and structural parameters on dynamic response are also discussed based on results obtained by using analytical solutions and finite element analyses. Next, a nonlinear finite element analysis system is developed to simulate the behaviors of the VLFS under dynamic loads. Finally, by using this analysis system, the response behavior of the VLFS supported with 25 dolphins, which is modeled as a horizontal elastic plate, supported with springs and dashpots through gap elements were investigated.

KEYWORDS

Horizontally elastic response, VLFS, Effect of mooring rigidity, Effect of shear rigidity

1 INTRODUCTION

In this paper, the eigen frequency characteristics of a VLFS under trial design are investigated using the combined model considering the shearing rigidity of the main structure and mooring effects. Effects of mooring characteristics and structural parameters on dynamic response are also discussed based on results obtained by using analytical solutions and finite element method analyses firstly. Next, a three dimensional, nonlinear finite element analysis is used to predict the dynamic response of a particular very large floating structure to the dynamic loads. The states of which mooring clearance and the ultimate strength mooring fender exists are numerically calculated, it is seen that the structure rigidity has a substantial effect on the result of VLFS mode and the eigen frequency, as well as the difference response due to the condition of incident wave. It is concluded that design should be considered with respect to the overall structure dynamic characteristics of the VLFS

2 BASIC STUDY

2.1 Outline of VLFS Under Trial Design

In this study, we deal with a very large floating structure (VLFS) under trial design, which is developed for the usage of a floating airport, for simplicity, we model the main body of the structure as beam supported with many dolphins shown in Fig.1 and indicate its main parameters in Table 1.

The dolphins attached to the fender as the shock-absorbing parts at the top end and driven into the base rock at the bottom end are also model as spring elements as shown in Fig.1. The numerical data for foundation spring and column elements are calculated out using a three-dimension finite element method and based on the experiment report1) as shown in Table2.

2.2 Eigen Frequency Characteristics

The solution of the real eigenvalue problem is very important for the following time history simulation analysis which is numerically difficult and time consuming, therefore, we investigate the eigen characteristics and normal modes of the VLFS by using both theoretical analysis and finite element methods at first.

For simplicity, we shall model the main structure as Timoshenko's beam on an elastic foundation, we can obtain the control elastically deflecting Eq. 1 as following.

$$EI\frac{\partial^4 v}{\partial x^4}+\rho A\frac{\partial^2 v}{\partial t^2}-\rho I(1+\frac{E}{k'G})\frac{\partial^4 v}{\partial t^2\partial x^2}+\frac{\rho^2 I}{k'G}\frac{\partial^4 v}{\partial t^4}+k_c(v+\frac{\rho\ I}{k'GA}\frac{\partial^2 v}{\partial t^2}-\frac{EI}{k'GA}\frac{\partial^2 v}{\partial x^2})=0 \qquad (1)$$

where, v: elastic deflection, ρA : linear density of main structure, EI :bending rigidity, $k'GA$: effective shearing rigidity, k_c : mooring rigidity.

By introducing the following constant variables into Eq. 1, we can re-write it as following.

$$\frac{\partial^4 v}{\partial x^4}-(\alpha^2+\beta^2)\frac{\partial^4 v}{\partial t^2\partial x^2}+\frac{k_p^4}{\omega_0^2}\frac{\partial^2 v}{\partial t^2}+\alpha^2\beta^2\frac{\partial^4 v}{\partial t^4}+k_p^4 v+\alpha^2\beta^2\omega_0^2\frac{\partial^2 v}{\partial t^2}-\gamma^2\frac{\partial^2 v}{\partial x^2}=0 \qquad (2)$$

where $\alpha^2=\frac{\rho A}{k'GA}$, $\beta^2=\frac{\rho I}{EI}$, $\gamma^2=\frac{k_c}{k'GA}$, $\omega_0^2=\frac{k_c}{\rho A}$, $k_p^4=\frac{k_c}{EI}$

constant α, β are the component of shearing rigidity and rotating inertia moment respectively, ω_0 is horizontal circular frequency when treating structure as rigid body, γ is the relationship between inertia and rigidity, and k_p indicates the relationship between bending rigidity and mooring rigidity.

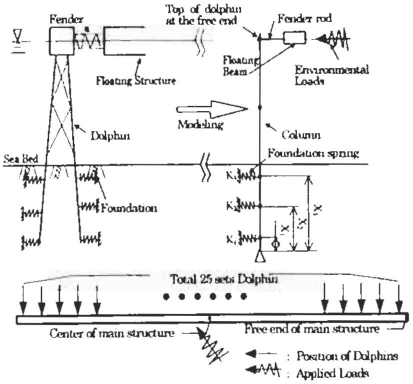
Fender
Top of dolphin at the free end
Fender rod
Floating Structure
Floating Beam
Environmental Loads
Modeling
Dolphin
Column
Foundation spring
Sea Bed
Foundation
K_3
K_2
K_1
x_3
x_2
x_1
Φ
Total 25 sets Dolphin
Center of main structure
Free end of main structure
: Position of Dolphins
: Applied Loads

Figure1 Combined model composed of VLFS and mooring system

TABLE 1

NUMERICAL DATA FOR COMBINED MODEL

Item	Data	Units
Length L	4560	m
Breadth B	1000	m
Linear density of main body ρA_M	3.713	10^6kg/m^3
Horizontal bending rigidity EI_H	1.090	10^{18} Nm^2
Shearing rigidity $k'GA$	2.377	10^{12} Nm^2

TABLE 2

NUMERICAL DATA FOR FOUNDATION SPRING AND COLUMN

Distance of the mounting point of foundation spring (x1,2,3)	8.45	37.50	66.55	m
Spring rigidity (k1,2,3) ×108	9.34	14.9	9.34	N/m
Height of dolphin H	22.5			m
Penetration depth h	75.0			m
Linear density of dolphin ρA_d	5.62×104			kg/m
Bending rigidity of dolphin EI_d	6.70×1013			Nm 2
Rigidity of fender rod for weak mooring	1.35×107			N/m
Clearance between fender and structure	0.4			m

Let us assume a solution in the form

$$v_j(x,t) = \Phi_j(x)\cos(\omega_j t) \tag{3}$$

where $\Phi_j(x)$ is the modes functions, ω_j is the eigen circular frequency.

By introducing Eq. 3 into Eq. 2, and satisfying the boundary conditions, we obtain the ordinary eigenvalue equation as following

$$\Phi_j'''' + [(\alpha^2+\beta^2)\omega_j^2 - \gamma^2]\Phi_j'' - (\frac{k_p^4}{\omega_0^2}\omega_j^2 + \alpha^2\beta^2\omega_0^2\omega_j^2 - \alpha^2\beta^2\omega_j^4 - k_p^4)\Phi_j = 0 \tag{4}$$

The resulting eigenvalue is given by the following

$$\lambda^4 + [(\alpha^2+\beta^2)\omega_j^2 - \gamma^2]\lambda^2 - (\frac{k_p^4}{\omega_0^2}\omega_j^2 + \alpha^2\beta^2\omega_0^2\omega_j^2 - \alpha^2\beta^2\omega_j^4 - k_p^4) = 0 \tag{5}$$

Hence, we conclude the solution

$$1 - \cos(\lambda_1 L)\cosh(\lambda_2 L) = (\frac{\lambda_1^2 s_2^2 s_3^2 - \lambda_2^2 s_1^2 s_4^2}{2\lambda_1\lambda_2 s_1 s_2 s_3 s_4})\sinh(\lambda_2 L)\sin(\lambda_1 L) \tag{6}$$

$$1 - \cos(\lambda_1 L)\cos(\lambda_2 L) = (\frac{\lambda_1^2 s_2^2 s_3^2 + \lambda_2^2 s_1^2 s_4^2}{2\lambda_1\lambda_2 s_1 s_2 s_3 s_4})\sin(\lambda_2 L)\sin(\lambda_1 L) \tag{7}$$

where $s_1 = \lambda_1^2 + \delta_1$ $s_2 = \lambda_2^2 - \delta_1$ $s_3 = \lambda_1^2 + \delta_2$ $s_4 = \lambda_2^2 - \delta_2$

The detailed theoretic eigenvalue ω_j can be calculated through the Eq.6 or Eq.7 and the results are tabulated in Table 3. As comparison, we also give the values obtained by the FEM methods in the same table.

3 FREQUENCY RESPONSE BEHAVIOR OF HORIZONTAL DEFLECTION

Frequency response of the elastic horizontal deflection of combined model under regular wave conditions had been computed using a finite element method, and the results of the response considering the shearing rigidity of main structure are also obtained. the results of the selected points are shown in from Fig. 2 to Figure 4.

Fig. 2 and Fig.3 are the frequency response of amplitude of horizontal deflection at the free end and the center of main structure under low mooring rigidity, Fig.4 is the frequency response of amplitude of deflection at the top end of dolphin located at the free end of the main structure.

It can be seen that the different harmonic vibration point exists from the dotted line and real line due to the effects of shearing rigidity of main structure. the difference is bigger in the second eigen circular frequency than the first one.

On the other hand, it can be seen that the frequency response of amplitude of horizontal deflection is small except for harmonic vibration points ,but it will become bigger when long wave appears.

4 NONLINEAR DYNAMIC FINITE ELEMENT ANALYSIS

The structure response to a dynamic load under the wave environment will become nonlinear, because of the existence of clearance between main floating structure and its mooring equipment and the disability of mooring fender or dolphin when the applied load exceed their ultimate strength. It is therefore necessary to predict the response in the design, and especially, evaluate the step of mooring dolphins under a critical status.

Thus, A nonlinear, three dimensional finite element modeling technique was developed for computing the dynamic response of a very large floating structure with the nonlinear elements. And a series of computation study were conducted to several sizes of mooring clearance and damaging path of the mooring equipment due to the difference incident angle.

4.1 Nonlinear Element

In our present work, we deal a combined model consisted of VLFS and its mooring equipment, we assume the clearance (gap) exists between VLFS and the mooring fender. So the VLFS, under the wave force applied or enforced displacement of the fender, will moves and deflects until the gap closes and continues to deflect with the gap closed. The characteristic of fender with clearance can be simplified as a gap element as shown Figure 5:(right) and the image of the fender behavior .can be illustrated as shown in Figure 5:(left)

On the other hand, the mooring fender has a ultimate strength, they will be broken if the applied force exceeds the ultimate strength under the severe circumstance, we consider the mooring fender has a relation between the deformation and applied force as shown in Figure 6. Once the fender is damaged it will not work, the image of some fender's behavior on this case can be illustrated as shown in Figure , and we take it out from model in the next numerical calculating time step. These two statuses also account for the geometric changes that may occur in the structure.

4.2 Numerical Calculation Method

When considering a problem in which dynamic (time integration) finite element analysis is to be used as commented above, because of the existence of nonlinear element such as mooring clearance and the damaged fender, the stiffness matrix is reconstructed in each time step.

TABLE 3

COMPARISON OF EIGEN ANGULAR FREQUENCY OF VLFS BY ANALYTICAL METHOD AND FEM

	Case	No *	Low*	High*
ω_0	 ω_{0H} ω_{0V}	0.000 (0.000) (0.000)	0.137 (0.137) (0.137)	1.027 (1.025) (1.026)
ω_1	$\alpha=0, \beta=0$	0.582	0.598	1.181
	$\alpha\neq0, \beta=0$ (FEM)	0.516 (0.517)	0.534 (0.534)	1.150 (1.147)
	$\alpha\neq0, \beta\neq0$	0.513	0.531	1.142
ω_2	$\alpha=0, \beta=0$	1.606	1.611	1.906
	$\alpha\neq0, \beta=0$ (FEM)	1.128 (1.130)	1.137 (1.138)	1.526 (1.526)
	$\alpha\neq0, \beta\neq0$	1.122	1.130	1.513
ω_3	$\alpha=0, \beta=0$	3.148	3.151	3.346
	$\alpha\neq0, \beta=0$ (FEM)	1.768 (1.772)	1.773 (1.777)	2.044 (2.048)
	$\alpha\neq0, \beta\neq0$	1.778	1.783	2.060

(*) mooring rigidity $k_c=0$ N/m^2 for case No, $k_c=6.963\times10^4$N/m^2,for case Low and $k_c=3.920\times10^4$N/m^2 for case High

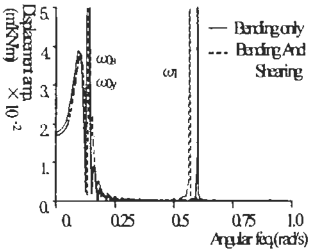

Figure 2: Frequency response amplitude of deflection at the top end of dolphin located at the free end of the structure under low mooring rigidity

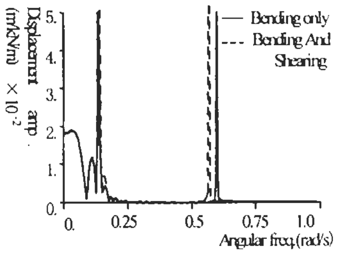

Figure 3: Frequency response amplitude of horizontal deflection at the free end of main structure under low mooring rigidity

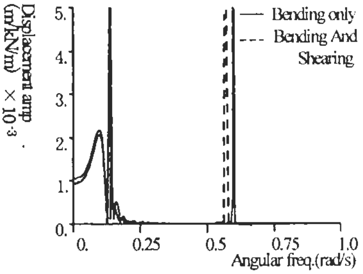

Figure 4: Frequency response amplitude of deflection at the top end of dolphin located at the free end of the structure under low mooring rigidity

The algorithm used consisted of a modified Newmark's family of equations with automatic time step feature and Newton-Raphson's Method.

4.3 Calculating Case and Results

4.3.1 Mooring clearance

As a study case, we calculated the time history of combined model under the regular wave force. The regular force is assumed as following.

$$F_i = F_0 \sin(k_\alpha x_i - \omega\, t) \qquad (8)$$

where F_i is wave force, ω ($=2\pi/T_w$)is circular frequency of wave force, x_i is the coordinates of the node, k_α ($=k/\cos(\alpha)$)is the degree of incident wave.

In numerical computation, we obtained the time history of the axial forces of each mooring fender and the deflection of the calculating points on the structure. We show only some selected figures due to page limited.

Figure is the time history of axial force of fender located at the center of the structure with gap 4.0cm, it can be seen that the curve of axial force is a discontinuous line due to the existence of mooring clearance between the fender and the structure, the long period wave curve with short period wave curve.

Figure and Fig. is the time history of deflection of the free end and the center in the same case. It should be noted that the two curves are similar but the phase is different, that is, the structure is not only moving as a rigid body, but also deflecting as an elastic structure. By analyzing the frequency characteristic of the curve data using FFT program, we got the distribution of frequency spectrum shown in Fig., it should be noted that the frequency of the first peak and second peak are very close to the yawing period and the first elastic eigen frequency in the horizontal.

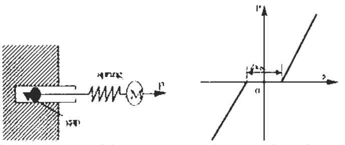

Figure 5: Characteristic of fender with clearance and model

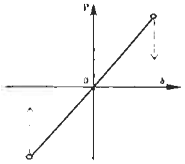

Figure 6: Characteristic of fender considering damage

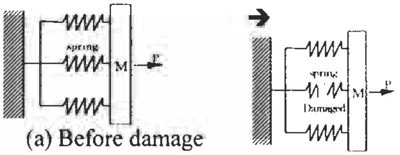

(a) Before damage

(b) Damaged

Figure 7: Change of model when fender was damaged

TABLE 4

CALCULATION CASES FOR MOORING CLEARANCE

Clearance	Condition for load
0.0 cm	Loading period 8.0 (s)
2.0 cm	Incident angle 60°
4.0 cm	Load amplitude 2.0×10^8 (N)

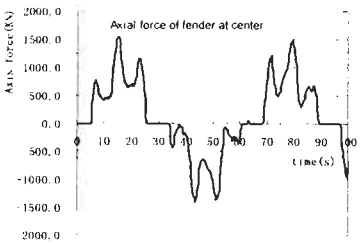

Figure 8: Time history of axial force for a selected fender

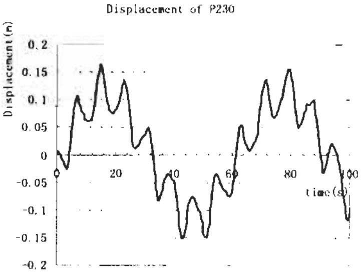

Figure 9: Time history of deflection of selected points on main structure

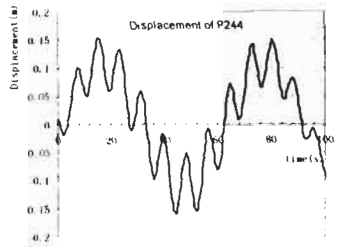

Figure 10: Time history of deflection of selected points on main structure

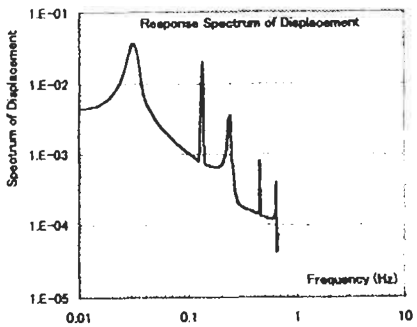

Figure11: Power spectral density of deflection for a selected point on main structure

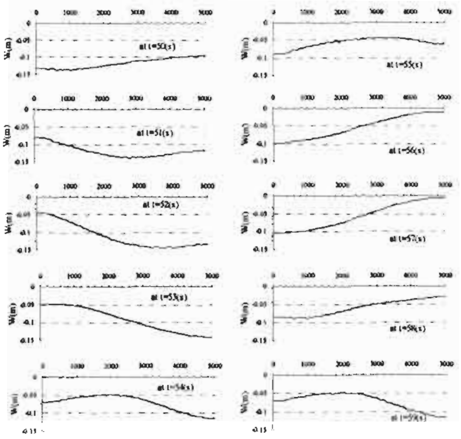

Figure 12: Deformed shape of main structure at a time

The elastic deformation and the movement of the structure are also obtained, which are shown in Fig. 12 with the centerline of the structure at some moment, It can be seen that the structure are moving from the 0-line, and at the same time deflecting horizontally. It can also be seen that the shape of deflection is similar to the first elastic mode of a horizontal beam.

4.3.2 Ultimate Strength

As the second numerical computation case, the strength of fender were stipulated to a ultimate value, when the axial force of fender exceed this value, the fender will be dealt as disability, and in the computing time step the matrix of the stiffness and the mass of the structure will be reconstructed by excluding this fender element. The angle of incident wave was changed to 30, 45, and 60 degree.

The successively damaged results of fender are tabulated in Table 5, and the time history of the deflection for selected points on the main body are given in Figure and Figure , the time history of axial force for selected fender is also shown in Figure .

It can be seen that the breach path of mooring fender is different, as well as the time of the first fender, which is broken, is different according to the incident angle. And the whole breaking process were divided into four stages in Table 5 according to the damaged time, it should be noted that the happening time of the each stage for the case of 30 degree incident wave is shortest, and is longest for the case of 60 degree incident wave, and no fender can survive in both cases.

On the other hand, it can be seen that the deflection response behavior on the structure is different from Figure and Figure . The fender, which is damaged, can be conformed from a time history of axial force like Figure .

5 CONCLUDING REMARKS

In this study, the eigen frequency characteristics were basically established, and then the nonlinear three dimension finite element analyzing technique was developed for computing the dynamic response of a very large floating structure to wave force or combined loads, the case of the existence of mooring clearance and the case of the geometric changes due to the occurrences of the fender's breaking were calculated numerically.

Effects of clearance and its size on the deflection of the structure were studied. Main structure is oscillating like rigid body, and also deflecting elastically.

Under the extreme wave loads, the survivability of the mooring fender was investigated and the path of breach can be traced by simulating calculation. Therefore this calculating system can be used to the design of mooring system and the management of VLFS system.

TABLE 5

COLLAPSING BEHAVIOR

Angle (deg.)	Stage 1	Stage 2	Stage 3	Final
30	2.5～3.75(s)	4.75～5.0(s)		8.25～8.5(s)
	25→22,24→23→21→20	→1,4,5,6,7,8,9,11,12,13,16→2,3,14,15		→20→21,22 surviving: no
45	6.25～7.0(s)	9.5～10.5(s)	11.7～14.5(s)	
	1,2,3→5,6→7→8	→23,24,25→20,21,22→19→18→17	→16→9→10	18.75(s)→11 22.5(s)→12 27.25(s)→14 Surviving 13
60	14.25～15.0(s)	35.25～35.50(s)	39.2～40.5(s)	40(s)
	14,15,16,17→12,13,18→11,19	→20,21,22,23→24,25	→1,2→3,4→6→7	→8,9,10 Surviving no

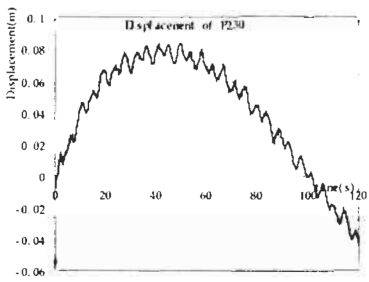

Figure 13: Time history of deflection of selected points on main body

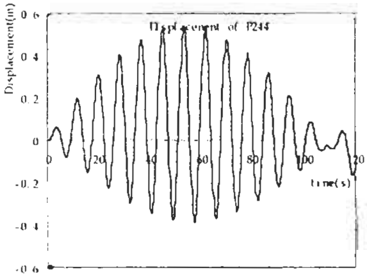

Figure 14: Time history of deflection of selected points on main structure

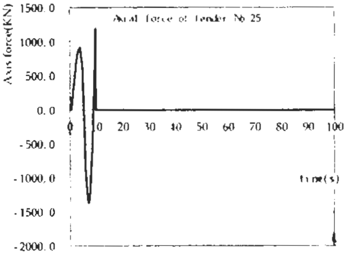

Figure 15: Time history of axial force for a selected fender

References

Hao LIU, Takashi TSUBOGO, Koji MASAOKA, Hiroo OKADA. (1999). a Study on the Horizontal Deflection Behavior of Very Large Floating Structures Considering Combined Effects with Mooring Systems, *Journal of the Kansai Society of Naval Architects*, Japan **232**, 117-126.

Yoshiyasu WATANABE. (1999). Seismic Behaviors of a Horizontally Elastic VLFS Supported with Dolphins, *Proc., 3rd International Workshop on Very Large Floating Structures (VLFS'99)*, Honolulu, USA, 335-342.

Toshiaki HISADA, Hirohisa NOGUCHI. (1995). Theory and Practice in Non-linear Finite Element Method, Maruzen.

Practical Design of Ships and Other Floating Structures
You-Sheng Wu, Wei-Cheng Cui and Guo-Jun Zhou (Eds)
© 2001 Elsevier Science Ltd. All rights reserved

EXPERIMENTAL STUDY ON THE HYDROELASTIC RESPONSE CHARACTERISTICS OF A PONTOON TYPE FLOATING STRUCTURE

T.Y. Chung[1], J.H. Chung[1], S.Y. Hong[2] and Y.J. Ji[3]

[1]Korea Institute of Machinery and Materials,
Yusung P.O. Box 101, Daejeon, 305-600, Korea
[2]Korea Research Institute of Ships and Ocean Engineering,
Yusung P.O. Box 101, Daejeon, 305-600, Korea
[3]Super Century Co., Ltd,
220 Kung-Dong, Yusung-Gu, Daejeon, 305-764, Korea

ABSTRACT

A model test with the scale ratio of 1/20 was carried out to investigate the hydroelastic response characteristics of a pontoon type floating structure in waves. In particular, the response-dependence on the water depth was investigated by the comparison with the other existing experimental results. As one of the most important findings, it was found that the hydroelastic response of a pontoon type floating structure decreases as water depth becomes shallow, which can be explained by the decreased wave exciting pressures and the increased added mass effects of the surrounding water with decreasing water depth.

KEYWORDS

Hydroelastic response, Pontoon-type very large floating structure, Model tests, Added mass effect

1 INTRODUCTION

The increasing demand for the use of ocean space is accelerating the study on very large floating structures. Hydroelastic behavior is one of the unique characteristics of very large floating structures and has been studied by many authors mainly theoretically or numerically (Kashiwagi 1999). The experiments on this type of structures are difficult because of the huge scale ratio of the real structure/model and the horizontal/vertical scale. Some experimental works (for example, Yago and Endo, 1996; Shin et al., 1999) have been done in the recent past in order to validate the theoretical or numerical approach.

Yago and Endo (1996) carried out tank tests using a scaled model to investigate hydroelastic response characteristics of the prototype structure that was constructed for the tests of very large floating structures at sea by the Technical Research Association of Mega-Float in Japan. The prototype structure is a pontoon type structure with the dimension of 300m length, 60m breadth, 2m depth and 0.5m draft, and installed at real sea having the water depth of 8m. The scale ratio of the model was 1/30, with 9.75m length. A series of tank test were conducted and vertical motions and bending moments were measured using potentiometers and strain gages, respectively in regular waves. Similar experiments were carried out by Shin et al. (1999) using a model having the scale ratio of 1/42.857 with 7m length for the same prototype structure and the experimental results were compared with the analytical ones.

In this paper, the experimental results using the model with the scale ratio of 1/20 for the same prototype structure were summarized and, in particular, they were compared with the other existing experimental data to investigate the response-dependence on the water depths chosen for the experiment.

2 DESIGN AND FABRICATION OF A TEST MODEL

An 1/20 scaled model of the prototype was designed and fabricated considering the size of the wave tank and capability of the wave maker of the Korea Research Institute of Ship and Ocean Engineering that has the dimension of 56m length, 30m breadth and 5m depth. The model was built up by mechanically bolting 15 units of aluminum honeycomb sandwich plates, each unit of which has the dimension of 1m(L) x 3m(B), using H-beam of the size of 3m length and cross section of 55x3 +39x3 mm. The total thickness of the model was 39mm, in which the thickness of face and bottom plates were 1mm respectively, and that of honeycomb core was 37mm. In order to get the desired draft of 25mm, 593 counter-weights, each having the weight of 1 kg, were uniformly distributed over the surface of the model. For simulating the dolphin fender mooring system of the prototype, the mooring device composed of horizontal bar and universal joints was also designed. The complete test model and the mooring device are shown in the figure 1 and 2, respectively.

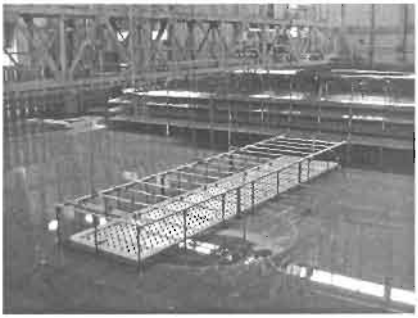

Figure 1 : The complete test model

For model tests, it is nearly impossible to fabricate a model to satisfy the similarity laws in both geometry and strength. In the hydroelastic model tests, it is common to build the model to satisfy the frequency similarity law between the exciting wave and the structure. The wave frequencies of real sea wave and the test wave in wave tanks have the following relationship by the similarity law and wave dispersion relations:

$$(f_{wave})_m = \sqrt{r} \times (f_{wave})_p \tag{1}$$

where r is the scale ratio and the subscripts m and p denote the model and the prototype, respectively. Therefore, the model should be built to satisfy the following relationship in the natural frequencies of the model and prototype structure:

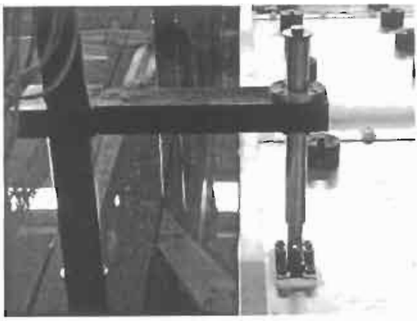

Figure 2 : The mooring device for the test

$$(f_{structure})_m = \sqrt{r} \times (f_{structure})_p \tag{2}$$

Since the pontoon type floating structure has very thin thickness compared to length and breadth, it can be analytically modeled as a thin plate and the hydroelastic motion of it can be described to the motion of a thin plate. The vibratory frequency of a thin plate can be expressed as follows:

$$f_{structure} \propto \frac{1}{a^2} \times \sqrt{\frac{EI}{\rho A}} \tag{3}$$

where a, EI and ρA are the length, the bending rigidity and the mass per unit length of a plate, respectively.

From the equations of (2) and (3), the bending rigidity of the model should satisfy the following relationship in order to satisfy the frequency similarity law.

$$(EI)_p = r^5 \times (EI)_m \tag{4}$$

We have performed the four-point bending tests on four specimens and the vibration test of one aluminum honeycomb sandwich plate in the air and confirmed that the test model has the 104% bending rigidity of the design value.

For more accurate model tests, especially in oblique waves, not only the similarity law for bending rigidity but also the similarity law for torsional rigidity should be satisfied in principle. However, it is almost impossible to make it so that the similarity law for torsional rigidity is not satisfied.

3 TEST CONDITIONS AND MEASUREMENTS ITEMS

As the water depths for model tests, two conditions were chosen; 0.4m and 1.3m. The water depth 0.4m corresponds to the water depth 8.0m at sea which is the real value of the water depth where the prototype floating structure has been installed and the water depth 1.3m corresponds to the water depth 26m at sea.

Incident waves having two different angles, 0 degree and 30 degree, were chosen, and the wave heights of 3cm, 6cm and 9cm, and the range of the wave lengths between 0.05 and 0.9 times of the model length were generated for the tests.

Vertical displacements of the test model were measured at 39 locations using potentiometers composed of pulley and torsional spring and strains due to bending were measured at 40 points using waterproof strain gages. In addition to this, 3 accelerometers were installed to measure the vertical accelerations and the absolute wave heights at 8 locations and relative wave heights at 4 locations using wave height meters were measured as shown in the figure 3.

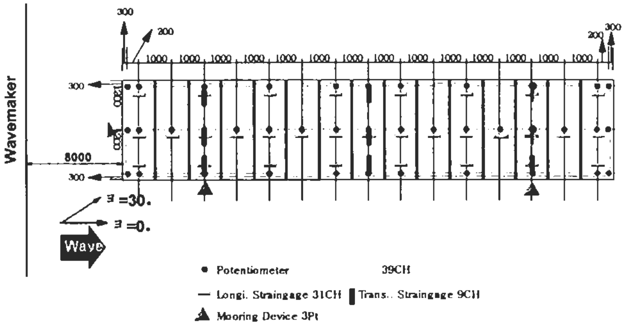

Figure 3 : Measurement items and locations

4 TEST RESULTS AND DISCUSSION

To investigate the response-dependence on the water depth, some of the test results were compared with the existing experimental data which were obtained by using different model scales for the same prototype floating structure and summarized in the figures 4, 5 and 6. Figure 4, figure 5 and figure 6 show the vertical displacement RAO at the centerline of the test model in regular waves with the incident angle 0 degree with $\lambda_\infty / L = 0.1$, 0.2 and 0.3, respectively. For the comparison of the test data in these figures, the wavelength in finite depth was converted to that in infinite depth. The main difference of the present test with the others (Yago and Endo, 1996; Shin, et al., 1999) is that the present test was carried out in the water depth corresponding to the water depth of the real sea, where the prototype floating structure is installed, by the similarity law.

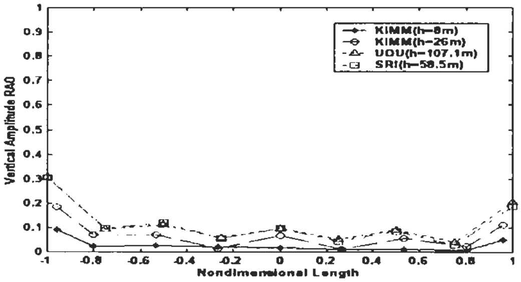

Figure 4 : The Vertical Displacement RAO($\lambda_\infty / L = 0.1$, Incident Angle=0 degree)

From the figures, some important findings are summarized as follows:

1) As generally known, the vertical displacement RAO has the largest value at the stem, and becomes smaller and has the smallest at the central part, and becomes lager again at the stern part.

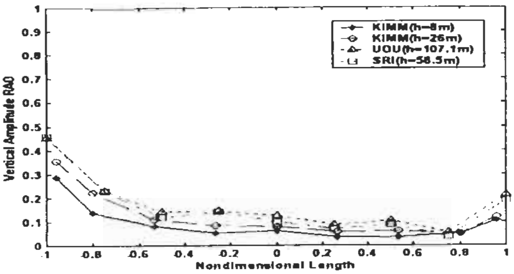

Figure 5 : The Vertical Displacement RAO($\lambda_\infty / L = 0.2$, Incident Angle=0 degree)

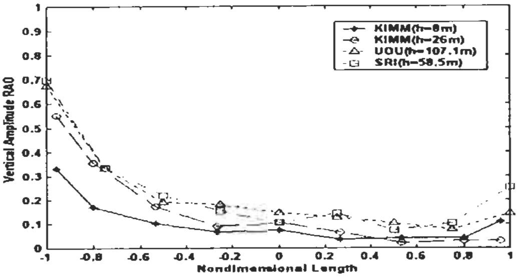

Figure 6 : The Vertical Displacement RAO($\lambda_\infty / L = 0.3$, Incident Angle=0 degree)

2) The vertical displacement RAO increases with the increase of wavelengths.
3) The vertical displacement RAO decreases in general with the decrease of water depths.

The reason why the vertical displacement RAO decreases with decreasing water depths can be explained by the fact that the wavelength becomes short in shallow water under the given wave period and wave with this short wavelength gives a relatively low pressure forces to the floating structure. In addition to this, the added mass in shallow waters which is much more than that in deep water can be added to one of the good reasons for the low vertical displacement RAO in shallow waters. As a reference, the table 1 shows the calculated wetted natural frequencies of the test model in different water depths obtained by the finite element analysis using MSC/NASTRAN. In the finite element analysis, the sea bottom was modeled as a rigid wall. As shown in the table 1, the wetted natural frequencies decrease with the decrease of water depths, which means the increase of added mass of the surrounding water.

As one of the test results, the typical longitudinal distribution of bending moments is shown in figure 7 and 8. As shown in these figures, the bending moments also increases with the increase of wavelengths. In the case of head sea, the maximum value occurs at the location of L/4 from the stem. In the case of oblique sea, the location of maximum value moves from the location of L/4 to the location of 3L/4 as the wavelength increases.

TABLE 1
CALCULATED WETTED NATURAL FREQUENCES OF THE TEST MODEL WITH THE VARIATION OF WATER DEPTH

Order & Mode	Calculated Natural Frequencies(Hz)		
	h=0.4m	h=1.3m	h=∞
1^{st}(Bending)	0.091	0.112	0.119
2^{nd}(Bending)	0.267	0.328	0.344
3^{rd}(Twisting)	0.407	0.470	0.472
4^{th}(Bending)	0.568	0.693	0.715
5^{th}(Twisting)	0.855	0.978	0.981

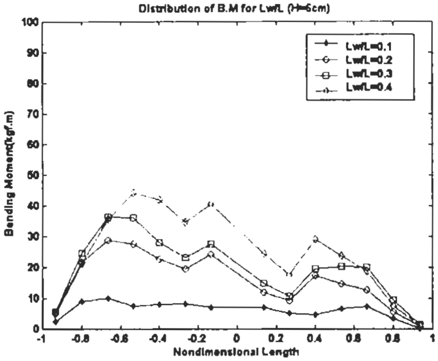

Figure 7 : The Longitudinal distribution of bending moments
(h=0.4m, H=6cm, Incident Angle=0 degree)

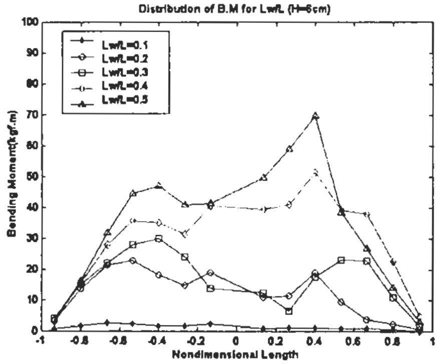

Figure 8 : The Longitudinal distribution of bending moments
(h=0.4m, H=6cm, Incident Angle=30 degree)

5 CONCLUSIONS

In this paper, an ocean engineering model basin test with the one twentieth model of the first phase pontoon of the Mega-Float project in Japan was carried out to investigate the hydroelastic response characteristics, especially the response-dependence on the water depth, of a pontoon type floating structure in waves. Compared with other existing experimental data, it was found that the hydroelastic response of a pontoon type floating structure decreased as water depth becomes shallow. This result could be explained by the decreased wave exciting pressures and the increased added mass effect of the surrounding water with decreasing water depth, which was confirmed by the wetted vibration analysis using the finite element method.

References

Kashiwagi, M. (1999). Research on Hydroelastic Responses of VLFS: Recent Progress and Future Work, *Proceedings of the 9th ISOPE Conference*, Brest, France.
Shin, H., Kim, S.K., Yang, Y.S., Park I.K. and Shin, H.S. (1999), A Study on Hydroelastic Responses of a Very Large Box-Shaped Floating Structure with Shallow Draft, *Proceedings of the 18th OMAE Conference*, Newfoundland, Canada.
Yago, K. and Endo, H. (1996), On the Hydroelastic Response of Box-Shaped Floating Structure with Shallow Draft(Tank Test with Large Scale Model), *Journal of The Naval Architects of Japan*, Vol.180, pp.341~352.

Practical Design of Ships and Other Floating Structures
You-Sheng Wu, Wei-Cheng Cui and Guo-Jun Zhou (Eds)
© 2001 Elsevier Science Ltd. All rights reserved

SIMULATION STUDY ON COASTAL ECOSYSTEM AROUND A VERY LARGE FLOATING STRUCTURE IN TOKYO BAY

D. Kitazawa[1], M. Fujino[2] and S. Tabeta[2]

[1]Department of Environmental and Ocean Engineering, Graduate School of Engineering, University of Tokyo, Japan
[2]Institute of Environmental Studies, Graduate School of Frontier Sciences, University of Tokyo, Japan

ABSTRACT

To realize a very large floating structure (VLFS), it is indispensable to examine various effects of the VLFS on marine environment. For environmental impact assessment in physical, chemical, and biological aspect, numerical simulation by means of the coastal ecosystem model is one of the useful tools. In the present paper, real time simulation is conducted for reproducing the marine environment around a Mega-Float model, which was moored off Oppama in Tokyo Bay from 1996 to 1998. As a result, it can be said that the impacts of the Mega-Float model are small because the size of the floating structure is comparatively small and exchange of seawater is effective in the sea area. Further, through this study, the present states of numerical simulation and its future assignments are discussed.

KEYWORDS

VLFS, Environmental impact assessment, Numerical simulation, Coastal ecosystem model, Real time simulation, Mega-Float model, Tokyo Bay

1 INTRODUCTION

To realize a very large floating structure (VLFS), it is indispensable to examine various effects of the VLFS on marine environment. Technological Research Association of Mega-Float (TRAMF), which was organized to promote research and development of the VLFS, moored a large floating offshore structure (hereafter called Mega-Float model) off Oppama in Tokyo Bay from 1996 to 1998 (Phase-1). In this project, a group of university researchers and the TRAMF cooperated to measure water temperature and salinity continuously around the Mega-Float model (Fujino et al. (1997)). Aside from this measurement, TRAMF carried out meteorological observations, water and benthic quality examinations (TRAMF (1998)). After the Phase-1 project, larger floating structure was moored in the same sea area from 1999 to 2000 (Phase-2), and water quality around the floating structure was examined (Fujino et al. (2001)).

TABLE 1

CHEMICAL AND BIOLOGICAL COMPARTMENTS IN COASTAL ECOSYSTEM MODEL

Group	Compartment	Group	Compartment
Organic Matter	Phytoplankton	Organic Matter	Diatom
	Zooplankton		Meiobenthos
	Particulate Organic Matter		Macrobenthos (Deposit-Feeder)
	Dissolved Organic Matter		Macrobenthos (Suspension-Feeder)
Nutrient	Cell Quota of Phosphorus		Aerobic Bacteria
	Cell Quota of Nitrogen		Anaerobic Bacteria
	Phosphate		Aerobic Detritus
	Ammonium		Anaerobic Detritus
	Nitrite		Sessile Organism
	Nitrate	Sulfide	Sulfide
Oxygen	Dissolved Oxygen	Thickness	Thickness of the Aerobic Layer

In the meantime, for environmental impact assessment of the VLFS, numerical simulation by means of the coastal ecosystem model is thought to be one of the useful tools. Recently, the model can reproduce general variations in marine environment by a method of real time simulation, in which boundary conditions change every time (Kitazawa et al. (2001)). And several simulations of the coastal ecosystem around a VLFS are also conducted and its effects on surrounding marine environment are discussed (Kyozuka et al. (1997), Kitazawa & Fujino (1999)). However, in these simulations, an imaginary VLFS is installed in the constant condition of marine environment in summer, and numerical results are not compared directly with the field data around the VLFS. Therefore, the purpose of the present paper is to simulate the coastal ecosystem around a Mega-Float model by a method of real time simulation, and to examine the effects of the floating structure on the surrounding marine environment by direct comparison of predictions with observations.

2 NUMERICAL MODEL

2.1 Coastal Ecosystem Model

Numerical model adopted in the present study is what was used by the authors previously. The model consists of physical and chemical-biological submodels, the latter of which is divided into pelagic and benthic submodels. In physical submodel, governing equations are as follows; the equations of fluid motion, the equation of continuity, the diffusion equations of water temperature and salinity, and the state equation of water density. And in the chemical-biological submodel, compartments summarized in Table 1 and interactions among these compartments are taken into account. Time variations of compartments in pelagic environment (listed in the left side of Table 1) are described by advection-diffusion equations. These equations in physical and chemical-biological submodel are solved by a finite difference scheme. Details of physical and chemical-biological submodels refer to Kitazawa and Fujino (1999), and Kitazawa et al. (2001), respectively. When a Mega-Float model is assumed to exist, activities of sessile organisms adhering to the floating structure are formulated according to Kitazawa et al. (2000).

2.2 Numerical Conditions

Figure 1 shows location of Tokyo Bay in Japan, and modeling of Tokyo Bay and of the sea area adjacent to the Mega-Float model. The sea area in Tokyo Bay is latticed with square grids in the horizontal direction, and multilevel model, in which the number of the layers is 10, is adopted in the vertical direction. To get detailed knowledge on the variation of current speed and water quality around the Mega-Float model, much finer grids are adopted in the sea area adjacent to the floating structure. Four kinds of square-grid are used; 1620m (Rank 1), 540m (Rank 2), 180m (Rank 3) and 60m (Rank 4). The Mega-Float model (Length: 300m, Width: 60m, Draft: 0.5m) is moored in the sea area off

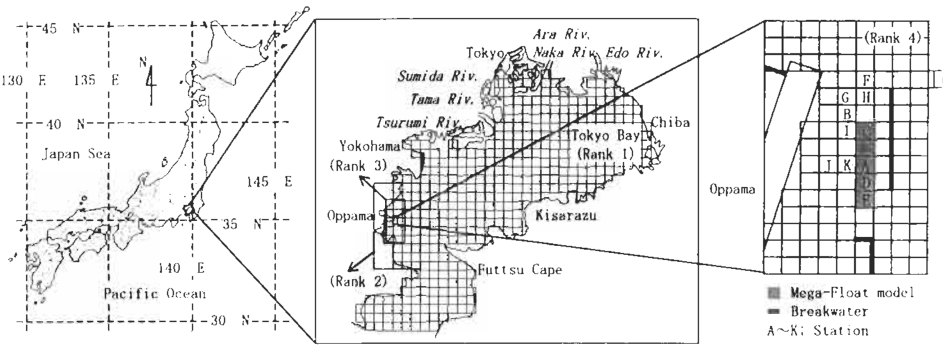

Figure 1: Location of Tokyo Bay in Japan, and modeling of Tokyo Bay and of the sea area adjacent to Mega-Float model.

Oppama (Rank 4), and the method of installing the floating structure refers to Fujino et al. (1996). At the bottom surface of the floating structure, the same friction stress as that at the sea bottom is considered. Further, the Mega-Float model is assumed to block off wind stress, heat and salinity fluxes, and exchange of oxygen through the sea surface. Predicted water quality and biomass of marine lives are compared with observations at 11 stations indicated in Fig.1. Stations A and C-E of these stations are located in the sea area, where the sea surface is covered with the Mega-Float model.

The simulated phenomenon is marine environment in Tokyo Bay from March 1, 1996 to March 1, 1997. To determine the initial condition for this simulation, real time simulation is conducted for three years using the observed meteorological data and rivers' inflow, until computed annual variation in marine environment approximately become stable. As numerical conditions for real time simulation, 4 kinds of tidal components, 6 rivers, meteorological data measured every 30 minutes around the Mega-Float model are taken into account. More details on the numerical conditions are described in Kitazawa et al. (2001). In the present study, real time simulation is conducted in two cases, where the floating structure is assumed to exist (Case 1), and where the floating structure is assumed not to exist (Case 2).

3 RESULTS AND DISCUSSIONS

3.1 The Effects on Oceanophysical Environment

Figure 2 shows the vertical profiles of the flow velocity at Stations C and I in the flood tide on January 9, 1997 (Case 1). The currents in the lowest layer at both stations are a little reduced due to the friction at the sea bottom. On the other hand, the velocity in the top layer at Station C is much smaller than that at Station I because the current under the Mega-Float model is weakened by the friction at the bottom surface of the floating structure. However, as depicted in Fig.3, residual current is not affected by the emplacement of the floating structure and directs to the southward as reported by Fujino et al. (1998). This characteristic of the residual current has an effect on the time variation of water temperature. Correlation coefficients of water temperature variations at Stations A and B from September 1 to September 24, 1996 are summarized in Table 2. Time lag indicates the difference between the phases of time variations at the both stations. If the lag is larger than zero, water temperature at Station A varies in prior to that at Station B. Correlation coefficients are more than 0.9 in every vertical point and the lag is smaller than zero. It means that time variation at Station B precedes that at Station A due to advection of seawater approximately to the southward. Further, absolute values of the lags are large in the top layer in both observation and prediction, and at 5m, 7.5m below the sea surface in prediction. This is because the current is weakened at the bottom surface of the floating structure, and at the sea bottom, respectively.

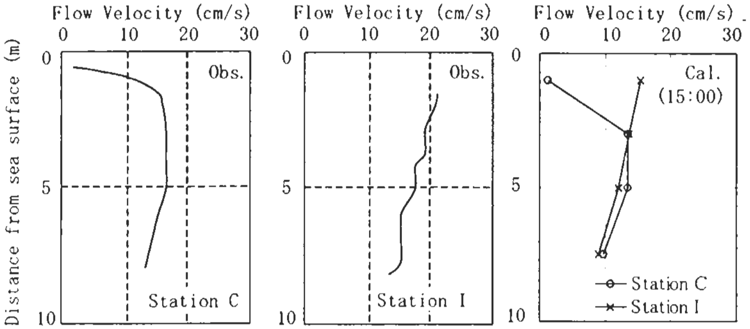

Figure 2: Vertical profiles of the flow velocity at Stations C and I in the flood tide on January 9, 1997 (Case 1).

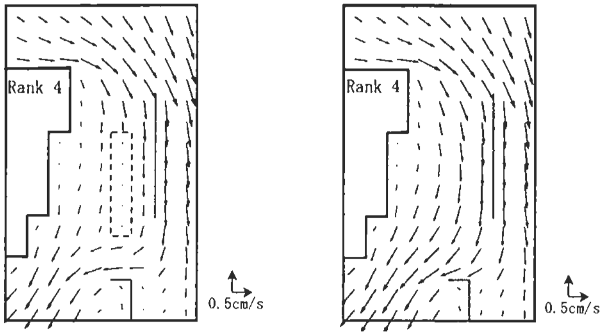

Case 1

Case 2

Figure 3: Horizontal distributions of residual current in the sea area adjacent to Mega-Float model.

TABLE 2
CORRELATION COEFFICIENTS OF WATER TEMPERATURE VARIATIONS

z (m)	Observation	Time lag (min.)	z (m)	Prediction	Time lag (min.)
-0.85	0.98	-20	-1	0.93	-20
-2.85	0.98	-10	-3	0.92	-10
-4.85	0.97	-10	-5	0.91	-20
-6.85	0.97	-10	-7.5	0.95	-30

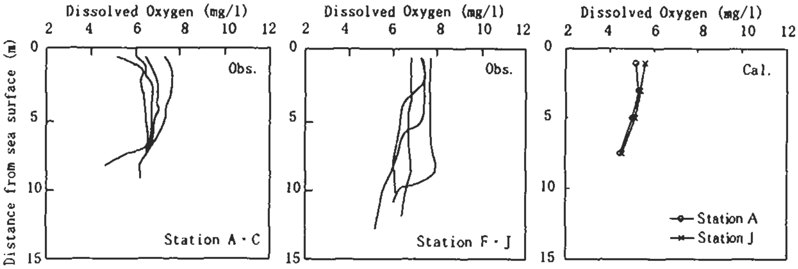

Figure 4: Vertical profiles of dissolved oxygen in August 27-29, 1996 (Case 1).

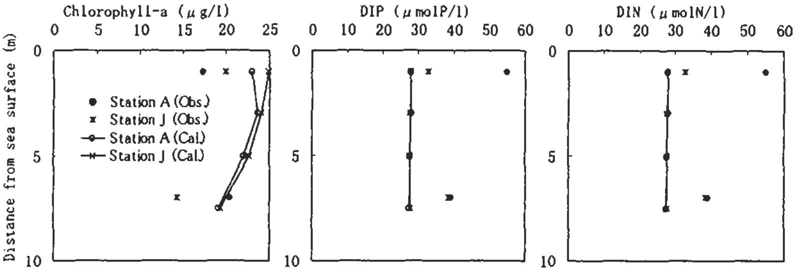

Figure 5: Vertical profiles of phytoplankton, dissolved inorganic phosphorus (DIP), and dissolved inorganic nitrogen (DIP) in August 27-29, 1996 (Case 1)

3.2 The Effects on Marine Chemical and Biological Environment

Vertical profiles of dissolved oxygen are shown in Fig.4. The observations are what were measured at Stations A, C, F, and J in August 27-29, 1996 (TRAMF (1998)). The predictions are the averaged values in the same period at Stations A and J. The amount of dissolved oxygen is a little small in the top layer at Station A. This is because dissolved oxygen is consumed by respiration of sessile organisms under the Mega-Float model. Further, vertical profiles of chlorophyll-a, dissolved inorganic phosphorus (DIP) and nitrogen (DIN) are depicted in Fig.5. The observations are attained at 1m below the sea surface and at 1m above the sea bottom (TRAMF (1998)). The amount of chlorophyll-a is a little reduced in the top layer at Station A due to filtering of phytoplankton by sessile organisms. As for DIP and DIN, observed concentrations of them are large under the Mega-Float model because sessile organisms excrete the nutrients into seawater, however the increases of DIP and DIN are not found in the prediction. This discrepancy is caused by the uncertain estimation of sessile organisms biomass. Figure 6 shows time history of sessile organisms biomass at Station E from March 1, 1996 to March 1, 1997. The observation is the average of sessile organisms biomass at 2 points around Station E, and is indicated by the amount of carbon converted from wet weight of sessile organisms (Tamai (1998)). Although it is reported that more than half of the observed sessile organisms is dead, the prediction is underestimated. Therefore, it is important to examine the amount of active sessile organisms and the ecology of them precisely.

Further, drop of the sessile organisms from the Mega-Float model to the sea bottom affects benthic quality and lives. Figure 7 shows the time history of macrobenthos biomass from March 1, 1996 to March 1, 1997. Both observation and prediction are the averaged values at 3 points, and are the sum of deposit-feeder and suspension-feeder. The biomass of macrobenthos is indicated by the amount of carbon in the same method as that of sessile organisms. In the numerical results, the biomass of

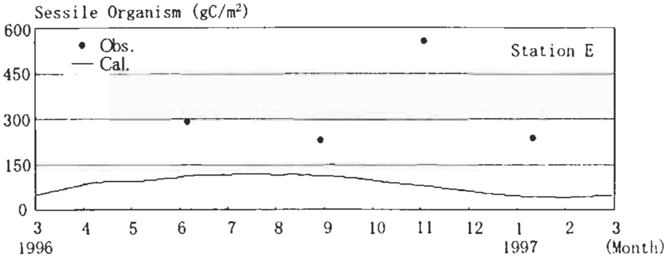

Figure 6: Time history of sessile organisms biomass from March 1, 1996 to March 1, 1997 (Case 1)

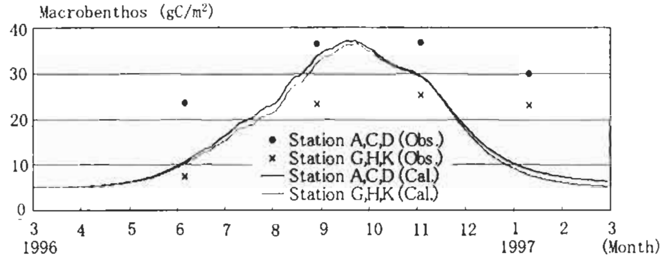

Figure 7: Time history of Macrobenthos biomass from March 1, 1996 to March 1, 1997 (Case 1)

macrobenthos is a little larger under the Mega-Float model because deposit-feeder increases by grazing bacteria, which multiply by making use of the detritus dropped from the floating structure. However, in the observation, the biomass of macrobenthos under the Mega-Float model is much larger than that at the sea bottom in the sea area, where the sea surface is not covered with the floating structure. To explain this observed result, for instance, change of benthic quality by sedimentation of detritus from the floating structure should be taken into account.

Finally, the horizontal distributions of dissolved oxygen and phytoplankton variations with the installation of the Mega-Float model are shown in Fig.8. The variations are expressed in terms of percentage, which is the ratio of difference in predictions to the predicted value in Case 2. The difference in predictions is defined by subtracting the values predicted in Case 2 from those predicted in Case 1. Both dissolved oxygen and phytoplankton decrease by a few percents, however it can be said that the impacts of the Mega-Float model are small. It is because the size of the floating structure is comparatively small, and seawater affected by the sessile organisms is transported to the southward with residual current, which is dominant in the sea area off Oppama.

4 CONCLUSIONS

In the present paper, the coastal ecosystem around a Mega-Float model is predicted by a method of real time simulation, and the effects of the floating structure on the surrounding marine environment are discussed. In physical viewpoint, friction stress between the floating structure and seawater reduces the flow velocity in the top layer. In chemical-biological aspect, the amounts of dissolved oxygen and chlorophyll-a are a little small in the top layer due to respiration and filtering by sessile organisms, respectively. And macrobenthos biomass increases by grazing the bacteria. However, it can be said that these impacts are small because the size of the Mega-Float model is comparatively small and residual current toward southward exists in the sea area off Oppama.

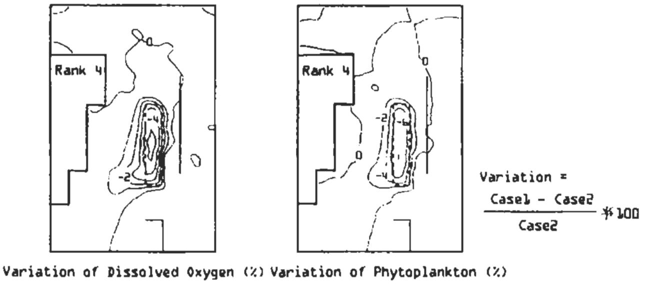
Rank 4
0
-4
-2
0
Rank 4
0
0
-2
-4
0
-4
Variation =
Case1 - Case2
Case2
*100
Variation of Dissolved Oxygen (%)
Variation of Phytoplankton (%)

Figure 8: Horizontal distributions of dissolved oxygen and phytoplankton variations at 1m below the sea surface in August 27-29, 1996

The size of the VLFS, which is expected to be constructed in the future, is perhaps much larger than that of the Mega-Float model. Further, the extent of the impacts depends on depth of the sea area, speed of the residual current, activities of marine lives, and so forth. Therefore, as future assignments, the impacts of the VLFS should be examined with sufficient caution on the size of the floating structure and the characteristic of the sea area.

References

Fujino M., Kagemoto H. and Hamada T. (1996). On the Sea-Covering Effect of a Huge Floating Structure on the Surrounding Water. *The Society of Naval Architects of Japan*, 393-402 (in Japanese).

Fujino M., Kyozuka Y., Tabeta S. and Ohkawa Y. (1997). Measurement of Marine Environment around Mega-Float Model in Tokyo Bay. *The 16th International Conference on Offshore Mechanics and Arctic Engineering*, 47-54.

Fujino M., Tabeta T., Kato T., Kitazawa D., Akiyama K., Matsuoka K. and Yukiura S. (2001). Field Measurement of Marine Environment around a Very Large Floating Structure in Tokyo Bay. *The 20th International Conference on Offshore Mechanics and Arctic Engineering* (in press).

Kitazawa D. and Fujino M. (1999). A Study on the Effects of a Very Large Floating Structure on Marine Environment. *The Third International Workshop on Very Large Floating Structures*, 297-306.

Kitazawa D., Fujino M. and Tabeta S. (2000). A Study on the Effects of a Very Large Floating Structure on Coastal Ecosystem in Tokyo Bay. *The Society of Naval Architects of Japan*, 59-72. (in Japanese).

Kitazawa D., Fujino M. and Tabeta S. (2001). Predictions of Coastal Ecosystem in Tokyo Bay by Pelagic-Benthic Coupled Model. *The 20th International Conference on Offshore Mechanics and Arctic Engineering* (in press).

Kyozuka Y., Hu C., Hasemi H., Nakagawa H. and Hikai A. (1997). An Ecohydrodynamic Model for Environmental Assessment of a Mega-Float in a Bay. *The 16th International Conference on Offshore Mechanics and Arctic Engineering*, 31-38.

Tamai K. (1998). Distribution and Production of Macrobenthos. *Marine Coastal Environment* (Edit. Hiarno T.), 244-253. (in Japanese)

Technological Research Association of Mega-Float. (1998). Measurement of the Ecosystem in the Real Sea around the Mega-Float Model.

Practical Design of Ships and Other Floating Structures
You-Sheng Wu, Wei-Cheng Cui and Guo-Jun Zhou (Eds)

© 2001 Elsevier Science Ltd. All rights reserved

EFFECTS OF A DRAFT ON HYDROELASTIC RESPONSES OF A PONTOON TYPE VERY LARGE FLOATING STRUCTURE

H. Maeda [1], T. Ikoma [1], C.K. Rheem [2] and M. Arita [1]

[1] Nihon University, Chiba, Japan
[2] University of Tokyo Tokyo, Japan

ABSTRACT

In this paper, the limitation of the zero draft assumption is examined. Then, the elastic motion and the wave drifting forces of a calculation model with 1000m in length and 250m in width are computed due to two calculation methods. Three-dimensional singularity distribution method is applied to the analysis of a finite draft body, and the pressure distribution method is applied to that of a zero draft body.

The authors conclude that the zero draft assumption is effective and practical for designing a VLFS in waves within wave frequency range. The hydrodynamics on a VLFS is calculated by the pressure distribution method with higher order boundary element in case of the zero draft assumption, while the three-dimensional singularity distribution method is applied to the finite draft case.

KEYWORDS

VLFS, Very large floating structure, Draft effect, Shallow draft assumption, Hydroelasticity, Elastic response, Momentum theory, Far field method, Near field method

1 INTRODUCTION

There are many examples on the elastic response analysis of a VLFS(Very Large Floating Structure) for which the shallow draft assumption is applied. The shallow draft assumption corresponds to the zero draft assumption. The effectiveness of the zero draft assumption has been confirmed already in case of rigid body motions on a ship or small scale offshore structure. In the same context, the shallow draft assumption is considered to be effective even for a flexible pontoon type VLFS without deeper investigation. However, there have been no big problems occur empirically yet, while there has been a few examples which investigated the effectiveness of the shallow draft assumption analytically. Kim et al. (2000) pointed out that there is not big discrepancy in the wave frequency range between the elastic deformation due to zero draft assumption and finite draft assumption, however, there are some discrepancy on elastic deformation in lower frequency or on critical angle of incident waves.

In this paper, the authors investigate the applicability of the zero draft assumption to the hydrodynamic forces on a VLFS. The 3D singular point distribution is applied to the finite draft assumption, while the pressure distribution method is applied to the zero draft assumption. The effectiveness of the shallow draft assumption is compared mainly on the elastic deformation and the steady wave drift force. The steady wave drift force is calculated by the momentum theory.

Several numerical procedures have been proposed and developed on hydroelastic responses of a pontoon type floating structure with a finite draft. Those procedures may take much computational time in the relatively high frequency range. Then zero draft assumption has been introduced in order to save computational time. (See, Maeda et al. (1996), Kashiwagi (1998), Ohmatsu (1998) and Kim et al. (1998)) The zero draft assumption has been partially verified by model tank tests, while the model tests may have some uncertainty and may not correspond to the full scale wave frequency range. The application area of the zero draft assumption is still not clear yet. Kim et al. (2000) verified about this problem, however, there are a few examinations on the zero draft assumption related to an analysis of a very large floating structure. In addition, few researchers verify the effectiveness of the assumption on wave drifting forces.

2 THEORY

It is assumed that the fluid is ideal fluid. The hydrodynamic forces are calculated by the linear potential theory. However the second order wave excitations are considered by the momentum theory using the linear velocity potentials. The coordinate system is the right hand Cartesian and the z-axis is positive upward. The coordinate system is illustrated in Figure 1. In addition, velocity potentials Φ, pressures P and vertical displacement η of a free surface or the structure are defined. Two methods are applied to the hydroelasticity analysis for the pontoon type very large floating structure. One is the three-dimensional singular distribution method for the analysis of finite draft bodies. Another one is the pressure distribution method for the analysis of zero-draft bodies.

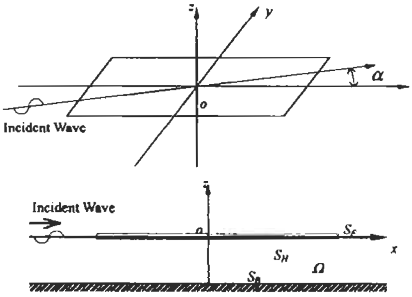

Figure 1: Coordinate system

2.1 Theory for a finite draft body

The 3-D singularity distribution method (3-D SDM) is used in the calculation in which the effect of the body's draft is considered. It is very general method for an analysis of hydrodynamic forces on offshore structure with arbitrary shapes. The authors modified our program code to calculate the elastic floating structure. The method for an analysis of the elastic motions is same as Nagata et al. (1997).

A theory to analyze the wave drifting force which is called as the second-order wave excitation generally is explained here. The momentum theory (far field theory) is applied.

The velocity potential ϕ in the fluid field at an arbitrary point is expressed as follows:

$$\phi_i(x,y,z) = -\iint_{S_H} \left(\frac{\partial \phi_i}{\partial n} - \phi_i \frac{\partial}{\partial n}\right) G(x,y,x;x',y',z')ds\,, \tag{1}$$

where G is Green's function. When a distance between the source and observation points becomes infinity, Green's functions (in this study) are:

$$G = -\frac{i}{2}\frac{1}{h+\dfrac{K}{k^2-K^2}}\cosh k(z+h)\cosh k(z'+h)\sqrt{\frac{2}{\pi KR}}\exp\!\left(-iKR+\frac{\pi}{4}i\right), \tag{2}$$

$$G = \frac{i}{2}K\exp k(z+z')\sqrt{\frac{2}{\pi KR}}\exp\!\left(-iKR+\frac{\pi}{4}i\right), \tag{3}$$

where eq. (2) is for shallow water depth, and eq. (3) is for deep water depth. Thus, the velocity potential at infinity field from the floating structure is expressed in the following equations.
for shallow water;

$$\lim_{R\to\infty}\phi_i = -\frac{i}{2}\frac{1}{h+\dfrac{K}{k^2-K^2}}\cosh k(z+h)\cosh kh\sqrt{\frac{2}{\pi KR}}e^{(\frac{\pi}{4}i)}\iint_{S_H}(\frac{\partial\phi_i}{\partial n}-\phi_i\frac{\partial}{\partial n})\frac{\cosh k(z'+h)}{\cosh kh}e^{-iKR}ds\,, \tag{4}$$

for deep water;

$$\lim_{R\to\infty}\phi_i = \frac{i}{2}\sqrt{\frac{2}{\pi KR}}\exp(\frac{\pi}{4}i)\iint_{S_H}(\frac{\partial\phi_i}{\partial n}-\phi_i\frac{\partial}{\partial n})\exp(-iKR)ds\,. \tag{5}$$

Now, if Kochin function is defined as follows,
for shallow water;

$$H(K,\alpha) = \iint_{S_H}(\frac{\partial\phi_i}{\partial n}-\phi_i\frac{\partial}{\partial n})\frac{\cosh k(z'+h)}{\cosh kh}e^{-iKR}ds\,, \tag{6}$$

for deep water;

$$H(K,\alpha) = \iint_{S_H}(\frac{\partial\phi_i}{\partial n}-\phi_i\frac{\partial}{\partial n})e^{-iKR}ds\,, \tag{7}$$

a final equation of the steady wave drifting force of a surge mode is obtained as following equation,

$$F_{dx} = -\frac{\rho K^2}{8\pi}\int_{-\pi}^{\pi}H_r H_r^* \cos\theta d\theta - \frac{\rho K}{8}\frac{ga}{\omega}\sqrt{\frac{KR}{2\pi}}(H_r + H_r^*)_{\theta=\alpha}\,. \tag{8}$$

While the drifting force of a sway mode is expressed as follows:

$$F_{dy} = -\frac{\rho K^2}{8\pi}\int_{-\pi}^{\pi}H_r H_r^* \sin\theta d\theta - \frac{\rho K}{8}\frac{ga}{\omega}\sqrt{\frac{KR}{2\pi}}(H_r + H_r^*)_{\theta=\alpha}\,. \tag{9}$$

The variables in the above equations are; 'ρ' is fluid density, 'g' is gravity acceleration, 'ω' is circular frequency, 'h' is water depth, 'i' means a complex value ($\sqrt{-1}$). But, subscript i stands for the component wave of 'i' and superscript '*' means a complex conjugate. And, K, k and R are defined as follows:

$$K = \frac{\omega^2}{g}, \quad K = k\tanh kh\,, \quad R = \sqrt{(x-x')+(y-y')+(z-z')}\,.$$

When the wave drifting forces are computed, the effect of the elastic motion is considered due to including or not including the radiation component in the velocity potentials.

2.2 Theory for a zero- draft body

The pressure distribution method is applied to the analysis of the hydrodynamic forces and the wave drifting forces under the zero-draft assumption. The velocity potential is obtained in the following equation:

$$\phi_i(x,y) = -\iint_{S_H} p_i(x',y')\cdot G dx'dy'\,. \tag{10}$$

Where G is the Green's function [1] for the shallow draft theory and S_H means an area of a body's bottom of a zero draft floating structure.
The steady wave drift forces in regular waves are given by the momentum theory, i.e. the far field theory as follows.
In this theory, H_i is defined as the Kochin function and can be expressed as follows:

$$H_i(k_i,\alpha_i) = \iint_{S_H} p_i(x',y')e^{-ik_i(x'\cos\alpha_i + y'\sin\alpha_i)}dS_H\,. \tag{11}$$

Using this Kochin function, steady wave drift forces of surge and sway modes in regular waves are given as follows:

$$F_{dx} = \rho g \frac{K_i \cdot k_i}{4\pi} \bar{k}_i \int_0^{2\pi} \left| A(k_i,\theta) \right|^2 (\cos\alpha_i - \cos\theta) d\theta, \tag{12}$$

$$F_{dy} = \rho g \frac{K_i \cdot k_i}{4\pi} \bar{k}_i \int_0^{2\pi} \left| A(k_i,\theta) \right|^2 (\sin\alpha_i - \sin\theta) d\theta. \tag{13}$$

Where,

$$\bar{k} = \begin{cases} \dfrac{K}{2} & (\text{ in deep water}) \\ \dfrac{h\cosh^2 kh}{2kh + 2\sinh kh} & (\text{ in shallow water}) \end{cases}, \tag{14}$$

and, 'A' is the total of Kochin function:

$$A(k_i,\theta) = H_D(k_i,\theta) + \sum_{r=1}^{M} q_{ri} H_r(k_i,\theta). \tag{15}$$

Here, q_{ri} is the first-order principal coordinate of r-th rigid and elastic mode. H_D is the Kochin function corresponds to the diffraction wave. Considering the second term in the right side of eq.(15), wave drift forces can be calculated even though the floating structure behaves an elastic motion.

3 RESULTS OF NUMERICAL CALCULATION

The corresponding model for the numerical calculations is illustrated in Figure 2. The model has 1000m in length, 250m in width. The water depth is 100m.

Variation of the draft is 2m, 5m and 8m for the finite draft cases, and the mass of the model corresponds to 2m, 5m to 8m equivalent draft, respectively. There is another case in which the mass distribution varies from 2m, 5m to 8m equivalent draft with the constant.

In the calculation due to the shallow draft assumption, the draft is zero, but the mass is considered in the elastic motion equations. The corresponding mass is the one for the equivalent draft of 2m, 5m and 8m.

The calculation results are shown in Figures. 3 to 12. In the figures, number of d0, d2, d5 and d8 stand for the draft on the hydrodynamic computational calculation. And m2, m5 and m8 mean the equivalent draft which corresponds to the distributed mass, i.e. m2 denotes the corresponding mass to the 2m equivalent draft. Position of the calculation of the vertical displacement is point 1 in Figure 2.

Figures 3 to 7 show the results of the vertical displacement at Point 1 in waves with 0 or 60 degrees of incoming wave angle. Horizontal axis of following figures is a circular frequency ω which corresponds to full scale wave condition. The response characteristics differ from each other in high frequency ranges because of the difference of the distributed mass. The equivalent draft for the distributed mass is as same as the corresponding draft itself in Figure 3. The effect of the zero draft assumption can be examined in Figures 4 to 7. The effect of the draft is smaller than that of the mass. The results due to the zero-draft theory agree with the finite draft one quantitatively and qualitatively.

Figures 8 to 10 show the steady wave drifting forces of surge or sway on the model. The elastic motion is not considered in the results of Figures 9 and 10. The results of the zero draft theory is very good agreement with that of the draft of 5m and 8m. The results of Figures 11 and 12 include the effect of the elastic motion of the model in 60 degrees wave. The wave drift force of surge becomes negative value in an oblique wave. The results of the zero-draft theory do not agree with the results of 2m in draft. The authors think that the cause is accuracy of the numerical calculation, i.e. the computation is severe in case of very shallow draft condition in the 3-D SDM.

4 CONCLUSIONS

Practically speaking we can conclude that the zero draft assumption(shallow draft assumption) is applicable to the calculation for hydroelastic behavior of a VLFS. The detail is as follows:

1) The zero draft assumption is very effective because the elastic response is mainly based on the

distributed mass, in other words, the hydrodynamic forces on a VLFS is almost independent of the draft of the structure.

2) In case of the very shallow draft condition, the numerical accuracy of 3-D SDM may get worse. Practically speaking, it is not necessary to use finer mesh for the calculation, but it is better to adopt the appropriate deeper draft to save the computational time.

3) The effectiveness of the zero draft assumption is verified w.r.t. not only the elastic deformation but also the steady wave drifting forces.

References

Maeda H., Masuda K., Miyajima S. and Ikoma T. (1996). Hydroelastic Responses of Pontoon Type Very Large Floating Offshore Structure. *Proceeding of the 15th international conference on Offshore Mechanics and Arctic Engineering* ASME **Vol.I**, 407-414

Kashiwagi M. (1998). A B-spline Galerkin scheme for calculating the hydroelastic response of a very large floating structure in waves. *Journal of Marine Science and Technology* **3**, 37–49

Ohmatsu S. (1998). Numerical calculation of hydroelastic behavior of pontoon type VLFS in waves. Proceedings of the *17th International conference on Offshore Mechanics and Arctic Engineering* ASME **CD-ROM OMAE98-4333**

Kim J.W. and Ertekin R.C. (1998). An eigen function-expansion method for predicting hydroelastic behavior of a hallow-draft VLFS. *Second International Conference On Hydroelasticity in Marine Technology (Hydroelasticity '98)*, 47–59

Nagata S., Yoshida H., Fujita T. and Isshiki H. (1997). THE ANALYSIS OF THE WAVE-INDUCED RESPONSES OF AN ELASTIC FLOATING PLATE. *Proceeding of the 16th international conference on Offshore Mechanics and Arctic Engineering* ASME **Vol.VI**, 163-178

Kim J.W. and Ertekin R.C. (2000). Hydroelastic Response of Mat-type VLFS: Effects of Non-Zero Draft and Mass Assumptions. *Conference Proceedings of OCEANS2000* MTS/IEEE **CD-ROM in Session 53**

Maeda H., Ikoma T. and Masuda K. (1998). Wave Drift Forces of a Very Large Flexible Floating Structure. *Proceedings of the 7th International Symposium on Practical Design of Ships and Mobile Units* ELSEVIER, 1037-1043

TABLE 1

PRINCIPAL PARTICULARS OF THE CALCULATION MODEL

Length of model (m)	1000
Width of model (m)	250
Draft of model (m)	2,5,8
Bending Stiffness per Width (kgf/m^2/m)	2×10^{10}

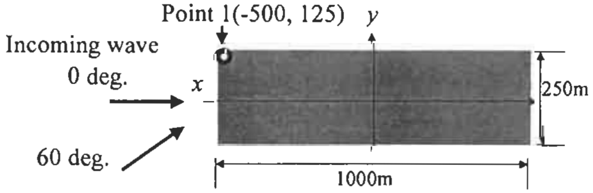

Figure 2: Calculation points of vertical displacement and angle of incoming waves

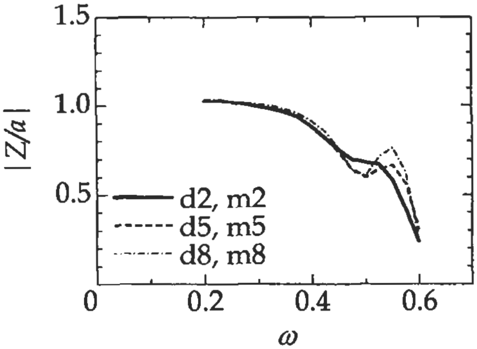

Figures 3: Vertical displacements in 60 degrees wave

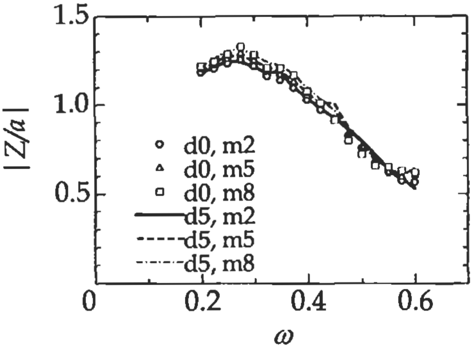

Figure 4: Vertical displacements in 0 degrees wave; effect of the zero-draft and mass

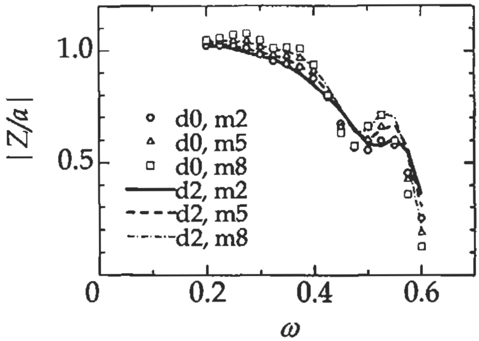

Figures 5: Vertical displacements in 60 degrees wave; zero draft and 2m in draft, (mass effect)

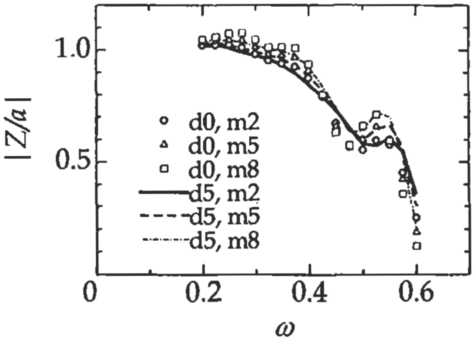

Figures 6: Vertical displacements in 60 degrees wave; zero draft and 5m in draft, (mass effect)

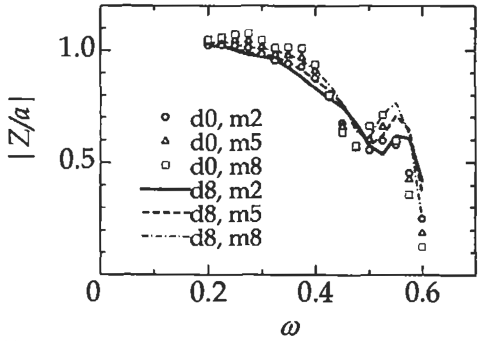

Figures 7: Vertical displacements in 60 degrees wave; zero draft and 8m in draft, (mass effect)

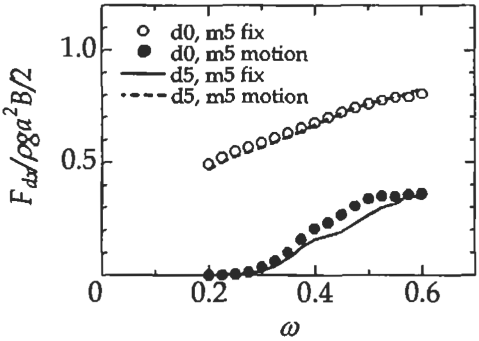

Figures 8: Steady wave drift forces on the model in 0 degrees wave

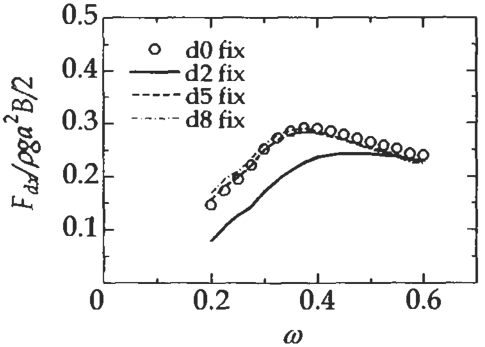

Figures 9: Steady wave drift forces of surge on fixed body in 60 degrees wave (effect of draft)

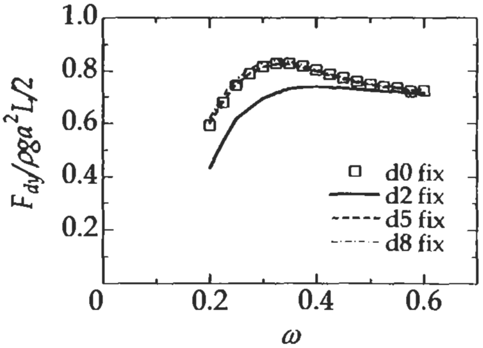

Figures 10: Steady wave drift forces of sway on fixed body in 60 degrees wave (effect of draft)

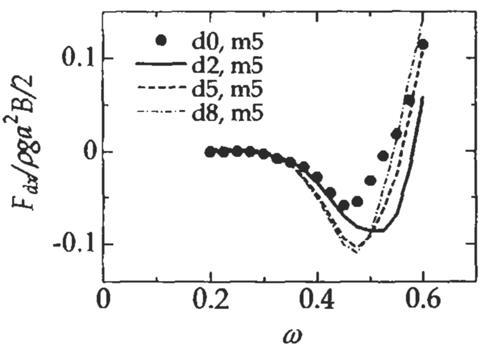

Figures 11: Steady wave drift forces of surge on body with elastic motion in 60 degrees wave (mass corresponds to 5m in draft, effect of draft)

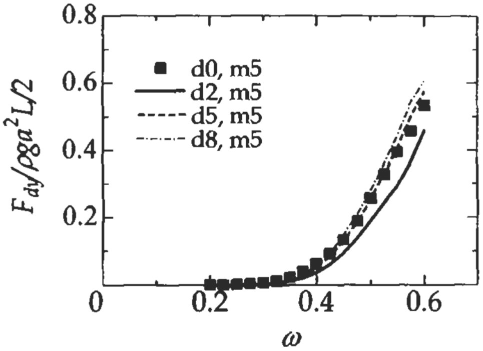

Figures 12: Steady wave drift forces of sway on body with elastic motion in 60 degrees wave (mass corresponds to 5m in draft, effect of draft)

Practical Design of Ships and Other Floating Structures
You-Sheng Wu, Wei-Cheng Cui and Guo-Jun Zhou (Eds)
© 2001 Elsevier Science Ltd. All rights reserved

A STUDY ON DECK WETNESS AND SLAMMING OF VERY LARGE FLOATING STRUCTURES

Hyunkyoung Shin[1], Ho-Young Lee[1], Choon-Gyu Lim,[1] Jeom-Moon Kang[2], Oi-Hyun Kim[2] and Myung-Cheol Yoon[2]

[1] School of Transportation Systems Engineering, University of Ulsan, Ulsan, Korea
[2] Hyundai Heavy Industry Co. Ltd., Ulsan, Korea

ABSTRACT

The length and breadth of a very large floating structure(VLFS) are determined by airplane types and airport facilities in the initial design stage. However, its depth is dependent on hydroelastic behaviors such as vertical responses as well as buoyancy. Generally speaking, VLFS of the pontoon type has rather small vertical motions except in both ends, where motions are much larger due to elasticity. In this paper, numerical predictions of deck wetness and slamming of VLFS with dimensions L×B×D=1,200m×240m×4.5m in waves are made. The source-dipole distribution method and the finite element method are employed for the hydroelastic behaviors in the frequency domain and the time domain.

KEYWORDS

Very large floating structure, VLFS, Time domain, Frequency domain, Memory effect function, Newmark β method, Hydroelastic responses, Irregular waves, Deck wetness, Slamming

1 INTRODUCTION

The typical configuration of the very large floating structure(VLFS) of the pontoon type is characterized by large horizontal dimensions compared with the incident wave. VLFS has small hydroelastic responses in the whole structure due to relatively small wave length, while the responses at both ends are large due to the elastic characteristics. Therefore, the deck wetness and slamming phenomena for VLFS must be checked in the initial design stage. A few researches on hydrodelastic behaviors of VLFS in irregular waves have ben made in the time domain(Ohmatsu(1998), Endo(1999), Lee and Shin(2000)).

In this paper, the source and dipole distribution method is employed for predicting hydrodynamic forces due to radiation and diffraction potentials, which is represented by Green function in finite depth. The added mass, wave damping coefficients and wave exciting forces calculated in the frequency domain are used to solve the equation of motion in the time domain. Newmark β method is applied for time integration considering memory effect function due to wave damping effects. Numerical prediction of the deck wetness and slamming are mde as a guideline to determine the depth of VLFS on the irregular waves. The results in the time domain are compared with those in the frequency domain.

2 FREQUENCY DOMAIN ANALYSIS

The Cartisian coordinates are defined with z=0 as the plane of undisturbed free surface and z=-h as the horizontal sea bottom(Fig. 1). Velocity potential Φ are expressed as follows.

$$\Phi = i\omega[\varsigma(\phi_I + \phi_d) + \sum_{j=1}^{3N} w_j \phi_j]e^{i\omega t} \tag{1}$$

where, N=Nx×Ny/4

Where ζ is the amplitude of incident wave, w_j complex amplitude of motion. Suffix d represents quantities related to the diffraction potential and suffix j represents heave, roll and pitch mode. The segmentation of panels are made such that the plate is subdivided into Nx in the x-axis and Ny in the y-axis and is composed of the group of N bodies. In the definition of radiation indices, the unit vertical motion of each body is described for representing elastic deformation due to radiation problems and one body is composed of four neighboring panels(Fig. 2).

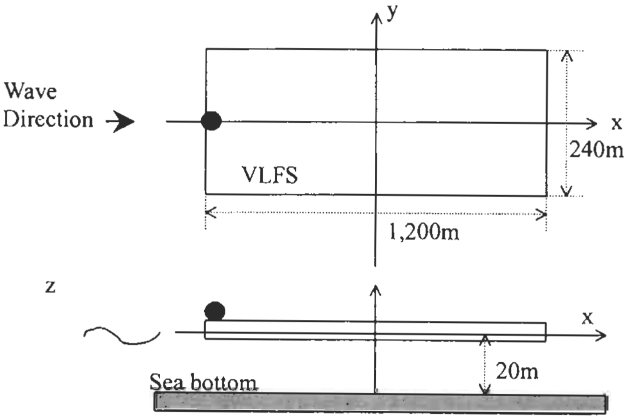

Figure 1: Cartesian coordinate system

As linear potential theory is assumed, the velocity potential must satisfy the Laplace equation, linear free surface boundary condition, sea bottom boundary condition and radiation condition at far field. The body boundary conditions for the radiation and diffraction problem are given as follows.

$$\frac{\partial \phi}{\partial n} = n_z \tag{2}$$

$$\frac{\partial \phi_d}{\partial n} = -\frac{\partial \phi_I}{\partial n} \qquad \text{on the body} \tag{3}$$

where, n_z : the direction cosine in the heave mode of motion.

The incident wave potential in Eqn. (4) satisfies the relation Eqn. (5).

$$\phi_I = \frac{g}{\omega^2}\frac{\cosh k_0(z+h)}{\cosh k_0 h} e^{i[k_0(x\cos\beta + y\sin\beta)+\omega t]} \tag{4}$$

$$\text{where,} \quad \omega^2 = gk_0 \tanh(k_0 h) \tag{5}$$

The velocity potential is obtained from Green's second identity as follows.

$$2\pi\phi(x) + \iint_{S_H} \phi(\xi)\frac{\partial G(\xi,x)}{\partial n_\xi}ds(\xi) = \iint_{S_H} \frac{\partial \phi(\xi)}{\partial n_\xi}G(\xi,x)ds(\xi) \tag{6}$$

Where S_H denotes the bottom of the pontoon-type VLFS sited on $z=-d$ and $G(\xi,x)$ denotes the Green function, which is given for the finite-depth case(Faltinsen and Michelson(1974)).
To solve the integral equation of radiation problem, the unknown potential is represented by unit vertical motion of a body of four neighboring panels. The vertical unit motion does not include the rotational motion and include only heave motion(Yago and Endo(1996)).
The body boundary condition of radiation potential is described in Eqn. (7) and (8).

$$\frac{\partial \phi}{\partial n} = (n_z)_1 = \{1,0,0,\dots,0,0\}^T \qquad \text{on the 1st body} \tag{7}$$

$$\vdots \qquad\qquad\qquad\qquad \vdots$$

$$\frac{\partial \phi}{\partial n} = (n_z)_N = \{0,0,0,\dots,0,1\}^T \qquad \text{on the Nth body} \tag{8}$$

To calculate these radiation potentials, the zero-th order panel method is employed. In diffraction problem, when Eqn. (3) is inserted in Eqn. (6), the diffraction potential is calculated. The radiation and diffraction potentials for N bodies are defined in Eqns. (9), (10), (11), and Fig. 2.

$$\phi_1 = [(\phi)_1 + (\phi)_2 + (\phi)_3 + (\phi)_4]/4 \tag{9}$$

$$\phi_2 = [(\phi)_1 - (\phi)_2 + (\phi)_3 - (\phi)_4]/4 \tag{10}$$

$$\phi_3 = [(\phi)_1 + (\phi)_2 - (\phi)_3 - (\phi)_4]/4 \tag{11}$$

where, ϕ_1, ϕ_2, and ϕ_3 : the potential of heave, roll and pitch motion.

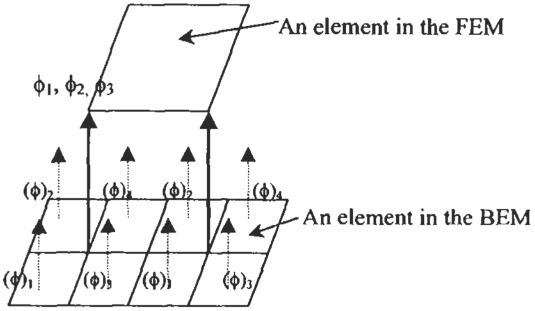

Figure 2: Discretization of a VLFS by quadrilateral elements.

The added mass and wave damping coefficients can be expressed as follows.

$$a_{kj} = -\rho \operatorname{Re}[\iint_{S_n} \phi_j n_k ds] \tag{12}$$

$$b_{kj} = -\rho\omega \operatorname{Im}[\iint_{S_n} \phi_j n_k ds] \tag{13}$$

where, j,k : 1, 2, 3, …, 3N

The wave exciting forces in the j-th bodies can be expressed by the incident wave potential and diffraction potential.

$$f_j = -\rho\omega^2[\iint_{S_n} (\phi_I + \phi_d)_j n_k ds] \tag{14}$$

3 TIME DOMAIN ANALYSIS

The equation of motion in the time domain can be derived by extending the equation for a floating body proposed by Cummins(1962). In this method hydrodynamic forces are expressed by time convolution of memory effect including wave damping effect and velocity of structure. VLFS is assumed to be a pontoon-type barge with the length L, the breadth B and the draft d. The thin plate theory can be used to describe vertical motions of it. The equation of motion can be given as follows.

$$\sum_{j=1}^{3N}[(M_{kj} + a_{kj}(\infty))\ddot{x}_j(t) + \int_0^t R_{kj}(t-\tau)\dot{x}_j(\tau)d\tau + (C_{kj} + K_{kj})x_j(t)] = F_j(t) \tag{15}$$

where, $$R_{kj}(t) = \frac{2}{\pi}\int_0^\infty b_{kj}(\omega)\cos(\omega t)d\omega \tag{16}$$

$$a_{kj}(\infty) = a_{kj}(\omega) + \frac{1}{\omega}\int_0^\infty R_{kj}(t)\sin(\omega t)dt \tag{17}$$

M : structural mass matrix
a : added mass matrix
b : damping matrix
R : memory effects function
C : restoring force matrix
K : stiffness matrix
F : wave exciting force

Eqn. 15 can be solved by using the numerical integration technique in each time step and the Newmark β method is employed here. To evaluate the retardation function, the wave damping coefficient should be known. In order to predict hydroelastic responses of VLFS in irregular waves, the seaway is represented by the ITTC spectrum.

$$S_\varsigma = \frac{A}{\omega^5}\exp(-\frac{B}{\omega^4}) \tag{18}$$

where, $$A = 172.75(H_{1/3}^2 / T_m^4) \tag{19}$$

$$B = 691./T_1^4 \tag{20}$$

$H_{1/3}$: significant wave height
T_m : mean period

The wave amplitude of m-th component for irregular wave is obtained by Eqn. (21) and (22).

$$\varsigma = \sum_{m=1}^{M} \varsigma_m \cos(\omega_m t + \varepsilon_m) \tag{21}$$

$$\varsigma_m = \sqrt{2S_\varsigma(\omega_m)\Delta\omega} \tag{22}$$

where ζ_m : wave amplitude
ω_m : wave circular frequency
ε_m : random phase angle
$\Delta\omega$: interval between wave circular frequencies

The wave exciting forces on the irregular waves are derived from Eqn. (14).

$$F_j = \sum_{m=1}^{M} \varsigma_m f_j e^{i\omega_m t + \varepsilon_m} \tag{23}$$

The deck wetness is defined when a bottom point of VLFS is below free surface and slamming when free surface is below a bottom point of VLFS in Eqn. (24) and (25).

$$z_r(t) = z(t) - \varsigma(t) > freebord \tag{24}$$
$$z_r(t) = z(t) - \varsigma(t) < -draft \tag{25}$$

where, Z_r: the local relative vertical motion

In the frequency domain, the response amplitude operator(RAO) of relative vertical responses in regular waves can be expressed as follows.

$$m_0 = \int_0^\infty \left(\frac{z_r}{\varsigma}\right)^2 S_\varsigma(\omega)d\omega \tag{26}$$

The relative responses for incident waves is described by the Rayleigh density function, the following relations in the frequency and time domain are satisfied for the probability of deck wetness and slamming.

$$P_{dw} = \exp[-f^2 / 2m_0] \tag{27}$$
$$P_{sl} = \exp[-d^2 / 2m_0] \tag{28}$$

where, f: freebord of VLFS
d: draft of VLFS

4 NUMERICAL RESULTS AND DISCUSSIONS

Fig.1 shows the VLFS model of length 1,200m, breadth 240m, depth 4.5m, draft 1.0m, and rigidity 4.559×10^9kg$_f$-m. The water depth is 20m. The location of slamming and deck wetness is expressed by circle in Fig. 1. VLFS is subdivided into 60×8 flat shell elements.

Fig.3 shows a wave spectrum used in the prediction. Its significant wave height is 4.81m, wave period is 15sec, and incident wave angle is 180 degree.

Fig. 4 shows the comparison of hydroelastic vertical displacements in the frequency domain analysis with those in the time domain analysis. The wave period is 8 seconds and its height is 2m. The responses predicted by two methods show good agreements and the time domain analysis method is validated.

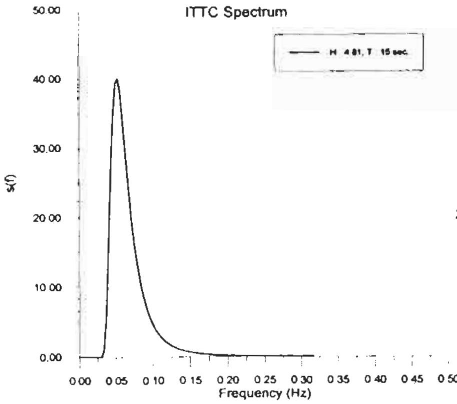

Figure 3:ITTC spectrum

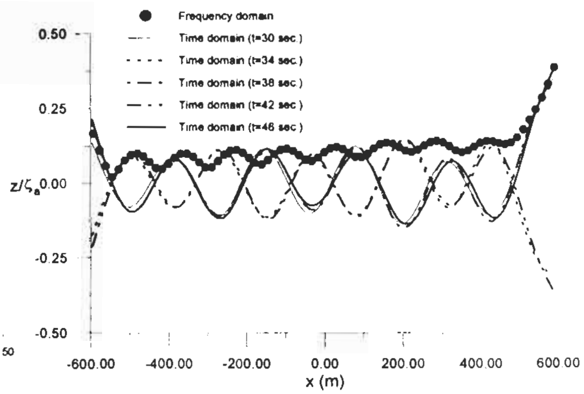

Figure 4: Comparison of relative vertical displacements in freency domain with those in time domain

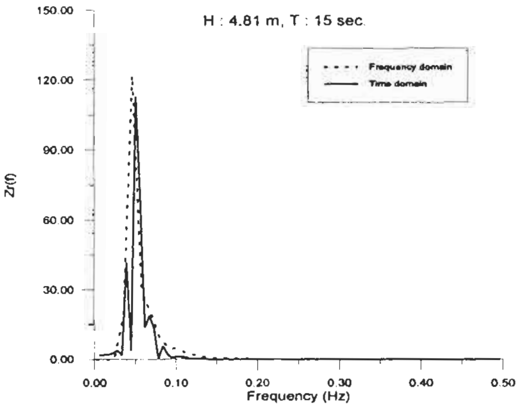

Figure 5: The relative response spectra ($H_{1/3}$:4.81m)

TABLE 1

THE PROBABILITIES OF THE SLAMMING AND DECK WETNESS

Sea state		Frequency domain	Time domain
$H_{1/3}$:4.81m T_m:15sec.	m_0	2.41	1.74
	Deck wetness probability(%)	7.9	3
	Slamming probability(%)	81	75

Fig.5 shows the relative response spectra calculated in the time and frequency domain
Table 1 shows the probabilities of the slamming and deck wetness in the long crested irregular waves. The value of m_0 in the frequency domain are greater than that in time domain.

5 CONCLUSIONS

Hydrodynamic forces of radiation and diffraction problems are estimated by using the source-dipole method and the structural bending rigidities are determined by the finite element method. The predictions of deck wetness and slamming of VLFS in time and frequency domain have been made.
VLFS is subdivided into 74×9 flat shell elements in the frequency domain. But it is subdivided into 59×7 flat shell elements in the time domain because of taking pretty long time for the analysis of hydroelasic motion. It makes is the difference between the results in the time domain and it in the frequency domain.

References

Yago, K. and Endo, H. (1996). On the Hydroelastic Response of Box-Shaped Floating Structure with Shallow Draft (Tank Test with Large Scale Model). *Journal of The Society of Naval Architects of Japan* **180**, 341-352

Endo, H. (1999). The Behavior of an Airplane Taking Off from Landing on a VLFS in Rough Sea Condition. *VLFS'99*, Honolulu, 212-218

Lee,H.Y. and Shin, H. (2000). Hydroelastic Responses of a Very Large Floating Structure in Time Domain. *Journal of Ocean Engineering and Technology*, KCORE **14:3**, 29-34 (in Korean).

Ohmatsu, S. (1998). Numerical Calculation of Hydroelastic Behavior of VLFS in Time Domain. *Proceeding of the Second International Conference on Hydroelasticity in Marine Technology*, OMAE, 89-97

Faltinsen, O.M. and Michelson, F.C. (1974). Motion of Large Structures in Waves at Zero Froude Number. *Int. Symp. the Dynamics of Marine Vehicles and Structures in Waves.*

Takaishi, Y., Masuda, K. and Minemura, K. (1999). Relative Wave Motion and Shipping Water on Deck of Mega-Float Structure. *VLFS'99*, Honolulu, 446-778

Practical Design of Ships and Other Floating Structures
You-Sheng Wu, Wei-Cheng Cui and Guo-Jun Zhou (Eds)

© 2001 Elsevier Science Ltd. All rights reserved

PROBABILISTIC ANALYSIS TOOLS FOR SURFACE SHIPS UNDER SEAWAY AND EXTREME DYNAMIC LOADS

Y. J. Lua[1] and P. E. Hess[2]

[1]Applied Mechanics Department, Engineering & Information Technology Group, Anteon Corporation
240 Oral School Road, Mystic, CT 06355-1208, USA
[2]Survivability, Structures, and Materials Directorate, Naval Surface Warfare Center
Carderock Division, West Bethesda, MD 20817-5700, USA

ABSTRACT

Two analysis tools, SIMLAB and PULSTR, have been developed for probabilistic vulnerability and reliability assessments of surface ships. These tools account for variability in material properties, geometric configuration, failure criterion, and loading parameters. SIMLAB is a stochastic finite element analysis system which integrates a nonlinear finite element code, DYNA3D, into a simulation-based computational framework. SIMLAB can generate a Gaussian, non-Gaussian, stationary, or non-stationary random loading process and assess ship vulnerability under extreme dynamic loads. The limit state function is based on the first crossing of the critical response quantity above a safe threshold during the loading process. PULSTR is a reliability-based analysis and design tool, which can be used in the preliminary stages of structural design. Both the Monte Carlo Simulation (MCS) and the first order reliability analysis (FORM) modules compute the probability of failure of a hull-girder under longitudinal bending. A hybrid approach (MCS/FORM) is developed to compute small probability of failure with a great computational efficiency and numerical accuracy. To demonstrate these analysis tools, SIMLAB is applied to an elastoplastic beam model subjected to a random excitation, and PULSTR is employed for the reliability assessment of a surface ship under its single and double hull configurations.

KEYWORDS

Hull girder, structural reliability, first excursion, random process, Monte Carlo simulation, first order reliability method, ultimate bending strength, double hull, hybrid approach, DYNA3D, stochastic finite element method

INTRODUCTION

Current structural design of surface ships is based on deterministic analysis methodologies and design rules/requirements which are highly dependent upon test data and at-sea experience. Analysts and designers are faced with numerous sources of uncertainty and product variability during ship design. In traditional ship structure designs, uncertain parameters are treated as deterministic variables and empirical factors-of-safety are used to account for uncertainties. Factors-of-safety are determined based on past experience, but do not guarantee safety or satisfactory performance, nor provide any information on how the different parameters of the ship structure influence safety. Thus, it is difficult to design a ship system with a uniform distribution of safety among the different components using factors-of-safety.

Surface ships must survive a hostile environment. Ship vulnerability assessment is important in identifying the levels of operational capability that must remain after a ship is damaged under extreme dynamic loads. Under extreme environments, experimental observations have shown that the loading process is non-Gaussian and non-stationary and the ship structural response is nonlinear. Nonlinear structural response is induced by the initiation and progression of multiple local damages, such as local in-elastic/plastic deformation, stiffener tripping, panel buckling, or fracture. The complexity of fluid-structure interaction phenomena renders the assumption on the loading process (i.e. stationary and Gaussian) invalid. The conventional approach, based on linear random vibration theories and peak statistics, is inapplicable for the probabilistic vulnerability assessment of surface ships subjected to an extreme environment. Therefore, it is imperative to develop a generalized, simulation-based, probabilistic analysis tool which has no limit on the nature of input random processes (Gaussian, non-Gaussian, stationary, or non-stationary) and system characteristics (linear or nonlinear).

The ship structural design process should maximize structural performance and minimize life-cycle costs and weight, while ensuring an acceptable risk of failure under operational, seaway and extreme dynamic loads. Reliability-based design uses probabilistic methods to measure all uncertainties and maximizes structural performance for an acceptable level of structural safety and reliability. Reliability-based ship structural design will provide the best solution in the light of the available knowledge, tools and consequent uncertainty (White et al., 1995). The two primary benefits of the reliability-based approach are: 1) a formal and traceable measure of risk or safety in a new ship design with the use of advanced materials and unconventional hull geometry; and 2) the ability to evaluate the relative importance of various design options on the safety of ship structural components and provide a consistent level of safety and efficiency throughout the ship (Mansour, 1990; Hess and Ayyub, 1997).

In order to perform the probabilistic vulnerability assessment of surface ships under extreme dynamic loads, a stochastic finite element tool, SIMLAB has been developed by integrating the nonlinear finite element code, DYNA3D, into a simulation based probabilistic analysis framework. SIMLAB can provide probabilistic failure prediction of a structural system characterized by both random variables and random processes (Lua, 2000). To demonstrate SIMLAB, an elastoplastic beam is subjected to a random excitation to explore the effect of material nonlinearity on probability of failure and peak statistics.

PULSTR is used to perform a reliability-based assessment of a surface ship structure at its preliminary design/analysis stage. The uncertainties associated with global hull geometry, panels, hard corners, stiffeners, and material properties are propagated into the hull ultimate strength prediction module. A hybrid approach which combines both the MCS and FORM solution modules has been developed to assess the reliability level of a Navy Combatant, Ship A, in both its single and double hull configurations.

OVERVIEW OF SIMLAB

SIMLAB is a general stochastic finite element system that integrates the nonlinear finite element code, DYNA3D, into a simulation based probabilistic analysis framework. Both random sampling and Latin Hypercube sampling techniques are used to generate random variables and random processes. The key components of the SIMLAB methodology are given in Figure 1.

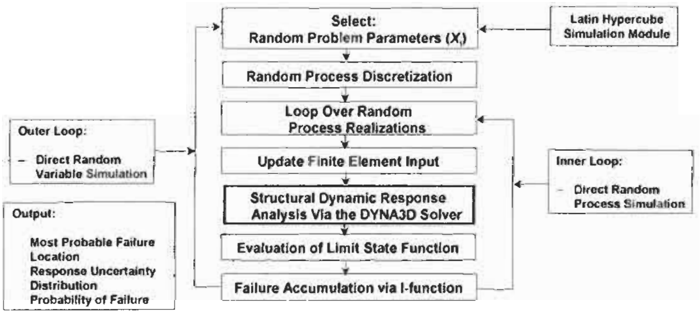
Select:
Random Problem Parameters (X)
Latin Hypercube Simulation Module
Random Process Discretization
Loop Over Random Process Realizations
Outer Loop:
– Direct Random Variable Simulation
Update Finite Element Input
Inner Loop:
– Direct Random Process Simulation
Structural Dynamic Response Analysis Via the DYNA3D Solver
Output:
Most Probable Failure Location
Response Uncertainty Distribution
Probability of Failure
Evaluation of Limit State Function
Failure Accumulation via I-function

Figure 1: Overview of SIMLAB Methodology

As shown in Figure 1, the outer loop simulates all random variables which characterize basic structural strength variables (material properties and geometric parameters). The inner loop simulates a random process (seaway/slamming loading). After selecting the material properties, hull geometric parameters, and applied loads, a finite element input file will be updated and a structural dynamic response analysis is performed using a FEM solver. The maximum response variable over the entire loading period at a critical location is stored and used in a limit state function.

Random Process Simulation Module

A random process simulation model has been developed to generate stationary Gaussian (g_{GS}), non-stationary Gaussian, non-Gaussian stationary, and non-Gaussian non-stationary processes. The spectral representation method developed by Grigoriu (1993) is employed for a Gaussian stationary process. Two approaches have been used in SIMLAB to generate a non-Gaussian process (g_{NG}) from the corresponding Gaussian process (g_G). In the first approach, we use a single parameter (random phase angle) based simulation model by Shinozuka and Jan (1972), along with a small number of frequency discretization points. In the second approach, a nonlinear transformation is introduced to generate a non-Gaussian process from the corresponding Gaussian process based on the mapping function developed by Sarkani et al. (1994).

Time Dependent Reliability Analysis via the First-Excursion Probability

Probabilistic vulnerability assessment of a ship structural component subjected to extreme dynamic loading can be formulated as a time-dependent reliability problem. The failure event is defined as the crossing of a critical response quantity above a safe threshold during the entire time history. Let $s(t, y)$ denote a critical response quantity of the structure and $r(t, y)$ denote the corresponding safe threshold (yield strength, or critical moment). The limit-state function defined in the random variables space (y) is given by $G(y) = \min_{t\in[a,b]} w(t, y)$, where $w(t, y)=r(t, y) - s(t, y)$. Note that even if $w(t, y)$ is continuously differentiable in y and t, the function $G(y)$ usually is not continuously differentiable due to the minimization operator used. The lack of uniqueness of the gradient of $G(y)$ at a point will result in a non-convergent solution in using the first order reliability method (FORM). Thus, the simulation-based stochastic finite element approach becomes very attractive in performing vulnerability assessment of ship structures under extreme dynamic loading.

EXAMPLE APPLICATION OF SIMLAB

An elastoplastic hull girder subjected to a stationary Gaussian process is considered here to investigate the effect of material nonlinearity on the statistical distributions of peak and extreme values. The hull girder is discretized into 24 beam elements. At each nodal point, a nodal mass is assigned to represent the sum of the structural mass (M_S), and the added mass (M_A). The structural mass consists of both the material mass (M_M) and the equipment mass (M_E). The safety margin for the *n-th* beam element is defined as

$$G_n(t, x_n) = \sigma_y^n - \sigma_{eff}^n(t, x_n) \qquad (1)$$

where σ_y^n is the yield strength of the *n-th* beam element and $\sigma_{eff}^n(t, x_n)$ is the VonMises stress of the *n-th* element at time *t*. The limit state function is given by

$$G = \min\{G_n(t, x_n)\}; \quad 1<n<M; \quad t \in [0, T] \qquad (2)$$

where M is the total number of beam elements and T is the termination time of response analysis.

In order to characterize the random temporal variation of the applied nodal force, a random process is used to describe the loading function *f(t)*. The spectral density function *S(ω)* using the significant wave height (H_m) of 5.0 *m* and the wave frequency (ω_m) of 52.36 *rps* is shown in Fig. 2a. Examples of loading histories generated from *S(ω)* are shown in Fig. 2b. In addition to the random loading process, a set of random variables are also used to characterize uncertainty in elastic modulus (E), yield strength (σ_y), sectional thickness (t), and total nodal mass (m_{node}^T).

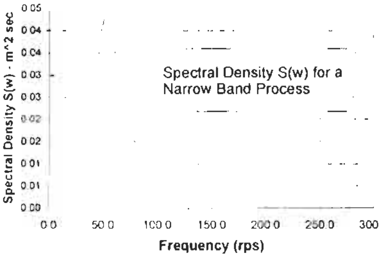

Figure 2a: Mean Square Spectral Density of Load Amplification Factor *f(t)*

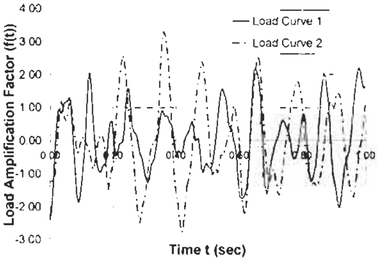

Figure 2b: Two Loading Curves Generated from the Gaussian-Stationary Random Process

One thousand (1000) simulations were performed using SIMLAB. The resulting total number of the first-excursion failure associated with Eq. (2) was 448. Thus, the simulated average value of probability of failure is 0.448. For a linear dynamic system subjected to a stationary narrow band Gaussian excitation, the statistical distributions of peak and extreme peak values can be described by a Rayleigh and a Gumbel distribution, respectively (see Mansour, 1990). To demonstrate whether these analytical peak distributions are still valid for the present nonlinear system, a comparison of CDFs of positive peak values with an equivalent Rayleigh distribution is shown in Figure 3a.

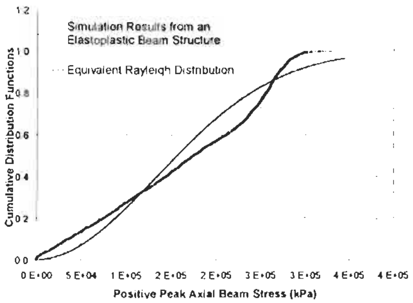

Figure 3a: Statistical Distribution of Positive Peak Values for the Elastoplastic Beam Model

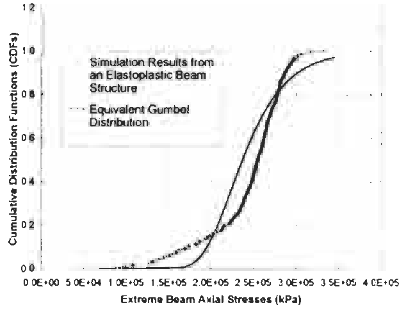

Figure 3b: Statistical Distribution of Extreme Peak Values for the Elastoplastic Beam Model

The statistical distribution of positive peak values has a large deviation from the equivalent Rayleigh distribution. Similarly, the statistical distribution of extreme peak values can no longer be described by an equivalent Gumbel distribution (see Figure 3b). A common feature can be observed from Figures 3a and 3b. In both the lower and the upper tail regions of these CDF curves, the CDF obtained from the simulated response data is larger than the one predicted from the corresponding analytical model, which is valid for a linear dynamic system subjected to a Gaussian process. Since the small failure probability of a structural system is governed by the tail CDF curve of the critical response parameter, we can conclude that the use of these analytical peak distributions for a nonlinear system will result in a conservative assessment of failure probability.

OVERVIEW OF PULSTR

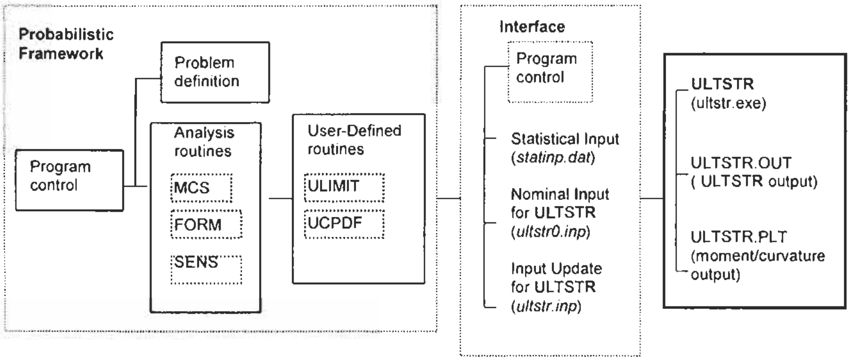
Probabilistic Framework
Problem definition
Program control
Analysis routines
MCS
FORM
SENS
User-Defined routines
ULIMIT
UCPDF
Interface
Program control
Statistical Input (statinp.dat)
Nominal Input for ULTSTR (ultstr0.inp)
Input Update for ULTSTR (ultstr.inp)
ULTSTR (ultstr.exe)
ULTSTR.OUT (ULTSTR output)
ULTSTR.PLT (moment/curvature output)

Figure 4: Block Diagram of PULSTR

PULSTR is a probabilistic version of the ULTSTR (ULTimate STRength) program. PULSTR allows designers to perform probabilistic analysis and design of a hull-girder under longitudinal bending. It is built on a macro command architecture which integrates a probabilistic analysis framework with the deterministic solver –ULTSTR- developed by Adamchak (1982). As shown in Fig. 4, PULSTR consists of three separate modules: 1) probabilistic analysis module; 2) interface module; and 3) ULTSTR response analysis module. To perform the probabilistic assessment of a hull girder, PULSTR requires the definition of a limit state function $G(x)$ through a user-defined subroutine, ULIMIT. The ULTSTR deterministic solver is integrated in ULIMIT using a system call to execute the ULTSTR response analysis module. While PULSTR provides fourteen (14) analytical statistical modes in its probability distribution library, an arbitrary user-defined probability distribution can be specified with the use of user-defined subroutine, UCPDF.

EXAMPLE APPLICATIONS OF PULSTR

In order to perform reliability assessment of a hull girder under random longitudinal bending, a limit state function $G(x)$ has to be defined with the user-defined subroutine, ULIMIT. For a given vector of random variables $\mathbf{x}(z_1, z_2, z_3, \ldots, z_n, M_{SW}, M_{WD})$ characterizing randomness in hull geometry, panel thickness, stiffener parameters, hard corner parameters, material parameters, and loading parameters (M_{SW}, M_{WD}), the limit state function can be expressed as

$$G(x) = M_{ult}(z_1, z_2, \ldots, z_n) - M_{app}(M_{SW}, M_{WD}) \qquad (3)$$

where M_{ult} is the ultimate resisting moment of a hull section computed by ULTSTR, and M_{app} is the resultant applied bending moment induced by the stillwater bending moment (M_{SW}) and the combined wave-induced and dynamic bending moment (M_{WD}). Since the probability of failure of a hull girder is in the range of 10^{-3} to 10^{-9}, the computational effort associated with a direct application of Monte Carlo simulation (MCS) will be prohibitively large, thus precluding its use for reliability assessment of surface ships. While the first order reliability method (FORM) provides an alternative way for evaluating the small probability of failure, the direct application of Eq. (3) in PULSTR's FORM solution module will result in a divergent solution because of 1) the oscillation of $G(x)$ near the design point (x^*); and 2) nonlinear dependence of the hull capacity M_{ult} on hull parameters z_i ($i=1, 2, \ldots, n$). To circumvent this difficulty, a hybrid approach is developed where a relatively small number of MCSs is performed to generate the statistical distribution of M_{ult} and the PULSTR's FORM solution module is applied next by replacing $M_{ult}(z_1, z_2, \ldots, z_n)$ in Eq. (3) with one independent random variable

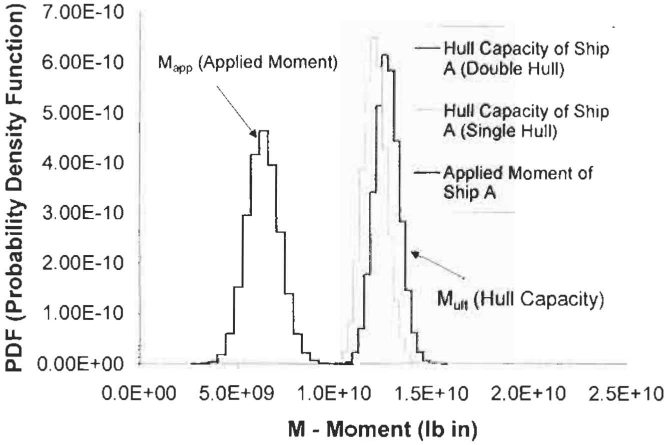

Figure 5: Comparison of PDF of M_{app} with PDFs of M_{ult} of Single and Double Hulls of Ship A

M_{ult}. The resulting significant reduction of the total number of random variables will make the FORM approach computationally efficient and numerically robust for computing the small probability of failure. The first-order reliability assessment of Ship A under its single and double hull configurations is performed using the hybrid approach in PULSTR. A comparison of PDFs of applied moment (M_{app}) and hull capacity (M_{ult}) is shown in Figure 5. Based on 250,000 simulations, a curve-fit CDF model is developed and used as the user-defined probability distribution of M_{ult} in UPCDF (see Fig. 4). Using PULSTR's FORM solution module, both the failure probability (P_f) and the reliability index (β) of Ship A are computed and given by

$$\begin{aligned} P_f &= 4.4317 \times 10^{-7}; \quad \beta = 4.915\,(\mathit{Single\ Hull}) \\ P_f &= 5.4417 \times 10^{-8}; \quad \beta = 5.3113\,(\mathit{Double\ Hull}) \end{aligned} \tag{5}$$

Since the PDF curve of hull capacity of the double hull is shifted along the positive x-axis (see Fig. 5), the resulting probability of failure (P_f) is about 8 times less than P_f of the corresponding single hull of Ship A. The computational efficiency of the hybrid approach can be demonstrated through comparison of the number of simulations (250,000) used with the number of simulations (3.482E+10) that would have been required if the direct MCSs were performed to compute the P_f with the same accuracy.

CONCLUSIONS

An overview of two probabilistic analysis and design tools, SIMLAB and PULSTR, has been given along with their applications to surface ships subjected to both extreme dynamic and seaway loading.

ACKNOWLEDGEMENT

The authors gratefully acknowledge the support of Dr. Roshdy Barsoum at Office of Naval Research and Dr. Jeff Beach at the Structures and Composites Department of Naval Surface Warfare Center of Carderock Division.

REFERENCES

Adamchak, J.C. (1982). ULTSTR: A Program for Estimating the Collapse Moment of a Ship's Hull Under Longitudinal Bending. DTNSRDC Report 82/076, U.S. Navy, NSWCCD.

Grigoriu, M. (1993). Spectral Representation Method in Simulation, *Prob. Eng. Mech.*, **8**, pp. 75-90.

Hess. P. and B. Ayyub. (1997). Variability in Geometry and Imperfections of Surface Ship Structural Scantlings. NSWCCD-TR-65-97/02.

Lua, Y. J. (2000). Probabilistic Vulnerability Assessment Tool for Surface Ship Under Extreme Dynamic Loads. *Ship Structure Symposium 2000*, in press.

Mansour, A. (1990). An Introduction to Structural Reliability Theory, SSC-351.

Sarkani, S., D.P. Hihl, and J. E. Beach (1994). Fatigue of Weded Joints Under Narrowband Non-Gaussian Loadings, *Prob. Eng. Mech.*, **9**, pp. 179 – 190.

Shinozuka, M. and Jan C-M (1972). Digital Simulation of Random Processes and Its Applications. *J. Sound Vib.* **25**(1), pp. 111 – 128.

Whirte, G., M. Bilal, E. Ayyub, E. Nikolaidis, and O. Hughes. (1995). Applications in Ship Structures. in *Probabilistic Structural Mechanics Handbook*, edited by C. Raj Sundararajan, pp. 575 – 607.

Practical Design of Ships and Other Floating Structures
You-Sheng Wu, Wei-Cheng Cui and Guo-Jun Zhou (Eds)
© 2001 Elsevier Science Ltd. All rights reserved

COMPREHENSIVE FUZZY APPROACH IN HAZARD IDENTIFICATION OF FORMAL SAFETY ASSESSMENT (FSA)

Ying-Qiu Chen[1] and Shao-Fen Lin[2]

[1]China Classification Society
40 Dong Huang Cheng Gen Nan Jie, Beijing 100006, China
[2]Department of Machinery of Navigation College, Jimei University
205 Rome, 175 Shi Gu Load, Jimei, Xiamen, Fujian Province, China

ABSTRACT

The paper presents an approach, which is used in hazard identification of Formal Safety Assessment (FSA) for ships, consisting of both fuzzy set theory application and database technology. An example of application concerned approach was given. This system will be applied to the application of decision making in the near future.

KEYWORDS

Risk Assessment, Database Technology, Fuzzy Set Theory

1 INTRODUCTION

There is a similar risk assessment procedure in the shipping or in the industry; namely it consists of three parts including the concerned persons, environment and the used facilities. Regarding a ship system, it should involve three parts; these are ships, navigation environment and crew. In the paper (Chen, 1998), the mathematics model for ship system is divided into seven sets which are as follows:

- ship set;
- crew set;
- environment set;
- relation set between ship and environment;
- relation set between ship and crew;
- relation set between crew and environment;
- relation set among ship, crew and environment.

At present, the " safety " and dangerous " all belong to fuzzy concepts, the difference between them will effect the final research results and decision made by top management level who decides the safety policy. For an example, study of FSA for bulk carriers, the dangerous means the happened event that will induce the following terms: lost of human lives, loses to property including the ship herself, consequential loses to stakeholders and the environment pollution.

There are so many factors which can be determined in the assessment procedures for bulk carriers, they could not be given as an obvious limitation and they cover not only random but fuzzy properties.

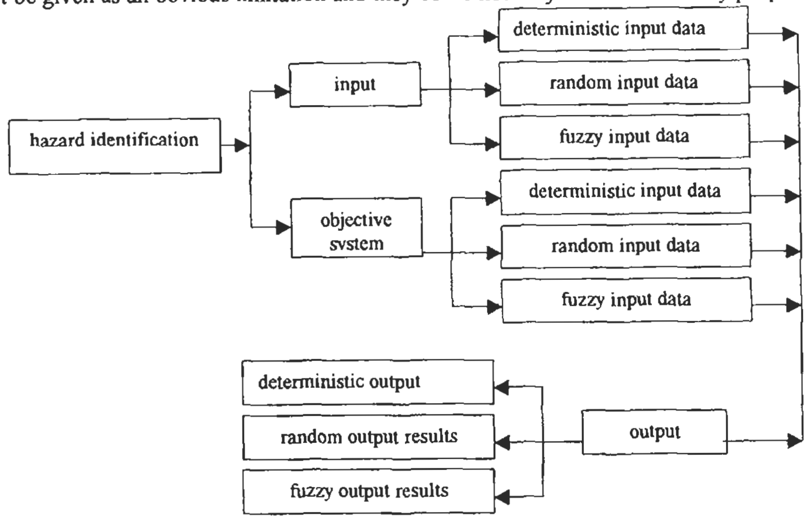
hazard identification
input
objective system
deterministic input data
random input data
fuzzy input data
deterministic input data
random input data
fuzzy input data
deterministic output
random output results
fuzzy output results
output

Figure1: Hazard identification of FSA

As mentioned above, the hazard identification of FSA covers so many non-deterministic factors either input subsystem or objective system in which the fuzzy factors in any part above will induce the output results with fuzzy (see Fig.1).

The paper presents a comprehensive fuzzy approach in the application of hazard identification of FSA, in the approach the ship system is regarded as a whole. So this is a common approach which can be used in assessment of many events in ship system.

2 COMPREHENSIVE FUZZY ASSESSMENT

2.1 One-Level Comprehensive Fuzzy Assessment (Lin and Chen, 1999)

One-Level Comprehensive Fuzzy Assessment follows the next orders:

1) Setting the factor set:

$$U=\{u_{1,}, u_{2,}, \ldots, u_m\}, \quad u_i \; (i= 1, 2, \ldots, m) \quad u_i \in U \text{ or } u_i \notin U \tag{1}$$

2) Setting the selected set:

$$V=\{v_1, v_{2,}, \ldots, v_n\} \qquad (i= 1, 2, \ldots, n) \tag{2}$$

3) Setting the weighting set:

$$\bar{A} = (a_{1,}, a_{2,}, \ldots, a_m) \tag{3}$$

$$\sum_{i=1}^{m} a_i = 1 \qquad \text{and} \qquad a_i \geq 0 \tag{4}$$

They can be regarded as " level of belonging to u_i ($i = 1, 2, \ldots, m$) ", the weighting set can be written as:

$$\bar{A} = a_1 \ / \ u_1 + a_2 \ / u_2 + \cdots + a_m \ / u_m \qquad (i = 1, 2, \ldots, m) \quad (5)$$

4) Fuzzy assessment of a single factor:
If we carry out an assessment with u_i (i= $1, 2, m$) within the assessed objectives and the membership degree of *ith* element V_j is r_{ij} , and then assessed set can be written as follows on the basis of the assessed results with *ith* factor u_i (i= $1, 2, \ldots, m$):

$$\ddot{R}_i = r_{i1} \ / v_1 + r_{i2} \ /v_2 + \cdots + r_{in} \ / v_n \qquad (6)$$

Obviously, it is a fuzzy sub-set in the selected set and is written as:

$$\bar{R}_i = (r_{i1} , r_{i2} , \cdots , r_{in}) \qquad (7)$$

Thus, we can obtain a matrix consisting of the membership degree with a single factor:

$$\bar{R} = \begin{bmatrix} r_{11} r_{12} \cdots\cdots\cdots r_{1n} \\ r_{21} r_{22} \cdots\cdots\cdots r_{2n} \\ \cdots\cdots\cdots\cdots\cdots\cdots \\ r_{m1} r_{m2} \cdots\cdots r_{mn} \end{bmatrix} \qquad (8)$$

Therefore the single factor set is also written as:

$$\bar{R}_i = r_{i1} \ /(u_i, v_1) + r_{i2} \ /(u_i, v_2) + \cdots + r_{in} \ /(u_i, v_n) \ \ (i = 1,2, \ldots, m; j = 1, 2, \ldots, n) \quad (9)$$

in which, (u_i, v_j) is the element of direct product set $U \times V$ and v_{ij} is the grade of reasonable relationship between u_i and v_j.

5) Comprehensive Fuzzy Assessment (CFA)
The sum of the elements in individual column in formula (8) is used to show the comprehensive effective of all factors, which is as follows:

$$R_j = \sum_{i=1}^{m} r_{ij} \qquad (j = 1,2,\ldots,n) \qquad (10)$$

If matrix $\bar{R}$ in the above formula (8) is multiplied by the weighting set $\ddot{A}$, then the obtained results can reflect the comprehensive effective of all factors, the procedure shows as follows:

$$B = \bar{A} \bullet \bar{R} \qquad (11)$$

The detail of the above procedure is:

$$\dot{B} = (a_1, a_2, \ldots, a_m) \begin{bmatrix} r_{11} r_{12} \cdots\cdots\cdots r_{1n} \\ r_{21} r_{22} \cdots\cdots\cdots r_{2n} \\ \cdots\cdots\cdots\cdots\cdots\cdots \\ r_{m1} r_{m2} \cdots\cdots r_{mn} \end{bmatrix}$$

$$= (b_1, b_2, \ldots, b_n) \qquad (12)$$

$$b_j = \bigvee_{i=1}^{m} (a_i \wedge r_{ij}) \qquad (j = 1,2,\ldots,n) \qquad (13)$$

is the comprehensive fuzzy assessment index which means the membership degree of *j*th element in the selected set.

6) The method of dealing with assessment index b_j

a. the maximum membership degree method

Taking the selected element v_L corresponding to the maximum assessment index max b_j as the results of assessment, i.e.

$$V = \{v_L \mid v_L \to \max_j \; b_j \} \tag{14}$$

b. the weighted-average method

Taking b_j as weighting value, the a single selected element v_j is operated with weighted-average procedure, its results are:

$$V = \sum_{j=1}^{n} b_j v_j / \sum_{j=1}^{n} b_j \tag{15}$$

If $\sum_{j=1}^{n} b_j = 1$ or the normalizing procedure is completed, the formula is simplified as follows:

$$V = \sum_{j=1}^{n} b_j v_j \tag{16}$$

For non-digital nature factors (e.g. working capacity of staff), then the selected set will be:

$$\text{V} = \{\text{excellent, good, medium, poor}) \tag{17}$$

The selected element should be equivalent to digital factors while the weighted-average method is still adopted.

2.2 Multi-Level Comprehensive Fuzzy Assessment

1) In case of existing multi-factors

a. It is very difficult to distribute the weighting value on the basis of actual cases. Sometimes, the weighting value mainly depends on the experience of the experts.

b. Non-meaningful assessment results (See Fig. 2).

2) Mathematical model

The above (right) gives an example of three level assessments.

2.3 All Kinds of Mathematics Model for Comprehensive Fuzzy Assessment

1) Model one: M $(\wedge, \vee)$, $b_j = \bigvee_{i=1}^{m} (a_i \wedge r_{ij})$ $\quad (j - 1,2,\dots,n)$

2) Model two: $M(\,*,\ \vee\,)$, in which, " * " means a common multiplication, we have:

$b_j = \bigvee_{i=1}^{m} (\; a_i r_{ij} \;)$ $\quad$ (*j*=1, 2, ..., n)

3) Model three: $M(\wedge, \oplus\,)$, in which, " $\oplus$ " means an operation of sum limited, i.e. $x \oplus y = \min(1, x+y)$, in the model, $b_j = \sum_{i=1}^{m} (a_i \wedge r_{ij}\;)$ (*j*=1, 2,..., n), the symbol $\sum_{i=1}^{m}$ is a sum of m numbers under $\oplus$ operation. Therefore, the above formula can be written as: $b_j = \min\{1, \sum_{i=1}^{m} (a_i \wedge r_{ij}\;)\}$ (*j*=1, 2, ..., n)

4) model four: $M(*,\oplus)$, i.e, $b_j = \sum_{i=1}^{m}(a_i r_{ij}\ )$ (j=1, 2, ..., n) or $b_j = \min\{1, \sum_{i=1}^{m}(a_i r_{ij}\ )\}$ (j=1, 2, ..., n)

5) Model five: $M(*,+)$and thus $b_j = \sum_{i=1}^{m} a_i r_{ij}$ (j=1, 2, ..., n)

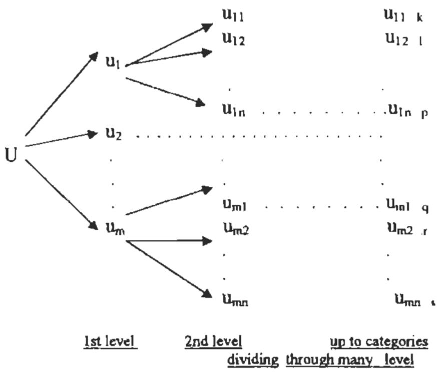
U
u1
u2
um
u11
u12
u1n
um1
um2
umn
u11 k
u12 l
u1n p
um1 q
um2 r
umn s
1st level
2nd level
up to categories dividing through many level

$$\bar{B} = \bar{A}\circ\bar{R} = \bar{A}\circ\begin{bmatrix} \bar{A}_1\circ\begin{bmatrix}\bar{A}_{11}\circ\bar{R}_{11}\\ \bar{A}_{12}\circ\bar{R}_{12}\\ \vdots\\ \bar{A}_{1n}\circ\bar{R}_{1n}\end{bmatrix}\\ \vdots\\ \bar{A}_m\circ\begin{bmatrix}\bar{A}_{m1}\circ\bar{R}_{m1}\\ \bar{A}_{m2}\circ\bar{R}_{m2}\\ \vdots\\ \bar{A}_{mn}\circ\bar{R}_{mn}\end{bmatrix}\end{bmatrix}$$

Figure 2: Multi-Level Comprehensive Fuzzy Assessment

3 APPLICATION OF THE COMPREHENSIVE FUZZY METHOD IN HAZARD IDENTIFICATION OF FORMAL SAFETY ASSESSMENT (FSA)

The all of kind of subsystem are as follows:

3.1 Crew Subsystem

Fig. 3 shows the collection procedure of the outside information.
A - information of ship navigation case; B - external force condition information; C - navigation condition and channel information; D - information of driving ship.
Crew will deal with the information and control the overall procedure of navigation (See Fig.4) .

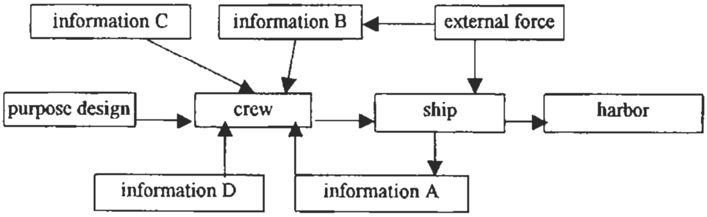
information C
information B
external force
purpose design
crew
ship
harbor
information D
information A

Figure 3: Collection procedure of the outside information

3.2 Environment Subsystem

Indeed, this is very complicated subsystem because ships will meet so many cases in its navigation not only natural condition but also men-made condition.

3.3 Ship Subsystem

The ship subsystem means an overall ship system including hull strength, stability, facilities, design approach and advanced grade of operation system.

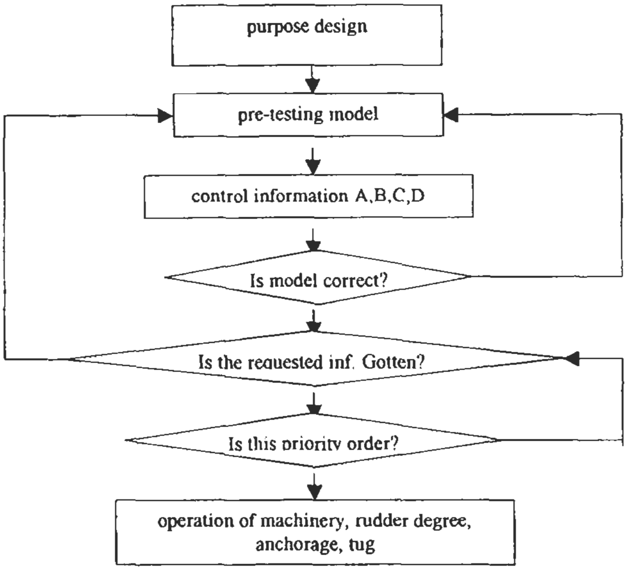
purpose design
pre-testing model
control information A,B,C,D
Is model correct?
Is the requested inf. Gotten?
Is this priority order?
operation of machinery, rudder degree, anchorage, tug

Figure 4: Check for information and control for overall procedure of navigation

3.4 Election of the Selected Set and Weighting Set

We must set up the corresponding selected element for each assessment factor and the selected set consists of the selected elements. In the paper, the selected set consists of the following seven levels:

{excellent, good, better, medium, poorer, poor, worse}

3.5 An Example-- hazard Assessment of Marine Power Plant for a Bulk Carrier

.1 basis factors: $U=\{u_1, u_2, u_3, u_4\}$:in which, u_1- engine; u_2- stern shaft; u_3- propeller; u_4- auxiliary engine.

.2 the selected set : $B=\{b_1, b_2, b_3, b_4, b_5, b_6, b_7\}$

In which, b_1- excellent from 90 to 100; b_2-good from 80 to 90; b_3 - better from 70 to 80; b_4 – medium from 60 to 70; b_5 - poorer from 50 to 60; b_6 - poor from 40 to 50; b_7 - worse from 30 to 40. The number of bj (j=1,2,3,4,5,6,7) are decided by investigation joined by the experts.

.3 the weighting set: $A=\{a_1, a_2, a_3, a_4\}$:In which, a_1 - 0.4; a_2 - 0.2; a_3 - 0.2; a_4 - 0.2. The value aj (j=1, 2, 3, 4) decided by the experts due to lack of database. The table 1 shows the selected set of the a single factor.

TABLE1

SELECTED SET OF THE A SINGLE FACTOR

Factor set	Basis factor		b_1	b_2	b_3	b_4	b_5	b_6	b_7
Marine power plant	u_1	engine	0.05	0.50	0.35	0.08	0.02	0.00	0.00
	u_2	stern shaft	0.00	0.30	0.55	0.15	0.00	0.00	0.00
	u_3	propeller	0.01	0.35	0.45	0.14	0.05	0.00	0.00
	u_4	auxiliary engine	0.00	0.20	0.60	0.10	0.05	0.05	0.00

The table 2 shows the results of comprehensive fuzzy assessment

TABLE 2
RESULTS OF COMPREHENSIVE FUZZY ASSESSMENT

Cal. Model	1	2	3	4	5	6	7	Assess. results
$M(\wedge, \vee)$	0.050	0.40	0.35	0.15	0.050	0.05	0.00	2
$M(*, \vee)$	0.020	0.20	0.14	0.032	0.010	0.01	0.00	3
$M(\wedge, \oplus)$	0.060	1.00	0.95	0.47	0.120	0.05	0.00	2
$M(*, \oplus)$	0.022	0.37	0.46	0.11	0.028	0.01	0.00	3
$M(*, +)$	0.022	0.37	0.46	0.11	0.028	0.01	0.00	3

If weighting set or input value of the selected set above are changed and the different results from table 1 and 2 will be obtained.

4 CONCLUSIONS

As mentioned above, the authors presented a new method applied to in the Hazard Identification of Formal Safety Assessment (FSA). It is a very useful tool and the corresponding software has been developed for the purpose. The next stage is that the relationship between hazard identification and risk assessment should be set up. In the study, other new method may be used and this is a task of the project.

References

Chen Yingqiu. (1998). A New Method for Assessment of Bulk Carrier Safety. *The report presented at the 3rd meeting of JRP*, Mumbai, India.

Lin Shaofen. (2000). Research on the First Cargo Hold Fuzzy Reliability of Bulk Carrier and Formal Safety Assessment. Thesis for Doctoral Degree, Harbin Industrial University..

Practical Design of Ships and Other Floating Structures
You-Sheng Wu, Wei-Cheng Cui and Guo-Jun Zhou (Eds)

© 2001 Elsevier Science Ltd. All rights reserved

ESTIMATING THE RISK OF CARGO SHIFTING IN WAVES – METHODOLOGY AND RESULTS

A. Ryrfeldt[1] and T. Källstam[2]

[1](b Ericson) Naval Architecture, KTH, SE-100 44 Stockholm, Sweden
[2]Center of Safety Research, KTH, SE-100 44 Stockholm, Sweden

ABSTRACT

An important cause for ship casualties is cargo shifting in rough seas. According to statistics approximately 10% of the founderings of general cargo ships are related to the shifting of cargo. Damage to cargo also means large costs to ship and cargo owners and insurance companies. This paper presents a methodology to calculate the long-term risk of initial cargo shift onboard a merchant vessel carrying unit cargo. Important applications of the methodology are the evaluation of new ship and cargo concepts, as a support for operational decisions and improvement of ship safety through risk estimations and assessment. In the methodology, models for the cargo shifting process, wave representation and calculation of ship motions have been combined with statistical models. The methodology has been used to perform case studies, indicating that the influence of factors such as stability, speed and lashings have a large influence on the risk of cargo shifting. The results confirm that the suggested methodology can be used to increase the understanding of factors influencing the risk of cargo shifting, which can affect design practice and operational aspects.

KEYWORDS

Cargo shifting, Risk analysis, Ship motions

1 INTRODUCTION

One of the major causes for ship casualties is the shifting of cargo, as can be seen from Lloyd's World Casualty Statistics (1999). According to these statistics approximately 10% of the founderings of general cargo ships are related to the shifting of cargo. Apart from being a threat to the vessel, cargo shifting causes damage to the cargo and thus costs to ship and cargo owners as well as insurance companies. Therefore cargo is secured to the vessel to prevent it from shifting, and much focus has been put on the lashing loads (e.g. Andersson et al. (1986)). However, ship owners and operators also need a tool for comparing risk levels, for example of different ships and different types of cargo on different routes. Although several studies have provided tools for evaluating the risk of unwanted events such as capsizing, grounding and collision, no such tools exist for estimating the risk of cargo shifting. The problem of cargo shifting is similar to that of estimating the risk of capsize as described by McTaggart (1998). The present paper describes a methodology for evaluating the risk with respect to cargo shifting. The risk is defined as the probability that at least one cargo unit will start to shift during a given time period. This probability is called the *risk of initial cargo shift*, and can be seen as a criterion for safe operation. This paper describes the methodology, which combines models for the interaction between waves, ship and cargo with statistical methods. Some case studies are included in order to evaluate the methodology and to show the influence of different parameters.

2 THE METHODOLOGY

Cargo shifting is a complex phenomenon, caused by the ship motions and largely influenced by the properties of cargo and lashings as well as operational aspects. During its time at sea a ship will encounter a large number of different conditions, defined by sea state, ship heading towards the waves, ship speed and loading condition. In each such condition the ship motions will be different and thereby also the forces acting on the cargo. Thus the probability of cargo shifting will differ in the various conditions. In order to estimate the total risk of cargo shifting during a year, or the ship's lifetime, the probability of shifting must be calculated in all conditions the ship will encounter during that time. In each condition the waves will have specific statistical properties and the ship will move in a certain way in response to these waves. These motions will induce forces on the cargo, which will shift if these forces are larger than what the cargo and its lashings can withstand. The total risk will depend on the probability of shifting in each condition and the probability that the ship will encounter each specific condition, as well as time. This section describes the cargo model used, and how the forces acting on the cargo are calculated from the ship motion response to waves. Further, a description is given of the statistical methods used for estimating the risk of shifting in a specific condition as well as the total risk. A thorough description of the methodology has been given by Ericson et al. (1999).

2.1 Cargo Model

A purely two-dimensional model of a cargo unit is used. This means that all forces act in the transversal plane of the ship, and that the pre-tensions in the lashings on each side are equal (see Figure 1). The cargo is assumed to be rigid, which means the lashing forces will be equal to the pre-tension until the cargo shifts. Shifting is defined as an initial motion, either by sliding or tipping. Thus, the risk presented is the risk of at least one initial motion of one cargo unit. For the case studies presented in this paper a model of a container is used. This container model is shown in Figure 1. The forces F and N are the forces corresponding to the combined effects of the ship motions, as described in the section

2.2 Ship Motion Induced Forces. If these forces are large enough in comparison to the pre-tensions and the friction, they will cause the cargo to shift. The tipping mode is neglected herein; since it can be shown that sliding is the critical mode for the studied type of cargo, see Ericson (2000). Sliding will occur if the total horizontal force is positive, that is if

$$F - F_f - 2\cdot(F_1 - F_2)\cdot\sin\varphi > 0\,. \tag{1}$$

The friction force (F_f) is found from vertical equilibrium, and the relation $F_f = \mu\cdot F_N$, where μ is the coefficient of friction. This means the friction force can be written as

$$F_f = \mu(N + 2\cdot(F_1 + F_2)\cdot\cos\varphi)\,. \tag{2}$$

Note that the friction force always acts in the opposite direction to the force F. Accounting for this and inserting the relation for the friction force from Eqn. (2) into Eqn. (1), gives the expression:

$$|F| - \mu(N + 2\cdot\cos\varphi\cdot(F_1 + F_2)) - 2\cdot\sin\varphi\cdot(F_1 - F_2)\cdot\text{sign}(F) > 0\,. \tag{3}$$

It should also be noted that in the methodology described herein, any cargo model can be used. For each cargo type an appropriate model should be used, taking into account its specific characteristics.

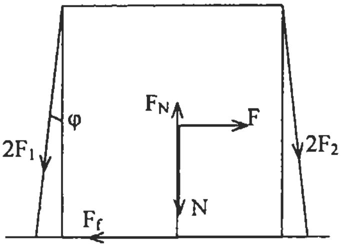

Figure 1: Geometry and forces acting on a container

2.2 Ship Motion Induced Forces

The forces F and N in the cargo model (and shown in Figure 1) are the combined effects of the ship motions influencing the cargo. Neglecting higher order terms the expressions for F and N are

$$F = m(a_v \cdot \sin\phi + a_h \cdot \cos\phi - z \cdot \ddot{\phi} + g \cdot \sin\phi) \qquad (4)$$

$$N = m(a_v \cdot \cos\phi - a_h \cdot \sin\phi + y \cdot \ddot{\phi} + g \cdot \cos\phi)$$

where	$a_v = a_{heave} - x \cdot a_{pitch}$	vertical acceleration
	$a_h = a_{sway} + x \cdot a_{yaw}$	horizontal acceleration (in the transversal direction)
	m	mass
	ϕ, $\ddot{\phi}$	roll angle and acceleration respectively
	x, y, z	longitudinal, transversal, and vertical distance from centre of rotation.

Since the horizontal and vertical forces (F and N) are non linear combinations of ship motions and since the phase shifts are important in evaluating the cargo shifting modes, the analysis must be made in the time domain. To calculate the time series of F and N the time series of the ship's roll angle and acceleration, and the vertical and horizontal accelerations are used. These time series can be calculated as the response to irregular waves by time-domain simulations, where the equation of motion is solved at each time step. However, in this kind of studies, where simulations must be done for a large number of situations, time-domain simulations are impractical due to long computational times. Therefore an indirect time-domain simulation technique has been used for estimating the forces acting on the cargo units. This technique, which is described in detail by Ericson (2000), has the benefit of being fast and giving reasonably accurate time series. However, it will not account for other non-linear effects than from combined responses, and will not be more accurate than spectrum theory for large motions. On the other hand, it is very time efficient and easy to use, since it is based on transfer functions calculated in the frequency-domain.

When simulating ship motions the time history of the waves is used. Irregular ocean waves can be viewed as superpositions of regular wave components of varying frequencies, as described by St. Denis and Pierson (1953). Irregular waves can therefore be simulated as a sum of regular waves with different frequencies, where the amplitude for each frequency can be found by discretizing a wave spectrum, which describes the statistical properties of the waves. In order to account for the stochastic properties of irregular waves random phases are used.

For a ship in an irregular wave system, the linear motion responses are the sum of the responses to the regular wave components in the wave system according to the superposition principle. When the transfer functions of the ship motions are available from linear strip calculation (e.g. as described by Salvesen et al. (1970)), the response of the motions or linear combinations of the motions can be added into an irregular response in the time-domain in the same way as the irregular wave system. Let $|\phi(\omega_i)|$ denote the amplitude transfer function of the roll motion for the regular component *i*. The time series for the roll motion will then be

$$\phi(t) = \sum_{i=1}^{I} a_i \cdot |\phi(\omega_i)| \cdot \cos(\omega_i \cdot t + \gamma_i + \delta_\phi(\omega_i)) \tag{5}$$

where $\delta_\phi(\omega_i)$ the phase transfer function, and a_i and γ_i are the wave amplitude and random phase for component *i* out of *I* components. The time series of the accelerations are calculated by the same principle. Insertion of these time series into Eqn. (4) gives F and N as functions of time.

2.3 Statistical Methods for Risk Calculation

The risk of cargo shifting is defined as the probability of at least one initial motion of a cargo unit onboard, during the studied time interval. This is equal to the complement of the probability of no cargo shift. The problem is similar to calculating the annual probability of capsize, as described by McTaggart (1998). If the studied time interval T is a year or more, it is reasonable to assume that the ship will encounter sea states according to the wave statistics. If the occurrence of sea states is assumed to be independent, the vessel can be assumed to encounter a number of independent conditions. For each condition *i* the probability of occurrence, denoted w_i, can be determined from wave statistics and knowledge of the ship operation. These probabilities of occurrence will have the property $\Sigma w_i = 1$. Further a sea state only has a short duration d, about 3 to 4 hours. It is assumed that the events of cargo shift during each condition lasting d hours are independent and identically distributed random variables. If the probability of no cargo shift during d hours in a certain condition is known as $p_i(d)$, the risk of cargo shifting can be written as

$$P = 1 - \left(\sum_i w_i p_i(d)\right)^{T/d} . \tag{6}$$

In estimating the risk of cargo shifting under a certain condition, or rather the probability of no shift p_i, the time series of the left-hand side of Eqn. (3) is used. If the value of this expression exceeds zero the cargo unit will start shifting. Therefore, the up-crossings of the time series through zero will be a measure of the risk of cargo shifting. If these up-crossings occur seldom, i.e. if the limit (in this case zero) is set high enough in relation to the mean value, the number of up-crossings occurring in disjoint time intervals can be asymptotically regarded as independent random variables. Further requirements for a Poisson process are the assumptions of stationarity and regularity (see Cramér & Leadbetter (1967)). These requirements are fulfilled for the simulated time series, and the events of up-crossings asymptotically form a Poisson process The Poisson parameter λ, i.e. the intensity, is the number of up-crossings per unit time. For a specific cargo unit *j* the probability of no cargo shift during d hours is

$$p_{i,j}(d) = e^{-\lambda_{i,j} d} . \tag{7}$$

Under the assumption that the individual cargo units are independent the probability of no cargo shift in a given condition will be the product of the probability of the individual units. However, due to the large number of cargo units onboard and the long computational time for time-domain simulations a sampling technique is used to reduce the number of calculations. Systematic sampling has been used since units close to each other have a similar probability not to shift. If the total number of cargo units is N and the sample size is n, a good estimate of the probability of no cargo shift in condition *i* is

$$p_i(d) = \prod_{j=1}^{n} \left(e^{-\lambda_{i,j} d}\right)^{N/n} . \tag{8}$$

3 CASE STUDIES AND RESULTS

In order to evaluate the methodology, case studies have been performed, where the risk of an initial cargo shift during one year has been calculated for various ship and cargo parameters. A typical Ro-Ro vessel (L_{pp} = 120 m and B = 20 m), in traffic between the Swedish and English east coasts, has been used. In each case the loading condition and ship speed has been assumed constant. This limits the number of situations the ship will experience to those defined by significant wave height, mean wave period and ship heading towards the waves. The cargo units have been assumed to be lashed containers, according to the cargo model described above, with $F_1 = F_2$. All cargo units are assumed to have equal properties, and the applied pre-tensions are according to the regulations of the Swedish Maritime Administration (1994). Sea states have been assumed to last for four hours. The probability of occurrence of the sea states is based on the wave statistics of Hogben et al. (1986), and the wave simulations are based on the Jonswap spectrum. The motion simulations have been made for four hours, with an increment of 0.05 rad/s and about 40 frequencies. In all cases the same wave realisations and sample of cargo units have been used in order to enable comparison.

In Figure 2 and Figure 3 the risk level is shown for three different shipping zones, which stands for areas of restricted operation with different cargo securing regulations, according to the Swedish Maritime Administration (1994). Zone A is sheltered waters, with the lowest requirement on pre-tension, and zone C is unrestricted operation, which imposes the strongest rules of securing. The route used for the case studies comprises both zone A and B. Thus the parameter influence is discussed for cargo lashed according to the regulations of zone B. As can be seen, for a ship operating in zone B with cargo secured for zone A the risk is significantly larger than when the cargo is secured for unrestricted operation (zone C). This points at the importance of securing the cargo according to the area in which the ship will operate. It is interesting to note that for the variation of GM_0, the parameter influence changes when the degree of pre-tension in the lashings is varied.

Figure 2 shows how the GM_0 of the vessel influences the risk of cargo shifting. GM_0, which influences the stability and natural roll period of a vessel, strongly influences the risk of cargo shifting and an unfortunate choice of GM_0 can have a large negative effect on the risk of cargo shifting. As can be seen the largest GM_0 results in the largest risk, which can be expected since a large GM_0 means a very stable and thereby stiff ship with large roll acceleration. However, a very low GM_0 (poor stability) will also result in a relatively high risk, since the roll amplitude is relatively high. The natural roll period is proportional to the inverse of GM_0, which means a vessel with a high GM_0 will have a low natural roll period. For the studied case the vessel with a GM_0 of 2.48 m has a natural roll period of 10 s. Since wave periods are generally in the range of 5 to 10 seconds, this means the stable ship will more often be subjected to waves exciting large roll motions.

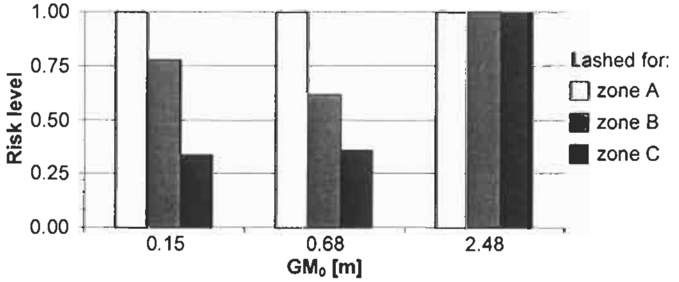

Figure 2: Risk of cargo shifting as a function of GM_0 (route in zone B, at a speed of 15 knots)

In Figure 3 the influence of speed is shown. The influence of speed mainly shows the importance of operational aspects. If the speed is reduced when severe ship motions are experienced the risk level can be reduced considerably. For example the risk at 10 knots is only one third of the risk at 15 knots. Naturally, constant speed in all sea states is unrealistic, especially at 20 knots.

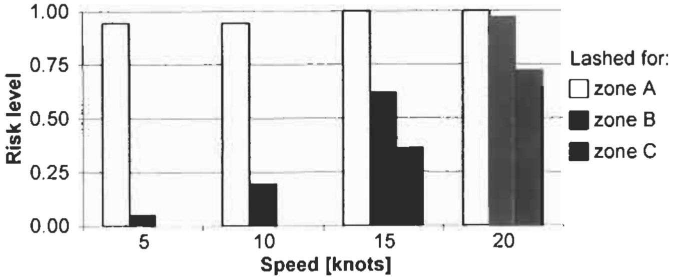

Figure 3. Risk of cargo shifting as a function of speed (route in zone B, at GM_0 0.68 m)

Calculations have also been made varying the cargo weight, the pre-tension in the lashings, and the coefficient of friction. The intervals of variation have been chosen based upon a study performed by Andersson et al. (1986). Figure 4 shows the relative risk as a function of the expected values of the cargo parameters. The relative risk is expressed as a percentage of the risk level when the actual cargo parameters are equal to the expected values. On the x-axis the cargo parameter values are given as a percentage of the expected value. It can be seen that even moderate changes in the cargo parameters can have a large influence on the risk of initial cargo shift. This points at the importance of proper lashing of the cargo, and of controlling the cargo parameters, such as friction.

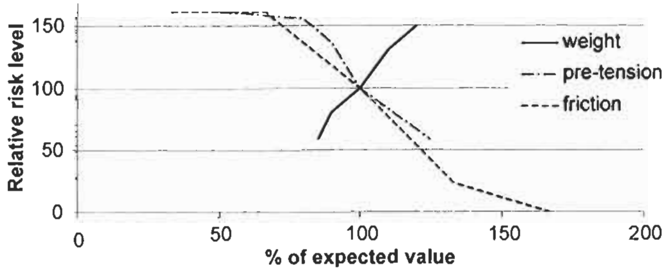

Figure 4: Relative risk of cargo shifting as a function of cargo parameters (route in zone B, $GM_0 = 0.68$, 15 knots)

4 DISCUSSION

In this paper a methodology for estimating the risk of initial cargo shift for a vessel carrying unit cargo has been presented. The benefit of the method is that the risk of initial cargo shift is evaluated in a large number of different situations that are weighted with respect to their probability of occurrence. The results from the case studies show that the method can be used for comparing risk levels. They also show how loading condition and speed have a large influence on the risk of cargo shifting. It is also shown that controlling the cargo parameters, and establishing routines for appropriate lashing of the cargo is an effective means of reducing the risk. Examining the risk of cargo shifting, and trying to optimise the vessel and its cargo with respect to low risk may have a large positive effect on the overall safety of the vessel.

As can be seen from the results the level of the risk of initial cargo shift is rather high. However, it should be noted that the risk of initial cargo shift is really the risk of getting potentially dangerous situations. The shift mode is set to an initial motion of the cargo, and the risk presented in the results is the probability that at least one such situation will occur during the studied time interval, which explains the rather high risk levels in the results. Furthermore, if the risk were calculated for the lifetime of a vessel instead of one year the risk would be one in all cases. This would imply that changes in ship handling, and cargo securing would have no effect on the risk of cargo shifting in the long run. However, the risk measure presented herein does not state anything about the frequency of occurrence of cargo shifts. It may be likely that a vessel will experience at least one cargo shift during its lifetime, but there is a difference between experiencing one or for example one hundred. An alternate risk measure, e.g. quantifying the most probable number of cargo shifts, may be of interest as a complement to the present measure, i.e. the risk of initial cargo shift.

An implementation of the methodology where consideration is taken to operational factors, such as speed reduction in severe weather, will give a more realistic, and probably lower, risk level. This could be done by simply reducing speed in waves with significant height above a specified limit. A more refined method would be to connect the speed reduction or alteration of course to appropriate comfort criteria and added resistance in waves. Statistical methods to account more realistically for differences in cargo and lashing equipment, as well as improved cargo models would also result in more realistic risk levels. An improved cargo model could comprise e.g. deformation of cargo and lashings, improved criteria for shifting, three dimensional models, and accounting for dynamical effects. Another area of further research is alternative methods for estimating the probability of cargo shift for a specific cargo unit in a specific condition, e.g. by the use of probability distribution curves. This would enable a reduction of the computational time, which is rather large due to extensive simulations. Since cargo shifting is most probable in severe sea conditions improved ship motion calculations, especially roll motion with rather strong non-linearity, is of interest.

References

Andersson, P., Koch, M. and Sjöbris, A. (1986). *Optimum Safety Factors for Securing of Cargo On Board Ships*. Research Report, MariTerm AB, Gothenburg, Sweden

Cramér, H. & Leadbetter, M. R. (1967). *Stationary and Related Stochastic Processes*. John Wiley & Sons, New York, US

Ericson, A. (2000). *Ship and Cargo Models for Studying the Risk of Cargo Shifting in Waves*. Licentiate Thesis, TRITA-FKT, ISSN 1103-470X, ISRN KTH/FKT/SKP/L--00/20--SE, Department of Naval Architecture, KTH, Sweden

Ericson, A., Källstam, K., Rutgersson, O., Thedéen, T. (1999). *Probabilistic Models for Ship Safety in Rough Seas – Final report for phase 1*. KFB-Report 1999:34, Stockholm, Sweden

Hogben, N., Dacunha, N. M. C. & Olliver, G. F. (1986). *Global Wave Statistics*. British Maritime Technology Limited, Feltham, UK

McTaggart, K. (1998). Ongoing work examining capsize risk of intact frigates using time domain simulation. *4th International Stability Workshop*. St. John's 27-29 September 1998

Lloyd's Register. (1999). *World Casualty Statistics 1998*. Lloyd's Register, London, UK

Salvesen, N., Tuck, E. O. and Faltinsen, O. (1970). Ship Motions and Sea Loads. *Trans. SNAME* **Vol 78**, 250-279.

St. Denis, M. and Pierson, W. J. (1953). On the Motions of Ships in Confused Seas; *Trans. SNAME* **Vol 61**, 280-357.

Swedish Maritime Administration. (1994). *Sjöfartsverkets författningssamling 1994:27 9§*. Swedish Maritime Administration, Sweden (in Swedish)

Practical Design of Ships and Other Floating Structures
You-Sheng Wu, Wei-Cheng Cui and Guo-Jun Zhou (Eds)

© 2001 Elsevier Science Ltd. All rights reserved

SHIP DESIGN USING PROBABILISTIC DAMAGE STABILITY RULES – A SENSITIVITY STUDY

Preben H. Lauridsen, Jørgen Juncher Jensen and Jan Baatrup

Department of Mechanical Engineering
Section for Maritime Engineering, Building 101E
Technical University of Denmark
DK 2800 Lyngby, Denmark

ABSTRACT

The current IMO resolutions contain two different probabilistic damage stability regulations: A.265 for passenger vessels and SOLAS Part B-1 for dry cargo vessels. However, ongoing harmonization studies as those presented in the IMO documents SLF 42/5 and SLF 43/3/2 aim at one single damage stability rule applicable to all kinds of ships. Such a harmonization requires due consideration of both the calculation of the attained index describing the probability of survival, and specification of a suitable minimum level, taking into account the consequences of loss of the vessel.

The present paper addresses the calculation of the Attained Index A. The first part considers the variation of A with the degree of details in the modelling of the compartmentation. The exemplified vessel is a recently built Danish ferry and both the SOLAS Part B-1 and the SLF 43/3/2 proposals are applied. The contributions from single and multiple compartment damages are identified. The reason for the different predictions from the two calculation procedures is discussed. The conclusions contain guidelines for the level of details needed in the geometrical definition of the vessel to predict the Attained Index A with acceptable accuracy.

The second part of the paper considers the variation of the Attained Index A with change in main parameters in the preliminary design phase. The main conclusions are that the height of the main deck may influence the attained index by up to 60 per cent for the present vessel, whereas the length of the machinery room can change A by up to 20 per cent. This illustrates the importance of the horizontal subdivision in the current probabilistic damage stability rules.

KEYWORDS

Ship design, Probabilistic damage stability, Attained Index A, Watertight subdivision

1 INTRODUCTION

One of the first decisions in the preliminary ship design phase concerns the degree of watertight subdivision needed to ensure a satisfactory stability of the vessel following a collision. Since the sinking of the 'TITANIC' the international community has issued and updated rules and regulations with the aim to avoid such disasters. The naval architect has to take these demands into account early in the design phase in order to reduce the adverse effects such measures usually have on the cargo handling and payload capacity of the ship. For passenger ships most national maritime authorities require that the margin line is not submerged in the case of a side shell damage of a predefined length. This demand can be transformed into so-called floodable length curves giving the naval architect immediate information on the necessary number and optimal positions of transverse bulkheads. The required damage stability is most often obtained by use of a deterministic approach where the residual stability for any location of the rule damage extent is checked against regulations laid down by the maritime authorities, notably the IMO. With only transverse bulkheads this can be done simultaneously with the floodable length calculations. If the residual stability is too low, longitudinal bulkheads can be inserted usually in a location at least one fifth of the ship's breadth inboard from the shell plating in way of the deepest subdivision load line, as this is the maximum penetration of a rule damage.

However, it has unfortunately been demonstrated in several accidents that the concept of rule damages of a predefined size does not always capture real life. This has led to the development of the probabilistic damage stability regulations, first issued in the seventies in IMO Resolution A.265 as an alternative to the deterministic approach for passenger vessels. Due to the heavier demands than those of the deterministic approach and the need for consideration of more damage cases, A.265 is, however, seldom used.

Restrictions are imposed on tankers and chemical carrier concerning the subdivision and residual stability as prescribed by IMO through the MARPOL and IBC codes, aiming mainly at reduction of the pollution in case of collision or grounding. For dry cargo vessels no general requirements existed before 1992 except for the position of an afterpeak and a collision bulkhead.

With the development of the probabilistic damage stability as introduced in SOLAS Part B-1 in 1992 for dry cargo ships and the ongoing harmonisation process towards uniform rules for all vessels, it has become very urgent for the naval architect to be able to fulfil these requirements in a rational manner. An Attained Index A now measures the residual stability of a vessel, taking into account all possible sizes of damage. Each damage is weighted by the possibility that such damage can be expected. The survivability of a given damage is measured in terms of a factor s, calculated from the properties of the associated residual stability curve. For a real vessel literally thousands of damage cases must be considered, cf. Koelman (1995), and only extensive use of dedicated computer programs, cf. Jensen, Baatrup and Andersen (1995), makes the procedure tractable.

Since only a single measure, the Attained Index A, obtained as a weighted average of contributions for all possible damages is used to assess the damage stability, it is not obvious how to use the regulations in the conceptual design phase to obtain the most appropriate subdivision. An infinite number of subdivision layouts might satisfy the regulations. Sen and Gerigk (1992) proposed the use of local attained indices, aiming at a uniform contribution to the Attained Index A along the length of the hull. This works well if only transverse bulkheads are considered and no constraints are made on the length of the compartments, but when longitudinal and horizontal bulkheads are included it is not straightforward to apply this procedure. Then it is more important in the initial design phase to be able to estimate rapidly the Attained Index A, based on a simplified layout of the subdivision, and to determine the sensitivity of A with respect to design parameters as bulkhead coordinates and centre of gravity. These two topics are addressed in the present paper.

2 EFFECT OF DEGREE OF DETAILS IN THE SUBDIVISION ON THE ATTAINED INDEX

In the probabilistic damage stability analysis the survivability factor s is calculated for any combination of adjacent damage compartments. Hence, if s=1 for a two compartment damage, the bulkhead separating these compartments can be omitted without changing the Attained Index A. Thus a good estimate of A can be expected even if several minor compartments are combined in a single compartment. This is often the case in the engine room and the side casing and will be illustrated in the following. The ship considered is a Ro-Ro passenger ferry with general arrangement and main dimensions as given in Figure 1. The subdivision shown corresponds to layout #1, defined in Table 1.

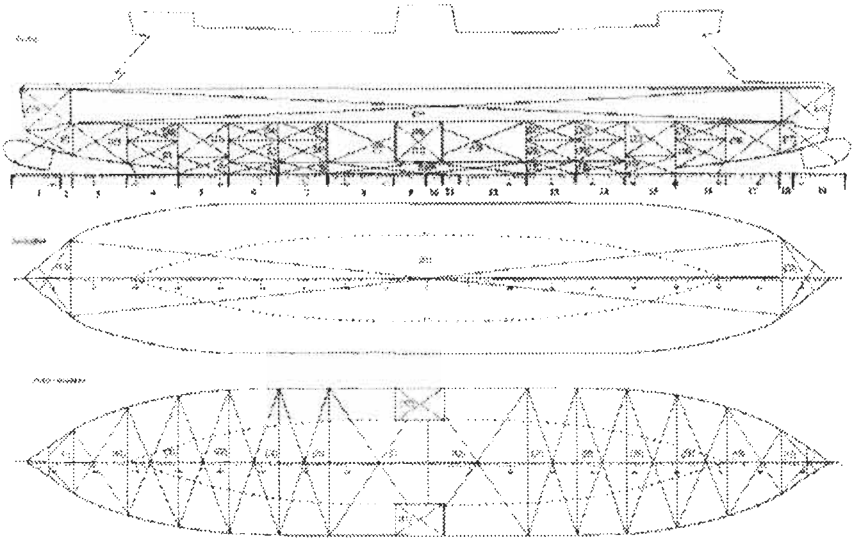

Figure 1: General arrangement of Ro-Ro passenger ferry. Length bpp: 134m, breadth moulded: 24.8m, design draught: 5.8m, GM (full load): 3.54m, service speed 18.5 kn, cars: 294, passengers: 900

Five different calculations of the Attained Index A have been made by use of more and more simplified layouts of the subdivision as defined in Table 1. For each layout both the current SOLAS Part B-1 regulations and the draft for harmonized regulations, given in IMO document SLF 43/3/2, are applied. In the harmonized regulations the residual stability curve for heeling angles greater than 30 degrees does not contribute to A for passenger vessels. Therefore, the SOLAS Part B-1 regulations are here limited to heeling angles up to 30 degrees. The reason for including SOLAS Part B-1 although only applicable to cargo ships is to estimate the sensitivity of A with respect to different formulations of the Attained Index. The results are shown in Tables 2 and 3 and in Figure 2.

TABLE 1
SUBDIVISION

Subdivision	Number of compartments	Description of layout
Layout #1	33	All longitudinal bulkheads except for heeling tanks removed
Layout #2	21	As #1, but all horizontal subdivisions below main deck removed
Layout #3	13	As #2, but transverse subdivisions removed below main deck to yield 4 large compartments
Layout #4	11	As #3, but volume below main deck reduced to 2 large compartments

TABLE 2

ATTAINED INDEX A USING SOLAS PART B-1

Subdivision	Number of compartments	1 damage zone	2 damage zones	3 damage zones	4 damage zones	5 damage zones	6 damage zones
As built	39						0.9742
Layout #1	33	0.2626	0.5770	0.8107	0.9253	0.9676	0.9737
Layout #2	21	0.2626	0.5768	0.8061	0.9157	0.9562	0.9603
Layout #3	13	0.2394	0.4928	0.6666	0.7381	0.7511	0.7518
Layout #4	11	0.1672	0.3325	0.4534	0.5148	0.5398	0.5445

TABLE 3

ATTAINED INDEX A USING HARMONISED REGULATIONS (SLF 43/3/2)

Subdivision	Number of compartments	1 damage zone	2 damage zones	3 damage zones	4 damage zones	5 damage zones	6 damage zones
As built	39						0.9826
Layout #1	33	0.2739	0.5863	0.8247	0.9401	0.9817	0.9875
Layout #2	21	0.2739	0.5863	0.8206	0.9324	0.9738	0.9794
Layout #3	13	0.2557	0.5231	0.7209	0.8141	0.8442	0.8494
Layout #4	11	0.2137	0.4323	0.5960	0.6771	0.7081	0.7136

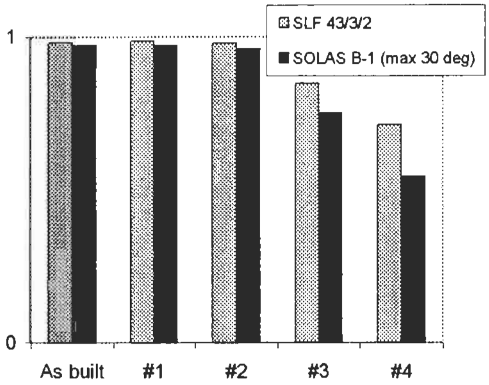

Figure 2: Comparison between Attained Index A obtained by different simplifications of the compartment layout and different probabilistic damage stability regulations

The present vessel has as-built a very high Attained Index A. The main reason is that s is equal to one for damage to the main deck running from fore to aft without any transverse or longitudinal subdivision. Only in the case of damage simultaneously to the main deck and the compartments below the deck, spanning more than 20 per cent of the length of the vessel, the survivability index s becomes less than 1. As seen from Tables 2 and 3 the main contributions to A come from the first four damage zones, each defined by two adjacent transverse bulkheads. It is therefore important to include damages extending over several compartments in the calculation of A already in the initial design phase. A comparison of the results for the simplified layouts #1-4 with the results for the as-built design shows that the omission of longitudinal (#1) and horizontal (#2) bulkheads below the main deck does not change A significantly. However, if also most of the transverse bulkheads are omitted, then the value of A decreases substantially. Thus, for the present vessel, as soon as the transverse bulkheads are fixed then a very good estimate of A can be obtained. It should be noted that the margin line does not enter into the probabilistic damage stability criteria, but that down-flooding points are included. These down-flooding points often have a significant influence on A.

The two different regulations yield qualitatively the same tendencies. The Attained Index obtained from SLF 43/3/2 is slightly larger than for SOLAS Part B-1. Careful study of the results reveals that the main reason is that the survivability index s generally becomes about 15 per cent larger using SLF 43/3/2 in the cases where $0<s<1$. The differences in the probability distributions for the damage location and extent are of lesser importance.

Another important parameter in the calculation of the Attained Index is the centre of gravity as given by GM in the intact conditions. A change of GM is easily included in the analysis as it only influences the index s and only through a change in the residual stability curve GZ:

$$G'Z(\theta) = GZ(\theta) + GG'\sin(\theta) \tag{1}$$

where G and G′ are the old and the new centres of gravity, respectively, and θ the heeling angle. For the subdivision defined in Table 1, the effect of changes of GG′ in the range ± 1m is given in Figure 3 using SOLAS Part B-1. For layout #3 a strong influence by such variation is seen because $0<s<1$ for damages to the main deck and either of the four large compartments below the main deck. For the layouts #1 and #2 $s = 1$ and for layout #4 $s = 0$ for similar damages for the range of GG′ shown in Figure 3 and hence the changes in GZ given by Eqn. 1 do not change A.

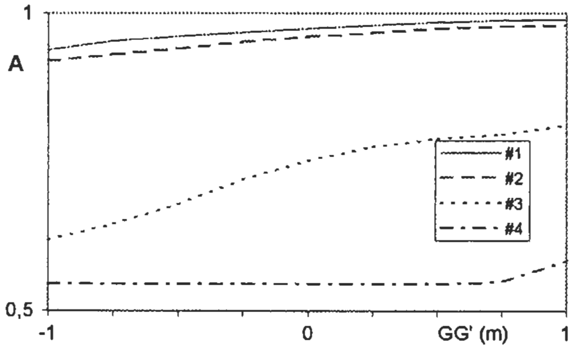

Figure 3: Variation of the Attained Index A with change in the vertical position GG′ of the centre of gravity. SOLAS Part B-1

3 SENSITIVITY OF THE ATTAINED INDEX WITH BASIC DESIGN PARAMETERS

To obtain the required Attained Index A the naval architect may need to change some design parameters. It is hence important to identify the parameters with most influence on A. This can be done by sensitivity analyses as shown in Figure 3 for the centre of gravity. Other important design parameters have been identified from the responses to a questionnaire to leading Danish naval architects regarding Ro-Ro ferries. Two main parameters are

- Length of machinery space
- Height of main deck above keel

The first should be as large as possible and the second should be as low as possible to lower the centre of gravity and to reduce the steel weight. In the sensitivity studies dealing with these parameters it is important to account for their influences on other parameters. In the present analyses the centre of gravity, the steel weight, the position of the vehicle deck and the down-flooding points are adjusted for changes in the distance H, measured from the tank top to the main deck. The length of the machinery space is supposed not to alter other pertinent parameters than the subdivision. The results from the sensitivity study are given in Figures 4 and 5. The vessel is the same as in the previous chapter but below the main deck it is divided into three main compartments. The machinery space is in the middle placed symmetrically with respect to midship. The layout is hence in between layouts #3 and #4.

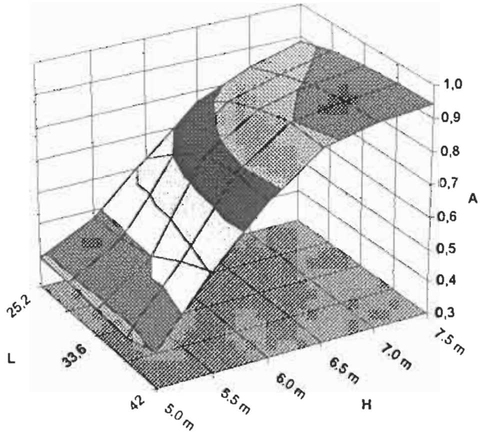

Figure 4: Attained Index A as a function of length L of machinery space and height H from tank top to main deck. SOLAS Part B-1

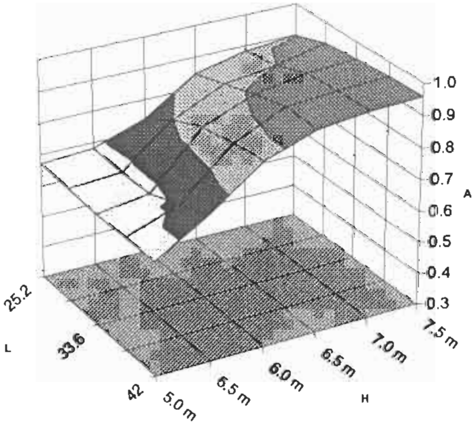

Figure 5: Attained Index A as a function of length L of machinery space and height H from tank top to main deck. SLF 43/3/2

The variation of A with the length of the machinery space is seen to be modest in the considered range of 25.2m to 42m. The Attained Index A has a maximum for L equal to about 38m, since the survivability factor s for simultaneous damage to the main deck and machinery space becomes less than one when L is larger than this value. Smaller values of L will give lesser s-values for simultaneous damage to the main deck and the compartments aft or fore of the machinery space. This is due to submergence of down-flooding points as a result of a large trim. The optimal length of L corresponds to about 30 per cent of the length of the vessel, but 40 per cent of the volume below the main deck.

The height H of the main deck above the tank top strongly influences the Attained Index A. The principal reason is that the probability of damage to the main deck decreases with its distance above the still water line. The draughts in full and partial load conditions are 5.8m and 5.52m, respectively and the height of the double bottom is 2m. The variation in Figures 4 and 5 thus corresponds to a main deck 1.2m to 3.7m above the draught in full load. For the as-built vessel H=6.5m. For H below this value large variations in A with H are seen, especially when the SOLAS Part B-1 Regulations are applied. This is due to the linear decrease of the probability of damage to the main deck with the distance from the water line. For SLF 43/3/2 this decrease first starts when the main deck is more than 3m above the water line and hence the main deck will be damaged with a probability of one for nearly all cases shown in Figure 5. The Attained Index A is, however, generally lower for SOLAS Part B-1 than for SLF 43/3/2 for the reason discussed in the previous chapter.

4 CONCLUSIONS

Based on the present parameter study the following recommendations can be given for use of the probabilistic damage stability regulations in the initial design phase:

- Define the hull form and insert the transverse and horizontal bulkheads required by the rules and those considered as necessary for separation of cargo, fuel, ballast and machinery
- Specify down-flooding points and centre of gravity G
- Calculate the Attained Index A. If it is lower than the required index R, then make a sensitivity analysis for A with respect to the positions of transverse and horizontal bulkheads to find the subdivision with maximum A. If still not sufficient, insert additional transverse bulkheads if possible, otherwise try to lower G, raise the down-flooding points or insert longitudinal bulkheads. The required changes are estimated by sensitivity analyses

References

Jensen J.J., Baatrup J. and Andersen P. (1995). Probabilistic Damage Stability Calculations in Preliminary Ship Design, Proc. PRADS'95, Vol.1, 1.565-1.577, Eds. H. Kim and J.W. Lee, The Society of Naval Architects of Korea, Korea

Koelman H.J. (1995). Damage Stability Rules in Relation to Ship Design. Proc. WEMT'95, 45-56, Eds. J.J. Jensen and V. Jessen, The Danish Society of Naval Architecture and Marine Engineering, Copenhagen, Denmark

Sen P. and Gerigk M.K. (1992). Some Aspects of a Knowledge Based Expert System for Preliminary Ship Subdivision Design for Safety, Proc. PRADS'92, Vol. 2, 1187-1197, Eds. J. Caldwell and G. Ward, Elsevier Publ. Ltd., UK

Practical Design of Ships and Other Floating Structures
You-Sheng Wu, Wei-Cheng Cui and Guo-Jun Zhou (Eds)
© 2001 Elsevier Science Ltd. All rights reserved

INTEGRATION OF FIRST-PRINCIPLE APPROACHES TO DESIGN FOR DAMAGE SURVIVABILITY

D. Konovessis[1] and D. Vassalos[1]

[1] The Ship Stability Research Centre, Department of Ship and Marine Technology,
University of Strathclyde, Glasgow, G1 1XN, UK

ABSTRACT

The paper elaborates on the development of a procedure for accommodating damage survivability in the ship design process cost-effectively. For passenger Ro-Ro vessels, damage survivability considerations make sense only when adequate subdivision criteria have been satisfied whilst allowing for other design considerations. The paper highlights and demonstrates that a ship design process could not possibly be optimal without involving the designer and hence any attempt to develop a fully automated procedure will be futile. The paper focuses on the development of the objective function, on the design parameters and on the integration of first-principles approaches, notably suitable Quantitative Risk Assessment (QRA) frameworks, to be included within the design for survivability optimisation process.

KEYWORDS

Design, Optimisation, First-Principles, Survivability, Quantitative Risk Assessment

1 INTRODUCTION

The approaches that can be deployed to allow for integration of safety considerations in the ship design process vary according to the stage the process has reached and the specific criteria compliance is sought for. A holistic approach should integrate the various methods available, taking into account the fact that the design information available at the initial phases of the design process is by no means complete or accurate and that as the process develops the quantity and quality of information increases, thus allowing for design assessment and analysis using advanced tools and techniques, until convergence is reached.

It should be highlighted, that the latter only reflects a physical demand, i.e. assessment at any stage of a process can only be based on the information available. The sequential nature of the well-known and established ship design spiral is no longer an issue to adhere to, given the technological advances of the last decade, particularly in computer science, for example work on distributed computer systems. However, in the every-day ship design practice, this sequential approach has been replaced by groups of naval architects working concurrently on different aspects of the project under development, co-ordination being offered by discussions, which usually result in implementation of design adjustments. It is argued, that it is essential to follow a methodology for effective design co-ordination, both for issues of concurrency and decision-making.

With this general frame in mind, it is argued that a "Design for Safety" paradigm could provide the vehicle for safety to constitute a focal issue for an improved ship design process, Vassalos et al. (2000). This paper deals with a specific issue within this vast subject, namely the provision of a procedure for the efficient integration of damage survivability considerations within the ship design process.

2 OPTIMISATION FOR SAFETY IN SHIP DESIGN

Design optimisation techniques have been developed with the aim to formalise the search for optimal solutions, to identify possible solutions beyond present state-of-the-art and effectively to reduce development time and associated costs. The general approach is to structure an optimisation function (and a set of design variables), which is considered against a set of optimisation criteria and design constraints and to produce a solution based on mathematical programming techniques. Obviously, due to the fact that the problem at hand is reduced to a function or a set of variables, there is a need for the mathematical formulation to represent the problem as accurately as possible in order to eliminate the chance of solving a fraction of the original problem. With rapidly advancing computer technology, computers are becoming more powerful, and correspondingly, there is an increase in the size and complexity of the problems being tackled, as well as the fact that new optimisation techniques can be developed and put into practice. Optimisation methods, coupled with modern tools of computer-aided design are also being used to enhance the creative process of conceptual and detailed design of systems.

Within the broad field of ship design, a large variety of design optimisation techniques have been successfully applied to solve either the general design problem (for example, determination of main dimensions and characteristics) or to provide optimal solutions to specific areas of ship design (for example, lines development or resistance). In the specific area of the assessment of safety in ship design there is a rather limited amount of work published. In the following, two areas that the proposed procedure is deemed appropriate are briefly described.

2.1 Probabilistic Rules-Based Optimal Design

The objective is the development of a procedure for optimal compartmentation and internal arrangements of passenger Ro-Ro ships adopting the probabilistic concept of damage stability. It proves necessary to evaluate first the robustness of a probabilistic rules-based design procedure in a range of scenarios and its sensitivity to the main design parameters involved in the assessment process, which will lead to the definition of suitable constraints. After setting up a framework of local and global optimisation techniques regarding ship compartmentation for enhanced damage stability characteristics, a formal integration within an overall computer-aided design procedure can be performed.

2.2 Quantitative Risk Assessment (QRA) –Based Optimal Design

An appropriately structured QRA framework provides the means for a unified measure of safety, represents an absolute measure for the risk levels of a vessel and quantifies the effect of risk reduction measures. To integrate such a framework within the ship design process efficiently, it is necessary to consider utilisation of appropriate design optimisation tools that perform the trade-offs and take into account identified safety-critical design features and established criteria. This way, an effective and efficient balance between risk reduction measures and cost benefits can be achieved. As a consequence of the optimisation procedure, the effects of optimal design features will be identified and assessed on a comparative basis, applying the consequence analysis tools and the risk-based techniques, including methods to analyse the profits/losses involved. Alternative design solutions will therefore be suggested, their selection being based on a sound economic application of the QRA-based design procedure.

3 ELEMENTS OF THE PROCEDURE

All design decision models developed so far, are based on a single economic criterion of merit, incorporating several constraints related to performance indicators, lately with the addition of some safety indicators of any type (deterministic, probabilistic or performance-based). In the context of the above described design goal, the current approaches are not sufficient, due to the fact that safety is not an integral part of the design process, but is taken into consideration as a design periphery issue at best, if not as a design afterthought. For this reason, the association of increased safety leading to increased incurred costs is considered to be the norm.

A clear and complete statement of the goal for the problem at hand is that a design procedure is sought to "*derive effective arrangements and layouts that maximise safety, whilst minimising the incurred costs*". This is a multiple criteria problem, the design solution of which depends on multiple design attributes, which in turn derive from the attained performance and characteristics of the alternatives under consideration.

To achieve such a goal a structured formulation of the criteria, parameters, constraints, objective function and mathematical models, needs to be developed. This will be based on the observation that an alternative to a single criterion of merit is the consideration of pair wise comparisons that employ valid criteria, which can also be extended to the consideration of a hierarchically decompositioned objective function that reflects and combines economic, performance and safety aspects. Such a formulation will lead to the following innovative aspects:

- The criteria to be considered need only be design-related, and not of conformance nature. More importantly, these criteria can be incorporated in the formulation of the objective function, as described below.
- The formulation allows for the development of a practically unconstrainted problem, in the sense that the various indicators (economic, performance, safety) are included in the objective function.
- The mathematical models ought to be of performance nature, at least for the assessment of damage survivability. This will allow the incorporation of first-principles approaches in the design process, which when combined with an overall QRA framework, accounts for an objective safety quantification process.

In the following, the formulation of the decision making process for the determination of the most effective internal configuration, given the vessel's hull, will be described. The focus will be on monohull passenger Ro-Ro vessels.

3.1 Development of the Objective Function

The objective function will be developed based on a method proposed by T.L. Saaty, known as the Analytic Hierarchy Process (AHP), Saaty (1980). The method consists of three principles: decomposition, comparative judgement, and priority synthesis.

Decomposition is the description of the problem in a hierarchical form. The elements of each level are independent of succeeding levels. The hierarchical structure starts at the top with a statement of a decision goal. The next lower levels contain the criteria by which the alternatives are measured by the degree to which they satisfy the goal. There can exist several such levels in the structure, detailing the selection criteria through the consideration of various decision attributes, such as fuel consumption and steel weight. The final lower level contains the actual alternatives from which the one that best satisfies the goal is selected.

An example of the various levels of an objective function of the problem at hand is as follows:

LEVEL 1	Goal	Derive effective subdivision arrangements and layouts that maximise safety, whilst minimising the incurred costs
LEVEL 2	Selection Criteria	• Income • Building cost • Operational cost • Machinery selection • Performance indicators • Safety indicators
LEVEL 3	Detailed Attributes	Lower level attributes, pertinent to the criteria above, that can be enumerated
LEVEL 4	Merit Function	Compose and iterate based on necessary improvements

This approach to construct the objective function is illustrated in Figure 1 in broad terms. Even though this kind of approach is widely used for problems related to selection and ranking of derived alternatives, the iteration proposed aims at the introduction of the approach at the design synthesis process. The objective of the iteration is not to alter any of the broad specifications (i.e. the goal or the selection criteria), but rather to allow focusing in specific areas of the process where attention should be paid.

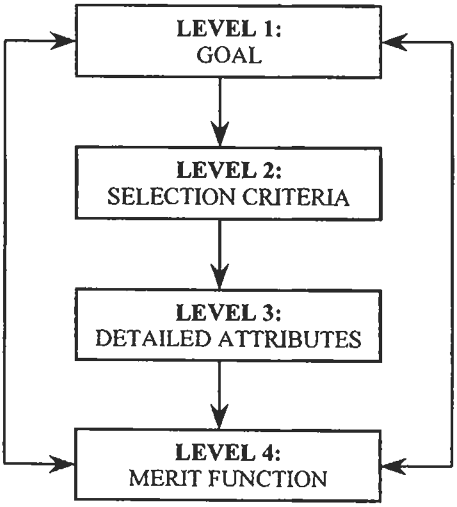

Figure 1: Objective Function

3.2 Design Parameters and Mathematical Model

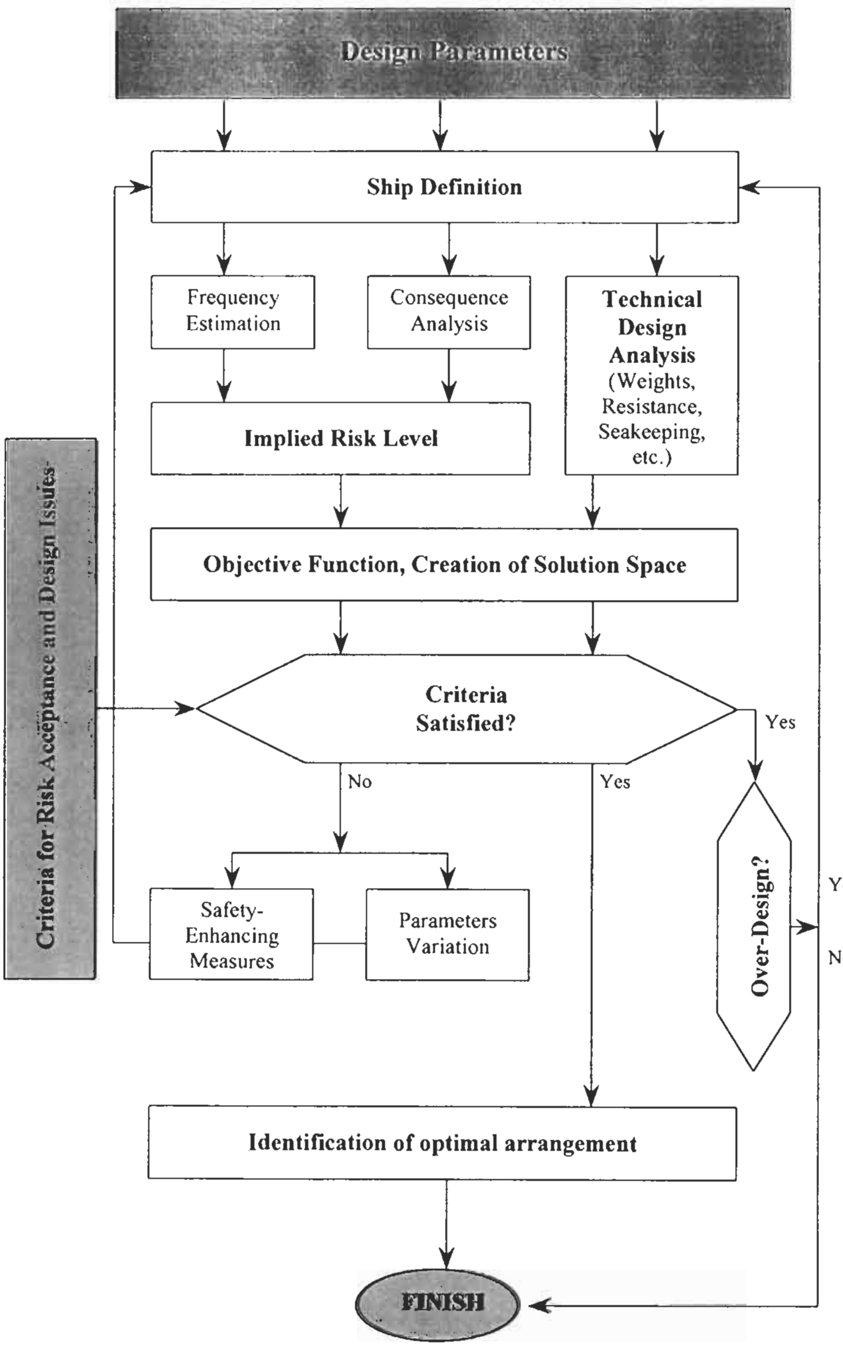
Design Parameters
Ship Definition
Frequency Estimation
Consequence Analysis
Technical Design Analysis (Weights, Resistance, Seakeeping, etc.)
Implied Risk Level
Objective Function, Creation of Solution Space
Criteria for Risk Acceptance and Design Issues
Criteria Satisfied?
Yes
No
Yes
Over-Design?
Yes
No
Safety-Enhancing Measures
Parameters Variation
Identification of optimal arrangement
FINISH

Figure 2: A QRA-Based Design Procedure (Single Risk DFX)

The desired goal in developing this procedure is to identify appropriate arrangements and layouts for passenger Ro-Ro vessels, by considering specific safety and techno-economic targets. The various characteristics/parameters to be considered are grouped in the following two categories:

- Hull-related parameters, for example L/B, flare, height of the main vehicle deck, shear, camber, presence of a ducktail, etc.
- Internal layouts and arrangements, i.e. possible layouts below (for example, pure transverse subdivision, combination of transverse and longitudinal subdivision, presence of a lower hold) and above the main vehicle deck (for example, presence of centre and/or side casings, transverse or longitudinal bulkheads, combinations).

The mathematical model to be considered utilises application of first-principles approaches for the determination of the probability of survival following large scale flooding, Vassalos & Konovessis (2001), within a QRA-based design framework. A comprehensive QRA framework for passenger Ro-Ro vessels has been developed during the Joint Northwest European Project, Spouge (1996). The various elements and the logical sequence of the procedure are illustrated in Figure 2. The procedure comprises of the following steps:

(1) Selection of risk acceptance criteria, as well as other design criteria, to be applied.
(2) Estimation of the frequency (probability) of an incident/accident occurring.
(3) Estimation of the cost of consequences.
(4) Estimation of the implied risk level and categorisation according to the severity of the consequences.
(5) Consideration of safety-enhancing measures to improve undesirable risk levels (these include both available risk control options as well as parametric studies).
(6) Setting-up of the optimisation problem and consideration of an objective function appropriate to perform trade-offs among the specified societal and techno-economic targets (criteria).
(7) All necessary iterations.

4 CONCLUSIONS

The elements of a procedure for the integration of a rational approach to damage survivability assessment within the ship design process have been described. A major conclusion is that classical optimisation techniques cannot be applied in isolation to derive effective solutions, but rather as a means to fine-tune an already developed solution that nearly satisfies the criteria. These should combine with environments that support decomposed objective functions where the behaviour of the various attributes can be readily assessed and decisions on design variations performed, which when integrated in appropriate design architectures can provide the necessary Design for Safety support, Duffy (1999).

References

Duffy A.H.B. (1999). Future Developments in Design for Safety Support. *WEGEMT Design for Safety Conference*, 25-28 October 1999, University of Strathclyde, Glasgow, UK.

Saaty T.L. (1980). *The Analytic Hierarchy Process: Planning, Priority Setting, Resource Allocation*, McGraw Hill Inc, New York, USA

Spouge J. (1996). Safety Assessment of Passenger Ro-Ro Vessels. *RINA International Seminar on The Safety of Passenger Ro-Ro Vessels*, Paper No. 7, 7 June 1996, London, UK.

Vassalos D., Oestvik I. and Konovessis D. (2000). Design for Safety: Development and Application of a Formalised Methodology. *The Seventh International Marine Design Conference (IMDC 2000)*, 21-24 May 2000, Kyongju, Korea, 151-165.

Vassalos D. and Konovessis D. (2001). Damage Survivability of Floating Marine Structures – A Probabilistic Approach. *The Twentieth International Conference on Offshore Mechanics and Arctic Engineering (OMAE 2001)*, 3-8 June 2001, Rio de Janeiro, Brazil.

Practical Design of Ships and Other Floating Structures
You-Sheng Wu, Wei-Cheng Cui and Guo-Jun Zhou (Eds)
© 2001 Elsevier Science Ltd. All rights reserved

RATIONAL DESIGN CRITERIA AND THEIR APPLICATION TO HULL FORM OPTIMISATION OF FLOATING SYSTEMS IN RANDOM SEAS

L. Birk and G.F. Clauss

Institute of Land and Sea Transportation
Technical University of Berlin, Germany

ABSTRACT

Efficient design of new floating systems requires more and more numerical tools to develop structures with excellent motion behaviour in briefer time spans. The paper presents a fully automated numerical procedure for optimum adjustment of shapes to environmental conditions. Rational design criteria based on short and long-term wave statistics are introduced and utilized as objective function in the optimisation process. Nonlinear programming algorithms vary the form parameters of the design and find a minimum of the objective function within a few iterations. The resulting hull shapes are characterized by minimized wave loads and motions. Optimization of a semisubmersible illustrates the efficiency of the proposed procedure.

KEYWORDS

Parametric design, Design criteria, Form optimisation

1 INTRODUCTION

Offshore operation of floating systems must cope with rough and hostile seas. Designs with favourable motion behaviour yield economic advantages avoiding restrained operation or weather induced downtime. Therefore, detailed performance analysis and optimization are necessary during initial design stages, when hull shapes can be adopted to sea states of the target location without introducing unnecessary expense. Currently best seakeeping behavior is obtained by expensive series of model tests or time consuming interactive design variations. In this paper a fully automated numerical procedure is described, which achieves an optimum adjustment of the shapes of floating systems to environmental conditions.

Automated hull design and optimization relies on the availability of a variety of software tools performing hydrodynamic analysis, assessment of motion behavior, parameter controlled shape generation and variation as well as nonlinear programming algorithms controlling the optimization process. Although automated optimization is increasingly perceived as a valuable tool in the design process, industry does not exercise this option regularly. In the past this may have been justified by substantial restrictions on the geometries handled, lack of computing power and unreliable analysis tools. A short overview of previous work on automated optimization of offshore structures is given by Birk (1998).

Today, automated optimization is mature enough to be a valuable tool in designing better floating systems (Birk and Harries, 2000). This approach shifts the main focus from repeated interactive work with CAD and CFD tools to the more important definition of objective functions, parametric description of hull properties and assessment of final results. The following section concentrates on rational design criteria suitable to compare motion behavior of different designs. For a detailed description of the optimization framework used in this research work the interested reader is referred to Birk (1998). Only a short review is presented below.

2 RATIONAL DESIGN CRITERIA

Automated assessment of design variants relies on rational criteria, i.e. an objective function which provides the scale necessary to compare different designs. Appropriate models of system behavior and environmental conditions have to be set up.

2.1 Modelling System Behaviour

The performance assessment of each design variant starts with computation of selected response amplitude operators of forces and motions. The application presented below utilizes results obtained by the well established 3D-diraction-radiation software package WAMIT®1 (Newman and Sclavounos, 1988). The program is based on linear potential theory and neglects viscous effects. Although higher order quantities and viscous effects may be important in special cases linear analysis based on potential theory will be generally sufficient when comparing different designs. The complex ratio of output and input signals $s(\omega)$ and $\zeta(\omega)$ for each wave frequency ω constitutes the transfer function or response amplitude operator (RAO) $H_{s\zeta}(\omega)=\frac{s(\omega)}{\zeta(\omega)}$ which gives a complete description of the corresponding hydrodynamic characteristics. Values of $H_{s\zeta}(\omega)$ are computed and stored for a larger number of wave frequencies and an appropriate number of wave headings.

In many cases motions of selected points $\underline{s}_r$ are of special interest. Within linear theory they are easily deduced from the translational and rotational motion vectors of the centre of gravity $\underline{s}_T$ and $\underline{s}_D$, i.e. $\underline{s}_r=\underline{s}_T+\underline{r}+\underline{s}_D$. The vector $\underline{r}$ describes the location of the reference point with respect to the centre of gravity. Since all quantities are harmonic with wave frequency ω amplitudes of velocities and accelerations are computed by simple multiplication of $\underline{s}_r$ by ω and $-\omega^2$ respectively.

2.2 Modelling environmental conditions

The hydrodynamic analysis yields transfer functions, which characterize the behavior in regular waves. In reality, the elevation of the ocean surface is irregular and of random nature. Hence, rational seakeeping criteria have to be based on a probabilistic description of random seas. For intervals ranging from one to three hours the statistical parameters of irregular seas do not vary much, i.e. the process is stationary (Barltrop and Adams, 1991). Gaussian distribution of wave elevations and Rayleigh distribution of wave heights are assumed. The description of these short- term sea states is commonly based on design spectra, representing the frequency dependent energy distribution of waves. The relevant parameters are significant wave height H_s and mean zero-up- crossing period T_0. The significant wave height is linked to the variance σ^2 of the random process by $H_s^2=16\sigma^2$ (Newland, 1975). The variance σ^2 represents the total energy of the sea state and is computed as the area contained in the design spectrum.

Observations of sea states (all directions)

T_0-class in [s]

H_s-class in [m]	5.0 0.0	7 0 5.0	9.0 7.0	11.0 9.0	13.0 11.0	15.0 13.0	17.0 15.0	19.0 17.0	21.0 19.0	23.0 21.0
12.0-15.0	0	0	0	1	1	0	0	0	0	0
11.0-12.0	0	0	0	1	2	0	0	0	0	0
9.5-11.0	0	0	0	1	0	0	0	1	0	0
9.0- 9.5	2	8	26	32	47	23	12	3	0	0
8.5- 9.0	0	4	7	25	15	7	3	0	0	0
8.0- 8.5	0	1	15	13	21	13	4	0	0	0
7.5- 8.0	2	10	31	35	40	26	9	2	0	3
7 0- 7.5	1	16	45	41	30	14	7	3	0	0
6.5- 7.0	5	21	35	34	31	18	8	1	0	0
6.0- 6.5	6	40	68	103	71	24	13	2	0	3
5.5- 6.0	3	34	97	120	78	33	15	3	0	2
5.0- 5.5	0	21	79	65	56	24	5	1	0	1
4.5- 5.0	3	34	71	80	25	14	2	0	1	1
4.0- 4.5	25	193	421	397	241	69	28	17	1	0
3.5- 4.0	25	204	480	411	195	58	28	7	2	1
3.0- 3.5	48	435	769	555	253	75	13	5	0	0
2.5- 3.0	96	681	1015	584	224	48	13	10	2	0
2.0- 2.5	229	1325	1455	620	185	65	13	6	1	2
1.5- 2.0	476	2049	1460	388	119	30	10	3	0	0
1.0- 1.5	1565	2860	1083	275	85	35	13	6	3	4
0.5- 1.0	2800	1448	321	123	42	6	3	6	5	48
0.2- 0.5	1558	179	46	20	8	8	4	6	5	63
0.0- 0.2	514	24	18	11	4	0	2	1	7	4

sum of observations $r_\beta = 33146$

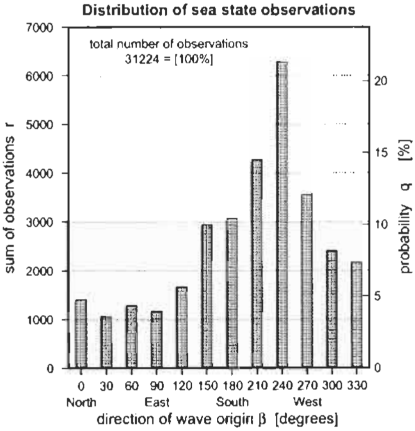

Figure 1. Long-term wave statistic of the Eastern Atlantic Ocean (Hogben and Lumb, 1967). Wave scatter diagram (left) and directional breakdown of occurrence of sea states (right).

Long-term statistics are necessary to comprise all sea states occurring during the time spread of interest, e.g. the lifetime of a structure. The occurrences of sea states are recorded in wave scatter diagrams. The table in Fig. 1 summarizes all sea state observations recorded at the Eastern Atlantic Ocean (Marsden Square 182; Hogben and Lumb, 1967). The respective numbers of observations r ij represent the joint probability distribution $q_{ij} = r_{ij} / \sum r_{ij}$ for a stationary sea state characterized by a zero-up-crossing period T_{0j} and a significant wave height H_{si}. The data may be subdivided according to the direction of waves β[2]. The number r_β denotes the sum of observations contained in the wave scatter diagram of sea states originating from direction β. The probability of sea states q_β having a selected direction β is shown in the histogram on the right of Fig. 1. Note that most of the waves in the selected area originate from a southwest direction. If interest is taken in shorter periods of time, an additional seasonal break-down of wave scatter diagrams may be applied (Hogben and Lumb, 1967).[2]

2.3 Linking system behaviour and environmental conditions

The application of spectral analysis in ship dynamics started with the fundamental publication of St. Denis and Pierson (1953). Natural seaway is interpreted as a random superposition of a great number of harmonic waves of different amplitudes ζ_{ai} and frequencies ω_i. The wave crests are assumed to be of infinite length. Each component wave contributes an amount of energy to the seaway proportional to its squared wave amplitude. The spectral density $S(\omega)$ represents the energy distribution as a function of wave frequency ω. We use Pierson-Moskowitz spectra for the fully developed wind seas in our example.

---

[2] Within this paper the term direction is assigned to the origin of incoming incident waves. The term heading refers to the direction in which the waves are propagating with respect to the positive x-axis of the body-fixed coordinate system.

Corresponding to the wave spectrum $S_\zeta(\omega)$ of the seaway the response spectrum $S_s(\omega)$ represents the energy distribution of the output signal. Utilizing the response amplitude operator $H_{s\zeta}$ wave and response spectra are related by

$$S_s(\omega) = \left|H_{s\zeta}(\omega)\right|^2 S_\zeta(\omega) \tag{1}$$

A significant double amplitude of system response $(2s_a)_s$, comparable to the significant wave height H_s, follows from the response spectrum:

$$(2s_a)_s = 4\sqrt{\int_0^\infty S_s(\omega)d\omega} \tag{2}$$

These significant double amplitudes characterize the behaviour of floating systems in stationary short-term sea states. Comparing systems by means of significant double amplitudes allows to select the most suitable design for a specific location and task, e.g. a lifting operation.

Development of new designs usually requires consideration of performance during longer time spans. In this case long-term wave statistics are applied. If operational requirements limit the significant double amplitude of response, e.g. acceleration, to $(2\ddot{s}_a)_{s,limit}$, expected downtime due to exceeding this limit can be evaluated. Applying the appropriate response amplitude operator Eqs. (1) and (2) are evaluated for all classes of zero-up-crossing periods T_{0i} in the wave scatter diagram. This yields the highest acceptable significant wave height as a function of zero-up- crossing periods T_{0i}:

$$H_{s,limit}(T_{0i}) = (2\ddot{s}_a)_{s,limit}\cdot\left(\frac{(2\ddot{s}_a)_s}{H_s}\right)^{-1} \tag{3}$$

The values $H_{s,limit}(T_{0i})$ are transferred into the wave scatter diagram and sea states are assigned to a feasible $(H_s < H_{s,limit}(T_{0i}))$ and an infeasible $(H_s > H_{s,limit}(T_{0i}))$ region. The summation of all occurrences of the infeasible region, $\sum_i\sum_k r_{ki}$, related to the total number of observations r_β, yields the expected probability of downtime P

$$P_{d\beta} = \frac{\sum_i\sum_k r_{kj}}{\sum_i\sum_i r_{ki}} \tag{4}$$

The index *k* ranges over all H_s-classes where $H_s(T_{0i})$ exceeds $H_{s,limit}(T_{0i})$

To account for the non-uniform distribution of wave directions the computed values of expected downtime $p_{d\beta}$ are multiplied by the probability of occurrence q_β. Summing up yields the averaged downtime considering all wave directions

$$P_d = \sum_{all\beta} P_{d\beta}\cdot q_\beta \tag{5}$$

Before we apply this rational design criteria to optimize a semisubmersible a short review of the optimization framework is given.

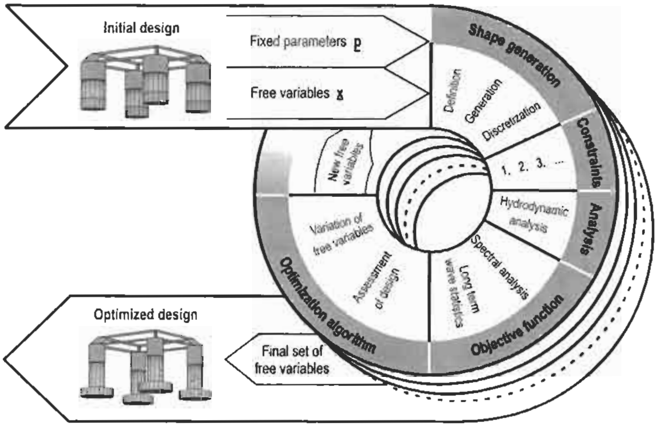
Initial design
Fixed parameters p
Free variables x
Shape generation
Definition
Generation
Discretization
Constraints
1, 2, 3, ...
Hydrodynamic analysis
Analysis
Spectral analysis
Long term wave statistics
Objective function
Assessment of design
Variation of free variables
New free variables
Optimization algorithm
Optimized design
Final set of free variables

Figure 2. Automated hull shape optimisation framework

3 OPTIMISATION FRAMEWORK

Fig. 2 illustrates the automated shape optimization process. The user prepares the optimization by selecting objective function, constraints and an appropriate parametric description of the hull geometry (see below). A subset of form parameters constitutes the vector of free variables x. The other parameters p are retained unchanged or are updated for each new design if they depend on free variables. Using this set of data the hydrodynamic shape optimization is started and no further user interference is required. The design is checked against the set of constraints before entering the time consuming stage necessary to evaluate wave-body interaction.

After processing of the initial design the loop of shape generation, check of constraints, hydrodynamic analysis and assessment of designs is repeated with changing free variables until a minimum of the objective function is obtained. Control of the process is conducted by a deterministic optimization algorithm (Tangent Search Method; Hilleary, 1966). Most optimization algorithms are composed for unimodal objective functions, i.e., functions with one well defined minimum. Nevertheless, they are successfully applied to multi-modal problems, if the user is aware of the fact that the results eventually represent local optima only. This fact is not detrimental at all, because each local minimum is still an improvement to the initial stage.

In contrast to ship hulls, surfaces of offshore structures are composed of clearly distinguishable components, e.g. columns and pontoons of semisubmersibles. This modular topology provides the key to an efficient parameter based shape description (Clauss and Birk, 1996; Huang, 1999). Each component is deed by two sets of form parameters (Fig. 3). One set comprises, e.g. volume, center of buoyancy etc and determines the volume distribution along the component axis (Fig. 3(a)). The other set defines the shape of the cross section (Fig. 3(b)). The form generation tool is implemented by means of the interpreter language Python (van Rossum, 2000). The object oriented features of the language enable the user to define template classes of body components which accelerate the process of setting up new optimization problems. The process of shape generation is illustrated in Fig. 4. After all components are generated from their form parameters, the procedure starts merging the components. If necessary a recess clearance is computed and blending patches are filled in to yield a completely seamless fitting of components.

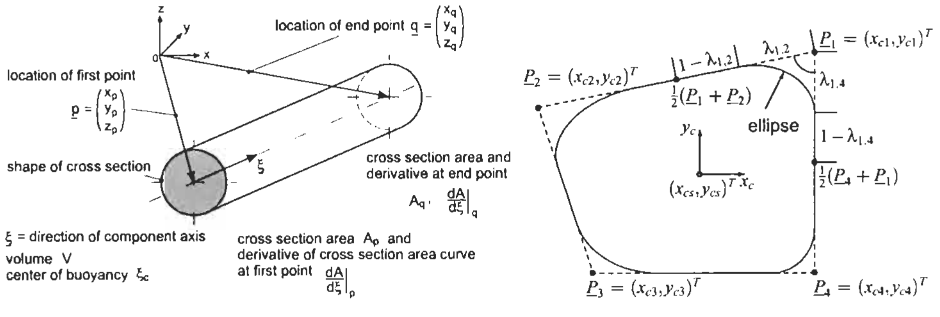
location of end point q
location of first point p
shape of cross section
cross section area and derivative at end point
ξ = direction of component axis
volume V
center of buoyancy ξc
cross section area Ap and derivative of cross section area curve at first point
P1 = (xc1,yc1)T
P2 = (xc2,yc2)T
P3 = (xc3,yc3)T
P4 = (xc4,yc4)T
ellipse
(xcs,ycs)T

(a) Form parameters of volume distribution (b) Form parameters of cross section

Figure 3. Shape definition of a single component by form parameters

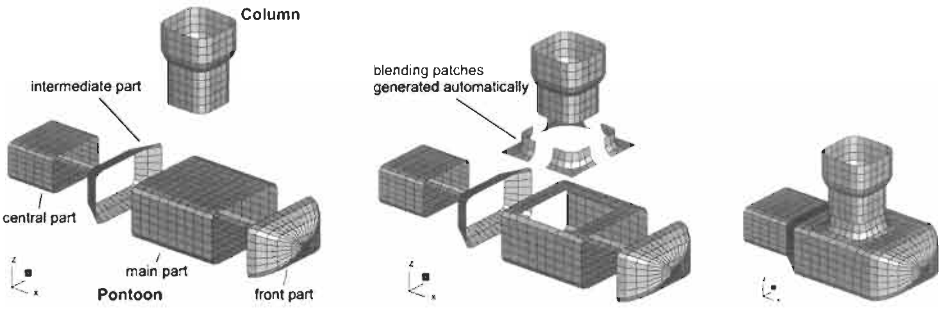
Column
intermediate part
central part
main part
Pontoon
front part
blending patches generated automatically

(a) Components generated from form parameters (b) Components prepared for merging (c) Merged components

Figure 4. Shape generation process

4 HULL FORM OPTIMIZATION

Motion of floating systems limits various offshore perations. Minimizing the total acceleration at a selected reference point provides a suitable method to improve motion behaviour in general. In order to include the statistical properties of sea states we minimize averaged downtime P d due to excessive acceleration according to Eq. (5). To enforce improvement for an extended range of T_0-classes a low limit of acceleration is selected, i.e., $(2\ddot{s}_a)_{s,\lim a} = 0.072 \cdot g$,g=9.81m/s^2 being the gravitational acceleration. The reference point is located 25m above sea level and shifted horizontally to the left forward column. Thus every mode of motion contributes to the total acceleration. The initial design of the semisubmersible is of standard shape with two pontoons and four columns. The x-axis (parallel to pontoon centreline) is pointing southwards. All designs are symmetric with respect to the *x*=0 and *y*=0 planes. Each pontoon half consists of four components: central, intermediate, main (underneath column), and rounded front part (Fig. 4). A broad range of hull shape variations is accomplished by five free variables:

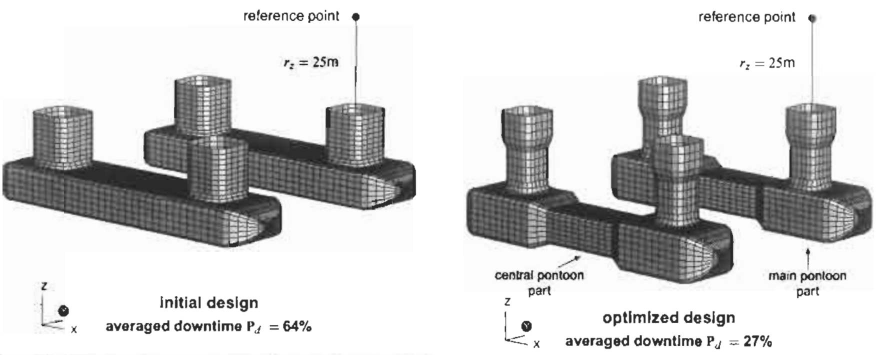

free variables	initial design	optimized design
pontoon cross section area ratio A_{pm}/A_{pc}	1.0	1.8875
pontoon breadth/height ratio B_p/T_p	2.0	1.4
pontoon centre line draught d_p	20.0m	30.0m
VCB/L of column from waterline ξ_{cc}	0.5	0.45
pontoon centre line shift Δy_p	0.0m	1.86m

constant form parameters	all designs
displacement $\forall$	50.000m^3
column centreline x- and y-separation	57.5m
pontoon length	95m

Figure 5. Geometric properties of initial design and the semisubmersible optimized with respect to downtime due to excessive accelerations at the reference point.

A_{pm} / A_{cm}	ratio of cross section areas of pontoon main part A_{pm} and central part A_{pc}.
B_p / T_p	ratio of width B_p and height T_p of pontoon cross section (all parts),
d_p	draught of pontoon centreline (all parts),
ξ_{cc}	normalized vertical centre of buoyancy of column $\xi_{cc} = VCB / L_c$, measured from waterline.
Δy_p	shift of pontoon centreline with respect to column centreline in direction of y-axis; breadth is increased when Δy_p is positive.

Fig. 5 presents the main geometric properties of initial and optimized semisubmersible design, respectively. The increase in pontoon centreline draught d_p decreases heave exciting forces. This ect is amplified by shifting displacement from the central pontoon part to the pontoon main part, i.e., A_{pm} / A_{cm} is increased, and the outward shift of the pontoon centreline by Δy_p=1:86m. Due to a decrease of ξ_{cc} a pronounced shoulder in the profile of the column is developed. Heave added mass and damping of the new configuration are adopted by reducing the B_p / T_p-ratio. The expected downtime P_d is decreased considerably for all wave directions. The optimisation process extends the region of feasible sea states especially where high probabilities of occurrence are present (Fig. 6).

The decrease in acceleration levels is reflected by a significant improvement of motion behaviour. Fig. 7 shows the response amplitude operators of surge (s_1), heave (s_3), roll (s_4) and pitch (s_5) motion. The wave heading is 120 deg, which corresponds to the most probable direction of sea states (β =240deg). In all cases and all ranges of wave frequencies lower motion amplitudes are achieved. Note that the amplitudes of heave motion are overestimated in the range of the resonance frequency and underestimated for the cancellation frequency. This is of course due to the lack of viscous effects in the hydrodynamic analysis. Indeed, the excessive heave resonance motions provide a positive side effect, preventing an increase of resonance frequency, which would constitute a serious security problem.

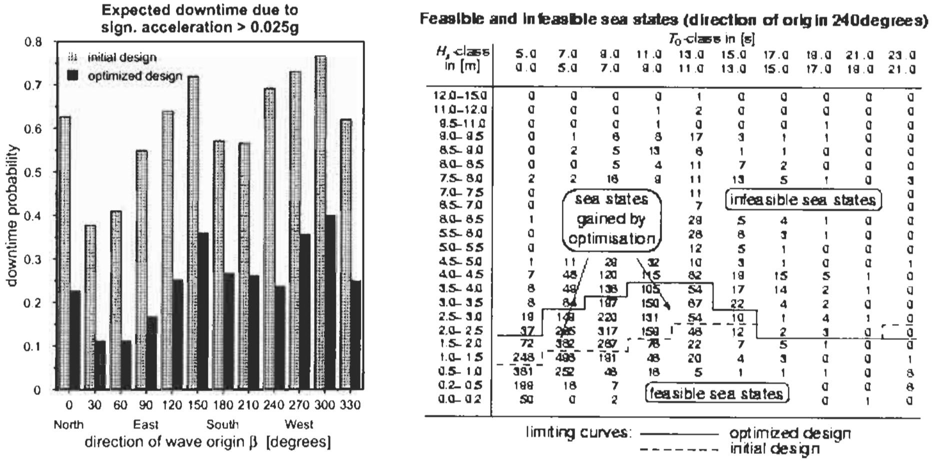

Feasible and infeasible sea states (direction of origin 240degrees)

H_s-class in [m]	T_0-class in [s] 5.0 0.0	7.0 5.0	9.0 7.0	11.0 9.0	13.0 11.0	15.0 13.0	17.0 15.0	19.0 17.0	21.0 19.0	23.0 21.0
12.0–15.0	0	0	0	0	1	0	0	0	0	0
11.0–12.0	0	0	0	1	2	0	0	0	0	0
9.5–11.0	0	0	0	1	0	0	0	1	0	0
9.0–9.5	0	1	6	8	17	3	1	1	0	0
8.5–9.0	0	2	5	13	6	1	1	0	0	0
8.0–8.5	0	0	5	4	11	7	2	0	0	0
7.5–8.0	2	2	16	9	11	13	5	1	0	3
7.0–7.5	0				11					0
6.5–7.0	0				7					0
6.0–6.5	1				29	5	4	1	0	0
5.5–6.0	0				28	8	3	1	0	0
5.0–5.5	0				12	5	1	0	0	0
4.5–5.0	1	11	29	32	10	3	1	0	0	1
4.0–4.5	7	48	120	115	82	19	15	5	1	0
3.5–4.0	8	49	138	105	54	17	14	2	1	0
3.0–3.5	8	84	197	150	67	22	4	2	0	0
2.5–3.0	19	149	220	131	54	10	1	4	1	0
2.0–2.5	37	265	317	159	48	12	2	3	0	0
1.5–2.0	72	382	267	78	22	7	5	1	0	0
1.0–1.5	248	498	191	48	20	4	3	0	0	1
0.5–1.0	381	252	48	18	5	1	1	1	0	8
0.2–0.5	199	18	7					0	0	8
0.0–0.2	50	0	2					0	1	0

Figure 6. Result of downtime minimization of a semisubmersible

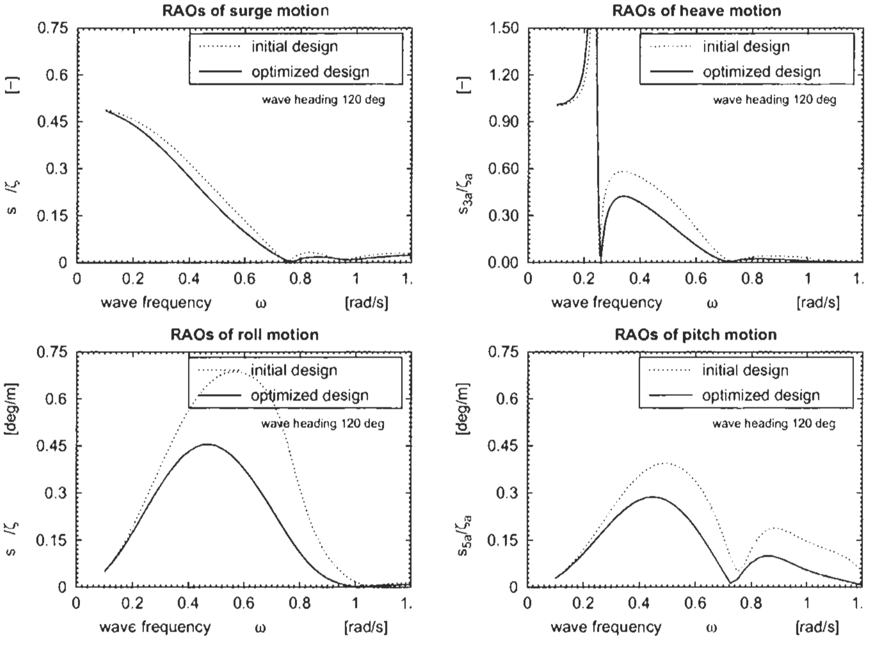

Figure 7. Comparison of motion behaviour of initial and optimized semisubmersible.

5 CONCLUSIONS

The paper presents rational design criteria based on short and long-term wave statistics. This allows to model realistic environmental conditions. The automated hull optimization based on these criteria successfully combines advanced analysis tools, numerical optimization methods and an automated, parameter controlled shape generation. The improvements in motion behavior of the designs are due to the precise adaption of important system parameters like added mass, damping by wave radiation, and exciting forces with respect to environmental conditions. Although the results are based on linear theory and obviously neglect higher order effects, the method is unmatched when comparing and optimizing designs. In summary, automated hydrodynamic hull optimization provides an efficient tool for the improvement of existing and the development of new system concepts in short time.

Acknowledgements

This work has been funded by the German Science Foundation (DFG).

References

Barltrop N. and Adams A. (1991). *Dynamics of Fixed Marine Structures*. Butterworth- Heinemann Ltd, Oxford, 3 rd edition.

Birk L. (1998). Hydrodynamic shape optimization of offshore structures. *PhD thesis*. Technische Universit at Berlin (D83), Germany.

Birk L. and Harries S. (2000). Automated optimization --- A complementing technique for the hydrodynamic design of ships and oshore structures. In *1st Int. Conf. on Computer Applications and Information Technology in the Maritime Industries (COMPIT)*. Potsdam, Germany.

Clauss G. and Birk L. (1996). Hydrodynamic shape optimization of large offshore structures. *Applied Ocean Research*. **18:4** 157-171.

Hilleary R. (1966). The Tangent Search Method of constrained minimization. *Tech.Rep./Res. Paper* 59, United States Naval Postgraduate School, Monterey.

Hogben N. and Lumb F. (1967). Ocean Wave Statistics. Her Majesty's Stationery Office, London.

Huang L. (1999). Anwendung von Freiformflachen beim arameter-gesteuerten Entwurf von Oshore-Plattformen. *PhD thesis*, Technische Universit at Berlin (D83), Germany. (In German).

Newland D. (1975). *Random Vibration and Spectral Analysis*. Longman Inc., New York.

Newman J. and clavounos P. (1988). The computation of wave loads on large offshore structures. *Proc. of BOSS Conf.*, pages 05.622, Trondheim, Norway.

St. Denis M. and Pierson W. (1953). On the motions of ships in confused seas. *Transactions, SNAME*. **61**.

van Rossum G. (2000). *Python Reference Manual*, Version 2. BeOpen PythonLabs.

Practical Design of Ships and Other Floating Structures
You-Sheng Wu, Wei-Cheng Cui and Guo-Jun Zhou (Eds)
© 2001 Elsevier Science Ltd. All rights reserved

THE APPLICATION OF A DECOMPOSITION AND REUSE APPROACH IN MARINE DESIGN

K. G. Tan[1] and P. Sen[2]

[1] Engineering Design Centre, Newcastle University,
Newcastle upon Tyne NE1 7RU, UK
[2] Department of Marine Technology, Newcastle University,
Newcastle upon Tyne NE1 7RU, UK

ABSTRACT

Decomposition and reuse are two practical approaches that could assist the solution of large marine design problems. Design Reuse has always been regarded as an attractive approach by marine designers, although the complexity of the problem and the relative novelty of individual designs do not always allow efficient application of design reuse paradigms. This paper discusses a decomposition and reuse approach in marine design. A well-known decomposition paradigm is used which allows identification of weakly connected model sub-structures that naturally exist within a design problem and permits the division of the overall design problem into sub-problems in accordance with these sub-structures. The reuse concept proposed in this paper is based on the reuse of design data. The aim is see how the designer can use existing design data as the basis for future designs without necessarily having to know how the data was derived, and without explicitly using iterative mathematical procedures.

KEYWORDS

Design decomposition, Reuse of design data, Multiobjective optimisation, Response surface.

1 INTRODUCTION

Marine design is a complex process which usually involves a multidisciplinary team of designers working on thousands of design variables. Designing of a new marine product therefore often requires the designer to decompose the overall design problem into a number of design tasks, so that a complex design problem is often broken down into a numberof smaller, manageable design sub-problems, in a divide-and-conquer manner, to deal with the complexity of the design task. This apporach often permits the reuse of past design data and knowledge in the decomposed domains. It is not surprising therefore that interest in design reuse have always been manifest in designers in all fields (Sivaloganathan and Shahin 1999).

Design is by nature an evolving process, and incremental improvements are made by designers based on past experience and knowledge gained in executing this process. Previously tried and tested designs are often re-used and improved upon to arrive at even better designs. This form of design reuse is routinely used in many areas of marine design. For example, many ships are designed from basis ships which are known to possess good performance characteristics. However, the complexity of a marine design problem does not always allow efficient application of design reuse paradigms. Decomposition breaks down complexity of design problems and hence allows designers to reuse design data in a relatively efficient manner.

This paper discusses some aspects of the application of a decomposition and reuse approach in marine design. The decomposition strategy employed allows identification of weakly connected model sub-structures that naturally exist within a design problem and attempts to divide the design problem into sub-problems in accordance with these sub-structures. Reuse of existing design data to solve the decomposed design problems further improves the efficiency and quality of the design solutions. A ship design example is used to illustrate the application of this decomposition and reuse approach in marine design.

2 DESIGN DECOMPOSITION

The motivations to decompose a design problem into a number of smaller sub-problems are: reduction of problem complexity, application of different targeted solution procedures on different sub-problems, carrying out problem-solving activities concurrently and utilising parallel computing opportunities.

While decomposition is a widely used problem-solving approach, there are significant variations in the criteria and strategies used for performing design decomposition in practice. Design decomposition strategies based on a combination of structures (physical components, logical objects, etc.), behaviours (action, force, process), disciplines, and goals or functional requirements (design properties that satisfy given requirements) have been observed (Koopman 1995). For designs that involve sequential flow of information sequential decomposition may be appropriate (Scott and Sen 1998). In addition, various methods for dealing with design sub-spaces problems exist, for example in the area of optimisation in design sub-space based on decomposition (Rao and Sen 1999).

When a design problem is broken down into a number of simpler sub-problems, the problem-solving procedures then involves solving such sub-problems of reduced complexity. It is desirable, therefore, to reduce the interactions between sub-problems (i.e. to reduce the co-ordination effort). However, many decomposition approaches do not take the magnitude of this co-ordination effort directly into consideration so that the decomposed sub-problems may have a relatively large number of variables that are common between the decomposed sub-problems. Put simply, the main problem may be decomposed into a number of highly coupled sub-problems requiring a relatively large co-ordination effort during the problem solving process. The additional co-ordination effort required in solving a series of highly coupled sub-problems might significantly undermine the initial objective of breaking down complexity by decomposition.

A hypergraph based approach to design decomposition is used in this paper. In this approach, a design problem is represented by a hypergraph. A hypergraph consists of nodes connected by hyperedges. A hyperedge connects two or more nodes. The objective of the hypergraph partitioning operation is to decompose a given hypergraph into a desired number of partitions (sub-hypergraphs) such that the hyperedges spanning across two or more partitions are minimised. The hypergraph partitioning approach has been applied in decomposition of Very Large Scale Integration (VLSI) circuit design problems, cell formation problems in flexible manufacturing systems and Finite Element Method (FEM) problems, to name but a few.

Hypergraph partitioning problems are known to be NP-hard. A number of hypergraph partitioning algorithms have been proposed in the literature. Essentially the algorithms make use of some heuristics and search methods to partition a given hypergraph into two or more partitions. Due to space constraint, detailed description of this class of problem and its solution mechanisms are not presented in this paper. Readers who are interested can refer to papers by Hendrickson and Leland, and Karypis *et al.* (Hendrickson and Leland 1995, Karypis. *et al.* 1997). A computer software system implementing a known multi-level hypergraph partitioning algorithm hmetis© (Karypis and Kumar 1998) is used in this paper. This algorithm is flexible enough to allow a designer to specify constraints in terms of partitions and association of nodes.

In the hypergraph representation of a marine design problem, the nodes can be used to model design/constraint equations, design activities or design tasks. The hyperedges can be used to model design variables that are required to connect the various nodes. The objectives of the hypergraph partitioning operation are therefore to produce equal (or near-equal) sized sub-problems (to yield sub-problems of roughly equal design effort) and to minimise the co-ordination effort in solving the decomposed sub-problems. In principle it is possible to have other objectives besides the two mentioned. Hence the result of the decomposition is a number of sub-problems each containing a number of design/constraint equations and a number of design variables. Some design variables will be associated with more than one sub-problem, and these are termed as linking variables.

Design decomposition by itself does not produce design solutions, hence the decomposed design sub-problems must be solved to provide overall solution(s) to the design problem.

3 DESIGN REUSE

Various forms of design reuse have been identified in practice: subsystem and component reuse (Culley 1998), software object reuse and design knowledge reuse (Chao *et al.*1998). Generally speaking, research work in reuse is mostly based on reuse of concepts and embodiments (Sivaloganathan and Shahin 1999). Relatively little work has been done on the reuse aspects of design data. Although design data has always been routinely reused, the reuse is usually associated with the invocation of complex and often iterative mathematical procedures (e.g. past design data is often re-used to perform design analysis e.g. powering estimation). The reuse concept proposed in this paper is based on the reuse of design data in such a manner that a designer can make full use of the data without having to know how it was derived, so that he can reuse the design data without explicitly using iterative mathematical procedures from which the data was originally derived. The purpose is to identify pockets of efficient designs for further detailed design analysis without the need to carry out relatively complex and time consuming analysis processes. This concept is rather similar to that of object oriented programming paradigm that has been successfully implemented in the field of computing science; the data should be active, it can be directly used without knowing the methods involved in the derivation and computation of complex data-entities.

The design reuse concept accommodates a three-pronged approach: *direct search* for a new design that has an exact match with existing design data, "*interpolation*" to obtain efficient solutions within a given range, and *extension* of existing design data to satellite applications. Design data can be stored and retrieved using a suitable form of database. For example, when a designer needs a preliminary design of a particular ship type based on a given specification a direct search of a relevant database may produce an exact match which will provide the designer with the necessary design data.

The result of a direct search, however, is more likely to produce a number of designs that are close to the given specification rather than an exact match. Hence the designer needs to perform "interpolation" between these using some form of iteration. The reuse approach suggests a form of "interpolation" that does not directly involve a user-driven iterative design process. Conceptually, this situation can be illustrated by a case in which a designer locates two designs both deviating somewhat from the desired specification. The question arises as to how one can find out or "interpolate" from the design data a new design (an emerging design) that meets the requirements of the given specification. The reuse approach proposes an objective-driven search (e.g. multiple objective optimisation) using relevant ship design knowledge to identify a range of efficient solutions for further consideration. These designs constitute the Pareto optimal set, where designs can only be improved with respect to one objective at the expense of others. The mechanics of the "interpolation" process is automated so that a designer is largely shielded from the background computations that are involved, partly as a result of reusing higher level knowledge (e.g. rule induction based relationships between variables) obtained from previous design efforts using the same database.

The reuse of design data can also be extended to satellite applications for which the data was not originally prepared. For example, a designer may only have a relatively small set of data concerning some aspects of ship performance. The designer may want to populate a relatively large database, which does not currently contain data elements concerning these aspects of performance, with approximated performance data elements based on the small set of design data that is available. In such a situation an approximate response surface to a set of given performance data. Artificial Neural Networks (ANN) and rule induction are two methods that can be employed within this reuse scenario for extending the reuse of design data, through this response surface approach, to satellite applications.

4 AN EXAMPLE APPLICATION

A small general cargo/container ship preliminary design application based on a decomposition and reuse approach is presented as an illustrative example in this section. The ship design problem is decomposed into two sub-problems. Design reuse approach is then used to deal with one of the sub-problems using the "interpolation" approach. The reuse of the design data is also extended to a satellite application. The satellite application is illustrated via the extension of existing design data to include seakeeping characteristics.

Suppose a set of design objectives is given: minimise transportation cost (F_1), maximise annual cargo carried (F_2), minimise lightship weight (F_3), minimise the probability of machinery space flooding (F_4) and minimise the probability of losing auxiliary power (F_5). The first three objectives are driven by economic considerations whereas the last two objectives are related to survivability of the vessel. Mathematically speaking, a ship design problem can be represented by a set of objectives and constraint equations over a finite number of design variables. For the illustrative example, the five objectives mentioned above can be expressed in terms of five formal objective functions. In addition to these five objective functions, eleven constraint equations are also to be taken into account to ensure feasibility.

4.1 Design Decomposition

In this example the given problem is decomposed into two sub-problems using the hypergraph partitioning approach mentioned in the previous section.

The objective functions can be represented in a tabular form. A partial table of the design problem is shown in Table 1. In Table 1, the nodes (functions) are listed in the rows and the hyperedges (design variables) are listed in the columns. For example, from Table 1, it can be seen that hyperedge (design variable) x_1 connects functions $F_1, F_2, F_3, \ldots, H_9$. In a complex problem (involving hundreds if not thousands of nodes and hyperedges), it is not immediately clear as to how the problem can be decomposed in such as way that the number of linking variables can be minimised. Hence the need for the algorithm.

TABLE 1

A PARTIAL TABLE SHOWING THE HYPERGRAPH REPRESENTATION OF THE DESIGN PROBLEM

	x_1	x_2	x_3	x_4	x_5	x_6	x_7	x_8	x_9	x_{10}	x_{11}	x_{12}	x_{13}	x_{14}	x_{15}	x_{16}	x_{17}	x_{18}	x_{19}	x_{20}	x_{21}	x_{22}	x_{23}	x_{24}	x_{25}	x_{26}	…	x_{33}
F_1	√	√	√	√	√	√																					…	
F_2	√	√	√	√	√	√																					…	
F_3	√	√	√	√	√																						…	
F_4	√							√	√									√	√								…	
F_5	√							√	√	√	√	√	√	√	√	√	√	√	√								…	
H_1	√	√																									…	
…															…												…	
H_8	√			√																√	√	√	√				…	
H_9	√	√	√	√	√	√																		√	√	√	…	

The result of the decomposition exercise is shown in Table 2. The two resultant sub-problems are semi-independent, and can be solved independently when the three linking variables x_1, x_3 and x_4 are co-ordinated. Sub-problem one is related to the economic objectives and their associated constraint functions. Sub-problem two is related to survivability objectives and their associated constraint functions. The two sub-problems could then be handled by two teams of designers: sub-problem one by the preliminary ship design team and sub-problem two by the safety analysis team. This illustrative example concentrates on solving sub-problem one as some concern is assumed to exist in this area. The design variables involved in this sub-problem are: x_1 (Length, L), x_2 (Breadth, B), x_3 (Depth, D), x_4 (Draught, T), x_5 (Speed, V), x_6 (Block coefficient, C_b) and x_7 (Waterplane coefficient C_w). The choice of variables involved in the sub-problem obviously depends on the mathematical models used.

TABLE 2

A PARTIAL TABLE SHOWING THE RESULT OF DESIGN DECOMPOSITION EXERCISE

	x_1	x_3	x_4	x_2	X_5	x_6	x_7	x_8	x_9	x_{10}	x_{11}	x_{12}	x_{13}	x_{14}	x_{15}	x_{16}	x_{17}	x_{18}	x_{19}	x_{20}	x_{21}	x_{22}	x_{23}	x_{24}	x_{25}	x_{26}	…	x_{33}
F_1	√	√	√	√	√	√																					…	
F_2	√	√	√	√	√	√																					…	
F_3	√	√	√	√	√																						…	
H_1	√			√																							…	
H_4		√		√																							…	
H_5	√	√	√	√	√	√																					…	
H_6	√					√																					…	
H_7		√	√	√	√		√																				…	
H_9	√	√	√	√	√	√																					…	
F_4	√							√	√									√	√								…	
F_5	√							√	√	√	√	√	√	√	√	√	√	√	√								…	
H_2	√		√																								…	
H_3	√	√																									…	
H_8	√		√																	√	√	√	√				…	
H_{10}	√		√																								…	√
H_{11}	√		√																								…	√

4.2 Design Reuse

As discussed above, a search in a database of good designs for design data that meets the design specification is the simplest and easiest form of design reuse. For a relatively simple design specification, a direct search on a design database may yield results that are suitable without further modification.

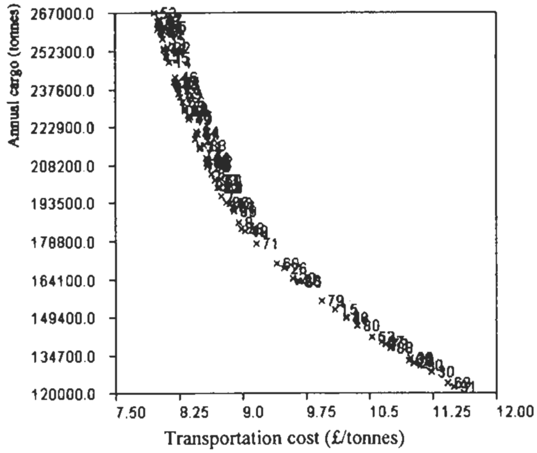

Figure 1: Annual Cargo Vs Transportation Cost.

However, the direct database search approach may not yield any design that exactly meets the design specification but may only identify some designs that are in reasonably close harmony with the given design specification. Hence, it is necessary to "interpolate" between these designs to obtain a desirable design that will meet the design specification. Such "interpolation" needs only involve the variables identified above as involved in sub-problem one. In this example, the design data is viewed as being active so that the designer need not know how the data is derived. Furthermore the data can be used without involving relatively tedious and often iterative mathematical procedures. As in object oriented programming approach, the "interpolation method" can be regarded as being attached with the data and can be used in a transparent manner. In this case an objective-directed search employing a genetic algorithm based multiobjective optimisation method was applied (Sen and Yang 1998) as the "interpolation" method. The necessary ship design knowledge (e.g. stability requirement, powering estimation, etc) is embedded within this method. The result of the interpolation is shown in Figure 1 which shows Pareto optimal solutions with respect to two economic objectives. For illustrative purpose, the range of the search is wide so that a clear range of efficient solutions can be shown. From Figure 1, a designer can then select efficient design solutions that most closely meet the specification.

As discussed before, reuse of design data can go beyond direct search and interpolation applications. It is possible to extend the design data to satellite applications. For example, suppose the designer would like to incorporate consideration of seakeeping characteristics (in terms of natural periods of roll, heave and pitch) into the main design database without carrying out full-scale analysis. His current database only has a relatively limited set of ships with known sea-keeping characteristics. If the database is reasonably large and populated with reliable data then an Artificial Neural Net (ANN) can be used to fit a response surface to the existing data. A three-layer feed-forward ANN with seven nodes in the input layer (nodes $i_1 - i_7$, length, breadth, depth, draught, block coefficient, waterplane coefficient and metacentric height), seven (nodes 1 – 7) in the hidden layer and three in the output layer (nodes $o_8 - o_{10}$, roll, heave and pitch period), was set up. This ANN was trained with a set of 110 training data from the designer's current database. A separate set of 16 test data was used to test the trained ANN. The approximate error given by the trained ANN for the test data was found to range from 0.00% to 2.00% with a majority of results being within 1.0%. The trained ANN is then able to give approximate roll, heave and pitch periods of all vessels within the database given the required seven inputs. In this manner, the database can be populated with extended data of seakeeping characteristics for future analysis.

5 DISCUSSION AND CONCLUSION

Consideration of reuse in design is usually related to components. Data reuse, although not uncommon, is rarely, if ever, discussed. And yet large and reliable databases of design data are often put together for future use. It can be observed that the use of such databases can be made more intelligent and rewarding by considering data reuse in a formal manner. It is obvious that it is possible to have decomposition without reuse and reuse without decomposition, but when used in combination it opens up new opportunities for either approach.

This paper addresses three common tasks performed by a designer: decomposing design problems into manageable tasks, applying past experience (knowledge and design data) and extending design knowledge. The first task relates to decomposition and the latter two to reuse. These tasks are illustrated through a preliminary ship design example.

The hypergraph partitioning approach used in the example in this paper is able to decompose a design problem into sub-problems with a minimum number of linking variables (hence co-ordination effort). Apart from design constraint equations, the hypergraph representation can also be used to model design activities and variables. The example design problem is decomposed into two sub-problems using this approach. The division of work shows a sensible pattern. Reuse concepts are then used to assemble candidate Pareto optimal designs for one of the sub-problems into which the original problem was decomposed. The reuse concept is then extended to include an associated satellite application. It is clear, on the basis of the above, that decomposition and data reuse have in-built capabilities that can be beneficially taken advantage of.

References

Chao, K. M.; Smith, P.; Hills W.; Florida-James, B. and Norman, P. (1998). Knowledge Sharing and Reuse for Engineering Design Integration, *Expert systems with applications.* **14:3**, 399.

Hendrickson, B. and Leland R. (1995). A Multilevel Algorithm for Partitioning Graphs, *Proceedings of Supercomputing 95, 1995 December, San Diego, CA,* 626–657.

Karypis, G.; Aggarwal, R.; Kumar, V. and Shekhar, S. (1997). Multilevel Hypergraph Partitioning: application in VLSI Domain, *34th Design Automation Conference, 1997 June, Anaheim, CA*, 526–529.

Karypis, G. and Kumar, V. (1998). hMetis, A Hypergraph Partitioning Package, Version 1.5.3 (User Guide), University of Minnesota, Department of Computer Science & Engineering, Army HPC Research Center, Minneapolis, MN 55455.

Koopman, P. J. (1995). A Taxonomy of Decomposition Strategies Based on Structures, Behaviors, and Goals, *9th International Conference Design Theory and Methodology, September Boston, ASME Publications DE 1995,* **83:2**, 611-618.

Rao, Z and Sen, P. (1999). Design Decomposition and Coordination of Multidisciplinary System Optimisation, *International Conference on Engineering Design, 12th August 1999,Munich, Germany, Wdk Workshop Design Konstruktion*, **2:26**, 733-738.

Sen, P. and Yang, J. B. (1998). *Multiple Criteria Decision Support in Engineering Design*, Springer-Verlag, London.

Scott, J. and Sen, P. (1998). Focusing Design Reuse Initiatives using the Design Structure Matrix System, *Engineering Design Conference 98*, 351–359.

Sivaloganathan, S. and Shahin, T. M. M. (1999). Design Reuse: An Overview, *Proceedings of the Institution of Mechanical Engineers. Part B, Journal of engineering manufacture.* **213:7**, 641-654.

Practical Design of Ships and Other Floating Structures
You-Sheng Wu, Wei-Cheng Cui and Guo-Jun Zhou (Eds)
© 2001 Elsevier Science Ltd. All rights reserved

EVALUATING DESIGN FOR UPGRADEABILITY: A SIMULATION BASED APPROACH FOR SHIPS AND MARINE PRODUCTS

I L Buxton and G H Stephenson

Dept of Marine Technology, University of Newcastle, Newcastle NE1 7RU, UK
School of Engineering, University of Northumbria, Newcastle, NE1 8ST,UK

ABSTRACT

Major engineering products like ships, offshore plant and power stations have lives of over 20 years. Technical and market changes may require mid-life upgrading, such as increasing capacity by jumboisation or installing new machinery or equipment. The question for the designer is how far to design for such upgradeability, e.g. by provision of additionally unused space or more powerful equipment than is required initially. A methodology has been developed for evaluating whether designs incorporating some upgrade capability from the start may be more economic than those which do not. A range of upgrade scenarios from 'bare minimum' to 'over-engineered' can be evaluated to show which are likely to show the greatest economic benefit in terms of NPV over the life cycle of the product. Since this depends on a probabilistic view of say market demand, a simulation model is needed to compare the alternatives. A spreadsheet-based evaluation has been developed which allows the user to incorporate stochastic values, and to investigate how much it is worth spending now in order to save later. Some results for a container ship are presented.

KEYWORDS

Design, Upgrading, Simulation, Container ship, Through life costs, Discounted cash flow.

1 BACKGROUND

Since 1995 a continuing research theme of the Engineering Design Centre (EDC) at the University of Newcastle, England, has been the use of estimates of product Through Life Cost (TLC) to support design decision making. The EDC concentrates on long life large made-to-order (MTO) products, which have a marketable output, such as ships, offshore production platforms or process plant. With guidance from the wide range of major companies that are sponsoring partners in the EDC, a generic approach to determining the TLC has been agreed. This uses Discounted Cash Flow (DCF) to arrive at a Net Present Value (NPV) for a MTO product. The method requires that all input variables are first defined and is, therefore, suitable for almost any application. A particular feature is the ability to build up a whole life cycle from cyclical activities, such as a voyage in the case of a commercial ship. The voyage is in turn broken down into loading, sailing and unloading. Costs and overheads can be up a whole life cycle from cyclical activities, such as a voyage in the case of a commercial ship. The voyage is in turn broken down into loading, sailing and unloading. Costs and overheads can be attributed to individual activities, voyages, maintenance/survey periods or years. Input values are assumed to be constant unless some step, percentage change or other function is added. The calculations simulate the life of the ship and are, by definition, fairly lengthy, so numerous tables and plots are available to users so that they can gain confidence in the numbers produced by checking at each stage. The change in NPV for any variation on the basic design is used to support design decision making.

Many MTO products undergo upgrading during their lives to meet changes in market requirements, to accommodate new technology or to meet new regulatory requirements. Hitherto, designing for such changes has rarely been addressed explicitly in design procedures. What has been lacking is a systematic means of comparing alternative upgrade scenarios, in order to assess which is likely to be the most cost effective.

Uncertainty and risk are important considerations in any attempt to predict future operating conditions because they determine the confidence that the designer can have in a decision. A means of adding a statistical distribution to one or more input parameters is important. In this case the NPV output values produced by the simulation of the ship's life also become a probability distribution. An upgrade, such as a jumboisation can be triggered, either at a fixed point in the life of the vessel or if certain conditions occur such as higher levels of demand. The spread of the results produced is a measure of the riskiness of the project and the extent to which additional expenditure may be justified.

2 DESIGN FRAMEWORKS

While testing the methodology on real cases provided by the partner companies, it became apparent that a generic approach to producing upgrade variations on a basic design does not exist. This contrasts the position where the requirement is to optimise the value of parameters defining the chosen components making up a design, for which many approaches are well known. There is a general recognition that many ships and manufacturing facilities experience either, at least one major change of operating conditions at some stage in their life, or there is a gradual change over time. Both may lead to the need for a significant upgrade, the cost of which could be significantly reduced in comparison to the increased revenue if provision had been made during the initial design and build. The value of this provision can be accounted for in the NPV if DCF techniques are used in assessing the total through life costs. A more obvious way of describing this approach is 'spend to save', which always requires a convincing justification if it is to be accepted by the project's financial backers. Other uncertainties can also be accommodated. For example, there may be significant additional 'regulatory' costs if say new safety standards were applied or an environmental levy on emissions was introduced. This introduces two elements of uncertainty, the extent and cost of the change, and the date from which it might be applicable. Both have probability distributions, so can be included in NPV calculations.

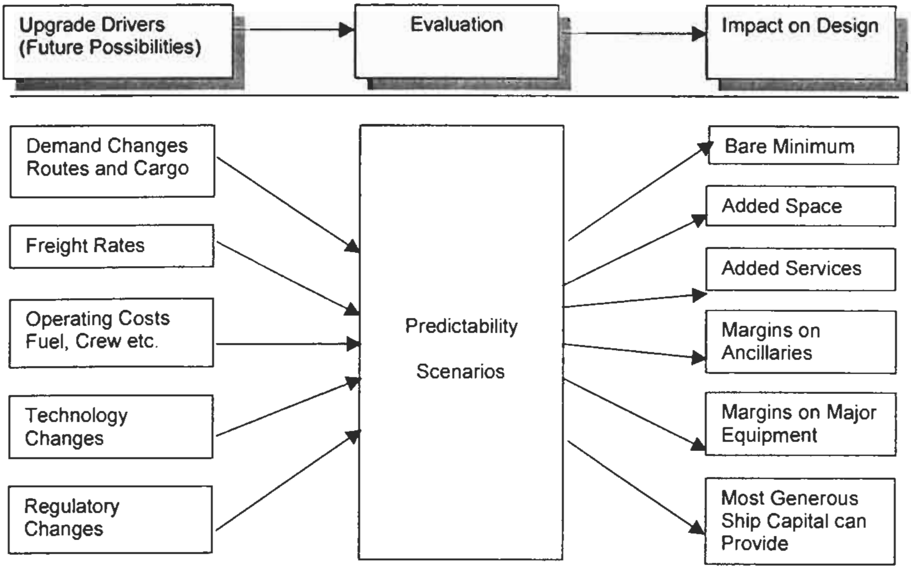
Upgrade Drivers (Future Possibilities)
Evaluation
Impact on Design
Demand Changes Routes and Cargo
Freight Rates
Operating Costs Fuel, Crew etc.
Technology Changes
Regulatory Changes
Predictability
Scenarios
Bare Minimum
Added Space
Added Services
Margins on Ancillaries
Margins on Major Equipment
Most Generous Ship Capital can Provide

Fig 1: Reasons for Upgrading and the Six Frameworks

To guide the designer through the problem, an approach using a hierarchy of design scenarios is suggested. The main factors which might give rise to a need for such changes, and some of the features which can be built into an initial design to minimise their impact are illustrated in Fig 1.

In response to these drivers for upgrading, it is proposed that the potential upgrade solutions can be classified into six broad frameworks, represented on the right hand side of Fig. 1. These range from a 'bare minimum' design for the current market, with no in-built upgrade potential, through four intermediate options, to a 'future-proof' version with substantial over-design. The six frameworks are:

Framework 1: A ship or plant designed only for today's requirement with minimal margins.
Framework 2: The basic requirements for some upgrades are built-in, such as additional hull strength, space for increased services or larger weight margins.
Framework 3: Additional services (power distribution, piping systems, ventilation etc.) to support an upgrade are provided, i.e. the design is "fitted for but not with".
Framework 4: Additional auxiliary equipment (e.g. bigger cranes, and bigger electrical generators) is provided.
Framework 5: Some items of major equipment (e.g. the main propulsion system in a ship) are oversized in anticipation of an upgrade.
Framework 6: The ship is designed and built as the most generous that capital can provide, i.e. overdesigned by today's requirements.

These frameworks are used in conjunction with the possible reasons for upgrading identified by the designer to evolve a set of alternative upgrade strategies at the concept design stage, with associated preliminary designs. The methodology described below can then be used to assist in choosing between them. It is obvious that to be attractive the through life benefits must be significantly greater than the initial 'extra' investment and this must show in the NPV for the ship, Fig. 2.

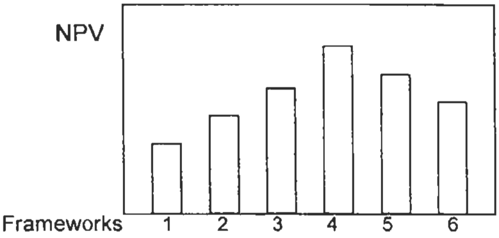

Fig. 2 Variation in NPV with increasing preparation for upgrade

Since the cost figures are subject to a degree of uncertainty, it is wise to add appropriate statistical probabilities to the key inputs so that the NPV comparisons appear with probability distributions. Fig. 3 shows the NPV distributions for three Frameworks: the basic design, a design with some built-in preparation for the upgrade and the 'over-engineered' design.

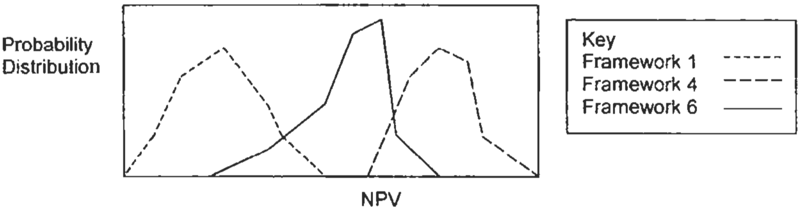

Fig 3 Typical distributions of NPV when uncertainty is added

In Fig. 3 the most attractive option, which has the highest NPV, is easily identified as Framework 4. The calculated figures can also be used to determine the probability that this Framework will always produce better financial results than the next best Framework, so should be taken into consideration if the difference between the mean values is small. Having determined an overall design philosophy for the ship by identifying the most appropriate Framework, it is then desirable to invoke a normal parameter optimisation technique to further refine the design.

3 METHODOLOGY

For each Design Framework selected for analysis, the basic methodology requires input data to generate a life cycle, which details each successive activity through from the start time of the intended simulation, e.g. start of procurement, to the disposal of the ship, offshore production platform or port facility. The duration of each activity must be estimated, while shipping demand, capacity, freight rates and operating costs may be assumed to change either progressively or at a particular point in time. Similarly, engine efficiency might be assumed to fall and the hull drag and maintenance requirements increase over time. Having established the life cycle, the cash flow balance can be found for each period by summing each of the contributing elements defined through additional input data. The total cash flow for each year is then discounted. The NPV for the Design Framework under consideration is the sum of the contributions from each of the years from start, through design and construction, operation, maintenance, upgrade (if triggered) to the final disposal.

When the required analysis takes into account the statistical probability of the value for any parameters in the simulation (e.g. fuel prices), then computation is more complex, but the methodology is the same.

The results from several Frameworks are then compared to support the decision as to how much preparation for an upgrade should be included in the initial build.

4 IMPLEMENTATION

The methodology has been implemented using a Microsoft^{TM} Excel Spreadsheet. The data is input to a number of sheets, each of which collects related items. For example, the first sheet defines the problem by requiring a definition of what the MTO product is and what it produces, the major stages of the life cycle, the currency to be used and the discount rate. Succeeding sheets detail all aspects of capacity and market demand and prices, costs, including product related production costs and overheads, both before and after any upgrade. The life cycle, event and annual cash flows appear as tables on later sheets from which the required summations and the resultant NPV are automatically produced. The entries in the tables are generated by macro programs, which calculate the appropriate data based on the current point in the ship's life. These tables, which may have hundreds of rows, can be checked to enable the user to confirm that the input data has produced the expected contribution to the summations.

Where statistical inputs are required, the Excel 'add-in' @Risk software from Palisade Corporation has been used to generate the distributions. This allows any cell to have any statistical distribution attached, so that for example a range of freight rates may be sampled. This employs a 'Monte Carlo' method in which the results of a number of individual simulations are collated to produce the final distribution and relevant statistical measures.

5 CONTAINER SHIP EXAMPLE

Ships are often upgraded about their mid-life. Some are designed with such expectations in mind, such as warships modernised with new weapon systems – an example of upgrading triggered by new technology. New regulations may also require ships to be upgraded, e.g. modifying passenger-vehicle roros to meet new damage stability standards.

The chosen example is jumboisation of a container ship. The growth in deep sea container shipping has been such over the last thirty years that not only are more ships required but larger ones. Many container ships have been jumboised, usually by adding a new section at midships. The same number of ships can then offer greater annual capacity at the same frequency of service.

If the ship has not been designed with jumboisation in mind, the original engine may not be able to maintain service speed. The main hull structure will require additional strengthening to withstand higher bending moments, shear forces and torsional moments. Auxiliary systems and fuel capacity may no longer be adequate for the larger vessel. However if a slightly larger engine and heavier scantlings had been built in from the start, both the cost of upgrading and the time out of service for adding the new section and modifying the systems will be reduced, and service speed maintained.

The example illustrates a 23-knot container ship designed around 1990 with a capacity of 3500 TEU, and examines whether it would have been worth designing for upgrading, given that the container market was then growing steadily. Such liner vessels are designed for an average load factor of around 70-80%, i.e. some voyages 100% full, others only half full. With an assumed growth rate of about 4% a year, such a ship will be fully utilised after about six years' service, but then not able to take all the cargo offered, so vulnerable to loss of market share. The owner may decide to 'do nothing', i.e. leave the ship unchanged, forego increased revenue and see his competitors take a greater market share; this may be regarded as Framework 1, the minimum ship. He may decide that the growth rate is such as to build an overlarge ship (and thus expensive) ship at the start, say one-third bigger, even though such a ship may be underutilised for about twelve years out of an assumed twenty year life (Framework 6). Or he might decide to pay a modest premium, by designing for jumboisation in the future, by installing a more powerful engine and increased scantlings and larger margins on equipment. (Framework 4)

The software enables all such variations to be explored, over differing life cycles. Estimates can be made of the different performance and construction costs of these three (or more) alternatives. The largest uncertainties lie in the prediction of future market trends, both in terms of cargo growth rate and in variation of freight rates. Other influences include fuel prices, and when to assume the upgrade will take place.

A typical ship in the fleet is taken, together with a typical service schedule. The basic 'cycle time' is a round voyage of 28 days with four ships providing a weekly frequency, all operating at 23 knots in service. Sea time is regarded as 'production' time, port time as 'idle time', while drydocking is part of maintenance time. Four types of 'production' are included: 20ft containers outward, 20ft homeward, 40ft outward, 40ft homeward. Different freight rates and growth trends are applied to each.

The key input data is summarised:

	Framework 1	Framework 4	Framework 6
TEU capacity as built/upgraded	3500	3500/4500	4800
Installed power, MW	30	34	36
Initial building cost $M	65	75	85
Proposed year of upgrade	-	7	-
Cost of upgrade, $M	-	6	-

Net freight rates of $750 per 20ft container and $1150 per 40ft were assumed, after container handling costs, assumed constant per box. Typical operating costs were assumed, with associated trends, e.g. escalation. NPV was then calculated for the life cycle of each Framework design.

A 'steady state' (deterministic) evaluation showed that Framework 4 (designed for upgradeability) produced a NPV $6M higher than Framework 1 (which is significant in terms of an investment of $65M). But it is useful to simulate the effect of random influences, such as variable freight rates. The @Risk software was then applied, with an assumed gaussian distribution of freight rate with a standard deviation of $70 (20ft) and $100 (40ft). 500 lifetimes were simulated. Fig 4 shows the probability density function, which has the following statistics:

	Mean NPV $M	Std Dev $M
Framework 4	17.64	4.09
Framework 1	11.34	3.86
Framework 6	-7.15	4.25

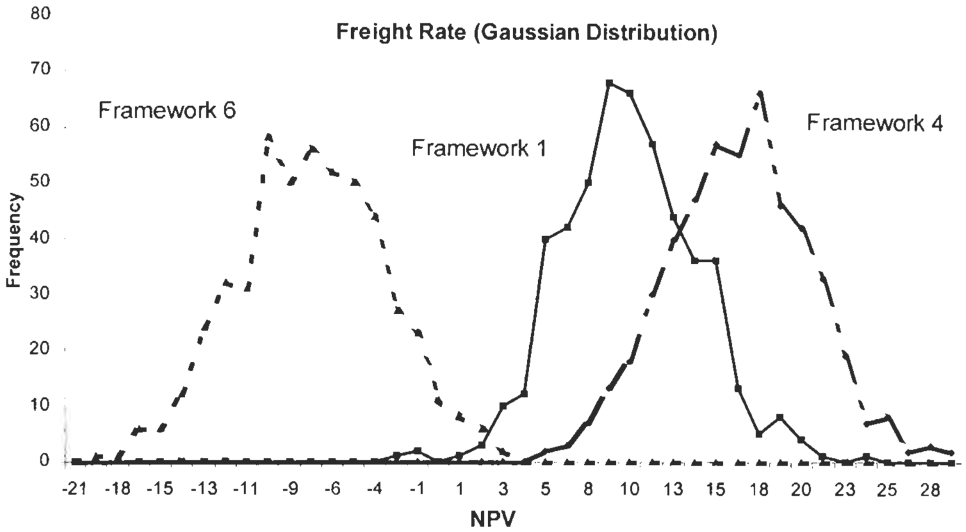

Fig 4. Distribution of NPVs for three Frameworks and variation in Freight Rate

While this shows a difference in mean NPV of $6.3M, this is only 50% higher than one standard deviation. The overlap in Fig 4 indicates that there is a probability that Framework 1 might actually be better than Framework 4, calculated by the program as 13.3%. There is a zero probability that 6 is better than 4, and less than 1% that 6 is better than 1, so the over-designed ship is clearly not an option.

So although the owner is paying a 'premium' of $10M by designing for jumboisation, it is more than repaid by its greater earning ability. Other variants which might be explored would be changes in growth rate trends, different extents of jumboising, and applying alternative statistical distributions for freight rate such as triangular or beta.

6 CONCLUSIONS

Simulation methods and DCF techniques are not new, but bringing them together into a formal procedure for evaluating alternative upgrading scenarios is new. With commercial pressures to minimise capital expenditure, even at the expense of operational difficulties later in a project's life, it is important to have agreed methods of assessing under what circumstances a degree of additional expenditure to facilitate later upgrading is justified. A simulation approach provides greater insight into the possible influence of changes in market trends or prices, as well as possible impact of new regulatory requirements on a project's life cycle cost. With the results presented as probabilities, the extent of risk can be gauged, so that the most cost-effective solution can be assessed. The methodology has been successful applied to a wide range of MTO products including offshore production platforms, process plant, power stations and steel mills. The familiarity of the spreadsheet and the availability of linked probabilistic software makes the introduction of such a method into an organisation straightforward.

Acknowledgements

Patrick Barber developed the original software and Jon MacGregor produced the container ship example.

Practical Design of Ships and Other Floating Structures
You-Sheng Wu, Wei-Cheng Cui and Guo-Jun Zhou (Eds)
© 2001 Elsevier Science Ltd. All rights reserved

MODEL-BASED SIMULATION FOR CONTAINER LOADING/UNLOADING

Soon-Sup Lee[1], Jong-Kap Lee[1], Hong-Tae Kim[1]

[1] Korea Research Institute of Ships and Ocean Engineering,
P. O. Box 23 Yusung, Taejon, 305-600, Korea

ABSTRACT

Recently, the greater part of a capacity of materials mobilization uses containers. The construction of new port and high-speed medium size container ship for the transportation of merchandise is very important.

The problem of ship stability is important because of the direct influence to the loss of the human-life, ship, and merchandise, etc. The stability of container ship during the sailing is not the problem because it is reflected in the design process. However, the assessment for ship stability during container loading/unloading in port depends on experience as yet.

In this paper, the model-based simulation system is introduced, which is able to assess ship stability during container loading/unloading, using ENVISION, the general-purpose simulation system.

KEYWORDS

Model-based simulation, CAD, CAE, Loading/unloading, High-speed medium size container ship, Stability assessment

1 INTRODUCTION

The emerging information and communication technologies of shipbuilding industrial environments are rapidly changing. To respond to the situation, a new paradigm has been matured with new concepts such as the concrete method. Especially, all the efforts are shown to be concentrated to realize the concept of Simulation Based Design(SBD) based on three dimensional Computer Aided Design(CAD) model.

In this paper, new methodology for design and operation of ship is suggested, and for the verification of suggested methodology, the system for stability assessment of ship during container loading/unloading was developed. The developed system consists of geometric modeling subsystem, basic calculation subsystem, and Computer Aided Engineering(CAE) subsystem. The function of the geometric modeling module is to perform the modeling of the hull form and compartment of the high-speed medium size container ship, and the shape of the container crane, the transfer crane, and the port. The function of basic calculation module is to provide the results of calculation of hydrostatics properties based on the extreme form associated to the displacement instill water. The function of CAE module is to provide the analysis for kinematics and dynamics motions. Interface to CAE/CAD/Simulation system such as SIKOB and ENVISION system is provided.

2 SBD TECHNOLOGIES

SBD is a new paradigm in which the total definition of a product is conceived, designed, manufactured, tested, trained, and supported for its useful life-cycle in a virtual environment.

In ship design, the SBD can have a powerful impact on the overall life-cycle of product development activities. By implementing the SBD system based strategies and techniques, the behavior ofproducts and process characteristics can be simulated in a Concurrent Engineering(CE) or Integrated Product and Process Design(IPPD) environment.

In the development of new concept ship, the SBD system will permit detailed evaluation of product and process design early in the life-cycle, reducing expensive surprises later during manufacturing and operational service. Also, it provides realistic operator interaction with the productduring the requirement and design process.

The SBD in ship design started in U.S. Department of Defense. Several prototype projects in navy ships have been performed to apply the SBD concepts through the Defense Advances Research Project Agency(DARPA) and its consecutive works, which was planned to maintain concurrent engineering design concepts in order to reduce the period of design and manufacturing,to economize, and to upgrade the quality of ships[1]. The well-known cases are U.S. Navy's LPD 17 simulation, General Dynamics Electric Boat Division(GDEB)'s NSSN submarine[2], and Gulf Coast Region Marine Technology Center(GCRMTC)'s Mobile Offshore Base(MOB) projects[3]. University of Strathclyde's safety simulations of RO-RO ferry ship and University of Michigan's ship motion simulations are typical examples in academic fields.

In Korea, SBD research has gained some interests in the commercial ship building industries and naval ships. Yet, the progress is far behind than the expectation.

SBD face several technological problems. Firstly, High Performance Computing(HPC) and HighPerformance Visualization(HPV), as well as high speed networking, are already under development program and it is expected that emphasis on advancing these technologies will continue.

Secondly, the integration of CAD/CAE/CAM is a critical element of the SBD system's capabilities as related to ship design in which the system must cope with the full spectrum of ship design engineering.

Thirdly, software standards and data exchange standards are needed for SBD to fully assimilate and utilize large number of existing codes[4][7].

3 SIMULATION OF SHIP STABILITY ON CONTAINER LOADING/UNLOADING

In this research, a system for assessment of ship stability for container loading/unloading was developed using SBD technologies. For the development of assessment system, the geometric models of the high-speed medium size container ship, port, and facility are implemented and interfaced to the CAE programs[5][6].

The Configuration of the system for container loading/unloading is shown in Figure 1.

3.1 Graphical User Interface

Graphical User Interface(GUI) is adopted to the commercial geometric modeling and simulation systems in order to increase the flexibility and efficiency of system.

GUI is designed considering the following items.

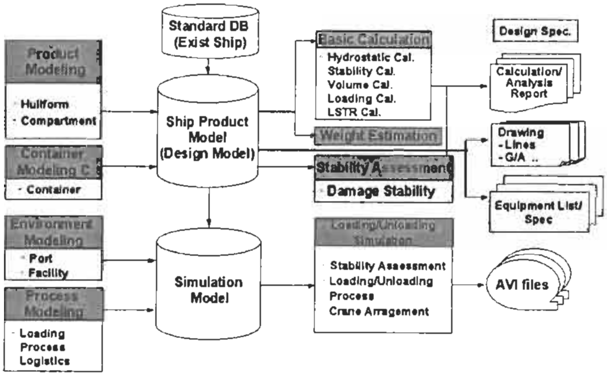
Standard DB
(Exist Ship)
Product Modeling
- Hullform
- Compartment
Container Modeling C
- Container
Environment Modeling
- Port
- Facility
Process Modeling
- Loading
Process
Logistics
Ship Product
Model
(Design Model)
Simulation
Model
Basic Calculation
- Hydrostatic Cal.
Stability Cal.
Volume Cal.
Loading Cal.
LSTR Cal.
Weight Estimation
Stability Assessment
- Damage Stability
Loading/Unloading Simulation
- Stability Assessment
Loading/Unloading
Process
Crane Arragement
Design Spec.
Calculation/
Analysis
Report
Drawing
- Lines
- G/A ..
Equipment List/
Spec
AVI files

Figure 1. System Configuration of Container Loading/Unloading

- Visualization of input data
    - Integration of each modules
- Visualization of final output and intermediate output

GUI of model-based container loading/unloading simulation system is developed using Graphical Simulation Language(GSL) and Command Line Interpreter(CLI) functions of ENVISION system, which is a commercial simulation system. All of the necessary commands and functions in developed system defined as the menu. Top level command is top level menu. Sub-menus are constructed as pull-down menus.

The hierarchy of menu of the developed system is shown in Figure 2. The input pad for principal particular, material, and stability criteria of ship is shown in Figure 3. In this paper, the criteria of stability assessment for ship are GM value and check collision between ship and port.

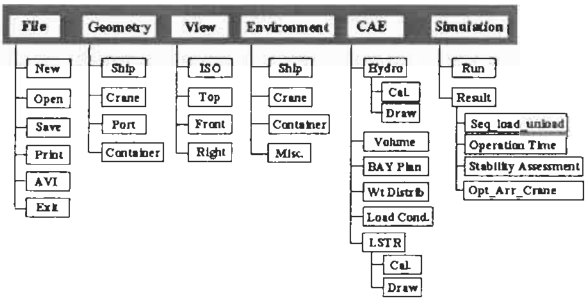
File
New
Open
Save
Print
AVI
Exit
Geometry
Ship
Crane
Port
Container
View
ISO
Top
Front
Right
Environment
Ship
Crane
Container
Misc.
CAE
Hydro
Cal.
Draw
Volume
BAY Plan
Wt Distrib
Load Cond.
LSTR
Cal.
Draw
Simulation
Run
Result
Seq_load_unload
Operation Time
Stability Assessment
Opt_Arr_Crane

Figure 2. GUI for Container Loading/Unloading Simulation System

3.2 Geometric Modeling

The 3D Design Model such as hull form and compartment Model, was developed using the commercial geometric modeling system, CATIA.

The hull form is the most fundamental model in a 3-dimensional product-model, which consists of shell plate model, hull compartment model, hull structural model, and is used all the way from initial to product designs.

A method to define a hull form is dictated by the requirement of accuracy in each design stage; in the initial design stage, the hull form is defined by a wire-frame model that is accurate enough for hydrostatic performance calculation. But, in the product design stage, the hull form is defined by a

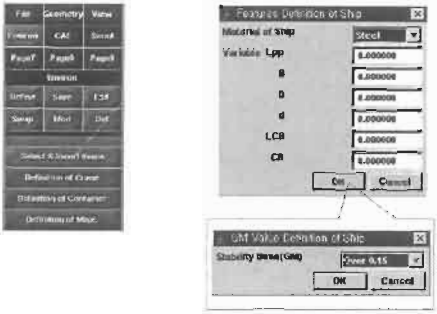

Material of Ship Steel
Variable Lpp 0.000000
B 0.000000
D 0.000000
d 0.000000
LCB 0.000000
CB 0.000000

Stability Base(GM) Over 0.15

Figure 3. Example of Definition of Principal Particular and Criteria for Stability Assessment

surface model as some geometry production information such as piece, material information, etc., is necessary at production job.

Recently, however, there has been research on constructing a product model itself in the initial design stage for integrated design process.

In this Paper, the hull form of the high-speed medium size container ship is defined by a surfacemodel.

The general arrangement of a ship is the process of assigning spaces for all the required functions and equipment, properly coordinated for location and access. The first step of general arrangement is locating the main spaces and their boundaries. The major surfaces are surfaces ofwater-tight transverse bulkhead and water-tight longitudinal members that become the boundarywalls of compartments. The boundary walls of compartments are composed of plane and free form surface such as hull form.

The cargo modeling is to define containers. The number of loaded container is 300 teu and all containers are located on deck.

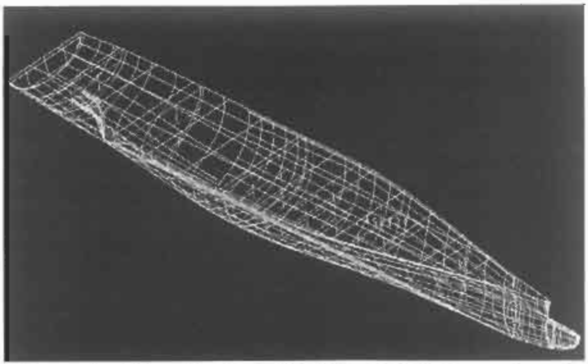

Figure 4. Visualization of Hull Form and Compartment

3.3 CAE Interface

The CAE programs used in developed system are hydrostatic calculation of ship, behavior assessment of facility, and stability assessment of ship during container loading/unloading. The stability assessment program of ship during container loading/unloading is developed using basic calculation program. The behavior assessment program of facilities is developed using calculation module of ENVISION system.

Interface between ENVISION system and CAE programs is implemented using visual C/C++ and interface function such as GSL and CLI function, in windows environment. Figure 5 shows the process of interface between ENVISION system and CAE programs.

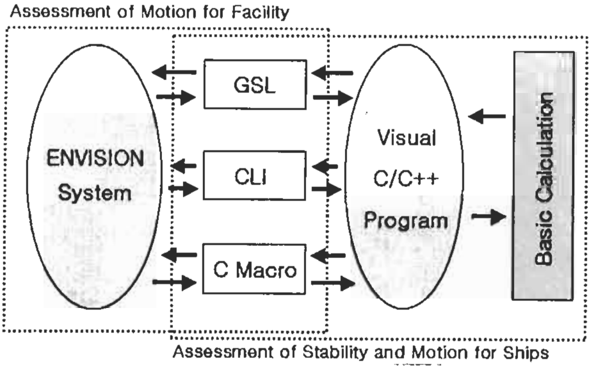
Assessment of Motion for Facility
ENVISION System
GSL
CLI
C Macro
Visual C/C++ Program
Basic Calculation
Assessment of Stability and Motion for Ships

Figure 5. The Process of Interface between ENVISION System and CAE Programs

Figure 6 shows the source of a collision examination program between ship and port using intersection method.

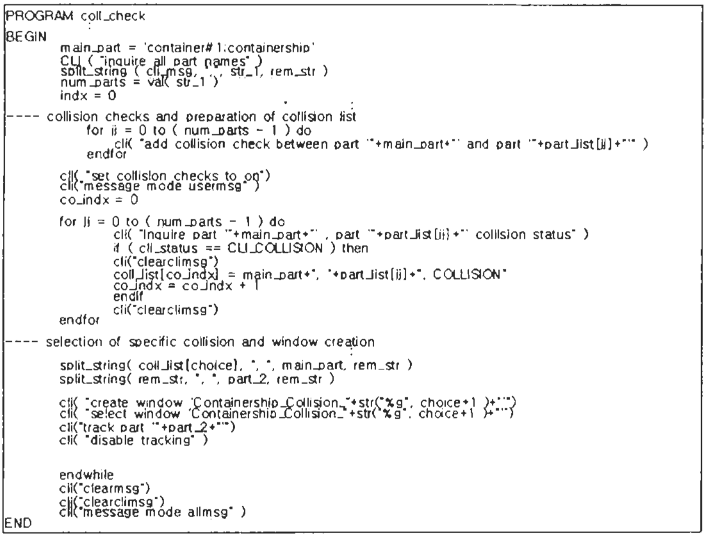

```
PROGRAM coll_check
BEGIN
        main_part = 'container# 1:containership'
        CLI ( "inquire all part names" )
        split_string ( cli_msg, ",", str_1, rem_str )
        num_parts = val( str_1 )
        indx = 0
---- collision checks and preparation of collision list
              for ij = 0 to ( num_parts - 1 ) do
                    cli( "add collision check between part '"+main_part+"' and part '"+part_list[ij]+"'" )
              endfor

        cli( "set collision checks to on")
        cli("message mode usermsg" )
        co_indx = 0

        for ji = 0 to ( num_parts - 1 ) do
                    cli( "Inquire part '"+main_part+"' , part '"+part_list[ij]+"' collision status" )
                    if ( cli_status == CLI_COLLISION ) then
                    cli("clearclimsg")
                    coll_list[co_indx] = main_part+", "+part_list[ij]+", COLLISION"
                    co_indx = co_indx + 1
                    endif
                    cli("clearclimsg")
        endfor
---- selection of specific collision and window creation

        split_string( coll_list[choice], ", ", main_part, rem_str )
        split_string( rem_str, ", ", part_2, rem_str )

        cli( "create window 'Containership_Collision_"+str("%g", choice+1 )+"'")
        cli( "select window 'Containership_Collision_"+str("%g", choice+1 )+"'")
        cli("track part '"+part_2+"'")
        cli( "disable tracking" )


        endwhile
        cli("clearmsg")
        cli("clearclimsg")
        cli("message mode allmsg" )
END
```

Figure 6. Source of a Collision Examination Program

3.4 Simulation of Container Loading/Unloading

The Container loading/unloading simulation is included in stability assessment of ship, assessment of process, and assessment for optimal position of cranes during container loading/unloading.

Figure 7 shows the procedures of simulation for container loading/unloading

The following items were considered in the development of container loading/unloading .

- The container loading/unloading simulation use hull form, compartment, port, and facilities model and CAE programs.
- The constraints such as sequence of loading/unloading and a moving distance of cranes, are permitted within limits of values defined in [environment] menu.
- When crane picked container up off the deck, stability assessment program is executed.
- When stability of ship disappeared during simulation, system is terminated with beep sound.

- View ports during simulation can be change using pocket menu.

The results of container loading/unloading simulation is as follows:

- The sequence Diagram of container loading/unloading
- The operation time of container loading/unloading
- The result of stability assessment for ship during container loading/unloading.
- The collision examination between ship and port during container loading/unloading simulation
- The optimal arrangement of cranes

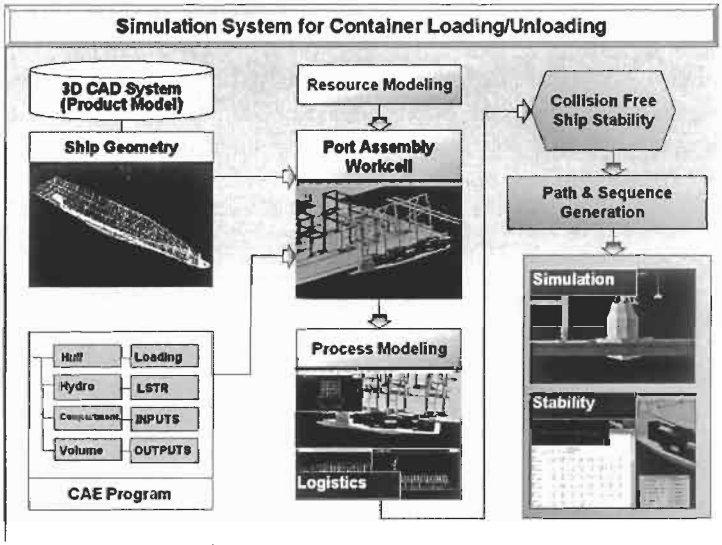
Simulation System for Container Loading/Unloading
3D CAD System (Product Model)
Ship Geometry
Resource Modeling
Port Assembly Workcell
Collision Free Ship Stability
Path & Sequence Generation
Simulation
Stability
Process Modeling
Logistics
Hull
Loading
Hydro
LSTR
Compartment
INPUTS
Volume
OUTPUTS
CAE Program

Figure 7. Procedures of Simulation for Container Loading/Unloading

The procedures of simulation for decision of the number and optimal position of crane using the operation time are shown in Figure 8. In this paper, the number of crane considered is within three cranes.

The optimization of container loading/unloading process is shown in Figure 9. To decide optimal process of container loading/unloading, the developed system only considers the operation time and not loading/unloading costs.

Figure 10 shows the visualization of container arrangement on deck and the visualization of cross sections for a frame. Figure 11 shows procedures of stability assessment for ship during container loading/unloading. The results of stability assessment use GM value. If GM value deviates from limits of stability criteria, system is terminated. Figure 12 shows the visualization for the results of stability assessment. Figure 13 shows collision examination between port and ship using intersection method.

4 CONCLUSIONS

In this paper, we investigated state-of-the-arts for SBD technologies and related researches, and developed container loading/unloading simulation system for high-speed medium size container ship using SBD technologies.

The shape of hull form, compartment, cargo, and facilities are defined using the 3D commercial geometric modeling system. The application programs for stability assessment of ship are in-house programs. The Graphical User Interface for the visualization and control of input/output data is adopted for the efficient use of developed system.

Finally, we developed simulation system for the visualization of stability and behavior of ship, the visualization of loading/unloading procedures, and the assessment of crane's optimal position using in-house CAE programs, graphical user interface, geometric model, and simulation function.

To support the effects of the external environment such as wind, wave, etc., the developed system has to be extended.

SBD technologies can be applied usefully to engineering parts such as virtual shipyard, marine accident simulation, marine safety, marine ergonomics, and so on.

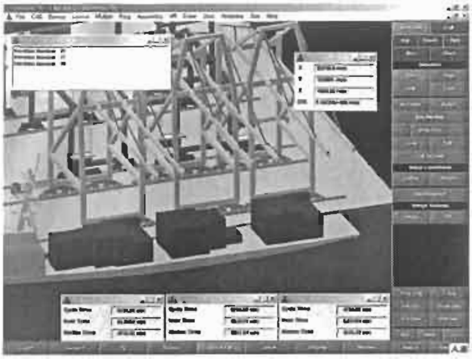

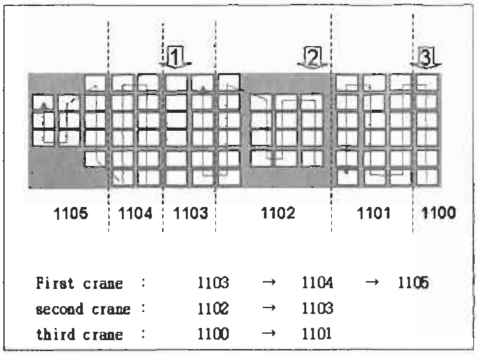

First crane : 1103 → 1104 → 1105
second crane : 1102 → 1103
third crane : 1100 → 1101

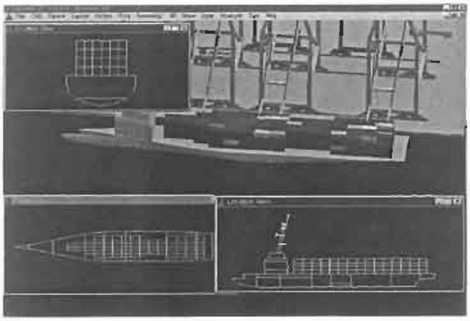

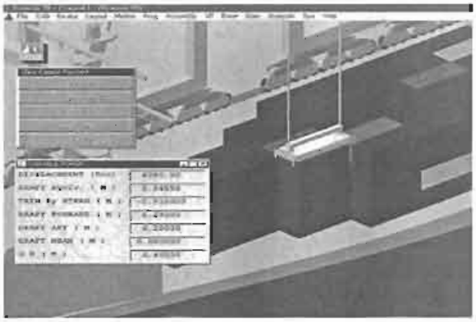

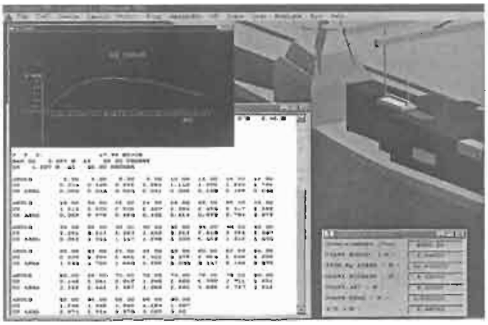

Figure 12. Visualization of Result for Ship Stability

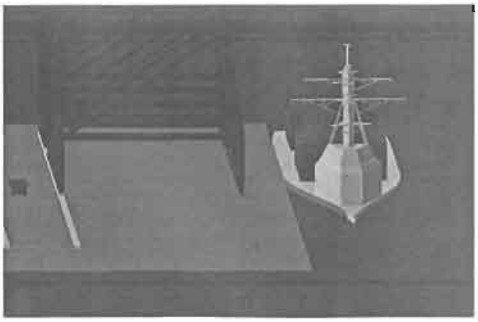

Figure 13. Collision Examination

References

[1] Jones G. and Hankinson T. (1994). Simulation Based Design for Ship Design and Acquisition. *Proceedings of ICCAS.* Bremen, Germany

[2] Ken Fast, Electronic Visualization System(EVS) at Electric Boat. *Proceedings of Deneb's User Group.* **996**

[3] John Cardner. (1998). Simulation of Mobile Offshore Base. Project Report. GCRMTC

[4] Lee J.K, et al. (2000). Development of Model-based CAE and Simulation Technologies for Ships and Ocean Engineering (III). Korea Research Institute of Ships and Ocean Engineering(in Korea)

[5] Lee S.S, et al. (1999). Simulation for Ship Stability According to Container Loading/Unloading. *Proceedings SNAK* (in Korea)

[6] Kim H.T. (2000). Evaluation of Safety for Container Loading/Unloading Using Modeling & Simulation Technologies. *Journal of Ships and Ocean Engineering* (in Korea). **29**, 161-166

[7] Kim E.C., et al. (2000). Development of Container Loading/Unloading and Transportation System for Next Generation (III)-Development of High-Speed Medium Size Container Ship. Korea Research Institute of Ships and Ocean Engineering (in Korea)

Practical Design of Ships and Other Floating Structures
You-Sheng Wu, Wei-Cheng Cui and Guo-Jun Zhou (Eds)
© 2001 Elsevier Science Ltd. All rights reserved

RESEARCH ON 3D-LAYOUT DESIGN OF SHIP COMPARTMENT BASED ON CBR

Jun-Hua Li, Ying-Fu Zhu, Wen-Ye Ying and Jun Lu

Huazhong University of Science & Technology, Wuhan, Hubei, China
Wuhan Ship Design and Development institute, Wuhan, Hubei, China

ABSTRACT

CBR(Case--Based Reasoning) is a new method for reasoning in AI. The core of CBR is the case presentation and the case-indexing model. This paper has developed the case-based reasoning for solving the 3D--layout design problem of ship compartments. The case presentation with object-oriented (O—O) in a compartment is presented. The O—O method is set up, by using classifing-decomposed relation and mixed knowledge expression of frames, rules and methods. The name, design-task are used in case indexing construction, a design-task-oriented indexing model based on artificial neural method and process for compartment layout based on CBR are put forward.

KEYWORDS

CBR, Naval ship compartment, Intelligent, 3D-layout

1 INTRODUCTION

In design process, experts always study old successful cases, and apply the experience to the new design problem. In ship design field, this method is usually called "Mother-Ship Modification Method". Case-Based Reasoning (CBR) is a kind of analogism . It expresses involved knowledge as cases. Each case composes of a design problem and its solution. Via memorizing the solution of the similar problem and properly adjusting the solution to suit the current problem, the solution of the current problem can be worked out.[1] Generally speaking, case-based design comprise three process: 1) presentation of case knowledge; 2) Indexing of relational cases; 3) Validation of the cased found.
This paper introduces the application of CBR technology in intelligent 3D layout design of ship compartment, it also introduces the stratagem of case indexing based on artificial neural method.

2 PRESENTATION OF CASE IN SHIP COMPARTMENT LAYOUT DESIGN

2.1 Object-oriented Knowledge Presentation Method of Compartment Layout Design

Knowledge presentation is a series of regulation describing objects and phenomena. It is a way of formalizing and symbolizing knowledge. The progress of artificial intelligence technology provides various means and methods to present and dispose knowledge. With the development of the object-oriented technology, it is possible to integrate several single knowledge presentation methods (such as frame, rule) into a compounded knowledge presentation form. The case of compartment layout design introduced in this paper adopts the object-oriented knowledge presentation method, and use frame case to describe object case. [2] Each object-oriented frame composes of relation slot, property slot, method slot and rule slot.

Relation slot present the static relationship of object with other objects, the essence of it is describing object in object. Via the presentation of relation slot, it's possible to realize the objective of integrated knowledge utilizing by decomposing the ship compartment layout design knowledge and presenting multi-knowledge in object.

Property slot describe the static relationship of object. A property slot can describe every feather of itself via many sides. Valueclass side presents the type of the slot value, inheritance side presents the inheritance feather of the slot value, and values side record the property value.

Method slot is used to record the method in object. It's a special dynamic process in frame. The structure of method includes name, message schema table, local variable definition and method structure body. Message transferring activates Method, and after the method is activated, the needed information is selected from the message sent and used by the method process body. Then the method process body is executed.

Rule slot is used to store generating rule set. Generating rule is grouped into many rule set according to diverse of their tasks and objective served. Each rule set stores in rule slot as a value, and a frame can have several rule slots to record different rule subset. Subset can be inherited. The use of rules depends on rule reasoning machine.

The BNF pattern of Frame knowledge presentation method in object-oriented compound knowledge presentation form is showed below:

```
<frame>::=unit:<frame name>in<knowledge library name>;
              {memberof: <class frame name>  {, <class frame name> };   }
<slot> {<slot>}
END unit ;
<slot>::=  memberslot | ownslot : <slot name>  from<frame name>;
           valueclass: <slot value class type>;
           ililieritance: <inheritance property>;
           {<user-defined side>;< side value>;}
          Values: <slot value>;
END slot;
<slot valueclass type>:: = integer | real | string | rules | METHODS | < class frame name>
<inheritance property>:: = override | union | METHODS
<frame name>:: =<character> {<character> |<number>}
<slot name>:: =<character> {<character> |<number>}
```

2.2 *Presentation of Case in Compartment Layout Design Based on Decomposition*

Case is a vital part of ship compartment intelligent layout design knowledge. At the same time, it is also the most important knowledge component of the Case-Based design model. Commonly, a case of ship compartment layout design composes of three parts: (1) data of compartment layout design case; (2) knowledge about solving the compartment layout design problem; (3) index of compartment layout design case. In this paper, the cases are presented by the method of object-oriented hierarchical structure decomposition.[2] By using this method, a complex 3D-layout design case can be decomposed to several easier cases, and every case can be decomposed hierarchy upon hierarchy. In each hierarchy, the case can be used independently. In the before mentioned, the result of compartment layout design is expressed by complex object structure. Because these objects have the format that is needed in case presentation and their properties can present result data of the compartment layout design, the object structure that present result of compartment layout design can present the case of compartment layout design directly. The object structure that is the result of the compartment layout design is always the instantiation of certain kind of layout design object class or the origin object. According to the inheritance principle in the object-oriented method, these cases can inherit the dynamic knowledge in the object class which they belong to. So using the object-oriented method to present knowledge of ship compartment layout design principle can present the data of compartment layout design case and solving knowledge of design conveniently. Fig.1 is the decomposition presentation of ship compartment layout design case.

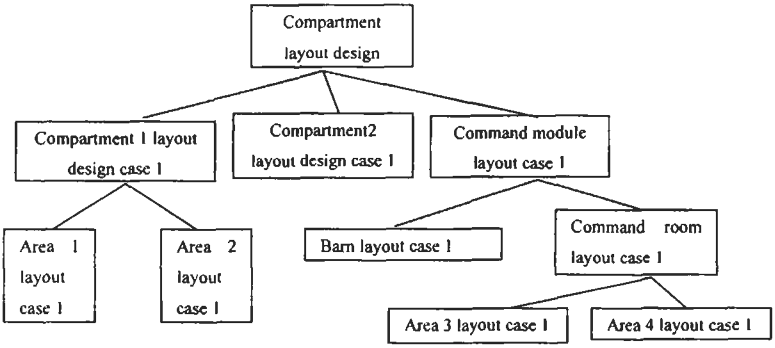
Compartment layout design
Compartment 1 layout design case 1
Compartment2 layout design case 1
Command module layout case 1
Area 1 layout case 1
Area 2 layout case 1
Barn layout case 1
Command room layout case 1
Area 3 layout case 1
Area 4 layout case 1

Figure 1: *the decomposition presentation of ship compartment layout design case.*

In the light of integration of hierarchical structure decomposition of the ship compartment layout design case and the object-oriented presentation method of ship compartment layout design knowledge, the compartment layout design case can be utilized not only as a whole, but also merely some parts of it. Therefore, as long as the design requirement of compartment design is identical with the object class, the new layout design objective will be composed from the subcase of different layout design objects according to compartment layout design knowledge.

Index of cases is another important part of case presentation of compartment design case. Index is the appearance property in compartment design case; index of cases is gist of selecting compartment layout design case based on case machine. The most convenient means to index a layout case is using a sequence of compartment layout design case feathers as the index of layout case. To each object class of layout design, an indexing type will be created in terms of its feather. In the process of layout design, when design object class is instantiated to a case of layout design object, the index object class also instantiated to the index of this object case, index object case include the record of index feather and the names of compartment layout cases needed indexed.

3 THE CASE INDEXING MODEL OF COMPARTMENT LAYOUT BASED ON NEURAL NETWORK

Before discussing the arithmetic, two notion are defined. One is degree of similitude which is the measurement of to what degree two compartment layout design case are similar. The second is dimension which describes compartment layout design space,it relates to the feather notion of compartment layout design case. If the layout case has N pieces of property, the presentation space of this case is called N-dimension space.

The selection of compartment layout design case can be described as following. Firstly use the case chain in the indexing object class to find relative indexing object class. Next, according to the objective of compartment layout design, finding out corresponding indexing object class. Then solving the case record in this object class structure, in another word, to find all relative index. Because these index object record all corresponding compartment layout design case, the relative case can be found. In these relative cases, the most similar case can be found via evaluating the degree of similitude between the new layout design task and the relative cases.

A compartment layout design task includes three parts. These are the objectives of layout design, initial qualification given and restriction must be gratified. In the compartment layout design process, the interaction of each sub-objective in the layout design task must be taken into account. In compartment layout design process, many objectives and many restrictions must be meet at simultaneity, and each objective and restriction belong to different property space.

Presently, there are three methods of case indexing based on CBR technology. They are Euclid distance, Manhattan distance and infinite distance. All the three methods of case indexing concern the weightiness of each property in the design case. In the process of solving problem of ship compartment layout design, determining weightiness of compartment layout design property is even more difficult. Based on foregoing analysis, this paper put forward the arithmetic to determine degree of similitude of ship compartment layout design case based on neural network. It is an indexing model, which look on a design task of compartment layout design as layout case index.

In the research of artificial neural network, BP(Back Propagation) arithmetic is widely studied and utilized. For determining degree of similitude of compartment layout design case, a BP network which have three layers and one output unit is constructed (see in Fig. 2).

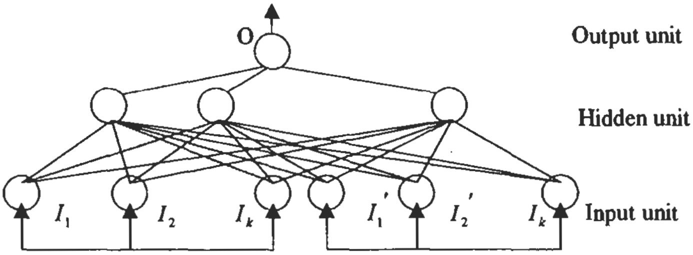

Figure 2: A three-layer BP network

In Fig.2, the input unit I composed of I_1 and I_2, I= { I_1 , I_2 }, and I_1={ I_i, i= 1, 2, …, k}, I_2= { I_i, i= 1, 2, …, k}, W_1 is the weightiness matrix between output layer and hidden layer, and W_2 is the weightiness matrix between input layer and hidden layer. BP is a recursive gradient arithmetic to minimize the unbiased variance between the actual output and the predicted output in the multi-layer BP network. The activation function of processing units is S type function, so the output of units express in Eqn. (1):

$$O_i = \frac{1}{1+e^{-S_i}} \tag{1}$$

In Eqn. (1), S_i present the weightiness sum of all input in certain unit, O_i present the output of that unit.

The aim to construct neural network is to acquired knowledge that ship design expert used in determining degree of similitude of ship compartment layout design case. In actual it is using neural network to present weightiness between sub-objective and properties in the design task of compartment layout design case, which is the rate of contribution to degree of similitude of ship compartment layout design case. So the network showed in Fig.2 has characteristics as following:

1. Input layer composes of two sets of unit I_1 and I_2. The two sets of unit have the same unit number and same unit sequence. They express different corresponding properties of the compartment layout design task.

2. Output layer have only one unit. The value of the unit is the degree of similitude of two compartment layout design cases inputted. The assign of weight is done by neural network. Supposing we have n pieces of compartment layout design cases and each case have m pieces of property which can be decomposed in the universal set of layout design task, the neural network would have 2m pieces of input unit. The design task properties of every two compartments layout design cases and the degree of similitude of these two compartment layout design cases construct a sample. The first one is the input, and the second is output. If we call the collection of design task property value a as C, $C_i=[a_{i1}, a_{i2}, \cdots, a_{im}]$, i=1, 2, ⋯ , n. If the input of the sample is I, $I_{ij} = [a_{i1}, a_{i2}, \cdots, a_{im}, a_{j1}, a_{j2}, \cdots, a_{jm}]$, i, j= 1, 2, ⋯, n. If O is the output of sample, Eqn. (2) is the corresponding matrix of sample input and output. In these matrixes, elements in corresponding position constitute a pair of samples.

$$\begin{bmatrix} I_{11} & I_{12} & \cdots & I_{1n} \\ I_{21} & I_{22} & \cdots & I_{2n} \\ \cdots & \cdots & \cdots & \cdots \\ I_{n1} & I_{n2} & \cdots & I_{nn} \end{bmatrix} \Longleftrightarrow \begin{bmatrix} O_{11} & O_{12} & \cdots & O_{1n} \\ O_{21} & O_{22} & \cdots & O_{2n} \\ \cdots & \cdots & \cdots & \cdots \\ O_{n1} & O_{n2} & \cdots & O_{nn} \end{bmatrix} \tag{2}$$

With regard to sample input of ship compartment layout design, this paper adopt following regulations:

$$I = \{I_1, I_2, I_3, I_4\}$$

In this equation, I_1 is the type of the naval ship compartment, I_2 is the size of the ship compartment, I_3 is the type and number of the equipments in compartment space, I_4 is the number, size and position of the passage in compartment space. The output matrix is a symmetric matrix, and its elements in leading diagonal are constant 1, which means every compartment layout design case is self -similitude. So the matrix can be present as a triangular matrix:

$$\begin{bmatrix} 1 & O_{12} & O_{13} & \cdots & O_{1n} \\ & 1 & O_{23} & \cdots & O_{2n} \\ & & 1 & \cdots & .. \\ & & & 1 & O_{(n-1)n} \\ & & & & 1 \end{bmatrix}$$

From this triangular matrix, we can find that n (n+1)/2 pieces of compartment layout design samples are needed to express the degree of similitude determinant. And the corresponding elements in upper triangular and lower triangular are of the same value. That is two compartment layout design cases input get the same output, and the only difference is the reversal of the case sequence. But with the samples of different sequence inputting into neural network together, the training effect will be better. Thus we still use n^2 pieces of samples in training.

In this way, the study is the process of giving n^2 pieces of compartment layout design samples, via n^2 times of study, the neural network then will contain the hidden rules for design expert to determine the degree of similitude of ship compartment layout design cases. To find the proper case corresponding with the current layout design task, the layout design objectives, initial conditions, restrictions and corresponding samples of n pieces of compartment layout design samples must be input, then the degree of similitude of them will be found. So, an array of cases arranged by their degree of similitude will be found, and we can select case based on it.

4 REASONING POLICY BASED ON LAYOUT DESIGN CASE

Naval ship compartment layout design reasoning policy based on CBR are showed as following.
(l) Firstly, to study and select the properties of compartment layout design problem, determining the compartment layout design objectives, initial conditions, and restrictions.
(2) By using the case-indexing model of compartment layout design based on neural network, to select a group of cases whose objective is like the current layout design and sort them by their degree of similitude. Search the most similar case to current problem in the compartment layout design case library and store it in the current workspace.
(3) Take the selected compartment layout design case as prototype of the solution, adjust and modify it, complete the conversion of case, until it satisfys the compartment layout design requirement. The conversion of case is realized by using compartment layout design knowledge inherited from layout design cases. The knowledge is derived from design class or design prototype.
(4) If the prototype cannot meet the requirements even after modifications and adjustments, it must be redesign. And the result of redesigning should store in cases in the new case form.

5 CONCLUSIONS

Using case presentation method and case-indexing policy based on neural network introduced , we can realize the intelligent ship compartment 3d-layout design based on CBR.
The neural network model introduced in this paper have two major advantages when compared with other case-indexing methods: 1) Neural network has ability of finding the hidden information in samples. Via training, neural network construct a model. The experience of design expert using to determine whether two ship compartment layout design cases are similar is hard to express by regular form, while using neural network can refine the experience of experts into the network. It's just the problem general methods are hard to solve. 2) Neural network has the ability of self-adaptation. Through the constant study, neural network can constantly modify the model to match the changing exterior conditions. The study of new compartment layout design case samples make neural network modify the weight matrix continuously. In this way, the experience of determining whether two ship compartment layout design cases are similar used by design expert can be expressed more accurately.

References

[1]MAO Quan.(1995). Research on Case Prototype Based Design Methodology and Design Support System, A Dissertation Submitted to Huazhong University of Science and Technology for the Degree of Doctor of Philosophy in Engineering
[2]Li Jun-Hua.(2000).Principles and Application on Intelligent 3D-Layout Design for Ship Compartments Based Compound Knowledge Model, A Dissertation Submitted to Wuhan Transportation University for the Degree of Doctor of Philosophy in Engineering

Practical Design of Ships and Other Floating Structures
You-Sheng Wu, Wei-Cheng Cui and Guo-Jun Zhou (Eds)
© 2001 Elsevier Science Ltd. All rights reserved

DEVELOPMENT OF A SOPHISTICATED HULL FORM CAD SYSTEM 'EZHULL' BASED ON A NON-MANIFOLD MODEL AND 'X-TOPOLOGY'

Kyu-Yeul Lee[1], Joong-Hyun Rhim[1], Sang-Uk Lee[1], Doo-Yeoun Cho[1] and Young-Bok Choi[2]

[1]Department of Naval Architecture & Ocean Engineering and Research Institute of Marine System Engineering, Seoul National University, San 56-1, Shinlim-Dong, Kwanak-Gu, Seoul 151-742, Korea
[2]EzGRAPH, Co. Ltd., Rm 1201, Union Center, Yoksam-Dong, Kangnam-Ku, Seoul, Korea

ABSTRACT

Hull design evolves from a wireframe model to a surface model through conceptual design, preliminary design, and production design. Hull form designers initiate designs using wireframe models with which they are familiar, and want to convert a wireframe model to surface model-whenever it is necessary. Therefore, hull form design system should support not only cross fairing and correct points ordering for a wireframe model but also be able to generate the surface from the wireframe model.

The EzHULL system developed in this research, provides an association based cross fairing and surface generation, using X-topology and non-manifold data structure. X-topology is the data structure for a wireframe model that supports the association based cross fairing. The association based cross fairing enables effective wireframe modification by automatically updating all hull lines related to a changed line. The non-manifold data structure stores both topological and geometric data of the surface model produced from the wireframe model. The geometric data of the surface model can be used to display the 3-D surface hull form to check the surface fairness at the early design stage of hull form. And, the topological information can be used to solve the points ordering problem that occurs in the wireframe based design system. An example of a twin skeg hull form showing the effectiveness of the developed system is included.

KEYWORDS

Hull form CAD system, cross fairing, surface model, non-manifold data structure

1 INTRODUCTION

The hull form design process is a multi-disciplinary operation involving cooperation between design departments. A CAD system in hull form design plays a fundamental role by sharing hull form data with other design processes [1]. Since the hull form normally evolves from a wireframe model to a surface model through conceptual design, preliminary design, and production design, it is necessary for a hull form CAD system to provide following features.

Wireframe Cross Fairing: The cross fairing is a basic and essential feature in a wireframe based hull design system. In the wireframe model, if one of crossing hull lines such as a station line or a waterline is modified for fairing, the other line should be altered to maintain the crossing points, this process is called 'cross fairing' in hull form design. In addition to the crossing lines, all other lines that are affected by them should also be rearranged automatically.

Direct Conversion from wireframe model to surface model: Hull form designers are used to dealing with lines plan represented by a wireframe model, and may estimate the performance of a ship based on a wireframe model. On the other hand, they also require that the hull form surfaces be displayed to check the surface fairness. Therefore, it is desirable to be able to perform immediate conversion from the wireframe model to the surface model to implement any necessary change into the wireframe model even at the early design stages of the hull form.

Correct points ordering during wireframe generation: When a new hull line is generated by intersecting a wireframe model with a certain plane, an intersection points ordering problem always occurs. Therefore, it is important to have the correct point ordering, especially with a complex multi-hull form such as twin skeg hull.

In this research, a hull form CAD system called 'EzHULL' was developed to perform the above tasks. Cross fairing features and conversion from wireframe model to surface model will be the main focus of this paper, and we will also discuss how these features help to significantly reduce time and cost of hull form design.

2 DATA STRUCTURE OF EzHULL

The data structure of EzHULL is composed of the wireframe and surface models that mutually represent the hull form. The wireframe data structure that efficiently supports the cross fairing is called 'X-topology'. The non-manifold data structure is used for storing the surface model produced from the wireframe model.

2.1 X-topology Data Structure

The X-topology is a basic data structure for hull form design using the wireframe model. Hull form designers usually perform cross fairing of the wireframe model by modifying the characteristic hull lines, such as the station line and the waterline. If a fitting point is moved on a waterline, they expect the waterline to be changed as a single unit curve and want the station lines crossing the waterline to move in concert. In the non-manifold data structure, however, a single waterline and station line are subdivided into several segments to represent edges that form face boundaries. Thus, in the EzHULL, a data structure that can manipulate hull lines as a suitable unit and support effective cross fairing of wireframe model has been developed and named 'X-topology', in addition to the non-manifold data structure for the surface model.

The X-topology has a hierarchical structure, which is similar to the non-manifold data structure, as shown in Fig 1. The 'X-edge', which represents hull lines of the wireframe model, is a base element of X-topology, and the collection of the X-edge forms the 'X-surface' that represents the imaginary surface. There are three types of X-edge, the B-line, S-line, and R-line. The B-line mainly represents the boundary curves, such as the deck line, the profile line, the midship section line, and the side- and bottom tangent line, whereas the S-line represents the interior form of the X-surface, and includes the station line and the waterline. Both the B-lines and S-lines are used for both fairing and forming the mesh of the X-surface. The R-line is only used for reference purpose and does not form the mesh of the X-surface.

2.2 Non-manifold Data Structure

In EzHULL, the hull surface data is represented as NURBS (Non-Uniform Rational B-Spline) surface patches. To improve the usability of the hull surface data, it is necessary to save the topological information that represents the relationships between surface patches as well as geometric information of them. To do this, EzHULL uses a non-manifold data structure that can store both the topological and geometric data of the hull surface without thickness [2]. Since the non-manifold data structure can deal with not only manifold data, such as, solid objects but also with non-manifold data, such as lines and surfaces, many commercial CAD systems have recently adopted non-manifold data structure. So, representing the hull surface data in the form of non-manifold data structure facilitates the transfer of surface data to the next process.

In EzHULL, geometric information, which is stored in the non-manifold data structure, is mainly used for verifying surface fairness by surface shading. The topological information is used for points ordering to generate a new hull line of the wireframe model. The non-manifold data structure is also used in the solid model-based compartment arrangement and the hydrostatics calculation system, which are currently being developed.

Fig. 1 shows an example of an afterbody wireframe model and the corresponding surface model. More detailed process which converts the 'X-topology' of the wireframe model into the non-manifold data structure of surface model, is described in Section 4.1

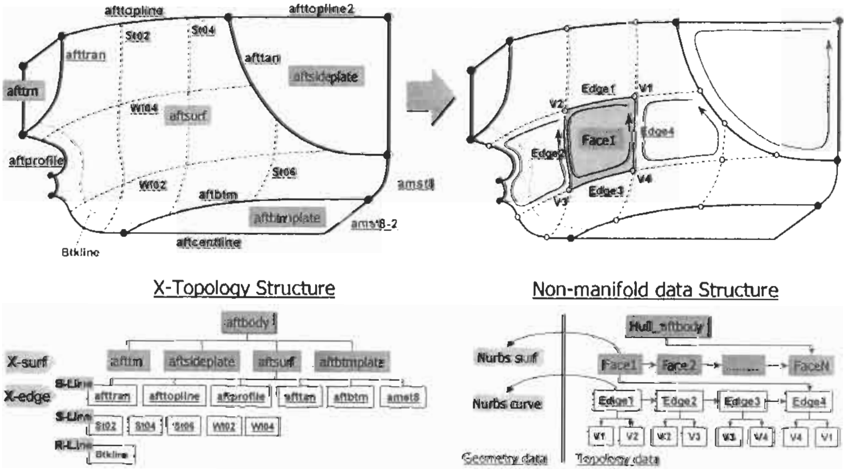
afttopline
afttopline2
St02
St04
afttran
afttan
aftsideplate
aftrn
Wl04
aftsurf
aftprofile
St06
Wl02
aftbtm
amst8
aftbtmplate
amst8-2
aftcentline
Btkline
Edge1
V1
V2
Face1
Edge4
Edge2
Edge3
V4
V3
X-Topology Structure
Non-manifold data Structure
aftbody
X-surf
aftrn
aftsideplate
aftsurf
aftbtmplate
B-Line
X-edge
afttran
afttopline
aftprofile
afttan
aftbtm
amst8
S-Line
St02
St04
St06
Wl02
Wl04
R-Line
Btkline
Hull_aftbody
Nurbs surf
Face1
Face2
....
FaceN
Nurbs curve
Edge1
Edge2
Edge3
Edge4
V1
V2
V2
V3
V3
V4
V4
V1
Geometry data
Topology data

Figure 1: Example of an afterbody wireframe model using the X-topology and corresponding surface model represented by non-manifold data structure

3 ASSOCIATION BASED CROSS FARING

3.1 Priority Order of the Association

In EzHULL, association based cross fairing is developed using the X-topology data structure to improve the efficiency of hull form design [3]. This association means the relationship between X-edges crossing each other, and X-edges of X-topology data structure are classified into three types: B-line, S-line, and R-line according to the priority order of the association. The B-line is the X-edge that has top priority, and is not affected by a change in any other line including other B-lines. Therefore, the principal lines of the hull form are represented as B-lines. Since the S-line has second priority compared to the B-line, it is affected by other B-lines, and the S-lines also affect each other. In other words, if a B- or S-line is modified, all crossing S-lines should be attached to it. When converting X-topology to non-manifold data structure, the S-lines and B-lines are subdivided at their crossing points into several curve segments that become boundary edges of surface patches. Finally, the R-line is attached to B-line and S-lines by the lowest priority, and a change of an R-line cannot affect any other line, including another R-line. So, the R-lines are usually used to describe the wireframe model in detail.

3.2 Procedure of Cross Faring Based on Association

The cross faring based on the association is implemented by an 'update line' operation, which is composed of several 'touch line' operations.

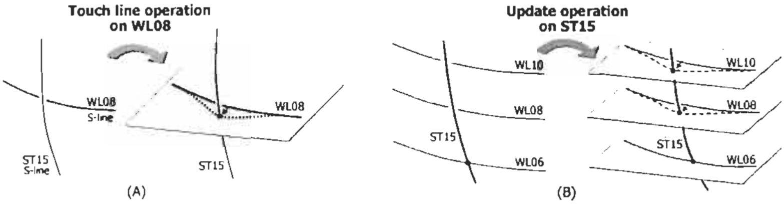

(A) (B)

Figure 2: Example of the 'touch line' operation (A) and the 'update line' operation (B) on station line

Performing 'touch line' operation on a target X-edge means attaching the target X-edge (except a B-line) to other X-edges that have higher or equal priority so as to cross them. Fig 2(A) shows that the target waterline WL08 is attached to the station line ST15 by a 'touch line' operation that consists of following 2 steps. In the first step, the plane of z=8.0m containing the target waterline WL08 is intersected with other X-edges that have higher or equal priority, i.e. the station line ST15 (S-line) in Fig. 2(A). In the second step, the target waterline WL08 is moved to pass the intersection point calculated in the first step. Then, a new waterline WL08 that crosses the station line ST15 is regenerated as the dotted line in Fig 2(A).

In contrast with the 'touch line' operation, the 'update line' operation is used to attach other X-edges that have equal or lower priority to the target X-edge. Thus, the 'update line' operation is implemented by several 'touch line' operations on other X-edges. In Fig 2(B), the update line operation on the station line ST15 is shown. Firstly, all X-edges that have equal or lower priority, for example the 3 waterlines WL06, WL08, and WL10, are searched using the priority order of association. Secondly, a 'touch line' operation is executed on each X-edge found in the previous step. Subsequently, the three waterlines WL06, WL08, and WL10 are attached to the station line ST15 as shown in Fig 2(B).

The process of association based cross fairing is to perform the update line operation on changed hull lines recursively, which means to perform the touch line operations on all hull lines associated with the changed lines. For example, when a B-line such as bottom tangent line is changed, all associated S-lines and R-lines should be modified to attach to the B-line by performing the update line operation. Then, the update line operation should be performed recursively for the modified S-lines until there are no more changes. Fig. 3 shows how the association based cross fairing reduces the effort required for hull form design with a wireframe model. If a hull form designer moves a point on the station line

ST15 (S-line) inspecting its curvature, the crossing waterlines WL06, WL08, and WL10 (S-lines) will be automatically changed by the update operation on ST15. Then, the change of the three waterlines causes a re-update of the buttock line and the gray station lines (R-lines). This automation of the cross fairing enables designers to manipulate the wireframe model more efficiently by inspecting the global curvature.

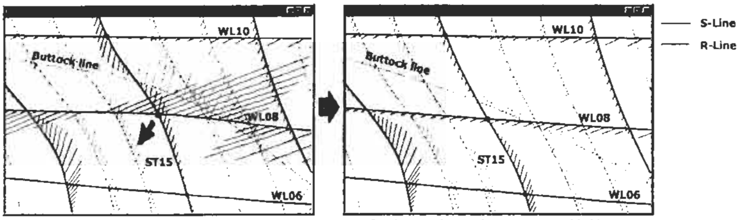
WL10
Buttock line
WL08
ST15
WL06
S-Line
R-Line

Figure 3: Example of the association based cross faring showing that all lines related to the changed station line ST15 are updated automatically

4 GENERATION OF SURFACE MODEL FOR NON-MANIFOLD DATA STRUCTURE

4.1 Process of Surface Model Generation

The surface model is generated from the X-surface mesh. The process of surface model generation is as follows. Firstly, the cross points (O) of the B-lines and S-lines are registered as nodes as shown in Fig 4(A) (at this stage, the R-lines are not involved). Fig 4(A) shows that no node is generated at the cross point between Btkline and WL02, because Btkline is a R-line. After all nodes are generated, each X-edge is divided into several segments at nodes. Later each node will be converted to a vertex and each segment to an edge of non-manifold data structure.

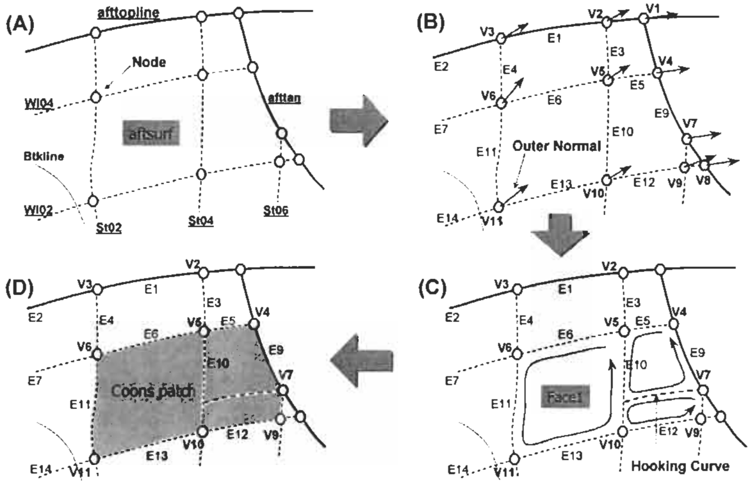
(A)
afttopline
Node
Wl04
aftsurf
afttan
Btkline
Wl02
St02
St04
St06
(B)
V1
V2
V3
V4
V5
V6
V7
V8
V9
V10
V11
E1
E2
E3
E4
E5
E6
E7
E9
E10
E11
E12
E13
E14
Outer Normal
(C)
Face1
Hooking Curve
(D)
Coons patch

Figure 4: Procedure for generating the non-manifold data structure of the surface model from the X-topology of the wireframe model

Secondly, loops of boundary edges of faces are identified, which represent the topology of surface patches in the non-manifold data structure. For loop search, the outer normal vector of each node is calculated approximately, as shown in Fig 4(B). Exploring the edges using the outer normal vectors, EzHULL automatically identifies all loops to be boundary of faces. Then, a series of Euler operators are applied for each loop, to construct the topology information. When this process is complete, the topological information of the non-manifold data structure is completely constructed.

Finally, EzHULL generates the geometric information of the non-manifold data structure with only the face boundaries. Since all surface patches are stored in the form of the tensor product NURBS in EzHULL, only rectangular surface patches are allowed for the geometric information of faces[4,5]. However, triangular or pentagonal faces occur frequently in the hull form design, and therefore, a degenerated NURBS surface patch is used for geometric data of the triangular faces. For pentagonal faces, a new edge called a 'hooking curve' is inserted to subdivide the pentagonal face into two rectangular faces as shown in Fig 4(C). After all faces are converted into rectangular faces, NURBS surface patches can be generated with the four edges of the faces using the bilinearly blended Coons patch method (Fig 4(D)). The bilinearly blended Coons patch can be easily converted to the mathematically equivalent of the NURBS patch [5].

4.2 Application of Surface Model

The surface Model is mainly used for following three purposes.

(1) Surface shading: After the geometric information of the surface model has been completely generated, the surface can be shaded with proper tessellation. As shown in Fig 5, designers can freely rotate and translate the shaded hull form, and easily understand the hull form 3-Dimensionally. In particular, the surface fairness can be inspected in detail by moving the light source.Designers can modify the wireframes more smooth based on the surface fairness.

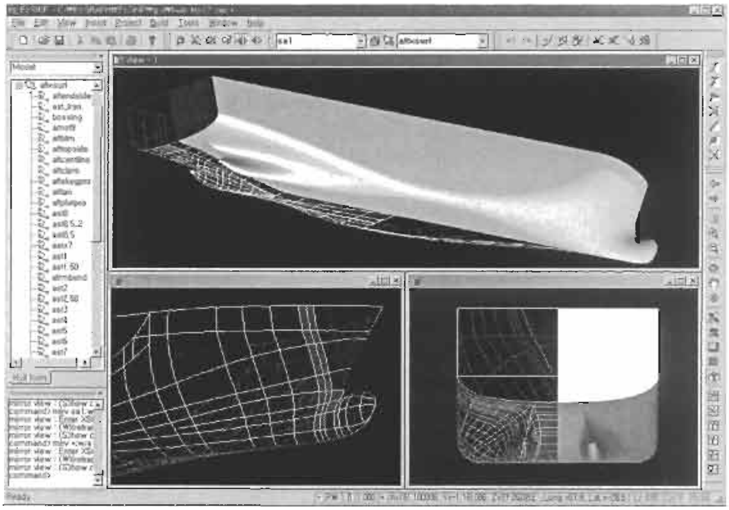

Figure 5: Shaded surface model of a twin skeg hull form produced from the wireframe model in EzHULL

(2) Points ordering: When a new hull line is generated by intersecting the wireframe model with a certain plane, an ordering problem of the intersection points invariably occurs. Suppose that a designer generates a 0.5m buttock line, for example. Then, all the points of the buttock line can be obtained by intersecting all station lines and waterlines with the infinite plane at y=0.5m. However, there is no general method available that allows the proper connection of the intersection points to determine the correct buttock line. This points ordering problem in the wireframe based system is one of the most difficult tasks. EzHULL solves this problem simply by using topological information stored in the non-manifold data structure. Using topological information, EzHULL can determine the partial order of intersection points on each surface patch, and then generate a new wireframe line by rearranging the segments of the partially ordered intersection points into a globally ordered points list (Fig. 6).

(3) Wireframe shading: The X-edges are converted into polylines for visualization and shaded using a technique which we call 'wireframe shading', which is a technique that shades the wireframe curves with a luminance calculated using a normal vector at each vertex of the polylines. The normal vector of a vertex is calculated by interpolating the outer normal vectors of section 4.1. If the wireframe model shaded using this technique, the lines with normal vectors directed towards the observer are bright, and the others are shaded. Therefore, the wireframe shading can give the pseudo 3D-effect and help to improve the presentation of the wireframe fairing, even for a complex hull form (Fig. 7).

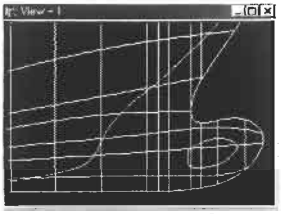

Figure 6: The buttock lines of a goose neck hull, which are generated using points ordering

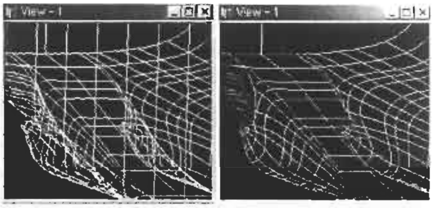

Figure 7: A twin skeg hull without wireframe shading (left) and with wireframe shading

5 CONCLUSIONS

EzHULL system developed in this research, provides an association based cross fairing and generates a surface from a wireframe model using X-topology and non-manifold data structure. The association based cross fairing offers designers an effective wireframe fairing, by monitoring how adjacent lines are affected when a particular line is changed. Direct conversion from a wireframe model to a surface model enables 3-D surface hull form to be visualized even at the earliest design stages. The topological information of the converted surface model helps to resolve the points ordering problem in the wireframe model and the geometric information is used to shade the wireframe model with a cubic effect. In addition to these features, EzHULL also provides convenient and intuitive wireframe editing system for planar and spatial curves, hull form variations and various facilities for hull form design. EzHULL[1] is now available as a commercial system, and it is our hope that the EzHULL system will give new vision to hull form designers.

References

1. Soon-Hung Han and Soon-Sub Lee. (1994). A Reference Model for the Computer-Aided Design of Hull Forms. *Transaction of the Society of Naval Architects of Korea* **31:4**, 15-22. written in Korean
2. Sang-Hun Lee and Kun-Woo Lee. (1996). Compact Boundary Representation and Generalized Euler Operators for Non-manifold Geometric Modeling. *Transactions of the Society of CAD/CAM Engineers* **1:1**, 1-19. written in Korean
3. Young-Bok Choi and Kyu-Yeul Lee. (1999). A Study on the Hull Form Design System on the Basis of the Associative Geometry Objects. *Transaction of the Society of Naval Architects of Korea* **36:4**, 105-115. written in Korean
4. Gerald Farin. (1999). *NURBS from Projective Geometry to Practical Use 2nd Ed*, AK Peters
5. Gerald Farin. (1997). *Curves and Surfaces For CAGD 4th Ed*, Academic Press

---

[1] Contact information: *http://www.ezgraph.co.kr*

Practical Design of Ships and Other Floating Structures
You-Sheng Wu, Wei-Cheng Cui and Guo-Jun Zhou (Eds)
© 2001 Elsevier Science Ltd. All rights reserved

A DESIGN MODIFICATION OF VLCC WITH WIDE WEB FRAME SPACE

Jae-Hyung Park, Chang-Hwan Jang and Joo-Ho Heo

Design Tech. R & D Team
Daewoo Shipbuilding & Marine Engineering Co.
1 Ajoo, Koje, KyoungNam, Korea

ABSTRACT

A new VLCC(Very Large Crude Oil Carrier) for improving productivity is suggested and the development procedures for the new VLCC are introduced. In the stage of initial design, a new VLCC with eight web frames and one swash bulkhead per one hold is suggested to reduce the number of web frame. Longitudinal structural members having sufficient longitudinal strength are introduced through conservative rule scantlings considering design still water bending moment and wave bending moment. 3-D cargo tank F.E. analyses have been performed to assess the structural adequacy of primary structural members such as floors, transverse webs, transverse bulkheads, swash bulkheads, girders and longitudinal bulkheads.
In the viewpoint of fatigue strength, hopper knuckle structure is apt to be weakened by opening and closing modes due to internal dynamic pressures and dynamic sea pressures. The fatigue strength of longitudinal connection is critical because the combined local stress components due to simultaneous internal and external pressure loads are to be added to the global stress components induced by hull girder wave bending. With these reasons, fatigue strength is calculated in longitudinal connection and hopper knuckle connection of the modified structural arrangement. The collision resistance is also investigated by comparing the new VLCC design and the original VLCC design.
Through this research, the newly designed VLCC is found to have enough strength with regard to yielding criteria, structural stability, fatigue strength and collision capacity.

KEYWORDS

Wide web frame space, Longitudinal strength, Hopper knuckle, Fatigue, Collision

1 INTRODUCTION

In the design of vessel, it is difficult to satisfy both aspects simultaneously, long-term operation life with minimum maintenance costs and structural design with the economic ship building costs.
Many research activities have been carried out for the development of new VLCC which has the long-term operation life and simple maintenance faculty in line with economical structural design [Park, et

al., 1999]. In this paper, engineering of VLCC for improving productivity is suggested and the development procedures for the new VLCC are introduced in the viewpoint of design.

2 STRUCTURAL ARRANGEMENT AND MID-SHIP SECTION

Main hull of cargo tank region of this vessel is consist of double side hull, double bottom, hopper tank and deck structures as same arrangement of original VLCC. Two longitudinal bulkheads divide the cargo tank part into center cargo tank and side cargo tanks and transverse bulkheads divide cargo tank into 5 tanks in longitudinal directions. Plane stiffened transverse bulkheads with three(3) rows of horizontal stringers on their forward sides subdivide the cargo region longitudinally. Nine web frames including one swash bulkhead exist in every hold in the design of original VLCC. However, to reduce the number of web fame, the structural design of new VLCC with wide web frame space is suggested.

Therefore, the suggested VLCC has eight web frames including one swash bulkhead in every hold as shown in Fig.1. That is, in the design of the new VLCC, total five web frames are reduced in comparison with the original VLCC design.

Hull section scantling, which have sufficient longitudinal strength, including stiffener and plate is calculated by considering total bending moment combined still water bending moment and design wave bending moment. Sagging and hogging conditions are considered in the design wave bending moments and still water bending moments.

Bending, shear and buckling strengths were considered in the definition of scantlings for longitudinal structural members. And minimum requirements of rules were also considered in the definition of the scantlings. Longitudinal strength is evaluated based on cross sectional area of the longitudinal member, position of the centroid, moment of inertia and section modulus.

According to the result of scantling for mid-ship section, longitudinal members of the subject VLCC have bigger scantlings in comparison with longitudinal members of original VLCC to satisfy longitudinal strength.

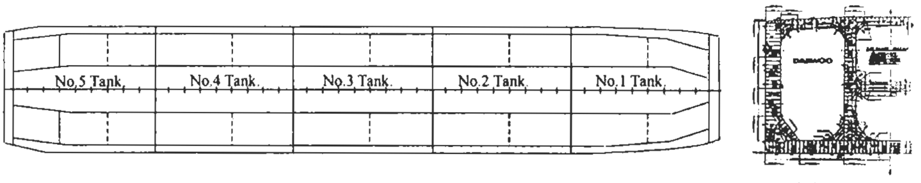

Figure 1: Structural arrangement and Midship section for new VLCC

3 CARGO TANK FE ANALYSIS

3-D Cargo Tank F.E. analysis is performed to assess the structural adequacy of the VLCC with wide web frame space and to define the scantling of the transverse members. Structural analysis has been carried out in accordance with the procedure outlined in the DNV's rule and guidelines[DNV, 1999].

3.1 Idealization for 3-D Cargo Tank Analysis

One and two half tanks in longitudinal direction were idealized in order to minimize boundary condition effects and the middle part of the model is used to examine the results of cargo tanks structural analysis. Only the port side with the full depth of the ship is idealized due to the symmetrical nature of loading conditions about the center line. 3-D FE model for cargo tank analysis is shown in Fig. 2.

The FE analysis of 3-D cargo tanks is performed by using shell, beam and truss elements to provide a satisfactory representation of the deflection and stress distribution within the structure. Longitudinal structure members(deck, bottom, inner bottom, side shell and bulkheads) are idealized by shell elements in order to take into account lateral pressure loads and to resist out of plane bending. Transverse structure members are also idealized by shell elements. The longitudinal stiffeners, vertical stiffeners attached to trans. BHD and face plate of horizontal stringers are idealized by beam elements in order to resist bending moment. The secondary structural members such as stiffeners on floors and webs etc. are idealized by truss elements in order to reflect axial load.

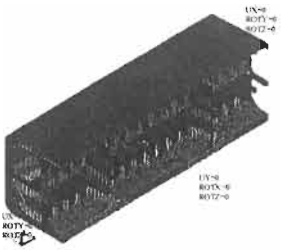

Figure 2: 3-D FE model

Half of the sectional properties are applied for the elements in the center line plane of the model, fore end plane and aft end plane of the model. Face plates and panel stiffeners of primary members are represented by line elements with a cross sectional area. The properties of curved face plate are defined by considering effective areas. Corrosion margin is considered in the definition of element properties. The number of mesh in double bottom floor and double side web are 4, the number of mesh between frames is 2 and the number of mesh between longitudinal stiffeners is 1.

3.2 Loading Conditions and Boundary Conditions

The most severe realistic load conditions of the ship are considered for the 3-D tank analysis. To investigate the response of the structure due to the local hydro-static and hydro-dynamic pressure, 8 load cases are considered. 5 cases are considered in sea-going condition and 3 cases are considered in harbor condition. Realistic combinations of external and internal dynamic loads are considered in sea-going conditions and the static loads are only considered in harbor conditions.

In order to consider shear force imbalance between downward loads and buoyancy, imbalance shear forces are calculated in way of the transverse bulkheads at inside longi. BHD, inner skin and side shell. To eliminate imbalanced shear forces, the calculated imbalance shear forces are re-acted to the same locations. The final 3-D cargo tank analysis shows the sum of the imbalanced shear forces is about 0.

For symmetrical nature of geometry and loading conditions, symmetrical constraints are applied at the centerline plane of the FE model. Symmetrical constraints are applied at the end of forward and aft plane of the FE model. Vertical fixed boundary is applied at the top node at the intersection of forward transverse BHD and side shell.

3.3 Analysis Results

Evaluation of stress results is performed by using element stress which is calculated at the middle surface of plate bending element. According to the results, the newly designed VLCC is found to have enough strength with regard to yielding criteria and structural stability.

4 EVALUATION OF FATIGUE STRENGTH

Fatigue strength has been considered as the one of main issues in the design of ship structure. That is, typical structural joints should be designed to sustain design service life without fatigue damage. Therefore, fatigue analyses for hopper knuckle connection and critical connections of longitudinals have been performed to evaluate whether these structural connections of subject vessel have sufficient fatigue strength in compliance with DNV's fatigue guidance[DNV, 1998].

4.1 Fatigue Loading

The only fluctuating loading components excluding static loading are considered as a fatigue loading, and the fluctuating loads covers wave bending moments, accelerations by ship motion and wave dynamic pressures. The detailed loading components such as external wave pressure, internal pressure and hull girder bending moment are defined in the probability level of loading to be 10^{-4}.

The accelerations due to ship motion produce the loads by cargo in hold or sea water in ballast tank, and these loads act on hold or ballast tank as inertia forces.

The dynamic external pressure is considered as the largest of the combined pressure dominated by pitch motion in head/quartering seas, or by roll motion in beam/quartering seas.

The dynamic internal pressures from liquid cargo or ballast water are calculated for acceleration components in vertical, transverse and longitudinal directions and the maximum pressure due to accelerations of the internal mass may be taken as the internal fatigue load.

4.2 Stress Combinations for Fatigue Analysis

A simplified approach to determine the distributions of long-term stress ranges for closed or semi-closed hull cross sections is expressed as Weibull distributions. Stress ranges for fatigue analysis are defined by combining local stress components due to simultaneous internal and external pressure loads with global stress components induced by hull girder wave bending.

The local dynamic stress components $\Delta\sigma_l$ are defined by external and internal dynamic pressures as following formula with a consideration of occurrence phase.

$$\Delta\sigma_l = 2\sqrt{\sigma_e^{\,2} + \sigma_i^2 + 2\rho_p\sigma_e\sigma_i} \tag{1}$$

The total local stress amplitude due to external and internal pressure loads are the sum of individual local stress components such as local secondary bending stress, local bending stress of longitudinal and local tertiary plate bending stress.

Global stress range is defined as the combination of vertical bending and horizontal components. Since two components of bending stress ranges, $\Delta\sigma_v$ and $\Delta\sigma_{hg}$, never occur at the same phase, global stress range $\Delta\sigma_g$ should be combined as

$$\Delta\sigma_g = \sqrt{\Delta\sigma_v^{\,2} + \Delta\sigma_{hg}^{\,2} + 0.2\Delta\sigma_v\Delta\sigma_{hg}} \tag{2}$$

The long-term sailing routes of the ship is considered by reduction factor f_e and the effect of mean stress is considered by reduction factor f_m.

Using the global and local stress ranges above, consequently, the stress range $\Delta\sigma_0$ for fatigue damage calculation is taken as [DNV, 1998]

$$\Delta\sigma_0 = f_m f_e \,\mathrm{Max}\left(\Delta\sigma_g + 0.6\Delta\sigma_l\,, 0.6\Delta\sigma_g + \Delta\sigma_l\right) \tag{3}$$

Stress range for fatigue analysis should include the effect of stress concentration due to detail structural geometry and welding geometry. Therefore, the stress concentration factor K is considered in the calculation of each stress component.

4.3 Fatigue Damage Assessment

When the distribution of long-term stress range follows Weibull distribution, fatigue damage ratio D indicating the intensity of cumulative damage is given by [DNV, 1998]

$$D = \frac{\nu_o T_d}{a}\sum_{n=1}^{N_{load}} p_n q_n^{\,m}\,\Gamma\!\left(1+\frac{m}{h_n}\right) \tag{4}$$

The S-N curves are adopted with welded joint, and it is assumed that the structure is exposed to corrosive effect of sour crude oil for half the ship life.

The fatigue damage can be calculated applying S-N curves for cathodic protection and corrosive environment equally. Simplified one-slope S-N curves have been used instead of bilinear curves with change in slope beyond 10^7 cycles. Considering the load conditions and corrosion effect, the resultant fatigue damage ratio leads to

$$D = \left[(D_{full})_{corrosive} + (D_{ballast})_{corrosive} + (D_{full})_{cathodic} + (D_{ballast})_{cathodic}\right] / 2 \qquad (5)$$

Each pair of load cases is used to calculate stress range which is defined as the difference of minimum and maximum stresses which are induced by minimum and maximum loading conditions, respectively. Stress range for damage ratio calculation is defined based on notch stress [Wagner, 1998].

4.4 Fatigue Analysis of Longitudinal Stiffener Connections

Fatigue analyses are performed in the connections of all longitudinal stiffeners except deck longitudinals. The effective length of beam for calculating local bending is varied due to the detail shape of longitudinal connections. Therefore, fatigue analyses for longitudinal connections are performed in typical web frame section, swash BHD and transverse BHD separately. Fatigue analyses for longitudinals at typical web frame section are performed in web frame section where maximum stress occurs from the result of cargo tank analysis. Fatigue analysis for longitudinals at transverse BHD are performed in fore and aft positions of the trans. BHD. FE model of 3-D cargo tank analysis is employed to obtain relative deformation that would be used in fatigue damage assessment of critical connections of longitudinal. The warping effect due to unsymmetrical section of longitudinal stiffener is also considered in the calculation of stress components.

According to the result of fatigue analysis of longitudinal connections, fatigue lives of longitudinal connections at aft position of transverse BHD are lower than longitudinal connections at fore position of transverse BHD due to the larger effective length of longitudinal.

Longitudinal stiffeners around design draft have most severe fatigue strength because of the maximum local bending stress due to external dynamic pressure. It can be found that all longitudinal stiffeners of the subject vessel have sufficient fatigue strength.

4.5 Fatigue Analysis of Hopper Knuckle Connection

Fatigue analysis for hopper knuckle connection is performed at the frame section having maximum stress by the result of 3-D cargo tank analysis. Fatigue analysis for this structure is performed in two steps. Global analysis (3-D cargo tank analysis for fatigue analysis) is performed to get global structural behavior and to get deflections results for the sub-model analysis. And then, the sub-model analysis is performed by using the local pressure and the displacements of the 3-D cargo tank model.

The sub-model extends two transverse floor spaces longitudinally to investigate the effect of docking bracket as shown in Fig. 3. Mesh sizes for critical zones are carefully controlled to get relevant geometric stress even by using t x t fine mesh.

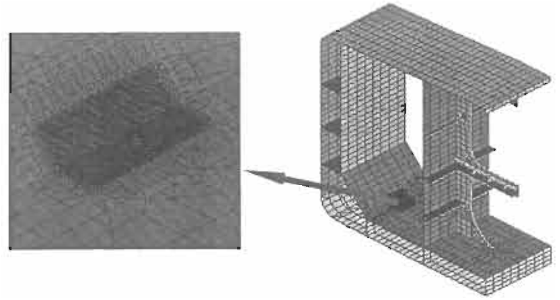

Figure 3: Local Model for the Fatigue Analysis of Hopper Knuckle

The stress components to be combined are the notch stresses, i.e. stresses including stress concentration factor of a structural detail depend on weld geometry, structural geometry and type of loading. Geometric stress is defined as a linear extrapolation of surface stresses at a distance 0.5t and 1.5t from the weld toe in case the thickness of parent metal being t. Transverse direction stress is similar to the principal stress in hopper structure. So, transverse direction stress is applied to evaluate fatigue life of hopper structure. The local stress resulted from hull girder bending moment is added to the local stress calculated from the sub-model analysis. Normal axial stress calculated by beam theory using hull girder bending moment is modified by considering geometry stress concentration induced by local geometry configuration of the sub model.

As a result, hopper knuckle of the new VLCC has sufficient fatigue life though the fatigue life is a little bit short in comparison with that of original VLCC.

5 EVALUATION OF COLLISION STRENGTH

Double hull tankers should be designed to have sufficient energy absorption capacity to reduce oil spillage in case of collision accident [Jang, et al., 1999]. Therefore, the hull resistance of subject VLCC against collision is investigated in the viewpoint of energy absorption capacity and resulting damage.

Contribution of each structural component such as side shell, side longitudinal bulkhead, stringer, web frame is investigated and energy absorption capacity and the amount of resulting damage are investigated according to the variation of ship speed with various plastic strain rate.

In this study, two types of VLCC are considered as struck ship and a 156,000 DWT oil tanker is considered as striking ship. The first struck ship is the new VLCC with wide web frame space and the other is original VLCC.

In each scenario, striking ship with ballast condition, moving ahead at a speed of 10 knots, collides with the struck ship. The struck ship is stationary and in full load condition. The position of collision is the middle of two successive web frames and struck ship's longitudinal center line is normal to the direction of motion of striking ship. The rolling, yawing and swaying of the striking ship are neglected.

5.1 Numerical Analysis

The explicit method to integrate the governing dynamic equations of a system with respect to time is used to simulate ship hull structural behavior in collision. Lagrange finite element method is also used by using a computer program MSC/DYTRAN [MSC, 1996]. The central difference method is used to perform this integration. As lumped mass is used, the mass matrix becomes a diagonal matrix and the equation of motion of each degree of freedom becomes independent and no matrix decomposition is necessary to obtain accelerations.

Plating and webs of web frame and longitudinal are modeled using Belytschko – Tsai shell elements and flange and small stiffeners are modeled using rod elements. The struck ship is modeled as deformable structures and striking ship is modeled as rigid bodies. In collision analysis, tearing of welding lines is important in areas where large damage occurs. Therefore, idealization of weld lines considering failure may be necessary in order to accurately predict collision damage. In this study, breakable joints are used to idealize welded connections.

Initially, as loads are applied, the two nodal points of each joint move together. When stresses acting on the weld satisfy a predefined failure condition (weld ultimate strength), the joint breaks up and internal forces are unloaded to the surrounding structure. Then each of two nodes may move independently. The weld failure of striking ship bow structure is not modeled because primary interest is focused on the behavior of the side structure of the struck ship.

5.2 Results

Collision force with penetration is shown in Fig. 4. The penetration is defined as the change of the distance between the center of gravity of the struck and striking ships. As collision starts the force increases until the side shell plate fails. Then force decreases rapidly, then increase again until failure of inner hull plate. Fig. 4 shows the collision forces of subject VLCC are higher than those of original VLCC. It reveals higher collision force is needed for new VLCC than the original VLCC.

As shown in Fig. 5, the absorbed energy of subject VLCC is higher than those of original VLCC. That is, the side structure of subject VLCC absorbs more energy than the original VLCC because softer structure absorbs more energy in collision.

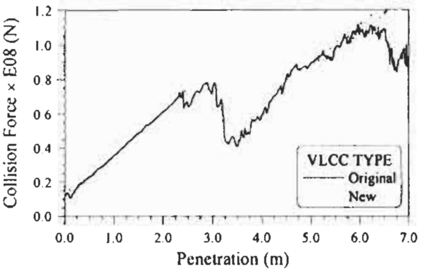

Figure 4: Collision Force Variation with Penetration

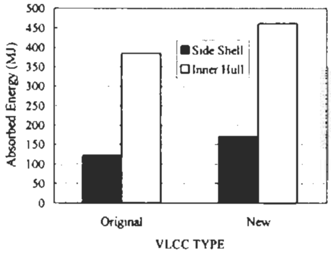

Figure 5: Comparison of Absorbed Energy

6 CONCLUSIONS

In this research, it can be found that the longitudinal structural members of the new VLCC have increased scantlings in comparison with the design of original VLCC. According to the results of 3-D cargo tank F.E. analyses, the transverse structural members of subject VLCC are reinforced.

By the result of fatigue assessment in longitudinal stiffeners and hopper knuckle connections, it can be found that the new VLCC has sufficient fatigue life. And it has been found that transverse stress is the dominant factor to cause the fatigue cracks for hopper knuckle connections.

In this paper, energy absorption capacity, damage mechanism and structural behavior according to the design modification for VLCC are studied. As the result of the evaluation of collision strength, the scantlings of both the new and original VLCCs are sufficient to endure the corresponding collision loads. In other words, the new VLCC as well as original VLCC is "safe" against oil leakage in the suggested scenario. And it shows the side structure of the new VLCC has a better collision capacity.

Through this research, the newly designed VLCC is found to have enough strength with regard to yielding criteria, structural stability, fatigue strength and collision capacity.

References

Chang- Hwan Jang, Jae-Hyung Park and Joo-Ho Heo (1999). Comparison of Collision Capacity for VLCC according to Design Modification. *Proceedings of the Annual Autumn Meeting.* SNAK, 445-448.

DNV(1999). Direct Strength Calculations. Rules for Classification of Ships.

DNV(1998). Fatigue Assessment of Ship Structures. Classification Notes No.30.7.

Jae-Hyung Park, Joo-Ho Heo, Young-Man Lee and Yeong-Soo Bae (1999). A Development of New VLCC for Productivity. *Proceedings of the Annual Spring Meeting.* SNAK, 435-438.

M. Wagner(1998). Fatigue Strength of Structural Members with In-Plane Notches. IIW.

MSC(1996). DYTRAN User's Manual Version 3.0.

Practical Design of Ships and Other Floating Structures
You-Sheng Wu, Wei-Cheng Cui and Guo-Jun Zhou (Eds)

© 2001 Elsevier Science Ltd. All rights reserved

OPTIMIZATION OF THE DESIGN OF SHIP STRUCTURES USING RESPONSE SURFACE METHODOLOGY

Makoto Arai[1] and Taito Shimizu[1]

[1]Department of Naval Architecture & Ocean Engineering, Yokohama National University,
79-5 Tokiwadai, Hodogaya-ku, Yokohama 240-8501, Japan

ABSTRACT

In this paper, the applicability of response surface methodology (RSM) to the design of ship structures is examined. This methodology involves the following mathematical techniques: a method of designing experiments that allows an efficient and accurate grasp of response features using a minimal number of analyses, the least squares method to obtain an approximate mathematical expression of the response, and the nonlinear optimization method to determine the optimal design, i.e., the minimum or maximum of the response. RSM allows easy estimation of changes on the response surface as changes are imposed on the design parameters. This is particularly effective in ship structural designs wherein trade-offs between design variables are inevitable. However, before RSM is applied to the actual design, the order of the approximate polynomial equation that represents the response surface, and the necessary number of response evaluations, etc., must be examined. Thus, the optimization of the transverse bulkhead structure of a crude oil tanker is performed as an example of the application of RSM, wherein the method's effectiveness together with the results of above-mentioned basic examinations are shown.

KEYWORDS

Optimization, Structural Design, Response Surface Methodology, Bulkhead Structure

1 INTRODUCTION

When a ship designer creates ship structural design, he first considers several combinations of design variables related to structural form, structural size, and so on. Next, he performs response analysis using FEM or some other method, and evaluates the performance of each design. Finally, he selects the best design from among the candidates.

However, this design-selection procedure carries with it the possibility that the selected combination of design variables may not always be the optimal one, due to the limited number of candidate designs analyzed.

Thus, response surface methodology (RSM) is applied in this study to optimize ship structural design. This methodology involves a few sets of mathematical techniques: the method of designing experiments to efficiently grasp the accurate features of a structural response using a minimal number of analyses, the least squares method to obtain an approximate mathematical expression of the response, and the nonlinear optimization method to determine the optimal design, i.e., the minimum or maximum response.

In this paper, as an example of the application of RSM to ship structural design, the optimization of the transverse bulkhead structures of an oil tanker is performed. The results obtained and the know-how accumulated in using this methodology for optimizing ship structural design are shown. Through the research shown in this paper, the advantages of the RSM are clarified; i.e., the behavior of the solution around the optimum is easily examined and the trade-off in the design can be carried out. Also, the methodology is shown to be very powerful means of rationally reducing the number of structural response analyses where efficiency of the analysis is very much expected.

2 RESPONSE SURFACE METHODOLOGY

2.1 Basic theories of RSM

A response surface is a curved surface that represents the relationship between the design variables x_i (i=1,....,n) and the response y. This relationship can be presented by the following equation:

$$y = f(x_1, \cdots\cdots, x_n) + \varepsilon \qquad (1)$$

where ε is the random error in y. There is no restriction in the form of function f that approximates the response surface. However, for the sake of simplicity, a polynomial to express the function f can be generally used. For example, if we use the second-order model with n design variables, the model becomes:

$$y = \beta_0 + \sum_{i=1}^{n} \beta_i x_i + \sum_{i=1}^{n} \sum_{j \geq i}^{n} \beta_{ij} x_i x_j + \varepsilon \qquad (2)$$

To obtain the form of the above equation, it is necessary to determine the unknown parameter β. For this purpose, we need a set of multiple design variables and the responses to those conditions (i.e., observations). To begin with, by replacing the second-order term (i.e., x_1^2, x_1x_2, x_2^2, etc.) with $x_m = x_1x_2$, etc., the equation is transformed to the first-order expression. Then, Eqn.2 can be expressed, in matrix notation, as

$$y = X\beta + \varepsilon \qquad (3)$$

where

$$y = \begin{Bmatrix} y_1 \\ y_2 \\ \vdots \\ y_k \end{Bmatrix} \qquad X = \begin{bmatrix} 1 & x_{11} x_{12} \cdots x_{1p} \\ 1 & x_{21} x_{22} \cdots x_{2p} \\ \vdots & \vdots \quad \vdots \ddots \vdots \\ 1 & x_{k1} x_{k2} \cdots x_{kp} \end{bmatrix} \qquad \beta = \begin{Bmatrix} \beta_0 \\ \beta_1 \\ \vdots \\ \beta_p \end{Bmatrix} \qquad \varepsilon = \begin{Bmatrix} \varepsilon_1 \\ \varepsilon_2 \\ \vdots \\ \varepsilon_k \end{Bmatrix}$$

Here, p+1 is the number of terms in the model in Eqn.2 in a linearlized expression, and k is the number of observations.

We assume that the values of ε are independently distributed as random variables with zero means and variances σ^2. In order to obtain the unknown parameter β, the least squares method is utilized. The least squares estimates (i.e., the best unbiased estimates), b, of the element β in Eqn.3 are

$$b = (X^T X)^{-1} X^T y \qquad (4)$$

It is possible to obtain an accurate approximate polynomial if the estimation accuracy of each component of b is high. For this purpose it is necessary to decrease the dispersion of each component of b. The variance-covariance matrix of the vector of estimates, b, is

$$Var(b) = Var(Cy)$$

$$= CVar(y)C^T$$

Here $C = (X^T X)^{-1} X^T$. Since $Var(y) = Var(\varepsilon) = \sigma^2 I$, then

$$Var(b) = \sigma^2 (X^T X)^{-1} \tag{5}$$

It is understood from Eqn.5 that the variance-covariance matrix $Var(b)$ consists of the components σ^2 and $(X^T X)^{-1}$. As mentioned above, σ^2 is the variance of the random errors that are related to the characteristics of the response y; thus it cannot be controlled. On the other hand $(X^T X)^{-1}$ is determined by the combination of the design variables. Therefore, the minimization of each component of $Var(b)$ is possible if we minimize the dispersion of $(X^T X)^{-1}$. In this way, estimation of at a high level of accuracy can be realized. This is the principle upon which the design of experiment is based. Taking advantage of the advancement of recent computer technology, a few numerical approaches of the design of experiment are proposed. In the design of experiment using a computer, a large number of candidate combinations of design variables are prepared beforehand, and the minimum number of combinations are selected from them by using the optimum criterion. In this paper, the D-optimal design, Khuri & Cornell (1996), is used. The D-optimal design is a method that determines a combination of design variables which maximizes the determinant of the matrix $M(= X^T X / k)$, which is called the moment matrix. In this method, by normalizing the coordinate of the design variable between –1 to 1, D-efficiency (D_{eff}), which is the corrected value of the moment matrix, is used as the criterion:

$$D_{eff} = \frac{\left(Det\left[X^T X\right]\right)^{1/p}}{k} \tag{6}$$

where p+1 is the number of unknown parameters in Eqn.3.

Each $(X^T X)^{-1}$ component decreases relatively if we choose the combination of the design variable which maximizes the D_{eff}; therefore, accurate parameters for the polynomial equation can be obtained.

2.2 Approximation of response surface using polynomial

In the actual design problems, the true solution may fluctuate or be discontinuous. In such cases, a decrease of the search accuracy or failure of the search algorithm is often brought about if the solution-search method uses the gradient of the response surface. In response surface methodology, on the other hand, the least squares method using the polynomial as seen in Eqn.2 is utilized and an alternative solution having a smooth surface is obtained. The search efficiency of the optimum solution is very good, since the optimization in the alternative response surface finishes almost in a moment. Moreover, this methodology has the advantage that it would be able to easily grasp the general property of the response by obtaining the approximate response surface which filters the small discontinuity or fluctuations which are, in some cases, inevitable (e.g., measuring errors in model experiments, etc.). This advantage is very effective in the initial design stage. If we consider the approximate polynomial to be a Taylor series expansion of the solution, it may be said that an approximation with sufficient accuracy is possible using a low-order polynomial if the region of interest is narrow. To approximate the response in a wider region, the introduction of higher order terms in the polynomial is considered. However, if we introduce higher terms, a rapid increase of computing time and unstable solutions are easily anticipated.

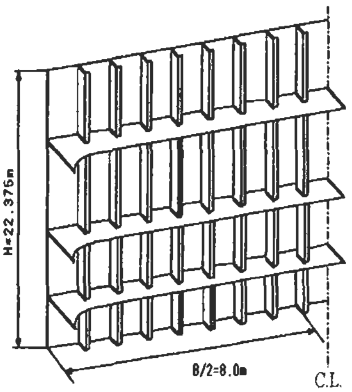

Figure 1:T.B.H.D.model

We must therefore evaluate the fitness criterion of the approximate polynomial function before we utilize it. And if the solution space is too large, it seems practical to sub-divide the space into some smaller regions and assign an accurate function to each of them. In this paper, we assume that the region of interest, which includes the optimum inside point, is comparatively narrow, and that the sub-division of the space is unnecessary.

3 EXAMPLES OF OPTIMIZATION BY RSM

3.1 Minimization of Bulkhead Structural Weight

3.1.2 Examination model

As a first example, we will show the results of the optimization of a transverse bulkhead of an oil tanker center tank as shown in Figure 1. The goal in this example is the minimization of structural weight. The number of vertical stiffeners n_{vs} and also the number of horizontal girders n_{hg} are considered design variables. For simplicity, those stiffening structures are assumed to be installed at equal intervals. Scantlings of bulkhead plates and stiffeners are determined by the section modulus requirements of NK (Nippon Kaiji Kyokai) rules, i.e., plate thickness and section modulus for stiffeners, taking into account of the space between the vertical stiffeners and that of the horizontal girders. Furthermore, the cross-sectional shape of the vertical stiffeners and horizontal girders are determined using the method described by Mano & Yoshida (1982) as the optimum shape (in view of the weight minimum) that satisfies the required section modulus. For the edges of the vertical stiffeners and horizontal girders, bracket plates of adequate size are installed. In this study, therefore, the independent design variables are n_{vs} and n_{hg} only, and the gross weight (W) of the transverse bulkhead structures are taken as objective functions.

3.1 2 Results of weight minimum optimization

There is no restriction in the order and the number of terms in the approximate polynomial used in this study. However, if the numbers of orders and terms of the approximate polynomial are unnecessarily increased, not only an increase in the calculation load but also instability of the approximation are anticipated. Therefore, in this paper, we will use the second- and third-order polynomial and examine the effect of those approximations.
The second-order model becomes:

$$W = \beta_0 + \beta_1 n_{vs} + \beta_2 n_{hg} + \beta_3 n_{vs}^2 + \beta_4 n_{vs} n_{hg} + \beta_5 n_{hg}^2 \tag{7}$$

And the third-order model becomes:

$$W = \beta_0 + \beta_1 n_{vs} + \beta_2 n_{hg} + \beta_3 n_{vs}^2 + \beta_4 n_{vs} n_{hg} + \beta_5 n_{hg}^2 + \beta_6 n_{vs}^2 n_{hg} + \beta_7 n_{vs}^3 + \beta_8 n_{vs} n_{hg}^2 + \beta_9 n_{hg}^3 \tag{8}$$

For the number of combinations (i.e., experimental points) of design variables necessary for determining the unknown parameters, we used twice the unknown parameter number. In this paper, as the first example, we compare the following three cases and will discuss the results.

Case 1: Second-order model with 12 experimental points
Case2: Third-order model with 20 experimental points
Case3: Exact solution

The region of interest is $15 \le n_{vs} \le 60$ and $1 \le n_{hg} \le 15$. Therefore, the number of candidate experimental points in the region is 690. In Case 3, all the responses at these 690 experimental points are evaluated. For Case 1 and Case 2, by using the D-Optimal design, the effective experimental points are selected, and the approximate response surfaces are computed using the least squares method. The results are shown in Figures 2 to 4. The results of the second-order model and the third-order model are considerably different. The result of the third-order model (Case 2) agrees more closely with the exact solution (Case 3). The reason for the difference between the result of second-order model (Case 1) and the exact solution (Case 3) is considered to be that the region of interest, in this example, is comparatively wide to approximate the response surface using the second-order model.

Figures 5 to 7 show the obtained results for these three cases. The result of the third-order model (Case 5) agrees closely with the exact solution (Case 6). The second-order model has a practical accuracy in estimating the peak value; however, the response surface is slightly deformed. Thc optimum design point, according to these results, is about σ^2 =37 to 38 and n_{hg} =10 to 11.

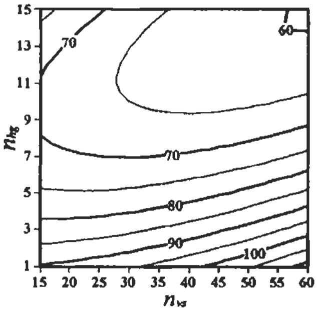

Figure 2: Hull steel weight (ton)
(Case 1: Second-order model)

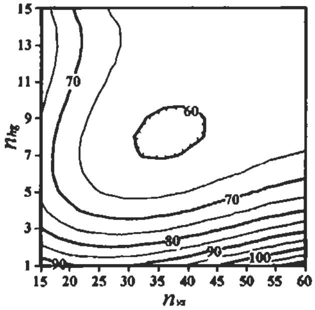

Figure 3: Hull steel weight (ton)
(Case 2: Third-order model)

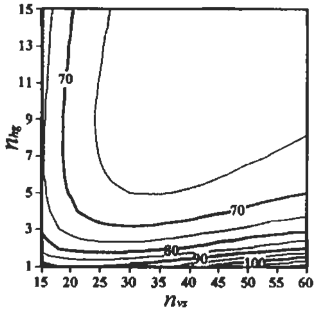

Figure 4: Hull steel weight (ton)
(Case 3: Exact solution)

Next, to examine the characteristics of the response near the peak value, re-calculation is carried out for a smaller region (i.e., $30 \leq n_{vs} \leq 60$ and $5 \leq n_{hg} \leq 15$).

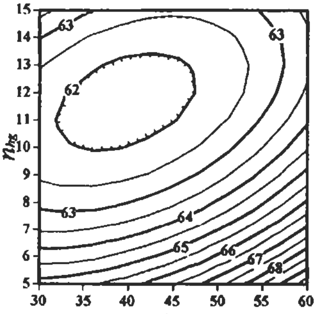

Figure 5: Hull steel weight (ton)
(Case 4: Second-order model)

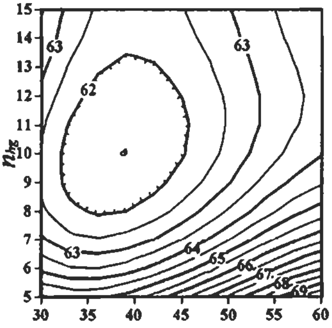

Figure 6: Hull steel weight (ton)
(Case 5: Third-order model)

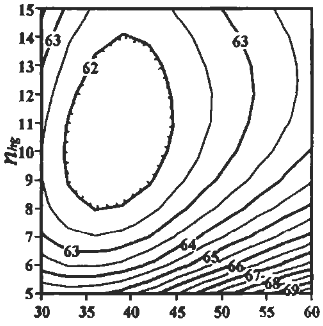

Figure 7: Hull steel weight (ton)
(Case 6: Exact solution)

Case 4: Second-order model with 12 experimental points
Case 5: Third-order model with 20 experimental points
Case 6: Exact solution

3.1.3 Optimization considering the construction cost

In the above section, optimization of the structure in the view of minimum weight was performed by changing the number of vertical stiffeners and horizontal girders. According to the results obtained, optimum value was found to be the combination in which the number of vertical stiffeners and horizontal girders is considerably more than the actual bulkhead structure (e.g., one actual tanker with the same tank size has $n_{vs} = 17$ and $n_{hg} = 3$).

If the number of vertical stiffeners and horizontal girders increases, the man-hours required for the construction of such transverse bulkheads increases. Such a design would be disadvantageous. Thus, in this section, the results of optimization that take into consideration not only weight of the material but also the construction cost of the structures will be shown. To begin with, total cost C is defined as the sum of the material cost and the construction cost as:

$$C = c_s \times W + c_w \times L_w \tag{9}$$

Here, c_s is the cost of steel building material per unit weight, and W is the total bulkhead weight. The second term in the right hand-side of Eqn.9 is the cost of construction which is assumed to be in proportion to the welding length D_{eff}. We can estimate L_w by the number of vertical stiffeners and horizontal girders. In this paper, c_s and c_w are assumed as:

$$c_s = 70{,}000 yen/ton \text{ and } c_w = 2{,}000 yen/m.$$

The response surfaces of the total construction cost are obtained on the basis of these assumptions. The third-order model is used. The obtained response surface of the total construction cost is shown in Figure 8. To confirm the accuracy of the response surface, the exact solution is also shown in Figure 9. The response surface by the third-order model agrees quite well with the exact solution. The results of both solutions are compared in Table 1. A slight difference between the two solutions exists in the number of optimum horizontal girders, since in this example n_{vs} and n_{hg} are treated as integers, while some errors due to polynomial approximation may also exist. However, the estimated peak response (i.e., the optimal value of total cost) obtained using RSM agrees very closely with that of the exact solution. As was indicated before, the actual ship with the same tank size has 17 vertical stiffeners and 3 horizontal girders. It is considered that in the actual ship, the vertical stiffeners are installed to correspond to the location of the longitudinal stiffeners, whose number is determined in regard to the longitudinal strength of the hull structure. Therefore, the obtained number of vertical stiffeners does not perfectly agree with the case regarding the actual ship; however, we can confirm that the optimum solution arrived at using this analysis approaches to the actual design by introducing the construction cost shown in Eqn.9.

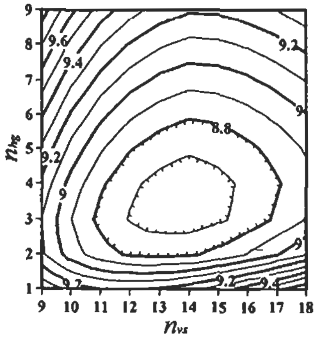

Figure 8: Total construction cost (10^6 yen), RSM

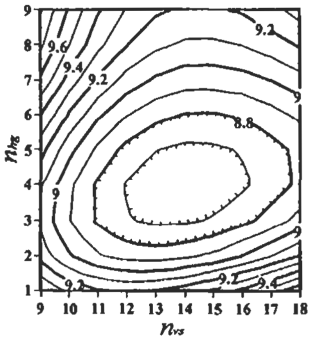

Figure 9: Total construction cost (10^6 yen), Exact solution

TABLE 1
COMPARISON OF OPTIMUL SOLUTIONS

	RSM	Exact sol.
n_{vs}	14	14
n_{hg}	4	3
Total cost in Yen	8,625,231	8,646,432

3.2 Optimization Based on the Stress Value of the Structure

As a second example of RSM application, a case is shown in which the maximum value of the stress that will be occurred in horizontal girders is made to be an objective function. In this example, the vertical positions of the horizontal girders (Figure 10) will be the design variables. In this study the number of horizontal girder is fixed as three. The loading condition is assumed to be the same as that in the first example shown in 3.1, i.e., full load water pressure on the transverse bulkhead. However, unlike the first example, for the sake of simplicity the plate thickness of all structures, dimensions, and the numbers of horizontal girders and vertical stiffeners, and the positions of vertical stiffeners are assumed to be constants. Therefore, only the intervals of three horizontal girders (i.e., x_1, x_2, x_3, x_4) are assumed to be design variables. Here, x_4 is a dependent variable (i.e., x_4 = tank depth $- x_1 - x_2 - x_3$). A second-order model is utilized to approximate the response as:

$$y = \beta_0 + \beta_1 x_1 + \beta_2 x_2 + \beta_3 x_3 + \beta_4 x_1 x_1 + \beta_5 x_2 x_1 + \beta_6 x_2 x_2 + \beta_7 x_3 x_1 + \beta_8 x_3 x_2 + \beta_9 x_3 x_3 \qquad (10)$$

The combinations of design variables chosen by the D-optimal criterion are shown in Table 2. Twenty FEM models that correspond to the experimental points, presented in Table 2, were prepared, and the finite element analyses were performed using MSC/NASTRAN. As examples of the analytical results, the case in which the low maximum stress is computed is shown in Figure 11, and the case in which the high maximum stress is computed is shown in Figure 12. Both figures show half of the transverse bulkhead of a center tank in consideration of the symmetric condition. For these cases, high von Mises stress occurs at the edge of the horizontal girders, with these regions whitely displayed in Figures 11 and 12. In this example, maximum stress is used as the objective function to be minimized.

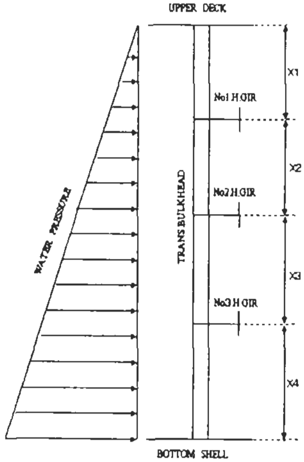

Figure 10: Design variables

TABLE 2
DESIGN VARIABLES SELECTED
BY D-OPTIMAL CRITERION

NUMBER	x_1	x_2	x_3	x_4
1	5,000	4,000	3,000	9,400
2	5,000	4,000	4,300	8,100
3	5,000	4,000	5,500	6,900
4	5,000	5,200	5,500	5,700
5	5,000	5,300	3,000	8,100
6	5,000	6,500	3,000	6,900
7	5,000	6,500	4,300	5,600
8	5,000	6,500	5,500	4,400
9	6,100	5,200	4,400	5,700
10	6,200	4,000	3,000	8,200
11	6,300	4,000	5,500	5,600
12	6,300	6,500	3,000	5,600
13	6,300	6,500	4,300	5,500
14	7,500	4,000	3,000	6,900
15	7,500	4,000	4,300	5,600
16	7,500	4,000	5,500	4,400
17	7,500	5,200	3,000	5,700
18	7,500	6,400	5,500	2,000
19	7,500	6,500	3,000	4,400
20	7,500	6,500	4,300	3,100

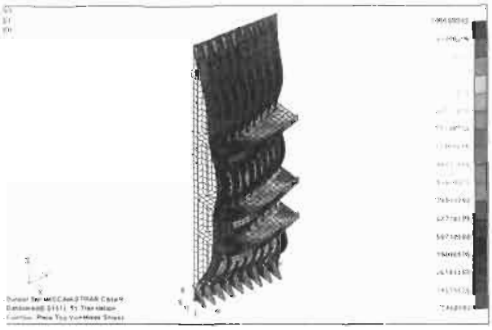

Figure 11: Case with low max. stress

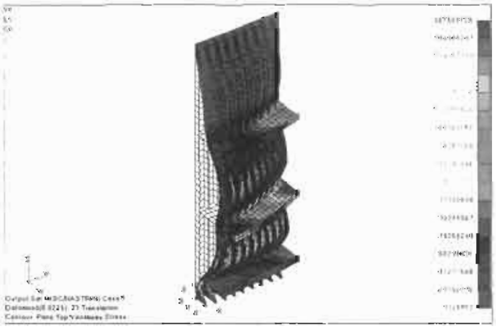

Figure 12: Case with high max. stress

The obtained response surface is shown in Figure 13. The parameters for the approximate polynomial are presented in Table 3. β_4 and β_9 are excluded, since the contribution of the terms of x_1^2 and x_3^2 in the Eqn.10 is judged to be negligible. The results of this example are summarized in Table 4, in which x_4 includes the depth of the bracket (1,300mm). The FE analysis is done for this optimum design point and the result is shown in Figure 14. According to Figure 14, the topmost (No.1) horizontal girder should be installed in a comparatively low position, and No. 2 and No. 3 horizontal girders are to be placed at well-balanced positions in order to support the vertical stiffeners.

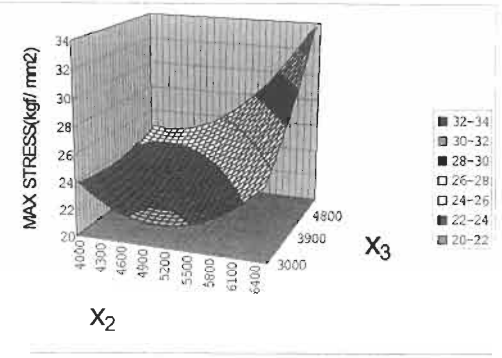

Figure 13: Response surface of maximum stress

TABLE 3
LEAST SQUARE ESTIMATION
OF EACH PARAMETER

Parameter	Least square estimation	Parameter	Least square estimation
β_0	166.906	β_5	1.8×10^{-6}
β_1	-0.012254	β_6	1.6×10^{-6}
β_2	-0.033251	β_7	0.5×10^{-6}
β_3	-0.007532	β_8	1.2×10^{-6}
β_4	—	β_9	—

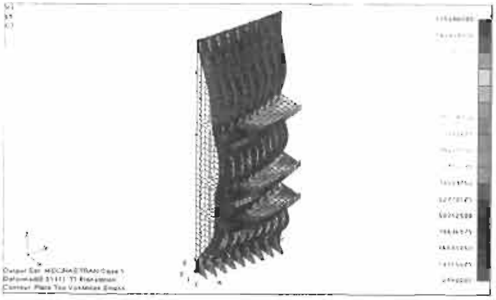

Figure 14: FE analysis for optimum design point

TABLE 4
OPTIMAL DESIGN-VARIABLE SET

Design variables & Max. stress	
x_1(mm)	7,500
x_2(mm)	5,045
x_3(mm)	3,000
x_4(mm)	5,853
Max. stress by R.S.M. (kgf/mm^2)	22.90
Max. stress by analysis (kgf/mm^2)	21.39

4 CONCLUSION

In this paper, the applicability of response surface methodology to hull structural design was examined. Optimization of bulkhead structures was carried out as analytical example, obtaining the following results:

(1) It is possible to determine response characteristics around the peak value through the use of low-order polynomial models (i.e., second-order or third-order models). The response surface around the peak can be used to discuss the trade-offs between design variables at the early stage of hull structural design.

(2) If the region of interest is wide, a higher-order model or the sub-division of the region is necessary, because a low-order model may produce an inaccurate and distorted response surface.

(3) If we use only structural weight as the objective function, the determined optimum bulkhead

design will include an excessive number of vertical stiffeners and horizontal girders compared to that used in actual ships. By including construction cost in the objective function, the optimum design approaches the actual design.
(4) RSM is powerful means of rationally reducing structural response analyses to obtain optimal design.

References

Arai, M., Shimizu, T., Suzuki, T. (2000). Optimization of Transverse Bulkhead Design by Response Surface Methodology, *Journal of Kansai Society of Naval Architects, Japan* **234**, 237-243.
Arai, M., Suzuki, T. Shimizu, T. (2000). On the Application of Response Surface Methodology to the Optimization of Ship Structural Design, *Journal of the Society of Naval Architects of Japan* **188**, 545-552.
Khuri, A. I., Cornell, J. A. (1996). *Response Surfaces, Designs and Analyses*, Marcel Dekker, Inc.
Mano, M., Yoshida, Y. (1982). Theories and Practice in Hull Structure Design, *Senpaku*, **55:610**, 32-39.
Nippon Kaiji Kyokai (1997). *Rules and Regulations for the Construction and Classification of Ships.*

Practical Design of Ships and Other Floating Structures
You-Sheng Wu, Wei-Cheng Cui and Guo-Jun Zhou (Eds)
© 2001 Elsevier Science Ltd. All rights reserved

A STUDY ON AN INFORMATION SYSTEM OF DAMAGES OF SHIP STRUCTURES

Y. Kawamura[1], T. Seki[2], T. Sakuragi[2] and Y. Sumi[1]

[1] Department of Naval Architecture and Ocean Engineering, Yokohama National University,
79-5 Tokiwadai Hodogaya-ku Yokohama 240-8501, Japan
[2] Formerly Graduate Students of Yokohama National University

ABSTRACT

Subcritical damages such as fatigue cracks and corrosion do not immediately cause a loss of serviceability or serious disaster such as oil spill from tankers. However, the maintenance of ship structures is very important to avoid such casualties. In this paper, a new concept of an information system of damages of ship structures is proposed in order to improve the safety and to support the maintenance of ships in service. In the proposed system, all information of damages in a certain ship is managed in one database, and appropriate action could be taken based on the assessment of these damages. In order to construct the database, object oriented data model of crack and corrosion damages with the structural data model of a single-hull tanker is developed. The prototype system is constructed on an object oriented database on an engineering workstation. For the efficient use of such system, the inspection with high detectability of damages and a convenient recording of the damages to the database are necessary. In this paper, a ship inspection supporting system by using a portable (wearable) computer and virtual reality technique is also proposed. The validity of the proposed systems is illustrated by some examples.

KEYWORDS

Information system, Damages of ship structures, Corrosion, Crack, Data model, Virtual reality, Portable (wearable) computer

1 INTRODUCTION

Generally, subcritical damages such as fatigue cracks and corrosion occur in ship structures during the service period. While such damages could cause a serious disaster, they may be comparatively light ones when they are detected so that such disasters can be prevented by appropriate countermeasures. For this purpose, it is necessary to grasp the state of the damages correctly and to evaluate them appropriately.

Recently, Computer Integrated Manufacturing System (CIMS) for ship building has been studied (for example Ship & Ocean Foundation 1989-94) and now the concept is practically applied in the design and manufacturing process in many shipyards. Furthermore, the concept of the life cycle support such as CALS concept is proposed in which not only the effectiveness of the design and manufacturing processes but also the effective operation and maintenance of ships are considered.

For the effective maintenance of the ship structures, a new concept of an information system of damages of ship structures has been studied by the authors (Kawamura *et al.* 1998, 2000). In this paper, we firstly describe about the concept of the information system and about the object oriented data model for crack damages used in the system. Second, the prototype system constructed on an object oriented database on an engineering workstation is demonstrated. Thirdly, based on the proposed information system, a ship inspection supporting system by using a portable (wearable) computer and virtual reality technique is described.

2 CONCEPT OF AN INFORMATION SYSTEM OF DAMAGES OF SHIP STRUCTURES

The role of the information system of damages of ship structures can be considered as (1) management of the health of an individual ship, (2) storage of the information related to the damages of the ship, and (3) estimation of the detected damages for the appropriate countermeasure. To realize such functions, we proposed a concept of an information system as shown in Fig.1(a). In this concept, the information about damages such as crack or corrosion obtained in surveys is stored in an Information Database. Since the detail information such as the location or the condition of the damages are important for the evaluation of damages, not only the information of damages itself but also the information about the 3-Dimensional (3D) hull structure of the ship is stored in the database. In the Assessment System for damages of ships, risk of the damages is assessed and repair plan or operation plan are drafted based on the information in the database. It is possible to say that the Information Database can be regarded such as a medical record for a certain ship and the Assessment System for damages of ships aids the evaluation and planning based on the information stored in the database. For the efficient use of the proposed information system, inspection with high detectability of damages and a convenient recording of the damages to the database are necessary. In this study, we also proposed a ship inspection supporting system by using a portable (wearable) computer as shown in Fig.1(b).

3 PROTOTYPE SYSTEM OF THE INFORMATION SYSTEM

3.1 Data Model for the Information System

The prototype of the information system of damages of ship structures was constructed assuming that the information of a certain ship is managed in a certain organization. The target ship of the prototype system is assumed to be a single-hull tanker, and a simple structure with 4 transverse spaces including transverse bulkhead is considered in the prototype system. Since the object oriented data structure is generally used in development of product model, an object oriented database (OBJECTIVITY 1993) is used for the data model of the information system.

As defined in the data model of CIMS, the ship hull structure is defined by Member-objects and Connect-objects which represent joint information such as weld or slots. For the damages, the data model for corrosion and crack was proposed by Kawamura *et al.* (1998). To construct the data model for damages, we consider that the data model can indicate (1) the location of the damage and the damaged structural members, (2) the condition of the damage such as configuration of the damage, and (3) the time when the damage is detected. Here, the definition of the crack at the intersection of longitudinals and transverse members is described as an example of the data model.

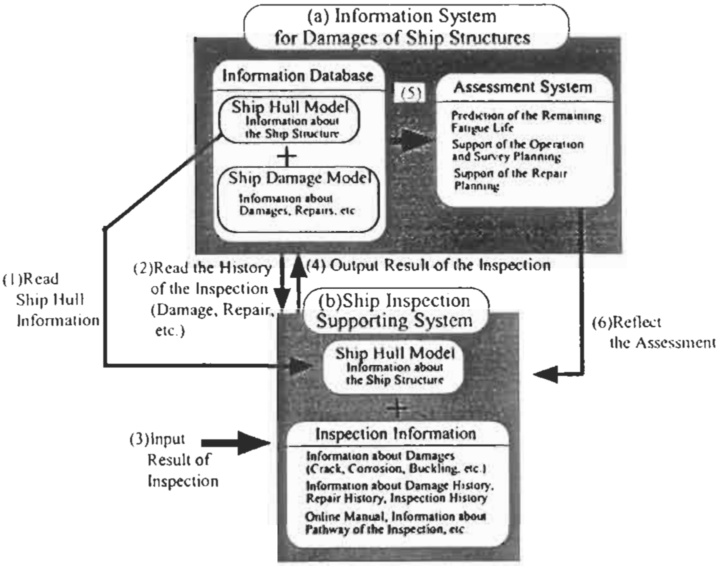
(a) Information System
for Damages of Ship Structures
Information Database
Ship Hull Model
Information about the Ship Structure
Ship Damage Model
Information about Damages, Repairs, etc
(5)
Assessment System
Prediction of the Remaining Fatigue Life
Support of the Operation and Survey Planning
Support of the Repair Planning
(1)Read Ship Hull Information
(2)Read the History of the Inspection (Damage, Repair, etc.)
(4) Output Result of the Inspection
(b)Ship Inspection Supporting System
Ship Hull Model
Information about the Ship Structure
(6)Reflect the Assessment
(3)Input Result of Inspection
Inspection Information
Information about Damages (Crack, Corrosion, Buckling, etc.)
Information about Damage History, Repair History, Inspection History
Online Manual, Information about Pathway of the Inspection, etc

Figure 1: Concept of an information system for damages of ship structures

Fig.2-left shows the process of typical crack propagation which is likely to occur at the intersection between longitudinal members and transverse members. In this process, first, a crack is generated at the end of fillet weld on the face plate (Fig.2- left (a)). After the crack penetrates and propagates in the web plate (Fig.2- left (b)), it reaches the shell plate and propagates as shown in Fig.2- left (c). Based on this observation, Crack-objects are defined by the combination of two crack geometries, SurfaceCrkGm-object(Fig.2(1)) and ThroughCrkGm-object(Fig.2(2)), which represent a surface crack and a through crack respectively. And the Crack-objects are related with corresponding Member-objects or Connect-objects in the ship hull structural model as shown in Fig.3. For example, when the crack penetrates on the shell plate, it is defined as the WebShellCrack-object which is represented by two ThroughCrkGm-objects and a SurfaceCrkGm-object, and related to the Member-objects (ShellPlate and etc.) and the Connect-object (LongiWeld). It is noted that the information about the time is defined in the Crack-objects and they are integrated in the LongiSectionCrack-object in order to represent the aging of the damage. Also based on this concept, cracks around the slot and etc. are similarly defined in the prototype system.

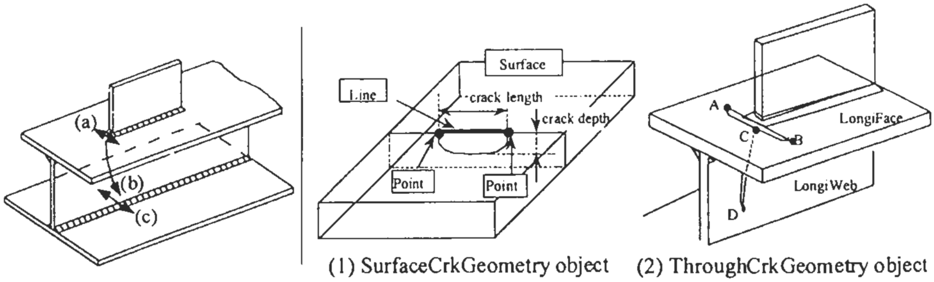
(a)
(b)
(c)
Surface
Line
crack length
crack depth
Point
Point
A
B
C
D
LongiFace
LongiWeb

(1) SurfaceCrkGeometry object (2) ThroughCrkGeometry object

Figure 2: Typical crack propagation and the definition of the crack geometry objects

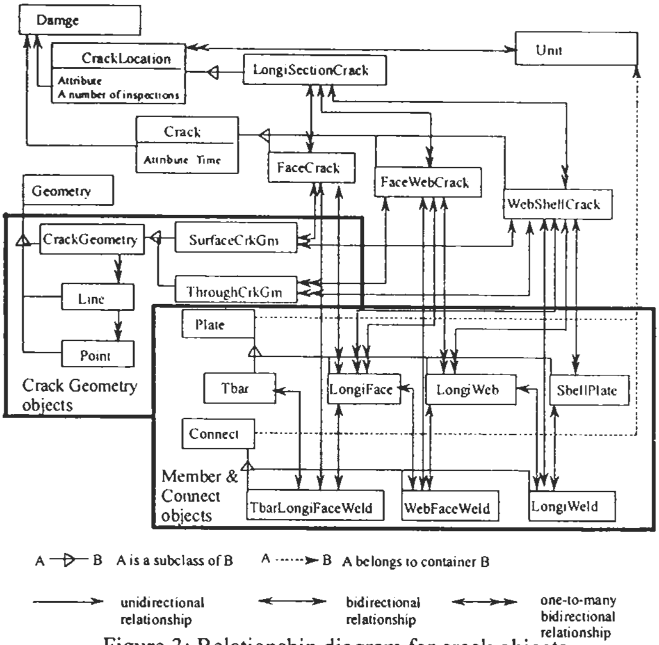
Damge
CrackLocation
Attribute
A number of inspections
Unit
LongiSectionCrack
Crack
Attribute Time
FaceCrack
FaceWebCrack
WebShellCrack
Geometry
CrackGeometry
SurfaceCrkGm
ThroughCrkGm
Line
Point
Crack Geometry objects
Plate
Tbar
LongiFace
LongiWeb
ShellPlate
Connect
Member & Connect objects
TbarLongiFaceWeld
WebFaceWeld
LongiWeld
A B A is a subclass of B
A B A belongs to container B
unidirectional relationship
bidirectional relationship
one-to-many bidirectional relationship

Figure 3: Relationship diagram for crack objects

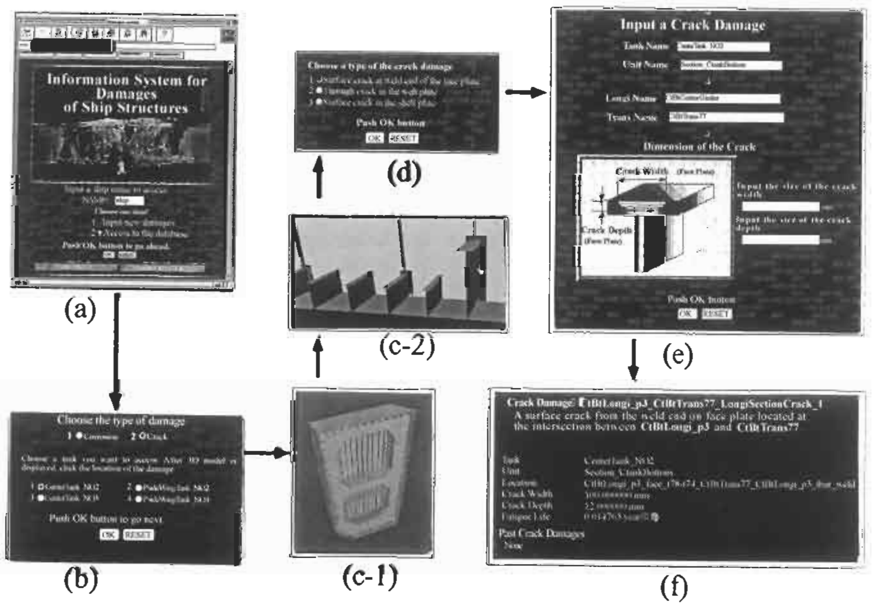
Information System for Damages of Ship Structures
(a)
Choose the type of damage
Push OK button to go next
OK RESET
(b)
(c-1)
(c-2)
Choose a type of the crack damage
Push OK button
OK RESET
(d)
Input a Crack Damage
Dimension of the Crack
Crack Width
Crack Depth
Push OK button
OK RESET
(e)
(f)

Crack Damage: CtBtLongi_p3_CtBtTrans77_LongiSectionCrack_1
A surface crack from the weld end on face plate located at the intersection between CtBtLongi_p3 and CtBtTrans77

Past Crack Damages
None

Figure 4: Input and evaluation process in the developed proto-type system

3.2 Demonstration of the Prototype System, Assessment of the Damages

Next, simple demonstration of the prototype system constructed based on the data model is shown in Fig.4. Since the sharing of the information by corresponding organizations is important for the proposed concept, the prototype system is accessible through WWW-browser on Internet. To input a detected crack damage into the system, the user selects the name of the ship and the name of the tank (Fig.4 (a)(b)). After the 3D structural model is shown in the browser by using VRML, the user walk through in the 3D structural model to choose the location of the damage (Fig.4(c-1)(c-2)). After the user choose the type of the damage (Fig.4(d)), the information of the damage can be input from the fill-form as shown in Fig.4(e).

For the assessment of the crack damages stored in the database, we consider to evaluate the possibility of unstable failure and fatigue life caused by the detected crack. In order to evaluate the stress intensity factors (SIF), the calculation method is defined in the database depending on the crack geometry. Necessary parameters for calculation are not only dimensions of crack and plates, but also the information about the load. In this study, we assume that the finite element shell analysis is carried out beforehand under a certain wave load, such as the load with excess probability $Q=10^{-8}$ derived from long-term prediction. And also it is assumed that the result of the analysis is stored in the FEM-objects defined in the database (Kawamura *et al.* 1998). For example, if the crack is a surface crack, the problem is assumed to be a plate with semi-elliptic center crack. By computing both tensile load and bending load from stress information stored in FEM-objects, SIF by tensile load and SIF by bending are calculated (Murakami *et al.* 1987), and the total SIF is used for evaluation of unstable failure by comparing it with fracture toughness (K_c) stored in the Material-object. Next, fatigue life assessment is carried out based on the Paris's law. In order to calculate the SIF range, equivalent effective stress range (DNV 1984) is used. Then, the fatigue life is computed by the SIF range and the parameters (c, m) stored in a Material-object. Fig.4(f) shows an example of the evaluation for the crack damage.

As shown above, the interface to use the information system of damages can be developed on WWW environment. It is possible to say that the proposed architecture of the information system is useful to construct a system to support evaluation and management of damages of ship structures.

4 SHIP INSPECTION SUPPORTING SYSTEM BY USING A PORTABLE COMPUTER

4.1 Concept of the Ship Inspection Supporting System

One of the important ship inspections is the close-up survey where a surveyor enters into tanks of the ship and directly watch and search damages existed in the tank. In the present inspection, after a surveyor enters into a tank, he looks around a place where damages likely to occur based on the survey program or on his experiential knowledge. When the surveyor detects damages, he records the situation of the damage. For example, the location of the damage may be recorded by writing down the tank number, longitudinal number and frame number into a memo pad. In a certain case, the damages may be sketched in the memo pad or a photo is taken by using a digital still camera. After the inspection, the detailed drawing of the damage is prepared from the recorded information, and the repair plan is made based on them. The problems of the present close-up survey process can be considered as follows.

(1) The performance of the inspection such as the detectability of damages is highly dependent on the knowledge and experience of the surveyor.

(2) Since there is no unified expression for damages detected in the inspection, it is difficult to utilize the result of inspection efficiently and rationally.

In this study, we proposed a ship inspection supporting system by using a portable (wearable) computer carried by the surveyor in the ship hull inspection in order to overcome the above problems. We consider the following three items as the role of the system.

(1) Electronic manual, by which efficient inspection is possible by surveyors with a little experience.

(2) The inspection support by displaying the information about the history of the inspection and about

the recorded past damages which is useful for the surveyor.

(3) Efficient recording of the result of the inspection such as detected damages or measured plate thickness and efficient input of the result of the inspection into the information database of damages.

Fig.1(b) and Fig.5(a) shows the concept of the proposed ship inspection supporting system. As shown in Fig.1(b), the concept is based on the information system of damages of ship structures described in the previous section. In the process with the inspection supporting system, the information such as the ship hull structures and past recorded damages is transferred from the information system to the inspection supporting system just before the inspection starts (Fig.1(1)(2)). When the surveyor enters into the target tank with the equipments shown in Fig.5(a), 3D computer graphics of the ship structure is displayed in the HMD. By utilizing the display of the ship structure, appropriate instructions by the electronic manual and accurate display of the information about past damages may be possible. When the damage is detected or the plate thickness is measured, the result of the inspection is not recorded in the traditional memo pad but directly recorded in the inspection supporting system (Fig.1(3)). Since the surveyor equips a Virtual Reality (VR) sensor which senses the position of the surveyor in real-time, the display of the 3D graphical model in Head Mount Display (HMD) can match to his actual view even if the inspector moves and the direction of his head changes in the tank. This helps the surveyor to recognize the location of the detected damages even in the complicated hull structure of the ship. After the inspection is finished, the collected data such as the damage information is send back to the information system of damages of ship structures (Fig.1(4)), so that immediate evaluation of the damages is possible(Fig.1(5)). In the inspection process, it is sometimes not so easy to use an input device such as the mouse for computers because the environment of the inspection is usually not so good (dark and with precarious foothold). For this reason, we proposed the utilization of a voice input system (Fig.5(a)-(3)) by which the surveyor can activate the computer command and input the detected damages to the inspection supporting system.

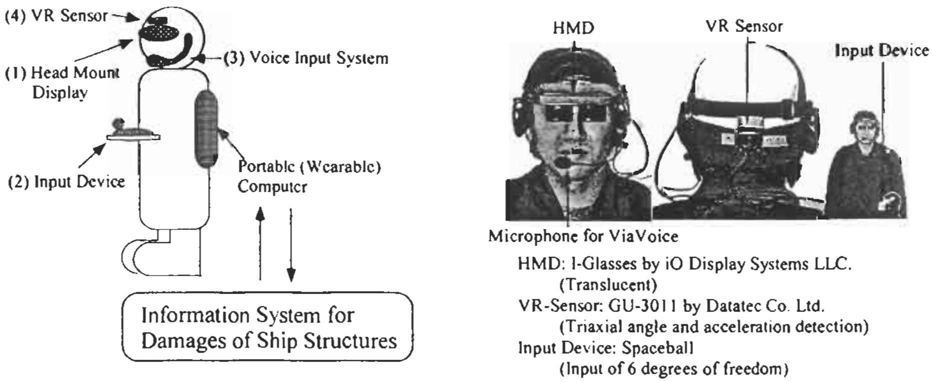
(4) VR Sensor
(1) Head Mount Display
(3) Voice Input System
(2) Input Device
Portable (Wearable) Computer
Information System for Damages of Ship Structures
HMD
VR Sensor
Input Device
Microphone for ViaVoice
HMD: I-Glasses by iO Display Systems LLC. (Translucent)
VR-Sensor: GU-3011 by Datatec Co. Ltd. (Triaxial angle and acceleration detection)
Input Device: Spaceball (Input of 6 degrees of freedom)

(a) Concept (b) Prototype system

Figure 5: Inspection style with the proposed ship inspection supporting system

4.2 The Prototype System

Based on the above concept, a prototype system is constructed as shown in Fig.5(b). HMD, VR-sensor and the input device are connected to a portable computer and integrated by using the software developed by the authors. For the development of the software, Visual C++ and WorldToolKit by SENSE8 Co.Ltd. which is a toolkit for virtual reality applications are used. For the development of the voice input system, a microphone and the speech recognition software, ViaVoice, with its toolkit for developers by IBM are used.

By using the developed prototype system, we carried out an experimental inspection for a simple and typical ship structural model. In the prototype system, the corresponding 3D model is not transferred from the information database but can be read from a text-file and displayed in the HMD, and also damage information is output to a text-file after the inspection. After reading the information about the structure and about the history of damages, the inspection starts. Here, the detection of the surface crack at the intersection between the face plate and the web stiffener is demonstrated in Fig.6. When the damage is detected, the surveyor selects the structural member on which the damage exists. In the concept of the proposed inspection supporting system, the display of the 3D graphical model in surveyor's HMD matches to the actual view. However, this function cannot be realized in the prototype system because of the difficulty in the position sensing by using the VR-sensor. By way of compensation, the surveyor can select the structural member by using the speech recognition function of the system. After the selection, a pointer-ball appears on the surface of the member in the equipped HMD. Then the surveyor can input the geometry of the crack by locating the pointer-ball following along the real crack geometry. After that, the data about crack size or some comments can be input by the surveyor's voice from the input dialog which is activated by the voice command.

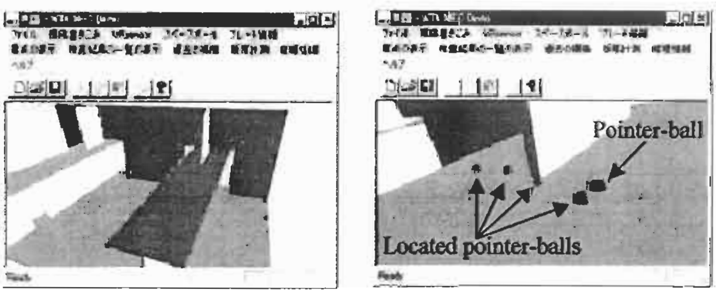

(a)Selection of a structural members (b) Locating the pointer-balls

Figure 6: Recording process of the detected crack damage

5 CONCLUSIONS

(1) A new concept of the information system for more advanced maintenance of ship structures is proposed. In the proposed system, the information about the damages is stored and managed in the database with the information of 3D ship hull structural model. A simple data model for the crack damage is proposed, and a prototype system is developed on Internet environment by using an object oriented database with 3D graphical interface by VRML. In order to demonstrate great potential of the system, a simple example of the assessment of damages is indicated.

(2) A concept of a ship inspection supporting system by using a portable (wearable) computer and virtual reality technique is proposed. The proposed inspection supporting system is carried by a surveyor during the inspection and helps surveyor by displaying the electronic manual and the history of damages of the ship. For the efficient recording of detected damages, utilization of a sensor and voice recognition system is proposed. Based on this concept, a prototype system is developed and validity of the concept is shown with the demonstration. By using this concept, the reasonable and labour-saving utilization of the inspection results is expected.

References

DNV. (1984). Fatigue Strength Analysis for Mobile Offshore Units, DETNORSKE VERITAS.

Kawamura Y., Seki T. and Sumi Y. (1998). A Study on the Information System for Damages of Ship Structures (in Japanese), *J. SNAJ.* **184**, 527-536.

Kawamura Y., Sakuragi T. and Sumi Y. (2000). A Study on a Ship Inspection Supporting System by Using Portable Computer (in Japanese), *J. SNAJ.* **188**, 737-743.

Murakami Y. *et. al.* (ed). (1987). *Stress intensity factors handbook* Vol I, II, Pergamon Press.

OBJECTIVITY. (1993). *Objectivity/DB manuals I, II, III.* Objectivity. Inc.

Ship & Ocean Foundation. (1989-94) Report on Development and Research of Shipbuilding CIM Frame Model (in Japanese).

Practical Design of Ships and Other Floating Structures
You-Sheng Wu, Wei-Cheng Cui and Guo-Jun Zhou (Eds)
© 2001 Elsevier Science Ltd. All rights reserved

BAYESIAN AND NEURAL NETWORKS FOR PRELIMINARY SHIP DESIGN

H. B. Clausen, M.Lützen, A. Friis-Hansen, N. Bjørneboe

Department of Mechanical Engineering,
Maritime Engineering Technical University of Denmark
DK-2800 Kongens Lyngby, Denmark

ABSTRACT

To ease the determination of the main particulars of a ship at the initial design stage it is convenient to have tools which, given the type of ship and a few other parameters, output estimates of the remaining dimensions. To establish such a tool, a database of the characteristics of about 87,000 ships is acquired and various methods for derivation of empirical relations are employed. A regression analysis is carried out to fit functions to the data. Further, the data is used to learn Bayesian and neural networks to encode the relations between the characteristics. On the basis of examples, the three methods are evaluated in terms of accuracy and limitations of use. For a chosen type of ship, here container vessels, the methods provide information on the relations between length, breadth, height, draught, speed, displacement, block coefficient and TEU capacity. Thus, useful tools are available for the designer when he is to choose the preliminary main characteristics of a ship.

KEYWORDS

Neural Network, Bayesian Network, Main Particulars, Preliminary Ship Design, Data Fitting.

1 INTRODUCTION

The main particulars of a ship are determined at a preliminary stage, based on more or less detailed customer requirements. The naval architect has to find a design with the 'optimal' main dimensions and often the approach is to consider ships with similar characteristics and use an iteration loop to modify the dimensions so that all specifications are met. Another approach is to use empirical relations for finding the initial design parameters. Many authors have refined this approach (e.g. Bertram and Wobig (1999), Watson and Gilfillan (1977)) by fitting regression lines to statistical data, yielding explicit empirical expressions for the relations between various parameters. However, the empirical expressions only give the relation between two parameters at a time irrespective of the rest. A method to find the simultaneous relations between more parameters is addressed with neural and Bayesian networks.

1.1 The Database

The database containing ship characteristics for the world fleet has been purchased from Lloyds' Maritime Information Services, London (LMIS). Container vessels are chosen as a subject of investigation in this paper, as they constitute a homogeneous group, which is still sufficiently complex (e.g. the Panmax size of some container vessels) to show the adaptability of the methods used. To obtain up-to-date estimates of the design parameters, only vessels from 1990 and later are included in the analyses. Unfortunately, some entries are missing for some vessels and therefore the study is based on records, for which all of the following data is available: TEU capacity, length, breadth, speed, draught, height and displacement. This means that 812 container vessels are analysed.

2 DATA ANALYSIS METHODS

2.1 Simple Regression

When empirical relations between the main dimensions are established, it is straightforward to use linear (or piecewise linear) functions to fit the dimensions. Piecewise linear functions require many subdivisions to yield low error measures and therefore, an alternative representation by power functions is chosen. This has the additional advantage that derived coefficients (as e.g. C_B) are simple power functions as well.

The loading capacity (e.g. deadweight, TEU or lane metres) can be used as an input for the regression analyses. These measures indicate the owner's needs and represent in very general terms the dimensions of the ship. The following power law relation between the loading capacity, LC, and the main particulars is chosen.

$$T = a(LC)^b \tag{1}$$

The parameter T is either of the main characteristics, and a and b are determined by use of the least squares method.

2.2 Neural Network

A feedforward neural network consists of a number of layers each transferring the weighted sum of its inputs to the next layer through transfer functions. Along with the weighted sum, a constant (also called bias) enters into the transfer function. The weights and biases are found in the learning phase, where an optimisation procedure in MATLAB minimises the output error, given known inputs and outputs.

2.2.1 Neural network topology

Normally, networks with biases, sigmoid layers and a linear output layer can approximate any continuous function to an arbitrary accuracy. The network used is a two-layer feedforward net with an input vector, one hidden layer, an output layer and an output vector. See Figure 1. The input vector is $\boldsymbol{P}$ and has the dimension R. Each of the two layers consist of S^x neurons (outputs), where x refers to the layer number. The input vector for each layer is connected to the neurons through a weight matrix, $\boldsymbol{W}^x$, and this weighted input is summed by the biases, $\boldsymbol{b}^x$, to yield the input, $\boldsymbol{n}^x$, for the transfer functions, $\boldsymbol{F}^x$. The output is kept in the vector $\boldsymbol{T}$.

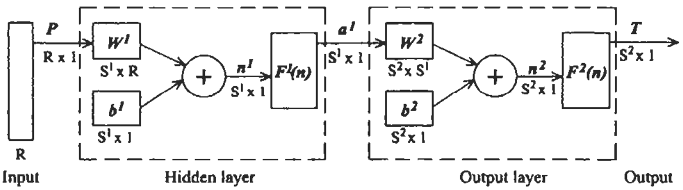

Figure 1: Structure of a neural network.

The data is normalised to assume values in the range [-1,1] to improve the learning convergence. This means that the outputs from the network must be returned through an equivalent postprocess to obtain real output values.

2.3 Bayesian Networks

A Bayesian network is a graphical representation of a set of uncertain quantities. It consists of a set of probabilistic nodes (ovals) and a set of directed arcs connecting the nodes. The nodes represent stochastic variables, defined as a set of discrete states and each state is associated with a probability measure. Arcs into variables indicate conditional probabilistic dependence so that the probability of a dependent variable B (child node) being in a particular state is given for each combination of the states of the preceding variables A (parent node). In a Bayesian network, directed loops are not allowed. See also Jensen (1996) for further details.

Although the diagram is compact and intuitive, it represents a complete probabilistic description of the problem. A central feature of Bayesian networks is that they allow inference based on observed evidence on any of the nodes. The inserted information is propagated through the network so that all variables in the model are updated in accordance with Bayes' rule.

2.3.1 Discretisation for bayesian networks

In the ship database the data set is organised as a matrix where each row represents the data for one particular ship and each column corresponds to a variable (for example L_{OA}). Each row may be seen as an instance (sample) drawn from a joint probability distribution over the variables in the data set. All the measured quantities may assume values from a continuous range of values. This makes discretisation necessary as Bayesian networks can only handle continuous probability distributions for very limited classes of models.

In this study, each variable is discretised individually. For each variable, a set of split-points must be chosen in order to divide the range into an appropriate number of intervals. Initially, the variables are

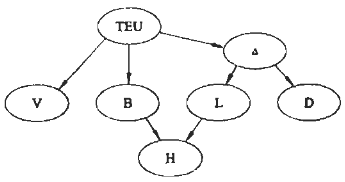

Figure 2: Bayesian network for container vessels.

discretised for equal number of ships in each interval. This approach has the characteristic that the dense part of the distribution is finely discretised so that the variable is well represented in these regions, whereas the sparse regions are represented by fewer and longer intervals. A pattern search algorithm is applied to optimise the locations of the discretising split-points, so that the categories become as uniform as possible. Each variable is discretised into 12 intervals, which is a rather crude, but to obtain reliable probability estimates, a reasonable number of data points in each interval is necessary.

Learning a Bayesian network is a task of constructing the network topology and estimating the associated probability tables, so that the underlying discretised data set is represented in the best possible way. In this study, the BNPC-algorithm by Cheng, Bell and Liu (2000) is used. Once the 'optimal' topology is found, the conditional) probabilities associated with each node are estimated.

3 SINGLE INPUT REGRESSIONS

In the following, the methods just described are used to predict the main particulars of container vessels. When the prediction is made on the basis of just one input parameter, this must in some sense be the governing one, in this case TEU capacity. Relations are found for length, L, breadth, B, velocity, V, draught, D, depth, H, and displacement, Δ.

3.1 Simple Regression

Expressed in the form of Eqn. 1, the power functions are fitted as given in TABLE 1 and shown in Figure 3(a).

TABLE 1

COEFFICIENTS OF FITTED POWER LAW FUNCTIONS

	L_{OA} [m]	B [m]	V [knots]	D [m]	H [m]	Δ [tonnes]
a	8.79	3.86	4.52	1.25	0.828	31.2
b	0.411	0.263	0.197	0.281	0.390	0.937

3.2 Neural Network

A network structure as shown in Figure 1 is used. It is found that the output of the network agrees well with the given data (i.e. no over-fitting) when the number of nodes or neurons in the hidden layer is three ($S^1 = 3$). The loading capacity (TEU) is assigned to the input P, and the output vector, $\boldsymbol{T}$, is ordered as shown below. Also shown are the normalisation matrices for the input P and the output $\boldsymbol{T}$.

$$T = \begin{bmatrix} \text{Length} & L \\ \text{Breadth} & B \\ \text{Speed} & V \\ \text{Draught} & D \\ \text{Depth} & H \\ \text{Displacement} & \Delta \end{bmatrix}$$

Input $P[min\ max]$

$$[95\ 6673]$$

Output $\boldsymbol{T}[min\ max]$

$$\begin{bmatrix} 69.2 & 347.0 \\ 13.3 & 42.8 \\ 10.0 & 26.3 \\ 3.0 & 14.5 \\ 5.0 & 24.4 \\ 295.5 & 142800 \end{bmatrix}$$

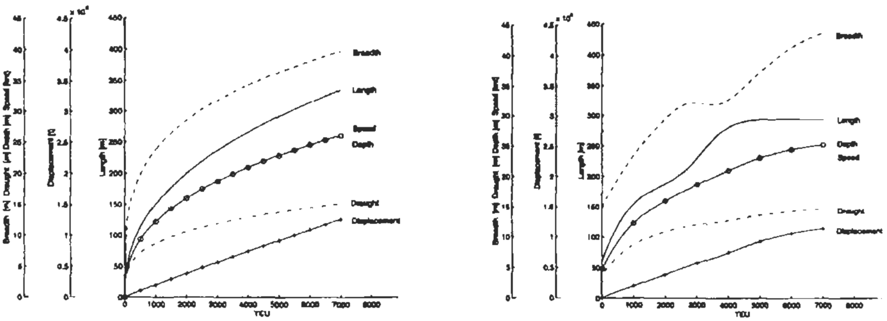

(a) Container vessel, power functions (b) Container vessel, neural network

Figure 3: Design parameters.

The weight matrices and bias vectors are

Hidden layer		Output layer	
Weight, W^1	Bias, b^1	Weight, W^2	Bias, b^2
$\begin{bmatrix} 2.52475 \\ 7.36627 \\ 4.93392 \end{bmatrix}$	$\begin{pmatrix} 0.08000 \\ 0.40853 \\ 5.86986 \end{pmatrix}$	$\begin{bmatrix} -0.08923 & 0.79895 & 3.03311 \\ 2.87692 & -1.09129 & 1.68256 \\ -0.01008 & 0.54992 & 3.15126 \\ 1.18918 & -0.23417 & 3.38025 \\ 1.42872 & -0.08277 & 3.01379 \\ 1.94908 & -0.27382 & 0.59050 \end{bmatrix}$	$\begin{pmatrix} -3.13720 \\ -2.26198 \\ -2.91564 \\ -3.25505 \\ -3.20148 \\ -1.57929 \end{pmatrix}$

The values predicted by the neural network are shown in Figure 3(b).

3.3 Bayesian Network

The Bayesian network shown in Figure 2 is learned by use of the following domain knowledge: The TEU capacity must be a root node, H and Δ are not connected and Δ is a cause of the TEU capacity.

3.4 Comparison of Methods

The average percentage error is calculated for each of the three methods. In this way, the tools may be compared in terms of their ability to predict each variable given a value of the TEU capacity. In the neural network model and the simple regression model the relation between the capacity and the other design parameters is given in terms of a continuous function based on least squares estimates. A Bayesian network expresses the updated probability distribution given the input (evidence) so that the uncertainty of the estimate is quantified. This information is neglected by the other methods, however it can be included.

The agreement is observed to be good for all three methods. The error plots in Figure 4 show that in spite of the crude discretisation in the Bayesian network, in some cases (for the variables L and B) the sum of squared errors is less than for the simple regression method. The figure also shows that the calculated errors are reasonably low and that all three methods have approximately the same level of relative error.

The results from the power function regression and the neural network are compared to the conditional mean of the distributions from the Bayesian network in the Figure 5(a) and 5(b) for the variables B

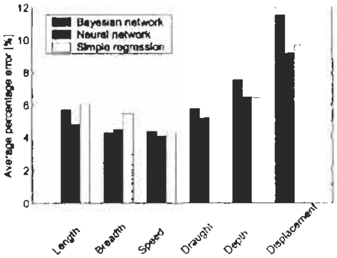

Figure 4: Comparison of average percentage error for power function regression, neural network and Bayesian network.

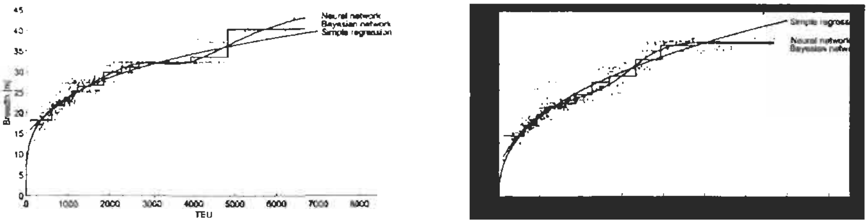

(a) Breadth, *B*. (b) Length, *L*.

Figure 5: Comparison of parameters calculated by use of a Bayesian network, power function regression and a neural network.

and *L*, respectively. For the breadth, it is seen that the Panmax behaviour is captured well by the neural and the Bayesian networks. However, the prediction of the output in the upper range differs for the three methods, which is due to the scattered and sparse data in that range. Good accordance for the length, *L*, is observed from the results of the neural and the Bayesian networks.

4 MULTIPLE INPUT REGRESSION

With a Bayesian network, it is possible to insert evidence on multiple variables without having to relearn the network. For multiple inputs, a designated neural network has to be learned for given inputs and outputs. The ability of the networks to use multiple, concurrent inputs (restrictions/demands) is shown by use of examples below.

4.1 Large Container Vessel

If for instance the main particulars of a 4100 TEU container vessel should be estimated, evidence is inserted in the Bayesian network on the state TEU $\in$ [3932, 4832] and propagation is performed. The probability distributions for the rest of the variables are now updated according to this evidence, of which bar charts of the displacement and the draught are shown in Figures 6(a) and 6(b), respectively. It is seen that a displacement range between approx. 72,000 and 94,000 tonnes and a draught of approx. 13 m are estimated by the Bayesian network to be more likely than other values. Still, there is a noticeable probability of the draught being as large as 14.5 m. The same range of capacity (TEU={3932, 4832}) is applied to the neural network and the power function regression, and they predict values near the estimate of the Bayesian network. The result of this computation is shown in Figures 6(a) and 6(b) as intervals labelled 'neural network, single input' and 'simple regression,' respectively.

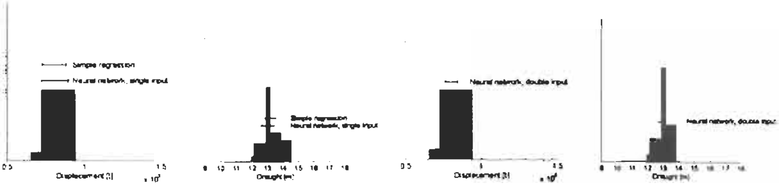

(a) (b) (c) (d)

Figure 6: Predictions of displacement and draught of a large container vessel in terms of probability distributions. (a) and (b) are restricted in TEU capacity, whereas (c) and (d) are restricted with respect to TEU capacity and Panmax dimensions.

It is further specified that the ship must not exceed the maximum dimensions of the Panama Canal ($L \leq 294.2$ m, $B \leq 32.3$ m, $D \leq 13.4$ m). This information can be inserted in the Bayesian network in the form of likelihood vectors. The dimension of the vector is equal to the number of states of the corresponding variable, and its elements are zero for impossible (unwanted) states and unity for possible states. When the new evidence is propagated the probability distributions are updated again. This does not change the distribution much for the displacement (Figure 6(c)), but as the draught is restricted its distribution changes, Figure 6(d). The Panmax requirements are not fulfilled by the estimates produced by the single input neural network, so a network with fixed TEU and breadth as inputs is trained. The results for displacement and draught are shown in Figures 6(c) and 6(d), respectively. With both TEU capacity and breadth specified, the neural network produces smaller variations in the predicted displacement and draught than the single input neural network.

4.2 Small Container Vessel

As another example, a smaller container vessel is considered. On the assumption of a capacity of approximately 950 TEU, evidence is inserted in the Bayesian network in the interval [846, 1062] and after propagation, the distributions of *L* and *D* are as shown in the bar charts of Figures 7(a) and 7(b). Here, a length between 140 and 160 m and a draught between 8 and 8.7 m are estimated to be the most probable. The predictions of a single-input neural network and the simple regression for the same range of TEU capacity are also shown.

By further requiring that the draught is limited to 8.5 m, the distributions from the Bayesian network of length and draught are as shown in the bar charts in Figures 7(c) and 7(d). The length and draught intervals mentioned above are now estimated to be even more likely. A neural network with capacity and draught as input is trained. The draught is set to 8.5 m and the result of inserting 846 TEU and 1063 TEU in the neural network is shown in Figures 7(c) and 7(d) as 'neural network, double input'. It should be noted that the evidence inserted in the Bayesian network ($D < 8.5$ m) is not fully equivalent to the input into the neural network ($D = 8.5$ m). This illustrates the flexibility of Bayesian networks.

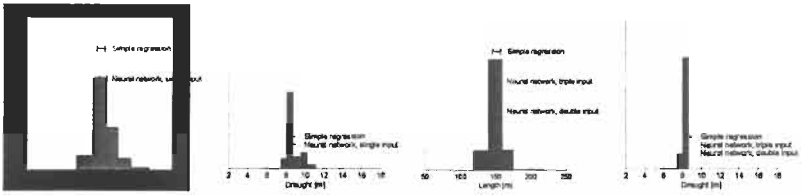

(a) (b) (c) (d)

Figure 7: Predictions of length and draught of small container vessel. (a) and (b) are restricted in TEU capacity, whereas (c) and (d) are restricted with respect to TEU capacity and draught.

Additionally, the requirement is added that the ship in question should have a service speed of minimum 18 knots. This does not change the distributions output by the Bayesian network for L and D. By training a neural network with capacity, draught and velocity and inserting TEUs as above, $D = 8.5$ m and $V = 18$ knots, the length and the draught shown as 'neural network, triple input' in Figures 7(c) and 7(d) are obtained.

Although not shown by graphs, these steps cause the distributions of L, Δ, B and H from the Bayesian network to be distributed with lower mean and variance. Thus, the range of the estimates of the main dimensions becomes narrower given the new information.

The above illustrates how evidence can be inserted in Bayesian networks and how a dedicated neural network can take multiple design requirements into account. This gives the designer the possibility of finding the most appropriate main characteristics given certain restrictions and demands, the Bayesian networks even quantify the uncertainties of the estimates.

5 CONCLUSIONS

New empirical formulae for the relation between main characteristics are derived and exemplified by predictions for container vessels. It is demonstrated that power functions will adequately describe the relation between TEU capacity and dimensions like displacement, length, draught, breadth, etc. The versatility of neural and Bayesian networks to take account of multiple design requirements is shown. Neural networks are simple to implement and yield smaller estimate errors, but as opposed to Bayesian networks they must be trained for each combination of inputs separately, and in the current configurations they do not yield information about the uncertainty of the given estimate.

References

Bertram, V. and Wobig, M.(1999), Simple Empirical Formulae to Estimate Main Form Parameter, *Schiff und Hafen*, **11**:118-121.

Cheng, J., Bell, D. and Liu, W. (2000), Learning Bayesian Networks from Data: An Efficient Approach Based on Information Theory, *Technical report*, University of Alberta.

Jensen, F.V. (1996), *An Introduction to Bayesian Networks*, Springer-Verlag, New York.

Lloyd's Maritime Information Services (2000), *Ship Characteristics*.

Watson, D.G.M. and Gilfillan, A.W. (1977), Some Ship Design Methods, *Transactions of the Royal Institution of Naval Architects*, **119**:279-303.

2. PRODUCTION

Practical Design of Ships and Other Floating Structures
You-Sheng Wu, Wei-Cheng Cui and Guo-Jun Zhou (Eds)
© 2001 Elsevier Science Ltd. All rights reserved

INNOVATION IN SHIP PRODUCTION WHAT CAN WE EXPECT ?

Hellmut Wilckens

Forschungszentrum des Deutschen Schiffbaus,
Bramfelderstrasse 164
22305 Hamburg, Germany

ABSTRACT

The paper deals by way of example with some aspects of innovative ship production. It is a European's viewpoint and it is meant to provoke an integrated vision of the total process from early design to delivery of the finished product. It points out the increasing value and importance of innovative IT tools along the process chain and leads to radically new concepts for the production of the hull structure. The paper indicates a potential for substantial productivity gains resulting from further increased efforts in research and development.

KEYWORDS

Ship production, Design, Production simulation, Accurate manufacturing, Laser welding product data technology

1 INTRODUCTION

Ship production has an extremely long tradition and yet only in the last decades it moved from a handicraft type heavy industry to industrial processing in the current sense.

Ship production has many appearances depending mainly on the product and the number of products per time unit. The making of a large warfare submarine, a luxury mega yacht or a 250.000 tdw crude oil tanker have nearly no similarities with respect to the approach, the technologies and the methods.

This paper aims at discussing -by way of example- some future aspects of the production processes of commercial vessels for cargo transportation and passengers. It deals mainly with the production of the hull structure.

This segment of the market is closely connected to the world trade development and especially the seaborne traffic, which in the last decade increased from roughly 17.1×10^{12} ton miles to 21.5×10^{12} ton miles i.e. by 25%, (Fearnleys) leading to an increase in the world fleet development from 667 million tdw to 778 million tdw i.e. 16% (Lloyds Register). This increase in trade and fleet size is paralleled by an unprecedented development in new types of ships, new operating methods and last but not least rapid development of production technologies and methods.

Comparing the shipbuilding industry with others, which often in the public opinion are considered as technology pushers, one fundamental difference becomes apparent. Taking complexity of the product and time to market as parameters the following Figure 1 illustrates the problem.

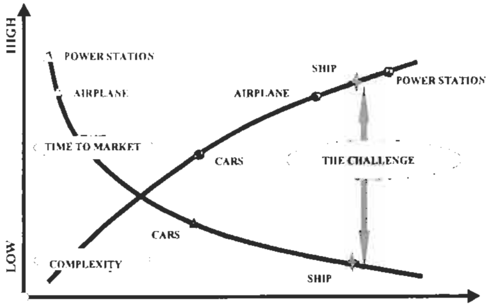

Figure 1: The Shipbuilding Challenge

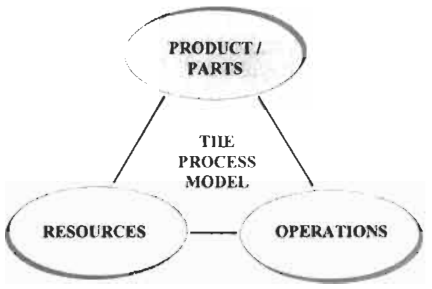

Figure 2: The Scalable Production Simulation Model

The high complexity of a modern Post Panmax container carrier, fully automated and with low crew, or a large cruise vessel compares easily with that of a modern airliner or a large thermal power station. However looking at the acceptable time to market the difference becomes evident: Time to market in shipbuilding is minimal and driven by the owners competitive demands always decreasing.

The gap between the two curves - complexity and time to market - is as I call it the shipbuilding challenge.

This challenge leads to the highest demands in concurrent engineering, design for production, distributed manufacturing and in innovative project control and management systems. Prototypes are not allowed. The prototype is the product. Zero Fault methods and processes are a necessity ('right first time').

2 INNOVATIVE IT-SOLUTIONS

Whereas in the past the production of ships was a relatively sequential chain of individual events at formally separate locations this is no longer possible in today's highly competitive market for various reasons:

- First and most important the clients have no time and want the product fast.
- Second and for the shipbuilder more important - the shorter the building period the shorter is the use of the very costly production facility and hence the resulting cost to the owner.

Simultaneous Engineering and Production (SEP) can be an answer but it is not enough. If the product definition phase - traditionally called design - is considered to be the first instance of generating of production related information, then it is obvious where and when the dialogue with production must start. Such dialogue however is meaningless if it is based on sketchy drawings and vague descriptions. This means innovative production methods require innovative early design i.e. product definition tools, based on consistent PDT.

Some years back the slogan "Design in Seven Days" (D7D) appeared. D7D means product definition from initial idea to basic structural lay out including global FEM analysis and production scheduling in seven working days. Today many researchers are trying to solve the underlying ambitions demand.

The link to production is simulation. Simulation in this context is the description of the total manufacturing process including the resources and operations necessary for assembling, machining, manufacturing and inspecting the product. This demands sufficient information about the product structure and its components in order to enable the modelling of fabrication sequences and their evaluation.

The modelling is based on a definition of the relationships between the elements of the product, the available or planned resources and the necessary operations as shown in Figure 2. By these definitions a scalable model can be obtained (electronic Bill of Process - eBoP).

For the use of this model a detailed analysis of the plant and the production process is necessary. The analysis in existing factories leads to an evaluation process, which also reveals the weak and strong points of the production line and the associated processes. The modelling leads additionally to considerations related to the necessity of single process steps or the avoiding of them. As a consequence of the introduction of simulation a deeper understanding of the complex relationship pattern of the many instances is generated.

The same simulation methods can be used in designing new or refurbishing existing plants. The decision making by the investor is then based on facts rather than promises or assumptions

Once the plant is modelled in the indicated manner the production process for an individual product can be simulated. Fig. 3 describes this in an abbreviated schematic view.

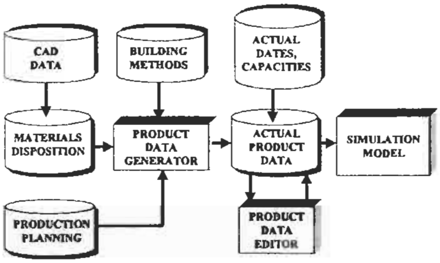
CAD DATA
BUILDING METHODS
ACTUAL DATES, CAPACITIES
MATERIALS DISPOSITION
PRODUCT DATA GENERATOR
ACTUAL PRODUCT DATA
SIMULATION MODEL
PRODUCTION PLANNING
PRODUCT DATA EDITOR

Figure 3: Data Flow for Production Simulation

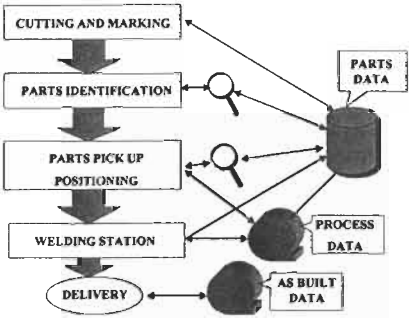
CUTTING AND MARKING
PARTS IDENTIFICATION
PARTS PICK UP POSITIONING
WELDING STATION
DELIVERY
PARTS DATA
PROCESS DATA
AS BUILT DATA

Figure 4: Series Production of Subassemblies

The model will yield information about bottlenecks (material, labour, plant etc.) but also information about the influence of design variants on production time and cost. Perhaps even more important: it creates a better and deeper understanding of the own production. The often discussed advantages of series production in shipbuilding, which basically are a result of more and better information downstream a line of series products, can now be harvested already in the first product. The gradient of learning curves is rapidly decreasing by adopting proper simulation techniques.

Typical calculation times for a medium sized Ro-Ro-vessel are in the order of 20 min, a time which allows for a true variant development and consequently also a qualified dialogue between all parties concerned. This can last but not least lead also to an improved dialogue between client and producer.

The modelling of plant and processes and finally the production is a task which can only be done in house. No software vendor can do the details; he can only supply good or better tools.

3 INNOVATIVE PRODUCTION

3.1 Accurate Manufacturing

The process chain analysis deals with the decomposition of the product and the subsequent detailed description of the production elements. This leads to a differential view of the individual elements with regard to productivity as defined above, i. e. the attempt to avoid all actions without contribution to the completion of the product.

Accuracy of production in steel hull fabrication is a target which may be used to demonstrate the new approach. Manufacturers of cutting machines are able to guarantee an accuracy of positioning of the cutting torch below 0,3 mm over a working area of for example 12m x 26m. This accuracy can be used to apply positioning marks or reference lines to the plates for further use in parts fitting.

In order to benefit from this low machine deviation the distance between cutting nozzle and marking torch must be kept constant. In reality however one may observe that due to changing geometric conditions in the plasma cutting head over time (anode burn out) the actual cutting line does not follow the theoretical one resulting in subsequent inaccuracies.

In consequence the efforts to increase cutting accuracy will yield no improvements if only the mechanical part of the machine is addressed. The real subject is the development of more accurate cutting nozzles of online accuracy control.

What is the effect of inaccuracies? Taking a buttweld in a 10mm plate with a design air gap of 2mm the increase of gap width by 2 times 0,3mm results in an increase in weld deposit of 30%. The unavoidable transverse shrinkage will increase correspondingly and will lead to stochastic buckling of the parts.

The only way to regain accuracy control is an on-line monitoring and control of cutting accuracy to below 0,1mm in the large plate cutting shop.

3.2 Autonomous Subassemblies Production

Another area in the production chain deals with the fabrication of small subassemblies consisting of flat plates and stiffeners. These are different in size and shape but principally they all belong to one "family". The production process of these can be regarded as series production and is likely to be fully automated. The following diagram illustrates this new subassembly factory concept.

From the cutting shops plates and profiles are moved into a parts recognition area where a camera identifies the parts by reading barcodes applied before cutting. The geometry information for these parts is taken from the CAD-database. In the next station the actual position of the plate on the conveyor is identified, in order to adjust the co-ordinates of the part to its actual random position.

Meanwhile a manipulator has picked up the stiffener profile(s) and positiones it onto the plate for tack-welding.

Once the subassembly is complete it is moved to the next station for robot welding. The last step is final measuring of contours of the subassembly and delivery of actual geometry data into the as built database.

One complete process step is avoided with corresponding gains in time and cost. By the use of such system marking work prior to or after cutting is not necessary and higher total accuracy can be achieved. The knowledge of the actual geometry of the subassemblies allows for process adjustments further downstream.

3.3 Laser Welding

This technology has been under discussion in the shipbuilding scene in Europe since the early nineties. Several large co-operative research projects dealt with the subject. The "Guidelines for Laser welding" by the Euracs-Classification societies are one of the results. All these early works considered CO_2 Lasers as the source of power. Meanwhile these Lasers have become very reliable and less expensive. As a result procedures for welding have been developed and some yards are using it in production.

Especially when working with relatively thin plate, like in passenger ship building, the advantages are very obvious. The very low heat input reduces thermal distortions to a minimum; rework for straightening becomes obsolete with consequential savings in process time and cost. Some yards quote 30% of all steelwork production hours as being rework.

However accuracy is not only to be achieved in the finished product; it is also a requirement in fitting the parts prior to welding because of the low tolerance of indigenous laser welding regarding gaps and steel composition. The idea to combine the sensitive Laser welding process with the more tolerant

GMA-process was an obvious answer. Several ways of combination were tested, of which the Hybrid Laser-GMA welding process showed the most significant advantages with respect to the mentioned tolerances and also regarding process stability and output performance.

The method shows very promising results again with thin plates (5-7mm) where welding speeds of more than 2 m/min can be achieved for one side full penetration welds. A typical process example is shown in figure 6.

The hybrid welding process can also be applied to fillet welding resulting in reduced angular distortions.

At this point in time one can state that Laser Hybrid welding with CO_2-Lasers and MAG is at the beginning of being state of the art.

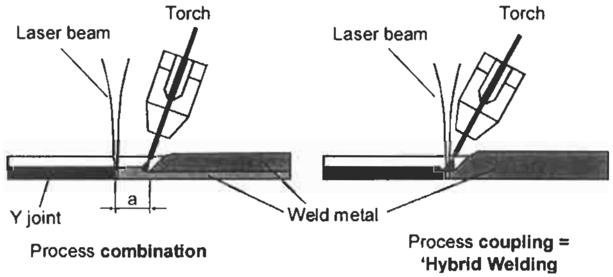
Laser beam
Torch
Laser beam
Torch
a
Y joint
Weld metal
Process **combination**
Process **coupling =**
'Hybrid Welding

Figure 5: Combination methods of GMA- and Laser Processes

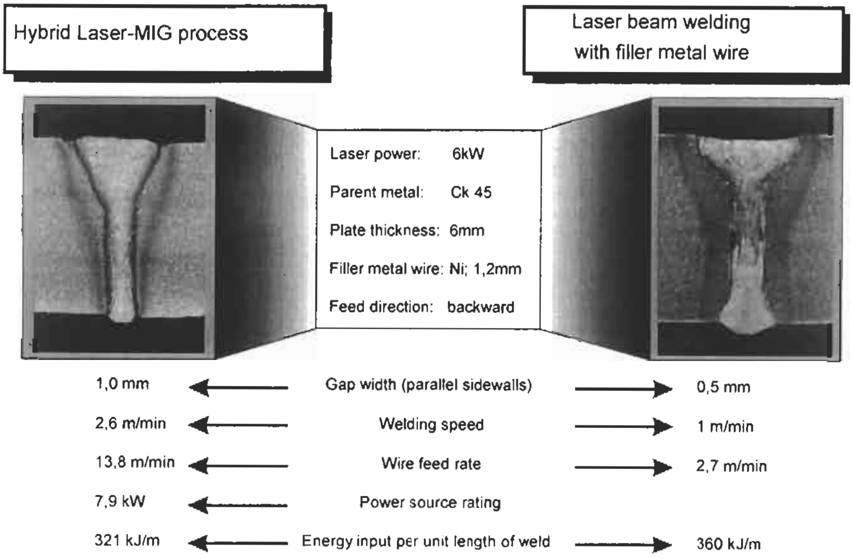
Hybrid Laser-MIG process
Laser beam welding
with filler metal wire

Laser power: 6kW
Parent metal: Ck 45
Plate thickness: 6mm
Filler metal wire: Ni; 1,2mm
Feed direction: backward

Hybrid Laser-MIG process		Laser beam welding with filler metal wire
1,0 mm	Gap width (parallel sidewalls)	0,5 mm
2,6 m/min	Welding speed	1 m/min
13,8 m/min	Wire feed rate	2,7 m/min
7,9 kW	Power source rating	
321 kJ/m	Energy input per unit length of weld	360 kJ/m

Figure 6: Comparison of Hybrid Welding with Laser Welding

The disadvantage of the CO_2-Laser is and will remain the relatively complicated beam handling systems. Due to its wave length of 10,6 µm the light can only be transmitted via mirror systems. This precludes the use of robots in large work spaces like in shipbuilding due to an excessive mechanical complexity of the beam handling systems.

But there are alternatives and the future of Laser-welding in that respect is just beginning: There are the Nd-Yag-Lasers and there will be the Diode Lasers. Here the wave length of the light is only 1,06 µm or slightly less. This makes the use of fibre-optics possible and consequently the beam handling is reduced to a flexible strand of fibres which easily can be fixed to a robot arm. In addition Diode Lasers will be very small as compared to what we are used to today as shown in Figure 7. By stacking a number of bars and combining several of these stacks into one unit the required output can be achieved. Today diode lasers with an output of 6 kW are available. The beam quality however is still a problem which needs to be solved.

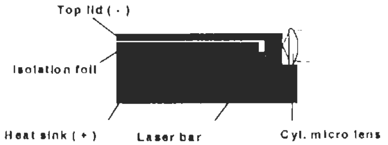
Top lid (-)
Isolation foil
Heat sink (+)
Laser bar
Cyl. micro lens

Cylindrical micro lenses for divergence concentrating and parallel beam

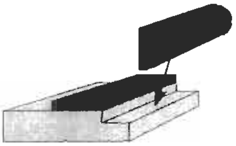

Micro assembling through adjusting glue

Figure 7: 50 W Diode Laser bar (28 x 13 x 1,5 mm)

Another present draw back is the cost and even the availability of stable high power diodes either as pump source or for direct Diode Lasers. The development work in this area is progressing fast and the following may illustrate a possibility for innovative production.

Earlier the concept of the fully automated sub-components line was developed. Here one can continue. The concept of "remote welding" may be an answer, provided a high beam quality as defined by the beam parameter product (θ_0 x w_0 mmxmrad) is achieved. Beam transmission without fibres can be arranged merely with optical systems i.e. zoom lenses and mirrors. Figure 8 illustrates the system set up.

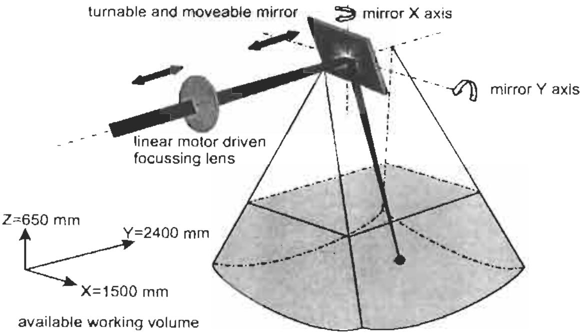
turnable and moveable mirror
mirror X axis
mirror Y axis
linear motor driven focussing lens
Z=650 mm
Y=2400 mm
X=1500 mm
available working volume

Figure 8: Principle of Remote Welding

Such arrangement could also be applied to long fillet welds in a panel line or even for egg box welding with a moving laser power source. This means that finally optronics are finding their way into the shipbuilding world.

It should not be forgotten that this is still along way and many problems not the least in the field of work safety are to be solved.

4 INTEGRATION ASPECTS

The new fabrication technologies and methods require considerable efforts regarding the integration of suitable IT- and Communication tools and systems. The individual special software solutions need to communicate often down to the shop floor level in a reliable manner and without loss of information. This parts highest demands on Product Data Technology (PDT) which in spite of all efforts over the last 15 years is still far from a common solution. The ISO-STEP approach created hopes and visions but the detailed problem solutions are only partially ready for use. If world leading CAD-vendors are not integrated the practical merits are questionable.

New solutions, which are independent from specific application systems, are appearing which use technologies offered by the world wide web (www). Some applications are already in use like digital document exchange between the yard and the classification society.

The requirements on PDT from the production technology point of view are manifold. In the planning stage detailed information about parts and processes are needed for the production simulation. As long as only the steel part is considered this is relatively easy; the additional inclusion of outfitting and machinery increases the complexity due to the large number of information suppliers.

A new task evolves from the necessity to update as built information along the process chain in order to adjust downstream process data according to the as built situation. The problem addresses the integration of sensor technology and data, CAD data and process data in a real time environment. Several research projects are presently ongoing in this particular problem scenario.

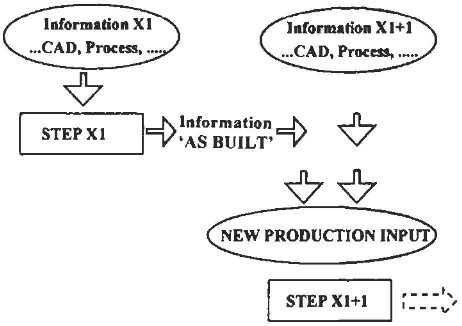

Figure 9: Principle of the Product State Model Approach

5 CONCLUSIONS

The paper has addressed only a few of the many upcoming new aspects of ship production. The underlying vision shows that ship production is still quite far away from harvesting the potentials which new technologies and methods can offer. Due to the special challenge of the industry new and more efficient solutions can not be purchased in the market or simply copied from other sectors. The innovations must be developed in house because only then a full understanding of the complexity and the interactivity is generated. On the other hand innovation requires also intense co-operation with other industry sectors, provided however the benefits are also transsectorial. The development of Laser technologies or of IT-CT-solutions are typical examples.

Practical Design of Ships and Other Floating Structures
You-Sheng Wu, Wei-Cheng Cui and Guo-Jun Zhou (Eds)
© 2001 Elsevier Science Ltd. All rights reserved

NEW PRODUCTION SYSTEM FOR VESSELS OF COMPOSITE MATERIALS USING AN ADJUSTABLE MOULD

Jong Oh Kwon[1], Jaesung Kim[1], Jung Chun Suh[1], Hyochul Kim[1]
Seung Hee Lee[2], Young Gill Lee[2], Kisung Kim[2], Jae Wook Lee[2]
Jae Moon Lew[3], Sanghong Lee[4], Jae Kyu Lee[4], Dae Sun Kang[5], Duk Soo Chung[5]

[1] Department of Naval Architecture and Ocean Engineering, RIMSE
Seoul National University , Seoul 151-742, Korea
[2]Department of Naval Architecture and Ocean Engineering, Inha University
[3]Department of Naval Architecture and Ocean Engineering, Chungnam National University
[4]Design and Research Center, Advanced Marine Tech.
[5]Korean Society of Ship Inspection and Technology

ABSTRACT

Hull form of a typical planing boat can be easily modified into a set of developable surfaces with minor modification. Then, the surfaces are developed onto a plane to manufacture thin laminated FRP plates on a flat bed. The plates are bended in an adjustable mould system defined by line elements to form the hull form. In the procedure, ruling lines are used as line elements representing the hull. Battens made of circular pipes are attached along the line elements and t-heir exact shapes and locations are maintained by wires and pin jigs. The plates are link together to complete the hull shape and additional laminas are stacked inside until necessary thickness is obtained. In order to verify the proposed method and to identify the possible flaws, a 1/3 scale model is constructed on the adjustable mould. The hull surface is divided into several pieces and developed onto aplane surface. At the fore body portion front of the 6th station, the hull shape varies rapidly in most case-s and a full scale mock-up of the fore body part has been constructed using 3mm plywood to evaluate t-he construction techniques morecarefully. It is found that the new production procedure can be successfully applied for the construction of planning vessels made of fiber reinforces plastics.

KEYWORDS

Adjustable mould, Developable surface, Fiber reinforced plastic, Planing boat

1 INTRODUCTION

Fiber-reinforced plastic (FRP) is a composite material with excellent physical and mechanical properties and relatively impervious to the degrading effects of a marine environment. There aremany potential advantages of FRP over other materials for small craft construction, such as the higher strength, the lower maintenance and the lighter weight etc. (Edmunds, 1999) However construction of the hull, deck or other structures of a ship usually necessitate a mould to mantain a desired shape by supporting laminas until completely cures. The method is suitable for the mass production of identical boats but even the minor variations in shapes to meet owner's requirements is not easy to achieve. To construct a ship of different shape, new mould should be constructed again and resulting higher cost and longer construction period.

The philosophy of using developable surfaces for ship hull construction has initially applied towarships to reduce construction costs and times. Application of the same idea to the merchantship has been carried out at Burmeister & Wain Shipyard recently. They reported 20% reduction in man-hours required to produce a hull that implements developable surfaces in its design.(Norskov & Lauritsen, 1985) It is well known that the use of a developable surface has several advantages over conventional one including lower labor costs in construction, smaller capita investment in equipment, ease of repair and simple tools for construction.(Calkins etc., 1989)

Applying the developable surface concept in steel ship, the hull surface can be formed by simple bending and welding of the developable plates. Using the same method in construction of a FRP ship needs extra stacking of laminas to obtain an adequate strength. Unlike the traditional FRP construction method using a mould, a new construction method using an adjustable mould is proposed in the present paper. In the method, hull surfaces are developed onto several plane pieces and thin FRP plates identical to the pieces are manufactured on a flat bed. The plates are simply bended along the generation lines to form the three-dimensional hull shapewith help of an adjustable mould. The construction of the ship is completed with additional stacking of FRP to obtain the required hull strength. The present paper briefly introduces a newmethod for FRP boat constructions and an adjustable mould including a newly designed jig system.

2 HULL DEVELOPMENT

A new effective and productive method for building small FRP fishing boats and planing boats is proposed in this section. The new method is applied to the construction of a small FRP fishing boat of 3 ton class. Figure 1 shows a typical fishing boats and Figure 2 shows the new hull form consists of developable surfaces. The box keel and the spray strips shown in the Figure 1 can be treated as appendages, therefore and hence only the main hull is drawn in Figure 2. Modification of the parent hull into the developable one, minor changes in the hull shapes are inevitable but the principal characteristics of the parent ship are almost preserved as shown in Table 1. Model tests are carried out at the speed of 15 knots to compare the resistance characteristics of the ships. It is found that the resistances of the ships are almost identical.

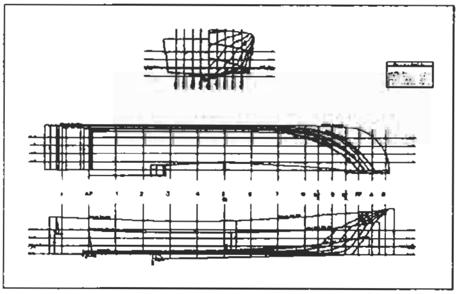

Figure 1: 3 Ton class parent hull

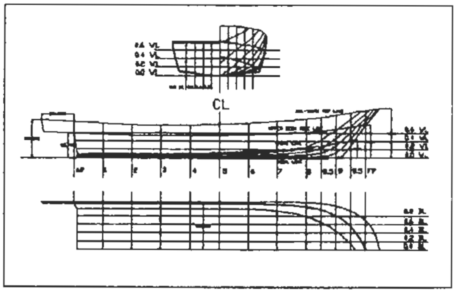

Figure 2: Lines of the developed hull

Figure 3 shows a drawing of typical developed plates of a planing hull.The plate between the keel and chine line is developed by the Apex method and the other two plates are generated by a Bezier surface method. (Yoon etc., 2000)

TABLE 1

PRINCIPAL PARTICULARS OF 3 TON CLASS BOAT

	Parent Hull	Designed ship	Change (%)
Length O.A.	8.15 m	8.14 m	-0.12
Length B.P.	6.5 m	6.5 m	0
Breadth (mld)	2.2 m	2.2 m	0
Draft (designed)	0.2 m	0.2 m	0
Displacement	1.68 ton	1.65 ton	-1.8

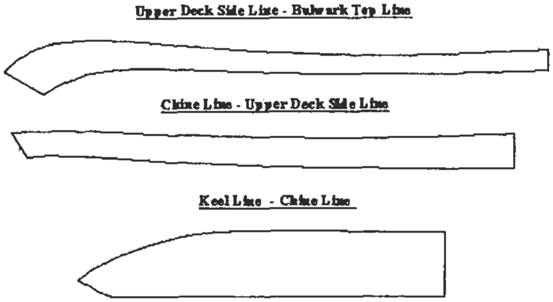
Upper Deck Side Line - Bulwark Top Line
Chine Line - Upper Deck Side Line
Keel Line - Chine Line

Figure 3: Developed plates of a typical fishing boat

3 CONSTRUCTION OF FRP BOAT

3.1 Configuration of the System

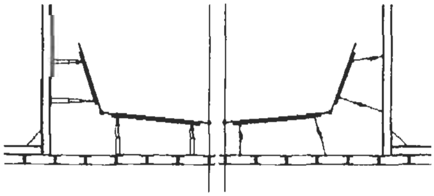

Figure 4: Schematic diagram of the adjustable system (side view)

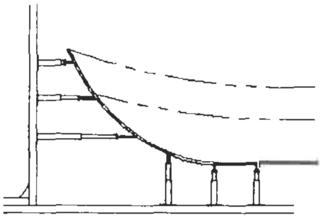

Figure 5: Schematic diagram of the mould system (transverse view)

An adjustable mould system is constructed on a precision bed as shown in the above figure. The frames of the mould are used as a reference frame when constructing the ship with composite materials. The procedures for construction of FRP ship on the adjustable mould are shown schematically in Figures 4 to 6. On the surface of the flat bed, vertical posts are installed firmly.

Vertical and horizontal pin jigs as well as metal rings for wire connections are attached on the surface of the mould and the vertical posts, respectively. Developable hull surfaces can be represented by the line elements. Battens made of circular pipes are attached along the line elements and their exact shapes and locations are maintained by wires and pin jigs. The plates are link together to complete the hull shape and additional laminas are stacked inside until necessary thickness is obtained. The battens are aligned with the line elements and their shapes are maintained by the pulling of the wire and the pushing from the pin jig.

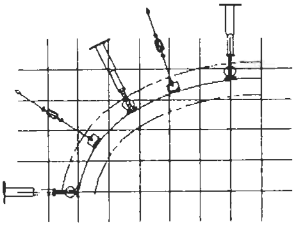

Figure 6: Top view of hull form

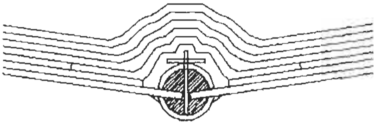

Figure 7: Joining method of developed plate

The Velcro attached on the hull surface prevents damages from wires and pin jigs. Number of the battens for definition of hull shape should be minimized to improve the productivity. Inner parts may help deforming the plate but is not recommended because bonding and stacking of extra layers inside is necessary in the procedure. The thickness of the plate should be determined carefully since the plate should be thin enough to deform hull shape easily in the elastic range but thick enough not to have excessive distortion during inner stacking and curing process. Stacking process is carried out inside of the developed pieces laid on the flat bed. To allow a scarp joint between the neighboring plates stacking should be planned to have thicker layer at the center and thinner on the boundaries. The developed pieces are bended in the elastic range to represent the hull shape and neighboring plates are assembled with mechanical devices as shown in Figure 7. The strength of the assembled plates shown in Figure 7 is not enough and so additional inner stacking process is necessary to guarantee adequate strength of the bonded plate. Box keels, strakes, spray strips and etc. are attached on the hull surface by the secondary bonding to complete the construction of the FRP boat.

3.2 Mock-up Test for Verification of the Construction Method

A 1/3 and a full scale models are constructed to verify the proposed method and to identify the possible flaws of the method. The hull surface is divided into several pieces and developed into a plane surface. Stacking processes for each piece should proceed cautiously not to cross over the bounding curves since each piece will be trimmed along the curves before the resin being completely cured and Figure 8 shows the procedure. Since the whole process of stacking laminas can be done on the flat bed, efficiencies go up with improvement in working condition, resin consumption downs and uniform quality can be maintained. The trimming of boundaries of the developed pieces before complete curing will improve environmental condition of ship yards by reducing dust production and since the scraps may be pressed to have less volume.

The 1/3 scale pieces shown in Figure 8 can be deformed within the elastic limit to form a developable hull perfectly as shown in Figure 9. At the fore body portion front of the 6th station, hull shape varies rapidly and a full scale mock-up is need to be constructed for evaluation of the construction techniques more carefully. However, construction of the fore body is the most difficult part of the process and hence a production precision bed is manufactured with I-beams to have uniform spacing of 500mm and a total working space of 4,000 mm× 4,000 mm. The pin jigs made of pipe are installed

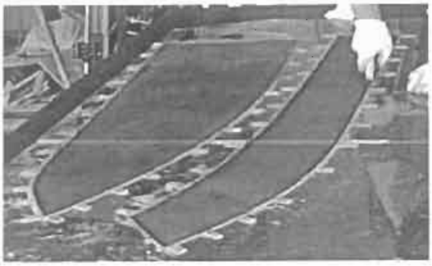
Figure 8: Trimming of boundary of developed piece

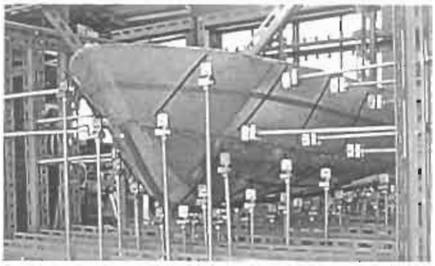
Figure 9: 1/3 scale mock-up

on the precision bed and designed to easily adjust their lengths. The length can be fine controlled with a screw attached at the end. Figure 10 shows the line elements installed with pin jigs and vertical members to define the hull geometry. It is seen also that special devices for jointing both halves are also installed along the centerline. In this mock-up, the hull plate is manufactured with plywood of 3mm thick instead of FRP plates for real ships. Each piece is fitted to corresponding parts of the hull surface with simple unidirectional bending. Figure 11 shows the competed hull shape in which new production procedure is successfully applied in representing the hull form even for the lower portion of the bow where curvature changes most severely. To represent the bow-lower part, however, special consideration in spacing and directions of the line elements and pin jigs are necessary. A structural analysis on the deformation process is necessary in that a plane FRP plate of uniform thickness being shaped into developable surfaces to consist a hull within the elastic limit. The ruling lines may be used as line elements for hull representation.

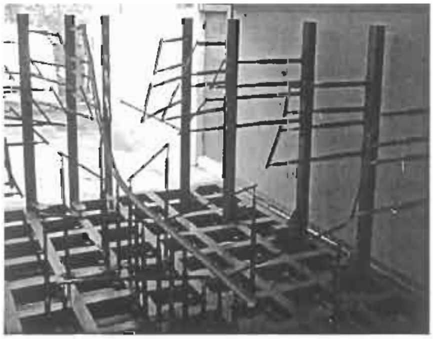
Figure 10: Pin jig and line element

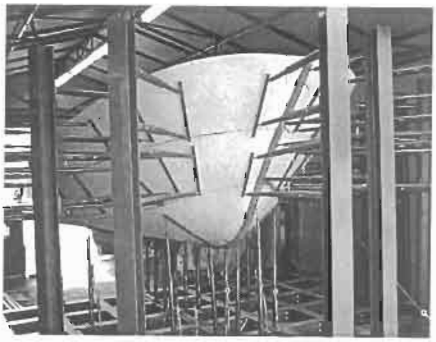
Figure 11: Bow shape supported by line elements

The plates should be thin enough to allow elastic deformation of the most severe curvature of the hull. And the number of line elements used for defining the hull shape should be minimized since the plates are to be deformed by applying force along the line. In the deformation process, the first loading point should be fixed in the space to be an origin of the process. If the thickness of the plates, arrangement in line elements and/or location of the origin are inappropriate, warping on the bounding contours will occur. After forming hull surface with the deformation process described above, the neighboring plates are jointed together and layers of laminas will be stack inside.

It is advised to carefully monitor deformations with optical devices since those occur during the cure of extra layers may spoil the accuracy in representing the hull shape. The roller used in the stacking may cause deformation also if the thickness of the plate is too thin. A new production procedure is possible in that line elements are placed on the ruling lines in the deformation process and after that structural members are placed simultaneously with inside stacking to maintain geometrical accuracies.

4 CONCLUDING REMARKS

A new method for construction of a FRP ship is proposed. In the method, hull shape is defined only by the line elements and conventional moulds for FRP construction method are not used. A 1/3 scale and a full scale mock-ups of a bow portion is manufactured on a proposed pin jig production system to identify and solve the difficulties for practical use. The major conclusions of the present paper are as follows:

(1) A typical hull form of a fishing boat can be developed without any changes in naval architectural characteristics by combining the Apex method and the Bezier surface method.
(2) Since the whole process of stacking laminas can be done on a flat bed, the loss of materials can be minimized and FRP plates of uniform qualities produced. Environmental hazard can also be reduced with improvement in trimming and scrap handling process.
(3) The shape of a developable hull can be represented by line elements placed along the ruling lines and supported by pin jigs attached on the precision bed. It is possible that the system can be used as an adjustable mould for deformation of plane plate to form a hull shape, if the number and rigidity of the elements are enough.
(4) The construction of a ship is completed if adjacent hull surface pieces are joined together and additional laminas stacked inside to have a necessary thickness. With the procedure, time and cost needed for mould construction can be eliminated.
(5) In the construction procedure, optical monitoring of the deformation occurs during the curing process is possible. The measurement will help final finishing of the hull surface after hardening.

Acknowledgement

This work was supported by the Ministry of Maritime Affairs and Fisheries. The authors thank to the graduate students, Mr. J. Jang, Mr. H. Ahn and Mr. J. Oh supported by BK 21 project for their help.

References

Arthur Edmunds. (1999). *Building a Fiberglass Boat*, Bristol Fashion Publications
Calkins D.E., Theodoracatos V.E., Aguilar G.D. and Bryant D.M. (1989). Small craft hull form surface definition in a high-level computer graphics design environment. T. *SNAME* **97**, 85-113.
Kim Byung Chul and Ha Chang Gil. (1997). The new method of FRP boat. *Korean Intellectual Property Office, Patent Application No. 97-38729*
Kim Hyoungki, Kwon Jongoh, Kim Jaesung and Kim Hyochul. (2000). An experimental study on optical measurement of deformation of hull surface element, *Proceedings of the Annual Autumn Meeting The Society of Naval Architects of Korea*, 261-264.
Kim Hyochul, Kim Jaesung and Lee Jaekyu. (2000). Mouldless method of construction of FRP Boat, *Seminar on the new method of construction of FRP vessel*, 84-94.
Kim Hyochul, Advanced Marine Technology Ltd. (2000). Method for production of vessels with composite material using on an adjustable mould. *Korean Intellectual Property Office, Patent Application No. 10-2000-0052754*
Lee Jaekyu, Kim Jaesung, Kwon Jongoh and Kim Hyochul. (2000). A production system of vessels with composite materials using on an adjustable mould, *Proceedings of the Annual Autumn Meeting The Society of Naval Architects of Korea*, 84 – 87.
Norskov and Lauritsen O. (1985). Practical Application of Single Curved Hull Definition-background, Application, Software and Experience. *Computer Applications in the Automation of Shipyard Operation and Design V, Elsevier Science* **11**, 485-491.
Yoon S.-H., Lee S.-H. and Lee Y.-G. (2000). A Study on the Hull Form of Developable Fishing Boat. *Proceedings of the Annual Spring Meeting of The Society of Naval Architects of Korea* , 88-91.

Practical Design of Ships and Other Floating Structures
You-Sheng Wu, Wei-Cheng Cui and Guo-Jun Zhou (Eds)
© 2001 Elsevier Science Ltd. All rights reserved

MOBILE AGENT BASED SUPPLY CHAIN MANAGEMENT IN SHIPBUILDING INDUSTRY

Jing-Yun Cheng, Bei Lu and Sheng-Kun Zhang

School of Naval Architecture and Ocean Engineering Shanghai Jiao Tong University
Shanghai, 200030, China

ABSTRACT

Now China shipbuilding industry faces the following serious problems: low productivity and long construction period. In order to cope with it, a mobile agent based supply chain management solution is provided. Firstly, summarizes the related research of supply chain management and intelligent agent and their application in shipbuilding industry. Secondly, a general commerce model which was developed by HAAS School of Business is used to design a shipbuilding supply chain management. Then implements a prototype which is based on IBM Aglet – a mobile Java agent development kit. The paper ends with some conclusions and suggestion for future research.

KEYWORDS

Shipbuilding, Supply Chain Management, Mobile Agent

1 INTRODUCTION

Shipbuilding is a typical make-to-order manufacturing, which is very complex and complicate. In order to survive in the competitive global shipbuilding market, each shipyard tries its best to take measure to decrease the cost, enhance the quality and etc. For shipyard in China, the difficulties confronted with are more serious. For example, in 1980s, the cost per tonnage is about 30 percent to 40 percent lower than shipyard in Japan. But since 1992, with the increasing of the cost of material, marine equipment and work force, then the shipbuilding cost has been increasing with 16.9 percent per year. Moreover, in other aspects such as quality, just in time delivery and level of management & technology, Chinese shipyard lags Japan, Korea, and European shipyards.

How can we cope with these challenges? In current global agile competition environment, only the enterprise who can put a stress not only on high quality, productivity, and reduced cost, but also on the ability to react quickly and effectively to changes in markets. During the implementation of agile manufacturing, supply chain management (SCM) has been utilized widely, which can reduce the cost, improve the productivity and efficiency of management, and shorten the period of product's R&D. In the commercial shipbuilding, according to statistics and ERIM research[5], the cost of material and equipment is about 50 percent of a delivered commercial ship, the percentage will be 75 higher in the passenger liner. So decrease the purchasing cost, simplify the procedure, and implement just in time purchasing is the critical factor to the enterprise. In shipbuilding industry, more and more shipyards begin to realize the importance of supply chain management. Japan, Korea and USA have initiated the related research on SCM and its implementation.

In this paper, 4 parts are divided. Section 2 of this article reviews the research on supply chain management and intelligent agent. Section 3 analyzes the business process model in shipbuilding SCM and designs the agent based supply chain. Section 4 brief describes the implementation of the prototype of a shipbuilding supply chain management system which based on mobile agent technology – IBM Aglet, the prototype mainly focuses on the purchasing of the material and marine equipment in the global market. Finally, the conclusion and future research is provided in section 5.

2 RELATED RESEARCH

Supply chain management began in 1980s. Supply chain management focuses on systems and processes to support the flow of information within and between organizations which occurs in the context of procurement, manufacturing, sales, distributions of goods, information and services [10]. The dynamic, unpredictable business environment of today further demands considerable process flexibility along the supply chain as a firm's set of commercial suppliers, customers, trading partners and even strategic allies – together defining its supply chain topology - may now shift both abruptly and frequently. In SCM, traditional EDI lacks the flexibility and efficiency required for the state of art electronic business. Even such web based e-commerce applications do not satisfy these joint requirements for process integration and flexibility, as most of web based supply chain technologies fail to closely integrate buyer and seller processes, they are developed predominately for either the buyer or seller, but not both [4].

Fortunately, recent emerging technology - Intelligent Agent provides the potential and capability for buyer-seller integration and flexibility in SCM [11]. There are many definition of intelligent agent, but at here, agent is defined as a component of software and/or hardware which is capable of acting exactingly in order to accomplish tasks on behalf of its user. It has the following attributes [11].

- Autonomous
- Social function
- Reactive
- Proactive
- Mobile

Fox [6] firstly use cooperative agent network to represent the supply chain, in which each agent represent one or multi function of supply chain, and coordinate with other agents to reach the optimal status. Swaminathan[11] use a multi agent framework to model the supply chain, in which exist two categories of element: structural elements and control elements. Structural elements including production elements (retailers, distribution centers, plants, suppliers) and transportation elements are modeled as agents. Control elements (inventory, demand, supply, flow and information controls) are used to help in coordinating flow of products in an efficient manner with the use of messages. Brugali[3] use the mobile java agent in supply chain management, which facilitate the enterprise response to the market's change, and optimize the whole supply chain. P.Dasgupta[8] use Java mobile agent technology to build a networked electronic trading system. T.Weitzel[12] provide an XML based B2B communication architecture that provide the solution to expensive and inflexible EDI connections.

There are many complex processes in shipbuilding industry, now more and more focus is put on SCM. Korea shipyard has initiated a project of electronic supply purchasing system. In USA, the

Shipbuilding Partners and Suppliers (SPARS) Consortium is established to deploy shipbuilding Supply Chain Virtual Enterprise which will integrate the shipbuilding supply chain composed of customers, partners, subcontractors, and suppliers. J.K.Lee[16] used intelligent agent in the scheduling system for shipbuilding In general, SCM in shipbuilding lags other industries, and has the following attributes[5].

- SCM in shipbuilding is hampered by a lack of consensus on the structure, function and dynamics of the integration of ship production and SCM.
- Shipbuilding lags in the use of electronic commerce technologies.
- Inaccurate production schedules affect many aspects of supply chain management, including increased supplier costs, problems with timeliness and completeness of vendor-furnished information, and diminished trust between the yard and its suppliers.
- Although people begin to implement SCM in shipbuilding industry, but not all shipyards realized its importance. Especially in China, no much focus even in the mind of manager of shipyard, the relation between shipyards and their suppliers is more adversarial than necessary, not win-win.

3 MODELING THE AGENT BASED SUPPLY CHAIN MANAGEMENT

Since SCM involves a set of activities in and between enterprises. It is necessary and convenient to analyze the process of SCM via a commerce model. This Commerce Model was originally developed for one of the prototypical courses on electronic commerce at the Haas School of Business and pertains to commerce in general[14]. See the figure 1, it consists of buyer, intermediary, seller, and a series of activities and interactions. The diagram depicts the process flow (from left to right) associated with a commercial relationship or transaction, a transaction or relationship can be seen to progress through each step along the process flow depicted in the model. Clearly these steps represent commerce at a very high level

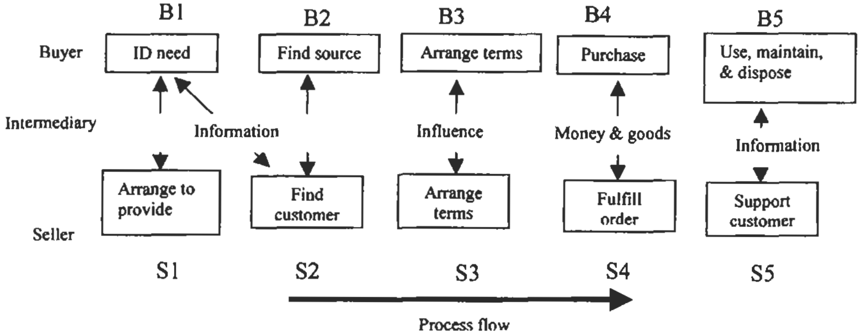

Figure1: General Commerce Model

From the buyer's perspective, the process begins with the identification of some need and proceeds through sourcing and purchasing to the use, maintenance and ultimate disposal of whatever product, service or information is purchased. The seller's process begins with some arrangement to provide a product, service or information (e.g., research and development, service process design, information acquisition, etc.) and proceeds through marketing and sales to customer support. The arrows connecting these high-level process steps are used to represent key items of exchange between buyer and seller, items which constitute the commercial activity proper. For example, information is exchanged at several points along the process flow, as are money and goods (or services, information, etc.) and even "influence," as delineated at the negotiation stage. In the actual activity, each the higher activity can be divided into sub-activity. For example, the fulfilling order can be divided into the receiving order, notifying the shipping and logistics schedule and so on. Moreover, many activities can be inserted into the buyer and seller, such as factory, warehouse, vendor, and financial department. Through the above two methods, the user can design any complicated SCM according to their need.

In the shipbuilding enterprise, the effective method in SCM is to purchase the steel, paint, marine apparatus and other materials according to the production schedule in the global market, and then reach the goal of purchasing under request, zero inventory and speeding the production. Based on HASS commerce model, we design an agent based SCM in shipyard. (See the Figure 2) The whole supply chain consists of user, an intermediary supply department and seller. The user represents different department in shipyard, such as design, engineering analysis, manufacturing, finance and other departments. The supply section represents various users, purchases on behalf on various needs. The seller is the suppler who can provide shipyard with the need product. They locate in worldwide. The whole enterprise activity consists of two flow, purchasing and fulfillment.

As shown in Figure 2, the commerce model is expanded to meet our need. For example, B1, B2 is divided into a series of activities, exchanges among the use, supply and seller. Such as market survey, complete PR form, research resource. Among, exchange internal to the organization is represented with X2', X5'. At the same time, the buying activity is divided and extended to the following activities (analyze the price, select resource, sign the order and receive product and make payment)

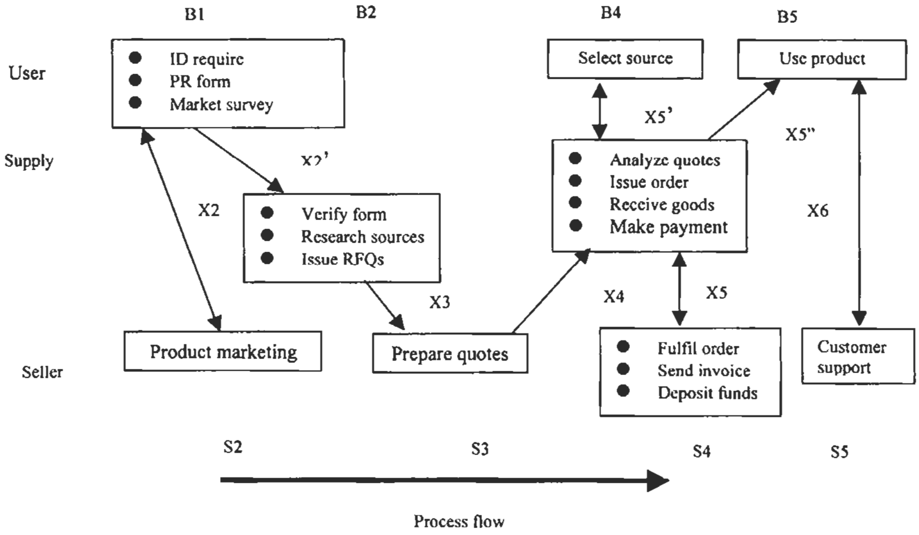
B1
B2
B4
B5
User
Supply
Seller
ID require
PR form
Market survey
Select source
Use product
X5'
X5"
X2'
X2
Verify form
Research sources
Issue RFQs
Analyze quotes
Issue order
Receive goods
Make payment
X6
X3
X4
X5
Product marketing
Prepare quotes
Fulfil order
Send invoice
Deposit funds
Customer support
S2
S3
S4
S5
Process flow

Figure 2: Enterprise Supply Chain Process

4 PROTOTYPE

Mobile Java agent –IBM Aglet is selected in our prototype of SCM, since the suppliers in shipbuilding SCM are located worldwide, and in current network band, the mobile agent can keep the data integration and security, combined with other characteristics, it can meet the need of agility of enterprise[2,8]. Moreover, IBM Aglet is free to use according the license.

Aglets are Java objects that can move from one host on the network to another. That is, an aglet that executes on one host can suddenly halt execution, dispatch to a remote host, and start executing again. When the aglet moves, it takes along its program code as well as the states of all the objects it is carrying. A built-in security mechanism makes it safe to host untrusted aglets. The details of IBM Aglet please refer to its ASDK[12].

In the implementation of supply chain, we simplified the purchasing process into 8 activities:

- Fill the buying request
- Verify the form
- Research resource
- Issue the RFQ
- Prepare the quotes
- Analysis the quotes
- Issue the order
- Use product

The fulfillment process can be simplified into 5 activities:

- Prepare quotes
- Arrange production
- Fulfill order
- Send invoice
- Customer support

The above activities include the major processes in the supply chain. As figure 3 show, the whole system consists of 3 parts, use, the buyer's subsystem and supplier's subsystem. This sub system can be exchanged. During the buying, customer can fill the order according the requirement of production planning and scheduling, send it to the intermediary- the buyer department of shipyard, then verify and integrated the requirement of different section, and form the buying list. This list is written with XML, which include:

- the price of product
- the highest available price
- the amount of product
- delivery time
- the URL for supplier
- the ID of supplier
- the ID of product for supplier

The buyer's subsystem consists of stationary agent, mobile agent, the potential supplier information and temporal log for recording transaction. The potential supplier information is acquired through research resource, market analysis, also it can add the new supplier to the information of supplier. The database of temporal transaction save the price and temporal transaction log when the mobile agent move, it's used for the final analysis. The seller subsystem consists of the stationary agent of supplier, the database of current supplier inventory, and interface of database and transaction log. The stationary agent is responsible for the transaction with buyer mobile agent, accept its price, and retrieve its inventory and its production plan to decide whether sign this transaction.

In the actual running, when supply department of shipyard verify the form, the buyer stationary agent firstly create a mobile agent, pass the mobile agent with the information from the list and supplier information. Mobile agent then visits every supplier according to the supplier information, the quantity of product and standard. During the negotiation, the standard of purchasing can be one of the following according to the different need, such as price, delivery time, or the combination of them. When the buyer's mobile agent arrives at the supplier, it has an interaction with seller agent. So seller agent can retrieve to decide whether the price meet the need, then reaches the temporal transaction, and the buyer builds the new proxy agent and returns the information to the buyer stationary agent, then visits the next supplier to go the same procedure. When the agent finished the prescribed itinerary. The buyer's agent select the optimal choice, sign the contract, for that is not optimal price supplier, cancel the proxy agent and temporal transaction, and pay the corresponded penalty money. Through this agent, the supply department can execute the purchasing based on their production scheduling. (The detailed implementations please see [15])

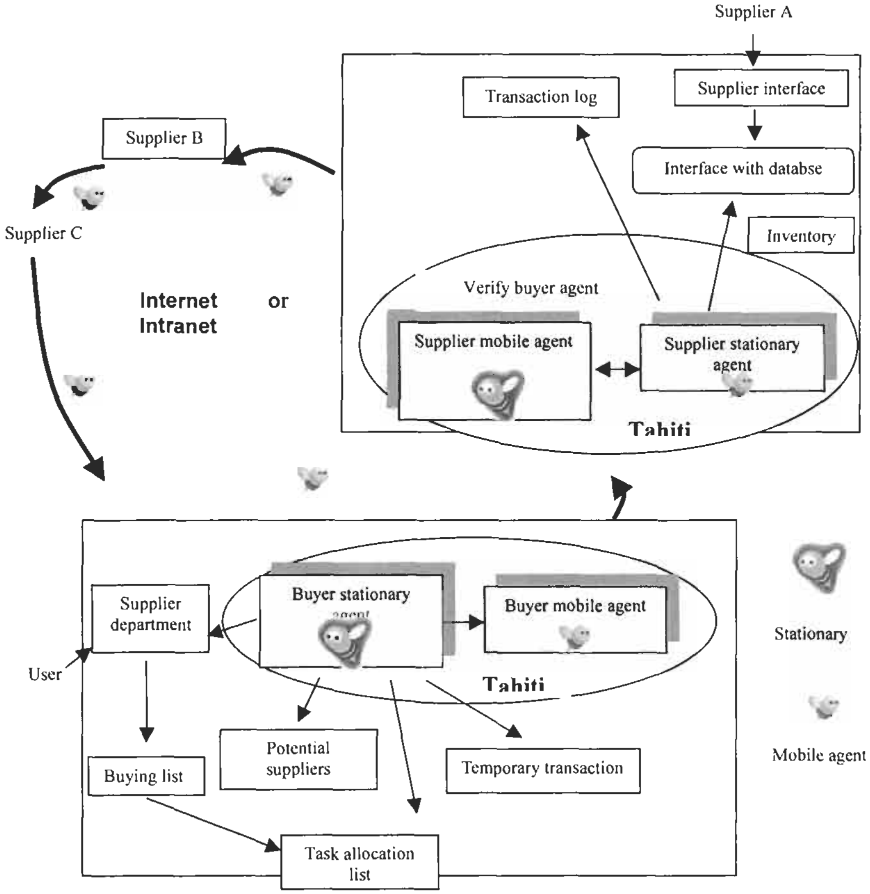
Supplier A
Transaction log
Supplier interface
Supplier B
Interface with databse
Supplier C
Inventory
Verify buyer agent
Internet or Intranet
Supplier mobile agent
Supplier stationary agent
Tahiti
Supplier department
Buyer stationary agent
Buyer mobile agent
User
Tahiti
Stationary
Potential suppliers
Buying list
Temporary transaction
Mobile agent
Task allocation list

Figure3: The Architecture of Mobile Based SCM

5 CONCLUSION

The paper researches the agent based supply chain management in shipbuilding industry, a general commerce model is used to model and design the supply chain management, and implement a prototype of SCM. From the above, mobile agent based supply chain can reduce the cost, inventory, shorten the production period, and finally reach the agile manufacturing. From our implementation, the result is encouraging, especially suitable for the global purchasing. But this system is quite simple, and currently the supply chain is mainly on purchasing. so the future research is mainly on the following,

1) In the shipbuilding SCM, quantitative and correct production plan and its executing is an important factor, so integration of supply chain management and production plan system is the next major research.
2) The dynamic attributes of supply chain management, such as later delivery, the quality of product will have a great impact on the whole SCM. So it's necessary to implement research on simulation of its dynamic attributes.

Acknowledgments

The author would like to thank Professor Mark.E.Nissen (Naval Postgraduate School, USA) for his suggestive discussion and kind assistance in the research.

References

1. Gebauer J., Buxmann P. (1999). Electronic Commerce and Supply Chain Management. *Proceeding of the 32nd Hawaii International Conference on System Sciences.*
2. Kiniry J., Zimmerman D. (1997). A Hands-on Look at Java Mobile Agents. IEEE Internet Computing.
3. Barbuceanu M., Teigen R., M.S.Fox. Agent Based Design and Simulation of Supply Chain Systems. *Proceeding of IEEE.*
4. Nissen M.E. (1999). Supply Chain Process and Agent Design for E-commerce. *Proceeding of the 32nd Hawaii International Conference on System Sciences.*
5. Fleischer M., Kohler R., Lamb T., Bongiorni H. B., Tupper N. (1999). Final Report of Shipbuilding Supply Chain Integration Project. *Environmental Research Institute of Michigan.*
6. Fox M.S., Chionglo J.F., Barbuceanu M. (1993). The Integrated Supply Chain Management System. Internal Report, Dept. of Industrial Engineering, Univ. of Toronto.
7. Mehra M.Nissen. (1998). Case Study: Intelligent Software Supply Chain Agents Using ADE. *Proceeding of 1998 AAAI conference workshop on software tools for developing agents.*
8. Dasgupta P., Narsimhan N., Moser L.E., Smith P.M. (1999). MAgNET: Mobile Agents for Networked Electronic Trading. IEEE Transaction on Knowledge and Data Engineering. **11:4.**
9. Clements P.E., Papaioannou T., Edwards J. (1997). Aglets: Enabling the Virtual Enterprise. ME-SELA '97. p425.
10. Chase R.B., quilanoN.J.A, Jacobs F.R. Production and Operation Research- Manufacturing & Service（Version 8）McGraw-Hill.
11. Shen W.M, Norrie D.H. (1999). Agented-based Systems for Intelligent Manufacturing: A State of Art Survey. *Knowledge and Information Systems.* **1:2**, 129-156.
12. Weitzel T., Buxmann P., Westarp F. (1999). A Communication Architecture for the Digital Economy 21st Century EDI. *Proceeding of the 32nd Hawaii International Conference on System Sciences.*
13. The Aglets Software Development Kit Http://www.trl.ibm.co.jp/aglets/
14. The Commerce Model for Electronic Redesign http://www.arraydev.com/commerce/jip/9702-01.htm
15. Cheng Jingyun. (2001). Internal Report on Agile manufacturing in shipbuilding industry. Shanghai Jiaotong University. China.
16. Jae Kyu Lee, Kyoung Jun Lee and etc. (1995). Intelligent Scheduling Systems for Shipbuilding. *AAAI* (Canada, August 1995).

Practical Design of Ships and Other Floating Structures
You-Sheng Wu, Wei-Cheng Cui and Guo-Jun Zhou (Eds)
© 2001 Elsevier Science Ltd. All rights reserved

ENERGY AND ENVIRONMENT DIMENSION IN SHIP MANUFACTURING PROCESSES

M. A. Shama

Department of Naval Architecture and Marine Engineering
Faculty of Engineering, Alexandria University, Alexandria 21544, Egypt

ABSTRACT

The main issues of energy and environment associated with shipyards manufacturing processes are presented. The direct and indirect demands of energy in the shipbuilding industry are clarified. The Life Cycle Analysis (LCA) in ship production is addressed with particular emphasis on the methods commonly used to reduce energy consumption and relevant harmful environmental impacts. The holistic approach of LCA is briefly outlined. The importance of rationalization of materials used in shipbuilding and ship scrapping is stressed. The modern approach of *Ship Design for Environment* is highlighted. The paper is concluded by stressing the importance of introducing the relevant energy and environment courses into the educational programs of Naval Architecture and Marine Engineering departments.

KEYWORDS

Shipbuilding, Energy, Environmental impacts, Pollution, Risk analysis, Life cycle analysis, Design for environment

1 INTRODUCTION

Awareness about environmental problems has increased significantly in recent years. There is now widespread appreciation of the serious health risks, degradation of natural resources, climate change and need for means of environmental protection. Energy consumption has adverse economic and environmental implications. Therefore, consumption of energy should be rationalized in order to improve the economics of the industry and protect the environment, particularly for energy intensive industries.

The shipbuilding and ship repair industries consume various types of energy for ship production and ship repair and therefore produce environmental problems. Identification of the size, scope and consequences of the harmful environmental impacts should receive some consideration. Solving pollution problems should be directed to pollution prevention, reduction and control. This philosophy should be reflected in the teaching curricula of the Faculties of Engineering. Future engineers should be properly equipped with adequate knowledge on energy and environment so as to understand and contribute to resolving the local, regional and global environmental challenges.

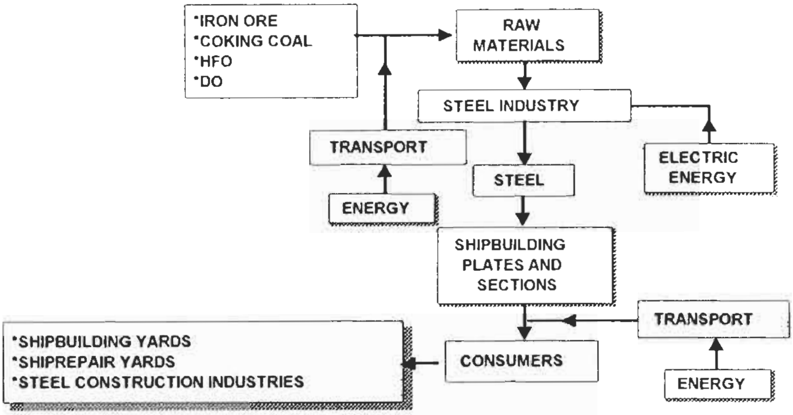
•IRON ORE
•COKING COAL
•HFO
•DO
RAW MATERIALS
STEEL INDUSTRY
TRANSPORT
ELECTRIC ENERGY
STEEL
ENERGY
SHIPBUILDING PLATES AND SECTIONS
TRANSPORT
•SHIPBUILDING YARDS
•SHIPREPAIR YARDS
•STEEL CONSTRUCTION INDUSTRIES
CONSUMERS
ENERGY

Figure 1: Indirect Energy used in Shipbuilding

2 TOTAL SHIPBUILDING SYSTEM

The total shipbuilding system is composed of several activities involving transportation, prefabrication, fabrication, post fabrication, outfitting, ship delivery and post delivery operations. The main elements of these activities involving environmental impacts are associated with the different materials used in ship construction, energy consumed in the various stages of fabrication, transport, construction, testing, maintenance and repair.

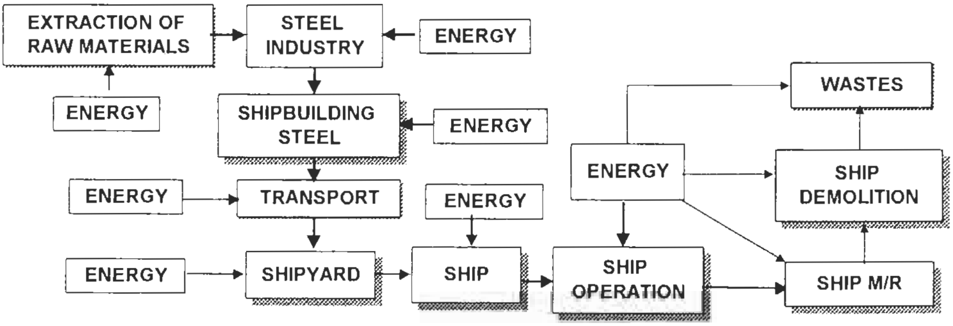
EXTRACTION OF RAW MATERIALS
STEEL INDUSTRY
ENERGY
ENERGY
SHIPBUILDING STEEL
ENERGY
WASTES
ENERGY
SHIP DEMOLITION
ENERGY
TRANSPORT
ENERGY
ENERGY
SHIPYARD
SHIP
SHIP OPERATION
SHIP M/R

Figure 2: Demands for Direct Energy

3 ENERGY USED IN THE SHIPBUILDING INDUSTRY

The energy demands for the shipbuilding industry could be divided into *direct* and *indirect* energy. The indirect energy is required for the manufacture and production of steel plates and sections, manufacture of main and auxiliary engines, manufacture of equipment and fittings, production of welding electrodes and coils, production of paints, etc., see Figure 1. The direct energy is required for the handling and transport of raw and fabricated materials, prefabrication and fabrication processes: cutting, forming of plates and sections, welding and assembly of steel plates and sections, construction of 2D and 3D blocks, assembly of blocks on berth/dock, outfitting and painting operations, tests and trials, see Figure 2. Figures 3,4 show the energy demands for ship plates forming and welding operations, (EE = Electric Energy, GE = Gas Energy).

For plate forming using line-heating method, acetylene is used for providing the required heat energy and CO_2 is the main polluting gas emitted. Assuming complete combustion of acetylene, the amount of emitted CO_2 could be estimated using the reaction equation for complete combustion as given by:

$$C_2H_2 + 2.5O_2 \Rightarrow 2CO_2 + H_2O$$

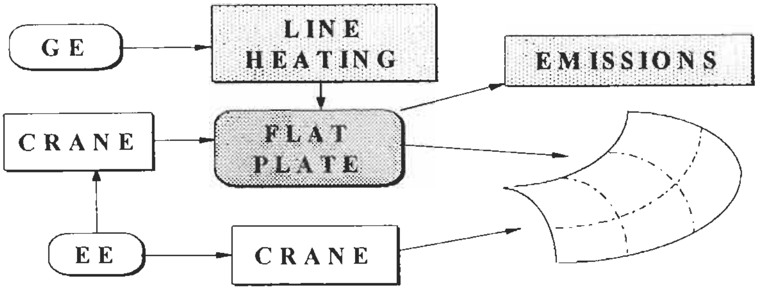

Figure 3: Energy Demands for Plate Forming, Line Heating

4 LIFE CYCLE ASSESSMENT IN SHIPBUILDING INDUSTRY

Life Cycle Assessment (LCA) adopts a holistic approach by analyzing the entire life cycle of a product starting with raw materials extraction processing and manufacture, materials transportation, product fabrication, transportation, distribution, operation, maintenance & repair and finally scrapping. The solid waste management hierarchy includes waste prevention, minimization at source, reuse, repair, recycle, incineration (with or without energy recovery) and landfill.

The holistic approach of LCA covers the energy consumption and associated environmental impacts over the entire life of a product. The main components of this holistic approach are:

- *Inventory analysis:* addresses the identification and quantification of energy and resources used and environmental releases to air, water and land.
- *Impact analysis:* addresses the technical qualitative and quantitative characterization and assessment of the ecological and human health consequences and resource depletion.
- *Improvement analysis:* addresses the evaluation and implementation of opportunities to reduce environmental burdens

LCA in the Shipbuilding Industry should include not only environmental impacts but should also include rational use of construction and outfitting materials, rational use of energy in all stages and phases of ship design, construction, outfitting, operation, maintenance, repair and finally ship scrapping. The main materials commonly used in the shipbuilding industry, which require rationalization are steel plates and sections, welding rods, castings, forged parts, timber, paints, etc. The rational use of these materials should not only reduce environmental impacts and energy consumption but should also have positive economic gains. The minimization of environmental impacts and wastes in ship construction could be achieved by the efficient use of all construction materials including steel plates, profiles, sections, welding rods, paints, etc. The measures commonly taken to save energy consumed in ship fabrication and construction are directed to the rationalization of inter-process transportation, reducing/improving bending & forming operations (2D and 3D forming), using large sizes of steel plates, particularly plate width, improving welding operations, improving accuracy of edge preparations, minimization of welding lengths, maximization of down-hand welding, minimization of cutting lengths of steel plates, widespread use of computer-aided marking and cutting, minimization of scrap using efficient methods of plate nesting, utilization of waste and minimization of rework.

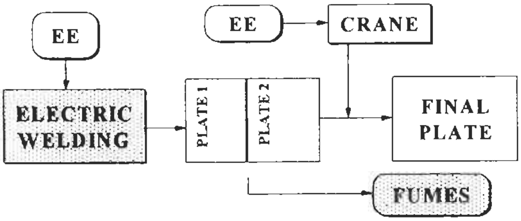
EE
EE
CRANE
ELECTRIC WELDING
PLATE 1
PLATE 2
FINAL PLATE
FUMES

Figure 4: Energy Demands for Welding

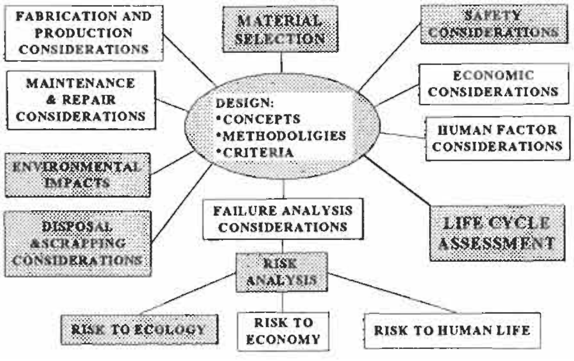
FABRICATION AND PRODUCTION CONSIDERATIONS
MATERIAL SELECTION
SAFETY CONSIDERATIONS
MAINTENANCE & REPAIR CONSIDERATIONS
ECONOMIC CONSIDERATIONS
DESIGN:
•CONCEPTS
•METHODOLIGIES
•CRITERIA
HUMAN FACTOR CONSIDERATIONS
ENVIRONMENTAL IMPACTS
FAILURE ANALYSIS CONSIDERATIONS
LIFE CYCLE ASSESSMENT
DISPOSAL &SCRAPPING CONSIDERATIONS
RISK ANALYSIS
RISK TO ECOLOGY
RISK TO ECONOMY
RISK TO HUMAN LIFE

Figure 5: Holistic Approach of ship design

5 EDUCATIONAL ASPECTS OF ENERGY AND ENVIRONMENT IN SHIPBUILDING

A brief statement of the main energy and environment courses relevant to the shipbuilding and ship repair industries is given below. These courses should improve the awareness of future engineers about energy consumption and environmental impacts resulting from the manufacturing processes in the shipbuilding and ship repair industries.

6 THE ENVIRONMENTAL ENGINEERING SYSTEM

The course on Environmental Engineering System should include design, construction, operation, maintenance and repair (M/R) and scrapping. Design is one of the main courses given in Faculties of Engineering that has a close connection with the relevant issues of energy and environment. The environmental dimension should be an integral part of the holistic approach of ship design, see Figure 5. The main objective of this holistic approach is to make safety, economy and environmental protection an integral part of the ship design process. Unfortunately, the inadequacy of design for safety is appreciated only after serious accidents have occurred. Design for safety, therefore, should include risk to human life and risk to environment. Risk management should, therefore, be an integral part of the holistic design approach. In the maritime sector, tragic accidents causing environmental disasters have focused world opinion on ship safety and environmental protection through the introduction of the International Safety Management code, (ISM).

The Factor of Safety commonly used in Engineering Design should, therefore, include not only safety of the structure but should also take into account risk to human life and risk to environment, as follows:

$$\gamma = \gamma_X . \gamma_Y . \gamma_Z$$

γ = Total Factor of Safety

γ_X = factor taking account of the safety of the system

γ_Y = factor taking account of the risk to human life

γ_Z = factor taking account of the risk to ecology

It is evident that the irrational increase in the magnitude of the total Factor of Safety of ship structure will not only reduce the probability of structural failure, the cost of failure, the harmful impact to the environment but will also increase the initial cost of ship structure through the irrational use of materials and resources. This indicates clearly that the magnitude of the Factor of Safety should be rationally selected so as to satisfy the requirements of safety, ecology, economy and sustainability.

7 RISK MANAGEMENT

The course on Risk Management should cover hazard assessment, risk analysis, development of accidental scenarios that could potentially lead to fatalities/injuries, development of methods and actions to reduce/prevent risk, calculation of risk taking into account the likelihood of the scenario and the probable negative consequences. Risk assessment is the process of assigning magnitudes and probabilities to adverse effects resulting from human activities. Risk could be assessed by using the probability density functions of both Demand and Capability. In this case the options to reduce risk are: increase capability (sometimes very costly), decrease demand (sometimes not feasible), decrease variability and uncertainty of capability (possible), decrease uncertainty of demand (not always feasible).

8 ENVIRONMENTAL PROBLEMS

The course on Environmental Problems should cover the main types, causes, scope, consequences, prevention, reduction and control of the negative environmental impacts. The impact of industry on air pollution, water pollution, (rivers, coastal water, seawater, ground water, lake water), noise pollution, climate change, ozone depletion, etc. should also be addressed. The course should clearly indicate the consequences of irrational use of resources, expected climate change due to the increase of greenhouse gases, etc. The contribution of the shipbuilding and ship repair industries to the local, regional and global environmental problems should be also introduced and highlighted. Unfortunately, there is very limited data available on energy consumption in the various stages of ship production. Also, there is scarce data available on the various types of the negative environmental impacts resulting from the different stages of ship production.

9 ENERGY AND ENVIRONMENT

The course on Energy and Environment should cover environmental and economic benefits resulting from introducing methods of increasing efficiency of production processes, cost-effective methods of handling unwanted effluents and methods of waste reduction. The course should clearly indicate the importance of using methods for energy conservation, raising energy efficiency in the various ship production processes, energy saving techniques, minimization of total energy consumption. minimization of wasted energy, controlling the environmental problems resulting from energy consumption, using safer, cleaner and more efficient technologies and systems for ship production. The course should also cover energy saving methods in ship operation, maintenance & repair and ship scrapping.

10 WASTE MANAGEMENT

The course on Waste Management may include the environmental and economic benefits from life extension, waste prevention/minimization at source, re-use, recycle, recover, repair/upgrade. incineration, (with/without energy recovery), dumping and landfill.

Ship scrapping is becoming an important industry in several countries. The outcome of ship scrapping includes usable materials, engines, equipment, fittings, etc. The various activities and operations used in this industry should be rationalized so as to protect our natural resources, save energy consumption, minimize environmental impacts and waste. The expected growth of this industry necessitates a thorough examination of the main issues of energy and environment associated with this fast growing industry. Waste management in ship scrapping should not only have significant economic opportunities but should also have positive impact on environmental protection.

11 CONCLUSIONS

The main conclusions drawn up from this paper are:

- In spite of the limited scale of local, regional and global negative environmental impacts of shipbuilding and repair industries, the identification, quantification and control of these negative impacts should receive serious attention.
- LCA in the shipbuilding industry could be used to assist shipbuilding and ship repair companies to quantify, assess and identify opportunities to minimize energy consumption and its impact to the environment, and to realize cost savings by making more effective use of available resources.
- The rational use of shipbuilding materials should not only reduce the harmful environmental impacts and energy consumption but should also have positive economic gains.
- Waste management in ship scrapping should not only have significant economic opportunities but should also have positive impact on natural resources and environmental protection.
- The teaching of Design courses should be more comprehensive than that normally given in our Faculties of Engineering and should cover the main issues of energy and environment.
- The environmental dimension in ship design should be an integral part of a holistic approach of ship design that takes account of safety, economy and environmental protection.
- In order to improve local, regional end global environmental protection, future shipbuilding and ship repair engineers should be well equipped with the necessary knowledge and tools for energy conservation and environmental protection.

References

Giustiniano D.F. and others. (1998). An Integrated Steel Workshop for Shipbuilding: A Real Application of Automation. JSP, Nov.

Glasson, & others. (1994). Introduction to Environmental Impact Assessment. UCL Press.

John Justus. (1991). Global Climate Change, Major Planning Issue. CRS.

Kura, Bhaskar and others. (1997). Comparison of Japanese and US Environmental Regulations Impacting Shipbuilding. JSP **13:3**.

Lindfors L. G. and others. (1995). Nordic Guidelines on Life- Cycle Assessment.

Richard L. Storch and others. (1995). Ship Production. second ed. SNAME.

Shama, M. A. (1997). Energy & Environment in Engineering Education. AEJ, September.

Shama, M.A. (1997). Implementation of Energy and Environmental Topics in Faculties of Engineering. Workshop, Faculty of Engineering, Alexandria University, March.

Shama, M. A. (1997). Climate Change, Causes and Consequences, an Engineering Overview. Workshop on Climate Change, Faculty of Engineering, Alexandria University, April.

Shama, M. A. (1997). Shipyard Engineering. Lecture Notes, Naval Architecture and Marine Engineering Dept., Faculty of Engineering, Alexandria University, Egypt.

Shama, M.A. (1998). Risk management. AEJ. **37:2**.

UNEP. (1995). Cleaner Production Worldwide. Vol. II.

Practical Design of Ships and Other Floating Structures
You-Sheng Wu, Wei-Cheng Cui and Guo-Jun Zhou (Eds)
© 2001 Elsevier Science Ltd. All rights reserved

STUDY ON HEAT TRANSFER BETWEEN GAS FLAME AND PLATE DURING LINE-HEATING PROCESS

Y. Tomita[1], N. Osawa[1], K. Hashimoto[1], N. Shinkai[2], J. Sawamura[1] and K. Matsuoka[1]

[1] Department of Naval Architecture and Ocean Engineering, Osaka University,
2-1, Yamadaoka, Suita, Osaka 565-0871 Japan
[2]Bureau Veritas Japan,
93, Edomachi, Chyuoh-ku, Kobe, Hyogo 651-0033 Japan

ABSTRACT

The transient 3-dimensional temperature distribution near the plate surface of the spot heating gas flame is measured in detail by a high performance L.I.F. measurement system. It has been found that the thermal-flow field within the combustion flame remains almost unchanged regardless of the temperature increase in the steel plate. A new hypothesis on the heat transfer during line heating process is built up based on the result of the L.I.F. experiment. This hypothesis is that the distributions of gas temperature near plate surface and local heat transfer coefficient depend only on the distance from the torch. The appropriateness of this hypothesis is proved by performing an inverse heat conduction analysis of a spot heating experiment.

KEYWORDS

Line heating, Heat transfer, L.I.F., Inverse heat conducting analysis

1 INTRODUCTION

Line heating process, which is one of the most characteristic works in the shipbuilding industry, is applied to the formation of curved hull plates. This work has not been carried out by the automatic operation, but by skilled workers. Recently the automatic operation has been strongly desired because of the decrease in skilled workers. In order to automate this process, heat transfer between flame and plate has to be evaluated theoretically.

The heat transfer during line heating process is a poorly understood phenomenon. Moshaiov and Latorre (1985) studied the temperature distribution of a plate using a distributed heat source moving along the plate surface. Tsuji and Okumura (1988) found that the heat flux distribution of flame could be expressed approximately by superposition of two gaussian distributions. Terasaki et al. (1999) derived the equations for thermal cycles of line heating. In these theories, a series of experiment is needed whenever plate size or plate thickness or torch speed changes even if torch nozzle, gas condition and torch height are unchanged. Furthermore, these theories are applicable only for the cases where torch travels at a constant speed in straight-line motion. These theories assume that the relative distribution pattern of heat flux around the stagnation point remains unchanged in time. Strictly speaking this assumption does not hold true, and this is the reason why the application of those theories is narrow.

It is needed to develop a new theory with wide application range on the bases of the true nature of thermal-flow filed within the gas flame and local heat transfer. In such study, it is necessary to measure the transient temperature distribution of gas flame near the plate surface accurately. Such measurement can be performed by laser induced fluorescence (L.I.F.) technique. Distribution of local heat transfer can be estimated by inverse heat conduction analysis.

In this paper, the transient 3-dimensional temperature distribution of the spot heating gas flame is measured in detail by a high performance L.I.F. measurement system. From the results of this experiment, a hypothesis on the distributions of gas temperature and local heat transfer coefficient is built up. The appropriateness of this hypothesis is proved by performing an inverse heat conduction analysis of a spot heating experiment.

2 MEASUREMENT OF GAS TEMPERATURE DURING SPOT HEATING BY USING L.I.F. TECHNIQUE

2.1 Experimental Apparatus

A methane gas is used as fuel gas. Table.1 shows the pressure and the flux of methane, oxygen and NO. The heating power of this torch is much lower than that of line heating torches used in shipyards. A square mild steel plate with sides 500mm long and 16mm thickness is arranged horizontally and a torch with a circle shaped nozzle of 0.9mm diameter is positioned above the plate. The center of the plate is heated by a flame of premixed methane and oxygen. The distance Z between the nozzle and the plate is arranged to be 12, 20 and 28mm.

2.2 Laser Optical System

The thermal field within the combustion flame is measured by the laser induced fluorescence (L.I.F.) technique and an optical measurement technique. Two wave-length L.I.F. technique, which utilizes NO in the measurement of temperature, is used.

The absorption band of NO exists near the 225nm, and the fluorescence is emitted in the band of 230nm~300nm. The characteristics of fluorescence and the wavelength of laser are selected so that they are suitable for the temperature range of 1000K~2000K. The outline of L.I.F. optical system is shown in Figure 1. Oscillated wavelength of YAG lasers and dye lasers is set to 10Mhz, which is the absorbed wavelength of NO. Laser beams 1 and 2 are gathered together at a beam combiner, and then they are irradiated to both a correction burner and an object flame of measurement.

The signals of fluorescence from target and correction burners are photographed on the upper and lower part of camera pictures by using two ICCD cameras, and the strength distribution of fluorescence NO molecules emits is measured. The measuring timing of the laser device and ICCD camera is controlled with delay-generator. Measured pictures are forwarded to a computer to analyze flame temperatures. The measured region is 200mm in width and 20mm high. The space resolution of the measured picture is 1.5 mm. From the instant when the torch is set up to home position laser beams are irradiated for 0.4sec by every 2 sec. Hereafter, t denotes the elapsed time since the measurement starts. The total numbers of laser irradiation is 12 times per each measurement.

2.3 Temperature Distribution within the Flame

Figure 2 shows the measured temperature distribution within the combustion flame at t=2sec and t=24sec for the case Z=20mm. Although plate heating face temperature increases significantly, the measured temperature distribution within the combustion flame is almost the same through the measurement. That is, the thermal-flow field becomes stable in extremely short time.

Figure 3 shows the averaged temperature distributions for the cases where Z=12, 20 and 28mm. The followings can be seen; 1) thin temperature boundary layers of about 1~2mm thickness are formed close the steel plate, 2) the temperature falls down rapidly upward from the plate surface and 3) the temperature around the nozzle rises when Z is small.

Figure 4 shows the averaged temperature distributions on the plane 1.5mm upward from the plate surface for the case where Z=12mm. This figure shows that lower temperature is observed on the center region of the plane, this is because the core of the gas flame, in which combustion does not occurs, touches the plate.

2.4 Discussion

The experimental results mentioned above indicate that thermal-flow field within the combustion flame remains almost unchanged. The local surface heat transfer between heating gas and steel plate is dominated by the turbulent energy of the flow field. These lead us to a hypothesis that the distribution of gas temperature near the plate surface and local heat transfer coefficient are time independent and they depend only on the distance from the torch.

The equation that expresses the relation between gas temperature right on the plate T_G, plate heating surface temperature T_S, heat flux from gas to plate q and local heat transfer coefficient α is given as

$$q = -\alpha T_S + \alpha T_G. \quad (1)$$

According to the proposed hypothesis, Eq. (1) leads to a linear relationship between q and T_S because we assume that α and T_G remain unchanged in time.

3 INVERSE HEAT CONDUCTION ANALYSIS OF SPOT HEATING EXPERIMENT

The discussion mentioned in the previous section is based on the result obtained from the experiment using a small torch whose heating power is much lower than that of the line heating torches used in shipyards. The proposed hypothesis should be verified in the experiment using a high power line heating torch. In this section, we shall show that a linear relationship between q and T_S, which is anticipated from the hypothesis, exists in the results of spot heating experiment using a high power line heating torch used in shipyards.

3.1 Experimental Apparatus

A circular mild steel plate of diameter 300mm and 6mm thickness is arranged horizontally and a torch with a #2000 nozzle is positioned above the plate. The center of the plate is heated by a flame of oxyacetylene. Table 2 shows the pressure and the flux of acetylene and oxygen. The heating power of this gas flame is higher by far than that of the methane torch used in the L.I.F. experiment. The distance between the nozzle and the plate is arranged to be 18.5mm. The time histories of the plate back face temperature are measured by using thermoelectric couples welded on the plate back surface. The outputs of thermocouples are recorded on a personal computer by every 0.5sec. The points, at which temperature is measured, are arranged in the radial direction from the center to the point 104mm apart from the center. Hereafter, r denotes the distance from the center. The intervals of the points are 4mm up to the point at which r=40mm, and 8mm for the points at which r>40mm. In the experiment, heating is ceased within about 10 seconds because the heating surface at the center melts about 0.5 mm deep at that time.

3.2 Inverse Heat Conduction Analysis

Figure 5 shows the measured distributions of plate back face temperature. From this figure, the time lay between the temperatures at the points is clearly observed, due to a thermal conductivity in the plate. Figure 5 also shows that the temperature on the back face does not always reach its maximum at the center.

The distribution of plate surface temperature and heat flux on the heating surface can be estimated by finite-difference inverse heat conduction analysis described in Beck et al. (1985).

Hereafter, T_B and T_S denote back and heating surface plate temperatures. ρ, c and κ are density, specific heat and heat conductivity of steel. t is the elapsed time since heating starts, and prefix Δ means the change over the time increment.

Heat conduction problem in this case is axial symmetric. The computational grid shown in Figure 6 is used. Hereafter, subscript i, i±1 denotes the i th and i±1 th grid point from the center, and i=1 when the point is at the center. The finite difference equations for temperature are obtained by integrating a heat conduction equation over the control volumes shown in Figure 7 and expressing the result in terms of neighboring grid point values.

Assuming that the back face of the plate is heat insulated, the following equations are derived. For the points at which r is not zero,

$$\nu\rho_i c_i \frac{\Delta T_{B,i}}{\Delta t} = \frac{1}{r_i}\left[\kappa_e r_e \left.\frac{\partial T_B}{\partial r}\right|_e - \kappa_w r_w \left.\frac{\partial T_B}{\partial r}\right|_w + \frac{r_{i+1}-r_{i-1}}{2}\frac{2\kappa_i r_i}{d^2}\left(T_{S,i}-T_{B,i}\right)\right]$$

$$;\ \left.\frac{\partial T_B}{\partial r}\right|_e = \frac{T_{B,i}-T_{B,i-1}}{r_i-r_{i-1}},\quad \left.\frac{\partial T_B}{\partial r}\right|_w = \frac{T_{B,i+1}-T_{B,i}}{r_{i+1}-r_i},\ \nu=\frac{1}{2}(r_{i+1}-r_{i-1}), \tag{2}$$

$$\kappa_i,\rho_i,c_i = \kappa,\rho,c|_{T=T_{B,i}}\,;\ \kappa_e,\rho_e,c_e = \kappa,\rho,c|_{T=(T_{B,i}+T_{B,i+1})/2}\,;\ \kappa_w,\rho_w,c_w = \kappa,\rho,c|_{T=(T_{B,i-1}+T_{B,i})/2}\,.$$

For the plate center, at which r=0,

$$\nu\rho_1 c_1 \frac{\Delta T_{B,1}}{\Delta t} = \nu\left(\frac{4}{D}\kappa_e \left.\frac{\partial T_B}{\partial x}\right|_e + \frac{2\kappa_1}{d^2}\left\{T_{S,1}-T_{B,1}\right\}\right)$$

$$;\ \left.\frac{\partial T_B}{\partial x}\right|_e = \frac{T_{B,2}-T_{B,1}}{D},\ \nu=D^2,\ D=r_2-r_1,\ \kappa_1,\rho_1,c_1=\kappa,\rho,c|_{T=T_{B,1}}\,;\ \kappa_e,\rho_e,c_e=\kappa,\rho,c|_{T=(T_{B,1}+T_{B,2})/2}\,. \tag{3}$$

In Eq. (2) and (3), d is the plate thickness, and subscripts n, s, e and w refer to north, south, east and west cell faces shown in Figure 7.

At each grid point, heating surface temperature $T_{S,i}$ can be calculated by Eq. (2) or (3). Surface heat flux $q_{S,i}$ is given by the following equation.

$$q_{s,i} = \left.\left(\kappa\frac{\partial T}{\partial z}\right)\right|_{S,i} \cong -2\kappa|_{T=T_B}\frac{T_{B,i}-T_{S,i}}{d} \tag{4}$$

The temperature dependence of the material properties used are shown in Figure 8. Figures 9 and 10 show the distributions of the estimated heating surface temperature T_S and heat flux q. Although any regularization is not given, results within acceptable stability is obtained. These figures show that both T_S and q on the heating surface reach their maximum at r=4mm, not at the center. The reason of this is that the core of the gas flame, in which combustion does not occurs, touches the plate in the same manner as the L.I.F. experiment shown in Figure 4. T_S and q are remarkably small at t=0.5sec because the moving of the torch to the home position has not finished at that time. T_S increases with time while q decreases after t=1.0sec.

3.3 Discussion

According to the hypothesis proposed in the previous section, surface heat flux q decreases as heating surface plate temperature T_S raises, and a linear relationship is established between them. Figure 11 shows the relations between T_S and q after t=1.0sec at various points. This figure shows that such linear relationship is approximately established.

From Eq. (1), distributions of local heat coefficient α and gas temperature right on the plate T_G can be obtained by performing a linear regression analysis on the relation of T_S and q. Figures 12 and 13 shows the calculated distributions of α and T_G.

Plate back face temperature T_B can be calculated from the estimated α and T_G by direct thermo conduction finite element analysis. Figure 14 shows the calculated and measured values of T_B. In this figure, it is found that calculated values agree well with the experimental results. It is considered that this result shows the accuracy of the inverse analysis, and it has also strongly supported the hypotheses proposed in this paper.

According to the proposed hypotheses, thermal-flow field and local heat transfer remain unchanged when the size and/or shape of plate is changed. It can be considered that the hypotheses approximately holds true during a line heating process when torch traveling speed is much smaller than the velocity of gas flow. This leads to an assumption that the relative distribution patterns of gas temperature and local heat transfer coefficient around the stagnation point during line heating with arbitrary torch traveling history are almost the same as those in spot heating using the same torch and gas condition. Therefore, it is anticipated that the temperature distribution in a plate during line heating with arbitrary torch traveling history and plate size can be calculated as far as a spot heating experiment with the same torch and gas condition is performed.

4 CONCLUSIONS

The transient 3-dimensional temperature distribution of the gas flame of the spot heating experiment using a small power methane torch is measured by a L.I.F. measurement system. The distributions of plate heating face temperature and heat flux during the spot heating experiment using a high power oxyacetylene line heating torch are calculated by inverse heat conduction analysis.

The main results are as follows:

1) For the spot heating experiment using a small methane torch, it has been found that the thermal-flow field within the combustion flame remains almost unchanged regardless of the temperature increase in the steel plate.

2) The hypothesis that, the gas temperature near the plate surface and local heat transfer coefficient are time independent and they depend only on the distance from the torch, is built up.

3) For the spot heating experiment using a high power line heating torch, the measured back face plate temperature agree well with the calculated ones which are derived from the plate heating face temperature and heat flux estimated by inverse heat conduction analysis. This result shows the accuracy of the inverse analysis, and it support the hypotheses proposed in this paper.

Acknowledgement

The measurement of temperature within the flame in L.I.F. experiment is carried out at Mitsubishi Heavy Industries, Co. Ltd. Inc. Nagasaki Research Institute. The authors would like to express to Dr. Watanabe, E. and Dr. Deguchi, Y. our deepest gratitude for their cooperation.

The measurement of plate back face temperature during spot heating with high power torch is carried out at Hitachi Zosen, Co. Ltd. Inc. Ariake Shipyard as a part of the research program of Panel SR246 of the Shipbuilding Research Association of Japan, sponsored financially by the Nippon Foundation. The authors would like to express to Mr. Ohsawa M. and Mr. Nakatani M. our deepest gratitude for their cooperation.

References

Moshaiov A. and Latorre R.(1985) Temperature Distribution During Plate Bending by Torch Flame Heating, *Journal of Ship Research* **29:1**, pp.1-11.

Tsuji I. and Okumura Y.(1977) A Study on Line Heating Process for Plate Bending of Ship Steels, *Trans. The West-Japan Soc. Naval Architects* **76**, pp.149-160 (in Japanese).

Terasaki T., Kitamura N. and Nakai M.(1999) Predictive Equation for Thermal Cycle Generated by Line Heating Method, *Trans. The West-Japan Soc. Naval Architects* **99**, pp.321-329 (in Japanese).

Beck J.V., Blackwell B. and St. Clair Jr., C. R.(1985) *Inverse Heat Conduction*, A Weley-Interscience Publication.

TABLE 1

FLUX AND PRESSURE OF CHEMICAL SPECIES USED IN THE L.I.F. EXPERIMENT

	flux (m^3/sec)	pressure (KPa)
NO	2.50×10^{-6}	98.07
O_2	2.83×10^{-5}	245.17
CH_4	2.67×10^{-5}	196.13

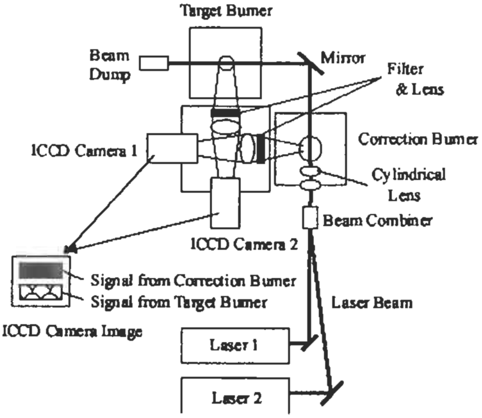
Target Burner
Beam Dump
Mirror
Filter & Lens
ICCD Camera 1
Correction Burner
Cylindrical Lens
Beam Combiner
ICCD Camera 2
Signal from Correction Burner
Signal from Target Burner
ICCD Camera Image
Laser Beam
Laser 1
Laser 2

Figure 1: Optical system

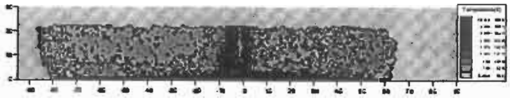

(a) t=2sec

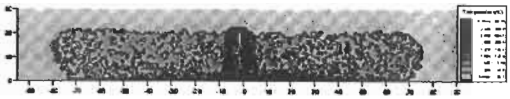

(b) t=24sec

Figure 2: Measured temperature distribution of gas flame in a transient state for the case where Z=20mm.

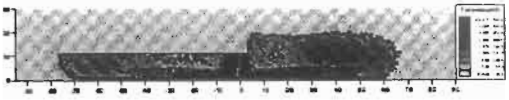

(a) Z=12mm

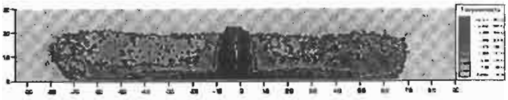

(b) Z=20mm

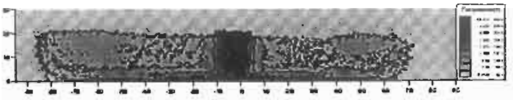

(c) Z=28mm

Figure 3: Averaged temperature distributions of gas flame

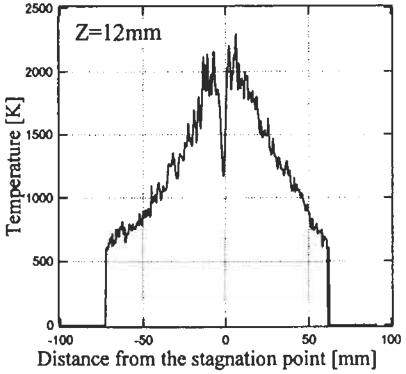

Figure 4: Measured gas temperature distribution on the plane 1.5mm upward from the plate surface for the case where Z=12mm

TABLE 2

FLUX AND PRESSURE OF CHEMICAL SPECIES USED IN THE SPOT HEATING EXPERIMENT

	flux (m^3/sec)	pressure (KPa)
O_2	0.0	6.92×10^{-5}
C_2H_2	4.62×10^{-7}	5.76×10^{-4}

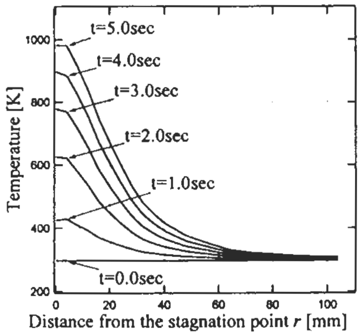

Figure 5: Distribution of plate back face temperature during the spot heating experiment

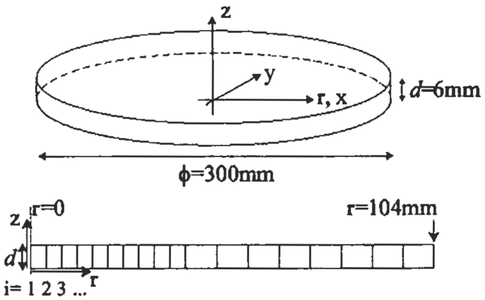
z
y
r, x
d=6mm
ϕ=300mm
z
r=0
r=104mm
d
r
i= 1 2 3 ...

Figure 6: Computational grid used in inverse heat conduction analysis

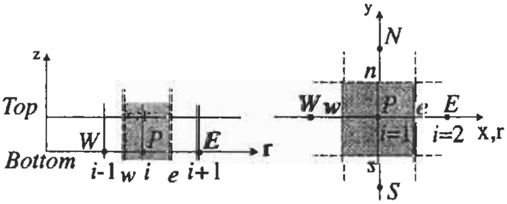
z
Top
Bottom
W
P
E
r
i-1
w
i
e
i+1
y
N
n
W
w
P
e
E
i=1
i=2
x,r
s
S

(a) for points with r>0 (b) for the plate center

Figure 7: Control volumes used in the inverse heat conduction analysis

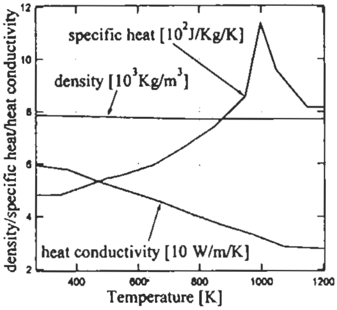

Figure 8: Temperature dependency of the material properties used in inverse heat conduction analysis

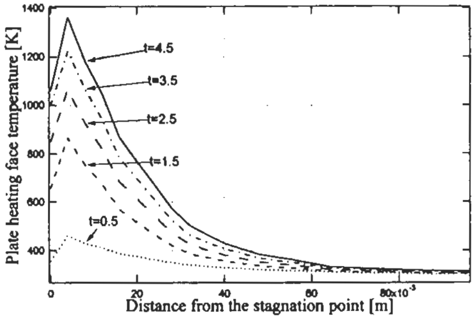

Figure 9: Estimated plate heating face temperature obtained by inverse heat conducting analysis

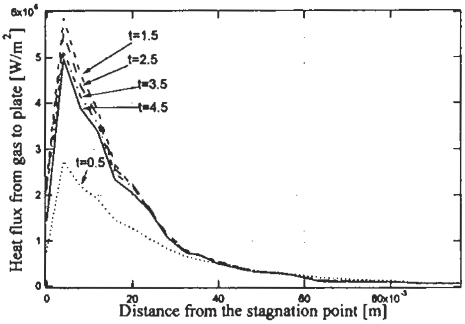

Figure 10: Estimated heat flux obtained by inverse heat conducting analysis

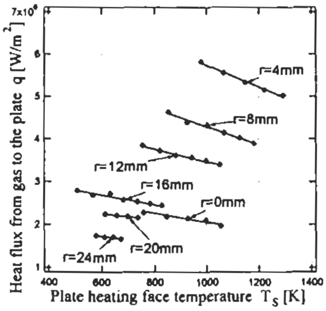

Figure 11: Relation between estimated plate heating face temperature and estimated heat flux

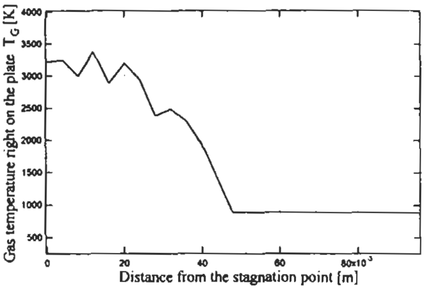

Figure 13: Estimated distribution of gas temperature right on the plate

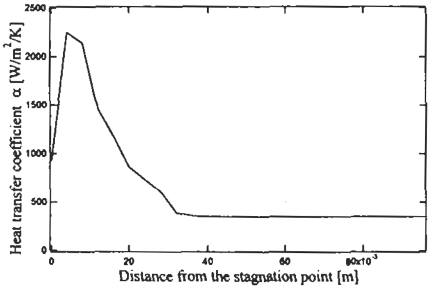

Figure 12: Estimated distribution of local heat transfer coefficient

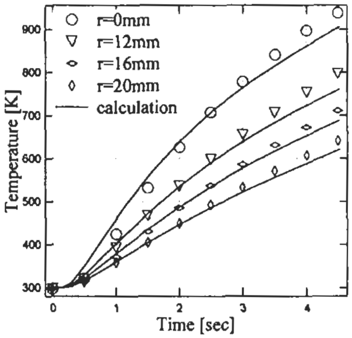

Figure 14: Comparison of calculated and measured plate back face temperatures

Practical Design of Ships and Other Floating Structures
You-Sheng Wu, Wei-Cheng Cui and Guo-Jun Zhou (Eds)
© 2001 Elsevier Science Ltd. All rights reserved

STUDY ON THE PROCESS TECHNOLOGY FOR LINE HEAT FORMING OF HULL FABRICATION

LIU Yujun, JI Zhuoshang, WANG Dong, DENG Yanping
School of Naval Archit. And Mar. Eng., Dalian Univ. of Technol., China

ABSTRACT

A simulation method of line heat forming of hull fabrication is proposed in this paper. The calculation methods of local contraction values for two kinds of complex curved Sail-Shaped plates are introduced. The mathematical models of the relation between the maximum retraction length and the parameters acting on the plates are established by theorems of stepwise regression and mathematical statistics. The Validity of the methods is presented on the basis of experimental data. The optimum design method of processing technical parameters is also discussed.

KEYWORDS

Shipbuilding, Hull fabrication, Line heat forming, Optimum design, Simulation method.

1 INTRODUCTION

The simulation method of line heat forming presented in this paper has been developed on the basis of the achievements of the first stage experimental research in China. This study has analyzed the practical conditions of China's shipbuilding industry, considered the characteristics of Chinese construction techniques, taken the advantages of longstanding co-operation between universities and shipyards, and made reference of the overseas research experience. The research has been divided into four stages. In the first stage, the essential local contraction values of the plate deformation, including contraction area and the maximum contraction length were studied, which are necessary for making complex developed curved surface from a plane plate. In the second stage, based on the processing data of ship plates, the mathematical model was established, which describes the relation between the local contraction value and the processing parameters of flame bending. In the third stage, according to the technical procedure of line heat forming, the optimal method was applied to determine the technical parameters in the processing of hull plates of known shapes. In the last stage, the feedback information of ship hull plates was collected to enrich, improve and correct the regression models.

2 CALCULATION METHOD OF ESSENTIAL LOCAL CONTRACTION VALUE FOR COMPLEX CURVED PLATE FORMING [1,2]

2.1 Calculation method of the local contraction value for symmetric sail-shaped plate and symmetric saddle-shaped plate

Symmetric sail-shaped plates and saddle-shaped plates being considered as a part of a circle, the equations for the maximum contract length $\triangle$L and contraction area $\triangle$A of curved plates are written as

Sailed-shaped plate:

$$\triangle L = \frac{8Hh}{L} \tag{1}$$

$$\triangle A = \frac{8HhB}{3L} \tag{2}$$

Saddle-shaped plate:

$$\triangle L = \frac{8Hh}{L} \tag{3}$$

$$\triangle A = \frac{16HhB}{3L} \tag{4}$$

where L, R and H are the length, radius and the height of the longitudinal arc respectively. B, r and h are the length, radius and height of the transverse arc across the contraction area respectively.

2.2 Expansion method of finite grid for sail-shaped plate

Hull plates are divided into finite grids. If the size of each grid is small enough, then the part of the curved surface in the grid can be considered as a plane panel. All these small planes make up the whole curved surface. When we imaginably unfold the bounded curved surface into a plane plate and allow the crannies among adjoining panels, several crevice lines lying on the unfolded plate would be observed. It is these crevice lines that indicate the essential local contraction values for the curved surface forming.

1) Determination of the reference line of the curved plate. The imaginary crevice lines are defined as the "reference lines". Obviously different layouts of the reference lines will result in different contraction values along the lines. After examination of different methods, geodesic line which links the central point of the short edge lying on the surface is chosen as the reference line.

2) Grid division of the hull plate. For the convenience of calculation, the curved surface between two ribs is regarded as a curved strip. Each strip is divided into small equal grids along the reference line.By substituting space planes for those small grids, the whole curved plate is divided into a certain number of small planes.

3) Development of the surface strip. The plan view of each surface strip is obtained by developing each surface strip from the reference line to its two edges with the help of the geodesic method. The developed form of the surface strip of the sail-shaped plate is a drum-shaped strip.

4) Joining of the strips. A developed view of the hull plate with crevices is obtained by joining the surface strips along the reference line in a proper sequence. These crevices are to be removed by line heat forming.

3 QUANTITATIVE ANALYSIS OF LOCAL DEFORMATION BY FLAME BENDING [3-5]

From the study on the relation between the integral shape and the local deformation values, it is known that complicated as the curved surface is, flame bending can be conducted on a quantitative basis if the local deformation can be determined. So it is necessary to define the different factors influencing local deformations, and this is one of the main technical difficulties in flame bending. Among the many technical parameters, transverse contractions and angular deformations are of great significance. This paper deals with the relation between transverse contraction and some main parameters.

3.1 Establishment of mathematical model

According to the analysis of the local deformation of the hull plate formed by line heat, plate width B_p (mm), plate length L_p (mm), plate thickness H_p (mm), transverse radius of curvature R_p (mm), heat line length L_h (mm), heat line intervals D_h (mm) and heat velocity V_h (mm/s) are determined to be the main influence factors, based on the sample data collected from the ship plate in Dalian New Shipyard. Three regression models are presented with the help of the stepwise regression method:

Model **I**:
$$y = b_0 B_p + b_1 L_p + b_2 H_p + b_3 R_p + b_4 L_h + b_5 D_h + b_6 V_h + b_7 + \varepsilon \tag{5}$$

Model **II**:
$$\begin{aligned} y = {} & b_0 B_p^2 + b_1 L_p^2 + \cdots + b_6 V_h^2 + b_7 B_p L_p + b_8 B_p H_p \cdots + b_{27} D_h V_h \\ & + b_{28} B_p + b_{29} L_p + \cdots b_{34} V_h + b_{35} + \varepsilon \end{aligned} \tag{6}$$

Model **III**:
$$y = C B_p^{b_0} L_p^{b_1} H_p^{b_2} R_p^{b_3} L_h^{b_4} D_h^{b_5} V_h^{b_6} \varepsilon \tag{7}$$

The results from model **I**:
$$\begin{aligned} L_S = {} & -0.000079859 R_p + 0.0024589 L_h - 0.00081704 D_h \\ & - 0.25506 V_h + 1.9592 + \varepsilon \end{aligned} \tag{8}$$

3.2 Validity of mathematical models

3.2.1 Significance test of population linear correlation

F-statistics can be obtained by analysis of variance, with a level of significance $\alpha = 0.05$, and F-distribution value of *(p, n-p-1)* degrees of freedom is found from F-distribution table. The calculation results for model **I**: $F = MSR / MSE = 21.534$, $F_{0.05}(\mathrm{p}, \mathrm{n-p-1}) = 2.4286$, as $F > F_{0.05}(\mathrm{p}, \mathrm{n-p-1})$ with a level of significance $\alpha = 0.05$, and hence H_1 (there is a nonzero at least for $b_1, b_2 \cdots b_p$) is accepted. That is to say, the linear relation significance exists between y and x_i in model **I**.

3.2.2 Goodness of fit inspection of regression function

TABLE 1.
GOODNESS OF FIT FOR REGRESSION MODEL **I**

complex correlation coefficient $C=\sqrt{\dfrac{SSR}{\sum_{i=1}^{n}(y_i-\bar{y})^2}}$	Multivariate determination of efficient $R^2 = SSR / SST$	multivariate adjusted determination coefficient $R_a^2 = 1 - \dfrac{SSE/dfE}{SST/dfT}$	estimator of standardization residual $P(\lvert e_i^* \rvert < 2)$
0.59520	0.35426	0.33781	0.96914

3.2.3 Significance test of regression parameters

The significance of the population linear correlation in the regression model doesn't mean each independent variable has a significant influence over dependent variables, so the significance test for each regression parameter is necessary. However, each regression parameter in the equation of stepwise regression algorithm is got on the condition that each factor significance is considered to be beyond certain significance. Thus, the significance test for each regression parameter may be ignored.

3.2.4 Calculation of Beta coefficients

As well known, **Beta** coefficient is an ideal indication to weigh the influence of each argument over function,

$$b_i^* = b_i \frac{\sqrt{\sum_{i=1}^{n}(x_{ij}-\bar{x}_j)^2}}{\sqrt{\sum_{i=1}^{n}(y_i-\bar{y})^2}} \qquad \begin{array}{l} i = 1, 2, \cdots, n \\ j = 1, 2, \cdots, p \end{array} \tag{9}$$

where **Beta** coefficient b_j measures the x variable of the j_{th} with other x variables kept fixed, and reflects the influence of alternation of one standard unit over y. Substituting b_i^* for b_i can measure the influence among variables under the condition of no-dimension number. The calculation results of **Beta** coefficient are shown in table 2:

TABLE 2. **Beta** coefficient of influence factors in model **I**:

R_p	L_h	D_h	V_h
-0.34523	0.26248	-0.27714	-0.56427

4 EXPERIMENTAL CORRECTION OF MATHEMATICAL MODELS FOR LINE HEAT FORMING

In the calculation of local contraction values, the curve plate is assumed as a theoretical hull without thickness. However, the practice of real ship plates processed by line heat forming shows that the influence of the thickness of plates shouldn't be ignore. So a series of experiments for regular plates of varied thickness are carriedout. In those experiments, quantitative analyses of the influence of plate thickness on local contraction values are made with other technical parameters kept fixed.

1) Fitting curve between the maximum local contraction lengths and the maximum longitudinal deformation of the whole plate. The local maximum contraction in relation to the maximum longitudinal deformation of each experimental plate of certain thickness is derived from the data of the experimental plates processed. The relation curve between the maximum local contraction and the maximum longitudinal deformation of plates of this thickness is obtained with the help of spline function. Similarly, a group of curves of plates of different thickness can be obtained.

2) Thickness correcting factors. According to the above fitting curves, correcting factors k_{di} are defined as:

$$k_{di} = \frac{L_{s,li}(w)}{L_s(w)} \frac{L_{s,10}(w)}{l_{s,20}(w)} \tag{10}$$

where suffix i is the number of experimental plates, and suffix 10 and 20 are the normal thickness of the experimental plates respectively. And the theoretical value of real ship plates is defined without suffix.

5 OPTIMUM DESIGN OF TECHNICAL PAREMETERS IN LINE HEAT FORMING

5.1 Optimum theorem and its characteristic

The method adopted in this paper is the mixed integer one, which combines the simple method and rotation coordinate methods and has the following characteristics:

1) Discrete or continuous optimal solutions can be obtained.
2) It can be used for continuous or discrete variables, or both of them.
3) Searching times are decreased greatly, because only the calculation of the discrete variables at nodes is necessary.

5.2 Optimal models

Given as the optimum solution is the optimal result x^*, which satisfies

$$f_i = (x^*) = \min f_i(x) \qquad i = 1,2,\cdots, n \tag{11}$$

and meets the constraining conditions

$$G_j(x) \le 0 \qquad j = 1,2,\cdots, m \tag{12}$$

where x, n and m are design variables (technical parameters), the number of objective functions and the number of constraints respectively.

6 CONCLUSION

1) Line heat forming is one of the most difficult processing procedures in ship construction. The new simulation method of flame bending presented in this paper has been proved to be highly efficient and practical in shipyards.

2) The understanding of the deformation mechanism in line heat forming is of great importance for the mechanization and automation in shipbuilding industry, and further research is necessary.

References

1. LIU Yujun, JI Zhuoshang, Dong Shoufu. (1995). Theoretical Analysis of Relationship Between Local Contraction and Integral Forming in Line Heating. *Shipbuilding of China*. **2**, 90-100 (in Chinese).
2. LIU Yujun, JI Zhuoshang, Dai Yinsheng. (1994). Regression Analysis of Parameters in Line Heat Forming for Hull Steel Plate. *Shipbuilding of China*. **1**, 65-73 (in Chinese).
3. JI Zhuoshang, LIU Yujun, SUN Zhenlie, et al. (1998). Study on Theory and Application for Hull Steel Plate by Line Heating. *Shipbuilding of China* (Supplement) 118-124 (in Chinese).
4. LIU Yujun, ZHANG Difu, JI Zhuoshang, et al. (1999). Study of Mathematical Models Construction Method for Plate Bending by Line Heating Based on BP Neural Network. *Journal of Dalian University of Technology*. **39:6** 797-801 (in Chinese).
5. LIU Yujun, WANG Dong, JI Zhuoshang, et al. (2000). Optimal Design of Hull Plate Processing Plan of Line Heating. *Journal of Dalian University of Technology*. **40:2** 207-209 (in Chinese).

Practical Design of Ships and Other Floating Structures
You-Sheng Wu, Wei-Cheng Cui and Guo-Jun Zhou (Eds)

© 2001 Elsevier Science Ltd. All rights reserved

NUMERICAL SIMULATION OF WELDING DISTORTIONS IN LARGE STEEL STRUCTURES

Lars Fuglsang Andersen

Section of Maritime Engineering, Department of Mechanical Engineering
Technical University of Denmark
DK-2800 Kgs. Lyngby, Denmark

ABSTRACT

The scope of the present paper is to describe a technique which combines several methods to predict welding distortions in large-scale industrial welding applications. The template is established in three steps: First, a general model is made allowing the essential welding mechanics to be captured in fillet welding. Subsequently, mesh grading techniques and dynamic meshing are used to enhance the computational efficiency. Finally, substructuring, global shell models and dynamically meshed models are combined in a template for further increase of the efficiency.

KEYWORDS

Large-scale welding applications, numerical welding simulation, dynamic meshing, templates.

1 INTRODUCTION

Geometrical distortions in the construction of steel structures are primarily caused by poor set-up of assemblies and thermomechanical processing such as welding. The distortions accumulate throughout the process chain and necessitate frequent compensation rework to maintain an acceptable distortion level. The present paper regards the assessment of welding distortions for analysis of manufacturing-related issues such as the effect of welding sequence. The paper provides mainly a summary of the work presented in Andersen (2000, 2001a,b,c), which addresses the following tasks:

- Find all pertinent parameters and establish a basic model, which can account for the essential welding mechanics in distortion prediction
- Increase the computational efficiency of welding simulation by the use of optimised mesh grading techniques and dynamic meshing
- Develop a template that enables each weld line of an assembly to be modelled in detail one at a time without neglecting the interaction between weld lines

The above techniques have proved to increase the computational efficiency significantly.

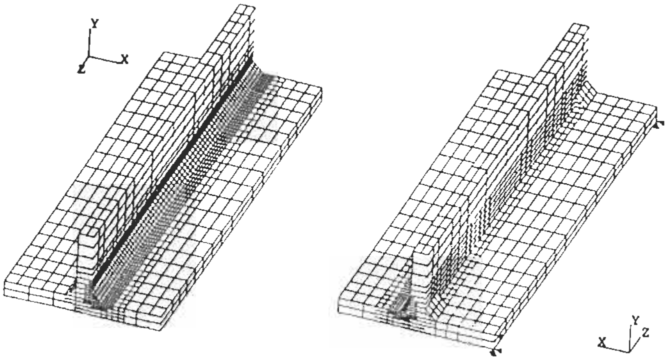

Figure 1: *Mesh topology employed for general models.*

2 BASIC MODEL

A basic model for fillet welding with the emphasis on the modelling of geometrical restraints was established in Andersen (2000,2001a). The general aspects of the model may be described as follows: The thermal and the mechanical analysis are sequentially coupled. The material is modelled as thermo-elasto-plastic with temperature-dependent material properties. The microstructural effects are included indirectly through the microstructural dependency on the cooling time and the austenisation peak temperature. A small strain implicit formulation, which disregards the geometrical non-linearities ,is applied to the mechanical analysis. Rate independent plasticity is assumed and modelled by use of the von Mises criterion, the associated flow rule and kinematic hardening. Further, transformation induced plasticity (TRIP) is accounted for.

The finite element applied is a version of the graded element developed by McDill et al. (1987). The 8-26 noded isoparametric hexahedron is similar to the familiar 8-noded linear brick but the constraints associated with mesh grading are embedded in the shape functions to ensure interelement compatibility. The variable number of nodes and the interelement compatibility make the graded element extremely efficient in mesh grading algorithms. An example of the mesh topology employed is shown in Figure 1.

Considerable effort was placed on the modelling of the geometrical aspects. The web and the base plate are allowed to move relatively to each other in welding, restrained at the beginning only by contact and tack welds. As the filler elements are activated, the parts are locked relatively to each other in the distorted configuration. The modelling of this phenomenon involves dynamic activation of fillet elements, dynamic coupling of parts and modelling of contact between web and base plate. It was shown that the modelling of these factors is essential for a physical correct prediction of the deformation pattern.

3 DYNAMIC MESHING

The basic model establishes the basis for the dynamic remeshing scheme developed in Andersen (2000, 2001c). In dynamic meshing it is exploited that the thermal and the mechanical activity are localised in the region of the heat source and the basic task is therefore to provide a dense mesh only where needed and thus, reduce the number of DOFs. The graded element introduced in the basic model has already

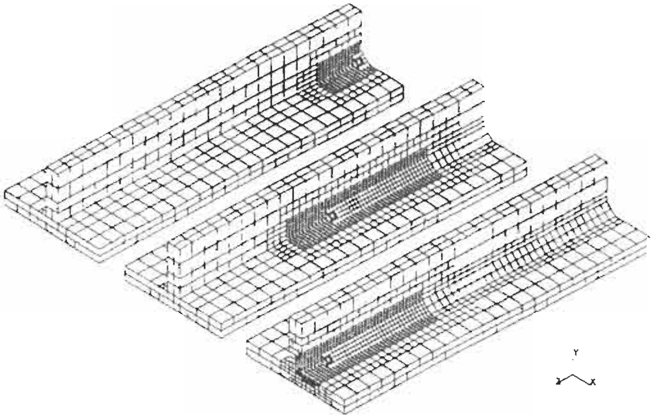

Figure 2: *Examples of meshes in dynamic meshing.*

attributed to increased efficiency and its superior mesh grading characteristics are essential to dynamic meshing. The dynamic mesh refinement scheme has been developed with the emphasis on displacements in the data mapping between meshes as distortion prediction is of primary interest to the present work. In Figure 2, three out of twelve meshes used for a simulation are shown, representing start, intermediate and final calculation. By investigation of the mesh density required in dynamic meshing, it was shown that accurate prediction of distortions can be obtained even if the mesh refinement is decreased considerably to increase the computational efficiency. The use of dynamic meshing enables simulation of welding applications which was previously far beyond the computational capability. As an example, the effect of tack weld positioning has been investigated for a large T-profile which contains more than 3.3 metres of weld in total and its size therefore surpasses most industrial welding applications. Altogether, 5 tack welds are applied to each T-profile, positioned at the weld line as indicated by the numbers in Figure 3. In welding, the first fillet is laid at the right side of the web, starting at the far end.

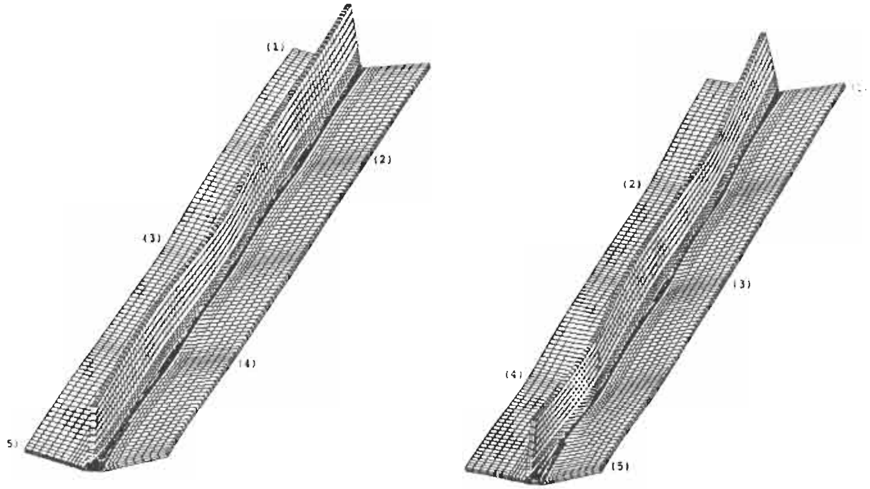

Figure 3: *Deformation mode depending on tack weld positions (scaling factor 30)*

It is interesting to notice that the deformation mode of especially the web is highly dependent on the tack weld positioning. In fact, the modes are directly opposite to each other and correspond therefore to the difference in tack weld positions. In the simulation it was found that the positions of the first few tacks were decisive for the general deformation mode as the influence of the succeeding tack welds is insufficient to cause large alterations once the deformation mode has been initiated.

The computation time used for each model is 120 hrs on a HP J5000 workstation, including the thermal and the mechanical simulation for both fillets. Holding the capability of the workstation against the standards of today, a considerable reduction in computation time is realistic.

4 THE LOCAL/GLOBAL TEMPLATE

The efficiency obtained by graded elements and moving mesh algorithms is inadequate when the objective is simulation of welding in large structures such as ship sections. The essential problem of dynamic mesh refinement is that the structure should be discretised at least to the level where geometry, stresses and deformation can be represented with adequate accuracy at ambient temperature. More precisely, unwelded regions should be discretised to represent geometry and restraints properly. The welded regions should also hold the stresses and deformations accumulated in welding and, hence, further discretisation is required. As a result the number of DOFs necessary to represent a given structure at the coarsest refinement level increases very quickly beyond what is computationally attainable when the size of the structure grows.

In the present context a template is defined by a bundle of techniques for welding simulation in large structures. Generally, templates are based on further approximations compared to the full simulation. The essence is how these approximations are chosen and how they affect the accuracy of the prediction. To predict the distortions of an assembly rather extensive requirements are imposed on the template to be developed. In addition to the factors essential to the local modelling, it is necessary further to account for the stiffness of the surrounding structure and to inclued the stress and deformation caused by preceding welding on the assembly. These factors are central to a template capable of predicting the effect of different welding sequences. A template denoted the Local/Global template or just the L/G template has been developed for the purpose in Andersen (2000, 2001b).

The subassembly chosen for analysis is a part of a transverse web frame in a container vessel and is particularly interesting as it has caused significant problems in production due to welding deformations. The global model of the subassembly is shown in Figure 4(a) and is composed of linear elastic shell elements.

As the global shell model is not suited for welding simulation, each weld line is represented by a local solid model, equivalent to the dynamically meshed models shown previously. The idea behind the L/G template is to link the local models to the global and thus enable a proper representation of both the boundary conditions for the local models and the accumulated distortions in the global model. Moreover, it is exploited that at large part of the structure can be modelled by substructures due to its linear elastic response at low temperatures. The steps in the L/G template may be described briefly as follows: The global model is substructured and included as boundary conditions for the first local model as illustrated by Figure 4(b). The welding response is calculated and the deformations are used to update the distortions of the global shell model as shown in Figure 4(c). The deformed global model is used to establish the boundary conditions in the modelling of the next weld line so that the interaction between weld lines is included in the modelling and the effect of welding sequence can therefore be accounted for. The specific calculation steps of the template and issues such as the updating of geometry, the combination of shells and solids, the extraction of boundary conditions and substructuring are addresses in detail in Andersen (2000, 2001b).

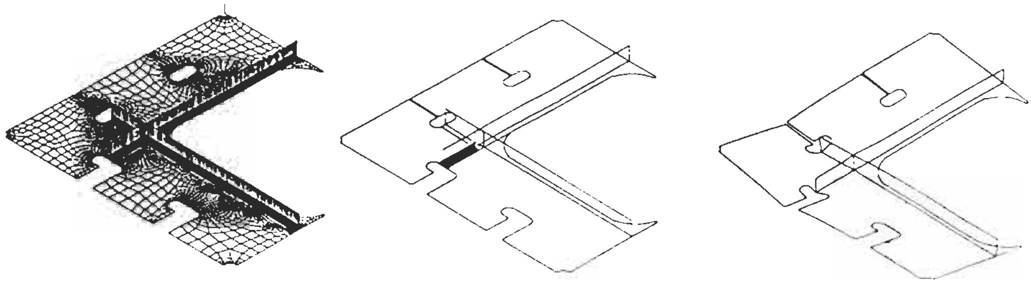

(a) (b) (c)

Figure 4: *The L / G template.*

The L/G template provides a method for simulation of welding in large assemblies. The template makes it possible to represent properly the accumulated distortions and the boundary conditions of the local solid models. The employment of local solid models offers further a detailed simulation of the welding response as the local models include dynamic activation of fillet elements, dynamic coupling of parts, the modelling of contact between parts and account for the positioning of tack welds. There are, however, also drawbacks related to the L/G template. First, it is presupposed that the welds are cooled to ambient temperature before the next weld is initiated. Secondly, the stresses cannot be represented in the weld line regions by the global model since the shell elements representing the local models have been made stress-free in the procedure used for displacement updating. Thirdly, and possibly most important, the modelling complexity of the implementation of the template is rather large. The use of dedicated subroutines facilitates, however, the application of the template and makes it relatively easy to modify e.g. the welding sequence. These disadvantages are, however, insignificant in comparison with the capability offered by the template, especially as there is no alternative available for welding simulation in large assemblies.

To illustrate the capability of the template the effect of welding sequence on the final displacement field is considered. The L/G template has been applied to the arbitrary welding sequences shown in Figure 5. The effect of welding sequence is illustrated in Figure 6 by comparison of the final y-displacements which results from weld sequence 1 with those resulting from weld sequence 2. The differences observed are not only related to the magnitude but also to the qualitative deformation pattern and it may be concluded that weld sequence 2 results in less deformation.

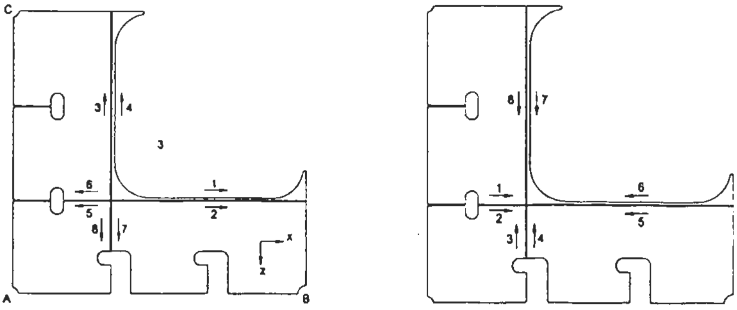

(a) Sequence 1. (b) Sequence 2.

Figure 5: *Welding sequences investigated.*

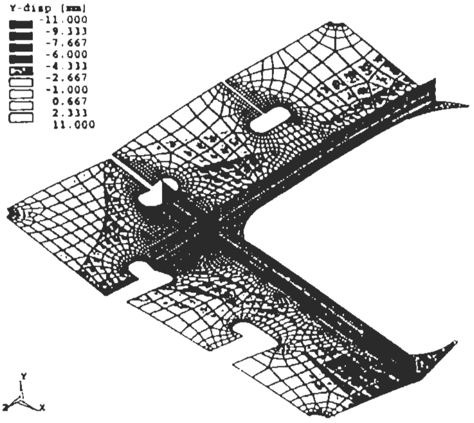
Y-disp [mm]
-11.000
-9.333
-7.667
-6.000
-4.333
-2.667
-1.000
0.667
2.333
11.000
Y
Z
X

(a) Weld sequence 1

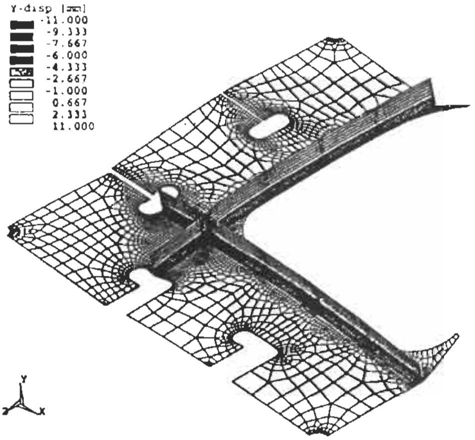
Y-disp [mm]
-11.000
-9.333
-7.667
-6.000
-4.333
-2.667
-1.000
0.667
2.333
11.000
Y
Z
X

(b) Weld sequence 2

Figure 6: *Final y-displacements resulting from weld sequences 1 and 2 (scaling factor 15).*

Figure 6: Final y-displacements resulting from weld sequences 1 and 2 (scaling factor 15).

5 COMPUTATIONAL EFFICIENCY

A significant increase in computational efficiency has been obtained by the techniques presented but seen in relation to the welding application, which contains more than 8 metres of weld, it is still a time consuming task to compute the welding distortions. The time used for one sequence adds up to approximately 290 hrs on an HP J5000 workstation. Considering the size of the subassembly this is very efficient seen from a simulation point of view, especially, if the capability of the workstation is taken into consideration. Even a low cost multi processor PC and the use of code parallisation will make it possible to reduce the computation time to less than 150 hrs. Hence, powerful workstations will reduce the computation time considerably and allow the L/G template to be applied to investigation of optimal welding sequences.

6 CONCLUSION

The above results illustrate that the L/G template can be applied to welding distortion prediction in large-scale industrial welding applications and that it can account for the effect of welding sequence. Thus, the basic capability needed for a welding response prediction tool has been established. Although, no experiments were made to validate the results, it is safe to conclude that the predicted level of magnitude is the same as the level observed for the application in production.

Acknowledgments

The author sincerely thanks Professor Dr. Techn, Jørgen Juncher Jensen, MEK, DTU for inspiration and ideas concerning the present work.

References

Andersen, L. F. (2000). Residual stresses and Deformations in Steel Structures, *PhD thesis*, Department of Naval Architecture & Offshore Engineering, Technical University of Denmark.
Andersen, L. F. (2001). Numerical Modelling and Simulation of Fillet Welding. *Journal of Engineering Materials and Technology.*
Andersen, L. F. (2001). Numerical Prediction of Welding Distortions in Large-Scale Structures. *Journal of Engineering Materials and Technology.*
Andersen, L. F. (2001). Welding Simulation with Emphasis on Computational Efficiency. *Journal of Engineering Materials and Technology.*
McDill, J., Goldak, J., Oddy, S., and Bibby, J. (1987). Isoparametric Quadrilaterals and Hexahedrons for Mesh-Grading Algorithms, *Communications in Applied Numerical Methods*, **3**, 155-163.

3. HYDROMECHANICS

Practical Design of Ships and Other Floating Structures
You-Sheng Wu, Wei-Cheng Cui and Guo-Jun Zhou (Eds)
© 2001 Elsevier Science Ltd. All rights reserved

SIMULATION OF VISCOUS FLOW OF MODERN SURFACE SHIPS USING THE FINFLO RANS SOLVER

Ting-Qiu Li, Jerzy Matusiak

Ship Laboratory, Helsinki University of Technology
P.O.Box 4100(Otakaari 4) FIN-02015 HUT, Finland

ABSTRACT

A FINFLO solver for simulation of a turbulent free-surface flow around a modern ship has been developed through resolving the RANS equations with the artificial compressibility that incorporates a treatment of the free-surface boundary conditions. Within a moving mesh system, a cell-centred finite-volume multigrid scheme and two turbulence models, the Baldwin-Lomax model and the Chien's low Reynolds number k-ε model, are implemented. A non-linear free-surface boundary condition is satisfied on the exact location of the surface. Test cases are three benchmarks recommended by the ITTC, the DTMB 5415 model, the KCS model and the HTC model, including the tanker model from the industry. The convergence performance and the effects of the grid size on the waves are investigated. The computational results are validated and they are in good correlation with the EFD data in terms of the free-surface waves and the total resistance coefficient.

KEYWORDS

Benchmark test , Viscous free-surface flow, Ships with a transom, FINFLO RANS solver, a moving mesh.

1 INTRODUCTION

A FINFLO-SHIP RANS version for simulation of a turbulent free-surface flow around a modern ship in a numerical water tank has been developed by our CFD group at Helsinki University of Technology (HUT). The capability of a numerical scheme provides the possibility for a ship design using the CFD techniques. In our approach, the RANS equations with the artificial compressibility are resolved by a cell-centred finite-volume multigrid scheme; an interface fitting method is implemented in order to capture explicitly the interface between water and air, which results in an exactly non-linear kinematic free-surface boundary condition is easy to be resolved. As a result, a high accuracy can be achieved for the ship waves, whereas approximately dynamic free-surface boundary conditions are employed on this surface. The steady state computations are performed on two selected transom types: a dry or a partially wetted transom. Our approach is an uncoupled algorithm. This implies that all three components of the velocities on the free surface are determined with the extrapolation.

To validate our approach, various types of ship geometry, such as the DTMB 5415 model, the KCS model, the HTC model and the tanker model, are used as the test cases with two turbulence models, the Baldwin-Lomax model and the Chien's low Reynolds number k-ε model. The convergence performance and the effect of the grid density on the free-surface waves are investigated. The results obtained are compared well with the experimental data provided by the KRISO, the INSEAN, the shipyard and the HSVA. For the former two test cases, an improvement for the free-surface waves has been achieved as compared with our latest work (Li et al., 2000), which has been presented in the workshop held recently at Gothenburg (Larsson, et al., 2000). Without doubt, the studies from CFD groups of various countries represent the major advances in this area, although just a few CFD groups completed these two cases in this workshop.

2 NUMERICAL METHODS

2.1 Mathematical Models

On the Cartesian co-ordinate (x, y, z, t) system, where the origin is fixed at the intersection of the bow with the still free surface, x is positive in the aft direction, y is positive towards the starboard and the z-direction is positive upwards, the RANS equations can be written in the compact form, namely

$$\frac{\partial U}{\partial t}+\frac{\partial (F-F_v)}{\partial x}+\frac{\partial (G-G_v)}{\partial y}+\frac{\partial (H-H_v)}{\partial z}=Q \tag{1}$$

where the variable $U=(\rho, \rho u, \rho v, \rho w, \rho k, \rho\varepsilon)^T$. The inviscid fluxes (F, G, H), the viscous fluxes (F_v, G_v, H_v) and the source term Q are expressed as, respectively

$$F=\begin{pmatrix}\rho u\\ \rho u^2+\psi\\ \rho vu\\ \rho wu\\ \rho uk\\ \rho u\varepsilon\end{pmatrix},\qquad G=\begin{pmatrix}\rho v\\ \rho uv\\ \rho v^2+\psi\\ \rho wv\\ \rho vk\\ \rho v\varepsilon\end{pmatrix},\qquad H=\begin{pmatrix}\rho w\\ \rho uw\\ \rho vw\\ \rho w^2+\psi\\ \rho wk\\ \rho w\varepsilon\end{pmatrix}. \tag{2}$$

$$Q=\begin{pmatrix}0\\0\\0\\0\end{pmatrix} the\ B-L\ \mathrm{mod}\ el;\qquad Q=\begin{pmatrix}0\\0\\0\\0\\ P-\rho\varepsilon-2\mu\dfrac{k}{d^2}\\ c_1\dfrac{\varepsilon}{k}P-c_2\dfrac{\rho\varepsilon^2}{k}-2\mu\dfrac{\varepsilon}{d^2}e^{-y'/2}\end{pmatrix} the\ k-\varepsilon\ \mathrm{mod}\ el \tag{3}$$

and

$$F_v=\begin{pmatrix}0\\ \tau_{xx}\\ \tau_{xy}\\ \tau_{xz}\\ \mu_k\left(\dfrac{\partial k}{\partial x}\right)\\ \mu_\varepsilon\left(\dfrac{\partial \varepsilon}{\partial x}\right)\end{pmatrix},\qquad G_v=\begin{pmatrix}0\\ \tau_{xy}\\ \tau_{yy}\\ \tau_{yz}\\ \mu_k\left(\dfrac{\partial k}{\partial y}\right)\\ \mu_\varepsilon\left(\dfrac{\partial \varepsilon}{\partial y}\right)\end{pmatrix},\qquad H_v=\begin{pmatrix}0\\ \tau_{xz}\\ \tau_{yz}\\ \tau_{zz}\\ \mu_k\left(\dfrac{\partial k}{\partial z}\right)\\ \mu_\varepsilon\left(\dfrac{\partial \varepsilon}{\partial z}\right)\end{pmatrix}. \tag{4}$$

ρ is the density of the fluid, the mean-velocity components in the x-, y- and z-directions are denoted by u, v and w, and ψ is the so-called piezometric pressure. For the k-ε model, k and ε are the turbulent kinetic energy and the dissipation of turbulence, respectively, d is the normal distance from the wall, and P is the production of turbulent kinematic energy.

The viscous stress tensors, τ_{ij} (i, j = 1, 2, 3), are defined as

$$\tau_{ij} = (\mu + \mu_t)\left(\frac{\partial u_i}{\partial x_j} + \frac{\partial u_j}{\partial x_i} - \frac{2}{3}(\nabla \cdot \vec{V})\delta_{ij}\right) \tag{5}$$

where $\mu=\rho\nu$ and $\vec{V} = u\vec{i} + v\vec{j} + w\vec{k}$. ν is the kinematic viscosity and δ_{ij} is the Kronecker's symbol. μ_t is the turbulent viscous coefficient determined by two turbulence models, the Baldwin-Lomax (B-L) turbulence model and the Chien's low Reynolds number k-ε model, without a wall function in the present case. The equation of the state of motion for a compressible fluid with the artificial compressibility is given by $\psi=c^2\rho$, where $c = \varsigma_t\sqrt{u^2 + v^2 + w^2}$ and ς_t is the constant.

*2.2 **Initial and Boundary Conditions***

2.2.1 Initial conditions

An uniform flow, a flat free surface and a constant distribution of the turbulent quantities are specified.

2.2.2 Boundary conditions

On the free surface: the wave height h (x, y, t) is evaluated by $\frac{\partial h}{\partial t} + u\frac{\partial h}{\partial x} + v\frac{\partial h}{\partial y} = w$. In the present case, three components of the velocities (u, v, w) are determined with the extrapolation, and the pressure ψ is updated by $\psi = \rho g h$. k and ε on this surface are given with the mirror conditions.

- On the wetted part of the hull surface: u = v = w = 0, k = k_{min} and $\mu = \mu_{min}$ are imposed, whereas the pressure on this surface is obtained by the Neumann approach.
- At the inlet: the uniform flow and the constant turbulence variables are given.
- At the outlet: all variables are extrapolated with a zero-gradient approach.
- On the centreline boundary and the external boundary: the mirror conditions for all variables are implemented.

*2.3 **Numerical Solution***

During the process of the resolution of the bulk RANS flow, the Roe's approach with the MUSCL type and a central-difference approach are separately implemented for the inviscid fluxes and the viscous fluxes; the solution vectors are updated by the DDADI-factorization with the local time step; and the convergence rate is improved by the V-cycle of the multigrid method. Once the solutions for the bulk RANS flow are given, the spatial derivative on the free surface is evaluated with a third-order upwind difference/the second-order nonessential oscillation (ENO) scheme; and the wave height is updated with the second-order explicit Adams-Bashforth scheme. Thus, the pressure on the free surface is adjusted. This procedure is repeated until the steady state is reached.

In the present approach, an asymptotical method for the treatment of the free surface is implemented. First, a zone used for an extrapolation of the free surface is specified, and it should be close the hull surface. Secondly, to maintain this zone as small as possible, the local filtering is applied, which covers this zone. Finally, the free surface in this zone is determined by a linear least-square fitting. The benefit is that problems, such as a high aspect ratio within the boundary layer and a numerical singularity at the contact line, can be avoided. Note that at a transom stern, the transom is dry for the KCS model and the HTC model using the dry-transom model but a partially wetted transom is maintained for the DTMB 5415 model and the tanker model. This implies that the water is enforced to detach from the base of the transom junction for the former; a flow adheres to the transom for the latter. Furthermore, a linear extrapolation for the wave height in the domain close to the transom is required due to the discontinuity edge of the transom. The details of this approach are given by Li (2001).

3 SIMULATION OF THE TEST CASES

3.1 Mesh

Figure 1 displays an initial O-O topology grid, where just one block mesh is applied for all test cases. Two grid levels, the 2-level (the coarse mesh) and the 1-level (the fine mesh) are used for the computations (see Table 1). This means that simulations are initiated on the coarse grid, and then the solution at the steady state is interpolated to the fine mesh. All calculation is carried out on a Silicon Graphics Origin2000 provided by the Centre for Scientific Computing (CSC).

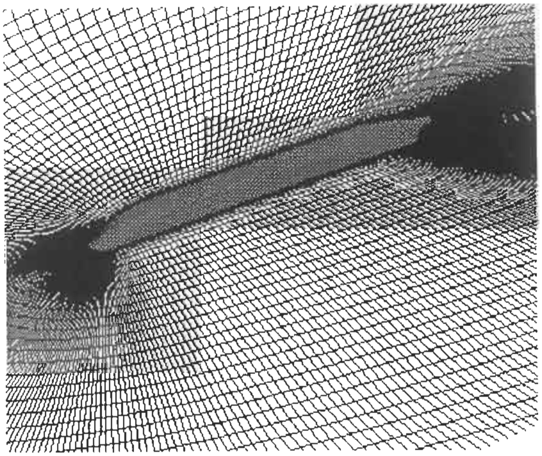

Figure 1: An initial single O-O mesh

TABLE 1
COMPUTATIONAL CONDITIONS FOR ALL THE TEST CASES

	KCS	DTMB 5415	Tanker	HTC
F_n	0.26	0.28	0.15	0.25
R_n	1.4×10^7	1.28×10^7	8.727×10^6	1.255×10^7
Coarse mesh	81×81×31	97×81×17	69×57×25	71×65×23
Fine mesh	161×161×61	193×161×33	137×113×49	141×129×45

3.2 Convergence History

Figure 2 shows convergence histories of the L_2 norm residuals for the momentums (U, V, W, P) and the total resistance coefficient, C_T, at the fine mesh for all the test cases, respectively. A monotone decreasing of these variables can be observed, except for the tanker model, where an oscillatory convergence is obtained. For all the test cases, C_T has converged to a certain value close to the corresponding data (see Fig. 2).

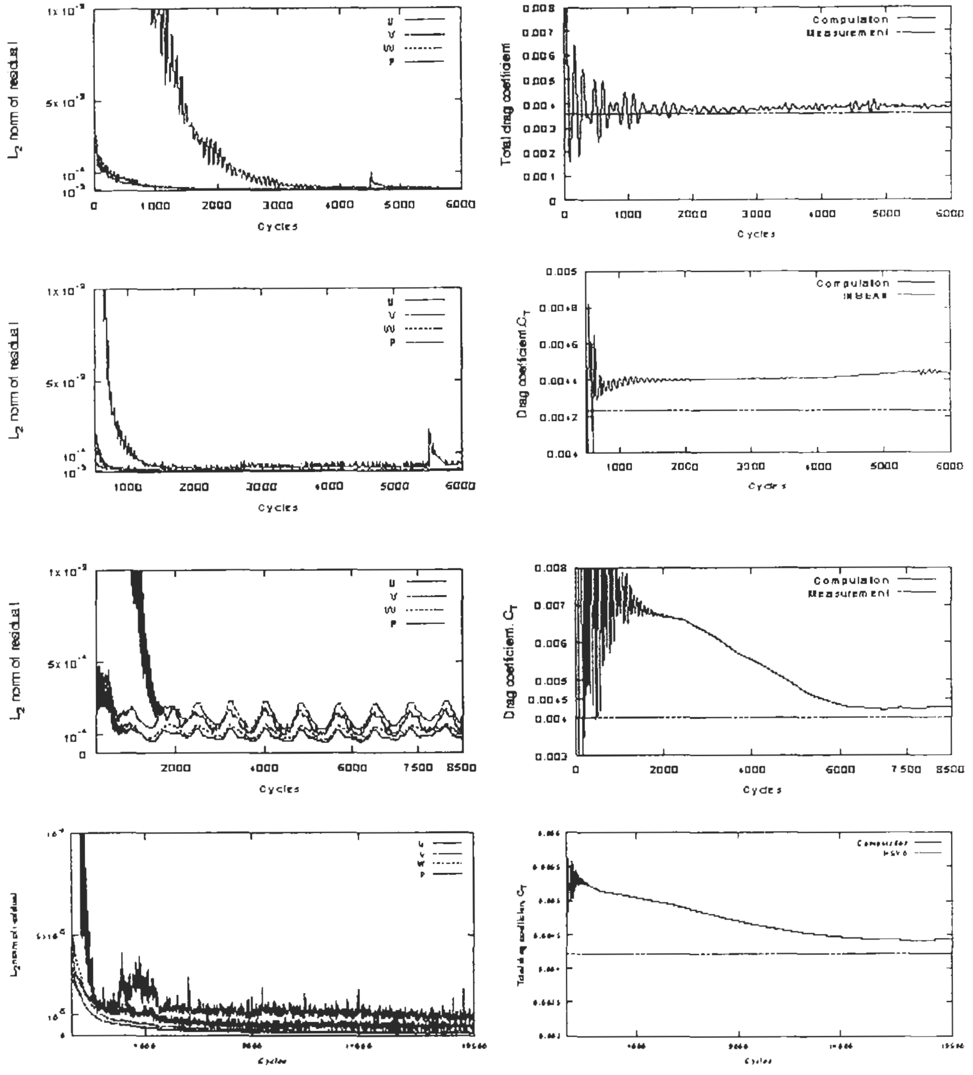

Figure 2: Convergence histories of (U, V, W, P) residuals and Ct at the fine mesh. The KCS model, the DTMB 5415 model, the tanker model and the HTC model from top to bottom

3.3 *Effect of Grid Density*

Figure 3 displays the wave profiles along the hull surface and the wave contours at two grid levels only for the KCS model and the DTMB 5415 model, where the origin (x/L=0.0) is at the midship and the bow is located at x/L=-0.5. The wave patterns close the hull surface are well correlated with the measurements. Furthermore, the results indicate that the influence of the two grid levels on the near-wall waves is weak. It is obvious that the results at the fine mesh are closer to the experimental data.

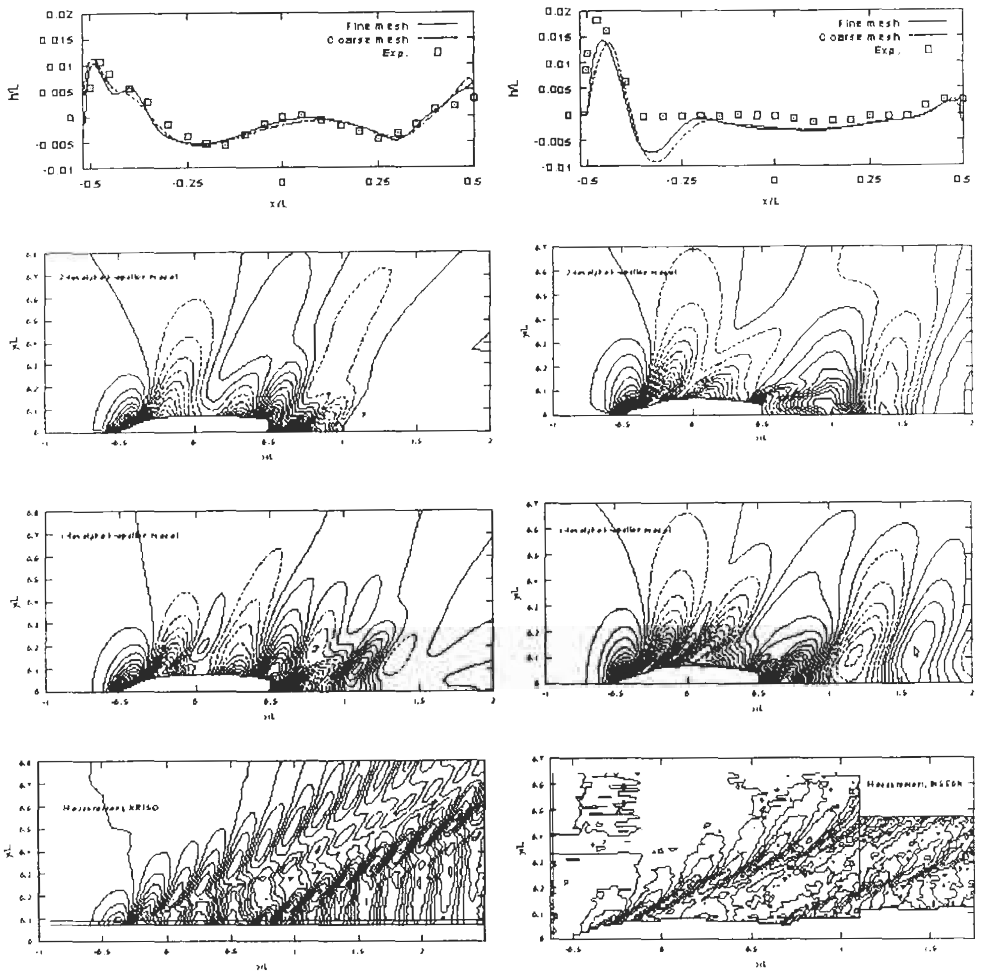

Figure 3: Effect of two grid levels on the waves. Left: the KCS model; right: the DTMB 5415 model. Solid lines for crests; dashed lines for trough; levels: 0.0005

3.4 Wave Patterns

Figure 4 shows the wave patterns at the fine mesh for the tanker model and the HTC model, respectively, using the B-L model and the k-ε model. The shape of the wave profiles along the hull is predicted well (see Figs. 3 and 4), except for the case with the DTMB 5415 model, where the steep crest wave crests are not predicted well and the first troughs are too deeper. Moreover, the effects of the turbulence model on the waves are insensitive. Note that the effects of the damping on the wave pattern, the diverging and the transverse wave systems, in the wake are obvious for the far-field waves, as shown in Figs. 3 and 4, due to viscous and/or the grid size.

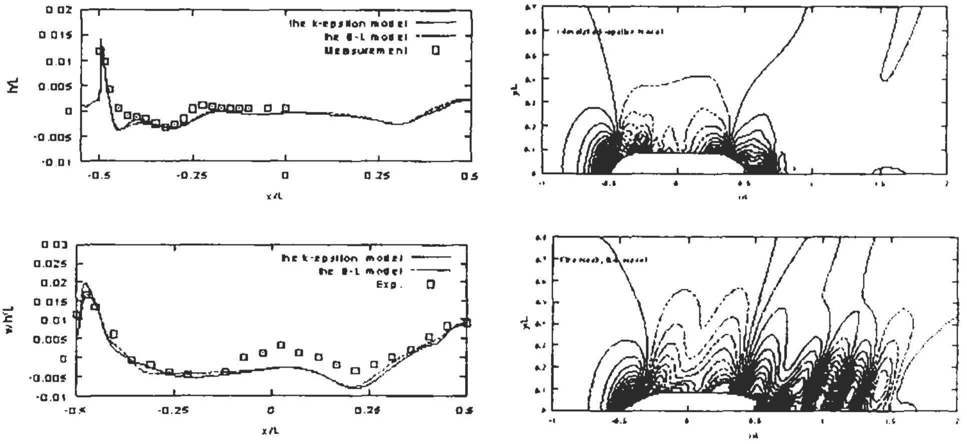

Figure 4: Surface-wave profiles and wave contours for the B-L model and the k-epsilon model. Top: the tanker model; bottom: the HTC model.

4 CONCLUSIONS

Utilizing our method, the FINFLO-RANS code with a moving mesh, the overall degree of accuracy has been achieved for simulation of a turbulent free-surface flow around a modern ship. This has be demonstrated with the benchmarks: the KCS model, the DTMB 5415 model, the tanker model and the HTC model, using the B-L model and the k-ε model, respectively. They are in very good agreement with the experimental data available. It is believed that the present study can provide the detailed and extensive information for analysis and design of ship.

Acknowledgements

The present work is sponsored by the Technology Development Centre (Tekes). Thanks are given to the members in CFD group at the HUT for their help.

References

Larsson, L., Stern, F., and Bertram V. (2000). A Workshop on Numerical Ship Hydrodynamic, Gothenburg 2000 Gothenburg, Sweden.

Li, T., Sachez-Caja, A., Marito, J. and Matusiak, J. (2000). Simulation of Free-Surface Viscous Flow around Two Ship Hulls Using RANS Solver FINFLO. A Workshop on Numerical Ship Hydrodynamics, Editors by Lars Larsson, Fred Stern and Volker Bertram, Gothenburg.

Li, Tingqiu, (2001). A Benchmark Test Case for a Viscous Free-Surface Flow around a Modern Ship: the HTC Model, the KCS Model, the DTMB 5415 Model and the Tanker Model. Report. Ship Laboratory, Helsinki University of Technology, Finland.

Practical Design of Ships and Other Floating Structures
You-Sheng Wu, Wei-Cheng Cui and Guo-Jun Zhou (Eds)
© 2001 Elsevier Science Ltd. All rights reserved

VISCOUS FLOW AROUND ROTATING SHIPS

Carlos Levi and Juan B. Villa Wanderley

Department of Ocean Engineering, Universidade Federal do Rio de Janeiro
Rio de Janeiro – 21945-970, Brazil

ABSTRACT

The present stage of viscous flow numerical analysis combined with computer technology latest advances made viable the mathematical treatment of robust and complex problems. Many heavy numerical problems that solutions would be just unthinkable not more than ten years ago may be now dealt with in a reliable and fairly accurate manner. A truly example of this kind of problem would be the calculation of hydrodynamic loads acting on rotating ships.

This paper discusses the numerical solution of viscous flow around slowly rotating arbitrary floating bodies in the presence of an incident flow. The solution of such a problem raises practical interest due to applications, for instance, as in the case of FPSO/FSO ships used in deep water oil production offshore.

In the present solution, the complete incompressible Navier-Stokes equations will be solved through a Finite Difference based-solver using generalized coordinates defined on a moving grid. The constitutive equations will be discretised in the space by second order central differences. Euler Explicit method performs the time-marching and the Successive Over Relaxation method solves the Poisson Equation at each iteration to calculate pressure distribution.

KEYWORDS

Viscous Flow, Rotating Ships, Finite Difference, Moving Grid

1 INTRODUCTION

Offshore oil and gas production is advancing fast towards water depth deeper and deeper. In the last couple of years, world records have been successively superceded. Oil industry is about to achieve production in fields approaching 2000m water depth while keeping on exploring new oil reservoirs in regions close to 3000m deep.

As water depth increases, the distance from oil field to mainland depots increases at similar rates and more hostile the ocean environment becomes. In such operational conditions the use of VLCC ship tanker has been proved to be technical and economically appealing.

Good hydrodynamic characteristics in severe sea environments, adequate storage capability and possibly the low prices of tanker hulls in the ship market are the main reasons to justify the increasing popularity of tanker hull based production systems (Floating Storage and Offloading – FSO and Floating Production Storage and Offloading – FPSO) among offshore oil producer companies.

The complete assessment of the dynamic behavior of moored tankers depends very much on the accuracy of the hydrodynamic loading and response evaluation that need be performed. Potential and viscous effects on the FSO/FPSO come into play equally important role on the acting flow around the ship hull. Furthermore, translational and rotational motions of the hull have to be incorporated all together into the analysis to produce a realistic picture of the physical problem.

Recently, Computational Fluid Dynamics (CFD) has been experiencing rapid advances due to both computer technology progress and efficient algorithms that have been developed to solve the Reynolds-averaged Navier-Stokes (RANS) equations used in the flow analysis around ship hulls, Ratcliffe (1998). The present work is a contribution to the numerical solution of the viscous flow around slowly rotating ship-like bodies in the presence of currents.

To tackle such a complex, robust numerical problem one has to search for a correct balance between accuracy and efficiency of the solution. The strategy is therefore to find a fair compromise between accuracy and computing time. Here, the authors adopted an algorithm specially tailored, and therefore unique, to perform an efficient solution in the usually time consuming three-dimensional incompressible viscous flow around arbitrary shapes.

In the present solution, the complete incompressible Navier-Stokes equations will be solved through a Finite Difference based-solver using generalized coordinates defined on a moving grid. The algorithm used to solve the set of incompressible flow equations was recently developed by Wanderley (2001). It assumes that water behaves as a slightly compressible fluid enough to provide the convenient coupling of the Continuity equation. The numerical solution benefits then from the coupling but avoids the need of any extra energy equation. Such a feature enables saving a lot of processing time, at the same time that does not imply in any sensitive burden on accuracy or stability of the solution. The constitutive equations will be discretised in space by second order central differences. Euler Explicit method performs the time-marching and the Successive Over Relaxation method solves the Poisson Equation at each iteration to calculate pressure distribution.

2 MATEHEMATICAL FORMULATION

2.1 Governing Equations

The complete discussion of the mathematical formulation of the slightly compressible approach to solve incompressible flow are presented in detail in Wanderley (2001). The basic idea behind the method was to include the time derivative term in the Continuity equation of the incompressible flow. But now, by introducing a new parameter into the flow equations based on the proper compressibility factor of the fluid, it was possible to avoid the need of any extra energy equation. The main benefits from that was to speed up enormously the convergence rate of the numerical solution without any loss of accuracy or numerical stability.

The 3-D slightly compressible N-S equations are written below in conservative form, in general curvilinear coordinates (ξ, η, ζ) and in the dimensionless form.

$$Q_t + E_\xi + F_\eta + G_\zeta + S = 0 \tag{1}$$

$$Q=\frac{1}{J}\begin{Bmatrix}\phi\\ u\\ v\\ w\end{Bmatrix},\quad (2)\qquad E_e=\frac{1}{J}\begin{Bmatrix}\phi U\\ uU+\phi\xi_x\\ vU+\phi\xi_y\\ wU+\phi\xi_z\end{Bmatrix},\quad E_v=\frac{M_\infty}{JR_e}\begin{Bmatrix}0\\ A_1u_\xi+A_2u_\eta+A_3u_\zeta\\ A_1v_\xi+A_2v_\eta+A_3v_\zeta\\ A_1w_\xi+A_2w_\eta+A_3w_\zeta\end{Bmatrix}\qquad (3)$$

$$F_e=\frac{1}{J}\begin{Bmatrix}\phi V\\ uV+\phi\eta_x\\ vV+\phi\eta_y\\ wV+\phi\eta_z\end{Bmatrix},\quad F_v=\frac{M_\infty}{JR_e}\begin{Bmatrix}0\\ A_2u_\xi+A_4u_\eta+A_5u_\zeta\\ A_2v_\xi+A_4v_\eta+A_5v_\zeta\\ A_2w_\xi+A_4w_\eta+A_5w_\zeta\end{Bmatrix}\qquad (4)$$

$$G_e=\frac{1}{J}\begin{Bmatrix}\phi W\\ uW+\phi\zeta_x\\ vW+\phi\zeta_y\\ wW+\phi\zeta_z\end{Bmatrix},\quad G_v=\frac{M_\infty}{JR_e}\begin{Bmatrix}0\\ A_3u_\xi+A_5u_\eta+A_6u_\zeta\\ A_3v_\xi+A_5v_\eta+A_6v_\zeta\\ A_3w_\xi+A_5w_\eta+A_6w_\zeta\end{Bmatrix},\quad S=\frac{1}{J}\begin{Bmatrix}0\\ 0\\ 0\\ M_\infty^2/F_n^2\end{Bmatrix}\qquad (5)$$

where

$$R_e=\frac{u_\infty L}{\upsilon},\quad M_\infty=\frac{u_\infty}{a_\infty},\quad C_p=\frac{p-p_\infty}{\frac{1}{2}\rho u_\infty^2}=\frac{\phi-1}{1/2M_\infty},\quad F_n=\frac{u_\infty}{\sqrt{gL}}$$

$$u=\frac{u^*}{a_\infty};\quad x=\frac{x^*}{L};\quad v=\frac{v^*}{a_\infty};\quad y=\frac{y^*}{L};\quad w=\frac{w^*}{a_\infty};\quad z=\frac{z^*}{L};\quad p=\frac{p'}{\rho a_\infty^2}$$

a_∞ *– sound speed;* L *– characteristic length;* u_∞ *– current speed*

$$\begin{aligned}U&=\xi_t+u\xi_x+v\xi_y+w\xi_z\\ V&=\eta_t+u\eta_x+v\eta_y+w\eta_z\\ W&=\zeta_t+u\zeta_x+v\zeta_y+w\zeta_z\end{aligned}$$

$$\begin{aligned}A_1&=\xi_x^2+\xi_y^2+\xi_z^2\\ A_2&=\xi_x\eta_x+\xi_y\eta_y+\xi_z\eta_z\\ A_3&=\xi_x\zeta_x+\xi_y\zeta_y+\xi_z\zeta_z\\ A_4&=\eta_x^2+\eta_y^2+\eta_z^2\\ A_5&=\eta_x\zeta_x+\eta_y\zeta_y+\eta_z\zeta_z\\ A_6&=\zeta_x^2+\zeta_y^2+\zeta_z^2\end{aligned}\qquad (6)$$

$$J=\begin{vmatrix}\xi_x&\xi_y&\xi_z\\ \eta_x&\eta_y&\eta_z\\ \zeta_x&\zeta_y&\zeta_z\end{vmatrix}$$

2.2 Boundary and Initial Conditions

No-slip condition is imposed over the body surface and the free-stream condition away from the ship. The no-slip condition implies that the fluid particles on the body surface are moving body velocity, say V_x and V_y.

$$u = V_x; \quad v = V_y; \quad w = 0; \quad \frac{\partial p}{\partial \eta} = 0 \tag{7}$$

On the body:

At infinity:

$$u = M_\infty; \quad v = 0; \quad w = 0; \quad \phi = 1 \tag{8}$$

Free-stream characteristics are applied everywhere in the flow to define the initial condition. Equations (13) below show the mathematical representation of this condition.

$$u = M_\infty; \quad v = 0; \quad w = 0; \quad \phi = 1 \tag{9}$$

2.3 Equation of Motion

Applying Newton's second law to the ship with mass *m* under hydrodynamics forces – lift L and drag D, one may obtain the dimensionless form of the equation of motion (10) that has to be solved for initial conditions (11). The equation of motion must be solved simultaneously with the Navier-Stokes equations to compute the ship velocity and ship position (y) that is used to regenerate the moving grid.

$$C_\mu \ddot{y} = C_L(R_e) \tag{10}$$

$$y(0) = 0; \quad \dot{y}(0) = 0 \qquad (11); \quad where: C_\mu = \frac{2m}{\rho D^2} \tag{12}$$

3 NUMERICAL SOLUTION

3.1 Beam-Warming Implicit Scheme

The Beam-Warming (1978) scheme is applied by using the Euler implicit method for time integration - equation (13), that is a convenient choice due to both simplicity and because it does not show restrictions to the step of integration.

$$Q^{n+1} = Q^n + \Delta t \left.\frac{\partial Q}{\partial t}\right)^{n+1} + O(\Delta t) \tag{13}$$

The time derivative is then eliminated from (17) by using the governing equation (1):

$$Q^{n+1} = Q^n - \Delta t\left(E_\xi^{n+1} + F_\eta^{n+1}\right) \tag{14}$$

The so called flux vectors E and F are evaluated in the n+1 time level. Newton's linearization procedure provides the flux vectors in the time level n:

$$E^{n+1} = E^{n} + \left.\frac{\partial E}{\partial Q}\right)^{n}\left(Q^{n+1} - Q^{n}\right) + \cdots \quad ; \qquad F^{n+1} = F^{n} + \left.\frac{\partial F}{\partial Q}\right)^{n}\left(Q^{n+1} - Q^{n}\right) + \cdots \tag{15}$$

Substituting (15) into equation (14), grouping ΔQ terms on the left-hand side of (14), and approximating partial derivatives by central differences, it is possible to write down the following equation:

$$\left\{I + \Delta t\left(\delta_{\xi} A^{n} - \delta_{\xi} M_{\xi}^{n}\right) + \Delta t\left(\delta_{\eta} B^{n} - \delta_{\eta} M_{\eta}^{n}\right)\right\}\Delta Q^{n} = -\Delta t\left(\delta_{\xi} E^{n} + \delta_{\eta} F^{n}\right) \tag{16}$$

where

$$E^{n} = E_{e}^{n} - E_{v}^{n},$$

$$F^{n} = F_{e}^{n} - F_{v}^{n}$$

$$A^{n} = \left.\frac{\partial E_{e}}{\partial Q}\right)^{n}, \qquad B^{n} = \left.\frac{\partial F_{e}}{\partial Q}\right)^{n}, \quad M_{\xi}^{n} = \left.\frac{\partial E_{v}}{\partial Q}\right)^{n}, \qquad M_{\eta}^{n} = \left.\frac{\partial F_{v}}{\partial Q}\right)^{n}$$

$$\delta_{\xi}(\;) = \frac{(\;)_{i+1,j} - (\;)_{i-1,j}}{2} \quad , \quad \delta_{\eta}(\;) = \frac{(\;)_{i,j+1} - (\;)_{i,j-1}}{2}$$

Equation (16) is a penta-diagonal system of algebraic equations that solution can be improved by convenient approximated factorization - Beam and Warming (1978). The left-hand side of (24) below, after proper factorization of (16), presents only ξ and η-derivatives in separate terms. Therefore, the numerical scheme of solution can be split into two steps. The first equation is solved for all interior grid points; then, the second equation is solved for all interior grid points using the previous values of f. In each step, the resulting block tridiagonal system of algebraic equations is solved by application of Thomas algorithm (Anderson, Tannehill and Pletcher, 1984).

$$\left\{I + \Delta t\left(\delta_{\xi} A - \delta_{\xi} M_{\xi}\right)\right\}^{n} f^{n} = (RHS)^{n} \tag{17}$$

$$\vdots$$

$$\left\{I + \Delta t\left(\delta_{\eta} B \;\; - \delta_{\eta} M_{n}\right)\right\}^{n} \Delta Q^{n} = f^{n}$$

$$\textit{where} \qquad (RHS)^{n} = -\Delta t\left(\delta_{\xi} E \;\; + \delta_{\eta} F \;\;\right)^{n} \tag{18}$$

Central difference schemes require artificial dissipation to improve stability – Pulliam (1980). Artificial dissipation suppresses high frequency oscillations and controls the odd-even uncoupling inherent to central difference schemes. The Von-Neumann linear stability analysis applied to the Beam-Warming central difference scheme shows that some artificial dissipation is required to improve stability.

$$\begin{gathered}\left(I + \Delta t\delta_{\xi} A^{n} - \Delta t\delta_{\xi} M_{\xi}^{n} + D_{\xi}^{(2)}\right) f^{n} = (RHS)^{n} + D^{(4)} \\ \\ \left(I + \Delta t\delta_{\eta} B^{n} - \Delta t\delta_{\eta} M_{\eta}^{n} + D_{\eta}^{(2)}\right)\Delta Q^{n} = f^{n}\end{gathered} \tag{19}$$

where

$$D_{\xi}^{(2)} = -\varepsilon_{i}\Delta t J^{-1}\nabla_{\xi}\Delta_{\xi} J; \; D_{\eta}^{(2)} = -\varepsilon_{i}\Delta t J^{-1}\nabla_{\eta}\Delta_{\eta} J; \; D^{(4)} = -\varepsilon_{e}\Delta t J^{-1}\left[\left(\nabla_{\xi}\Delta_{\xi}\right)^{2} + \left(\nabla_{\eta}\Delta_{\eta}\right)^{2}\right] J Q^{n}$$

3.2 Grid Generation

An algebraic grid generator using the multi-surface method – Fletcher (1988) - is used to generate the grid points over and around the ship hull (body fitted grid). The grid is locally orthogonal to the body surface to facilitate the implementation of the boundary condition on the body. To concentrate grid points next to the bow and bow surface, an exponential stretching is used in both stream-wise (ξ) and transversal (η) directions (see Figure 1)

3.3 Free Surface

The free surface is embedded in the grid generated around the ship model and its geometry is obtained by satisfying the free surface conditions:

- pressure is equal to the atmospheric pressure everywhere on the free surface; fluid particles on the
- free surface should remain on the free surface:

$$h_t + uh_x + vh_y - w = 0 \tag{20}$$

3.4 Equation of Motion

The equation of motion is solved simultaneously with the Navier-Stokes equations to compute the velocity and position of the ship. The velocity and position of the ship hull are used to impose the no-slip condition on the body surface and to relocate the ship to generate the new grid points at each time step. The Lax-Wendroff method and Euler explicit method were used to compute the new position and velocity of the ship respectively. The lift coefficient C_L is obtained from pressure and skin friction distribution on the ship surface defined at previous time-step:

$$y^{n+1} = y^n + V_y^n \Delta t + \frac{1}{2} a_y^n \Delta t^2 \tag{21}$$

$$V_y^{n+1} = V_y^n + a_y^n \Delta t \tag{22}$$

where

$$a_y^n = \frac{C_L^n}{C_\mu} \tag{23}$$

To start the time-marching procedure, the initial conditions are taken as:

$$\begin{aligned} y^0 &= 0 \\ V_y^0 &= 0 \end{aligned} \tag{24}$$

4 RESULTS

Previous work – Wanderley (2001) - described results and comparisons done for 2-D incompressible flow around a circular cylinder. Table I reproduces some of the results presented there to demonstrate the very good agreement that with other incompressible methods. On the other hand, the algorithm discussed here presents a very much higher efficiency compared with other methods, lowering significantly the computer time necessary to reach the same level of accuracy.

Applications on 3-D incompressible flow have shown the same positive performance opening concrete possibilities for practical simulations of interest where the amount of computing time is a serious burden. The results discussed below are still preliminary from the point of view of its scope and validation. But they serve to evaluate the potential qualities of the proposed algorithm.

A stationary Wigley hull in incompressible flow at $R_e=1\text{x}10^4$ and $F_r= 0.25$ is considered as an illustrative example:

$$\frac{y}{B}=\frac{1}{2}\sqrt{1-\left(\frac{2x}{L}\right)^2}\sqrt{1-\left(\frac{z}{d}\right)^2} \qquad (25)$$

where

B – max *imum breadth* : L – *total length* ; d – max *imum draft*

TABLE 1

COMPARISONS FOR 2-D FLOW AROUND CIRCULAR CYLINDER (FROM WANDERLEY (2001)
1) Tritton, Exp.(1959) ; 2)Constanceau Bouard (1977); 3) Rengel, Sphaier (1999) 180x160; 4) Wanderley (2001), 100x100 ε_c=6x10^{-2} ; 5) Wanderley (2001), 180x160, ε_c=6x10^{-2} ; 6) Wanderley (2001), 100x100, ε_e=1.0.

References	*Cd*	*L/d*	*a/d*	*b/d*	θ_s	*Time*[*] *(hours)*
1	1.57	-	-	-	-	-
2	-	2.13	0.76	0.59	53.5	-
3	1.61	2.23	0.72	0.58	54.06	11:00
4	1.60	2.20	0.72	0.60	54.60	00:42
5	1.61	2.20	0.71	0.60	54.01	02:06
6	1.58	2.20	0.73	0.59	54.26	00:42

A 100x100x40grid was generated around a model ship, defined in (25), with B/L= 0.10 and d/L=0.0625. Exponential stretching parameter equal to 1.060 in the radial direction has been applied. The minimum distance between the body surface and the external boundary was taken equal to 10 ship length (see Figure 1). Graphical displays of the numerical solution of the flow are shown in Figure 2. These results have been generated by a PC- Pentium III – 64 MB RAM and 500Mhz. The convergence has been reached after 22 hours of processing time, a computational effort relatively low if one compares to other known alternatives.

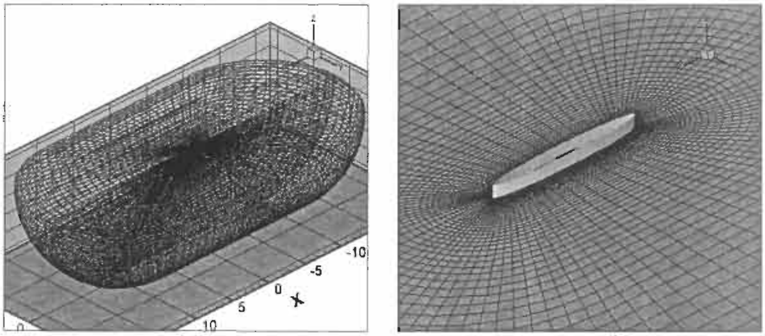

(a) (b)

Figure 1. Computational Grid in the Physical Domain: 100x100x40 (a) Amplified View (b)

---

[*] PC-Pentium III – 550 MHz; *Residue*=$1.0x10^{-9}$

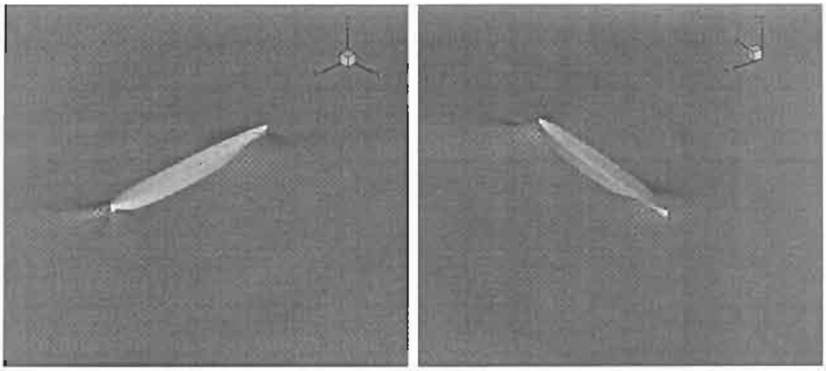

Figure 2: Graphical representation of the 3-D flow around modified Wigley hull
R_e= 10 000; F_r= 0.25.

References

Anderson, D. A., Tannehill, J. C., and Pletcher, R. H. (1984). Computational Fluid Mechnics and Heat Transfer. McGraw-Hill, New York.

Beam, R. M., and Warming, R. F. (1978). An Implicit Factored Scheme for the Compressible Navier-Stokes Equations. *AIAA Journal* **16:4**, 393-402.

Constanceau, M., and Bouard, R. (1977). Experimental Determination of the Main Features of Viscous Flow in the Wake of a Circular Cylinder in Uniform Translation Steady Flow, *Journal of Fluid Mechanics*, **79**, 231-256.

Fletcher, C. A. J. (1988). Computatinal Techniques for Fluid Dynamics. Springer-Verlag, Berlin, Germany.

Hino, T. (1987). Numerical Simulation of a Viscous Flow with a Free Surface around a Ship Model. *Journal of the Society of Naval Architects of Japan* **161**.

Kloker, M., and Konzelmann, U. (1993). Outflow Boundary Conditions for Spatial Navier-Stokes Simulations of Transition Boundary Layer. *AIAA Journal* **31:4**.

Pulliam, T. H., and Steger, J. L. (1980). Implicit Finite-Difference Simulations of Three-Dimensional Compressible Flow. *AIAA Journal* **18:2**, 159-167.

Pulliam, T. H. (1986). Artificial Dissipation Models for the Euler Equation. *AIAA Journal* **24:12**, 1931-1940.

Rengel, J. E., and Sphaier, S. H. (1999). A Projection Method for Unsteady Navier-Stokes Equation with Finite Volume Method and Collocated Grid, Hybrid Methods in Heat and Mass Transfer, **1:4**.

Ratcliffe, T. (1998). Validation of the free surface Reynolds-averaged Navier-Stokes and potential flow codes – Proceedings, *22nd ONR Symposium on Naval Hydrodynamics.*

Schlichting, H. (1979). Boundary Layer Theory. McGraw-Hill, New York.

Steger, J. L. (1978). Implicit Finite Difference Simulation of Flow About Arbitrary Two-Dimensional Geometry. *AIAA Journal* **16**.

Tritton, D. J. (1959). *Journal of Fluid Mechanics*, **6**, 547.

Wanderley, J. B. V., and Levi, C. A. (2000). Simulation of Vortex-Induced Vibrations on a Circular Cylinder by the Numerical Solution of the Compressible Navier-Stokes Equations. Workshop on Vortex-Induced Vibrations of Offshore Structures. São Paulo, Brazil.

Wanderley, J. B. V. (2001). An Algorithm for Slightly Compressible Flows. Proceedings of the 20th International Offshore Mechanics and Arctic Engineering (OMAE) Conference. Rio de Janeiro, Brazil

Practical Design of Ships and Other Floating Structures
You-Sheng Wu, Wei-Cheng Cui and Guo-Jun Zhou (Eds)
© 2001 Elsevier Science Ltd. All rights reserved

NUMERICAL SIMULATION OF FLOWS OVER UNDERWATER AXISYMMETRIC BODIES WITH FULL APPENDAGES

Zhen-Yu Huang and Lian-Di Zhou

China Ship Scientific Research Center, Wuxi 214082, China

ABSTRACT

The numerical method based on flux-difference splitting LU decomposition, implicit high-resolution third-order Essentially Non-Oscillatory (ENO) schemes is constructed for efficient computations of steady-state solution to the three-dimensional, incompressible Navier-Stokes equations in curvilinear coordinates. The flowfields over underwater axisymmetric bodies with a fairwater and four stern appendages are calculated.

The numerical results show that the circumferential-mean non-dimensional velocity profiles at propeller are in good agreement with the experimental data, which can satisfied with the need of wake profile accuracy in the design of propuslor blade. Meanwhile the circumferential distributions of numerical non-dimensional velocity at the propeller plane are also similar with the experimental data, which can be used to predict the water noise generated by vehicle propulsor.

KEYWORDS

Essentially Non-Oscillatory (ENO) Schemes, Flux Splitting, LU Decomposition, Computational Fluid Dynamics (CFD)

1 INTRODUCTION

The flow over an appended body during level flight is characterized by thick boundary layers, vortical flow structure generated by hull/appendage junctures, and appendage turbulent wakes. The spatial nonuniformity and temporal fluctuations of the flow into propulsor significantly affect propulsor noise. For a long period the model experiment is the main way to get data for the flow field over an appended body, but are still limited. CFD numerical methods for the design of submarines and other ships are successfully applied in shipbuilding industry, which can shorten the time needed in the ship design and save lots of research fund. The goal of this paper is to present a CFD numerical method which can be used to study the flow field over underwater bodies with a fairwater and four stem appendages.

The schemes based on flux-difference splitting, implicit high-resolution are constructed for computations of steady-state solutions to the three-dimensional, incompressible conservative Navier-Stokes equations in curvilinear coordinate. These schemes use third-order-accurate Essentially Non-Oscillatory(ENO) differencing for inviscid flux and second-order central differencing for the viscous shear flux. Up to third-order-accurate Essentially Non-Oscillatory(ENO) differencing is achieved through flux reconstruction. The implicit, first-order LU decomposition scheme is applied to flowfield computations of underwater bodies with full appendages.

2 GOVERNING EQUATIONS

Artificial compressibility method, which adds a time-derivative of the pressure to the continuity equation of incompressible Navier-Stokes, can couple the equations of motion with the continuity equation. Then one can apply the most efficient implicit time-dependant methods to the incompressible Navier-Stokes equations, i.e. the complete set of governing equation can be solved simultaneously.
The Navier-Stokes equations in conservation law form for an incompressible, three-dimensional flow are written as

$$Q_t + (E^* - E_v^*)_x + (F^* - F_v^*)_y + (G^* - G_v^*)_z = 0 \tag{1}$$

E^*, F^*, G^* are inviscid flux vectors, E_v^*, F_v^*, G_v^* are viscous flux vectors (Peter, et al. 1988).
Following the artificial compressibility method, the dependant variable vector Q in Eq.(1) are defined as

$$Q = (p, u, v, w)^T \tag{2}$$

Considering a coordinate transformation of the form $\xi = \xi(x, y, z)$, $\eta = \eta(x, y, z)$, and $\varsigma = \varsigma(x, y, z)$, Eq.(1) can be rewritten in strong conversation law form.

$$(Q/J)_t + (E - E_v)_\xi + (F - F_v)_\eta + (G - G_v)_\varsigma = 0 \tag{3}$$

The flux vectors E, F, G are linear combination of E^*, F^*, G^* in Eq. (1). For example, E can be written as

$$E = (\xi_x / J)E^* + (\xi_y / J)F^* + (\xi_z / J)G^* \tag{4}$$

Where J is the Jacobian of the coordinate transformation.

3 NUMERICAL SCHEMES

3.1 High Resolution Schemes for Inviscid Flux

Because of the complicity of the flowfield structure around the underwater bodies with full appendages, Essentially Nonoscillatory (ENO) schemes, which was developed by Harten et al, are applied in the numerical simulations of this paper. ENO schemes, which use adapted stencil, are uniformly high-order accuracy throughout even at critical points
Following Yang(1992), third-order nonoscillatory schemes are given below. Take δE_ξ in direction ξ of Eq. (3) as an example, let $A = \frac{\partial E}{\partial Q}$, $(\Lambda_E)_{i+\frac{1}{2}} = (\lambda_1, \lambda_2, \lambda_3, \lambda_4)$ are eigenvalue diagonal matrix of A.
R、L are right and left eigenvector matrices of eigenvalue diagonal matrix Λ_E. Then we can get $A = R\Lambda_E L$. The spatial difference of E_ξ can be reached by using finite volume method

$$E_\xi = E_{i+1/2}^{\mathrm{ENO3}} - E_{i-1/2}^{\mathrm{ENO3}} \tag{5}$$

And
$$E_{i+1/2}^{\mathrm{ENO3}} = \frac{1}{2}(E_i + E_{i+1} + R_{i+1/2}\Phi_{i+1/2}^{\mathrm{ENO3}}) \tag{6}$$

let $\alpha_{i+1/2} = L(Q_{i+1} - Q_i)$, the components of $\Phi_{i+1/2}^{\mathrm{ENO3}}$ can be defined as

$$\Phi_{i+1/2}^{\mathrm{ENO3}} = \sigma(\lambda_{i+1/2})(\beta_i + \beta_{i+1}) + \begin{cases} \overline{\sigma}(\lambda_{i+1/2})(\overline{\beta}_i + \overline{\beta}_{i+1}) - \psi(\lambda_{i+1/2} + \gamma_{i+1/2} + \overline{\gamma}_{i+1/2})\alpha_{i+1/2}, & |\alpha_{i-1/2}| \le |\alpha_{i+1/2}| \\ \hat{\sigma}(\lambda_{i+1/2})(\hat{\beta}_i + \hat{\beta}_{i+1}) - \psi(\lambda_{i+1/2} + \gamma_{i+1/2} + \hat{\gamma}_{i+1/2})\alpha_{i+1/2}, & |\alpha_{i-1/2}| > |\alpha_{i+1/2}| \end{cases} \tag{7}$$

Where the σ, $\overline{\sigma}$, and $\hat{\sigma}$ functions are given by:

$$\sigma(z) = \frac{1}{2}(\psi(z) - Bz^2) \tag{8}$$

$$\overline{\sigma}(z) = \frac{1}{6}(2|z| - 3B|z|^2 + B^2|z|^3) \tag{9}$$

$$\hat{\sigma}(z) = \frac{1}{6}(B^2|z|^3 - |z|) \tag{10}$$

$$\psi(z) = \begin{cases} |z| & |z| \ge \varepsilon \\ (z^2 + \varepsilon^2)/\varepsilon & |z| < \varepsilon \end{cases} \tag{11}$$

Where ε is a small positive constant. B is the value of $\Delta t / \Delta\xi$. One can find that the value of $\Phi_{i+1/2}^{\mathrm{ENO3}}$ is self-adapted with the distribution of physics of flowfield. And

$$\beta_i = \min\mathrm{mod}[\alpha_{i+1/2}, \alpha_{i-1/2}] \tag{12}$$

$$\overline{\beta}_i = \overline{m}[\Delta_-\alpha_{i-1/2},\ \Delta_+\alpha_{i-1/2}] \qquad |\alpha_{i-1/2}| \le |\alpha_{i+1/2}| \tag{13}$$

$$\hat{\beta}_i = \overline{m}[\Delta_-\alpha_{i+1/2},\ \Delta_+\alpha_{i+1/2}] \qquad |\alpha_{i-1/2}| > |\alpha_{i+1/2}| \tag{14}$$

$$\gamma_{i+1/2} = \sigma(a_{i+1/2})\begin{cases} (\beta_{i+1} - \beta_i)/\alpha_{i+1/2} & \alpha_{i+1/2} \neq 0 \\ 0 & \text{otherwise} \end{cases} \tag{15}$$

$$\overline{\gamma}_{i+1/2} = \overline{\sigma}(a_{i+1/2})\begin{cases} (\overline{\beta}_{i+1} - \overline{\beta}_i)/\alpha_{i+1/2} & \alpha_{i+1/2} \neq 0 \\ 0 & \text{otherwise} \end{cases} \tag{16}$$

$$\hat{\gamma}_{i+1/2} = \hat{\sigma}(a_{i+1/2})\begin{cases} (\hat{\beta}_{i+1} - \hat{\beta}_i)/\alpha_{i+1/2} & \alpha_{i+1/2} \neq 0 \\ 0 & \text{otherwise} \end{cases} \tag{17}$$

$$\overline{m}(y,z) = \begin{cases} y & , |y| \le |z| \\ z & , |y| > |z| \end{cases} \tag{18}$$

The other fluxes of three dimensional N-S equations (Eq.(3)) can be defined with the similar way.

3.2 Lu Decomposition for Time Derivative

By using Finite Volume Method, the integrated form of Eq. (3) can be written as

$$\frac{\partial}{\partial t}[\frac{1}{V}\int_V J^{-1}QdV] + \frac{1}{V}\int_S H \bullet d\bar{S} = \frac{1}{V}\int_V DdV \tag{19}$$

Where S is the surfaces around the cell, $d\bar{S}$ is the normal vector of each surface, and H is the tensors and its vector components in three directions are

$$
\begin{aligned}
H &= iH_{(\xi)} + jH_{(\eta)} + kH_{(\varsigma)} \\
H_{(\xi)} &= E - \frac{1}{\mathrm{Re}} E_v \\
H_{(\eta)} &= F - \frac{1}{\mathrm{Re}} F_v \\
H_{(\varsigma)} &= G - \frac{1}{\mathrm{Re}} G_v
\end{aligned}
\tag{20}
$$

If Eq.(19) is applied over a hexahedral cell($\Delta\xi=\Delta\eta=\Delta\varsigma = 1$), time discretion uses first -order-accurate differencing, inviscid terms use implicit difference, viscous terms are explicit central difference, we can rewrite Eq. (3) as

$$
\begin{aligned}
&J^{-1}(Q^{n+1}_{i,j} - Q^{n}_{i,j}) + \Delta t\{[E^{n+1}_{i+1/2} - E^{n+1}_{i-1/2}] + [F^{n+1}_{j+1/2} - F^{n+1}_{j-1/2}] + [G^{n+1}_{k+1/2} - G^{n+1}_{j-1/2}]\} \\
&= \frac{\Delta t}{\mathrm{Re}}\{[E^{n}_{v i+1/2} - E^{n}_{v i-1/2}] + [F^{n}_{v j+1/2} - F^{n}_{v j-1/2}] + [G^{n}_{v k+1/2} - G^{n}_{v k-1/2}]\}
\end{aligned}
\tag{21}
$$

The definition of $(\Lambda_E)_{i+1/2}$ and $A = (\partial E / \partial Q)_{i+1/2}$ are same as last section. Let

$$
(\Lambda^{\pm}_E)_{i+1/2} = [(\Lambda_E)_{i+1/2} \pm |(\Lambda_E)_{i+1/2}|]/2 \tag{22}
$$

If L_E 、 R_E are the left and right eigenvector matrices of matrix A, we can get

$$
A^{\pm} = R_e \Lambda^{\pm}_E L_E \tag{23a}
$$

Similarly

$$
B^{\pm} = R_F \Lambda^{\pm}_F L_F \tag{23b}
$$

$$
C^{\pm} = R_G \Lambda^{\pm}_G L_G \tag{23c}
$$

Let $Q^{n+1}_{i,j} - Q^{n}_{i,j} = \Delta Q^{n}_{i,j}$, LU decomposition expression of Eq. (3) can be written as

$$
\begin{aligned}
&J^{-1}[I + \Delta t J(A^{+} + B^{+} + C^{+})][I - \Delta t J(A^{-} + B^{-} + C^{-})]\Delta Q^{n}_{i,j} \\
&= -\Delta t\{[E^{n}_{i+1/2} - E^{n}_{i-1/2}) + (F^{n}_{j+1/2} - F^{n}_{j-1/2}) + (G^{n}_{k+1/2} - G^{n}_{k-1/2})]\} \\
&+ \frac{\Delta t}{\mathrm{Re}}\{[E^{n}_{v i+1/2} - E^{n}_{v i-1/2}] + [F^{n}_{v j+1/2} - F^{n}_{v j-1/2}] + [G^{n}_{v k+1/2} - G^{n}_{v k-1/2}]\}
\end{aligned}
\tag{24}
$$

3.3 Turbulence Model

The effect of turbulence fluctuations, which can be resolved on the computational grid, are approximated with the Smagorinsky model.

$$
\mu_t = (C_s L)^2 |S_{ij}| \tag{25}
$$

$$
S_{ij} = \frac{1}{2}\left(\frac{\partial u_i}{\partial x_j} + \frac{\partial u_j}{\partial x_i}\right) \tag{26}
$$

in which the model coefficient $C_s = 0.1$ and length scale is the geometric mean of the grid spacing

$$
L = (\Delta x \Delta y \Delta z)^{1/3}.
$$

4 RESULTS

The flowfields around the underwater axisymmetric bodies with full appendages are computed as steady-state solutions to the incompressible Navier-Stokes equations. The full appendages include a fairwater and four stern appendages. The numerical velocity distribution and nominal wake at the propeller are compared with the experiment data measured in the wind tunnel. The Reynolds number in the calculation and experiment are 6.0×10^{6}. The complete calculation was carried out by two steps. The flowfields around the body and a fariwater are numerically simulated firstly, which can provide the inlet boundary condition for the following fine simulation of flowfield around stern part of body and four stern appendages.

The numerical dimensionless circumferential-mean velocity along the radius of the propeller are presented in Fig. 1, which are in good agreement with the experimental data. The details of numerical dimensionless circumferential-mean velocity and the experimental data can also been found in Table 1. Except few points, the relative error between the numerical results and the experimental data is less than 3%, their average relative error is only 2.107%, the accurate numerical nominal wake at propeller can be used as input data of vehicle propulsor blade design. The numerical dimensionless circumferential velocity distribution at different radius station are showed in Fig. 2(a)-Fig. 2(g). There are difference between the numerical results and the experimental data, but their phases are similar, so the calculated circumferential velocity can be applied to the optimization and evaluation of hydrodynamics noise of vehicle propulsor. The code developed in this paper has been used in the design and optimization of new underwater bodies with full appendages.

TABLE 1
COMPARISON OF NUMERICAL CIRCUMFERENTIAL VELOCITY
WITH EXPERIMENTAL DATA

Relative radius	Numerical results	Experiment data	Relative error (%)
0. 217	0. 4866	0. 4833	0. 68
0. 300	0. 5177	0. 4911	5. 42
0. 400	0. 5471	0. 5319	2. 88
0. 518	0. 5935	0. 5993	-0. 97
0. 678	0. 6681	0. 6814	-1. 95
0. 840	0. 7387	0. 7479	-1. 23
1. 000	0. 7933	0. 8064	-1. 62

5 CONCLUSIONS

Based on flux-splitting, implicit high-resolution schemes have been constructed for efficient calculations of steady-state solutions to the three dimensional, incompressible Navier-Stokes equations in curvilinear coordinates. The third-order-accurate efficient ENO has been applied in the calculations, which can capture the details of the flowfield around underwater bodies with full appendages. The numerical results agree quite well with the experimental data. The schemes and code developed in this paper can be applied in the design of underwater vehicle propulsor and in the optimization and evaluation of its hydrodynamics noise. Also the code can be used in the optimization and design of shapes of vehicle body and its appendages.

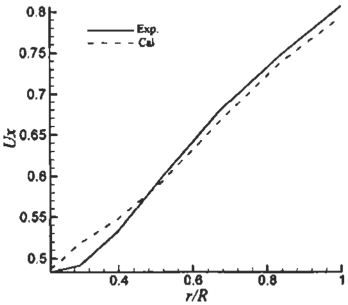

Figure 1: Comparison of numerical circumferential-mean velocity at propeller plane with experimental data

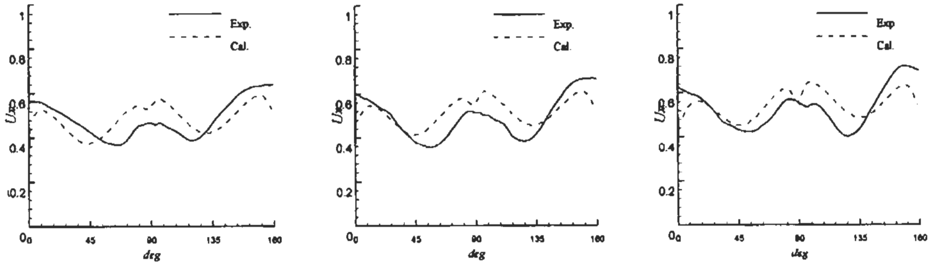

(a) r/R=0.217

(b) r/R=0.300

(c) r/R=0.400

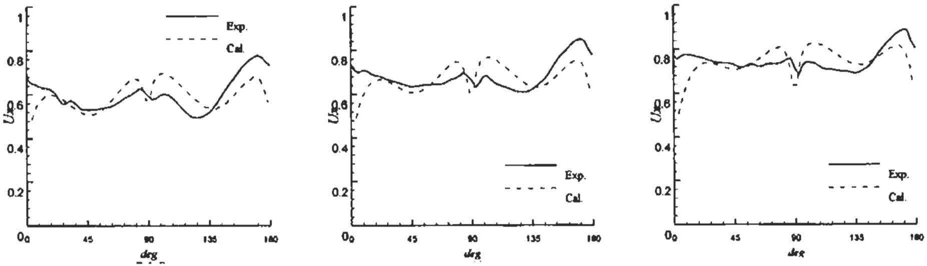

(d) r/R=0.518

(e) r/R=0.678

(f) r/R=0.840

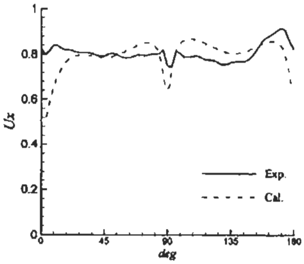

(g) r/R=1.000

Figure 2: Circumferential variation of axial velocity at difference radius station of propeller

Reference

Peter M. Hartwich, Chung Hao Hsu. (1988). High-resolution upwind schemes for the three-dimensional incompressible Navier-Stokes equations, *AIAA* J, **26:11**, 1321-1326

Huang Zhenyu. (1999). Numerical simulation of jet flows and nozzle flows, *Doctorial dissertation*, Beijing Institute of Technology (in Chinese)

Yang J. Y. (1992). High-resolution, nonoscillatory schemes for unsteady compressible flows, *AIAA* J, **30:6,** 1570-1575

Huang Zhenyu. (1999). Flowfield calculation with high resolution ENO, *The proceedings of eighth international space conference of pacific-basin societies(8th ISCOPS)*, Xi'an China, 691-697

Huang Zhenyu, Xu Wencan. (2000). Flowfield calculation with high resolution ENO, *ACTA* Aerodynamica SINICA, **18:1**, 14-21 (in Chinese)

Huang Zhenyu, Xu Wencan. (1999). Numerical simulation of turbulent jet, *Journal of Beijing Institute of Technology*, **19:6**, 691-695 (in Chinese)

Huang Zhenyu, Zhou Liandi and Zhao Feng, (2000). High-resolution schemes in simulation of flowfield around submarines, *Technical Report 00867*, CSSRC (in Chinese)

Practical Design of Ships and Other Floating Structures
You-Sheng Wu, Wei-Cheng Cui and Guo-Jun Zhou (Eds)
© 2001 Elsevier Science Ltd. All rights reserved

VISCOUS FLOW CALCULATIONS USED FOR DREDGER DESIGN

M. Hoekstra [1], A. de Jager [2] and H.H. Valkhof [1]

[1] MARIN, P.O. Box 28, 6700 AA Wageningen, the Netherlands
[2] IHC Holland NV Dredgers, P.O. Box 1, 2960 AA Kinderdijk, the Netherlands

ABSTRACT

For a single screw Hopper Dredger, which meanwhile has been constructed and is operating successfully now, as shown below, IHC HOLLAND NV DREDGERS (IHC) studied the viscous flow and the related wake distribution with the aid of MARIN's viscous flow code PARNASSOS. Due to the very short building time, demanded by the owner, the yard was forced to skip the usual model test programme. Instead, computational fluid dynamics was chosen to verify the design and to make sure that a reasonable inflow for the propeller was obtained, a necessary condition for the avoidance of vibration problems. The study concerns the viscous flow calculations for a preliminary and modified hull form at model and full scale Reynolds numbers, while for a few calculations the effect of the propeller has been included.

KEYWORDS

Propeller, Computational fluid dynamics, Viscous flow, Wake distributions, Reynolds number

1 INTRODUCTION

The design and construction of dredgers is the core business of IHC. An important contingent of these dredgers is of the trailing suction hopper type. The hull form of such vessels is characterized by a high block coefficient, a low L/B ratio and a high B/T ratio. Because of these characteristics and the high power density of the propeller, hopper dredgers have typically twin-screw propulsion. Nozzles are nearly always applied in view of the need of high thrust during dredging at low speeds.

As an exceptional case, IHC received recently an order for a *single-screw* Hopper Dredger. This vessel happened to be the first single-screw dredger for the yard since 28 years, all intermediate hopper newbuildings being twin-screw ships. The performance of that former single-screw case – in the sequel referred to as "the old hull" - had been disappointing. The combination of the full aft body, the heavily loaded propellers and the small propeller-hull clearance led to unacceptably high vibration levels, which had to be remedied by expensive retro-fit solutions.

Such incidents, which put a burden on the relation with the client and certainly cause damage to the reputation of the yard, should preferably be avoided. However, the client's choice of a single-screw Hopper Dredger because of its relatively low price is of course legitimate. This brings out the need for an early detection of possible problems with a new design. In this respect, model tests play an important role. However, time constraints ask for checks even at a pre-model testing stage. In this paper we show that computational fluid dynamics can assist to avoid major problems.

2 THE CASE

Early 2000, IHC got an order from a small French dredging company to build a low- budget single-screw hopper dredger in an extremely short delivery time of less than 11 months. The block coefficient of 0.85, the thrust loading coefficient of 2.7, the propeller power density of 420 kW/m^2 and small propeller-hull clearances all pointed to a serious risk of vibration problems. It was clear therefore that the design of the aft body should be thoroughly investigated, but lack of money (low budget) and time (very short building period) seemed to frustrate that. At least model tests were under the given circumstances no viable option. The application of computational fluid dynamics, in particular the PARNASSOS code, was proposed by MARIN as an alternative to check the lines of the aft body and to investigate possible shortcomings.

3 DESIGN CONSIDERATIONS

Hopper dredgers have undergone drastic changes during the last decades as a result of changing demands of the owners. Not only the loading capacity has increased, also the operation range and the maximum speed. Besides, more stringent requirements on the comfort for the crew are imposed nowadays. Hence, the design has become critical, particularly with regard to vibration hindrance, basically caused by poor inflow to the propeller.

From the beginning it was clear that the hull form of the old vessel was not a proper starting point for the new design. The aft body of that hull may be classified as V-shaped, which for high-block ships naturally lead to steep buttocks. Ships based on such a design concept often suffer from a bad wake field at the propeller location, notably in the top sector of the propeller disk.

To improve the design, a pram-with-gondola-type afterbody was suggested by MARIN. Displacement volume was brought to the sides resulting in a significant reduction of the buttock slope. To accommodate the engine, a rather wide gondola was needed. Special attention was paid to the orientation of the knuckle line at the location where pram and gondola merge. A compromise was necessary in view of the variety of operating conditions: loaded, empty, unrestricted and restricted water depth. The aft body shape of the proposed hull form is shown in Figure 1.

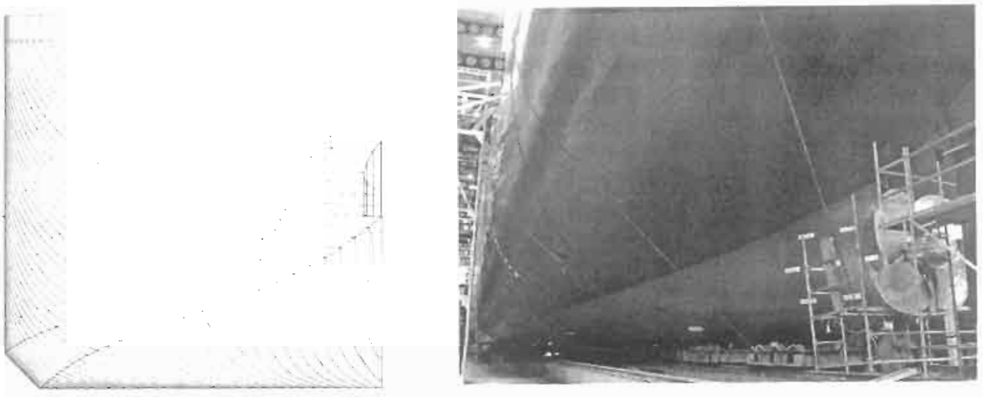

Figure 1: Aft body design; frame lines (left)
and ship in construction dock (right)

To check the design, model tests would normally have been the next step. Instead, a set of numerical flow simulations was carried out with PARNASSOS. It was considered by the yard to be the only reasonable option that the circumstances permitted.

4 VISCOUS FLOW SIMULATIONS

PARNASSOS is a numerical tool developed at MARIN to simulate the steady viscous flow around a ship, under the assumption that the wave-making of the ship can be neglected. The underlying mathematical model is the combination of the full Reynolds-averaged Navier-Stokes (RANS) equations and a one-equation transport equation for the eddy viscosity. If required, the action of the propeller can be included by representing the propeller as an actuator disk. The results of PARNASSOS include the complete velocity field and the pressure distribution around the stern of the ship as well as the viscous resistance of the hull. This allows streamlines to be traced and possible separation zones to be detected. Details on the method can be found in e.g. Hoekstra (1999), Hoekstra & Eça (1998). Another example of its application to practical design problems can be found in Valkhof *et al.* (1998).

All calculations to be presented here are based on the use of a single block grid of H-O topology, containing between 620,000 and 930,000 nodes, wrapped around the afterbody. The ship has an immersed transom; in order to avoid the complication of the recirculating flow zone aft of the transom in the numerical simulations, the hull was smoothly extended. Moreover, the rudder and the headbox above it were removed.

The following series of calculations was carried out for the new design:

Draught condition	Reynolds number	Propeller
loaded	$7.96*10^{6}$ (model scale)	no
loaded	$3.73*10^{8}$ (full scale)	no
loaded	$7.96*10^{6}$ (model scale)	yes
empty	$8.68*10^{6}$ (model scale)	no

Some representative results will now be shown and discussed. First the limiting streamlines (the numerical equivalent of the paint test) are displayed for the loaded condition without propeller; Figure 2 shows the situation at model scale (top) and at full scale (bottom) .

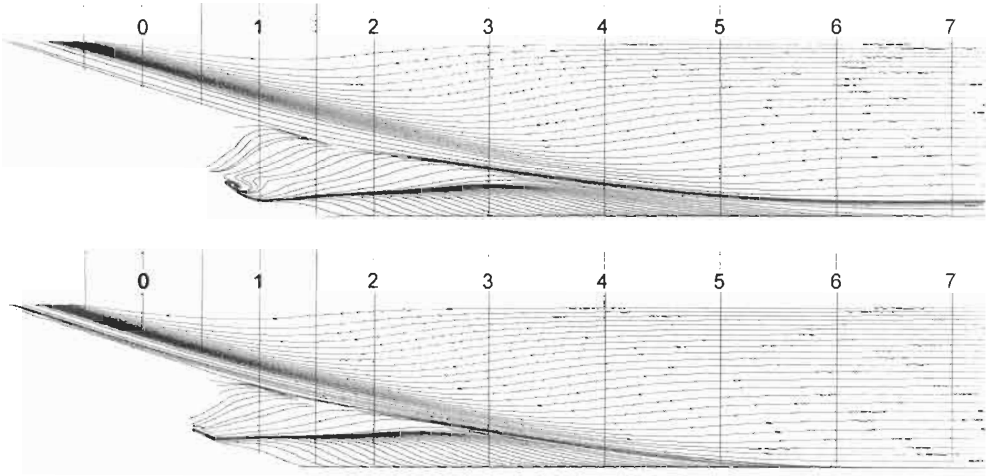

Figure 2: Comparison of limiting streamlines in loaded condition
at model scale (top) and at full scale (bottom)

Figure 2 clearly indicates for model scale conditions a confluence of limiting streamlines on the gondola, representative for the formation of a longitudinal vortex. Close to the stern a small region of flow reversal occurs on the gondola. By changing the Reynolds number so as to simulate the situation at full scale, the flow reversal zone on the gondola disappears, while the confluence of limiting streamline occurs clearly at a higher position. A comparison of the axial velocity distribution at x/Lpp = 0.95 (i.e. 0.05 Lpp ahead of the aft perpendicular) at model and full scale is shown in Figure 3.

The results for the model scale condition with running propeller revealed that the propeller is able to remove the flow-reversal zone on the gondola. But difficulties were now seen to appear above the propeller, slightly ahead of it. Such trends were to be expected, but PARNASSOS gives quantitative information, which allows a direct qualification of the hull design.

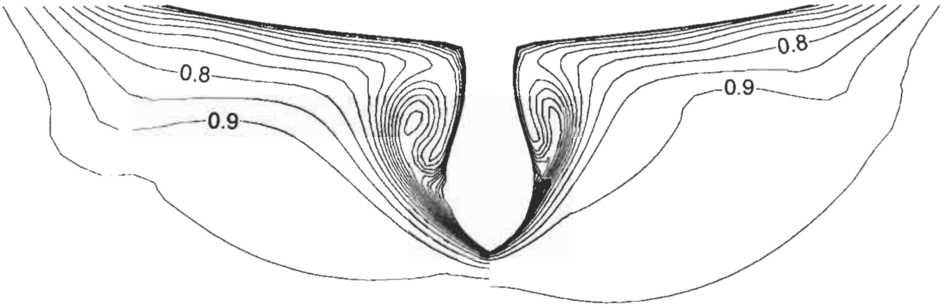

Figure 3: Axial velocity field at Station1 (x/Lpp = 0.95) at model scale (left) and full scale (right)

A change in loading condition can affect the flow conditions at the aft end of the ship considerably. The flow around the empty hull (draught forward 1.75 m, draught aft 3.10 m) was therefore simulated as well. Figure 4 gives a comparison of the nominal wake in the propeller plane at loaded and empty condition. Although similar flow features appear, the position of the longitudinal vortex is different; hence the wake field patterns differ significantly and the mean wake fraction is greater for the empty condition. So, as anticipated, this condition is more critical for the design.

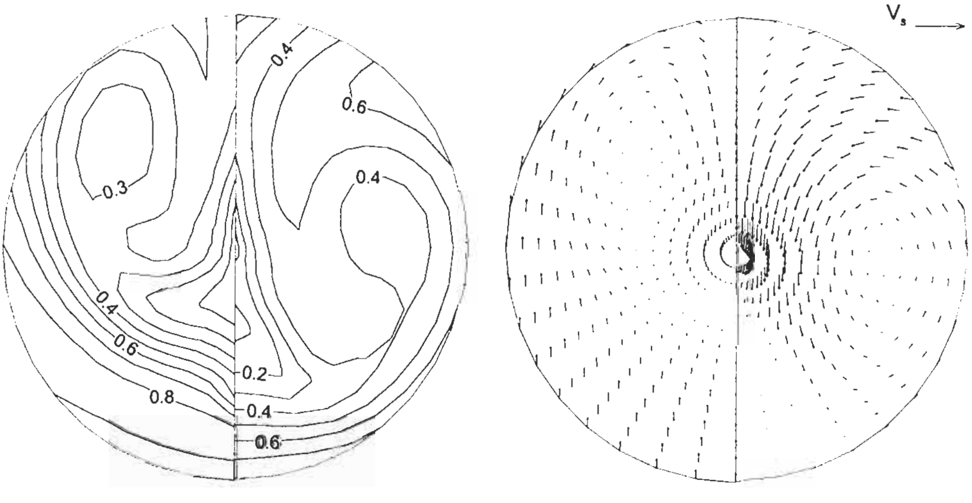

Figure 4: Wake field in the propeller plane calculated for loaded (left) and empty (right) condition

Because of the small flow reversal zone above and slightly ahead of the propeller, a hull form modification was suggested, which essentially consisted of a forward extension of the headbox above the rudder to about station 1 (i.e. 5 per cent of Lpp ahead of the aft perpendicular). Thus a kind of tunnel roof was constructed to reduce the buttock slope locally. The flow around this modified hull with headbox was subsequently analysed for the loaded condition with active propeller at model scale. Unfortunately, the results did not give the improvements hoped for. The small flow reversal zone persisted and was brought closer to the propeller. So it was decided to reject the hull modification. Because there was no time left for further exercises the hull design was accepted as maybe not perfect but certainly good enough to guarantee an acceptable inflow to the propeller.

5 PROPELLER DESIGN

For the propeller design two sets of data concerning the wake field in loaded and empty condition were delivered by the PARNASSOS code: the wake field plots of axial, radial and tangential velocity components (as normally delivered after conduction of a wake field model test), and, in addition, the pressure distribution over the propeller plane. Because the nominal wake field for both the model scale and full scale situation was provided, as well as the flow field with active propeller, the propeller designer got in fact more information than usual. He assessed the wake fields as "quite normal", which ensured the yard that the job was well done for this single-screw full-block aft body.

After completion of the propeller design, the propeller manufacturer informed the yard about the cavitation characteristics of the propeller by means of plots of the blades in positions where cavitation was calculated (see Figure 5).

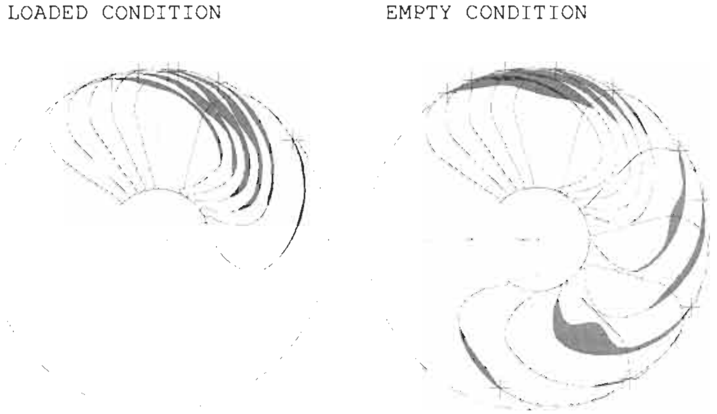
LOADED CONDITION EMPTY CONDITION

Figure 5: Cavitation characteristics of the calculated positions

The worst case for the propeller is the empty condition, as can be easily seen in the wake field. Due to the wake peak at 180° (bottom) sheet cavitation inception will occur at the leading edge. At blade position 120° the leading edge at low radius is close to the wake peak. At blade position 150° the leading edge is out of the peak and no sheet cavitation will occur. It was recognized, however, that the effective wake showed a decreased wake peak. This justified the assumption that the predictions (based on the nominal wake) were slightly pessimistic. In loaded condition only sheet cavitation was predicted to occur in top position in the range from -60° to 60°.

For the dredging condition (initially empty) the margin against bubble cavitation at 12 o'clock position was estimated as just above 50 per cent.

These cavitation patterns and margins could be assessed as 'acceptable' and the propeller has been manufactured according to this design.

6 FULL SCALE TRIALS

After completion of the sea trials, during which extensive speed and vibration measurements have been carried out, it could be concluded that the vessel satisfied all targets. The attained trial speed in loaded condition was even significantly higher than the speed predicted based on previous experience. The speed-power prediction together with the attained speed during speed runs is indicated in Figure 6.

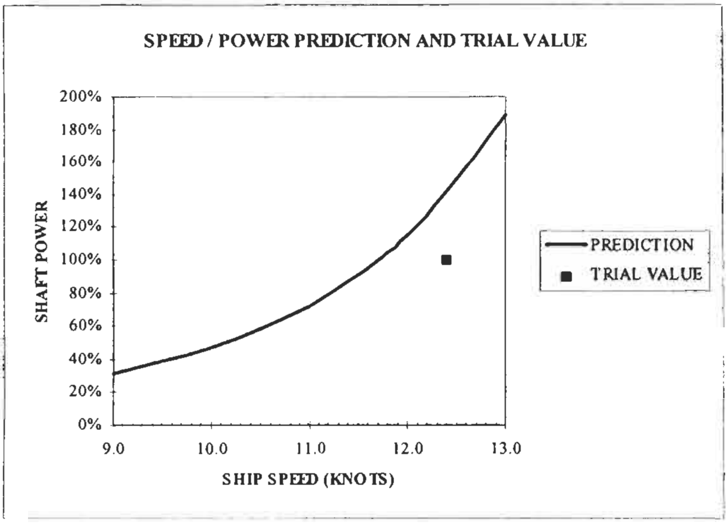

Figure 6: Power prediction together with the attained speed during speed runs

We like to point out that with model tests a better estimate of the trial speed would have been possible. PARNASSOS did not provide a speed-power prediction because the flow simulation was incomplete (no waves, flow around fore body not calculated to reduce costs). So, it is concluded that even for low-budget vessels it is recommendable – if time permits - to conduct at least a propulsion test to verify the attained speed. In the present case, a lighter engine and gearbox and smaller propeller would have sufficed. The extra expenses of overpowering amply exceeded the costs of model tests.

The measured vertical vibration levels at a blade frequency of 17 Hz. in empty condition (worst case) in the aft body are indicated in the table below:

Position	Vertical speed (mm/s)
Steering gear room	4.1
Main deck	2.8
Mess room	3.5
Wheel house	4.8
Bridge wing	4.3

Adverse comments are according to interim guidelines of Bureau Veritas “not probable” with these values.

7 CLOSURE

In an unusual procedure, dictated by short delivery time, a dredger design was verified by computations rather than model tests. Thus the aims of the yard, viz. to obtain reasonable inflow for the propeller and wake information for the propeller design, were achieved. In a very short period of time, calculation results were made available so that a technical assessment was possible. This manner of hull examination proved to be so fast that, while realizing the critical delivery time, a design alternative could be investigated. Full scale trials with the vessel constructed according to the chosen design later revealed a satisfactory performance in all critical aspects.

Meanwhile, similar computational analyses have been carried out with success for twin-screw dredgers as well. Flow simulation for these hulls, which are based on the twin-gondola concept, is a challenge for the numerical analysts, because of the complex geometry, and hence complex flow phenomena. The next step will be to include the effects of restricted water depth.

References

Hoekstra, M. (1999). Numerical simulation of ship stern flows with a space-marching Navier-Stokes method. *PhD thesis*, Delft University of Technology, the Netherlands.

Hoekstra, M. and Eça, L. (1998). PARNASSOS: an efficient method for ship stern flow calculation. In *proceedings of 3rd Osaka Colloquium on Ship Viscous Flows*, Osaka, Japan.

Valkhof, H.H., Hoekstra, M. & Andersen, J.E. (1998). Model tests and CFD in hull form optimization. *Transactions SNAME.*

Practical Design of Ships and Other Floating Structures
You-Sheng Wu, Wei-Cheng Cui and Guo-Jun Zhou (Eds)
© 2001 Elsevier Science Ltd. All rights reserved

FULLY NONLINEAR WAVE COMPUTATIONS FOR ARBITRARY FLOATING BODIES USING THE DELTA METHOD

Tzung-Hang Lee and Chang-Lung Chen

Department of Mechanical Engineering
Tamkang University, Taipei China

ABSTRACT

Fully nonlinear water wave problems are solved using Eulerian-Lagrangian time stepping methods in conjunction with a desingularized approach to solve the mixed boundary value problem that arises at each time step. In the desingularized approach, the singularities generating the flow field are outside the fluid domain. This allows the singularity distribution to be replaced by isolated Rankine sources with the corresponding reduction in computational complexity and computer time.

Examples of the use of the method in three-dimensions are given for the exciting forces acting on a modified Wigley hull and Series 60 hull are presented.

KEYWORDS

Fully nonlinear, Eulerian-Lagrangian, Time stepping, Isolated Rankine sources

1 INTRODUCTION

When body motion becomes large, nonlinear waves are generated and higher-order hydrodynamic forces appear. These phenomena can not be explained by linear theory since nonlinear effects are essentially excluded. Therefore, time-domain calculations are necessary for fully nonlinear problems since frequency-domain computations are only good for linear problems or a few very specific body-exact problems.

Longuet-Higgins & Cokelet [8] first introduced the mixed Eulerian-Lagrangian time-stepping scheme for solving two-dimensional fully nonlinear water wave problems. Faltinsen [6] used a similar scheme to study the nonlinear transient problem of a body oscillating on a free surface.

Vinje & Breving [12] continued the approach of Longuet-Higgins & Cokelet[8] to include finite depth and floating bodies but retained the assumption of spatial periodicity. Baker, Dommermuth & Yue [5] used the mixed Eulerian-Lagrangian method and postulated a far-field boundary matching algorithm by matching the nonlinear computational solution to a general linear solution of transient outgoing waves.

The desingularization method was first developed by von Karman [13] in which an axial source distribution was used to determine the flow about an axisymmetric body. A non-singular formulation of the boundary integral equation method was proposed by Kupradze [7]. The exterior Dirichlet problem was solved by using an auxiliary surface located outside the computational domain. Webster [14] investigated the numerical properties of the desingularization technique for the external potential flow around an arbitrary, three-dimensional smooth body. He concluded that the use of this desingularization technique greatly improved the accuracy of the solution.

Cao, Schultz & Beck [2, 3, 4] solved nonlinear problems for waves generated by a free surface pressure disturbance or a submerged body by combining the time-stepping scheme and the desingularized boundary integral equation method. Cao, Lee & Beck [1] extended the method to study nonlinear water wave problems with floating bodies, Scorpio et al [9] used a multipole accelerated desingularized method to compute nonlinear water waves. Lee & Cheng [10, 11] used the desingularized method to solve fully nonlinear wave calculations for arbitrary float bodies.

2 FULLY NONLINEAR PROBLEM FORMULATION

As shown in Fig.1, cartesian coordinates that refer to an absolute inertial frame are used. The z-axis points upward and the x - y plane is coincident with the still water level. The fluid domain, D, is bounded by the free surface, S_f, the body surface, S_b, the bottom surface, S_h, and the enclosing surface at infinity, S_∞.

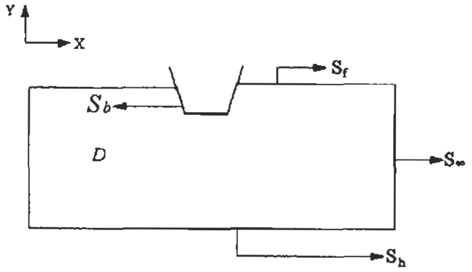

Figure 1: Problem definition and coordinate system

The desingularized boundary integral equations for the unknown strength of the singularities $\sigma(\vec{X}_s)$ are :

$$\iint_\Omega \sigma(\vec{X}) \frac{1}{|\bar{X}_f - \bar{X}_s|} d\Omega = \phi o(\bar{X}_f) \qquad (\bar{X}_f \in \Gamma_d) \tag{1}$$

and

$$\iint_\Omega \sigma(\vec{X}) (\frac{1}{|\bar{X}_f - \bar{X}_s|}) d\Omega = \chi(\bar{X}_f) \qquad (\bar{X}_f \in \Gamma_n) \tag{2}$$

where

$\bar{X}_s$ is the point on the integration surface ; $\bar{X}_f$ is the field point on the real boundaries ;
ϕ_0 is the given potential value at X_f ; χ is the given normal velocity at X_f ;
Γ_d is the surface on which ϕ_0 is given ; Γ_h is the surface on which χ is given

3 DISCRETIZATION AND SINGULARITY DISTRIBUTION

To solve the integral equation for $\sigma(\vec{X}_s)$, the collocation method is used. Field points are chosen along the real boundary and sources are distributed outside the computational domain. A set of field points and the corresponding source points are chosen along the contours, S_f, S_b, and S_h, as shown in Fig. 2.

In the DELTA method, the sources are distributed on the integration surface so that the source points never coincide with the field points and the integrals are nonsingular. In addition, a simple isolated sources rather than a distribution is used. The equivalent accuracy in the solution is then obtained.

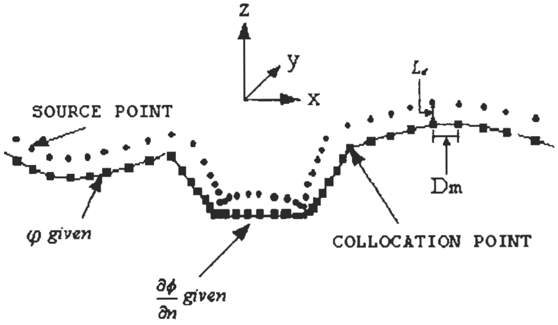

Figure 2: Model for numerical simulation

The singularities are distributed above the field points on the free surface in the normal direction of the boundaries. Inside the body, the isolated singularities are placed along the normal direction from the field points in the body surface. Numerical difficulties may occur in the vicinity of a sharp edge. One of the difficulties is that the singularity distribution may cross over thc bisector of two body surfaces or even the other side of the body surface since the desingularization distance is proportional to the local grid size.

These types of difficulties can be avoided by careful discretization and desingularization. The desingularization distance near a sharp corner is modified so that the singularities are distributed on the bisector of the two body surfaces to avoid the cross over of the singularities beyond the centerline or the body surfaces.

The nondimensional desingularization distance is set to be

$$L_d = l_d(Dm)^{\alpha} \tag{3}$$

Where l_d reflects how far the integral equation is desingularized, D_m is the non-dimensional local mesh size (usually the square root of the local mesh area in 3-D problems and the local mesh size in 2-D problems). α is a parameter associated with the convergence of the solution as the mesh is refined. Cao, Schultz & Beck [2] conducted numerical tests in which an integral of a constant source distribution over a square flat surface is evaluated at a point above the center of the square with a distance given by Eqn. 3 They found that $\alpha = 0.5$ and $l_d = 1.0$ are about the optimum values for the performance of the desingularization method.

A linear system of $m \times m$ algebraic equations is set to be

$$A_{m\times m} \cdot \vec{X}_m = \vec{B}_m \tag{4}$$

where	m	is the total number of field points ;
	$A_{m\times m}$	is the influence function matrix with $m \times m$ elements ;
	$\vec{X}_m$	is the unknown source strength vector, $\sigma(\vec{X}_m)$,to be solved ;
	$\vec{B}_m$	is the known vector which contains the values of ϕ at the field points on the free surface and the values of $\partial\phi/\partial n$ at the field points on the body

Once Eqn. 4 is solved, $\nabla\phi$ can be evaluated on S_f, and the combined free surface boundary conditions on the free surface can be integrated in time.

Nondimensionalization

The fundamental variables, ρ, g and L are used to nondimensionalize all the other variables, ρ is the density of the fluid, g is the gravitational acceleration and L is the initial draught of the body. Thus,

$\bar{L} = 1.0$	is the nondimensional draught ;	$\bar{D} = \frac{D}{L}$	is the nondimensional position ;
$\vec{x} = \frac{\vec{X}}{L}$	is the nondimensional vector ;	$\bar{B} = \frac{B}{L}$	is the nondimensional radius ;
$\bar{D}_m$	is the nondimensional panel size ;	$\vec{V}_b = \frac{\vec{V}_b}{\sqrt{gH}}$	is the nondimensional body velocity

The nondimensionalized system, the bar system, will be used but bars on all the variables will be dropped from now on. The numerical results shown in this thesis are all based on nondimensionalized variables unless otherwise mentioned. Also, ρ_{air} is the air pressure and is taken as zero. Consequently, the nondimensional governing equation and boundary conditions are

$$\Delta\phi = 0 \qquad (on\ S_f) \tag{5}$$

$$\frac{D\vec{X}_f}{Dt} = \nabla\phi \qquad (on\ S_f) \tag{6}$$

$$\frac{D\phi}{Dt} = \frac{1}{2}\left|\nabla\phi\right|^2 - z_f \qquad (on\ S_f) \tag{7}$$

$$\frac{\partial\phi}{\partial n_b} = \vec{V}_b \bullet \vec{n}_b \qquad (on\ S_b) \tag{8}$$

$$\frac{\partial\phi}{\partial n_h} = \vec{V}_h \bullet \vec{n}_h \qquad (on\ S_h) \tag{9}$$

$$\nabla\phi \to 0 \qquad (on\ S_\infty) \tag{10}$$

4 NUMERICAL COMPUTATION RESULTS

Figs. 3~4 show the mesh of the free surface profiles due to the motion of the wigley ship model. The froude no.(Fn) is 0.316. The time(t) histories shown in the figs. 3~4 are 0, 20 respectively.
Figs. 5~6 show the mesh of the free surface profiles due to the motion of the Series 60 ship model.The froude no.(Fn) is 0.316. The time (t) histories shown in the figs. 5~6 are 0, 35 respectively.

5 CONCLUSIONS

The conclusions of this work are summarized as followings:
1.The desingularization method is robust in simulating the motions of floating bodies with complicated

shapes.

2.The desingularization method shows no difficulty in treating the body-free surface intersection point.

3.For the desingularization method, no special treatment for the coefficient of the influence matrix is necessary. The stability of the desingularization method is better than that of the conventional boundary integral equation method.

4.The desingularization method is promising for further application to floating structures with arbitrary shape undergoing arbitrary motion.

References

[1] Beck, R.F., Y.Cao and T-H. Lee (1993), "Fully Nonlinear Water Wave Computations Using the Desingularized Method," *Proceeding 6th, International Conference on Numerical Ship Hydrodynamics*, University of Iowa.

[2] Cao, Y., W.W.Schultz and R.F.Beck (1991a), "Three-dimensional, Desingularized Boundary Integral Methods for Potential Problems," *International Journal of Num. Meth. Fluids*, Vol.12, pp. 785-803.

[3] Cao, Y., W.W.Schultz and R.F.Beck (1991b), "Two-dimensional Solitary Waves Generted By a Moving Disturbance," *6th International Workshop on Water Waves and Floating Bodies*, Woodshole, MA, USA.

[4] Cao, Y., W.W. Schultz and R.F.Beck (1990), "Three-dimensional unsteady computation of nonlinear waves caused by under water disturbance," *Proceedings 18th Symposium on Naval Hydrodynamics*, Ann Arbor, MI, USA, pp.417-427.

[5] Dommermuth, D.G. and D.K.-P.Yue (1988), "Study of Nonlinear Axisymmetric Body-Wave Interactions," *Proceedings 16th Symposium of Naval Hydrodynamics*, Berkeley.

[6] Faltisen,O.M.(1977),"Numerical Solution of Transient Nonlinear Free Surface Motion Outside or Inside Moving Bodies," Proceedings 2nd Conference On Numerical Ship Hydrodynamics," U.C. Berkeley, pp.347-357, University Extension Publications.

[7] Kupradze, V. (1967), "On the Approximate Solution of Problems in Mathematical Physics," *Russ. Math. Surveys*, Vol.22, pp.59-107.

[8] Longuet-Higgins M.S. and C.D.Cokelet (1976), "The Deformation of Steep Surface Waves on Water," *I.A Numerical Method of Computation Proceedings of Royal SocietyLondon,*A350, pp. 1-26.

[9] Scorpio S., R.F.Beck and F.Korsmeyer (1996), "Nonlinear Water Wave Computations Using a Multipole Accelerated, Desingularized Method", *Proceedings 24th Symposium of Naval Hydrodynamics*, pp.34-43

[10] T.H.Lee & Cheng (1999), "Fully Nonlinear Wave Calculations for Arbitrary Floating Bodies," *Proceedings of the 23th National Conference on Theoretical an Applied Mechanics*, Hsinchu, Taiwan, China.

[11] T.H.Lee & Cheng (2000), "Applications of Desingularization Techniques in Fully Nonlinear Wave Calculation for Arbitray 2-D Floating Bodies," *the 7th National Conference on Computational Fluid Dynamics*, Kenting, Taiwan, China Vol.1, D-39.

[12] Vinje, T.and P.Breving (1981), "Nonlinear Ship Motions," *Proceedings 3rd Int. Conference on Numerical Ship Hydrodynamics*, Paris.

[13] von Karman, T.,(1930), "Calculation of Pressure Distribution on Airship Hulls," *NACA Technical Memorandum* No. 574.

[14] W.C.Webster (1975), " The Flow About Arbitrary, Three-Dimensional Smooth Bodies," *J. Num. Ship Research*, Vol.19, pp.206-218.

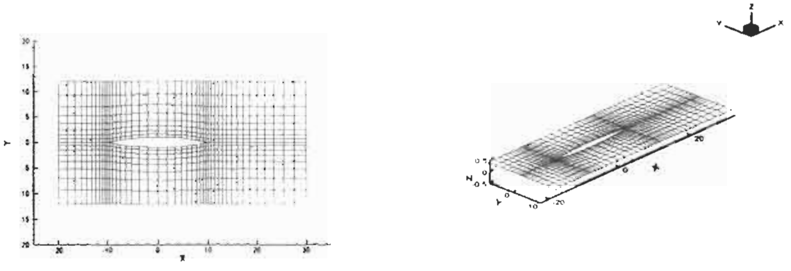

Figure 3: the mesh of the free surface, Fn=0.316, t=0, (Wigley ship model)

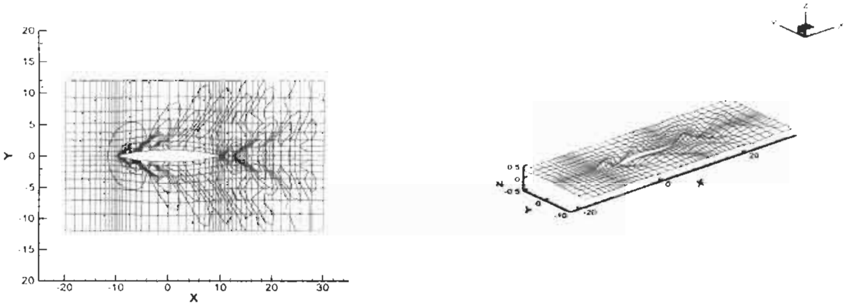

Figure 4: the mesh of the free surface, Fn=0.316, t=20 sec, (Wigley ship model)

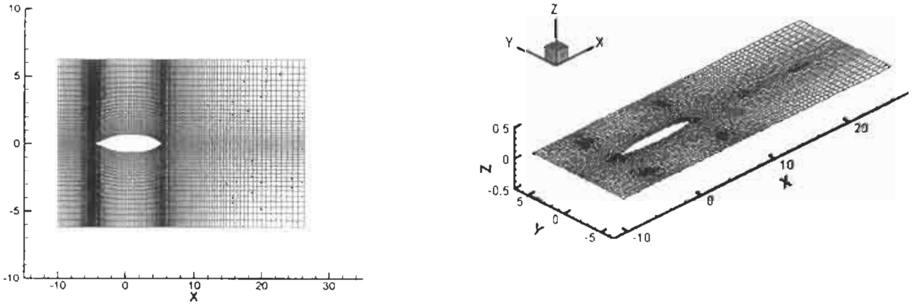
10
5
Y 0
-5
-10
-10
0
10
20
30
X
Z
Y
X
0.5
Z 0
-0.5
5
Y 0
-5
-10
0
10
X
20

Figure 5: the mesh of the free surface, Fn=0.316, t=0, (Series 60 ship model)

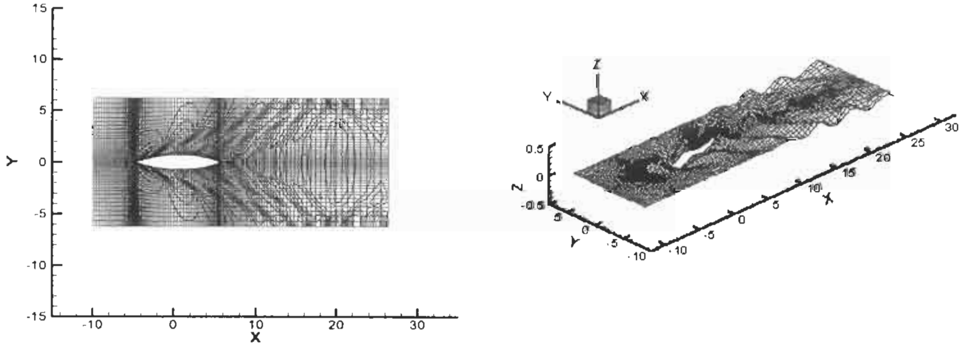

Figure 6: the wave of free surface in acceleration, Fn=0.316, t=35 sec, (Series 60 ship model)

Practical Design of Ships and Other Floating Structures
You-Sheng Wu, Wei-Cheng Cui and Guo-Jun Zhou (Eds)
© 2001 Elsevier Science Ltd. All rights reserved

FLOW BEHAVIOR AROUND TANDEM OIL FENCES

Dong Gi Han[1], Choung M. Lee[1] and Sang J. Lee[1]

[1]Department of Mechanical Engineering
Pohang University of Science and Technology, Korea

ABSTRACT

The present paper presents the results of the experimental and numerical investigation on the flow and oil droplets behaviors about a set of tandem oil fence deployed in a uniform current. A numerical solver of the Reynolds averaged Navier-Stokes equation and the Lagrangian particle trajectories are utilized to trace the oil droplets around the two fences, and assessment of the effectiveness of a tandem fence is made. Laboratory experiments are carried out to check the validity of the numerical predictions.

KEYWORDS

Oil fence, Oil leakage, Flow passing a tandem fence, PIV method, Lagrangian particle-tracking method, Free-surface effect , Entrainment failure, critical leakage zone.

1 INTRODUTION

The only mechanical device used in deterring the spreading of spilt oil in water is oil fence that normally consists of the float, skirt and ballast rope or chain. However, when the environment condition such as current, wind and wave, exceeds certain limits, the oil fences become useless since the oil would either leak beneath the fence or spill over the fence. Yet, there are some water zones that definitely need to be protected from the oil contamination such as fishing farm area, cooling-water intake area for a nuclear power plant, marine sports and recreational area, and marine ecologically sensitive area. In these areas, the chemical dispersants are not favorable substances because of the possible secondary pollution hazards. Short of any better conceivable devices for prevention of the spilt-oil spreading, the idea of tandem fence has been proposed by Comrack(1983), Delvigne(1987), Lo(1996) and Lee et al.(1998). A computational assessment method for tandem-fence effectiveness was introduced by Lee et al.(1998), which tracks the motion of oil patches around and between the two fences. The variables considered in this method were current(or towing) speed, and fence separation distance under the assumption of an identical draft for the two fences, deep water and flat free surface. In the present investigation, the effects of the variation of the drafts of the two fences, the water depth and the deformable free surface on the tandem-fence effectiveness are investigated.

2 THEORY

The right-handed Cartesian coordinate system as shown in Figure 1 is employed. The fluid field in the presence of a set of tandem fence is assumed steady, viscous and incompressible, which is represented by

$$\nabla \cdot \boldsymbol{u} = 0 \tag{1}$$

$$\rho \boldsymbol{u} \cdot \nabla \boldsymbol{u} = -\nabla p + \mu \nabla^2 \boldsymbol{u} \tag{2}$$

where $\boldsymbol{u}$ is the fluid velocity, ρ the density of water, p the pressure and μ the fluid viscosity. For the given free stream velocity U, the fluid boundaries are the free surface, the rigid two fences, and the water-bottom surface. On the latter two boundary surfaces, no-slip condition is imposed, and on the free surface, a vanishing normal velocity condition is imposed i.e. the free surface remains flat.

Lagrangian Particle Tracking

Once the flow velocity field is known, the motion of an oil droplet of diameter d_e can be found by solving the following equation of motion given by Maxey et al. (1983) and Berlemont et al.(1990):

$$\rho_0 \frac{d\boldsymbol{u}_d}{dt} = -\rho C_A \frac{d\boldsymbol{u}_r}{dt} - \frac{\rho}{2} C_D \frac{A_e}{V} |\boldsymbol{u}_r| \boldsymbol{u}_r + (\rho_0 - \rho)\boldsymbol{g} + \rho \frac{D\boldsymbol{u}}{Dt} \tag{3}$$

where ρ_0 is the density of oil, $\boldsymbol{u}_d$ the droplet velocity, C_A the added mass coefficient normalized by the droplet volume V, $\boldsymbol{u}_r(=\boldsymbol{u}_d - \boldsymbol{u})$ the relative velocity of the droplet to the fluid velocity, C_D the drag coefficient normalized by $\rho|\boldsymbol{u}_r|^2 A_e$, $A_e(=\pi d_e^2/4)$ the equivalent cross-section area of the droplet, $\boldsymbol{g} = (0, -g, 0)$ the gravitational acceleration, and D/Dt the substantial time derivative. The coefficients C_A and C_D are obtained by the formulae given by Clift et al(1978).

3 NUMERICAL METHOD

The computations are carried out under the assumption that the fences are very long such that the flow field is two dimensional. The Navier-Stokes equations are solved by the finite-difference scheme with body-fitted grids, standard k-ε turbulence model of Jones and Launder (1972), and SIMPLE C algorithm for the velocity-pressure correction to satisfy the continuity Eqn. 1. The computation domain is x= (-15D, 25D) and y=(0, -15D), and the boundary conditions for the steady, viscous flow case are

$$\boldsymbol{u} = (U, 0) \quad \text{at} \quad x = -15D \tag{4a}$$

$$\frac{\partial u}{\partial x} = 0 \quad \text{at} \quad x = 25D, \text{ and} \quad v = 0 \quad \text{at} \quad y = 0, -15D \tag{4b}$$

where D is the fence draft. The exact free-surface condition is that the free surface remains as a material surface which allows the deformation. However, in the present work, mainly due to the numerical complexity and uneconomical computation time involved, the v = 0 condition is adopted.

4 EXPERIMENTAL METHOD

4.1 Experimental Facilities and Procedures

The experiment for obtaining flow velocity field by PIV(Particle Image Velocimetry) method of Shin et al.(2000) was carried out at a circulating water channel of which the test section size was

$300^w \times 200^h \times 1200^l$(mm). A schematic diagram of the fence model and coordinate system used in this study is shown in Figure 1. The draft(D) and width(W) of the oil fence are 40mm and 300mm, respectively and the fence model has a flat end with a thickness(B) of 5mm made of acrylic material. The free stream velocity was uniform at 10cm/s and its corresponding Reynolds number (Re) and Froude number (Fr) based on the fence draft are about 4000 and 0.16, respectively. The free stream turbulence intensity is about 0.5% at this velocity. The experiment is conducted for two free-surface conditions i.e. open and closed free surface between the tandem fences.

4.2 Droplet Tracking

The experiment to obtain the trajectories of paraffin balls(1) of different sizes which are released in the upstream of a model fence is carried out at a larger circulation water channel of $1m^w \times 1m^h \times 4.2m^l$ in order to increase the Reynolds number to the order of $10^4 \sim 10^5$ and make the balls to escape beneath the fence, which cannot be done with the smaller channel. The fence draft was increased to 150mm and the Froude number to 0.292. The tracking of the motion of the balls is done by CCD camera as schematically shown in Figure 2a and a sample photograph of the trajectory in Figure 2b.

5 RESULTS AND DISCUSSIONS

In Figure 3 the variations of the horizontal velocity profiles at several longitudinal locations obtained by the PIV method and computations are shown.

Since our major interest lies in the flow behavior in the upper layer close to the free surface, attention should be given to this region i.e. Y/D>-1.0, Due to the light density of the oil, the oil leaked below the fore fence would tend to float up to the free surface. Thus, if it is assumed that the oil layer covers the free surface between the tandem fence, it is our focal subject to find out if the computational method of the flow field with the closed free-surface assumption would be valid or not.

Several interesting phenomena can be observed from Figure 3. In Figure 3a, a comparison of the computed and experimental results is shown. If we focus our observation in the region of Y/D > -1.0, we can conclude in general that the computational method with the closed free-surface condition is reasonable. In Figure 3b in the region of Y/D > -1.0 and 1.81 < X/D <5.85, back flows exist for the tandem fence and the magnitude is greater for the open free surface than the closed free surface. The greater back flow in the upper fluid zone is favorable in view of trapping the leaked oil. The computational results in Figure 3b show under predicts the back flow velocity, which implies that the computational results are on the more conservative side than the experimental results in assessing the tandem-fence effectiveness.

When a fence is deployed, the fence will block the movement of an oil slick, and the accumulated oil in front of the fence forms a triangular shape. The initial stage of the leakage takes place by the oil droplets sheared off the surface of the oil layer. Depending on where these droplets start their motion, they could be reattached to the oil layer or leaks below the fence. The computational method can predict a zone in the upstream of the fence in which oil droplets having started their movement will escape below the fence.

In Figure 4 the demarcation lines called as "Leakage Line" are shown for two oil droplet sizes and two Froude numbers. If the droplets begin their movement below the leakage line, they could leak below the fence. The dotted lines are for the deformed fence. One can observe from this figure that the bigger a droplet, the lesser the current speed and the lesser the fence deformation, the lesser the chance of oil leakage.

---

(1) The laboratory experiments using a paraffin ball and the equivalent diameter oil droplet were conducted by Lee et al.(1998) and found they exhibited the same trajectories

In Figure 5 the trajectories of a spherical paraffin ball of diameter of 5mm and density of 900kg/m^3, which is supposed to represent an oil droplet, are shown. The solid curve is the computed trajectory by Eqn.3 and symbols are the repeated experimental results. The particle release point (x_0, y_0) for Figure 5a is (x_0/D, y_0/D) = (-2.0, -0.6) and for Figure 5b (-0.8, -0.6). It can be seen from Figure 5 that the experimentally obtained trajectories from the releasing point nearer to the fence show an inconsistent behavior behind the fence. The main reason is due to the unsteady nature of the tip vortex emanating from the tip of the fence. Although no attempt was made to obtain more accurate time-averaged trajectories from the experiment due to the impracticality of repeating the tests for over at least fifty times, it is assumed the computed trajectory may represent the reasonable time-averaged values.

Based on the analysis described above, it is thus concluded that the evaluation of the containment effectiveness of a set of tandem fence by the flow-field computation based on the present Navier-Stokes solver with k-ε turbulence modeling and vanishing velocity condition on the free surface is reasonable.

Computation for the trajectories of the oil droplet of various sizes is carried out for the draft ratio (D_1/D_2) of 0.5, 1.0, and 2.0 where D_1 and D_2 are the drafts of the fore and the aft fence, respectively. From the results it is concluded that $D_1/D_2 = 1.0$ is more effective than the other two ratios.

The effect of the water depth on the tandem-fence effectiveness is investigated by computing the trajectories of the oil droplets for different values of water depth ranging from 2D to 15D. It was found that the shallower the depth, the longer the oil trajectory between the fences, which is not favorable in the viewpoint of the oil trapping between the fences.

6 CONCLUSIONS

From the results of the present investigation, the following conclusions are drawn :

1) The present flow-field computation by the Navier-Stokes solver with the k-ε turbulence modeling and the free-surface condition of vanishing vertical velocity together with the Lagrangian particle-tracking method seems a reasonable tool in evaluating the effectiveness of tandem fences,
2) The condition of lower current speed, larger oil-droplet size, and smaller fence-skirt deformation would lead to a lesser chance of oil leakage below the fore fence,
3) An identical draft for both fences of a tandem fence seems more effective than other combinations of the fore and aft fence drafts, and
4) In the shallow water region, deployment of a tandem fence with larger draft would not necessarily increase the oil-trapping effectiveness. It is recommended to leave the gap between the fence tip and the water bottom more than twice the fence draft.

Acknowledgment

The authors express their appreciation for the supports granted by Advanced Fluids Engineering Research Center of Pohang University of Science and Technology through Korea Science and Engineering Foundation. They also acknowledge the assistances of their graduate students, Messrs Min S. Koh and Sang K. Chung in carrying out the present investigation.

References

Comrack, D. (1983). Response to Oil and Chemical Marine Pollution. Applied Science Publishes. New York.

Delvigne, G.A.L. (1987). Laboratory Experiments on Oil Spill Protection of a Water Intake. Oil in Fresh Water : Chemistry, Biology, Countermeasure Technology (Eds. Vandermulen, J.H, and Hurdey, S.E.), Pergamon Press, 446-458.

Lo, Jen-Men. (1996). Laboratory Investigation of Single Floating Booms and Series of Booms in the Prevention of Oil Slick and Jellyfish movement. *Ocean Eng.* **23**, 519-531.

Lee, C.M, Kang, K.H. and Cho, N.S. (1998). Trapping of Leaked Oil with Tandem Oil Fences with Lagrangian Analysis of Oil Droplet Motion. *J.OMAE, ASME Trans.* **120**, 519-531.

Maxey, M.R and Riley, J.J. (1983). Equation of Motion for a Small Rigid Sphere in a Nonuniform Flow. Phys. of Fluids. **26**, 883-889.

Berlement, A., Desjonqueres, P. and Gouesbet, G. (1990). Particle Lagrangian Simulation in Turbulent Flows. Int'l *J. Multiphase Flow*. **16:1**, 19-34.

Clift, R, Grace, J. R. and Weber, M.E. (1978). Bubbles, Drops, and Particles, Academic Press.

Jones, W.P. and Launder, B.E. (1972). The Prediction of Laminarization with a Two-Equation Model of Turbulence. *Int'l J. Heat and Mass Transfer* **15**, 301-314.

Shin, Dae Shik, Choi, Jay Ho and Lee, Sang-Joon. (2000). Velocity Field Measurement of Flow inside Snout of Continuous Hot-Dip Galvanizing Process Using a Single-Frame PIV Technique. *The Iron and Steel Institute of Japan Journal.* **40:5**, 484-490.

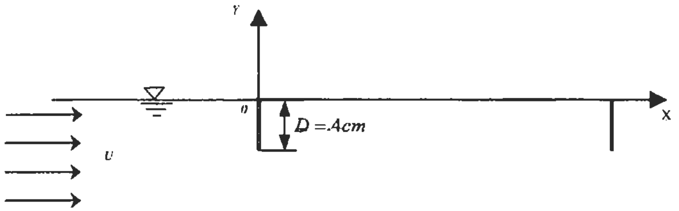

Figure 1: Schematic diagram of experimental set-up and coordinate system

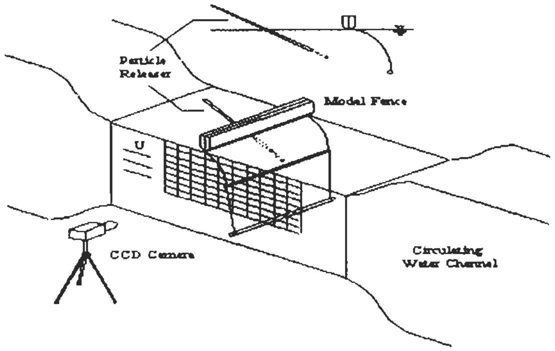

Figure 2a: Experimental setup for measuring the trajectory of paraffin balls

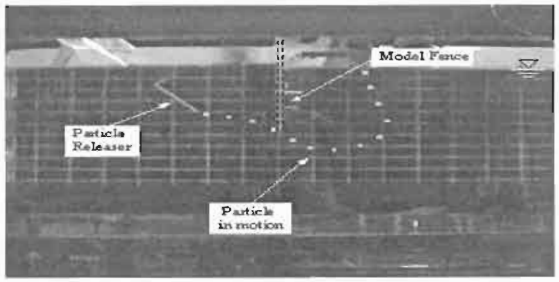
Model Fence
Particle Releaser
Particle in motion

Figure 2b: Photograph of the trajectory of a paraffin ball

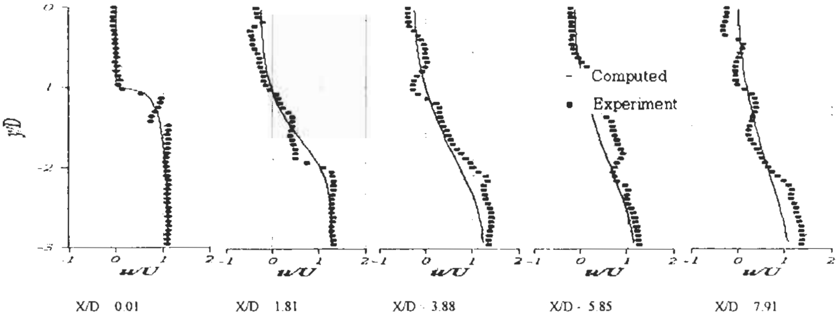

a) Single Fence

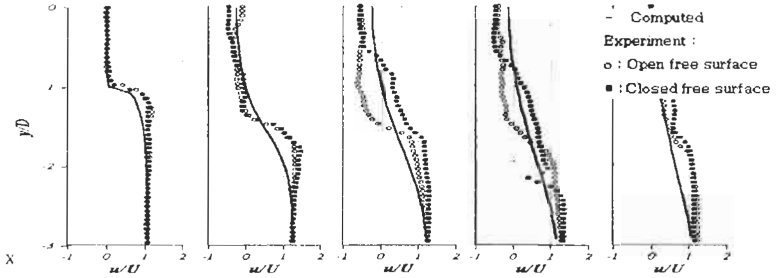

(b) Tandem fence with separation distance of 8D

Figure 3: Comparison of horizontal velocity profiles obtained by computation and experiment at Fr = 0.16

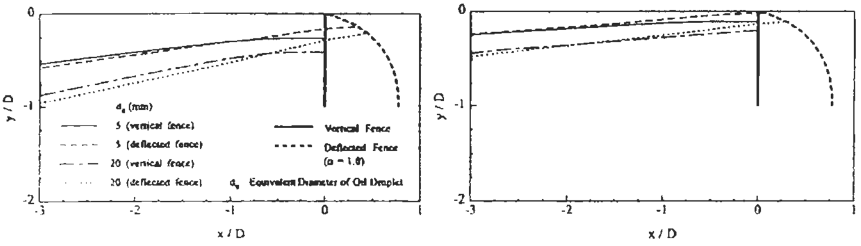

(a) Fr = 0.116 (b) Fr = 0.232

Figure 4: Leakage lines of vertical fence and deflected fence for different oil droplet diameters and current speeds

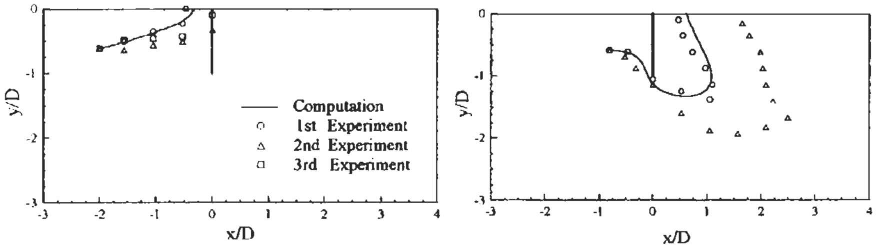

(a) $(x_0, y_0)/D$ = (-2.0, -0.6) (b) $(x_0, y_0)/D$ = (-0.8, 0.6)

Figure 5: Trajectories of paraffin balls around the vertical model fence for different initial release points at Fr = 0.29, Re = 53100

Practical Design of Ships and Other Floating Structures
You-Sheng Wu, Wei-Cheng Cui and Guo-Jun Zhou (Eds)
© 2001 Elsevier Science Ltd. All rights reserved

A CFD-BASED PARAMETRIC STUDY ON THE SMOKE BEHAVIOR OF A TYPICAL MERCHANT SHIP

Eunseok Jin, Jaedon Yoon and Yongsoo Kim

Daewoo Shipbuilding & Marine Engineering Co., Ltd.,
1-Aju-Dong, Koje-City, Kyungnam, 656-714 Republic of Korea

ABSTRACT

In this paper, a CFD based parametric study is introduced, which is intended to investigate the smoke behavior depending on the funnel and accommodation arrangement. Corresponding calculation results were analyzed systematically and a simple measure was obtained, which hopefully could be applied to the preliminary design of funnel and accommodation arrangement. In modeling the geometry, elements having minor effects on the flow field were excluded and its reasonableness was proved by some pre-calculations. But, the remaining elements that have considerable effects were modeled and the analyses were performed in pretty realistic conditions. Properties that have significant effects on the behavior were chosen as parameters to be investigated. Each parameter was varied in a given range. Calculations were performed for all models resulting from the parameter variations. Analyzing all the calculation results, influences of the parameters on the smoke behavior and a simple measure to predict the smoke exhaust performance was obtained.

KEYWORDS

CFD, Parametric study, Smoke behavior, Funnel height, Deckhouse height, Funnel position, NO_2 iso-surface, Particle track

1 INTRODUCTION

For last several years DSME (Daewoo Shipbuilding and Marine Eng. Co., Ltd.) has practiced numerous model tests and CFD analyses concerning the smoke exhaust performance of the funnel. Through these experiences, now DSME has a good knowledge of a flow around the funnel and especially, its ability of CFD analysis is on a fairly high level. But there is no standard to use properly in the funnel design. By the way, recently, owner's requirements for the model test or CFD analysis to guarantee the smoke exhaust performance are increasing and thus the related costs are increasing. Therefore, a proper method to estimate the smoke exhaust performance is highly required.

The behavior of the smoke exhausted from ship funnel is important in relation to the onboard hazard such as pollution, high temperature, machinery malfunction and so on. And it strongly depends on the funnel and accommodation arrangement. Therefore, it is required to estimate the smoke exhaust performance of a ship in advance to derive desirable arrangement of funnel and accommodation. The estimation can be made in various ways e.g., model test, CFD and preferably simple empirical formula or statistical methods that can be obtained through full-scale ship observations, model tests or CFD analyses. To obtain useful formula or tables that can be used in the estimation of the smoke exhaust performance, numerous cases must be analyzed. Using CFD in this kind of analysis has merits in cost over model tests. Moreover, when CFD is used, simulation results can be observed more closely than in model tests both qualitatively and quantitatively.

The objective of this study was to observe the influences of the funnel and accommodation arrangement on the smoke behavior through a CFD-based parametric study. Also, if possible, a simple measure to expect the smoke exhaust performance was to be obtained. For these purposes, three parameters were chosen and calculations were executed for the models obtained through the variations of the parameters. Each calculation result was analyzed with several appropriate methods prepared beforehand.

2 CALCULATION MODEL

The ship adopted as a model of the analysis is an oil carrier having the shape presented in Figure 1. The result of the analyses using this model could be referred to in the design of the ships of similar shape.

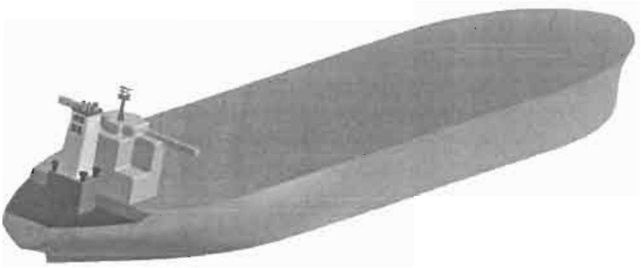

Figure 1: Model of the Calculation

In the analysis of the flow around a ship funnel using CFD, calculation model must be carefully chosen. It requires much effort to describe the like hull and other appendages such as radar mast or on-deck pipe system due to their complicated shapes or small sizes. Besides, if they are included in the analysis, calculation time will increase according to the increased mesh size to describe the complex geometry. On the other hand, among those there can exist one or more elements that have little influence on the flow around the funnel. For the efficiencies in the modeling and calculation procedure, it is better to exclude the elements having minor effect on the flow field from the model.

Thus prior to the main calculation, effects of hull, radar mast and on-deck pipe system on the flow around the funnel was investigated through several calculations. As a result of those calculations, the hull had a significant effect on the flow around the funnel, while the effect of the radar mast and on-deck pipe system was so small. Consequently, the radar mast and on-deck pipe system might be excluded from the model, but the hull must be included.

The effect of bow shape was considered by changing the bow part of the hull into a vertical prism of which the section has the same shape as the deck plane. The intention of this analysis is to make the hull modeling procedure efficient, i.e., if the difference between the result of the bow-modified model and that of the original model is not great, the modified bow shape is adopted in the modeling. The result of this analysis is that the difference between the two cases is not significant.

Following the above discussion, the model having the shape in Figure 2 was chosen. The radar mast and on-deck pipe system were excluded and bow part of the hull was replaced with a vertical prism.

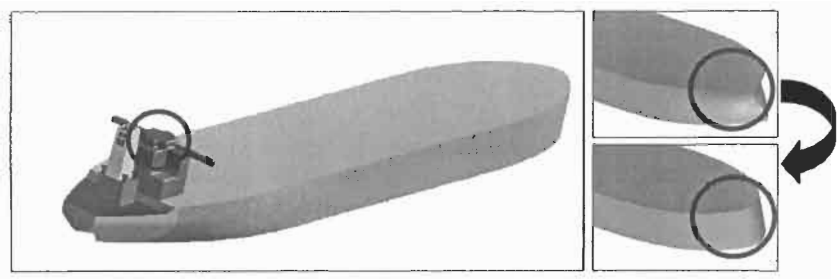

Figure 2: Model Used in the Parametric Study

3 PARAMETRIC STUDY

3.1 Parameters

Among the elements that are expected to influence the flow field around the funnel, deckhouse height, funnel height and funnel position were chosen as parameters. Their definitions are shown in Figure 3. Variations of parameters are also listed in Figure 3, where the abbreviations DH, FH and FP stand for deckhouse height, funnel height and funnel position respectively. These abbreviations mean the same throughout this paper. Deckhouse height varies with the step of 2 m and DH2 has the same deckhouse height as the original model. Funnel height variation follows the way that the ratio of funnel height to deckhouse height changes with the step of 0.15. The original value of the funnel height to deckhouse height ratio is 1.307, so the closest case to the original model is FH3. Concerning the funnel position, three cases are applied and the funnel position of FP2 is the same as the original model. Following these variations, 60 cases were produced.

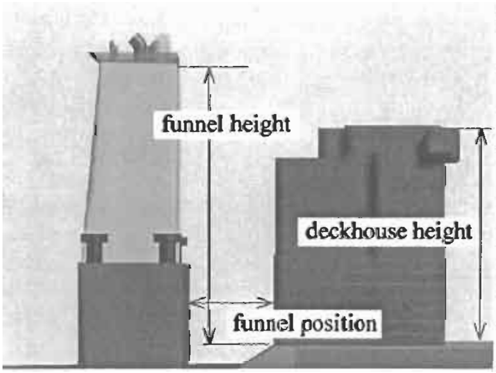

Deckhouse height

Case	Original	DH1	DH2	DH3	DH4
DH	**21.5**	19.5	21.5	23.5	25.5

Funnel height

Case	Original	FH1	FH2	FH3	FH4	FH5
FH/DH	**1.307**	1.00	1.15	1.30	1.45	1.60

Funnel position

Case	Original	FP1	FP2	FP3
FP	**7**	5	7	9

Figure 3: Parameter Definition and Variation

3.2 Calculation

3.2.1 Calculation domain and mesh

Calculation domain was set as shown in Figure 4. For an efficient mesh generation, calculation domain was divided into a cylindrical inner part surrounding the ship and a cubic outer. These two domains were filled with tetrahedral meshes. Total number of the meshes is about 500,000.

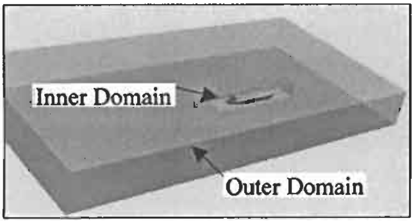

Domain	Domain size: L×B×H (m)
Ship	332×58×63
Inner Domain	500×120×85
Outer Domain	2000×1000×200

Figure 4: Calculation Domain

3.2.2 Calculation setting

The ship is advancing with its speed in a wind. And nitrogen dioxide is included in the exhaust gas with the concentration of 1200 ppm. Although many other noxious gases are included in real exhausts, they need not be included in the analysis because their concentrations are generally too low to cause on-board pollution.

Principal features of the analysis are summarized in TABLE 2. Multiple species model was adopted in order to simulate the dispersion of nitrogen dioxide and energy equation was included into the governing equation set because of the high temperature at the exits of the exhausts.

TABLE 1

PRINCIPAL FEATURES OF THE ANALYSIS

Coordinate system	Right-handed cartesian coordinate system, vertically upward z-axis
Problem type	3D steady state, energy equation included
Solver	Segregated explicit
Turbulence model	RNG k-ε model with standard wall function
Discretization	Standard for pressure, fist order upwind for all the other variables

3.3 Evaluation of the Smoke Exhaust Performance

Some measures are required to judge the smoke exhaust performance from simulation results. Those can be prepared considering the problems caused by exhaust gas from the funnel exhausts. For a common merchant ship, the problems caused by exhaust gas can be divided into two categories. The first is the dispersion of the noxious gases, and the second is the possibility of pollution caused by ash included in the exhaust. In this study, following items are introduced for the purpose of the evaluation of the smoke exhaust performance:

3.3.1 Dispersion of the noxious gas

As mentioned before, nitrogen dioxide was adopted as a typical noxious gas. It starts with concentration of 1200 ppm and disperses rapidly. If its concentration at the deckhouse, engine room intake or other principal points is higher than a certain value, there exists a possibility of health problem of the crews. Two methods were adopted to inspect the dispersion of nitrogen dioxide. The first is to observe the shape of the iso-surface of NO_2 concentration. The region covered with the iso-surface is polluted by NO_2 beyond the limitation. An example of the NO_2 iso-surface is shown in Figure 5-(a). The iso-value used in this example is 3 ppm, which is the long-term (8 hours) exposure limit for nitrogen dioxide recommended by HSE (Health and Safety Executive), and this value is used as a criterion for the judgement of safety through this study. The second method is to check the NO_2 concentrations at specific points. In Figure 6, the checking points used in the analysis are presented.

3.3.2 Particle track

To simulate the ash included in the exhaust, particles, whose density and size are similar to those of the real ash, were modeled. By observing the trajectories of these particles released from exhausts, the possibility of pollution of hull surface can be estimated. An example of particle trajectory is shown in Figure 5-(b).

In summary, measures used in the evaluation of the smoke exhaust performance are NO_2 3 ppm iso-surface, particle trajectory and NO_2 concentrations on Surface 1, Surface 2, E/R intake and Deckhouse in Figure 5-(c).

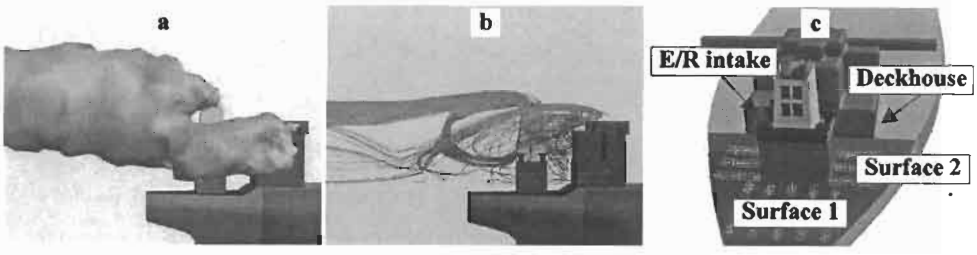

Figure 5: NO_2 3 ppm Iso-surface (a), Particle Trajectory (b) and Checking Points of NO_2 Concentration (c)

3.4 Results

As the first step, the effect of the parameter variation was investigated. The investigation was based on the changes of the evaluation items i.e., NO_2 iso-surface shape, particle trajectory and the NO_2 concentrations on the checking points.

As typical examples, change of NO_2 iso-surface according to the deckhouse height and the funnel height are presented in Figure 7 and Figure 8 respectively. As shown in these two figures, there is no significant change in the smoke behavior according to the deckhouse height variation, but the exhaust performance shows significant improvement as the funnel height increases. Generally, the wake generated by the deckhouse becomes weaker as it becomes farther from the deckhouse. According to this physics, smoke exhaust performance would improve as the funnel is moving farther from the deckhouse. But when the results are compared with respect to each funnel position, such tendency does not appear so obviously. It is likely that this is due to the fact that the funnel location is within the range where the flow pattern is still quite irregular. But when all the evaluation results obtained following the procedure showed in TABLE 2, it can be concluded that it's beneficial to the exhaust performance to locate the funnel as far away from the deckhouse as possible. To observe the influence of the funnel position on the smoke behavior clearly, the variation range of the funnel position needs to be larger. But such variation of funnel position would be beyond the scope of the real design practice.

TABLE 2 shows the second step, i.e., evaluating procedure of the smoke exhaust performance. Judging rules adopted in this evaluation are tabulated in TABLE 3. In TABLE 2, the first two rows ('NO_2 Iso-surface' and 'Particle Track') are results obtained by observing the shape of NO_2 3 ppm iso-surface and particle trajectory. The third ('NO_2 on Surface 1') and the fourth ('NO_2 on Surface 2') were obtained from the inspection of the distributions of NO_2 concentrations on Surface 1 and Surface 2 respectively. The last two are maximum NO_2 concentrations on Deckhouse and E/R intake. As for the name of checking points, reference can be found in Figure 5-(c). The last item 'Exhaust Performance' is the gradation of the exhaust performance obtained by summarizing results of all the items. If any of the first four items is 'absolutely unsatisfactory' (×), the final result becomes 'absolutely unsatisfactory', and the exhaust performance also becomes 'absolutely unsatisfactory' if the maximum NO_2 concentration on E/R intake or Deckhouse is higher than 3 ppm, even if there is no 'absolutely unsatisfactory' in the results of the first four items.

When all the evaluation results of the smoke exhaust performance are investigated, dependence of the smoke exhaust performance on the deckhouse height and the funnel height reveals clearly. The smoke exhaust performance does not significantly depend on the deckhouse height while it is highly dependent on the funnel height, i.e., it improves with the increase of the funnel height. From the inspection of the relation between the funnel height and the exhaust performance it is concluded that the smoke exhaust performance will be satisfactory if the ratio of funnel height to deckhouse height is 1.3 or larger. When it comes to the funnel position, as mentioned before, it's beneficial to the smoke exhaust performance to locate the funnel as far away from the deckhouse as possible.

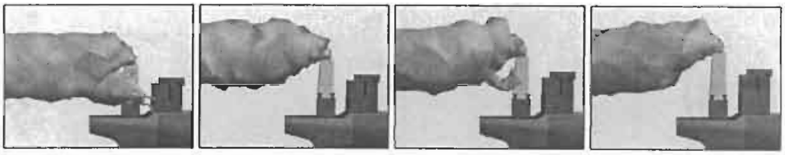

Figure 6: An Example of Change of NO_2 iso-surface according to the deckhouse height

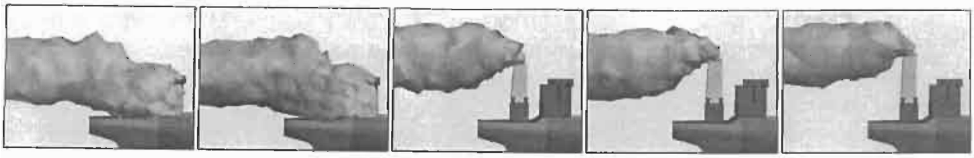

Figure 7: An Example of Change of NO_2 iso-surface according to the funnel height

TABLE 2

EXAMPLES OF EVALUATION OF THE SMOKE EXHAUST PERFORMANCE

Item	Case 1	Case 2	Case 3	Case 4
NO_2 Iso-surface	○	×	×	△
Particle Track	◎	×	×	◎
NO_2 on Surface 1	◎	○	○	○
NO_2 on Surface 2	○	△	△	○
Max. NO_2 on Deckhouse side	0.72	0.53	2.79	2.20
Max. NO_2 on E/R Intake	2.63	2.02	6.06	9.15
Exhaust Performance	○	×	×	×

TABLE 3
JUDGING RULES OF THE SMOKE EXHAUST PERFORMANCE

Level	Judging Rule
⊚	Absolutely Satisfactory, Smoke is hardly disturbed, No possibility of pollution
○	Marginally Satisfactory, Smoke is disturbed a little, No possibility of pollution
△	Marginally Unsatisfactory, Smoke is disturbed significantly, a little possibility of pollution
X	Absolutely Unsatisfactory, Smoke is severely disturbed, Pollution occurs surely

4 CONCLUSIONS

Before the main calculation, influence of the hull and other appendages on the flow around the funnel was investigated through several calculations. It was concluded that the hull must be modeled, but the radar mast and on-deck pipe system need not to be modeled due to their minor effects on the flow field around the funnel.

The smoke exhaust performance is not directly influenced by the deckhouse height but it improves with the increase of the funnel height. In practical design, the funnel would show a satisfactory smoke exhaust performance when the ratio of funnel height to deckhouse height is 1.3 or larger. The effect of the funnel position on the smoke behavior did not appear obviously when the calculation results were inspected with individual measures because the range of the variation was somewhat small. But when all the estimation results were taken into consideration, it could be concluded that it's beneficial to the smoke exhaust performance to locate the funnel as far away from the deckhouse as possible.

The quantitative accuracy of the results in this study is not guaranteed, so caution is required when this paper is referred to. The quantitative validity of the analysis of the smoke exhaust performance using CFD needs to be verified for the direct use of the results, and this verification work can be executed in the near future.

References

[1] (1986). A Method to Predict Stack Performance. *Naval Engineering Journal.* 35-46

[2] (1998). *Fluent User's Guide*, Fluent Inc.

[3] Gary J. Baham and Donald McCallum. (1977). Stack Design Technology for Naval and Merchant Ships. *SNAME Transactions* **85**, 324-349

[4] Jaedon Yoon, Eunseok Jin and Yongsoo Kim. (2000). Design of the Accommodation and Funnel in a Merchant Ship for Favorable Smoke Emission Performance. *The 5th Korean Fluent Users' Group Meeting.*

[5] (2000). Occupational Exposure Limits 2000. *Health and Safety Executive.*

[6] (1998 ~ 2000). Internal R&D Reports, *Daewoo Shipbuilding and Marine Engineering Co., Ltd.*

Practical Design of Ships and Other Floating Structures
You-Sheng Wu, Wei-Cheng Cui and Guo-Jun Zhou (Eds)
© 2001 Elsevier Science Ltd. All rights reserved

APPLICATION OF CFD TO ASSESSMENT AND DESIGN OF THE AIR-VENTILATION SYSTEM IN THE REEFER CONTAINER HOLDS OF CONTAINER CARRIERS

Bong Jun Chang

Maritime Research Institute, Hyundai Heavy Industries Co., Ltd. Ulsan 682-792, Korea

ABSTRACT

A CFD methodology, based on Finite Volume Method, is applied to the assessment of the air-ventilation system in the 3-dimensional reefer container holds of a container carrier ship and to the re-design of the ventilation system to reduce the labor costs. In order to understand the airflow pattern inside the hold, the flow and temperature distributions between a reefer container column and a ventilation duct are calculated. Using the flow characteristics obtained from the calculated results, the ventilation system is re-designed, and finally, in the 3-dimensional whole hold, the flow and temperature induced by the re-design system are simulated and qualitatively compared with those by the original system. In these simulations, the flow is assumed to be steady in order to save computational costs and the gravity is added to governing equations to consider the effect of the density change due to the temperature change on flow patterns. As conclusions, the performance of the re-designed system similar to that of the original system, but 40% of the labor cost is saved. However, in order to obtain the quantitative information from simulated results, the detailed measurements must be conducted and numerical methodology applied here must be adjusted.

KEYWORDS

CFD, Ventilation, Reefer, Container, Flow, Temperature, Heat, Finite-Volume-Method

1 INTRODUCTION

Inside the one or two holds of container carriers, ventilation systems are built to keep the performance of reefer containers or exhaust the gas, which may leak from dangerous cargoes. However, these ventilation systems have been often designed by the intuition and experience of designers without understanding the flow characteristic inside the holds.

There are two popular methods to understand these flow characteristics; the first is the model measurement, and the second is the numerical simulation, commonly based on Computational Fluid Dynamics(CFD). The former may give us the reliable results, but require expensive costs for us to understand global flow characteristics and temperature distributions[5]. Present CFD methodologies cannot be said to be perfect, especially in the respect of turbulent flows around complex bodies, but state-of-the-art CFD codes are beginning to tackle complex geometries and flow conditions, recently with the rapid increase of computer capacity and the development of numerical algorithms[2,9]. Furthermore, the usefulness and advantage in using CFD to analyze ventilation performance have been pointed out by studies in several engineering-fields such as the building construction[1,3,4,8] and the fire safety [5,10,11].

The purposes of this study are to understand flow and temperature characteristics in reefer container holds and then to find how to re-design the economical ventilation system. For the sake of these purposes, the STAR-CD, a commercial CFD code is used. However, in this paper, quantitative information from this application is not drawn because the details of numerical methodologies used here are not verified with systematic experiments

1.1 Backgrounds

As a typical example, Figure 1 shows the ventilation systems inside the reefer container holds. Six ventilation units were installed, and each ventilation unit consisted of a fan and two duct columns. To inhale the air heated by each reefer container, even at the bottom of the hold, the long ducts reached down. However, a simple natural law, the moving-up of the heated air, was passed over in designing this system.

In this paper, the flow and temperature characteristics between one duct and one container-column are studied, like cascade foils. Then, based on these studies, duct system is re-designed. Finally the performances of original and re-designed system in the three-dimensional hold are calculated and compared.

2 NUMERICAL APPROACHES

Figure 2 shows the geometrical model of the original ventilation system for the present numerical calculation at the design condition, when the containers are fully stored in the hold. For simplicity, it is assumed that the half capacity of the fan is attached to each of separated duct columns and flows at the narrow gap between containers are neglected.

On the numerical methodologies applied, the finite volume method(FVM) are well known and extensively documented[2]. Hence, in this paper, only the main features of the methodologies are summarized in Table 1. In these simulations, the flow is assumed to be steady and a relative simple algorithm, SIMPLE, is applied. Also, the effect of the density change, due to the temperature change, on flow patterns are considered as the gravity is added to governing equations. The Re-Normalized Turbulence(RNG) model is used because this model is known to be appropriate for circulating flows[2].

TABLE 1

MAIN FEATURES OF NUMERICAL METHODOLOGIES

Code Name	STAR-CD
Numerical Algorithm	SIMPLE (steady)
Difference Scheme	SFCD(Self-Filtered CD)
Turbulence Model	RNG k, ε
Solved Variables	Velocity, Pressure, k, ε , Temperature, Density
Convergent Criteria	1.0E-03

Table 2 shows the details of boundary conditions for these calculations. The fan is installed to exhaust the heated air, and the temperatures on the deck and the side-hull surfaces are assumed to be 65° and 42° Celsius degree, respectively. These conditions are obtained from the rules to consider when a ship operates in tropical oceans. For the turbulent flow on the solid surfaces, wall function is used.

TABLE 2

THE DESCRIPTION OF BOUNDARY CONDITIONS(SEE FIGURE 2)

Surface	Name	Details
S1	Fan	Q=960 m3/Min,
S2	Reefer	No-slip, Heat 5.23KW
S3	Side Hull	No-slip, T=42°C
S4	Deck	No-slip, T=65°C
S5	Air-In	No-slip, T=35°C
Others	Wall	No-Slip, T=35°C

3 CALCULATED RESULTS

In order to understand the flow pattern inside the hold with a relatively low computational cost, the flow between a duct and a container column is simulated as shown in Figure 3, like approaches for cascade foils. The capacity of a fan at the end of a duct is assumed to be half of the original fan, i.e. 480 m^3/MIN. On the both surfaces in the lateral direction, symmetric boundary conditions is applied

3.1 Cascade Approach for a Duct and a Container Column

Figure 4 shows the flow and temperature distributions on the longitudinally cut-surfaces as determined in Figure 3. The calculated results around upper, middle, lower parts of the duct are plotted separately. The major drawbacks of the flow and temperature in the original system are summarized as follows:

- The suction flow does not reach the surface of reefer containers to generate the heat. As the result, the heated flow does not move into the duct.
- At the end of duct, the relatively cool air is inhaled.

TABLE 3

THE SIZE OF THE ORIGINAL AND MODIFIED DUCT SYSTEM

Duct	Original (12 Duct Column)	Modified (6 Duct Column)
Width ×Thickness	0.8m × 0.6m	1.25m × 1.0m
Hole Width	0.4m	1.2m
Hole Height	0.3m	0.3m

From the results, we find that it is necessary to make the velocity at the hole increased and only heated air inhaled. However, the increase of fan capacity requires additional costs. Hence, the duct system is modified in following ways:

- To make the duct short, not to inhale the relatively cool air
- To adjust the hole size to make the suction flow velocity increase.

After studying the effect of the duct length and the hole size on the temperature and velocity distributions, the ventilation system is modified. Also, it is concluded that the number of the duct column may be reduced if the each duct is efficiently designed. Figure 5 shows the calculated results of the finally modified system using the cascade approach. In the system, a duct is used to two columns of reefer containers. The fan capacity is adjusted to total fan capacity, 960 M^3/MIN, in the calculation. Table 3 shows the size of hole on the duct in the original and modified systems.

3.2 Whole Domain Approaches

Figure 6, 7, 8 and 9 show the temperature and velocity distributions in the whole hold by the original and modified duct systems. The branch of original duct system is assumed to be separate, so as to use relatively simple meshes. However, it is considered that the effect of this simplification on the flow near duct columns is small.

As shown in the figures, there are relatively strong flows in the lateral direction inside the hold. This flow will be expected to suppress the locally high temperature. However, in the hold, the locally high temperature regions are predicted and the positions of the regions coincide with the center of the circulations in lateral direction.

In modified system, also, there is a high peak region in the middle of the hold with the modified system, but this region have a relatively weak influence on the performance of reefer containers, because there is no reefer container.

From these calculations, it is concluded that the global performance of modified system similar to that of the original system even though they give locally different distributions of the temperature. And, furthermore, the high temperature regions near the reefer containers disappear in the modified system.

4 CONCLUSIONS

In this paper, the flow and temperature distributions inside the hold for the reefer containers are studied using a CFD code, STAR-CD. Although the numerical methodologies applied here are not verified through the comparison with systematic experiments, this approach gives us the information on the flow characteristics inside the hold, and allows qualitative comparison with the performance of different systems.

Finally, from the information obtained by the present approaches, the design guides for ventilation ducts in the reefer container holds are suggested as following:

- The duct column need not reach the reefer container at the bottom of the hold, because the heated air moves up naturally.
- The relatively strong suction flows had better be generated in the upper region of the hold
- Due to the lateral flows in the hold, it is considered that the number of the duct column may be reduced if the each duct is efficiently designed

Finally, for the quantitative evaluation of the performance, it is necessary to collect systematically experimental data.

References

1. Awbi H.B. (1988), Energy efficient room air distribution, *Renewable Energy*, vol. 15, no. 1, pp. 293-299

2. Chang B.-J. (1997), Application of CFD to Marine Propellers and Propeller-Hull Interactions, *Phd dissertation*, Imperial College, London

3. Chow W.K. (2001), Numerical studies of airflows induced by mechanical ventilation and air-conditioning (MVAC) systems, *Applied Energy*, vol. 68, no. 2, pp. 135-159

4. Chung I.-P. and Dunn-Rankin D. (1998), Using numerical simulation to predict ventilation efficiency in a model room, *Energy and Buildings*, vol. 28, no. 1, pp. 43-50

5. Demmers T.G.M., Burgess L.R., Phillips V.R., Clark J.A., and Wathes C.M. (2000), Assessment of Techniques for Measuring the Ventilation Rate, using an Experimental Building Section, *Journal of Agricultural Engineering Research*, vol. 76, no. 1, pp. 71-81

6. Fujita A., Kanemaru J.-i., Nakagawa H. and Ozeki Y. (2001), Numerical simulation method to predict the thermal environment inside a car cabin, *JSAE Review*, vol. 22, no. 1, pp. 39-47

7. Gan G. and Riffat S.B. (1998), A numerical study of solar chimney for natural ventilation of buildings with heat recovery, *Applied Thermal Engineering*, vol. 18, no. 12, pp. 1171-1187

8. Papakonstantinou K.A., Kiranoudis C.T. and Markatos N.C. (2000), Numerical simulation of air flow field in single-sided ventilated buildings, *Energy and Buildings*, vol. 33, no. 1, pp. 41-48

9. *STAR-CD User Guide v3.100*, (1999), Computational Dynamics Ltd.

10. Wen J.X. and Huang L.Y. (2000), CFD modelling of confined jet fires under ventilation-controlled conditions, *Fire Safety Journal*, vol. 34, no. 1, pp. 1-24

11. Wu Y. and Bakar M.Z.A. (200), Control of smoke flow in tunnel fires using longitudinal ventilation systems - a study of the critical velocity, *Fire Safety Journal*, vol. 35, no. 4, pp. 363-390

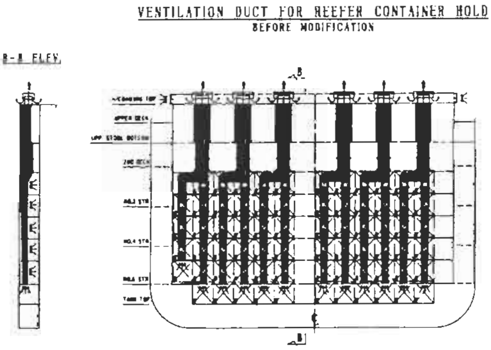

Figure 1 : Sketch of the original ventilation system (Left : transverse view, Right : longitudinal view)

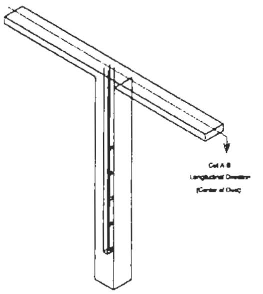

Figure 2 : Geometrical model for cascade approach

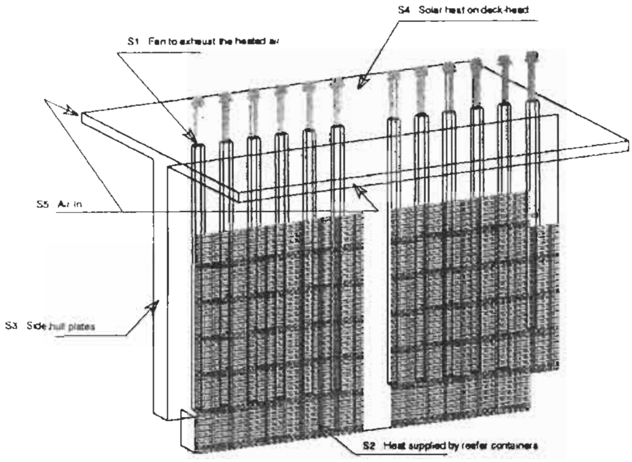
S4 Solar heat on deck-head
S1 Fan to exhaust the heated air
S5 Air in
S3 Side hull plates
S2 Heat supplied by reefer containers

Figure 3 : Calculation domain for cascade approach

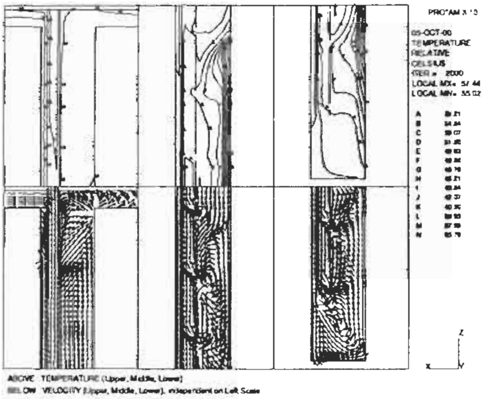

Figure 4 : Flow and temperature in original system (Cascade)

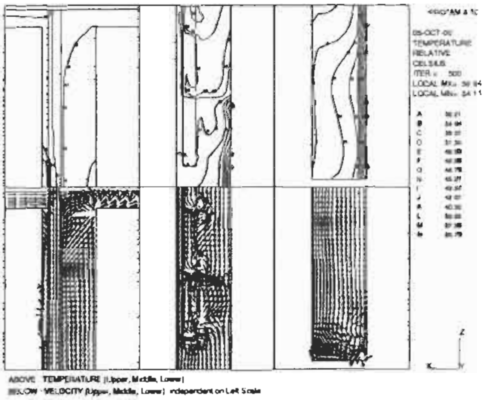

Figure 5 : Flow and temperature in new system (cascade)

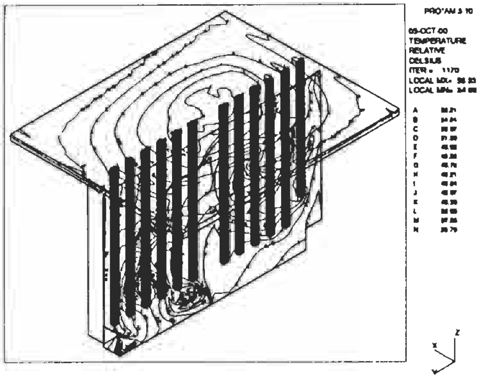

Figure 6 : Temperature distribution by original system

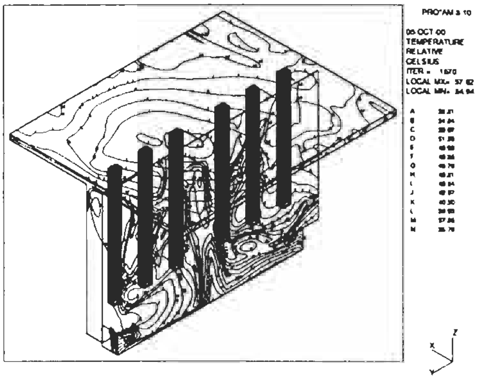

Figure 7 : Temperature distribution by new system

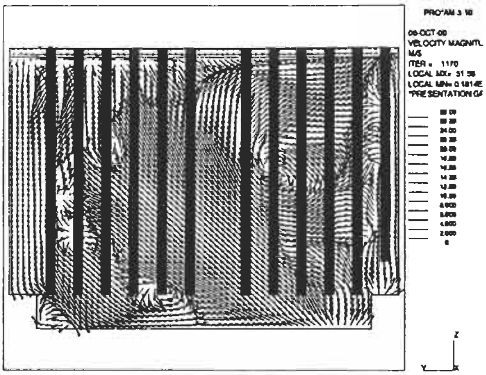

Figure 8 : Flow pattern by original system

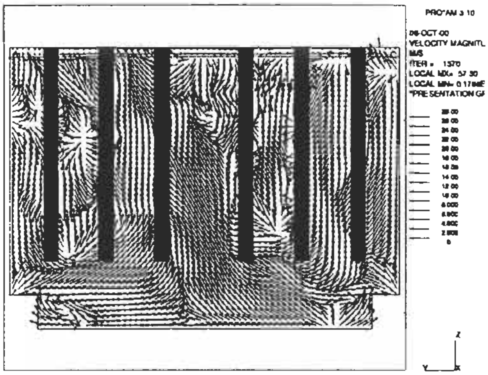

Figure 9 : Flow pattern by modified system

Practical Design of Ships and Other Floating Structures
You-Sheng Wu, Wei-Cheng Cui and Guo-Jun Zhou (Eds)
© 2001 Elsevier Science Ltd. All rights reserved

WASH AND WAVE RESISTANCE OF SHIPS IN FINITE WATER DEPTH

Qinzheng Yang[1], O. M. Faltinsen[1] and Rong Zhao[2]

[1] Department of Marin Hydrodynamics, Norwegian University of
Science and Technology, N-7491 Trondheim, Norway
[2] MARINTEK A/S, P. O. Box 4125 Valentinlyst, Trondheim, Norway

ABSTRACT

A linear theory to predict wash and wave resistance of ships in finite water depth is developed. The hull is assumed slender and the water depth is constant. The method uses the 3-D Green's function in finite water depth, that satisfies the classical linear free surface condition. Both sub- and supercritical speed are studied. The thin ship theory is used. The Green's function is studied carefully by different approaches. Wave resistance is predicted both by direct pressure distribution and by the far field wave systems. Vertical force and pitch moment are also examined. The results are compared with experiments and shallow water slender body theory. Wash is discussed by systematically examining the wave resistance for different water depths and depth Froude numbers.

KEYWORDS

Thin Ship Theory, Wave Resistance, Finite Water Depth, Wigley Hull, Trim, Sinkage, Wash

1 INTRODUCTION

With the introduction of high speed ships, there has been increasing attention for the impact of ship wash on safety and environment. The great increase of wave resistance in shallow water when approaching critical speed is important in ship design. Also the sinkage and trim must be considered in particular for small clearances between the ship bottom and the sea floor.

To solve the related steady motion problem we could use Rankine singularities. This requires singularity distributions over both the hull, free surface and in principle a control surface at infinity. This leads to a large equation system of unknown singularity densities. An advantage of using a Rankine method is that nonlinear free surface problems can be handled. However we have chosen to linearize the problem and use thin ship theory (Michell (1898)) with a Green's function satisfying the classical linear free surface condition, wave radiation condition and boundary condition on a horizontal sea floor. Given that the ship is slender and the problem can be linearized, we believe that using this

Green's function is advantageous in accurately determining the far field wave picture (wash). The method can be generalized to handle multihull vessels. An important effect for high speed vessels is flow separation from a transom stern. This is not focused on in the present paper. We assume infinite horizontal extent of the fluid domain. In confined areas like in a channel, additional effects have to be considered when the water depth Froude number is close to 1. Unsteady wave effects and upstream propagating solitary waves may occur (Chen and Sharma(1995)). It is possible to combine the present method with a nonlinear shallow water theory accounting for variable water depth. This will enable us to analyse wash on a beach. Examples of wash are given in the present paper. This ought to be related to criteria for acceptable wash. However this is not further pursued here. We are instead qualitatively discussing wash by relating it to wave resistance. The present method has been tested for a Wigley hull. The importance of water depth and ship length Froude number is discussed. Comparisons are made with experiments and slender body theory in shallow water.

2 THEORY

The fluid is assumed inviscid, incompressible and homogenous. The fluid motion is steady in a reference frame following the ship motion. Surface tension is neglected and the free surface slope is assumed sufficiently small so that linear theory can be applied. A Green's function G satisfying the Laplace equation in the fluid domain except at the source point, linearized kinematic and dynamic free surface conditions at the mean free surface, no penetrating conditions at the sea floor, and radiation conditions at infinity is used. Thin ship theory is applied. The ship is then represented by a centreplane source distribution proportional to the longitudinal rate of change of local beam. The Green's function is given by for instance Wehausen and Laitone(1960), Kostyukov(1968) and Lunde(1951). We rearrange the result and decompose it into three parts: images of Rankine sources, a local disturbance part and the downstream wave part. Cartesian coordinates are used with x to be the direction of the forward velocity U, y is transverse and z is vertical and positive upwards. The coordinate system is fixed relative to the ship and the origin is in the mean free surface. The final results are normalized with respect to the water depth H. Then we have

$$G=\frac{1}{r}+\frac{1}{r_2}-\frac{1}{\pi}\int_0^\infty\int_{-\pi}^{\pi}\frac{e^{-k}\cosh(k(1+\zeta))\cosh(k(1+z))e^{ik((x-\xi)\cos\theta+(y-\eta)\sin\theta)}}{\cosh k}dk\,d\theta \tag{1}$$

$$-\frac{2}{\pi}\int_{-\frac{\pi}{2}}^{\frac{\pi}{2}}d\theta\int_0^\infty\frac{\cosh(k(1+z))\cosh(k(1+\zeta))\exp(ik(|x-\xi|\cos\theta+(y-\eta)\sin\theta))-f(\theta,k)}{\cosh^2 k(kF_h^2\cos^2\theta-\tanh k+i\varepsilon\cos\theta)}dk \tag{2}$$

$$-4iH(\xi-x)\left(\int_{\theta_0}^{\frac{\pi}{2}}+\int_{-\frac{\pi}{2}}^{-\theta_0}\right)\frac{\cosh(K_0(1+z))\cosh(K_0(1+\zeta))\exp(iK_0(|x-\xi|\cos\theta+(y-\eta)\sin\theta))}{\cosh^2 K_0(F_h^2\cos^2\theta-1/\cosh^2 K_0)}d\theta \tag{3}$$

where the source point is at $(\xi,\ \eta,\ \zeta)$ and the field point is at $(x,\ y,\ z)$. Further $r^2=(x-\xi)^2+(y-\eta)^2+(z-\zeta)^2$, $r_2^2=(x-\xi)^2+(y-\eta)^2+(z+2+\zeta)^2$, $\theta_0=\arccos(1/F_h)$ for $F_h>1$ and $\theta_0=0$ for $F_h<1$. $F_h=U/\sqrt{gH}$ is the depth Froude number and $K_0=K_0(\theta)$ is the real positive root of $K_0F_h^2\cos^2\theta-\tanh K_0=0$. $H(x)$ is the Heaviside step function. ε is a small positive number proportional to the Rayleigh's viscosity. The latter takes care of the radiation condition. Further $f(\theta,k)$ is a function of θ and k that removes the singularity at $k=0$. It follows by Fourier transform that expression (1) is the sum of infinite number of sources and sinks which are images of the source located at (ξ,η,ζ) with respect to $z=0$ and $z=-1$ so that the boundary conditions $\varphi=0$ at $z=0$ and $\partial\varphi/\partial z=0$ at $z=-1$ are satisfied. Part (2) is even in $x-\xi$ and important near the source and behaves like $\log R$ far away from the source for subcritical case. Here

$R^2 = (x-\xi)^2 + (1-F_h^2)(y-\eta)^2$. Part (3) includes the far-field downstream wave systems. Expression (2) is a double integral with singularities. Because of the highly oscillatory properties of the integrand, and also because it has no influence to the wave resistance (Newman (1976)), this has not been extensively studied in the literature. But this part is important for prediction of sinkage and trim. We must be careful with the singularities in expression (2). The properties of the singularities are not the same for subcritical and supercritical case. For subcritical case, $k = 0$ is not a singularity if $f(\theta,k)$ is properly chosen. We can then integrate with respect to k first. For supercritical case, $k = 0$ is a singularity for some values of θ. We must then integrate first with respect to θ in order for the integration to have a meaning. Two different methods are used to calculate the local disturbance. One is to keep ε as a small positive number and do the double integration. This method is direct, no singularities involved and the sequence of integration is unimportant. But the accuracy cannot be guaranteed, and a lot of CPU time is needed because of the highly oscillatory integrand. When using this method, we select $f(\theta,k) = 1/\cosh^2 k$ for all the k and θ in order to have a continuous integrand. Another method is to take one variable as a complex number, and use Cauchy's theorem to find some suitable integration path in the complex plane. For subcritical case, a steepest descent path is easy to find for k and for supercritical case, principle value integration plus residues has been used. For subcritical case, we select $f(\theta,k) = 1/\cosh^2 k$ for $k < a$ and 0 for $k \geq a$. Here a is a small positive number less than k_s. k_s is the smallest k that the dispersive relation $kF_h^2 \cos^2\theta - \tanh k = 0$ has a real solution. We can always find such an a at subcritical case. The reason we choose $f(\theta,k) = 0$ for $k \geq a$ is that finding the steepest descent path is simple. Table 1 presents some results for subcritical case by these two different methods. $a = 0.1$ is used. Because of the different selection of $f(\theta,k)$, there is a constant difference between the two methods. It should be noted that this constant difference does not influence the predicted values of free surface, force and moment.

We will now show that part (2) has a logarithmic far-field behavior for subcritical case. For the integrand, we can make a Taylor expansion about $k = 0$ but keep the highly oscillatory term $\exp(ik(|x-\xi|\cos\theta + (y-\eta)\sin\theta))$. The leading order term will be $(\exp(ikr)-1)/k/(F_h^2\cos^2\theta - 1)$, where $r = |x-\xi|\cos\theta + (y-\eta)\sin\theta$. Integration gives $\int_0^a (\cos(kr)-1)/k\,dk = Ci(ar) - \ln(ar) - \gamma$, where $Ci(z)$ is Cosine Integral defined by equation 5.2.2 in Abramowitz and Stegun(1964) and γ is Euler's Constant. For large r, $Ci(ar) \to 0$ and the leading order term will be $(2/\pi)\int_{-\pi/2}^{\pi/2} \ln(ar)/(F_h^2\cos^2\theta - 1)d\theta$. Numerical evaluation of this expression is easy and there is only a constant difference between this expression and the result $\ln((x-\xi)^2 + (1-F_h^2)(y-\eta)^2)/(1-F_h^2)^{0.5}$ from shallow water slender body theory by Tuck (1966). The evaluation of part (2) is slow in general. Chebyshev polynomials can be used to approximate the results as Newman (1987) did for the deep water Green's function. Five variables $x-\xi, y-\eta, z, \zeta, F_h$ are involved in this function. We can decompose it into two sub-functions. Each involves four variables. One is function of $x-\xi, y-\eta, z+\zeta, F_h$. The other is function of $x-\xi, y-\eta, z-\zeta, F_h$.

The wave part (3) is the integration of residues. We can choose to integrate over θ as in expression (3) or to integrate over k as follows:

$$-4iH(\xi - x)\int_{K_0}^{\infty} dk \frac{\cosh(k(1+z))\cosh(k(1+\zeta))(e^{ik(|x-\xi|\cos\theta_0 + (y-\eta)\sin\theta_0)} + e^{ik(|x-\xi|\cos\theta_0 - (y-\eta)\sin\theta_0)})}{2kF_h^2\cos\theta_0\sin\theta_0\cosh^2 k} \qquad (4)$$

Here $K_0 = 0$ if $F_h > 1$ and K_0 is the positive root of $K_0F_h^2 - \tanh K_0 = 0$ if $F_h < 1$, and $\theta_0 = \arccos((\tanh k/k)^{0.5}/F_h)$. The integrand is highly oscillatory when the field point is far away from the source point. A fast convergence method is used to speed up the calculation (See p. 297 and

72 in Dahlquist(1974)). In order to study the wave systems behind the source, we study the change of the phase of the integrand in expression (4). Due to symmetry only positive $y-\eta$ needs to be studied. The phase function $k(|x-\xi|\cos\theta_0+(y-\eta)\sin\theta_0)$ increases monotonically with increasing k and will give no wave contribution far away. If $\alpha=\arctan((y-\eta)/|x-\xi|)$ is larger than some value β, the phase function $k(|x-\xi|\cos\theta_0-(y-\eta)\sin\theta_0)$ will decrease monotonically with increasing k and will not give any wave contribution. If α is less than β, this phase function will have one local maximum and/or minimum. Thus β determines the wave angle behind the source. For subcritical case, the phase function will have both local minimum and maximum, which corresponds to respectively the transverse and divergent wave systems. For supercritical case, it has only one local maximum which corresponds to the divergent wave systems. Fig 1 shows the relationship between wave angle and F_h. If $F_h <\sim 0.6$, the wave angle is almost the same as in deep water ($19^0 28'$), and approaches 90^0 when reaching the critical speed. It then decreases with increasing speed.

Michell's thin ship theory is used to determine the densities of the source distribution on the centreplane S_0 of the ship. This gives the velocity potential $\phi=\frac{U}{2\pi}\iint_{S_0} d\xi d\zeta \frac{\partial f(\xi,\zeta)}{\partial \xi} G(x,y,z;\xi,0,\zeta)$ due to the presence of the ship. Here $y=f(x,z)$ descirbes the hull surface for $y>0$. By expressing the hydrodynamic pressure as $p=\rho U\phi_x$, the corresponding longitudinal force F_1, vertical force F_3 and pitch moment F_5 about the $y-axis$ are:

$$F_1=\rho U\iint_{S_B}\phi_x n_1 ds \approx 2\rho U \iint_{S_0}\frac{\partial f(x,z)}{\partial x}\phi_x ds$$

$$=\frac{\rho U^2}{\pi}\iint_{S_0} dxdz \frac{\partial f(x,z)}{\partial x}\iint_{S_0} d\xi d\zeta \frac{\partial f(\xi,\zeta)}{\partial \xi} G_x(x,0,z;\xi,0,\zeta) \tag{5}$$

$$F_3=\frac{\rho U^2}{2\pi}\iint_{S_B} dsn_3 \iint_{S_0} d\xi d\zeta \frac{\partial f(\xi,\zeta)}{\partial \xi} G_x(x,y,z;\xi,0,\zeta) \tag{6}$$

$$F_5=-\frac{\rho U^2}{2\pi}\iint_{S_B} dsn_3 x \iint_{S_0} d\xi d\zeta \frac{\partial f(\xi,\zeta)}{\partial \xi} G_x(x,y,z;\xi,0,\zeta) \tag{7}$$

Here S_B is the mean wetted ship hull surface, ρ is the mass density of water and n_3 is the z-component of the normal vector to the body surface. Positive normal direction is into the body. We can use the pressure at the centreplane in the integration of F_3 and F_5, but must integrate over S_B in order to properly account for area. By decomposing the Green's function into an odd and even function in $x-\xi$, we can see that the only non-vanishing contribution to F_1 is coming from the odd term. This gives:

$$F_1=-\frac{4\rho U^2}{\pi}\int_{\theta_0}^{\pi/2}\frac{(P^2+Q^2)k\cos\theta}{\cosh^2 k(F_h^2\cos^2\theta-1/\cosh^2 k)}d\theta \tag{8}$$

where $P+iQ=\iint_{S_0} dxdz f_x(x,z)\cosh(k(1+z))\exp(ikx\cos\theta)$. This is a well known result (Lunde (1951)).

We then have two equations to calculate the wave resistance, either Eq. (5) or Eq. (8). This can be used to check the accuracy of the results.

3 RESULTS FOR WIGLEY HULL

Wigley's (1942) parabolic hull is used in the case studies. The hull surface for $y>0$ is given by:

$$\frac{y}{B/2}=\left[1-(\frac{x}{L/2})^2\right]\left[1-(\frac{z}{T})^2\right]$$

Here the origin for x, y and z is on the centreplane at the waterplane amidships. L, B and T are respectively the length, beam and draught, where $B/L = 0.1$ and $T/L = 0.0625$ in our case. We divided the centreplane into panels and the source density on each panel was taken as constant and equal to its value at the middle of the panel. Convergence studies were done by using different number of panels and the wave resistance results obtained by Eq. (5) were compared with results by Eq. (8). We used either $50(10\times5)$, $120(20\times6)$ or $240(30\times8)$ panels to calculate the wave resistance. Here the first number in the brackets is the number of panels in longitudinal direction and the second number is the number of panels in vertical direction. The panel size is small at bow and stern and near the free surface. Results for $H/L = 0.1$ are shown in Table 2. For high Froude numbers, even 50 panels can give good results, but for low Froude number, more panels are needed. One reason is that the resistance at low speed is small. Another reason is that the decreasing wave length of the transverse wave systems with decreasing speed requires more panels in the longitudinal direction.

In Fig 2, the wave resistance coefficient $Cw = -2F_1/\rho U^2 S$ in deep water and finite water depth $H/L = 0.1$ are presented. Here S is the area of the mean wetted hull surface. When F_h is less than ~0.6, the influence of water depth is small. The reason is that the wave lengths associated with the far-field wave systems are small relative to the depth and the waves cannot be influenced by the sea floor. We can also see from Fig 1 that the wave angle is almost the same as that in deep water. The influence of the sea floor is large close to the critical speed ($F_h = 1$). At high Froude numbers, the influence is small again. The reason is that the divergent wave systems are dominant for high Froude numbers. Since the wave lengths of the divergent wave systems are small, the influence from the sea floor is small. Fig 3 shows comparisons with experimental and theoretical results by Everest and Hogben (1970) when $H/L = 0.425$. The agreement with the experiments is quite good but there are some differences with the theory by Everest and Hogben (1970). There is no great change of wave resistance when the speed passes through the critical speed. This can also be clearly seen from Figs 4 and 5. Figs 4 and 5 present the shallow water resistance ratio $r = R_h/R_\infty$ as a function of H/L and F_h. Here R_h is the wave resistance in finite water depth and R_∞ is the wave resistance in deep water at the same speed. These results are similar but not the same as presented by Hofman and Kozarski (2000). When F_h is near 1 and H/L is small, the wave resistance ratios r are very large and cannot be clearly seen from Fig 4. We use Fig 5 to show these results. We can see that the wave resistance ratio can be larger than 50 when the clearance between the ship bottom and the sea floor is small and the speed is near critical. Obviously we should then question the linear theory (Lea and Feldman (1972)). Fig 4 shows that the influence of the sea floor is small when H/L is larger than 0.4. When doing model tests in a towing tank such as MARINTEK, the water depth is 5.5 m, the highest towing speed is about 8 m/s. The depth Froude number may then be larger than 1. If for instance a model length L=5.5 m is used, the ratio H/L=1 and the curve lies at far right of Fig 4. The wave resistance ratio r is then almost equal to 1 even near the critical speed.

Figs 6-8 present comparisons with the shallow water slender body theory by Tuck (1966) when $H/L = 0.1$. From those figures, we can see that the two theories agree quite well except in the vicinity of the critical speed. The vertical force at supercritical speed and the pitch moment and wave resistance at subcritical speed are zero by slender body theory. The reason is that the slender body theory only considers the local disturbance at subcritical speed while predicts the wave systems at supercritical speed. Further the for and aft symmetry of the Wigley hull matters.

Wash is calculated by keeping only the wave part of the Green's function. Figs 9 and 10 show pictures of wash at respectively subcritical and supercritical speed. For Fig 9, F_h is equal to 0.9. Measured from the figure, the wave angle is about 35^0. We can see both transverse and divergent wave systems. But the divergent wave systems are dominant. For Fig 10, F_h is equal to 1.2. The wave angle is about 50^0 measured from the figure. We can only see the divergent wave systems. The wave angles are in good agreement with the results in Fig 1. Wash has a close relationship with the corresponding wave resistance. We can therefore get some information on how to minimize wash from Figs 4 and 5. The shallow water wave resistance ratio r is about 1.5 for $F_h = 0.9$, $H/L = 0.1$ and is about 4 for $F_h = 1.2$, $H/L = 0.1$. This means that the wash at $F_h = 0.9$ is favorable. By using Figs 4 and 5 we could minimize wash by changing F_h. For $F_h = 1.2$, we should actually increase F_h. If we increase the speed by ~10%, r will decrease from ~4 to ~2. But for $F_h = 0.9$, the change of F_h will not improve the wash problem. Both increase and decrease of F_h will increase the value of r if the change of F_h is confined to ± 10%. We should note that a large value of shallow water wave resistance ratio r is not necessarily corresponding to large value of wave resistance if there is a large difference between F_h. It should also be noted that r can be less than 1 which means that shallow water can have a positive effect on wash.

4 CONCLUSIONS

Steady forward ship motions in finite water depth are numerically investigated by thin ship theory and steady Green's function satisfying classical linear free surface condition in finite water depth. Both the wave part and the local disturbance of the Green's function are studied carefully. The local disturbance is numerically difficult to handle. The longitudinal force F_1, vertical force F_3, pitch moment F_5 and wash are calculated. The local disturbance part of the Green's function is important in calculating F_3 and F_5. The present methods have been tested for a Wigley hull, and the results are compared with experiments and Tuck's shallow water slender body theory. The shallow water theory is limited to small water depth while the present theory applies to any water depth. Wash is discussed by systematically presenting results for the wave resistance.

References

Abramowitz, M. and Stegun, I. A.(1964), *Handbook of Mathematical Functions with Formulas, Graphs, and Mathematical Tables*, Dover Publications, New York.

Chen, X.-N. and Sharma, S.D.(1995), A Slender Ship Moving at a Near-critical Speed in a Shallow Channel, *J. Fluid Mech.*, . **291**, pp. 263-285.

Dahlquist, G., Björck,Å. and Anderson, N.(1974). Numerical Method, Prentice-hall, Inc. Englewood Cliffs, New Jersey.

Everest, J. T. and Hogben, N.(1970). An Experimental Study of the Effect of Beam Variation and Shallow Water on Thin Ship Wave Predictions. *Trans RINA*.

Hofman, M. and Kozarski, V.(2000). Shallow Water Resistance Charts For Preliminary Vessel Design. *Int. Shipbuild. Progr.* **47: 449**, pp61-76.

Kostyukov,A.A.(1968),Theory of Ship Wave and Wave Resistance, Effective Communications Inc. Iowa City, Iowa.

Lea, G. K. and Feldman, J. P.(1972). Transcritical Flow Past Slender Ships. *9th Symp. Naval Hydrodynamics,* Paris, 1527-1539.

Lunde, J.K.(1951). On the Linearized Theory of Wave Resistance for Displacement Ships in Steady and Accelerated Motion. *Trans SNAME* 25-85.

Michell, J. H.(1898), The Wave Resistance of a Ship, *Phil. Mag.*, London, England,vol. **45**, pp. 106-123.

Newman, J. N. (1976), Linearized Wave Resistance Theory, *Proc. Int. Sem. on Wave Resistance*, pp.31-43. Soc. Nav. Arch. of Japan, Tokyo.

Newman, J. N. (1987), Evaluation of the Wave-Resistance Green Function: Part 1—The Double Integral. *J. Ship Res.* 31: 2, June, pp. 79-90.

Tuck, E. O. (1966), Shallow Water Flows Past Slender Bodies. *J. Fluid Mech.* **26**, pp. 89-95.

Wehausen, J. V. and Laitone, E.V.(1960), Surface Waves in *Handbuch der Physik*, Springer-Verlag, Berlin, Vol. 9, 446-778.

Wigley, W.C.S.(1942), Calculated and Measured Wave Resistance on a Series of Forms Defined Algebraically. *Trans. RINA*, Vol. **84**, 52.

TABLE1: COMPARISON BETWEEN TWO METHODS FOR CALCULATING LOCAL DISTURBANCE OF GREEN'S FUNCTION

(F_h=0.319, y=0, z=0, $\xi=0$, $\eta=0$, ζ=-0.1)

Method	x=0	x=0.1	x=0.3	x=0.7	x=0.9
Rayleigh's Viscosity	18.39429635	7.927961571	2.14054444	-0.610965748	-1.21626098
Cauchy's Theorem	29.72203588	19.25516810	13.46755223	10.71625231	10.11112379
Difference	-11.32773953	-11.32720653	-11.32700779	-11.32721885	-11.3273847

TABLE 2: CONVERGENCE STUDIES OF Cw FOR A WIGLEY UULL ($H/L=0.1$)

F_h	0.411096	0.600633	0.885438	1.075174	1.264911	1.549516	1.834121	2.213594
50 panels	-0.00063	0.000671	0.002456	0.011580	0.006733	0.004535	0.003511	0.002708
120 panels	0.000194	0.000476	0.002494	0.011725	0.006820	0.004598	0.003553	0.002750
240 panels	0.000169	0.000477	0.002505	0.011715	0.006818	0.004599	0.003556	0.002755
Eq. (8)	0.000170	0.000483	0.002516	0.011689	0.006808	0.004596	0.003557	0.002759

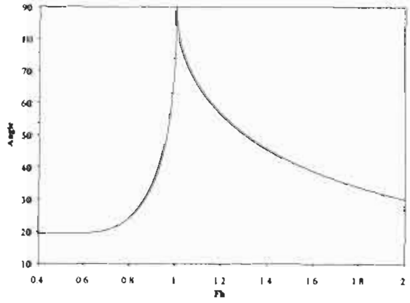

Figure1: The relationship between the wave angle and the water depth Froude number

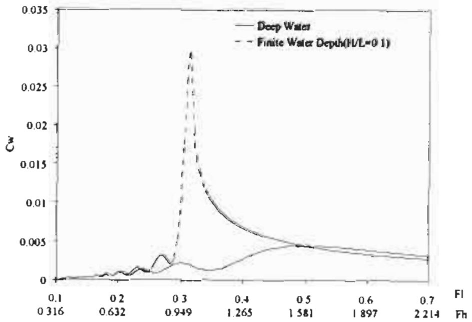

Figure 2: Wave resistance coefficient in deep water and finite water depth

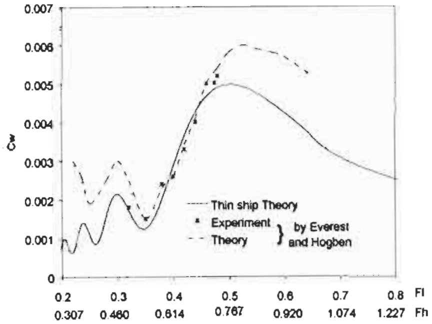

Figure 3: Comparisons of predicted wave resistance with experimental and theoretical results by Everest and Hogben (H/L=0.425)

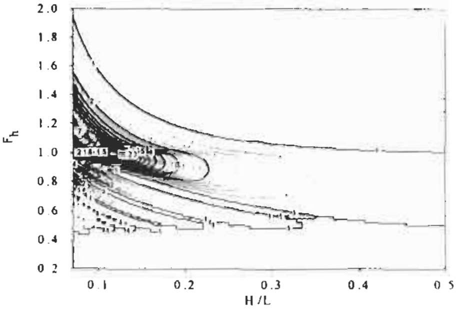

Figure 4: Shallow water wave resistance ratio $r = R_h / R_\infty$ as a function of H/L and F_h (see more details in Fig. 5)

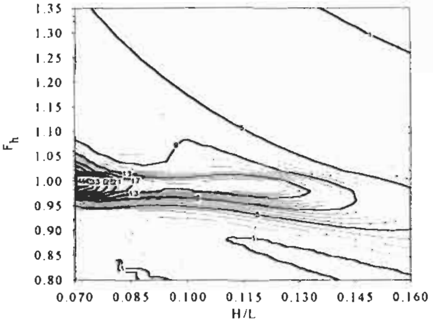

Figure 5: Shallow water wave resistance ratio $r = R_h / R_\infty$ as a function of H/L and F_h

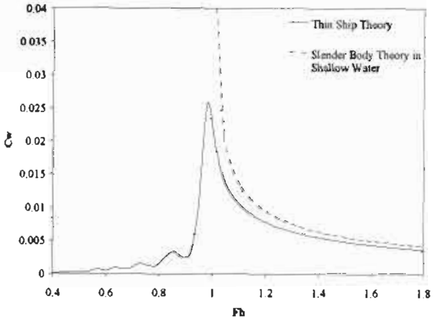

Figure 6: Wave resistance by thin ship theory and the shallow water slender body theory by Tuck (1966) (H/L=0.1)

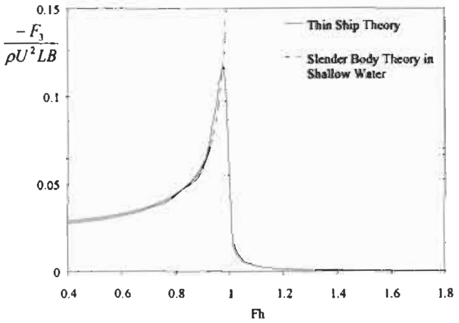

Figure 7: Vertical force F_3 by thin ship theory and the shallow water slender body theory by Tuck (1966) (H/L=0.1)

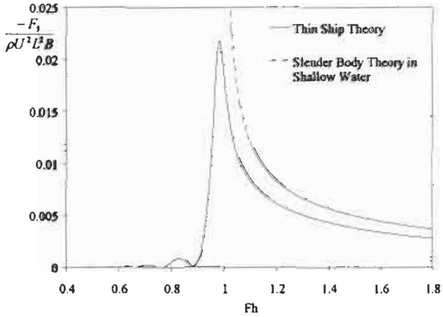

Figure 8: Pitch moment F_5 by thin ship theory and the shallow water slender body theory by Tuck (1966) (H/L=0.1)

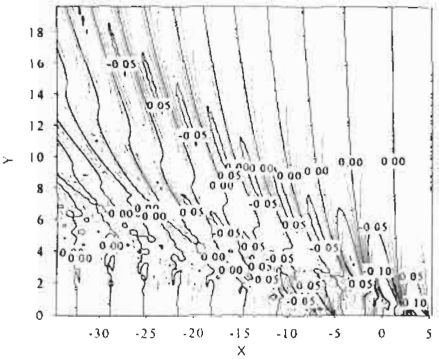

Figure 9: Predicted wash for Fh=0.9. The ship is located at -5<x<5 and $H/L = 0.1$. The numbers associated with the different lines are wave elevation divided by water depth.

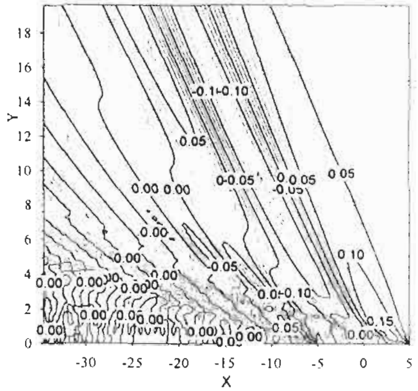

Figure 10: Predicted wash for Fh=1.2. The ship is located at –5<x<5 and H/L=0.1. See figure capture for Fig. 9.

Practical Design of Ships and Other Floating Structures
You-Sheng Wu, Wei-Cheng Cui and Guo-Jun Zhou (Eds)
© 2001 Elsevier Science Ltd. All rights reserved

ON SCALE EFFECT OF THE RESISTANCE DUE TO STERN WAVES INCLUDING FORWARD-ORIENTED WAVE BREAKING JUST BEHIND A TRANSOM STERN

Tadao Yamano[1], Yoshikazu Kusunoki[1], Fumiyasu Kuratani[1], Teturo Ikebuchi[2] and Isao Funeno[2]

[1]Department of Practical Life Studies, Hyogo University of Teacher Education
942-1, Shimokume, Yashiro-cho, Kato-gun, Hyogo, 673-1494 Japan
[2]Fluid Dynamics Research Department, Akashi Technical Institute, Kawasaki Heavy Industries Ltd.
1-1, Kawasaki-cho, Akashi, 673-8666 Japan

ABSTRACT

When a ship with a wide immersed transom stem runs on a deeper draft, forward-oriented wave breaking often occurs just behind the transom stem. Stem waves in such condition consist of two main components: the forward-oriented wave breaking and remained following waves. An example of such stern waves is shown in Figure 4. In our previous papers[1,2], we have developed a method to treat the former one and have clarified that it has scale effect and its resistance coefficient decreases with increase of model ship size. Purpose of this paper is to develop a method to treat the latter ones and then to clarify scale effect of such stem waves. We have developed a method to estimate resistance due to the latter ones. After the studies by those methods, we have come to the conclusions: Resistance increases largely, if the latter ones change to the former one. The latter one resistance coefficient increases only slightly with increase of model ship size. Resistance coefficient due to such stern waves is largely affected by the former one and, therefore, decreases with increase of model ship size.

KEYWORDS

Stern waves, Forward-oriented wave breaking, Remained following waves, Resistance, Scale effect

1 INTRODUCTION

Most of the recent container ships have rather wide immersed transom sterns to keep necessary transverse stability with much more containers on deck compared with those of two decades ago. When such a ship runs on a deeper draft than its design draft, forward-oriented wave breaking with high turbulence intensity often occurs just behind the transom stern. The phenomenon accompanies large momentum loss and accordingly generates large hull resistance. Research on the phenomenon is, therefore, important for energy saving for such ships. Regarding prevention or decrease of the phenomenon, one of the authors has conducted some studies[3,4,5,6]. Occurrence mechanism and characteristics detail of the phenomenon have, however, not yet completely been clarified.

In our previous papers[1,2], our studies have been concentrated on the forward-oriented wave breaking. A method to treat the phenomenon has been developed. An important result of the studies using the method is that it has been clarified that the phenomenon has scale effect and non-dimensional coefficient of resistance due to the phenomenon decreases with increase of model ship size. The result indicates, on the other hand, that height of the remained following waves, which are generated by stern end, not broken and propagated afterwards, increases with increase of model ship size to the contrary.

In the following, we study the remained following waves at first, and then we try to clarify scale effect of stern waves which consist of these two different main components.

2 A METHOD TO TREAT STERN WAVES INCLUDING FORWARD-ORIENTED WAVE BREAKING JUST BEHIND A TRANSOM STERN

To study such stern waves as described above, a method to estimate resistance due to the remained following waves, one of two main components of such stern waves, is further necessary and now it lacks. We, therefore, propose and evaluate a method for it in the following.

2.1 A Method to Estimate Resistance due to Remained Following Waves

We approximate water flow just behind a transom stern with the two-dimensional trochoidal wave as we have conducted in our previous study[1,2]. Figure 1 shows the coordinate system to be used.

Amount of kinetic energy dE_{kin}, which an infinitesimal part of the trochoidal wave with length $2\pi R$ (a wave length), breadth b and depth dy_0 has, can be described as follows[7]:

$$dE_{kin} = \pi \rho b g r_0^2 \{e^{2y_0/R} - (r_0/R)^2 e^{4y_0/R}\} dy_0 \tag{1}$$

where

dE_{kin} $(kgfm)$: amount of kinetic energy which an infinitesimal part of two-dimensional trochoidal wave has

ρ $(kgfs^2/m^4)$: density of water

$b(m)$: breadth of the infinitesimal part

$g(m/s^2)$: gravitational acceleration

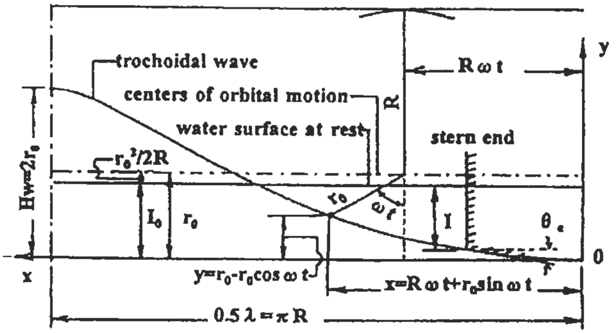

Figure 1: Coordinate system

$r_0(m), R(m)$: auxiliary variables in trochoidal wave equation[1,2]

$y_0(m)$: depth of a flow line below water surface (hull bottom) at the stern end

To maintain the wave system, amount of kinetic energy which is equal to integration of dE_{kin} over water depth from water bottom $(y_0 = -h)$ to water surface $(y_0 = 0)$ has to be supplied to the wave system per a wave length. This meets with wave resistance R_{fw}. This relation can be described as follows:

$$R_{fw} v_0 = \int_{-h}^{0} (dE_{kin} / T) dy_0 \tag{2}$$

where

$R_{fw}(kgf)$: resistance due to following waves behind a transom stern

$v_0(m/s)$: ship speed

$T(s) = 2\pi/\omega$: period of the following wave, where $\omega = (g/R)^{1/2}$

$h(m)$: water depth

If we suppose that the water flow layer at the water depth from a level ($y_0 = -y_c$) to water surface ($y_0 = 0$) at the stern end breaks, then we can estimate resistance due to not broken and remained following waves which come from the water flow layer at the water depth from water bottom ($y_0 = -h$) to the level ($y_0 = -y_c$) at the stern end using Eqn. (2) as follows:

$$\begin{aligned} R_{sfw} &= (1/v_0 n) \int_{-h}^{-y_c} (dE_{kin}/T) dy_0 \\ &= (\rho\, B_m g^{3/2} / 2v_0 n) \int_{-h}^{-y_c} (r_0{}^2 / R^{1/2}) \{ e^{2y_0/R} - (r_0/R)^2 e^{4y_0/R} \} dy_0 \end{aligned} \tag{3}$$

where

$R_{sfw}(kgf)$: resistance due to the remained following waves

$B_m(m)$: mean breadth of immersed transom stern end plane

$n(-)$: coefficient representing three dimensional effect, where is used n = 3 which is the value used in the equation for forward-oriented wave breaking resistance R_{swbf} in our previous papers[1,2].

$y_c(m)$: thickness of water flow layer which breaks

Integration in Eqn. (3) is convenient to be conducted separated into two parts as follows, since R and r_0 have constant values R_δ and $r_{0\delta}$ respectively over the water depth from $y_0 = -h$ to $y_0 = -\delta$:

$$\int_{-h}^{-y_c} = \int_{-h}^{-\delta} + \int_{-\delta}^{-y_c} \tag{4}$$

where

$r_{0\delta}(m), R_\delta(m)$: values of r_0 and R at $y_0 = -\delta$

$\delta(m)$: boundary layer thickness at the stern end

$h(m)$: water depth (supposed to be infinite)

Finally, we can obtain the following equation:

$$\begin{aligned} R_{sfw} = (\rho B_m g^{3/2} / 2v_0 n) [& \int_{-\delta}^{-y_c} (r_0{}^2 / R^{1/2}) \{ e^{2y_0/R} - (r_0/R)^2 e^{4y_0/R} \} dy_0 \\ & + (r_{0\delta}{}^2 R_\delta{}^{1/2} / 4) \{ 2e^{-2\delta/R_\delta} - (r_{0\delta}/R_\delta)^2 e^{-4\delta/R_\delta} \}] \end{aligned} \tag{5}$$

2.2 Verification of the Method

2.2.1 Comparison of estimated resistance with measured one

Measurement.

TABLE 1
PRINCIPAL PARTICULARS
(M.S.NO. CA)

$L_{WL}(m)$	7.385
$B\ (m)$	0.8833
$d\ (m)$	0.3072(Full-1)
$d\ (m)$	0.3292(Full-2)

Yamano et al.[3] show residual resistance coefficient r_r curves on two conditions Full-1 and Full-2 of a ship CA's 1/36.3 scale model (hereafter called M.S.NO.CA). Principal particulars of M.S.NO.CA are shown in Table 1. Comparison of model ship wave photographs taken at the model test between the two conditions reveals that the most different point in waves between the two conditions is the forward-oriented wave breaking just behind the transom stern. This is considered to mean that the r_r difference between the two conditions is mainly due to the difference of R_{swbf}. Let the difference of R_r obtained from r_r between the two conditions be δR_r.

Estimation. We can estimate R_{sfw} and R_{swbf} on each of the two conditions Full-1 and Full-2 by the methods we have developed. Let the difference of estimated stern wave resistance $R_{sw}=R_{swbf}+R_{sfw}$ between the two conditions be δR_{sw}.

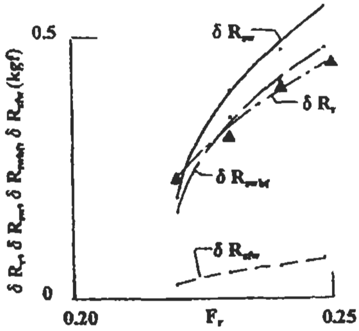

Figure 2: Comparison of estimated stern wave resistance δR_{sw} with measured

Comparison. Figure 2 shows comparison of δR_{sw} with δR_r. Both results agree fairly well in their tendency of change with Froude number $F_r = v_0 / \sqrt{gL_{WL}}$. In **Figure 2**, we show also δR_{swbf} and δR_{sfw} besides δR_{sw}, where $\delta R_{sw} = \delta R_{swbf} + \delta R_{sfw}$. Figure 2 shows that most part of δR_{sw} is occupied by δR_{swbf}, which confirms that above-described our assumption regarding the components of δr_r is correct.

From above discussion, we can say that we can use the method we have developed in this paper together with those developed in our previous study[1,2] to study characteristics of stern waves including the forward-oriented wave breaking just behind a transom stern.

3 SCALE EFFECT OF STERN WAVES INCLUDING FORWARD-ORIENTED WAVE BREAKING JUST BEHIND A TRNSOM STERN

3.1 Comparison of Following Wave Resistance with Forward-oriented Wave Breaking Resistance

Figure 3 shows estimated scale effect of water flow just behind the transom stern of M.S.NO.CA at $F_r = 0.25$ on Full-2 condition. At each of three similar hulls in Figure 3, water flow layer at the water depth from $y_0 = -\delta$ to $y_0 = -y_c$ does not break and propagates afterwards as following waves. We can estimate resistance due to the remained following waves from this water flow layer $R_{sfw-\delta-y_c}$ by Eqn. (5) as follows:

$$R_{sfw-\delta-y_c} = (\rho\ B_m g^{3/2} / 2v_0 n) \int_{\delta}^{-y_c} (r_0{}^2 / R^{1/2}) \{e^{2y_0/R} - (r_0/R)^2 e^{4y_0/R}\} dy_0 \qquad (6)$$

If this water flow layer broke forwards, we could estimate resistance due to the forward-oriented wave breaking $R_{swbf-\delta-y_c}$ by the equation developed in our previous study[1,2] as follows:

$$R_{swbf-\delta-y_c} = (\rho\ B_m / n) \int_{-\delta}^{-y_c} u_0^{\ 2} dy_0 \qquad (7)$$

where

$u_0 (m/s)$: water flow velocity at the stern end

For each of three similar hulls shown in Figure 3, we have estimated $R_{sfw-\delta-y_c}$ and $R_{swbf-\delta-y_c}$. Table 2 shows comparison of $C_{sfw-\delta-y_c} = R_{sfw-\delta-y_c} /(1/2)\rho B_m I v_0^{\ 2}$ with $C_{swbf-\delta-y_c} = R_{swbf-\delta-y_c} /(1/2)\rho B_m I v_0^{\ 2}$, where I is stern end immersion.

TABLE 2
COMPARISON OF C_{sfw} WITH C_{swbf}
(M.S.NO.CA AND SIMILAR HULLS)

$L_{WL}(m)$	0.7478	7.385 M.S.NO.CA	269.2
(1) $C_{swbf-\delta-yc}$	2.14	0.979	0.329
(2) $C_{sfw-\delta-yc}$	0.0108	0.0071	0.0030
(1) / (2)	198	139	110

Condition: $F_r = 0.25$, Full-2

Suffix $_{-\delta-yc}$ means "due to flow layer at the water depth from $y_0 = -\delta$ to $y_0 = -y_c$"

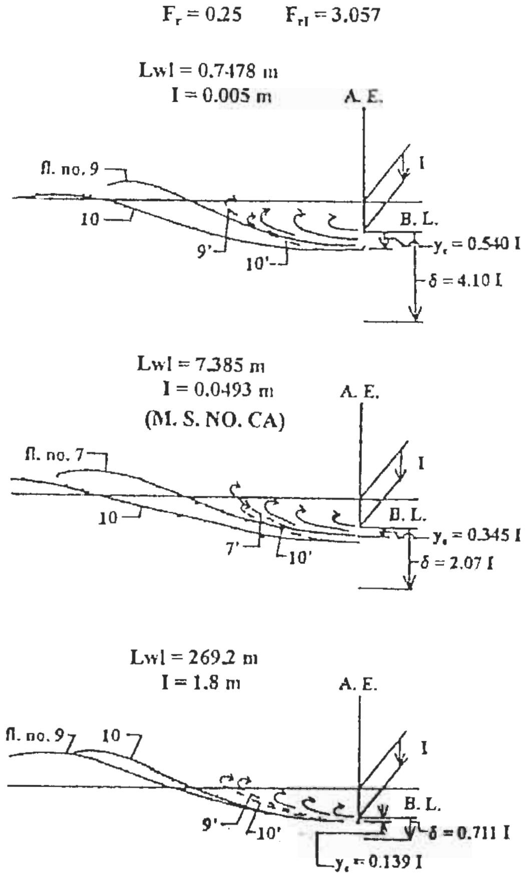
$F_r = 0.25$ $F_{rI} = 3.057$
Lwl = 0.7478 m
I = 0.005 m
A. E.
fl. no. 9
10
9'
10'
I
B. L.
$y_c = 0.540$ I
$\delta = 4.10$ I
Lwl = 7.385 m
I = 0.0493 m
(M. S. NO. CA)
A. E.
fl. no. 7
10
7'
10'
I
B. L.
$y_c = 0.345$ I
$\delta = 2.07$ I
Lwl = 269.2 m
I = 1.8 m
A. E.
fl. no. 9
10
9'
10'
I
B. L.
$\delta = 0.711$ I
$y_c = 0.139$ I

Figure 3: Scale effect of water flow just behind a transom stern on Full-2
(M.S.NO.CA and similar hulls)

We can see from Table 2 that resistance increases by more than 100 times, if the following waves change to the forward-oriented wave breaking. This result clearly indicates that the forward-oriented wave breaking causes large hull resistance, though the phenomenon occurs only in a limited thin water flow layer just below the water surface. We, therefore, can say that to prevent or to decrease the forward-oriented wave breaking is sure to be effective for energy saving for this type of ships.

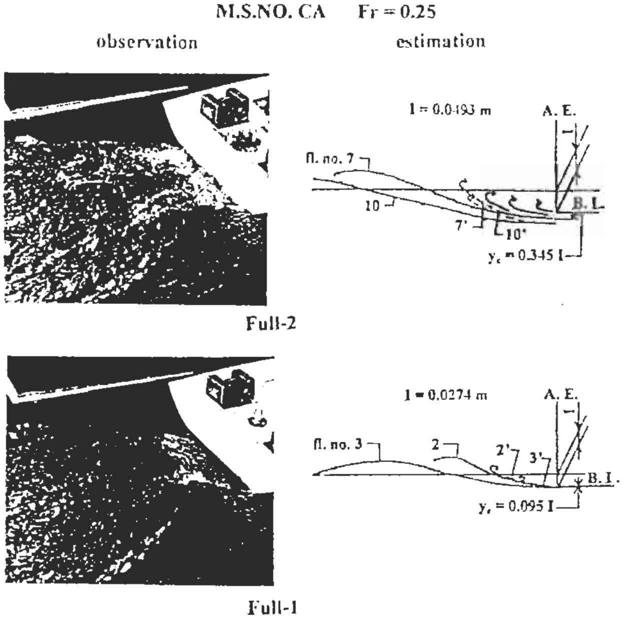
M.S.NO. CA Fr = 0.25
observation
estimation
l = 0.0493 m
A. E.
fl. no. 7
10
7'
10'
B. L.
y_c = 0.345 l
Full-2
l = 0.0274 m
A. E.
fl. no. 3
2
2'
3'
B. L.
y_c = 0.095 l
Full-1

Figure 4: Comparison of estimated water flow with observed water surface (M.S.NO.CA)

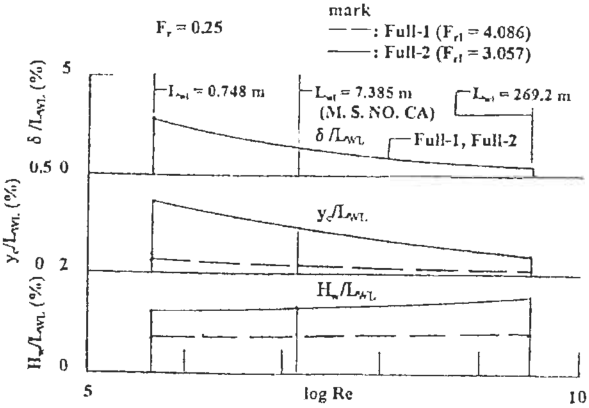

Figure 5: Scale effect of boundary layer thickness δ , thickness of flow layer which breaks y_c and remained following wave height H_w (M.S.NO.CA and similar hulls)

3.2 Scale Effect of Water Flow just behind a Transom Stern

Figure 3 shows scale effect of water flow just behind the transom stern of M.S.NO.CA at $F_r = 0.25$ on Full-2 estimated by our method[1,2]. Reliability of Figure 3 can be understood by Figure 4. Figure 4 compares estimated water flow with observed water surface on Full-1 and Full-2 for M.S.NO. CA. We can see from Figure 4 that the estimated water flow can explain fairly well the difference of forward-oriented wave breaking and that of remained following waves seen between the two observed water surfaces. Figure 5 summarizes change with Reynolds number $R_e = v_0 L_{WL} / \nu$ of δ / L_{WL}, y_c / L_{WL} and H_w / L_{WL} for each of the two conditions, where H_w is remained following wave height. δ / L_{WL} decreases with increase of model ship size. This causes decrease of y_c / L_{WL} and also increase of H_w / L_{WL}.

We can also see by comparing above estimated data on Full-1 with those on Full-2 that such tendency becomes more remarkable on condition with higher value of y_c / L_{WL}.

Regarding H_w / L_{WL}, above estimated tendency is seen in the wave heights measured on two similar model ships with L_{pp} of 2m and 10m by Miyata et al.[8].

3.3 Scale Effect of the Resistance due to Stern Waves Including Forward-oriented Wave Breaking just behind a Transom Stern

We have estimated forward-oriented wave breaking resistance R_{swbf} and remained following wave resistance R_{sfw} for each of three similar hulls in Figure 3 on Full-1 and Full-2 by the methods we have developed. Figure 6 summarizes the result. Non-dimensional coefficient of the former one $C_{swbf} = R_{swbf} / (1/2) \rho B_m l v_0^2$ decreases with increase of model ship size, and that of the latter one $C_{sfw} = R_{sfw} / (1/2) \rho B_m l v_0^2$ slightly increases to the contrary. Stern wave resistance coefficient $C_{sw} = C_{swbf} + C_{sfw}$ decreases with increase of model ship size. This tendency is more remarkable on Full-2 with higher value of y_c / l. Scale effect tendency of the stern wave resistance coefficient C_{sw} is almost same as that of the forward-oriented wave breaking resistance coefficient C_{swbf}. This is because the forward-oriented wave breaking resistance R_{swbf} is much larger compared with the following wave resistance R_{sfw} as shown in Table 2 and, therefore, occupies larger part of the stern wave resistance R_{sw}, even if the phenomenon occurs only slightly.

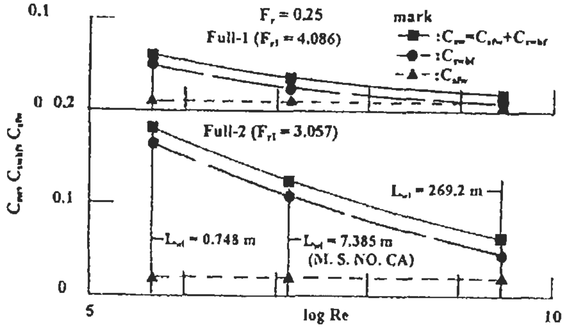

Figure 6: Scale effect of stern wave resistance and its components (M.S.NO.CA and similar hulls)

4 CONCLUSIONS

Results of this research can be summarized as follows:

(1) We have proposed a method to estimate resistance due to remained following waves, one of two main components of stern waves, and have demonstrated its usefulness.

(2) We have clarified the following characteristics of stern waves including forward-oriented wave breaking just behind a transom stern by the methods we have developed:

1) Amount of resistance increases by more than 100 times, if following waves from a part of flow layer near water surface change to forward-oriented wave breaking.

2) Forward-oriented wave breaking resistance coefficient decreases with increase of model ship size. On the other hand, remained following wave resistance coefficient increases only slightly with increase of model ship size.

3) Non-dimensional coefficient of resistance due to stern waves including the forward-oriented wave breaking just behind a transom stern is largely affected by the phenomenon because of its characteristics described in above 1) and, therefore, decreases with increase of model ship size.

Acknowledgments

We would like to thank Prof. H. Miyata, the University of Tokyo for his encouragement and discussions. Thanks are extended to Prof. T. Suzuki, Osaka University, Prof. T. Okuno, Osaka Prefectural University and Dr. Y. Iwasaki, Kawasaki Heavy Industries Ltd. who have cooperated with the authors in completing this research. Thanks are extended further to Dr. T. Atsuta and Mr. T. Isozaki, Akashi Technical Institute, Kawasaki Heavy Industries Ltd. who have supported the authors in many respects. The authors acknowledge that Grant-in-Aid for Scientific Research from the Ministry of Education, Science, Sports and Culture of Japan has partly supported this research.

References

1. Yamano T., Ikebuchi T. and Funeno I. (2000). On Forward-oriented Wave Breaking just behind a Transom Stern. *J Soc Nav Archit Jpn* **187,** 25-32
2. Yamano T., Hibino N. and Kuratani F. (2000). On Scale Effect of the Resistance due to Wave Breaking just behind a Transom Stern. *Proceedings of IMDC 2000*, 567-577
3. Yamano T., Iwasaki Y., Taguchi K. and Maeda N. (1994). Development of a New Stern Form for Ocean Going Fine Ships. *J Kansai Soc Nav Archit Jpn* **221,** 25- 33
4. Okamoto H., Tanaka A., Yamano T., Inui T. and Miyata H. (1982). Resistance Reduction by Stern-End-Bulb (Third Report). *J Soc Nav Archit Jpn* **152,** 22-31
5. Yamano T., Iwasaki Y., Taguchi K. and Maeda N. (1994). Some Methods to Reduce Stern Waves. *Proceedings of IMDC'94*, 609-623.
6. Iwasaki Y., Tahara,Y., Okuno T., Himeno Y. and Yamano T. (1996). Studies on Relationship between Water Surface behind Stern and Stern End Form of Fine Ships. *J Soc Nav Archit Jpn* **180,** 13-20
7. Lap A. J. W. (1955), *Fundamentals of Ship Resistance and Propulsion*, NSMB Publication, Wageningen, The Netherlands
8. Miyata H., Tsuchiya Y. and Inui T. (1981). Resistance Reduction by Stern-End-Bulb (Second Report). *J Soc Nav Archit Jpn* **152,** 1-10

Practical Design of Ships and Other Floating Structures
You-Sheng Wu, Wei-Cheng Cui and Guo-Jun Zhou (Eds)
© 2001 Elsevier Science Ltd. All rights reserved

NUMERICAL AND EXPERIMENTAL EVALUATION OF THE HULL CHARACTERISTICS OF TWO-SEMI-DISPLACEMENT FAST MONOHULLS

C. M. P. Sampaio[1], K. Nishimoto[1], C. H. Miyagi[1], K. Hirata[2] and I. Miwa[2]

[1] Dept. Naval Architecture and Ocean Engineering – Escola Politécnica – University of São Paulo,
Cidade Universitária, São Paulo, 05508-900 Brasil
[2] Hydrodynamic Division of Technological Research Institute of São Paulo - IPT/SP;
Cidade Universitária, São Paulo, 05508-901, Brazil

ABSTRACT

For this study, two semi-displacement monohull types had been considered; a round bilge type and a hard chine hull, this as suggested by the 1986 ITTC Committee. For the experimental evaluation two models were constructed in FRP. To compare the results both hull forms have been developed in CAD and discretized and the resistance components evaluated with the software SHIPFLOW. The numerical procedure gives an estimation of the sinkage, trim and wave resistance component whose values were compared with the experimental ones. The friction resistance component has been estimated through the use of the 1978 ITTC line and the form factor based on suggested values. The agreement of wave component is reasonable around medium Froude numbers but the difference increases with speed. In spite of this deficiency the software has permitted a systematic study of the effects of the variation of the stern wedge angle whose optimum value agrees with the original angle. It has been verified that for different displacement different wedge angle should be adopted. Besides this analysis it was verified that the positioning of the bilge keels were in agreement with the computed streamlines.

KEYWORDS

Semi-displacement hull, Numerical optimization, Stern wedges, Experimental evaluation, Calm water resistance, ITTC high-speed model

1 INTRODUCTION

The present work has its origin on the increased importance of high-speed transportation worldwide and the necessity to start some research in this field. The opportunity appeared as a result of new resources for upgrading the experimental installations of IPT/SP and the possibility to carry on some experimental and numerical analysis with two semi-displacement hulls.

The numerical calculation is based on the software SHIPFLOW (FLOWTECH) which is a well-known software. The software employs the zonal approach that is the fluid domain around the hull is divided in three characteristic procedures: the potential flow, the boundary layer and the true viscous flow analysis. In spite of some restrictions on absolute values, the common CFD techniques offer great possibilities as optimization tools for preliminary design.

Therefore, the first objective of this research was to compare the experimental and numerical techniques, to get acquainted with modern numerical tools for hull design and to verify the optimization capabilities with some particular problems, for example, the choice of the stern wedge and the positioning of appendages

2 THEORETICAL BACKGROUND

The traditional procedure to estimate the ship's resistance in calm water is based of the Froude's hypothesis which is given by:

$$C_T(Fn,\mathrm{Re}) = C_R(Fn) + C_F(\mathrm{Re}) \tag{1}$$

However, the present recommended procedure (ITTC-1978) is based on the separation of the resistance components into a viscous term and wave term as shown below.

$$C_T = C_W(Fn) + C_V(\mathrm{Re}) \tag{2}$$

The viscous resistance component depends on Reynolds number and is, itself, divided by the friction line term and a form factor term, k, that takes into account the actual body shape.

$$C_V(Rn) = (1+k)(Fn)\cdot C_F(\mathrm{Re}) \tag{3}$$

The wave resistance coefficient, C_W can be divided in the wave pattern component C_{WP} and, for high-speed vessels, an additional component related to the generation of spray.

3 HULL CHARACTERISTICS

Two high-speed semi-displacement hulls were analyzed the first, a round bilge type and the second, a hard chine type. The main geometric characteristics are given on Table 1 and the body plans are shown in Figure 1. The scale models were built in FRP and tested on the 280,0 m towing tank of the Technological Research Institute – IPT/SP.

The round bilge vessel has a design displacement of $\Delta \cong 215$ ton, but its final operational displacement is greater. It was designed with a stern wedge with an angle of 6.9°, spray rails and bilge keels. The model was built on the scale $\lambda = 1/18{,}5$ and a strip of pins for turbulence stimulation (NPL standard) attached. The second vessel, the hard chine model recommended by 19th HSMV Committee of ITTC, is described by Tanaka (1990) and was built without any turbulence stimulation. The model scale adopted was $\lambda = 1/11{,}6$ and, in spite of the proposed test conditions include appendages, these were not included but will be installed in future experiments.

4 EXPERIMENTAL AND NUMERIC CONDITIONS

The towing tests for the round-bilge models were carried on for a speed range of $0{,}25 < Fn < 0{,}65$

while the ITTC hard-chine model the range was 0,05 < Fn < 0,70 because of the limitation on the carriage speed. Since then a new motor and control system was implemented and the high limit should be increased to Fn = 1,0.

TABLE 1
SHIP'S AND MODEL'S GENERAL DIMENSIONS

Model		ITTC	RB
L_{BP}	[m]	2,00	2,297
B_M	[m]	0,488	0,405
d_F	[m]	0,0774	0,100
d_M	[m]	0,0749	0,100
d_A	[m]	0,0724	0,100
∇	[m^3]	0,02897	0,0308
S	[m^2]	0,8043	0,772

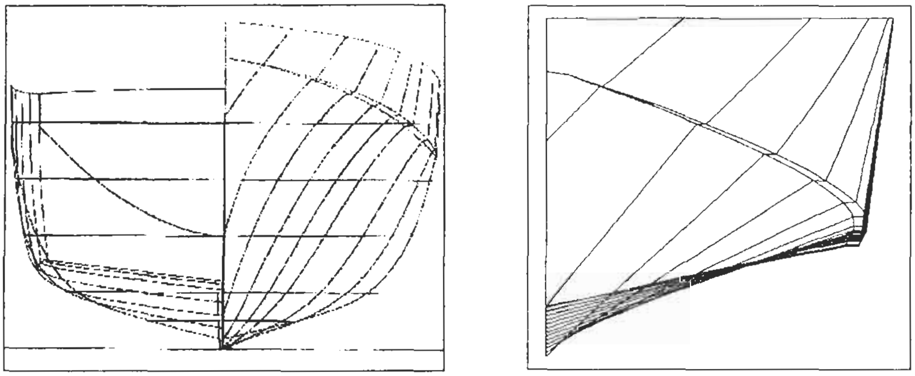

Figure 1: Hull Body Plans

The numerical simulation was carried on by the software SHIPFLOW (FLOWTECH) in its potential and boundary layer modes. The round-bilge vessel was panelized by the automatic panel generation as suggested by the program (451 on the hull and 1370 on the free surface) while, for the ITTC model, a greater number of panels were required because of the sharp change of the body plan. The number of panels on the hull is 1100 (Figure 2) and, at the free surface, 1836. The calculation was performed for a speed range of 0,35 < Fn < 0,65 as, for lower speeds, the detachment condition on the transom stern is invalid and, for higher speeds, the limitation on the experimental towing tests. All the runs were done with a dynamic condition for sinkage and trim but, for the wave calculation, only the linear option was adopted.

5 EXPERIMENTAL AND NUMERICAL RESULTS

The first part of this item is related to the analysis of the round-bilge vessel. Its experimental and numerical values are compared and the optimization of the stern wedge, for different displacement conditions, carried on. This work also studied the capability of the software for preliminary positioning of the bilge keels. In the second part, the experimental and numerical results for the ITTC hard-chine model were analyzed and the possible advantages of stern wedges considered.

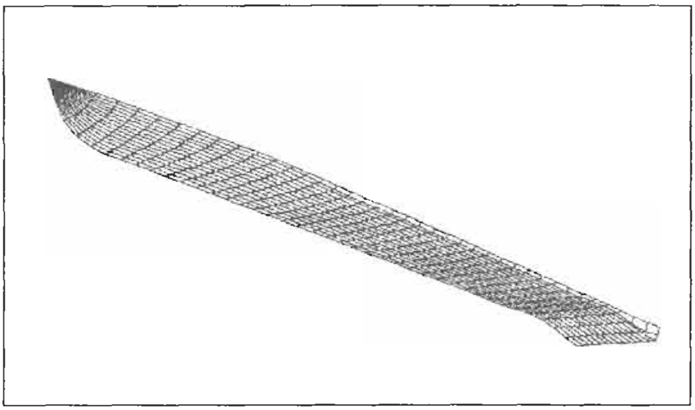

Figure 2: ITTC Model Panelization

5.1 Round-Bilge Hull Results

The results of the round-bilge hull are shown in Figure 3. The residual resistance coefficient (with/without spray rails) from the towing tank tests are compared with the numerical wave resistance coefficient. It is interesting to note that both curves profile is very similar. The numerical values were increased by a constant form factor (1 + k) = 1,3 as suggested by Couser (1997). As explained in Sahoo (1999) the only way to estimate the total resistance is by the adoption of a wave-resistance correction factor, which was defined as:

$$K(Fn) = \frac{C_{\mathrm{Re}xp} - (C_{Wnum} + kC_{FITTC})}{C_{Wnum}} \tag{4}$$

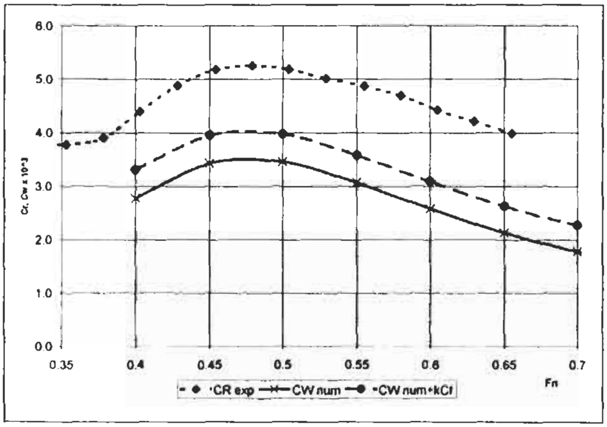

Figure 3: Comparison of C_R, C_W, C_{WK} (form factor) vs. F_n

The introduction of stern wedges is usually advantageous for high-speed vessels but its choice depends on specific conditions of the vessel. As already written, the vessel was designed for a displacement of 215 ton but the actual one has around 250 ton. The original stern wedge has a constant length ratio of L_W/L_{BP} = 3,4 % and, approximately, a wedge angle of $\alpha = 6,9^{\circ}$. The systematic variation of the wedge

angle was carried on for both displacements and is shown in Figure 4. For the lower displacement the optimum wedge angle agreed with the designed hull while, for the higher one, the wedge angle should be increased to α = 10,9°.
To verify the potentialities of the software for preliminary studies the flow lines were calculated and the positioning of the bilge keel checked. The results of this work is shown in Figure 5 were the numerical results are compared with two previous options, one suggested by a Brazilian shipyard and the second, obtained by flow analysis on towing tank. It is clear that the agreement between the numerical result and towing tank are consistent.

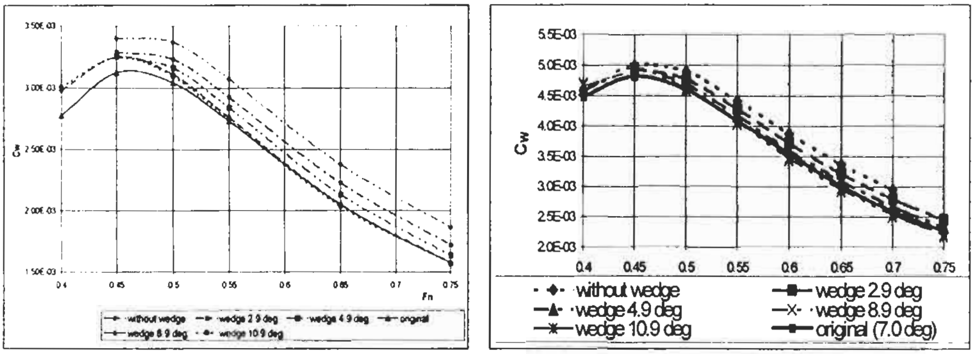

Figure 4: C_W vs. F_n for different stern wedge angles (α)

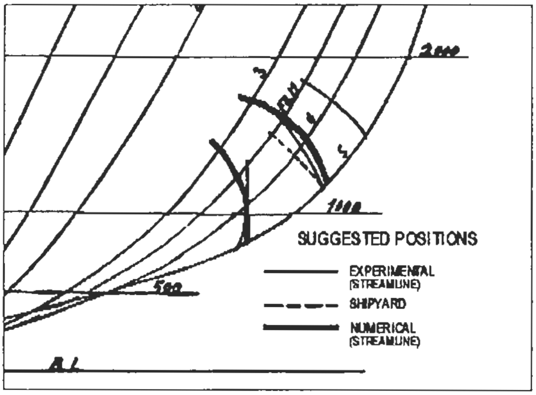

Figure 5: Positioning of Bilge Keels

5.2 ITTC Model Results

The total resistance coefficient, C_T , the sinkage and trim obtained in the towing tank are compared with the values collected by Tanaka (1990) in Figure 6. The sinkage and trim agree reasonable well but the total resistance coefficient are lower as the appendages were not included.

The numerical wave resistance coefficient is compared with the wave pattern term in Figure 7 and plotted in Figure 8 for comparison with the residual resistance coefficient, C_R, calculated by the original Froude hypothesis. A second line was included in which the C_W value was increased of the form factor (1+k) = 1,4 as suggested by Tanaka (1990). As expected for this speed range the spray component has a significant contribution on the total resistance.

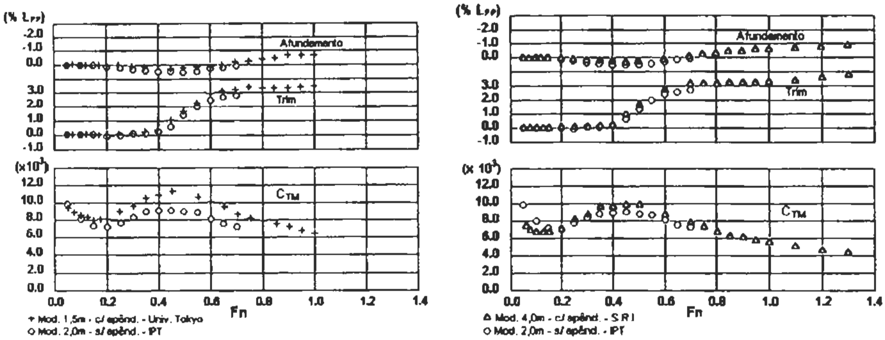

Figure 6: Comparison of C_T, sinkage and trim among the 2 m IPT/ST Model, 1,5 m U.Tokyo (left) and 4 m SRI Model (right)

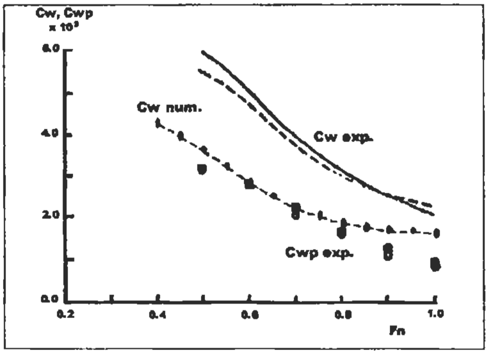

Figure 7: Comparison wave pattern C_{WP}

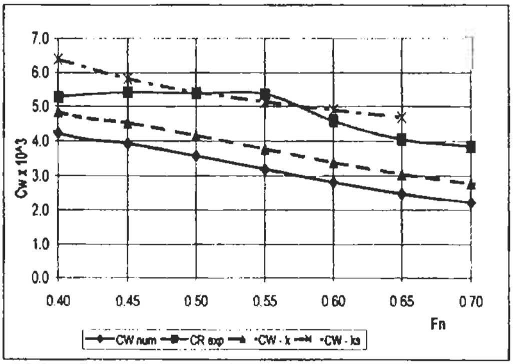

Figure 8: Comparison of C_R, C_W, C_{WK} (form factor) and $C_{WK\text{-}S}$, (form factor + spray factor) vs. F_n

Finally, to analyze the effects of stern wedges, wedges were included in the numerical model. These have a constant length ratio, L_W/L_{BP} = 7 % and the angles were varied systematically. The results are presented in Figure 9 where it can be clearly observed that the benefits of the stern wedges depend on wedge's angle and are restricted for a specific speed range.

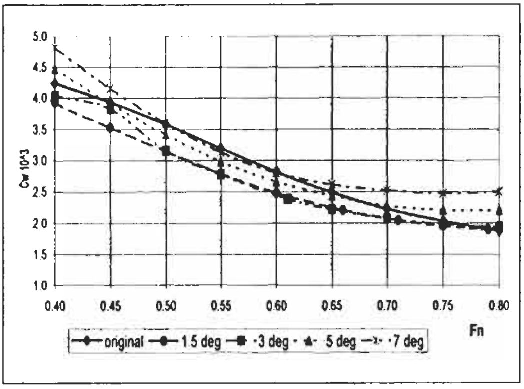

Figure 9: C_W vs. F_n for different stern wedge angles (α)

6 CONCLUSIONS

One important conclusion is that the numerical procedure is extremely powerful for the preliminary choice of the hull form. The possibility to choose the optimum stern wedge angle and the position of the bilge keel are useful design tools. For the absolute estimation of the ship's resistance it is necessary to make use of experimental results however, the use of the correction factor, of the same magnitude for both vessels, permits a first estimation. The experimental procedure compare favorable with previous results and it is hoped that future test will include a broader speed range.

Acknowledgements

The authors would like to thank Mr. A. A. B. Lleyda for the help in the computations, Mr. L. F. P. de Castro of the Navy Engineering Department for the interest on the research. We are also grateful for the support given by the Research Foundation of São Paulo for the construction of the models. Finally, the numerical computations were based on the results given by the software SHIPFLOW of FLOWTECH, without it the comparison with the experimental results would not be possible.

References

Couser, P. R., Molland, A. F., Armstrong, N. A. and Utama, I. K. A. (1997). Calm Water Powering Predictions for High Speed Catamarans, *Proceedings of the Fourth International Conference on Fast Sea Transportation -FAST'97,* Baird Publications, 765 –772.

Karafiath, G. and Fisher, S. C. (1987). The Effect of Stern Wedges on Ship Powering Performance, *Naval Engineers Journal*, 27–37.

Tanaka, H. ; Nakatake, K. ; Araki, S. ; Nakato, M. and Ueda, T. (1990). Cooperative Resistance Tests with Geosim Models of a High-Speed Semi-Displacement Craft. *Journal of the Society of Naval Architects of Japan* **Vol. 169**, 55–64.

Sahoo, P. K. ,Doctors, L. J. and Renilson, M. R. (1999). Theoretical and Experimental Investigation of Resistance of High-Speed Round-Bilge Hull Forms., *Proceedings of the Fifth International Conference on Fast Sea Transportation -FAST'99*, 803-814.

Practical Design of Ships and Other Floating Structures
You-Sheng Wu, Wei-Cheng Cui and Guo-Jun Zhou (Eds)
© 2001 Elsevier Science Ltd. All rights reserved

EMPIRICAL PREDICTION OF SHIP RESISTANCE AND WETTED SURFACE AREA USING ARTIFICIAL NEURAL NETWORKS

Kourosh Koushan

Norwegian Marine Technology Research Institute (MARINTEK)
P.O.Box 4125 Valentinlyst, 7045 Trondheim, Norway

ABSTRACT

New empirical methods are presented for prediction of ship resistance and wetted surface area of ships based on analysis of database of tests performed in the towing tank of MARINTEK. Artificial neural networks method is applied for analysis of the database. The methods are verified using several towing test results available. These methods show generally reliable simulation of residual resistance and wetted surface area of the ships.

KEYWORDS

Ship resistance, Residual resistance, Wetted surface, Empirical method, Artificial neural networks, Database, Simulation

1 INTRODUCTION

There has been a significant development in the field of numerical calculation of ship resistance in the recent decade. These have led to useful tools for detail analysis of ships. Inevitably require all these tools a complete physical description of vessel. However at an early design stage require naval architects often a tool for reliable prediction of ship resistance based on few main parameters, usually Froude number and some geometric coefficients. Again there have been remarkable efforts to cope with this situation and several empirical methods are developed and optimised over the years applying regression analysis, e.g. Holtrop (1984) and Hollenbach (1998).

Experience has shown that all these methods can predict some cases very well whereas in some other cases predictions might not be as reliable. The method presented in this paper applies artificial neural networks (ANN) for the analysis of the extensive database of towing test results performed at MARINTEK in recent two decades to predict residual resistance coefficient. ANN method allows for non-linear effects and interdependence of input parameters. The database is divided into several ship categories and a network is designed for each category, allowing a more accurate prediction for each category. For the first time a reliable empirical method is developed for prediction of resistance of offshore vessels and car ferries. Objective of the method is to keep the number of input parameters as low as possible however at the same time deliver a reliable prediction, which can help the designer at an early design stage.

Every resistance prediction method requires also a reliable prediction of wetted surface area of the vessel, to be able to predict not only the resistance coefficient but also the resistance force. Presented method includes prediction of wetted surface area based on main geometric parameters using ANN method. Again different networks are designed for each ship category.

ANN method offers the unique capability of easy adaptation to new data, which makes the developed methods quasi-dynamic models. That means with the access to new measurement data, developed networks can be upgraded with minimum amount of efforts. Networks are translated to DLLs that can be implemented easily to existing software.

2 SHIP RESISTANCE FROM MODEL TESTS

MARINTEK's standard definition of residual resistance coefficient is used. It is assumed that the total resistance coefficient C_T is divided mainly into the viscous resistance and the residual resistance coefficient C_R, where the latter is due to vorticity, wave making and wave breaking. The following equation is applied for resistance coefficients:

$$C = \frac{R}{\rho/2 \cdot S \cdot V^2}$$

Where R is the resistance, ρ is the density of water, S is the wetted surface area and V is the ship velocity. The residual resistance coefficient is defined as:

$$C_R = C_{Tm} - C_{Fm} \cdot (1 + k_o) - C_{AA} - C_{BD}$$

The base drag coefficient C_{BD} is calculated applying the wetted area of the transom stern S_B.

$$C_{BD} = \frac{0.029 \cdot (S_B / S)^{3/2}}{(C_F)^{1/2}}$$

The air resistance coefficient C_{AA} is calculated using transverse projected area above the waterline A_T.

$$C_{AA} = 0.001 \cdot \frac{A_T}{S}$$

The frictional resistance coefficient C_F is based on the ITTC-57 correlation line, which is a function of Reynolds number Rn.

$$C_F = \frac{0.075}{(\log Rn - 2)^2}$$

The form factor k_o is calculated as:

$$k_o = 0.6 \cdot \frac{C_B}{L_{WL}} \sqrt{T_{AP} + T_{FP}} \cdot B + 145 \cdot \left(\frac{C_B}{L_{WL}} \sqrt{T_{AP} + T_{FP}} \cdot B \right)^{3.5}$$

The total ship resistance coefficient is defined as:

$$C_{Ts} = C_{Rm} + (C_{Fs} + \Delta C_F) \cdot (1 + k_o) + C_A + C_{AAs} + C_{BDs}$$

Residual resistance coefficient C_R can be predicted by the artificial neural networks presented in this paper. The result is correlated against full-scale trials applying a resistance correlation coefficient C_A, which usually varies for different towing tanks. MARINTEK usually applies resistance correlation coefficient values between $-0.20 \cdot 10^{-3}$ and $-0.23 \cdot 10^{-3}$ for conventional ships.

The roughness allowance ΔC_F is calculated using hull surface roughness H in μ (= 10^{-6} m). Typical value of hull surface roughness is 150 μ. Only positive values of ΔC_F are used.

$$\Delta C_F = \left[110.31 \cdot (H \cdot V_s)^{0.21} - 403.33\right] \cdot C_{FS}^2$$

3 DATABASE

Analyses are based on measurements performed in the towing tank at MARINTEK in recent two decades. Special cases did not take part in analysis. The database includes 487 ships and 3481 measurement points. Analyses of the database are performed using Artificial Neural Networks Method. A preliminary analysis of the database shows that higher accuracy can be achieved by using different neural networks for different categories of ships.

Therefore one ship type or several similar ship types are grouped in one category. This allows using different input parameters according to sensitivity analysis performed for each group. In addition pre-weighting of input parameters can be tuned applying sensitivity analysis results. The pre-study led to five categories. Categories, number of ships in each category and number of measurement points in each category are presented in **TABLE 1**. If a ship type is not represented in the selected categories, closest category may be selected for the prediction.

TABLE 1

SHIP CATEGORIES AND CORRESPONDING NUMBER OF SHIPS AND MEASUREMENTS IN EACH CATEGORY

Category	Car ferries	Passenger & cargo	Tanker & bulk	Offshore	Fishery
No. of ships	26	163	158	64	76
No. of measurements	228	1142	935	525	651

TABLE 2

SELECTED INPUT PARAMETERS AND THEIR VALIDITY RANGE FOR EACH CATEGORY

(Residual resistance prediction)

	Z	$10^*B_{WL}/L_{WL}$	$100^*T/L_{WL}$	$100^*LCB/L_{WL}$	10^*C_{BWL}	10^*FN	10^*C_M
Car ferries	1 – 2	1.25 – 2.20	3.05 – 5.75	-	3.00 – 6.30	1.6 – 3.50	6.30 – 9.85
Passenger & cargo	1 – 2	1.15 – 3.41	2.65 – 8.22	-5.00 – 3.22	4.15 – 8.10	1.1 – 3.70	5.80 – 10.00
Tanker and bulk	-	1.30 – 2.20	3.7 – 7.30	-1.20 – 4.50	6.35 – 8.60	1.1 – 2.62	-
Offshore	1 – 2	1.96 – 2.80	5.95 – 9.70	-3.90 – 1.02	4.71 – 7.15	1.8 – 3.50	8.15 – 100
Fishery	-	1.79 – 3.50	6.00 – 19.0	-4.10 – 3.42	3.77 – 6.90	1.75 – 4.0	6.60 – 9.55

The input parameters chosen for each category and their validity range are presented in **TABLE 2** for residual resistance prediction and in **TABLE 3** for prediction of wetted surface area. Z is the number of propellers, B is the breadth, L_{WL} is the length of waterline, LCB is the longitudinal centre of buoyancy relative to $L_{pp}/2$ (half of length between perpendiculars, positive forward), C_B is the block coefficient, FN is the Froude number, C_M is the mid-ship coefficient and T is the mean draught.

In case of prediction of wetted surface area, a category is defined containing all available data, this category is called "All". Though the validity range of this category is broader, however the prediction results may be not as accurate.

TABLE 3
SELECTED INPUT PARAMETERS AND THEIR VALIDITY RANGE FOR EACH CATEGORY
(Wetted surface area prediction)

	C_M	C_{BWL}	B_{WL}/T	T/L_{WL}
Car ferries	-	0.299 – 0.641	3.290 – 4.956	-
Passenger & cargo	0.571 – 1.000	0.415 – 0.812	2.460 – 7.700	0.0261 – 0.0824
Tanker and bulk	-	0.616 – 0.864	2.179 – 5.037	0.0368 – 0.0764
Offshore vessels	-	0.468 – 0.719	2.301 – 3.789	0.0584 – 0.0981
Fishery	-	0.374 – 0.695	1.833 – 3.066	0.0597 – 0.1908
All	0.571 – 1.000	0.299 – 0.864	1.833 – 7.700	0.0261 – 0.1908

The networks are verified within valid range of input parameters in the database.

4 VERIFICATION

There are different statistical coefficients, which can define the quality of a prediction. Average mean squared error *AMSE*, average absolute error *AAE*, standard deviation of error *St.Dev.* and Pearson correlation coefficient *r* are used here. Pearson correlation coefficient *r* reflects the extent of a linear relationship between two data sets X (measurement) and Y (prediction).

$$AMSE = \frac{\sum (X-Y)^2}{\sum X} \cdot 100$$

$$AAE = \frac{\sum ABS(X-Y)}{\sum X} \cdot 100$$

$$St.Dev. = \frac{\sqrt{\frac{1}{n}\sum\left[(X-Y)-\frac{1}{n}\sum(X-Y)\right]^2}}{\frac{1}{n}\sum X} \cdot 100$$

$$r = \frac{n\sum(X \cdot Y)-\sum X \cdot \sum Y}{\sqrt{\left[n\sum X^2-\left(\sum X\right)^2\right]\left[n\sum Y^2-\left(\sum Y\right)^2\right]}} \cdot 100$$

TABLE 4 presents results of verification of predicted residual resistance coefficient related to measured residual resistance coefficient, TABLE 5 presents corresponding values for total resistance coefficient and TABLE 6 for wetted surface area.

TABLE 4

CORRELATION FACTOR, STANDARD DEVIATION IF ERROR, AVERAGE MEAN SQUARED ERROR AND AVERAGE ABSOLUTE ERROR RELATED TO PREDICTION AND MEASUREMENT RESULTS OF RESIDUAL RESISTANCE COEFFICIENT

	Total database				Verification set			
	r	St.Dev.	AMSE	AAE	r	St.Dev.	AMSE	AAE
Car ferries	96%	14%	3%	11%	96%	15%	4%	12%
Passenger & cargo	98%	13%	2%	8%	97%	14%	2%	9%
Tanker and bulk	99%	13%	1%	8%	98%	15%	1%	10%
Offshore vessels	98%	10%	5%	8%	97%	12%	6%	9%
Fishery	97%	13%	7%	10%	96%	15%	9%	12%

The number of input parameters is kept low to obtain an easy to use method. This has the consequence that design details and appendages like bulbous bow are not used as input. Experience has shown that appendages may result up to 10% difference in total resistance. In general an average accuracy of approximately 96% can be expected from total resistance coefficient prediction. As expected the accuracy is higher in case of tankers and bulk carriers, due to more homogenous ship geometries in this category. On the contrary fishery vessels have less homogenous forms leading to a lower accuracy for this category.

TABLE 5

CORRELATION FACTOR, STANDARD DEVIATION OF ERROR, AVERAGE MEAN SQUARED ERROR AND AVERAGE ABSOLUTE ERROR RELATED TO PREDICTION AND MEASUREMENT RESULTS OF TOTAL RESISTANCE COEFFICIENT

	Total database				Verification set			
	r	St.Dev.	AMSE	AAE	r	St.Dev.	AMSE	AAE
Car ferries	96%	5%	1%	4%	96%	5%	1%	4%
Passenger & cargo	97%	3%	0%	2%	97%	3%	1%	2%
Tanker and bulk	98%	2%	0%	1%	97%	2%	0%	2%
Offshore vessels	98%	5%	2%	4%	97%	6%	3%	5%
Fishery	97%	6%	3%	5%	96%	7%	4%	6%

TABLE 6

CORRELATION FACTOR, STANDARD DEVIATION OF ERRORS, AVERAGE MEAN SQUARED ERROR AND AVERAGE ABSOLUTE ERROR RELATED TO PREDICTION AND MEASUREMENT RESULTS OF WETTED SURFACE AREA

	Total database				Verification set			
	r	St.Dev.	AMSE	AAE	r	St.Dev.	AMSE	AAE
Car ferries	87%	3%	0%	2%	90%	3%	0%	3%
Passenger & cargo	84%	3%	0%	2%	78%	4%	0%	3%
Tanker and bulk	77%	2%	0%	2%	93%	1%	0%	1%
Offshore vessels	69%	4%	0%	3%	55%	4%	0%	3%
Fishery	70%	4%	0%	3%	58%	4%	0%	3%
All	70%	4%	0%	3%	67%	4%	0%	3%

5 INTRODUCTION OF ARTIFICIAL NEURAL NETWORKS

There is no universally accepted definition of an artificial neural networks method (ANN). But perhaps most people in the field would agree that an ANN is a network of many simple processors (processing elements), each probably having a small amount of local memory. The processors are linked by communication channels (synapses), which usually carry numeric data, encoded by any of various means. The units run only on their local data and on the inputs they receive via the communication channels.

Most artificial neural networks have some sort of "training" rule whereby the weights of synapses are adjusted on the basis of data. In other words, artificial neural networks "learn" from examples (as children learn to recognise cats from examples of cats) and show some capability for generalisation beyond the training data. Simple linear regression (a minimal feedforward net with only two processing elements plus bias) is usefully regarded as special cases of artificial neural networks. Artificial neural networks are used in many different fields in recent years. A few engineering application examples:

- Rudder force prediction (Koushan et al 1998)
- Propeller induced pressure pulses (Koushan 2000)
- Robot control
- Pattern recognition

Figure 1 demonstrates main components of a feed-forward recall artificial neural network. These are input layer, synapses, one or more hidden layers (axons) and an output layer.

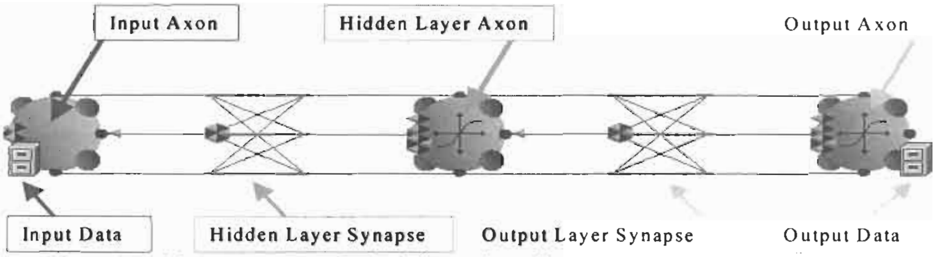

Figure 1: Main components of a feed forward recall network with a single hidden layer

Input layer is used to feed the network with data. This layer normalises usually data between 0 and 1 or between -1 to 1 depending on activation function used. Synapse is connecting different layers. Hidden layer is made of one or more processing elements and corresponding activation function, which transforms the input of processing element. Typical activation functions are linear, sigmoid and tanh functions. Output layer operates usually like a hidden layer and can in addition denormalise the output.

There are different procedures for training the network. Typical procedure is back propagation. In a backpropagation procedure, network starts with a random set of weights. Then output is compared to input and the error is verified. Then these errors are propagated backwards through the network to find better weights. Again there are different ways of reaching optimal weights by means of errors. Apart from weights and activation functions, number of hidden layers and number of processing elements in each hidden layer must also be optimised during the training. Usually one half part of database is used for training whereas the other half is used for verification of the network, i.e. the network does not “see” verification set during optimisation process.

6 CONCLUSIONS

The method presented is a novel procedure for prediction of total resistance. A reliable prediction method is presented for the first time for prediction of total resistance of offshore vessels. To keep the method easy-to-use the number of input parameters are limited. This has the consequence of ignoring design details like bulbous bow and appendages. These details may result up to 10% difference in the total resistance. Adding more input parameters will increase the accuracy for special cases, however without access to sufficient additional exemplars this may reduce generalisation of the method. The method can be further developed with the access to new measurement data.

References

Hollenbach, K. U. (1998). Estimating Resistance and Propulsion for Single-Screw and Twin-Screw Ships. *Ship Technology Research*. **45**, 72-76.

Holtrop, J. (1984). A Statistical Re-analysis of Resistance and Propulsion Data *Shipbuilding Progress*. **31:363**. 272-276.

Koushan; K.; Mesbahi, E. (1998). Empirical Prediction Methods for Rudder Forces of a Novel Integrated Propeller-Rudder System. *Proceedings of OCEANS '98*. 532-537. Nice. France

Koushan, K. (2000). Prediction of Propeller Induced Pressure Pulses Using Artificial Neural Networks. *1st International Conference on Computer Applications and Information Technology in the Maritime Industries*. 248-254. Potsdam. Germany

Practical Design of Ships and Other Floating Structures
You-Sheng Wu, Wei-Cheng Cui and Guo-Jun Zhou (Eds)
© 2001 Elsevier Science Ltd. All rights reserved

A NEW METHOD FOR RESISTANCE AND PROPULSION PREDICTION OF SHIP PERFORMANCE IN SHALLOW WATER

T. Jiang

European Development Centre for Inland and Coastal Navigation
D-47057 Duisburg, Germany

ABSTRACT

To improve the resistance and propulsion prediction of ships in shallow water, model tests were performed with an inland ship-model and a container ship-model at different water-depths in the Shallow Water Towing Tank Duisburg (VBD). After an introduction of an effective ship speed, defined by the mean sinkage which combines the blockage effect near the ship and the effective depth-effect under the ship, a new method is proposed for resistance and propulsion prediction of the ship performance in shallow water. For the subject two ships in the subcritical speed range and in a not too extremely shallow water, it has been found that the total resistance could be considered as a unit function of the effective speed and independent of the water depth. Furthermore, at a ship self-propulsion point corresponding to the effective speed, it has been shown that the delivered power at propeller could be considered as a unit function of the blockage speed. Since the mean sinkage can be accurately calculated by means of the potential theory, for instance using an extended shallow-water approximation, this new method could impact the resistance and propulsion prediction of the ship performance in shallow water.

KEYWORDS

Resistance and propulsion prediction, Ship performance, Shallow water, Effective speed.

1 INTRODUCTION

For designing new ships, resistance and propulsion predictions are a central task not only for a towing tank but also at a design company. For ships sailing in shallow water, the corresponding predictions at different water depths are an additional part of the contract. Depending on the individual requirements two methods are commonly in use. For a ship which mainly operates in deep water, e.g. a seagoing ship, empirical formulae and diagrams are often applied to predict the increased resistance and the additional power demand. For a ship which mainly operates in shallow water at different depths, e.g. an inland ship, the more expensive, additional model tests can be performed at the water-depths interested.

In the empirical approximation of the above problem, the basic consideration is to correct or to include the boundary effects caused by the water bottom and channel walls. Physically, this is equivalent to the different blockage correction caused by ships moving in a towing tank and in an operating area considered. A large number of theoretical and experimental investigations has been devoted to this problem. As documented by Gross and Watanabe (1972), there are two methods for correcting these boundary effects. One is to correct the resistance and the other to correct the speed. These two methods are combined in the so-called Schlichting's hypothesis (1934). According to his hypothesis the wave resistance is the same at the same wave length corresponding to different speeds in deep and shallow water and the viscous resistance is the same at the same speed relative to the water at different water-depths. The speed change due to the blockage effect can be empirically estimated either by using the simple control parameter defined by Schlichting (1934) without correcting the wall effects or by using a control parameter based on the hydraulic radius given by Landweber (1939), which is also applicable for a real shape of the channel section. The speed change at each parameter value can be either read in the corresponding diagrams or calculated from the empirical formulae, e.g. Lackenby (1963). For narrow channels, like many small towing tanks, the mean flow theory based on the one-dimensional continuity and Bernoulli's equation has been widely used. These tow equations lead to a mean flow over the whole channel section. The mean flow change near the ship's surface can then be obtained by means of an empirical factor, e.g. Emerson (1959) using a constant value independent of the speed and Kim (1963) using a factor depending on speed and block coefficient.

The present study focuses on a physically reasonable and practically applicable method for resistance and propulsion prediction of ships in shallow water at a subcritical speed. After analyzing the resistance characteristics at different water-depths, a new method is proposed for predicting the total resistance which can be considered as a unit function of the effective speed defined by the mean sinkage. Accordingly, the propulsion tests will be conducted at a ship self-propulsion point corresponding to the effective speed. It can be shown that the delivered power at propeller seams to be a unit function of the blockage speed. In comparison to the earlier empirical approximation, the new method includes one additional information, namely the mean sinkage, which is an individual quantity depending both on the ship geometry and speed as well as on the geometry configuration of the operating area. Since the mean sinkage can be accurately calculated by means of the potential theory, for instance using an extended shallow-water approximation, this new method could impact the resistance and propulsion prediction of the ship performance in shallow water.

2 RESISTANCE PERFORMANCE

The experiments reported here were conducted in the main towing tank (200 m x 9.81 m x 1.2 m) of the Duisburg Shallow Water Towing Tank (VBD). Its water depth can be adjusted to any value between 0-1.2 meter. Two ships were chosen for model tests. One is an inland-ship with a ducted propeller and its model of scale 14 has a length at the load waterline 7.857 m, a beam 0.818 m, a draft 0.214 m and a wetted surface 9.059 m^2, see the body plan in Fig. 1. More details could be found in the work of Lochte-Holtgreven et al.(2001). The other is a typical containership model with a conventional single screw. It has a length-beam ratio 6.08 and a beam-draft ratio 2.9. The model has a draft 0.255 m and a wetted surface 4.0 m^2.

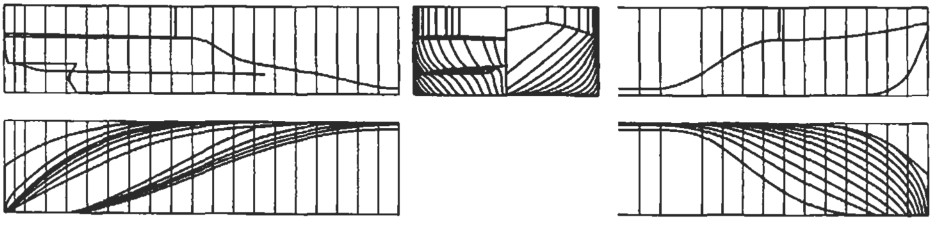

Figure 1: Body plan of the subject inland ship

For the inland ship the water depth was adjusted to ratios of the water depth to the draft h/T=1.5, 2.0, and 3.0 and for the subject container ship to h/T=2.0, 2.6, and 4.0 . The resistance tests were conducted by free trim and sinkage. The measured total resistance and sinkage for the inland ship model are plotted in Fig. 2 as a function of the towing speed, e.g. the speed over ground. The towing speeds were all at the depth-Froude numbers $F_{nh} \leq 0.7$. In this subcritical speed range, the sinkage and the total resistance monotonously increase with the increased towing speed at the same water depth and with the decreased water depth at the same towing speed.

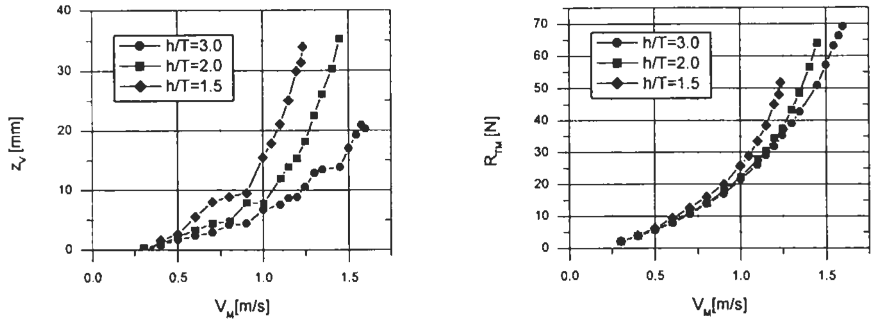

Figure 2: Characteristics of sinkage and measured resistance of the subject inland ship model

3 ANALYSIS METHOD

3.1 Introduction of a Mean Effective Speed Based on the Mean Sinkage

Referring to the definition of an effective depth-Froude number given by Graff (1963), a mean effective speed V_E based on the mean sinkage z_V is introduced here

$$V_E = \sqrt{(V^2 + 2g\,z_V)\Big/(1-\frac{z_V}{h})} = V\sqrt{(1+\frac{2g\,z_V}{V^2})\Big/(1-\frac{z_V}{h})} \qquad (1)$$

where g denotes the acceleration due to gravity and V the ship speed. This effective velocity combines the blockage effect near the ship and the effective depth-effect under the ship. The former is important for the viscous effect and the latter for the wave effect. According to Horn (1932), the mean deformation of the water surface under the ship can be assumed to be equal to the mean sinkage z_V. Therefore, the mean near-ship water-velocity relative to the ship can be obtained by means of Bernoulli's equation:

$$V_B = \sqrt{V^2 + 2g\,z_V} \qquad (2)$$

For a measured sinkage z_V, the velocity V_B defined by equation (2) combines both potential and viscous effects. Since the viscous effect on the mean sinkage is negligible small, the velocity V_B can be called as a blockage speed near the ship. It implies that the blockage velocity can be estimated by means of potential calculations. However, the viscous effects on the ship are more associated with the blockage speed, since the local friction is a function of the local velocity relative to the ship's surface, not necessarily of the ship speed over the ground.

3.2 Model Resistance as a Function of the Effective Speed

Now by re-construction of the total resistance measured at different water-depths as a function of the effective speed, Fig. 3 and 4 show that the model resistance of the subject inland ship and the container ship, respectively, is almost a unit function of the effective velocity and independent of the water-depths tested. The novel result leads to a new hypothesis for the total resistance of ships in shallow water:

For a ship moving at a subcritical speed and in not extremely shallow water, the total resistance could be considered as a unit function of the effective velocity and independent of the water depth.

For the two subject ships tested, this hypothesis holds for a speed $F_{nh} \le 0.7$ and a water depth h/T ≥ 1.5. If this hypothesis could be systematically validated for other ships, it would substantially impact the resistance prediction of ships in shallow water.

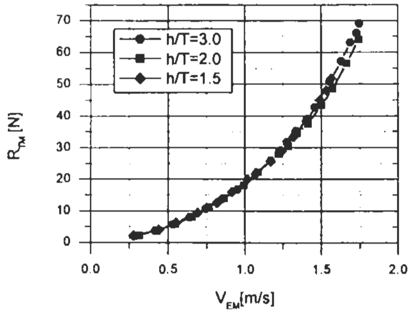

Figure. 3: Total model resistance as a function of the effective speed for the subject inland ship

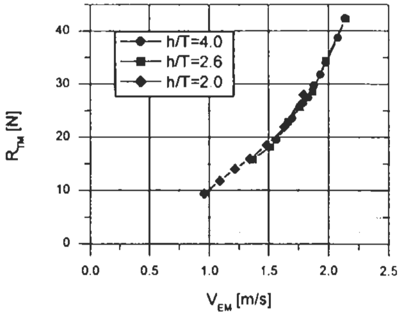

Figure 4: Total model resistance as a function of the effective speed for the subject container ship

3.3 Unit Form-Factor Based on the Effective Speed

The uniform total model resistance should also lead to a unit form-factor, if the model speed V_M for the identification of the form factor is replaced by the effective speed V_{EM}. The well-known Hughes-Prohaska formula reads now

$$\frac{C_{TME}}{C_{FOME}} = (1+k)_E + y \cdot \frac{F_{nE}^4}{C_{FOME}} \qquad (3)$$

here the model resistance is normalized by $\rho/2 \cdot S_M \cdot V_{EM}^2$ instead of by $\rho/2 \cdot S_M \cdot V_M^2$. The Froude number F_{nE} and Reynolds number R_{nEM} for the ITTC friction line refer also to the effective speed. The resulting form factor should be thus called as an effective form-factor.

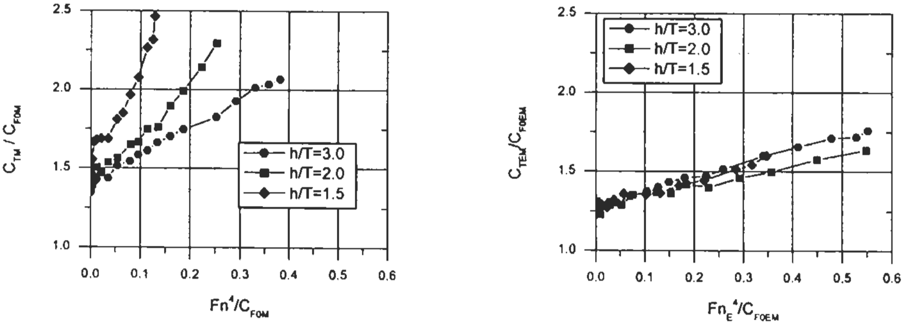

(a) Conventional evaluation based on the towing speed

(b) New evaluation based on the effective speed

Figure 5: Hughes-Prohaska form-factor at different water depths for the inland ship

4 RESISTANCE PREDICTION

Considering the special feature of the model resistance as a unit function of the effective speed, the conventional prediction of the ship resistance by means of the common form-factor method can be demonstrated as follows:

- Estimating the model wave resistance $R_{WM}(V_{EM})$ as a function of the effective speed V_{EM}
$$R_{WM}(V_{EM}) = R_{TM}(V_{EM}) - R_{VM}(V_{EM}) = R_{TM}(V_{EM}) - (1+k)_E C_{FOEM}\, \tfrac{1}{2}\rho_M \cdot S_M \cdot V_{EM}^2 \tag{4}$$
with the ITTC friction line $C_{FOEM} = 0.075/(\log R_{nEM}\text{-}2)^2$ for a Reynolds number corresponding to the effective speed at model scale $R_{nEM} = V_{EM} \cdot L_M / \nu_M$;
- Evaluating the ship speed $V_S = V_M\sqrt{\lambda}$ as well as the effective speed $V_{ES} = V_{EM}\sqrt{\lambda}$;
- Predicting the ship resistance at the corresponding water-depth tested
$$R_{TS}(V_S) = R_{VS}(V_{ES}) + R_{WS}(V_{ES}) = [(1+k)_E C_{FOES} + C_A]\tfrac{1}{2}\rho S V_{ES}^2 + \rho/\rho_M R_{WM}\lambda^3 \tag{5}$$
with the ITTC friction line $C_{FOES} = 0.075/(\log R_{nES}\text{-}2)^2$ and for the effective Reynolds number at the full scale $R_{nES} = V_{ES} L_S / \nu_S$;
- Predicting the ship resistance at the water-depth h/T=Prediction from the available model test h/T=Test:
$$\begin{aligned}\left[R_{TS}(V_S)\right]_{h/T=\text{Prediction}} &= \left[R_{VS}(V_{ES})\right]_{h/T=\text{Prediction}} &&+ R_{WS\,h/T=\text{Test}}(V_{ES\,h/T=\text{Prediction}}) \\ &= \left[(1+k)_E \cdot C_{F0ES} \cdot \tfrac{1}{2}\rho \cdot S \cdot V_{ES}^2\right]_{h/T=\text{Prediction}} &&+ \rho/\rho_M \left[R_{WM}\right]_{h/T=\text{Test}} \cdot \lambda^3\end{aligned} \; . \tag{6}$$

According to the prediction mentioned above, the measured resistance at h/T=3.0, 2.0 and 1.5, see the full-filled symbols in Fig. 6, was directly converted to its full scale value via equation (5) and then compared with those predicted by means of the model test at the water depth h/T=3.0 via equation (6), where the measured sinkage at h/T=2.0 and 1.5 was used to determine the corresponding effective speed. As shown in Fig. 6, the agreement is generally acceptable. Similar agreement was also found at different scales for the same inland ship, see Lochte-Holtgreven et al.(2001). However, it was shown in their work, there is a disagreement for the extremely shallow water at h/T=1.2. Generally speaking, the proposed method is only valid for a subcritical speed $F_{nh} \leq 0.7$ and in a not too extremely shallow water.

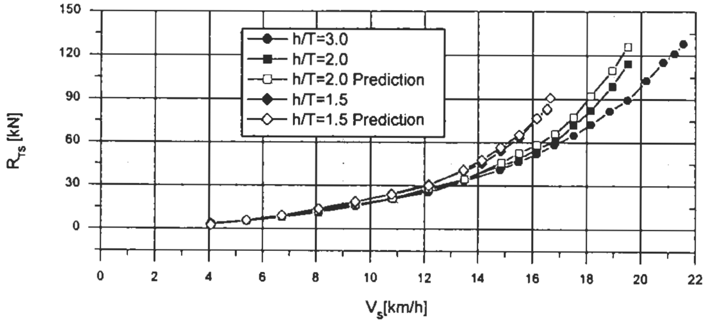

Figure 6: Comparison of the predicted ship-resistance via equation (5) with those from the direct conversion via equation (6) for the subject inland ship

The excellent agreement for h/T=1.5 in Fig. 6 demonstrates the quality of the proposed method for predicting the ship resistance in shallow water. More importantly, it implies that the model tests at h/T=1.5 could be entirely saved if the corresponding sinkage is realistically approximated, for instance by empirical formulae for ships moving at a narrow channel and by numerical calculations based on the potential theory. Fig. 7. compares the predictions based on the measured sinkages and the empirical estimations by Emerson (1959). Fig. 8 compares the predictions based on the measured sinkages and the numerical calculations by Jiang (2000) using an approximation based on the extended shallow-water theory. For the geometry configuration of the VBD towing tank the agreement is equally remarkable for both sinkage estimations. However, since the numerical estimation can be applied for general shallow water cases, the combination of the proposed prediction method with the well-established shallow-water approximation could be a new method for the resistance prediction of ships in shallow water.

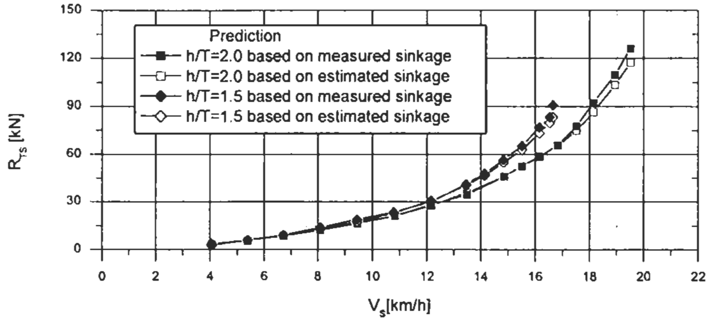

Figure 7: Comparison of the predicted ship-resistance using measured and empirically estimated sinkage

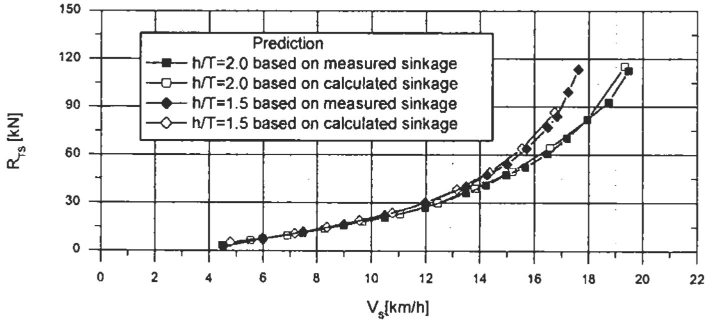

Figure 8: Comparison of the predicted ship-resistance using measured and calculated sinkage

5 PROPULSION PERFORMANCE

Since the propulsion tests can be conducted by means of the so-called English method, in principle the self-propulsion point at any considered propeller loading can be found. For a ship in shallow water, the ship self-propulsion point should correspond a towing force defined by

$$F_{DE}(V_M) = (C_{FOEM} - C_{FOES} - C_A)\tfrac{1}{2}\rho_M S_M V_{EM}^2 \tag{7}$$

where C_A is an empirical model-ship correction allowance.

The delivered propeller-power at the ship self-propulsion point defined above is plotted in Fig. 9 versus the effective speed for the water depth h/T=4.0, 2.6 and 2.0. For this subject container ship, the delivered power at the same effective speed is slightly higher in deeper water. This means the propulsion features could not be assumed as a unit function of the effective speed. However, if the delivered propller-power at the ship self-propulsion point is plotted now versus the blockage speed defined by equation (2), as shown in Fig. 10, it can be found that the delivered power at propeller can be considered as a unit function of the blockage speed and independent of the water depth. If this would be true, it would lead to a new hypothesis for the propulsion performance:

The delivered power at propeller at the ship self-propulsion point corresponding to the effective speed could be considered as a unit function of the blockage speed and independent of the water depth.

Physically, the wave effect included in the effective speed is less important or may be not reasonable for the propulsion characteristics behind the ship. However, due to possible errors in the measurements for one specific ship, this hypothesis has to be proved by analyzing measurements of other ships.

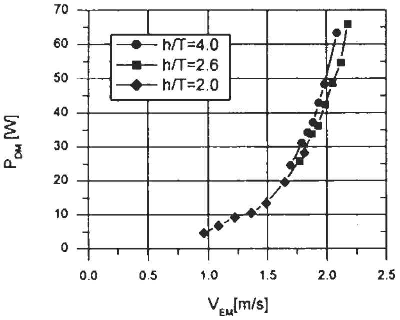

Figure 9: Delivered power at propeller as a function of the effective speed

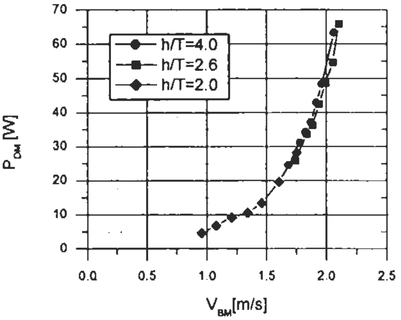

Figure 10: Delivered power at propeller as a function of the blockage speed

6 CONCLUSIONS

Based on a novel analysis of model tests for an inland ship-model and a container ship-model at different water-depths conducted in the Shallow Water Towing Tank Duisburg (VBD), a new method is proposed for resistance and propulsion prediction of the ship performance in the subcritical speed range and in a not too extremely shallow water by using an effective and blockage speed defined by the mean sinkage. Whereas the total resistance is found to be a unit function of the effective speed and independent of the water depth, the delivered power at propeller at a ship self-propulsion point corresponding to the effective speed could be considered as a unit function of the blockage speed.

Acknowledgement

This work was partially supported by the Ministry of Education and Research (BMBF) of the Federal Republic of Germany. The author is grateful to Mr. Lochte-Holtgreven for conducting the model experiments.

References

Emerson, A. (1959): Ship Model Size and Tank Boundary Correction. *Journal of North East Coast Engineers.*

Graff, W., Kracht, A. and Weinblum, G. (1964) : Some Extensions of D.W. Taylor's Standard Series, *Transactions of Society of Naval Architects and Marine Engineers, Vol. 72.*

Gross, A. & Watanabe, K.(1972): On Blockage Correction. *Proceedings of the 13th ITTC, Berlin/Hamburg.*

Horn, F. (1932): *Hydrodynamische Probleme des Schiffsantriebs.* Editor: G. Kempf und Foerster

Jiang, T. (2000): *Ship Waves in Shallow Water.* Habilitation Thesis, Mercator University Duisburg, Germany.

Kim, H.C.(1963): Blockage Correction in a Ship Model Tank. *Report of Michigan University No.04542, Part III.*

Lackenby, H. (1963): The Effect of Shallow Water on Ship Speed. *The Shipbuilder and Marine Engine-Builder.*

Landweber, L.(1939): Tests of a Model in Restricted Channels. *TMB-Report 460.*

Lochte-Holtgreven, H., List, S. & Jiang, T.(2001): Widerstandsprognose für Schiffe auf flachem Wasser. *VBD-Bericht Nr. 1532.*

Schlichting, O.(1934): Schiffswiderstand auf beschraenkter Wassertiefe. *Jahrbuch d. STG, Bd. 35.*

Practical Design of Ships and Other Floating Structures
You-Sheng Wu, Wei-Cheng Cui and Guo-Jun Zhou (Eds)
© 2001 Elsevier Science Ltd. All rights reserved

LOWER FRICTIONAL RESISTANCE CHARACTERISTICS OF FOUL RELEASE SYSTEMS

M. Candries[1], M.Atlar[1], A. Guerrero[2] and C.D. Anderson[3]

[1]Department of Marine Technology, University of Newcastle-upon-Tyne,
Newcastle-upon-Tyne, NE1 7RU, UK
[2]Canal de Experiencias Hidrodinamicas (CEHIPAR),
El Pardo, 28048 Madrid, Spain
[3]International Coatings Ltd.
Stoneygate Lane, Felling, Tyne and Wear, NE10 0JY, UK.

ABSTRACT

The roughness and drag characteristics of two antifouling paint systems are investigated; a state-of-the-art (Tributyl)tin-free Self-Polishing Co-Polymer (SPC) and a non-toxic Foul Release system. Towing tank experiments have confirmed that the total resistance of a 6.3m long plate coated with the Foul Release coating system was on average 1.4% lower than when it was coated with the tin-free Self-Polishing Co-polymer. The roughness characteristics were measured with both a stylus instrument and an optical measurement system. Correlation with the measured drag has shown that the roughness of the Foul Release cannot be characterised solely by a height parameter, such as the parameter Rt50. The texture of the Foul Release surface is significantly different from SPC systems as is evident from parameters such as the average absolute slope Sa and the correlation length τ of the roughness profile. Roughness and drag seem to correlate well when the parameter h, which takes the slope and curvature of the surface into account, is used to characterise the roughness.

KEYWORDS

Foul Release, Roughness, Resistance, Antifouling, Roughness function, Friction, Coatings

1 INTRODUCTION

The intended worldwide ban on the application of TBT Self-Polishing Co-Polymers from 2003 and the complete prohibition of their presence on ships from 2008 will have profound consequences for the marine industry. While much attention has been spent on the antifouling efficacy and ecological repercussions of the proposed alternatives to TBT-SPCs, no study has paid attention to the roughness and drag characteristics of these new paint systems, to the authors' knowledge. A research project set up at the University of Newcastle-upon-Tyne has compared these characteristics, for a tin-free SPC.

which prevents fouling of the hull by a well-controlled release of a copper-based toxin, and for a Foul Release system. The Foul Release system is a non-toxic silicone elastomer onto which fouling organisms have great difficulty attaching. If vessels are stationary for extended periods, settlement can occur, but there is only weak bonding between the fouling and the Foul Release surface. Consequently, the organisms can be removed by the hydrodynamic forces against the hull when the vessel is travelling fast enough. The speed at which most fouling organisms can release has been measured at the Florida Institute of Technology by towing experiments (Kovach and Swain, 1998). These trials have shown that, with the current Foul Release technology, speeds in excess of 15 knots are required to prevent most fouling types settling.

The following sections describe two sets of towing tank experiments, which have been carried out with flat plates to study the resistance increase caused by the application of the different paint systems. A detailed roughness analysis was carried out with a stylus instrument and an optical measurement system. Both findings have been correlated.

2 DRAG EXPERIMENTS

The first set of experiments involved a 2.55m long plate that was towed in the 40m long, 3.75m wide and 1.2m deep tank of the University of Newcastle-upon-Tyne. The aluminium plate was towed over a speed range up to 2m/s. The measurements were taken with the three different surfaces, which were the aluminium reference surface, the 3-coat SPC antifouling scheme and the 3-coat Foul Release system. The measurements showed that the drag increase for the Foul Release was significantly lower than for the SPC surface (Candries et al., 1998). Because of the limited speed range and run-length, it was decided to repeat the experiments with a large plate over a much larger speed range.

The second set of experiments was carried out over a speed range up to 8m/s, with a 6.3m long plate, in the 320m long CEHIPAR Calm Water Tank. The design of the aluminium plate was based on the NSRDC friction plane model 4125, which has been used for similar experiments at the David Taylor Model Basin (West, 1973). The total resistance of the plane was measured with the dedicated dynamometer of the carriage for the same three different surfaces: the aluminium reference surface, the surface coated with a 3-coat SPC antifouling scheme and the surface coated with a 3-coat Foul Release system. Figure 1 shows the total resistance coefficients for the three surfaces plotted against the Reynolds number. Above a Reynolds number $Re = 2\cdot10^7$, the Foul Release surface exhibits a drag which is on average 1.56% higher than the aluminium surface, and the SPC surface exhibits a drag which is on average 2.91% higher than the aluminium reference. In other words, the total drag coefficient of the Foul Release surface was on average 1.41% lower than the SPC surface (Candries and Atlar, 2000).

2 ROUGHNESS MEASUREMENT

The roughness measurements were initially carried out with the BMT Hull Roughness Analyser, which is the standard instrument for use on ship hulls. The stylus instrument measures Rt50, which is the highest peak to lowest valley perpendicular to the mean line over a length of 50mm. When the stylus has traversed the evaluation length, fifteen readings of Rt50 and an average, the Mean Hull Roughness (MHR) are printed out. The instrument was used throughout both sets of the towing tank experiments. In general, 10 and 20 MHR values for the small and large plate respectively were averaged to obtain the overall Average Hull Roughness (AHR). It was observed from the beginning that the measurement of the Foul Release surface required a special treatment in that the coated surface had to be wetted slightly in order to get meaningful readings. If the surface was dry, the stylus hopped over the rubberlike material, whereas if the surface was too wet, the gauge skidded very easily; both practices would give erroneous readings (Anderson et al., 1999). Table 1 presents the average roughness in microns for the three surfaces obtained from both sets of experiments.

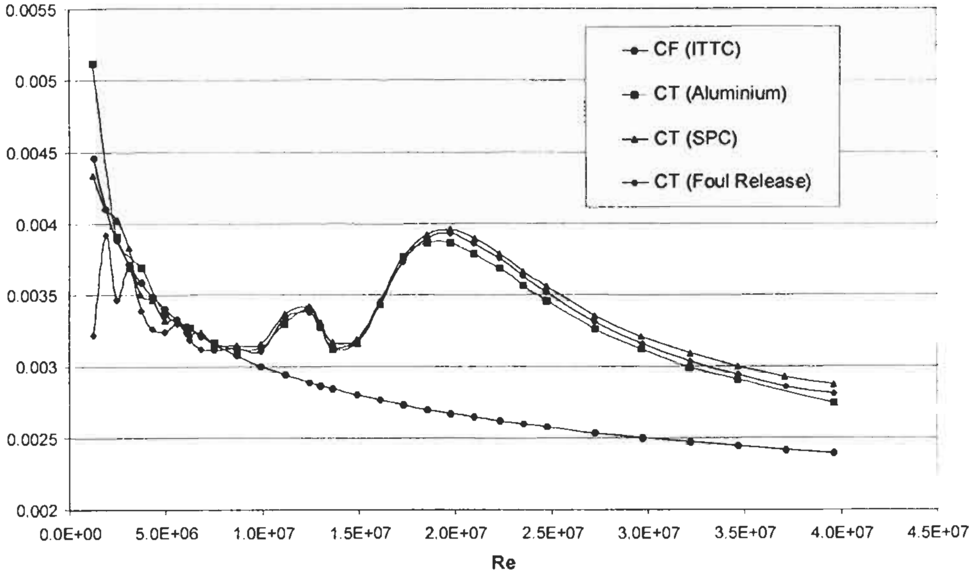

Figure 1: Total resistance coefficients against Reynolds number in the CEHIPAR Calm Water Tank

TABLE 1

AVERAGE HULL ROUGHNESS (IN µM) OF THE THREE TESTED SURFACES IN BOTH SETS OF EXPERIMENTS

Average Hull Roughness	*Newcastle Experiments (2.55m long plate)*	*CEHIPAR experiments (6.3m long plate)*
Aluminium	17	18
TBT-free SPC	75	39
Foul Release	48	62

As shown in Table 1, the roughness of the aluminium reference surface was virtually identical for both sets of experiments, but in contrast to the first experiments, the roughness of the Foul Release surface was higher than the roughness of the SPC surface in the second set of experiments. This oddity can be explained by the poor surface condition prior to the application of the Foul Release surface in the second set of tests. The SPC coating had been stripped off with the intention of leaving the primer on, but there were large patches where the aluminium was exposed. Thus, instead of applying the Foul Release system on a smooth aluminium surface like in the first set of experiments, the Foul Release tiecoat and topcoat were applied on an uneven primer surface with an average roughness of 37µm. In contrast, the SPC surface was much smoother for the second set of experiments due to a better paint application than in the first set of experiments.

If one compares Table 1 with Figure 1, one notices immediately that the resistance of a surface coated with a Foul Release system does not correlate with the roughness parameter Rt50.

Consequently, a UBM optical measurement system was used to analyse small sample plates (20 by 25cm) coated with the two paint systems described in the previous section. The instrument works by the focus-detection principle whereby the vertical displacement of the objective is measured by an infrared laser diode as light source. The instrument has a vertical range of 0.5mm and a resolution of less than 50nm.

The roughness of the surfaces has been investigated by analysing a wide range of parameters. The amplitude parameters, characterising how the roughness varies at right angles to the surface, can be subdivided into extreme-value parameters (e.g. Rt), average parameters and properties of the height distribution. Texture parameters, which describe how the roughness varies in the plane of the surface, included counts of extrema and crossings with the mean line, the average absolute slope Sa, and the correlation length τ. A fractal approach, which essentially scrutinises the surface for self-similarity, was included by computing the fractal dimension.

The measurements were carried out for a range of long wavelength cut-offs and sampling intervals (equal to half the Nyquist short wavelength cut-off). In accordance to the standards for roughness measurement as suggested by Medhurst (1990), 3 transversal and 3 longitudinal measurements were taken for each set of bandwidth parameters.

Two typical examples of the measured roughness profiles of the SPC and the Foul Release surface are shown in Figures 2 and 3 respectively for a long wavelength cut-off of 5mm and a sampling interval of 50μm, filtered by a 81-part moving-average method. All parameters have been averaged over 10 cut-off length intervals.

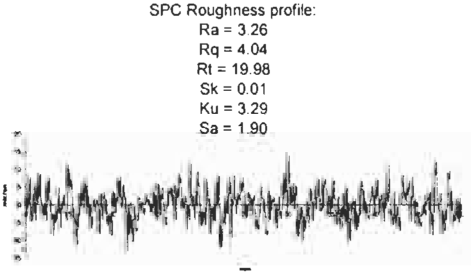

Figure 2: Typical profile of the SPC surface surface

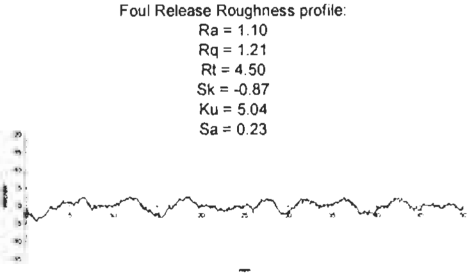

Figure 3: Typical profile of the Foul Release surface

Figures 2 and 3 show that the amplitude parameters (centre-line average roughness Ra, RMS roughness height Rq and maximum peak to valley height Rt) are in this case lower for the Foul Release surface than for the SPC surface. Moreover, the "spiky" SPC surface clearly exhibits a great deal more of short-wavelength roughness. In other words, the "open" texture of the Foul Release surface is very different from the "closed" SPC surface, as partially indicated by the average absolute slope Sa (in degrees), which differs by an order of magnitude. Further computations show that the correlation length is also an order of magnitude larger for the Foul Release surface than for the SPC surface. This further indicates the low-amplitude undulating character of the Foul Release surface, which in effect is essential to its efficacy as an antifouling system. The surface area available for adsorption and attachment of fouling organisms increase with roughness. The valleys of rough surfaces are penetrated by marine adhesives and hence foulants will more readily attach. Moreover, the foulants also find shelter from shear and abrasion in the crevices and thus roughness also poses a threat to the hydrodynamical removal of the organisms.

3 CORRELATION OF THE ROUGHNESS AND DRAG

Townsin and Dey (1990) correlated the roughness and drag of a very wide range of coated surfaces and found that the resistance of smooth newly painted surfaces correlated well with the parameter Rt50. Their main argument for the use of a single height parameter to characterise the roughness was that the texture of a newly painted surface must depend principally on the rheology of the paint. There is no in-service damage which might affect the texture and only a height parameter is required to differentiate one from another. This argument may hold for newly painted SPC surfaces, but it does not hold for Foul Release surfaces since its surface texture is already significantly different immediately after application.

Townsin and Dey (1990) had found that a composite roughness parameter, h, correlated well with the drag increase of the entire range of painted surfaces. The parameter h is equal to $m_0(m_4/m_2)^{0.5}$ whereby m_0, m_2 and m_4 are the first even spectral moments of the roughness profile, which are directly related to the variances of the height, slope and curvature respectively. The drag increase is characterised by the roughness function $\Delta U/u_\tau$ as defined by Hama (1954). Granville's indirect method was used to convert the total drag as measured from the towing tank experiments to the roughness function at the trailing edge, using the equation (Granville, 1987):

$$\Delta U/u_\tau = \left(\sqrt{\frac{2}{C_F}}\right)_s - \left(\sqrt{\frac{2}{C_F}}\right)_r - 19.7\left[\left(\sqrt{\frac{C_F}{2}}\right)_s - \left(\sqrt{\frac{C_F}{2}}\right)_r\right] + 2.5B_1'\left(\sqrt{\frac{C_F}{2}}\right)_r$$

The frictional resistance of the rough, painted surfaces is subtracted from the smooth aluminium reference values at equal values of ReC_F. The frictional resistance coefficients C_F were obtained from subtracting the wave resistance coefficients, as computed by a dedicated computational fluid dynamics tool, from the measured total resistance coefficients shown in Figure 1. The frictional resistance of the aluminium reference surface was found to be in excellent agreement with the Schoenherr friction line. Consequently, iteration of the Schoenherr equation was carried out to obtain $(2/C_F)^{0.5}$ of the aluminium surface at the respective ReC_F values of the painted surfaces. The associated value of the roughness Reynolds number $h^+ = hu_\tau/\nu$ for the given value of ReC_F is then applied with the h values obtained from the optical roughness measurement:

$$hu_\tau/\nu = \left(\frac{ReC_F}{2}\right)\left(\frac{h}{L}\right)\left(\sqrt{\frac{2}{C_F}}\right)_r\left[1 - 2.5\left(\sqrt{\frac{C_F}{2}}\right)_r + 2.5(3.75 + B_1')\left(\frac{C_F}{2}\right)_r\right]$$

Figure 4 shows the roughness function of the two painted surfaces plotted against $\log(hu_\tau/\nu)$.

In Figure 4, the results of four other painted surfaces, which were tested by Dey with rotating drums (Dey, 1989), are included for the sake of comparison. Also plotted is the line of Colebrook-White form which Townsin and Dey (1990) had found to indicate the trend of 28 different painted surfaces. The influence of a different roughness parameter appears as a shift in the abscissa of the data in Figure 4, where the data seem to correlate quite well. The parameter h of the Foul Release surface was increased in view of the fact that the sample plates analysed by the optical measurement system did not exhibit the same underlying conditions in terms of surface preparation. This was done by calculating m_0 as the square of Rq, which in turn was calculated via a correlation relationship with Rt. The value of Rt was taken as the value measured by the BMT Hull Roughness Analyser. It is believed that the effect of the poor surface preparation was less significant on the absolute slope and the curvature of the surface, but the data could possibly shift slightly towards the right. Further investigation and the acquisition of more data is needed to validate the trends observed in Figure 4.

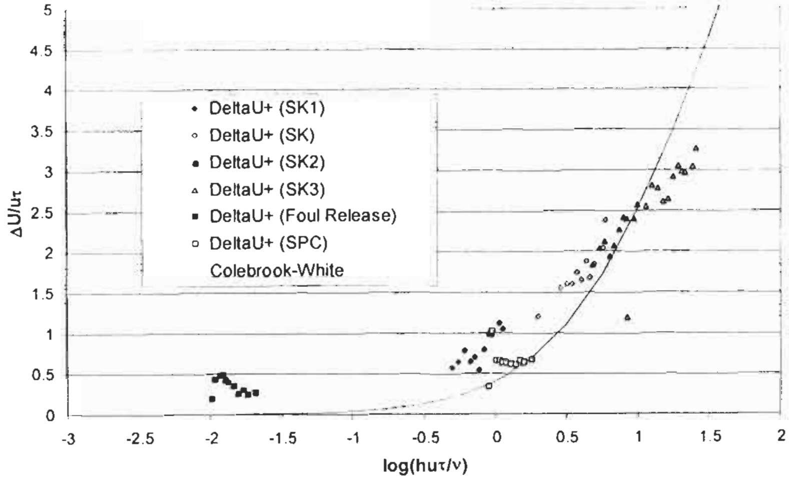

Figure 4: The roughness function of the surfaces tested by the authors and by Dey (1989) plotted against log(hu_τ/ν)

To complement the above analysis, water tunnel tests are currently underway in the Emerson Cavitation Tunnel of Newcastle University to measure the boundary-layer characteristics of the painted surfaces using Laser Doppler Velocimetry. In addition, further drag measurements with rotating drums and detailed analysis of the roughness of the test surfaces are planned.

4 CONCLUSIONS

A systematic investigation of the resistance and roughness of two state-of the-art alternatives to TBT-SPC has been undertaken. The resistance of a tin-free SPC and a non-toxic Foul Release system has been measured in a 320m long towing tank on a 6.3m long friction plate. For the Foul Release surface, the resistance of the flat plate between a Froude number of 0.5 and 1 was on average 1.56% higher than the aluminium reference surface; for the SPC surface, the total resistance was on average 2.91% higher than the aluminium surface. In terms of frictional resistance, the differences were 2.09 and 3.84% respectively.

Surface profilometry of coated sample plates has shown that the texture of a Foul Release surface is significantly different from the texture of a tin-free SPC surface, exhibiting a low-amplitude undulating character. In order to correlate the roughness functions measured from the drag experiments with the surface characteristics, it is necessary to take a measure for the texture into account, in addition to a measure for the height of the profile. The first results seem to indicate that the parameter h as suggested by Townsin and Dey (1990) correlates the measured roughness fairly well with the measured drag.

Acknowledgements

This research project is funded by EPSRC Research Grant No. 98316366 and by International Coatings Ltd. The large plate experiments at CEHIPAR were made possible by the European Community programme CEHMAR, which promotes the mobility and opportunities of researchers. The authors wish to thank the CEHIPAR staff for their contribution to the experiments, and Sabino Quirros and Josu Intxaurraga from International Coatings Ltd. Spain for their help in the paint application. Trevor Wills (Akzo Nobel Technology Centre) is thanked for his help with the optical measurement of the surfaces. Dr. Townsin is thanked for his helpful comments and suggestions throughout the course of this project.

References

Anderson C.D., Townsin R.L. and Candries M. (1999). Idiosyncracies of low surface energy (Foul Release) antifoulings: drag, roughness and maintenance. *10th International Congress on Marine Corrosion and Fouling*, Melbourne, Australia.

Candries M., Atlar M., Mitchell G.H.G. and Lamb D. (1998). Flat plane towing experiments with two coatings, *Report No. MT-1998-034*, Department of Marine Technology, University of Newcastle-upon-Tyne.

Candries M. and Atlar M. (2000). Influence of Two Different Antifoulings on the Resistance of Roughness of a Flat Plate, *Report No. MT-2000-102*, Department of Marine Technology, University of Newcastle-upon-Tyne.

Dey S.K.(1989). Parametric Representation of Hull Painted Surfaces and the Correlation of Fluid Drag, *PhD Thesis*, Department of Marine Technology, University of Newcastle-upon-Tyne.

Granville P.S. (1987). Three indirect methods for the drag characterisation of arbitrary rough surfaces on flat plates, *Journal of Ship Research*, **31**, 70-77.

Hama F.R. (1954). Boundary-layer characteristics for smooth and rough surfaces, *Trans. S.N.A.M.E.*, **62**, 333-358.

Kovach B.S. and Swain G.W. (1998). A boat mounted foil to measure the drag properties of antifouling coatings applied to static immersion panels, *Proc. Int. Symp. Seawater Drag Reduction*, July 22-24, Newport, Rhode Island.

Medhurst J.S. (1990). Outline of a draft international standard for the measurement and characterisation of roughness topography in fluid flow, *Marine Roughness and Drag Workshop*, R.I.N.A., London.

West E.E. (1973). The effect of surface preparation and repainting procedures on the frictional resistance of old ship bottom plates as predicted from NSRDC friction plane model 4125. *Report 4084*, Naval Ship Research and Development Center, Bethesda, Maryland.

Thomas T.R. (1999). *Rough Surfaces*, Second Edition, Imperial College Press, London.

Townsin R.L. and Dey S.K. (1990), The correlation of roughness drag with surface characteristics, *Marine Roughness and Drag Workshop*, R.I.N.A., London.

Practical Design of Ships and Other Floating Structures
You-Sheng Wu, Wei-Cheng Cui and Guo-Jun Zhou (Eds)
© 2001 Elsevier Science Ltd. All rights reserved

EVALUATION AND COMPUTER PROGRAM ON THE SPEED TRIAL ANALYSIS METHOD OF THE ONGOING WORK IN ISO/TC8

Eun-Chan Kim[1], Hyun Se Yoon[1], Sa Young Hong[1], Yoon-Rak Choi[1]

[1] Korea Research Institute of Ships and Ocean Engineering,
P. O. Box 23 Yusung, Taejon, 305-600, Korea

ABSTRACT

The ISO Draft International Standard 15016, entitled "Guidelines for the assessment of speed and performance by analysis of speed trial data", was developed by the working group ISO/TC 8/SC 9/WG 2. This paper presents the structure of computer program based on the ISO/DIS 15016. The computer program is constructed to optimize the structure, to emphasize the graphic function and to implement the GUI at WINDOWS environment. Various analysis methods for resistance increase due to ship motion, wave diffraction, wind, steering, drifting, water temperature and salt content, deviation of displacement, hull and propeller surface roughness, and shallow water effects are contained in this computer program. The output result of this computer program was compared with an example of ISO/DIS 15016.

KEYWORDS

ISO, Speed, Trial, Analysis, Program, Resistance, Increase, Wave, Wind

1 INTRODUCTION

Four objectives of speed trials are described in the report of the Performance Committee of the 16th ITTC. Four objectives are to fulfill contractual obligation, to obtain performance data, to determine the relationship between ship speeds and propeller revolutions, and to obtain ship-model correlation allowance. To fulfill contractual obligation, the primary purpose of speed trials is determining ship performance in terms of speed, power and propeller revolution under prescribed ship conditions. The speed trial results should be analyzed under the contractually stipulated conditions which usually are no wind, no wave, no current, deep water, smooth hull and smooth propeller surface conditions.

The ISO/DIS 15016 (ISO/TC8, 2000), entitled "Guidelines for the assessment of speed and performance by analysis of speed trial data", was developed by the working group ISO/TC 8/SC 9/WG 2. This guideline contains a basic procedure for the speed loss and various procedures for correction of speed trials covering all influences. Several methods are suggested to correct all influences in this guideline.

All of the symbols are used according to the ISO/DIS 15016 and ITTC standard symbols.

2 SPEED TRIAL ANALYSIS PROCEDURE OF ISO/DIS 15016

The analysis procedure of ISO/DIS 15016 is divided into six steps. This analysis procedure is based on Taniguchi-Tamura's Method (Taniguchi etc., 1966). Various calculation methods of resistance increase due to the disturbances and the deviations are suggested to use at annex of ISO/DIS 16016. In this guideline, it has described that the methods presented in the annexes are the latest one available today, other scientifically-based method including model tests may be adopted as agreed between shipyard and ship owner.

Calculation of resistance increase due to waves is divided into two stages. One is pre-calculation of response function of added resistance in regular waves prior to speed trials. The other is main calculation to be made on board for particular irregular waves during trials. When both seas and swell are observed and are to be taken into account, the total resistance increase is given by the sum of resistance increase due to seas and swell calculated independently. The calculation of resistance increase due to waves is based on Maruo's formula (Maruo, 1960). In short waves, diffraction of incident waves is observed around the bow, and this causes the main resistance in waves. As the correction of this effect, Faltinsen's formula (Faltinsen etc., 1980), Kwon's formula (Kwon, 1982) and Fujii-Takahashi's formula (Fujii etc., 1975) are suggested to use. For the resistance increase due to waves, the Townsin-Kwon's method (Townsin etc., 1993) is suggested to use also. When the calculation of resistance increase of ships in irregular waves, ITTC standard spectrum and JONSWAP spectrum are respectively used for the frequency distribution of incident waves for seas and swell.

The analysis method of resistance increase due to wind is suggested to use. The wind resistance coefficients should be based on data which is derived from model tests in wind tunnel or test results of similar ship. The formula for resistance increase due to steering required by course keeping and the formula of resistance increase due to drifting are suggested to use. For speed loss due to shallow water, the Lackenby's formula (Lackenby, 1963) is suggested to use also.

3 COMPUTER PROGRAM OF SPEED TRIAL ANALYSIS

The flowchart of analysis program is shown in Figure 1. All of the suggested methods from ISO/DIS15016 are contained in this program. Resistance increase due to displacement deviation is calculated as equation 1.

$$R_{ADIS} = 0.65\, R_{TS}\left(1 - \frac{\Delta_O}{\Delta}\right) \tag{1}$$

The effect of water temperature and density are applied as equation 2 before the initial correction of resistance increase.

$$R_{AS} = R_{TS}\left(1 - \frac{\rho_0}{\rho}\right) + \frac{1}{2}\rho\, S\, V^2 (C_F - C_{F0}) \tag{2}$$

For the effect of hull surface roughness, resistance increase is calculated according to the formula as equation 3 which is derived from the model-ship correlation allowance formula of 1978 ITTC performance prediction method (ITTC, 1978).

$$R_{hull} = \frac{1}{2}\rho S\, V^2 \frac{105}{L^3}\left(k_S^{\frac{1}{3}} - k_{S0}^{\frac{1}{3}}\right)\cdot 10^{-3} \tag{3}$$

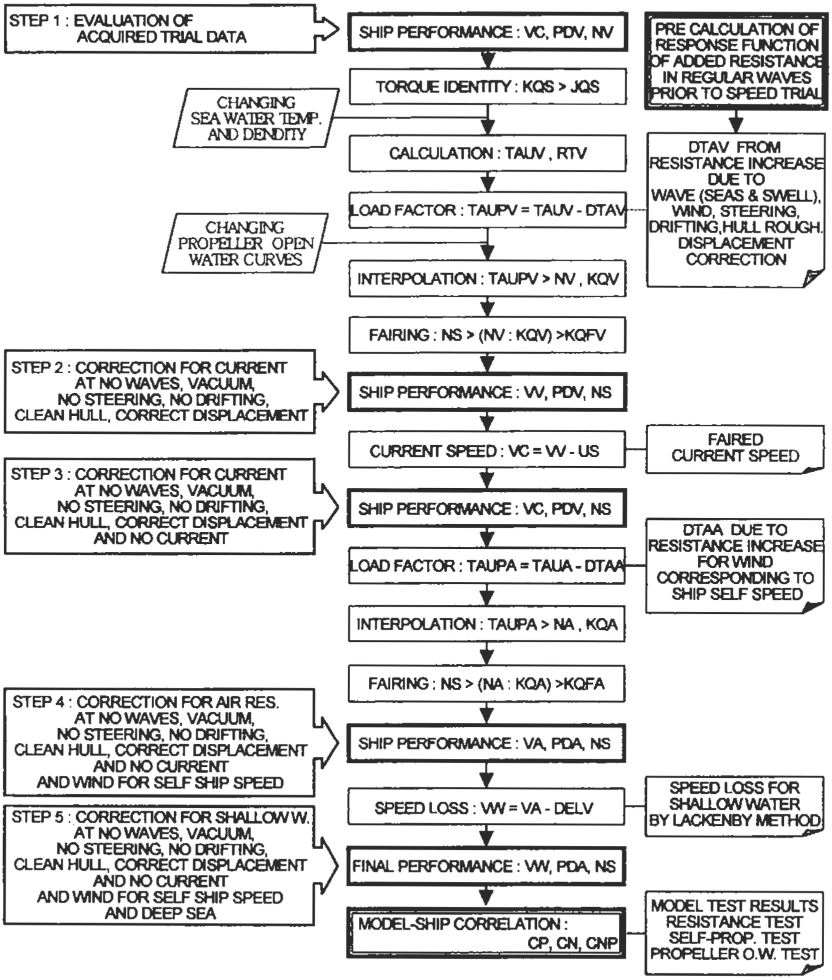
STEP 1 : EVALUATION OF ACQUIRED TRIAL DATA
SHIP PERFORMANCE : VC, PDV, NV
PRE CALCULATION OF RESPONSE FUNCTION OF ADDED RESISTANCE IN REGULAR WAVES PRIOR TO SPEED TRIAL
TORQUE IDENTITY : KQS > JQS
CHANGING SEA WATER TEMP. AND DENDITY
CALCULATION : TAUV , RTV
DTAV FROM RESISTANCE INCREASE DUE TO WAVE (SEAS & SWELL), WIND, STEERING, DRIFTING,HULL ROUGH. DISPLACEMENT CORRECTION
LOAD FACTOR : TAUPV = TAUV - DTAV
CHANGING PROPELLER OPEN WATER CURVES
INTERPOLATION : TAUPV > NV , KQV
FAIRING : NS > (NV : KQV) >KQFV
STEP 2 : CORRECTION FOR CURRENT AT NO WAVES, VACUUM, NO STEERING, NO DRIFTING, CLEAN HULL, CORRECT DISPLACEMENT
SHIP PERFORMANCE : VV, PDV, NS
CURRENT SPEED : VC = VV - US
FAIRED CURRENT SPEED
STEP 3 : CORRECTION FOR CURRENT AT NO WAVES, VACUUM, NO STEERING, NO DRIFTING, CLEAN HULL, CORRECT DISPLACEMENT AND NO CURRENT
SHIP PERFORMANCE : VC, PDV, NS
DTAA DUE TO RESISTANCE INCREASE FOR WIND CORRESPONDING TO SHIP SELF SPEED
LOAD FACTOR : TAUPA = TAUA - DTAA
INTERPOLATION : TAUPA > NA , KQA
FAIRING : NS > (NA : KQA) >KQFA
STEP 4 : CORRECTION FOR AIR RES. AT NO WAVES, VACUUM, NO STEERING, NO DRIFTING, CLEAN HULL, CORRECT DISPLACEMENT AND NO CURRENT AND WIND FOR SELF SHIP SPEED
SHIP PERFORMANCE : VA, PDA, NS
SPEED LOSS : VW = VA - DELV
SPEED LOSS FOR SHALLOW WATER BY LACKENBY METHOD
STEP 5 : CORRECTION FOR SHALLOW W. AT NO WAVES, VACUUM, NO STEERING, NO DRIFTING, CLEAN HULL, CORRECT DISPLACEMENT AND NO CURRENT AND WIND FOR SELF SHIP SPEED AND DEEP SEA
FINAL PERFORMANCE : VW, PDA, NS
MODEL-SHIP CORRELATION : CP, CN, CNP
MODEL TEST RESULTS RESISTANCE TEST SELF-PROP. TEST PROPELLER O.W. TEST

Figure 1: Flowchart of speed trial analysis

For the effect of propeller surface roughness, propeller open-water characteristics are corrected according to the formula as equation 4 which is derived from the propeller scale effect correction formula of 1978 ITTC Performance Prediction Method.

$$K_{TSR} = K_{OTS} + \Delta C_D \, 0.3 \, \frac{P}{D} \frac{c}{D} Z$$

$$K_{QSR} = K_{OQS} - \Delta C_D \, 0.25 \, \frac{c}{D} Z \tag{4}$$

$$where \quad \Delta C_D = 2\left(1 + 2\frac{t}{c}\right)\left[\left(1.89 + 1.62\log\frac{c}{k_{P0}}\right)^{-2.5} - \left(1.89 + 1.62\log\frac{c}{k_P}\right)^{-2.5}\right]$$

For the wind resistance coefficients, the JTTC standard curve and twenty-two Blendermann's curves can be selected as an option (Blendermann, 1991). It needs lots of interpolation routines in this program. Table 1 shows various interpolation methods used in this program. The computer program is constructed to emphasize the graphic function and to use the GUI at WINDOWS environment. Figure 2 shows interpolation step to derive K_{QFV} from N_V-K_{QV} curve.

As a post-calculation, model-ship correlation analysis is included in this program. This routine is constructed according to the 1984 ITTC trial analysis method (ITTC, 1984).

TABLE 1

INTERPOLATION METHODS

Calculation	Interpolation Method
V : t, w, η_R	2nd Degree Polynomial
J : K_Q	2nd Degree Polynomial
J : TAU(=K_T/J^2)	2nd Rational Function
N : K_Q	Least Square
Time : Current	Cubic Spline
V : P_D, N	Least square or Cubic Spline

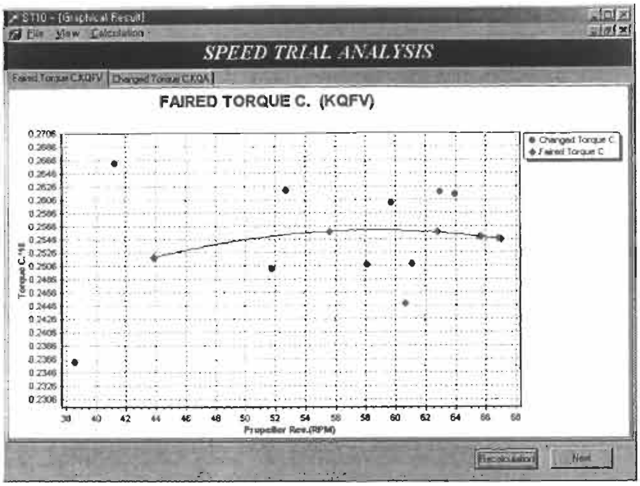
ST10 - [Graphical Result]
File
View
Calculation
SPEED TRIAL ANALYSIS
Faired Torque C.KQFV
Changed Torque C.KQA
FAIRED TORQUE C. (KQFV)
Changed Torque C
Faired Torque C
Torque C.*10
0.2706
0.2686
0.2666
0.2646
0.2626
0.2606
0.2586
0.2566
0.2546
0.2526
0.2506
0.2486
0.2466
0.2446
0.2426
0.2406
0.2386
0.2366
0.2346
0.2326
0.2306
38
40
42
44
46
48
50
52
54
56
58
60
62
64
66
68
Propeller Rev.(RPM)
Recalculation
Next

Figure 2: A sample of interpolation

4 DISCUSSION OF RESULTS

Table 2 shows the analysis result for a 300K VLCC which uses similar ship and same trial data with the example results of ISO/DIS 15016. All of these calculation results of resistance increase due to the disturbances and the deviations give good agreement with the calculation results taken from the example of ISO/DIS 15016.

Table 3 shows the comparison between the results of resistance increase due to waves by this program and of ISO/DIS 15016 examples. The resistance increase due to ship motion is calculated following the Maruo's method using strip method results, and the resistance increase due to wave diffraction is calculated using the Faltinsen's method (Hong etc., 2001). Making clear comparison between two results is impossible because the hull form offsets are not mentioned and the components of resistance increase due to waves are not available in the example.

TABLE 2

A SAMPLE OUTPUT FOR THE 300K VLCC WHICH IS A EXAMPLE OF ISO/DIS 15016

```
    ---------------------------------------------------------------
     ADDED RESISTANCE CORRECTION BY SPEED TRIAL ANALYSIS PROGRAM ST10D
    ---------------------------------------------------------------
                              PROGRAMED BY KRISO ACCORDING TO ISO/DIS15016

FILE NAME : 300i.inp                             TRIAL DATE   : 2000-08-03
SHIP NAME : ISOSAMH       PROP.NAME : ISOSAMP    WEATHER      : CLOUD
* LPP     = 318.000 M     * NO.PROP.=       1    COURSE       : OFF-JAPAN
* BREADTH =  58.000 M     * NO.BLADE=       4    * SEA DEPTH  :   100.0     M
* DEPTH   =  29.000 M     * DIAMETER=   9.500 M  * ROUGH.HULL = 0.000180    M
DRAFT                     * PRO70   =  0.8737              STD. = 0.000150    M
*      MEAN=  18.500 M    * EAR     =  0.4300    * ROUGH.PROP. = 0.000036   M
*        FP=  18.500 M    * CHR     =  0.3000              STD. = 0.000030    M
*        AP=  18.500 M                           * CLEAN.HULL =      2.5 MONTH
*       MID=  18.500 M    RUDDER                 * CLEAN.PROP. =     0.2 MONTH
* LWL     = 320.000 M     * AREA    =   95.00 M2 * AIR TEMP.  =   20.00   DEG
* S       = 25800.0 M2    * HEIGHT  =  14.200 M  *       DENSIYT=   1.225 KG/M3
* SBK     =   180.0 M2    * AREA R. =  0.0162    * WATER TEMP. =  20.00 DEG:S
* AT      =  1132.0 M2                           *          DENS. = 1024.00 KG/M3
* AL      =  3900.0 M2    ENGINE    : ISOSAME    *        K.VIS. = 1.0423 E6M2/S
* CM      =  0.9972 M3    * MCR BHP =  30000. PS * W.STD.TEMP. =  15.00 DEG:S
* DISV    = 267324.  M3   * MCR REV.=  67.00RPM  *          DENS. = 1024.00 KG/M3
     STD. = 269997.  M3   * ETAT    =  0.9709    *        K.VIS. = 1.1873 E6M2/S

MODEL TEST RESULTS
---------------------------------------------------------------------------
PREDICT METHOD: 2-D, KRISO-2D  SCALE= 39.0000                DELCF = -0.000200
---------------------------------------------------------------------------
* VS(KNOT):  6.00 11.00 12.00 13.00 14.00 15.00 16.00 17.00 18.00 19.00
---------------------------------------------------------------------------
* CRM*1000: 0.779 0.779 0.767 0.754 0.747 0.744 0.751 0.760 0.780 0.800
* TM      : 0.130 0.130 0.130 0.130 0.130 0.130 0.130 0.130 0.130 0.130
* WM      : 0.450 0.450 0.450 0.450 0.450 0.450 0.450 0.450 0.450 0.450
* WS      : 0.334 0.334 0.334 0.334 0.334 0.334 0.334 0.334 0.334 0.334
* ETARM   : 1.000 1.000 1.000 1.000 1.000 1.000 1.000 1.000 1.000 1.000

PROPELLER OPEN-WATER CHARACTERISTICS AT FULL SCALE
---------------------------------------------------------------------------
* J        :0.50000.55000.60000.65000.70000.7500
---------------------------------------------------------------------------
* KTS      :0.22310.21190.19070.16890.14650.1241
* KQS*10   :0.33350.31140.28930.26600.24150.2170
* KTR      :0.22300.21180.19060.16880.14640.1240
* KQR*10   :0.33420.31210.29000.26670.24220.2177

WATERLINE OFFSETS : X(METER:FWD+)/Y(METER:ALL-)
---------------------------------------------------------------------------
 159.00 151.05 143.10 135.15 127.20 111.30  95.40  63.60  28.62   0.00 -15.90
 -47.70 -79.50 -95.40-111.30-127.20-135.15-143.10-151.05-159.00-164.41-165.20
   0.00  -8.24 -15.17 -19.73 -23.05 -27.28 -28.63 -29.00 -29.00 -29.00 -29.00
 -29.00 -29.00 -28.30 -25.87 -21.89 -19.25 -16.68 -13.85  -9.77  -6.46   0.00

WIND RESISTANCE C.: WIND DIRECTION(DEG.:BOW=0)/COEFFICIENT(CAA0*K)
---------------------------------------------------------------------------
   0.00  10.00  20.00  30.00  40.00  50.00  60.00  70.00  80.00  90.00 100.00
 110.00 120.00 130.00 140.00 150.00 160.00 170.00 180.00
   0.94   0.85   0.95   0.95   0.81   0.69   0.49   0.26   0.04  -0.12  -0.30
```

```
  -0.32  -0.45  -0.51  -0.59  -0.64  -0.63  -0.61  -0.55
-------------------------------------------------------------------------------


SPEED TRIAL RESULTS
-------------------------------------------------------------------------------
RUN NUMBER             :     1       2       3       4       5       6       7       8       9      10
-------------------------------------------------------------------------------
LOAD CONDITION         :   0.25    0.25    0.50    0.50    0.75    0.75    0.90    0.90    1.00    1.00
WIND DIRECTION   (DEG) : S 10.0  P145.0  S 10.0  P135.0  P  5.0  P150.0  P136.0  P  5.0  P145.0  S 10.0
WIND VELOCITY    (M/S) : 13.500   4.000  15.000   2.800  16.000   0.700   0.400  16.500   0.000  16.500
RUNNING DIRECTION      : 20.     200.     20.     200.     20.     200.     200.     20.     200.     20.
SHIP SPEED      (KNOT) :  8.570  10.810  11.760  13.960  14.030  15.710  16.360  15.110  16.400  15.400
PROPELLER REV.   (RPM) :  43.90   43.80   55.60   55.60   62.80   62.80   65.60   65.70   67.00   66.80
SHAFT POWER       (PS) :  7767.   7525.  15435.  15150.  22032.  22018.  24928.  25160.  26868.  26452.
CURRENT SPEED   (KNOT) : -1.010   1.010  -0.990   0.990  -0.840   0.830   0.600  -0.600   0.530  -0.530
WAVE  PERIOD     (SEC) :   3.90    3.90    3.90    3.90    3.90    3.90    2.80    2.80    2.80    2.80
WAVE  HEIGHT       (M) :   1.00    1.00    1.00    1.00    1.00    1.00    0.50    0.50    0.50    0.50
WAVE  INCD.ANG.  (DEG) :  170.0   350.0   170.0   350.0   170.0   350.0   350.0   170.0   350.0   170.0
SWELL PERIOD     (SEC) :  10.59   10.59   10.59   10.59   11.32   11.32   11.32   11.32   11.32   11.32
SWELL HEIGHT       (M) :   2.00    2.00    2.00    2.00    2.50    2.50    2.50    2.50    3.00    3.00
SWELL INCD.ANG.  (DEG) :   40.0   220.0    40.0   220.0    40.0   220.0   220.0    40.0   220.0    40.0
RUDDER ANGLE     (DEG) :    1.0     1.0     1.0     1.0     1.0     1.0     1.0     1.0     1.0     1.0
DRIFT  ANGLE     (DEG) :    0.2     0.2     0.2     0.2     0.2     0.2     0.2     0.2     0.2     0.2

CORRECTION METHOD OF ADDED RESISTANCE :
-------------------------------------------------------------------------------
* SEA WAVE AND SWELL          2 : SEA WAVE AND SWELL
* EFFECT OF SHIP MOTION       1 : MARUO METHOD
* EFFECT OF WAVE DIFFRACT.    1 : FALTINSEN METHOD
* EFFECT OF STEERING          1 : SR208 METHOD
* EFFECT OF DRIFTING          1 : SR208 METHOD
* EFFECT OF HULL ROUGHNESS    1 : ITTC METHOD
* EFFECT OF PROP.ROUGHNESS    1 : ITTC METHOD
* EFFECT OF SHALLOW WATER     1 : LACKENBY METHOD
* EFFECT OF DISPLACEMENT      1 : FACTOR 0.65 METHOD
* EFFECT OF TEMP.& DENSITY    1 : ITTC METHOD
* EFFECT OF CURRENT           1 : INPUT SPEED
* WIND RESISTANCE COEFF.    B07 : TANKER, LOADED FROM BLENDERMANN CHART

-------------------------------------------------------------------------------


-------------------------------------------------------------------------------
RUN NUMBER             :     1       2       3       4       5       6       7       8       9      10
-------------------------------------------------------------------------------

STEP I : EVALUATION OF ACQUIRED DATA
-------------------------------------------------------------------------------
SHIP SPEED      (KNOT) :  8.570  10.810  11.760  13.960  14.030  15.710  16.360  15.110  16.400  15.400
DELIVERED POWER   (PS) :  7541.   7306.  14986.  14709.  21391.  21377.  24203.  24428.  26086.  25682.
PROPELLER REV.   (RPM) :  43.90   43.80   55.60   55.60   62.80   62.80   65.60   65.70   67.00   66.80
TORQUE COEFFICIENT     : 0.2844  0.2775  0.2782  0.2731  0.2756  0.2754  0.2736  0.2749  0.2768  0.2749
PROP.ADVANCE RATIO     : 0.6121  0.6271  0.6255  0.6365  0.6311  0.6315  0.6354  0.6327  0.6286  0.6325
WAKE FRACTION          : 0.0349  0.2178  0.0897  0.2197  0.1305  0.2230  0.2158  0.1533  0.2095  0.1555
THRUST DEDUCTION       : 0.1300  0.1300  0.1300  0.1300  0.1300  0.1300  0.1300  0.1300  0.1300  0.1300
LOAD FACTOR            : 0.4948  0.4548  0.4590  0.4315  0.4447  0.4438  0.4341  0.4408  0.4510  0.4412
SHIP RESISTANCE   (KN) :  720.2   691.7  1119.0  1089.1  1408.1  1406.8  1520.1  1535.2  1612.6  1587.6

STEP II : CORRECTION FOR VARIOUS RESISTANCE INCREASE
-------------------------------------------------------------------------------
MOTION,SEA WAVE   (KN) :    0.0     0.0     0.0     0.0     0.0     0.0     0.0     0.0     0.0     0.0
MOTION,SWELL      (KN) :    0.9    92.8     7.3   101.6    17.9   123.9   119.3    17.6   171.4    24.2
```

```
DIFFRACT,SEA WAVE(KN):    28.1    0.0   33.9    0.0   38.1    0.0    0.0   12.7    0.0   12.9
DIFFRACTION,SWELL(KN):     0.0   48.9    0.0   54.1    0.0   71.9   73.2    0.0  105.5    0.0
DIRECT.C. FOR WIND   :   0.850 -0.623  0.850 -0.547  0.850 -0.640 -0.547  0.850 -0.623  0.850
WIND EFFECT      (KN):   107.4   -6.9  132.6   -3.0  150.9   -0.2   -0.1  160.5    0.0  160.4
STEERING EFFECT  (KN):     0.5    0.7    0.9    1.1    1.2    1.4    1.6    1.4    1.6    1.4
DRIFTING EFFECT  (KN):     0.1    0.1    0.1    0.2    0.2    0.2    0.2    0.2    0.2    0.2
HULL ROUGHNESS   (KN):    13.2   21.0   24.8   34.9   35.3   44.3   48.0   40.9   48.2   42.5
DISPLACEMENT     (KN):    -4.7   -4.5   -7.3   -7.1   -9.2   -9.1   -9.9  -10.0  -10.5  -10.3
TEMP.DENS.K-VISC.(KN):    -6.1   -9.3  -10.8  -14.8  -14.9  -18.3  -19.7  -17.1  -19.8  -17.7
TOTAL RES.INCR.  (KN):   139.4  142.8  181.5  167.1  219.5  214.1  212.7  206.3  296.8  213.7
LOAD FACTOR DIFFERENT:  0.0957 0.0939 0.0744 0.0662 0.0693 0.0675 0.0607 0.0592 0.0830 0.0594
CHANGED LOAD F. TAUPV:  0.3991 0.3609 0.3845 0.3653 0.3754 0.3763 0.3733 0.3816 0.3680 0.3818
CHANGED ADVC.R.  JQSV:  0.6502 0.6672 0.6564 0.6652 0.6605 0.6601 0.6614 0.6577 0.6639 0.6576
CHANGED REV.(RPM)  NV:   41.33  41.17  52.98  53.20  60.01  60.08  63.02  63.20  63.44  64.25
CHANGED TORQUE C. KQV:  0.2666 0.2582 0.2635 0.2592 0.2615 0.2617 0.2611 0.2629 0.2599 0.2629
FAIRED TORQUE C. KQFV:  0.2620 0.2621 0.2614 0.2614 0.2617 0.2617 0.2619 0.2620 0.2621 0.2621
PROP.ADVC.RATIO   JTV:  0.6581 0.6581 0.6594 0.6594 0.6588 0.6588 0.6583 0.6583 0.6580 0.6580
LOAD FACTOR     TAUTV:  0.3816 0.3817 0.3788 0.3788 0.3801 0.3801 0.3812 0.3813 0.3819 0.3818
SHIP SPEED (KNOT)  VV:   9.243 11.380 12.439 14.510 14.694 16.444 17.003 15.772 17.222 16.072
DELIV.POWER  (PS) PDV:   6947.  6900. 14080. 14080. 20311. 20311. 23173. 23280. 24703. 24480.
PROPELLER REV.(RPM)NS:   43.90  43.80  55.60  55.60  62.80  62.80  65.60  65.70  67.00  66.80

STEP III : CORRECTION FOR CURRENT
---------------------------------------------------------------------------

CURRENT S.SPEED(KNOT):  10.253 10.370 13.429 13.520 15.534 15.614 16.403 16.372 16.692 16.602
CURRENT ADVC.RATIO   :  0.6581 0.6581 0.6594 0.6594 0.6588 0.6588 0.6583 0.6583 0.6580 0.6580
CURRENT WAKE FRACTION:  0.1327 0.1445 0.1597 0.1653 0.1802 0.1844 0.1897 0.1869 0.1871 0.1851

STEP IV : CORRECTION FOR WIND RESISTANCE DUE TO SELF SPEED
---------------------------------------------------------------------------

DIRECT.C. SELF WIND  :   0.940  0.940  0.940  0.940  0.940  0.940  0.940  0.940  0.940  0.940
WIND RESISTANCE  (KN):   -18.1  -18.5  -31.1  -31.5  -41.6  -42.0  -46.4  -46.2  -48.0  -47.5
THRUST DEDUCTION,WIND:  0.1300 0.1300 0.1300 0.1300 0.1300 0.1300 0.1300 0.1300 0.1300 0.1300
LOAD FACTOR DIFFERENT:-0.0108-0.0111-0.0115-0.0116-0.0121-0.0122-0.0123-0.0123-0.0123-0.0122
CHANGED LOAD F. TAUPA:  0.3924 0.3928 0.3903 0.3904 0.3921 0.3923 0.3935 0.3935 0.3942 0.3940
CHANGED ADVC.R.  JQSA:  0.6531 0.6529 0.6540 0.6539 0.6532 0.6532 0.6526 0.6526 0.6523 0.6524
CHANGED REV.(RPM)  NA:   41.15  42.07  53.18  54.11  60.67  60.72  63.87  63.69  64.56  64.76
CHANGED TORQUE C. KQA:  0.2645 0.2646 0.2640 0.2641 0.2644 0.2645 0.2647 0.2647 0.2648 0.2648
FAIRED TORQUE C. KQFA:  0.2643 0.2643 0.2641 0.2641 0.2646 0.2646 0.2649 0.2650 0.2651 0.2651
PROP.ADVC.RATIO   JTA:  0.6534 0.6534 0.6538 0.6538 0.6528 0.6528 0.6522 0.6521 0.6518 0.6518
LOAD FACTOR     TAUTA:  0.3920 0.3920 0.3911 0.3911 0.3934 0.3934 0.3949 0.3949 0.3957 0.3956
SHIP RES.    (KN) RTA:   649.7  646.7 1040.8 1040.8 1331.4 1331.4 1455.3 1459.8 1519.6 1510.3
SHIP SPEED (KNOT)  VA:  10.176 10.293 13.310 13.400 15.386 15.465 16.243 16.212 16.526 16.438
DELIV.POWER  (PS) PDA:   7008.  6960. 14226. 14226. 20538. 20538. 23438. 23547. 24989. 24763.
PROPELLER REV.(RPM)NS:   43.90  43.80  55.60  55.60  62.80  62.80  65.60  65.70  67.00  66.80

STEP  V : CORRECTION FOR SHALLOW WATER EFFECT
---------------------------------------------------------------------------

SHIP S.,SHALLOW(KNOT):  10.190 10.307 13.324 13.414 15.399 15.478 16.256 16.225 16.540 16.452
```

5 CONCLUSIONS

The structure of the computer program for speed trial analysis are presented. It is made according to the ISO/DIS 15016 entitled "Guidelines for the assessment of speed and performance by analysis of speed trial data". In this computer program, various analysis methods for resistance increase due to ship motion, wave diffraction, wind, steering, drifting, water temperature and salt content, deviation of displacement, hull and propeller surface roughness, and shallow water effects are contained. The computer program is constructed to optimize the structure, to emphasize the graphic function and to implement the GUI at WINDOWS environment.

For the comparison with the example of ISO/DIS 15016, the present results of resistance increase due to waves showed small difference with the example. It needs further cooperative study of the components of resistance increase due to waves for various hull forms, loading conditions, heading angles and ship speeds using same input data

TABLE 3

COMPARISON OF THE RESULTS OF RESISTANCE INCREASE DUE TO WAVES

Resistance(KN)	Speed (knots)	8.57	10.81	11.76	13.96	14.03	15.71	16.36	15.11	16.40	15.40
Present Program	Motion, Sea Wave	0	0	0	0	0	0	0	0	0	0
	Motion, Swell	1	93	7	102	18	124	119	18	171	24
	Diffract, Sea Wave	28	0	34	0	38	0	0	13	0	13
	Diffract, Swell	0	49	0	54	0	72	73	0	106	0
	Total	29	142	41	156	56	196	192	31	277	37
ISO Example	Total	31	119	31	107	31	183	180	8	265	8

References

Blendermann, W. (1990,1990,1991). Chapter 3.1 External Forces, Wind Forces of Manoeuvring Technical Manual, *Schiff & Hafen* **1990:2**, 41-43, **1990:3**, 55-58, **1991:4**, 39-41

Faltinsen, O. M., Minsaas, K. J., Liapis, N. & Skjordal, S. O. (1980). Prediction of resistance and propulsion of a ship in a seaway, *Proceedings 13th ONR*, 505-529

Fujii, H. & Takahashi, T. (1975). Experimental study on the resistance increase of a large full ship in regular oblique waves, *Journal of SNAJ* **137**, 132-137

Hong, D. C., Hong, S. Y. & Kim, E. C. (2001). On the Calculation of Added Resistance of a Ship by Maruo's Formula, *Proceedings of Korea Committee for Ocean Resources and Engineering 2001*

ISO/TC8 (2000). *Guidelines for the Assessment of Speed and Power Performance by Analysis of Speed Trial Data,* Draft International Standard ISO/DIS 15016

ITTC Performance Committee (1978). Report of Performance Committee, *Proceedings 15th ITTC*

ITTC performance Committee (1984) Report of Performance Committee, *Proceedings 17th ITTC*

Kwon, Y. J. (1982). *The Effect of Weather, Particularly Short Sea Waves, on Ship Speed Performance*, Ph.D Thesis of University of Newcastle upon Tyne, UK

Lackenby, H. (1963). The Effect Shallow Water on Ship Speed, *Shipbuilder* **70:672**

Maruo H.(1960). On the increase of the resistance of a ship in rough seas(2nd report), *Journal of SNAJ* **108**

Taniguchi, K. & Tamura, K. (1966). On a New Method of Correlation for Wind Resistance Relating to the Analysis of Speed Trial Result, *Appendix 11 of the Performance Committee Report of 11th ITTC*, Tokyo, 144-149

Townsin, R. L., Kwon, Y. J., Baree, M. S. & Kim, D. Y. (1993). Estimating the influence of weather on ship performance, *Transaction RINA* **135**, 191-209

Practical Design of Ships and Other Floating Structures
You-Sheng Wu, Wei-Cheng Cui and Guo-Jun Zhou (Eds)
© 2001 Elsevier Science Ltd. All rights reserved

A TEST PROCEDURE AND EVALUATION METHOD FOR SEAKEEPING TRIALS WITH ADDRESS TO BROACHING-TO

Olov Lundbäck

Naval Architecture, KTH, S-100 44, Stockholm, Sweden

ABSTRACT

Modern semiplaning hulls often suffer from broaching-to and problems with manoeuvring in following seas. The aim of the presented work is to develop a method to assess the manoeuvring characteristics of a ship in following sea, e.g. if the ship is able to steer in a certain sea condition. A test procedure and a method for evaluating test data from trials in following sea have been developed. The presented method is used to calculate forces that the waves exert on the ship, using measurement data as input. In order to do this a two dimensional manoeuvring equation has been employed. The calculated wave forces seems to be of a reasonable magnitude.

KEYWORDS

Broaching-to, Following sea, Measurements, Manoeuvring, Waves, Semi planing, Full scale, Free running.

1 INTRODUCTION

Modern fast ships are often imposed to difficulties of manoeuvring combined with resonant or excessive rolling in following seas. These problems are usually addressed as Broaching-to. The problems are most common for ships able to operate at $F_n>0.3$ and with a length less than 150m. In this category there is a wide variety of ships, for example fast ferries for transport of passengers and cars; pilot boats and patrol crafts. The Navies in Finland and Sweden are using a large number of small fast craft and have consequently experienced problems concerning manoeuvring and seakeeping in following sea. Hence, a co-operative research programme in Finland and Sweden has been initiated. The aim of the first part of the programme is to find test procedures that could be used to evaluate the characteristics of a ship or model in following sea. A method for evaluating test data has also been tried out.

This paper presents a part of the work with full scale and model trials in Sweden. The present work is a continuation of the work presented by Lundbäck & Rutgersson (2000), where standard manoeuvring tests were performed in waves.

The presented evaluation method use manoeuvring equations in combination with test data to calculate the wave induced forces. The approach is similar to the one used by Nomoto (1966), but here terms considering wave forces have been added to the equations. Manoeuvring trials are performed in calm water to determine manoeuvring coefficients. Data from seakeeping trials in following sea are then used to determine the influence from the waves on the manoeuvring of the ship.

To assess the ship's controllability the wave-induced forces are compared to the force that the rudder can produce.

2 METHOD FOR CALCULATION OF WAVE FORCES

We want a method to assess the forces that the waves exert on the ship. To do this we use measurements. For full-scale trials it is most convenient to use a dynamic model, using measurement data as input and hereby assess the forces on the ship. In calm water the method used by Nomoto (1966) is shown to be successful for evaluating data from free running tests. This method takes into account manoeuvring equations of yaw and sway. But the sway is eliminated by an algebraic procedure. Hence only the yaw velocity and its time derivatives are left as degrees of freedom for the ship. This is a strong advantage, because the yaw rate and its derivatives are almost orthogonal or have a large difference in frequency content. This makes it possible to determine the coefficients in the dynamic equation by data analysis. Other forms of equations for describing the dynamics would need a very difficult data analysis, if possible at all, to determine the coefficients of the equations.

For slow manoeuvres we can use the following linear equations that describes the sway and yaw:

$$m(\dot{v} + u \cdot r) = Y_{\delta}\delta + Y_{v}v + Y_{\dot{v}}\dot{v} + Y_{r}r + Y_{\dot{r}}\dot{r} \tag{1}$$

$$I_{zz}\dot{r} = N_{\delta}\delta + N_{r} + N_{\dot{r}} + N_{v}v + N_{\dot{v}}\dot{v}$$

The notations are described in the section "nomenclature".

By adding terms accounting for the waves and eliminating the sway velocity. the following equation is obtained:

$$k_1\ddot{r}(t) + k_2\dot{r}(t) + r(t) + k_3\dot{\delta}(t) + k_4\delta(t) + N_w(t) = 0\,, \tag{2}$$

where the following yields for N_w:

$$N_w(t) = k_5\dot{y}_w(t) + k_6 y_w(t) + k_7\dot{n}_w(t) + k_8 n_w(t)\,. \tag{3}$$

These equations are deduced in appendix. In following sea generally and in the context of broaching particularly we consider only low frequencies of encounter, i.e. $\omega_e \to 0$. This means that the terms $\dot{y}_w(t), \dot{n}_w(t) \to 0$. From calm water trials we know the coefficients k_1, k_2, k_3 and k_4. In the seakeeping trials r and δ are measured. This means that a sum of the yawing moment and sway force can be determined. This sum is the wave induced generalised force, denoted N_w and takes the form

$$N_w(t) = k_6 y_w(t) + k_8 n_w(t)\,. \tag{4}$$

N_w can be compared to the maximum generalised force that the rudder can produce in order to check whether the ship is able to steer or not. This is described in the section "criteria".

3 TEST PROCEDURE

Tests are performed in both calm water and in waves. The calm water tests are used to determine the coefficients k_1,..,k_4 in Eqn. 2. Then data from seakeeping tests in following sea are used in combination with Eqn. 2. to calculate the generalised force, N_w that the waves exert on the vessel.

In calm water two types of tests are performed, first circle tests or spiral tests are performed, secondly zig-zag tests are performed. The circle tests are performed keeping the rudder angle constant, then all terms in Eqn. 2. that contain time derivatives are approaching zero after some time. This means that the coefficient k_4 of Eqn. 2. can be uniquely determined.

The zig-zag test is a way of oscillating the ship in the horizontal plane. This test is described in e.g. Lewis (1989). Zig-zag tests are used to determine all coefficients in Eqn. 2. except k_4, which is determined by circle tests. In this work system identification by the least square method has been used to determine these coefficients. Trials are carried out at different speeds to account for speed dependency of the coefficients in Eqn. 2. It was found that the frequency of the steering oscillation affects the accuracy of the coefficients. In the present work a rudder angle of 15° and a course deviation of 5° have been used and were found to give good results.

Sea keeping tests are carried out by setting a course of 30°-60° relative to the waves, when the right course is reached the helmsman tries to keep the course as constant as possible.

4 CRITERIA

Assume that a broaching situation is a relatively slow process so that it can be considered as quasi static. This will lead to that $r, \dot{r}, \ddot{r}, \dot{\delta} \rightarrow 0$. Then Eqn. 2. approaches the following:

$$k_4\delta(t) + N_w(t) = 0 \tag{5}$$

To be able to steer the ship, according to (5), the following relationship must be satisfied:

$$\left|k_4\delta_{\max}(t)\right| > \left|N_w(t)\right| \tag{6}$$

Where $\delta_{\max}$ is the maximum rudder angle or the angle at which the rudder is stalling. The relation (6) could be used as a criterion for steering ability in following sea at low frequencies of encounter. Depending on the maximum rate of change of rudder angle there could also be a need for a margin between $k_4\delta_{\max}$ and N_w.

In addition to (6) it could be convenient to use a criteria for the roll angle, which has been investigated by other projects, for example NORDFORSK (1987). The characteristics of the roll angle should be such that the ship can serve its purpose as a working platform or as means of transport.

5 CALCULATED GENERALISED FORCES

The method outlined above has been used to calculate wave forces for different ships and ship models. In this section two examples are shown from measurements on a patrol craft, which is 22.5m between the perpendiculars. The measurements have shown that the generalised force N_w is unambiguously increasing with the amplitude of the waves.

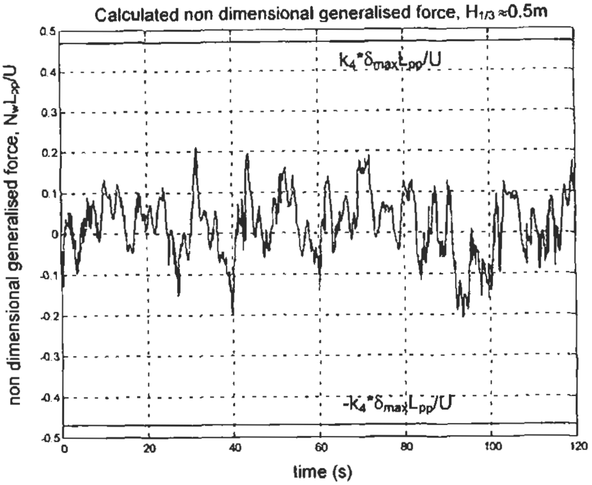

Figure 1: Calculated non dimensional generalised force for the patrol craft HMS Sandhamn at a significant wave height of approximately 0.5m, $F_n\approx0.4$.

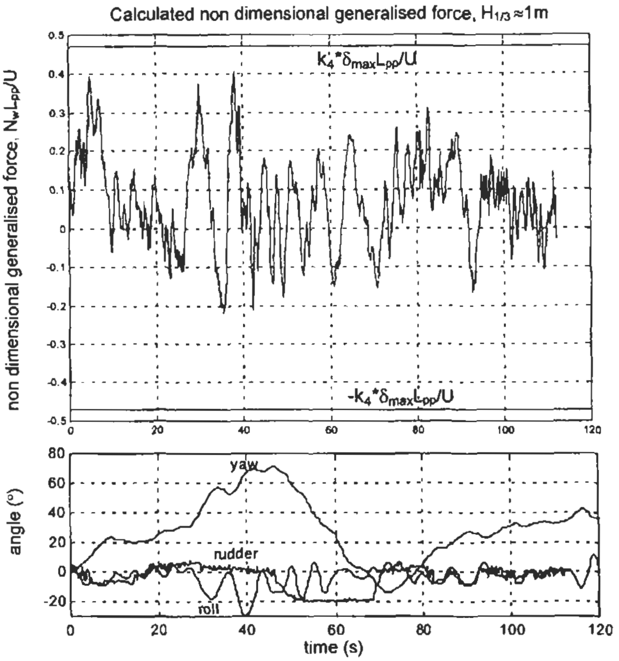

Figure 2: Calculated non dimensional generalised force for the patrol craft HMS Sandhamn at a significant wave height of approximately 1m, $F_n\approx0.4$ (during the first 40 seconds).

Figure 1 and Figure 2 show data from two different measurement occasions carried out in the waters outside of Malmö in Sweden. On the occasion shown in Figure 1, the weather was relatively calm and the ship could be manoeuvred without problems, the significant wave height was approximately 0.5m. On the occasion shown in Figure 2 the waves caused the ship severe manoeuvring problems and the captain decided to go directly back to the harbour at the time of the measurement, the significant wave height was 1m. The wave height was estimated by the captain of the ship. These values were compared to data from a nearby sited wave buoy. Data from the wave buoy and the estimation of the captain were in good agreement.

On the occasion with 0.5m waves there were no problems manoeuvring the ship, consequently there was a good margin between the generalised force N_w and the criteria limit $k_4\delta_{max}$.

On the occasion with 1m waves the ship was close to broach and the maximum of the generalised force, N_w approaches the limit $k_4\delta_{max}$. In agreement with the used criteria the ship is still possible to steer, but it is becoming very difficult to manoeuvre in a safe manner.

6 VALIDITY OF THE METHOD AND POSSIBLE IMPROVEMENTS

There could be problems using a linear model both in calm water and waves. In order to use a linear model the manoeuvres need to be "slow". A normal zig-zag manoeuvre that is used to determine the coefficients is rather fast. When the coefficients are determined in this way we could get an error because of non-linear effects. However the model and the test data show good agreement. But the agreement was improved by letting the hydrodynamic forces be a non-linear function. Polynomials up to 7th order have been tested. When using a polynomial of 7th order, the fitted data and the measured yaw rate were practically coinciding. However the higher order models have not been mathematically studied and proved. The tests in waves were performed by trying to keep the course as constant as possible. Then the yaw rates were quite low. This means that the error due to non-linear effects is small. An exception is when a broach occurs. Although, in full-scale such trials should be avoided due to safety reasons.

The sway force and yaw moment seem to be relatively well described by assuming that they only depend on motions in the sway and yaw directions. The accuracy of the calculated wave forces would probably be improved by accounting for the coupling between sway, roll and yaw. However accounting for the coupling between sway, roll and yaw would require tests for this purpose. Other degrees of freedom would be rather complex to handle, as it would require a difficult and yet uncertain data analysis. Further it is uncertain if the accuracy would be improved. We would also need very sophisticated measurement sensors to account for further degrees of freedom.

The hydrodynamic coefficients are assumed to be constant in the employed model. This is a rather large simplification, but from the test data this approximation does not seem to give too large errors. Depending on the way that the wave forces are defined, it can further be argued that the variation in the hydrodynamic coefficients should be included in the wave-induced forces. In the presented equation these effects are included.

The criterion for ability of steering is valid only at low frequencies of encounter. If the encounter frequency is high the assumptions are violated and it could be possible to control the ship even if the generalised force N_w is exceeding $k_4\delta_{max}$.

APPENDIX

Deducing a Linear Equation for Manoeuvring in Waves

Start with the two-dimensional linear manoeuvring equation. The notations are described in the section "nomenclature".

$$\begin{aligned} m(\dot{v}+u\cdot r) &= Y_{\delta}\delta+Y_{v}v+Y_{\dot{v}}\dot{v}+Y_{r}r+Y_{\dot{r}}\dot{r} \\ I_{zz}\dot{r} &= N_{\delta}\delta+N_{r}+N_{\dot{r}}+N_{v}v+N_{\dot{v}}\dot{v} \end{aligned} \tag{7}$$

Add terms representing the wave induced sway force (y_w) and yaw moment (n_w) to the equations, but assume that the hydrodynamic coefficients are constant also in waves.

$$\begin{aligned} m(\dot{v}+u\cdot r) &= Y_{\delta}\delta+Y_{v}v+Y_{\dot{v}}\dot{v}+Y_{r}r+Y_{\dot{r}}\dot{r}+y_{w} \\ I_{zz}\dot{r} &= N_{\delta}\delta+N_{r}+N_{\dot{r}}+N_{v}v+N_{\dot{v}}\dot{v}+n_{w} \end{aligned} \tag{8}$$

Laplace transformation of (8) gives the following:

$$\begin{aligned} &(Y_{\dot{v}}-m)v(0)+Y_{\dot{r}}r(0)+[(m-Y_{\dot{v}})s-Y_{v}]v(s)+(-Y_{\dot{r}}s+m\cdot u-Y_{r})r(s)-Y_{\delta}\delta(s)-y_{w}(s)=0 \\ &N_{\dot{v}}v(0)+(N_{\dot{r}}-I_{zz})r(0)+(-N_{\dot{v}}s-N_{v})v(s)+[(I_{zz}-N_{\dot{r}})s-N_{r}]r(s)-N_{\delta}\delta(s)-n_{w}(s)=0 \end{aligned} \tag{9}$$

We make the assumption that there is no motion initially i.e. v(0)=r(0)=0. Then the first terms of (9) vanish and the equation becomes:

$$\begin{aligned} &[(m-Y_{\dot{v}})s-Y_{v}]v(s)+(-Y_{\dot{r}}s+m\cdot u-Y_{r})r(s)-Y_{\delta}\delta(s)-y_{w}(s)=0 \\ &(-N_{\dot{v}}s-N_{v})v(s)+[(I_{zz}-N_{\dot{r}})s-N_{r}]r(s)-N_{\delta}\delta(s)-n_{w}(s)=0 \end{aligned} \tag{10}$$

Now we solve the "sway-equation" from (10) for v(s).

$$v(s)=\frac{(Y_{\dot{r}}s-mu+Y_{r})r(s)+Y_{\delta}\delta(s)+y_{w}}{(m-Y_{\dot{v}})s-Y_{v}} \tag{11}$$

Inserting (11) in the "yaw-equation" from (10) and multipling the equation by $(m-Y_{\dot{v}})s-Y_{v}$ gives:

$$\begin{aligned} &[((m-Y_{\dot{v}})s-Y_{v})(I_{zz}-N_{\dot{r}})s+(-N_{\dot{v}}s-N_{v})(Y_{\dot{r}}s-mu+Y_{r})-N_{r}((m-Y_{\dot{v}})s-Y_{v})]r(s) \\ &+[Y_{\delta}(-N_{\dot{v}}s-N_{v})-N_{\delta}((m-Y_{\dot{v}})s+Y_{v})]\delta(s)+(-N_{\dot{v}}s-N_{v})y_{w}(s)+[(m-Y_{\dot{v}})s-Y_{v}]n_{w}(s)=0 \end{aligned} \tag{12}$$

Then collect the terms in powers of s:

$$\begin{aligned} &\{[(m-Y_{\dot{v}})(I_{zz}-N_{\dot{r}})-N_{\dot{v}}Y_{\dot{r}}]s^{2}+[-Y_{v}(I_{zz}-N_{\dot{r}})-N_{\dot{v}}(-mu+Y_{r})-N_{v}Y_{\dot{r}}-N_{r}(m-Y_{\dot{v}})]s \\ &+N_{v}(mu-Y_{r})+N_{r}Y_{v}\}r(s)+[Y_{\delta}(-N_{\dot{v}}s-N_{v})-N_{\delta}((m-Y_{\dot{v}})s-Y_{v})]\delta(s) \\ &+(-N_{\dot{v}}s-N_{v})y_{w}(s)-[(m-Y_{\dot{v}})s-Y_{v}]n_{w}(s)=0 \end{aligned} \tag{13}$$

Perform an inverse Laplace transformation.

$$\begin{aligned} &[(m-Y_{\dot{v}})(I_{zz}-N_{\dot{r}})-N_{\dot{v}}Y_{\dot{r}}]\ddot{r}(t)+[-Y_{v}(I_{zz}-N_{\dot{r}})-N_{\dot{v}}(-mu+Y_{r})-N_{v}Y_{\dot{r}}-N_{r}(m-Y_{\dot{v}})]\dot{r}(t) \\ &+[N_{v}(mu-Y_{r})+N_{r}Y_{v}]r(t)+[-Y_{\delta}N_{\dot{v}}-N_{\delta}(m-Y_{\dot{v}})]\dot{\delta}(t)+[N_{\delta}Y_{v}-Y_{\delta}N_{v}]\delta(t)-N_{\dot{v}}\dot{y}_{w}(t) \\ &-N_{v}y_{w}(t)-(m-Y_{\dot{v}})\dot{n}_{w}(t)+Y_{v}n_{w}(t)+[Y_{v}-m]\dot{n}_{w}(t)=0 \end{aligned} \tag{14}$$

Or written in a shorter notation.

$$c_{1}\ddot{r}(t)+c_{2}\dot{r}(t)+c_{3}r(t)+c_{4}\dot{\delta}(t)+c_{5}\delta(t)+c_{7}\dot{y}_{w}(t)+c_{6}y_{w}(t)+c_{8}\dot{n}_{w}(t)+c_{9}n_{w}(t)=0 \tag{15}$$

where the coefficients $c_1,..,c_7$ can be identified from (14)

Divide eq. (15) by c_3. Then the equation can be written as follow:

$$k_{1}\ddot{r}(t)+k_{2}\dot{r}(t)+r(t)+k_{3}\dot{\delta}(t)+k_{4}\delta(t)+k_{5}\dot{y}_{w}(t)+k_{6}y_{w}(t)+k_{7}\dot{n}_{w}(t)+k_{8}n_{w}(t)=0 \tag{16}$$

Collect all terms that considers the waves in one term and call it N_w:

$$k_{1}\ddot{r}(t)+k_{2}\dot{r}(t)+r(t)+k_{3}\dot{\delta}(t)+k_{4}\delta(t)+N_{w}(t)=0$$

where the following yields for N_w:

$$N_{w}(t)=k_{5}\dot{y}_{w}(t)+k_{6}y_{w}(t)+k_{7}\dot{n}_{w}(t)+k_{8}n_{w}(t)$$

7 CONCLUSIONS

- It seems as linear equations describing the yaw and sway work well to describe the course keeping in waves, except when the ship is subject to broaching-to. Further these equations can be used to analyse a zig-zag or circle test in calm water if the sway and yaw velocities are not too high.
- The proposed criterion for ability of steering appears to be reasonable. The ship behaviour is in good agreement with the criterion.
- It can be assumed that the hydrodynamic coefficients are constant.
- The method could be improved in some ways. Most interesting would be to include non-linear terms in the governing equation and to account for the roll-yaw-sway-coupling.

Nomenclature

m = mass

I_{zz} = yaw moment of inertia

t= time

v = sway velocity

r = yaw velocity

δ = rudder angle

y_w = wave induced sway force

n_w = wave induced yaw moment

Y = hydrodynamic sway force

N = hydrodynamic yaw moment

$Y_\delta = \frac{\partial Y}{\partial \delta}$

$Y_v = \frac{\partial Y}{\partial v}$

$Y_{\dot v} = \frac{\partial Y}{\partial \dot v}$

$Y_r = \frac{\partial Y}{\partial r}$

$Y_{\dot r} = \frac{\partial Y}{\partial \dot r}$

$N_\delta = \frac{\partial N}{\partial \delta}$

$N_r = \frac{\partial N}{\partial r}$

$N_{\dot r} = \frac{\partial N}{\partial \dot r}$

$N_v = \frac{\partial N}{\partial v}$

$N_{\dot v} = \frac{\partial N}{\partial \dot v}$

N_w = wave induced generalised force

s= frequency parameter

F_n= Froude's number

U=absolute value of ship speed

References

Lewis E. V., Ed. (1989). Principles of Naval Architecture Vol. III, The Society of Naval Architects and Marine Engineers.

Lundbäck, O., Rutgersson, O. (2000). Full Scale Trials for Use in the Prediction of Broaching-to, *Proc. of 7th International Conference on Stability of Ships and Ocean Vehicles 2000*, Launceston, Australia, **Vol A**, 481-491.

Nomoto K. (1966). Researches on the Manoeuvrability of Ships in Japan, The Society of Naval Architects of Japan.

NORDFORSK (1987). Assessment of Ship Performance in a Seaway, NORDFORSK, Copenhagen, Denmark

Practical Design of Ships and Other Floating Structures
You-Sheng Wu, Wei-Cheng Cui and Guo-Jun Zhou (Eds)
© 2001 Elsevier Science Ltd. All rights reserved

EXPERIMENTAL INVESTIGATION OF BANK EFFECTS UNDER EXTREME CONDITIONS

D.-Q. Li, M. Leer-Andersen, P. Ottosson and P. Trägårdh

SSPA Sweden
P O Box 24 001, SE-400 22 Göteborg, Sweden

ABSTRACT

Experiments on bank effects in extreme conditions were carried out for three ships: a low speed displacement tanker, a mono-full ferry and a catamaran. The last one is a large high-speed craft. Five long bank models were tested. The influence of propeller loading on bank effects and the wave pattern during bank passage were also studied. For the tanker, results indicated that there is a critical water depth to draught ratio (*h/T*) approximately 1.10, where the sway force changes from a suction force to a repulsion force. It was found that the sway force and the yaw moment are not always proportional to ship speed squared. A working propeller induces a suction force and a bow-away moment. In the wave systems created by the tanker and the ferry, Bernoulli wave is significantly magnified and dominant. Interaction between Bernoulli wave and wash waves was observed in the catamaran's wave system.

KEYWORDS

Bank effects, Sway force, Yaw moment, Wash wave, Bernoulli wave, Propeller loading.

1 INTRODUCTION

When a ship manoeuvres parallel and in close proximity to the wall of a quay or a canal, a hydrodynamic interaction between the ship and the wall, known as *Bank Effect*, occurs. Usually it is a low-speed displacement ship that encounters bank effect. Research has thus been focused primarily on *low-speed ships* in the past. With the contemporary trend in building high-speed vessels of ever-increasing size, however, bank effects also occur with *large high-speed* ships. The increase in ship size reduces the margin between the ship and the bank. In other words, ships today are being operated more often under extreme conditions. For example, operating a ship in shallow water with a keel clearance of 10% of draught is not unusual today. Since the behaviour of fast ships when passing banks has not been tested before, there is a need to identify their characteristics in these situations.

SSPA conducted many research studies on bank effects during 1970s, see Norrbin (1970 & 1975). The earlier work, performed with simplified bank models and low-speed ships, showed that a ship is subjected to a suction force and a bow-away moment. Further, these hydrodynamic loads were believed to be proportional to the square of speed. Recent experiments, however, have shown that this is not always true, see Dand (1981) and Vantorre (1995). If a ship is passing a bank in very shallow water (e.g. $h/T < 1.15$) and is close to the bank, the sway force changes direction and becomes a repulsive force pushing the ship away from the bank. This means that a somewhat different manoeuvre must be performed in this case, as compared with the case where the ship experiences a suction force. It is important to understand bank effects and thereby to plan suitable manoeuvres in extremely shallow and constrained water.

In the present work, the experiments were conducted with three ship models: a tanker, a mono-hull ferry and a catamaran ferry. The last one is of the large high-speed craft type, whose response to bank effects has not been tested before and whose waves have been reported to cause serious impact along coastal lines. With this in mind the waves generated by ships during bank passage were measured. The focus for the tanker and the ferry was on extreme shallow water and near bank cases, while for the catamaran it was on high-speed conditions. Principal results are presented here while the complete report is found in Li (2000).

2 TEST ARRANGEMENT AND PROGRAM

The bank models include a vertical bank, a sloping bank with a 30° inclination, and three flooded banks. All are 25 meters long to enable stationary results to be acquired. Table 1 gives the main ship dimensions and a summary of the test conditions. Banks are placed on the port side, i.e., a negative sway force Y means a suction. The variables measured were speed; trim; resistance; roll moment; sway force; yaw moment; wave heights at 5 transversal locations; and pressure on the wall and the bottom.

TABLE 1

MAIN DIMENSIONS AND THE TEST CONDITIONS

	Main dimension			Test conditions			
	Tanker	**Ferry**	**Catamara**	**Parameters**	**Tanker**	**Ferry**	**Catamaran**
Scale	1:46.25	1:37.5	1:40.0	Fn	0.04 ~ 0.13	0.05 ~ 0.17	0.16 ~ 0.69
L_{pp}[m]	5.146	4.965	1.723	h/T	1.06,1.12,1.2,1.4 17	1.1, 1.2, 2.5	1.1, 1.5, 2.5
B [m]	0.930	0.773	0.105	y/B	-0.6 ~ -1.5	-0.6, -1.2, -2.5	-0.5, -1.2, -2.5
T [m]	0.292	0.165	0.084	self-propelled	at 3 loadings	-	-
C_B [-]	0.816	0.695	0.466	Bank slope α	30 ° & 90 °	30 °	30 °

3 SWAY FORCES AND YAW MOMENTS

3.1 Influence of Ship Speed Fn

The sway force coefficient Y' and the yaw moment coefficient N' of the tanker passing the vertical bank at different h/T and ship-bank distances y/B are plotted against Froude number F_n in Figure 1. It is seen that the relationship proposed by the earlier researchers that Y and N vary with U^2, did not always hold in the current study. This is especially true in very shallow water (e.g. $h/T < 1.10$). Even at a moderate water depth $h/T = 1.4$, the Y' seemed to increase with speed to an order higher than two. This observation agreed with that by others, e.g., Vantorre (1995) and Dand (1981). Another interesting phenomenon found here was that the Y' was a repulsive force at h/T=1.06. This phenomenon began to be apparent at F_n=0.085, h/T=1.12 and y/B=-0.6.

The change of sign of the sway force appears to closely depend on two variables, namely the water depth and the ship speed. It is believed that there is a large stagnation area between the bank and the fore part of hull in this case which produces higher pressure on the near bank side and results in an integrated repulsive force and a large bow away moment. The repulsion phenomenon in bank effects resembles very much an airplane's Wing In Ground (WIG) effects.

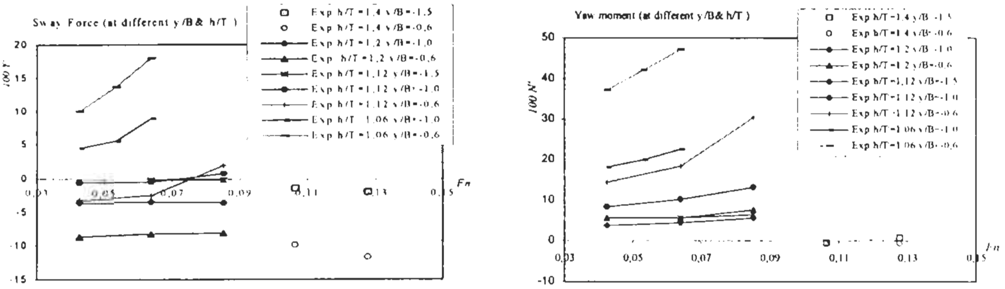

Figure 1: *Y′* (left) & *N′* (right) vs. *Fn* at different *h/T* and *y/B*, tanker with vertical bank

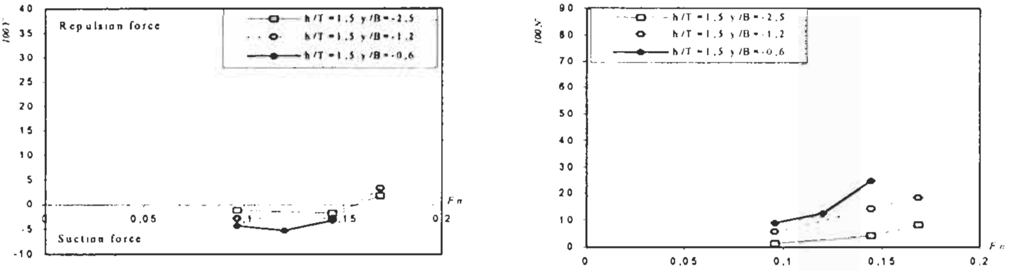

Figure 2: The *Y′* and *N′* as function of F_n at *h/T* = 1.5, ferry model with sloping bank

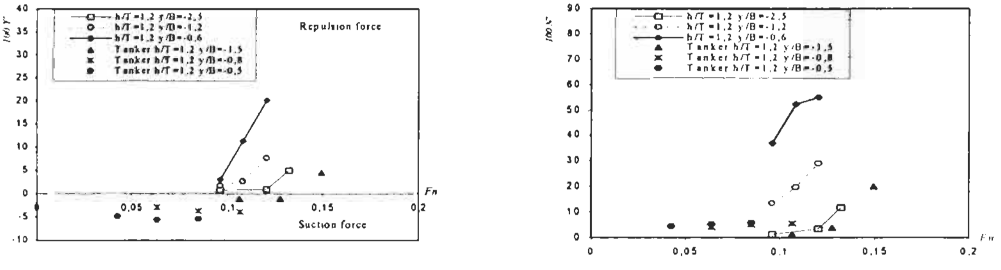

Figure 3: The *Y′* and *N′* vs. F_n at *h/T* = 1.2, ferry model compared with Tanker model, sloping bank

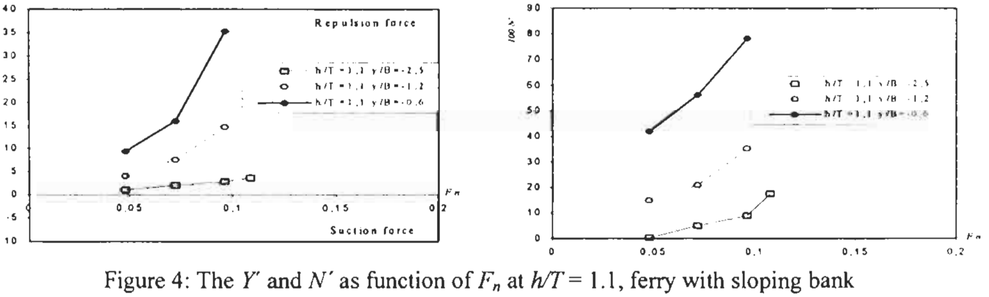

Figure 4: The *Y′* and *N′* as function of F_n at *h/T* = 1.1, ferry with sloping bank

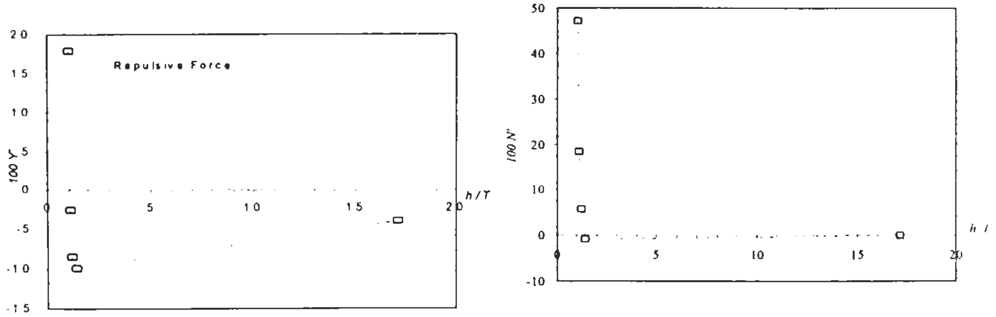

Figure 7: Y' and N' versus h/T at Fn=0.06 and y/B=-0.6, tanker with vertical bank

3.4 *Influence of Propeller Loading C_T*

Figure 8 shows an example where Y' and N' vary with the propeller loading coefficient C_T.

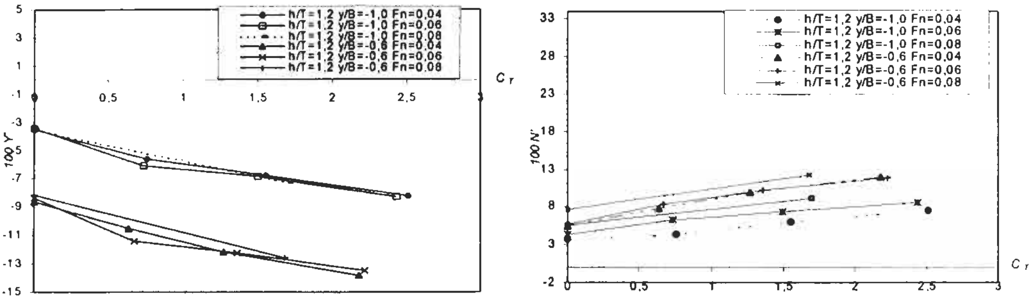

Figure 8: The Y' and N' variation with the propeller loading coefficient C_T at h/T=1.2

It is clear that a rotating propeller contributes to an additional suction force and a bow-away moment (compared with the case without a propeller, i.e. C_T= 0). The heavier the propeller loading, the larger the contribution. There seems to be a linear relation between the increment of Y' (and N') and C_T.

3.5 *Influence of Bank Inclination*

The sloping bank has a fixed inclination angle α=30°. The variations of Y' and N' values with speed for the tanker when passing the sloping bank were compared with those when passing the vertical bank at h/T=1.2 in Figure 9. It was found that:

- At low speeds, the Y' and N' values are less than those due to a vertical bank;
- At high speeds, significantly higher Y' and N' values are created compared with a vertical bank. Moreover, the Y' changes into a repulsion force at high speeds.

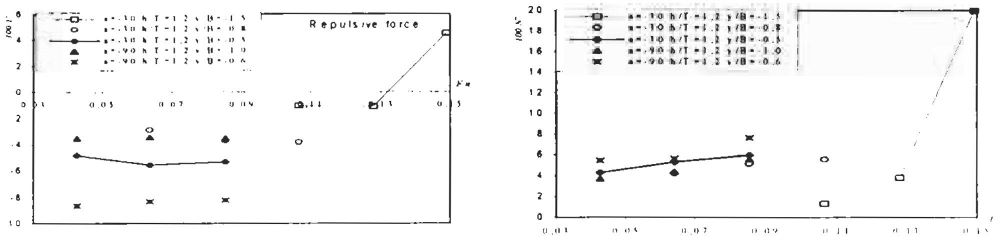

Figure 9: *Y′* and *N′* vs. *Fn*, comparison between the vertical and the sloping banks

4 WAVE MEASUREMENT

4.1 Waves by the Tanker Model

The wave elevations resulted from the tanker passing a vertical bank are depicted in Figure 10. The legend numbers in the figure are the wave gauge numbers. The wave on the port side is represented by No. 1 while the wave profiles on the starboard side are represented by Nos. 2~5. Furthermore, the wave heights and the x-positions are non-dimensionalised by ship length L_{pp}. As seen in the figure, large waves are observed on the starboard side and the port side (the near-bank side) of the hull, with the amplitudes on the port side substantially larger than those on the starboard side. This wave is a Bernoulli wave, whose amplitude is amplified so much that it becomes a dominant wave component.

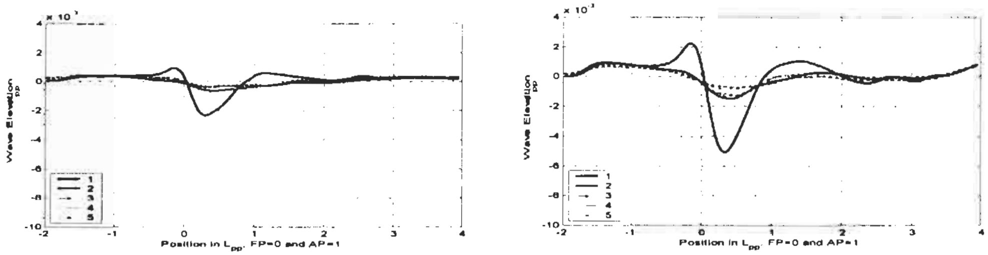

Figure 10: Waves at F_n = 0.06 (left) and 0.08 (right), tanker at *h/T* =1.2 and *y/B* =-0.6 with vertical bank

4.2 Waves by the Ferry Model

The waves created by the ferry are quite similar to those created by the tanker. They differ mainly forward of the bow, where a water level rise is noticed in the waves generated by the ferry.

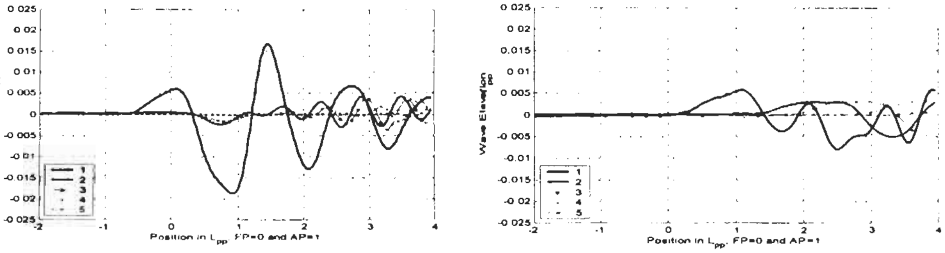

Figure 11: Waves by catamaran at F_{nh}=0.85 (left) and 1.99 (right) in *h/T*=2.5 & *y/B*=-1.2, sloping bank

4.3 Waves by the Catamaran Model

Waves generated by the catamaran take different forms at different speeds. Figure 11 shows the waves at a sub-critical speed (left) and a supercritical speed (right). At sub-critical speeds, the most significant and dominant wave is a Bernoulli wave occurring on the near-bank side, while on the free-water side the wash wave is dominant. At trans-critical speeds, the waves beside the hull are a mixture of Bernoulli waves and wash waves. At supercritical speeds, wash waves become most significant.

5 CONCLUSIONS

- The sway force and yaw moment vary with ship speed in a more complex manner, not necessarily proportional to the square of speed.
- The sway force will turn into a repulsive force when a ship is operated in extreme shallow water and close to bank in the same time. Both the sway force and the yaw moment can become surprisingly large in this case. If this occurs, a proper manoeuvre would be to run a small drift angle towards the bank side while also setting a rudder angle towards the bank side.
- The sloping bank with a 30° inclination reduces bank effects at low speeds but intensify bank effects at high speeds.
- A rotating propeller induces a suction force component to the sway force and a bow-away moment component to the yaw moment. The higher the propeller loading, the larger the contribution.
- The Bernoulli wave is amplified and becomes a dominant component in the waves caused by the tanker and the mono-hull ferry. Its impact should not be ignored in shallow water. Interaction between Bernoulli wave and wash waves was observed in the catamaran's wave system.

References

Ch'ng P.W. Doctors L.J. & Renilson M.R. (1993). A method of calculating the ship-bank interaction forces and moments in restricted water. *International Shipbuilding Progress* **40:421**, 7-23.
Dand I.W. (1981). On ship-bank interaction. *Transactions of RINA*, **124**.
Li D.-Q. (2000). Bank effects under extreme conditions. *SSPA report No. 20000028-1.*
Norrbin N.H. (1970). Theory and observations on the use of a mathematical model for ship manoeuvring in deep and confined waters, *Proc. 8th Symposium on Naval Hydrodynamics*, Canada.
Norrbin N.H. (1975). Manoeuvring in confined waters: Interaction phenomena due to side banks or other ships. *14th ITTC Appendix VIII __ Report of Manoeuvrability Committee.*
Vantorre M. (1995). Experimental study of bank effects on full form ship models. *Mini symposium on ship manoeuvrability*, Fukuoka, Japan,. 85-102.

List of symbols

L, B, T	length, breadth and draught of a ship
y	horizontal distance from ship centreline to the conjunction of bank wall and bottom (negative on the port side)
α	bank slope angle (90° on a vertical bank, positive on the starboard side)
Y	the sway force on the ship due to the bank effect, positive when pointing to starboard
N	the yaw moment on the ship due to the bank effect
Y'	the sway force coefficient, $Y' = Y/(\frac{1}{2}\rho U^2LT)$
N'	the yaw moment coefficient, $N' = N/(\frac{1}{2}\rho U^2LBT)$
F_{nh}	Froude number based on water depth, $F_{nh} = U/\sqrt{(gh)}$
C_T	propeller loading coefficient, $C_T = Tp/(\frac{1}{2}\rho D^2U^2)$

Practical Design of Ships and Other Floating Structures
You-Sheng Wu, Wei-Cheng Cui and Guo-Jun Zhou (Eds)
© 2001 Elsevier Science Ltd. All rights reserved

EFFECTS OF DIFFERENT THREE DIMENSIONAL FORMULATIONS ON THE SEAKEEPING COMPUTATIONS OF HIGH SPEED HULLS

D. Bruzzone[1], P.Gualeni[1] and L. Sebastiani[2]

[1]Department of Naval Architecture,University of Genova,
Via Montallegro,1 16145 Genova Italy
[2]CETENA Via Ippolito d'Aste, 5 16121 Genova Italy

ABSTRACT

The present interest in high speed hulls reflects also in their seakeeping performance so, with the aim to have proper methodologies to deal with this problem, the speed of advance must be taken into account by suitable methods. In this paper two different Green function formulations for the radiation and diffraction problems related to the evaluation of the wave induced motions, are comparatively studied. Both the involved methodologies are into the frequency domain. The first formulation is based on the Green function which analytically satisfies the Kelvin free surface condition taking into account the effects of the forward speed. The second formulation is based on the simpler Green function involved by a distribution of Rankine sources on the ship and on a portion of the free surface. The emphasis of the paper is directed toward the practical application of the foregoing methodologies to high speed vessels, so suitable hull forms for such vehicles are chosen, among which a round bilge hull of a frigate and an hard chine hull of a fast ferry. The results regarding the coefficients of equation of motion, the exciting forces and the responses are comparatively examined and discussed. It turns out that the proper speed effects into the free surface condition have significant influence on computed results and differences are evidenced in the results produced by the two formulations.

KEYWORDS

Fast marine vehicles, Seakeeping, Three dimensional methods, Green functions, Boundary elements.

1 INTRODUCTION

Notwithstanding strip theory can still be considered as the most spread practical computational tool for ship motion evaluation, algorithms based on three dimensional theories are gaining more and more consideration among designers. This fact may be considered as a consequence of the recently increased computing power, now available at lower costs, and of the refinement of these methodologies due to growing research and application cases. In principle, these methods, besides capturing all the three dimensional components of the flow, can properly allow for the speed effects in the free surface condition of the boundary value problems involved by the ship motion computations. It follows how this capability is particularly suitable in the field of high speed vehicles, where two dimensional methods might result as inadequate.

It can be stated that the solution of the boundary value problems for radiation and diffraction are developed following essentially two main approaches: one is based on the so called analytic Green function, the other is based on a simpler formulation involving only Rankine singularities.

From an historical point of view, the first method can be considered as the natural successor of the strip theory in that the Green function is extended from two to three dimensions, further accounting for the speed effects into the free surface condition; first applications were reported for instance by Chang (1997) and by Inglis and Price(1982). The latter methodology was born as the evolution towards the unsteady problem solution of a method originally introduced for the steady free surface waves evaluation, including wave resistance, see for example, Nakos and Sclavounos (1990).

The main problem of the first method has just been recognised as the difficulty in the evaluation of the forward speed effects which led to analytical instabilities in the integrands of the Green function formulation. It seems that recently proposed methodologies, like Brument and Delhommeau (1997), has satisfactory overcome this obstacle. On a similar methodology is based the code PRECAL, which has been used for part of the computed results presented in this paper. In addition to the complete forward speed Green function, the zero speed option has also been applied.
The second method here adopted (Bruzzone et al., 1997) allows also to consider basic steady flows , necessary for the solution of the unsteady problem, alternative to the free stream velocity, as the double model flow or the steady free surface flow (Bruzzone and Gualeni, 1999). On the contrary it requires an adequate additional representation of the free surface by panels and presents limitations at the lower reduced frequencies.

In the following, the basic features of the methodologies are briefly outlined and applications with a critical analysis of results are reported.

2 OUTLINE OF THE COMPUTATIONAL MODELS

The computation of the forces and motions requires the solution of a given set of boundary value problems. For their mathematical description a right-handed reference frame is chosen moving with the ship speed U, where the x axis coincides with the longitudinal waterline symmetry axis in still water and the z axis is positive upward. Assuming the usual hypothesis of irrotational flow, these problems can be stated in terms of a series of velocity potentials: six unknown radiation potential, one for each considered motion Φ_k $(k=1\text{-}6)$, a known incident wave potential Φ_I and a unknown diffraction potential Φ_7. In addition it is necessary to consider a steady potential. In the seakeeping problem, at a an increasing order of approximation, the latter can be generally chosen as the free stream potential Ux, the double model potential Φ_D or the steady free surface potential Φ_S, and is here generically indicated as "basis or reference potential" Φ_R.

If regular linear waves and linear responses are supposed, all the unsteady potentials $\Phi_I \div \Phi_7$ may be expressed in the form $\Phi_j = \varphi_j \exp(i\omega t)$ where ω is the frequency of encounter. Besides the Laplace equation in the fluid domain, a body boundary condition, a free surface boundary condition and a suitable radiation condition must be enforced. The body boundary condition may be written as:

$$\frac{\partial \varphi_k}{\partial n} = i\omega n_k + m_k \quad \text{for } k = 1,\dots,6 \text{ and } \quad \frac{\partial \varphi_7}{\partial n} = -\frac{\partial \varphi_I}{\partial n} \tag{1}$$

where n_k are the components of the generalised normal to the wetted hull surface : $(n_1, n_2, n_3) \equiv \mathbf{n}$, $(n_4, n_5, n_6) \equiv \mathbf{x}_b \times \mathbf{n}$; and m_k are defined as : $m_1, m_2, m_3 = -(\mathbf{n}\cdot\nabla)\nabla\Phi_R$ $m_4, m_5, m_6 = -(\mathbf{n}\cdot\nabla)(\mathbf{x}_b \times \nabla\Phi_R)$. with $\mathbf{x}_b$ representing a generic point on the hull.

The linearised free surface boundary condition requires, for each potential complex amplitude φ_j:

$$L(\varphi_j) = [-\omega^2 + g\frac{\partial}{\partial z} - 2i\omega\nabla\Phi_R\cdot\nabla + \nabla\Phi_R\cdot\nabla(\nabla\Phi_R\cdot\nabla) + \frac{1}{2}\nabla(\nabla\Phi_R\cdot\nabla\Phi_R).\nabla](\varphi_j) = 0 \tag{2}$$

When the complex amplitudes of the potentials have been determined the exciting forces F_j and the hydrodynamics coefficients $T_{jk} = -\omega^2 A_{jk} + i\omega B_{jk}$ may be determined according to the formulas:

$$F_j = \iint_{S_B} n_j(i\omega + \nabla\Phi_R\cdot\nabla)(\varphi_I + \varphi_7)dS \quad \text{and} \quad T_{jk} = \iint_{S_B} n_j(i\omega + \nabla\Phi_R\cdot\nabla)\varphi_k dS \tag{3}$$

in which S_B represents the body surface.

All the potentials are expressed in term of appropriate singularities. In the Green function method they are distributed only on the body surface and satisfy condition (2), in which Φ_R is the free stream potential $-Ux$. In the formulation adopted in the present paper, due to Bessho (1977), and incorporated into the PRECAL code, considering a singularity at $Q \equiv (x_0, y_0, z_0)$, we have for a field point $P \equiv (x,y,z)$:

$$G(\underline{x}, \underline{x}_0) = \frac{1}{4\pi}\left(\frac{1}{R_1} - \frac{1}{R_2}\right) - \frac{i}{2\pi}k_0 \int_{\alpha-\pi}^{\frac{\pi}{2}+\psi-i\varepsilon} \frac{k_1\exp(k_1 w) - \mathrm{sgn}(\cos(\mathrm{Re}(\theta)))k_2\exp(k_2 w)}{\sqrt{1+4\beta\cos\theta}}d\theta \tag{4}$$

with $R_1 = |P-Q|$, $R_2 = |P-Q^*|$, $Q^* \equiv (x_0, y_0, -z_0)$; $\psi = \cos^{-1}(X/\sqrt{X^2+Y^2})$; $\varepsilon = sinh^{-1}(|Z|/\sqrt{X^2+Y^2}$

$k_1 = \frac{1}{2\cos^2\theta}\left(1 + 2\beta\cos\theta - \sqrt{1+4\beta\cos\theta}\right)$ $\quad k_2 = \frac{1}{2\cos^2\theta}\left(1 + 2\beta\cos\theta + \sqrt{1+4\beta\cos\theta}\right)$

$w = Z + i(X\cos\theta + Ysin\theta)$, $\beta = U\omega/g$, $k_0 = g/U^2$, $X = k_0(x - x_0)$, $Y = k_0|y - y_0|$, $Z = k_0(z + z_0)$

$\alpha = \cos^{-1}(1/4\beta)$ for $\beta \geq 1/4$ $\quad \alpha = -i\cos^{-1}(1/4\beta)$ for $\beta > 1/4$

In the Rankine source approach, the various potentials are expressed as:

$$\varphi(P) = \int_{S_{F_0}+S_{H_0}} [1/R(P,Q)]\cdot\sigma(Q)\cdot dS(Q) \tag{5}$$

with $R(P,Q) = |P-Q|$. In this method, the steady potential may be indifferently assumed as one of the three alternatives listed before. Opposite to this higher flexibility in the enforcement of condition (2), it must be considered that the singularities must be distributed on the hull and on a portion of the still water surface. Due to the limited extension of this latter part, the radiation condition and the wave propagation are more difficult to deal with. In the present methodology (Bruzzone et al., 1997), flat panels are employed and their influence on the collocation points is computed according Hess and Smith (1967). The second order derivatives on the free surface are computed using a four point upstream operator in the longitudinal direction and an outward difference operator in the lateral direction. Only wave frequencies for which $\omega U/g > 0.25$ can be considered in the calculations.

3 APPLICATIONS AND RESULTS

With the aim of assessing the relative performance of such methodologies and in order to get insight for their correct application to high speed ships, two cases are considered here: a round bilge hull of a frigate, for which some experiments are reported in Gerritsma and Smith (1967), and a high speed ferry with an hard chine deep-vee hull with length L = 128.6 m at speeds V = 30 knots and V = 40 knots.

A panel representation of both the considered hulls is given in fig.1. All the computations have been carried out for head waves. Besides the 3-D methods, also a strip theory has been applied in order to assess and compare the different sensitivity among all the most widely used tools in seakeeping calculations.

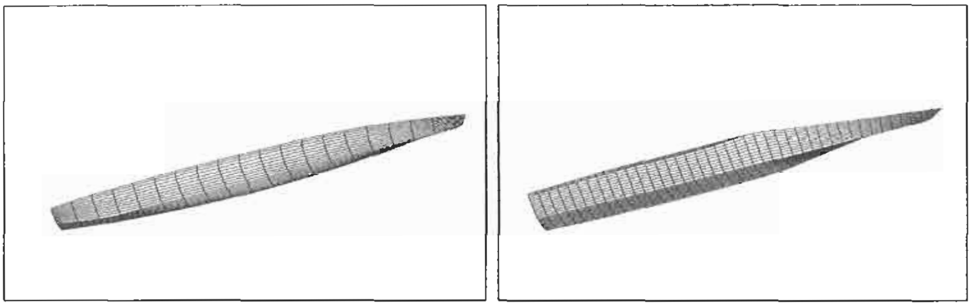

Figure 1: View of the grids for modelling the frigate hull (left) and the fast ferry hull (right)

To have a more significant comparison between the results from the formulations, only the free stream potential $-Ux$ has been considered as steady reference potential into the Rankine source method.

In fig. 2 the heave and pitch amplitude operators for the round bilge hull at Fn=0.45 are presented. It seems that the methods based on forward speed Green's function and Rankine sources overestimate the peak values. Appreciable differences between them are not noted as regard the heave motion, while for the pitch motion the Rankine source method fits better with experimental data.

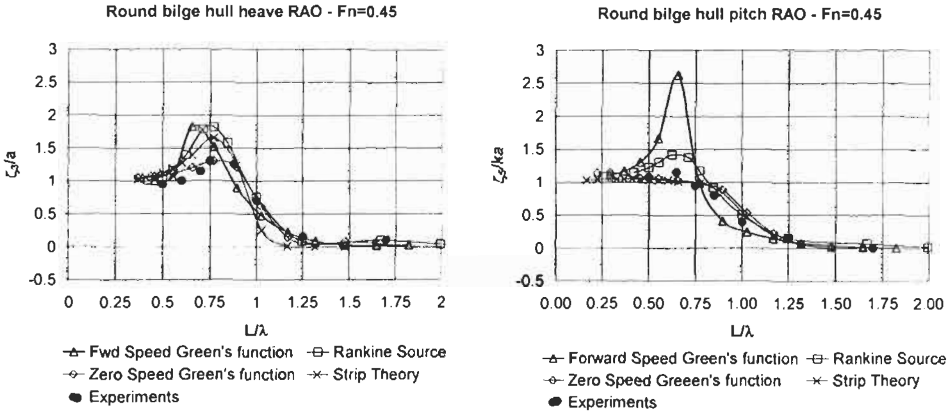

Figure 2: Heave and Pitch RAO for a round bilge frigate hull at Fn=0.45

In figure 3 the vertical motions transfer functions are presented for the hard chine hull. From the pitch motion operators at both speeds, it seems that all the methods capture the same peak frequency value. As far as the amplitude response is concerned, at the peak value, the methods based on the forward speed Green's function and on the Rankine sources give the highest value. When observing heave motion operators, it appears that strip theory and zero speed Green's function methods do not give evidence to any resonance, while both the forward speed Green's function and the Rankine source methods show the presence of peak frequency in the results. In this case the Rankine source method has the highest amplitude value and, moreover an oscillation for higher frequencies is observed, probably due to numerical problems, dealing with grid definition.

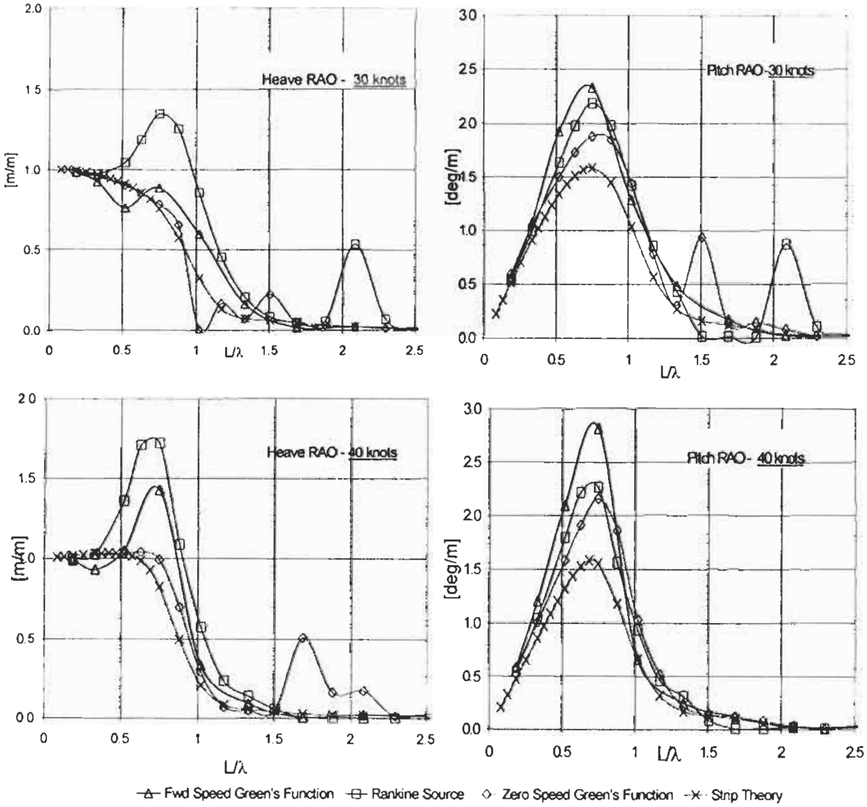

Figure 3: Heave and Pitch RAO for a fast monohull at 30 knots and 40 knots

An overall consideration about results could suggest that the capability to evaluate the forward speed effects can lead to substantial difference in significant results.

Diagonal added mass and damping coefficients for the fast monohull are presented versus non dimensional frequency of encounter $\omega\sqrt{L/g}$ in figure 4, with the non-dimensional expressions as follows $A_{33}/\rho\nabla$, $A_{55}/\rho\nabla L^2$, $(B_{33}/\rho\nabla)(\sqrt{L/g})$, $(B_{55}/\rho\nabla L^2)(\sqrt{L/g})$.

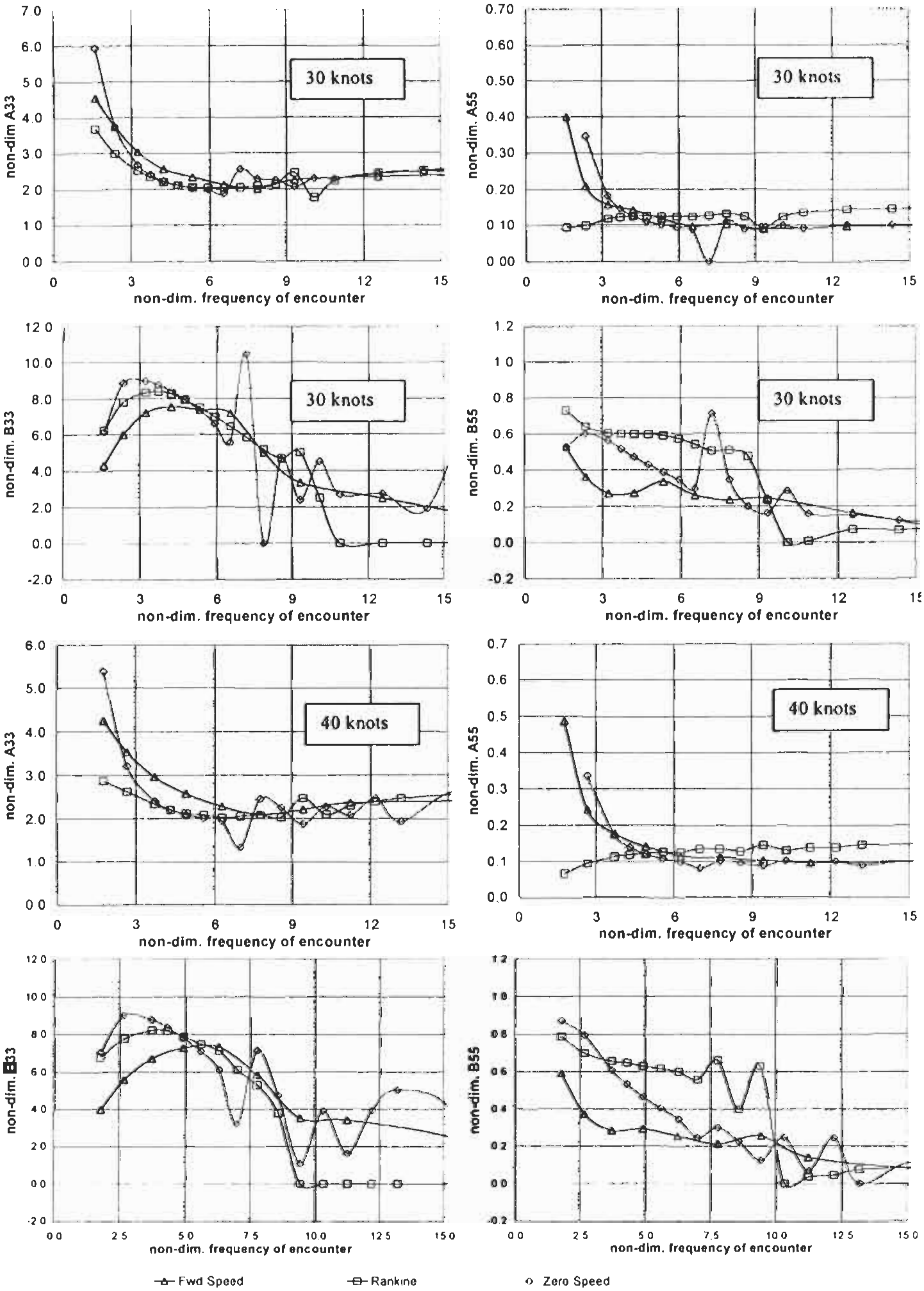

Figure 4: Diagonal Added mass and Damping coefficients for a fast monohull at 30-40 knots

It appears that added mass coefficient results present a rather coherent behaviour among all the methods while more relevant discrepancies are shown as far as damping coefficients are considered. The curves deriving from the application of the Green's function without forward speed effects into the free surface equation show a questionable oscillating behaviour in both the added mass and damping coefficients, which is reflected in the response amplitude operators. Some oscillations can be noted also in the results from the Rankine source method, at the higher frequencies. It is supposed that it can be due to the choice of the free surface panel dimensions. In fact, in convergence tests, that have been carried out before the final computation, this problem was not noted when using a coarser grid. On the other hand, some sort of aliasing may probably occur also with denser grids, at particular frequencies.

4 CONCLUSIONS

Notwithstanding the fact that modern tools, other than strip theory, are available for seakeeping calculations, they are not so much exploited in the design process, neither in those cases where strip theory is in principle not adequate. This comparative study has shown that among the selected potential methods, i.e. forward speed and zero speed Green's functions and Rankine source methods, some not negligible differences in results are obtained. For both the examined hulls the forward speed Green's function produces the highest pitch resonance while the Rankine source gives the highest heave resonance on the amplitude response operators. Higher instabilities and oscillations in the results have been obtained for the hard chine hull. In both cases it has turned out that the consideration of the speed into the free surface boundary condition, allowed by the Rankine source method and by the forward speed Green function, leads to appreciable differences with respect to older or more approximate theories. Further investigations should be performed for the fast ferry hull, when experimental data will be available.

References

Brument A., Delhommeau G. (1997). Evaluation Numérique de la Fonction de Green de la Tenue à la Mer avec Vitesse d'Avance. *6e Journées de l'Hydrodynamique*, 147-160.

Bruzzone D., Gualeni P., Sebastiani L. (1997). Steady and Unsteady motions by a Rankine Source Method" *XII Int. Conf. On Hydrodynamics in Ship Design*, Szklarska Poreba, 71-87.

Bruzzone D. and Gualeni P. (1999). Application of a Rankine Source Method for the Seakeeping Problem with Investigation on Effects of Different *Linearisations proc. of the 13th int. Conf. Hydrodynamics in Ship Design* Gdansk, 184-193.

Chang. M. (1977). Computation of three-dimensional Ship Motions with Forwars Speed. *proc.* of *the 2nd Conf. On Numerical Ship Hydrodynamics*, Nantes, 124-135.

Hess J.L. and Smith A.M.O. (1964). Calculations of Non-lifting Potential flow About Arbitrary Three-dimensional Bodies *Journal of Ship Research*, **8**, 22-44.

Inglis R.B.and Price W.G. (1982). A three dimensional ship motion theory: calculation of wave loading and response with forward speed. *Trans. RINA*, **124**, 183-192.

Gerritsma J.and Smith W.E. (1967). Full Scale Destroyer Motion Measurements. *Journal of Ship Research*, **11**, 1-9.

Nakos D.E. and Sclavounos P.D. (1990). Ship Motions by a 3-D Rankine Panel Method, *18th Naval Hydrodynamic Conference*, Ann Arbor.

Practical Design of Ships and Other Floating Structures
You-Sheng Wu, Wei-Cheng Cui and Guo-Jun Zhou (Eds)
© 2001 Elsevier Science Ltd. All rights reserved

MEASUREMENT OF SHIP MOTION DURING MODEL TESTS AND FULL SCALE SEAKEEPING TRIALS

Nan Xie, Guo-Liang Qian, Huan-Qiu Gao, Na-Xin Wei

China Ship Scientific Research Center, Wuxi,214082, China

ABSTRACT

A measurement system has been developed for recording ship motions during model tests and seakeeping trials. The system consists of accelerometers, angular rate sensors and a PC with data logging and analysis software. The non-linear iterative approach is used for the data processing. Model tests at wave basin and full scale ship trials were conducted to verify the system. The comparison of the ship motions measured by the present system with that by other systems is satisfactory. The present method provides a reliable and inexpensive alternative to other systems, e.g. gyro-stabilized platform or optical tracking devices.

KEYWORDS

Seakeeping, Measurement, Ship motion, Model tests, Full scale trial

1 INTRODUCTION

The strap-down system has been used to measure ship motions by many authors. To measure the wave induced motions of a vessel in six degree of freedom during full scale seakeeping trial, gyro-stabilized platforms can be used. The gyro systems have a sufficient accuracy and the analysis is straightforward, the drawbacks are fairly high initial and maintenance costs and a short operational life. Accelerometers and angular rate sensors are reliable, inexpensive and virtually maintenance free whereas using them to determine accurately the motions of a ship requires careful analysis.

Miles [1] was the first researcher to use seven accelerometers on the model to measure the six-degree of freedom motions of a ship and model tests were conducted to verify the method, his system can also be applied in full scale experiments. Hong et al [2] have developed such a system for full-scale seakeeping trial. Grigoropoulos [3] also presented a similar system and verified by model tests in towing tank. While Rantanen et al [4] have developed another system which uses were made of four accelerometers and two angular rate sensors. Their system has been successfully used for seakeeping trials on fast naval vessels.

In the present paper, a new system for measuring ship motions, which consists of three accelerometers and three angular rate sensors, is presented. The analysis approach has been formulated on the basis of Miles' work. The measurement system includes angular rate sensors to make the system more compact and to simplify the analysis. Full scale seakeeping trials and model experiments were conducted to verify the system. Comparisons between ship motions measured by the present method and that by other system are satisfactory.

2 MATHEMATICAL FORMULA

We aim to derive the body motion from the measured accelerations and angular rates. We use two coordinate systems: an inertial system $Ox_0y_0z_0$ moving with the average speed of the body, and a body fixed system $Cxyz$ which coincides with the inertial one in absence of body oscillations. The x_0 axis points in the mean forward direction of the ship. The positive direction of the vertical z_0 axis is downwards. The origin of the local coordinate system ($Cxyz$) moving with the ship is located at C where the accelerometers and angular rate sensors are fixed.

The rotation of the local coordinate system is uniquely defined by the Euler angles [5] roll, ϕ, pitch, θ, and yaw, ψ. For small angular motions as a linear approximation, The Euler angles coincide with the rotational displacements around the coordinate axes (xyz) fixed to the ship. If the three components of the angular velocity vector ($\omega_x, \omega_y, \omega_z$) are known in the ship coordinate system, the roll, pitch and yaw angles may be solved from the equations:

$$\dot{\phi} = \omega_x + tg\theta(\omega_y \sin\phi + \omega_z \cos\phi) \tag{1}$$

$$\dot{\theta} = \omega_y \cos\phi - \omega_z \sin\phi \tag{2}$$

$$\dot{\psi} = \frac{\omega_y \sin\phi + \omega_z \cos\phi}{\cos\theta} \tag{3}$$

Equations (1) and (2) must first be solved by iteration after which the yaw angular displacement is obtained from (3). When the angular displacements have been calculated, the translational displacements can be determined. Let $\vec{a}_C = [a_x, a_y, a_z]^T$ be the acceleration vector at point C in the ship coordinate system. Transformed to the inertial coordinate system, the acceleration is:

$$\vec{a}_{OC} = [A][\vec{a}_C] + [\vec{G}] \tag{4}$$

where

$$[A] = \begin{bmatrix} \cos\theta\cos\psi & \sin\phi\sin\theta\cos\psi - \cos\phi\sin\psi & \cos\phi\sin\theta\cos\psi + \sin\phi\sin\psi \\ \cos\theta\sin\psi & \sin\phi\sin\theta\sin\psi + \cos\phi\cos\psi & \cos\phi\sin\theta\sin\psi - \sin\phi\cos\psi \\ -\sin\theta & \sin\phi\cos\theta & \cos\phi\cos\theta \end{bmatrix} \tag{5}$$

and

$$[\vec{G}] = \begin{bmatrix} -g(\cos\phi\sin\theta\cos\psi + \sin\phi\sin\psi) \\ -g(\cos\phi\sin\theta\sin\psi - \sin\phi\cos\psi) \\ -g(\cos\phi\cos\theta - 1) \end{bmatrix} \tag{6}$$

The matrix $[A]$ is a general transformation matrix between the inertial and the ship fixed coordinate systems. The components of the transformation matrix may be computed at any instant of time on the basis of the Euler angles. The vector $[\bar{G}]$ is included because the vertical acceleration has been set to zero, when the ship is at rest, both in the measurements and in the analysis, and not to the gravitational acceleration, g.

3 MEASUREMENT SYSTEM

The present measurement system consists of three accelerometers, three angular rate sensors, amplifier and a PC with data logging and analysis software. Measurement range of the accelerometers is ± 2g, the accuracy and non-linearity are 0.1% and 0.05% respectively. Measurement range of the angular rate sensor is $\pm 90^0/s$, the accuracy and non-linearity are 0.02% and 0.5% respectively. The accelerometers a_x, a_y, a_z in Fig 1 measure the longitudinal, transverse and vertical acceleration respectively. Three angular rate sensors have recorded the angular velocities about the longitudinal, transverse and vertical axis respectively. In the old version of the ship motion measurement, also these angular velocities were measured by accelerometers [1][2][3]. In the work of Rantanen et al [4], four accelerometers and two angular rate sensors are used, in which a fourth accelerometer, a_4, also measures the transverse acceleration and is situated towards the bow from the measurement station. The signals from the transverse accelerometers a_y and a_4 have been used for determining the angular velocity about the vertical axis, ω_z, see [4]. Fig.2 shows the diagram of the present measurement system. The digital data is stored on the data disk for analysis.

The analysis starts by solving the roll and pitch time histories. Initial estimates of the roll and pitch angle are determined according to Miles [1] by using the linearized form of equation (4) for the longitudinal and transverse accelerations, which are assumed to have mean values of zero. The mean values of roll and pitch are thus:

$$\bar{\phi}_0 = -\bar{a}_y / g \tag{6}$$

$$\bar{\theta}_0 = \bar{a}_x / g \tag{7}$$

The roll and pitch angles are determined by solving iteratively the following equations:

$$\dot{\phi}^{(n+1)}(t) = \omega_x(t) + tg\theta^{(n)}(t)[\omega_y(t)\sin\phi^{(n)}(t) + \omega_z(t)\cos\phi^{(n)}(t)] \tag{8}$$

$$\dot{\theta}^{(n+1)}(t) = \omega_y(t)\cos\phi^{(n)}(t) - \omega_z(t)\sin\phi^{(n)}(t) \tag{9}$$

The first approximations for the time histories of roll and pitch angular velocities are obtained by setting the initial values (6), (7) for the roll in (8) and pitch angle in (9). Integration in the frequency domain and inverse FFT give the roll and pitch time histories. The iteration is finished when the RMS values of both angular motions differ less than 0.5% from the values computed on the previous iteration. Usually two or three iteration rounds are enough. When roll and pitch known, the yaw angular velocity may be determined by (3).

Components of the translational motion are obtained by integrating twice the respective accelerations in (4). If the point C is not G, the center of gravity of the ship, the global acceleration vector at point G of the ship is obtained from:

$$\vec{a}_{OG} = [A][\vec{a}_C] + [A][B]\vec{\rho}_{CG} + [\vec{G}] \tag{10}$$

where

$$[B]\vec{\rho}_{CG} = \dot{\vec{\omega}} \times \vec{\rho}_{CG} + \vec{\omega} \times (\vec{\omega} \times \vec{\rho}_{CG}) \tag{11}$$

here $\vec{\rho}_{CG}$ is the position vector between the point C and G, the translational displacements of the ship at point G, surge、sway and heave can be obtained by integrating (10) twice.

All integrals and derivations are made in the frequency domain. Velocities are obtained from accelerations by changing the real and imaginary parts of the Fourier coefficients of the acceleration using the following formulas:

$$\mathrm{Re}\{V_i\} = \mathrm{Im}\{A_i\} / \omega_i \tag{12}$$

$$\mathrm{Im}\{V_i\} = -\mathrm{Re}\{A_i\} / \omega_i \tag{13}$$

where A_i, V_i are Fourier coefficients of acceleration and velocity respectively, and ω_i is the circular frequency of the *ith* frequency component. Fourier coefficients to calculate displacements from accelerations are determined by:

$$\mathrm{Re}\{X_i\} = -\mathrm{Re}\{A_i\} / \omega_i^2 \tag{14}$$

$$\mathrm{Im}\{X_i\} = -\mathrm{Im}\{A_i\} / \omega_i^2 \tag{15}$$

here X_i is Fourier coefficients of displacement.

Before integration, the signals are band-pass filtered in the frequency domain. This can be done by selecting a pair of suitable lower and higher cut-off frequencies on the basis of the spectrum of the signal. The cut-off frequencies are then given as input to the analysis program. The time history of the integrated quantity can be finally determined by means of an inverse FFT.

4 VERIFICATION OF THE MEASUREMENT METHOD

The method was first evaluated by computer simulation using typical motion spectra. Subsequently, the system was installed onboard of a ship during seakeeping trial. The results are published in [6]. The agreement between the motions measured by present method and that by gyro is good. In order to make further verification for the system, dry tests using a 3DOF platform and model tests in a seakeeping basin are carried out. In the dry tests, the measurement device is put on a platform which can move with three degree of freedom of motion (roll, pitch and heave) at both regular and random way, see Fig.3. The motions measured by the present system are compared with the driving signals of the platform, typical results are shown in Fig.4.

Also, model tests were conducted for a container vessel in the wave basin of China Ship Scientific Research Center at different headings and regular and irregular waves. The motions of the model in waves are measured by using the present system and a six-degree of freedom motion tracer simultaneously. Fig.5 shows sample comparison between the ship model motions measured by the six-DOF motion tracer and that derived from the present system. The agreement is estimated satisfactory, enhancing the confidence in the reliability of our method.

5 CONCLUSIONS

A system developed for measuring the motion of a ship in six degree of freedom by using accelerometers, rotational rate sensors has shown promising accuracy in both model tests and full scale seakeeping trials.

The system may also be used in commercial applications for monitoring the safety of the passengers, crew, cargo and the vessel when the analysis has been automated and the output is presented in a relevant way. Another application of the system may be in weather routing for providing reliable data on the actual sea conditions and motions of the vessel. The system can be combined with a long term measurement to collect data on operating conditions of ships to be used in ship design. The present system also has advantages over the 6-DOF-motion tracer when model tests of high-speed vessel is performed.

References

[1] Miles M.D. (1986). Measurement of six degree of freedom model motions using strap-down accelerometers, 21st ATTC, Washington D.C.
[2] Hong S.Y. and Lee J.S. and Hong S.W. (1992). Development of a digital motion measuring system in a real seaway, *Journal of Society of Naval Architecture of Korea*, **29:3**.
[3] Grigoropoulos G.J. and Politis C.G. (1999). A system for measuring the six degrees of motions of a moving body, *Ship Technology Research*, **46**.
[4] Rantanen A., Holmberg, J. and Karppiner, T. (1995). Measurement of encountered waves and ship motions during full-scale seakeeping trials, Symposium on Ship Motion in Rough Weather, U.K.
[5] Lewis E.V. (1989). *Principles of Naval Architecture, Vol.III, Motions in Waves and Controllability.* Published by SNAME.
[6] Xie N. Qain G. L. and Gao H.Q. (1998). Measurement of six degrees of freedom of ship motions during full-scale seakeeping trial, *Journal of Ship Technology*, No.1.
[7] Xie N. Qian G.L. and Gao H.Q. (1999). Experimental verification of the strapdown ship motion measurement system, Report of China Ship Scientific Research Center, No.99265.

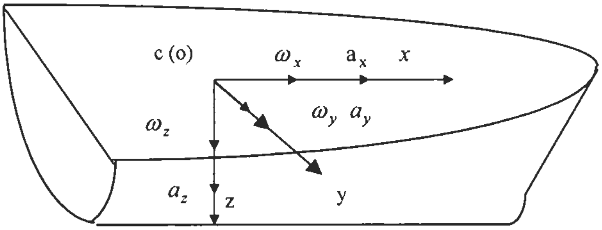
c (o)
ω_x
a_x
x
ω_y a_y
ω_z
a_z
z
y

Figure 1: Definitions and the coordinate system

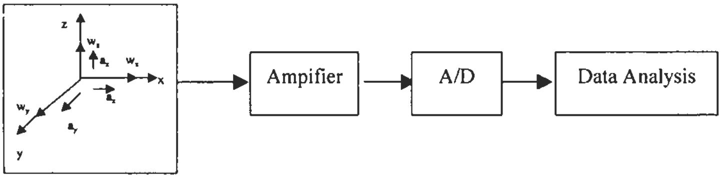
z
w_z
a_z
w_x
x
a_x
w_y
a_y
y
Ampifier
A/D
Data Analysis

Figure 2: Flow chart of the measurement system

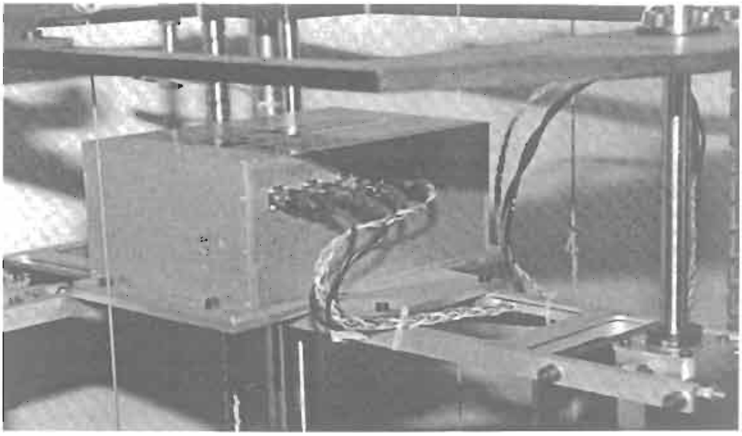

Figure 3: The system testing at the 3 DOF moving platform

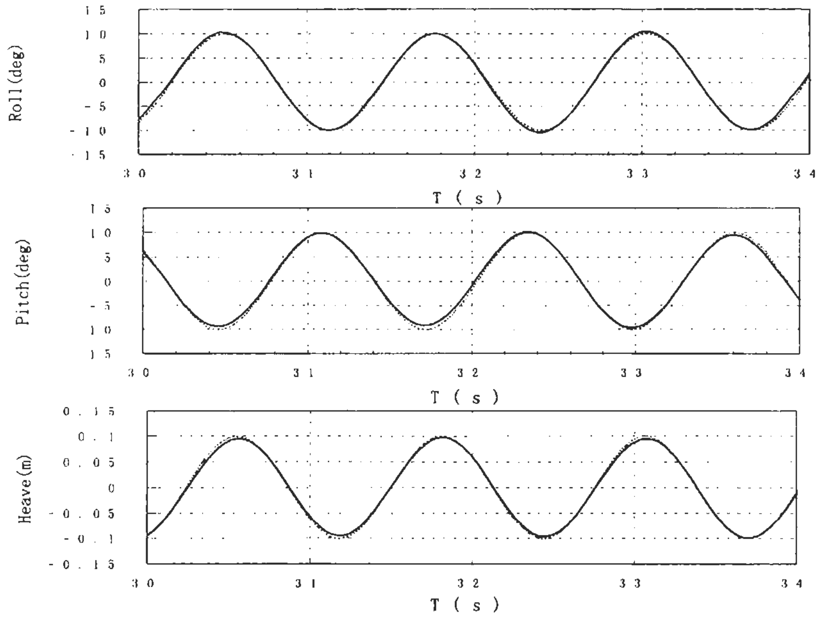

Figure 4: Motions of the 3DOF platform measured by present system and the driving signals

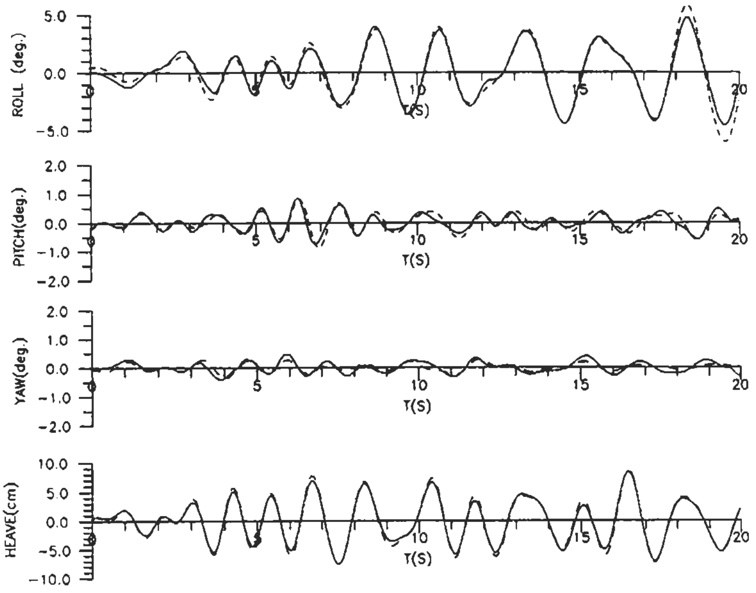

Figure 5: Motions of a container vessel model measured by two system

—— By present syst~~em,~~--- by 6-DOF motion tracer

Practical Design of Ships and Other Floating Structures
You-Sheng Wu, Wei-Cheng Cui and Guo-Jun Zhou (Eds)

Crown Copyright © 2001 Published by Elsevier Science Ltd. All rights reserved

DEVELOPING SEAKEEPING PERFORMANCE CRITERIA FOR A HELICOPTER PILOT TRAINING VESSEL

P. Crossland and M.C. Johnson

Centre for Marine Technology
Defence Evaluation and Research Agency
Haslar, Gosport, Hampshire, PO12 2AG, UK

ABSTRACT

The current approach to procuring new equipment in the UK MOD is to specify as completely as possible the requirements rather than to make recommendation for possible design solutions. In terms of a new vessel the requirements will include the expected performance in rough weather. It is important that throughout the whole procurement cycle the customer and the contractor must be confident that the replacement vessel will eventually meet those requirements. However, in order to do this a set of performance criteria must be established; criteria that actually represent the limitations on the ability for the vessel to undertake its allotted task. This paper describes a practical method for developing performance requirements of a vessel used to support aircrew training, which was then used in the performance specification of a replacement vessel.

KEYWORDS

Seakeeping, Seakeeping criteria, Sea trials, Ship motion prediction, Operability

1 INTRODUCTION

There is a clear link between designing a ship with poor seakeeping qualities and the cost of days lost due to excessive motions curtailing the operation, or in the case of this craft lost training days or aircraft flying time. Despite this, seakeeping performance is not usually sufficiently well specified to have any confidence that the ship and system will be designed to meet the requirements. The UK Defence Logistics Organisation (DLO) is in the process of updating all its aircrew training vessels; currently three different classes of vessel are used to support the training. This paper describes a method of developing performance criteria for inclusion in a procurement specification for the new craft such that its seakeeping performance at least matches that of the craft it is due to replace. This methodology begins with an extensive set of trials where the motions of an existing vessel, the RTTL, were measured as the ship performed a set of straight course runs. Thirteen runs were performed to expose the vessel to seas from all directions of the compass at 30 degree heading intervals. During the trials simultaneous measurements of the directional sea state were made using a fully directional wave rider buoy. From these data a systematic approach was used to generate the criteria set giving the limits of the motions and derived responses at which the vessel is considered operable, based on the limitations of the activities and systems used in the aircrew training task. The trials data were used to validate the results from computer predictions, which in turn were then used to assess performance in likely-to-be-encountered wave conditions. These predictions were compared with the criteria set to obtain a measure of operability of the existing craft.

2 ROLE AND DESCRIPTION OF CURRENT VESSELS

The craft are used for the following tasks; winch training for helicopter crews, sea survival training, patrolling the sea danger area of coastal live firing ranges, target towing for aircraft and land ranges, fast attack craft threat simulation, recovering air sea rescue apparatus and air dropped torpedoes and Search and Rescue. The operators report that it is the ability to carry out the deck winch training task, in particular during the training of novice pilots and rear-end crew, which is of major concern with regards to the seakeeping performance of the craft, see figure 1.

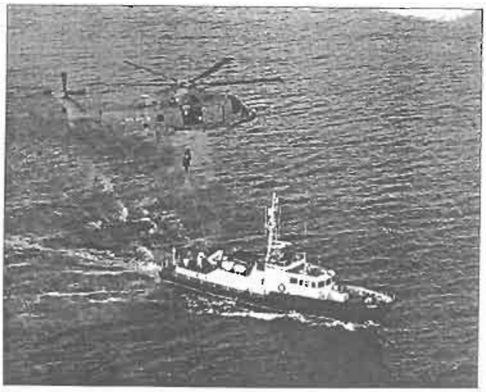

Figure 1: Winch training

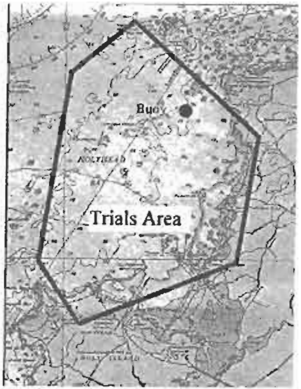

© Crown Copyright 1979

Figure 2: Trials Area

The vessel examined in this paper is the Spitfire class Rescue Target Towing Launch (RTTL) Mk 3, HURRICANE, dating from the early eighties (Figure 1). They have length 24m, beam 5.5m and displace 70 tonnes. The stern, transom or foredeck are used for landing a winchman. Man overboard rescue is achieved by deployment of a small boat. A platform for deck winching training and a safety boat for 'survivors' in the water during wet winching is required day and night. These craft operate in specific locations around the UK; the training of novice aircrew takes place at Holyhead Bay, North West Wales, shown in Figure 2.

3 SEAKEEPING TRIALS

The trials area was in Holyhead Bay, covering an area shown in Figure 2. This area was chosen to meet a series of compromises; the need for a large area so not to restrict the trials, the need to undertake the trials in a typical operational area and the need to deploy the wave buoy away from the ferry routes. Thirteen runs were performed at a typical working speed of 7 knots so that the ship was exposed to the seas in all directions of the compass at 30° intervals, forming a 'star' trajectory similar to that shown in

Figure 3. For each trajectory, six degrees of freedom - roll, pitch angle and yaw rate and three orthogonal linear acceleration were measured in body axes in the wheelhouse.

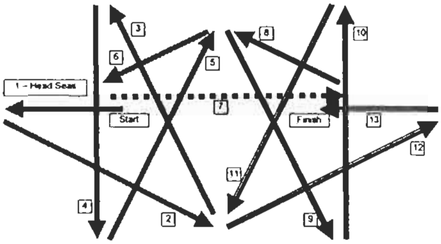

Figure 3: Star trajectory

In general, longer runs were performed in following and quartering seas and shorter runs in head seas, with the aim of encountering around 100 waves per run. In a symmetrically spread sea state, pairs of relative headings should give similar ship motion results; e.g. 30° and 330° are both quartering seas, but 30° is to port and 330° is to starboard.

A fully directional wave buoy was deployed in the trials area at the location indicated in Figure 2. The wave rider buoy measured for periods of 20 minutes and reported conditions hourly. Figure 4 shows the variation in spectral energy, wave direction and spreading at each frequency and the average parameters over the duration of the trial. The JONSWAP (Hasselmann *et al*, 1980) idealised spectra given in Figure 4 fits the observed spectrum very well. A visual estimate of the wave conditions was a high sea state 3 (reasonably long crested) coming from a direction 310° magnetic, which remained consistent throughout the day of the trial. The subjective view of the operators was that these were challenging conditions for the ship to perform the deck winching training task.

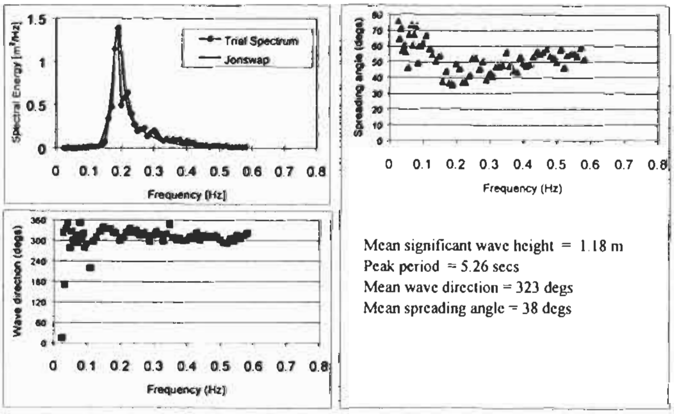

Mean significant wave height = 1.18 m
Peak period = 5.26 secs
Mean wave direction = 323 degs
Mean spreading angle = 38 degs

Figure 4. Average wave parameters

According to Tucker (1991) the spreading angle can be related to a cosine even power spreading function that can be easily used in ship motion prediction packages; the spreading function assumes even spreading across the entire frequency range. In the case of these trials $\cos^{12}$ spreading gives the most appropriate model of the wave conditions encountered.

4 THE TRAINING CRAFT CRITERIA SET

The key issue in specifying and assessing the operational performance of any type of ship is to establish a set of criteria linking the ability to perform the tasks with the ship motions. The ship motions themselves may present operational limits, or influence the human or equipment limitations for the support activities the ship must perform. In the case of the craft in this report, the criteria developed concentrate on the deck winching training exercise involving novice aircrew that was regarded by the crew as the most important task. Crossland (1998) gives some guidance on establishing criteria for ship tasks but does not include something as specific as winching training. Nevertheless, the systems approach advocated in this reference can be applied to the winching activity. The activities, systems and tasks used for this type of training must be established to form a criteria set for assessing the effects of ship motions and related phenomena on the effectiveness of the support ship. The two principal tasks involved in winching training where the vessel seakeeping is important are (a) transferring the winchman from the helicopter to the craft safely and (b) recovering personnel and their survival rafts from the sea during wet winching training. For winching a person on to the craft the types of limiting events are classified in Table 1.

TABLE 1

LIMITING EVENTS

Activity	Risk	Limiting event	Comments
Crew operations on deck	Crew falling Overboard	Lateral acceleration MII	Crew cannot balance due to excessive ship motions
Winchman Recovery	Crew falling Overboard	Vertical and lateral Acceleration, roll, pitch	Crew can safely receive the winchman from the helicopter
Winchman Recovery	Injury to Winchman	Vertical velocity	High vertical velocities on impact may injury a person
Tracking moving deck	Winchman Missing Landing zone	Lateral, longitudinal Displacement	Problems with directional stability in stern seas may be a problem
Crew tolerance	Motion Sickness Amongst the Crew	MSI	Excessive vertical acceleration for prolonged periods will induce sickness
Hull limits	Risk to hull	Wetness index Slamming index	Severe slamming will damage hull; severe wetness will damage equipment and injure personnel on the weather deck.

During normal operations, a rescue/safety boat is deployed from the 'mother' craft. The winching training task would be restricted by the inability to deploy/recover the rescue boat safely in the event of the winchman falling into the sea. The limiting events in this case are lateral and vertical motions at the launch position. A criteria set using the above limiting events has been developed as shown in Table 2. It shows both location-independent criteria (i.e. roll and pitch angles), and location-dependent criteria. The ship is deemed no longer operational if any one of the criteria is exceeded.

In Table 2 the roll, pitch and acceleration criteria are taken from the RMS values measured during the trials where it was deemed that the limit to operational performance had been reached. The wetness and slamming criteria are given in Crossland (1998). Wetness Index is the probability of relative motion exceeding freeboard at the FP. Slamming Index is the probability of severe slamming, based on the theory of Ochi (1964). Motion Sickness Incidence (MSI) is defined as the percentage of crew who vomit after two hours exposure to the ship motions, from O'Hanlon and McCauley (1974). Motion Induced Interruptions (MIIs) are incidences where ship motion causes the person to stumble or fall, see Graham *et al* (1992). In the absence of data for tolerable impact velocities on people an estimate has been made based on the impact velocity of a person jumping from a height of two metres. Using Newton's equations of motion this gives an impact speed of 4.64 m/s. By assuming that the vertical velocity peaks are Rayleigh distributed means that this impact speed will be exceeded about 1 in 100 times for the RMS vertical velocity given in Table 2.

TABLE 2

CRITERIA SET

Limiting event	Location	Unit	Criterion
RMS Roll		Degrees	5
RMS Pitch		Degrees	2.5
Wetness index	FP	Per hour	30
Slamming index	Station 5	Per hour	20
MSI	Wheel house	Percent who vomit	30
MII	Landing zone	Per minute	2
RMS vertical Acceleration	Landing zone	G	0.14
RMS lateral Acceleration	Landing zone	G	0.12
RMS vertical Velocity	Landing zone	M/s	1.5

5 OPERATIONAL EFFECTIVENESS

The seakeeping trials results are invaluable in that they present an unequivocal measurement of the motions of the vessel. However, the data cannot be used directly to quantify the seakeeping performance in a wide range of sea conditions, since the trial represents only a snapshot of all the possible wave conditions the vessel might encounter in its lifetime. A computer assessment of the operability of the ship gives the only alternative to overcome this issue. Initially, the trials data are used to validate the computer model which in turn can be used to generate the motion responses in wider set of sea conditions.

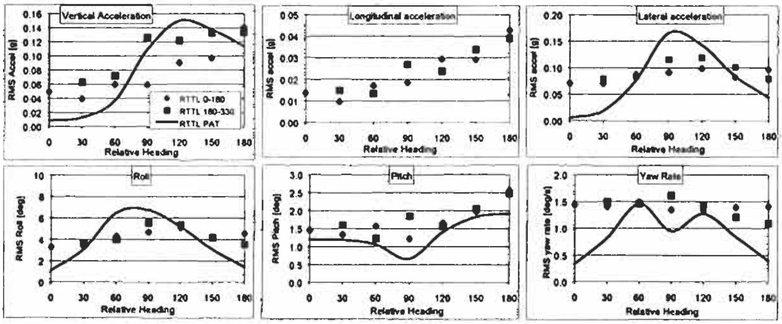

Figure 5: Predicted and measured motions

Predictions made using a strip theory ship motion package (PAT-95, Montgomery and Crossland, 1995) are compared with the trials results in Figure 5. In general the PAT-95 predictions show quite good qualitative and quantitative agreement with the trials results which in principal agree with the model validation shown in Lloyd and Crossland (1989). Some discrepancy may be attributed to the wave descriptions used in each of the PAT models, which are smoothed, idealised and averaged versions of the trials wave conditions, but in general the results confirm that the computer models are satisfactory.

In order to get a representative measure of the ability of the ship to undertake its task effectively a series of calculations in all possible sea conditions are undertaken. In this context, operational effectiveness is a measure of the ability of the craft to put to sea and achieve its mission under the environmental conditions encountered. This is defined as the percentage of time the craft can perform its allotted task for a given combination of environmental factors. Johnson (1999) describes PATOP98, a suite of programs that performs an operability analysis based on the method outlined in Crossland (1998) for a ship at any one speed in a specified operating environment. The suite uses PAT-95 in a controlled series of runs from which the relevant data are extracted and used in operability analysis. The analysis determines the limiting significant wave height for each modal period in a range defined by wave scatter diagrams. Once the operating scenario has been specified and the conditional frequency distribution of wave direction has been determined from suitable wave atlases, it is possible to determine all relevant ship motions from the short term responses for every combination of ship course and heading. Some of these responses may exceed the maximum permissible value set by the chosen criteria. If this is the case then the operation has a high risk of failure and the ship may not achieve its mission.

Real data describing the long term environmental conditions that are likely to be encountered by the ship are required to ensure the assessments are performed using representative wave conditions. These environmental data can be found as scatter diagrams available in wave atlases. It is necessary to represent the individual boxes of these scatter diagrams by wave spectra. Ideally, operability assessment should be made using long term wave data gathered at the sites where the RTTL will be operating. Unfortunately, statistics of the quality required are not typically available at these locations, and wave atlas statistics that are typically of good quality, cover vast open ocean areas that are not appropriate in this case. As a compromise, long term wave statistics from permanently moored buoys and ships were considered. It was decided that data from Sevenstones was the most suitable. This coastal zone experiences short, low period waves for much more of the year than the open ocean. This is an important factor when considering the operability of ships, particularly relatively small craft like the DLO vessels, in these regions.

Figure 6 gives results of the PATOP98 operability analysis for the RTTL operating at Sevenstones. The figure shows a polar diagram of the envelope of limiting wave height for the vessel at each relative heading to the predominant waves and an associated Percent Time Operable at each heading. The Percent Time Operable (PTO) at each relative heading is accumulated over all the possible sea states defined in the Sevenstones area given their frequency of occurrence during the year. The title text indicates the Overall PTO averaged over all the possible relative headings. No weighting has been applied in determining this average; it is assumed that the ship is equally likely to travel in any heading. Limiting heights in the range 180°-360° are not plotted as these will be a mirror image of the 0°-180° results (the sea state is symmetrical about the principal direction). Larger envelopes indicate higher operability. A dotted line indicating the boundary between upper Sea State 3 and lower Sea State 4 is indicated at 1.25m Significant Wave Height. Postural control (MIIs) at the winch landing position is clearly a problem at most headings. It is this criterion that limits the operational performance of the craft.

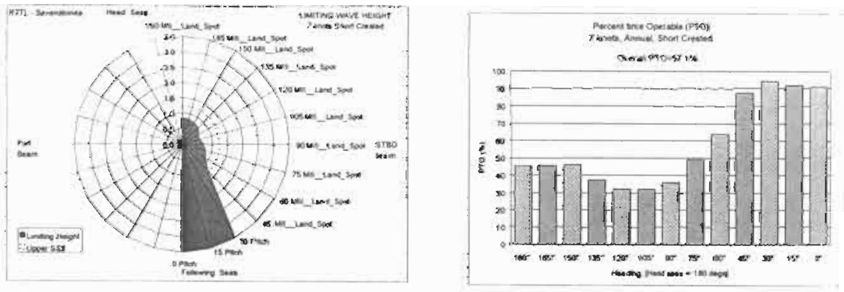

Figure 6: Limiting significant wave height and PTO of the RTTL at Sevenstones

It is the limiting wave height and PTO diagrams of Figure 6, derived from the criteria set of Table 2, that give the most objective measure of the craft's seakeeping ability in its operational area, and give the target which replacement vessels should match or surpass.

6 CONCLUSIONS

This paper has demonstrated a practical approach to quantifying the seakeeping performance of an existing craft. The data measured on dedicated trials has been combined with existing standards to make the key step of generating a set of performance criteria. Additionally, the seakeeping trial results have been used to validate a strip theory ship motion code. By applying the criteria set to the predicted ship motions from a wide range of sea states in the operating area allows the operability of the existing vessel to be calculated. Both the criteria set and the operability analysis can be used to aid the development of performance specification for a replacement craft.

Acknowledgements

The authors would like to thank the UK Defence Logistics Organisation for supporting the work from which this paper was derived and for their valuable comments on the first draft.

The authors would also like to thank the Master and crew of RTTL Hurricane for their cooperation during the trials.

References

Crossland P. (1998). NATO NG/6 on Ship Design, Specialist Team on Seakeeping. A rational approach to specifying seakeeping performance in the ship design process. *RINA International Conference WARSHIP '98*. London.
Graham, R., Baitis, A.E., and Meyers, W.G. (1992). On the Development of Seakeeping Criteria. *Naval Engineers Journal*.
Hasselmann D E, Dunckel M and Ewing J A. (1980). Directional spectra observed during JONSWAP 1973, *Journal of Physical Oceanography* **10**, 1264-1284
Johnson M C. (1999). Patop98 User Guide. DERA Technical Report DERA/MSS6/TR990530
Lloyd ARJM, Crossland P. (1989). Motions of a Steered model warship in oblique waves. *Trans RINA*, **31**.
Montgomery P, Crossland P. (1995). User Guide for the PAT-95 Suite of Ship Motion Computer Programs. *DERA Customer Report DRA/SS/SSHE/CR95030*.
Ochi, M.K. and L.E. Motter. (1973). Prediction of Slamming Characteristics and Hull Responses for Ship Design. *Transactions of the Society of Naval Architects and Marine Engineers*. **81**.
OHanlon, J.F. and McCauley M.E. (1974). Motion Sickness Incidence as a Function of Frequency and Acceleration of Vertical Sinusoidal Motion. *Aerospace Medicine*.
Tucker M.J. (1991). Waves in Ocean Engineering: Measurement, Analysis, Interpretation. Ellis Horwood.

© British Crown Copyright DERA 2001. Published with the permission of the Defence Evaluation and Research Agency on behalf of the Controller HMSO

Practical Design of Ships and Other Floating Structures
You-Sheng Wu, Wei-Cheng Cui and Guo-Jun Zhou (Eds)

© 2001 Elsevier Science Ltd. All rights reserved

DYNAMIC BEHAVIOUR OF RIGID MONO- AND MULTI-HULLED VESSELS IN WAVES, INCORPORATING NON-LINEAR EXCITATION

P. A. Bailey, E. J. Ballard and P. Temarel

School of Engineering Sciences, Ship Science, University of Southampton,
Southampton, SO17 1BJ, UK

ABSTRACT

A time domain model for the prediction of ship motions in waves is presented in this paper. Fluid forces and moments acting on the ship are represented by convolution integral expressions thus accounting for fluid memory effects. The required impulse response functions are obtained from transforms of frequency domain data evaluated using a three-dimensional potential flow analysis based on a source distribution over the mean wetted surface of the vessel. Convolution integrals are used to describe both the radiation and diffraction contributions to the ship motion problem. Non-linear restoring and Froude-Krylov excitation forces are determined at each time step using the instantaneous underwater portion of the hull. Results are presented in head and oblique regular waves for a fast hull form, namely an NPL round bilge series, in both mono-hull and catamaran configurations. Initially the wave amplitude conforms to the concept of linearity, allowing for the validation of the numerical procedures. Subsequently the effects of non-linear excitation are investigated by increasing the amplitude of the regular waves.

KEYWORDS

Rigid body motions, Seakeeping, non-linear, Wave excitation, Multi-hulled vessels.

1 INTRODUCTION

Modelling of ship motions in the time domain allows for the evaluation of responses to arbitrary and/or transient excitation. Such a method enables, for example, the influence of control surfaces and excitation by random waves to be accounted for in a way that is not possible using conventional frequency domain approaches. The fluid memory effect, exemplified by the generation of motion induced surface waves, introduces a dependence of the forces and moments on past motion/excitation. The use of impulse response functions and a convolution integral formulation for the fluid actions allows for the generation of a time domain model that is capable of incorporating the aforementioned influences and excitations. Bailey et al (1998a) presented a mathematical model for the manoeuvring of a ship in a seaway that is also capable of simulating the conventional seakeeping behaviour and manoeuvring in calm water, as illustrated for a Mariner ship by Bailey et al (2001a). These investigations were further extended to include the influence of diffracted waves and applied to a Series 60 hullform, Bailey et al (2000a). The fundamental building blocks of these investigations are the use of frequency domain hydrodynamic data to generate the requisite impulse response functions and transforms between the equilibrium axes and the body fixed axes of conventional seakeeping and manoeuvring theories, respectively, as shown by Bailey et al (1998a, 2001a). The determination of the frequency domain data relies on a suitable singularity distribution over the mean wetted surface of the ship, Inglis and Price (1982), Bailey et al (1999, 2000b),

Although the mathematical model developed is capable of simulating the dynamic behaviour of a ship travelling in waves in all six degrees of freedom, results presented in this paper are focused on the symmetric motions of heave and pitch. A fast hull form from the extended NPL round bilge series, namely model 5b, is used to illustrate the applicability of the methodology. The motions of this hull form are predicted when travelling at various speeds and headings in mono-hull and catamaran (demi-hull separation = 0.2L) configurations. Comparisons are made with available experimental measurements, Bailey et al (1999), Molland et al (2000).

2 AXIS SYSTEMS AND EQUATIONS OF MOTION

Seakeeping theory has traditionally referenced the rigid body motions of a vessel to equilibrium axes. However, it has been shown by Bailey et al (2000a) that the behaviour of the frequency domain added mass and damping calculated with respect to these axes results in problematic evaluation of the corresponding impulse response functions. Bailey et al (2001a) demonstrated that frequency domain data transformed to a body fixed set of axes is more amenable to the calculation of impulse response functions.

For a ship travelling with forward speed $\overline{U}$ in regular waves encountered at arbitrary heading, the heave and pitch (denoted by displacements $z^{\bullet}$ and θ) equations of motion referenced to a right handed body fixed axis *Cxyz* can be written as

$$\begin{bmatrix} m & 0 \\ 0 & I_{yy} \end{bmatrix}\begin{bmatrix} \dot{w} \\ \dot{q} \end{bmatrix}+\begin{bmatrix} 0 & -m\overline{U} \\ 0 & 0 \end{bmatrix}\begin{bmatrix} w \\ q \end{bmatrix}=\begin{bmatrix} Z_{\dot{w}} & Z_{\dot{q}} \\ M_{\dot{w}} & M_{\dot{q}} \end{bmatrix}\begin{bmatrix} \dot{w} \\ \dot{q} \end{bmatrix}+\begin{bmatrix} Z_{w} & Z_{q} \\ M_{w} & M_{q} \end{bmatrix}\begin{bmatrix} w \\ q \end{bmatrix}+\begin{bmatrix} Z_{z^{\bullet}} & Z_{\theta} \\ M_{z^{\bullet}} & M_{\theta} \end{bmatrix}\begin{bmatrix} z^{\bullet} \\ \theta \end{bmatrix}+\begin{bmatrix} Z(t) \\ M(t) \end{bmatrix}, \quad (1)$$

where w and q are the heave and pitch velocities, respectively, terms such as $Z_{\dot{w}}, M_{q}$ are the oscillatory coefficients and $Z(t)$ and $M(t)$ represent the excitation. Alternatively, Bailey et al (2001a) have shown that these equations of motion can be written using a convolution integral formulation in the following way:

$$\begin{bmatrix} \dot{w}(t) \\ \dot{q}(t) \end{bmatrix}=M^{-1}\begin{bmatrix} f_3(w,q,z^{\bullet},\theta,t) \\ f_5(w,q,z^{\bullet},\theta,t) \end{bmatrix}, \quad (2)$$

where

$$\begin{aligned} f_3 &= Z_{\tau}+Z_{\alpha}+\widetilde{Z}_{w}(\infty)w+\widetilde{Z}_{q}(\infty)q+mq\overline{U} \\ f_5 &= M_{\tau}+M_{\alpha}+\widetilde{M}_{w}(\infty)w+\widetilde{M}_{q}(\infty)q. \end{aligned} \quad (3)$$

In these equations the contributions of weight, buoyancy and incident wave excitation are denoted by the terms with subscript α. The detail of these terms will be elaborated upon in later sections. The mass matrix is given by

$$M = \begin{bmatrix} m - \widetilde{Z}_{\dot{w}}(\infty) & -\widetilde{Z}_{\dot{q}}(\infty) \\ -\widetilde{M}_{\dot{w}}(\infty) & I_{yy} - \widetilde{M}_{\dot{q}}(\infty) \end{bmatrix},$$

where terms such as $\widetilde{Z}_{\dot{w}}(\infty)$ and $\widetilde{M}_{\dot{w}}(\infty)$ are the infinite frequency values of the acceleration oscillatory coefficients. The terms with subscript τ are the radiation forces and moments and are expressed as follows

$$\begin{aligned} Z_\tau &= \int_0 z_w(\tau)w(t-\tau)d\tau + \int_0 z_q(\tau)q(t-\tau)d\tau \\ M_\tau &= \int_0 m_w(\tau)w(t-\tau)d\tau + \int_0 m_q(\tau)q(t-\tau)d\tau. \end{aligned} \tag{4}$$

The impulse response functions used in the convolution integrals in the previous equations can be calculated using either the velocity or acceleration frequency domain data. The transformation of the frequency domain data from an equilibrium to a body axis representation enables the calculation of terms such as $\widetilde{M}_w(\omega_e)$ and $\widetilde{M}_{\dot{w}}(\omega_e)$, the frequency dependent velocity and acceleration oscillatory coefficients, respectively, Bailey et al (1998a, 1998b, 2000a). For example

$$z_w(\tau) = \frac{2}{\pi}\int_0^\infty \widetilde{Z}_w(\omega_e)\cos(\omega_e\tau)d\omega_e = -\frac{2}{\pi}\int_0^\infty \omega_e\widetilde{Z}_{\dot{w}}(\omega_e)\sin(\omega_e\tau)d\omega_e .$$

Numerical experiments have shown that the impulse response function calculated using the velocity derivative data converges faster than its equivalent determined using the acceleration data, hence the velocity data is used in preference.

The relevant frequency domain data is obtained using a three-dimensional potential flow analysis, based on the conventional equilibrium axis system, with a singularity distribution over the mean wetted surface. In this investigation two types of singularity are used, a pulsating source and translating, pulsating source. Both of these source types satisfy a linearised free surface condition as well as the radiation condition at infinity. The pulsating source method accounts for forward speed in a limited fashion, using corrections to the zero speed solution much the same as are used for strip theory, Beck et al (1989). The translating, pulsating source on the other hand accounts for forward speed effects in the linearised free surface condition, but does so at considerable computational expense. It has been shown that for monohulls at moderate forward speeds the results of the two methods are quite similar, Inglis & Price (1982), Bailey et al (1999), hence results for the monohull use the simpler and faster method. However, for a catamaran model the translating pulsating source is required to fully account for interaction between the hulls.

3 WAVE EXCITATION

It can be argued that observed differences between theoretical linear motion predictions and experimental results can be attributed, to some extent, to the nature of the excitation, particularly for ships with large flare. To this end, it is possible to introduce a non-linear component of excitation into an otherwise linear system, the integration of the Froude-Krylov wave excitation pressure over the instantaneous wetted surface yielding such a contribution. The wave excitation and restoring terms, denoted with subscript α, in Eqn. 3 can be represented as

$$
\begin{aligned}
Z_\alpha &= Z_\alpha{}^D + Z_\alpha{}^F + Z_z.z^\bullet + Z_\theta \theta \\
M_\alpha &= M_\alpha{}^D + M_\alpha{}^F + M_z.z^\bullet + M_\theta \theta,
\end{aligned}
\tag{5}
$$

where the superscripts D and F refer to the linear diffraction and the non-linear Froude-Krylov components respectively. The non-linear restoring forces and moments are denoted by the subscripts $z^\bullet$ and θ respectively.

It has been shown by Bailey et al (2000a) that linear diffraction excitation actions can be represented using a convolution type formulation. Calculation of these wave excitation impulse response functions is more difficult than the calculation of the radiation impulse response functions, since the influence of a wave prior to its reaching the reference point must be accounted for. This means that the diffraction excitation impulse response functions are non-zero for $\tau < 0$, Bailey et al (2000a), King et al (1988), and unlike the radiation impulse response functions their calculation requires both the real and imaginary parts. For example,

$$Z_\alpha{}^D = \int_{-\infty}^{\infty} z^D(\tau)\alpha(t-\tau)d\tau$$

where $$z^D = \frac{1}{\pi}\int_0^{\infty} \{\Xi_z{}^R(\omega_e)\cos(\omega_e\tau) - \Xi_z{}^I(\omega_e)\sin(\omega_e\tau)\}d\omega_e \quad \text{for all } \tau,$$

$\alpha(t)$ denotes the wave elevation and Ξ_z is the frequency domain diffraction term, transformed to the body fixed axis system.

The non-linear portion of the wave excitation terms in Eqn. 5 are made up of two components. These are the non-linear Froude-Krylov and restoring forces and moments. They are determined up to the intersection of the incident wave surface and the ship in its perturbed state at each time step.

The entire surface of the ships hull, including the portion above the waterline, is discretised using a mesh of quadrilateral panels. This allows a single mesh to be used to represent a range of ship loading conditions. At each time step the instantaneous underwater portion of the hull is extracted. Special consideration must be given to panels that cross the incident free surface. Panels that are entirely above the surface are ignored and those that cross the surface are either split or replaced with two smaller panels. The static and Froude-Krylov pressures are then calculated at the centre of each panel. The contribution of the force on each panel to the overall forces and moments is determined using the area of the panel and its normal. The total Froude-Krylov and buoyancy forces are then calculated by summing the contributions from all the panels. Care has been taken to ensure that the splitting, adding or destroying panels does not introduce step changes in the resulting forces and moments, Bailey (2001b).

4 TIME DOMAIN SIMULATION TECHNIQUES

The time domain simulation of the vessel's motions is undertaken using a fourth order Runge-Kutta method of solution, Bailey et al (2001a), in which the vessels velocity and displacement are calculated for a series of time steps of fixed increment. At each step, the convolution integrals are evaluated using a numerical convolution method, whereby the velocity and impulse response functions are represented using a series of discrete points. These convolution integrals are evaluated using trapezoidal summation. To account for the fact that the time steps of the velocity and impulse response functions may be different, the time steps of the impulse response function are used in this evaluation and the velocity trace is linearly interpolated.

5 DISCUSSION OF RESULTS

The length of the vessel used in the calculations is 4.5m in both mono-hull and catamaran configurations. The mean wetted surface, to a draught of 0.2m, was idealised using 554 four-cornered panels for the NPL mono-hull. 640 panels were used to idealise the entire surface of the mono-hull, to a depth of 0.35m. The first idealisation is used to evaluate frequency domain hydrodynamic/oscillatory coefficients and diffracted wave excitation, whilst the second is employed when generating the instantaneous underwater surface to evaluate the non-linear incident wave excitation and restoring forces and moments. In the same way, the mean wetted surface of the catamaran is idealised using 390 panels per demi-hull for the frequency domain analysis, whilst the entire surface to a depth of 0.4m is idealised using 415 panels per demi-hull for the evaluation of the non-linear components. The idealisations used provide a reasonably good panel aspect ratio, approximately 2, which is particularly important in ensuring a good convergence in the frequency domain data calculated using the translating, pulsating source distribution, Bailey et al (2000b).

The pitch-pitch radiation impulse response function is illustrated in Figure 1(a) for both mono-hull and catamaran configurations, albeit at different speeds. The trends of the impulse response function for the catamaran configuration requires further investigation as demi-hull separation increases. The variation of the predicted heave displacement with time is also shown in Figure 1(b). The simulation shown corresponds to the mono-hull travelling in head regular waves at Fn = 0.53, encountered at $\omega_e' = \omega_e\sqrt{L/g} = 5.42$ and amplitude α = 0.05625m. The simulated heave displacement quickly converges to a steady state sinusoidal variation with time that has a non-zero mean value, zero representing the still water equilibrium position, due to the relatively large wave amplitude used (approximately a quarter of the draught). The motion amplitudes are obtained from a Fourier fit of the steady state part of the time records, e.g. as shown in Figure 1(a) starting from 42 seconds.

The predicted heave and pitch transfer functions for the mono-hull in regular head waves are shown in Figures 2 and 3. These are for slow and moderate speeds corresponding to Fn = 0.2 and Fn = 0.53, respectively. The transfer functions (or RAOs) are defined as heave or pitch amplitude per wave amplitude α. The time domain predictions (two wave amplitudes α=0.001m and α=0.05625m), are compared with the frequency domain predictions, both using a pulsating source distribution, and experimental measurements carried out with a 1.6m model, Bailey et al (1999). For the lowest speed used, i.e. Fn = 0.2, frequency and time domain predictions are all in close agreement. Nevertheless, small differences are observed for the highest wave amplitude, especially for the pitch RAO around resonance, resulting in closer agreement between the time domain prediction (α=0.05625m) and experiments carried out using the same wave amplitude. For the moderate speed, Fn = 0.53, there is once again very close agreement between the time domain predictions with the smallest wave amplitude and frequency domain results. The differences using the larger wave amplitude are now more clearly seen, especially for the pitch RAO. The time domain predictions are closer to the experimental measurements using the same amplitude. It is worthwhile noting that the time domain method results in accurate predictions of the pitch RAO magnitude at resonance, although the frequency of resonance is still overestimated.

For the NPL catamaran configuration frequency and time domain predictions for heave and pitch RAOs are compared for a moderately high speed, Fn = 0.65, whilst the vessel is travelling in oblique regular waves (heading of 150 degrees), as shown in Figure 4. Experimental measurements carried out with a model of 4.5m are also shown, Molland et al (2000). When the wave amplitude is low (α=0.001m), there is good agreement between time and frequency domain RAOs, both evaluated using a translating, pulsating source distribution. Increasing the wave amplitude to α=0.01m appears to result in small differences in the predicted RAOs, unlike the trend observed in the mono-hull for Fn = 0.53, albeit with a larger wave amplitude. Consequently the differences observed between theoretical predictions (either frequency or time domain) and experimental measurements persist, especially in pitch RAOs. At this speed it is known that the transom runs dry, which may have an effect on the pitch damping values and corresponding impulse response functions. Furthermore, the omission of roll when determining the perturbed attitude of the ship relative to the regular incident wave at any time instant may also have an influence on the result of the time domain simulation.

6 CONCLUSIONS

The applicability of a time domain method, formulated using body fixed axes, impulse response functions for radiation and diffraction influences and non-linear incident wave and restoring actions, in predicting motions for mono- and multi-hulled vessels travelling in regular waves has been illustrated for various speeds and headings.

The validity of the numerical procedures involved, such as the evaluation of impulse response functions, the time stepping scheme and the generation of the instantaneous free surface, have been demonstrated by comparison with frequency domain predictions of heave and pitch RAOs.

For the NPL round bilge hull form, in mono-hull configuration, it was shown that the influence of the non-linearities in the incident wave excitation and restoring actions is very small at low speeds. However, these influences become more significant at moderate speeds. The predictions provided are in closer agreement with experimental measurements, by comparison to frequency domain and small amplitude time domain predictions.

For the same fast hull form in catamaran configuration and moderately high speeds, the requisite frequency domain data were obtained using a translating, pulsating source distribution over the mean wetted surface to better idealise the interactions between the demi-hulls. The applications of the partly non-linear time domain method in oblique regular waves has, so far, shown that the non-linearities in the incident wave excitation and restoring actions do not appear to have a significant influence on predicted heave and pitch RAOs. The effects of pitch damping, and consequent influences on relevant impulse response functions, are thought to be likely causes. These may arise from the transom running dry at this speed.

Further work is required, especially in the catamaran configurations, to assess the influence of:
(i) the nature of the idealisation of the mean and instantaneous wetted surfaces (i.e. panel aspect ratio) on the predicted impulse response functions and time domain simulations,
(ii) inclusion of antisymmetric motions, such as roll, and
(iii) larger wave amplitudes, similar to those used in the experimental measurements.

References

Bailey, P.A., Price, W.G. and Temarel, P. (1998a). A Unified Mathematical Model Describing the Manoeuvring of a Ship Travelling in a Seaway. *Trans. RINA* **140**, 131-149.

Bailey, P.A., Hudson, D.A., Price, W.G. and Temarel, P. (1998b). The Measurement and Prediction of Fluid Actions Experienced by a Manoeuvring Vessel. In Proc. *Intl. Symposium and Workshop on Forces Acting on a Manoeuvring Vessel, MAN'98*, 117-123, Val de Reuil, France.

Bailey, P.A., Hudson, D.A., Price, W.G. and Temarel, P. (1999). Theoretical and Experimental Validation of the Seakeeping Characteristics of High Speed Mono and Multi-Hulled Vessels. *FAST'99: Fifth International Conference on Fast Sea Transportation*, Seattle, 429-441.

Bailey, P.A., Ballard, E.J., Hudson, D.A. and Temarel, P. (2000a). Time Domain Analysis of Vessels in Waves Accounting for Fluid Memory Effects. In Proc. *NAV2000, International Conference on Ship and Shipping Research* , Volume II, pages 9.4.1-9.4.11, Venice, Italy.

Bailey, P.A., Hudson, D.A., Price, W.G. and Temarel, P. (2000b). Comparisons Between Theory and Experiment in a Seakeeping Validation Study, *Trans. RINA*, paper 261, 2000.

Bailey, P.A., Hudson, D.A., Price, W.G. and Temarel, P. (2001a). Time Simulation of Manoeuvring and Seakeeping Assessments Using a Unified Mathematical Model. *Trans. RINA*, Accepted for publication 2001.

Bailey, P.A., Hudson, D.A., Price, W.G. and Temarel, P. (2001b). A Simple yet Rational Approach to the Panelling of a Hull Surface. *Trans. RINA*, Accepted for publication 2001.

Beck, R.F., Cummins, W.E., Dalzell, J.F., Mandel, P. and Webster, W.C. (1989). *Principles of Naval Architecture*, Volume 3, Chapter 8, SNAME.

Inglis, R.B. and Price, W.G. (1982). A Three Dimensional Ship Motion Theory: Comparison Between Theoretical Predictions and Experimental Data of the Hydrodynamic Coefficients with Forward Speed, *Trans. RINA* **124**, 141-157.

King, B.K., Beck, R.F. and Magee, A.R. (1988). Seakeeping Calculations with Forward Speed Using Time Domain Analysis. In *17th Symposium on Naval Hydrodynamics*, pages 557-596, The Hague, Netherlands.

Molland, A.F., Wellicome, J.F., Temarel, P., Cic, J. and Taunton, D.J. (2000). Experimental Investigation of the Seakeeping Characteristics of Fast Displacement Catamarans in Head and Oblique Seas, *Trans. RINA*, paper 255.

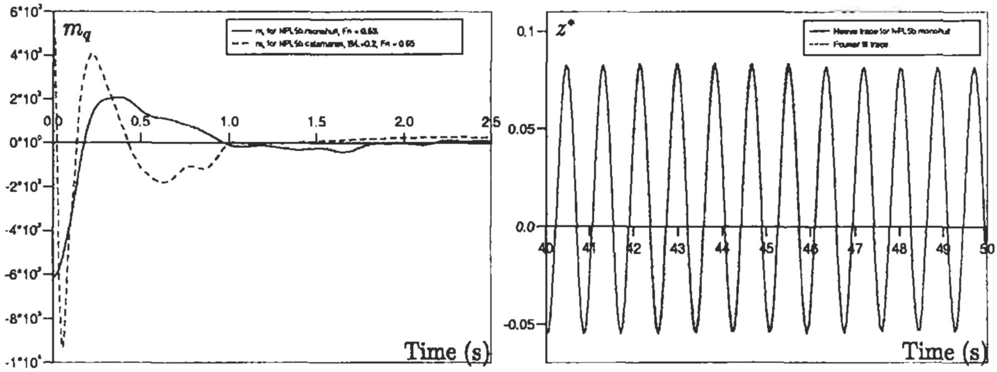

a) b)

Figure 1: (a) Pitch-pitch (m_q) impulse response functions for mono-hull and catamaran configurations and (b) heave response trace for mono-hull, Fn = 0.53, Heading = 180deg, $\alpha = 0.05625$m, $\omega_e' = 5.42$

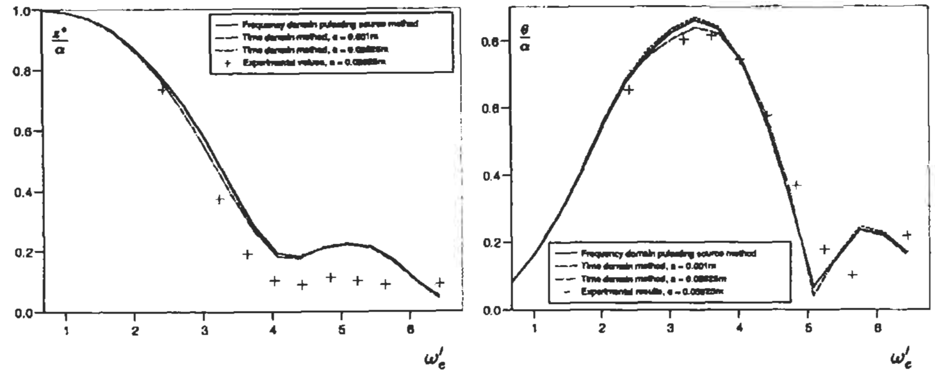

Figure 2: Heave and Pitch RAOs for a NPL5b mono-hull in regular head waves of variable amplitude. L=4.5m, Fn=0.2.

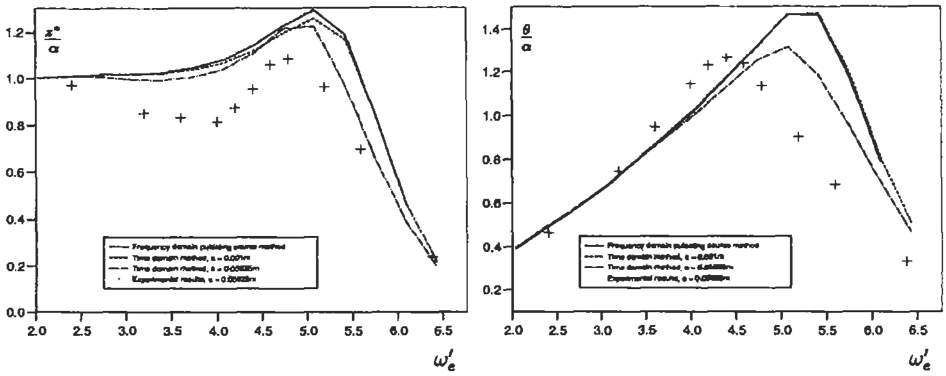

Figure 3: Heave and Pitch RAOs for a NPL5b mono-hull in regular head waves of variable amplitude. L=4.5m, Fn=0.53.

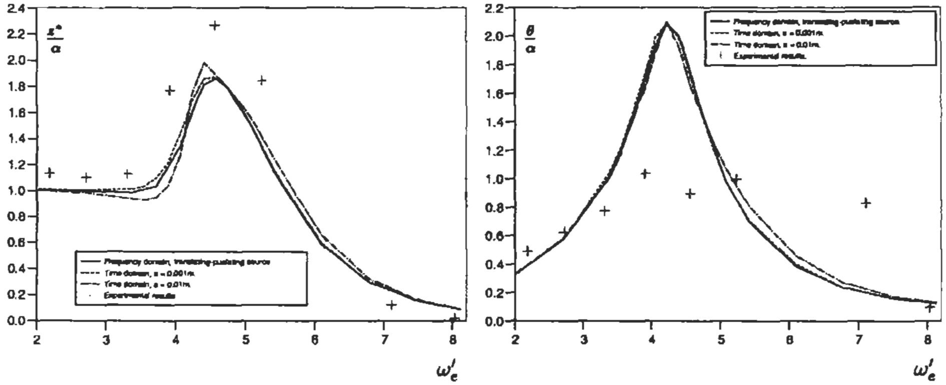

Figure 4: Heave and Pitch RAOs for a NPL5b catamaran in oblique regular waves (150 degree heading), L=4.5m, S/L=0.2, Fn=0.65

Practical Design of Ships and Other Floating Structures
You-Sheng Wu, Wei-Cheng Cui and Guo-Jun Zhou (Eds)
© 2001 Elsevier Science Ltd. All rights reserved

TIME-DOMAIN SIMULATIONS AND MEASUREMENTS OF LOADS AND MOTIONS OF PLANNING HIGH-SPEED CRAFT IN WAVES

K. Garme

Division of Naval Architecture, Royal Institute of Technology, KTH
Stockholm, S-100 44, Sweden

ABSTRACT

A 2-dimensional non-linear time-domain simulation model tailored for planing hulls in head seas, is presented together with results from model experiments, studying motional response and hull pressure distribution. A wave equation representation of the wave measurement is used in the numerical simulations enabling direct comparisons between simulated and measured time series. Compared quantities are heave and pitch motions; accelerations at bow and centre of gravity; and simulated section loads compared with integrated section wise pressure measurements. It is concluded from the measurement results that the difficulties to model planing calm water performance, noticed by many authors, are above all due to the flow at transom. It is also shown that with a simple correction of the excitation force close to the stern the performance of the simulation model is improved in calm water as well as in waves. The modified simulation model accurately repeats all measured quantities also at severe wave conditions when the hull occasional leaves the water and reenters with the characteristic slamming response all along the hull.

KEYWORDS

Time-domain simulation, Seakeeping, Pressure measurement, Planing, HSC, Slamming

1 INTRODUCTION

An absolute condition for a successful structural design is a realistic picture of what situations, in terms of loads and motions; the ship has to withstand during its lifetime. Striving towards an optimised design, the better knowledge of the load condition, the closer the designer can get to the optimum. The water pressure on the hull is simultaneously the origin of structure load and the cause of the rigid body response, defining the seakeeping performance and human comfort. The research project on loads and motions of HSC, tries to catch the situation starting from the dynamic pressure distribution leading to its effect on structure and motions. This work reviews a time-domain simulation model for a planing monohull in head seas and model experiments on such craft. A method to create a wave model from a measured wave signal is described and used to enable validation of the simulation model by direct comparison with measured time series.

2 SIMULATION MODEL

The time-domain simulation model is based on 2-dimensional potential theory. It has been developed with the starting point that the classical analogy of a planing hull in calm water and the water entry of a 2-dimensional section can be generalised to approximate the hydrodynamic loads on a slender planing hull during transient conditions in waves (Garme 2000). The section forces are formulated in terms of added mass coefficients and incident local flow velocities and integrated along the hull to formulate the equations of motions. The added mass high-frequency coefficients are dependent of the local draught and pre-calculated, stored and collected by the time-stepping procedure. The incident flow velocity is a function of water particle velocity, ship forward speed and hull motion. The local sectional draught is calculated as the distance between the keel line and the hull-wave surface intersection. The local water surface deformation, pile-up, is added to the wave height. This is, at least approximately, to satisfy the kinematic free-surface condition. For hard chine sections the pressure decreases sharply when the chine is wetted. This is an important effect to model, and is caught by adding the pile-up to the draught. The 2-dimensional hydrodynamic problem is solved with a panel method based on the Tulin & Hsu (1986) approach dividing the singularity distribution into a source distribution treating the incident velocity and a vortex distribution handling the sideways surface flow. The latter satisfies a Kutta condition in the transverse direction. The equations of motions are solved with a predictor-corrector method. The local draught, hydrodynamic coefficients and local incident velocity is updated at each time-step and at every iteration step during the iteration for dynamic equilibrium. This procedure makes the coefficients in the equations of motions time dependent and the solution non-linear. The simulation model is presently limited to constant forward speed and head seas and assumes the waves to be uninfluenced by the vessel besides the pile-up phenomenon.

3 MODEL EXPERIMENT

The model test set-up (in the following referred to as KTH HSC) was aimed to fulfil two major goals; first to gain high-resolution validation data for the simulation model and second to get a good picture of the pressure distribution at the most exposed parts of the hull. The latter in order to study how important the shape and dynamics of the load are to the structural response. A well-defined model situation, with as few variables as possible, was provided for by the choice of a prismatic hull, towed at a strait path, free to move in heave, roll and pitch. The prismatic hull (L_{oa}=1.05 m, B=0.25 m deadrise 22° and weight 6.5 kg) was basically a 1:10 scale model of the Swedish combat craft 90E on which full-scale trials were performed during the late nineties, Rosén (1998). Rosén & Garme (1999) compared those trials with simulations and the new model results complete a chain of data from full-scale to simulation.

The model was instrumented for hull pressure distribution measurement, by a matrix of 20 pressure transducers. The rigid body acceleration was recorded by 3 vertical accelerometers, with a resolution high enough to catch the transient characteristics of the slamming event. This demanded for a sampling frequency of 2.5 kHz. Rigid body motions, wave elevation and hull resistance were also measured.
The pressure transducers were concentrated to the bow area were the most severe slamming occurs and to an area close to the transom where the pressure somehow adjusts to atmospheric. The location of the pressure transducers and accelerometers are shown in Figure 1.

The test program comprised calm water, regular and irregular waves, and a variation of forward speed and relative headings. Tests were performed at three speeds aimed to represent displacement, semiplaning and planing conditions. The head and bow sea cases were the objectives of the study and the relative heading was stepped as 150°, 165° and 180° (180° defined as head seas). In regular waves tests were performed with 4-5 wave frequencies chosen to trig heave and pitch motion close to resonance. Each run was repeated with different wave amplitudes. For the irregular waves PM spectrum was used. Each spectrum was generated as a continuous spectrum in standard manner and as a discrete spectrum consisting of five wave components. The latter wave representation was used to simplify a direct evaluation of the measured time series with corresponding simulated ones.

The tests were performed at CEHIPAR, Madrid, within the EU TMR-ALSF project and are described in detail by Rosén & Garme (2001) and more generally in Garme & Rosén (2000).

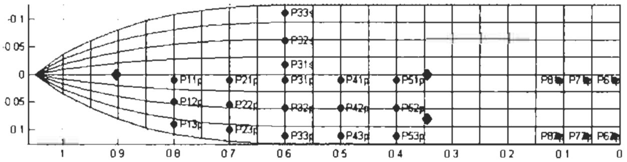

Figure 1: Test set-up and pressure transducer and accelerometer location. At all tests 20 transducers were in use. The transducers at position P51-3 were moved to position P11-P13 for all runs in waves.

4 WAVE MODEL

Generally, seakeeping experiments are evaluated as transfer functions and significant values. If, on the other hand, the experiments are to validate a time-domain simulation model it is preferable to compare measured time series and simulations. Here the measured wave signal was used to create a wave model for the simulation. The wave model gives the wave elevation and water particle velocities as a function of time and space and contains consequently all necessary information to expose the numerical hull to practically exactly the same waves as the physical ship model. The method for wave modelling, Garme & Hua (1999), is based on a simple linear fit of trigonometric functions to the measured wave elevation time series. The method works well especially on waves consisting of only a few wave components (see Figure 4). For this reason the discrete 5-component irregular waves were used in the experiments. As will be seen in the next section short sequences of more complex waves are also repeated well by this method (Figure 6).

5 RESULTS

The simulation model for hull motions and loads given in Garme (2000), showed promising agreement with the Fridsma (1969) results. However, a general discrepancy with a too low running trim in calm water and too large pitch at resonance in regular waves was noticed. Questions arose whether this was due to 3-dimensional effects in the bow or at transom or due to inaccuracies in the added mass calculation or in the estimate of the pile-up. The model pressure measurements show clearly that the pressure decreases rapidly in the absolute vicinity of the transom and that the 2-dimensional model is not valid there. Physically the 2-dimensional model does not satisfy the Kutta condition at the transom in the alongships direction of the flow. This is a local effect but, as it turns out, of major importance for the centre of pressure and thereby the running trim. Table 1, shows calm water performance predicted by different methods of which both the KTHSIM2 and the Savitsky (1964) results are close to the measurements.

TABLE 1.

CALM WATER TRIM AND RISE OF CG. MEASURED AND CALCULATED RESULTS OF THE FRIDSMA (1969) HULL CONFIGURATIONS A & B (PRISMATIC HULLS, L/B=5 AND DEADRISE 20°) AND OF THE EXPERIMENTS ON THE KTH HSC. RESULTS ARE PRESENTED FROM SIMULATION MODEL KTHSIM1 AND KTHSIM2 AND FROM THE SAVITSKY (1964) METHOD.

Hull	Measurement		KTHSIM1		KTHSIM2		Savitsky (1964)	
Speed coef. $C_v = V/\sqrt{L}$ [kn/$\sqrt{\text{ft}}$]	Trim [deg]	rise CG [% B]	Trim	rise CG	Trim	rise CG	Trim	rise CG
Fridsma A, deadrise 20°, Cv=4	4	6	3.4	4.7	4.2	3.8	4.4	4.6
Fridsma B, deadrise 20°, Cv=6	4	13	3.6	9.8	4.3	11.1	3.9	11.2
KTH HSC, deadrise 22°, Cv=4.7	6	9	4.4	7.0	6.2	10.2	5.5	10.1

The KTHSIM1 are the Garme (2000) simulation model in its original formulation and the KTHSIM2 is the same model but with a modification of the excitation force at the three aftermost sections (x=0-0.1 m). The correction is a function of forward-speed and based on the differences between the measurements and results from KTHSIM1 run in captive mode, in calm water, at the same speeds, trim and global-CG as the KTH HSC model (Figure 2).

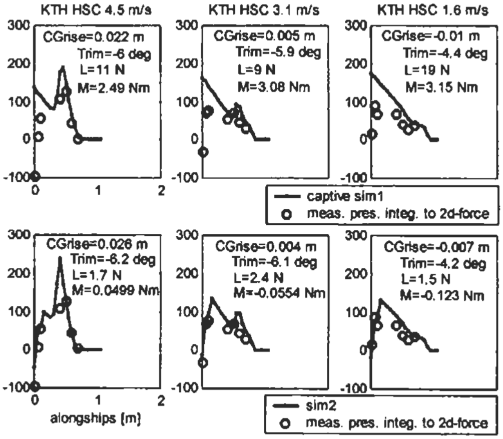

Figure 2: Measured and simulated section forces at calm water run. The upper row shows simulated (KTHSIM1) section forces with the model fixed at the model test trim and CG position and a section-wise integration of the measured pressure. At the lower row, the hull is free to move and has found its equilibrium by the modified simulation model (KTHSIM2). The CGrise and trim values in the upper row are the measured ones and constants in the captive mode simulation, in the lower row those are the simulated equilibrium. L and M are in both rows of graphs the calculated lift force and moment.

The modified simulation model, KTHSIM2, improves the agreement on the pitch response of the Fridsma (1969) configurations without detoriation of the other responses, examples for the configuration A and B are shown in Figure 3.

Using the wave model determined from the measurements the performance of the KTHSIM2 model is demonstrated by comparisons of simulated and measured time series. Two sequences are shown where the ship model is run in irregular head seas corresponding to the full-scale speed of 28 knots. Figure 4 and Figure 5 show simulated and measured rigid body responses at $H_{1/3}$=0.75m. The condition is severe with bow acceleration as large as 5g. Increasing the wave height to $H_{1/3}$=1.0m the situation becomes even more violent (Figure 6 and Figure 7). During this sequence the hull completely leaves the water (at 18.2s) and reenters a moment later appreciating a vertical acceleration of approximately 9g at the bow and 4g at the CG. The simulation model keeps good track of all responses and it is worth

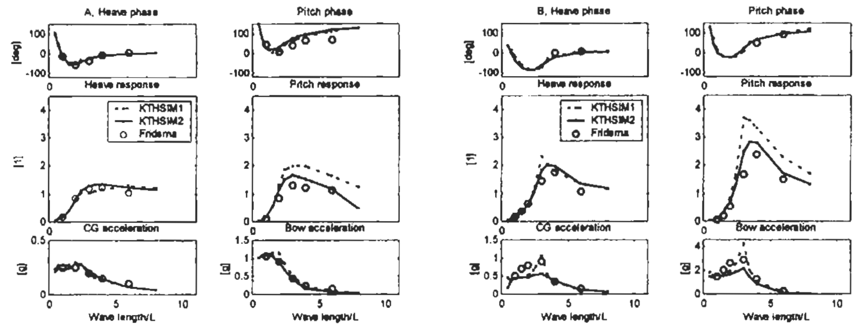

Figure 3: Examples on the agreement between simulations (KTHSIM1) & (KTHSIM2) and measurements of Fridsma (1969) configurations A and B in regular waves.

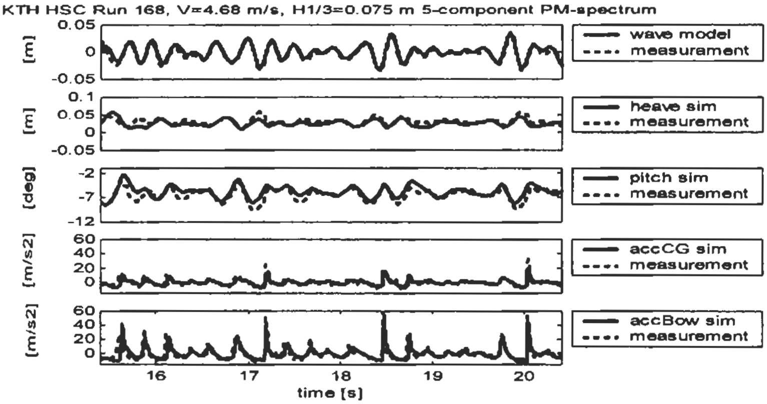

Figure 4: Simulated and measured time series. Quantities are in model scale.

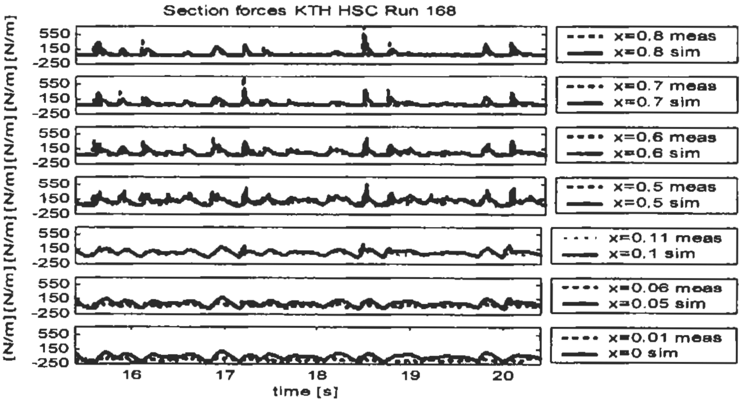

Figure 5: Comparison of calculated section forces and section wise integration of the pressure measurement. The x-position refers to the coordinate system in Figure 1. Quantities are in model scale.

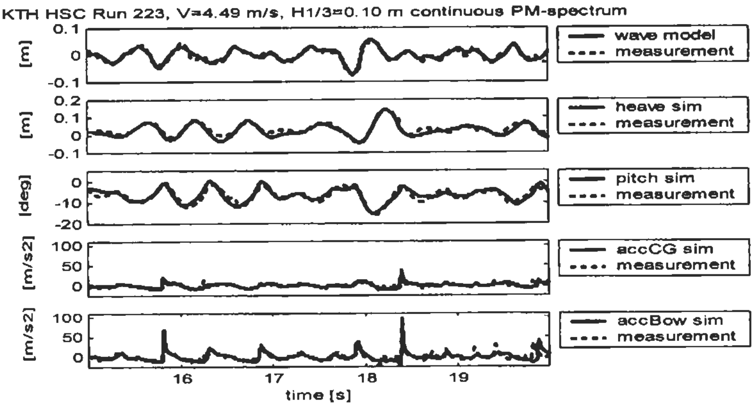

Figure 6: Simulation of a sequence in sever head seas where the complete hull leaves the water and reenters (18.1<time<18.5). A wave equation of 30 wave components models the wave measurement of the continuous spectrum.

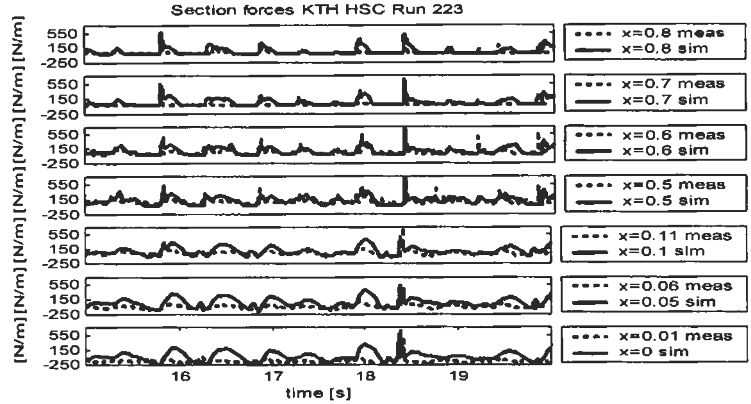

Figure 7: The simulated section forces are plotted together with a section-wise integration of the pressure measurement. Notice the slamming load along the hull. The load fluctuations at the aftmost sections are too pronounced in the simulation.

noting the section forces in Figure 7, where the typical slamming load occurs almost simultaneously over the complete hull length.

6 SUMMARY AND CONCLUSIONS

A 2-dimensional simulation model for the loads and motions of a planning hull in head seas is reviewed together with model experiment results and a method to create a wave model linking the simulations and measurements. The experimental results show on low pressure and even suction close to the transom. With a correction of the simulated excitation force at the aftmost sections (approx. 10% of the hull length) the agreement between simulations and model tests becomes very good. The calm water performance is of course good since the correction, based on calm water pressure measurements, was tailored for this but also the dynamic results are very close to the measurement. The pitch and heave responses, as well as the non-linear and transient acceleration signals, are well predicted by the simulation. The simulated local forces stick close to the integrated pressure measurements, especially at the fore sections. In the aft, the measured load-fluctuation in waves is less pronounced than the simulated. This can be due to the fact that the wave profile is not undeformed as the simulation model assumes. The wave equation method, which enabled the direct comparison of simulated and measured time-series, is shown to work well also in this high-speed application. The comparison between simulated and measured motions, accelerations and section forces give a good picture of both the loads the structure is exposed to and the excitation of the seakeeping and human comfort situation.

The 2-dimensional simulation approach, where the Kutta condition in the transverse plane is satisfied and where the pile-up is taken into account estimates the forces on the hull well except in the absolute vicinity of the transom. In that region a local model should be superimposed to correctly model the flow and satisfying the Kutta condition in the alongships direction. The simple correction of the excitation forces closest to the transom shows remarkably good results. The author believes that a fast and accurate simulation model allowing six degrees of freedom and any relative course angle can be formulated based on the present model. To achieve this the effort should be put on accurate pre-calculation of the hydrodynamic coefficients and pile-up and to find proper transom pressure corrections.

References

Fridsma G. (1969). A Systematic Study of the Rough-Water Performance of Planing Boats, *Davidson Laboratory report 1275*

Garme, K. & Hua, J. (1999). A Method to Analyse Seakeeping Model Measurements in Time Domain, *Proc. 9th Int. Offshore and Polar Engineering Conference ISOPE*, France

Garme, K. (2000). Time-Domain Model for Planing High-Speed Vessels in Head Seas, Licentiate Thesis TRITA-FKT 2000:07, ISSN 1103-470x, Royal Institute of Technology (KTH), Stockholm, Sweden

Garme K. & Rosén A. (2000). Experimental Pressure Investigation on a High-Speed Craft in Waves, *Proc. Hydrodynamics of high speed craft*, RINA, UK

Rosén, A. & Garme, K. (1999). Slamming Studies on High Speed Planing Craft Through Full-Scale Trials and Simulations, *Proc. 5th International Conference on Fast Sea Transportation FAST*, USA

Rosén A. & Garme K. (2001). Pressure Investigation on a High-Speed Craft in Waves, TRITA-FKT 2001:11, ISSN 1103-470X, Royal Institute of Technology (KTH), Stockholm, Sweden

Rosén, A. (1998). Full-Scale Trials on a Small High Speed Naval Craft with Focus on Slamming. *Proc. 17th Int. Conference on Offshore Mechanics and Arctic Engineering OMAE*, Portugal

Savitsky D. (1964). Hydrodynamic Design of Planing Hulls, *Marine Technology* **1:1**

Tulin M. P. and Hsu C.C. (1986). *Theory of High-Speed Displacement Ships with Transom Sterns*, Journal of Ship Research **30:3**

Practical Design of Ships and Other Floating Structures
You-Sheng Wu, Wei-Cheng Cui and Guo-Jun Zhou (Eds)
© 2001 Elsevier Science Ltd. All rights reserved

ANALYSIS OF RINGING BY CONTINUOUS WAVELET TRANSFORM

S.H. Kwon[1], H.S. Lee[1], J.S. Park[1], M.K. Ha[2], Y.J. Kim[3]

[1]Department of Naval Architecture and Ocean Engineering, Pusan National University,
30, Kumjung-Ku, Pusan 609-735, Korea
[2]Shipbuilding and Plant R&D Center, Samsung Heavy Industries Co, Ltd., Koje 656-710, Korea
[3]Department of Naval Architecture and Marine Systems Engineering, Pukyong National University,
599-1, Nam-Ku, Pusan 608-737, Korea

ABSTRACT

The present study investigated ringing phemomenon by using continuous wavelet transform. The used mother wavelet is the Morlet wavelet. Experiments were done in a wave tank. Breaking waves were generated to understand the ringing phenomenon. The model tested was a surface piercing circular cylinder. The time series of the wave height and the force acting on the cylinder were measured. They were analyzed by using continuous wavelet transform. The scalograms of the time series of the wave height and those of the forces revealed the fact that high frequency components were generated at the onset of the breaking wave impact in the time domain. This can be hardly detected if one relied on traditional spectral analysis. The coherence analysis supported the above mentioned results.

KEYWORDS

Ringing, Continuous Wavelet Transform, Breaking Waves, Coherence Analysis, Spectral Analysis, Circular Cylinder

1 INTRODUCTION

The motivation of the present analysis was based on the fact that wavelet transform is an excellent tool in analyzing transient signals. Ringing is a typical transient phenomenon in the fileds of ocean engineering. Ever since the ringing phenomenon was known during the Hutton TLP design, subsequent model tests and analytic works have been undertaken (C.H.Kim, 1996, 1997; Stansberg, 1995; Marthinsen, 1996; Welch, 1999). The objective of the present study is to apply the continuous wavelet transform (CWT) to the ringing analysis. As a first attempt in applying the CWT to ringing phenomenon, the authors carried out the CWT analysis with experimental data.

The experiment was carried out in a wave tank. A vertical circular cylinder was placed in the incoming breaking waves. Since experiments were carried out with fixed cylinder, it was the excitation not the ringing response to be investigated in the present study. The time histories of wave elevation and the forces acting on the cylinder were measured and analyzed. The spectra of the wave and forces were also presented. The spectral analysis gives only energy content in the frequency domain. However, by using the CWT, the information in frequency domain as well as that in time domain can be obtained. Coherence analysis was also carried out to demonstrate the ability of CWT in locating the time evolution of ringing phenomenon.

2 CONTINOUS WAVELET TRANSFORM

A CWT of a signal s(t) is given by

$$W_S(a,b) = \frac{1}{\sqrt{|a|}} \int_{-\infty}^{\infty} \psi^*\left(\frac{t-b}{a}\right) s(t)\,dt \qquad (1)$$

where ψ is wavelet function, a is the scaling parameter, and b is the transformation parameter, and $*$ represents complex conjugate. It can be stated that CWT is the sum over all time of real signal s(t) multiplied by the scaled, shifted wavelet function. The parameters a and b vary continuously. The wavelet function used in the present analysis is Morlet wavelet. The formulation of this wavelet function is show below

$$\psi(t) = \pi^{-\frac{1}{4}}\left(e^{-i\omega_0 t} - e^{-\frac{\omega_0^2}{2}}\right)e^{-\frac{t^2}{2}} \qquad (2)$$

The second term is added to satisfy the so-called admissibility condition. However, for large ω_0 ($\omega_0 \geq 5.5$), the correction term is numerically negligible. Thus the complex valued Morlet wavelet can be approximated by

$$\psi(t) = \pi^{-\frac{1}{4}} e^{-i\omega_0 t} e^{-\frac{t^2}{2}} \qquad (3)$$

Fourier transform of this wavelet is of the form

$$\hat{\psi}(\omega) = \pi^{-\frac{1}{4}} e^{-\frac{(\omega-\omega_0)^2}{2}} \qquad (4)$$

Figure 1 shows real and imaginary part of the Morlet wavelet. Its spectrum is shown in Figure 2.

3 MODEL TESTS

The experiment was carried out in a 2.5m wide, 40m long, and 1.2m deep wave tank. Wave loads were measured on vertical surface piercing cylinder of 0.10m diameter. The draft of the cylinder was 1.08m. The total length of the cylinder was 1.5m. The column of the cylinder was fixed to a load cell, which was fixed to a carriage frame. Two wave gauges were attached to front and back of the cylinder. The experimental setup is illustrated in Figure 3. The breaking waves were generated by using three parameters i.e., location of the generated wave from the wave maker, maximum stroke, and duration of the wave maker operation. The three parameters used were 23m, 0.2m, and 29.5 seconds for the location, the maximum stroke, and the duration, respectively. The time histories of the wave elevation measured at the front of the cylinder and forces acting on the cylinder were shown in Figures 4 and 5.

4 RESULTS AND DISCUSSION

The time histories of the forces illustrated in Figure 5 show that the signals are oscillating at the natural frequency of the cylinder after the impact of the breaking wave. The CWT of the wave elevation and the forces are shown in Figures 6 to 7. ω_0 in Eqn. 4. was taken to be 5 for the calculation of the CWT. The high frequency components start appearing at about a=6 in Fig 6. These newly generated high frequency components are believed to be responsible to the resonance of the cylinder. The high frequency force components were also generated at the onset of the breaking wave impact as shown in Figure 7. The spectra of the wave and forces are shown in Figures 8 and 9. The spectrum of the generated breaking wave shown in Figure 8 is widely spread over the frequency range. The natural frequency of the cylinder estimated from the force spectrum is 2.8Hz. Therefore, the natural frequency of the cylinder tested in this study was within the band of the wave spectrum. This indicates the fact that the ringing can be understood as a natural frequency resonance of the structure due to the breaking wave impact. The coherence analysis with the results of CWT was also carried out. In analogy with Fourier energy density spectrum, a wavelet spectrum for a data x(t) can be readily defined

$$S_X(a,b) = W_X(a,b)W_X^*(a,b) = |W_X(a,b)|^2 \qquad (5)$$

A cross wavelet spectrum for the analysis of two simultaneously measured data x(t), y(t) can be defined as

$$S_{XY}(a,b) = W_X(a,b)W_Y^*(a,b) \qquad (6)$$

The wavelet coherency and wavelet coherence can be accordingly defined as

$$\Gamma(a,b) = \frac{S_{XY}(a,b)}{\sqrt{W_X(a,b)W_Y(a,b)}} \qquad (7)$$

$$\Gamma^2(a,b) = \frac{[\mathrm{Re}S_{XY}(a,b)]^2 + [\mathrm{Im}S_{XY}(a,b)]^2}{W_X(a,b)W_Y(a,b)} \qquad (8)$$

where Re and Im represent real part and imaginary part of complex value respectively.
The cross section of the wavelet spectrum of the wave and the force acting on the cylinder at b=0.25 are illustrated in Figures 10. The real part and imaginary part of the coherence and its phase are shown in Figures 11. The maximum coherency occurs at the zero phase points. The maximum coherence which is responsible to the ringing seems to have occurred at translation scale a= 6.9. The present study carried out using CWT was able to detected not only frequency components which seems to responsible for the ringing but also the specific time duration of the phenomenon. This result can not be obtained if the traditional Fourier analysis was adopted.

5 CONCLUSIONS

The analysis of ringing was carried out using CWT. The traditional spectral analysis was also carried out. The CWT of the wave elevation and force time histories illustrate the appearance of high frequency components which are believed to trigger the ringing phenomenon in the time domain. This feature is superior characteristics of CWT over traditional spectral analysis. The coherency analysis can be also used to locate the exact time of the maximum coherence between wave and the structure. It is concluded that ringing is a natural frequency resonance of the structure due to the breaking wave impact.

References

Kim C.H., Xu Y., Zou J. and Won Y.S.(1996). A Model for Weak Impacting Force on Vertical Truccated Cylinder Due to Steep Asymmetric Wave. *Proceedings of the Sixth International Offshore and Polar Engineering Conference* **vol.3**, 215-220.

Kim C.H., Zhao C.T., and Xu Y. (1997). Spring and Ringing Due to Laboratory-Generated Asymmetric Waves. *International Journal of Offshore and Polar Engineering* **7:1**, 30-35.

Marthinsen T., Stansberg C.T., and Krokstad J.R. (1996). On the Ringing Excitation of Circular Cylinders. *Proceedings of the Sixth International Offshore and Polar Engineering Conference* **vol 1**, 196-204.

Stansberg C.T., Huse E. Krokstad J.R., and Lehn E. (1995). Experimental Study of Non-Linear Loads on Vertical Cylinders in Steep Random Waves. *Proceedings of the Fifth International Offshore and Polar Engineering Conference* **vol 1**, 75-82.

Welch S., Levi C., Fontain E., and Tulin M.P. (1999). Experimental Study of the Ringing Response of a Vertical Cylinder in Breaking Wave Groups, *International Journal of Offshore and Polar Engineering* **9:4**, 276-282.

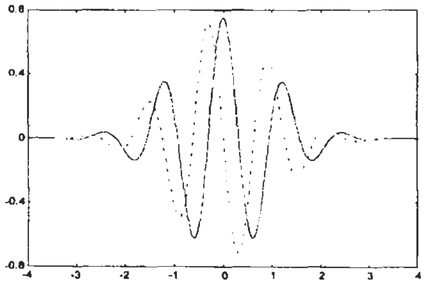

Figure 1: Real & imaginary part of Morlet wave

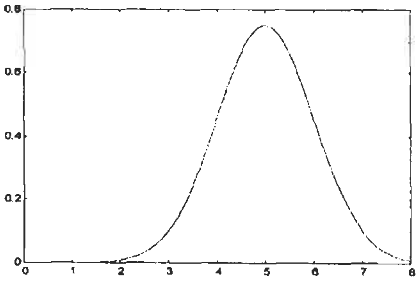

Figure 2: Spectrum of Morlet wave

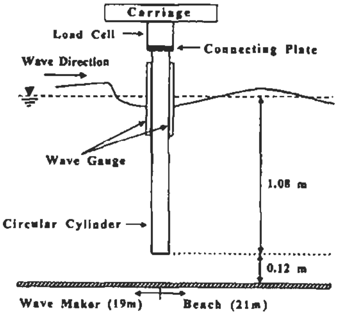

Figure 3: Experimental Setup

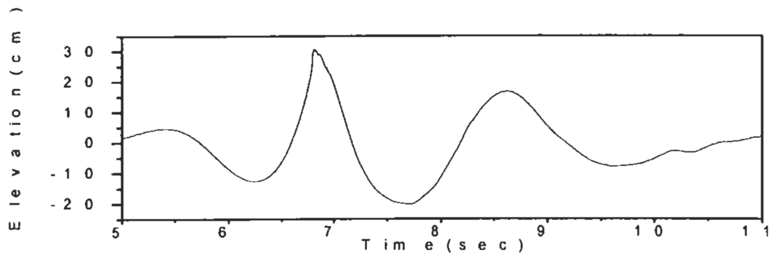

Figure 4: Time history of wave elevation

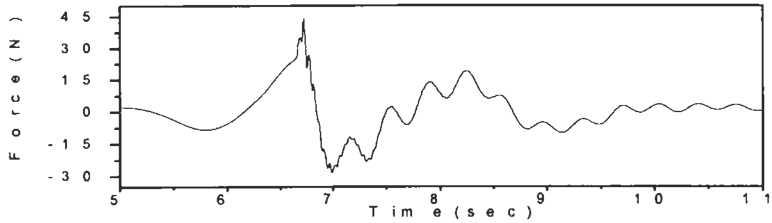

Figure 5: Time history of force

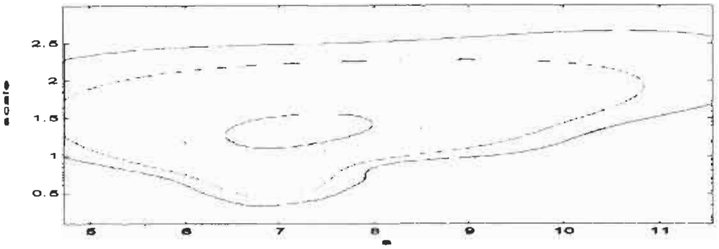

Figure 6: Scalogram for wave

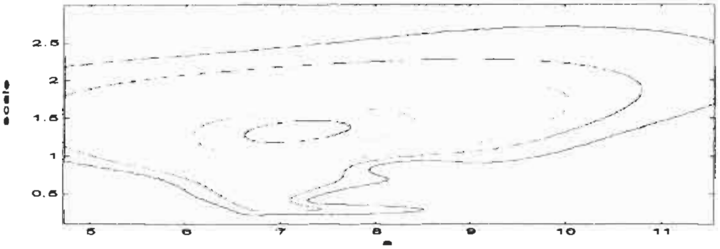

Figure 7: Scalogram for force

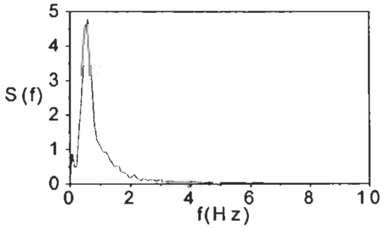

Figure 8: Spectrum of wave

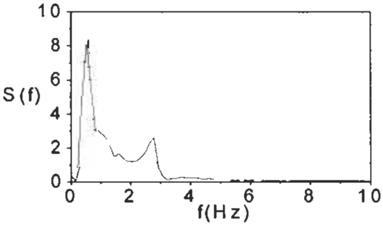

Figure 9: Spectrum of force

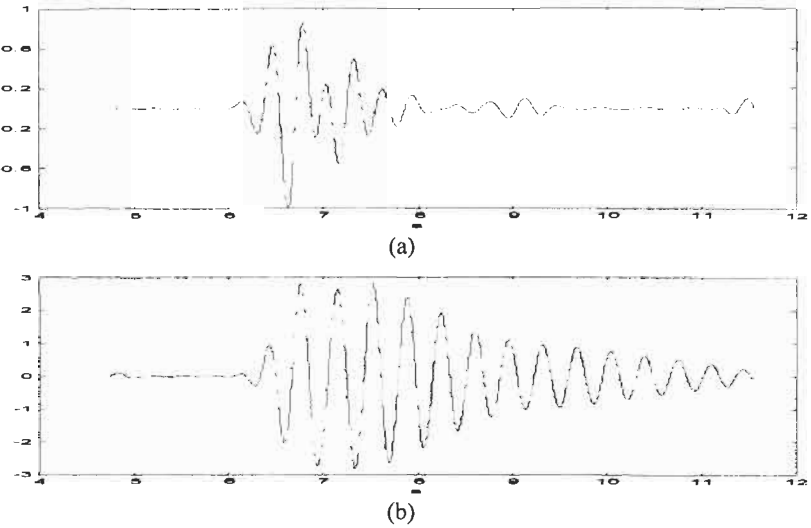

Figure 10: Wavelet spectrum of wave elevation at b=0.25(a), wavelet spectrum of force at b=0.25(b)

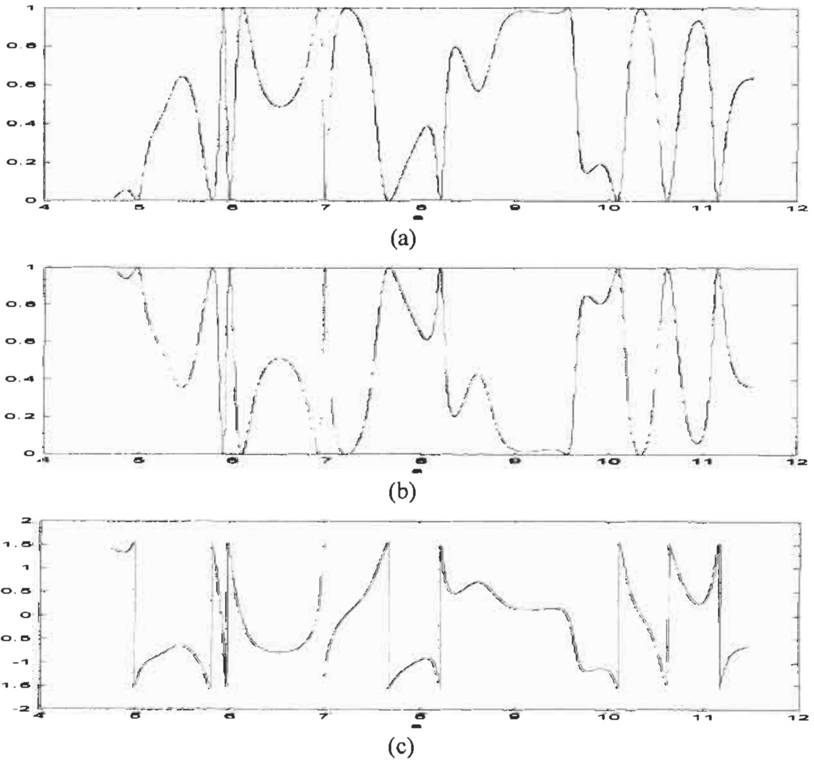

Figure 11: Real part of Coh^2(a), imaginary part of Coh^2(b), phase of coherence(c)

Practical Design of Ships and Other Floating Structures
You-Sheng Wu, Wei-Cheng Cui and Guo-Jun Zhou (Eds)
© 2001 Elsevier Science Ltd. All rights reserved

GREEN SEA AND WATER IMPACT ON FPSO IN STEEP RANDOM WAVES

C. T. Stansberg [1] and S.I. Karlsen [1]

[1] Norwegian Marine Technology Research Institute A/S (MARINTEK)
N-7450 TRONDHEIM, Norway

ABSTRACT

Results from 1:55 scaled model tests with an FPSO in irregular waves are presented. Interactions leading to green sea events in steep random waves, and the resulting impact loads, are investigated. This includes water on deck as well as bow slamming. In particular, storm sea states with moderate wavelengths are considered. The measuring equipment include wave probes in a grid at the bow and on the front deck, vessel motions, as well as load and pressure cells on the deck house and on the bow. High-resolution video recordings are also included. The results show that critical events often occur in steep and energetic nonlinear waves. The ship pitch motion is also essential, both with respect to the amplitude and the relative phase. Wave spectra with moderate wave periods may therefore be more critical than long waves. The water propagation on deck and resulting impact loads vary significantly from one event to another, probably due to influence from incoming wave properties.

KEYWORDS

Green sea; Wave impact; Bow slamming; FPSO; Model tests; Random waves.

1 INTRODUCTION

In recent years there has been some focus on damages on FPSO bow and deck structures, arising from events with extreme wave-structure interaction in rough sea states. Some examples from water on deck events on Norwegian production ships have been given in Ersdal & Kvitrud (2000), while severe bow damage has been reported on a UK vessel West of Shetland (MacGregor et. al., 2000). A detailed theoretical description of these problems is complex, since highly nonlinear interaction effects are involved, in combination with nonlinear incoming waves. Various numerical approaches are in development, see e.g. Greco & Faltinsen (2000), but complete numerical models for design use still do not seem be generally available, and predictions must be based on simplified models in combination with experiments. Thus model test data are important in the understanding and modelling of the physical mechanisms. (Buchner (1995), Buchner & Voogt (2000), Gorf et. al. (2001).

In the present work, new model tests with a turret-moored FPSO carried out in scale 1:55 are reported. The purpose of the tests is to observe and measure green sea (water on deck) and their impact load effects, as well as bow slamming phenomena, in realistic steep North Sea storm conditions. In particular, random (irregular) storm wave spectra with moderate peak periods in the range 12 – 14 seconds are included, since the vessel motion is then out of phase with the wave, and do play a role for the wave impact events. The tests are planned for systematic research purposes, and not for any specific system or field. The results are presently being applied in the development of a new design tool (Hellan et. al., 2001a, 2001b).

2 DESCRIPTION OF EXPERIMENT

The model tests were carried out in MARINTEK's 50mx80m Ocean Basin. A 1:55 scaled model of a turret moored 100 000 tons monohull vessel, with length Lpp=200m, was selected for the experiments. The model was moored at the centre of the basin with a realistic10-line catenary system in 84m water depth. One bow shape was investigated, with four different bulwark heights: 0.00m -1.65m - 3.10m - and 4.40m), while further tests with alternative bow shapes are planned in the future. The vessel pitch period was 9.0s. All data in the following are given in full scale, unless where otherwise is informed.
The measuring equipment on the forecastle deck is shown in Figure 1, seen from above. A 10-staff wave array was installed in order to record the water flow on deck, and 4 relative-wave elevation gages were fixed to the front of the bow. The wave disturbance was found from the relative wave signal by correcting for the vertical bow motion. Prior to the tests, the undisturbed wave elevation was measured at the bow region and at COG. Three load panels, each measuring the integrated force on an area 2.75m x 2.75m, were installed on the deck house wall. Five 3.85m x 1.65m panels were installed on the upper part of the bow. The force sensors were made particularly stiff, with natural periods 175 Hz (full scale, in water). In addition, two pressure cells were installed on the bow. Vessel motions in 6 DOF were measured by an optical recording system with accuracy better than 0.001m (model scale). The sampling rate was 647 HZ (full scale) for the load and pressure measurements, and 11 Hz for the other channels. Continuous recordings simulating 3 hours storms were made of all the channels.
Continuous video recordings of all tests were made with a 4-camera high-resolution system, including two cameras from the side, one viewing forward from the top of the deck house ("captain's view"),

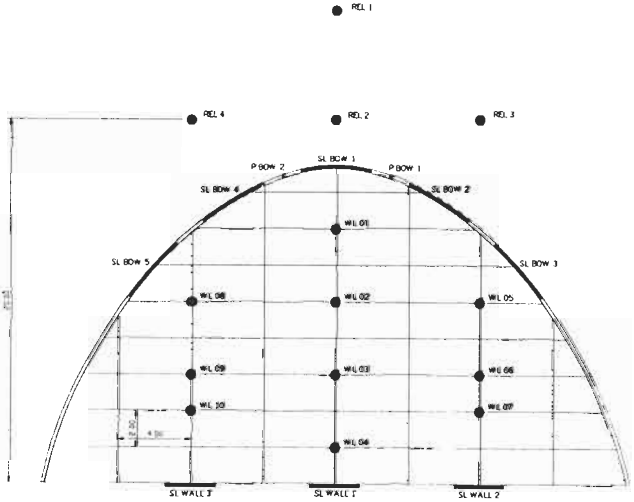

Figure 1: Measuring equipment on deck.

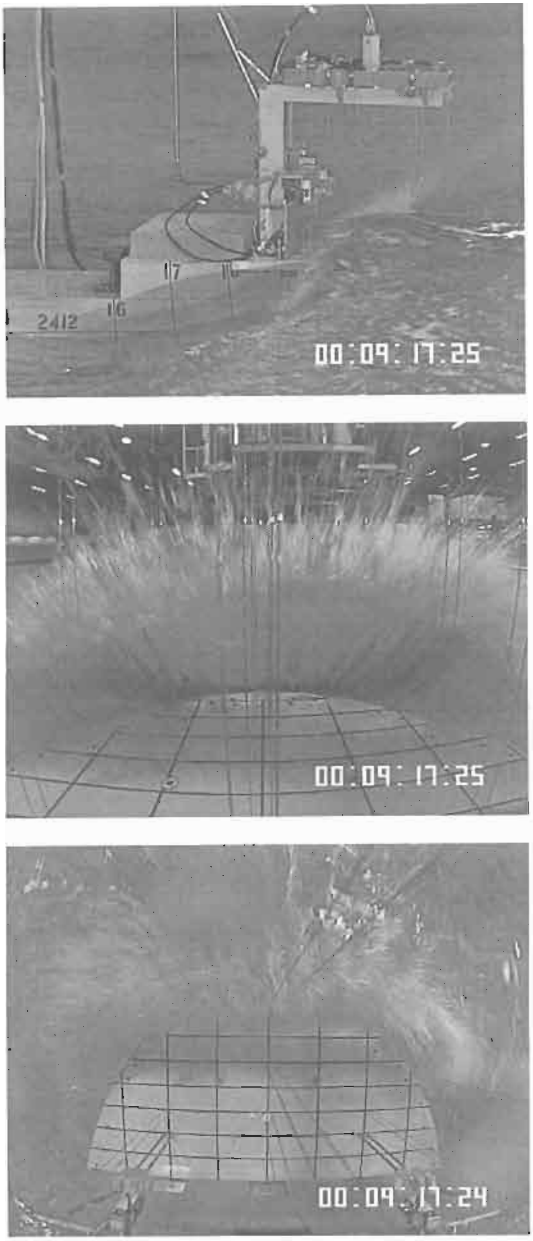

Figure 2: Photos from test in irregular waves: Side, forward and downward views.

and one viewing downwards on the front deck. An example with pictures from three of the cameras, showing one of the most extreme and steep random wave events, is presented in Figure 2. The impact from the energetic wave can be observed through the shape of the disturbed wave.

The irregular wave conditions are described in Table 1. No wind nr current was included. All tests were modelled as 3-hours storms (full scale). In addition, a few regular wave tests were also run.

TABLE 1

TEST CONDITIONS, IRREGULAR WAVES

Irreg. wave ident.	Sea state description
A	Hs=10.0m Tp=14.0s PM spectrum,
B	Hs=12.0m Tp=12.0s TH (2-comp.) spectrum,
C	Hs=12.0m Tp=12.0s JONSWAP (1-comp.) spectrum
D	Hs=14.0m Tp=14.0s TH (2-comp.) spectrum
E	Hs=16.0m Tp=14.0s TH (2-comp.) spectrum
F	Selected sequence from sea state C repeated 12 times

PM means "Pierson-Moskowitz", and TH is a 2-component spectrum (Torsethaugen,1993). Except from sea state A, all wave conditions represent quite steep storm North Sea conditions. In the following analysis, only Spectra B, C and D are included. See Figure 3. Spectrum E was run in order to observe the statistical variation between repeated, "identical" extreme wave events, with focus on the load measurements. All tests were run in head seas (0 deg), and with four bulwark heights.

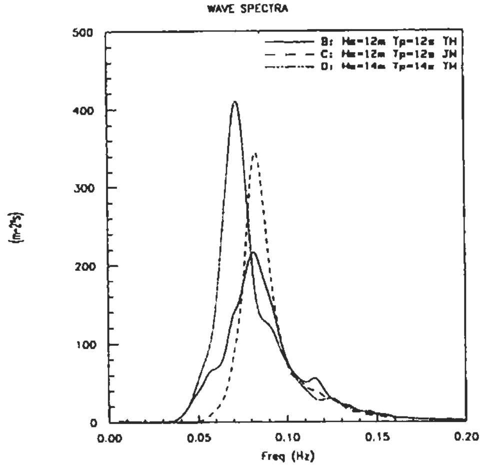

Figure 3: Wave spectra B, C & D

3 RELATIVE WAVE MOTION AND PROBABILITY OF EXCEEDANCE AT BOW

Results from relative wave measurements made 2m in front of the bow (Probe REL2), for the three different irregular wave conditions B, C & D, are presented in Figure 4 (left). Probability distributions of peak values from 3-hours records are compared to each other. The results are for cases with bulwark 1.65m, but they are also very similar to those without bulwark. Weibull-scaled axes are used. The Rayleigh model for spectrum B is also shown. The deck level at 12.8m is marked with vertical dashed line. Exceedence probabilities derived from the measured distributions are shown in Table 2.

From Fig. 4 and additional results it is found that the probability of relative waves exceeding the deck level and the bulwark heights is clearly higher than predicted from a Rayleigh model. One explanation is the nonlinear contributions in high and steep incoming waves. The crest height probability distributions in Figure 4 (right), where the deviation from the Rayleigh prediction is clearly documented for case B, strongly indicate this. The role of nonlinear waves in the green sea problem has been investigated and discussed further on basis of the present experiments in Stansberg & Nielsen (2001), where it is found that serious green water events are to a large extent determined by energetic nonlinear waves, in combination with a negative bow motion. The *highest* relative wave peaks in Figure 4a are, however, close to the Rayleigh estimates, probably as a result of very large pitch motion - which is found to be slightly over-predicted by the Rayleigh model. Nonlinear effects were found to be of minor importance for the ship motion (Hellan et. al. 2001a).

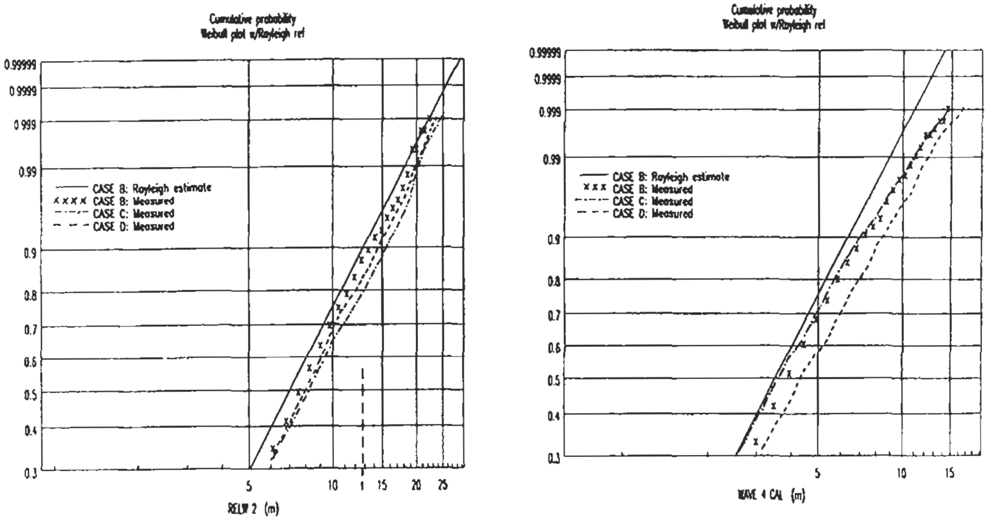

Figure 4: Peak value probability distributions. Left: Relative wave #2. Right: Incoming wave crests

TABLE 2
PROBABILITY OF PEAK VALUE EXCEEDANCE AT GIVEN LEVELS OF FREEBOARD

Test no.	Wave spectrum	Level 12.8m (deck level)	Level 14.45m (bulw. 1)	Level 16m	Level 18m	Level 20m
1130	B	12%	8%	6%	2%	0.7%
1140	C	20%	14%	9%	5%	1.0%
1150	D	15%	10%	8%	3%	1.0%

We also see from Fig. 4 that the three cases differ somewhat. The most serious condition is in fact not the 14m sea state (D), but rather the 12m case with a single-peaked JONSWAP spectrum (C), although the maximum incoming crests are clearly higher for case D. This is due to the relative phase of the pitch motion, which is very sensitive to the wave period. Thus for 14s waves, the bow motion is 60 deg out of phase with the wave; and for 12s it is 90 deg,. The narrow-peaked 12s spectrum is more critical than the broader one probably because more energy is then concentrated at shorter periods (see Fig. 2).

4 WATER PROPAGATION ON DECK

The maximum level of the water propagating along the centre line of the forecastle deck is illustrated in Figure 5, for four selected wave events with massive green water on deck (the identifications A-D should not be confused with the spectra in Table 1). The corresponding level at the relative-wave probe REL2 in front of the bow is also included for comparison (the freeboard deck level 12.8m is subtracted). Different types of behaviour are observed. In some cases the water level is rapidly decreasing after a short distance, as in a dam-breaking type of mechanism. This is mainly a result of a large negative bow motion (≈ 10 - 15 m), while the initial wave particle velocity is not necessarily very high. In other cases, the event is more determined by the kinematics of the incoming wave itself (combined with negative bow motion ≈ 2 – 5 m), and the water level shows a less rapid decrease with the propagation. The latter cases seem to be more critical for impact loads than the "dam-breaking" type (see below).

Results for all four bulwark heights are included in the figure. They indicate that for high relative-wave motions clearly over-topping the bulwark, the actual height of the bulwark is not very critical. But a high bulwark does certainly prevent or reduce green water events, although the waves may still lead to a vertical flow upwards across the bulwark and on to the deck.

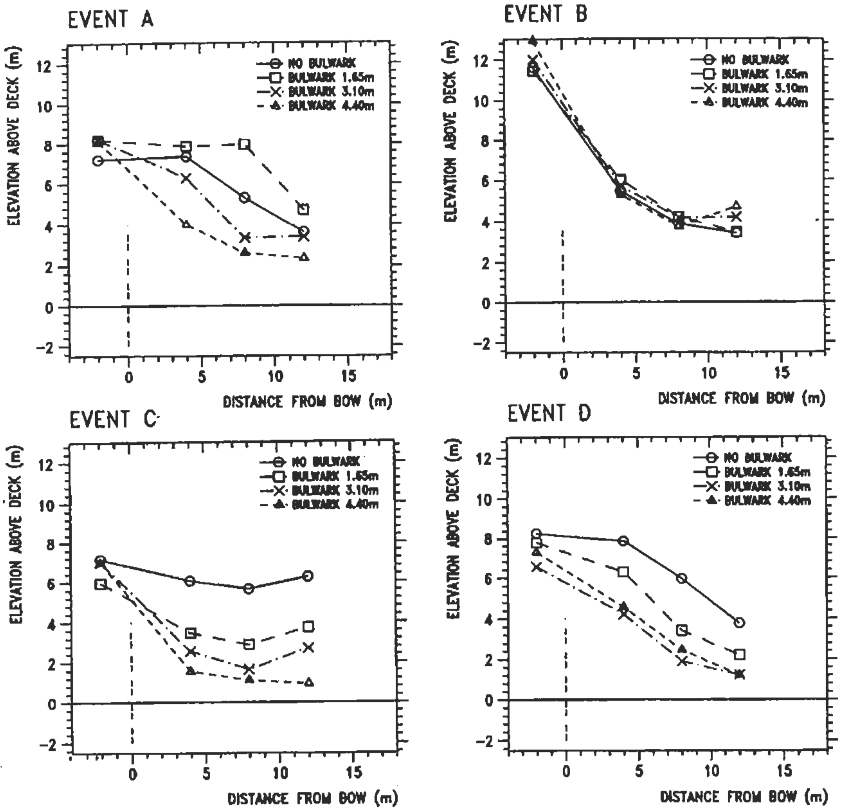

Figure 5: Water propagation on deck - four green sea events. The bulwark location is also indicated.

The velocity of the initial water flow on the deck has been preliminary estimated to be up to 8 – 9 m/s, based on predictions made from the measured elevation assuming second-order free-surface wave kinematics (Stansberg & Gudmestad, 1996). Steep waves give highest velocities. These values agree with estimates made from time lags observed between the probe measurements. After further 10–15m on the deck, the time lags indicate an increase up to approximately 15 m/s in the extreme cases.

The correlation between the elevation in front of the bow and the resulting water on deck 4m aft of the bow (WL1), is shown in Figure 6 (left), for the case with no bulwark. Events with large relative waves or large amounts of water on deck have been selected. In some cases, there is almost a one-to-one correlation, while in other cases, the water level has been reduced to 50% at this location. The one-to-one cases are due to steep waves, while the others are more a direct result of large negative bow motion and a resulting “dam-break”-like behaviour .

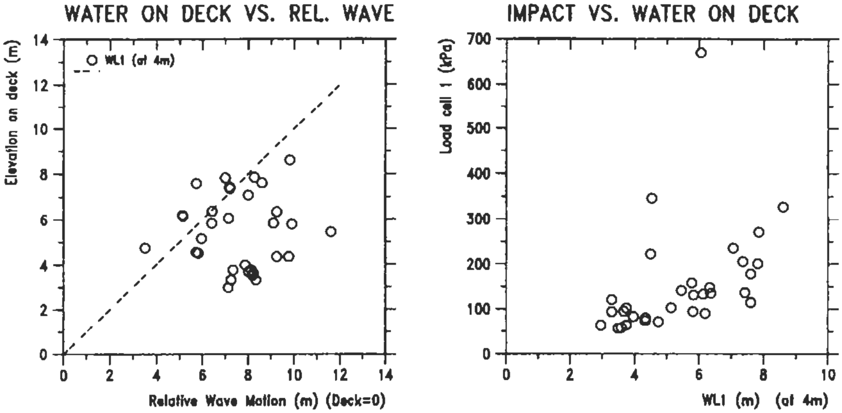

Figure 6: Correlation between relative wave, water on deck and impact load.

5 IMPACT LOAD MEASUREMENTS

Figure 6 (right) shows the correlation between the water on deck at 4m (WL1) and the resulting impact loads on the deck house, for the events in Fig. 6 (left). In most cases there seems to be, approximately, a quadratic correspondence, although there is some scatter. Similar observations were also made in Buchner & Voogt (2000). A few events differ from the others, with very high loads. They are due to particularly steep waves. A detailed force signal example is shown in Figure 7, for one of the most extreme cases. Critical loads are characterised by a very short rise time (less than 0.1s, full scale), and a peak duration of about 0.1 – 0.2s. The recordings indicate that the measuring equipment has been able to record the physical behaviour of the impact, with minor influence from the natural periods of the sensors. Peak pressure levels, averaged over a panel area of 7 m^2, vary typically from 100 to 700 kPa. (Integrating the load signals over time, we find that the *momentum* shows a much less variation).

Similarly, force signals from load cell recordings on the bow are shown in Figure 8, for an event with a very high slamming force measurements.The shape of the bow slam signals are typically similar to those for the deck house loads, but they are generally shorter and may become higher. Again, the forces are integrated over the area of the panels (6.3 m^2). For comparison, direct measurements of the pressure from pressure cells located in the same area (see Fig. 1) are shown in Figure 8b, which confirm the force panel measurements.
From a preliminary study of tests with repeated “identical” conditions (spectrum E), it is found that although vessel motions and relative waves repeat very well, the peak load measurements show some scatter. Further analysis of this, and of the above load data in general, is to be carried out in the future, for the calibration of a numerical procedure (Hellan et. al. 2001b).

6 DISCUSSION WITH CONCLUDING REMARKS

One main experience from this experimental case study is that the most critical green sea and impact events observed in steep random wave conditions are mostly generated by steep and energetic waves or wave groups. Nonlinear effects in the incoming waves, including the kinematics, play an important role, and this connection should be investigated further. The ship motion is also important. Thus relative short and steep waves are more critical than longer waves, due to the phase lag of the pitch motion. Large pitch amplitudes can worsen the problem. The bulwark height has some reduction influence on the overtopping water, but the effect decreases with the height of the incoming water.

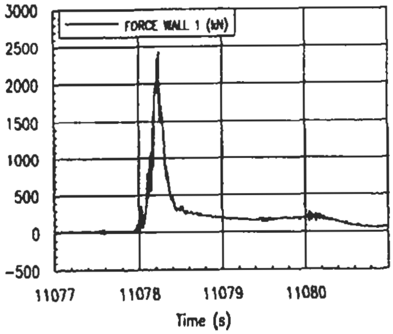

Figure 7: Impact signal from force sensor on deck house.

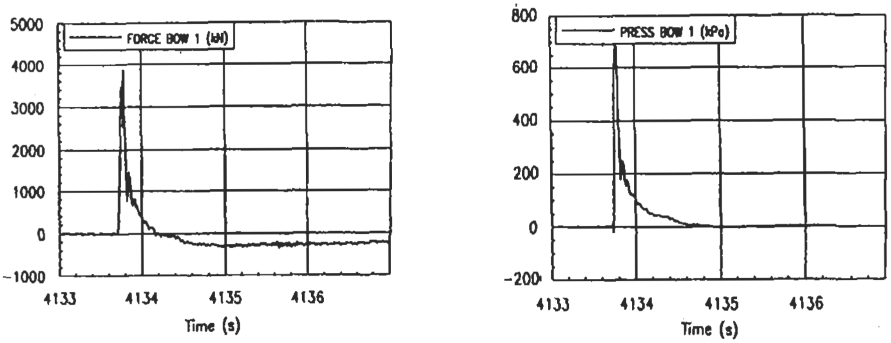

Figure 8: Impact signals from force and pressure sensors on bow

It has been observed that the most critical impact load events, with average pressures above 200 kPa over areas more than 5 m^2, occur as very rare events, and it is a challenge to become able to predict their probability. The present tests, simulating 3 hours storm duration, give an indication of their presence in a random sea, while further studies of longer records (or additional 3-hours realisations) should be carried out for more detailed studies of the statistics. Use of numerical models in combination with model test data (Hellan et. al. 2001b) also contributes to this. Another challenge is the laboratory modelling of random extreme waves, as discussed in Stansberg (2001): What are the requirements, what are the limitations, and what is observed? The measuring statistics and use of peak impact loads obtained from model tests should also be evaluated further.

Acknowledgements

Parts of this work has been carried out within the Norwegian Joint Industry Project "Design Loads ind Integrity Assessment for Wave Impact on Bow and Deck Structures", sponsored by APL, Golar-Nor, Navion, Norsk Hydro, The Norwegian Petroleum Directorate, Rolls-Royce Marine, Statoil and MARINTEK. The support from the sponsors is gratefully acknowledged.

References

Buchner, B. (1995). On the Impact of Green Water Loading on Ship and Offshore Unit Design. *Proc. Vol. 1, PRADS'95*, The Society of Naval Architects of Korea, Seoul, Korea.

Buchner, B. and Voogt, A. (2000). The Effect of Bow Flare Angle on FPSO Green Water Loading. *Proc., the 19th OMAE Conf.*, Paper No. OSU OFT-4092, New Orleans, LA, USA.

Ersdal, G. and Kvitrud, A. (2000). Green Water on Norwegian Production Ships. *Proc., the 10th ISOPE Conf.* Seattle, WA, USA.

Gorf, P., Barltrop, N., Okan, B., Hodgson, T and Rainey, R. (2001). FPSO Bow Damage in Steep Waves. *Rogue Waves 2000 Workshop*, held at IFREMER, Brest, France, Nov. 2000.

Greco, M., Faltinsen, O. and Landrini, M. (2000). Basic Studies of Water on Deck. *Proc., 23rd Symp. on Naval Hydrodynamics*, National Academy Press, Val de Reuil, France.

Hellan, Ø., Hermundstad, O.A. and Stansberg, C.T. (2001a). Designing for Wave Impact on Bow and Deck Structures. *Proc., the 11th ISOPE Conference*, Stavanger, Norway.

Hellan, Ø., Stansberg, C.T., Hoff, J.R. and Hermundstad, O.A. (2001b). A Practical Design Tool for Wave Impact on Bow and Deck Structures. *Proc., PRADS 2001 Conf.*, Shanghai, China.

MacGregor, J.R., Black, F., Wright, D. and Gregg, J., (2000). Design and Construction of the FPSO Vessel for the Schiehallion field, *Trans., The Royal Institution of Naval Architects*, London, UK.

Stansberg, C.T. (2001). Random Waves in the Laboratory: What is Expected for the Extremes? Proc., Rogue Waves 2000 Workshop, held at IFREMER, Brest, France, Nov. 2000.

Stansberg, C.T. and Gudmestad, O.T. (1996). Nonlinear Random Wave Kinematics Models Verified Against Measurements in Steep Waves. *Proc. Vol. 1A, the 15th OMAE Conf.*, Florence, Italy, 15-24.

Stansberg, C.T. and Nielsen, F.G. (2001). Nonlinear Wave-Structure Interaction on Floating Production Systems. *Proc., the 11th ISOPE Conf.*, Stavanger, Norway.

Torsethaugen, K. (1993). A Two-Peak Wave Spectrum Model. *Proc., Vol. II, 12th OMAE Conf.*, Glasgow, Scotland, 175-180.

Practical Design of Ships and Other Floating Structures
You-Sheng Wu, Wei-Cheng Cui and Guo-Jun Zhou (Eds)
© 2001 Elsevier Science Ltd. All rights reserved

LONG TERM PREDICTION METHOD OF SHIPPING WATER LOAD FOR ASSESSMENT OF THE BOW HEIGHT

Yoshitaka OGAWA, Harukuni TAGUCHI, Iwao WATANABE and Shigesuke ISHIDA

Ship Dynamics Division, Ship Research Institute, Ministry of Land, Infrastructure and Transport,
6-38-1 Shinkawa, Mitaka, Tokyo, 181-0004, Japan

ABSTRACT

Model test in regular and irregular waves was carried out in order to develop a long-term prediction method of shipping water load on the bow deck. Model of a tanker for Japanese domestic voyage was used. From the result of test in regular waves, the relation between shipping water load and relative water height at stem was discussed. It was found that shipping water load is proportional to the square of the water elevation over the bow top. Based on this relation, probability density function of shipping water load in short-term prediction was proposed. It was confirmed that proposed function shows a good agreement with the measured distribution in irregular waves, especially the tail of it, better than the conventional function. Applying this function to the long-term prediction of shipping water load, it was concluded that the present method might be more rational than conventional method to predict shipping water load.Using this prediction method, assessment of bow height of Japanese domestic ship from the viewpoint of deck wetness was carried out. From the result of assessment, a draft of rule on load lines for "the limited greater coastal area", which is a new navigation area in Japan and is needed to set the new rule, was shown.

KEYWORDS

Load lines, Deck wetness, Long-term prediction, Probability density function, Shipping water load, Bow height

1 INTRODUCTION

In Japan, the rule on load lines for domestic ships is relaxed compared to the international rule. The navigation area in Japan had been divided to two, namely the coastal area and the greater coastal area. These areas are shown in Figure 1. The requirements for ship navigating in the greater coastal area are severer than in the coastal area in the consideration of the sea conditions and so forth. Recently a new navigation area "the limited greater coastal area", which is located among the coastal area and the greater coastal area, has been introduced for the efficiency of domestic transportation. In the present, the requirements for the greater coastal area are applied to the limited greater coastal area in spite of the difference of sea conditions. The setting of the rational rule for the limited greater coastal area is needed

It is well known that deck wetness, which is one of factors for the basis of the rule on load lines, sometimes causes serious damage to the bow deck itself and structures on the deck. Many studies have been carried out on this phenomenon. It was found that the occurrence of deck wetness could be determined by the comparison of relative water height at stem with bow top height. However, only a few of the studies (Takezawa (1977)) gave us quantitative information about water volume on deck, impulsive load and the relation between them and ship motion. A practical prediction method, which can be made use of by designers and rule-making people, is needed.

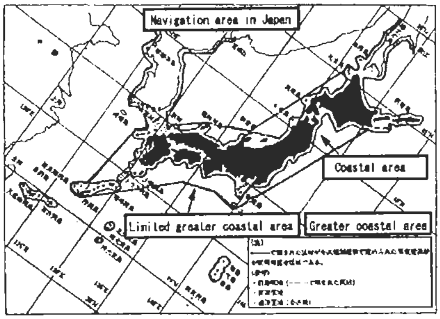

Figure 1 : Navigation area in Japan

An experiment was carried out using a Japanese domestic tanker model in regular and irregular waves in order to measure the shipping water height distribution, its load and pressure due to deck wetness. The limiting condition, e.g. model speed, wave steepness, of the occurrence of deck wetness was clarified. The relations among the key quantities relating to deck wetness mentioned above are discussed. Based on this relation, a prediction method in irregular seas for shipping water load was proposed. Applying this method, estimation of the bow height for ship navigating in the limited greater coastal area was carried out from the viewpoint of deck wetness. From the result of this estimation, a draft of rule on load lines for "the limited greater coastal area" was shown.

2 MODEL TESTS

2.1 Model Configuration

A detailed explanation of model configuration in regular waves had been given in another paper (Ogawa (1998)). The part, which has relation with this study, is shown once again. The free running test was carried out for a Japanese domestic tanker in regular and irregular head seas. The principal particulars are shown in Table 1. The setup of measuring instruments around the bow deck is shown in Figure 2. A load cell was attached under the bow deck that is separated from the main body of the model for measuring shipping water load directly. Area of separated deck of domestic tanker was $0.158m^2$. An accelerometer was attached beside the load cell to exclude the effect of inertia of the bow deck plate. Five mean water height probes, combinations of wave probes at a cross section, were attached on the bow deck from F.P. to S.S. 9. Shipping water volume was estimated by integrating the mean water height at each cross section. A wave probe was also attached at stem. A video camera was attached to observe the behavior of shipping water.

2.2 Wave Condition

Test in regular waves was carried out at various wave length $\lambda/L=0.6$ to 1.5 (λ : wave length L: ship length) to observe severe deck wetness. Wave steepness H/λ was 1/30 (H : wave height) and ship speed was constant (Fn=0.1). It is found that deck wetness occurred at $\lambda/L=1.0$ to 1.5 when relative water height is larger than the bow top height. For measuring a severe shipping water load at these wave length, test at various wave steepness and ship speed was also carried out.

Test in irregular waves was carried out in the following condition. Wave period T=1.459sec, significant wave height $H_{1/3}=0.174$m and ship speed Fn=0.1. The encounter waves were 400 in number. The ISSC spectrum was used for wave spectrum of irregular waves.

TABLE 1

PRINCIPAL PARTICULAR

	Ship	Model
Lpp(m)	72.0	4.0
B(m)	11.5	0.638
D(m)	5.3	0.292
d(m)	4.74	0.263
Bow height(m)	2.45	0.136
GM(m)	1.37	0.076
Cb	0.68	0.680
Disp.(ton)	2720	0.466

3 RESULT OF TESTS

Relation between shipping water load F and the exceeded height δ, which is the water elevation over the bow top, is shown in Figure 3. From the experimental results in regular waves, it is found that the shipping water load has a relation with the exceeded height as the following expression

$$F = \alpha\rho g B(\eta_{max} - f)^2 = \alpha\rho g B\delta^2 \qquad (1)$$

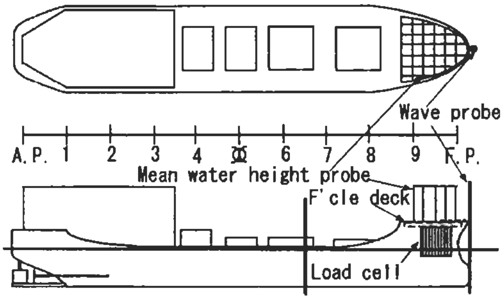

Figure 2 : Setup of measuring instruments

where, α is the coefficient, ρ is a density of water, g is the acceleration of the gravity, B is a breadth of ship, η_{max} is the amplitude of relative water height and f is the bow height at stem. Marks and line in Figure 3 indicate the experimental results and approximated value by equation (1) respectively. Values were converted to the ship scale. The coefficient α was determined by the experimental results in regular waves. As for the domestic tanker, coefficient α was 0.57.

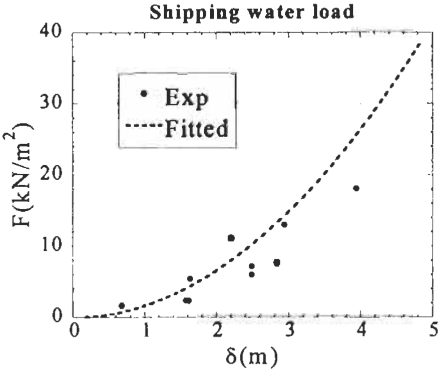

Figure 3 : Relation between shipping water load and relative water height at stem (Fn=0.1)

4 PREDICTION FOR THE PROBABILITY OF SHIPPING WATER LOAD

In this section, a prediction method for shipping water load in irregular waves is proposed. Analysis was carried out under the assumption that is shown below.

- Spectrum of ship motion, relative water height and so on are narrow band spectrum.
- Deck wetness is occurred when the relative water height at stem exceeded bow height.

Results that is shown below is only in the head seas ($\chi = 180°$).

4.1 Exceedance of Probability of Shipping Water Load

The probability density function of shipping water load $p_F(F)$ is expressed with the following equation by the probability density function of relative water height at stem $p_\eta(\eta_{max})$ as

$$p_F(F)dF = p_\eta(\eta_{max})d\eta_{max} \tag{2}$$

Assuming that the spectrum of relative water height is in narrow band, probability density function of relative water height $p_\eta(\eta_{max})$ is given by Rayleigh distribution. By combining equation (1) and (2), the probability density function of shipping water load is obtained as

$$\begin{aligned} p_F(F) &= p_\eta(\eta_{max})\frac{d\eta_{max}}{dF} \\ &= \frac{1}{2\alpha\rho g B(\eta_{max} - f)} \cdot \frac{\eta_{max}}{\sigma_\eta^2} \exp\left\{\frac{-\eta_{max}^2}{2\sigma_\eta^2}\right\} \\ &= \frac{f \cdot \sqrt{\alpha\rho g B} + \sqrt{F}}{2\alpha\rho g B \sigma_\eta^2 \sqrt{F}} \cdot \exp\left\{-\frac{\left(f \cdot \sqrt{\alpha\rho g B} + \sqrt{F}\right)^2}{2\sigma_\eta^2 \alpha\rho g B}\right\} \end{aligned} \tag{3}$$

where σ_η is standard deviation of relative water height. The exceedance of probability of shipping water load $P(F>F_0)$ can be expressed by the integral of equation (3) as

$$P\ (F > F_0) = \int_{F_0}^{\infty} p_F(F)dF = \exp\left\{-\frac{\left(f\cdot\sqrt{\alpha\rho g B}+\sqrt{F_0}\right)^2}{2\sigma_\eta^2\alpha\rho g B}\right\} \quad : F_0>0$$

$$P(F > F_0) = p_F(0)dF = 1-\int_f^{\infty} p_\eta(\eta_{max})d\eta = 1-\exp\left\{-\frac{f^2}{2\sigma_\eta^2}\right\} \quad : F_0=0 \qquad (4)$$

4.2 Short-term Prediction of Shipping Water Load

Comparison between the measured and estimated exceedance of probability of shipping water load of domestic tanker is shown in Figure 4. Values were converted to the ship scale. Measured standard deviation of relative water height was used in equation (4). As for the domestic tanker, standard deviation is 0.140m. It is found that the present method agrees well with the experimental results. It is concluded that the present method is practical enough to estimate shipping water load.

4.3 Long-term Prediction of Shipping Water Load

From the exceedance of probability, the long-term prediction of shipping water load can be evaluated as

$$q(F > F_0) = \int_0^{\infty}\int_0^{\infty} P\ (F > F_0)\cdot P(H,T)dHdT \qquad (5)$$

where P(H, T) is the joint probability of wave height H and wave period T. Standard deviation of relative water height that is an input for evaluating the exceedance of probability was estimated by the strip method (NSM). Comparison between conventional method, which is proposed by Fukuda (Fukuda(1973)), and present method is shown in Figure 5. Values in Figure 5 indicate mean value per unit area. It is found that the difference between present method and conventional method is large. According to the design manual (KSNAJ(1983)), design load of shipping water load is defined as 0.98Lpp(KN/m^2). Design load of shipping water load of present tanker becomes 70.6(KN/m^2). From the viewpoint of the probability of occurrence, it is concluded that the present method may be more rational than conventional method to predict shipping water load.

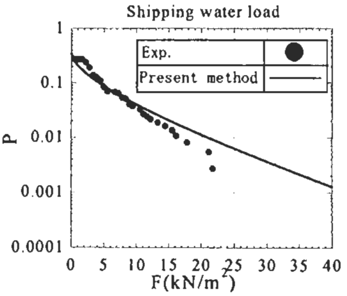

Figure 4 : Comparison between measured and estimated exceedance of probability of shipping water load (χ =180° , T=1.459sec, $H_{1/3}$=0.174m, Fn=0.1)

5 ASSESSMENT OF DOMESTIC RULE ON LOAD LINES

From the viewpoint of the probability of occurrence of deck wetness and severe shipping water load, bow height of domestic ships in the limited greater coastal area, which is necessary for a domestic ship to navigate safety, was estimated. It was assumed that deck wetness was occurred when relative water height is greater than the bow height. Severe shipping water load was defined by rules and design criteria. 18 ships for Japanese domestic voyage were used in calculation. Strip method (NSM) was used for estimation of ship motion and relative water height. Hindcast data of Japanese domestic area, which is provided by the Japan Weather Association (JWA), was used for wave diagram that is the input of long-term prediction.

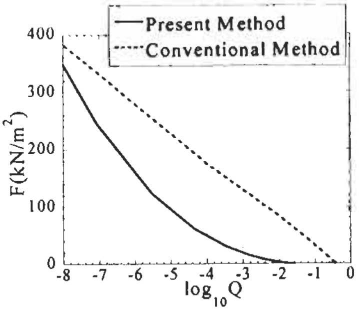

Figure 5 : Comparison between conventional and present method for long-term prediction of shipping water load ($\chi = 180°$)

5.1 The Probability of Occurrence of Deck Wetness

At first, the probability of occurrence of deck wetness in the greater coastal area was estimated. The bow height of each ship was set to the minimum bow height according to the present domestic rule. Next, the bow height in the limited greater coastal area was estimated in order to equate the probability of occurrence with the one in the greater coastal area. Wave diagram in the limited greater coastal area is used for the input of long-term prediction.

The ratio of estimated bow height in the limited greater coastal area to the presently required bow height in the greater coastal area is shown as marks in Figure 6 (a). Line indicates the approximated line of each value. The ratio becomes larger as the ship length becomes shorter. It is considered that the difference between estimated bow height and the presently required bow height is caused by the difference of the sea condition. It is found that the effect of the sea condition on the long-term prediction is relatively small as the ship length becomes shorter.

5.2 The Probability of Occurrence of Shipping Water Load

At first, the probability of occurrence of severe shipping water load in the greater coastal area was estimated. The bow height of each ship was set to the minimum bow height according to the present rule for ships in the greater coastal area. The threshold value of shipping water load was determined as

(a) Design manual (KSNAJ(1983))

(b) Design load defined in the rule of the Nippon Kaiji Kyokai (NK) on ship structure

(c) Design load defined in the unified requirements of IACS (UR-S21).

Next, the bow height, which is necessary in the limited greater coastal area to equate the probability of occurrence with the one in the greater coastal area, is estimated. The ratio of estimated bow height in the limited greater coastal area to the presently required bow height in the greater coastal area is shown in Figure 6 (b). The correlation between ratio and ship length is similar to the one from the viewpoint of probability of occurrence of deck wetness. It is found that required bow height from the viewpoint of occurrence of deck wetness is severer than the one from the viewpoint of occurrence of severe shipping water load. It is concluded that bow height should be decided by the probability of occurrence of deck wetness to satisfy each requirements.

5.3 Assessment of Bow Height for Ships in the Limited Greater Coastal Area

Based on the estimations, the bow height in the limited greater coastal area can be determined by multiplying the correction coefficient C by the bow height in the greater coastal area as follows:

$Lpp > 100(m)$:$C=0.78$

$Lpp < 100(m)$:$C=1.0-0.0022 \times Lpp$.

This correction coefficient is shown in Figure 6 (a) by solid line. It is found that this correction coefficient agrees well with estimated value. It is considered that using these prediction methods can estimate the bow height from the viewpoint of deck wetness rationally.

6 CONCLUSIONS

Prediction method for shipping water load in irregular waves was proposed and validated. Using this prediction method, assessment of bow height of Japanese domestic ships from the viewpoint of deck wetness was carried out. The conclusions are as follows.

The correlation between shipping water load and the exceeded height δ , the relative water height at stem exceeded the bow height, is strong. The probability density function of shipping water load was proposed. It is confirmed that present method agrees well with experimental results.

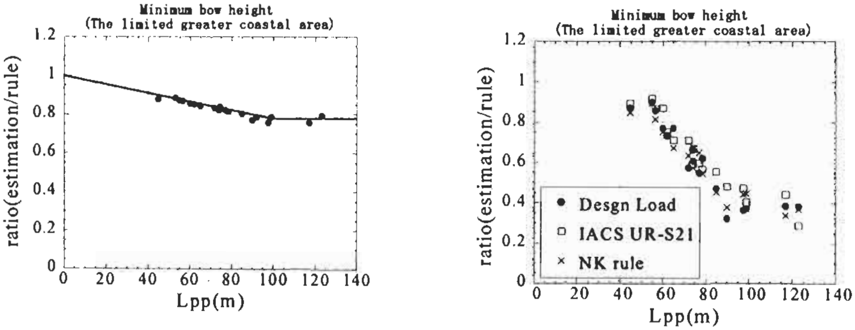

(a) Probability of occurrence (b) Shipping water load

Figure 6 : Estimation of minimum bow height from the viewpoint of deck wetness

From the comparison with long-term prediction between present method and conventional method, it is concluded that the present method may be more rational than conventional method to predict shipping water load.

Using these prediction methods, bow height can be estimated rationally from the viewpoint of deck wetness.

Acknowledgements

A part of the present study was carried out as the part of the cooperation project (RR45) with the Shipbuilding Research Association of Japan that is supported by the Nippon Foundation.

References

Fukuda, J. et. al. (1973). Predicting the Long-Term Trends of Loads on Deck due to Shipping Water.

Transaction of The West Japan Society of Naval Architects **45,** 95-114
Ogawa, Y. et. al. (1998). A Practical Method for Shipping Water Height and its Load on Deck. Proc. 7th International Symposium on Practical Design of Ships and Mobile Units. 535-543

Takezawa, S. et. al. (1977). On deck wetness and impulsive water pressure acting on the deck in the head seas. Journal of The Society of Naval Architects of Japan **141,** 86-96

The Kansai Society of Naval Architects, Japan. (1983). Design Manual ver.4. KAIBUNDO

Practical Design of Ships and Other Floating Structures
You-Sheng Wu, Wei-Cheng Cui and Guo-Jun Zhou (Eds)
© 2001 Elsevier Science Ltd. All rights reserved

A PRACTICAL DESIGN TOOL FOR WAVE IMPACT ON BOW AND DECK STRUCTURES

Øyvind Hellan, Jan Roger Hoff and Carl Trygve Stansberg

Norwegian Marine Technology Research Institute A.S. (MARINTEK)
7450 Trondheim, Norway

ABSTRACT

There is a growing need to establish reliable engineering tools for prediction of loads and structural responses from local wave impact on bow and deck structures. State-of-the-art tools describe the linear and some non-linear contributions quite well, but taking into account all non-linear effects ranging from steep and extreme waves, through water propagation and impact forces, and finally to the coupling with structural responses, is still in its development. Fully non-linear modelling is clearly a goal, but presently, practical tools have to be based on some kind of simplifications and make use of extensive experimental calibration. The challenge is then to make the proper (and as few as possible) simplifications, and to combine this reasonably in a complete procedure starting with the random sea and ending up with a final structural integrity assessment.

In the present work, such a complete design tool is described. A time-domain design code is being developed, based on a combination of a second-order random wave kinematics model with a non-linear water propagation and local pressure formulation, which is finally used as input in an structural analysis of the local structure. Empirical verification and calibration against model test data form an essential part of the development. The study is initially directed towards FPSO's, but an extension to air-gap and run-up problems on floating platforms is also planned.

The work is carried out through the Norwegian Joint Industry Project "Design Loads and Integrity Assessment for Wave Impact on Bow and Deck Structures".

KEYWORDS

Floating production, Platform, FPSO, Wave impact, Green sea, Slamming, Run-up

1 BACKGROUND

Wave impact and green sea incidents in steep storm wave conditions have been reported to cause a number of damages on bow and deck structures on floating production systems in the North Sea / Atlantic frontier area (Ersdal & Kvitrud, 2000; MacGregor et. al., 2000). This results in a need for improved analysis and prediction tools that are more accurate than existing standard procedures.

Critical situations include such as bow stem slam and green sea on FPSOs, large waves hitting platform decks, and local diffraction and run-up around platform columns.

Significant research activities have already been established on different aspects of this subject. This includes theoretical and experimental studies on green water (Buchner 1995, Buchner & Voogt 2000, Greco et. al. 2000, Faltinsen et. al. 2001), slamming force modelling (Zhao & Faltinsen 1993, Zhao et. al. 1996) and fully non-linear flow and wave diffraction models (Guignard et. al. 1999, Ferrant 1999). Since parts of the problems are considerably complex and highly non-linear, this includes, to some extent, long-term research studies, from which significant developments are expected after some time. Such studies are important steps for future design models.

So far, however, a consistent design tool combining the complete chain of different load and response effects in a generally accepted way does not seem to be available today, although various empirical methods are in use on different elements in the procedure.

2 A NEW DESIGN TOOL

The objective of the present work is to establish reliable tools for prediction of loads and structural responses from local wave impact on bow and deck structures on FPSOs and floating platforms, based on an analytical formulation with empirical calibration to measured data. Thus the overall aim is to predict:

- probability of bow stem slamming and/or water on deck on FPSO
- probability of water hitting platform deck
- slamming loads
- assessment of structural integrity

A software package for practical engineering use is developed. The probability and nature of random, steep non-linear wave events in a stochastic sea description is coupled with slamming force models and structural response analysis based on available experience in combination with model test calibration. The work is to a large extent making use of and combining existing tools and modules already available. Model test verification and calibration plays an important role. Empirical corrections can be applied to the calculated local wave elevation around the bow as well as to the horizontal velocity of the water flowing across the bulwark.

The development is carried out within the Norwegian Joint Industry Project "Design Loads and Integrity Assessment for Wave Impact on Bow and Deck Structures" (MARINTEK, 1999). The plan for the whole project includes analysis of FPSOs (Phase I) and floating platforms (Phase II). This paper gives a description of the water on deck analysis for FPSOs. A particular FPSO research study carried out for the purpose of this project is then presented, and preliminary results are shown. The bow slamming analysis has been outlined in Hellan et. al. (2001).

3 WATER ON DECK LOADS

The different parts of the problem are shown in Figure 1, which also illustrates the interface between the different parts of the analyses.

3.1 Water Kinematics and Relative Motions

Incoming waves are simulated by a second-order random wave model, which describes the water elevation as well as the kinematics. Vessel motions are calculated by linear ship motion analysis, such as 3D diffraction or strip theory. The diffracted wave field is calculated taking into account linear 3D diffraction, either by full diffraction analysis, by empirical correction or from experiments.

Relative motions are then estimated by combining the linear vessel motions, second-order incoming wave and linear diffraction. Particle velocities for waves exceeding the vessel's freeboard are estimated from the second-order incoming wave without diffraction. Systematic model test observations are used in checking and calibration of the models. Empirical corrections can be taken into account, depending on the need and the actual application. The approach and its simplifications are further discussed in Stansberg & Nielsen (2001).

The relative motions are used to assess the probability of water on deck. The volume and velocity of water entering the vessel is calculated at selected points around the bulwark as continuous time series of $h_i(t)$ and $v_i(t)$ obtained from the water kinematics above.

3.2 Water Propagation and Local Loads

Preliminary findings from model tests indicate two types of water entry: Water flow on the deck continuously from the bow and backwards, and "jets" from extreme waves. So far in this work, the focus is on continuous water flow from the bow and backwards, with "jet" entry handled through empirical corrections.

The non-linear water propagation across the deck is modelled by a shallow water approach, extended from Huang (1995). The formulation includes non-stationary boundary conditions in terms of surface elevation and velocity. Dam breaking can be handled as a special case, but in the present project the water will have a prescribed horizontal velocity across the boundary, and the water elevation will typically rise from zero during a water-on-deck event.

Loads on deckhouses and other large objects are calculated with a similarity solution (Zang et.al, 1996), where the impacting water is described by an infinite wedge with an angle α that travels across the deck with velocity v just before the impact on a vertical wall. The two parameters α and v are predicted by the shallow-water method. Greco et al (2000) demonstrates that a similarity solution is a reasonable approximation during the first phase of the impact, but becomes increasingly conservative at later stages. The important issue is however that the similarity solution gives a reasonable approximation when the maximum structural responses occur.

Forces on piping and secondary structures in the water flow are calculated using Morison's equation with the calculated water particle velocities.

3.3 Structural Integrity Assessment

Calculated impact loads are transferred to standard FE systems (NISA, SESAM, ASAS) for simulation of the structural response for each specific impact history. If local FE models are available, the predicted slamming loads are mapped onto existing FE models as nodal forces or distributed pressure loads.

Integrity assessment of multi-stiffened plate structures under water impact loading is based on Biggs' and Baker's methods (Biggs 1963, Jones 1973, Baker et al 1983, NORSOK 1998). The structural response and capacity is idealised by non-linear 1 DOF spring characteristics, and the structural response simulated by Duhamel integrals of the structural response under impulse loading with a specified build-up and decay rate. Limiting criteria are specified in terms of maximum deformations or maximum strains. A series of analyses are then carried out to establish the combination of peak pressure, p, and impulse duration, t, that matches the failure criteria for the given structure and impulse shape.

Further discussion on integrity assessment and acceptance criteria are given in Hellan et. al (2001).

4 CASE STUDY WITH PRELIMINARY RESULTS

The following shows results from a case study currently being carried out with an FPSO in conditions typical of the Norwegian sector of the North Sea. Simulations are compared with model tests and theoretical solutions. The model tests were carried out in MARINTEK's Ocean Basin and are described in more detail in Stansberg & Karlsen (2001).

4.1 Wave Kinematics and Relative Motion

Vessel motions and wave amplification around the hull are calculated from linear 3D diffraction analysis with WAMIT. The disturbed wave surface elevation is calculated by combining the linear diffraction and a second-order model for the incoming wave, and then using an empirical correction factor (see below). Particle velocities are estimated from the second-order incoming wave (without taking the diffracted wave-field into account).

Figure 2 shows the calculation domain for the wave kinematics analysis. The dotted line shows the water line of the vessel, while the ×'es mark the points where surface elevation and particle velocities are determined at selected points along the bulwark, at the bow waterline and at some points ahead of the vessel. Figure 3 shows visual snap-shots from a time-domain simulation in irregular waves.

In Figure 4, time series samples from preliminary simulations of the water elevation overtopping the bow are compared to 1:55 scaled model tests and to a linear model without 3D diffraction. Two green sea events observed in model tests are selected, from a 3-hr record in a 100-year irregular wave condition with Hs=12m, Tp=12s. This is a rather steep wave condition. In the present analysis the non-linear model has been empirically adjusted by a factor of 1.1, based on matching with a large number of observed events. (The effect of this correction on the maximum overtopping was typically 1m increase). The prediction works reasonably well, although the predicted extreme levels are still somewhat low in the most extreme wave events. For most of the other green sea events (event 1 + cases not shown here), the agreement is quite good. The deviation, and need for further empirical adjustment, is increasing with increasing steepness of the wave front. Further comparison and discussion of the method is given in Hellan et.al. (2001) and Stansberg & Nielsen (2001).

4.2 Water on Deck

The water propagation across the deck is modelled by a shallow water approach. When entering at the most forward part of the bow, the water has a velocity in the longitudinal direction. Water entering from the sides of the bow has a transverse velocity component towards the middle of the deck. These water flows meet at the centre of the deck and forms a high water "tongue" which propagate at high velocity along the middle of the deck. Figure 5 shows simulated water propagation across the deck of the case vessel based on a dam breaking mechanism. Figure 6 shows simulated water propagation with boundary conditions (elevation and velocity) taken from the wave kinematics analysis above. Boundary conditions at selected points along the bulwark are shown in Figure 7 (freeboard exceedance) and Figure 8 (velocities). The locations of the points along the bulwark are indicated in Figure 2. The boundary conditions produce a flow pattern different form the dam breaking case, e.g. the water "tongue" is less pronounced when the boundary conditions are taken into account. Figure 9 and Figure 10 show the surface elevation of the water flow along the centreline deck, as predicted by a dam breaking model and the present model. When the water flow reaches the deckhouse position, the calculated water flow velocity and surface angle (at the centreline of the vessel) is 4-5 m/s and 20° for the dam breaking case, compared to 12 m/s and 13° with boundary conditions at the bulwark.

4.3 Local Loads

Figure 11 shows model test measurements of impact forces on the deckhouse of the case study vessel. 2.75×2.75 (in full scale) meters stiff force panels were applied. Figure 12 shows calculated forces for a wave of similar height from the same sea state. Also shown are forces based on water flow from a dam breaking case.

As long as the calculations are not based on the actual measured wave, only a qualitative comparison is possible: The dam breaking mechanism leads to an under prediction of local loads in the present case.

When the water flow is based on boundary conditions from wave kinematics analysis, the predicted force on the panel is in the same range as the measured event. The error bars illustrate the effect of different linearisation of the front of the water flow: The similarity solution is based on a wedge of water with constant angle α, whereas the simulated water flow has a concave shape at the front (see Figure 10). The predicted build-up rate of the forces is somewhat slower than in the measured event, and the present formulation is unable to capture the decay in forces. This is also due to inherent assumptions in the similarity solution, which assumes an infinite wedge of water flowing onto the wall, and neglects gravity effects. However, this development is still in progress, and considering it's simplicity, the similarity solution shows promising results.

5 CONCLUDING REMARKS

A simplified approach for design and integrity assessment for wave impact on bow and deck structures has been described in the present paper. The approach is based on a combination of presently available theory, with the aim to end up with a practical and robust tool taking into account the most essential linear and non-linear physical effects. The main physical effects have been discussed through a research case study of an FPSO operating in conditions typical of the Norwegian sector of the North Sea. Simulations are in qualitative agreement with model tests and theoretical solutions. Work is still in progress, but the methodology shows promising results.

Acknowledgements

This work has been carried out within the Norwegian Joint Industry Project "Design Loads and Integrity Assessment for Wave Impact on Bow and Deck Structures", sponsored by the Norwegian Petroleum Directorate, Norsk Hydro, STATOIL, APL, NAVION, Rolls Royce Marine and PGS. Permission to publish is gratefully acknowledged. Thanks are also due to Mr. Atle Johansen, Dr. Vibeke Moe and Dr. Ole A. Hermundstad for valuable contributions.

References

Baker, W.E., Cox, P.A., Westine, P.A., Kulesz, P.S. and Strehlov, R.A. (1983). *Explosion Hazards and Evaluation.* Elsevier Scientific Publishing Company, Amsterdam, Holland.
Biggs, J.M. (1963). *Introduction to Structural Dynamics.* McGraw-Hill New York, USA.
Buchner, B. (1995). On the Impact of Green Water Loading on Ship and Offshore Unit Design. *Proc. Vol. 1, PRADS'95,* The Society of Naval Architects of Korea, Seoul, Korea.
Buchner, B. and Voogt, A. (2000). The Effect of Bow Flare Angle on FPSO Green Water Loading. *Proc, the19th OMAE Conf.,* Paper No. OSU OFT-4092, New Orleans, LA, USA.
Ersdal, G. and Kvitrud, A. (2000). Green Water on Norwegian Production Ships. *Proc, the 10th ISOPE Conf.,* Seattle, WA, USA
Faltinsen O.M., Greco M., Landrini M. (2001). Green Water Loading on a FPSO. *Proc. OMAE 2001,* Rio de Janeiro, Brazil.
Ferrant, P. (1999). Fully Non-linear Diffraction of Regular Waves by a Multicolumn Structure. *Proc, Vol. III, 9th ISOPE Conf.,* Brest, France.
Greco M. Faltinsen O.M., Landrini M. (2000). A Parametric Study of Water on Deck Phenomena. *Proc. Int. Conf. on Ship and Shipping Research,* NAV'2000, Venice.
Greco M., Faltinsen O.M., Landrini M. (2001). Green Water Loading on a Deck Structure. *Proc, 16th Int. Workshop on Water Waves and Floating Bodies.*
Guignard, S., Rey, V. and Marcer, R. (1999). New Method for Simulation of Non-linear Wave Effects. *Proc, Vol. III, 9th ISOPE Conf.,* Brest, France, 382-387.

Hellan, Ø., Hermundstad, O.A., and Stansberg, C.T. (2001). Design Tool for Green Sea, Wave Impact, and Structural Response on Bow and Deck Structures. *OTC Paper No. 13213*, Offshore Technology Conference, Houston, TX, USA.

Huang, Z.-J. (1995). Non-linear Shallow Water Flow on Deck and Its Effect on Ship Motion. *Ph.D. thesis*, Technical University of Nova Scotia, Halifax, Nova Scotia.

ISSC (2000). Report from the 14th International Ship and Offshore Structures Congress (ISSC). Technical Committee I.1: Environment, Nagasaki, Japan.

Jones, N. (1973). Slamming Damage. *Journal of Ship Research* **17:2**.

MARINTEK (1999). Design Loads and Integrity Assessment for Wave Impact on Bow and Deck Structures: Proposal for a Joint Industry Project, Proposal T99-51.063, Trondheim, Norway,

NORSOK N-004 (1998). Design of Steel Structures, Annex A, rev. 1.

Stansberg, C.T. and Karlsen, S.I. (2001). Green Sea and Water Impact on FPSO in Steep Random Waves, to be published at the PRADS'01 Conference, Shanghai, China.

Stansberg, C.T. and Nielsen, F.G. (2001). Non-linear Wave-Structure Interaction on Floating Production Systems. *Proc. the 11th ISOPE Conference*. Stavanger, Norway.

WAMIT Version 5.0. (1993). A Radiation-Diffraction Panel Program for Wave-Body Interaction. Report, Dep. of Ocean Eng., MIT, Cambridge, Mass., USA.

Zhao R. and Faltinsen O.M. (1993). Water entry of two-dimensional bodies, *Journal of Fluid Mechanics* **246**, 593-612.

Zhao R., Faltinsen O.M. and Aarsnes, J.V. (1996). Water entry of arbitrary two-dimensional sections with and without flow separation, *Proc. 21st Symp. Naval Hydrodynamics*, Trondheim, Norway. 408-423.

Zang, S., Yue, D.K.P and Tanizawa, K. (1996). Simulation of plunging wave impact on a vertical wall, *Journal of Fluid Mechanics* **327**, 221-254.

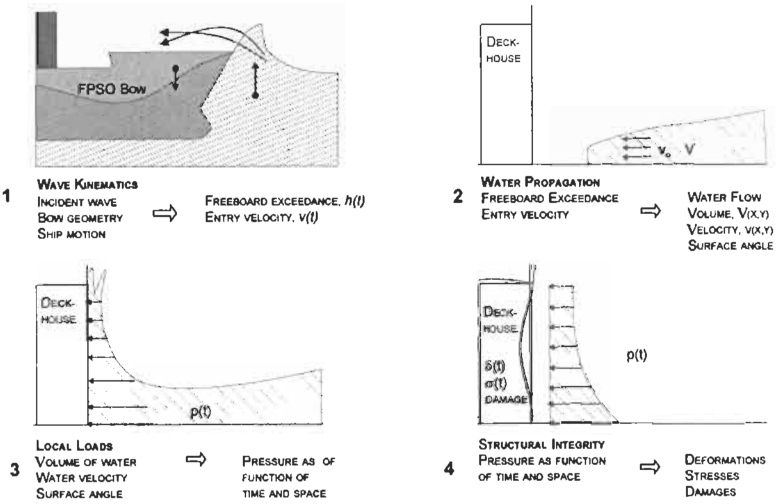
FPSO Bow
1
WAVE KINEMATICS
INCIDENT WAVE
BOW GEOMETRY
SHIP MOTION
⇨
FREEBOARD EXCEEDANCE, h(t)
ENTRY VELOCITY, v(t)
DECK-HOUSE
v₀
V
2
WATER PROPAGATION
FREEBOARD EXCEEDANCE
ENTRY VELOCITY
⇨
WATER FLOW
VOLUME, V(X,Y)
VELOCITY, v(X,Y)
SURFACE ANGLE
DECK-HOUSE
p(t)
3
LOCAL LOADS
VOLUME OF WATER
WATER VELOCITY
SURFACE ANGLE
⇨
PRESSURE AS OF
FUNCTION OF
TIME AND SPACE
DECK-HOUSE
δ(t)
σ(t)
DAMAGE
p(t)
4
STRUCTURAL INTEGRITY
PRESSURE AS FUNCTION
OF TIME AND SPACE
⇨
DEFORMATIONS
STRESSES
DAMAGES

Figure 1: Calculation procedure, water on deck

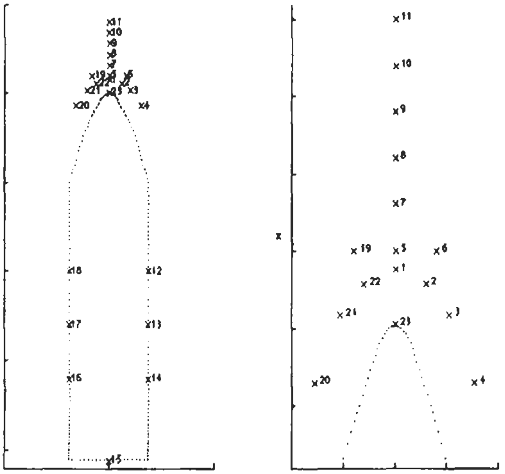
x11
x10
x9
x8
x7
x19 x5 x6
x1
x22 x2
x21 x23 x3
x20 x4
x18 x12
x17 x13
x16 x14
x15
x

Figure 2: Calculation domain for Wave Kinematics

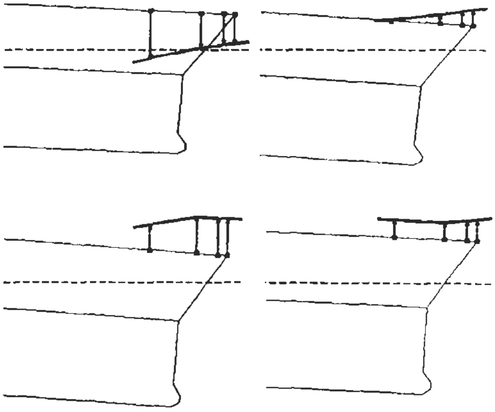

Figure 3: Snap shots from numerical simulation in irregular sea

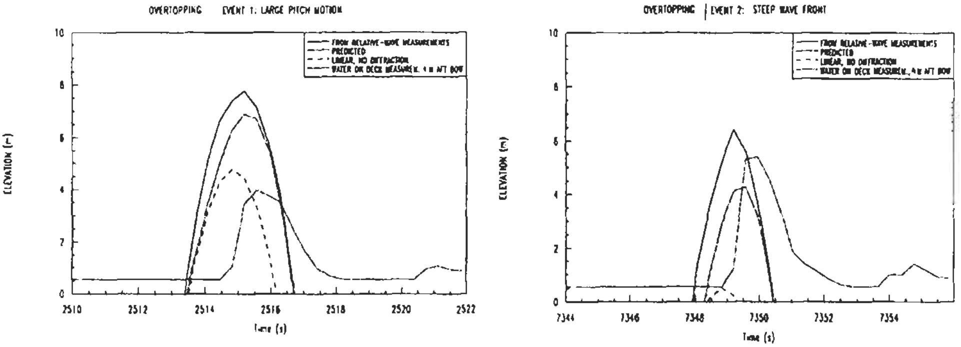

Figure 4: Predicted and measured time series of overtopping at bow, in two different events. Full line: relative-wave measurement. Dot-dashed: present method. Dashed: linear, no diffraction. Dot-dot-dashed: measured water on deck, 4m aft.

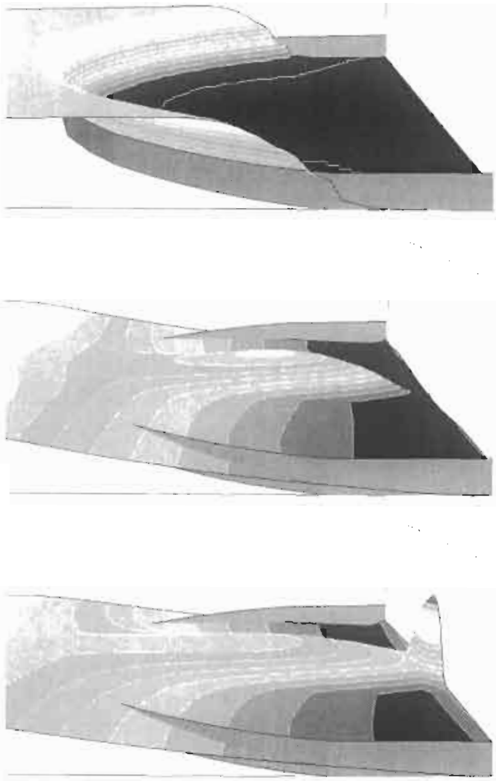

Figure 5: Simulation of water propagation for case vessel according to a dam breaking model. Deck movement neglected

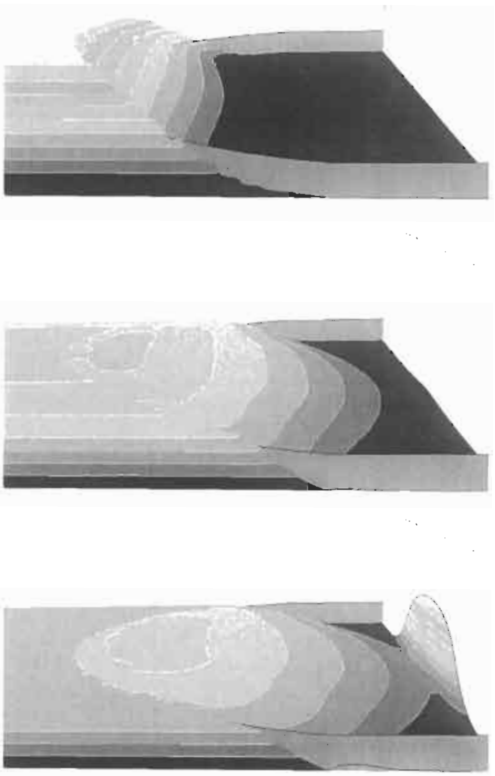

Figure 6: Simulation of water propagation for case vessel with boundary conditions from wave kinematics analysis. Deck movement neglected

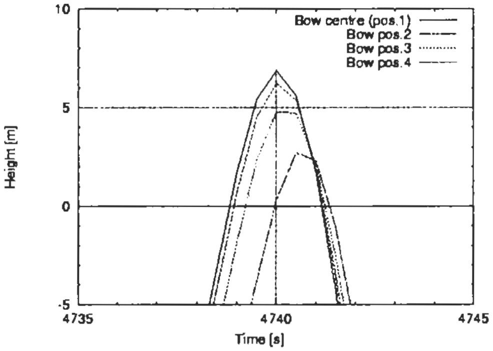

Figure 7: Boundary conditions for water flow deck: Freeboard exceedance at bulwark (ref. Figure 2)

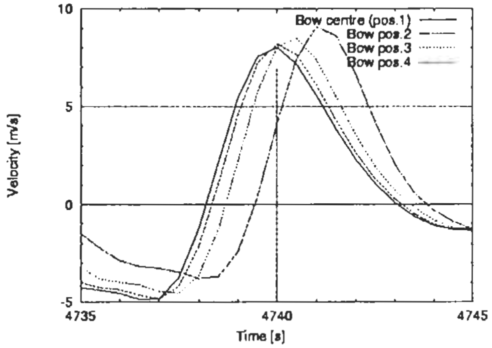

Figure 8: Boundary conditions for water flow deck: Velocity at bulwark (ref. Figure 2)

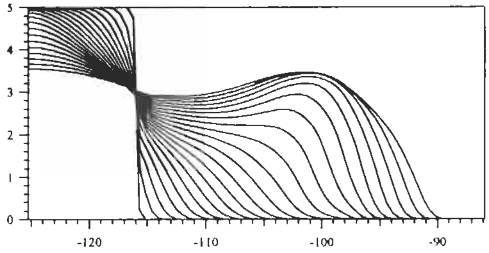

Figure 9: Water flow along centreline of the vessel: Surface elevation according to dam breaking model.

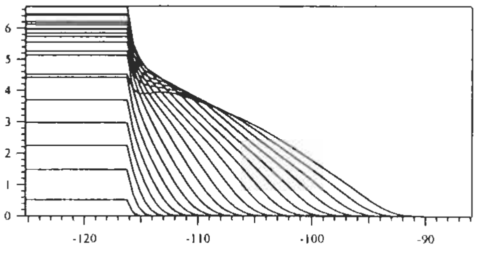

Figure 10: Water flow along centreline of the vessel: Surface elevation with boundary conditions from wave kinematics analysis.

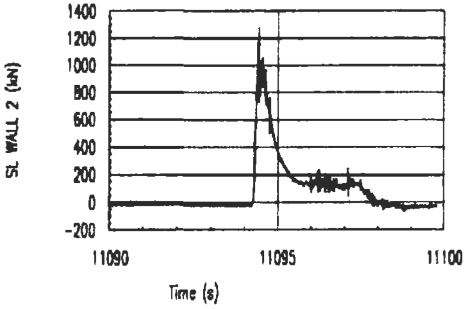

Figure 11: Measured forces from water impact on deckhouse wall

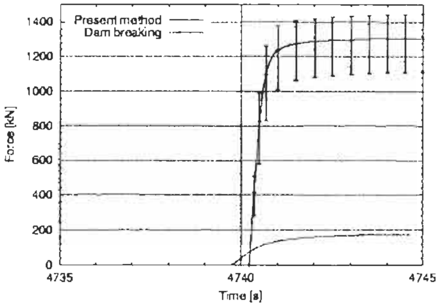

Figure 12: Calculated forces from water impact on deckhouse wall. Water propagation based on boundary conditions from wave kinematics analysis, and on dam breaking.

Practical Design of Ships and Other Floating Structures
You-Sheng Wu, Wei-Cheng Cui and Guo-Jun Zhou (Eds)
© 2001 Elsevier Science Ltd. All rights reserved

WAVE IMPACT ON DECKS OF FLOATING PLATFORMS

Rolf Baarholm[1], Odd M. Faltinsen[1] and Kjell Herfjord[2]

[1]Department of Marine Hydrodynamics, NTNU, N-7491 Trondheim, Norway
[2]Norsk Hydro Research Centre, P.O. Box 7190, N-5020 Bergen, Norway

ABSTRACT

Two methods for predicting wave impact loads underneath decks of offshore platforms are presented. These are a Wagner based method (WBM) and a non-linear boundary element method (BEM). Experiments of wave impact on a fixed idealized deck in 2-D flow conditions have been performed to validate the theories. A procedure for accounting for 3-D effects is suggested. At present only the WBM can account for motions of the platform and compute the rigid body responses due to impact. This method is used to study the loads on the deck and the rigid body responses of a semi-submersible due to regular incident waves. Stokes second order theory is used to describe the incident waves. It is shown that the impact can cause an important suction force and resulting downward heave motion.

KEYWORDS

Wetdeck slamming, Rigid body response, Air gap.

1 INTRODUCTION

It is common practice to design the lower deck of offshore platforms to be above the maximum predicted level that waves can reach. However, *e.g.* limited field data may give considerable uncertainties in the expected value for the maximum water level. For bottom-mounted platforms subsidence may increase the risk of wave impacts with time. It has been customary for floaters to neglect any probability of waves reaching the deck, relying on the air gap to provide a sufficient margin of safety. The deck height of floaters is limited by weight and stability considerations, and this makes the air gap a substantial cost driver for the platform. In the design of new floaters, one might allow some extreme waves to hit the deck structure. Reduction of the deck height of existing floaters may occur when they are in damaged condition or due to failure in ballast systems. The deck clearance of existing floaters may be decreased if higher production is desired. Increased storage capacity and deck weight must then be compensated by reduced deck clearance, which implies higher risk of wave impacts. This is the motivation for this study.

2 THEORY

Two-dimensional potential flow is initially assumed. This implies head sea on a floater with lateral symmetry, and that diffraction due to vertical platform members is neglected. The latter is a reasonable assumption for survival conditions where the wavelengths are long relative to the cross-dimensions of the platform legs. In this case the platform will oscillate in three degrees of freedom (surge, heave and pitch). It is further assumed that hydroelasticity is not important for the loading. The fluid flow can be described by the total velocity potential $\Phi = \phi + \varphi_I$, where ϕ is the velocity potential due to the impact and φ_I is the known incident wave potential. In this work the incident waves are regular and described by Stokes' second order theory. A boundary value problem for ϕ is set up. The two-dimensional Laplace equation becomes the governing equation in the fluid domain. The effect of gravity is neglected, leading to the high frequency dynamic free surface condition, $\phi = 0$. When solving the boundary value problem (BVP), this condition is applied on the straight line $z = 0$. The local (x,z)-coordinate system has its origin in the center of the instantaneously wetted length with the positive x-axis running downstream along the deck and the z-axis pointing upwards. This condition implies that no waves will be generated. Furthermore, a boundary condition must be imposed on the impermeable instantaneous wetted body surface. For impact with small local dead-rise angle this condition may be approximated as $\partial\phi/\partial z = -V_R(x,t)$ on $z = 0$. $V_R(x,t)$ is the relative normal velocity between the body and the fluid. The impact velocity gets contributions from both the fluid particle velocities in the incident wave and from the rigid body velocity of the deck. The resulting boundary value problem is on the same form as the two-dimensional lifting problem discussed in Newman (1977). Newman solved this problem by using a vortex distribution along the wetted body surface. An identical procedure is used to solve the present problem. A linear spatial distribution of V_R along the wetted length is assumed, *i.e.* $V_R = V_0 + V_1 x$ for $|x| \le c(t)$ and $z = 0$. The BVP can then be solved analytically at each time step. This yields

$$\phi = -V_0\sqrt{c^2 - x^2} - \frac{1}{2}V_1 x\sqrt{c^2 - x^2} \quad \text{on} \quad z = 0 \quad \text{and} \quad |x| \le c \tag{1}$$

for the perturbation velocity potential on the body and

$$\frac{\partial\phi}{\partial z} = \frac{V_0|x|}{\sqrt{c^2 - x^2}} + \frac{1}{2}\operatorname{sgn}(x)V_1\left(\sqrt{c^2 - x^2} - \frac{x^2}{\sqrt{c^2 - x^2}}\right) - V_0 - V_1 x \quad \text{on} \quad z = 0 \quad \text{and} \quad |x| > 0 \tag{2}$$

for the impact induced vertical velocity on the free surface. The evolution of $c(t)$, which determines the wetted length, is unknown and must be solved numerically. Water hits initially the front end of the deck and during the initial increase in wetted surface it is the downstream intersection point that changes, while the upstream intersection is fixed at the front end of the deck. The free surface is discretized by fluid particles that are stepped in time. Let superscript j denote a time instant and subscript i denotes a fluid particle, so that P_i^j is the position of particle i at time step $t = t^j$, see Figure 1. The vertical velocity given in Eqn. 2 dominates the fluid velocity close to the intersection points, and the horizontal velocity due to φ_I is therefore disregarded in this region. The new downstream intersection point c^{j+1} is determined a priori while the time increment $\Delta t^j = t^{j+1} - t^j$ is found by a local analysis as the time the particle P_i needs to cover the vertical distance Δz. The time increment can be written as $\Delta t^j = \left(dt/dc\right)_m \left(c_i^{j+1} - c_{i-1}^j\right)$ where $\left(dt/dc\right)_m$ is found by using a local "corner flow" velocity potential valid near the intersection point, matching this with Eqn. 1 and averaging over the time step. The local solution is introduced due to the singular nature of the fluid velocity at the intersection points. The details in this procedure are given in Baarholm (2001). Once the time increment is determined, the free

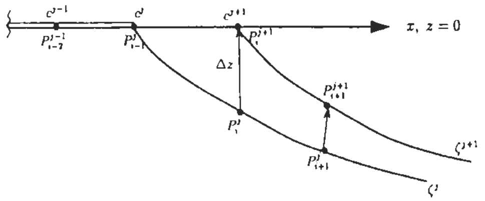

Figure 1: Stepping of free surface.

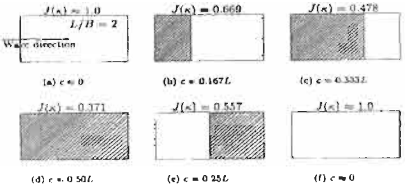

Figure 2: The variation of $J(\kappa)$ as a wave propagates along a deck.

surface particles are moved with their local velocities due to both ϕ and φ_I, and the new free position ζ^{j+1} is found. A fourth order Runge-Kutta scheme is used to integrate ζ in time. To find the velocities due to φ_I in the "wave zone" above the mean free surface $z_0 = 0$, Taylor expansion about $z_0 = 0$ consistent with the theoretical derivation of Stokes' second order theory is applied. Once the downstream intersection point has reached the aft end of the deck, it is kept fixed there during the water exit phase, *i.e.* when the wetted area diminishes. During water exit the upstream intersection point is determined by a von Karman type approach, *i.e.* as the intersection between the deck and the incident wave. For a floater this intersection point may not exist in the theoretical solution, and the upstream intersection point is then let to propagate downstream with the phase velocity of the incident wave. The dynamic free surface condition, $\phi = 0$, can strictly speaking only be justified in the water entry phase. The normal force on the deck due to ϕ can be determined as $d\left(A_{33}^{(\infty)}V_0\right)/dt$, where $A_{33}^{(\infty)}$ is the high frequency limit added mass of the wetted deck area. For a deck with wetted length equal to $2c$ and breadth equal to B, $A_{33}^{(\infty)} = 0.5\rho\pi c^2 B$ if 2-D theory is applied. However, due to finite breadth 3-D effects will reduce the added mass. These effects will depend on the wetted area's aspect ratio $\kappa = 2c/B$, *i.e.* the three-dimensional added mass can be expressed as $A_{33}^{(\infty)} = 0.5J(\kappa)\rho\pi c^2 B$, where $J(\kappa)$ is a correction factor accounting for 3-D effects. Blagovenshchensky (1962) suggests the following empirical based formula for the correction factor

$$J(\kappa) = \frac{1}{\sqrt{1+\kappa^2}}\left\{1 - \frac{0.425\kappa}{1+\kappa^2}\right\} \tag{3}$$

Meyerhoff (1970) has shown that Eqn. 3 yields results that are in good agreement with theoretical results obtained from three-dimensional potential theory. Eqn. 3 suggests that the importance of 3-D effects vary significantly when a wave hits the front end of a deck and propagates downstream. It is important in practice to account for this when computing the impact loads on the deck. Figure 2 illustrates how $J(\kappa)$ may vary for a deck with $L/B = 2$, where L is the length of the deck. The wetted area is shaded. Note that the time intervals between each sketch in the Figure 2 are not identical. The $J(\kappa)$-coefficient is equal to unity at the initial impact but it decreases as the wetted length increases. When the deck is fully wetted $\kappa = 2$ and $J(\kappa) = 0.371$, *i.e.* the added mass is only 37.1% of the value obtained by two-dimensional theory. Taking this into account, the vertical component of the force acting underneath the deck can be written as

$$F_3 = -\rho\pi c B n_3\left(J(\kappa)\dot{c} + \frac{1}{2}\dot{J}(\kappa)c\right)V_0 - \frac{1}{2}\rho\pi c^2 B J(\kappa) n_3 \dot{V}_0 + F_{3,I}, \tag{4}$$

where n_3 is the vertical component of the deck's unit normal vector **n**. **n** is defined to be positive into the fluid. The first term in Eqn. 4, $\dot{A}_{33}^{(\infty)}V_0$, is denoted as the slamming force and it is governed by the rate of change of the wetted area, while the second term, $A_{33}^{(\infty)}\dot{V}_0$, is an added mass force. One should note that Eqn. 4 uses the same $c(t)$ as found by 2-D theory. This is strictly speaking incorrect. As described in Kaplan (1992), the slamming term is set equal to zero during water exit. $F_{3,I}$ is the vertical component of the Froude-Kriloff force. This is written as $\rho\Omega(t)\left(g+a_3(t)\right)$, where $\Omega(t)$ is the instantaneous submerged volume due to the incident wave, g is the acceleration of gravity and $a_3(t)$ is the average vertical fluid acceleration in the undisturbed wave across the wetted area. Similarly, one can derive expressions for the impact induced surge force and pitch moment, see Baarholm (2001). The pitch moment due to the Froude-Kriloff pressure is estimated by integrating over the area intersected by the incident wave.

Before impact occurs, the platform experiences linear wave-induced motions. It is assumed that the total motion of the platform can be written as $\vec{\eta}=\vec{\eta}_w+\vec{\eta}_s$ where $\vec{\eta}_s$ is the slamming induced rigid body motion and $\vec{\eta}_w$ is found from a linear motion analysis of the platform. The slamming induced rigid body responses follow by solving

$$(\mathbf{M}+\mathbf{A})\ddot{\vec{\eta}}_s+\mathbf{C}\vec{\eta}_s=\mathbf{F}_{exc} \qquad (5)$$

M, **A** and **C** are the inertia, added mass and restoring matrices, respectively. $\mathbf{F}_{exc}$ contains the impact-induced surge, heave and pitch loading on the deck described above. The added mass coefficients are associated with the high frequency limit $\omega\rightarrow\infty$, and the asymptotic values for these coefficients for the submerged volume must be evaluated beforehand, and the added masses due to the wetted deck area are added. Eqn. 5 is integrated in time using a fourth order Runge-Kutta scheme, with initial conditions $\vec{\eta}_s(t_0)=[0,0,0]^T$ and $\dot{\vec{\eta}}_s(t_0)=[0,0,0]^T$.

A non-linear boundary element method has also been developed to solve water impact underneath decks of offshore platforms. At present the method is limited to solve impact on fixed decks, but it provides several improvements relative to the Wagner based method described above. As for the WBM, two-dimensional potential theory is assumed and the total velocity potential is written as $\Phi=\phi+\varphi_I$, where the perturbation velocity potential, ϕ, is unknown and the incident wave potential, φ_I, is described by Stokes' second order theory. A boundary value problem for ϕ is set up by imposing exact boundary conditions according to Stokes second order theory. The exact dynamic free surface condition with gravity included and the exact kinematic free surface condition are imposed on the exact free surface. The exact body boundary condition is imposed on the wetted part of the underside and the front side of the deck. The resulting boundary value problem is solved as an initial value problem with initial condition $\phi=0$ on the incident free surface at the time instant of first impact. The perturbation velocity potential inside the fluid domain is represented by Green's second identity. The procedure for solving the BVP is described in Baarholm and Faltinsen (2001). The velocity potential on the free surface and the free surface elevation are integrated in time by using the dynamic and kinematic free surface conditions, respectively. Special care is necessary in describing the motion of the free surface, and a time integration scheme similar to the one described in Zhao and Faltinsen (1993) is implemented. A major improvement made by the BEM compared to the WBM is the evaluation of the body/ free surface intersection points, especially during the water exit phase. Baarholm and Faltinsen (2000) presented experiments for wave impact on an idealized fixed horizontal deck in two-dimensional flow condition. These showed that the upstream body/ free surface intersection behaves very differently from the intersection with the undisturbed wave profile. Figure 3 shows the free surface as the upstream intersection moves from the front side to the bottom plate of the deck. The BEM accounts for the free surface deformation on the upstream side of the body. As the fluid reaches the aft end of the deck, the fluid flow leaves the deck tangentially, see Figure 4. To account for this a Kutta condition is imposed. This ensures that the flow leaves the deck tangentially and that the velocity potential is continuous at the downstream intersection point. During the final part of the water exit phase the downstream intersection point starts to move forward again towards the upstream intersection and the water leaves the structure somewhere on the aft part of the deck. Also in this final stage a Kutta condition is required in the BEM to obtain stable solutions. The evaluation of the intersection points is discussed in more details in Baarholm and Faltinsen (2001). The vertical force on the deck is computed by either using direct pressure integration or by imposing conservation of fluid momentum.

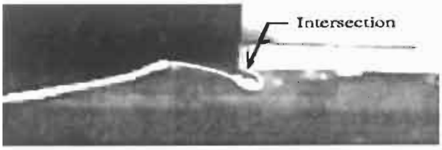

Figure 3: Upstream intersection as the fluid flow detaches from the front end.

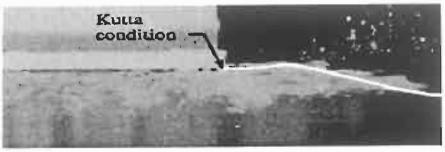

Figure 4: Fluid flow at aft end of the deck. The fluid leaves the deck tangentially.

In general, the water entry/ water exit process yields a vertical force history where the structure experiences a positive slamming dominated force (upward directed) during the initial water entry phase, followed by a negative added mass dominated force, due to negative fluid particle accelerations in the wave crest. Figure 5 shows a typical comparison between experimental results and theoretical results by the WBM and the BEM. Two experimental realizations are shown to illustrate the repeatability of the experiments. The model used was 0.63 m long and 0.56m wide and it covered the entire width of the wave tank, thus $J(\kappa)=1.0$. The WBM and the BEM describe the water entry phase well. The duration of the water entry process and the resulting impact force are well predicted by both theories. For the water exit phase the results from the two theoretical methods deviate more. The WBM overestimates the magnitude of the largest negative force and it underestimates the duration of the water exit process. The BEM, however, yields results for both the magnitude of the negative force and the duration of the water exit process that compare well with the experiments.

3 CASE STUDY: WAVE IMPACT ON A SEMI-SUBMERSIBLE

A case study of wave impact on a floater in extreme waves has been performed. The emphasis has been on the impact loads and on the rigid body response. Since the BEM is not applicable for floaters at the present time, the WBM has been used to compute the loads on the deck. WAMIT has been used to determine the transfer functions for the linear wave induced motions and the high-frequency added mass matrix for the submerged hull. The panel model of the platform is shown in Figure 6. The draft of the platform is 29m and the length of the sides is 84.48m. The cross-sections of the pontoons and the columns are rounded rectangles with dimensions 16.64m × 8.40m and 16.64m × 16.64m, respectively. This yields a displaced volume of 59114m^3. The radius of inertia for pitch is $r_{55} = 32.68\,\text{m}$, and the center of gravity is located 28m above the keel. The deck dimensions are $90\text{m}\times 90\text{m}$. Norwegian standards (NPD) requires the deck height to be sufficient for the probability of structural damage due to impact to be less than 10^{-4} per year when all uncertainties are accounted for. 10000 years extreme waves are therefore assumed in this study. Contour curves for 10000 years sea states (H_S, T_P) at two different locations, the Northern North Sea (NNS) and the Aasgard field, are shown in Figure 7. Representative regular waves are found by using the wave height of the most probable highest wave, $H = H_S\sqrt{\ln N/2}$, during a 3hrs long sea state with T_P as the corresponding wave period T. N is for simplicity taken as $10800\text{s}/T_P$. Simulations are performed to evaluate reduction in the air gap relative to still water level for sea states on the two contour curves, see Figure 8.

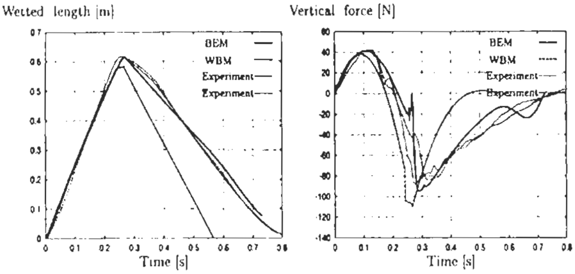

(a) Wetted length (b) Vertical impact force

Figure 5: Comparisons between experiments and theory. Wave period T=1.25s, wave height H=0.14m, and deck height $\eta_{ag0} = 0.06\,\text{m}$.

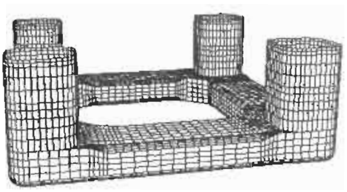

Figure 6: Panel method for the floater used in the case study.

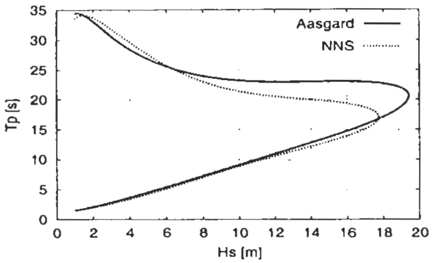

Figure 7: 10000 years sea states.

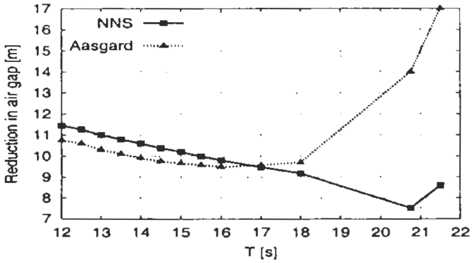

Figure 8: Reduction of air gap for platform in regular waves relative to the air gap in still water.

Different criteria for the maximum wave steepness exist, see *e.g.* Haver and Nyhus (1986). In this work periods less than 12 s are not considered. For $T < 16.5$ s the NNS contour curve yields the most critical waves, while the Aasgard curve yields the most critical wave conditions for longer waves. Note that the air gap diminishes rapidly as T approaches 21.5s. This is because the platform experiences cancellation in heave for this period according to the WAMIT computations. However, viscous forces are important in this region and full heave cancellation will not occur. This is not included in the WAMIT calculations. Still, this period may be the most critical period at the Aasgard field. The cancellation period should be considered when designing a floater for a given location. Note that close to this period the wave may initially hit deck somewhere between the front and aft ends of the deck. For NNS the wave height corresponding to the high periods are smaller and they are therefore less critical. The deck height of the platform is set equal to 11.0m. This is not necessarily a realistic value. Design deck heights are usually larger. For NNS wave conditions and for second order incident waves impact occurs for wave periods between 12 and 13 seconds. For higher wave periods the waves will pass under the deck. Figure 9 and Figure 10 show the vertical heave force and the resulting wave induced heave displacement for wave periods equal to 12s, 12.5s and 13s. The corresponding wave heights are 25.41m, 26.48m and 27.50m, respectively. T=12s gives the largest loads and thus the largest rigid body responses. The negative added mass force is the dominating force and this gives the platform a negative heave displacement. Due to dynamic effects, the negative displacement increases after the wave has detached from the deck. For T=12s the platform is pulled down 4.02m due to the wave impact. The largest pitch displacement for this period is also negative with magnitude equal to 0.026rad. These rigid body responses are important to take into account when impact occurs for two consecutive large waves. The maximum vertical acceleration of the deck for T=12s is approximately equal to 0.96m/s^2.

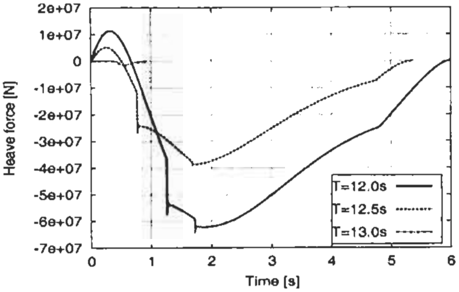

Figure 9: Impact induced heave force.

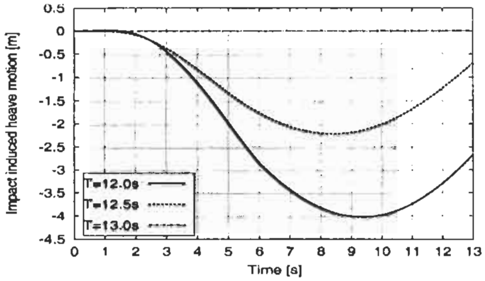

Figure 10: Impact induced heave motion.

The maximum magnitude of the negative force for 12s is more than 50% larger than for T=12.5s. This is partly due to due to larger wetted area. The maximum wetted areas are 33.6m and 26.1m for T=12s and T=12.5s, respectively.

Uncertainties from a number of sources are connected to the above computations. The contour curves for 10000 yr. sea states are based on extrapolation of measurements, and also the contour curve approach itself is approximative. In principle, full long term statistics should have been applied. Further, the highest wave is represented by second order regular waves. For steep waves this may not be good enough, and an "infinite" order wave theory should have been used. This would lead to a larger reduction of the air gap, and impact would have occurred for a larger range of wave periods. From Figure 5 it can be noted that computations with the WBM are not satisfactory for the water exit phase. To get better predictions of body/ free surface intersections and the impact loading, a non-linear boundary element method should be used.

Acknowlegdements

Norsk Hydro has financed the study. Statoil are acknowledged for providing the contour curves.

References

Baarholm, R. (2001). *Theoretical and experimental studies of wave impact underneath decks of offshore platforms*. Doctoral dissertation, NTNU, Trondheim, Norway.

Baarholm, R. and Faltinsen, O. M. (2000). Experimental and Theoretical Studies of Wave Impact on an Idealized Platform Deck. *In Proc. 4th Int. Conf. on Hydrodynamics (ICHD2000)*. 181-186.

Baarholm, R. and Faltinsen, O. M. (2001). A boundary element method for solving water impact on a platform deck. *In Proc. 20th Int. Conf. on Offshore Mech. and Arctic Eng. (OMAE2001).*

Blagovenshchevsky, S. N. (1962). *Theory of ship motion*, Dover, New York, USA.

Haver S. and Nyhus K. A. (1985). A wave climate description for long term response calculations. *5th Int. Symp. on Offshore Mech. and Arctic Eng.* Tokyo.

Kaplan, P. (1992). Wave impact on Offshore platforms: Re-examination and New Interpretations, In *Proc. 20th Offshore Tech. Conf.* (OTC1992), 79-86.

Meyerhoff W. K. (1970). Added masses of thin rectangular plates calculated from potential theory. *J. Ship Research*. 100-111.

Newman , J. N. (1977). *Marine Hydrodynamics*, MIT Press, Cambridge, USA.

Wagner, H. Über Stoβ- und Gleitvorgänge and der Oberfläche von Flüssigkeiten. *Zeitschr. für angewandte Mathematik und Mechanik.* **12:4**, 193-214.

Zhao R. and Faltinsen O. M. (1993). Water Entry of Two-Dimensional Bodies. *J. Fluid Mech*, **246**, 593-612.

Practical Design of Ships and Other Floating Structures
You-Sheng Wu, Wei-Cheng Cui and Guo-Jun Zhou (Eds)
© 2001 Elsevier Science Ltd. All rights reserved

IMPACT PRESSURE ANALYSIS ON HIGH-SPEED CRAFT IN WAVES, THROUGH FE-ANALYSIS ON FULL-SCALE AND MODEL MEASUREMENT DATA

Anders Rosén

Division of Naval Architecture, KTH, Stockholm, Sweden

ABSTRACT

The paper discuss a method to re-construct three-dimensional propagating impact pressure distributions, from recordings with an arbitrary matrix of pressure transducers on a hull. With pressure measurements made with several transducers, on a small high-speed craft in both full-scale and model scale, the method is used to formulate realistic load cases for FE-analysis. Resulting structural responses are calculated and compared with full-scale strain measurements, indicating that the re-constructed pressure distributions well resembles the actual load. Further use of the method is discussed, for example investigation of the real pressure distribution influence on panel boundary conditions, and time domain simulation of structural response when the method is used together with methods for seakeeping simulation.

KEYWORDS

HSC, Impact pressure distribution, Full-scale trials, Model tests, Structural response, Design methods

1 INTRODUCTION

The usual approach in high speed craft design can be illustrated by the following quotation taken from the frequently referred work by Allen & Jones (1978) : "Each occurrence of hull-water impact is a unique event. The magnitude and shape of the resulting pressure distribution depend on a number of parameters.....During its operational lifetime, a hull will be subjected to countless variations in these parameters.....From a design standpoint, there is need for something more than just the three-dimensional pressure distribution, e.g. a method which, ideally, can minimize the uniqueness and provide a simple description of the impact phenomenon". With this approach several different semi-empirical methods have been developed, relating vertical impact acceleration with design pressure for the different structural members. A short review of these methods is given below.

The design pressure formulated in Allen & Jones (1978) is expressed as,

$$p_D \sim (\frac{m \cdot a_{cg}}{A_R} \cdot k) \tag{1}$$

Here m is the mass displacement of the craft. A_R is the reference area on which the total impact force $m \cdot a_{cg}$ is assumed to work. The area reduction factor, k, is a function of the ratio between the design area, A_D, i.e. load carrying area for the structural member in question, and the reference area. The area reduction factor is a way to take the non-uniformity of the pressure distribution, and the pronounced pressure peak, into account through giving relatively higher pressure the smaller the design area is, (e.g. for A_D / A_R=0.1 $k \approx$2, and for A_D / A_R=0.01 $k \approx$4). Similar approaches are found in the classification rules.

Considering the design acceleration, a_{cg}, one approach is to choose a level based on the type of service the craft will be used for and the endurance and motivation of the crew in that service, from a comfortability point of view, (e.g. Koelbel (1995)). Hereby a craft can be classified as a 4g-craft or a 6g craft etc.

There are different expressions relating vertical acceleration in the centre of gravity, with significant wave height $\overline{H}_{1/3}$ and speed V, and combinations of some hull parameters, like length L, beam B, deadrise β, trim angle τ, etc, (e.g. Savitsky & Brown (1976)),

$$a_{cg} \sim (\overline{H}_{1/3}, V, \text{hull parameters}) \tag{2}$$

With these expressions the possible service, $V \sim \overline{H}_{1/3}$, due to the chosen acceleration level, can be checked. In these methods the acceleration, a_{cg}, is normally formulated as the statistical average of the one tenth or one hundredth highest vertical acceleration in the centre of gravity, the design pressure, p_D, is formulated as static and uniform, and the structural elements on which the pressure works are assumed to be clamped.

Now, lets go back to the quotation above, where the transient propagating impact pressure is addressed as "just the three-dimensional pressure distribution". What does it actually look like this distribution in a full-scale situation? How does it propagate and redistribute during an impact? And, is it possible to monitor the impact pressure distribution on a craft in irregular seas with a limited number of transducers?

At continuous pressure measurements on high-speed craft in waves, with high resolution in time as well as in space, i.e. high sampling frequency and several transducers, an immense amount of data is generated. The method for re-construction of the three-dimensional pressure distribution at every time instant presented below, offers a tool to handle these data, that enables detailed water-hull interaction analysis at every time instant of each impact occasion. Thus, it is an attempt to deal with the three-dimensional pressure distribution itself.

2 PRESSURE DISTRIBUTION RE-CONSTRUCTION

The method is simply based on linear interpolation and extrapolation. It requires at least two transducers in the longitudinal direction of the craft and two in the transverse direction. It can easily be adopted to arbitrary sized matrices of pressure transducers, and arbitrary hull shapes. Of course, the higher resolution of the transducer matrix, and the larger area it covers, the better is the resulting re-construction.

Extensive full-scale trials and model tests have been performed on a small planing craft in waves, (see Rosén & Garme (1999), and Garme & Rosén (2000)). The craft is 10 metres long, has a displacement of 6.5 tonnes and a maximum speed of +40 knots. In Figure 1 the hull and transducer set-up in the full-scale trials is shown. In the model tests a matrix of 3x4 pressure transducers covered an even larger area of the hull. In Figure 2 a sequence of continuous pressure recordings in full scale is given, showing an impact occasion. These data are used below when describing the method.

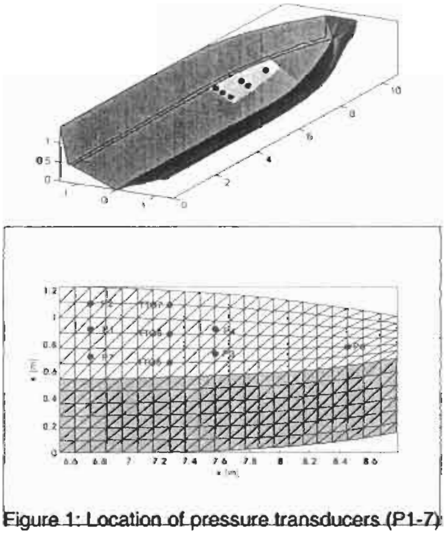

Figure 1: Location of pressure transducers (P1-7) and strain gauges (TTG5-7).

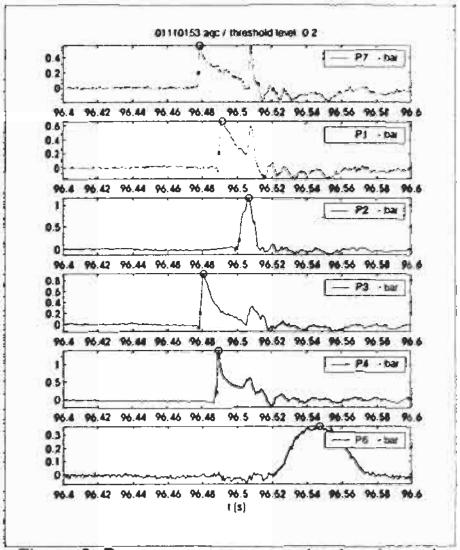

Figure 2: Pressure measurements at an impact.

The first step is to locate the puls front (the spray root) at every time instant. The moment $t_{rise,i}$ when the pressure abruptly rise at the particular transducer i, is assumed to be the moment when the puls front reaches that location. The spacing $(s_{trans,j} - s_{trans,i})$ between two successive transducers is of course known, and with the time lag $(t_{rise,j} - t_{rise,i})$ between puls front passings, the speed of the puls is determined simply as,

$$v_{ij} = (s_{trans,j} - s_{trans,i}) / (t_{rise,j} - t_{rise,i}) \qquad (3)$$

Sections with several transducers gives one speed for each transducer spacing. On sections with only one transducer, the speed is taken from the closest section having several transducers.

For each puls front passing between two successive transducers i and j, the position of the puls front, $s_{front,ij}(t_k)$ is determined for time steps, t_k, with desirable resolution,

$$s_{front,ij}(t_k) = s_{trans,i} + v_{ij}\,(t_k - t_{rise,i}) \tag{4}$$

The puls front position is extrapolated below the lowest transducer on a section and above the highest, of course giving less accurate position the further the extrapolation is made.

The puls front positions at the different sections are connected with splines with a desirable resolution in the x-direction. The resulting puls front locations from the recordings in Figure 2 are given in Figure 3 for a number of time steps.

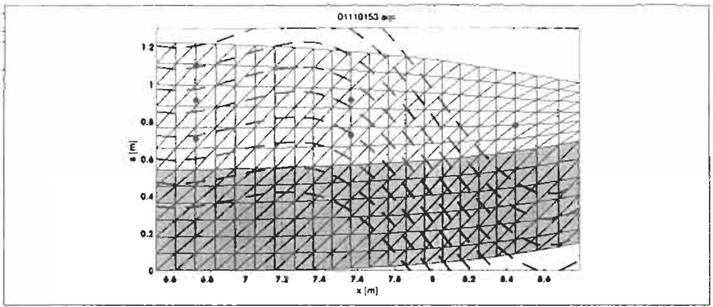

Figure 3: Position of the pressure puls front at a few time steps, derived from the measurements in Figure 2.

The peak pressure $p_{max,i}$ occurring at each transducer during an impact is identified, and the pressure gradient for the peak pressure between successive transducers is determined as,

$$(dp/ds)_{ij} = (p_{max,j} - p_{max,i})/(s_{trans,j} - s_{trans,i}) \tag{5}$$

The assumption is made that the peak pressure occurs right at the puls front, and the peak pressure in each puls front location $s_{front,ij}(t_k)$ is calculated as,

$$p_{peak,ij}(t_k) = p_{max,i} + dp_{ij}(t_k) \tag{6}$$

where,

$$dp_{ij}(t_k) = (dp/ds)_{ij} \cdot (s_{front,ij}(t_k) - s_{trans,i}) \tag{7}$$

The pressures in the 'tail' is moved along with the puls front, and scaled percentually as,

$$p = p \cdot k_{ij}(t_k) \tag{8}$$

where,

$$k_{ij}(t_k) = p_{peak,ij}(t_k)/p_{max,i} \tag{9}$$

The resulting two-dimensional pressure distribution, re-constructed from the measurements in the section with three transducers in Figure 2, can be seen in Figure 4. Each pressure value in the two dimensional distribution, at each different section is connected with splines with corresponding values at the other sections. The resulting three-dimensional pressure distribution can be seen in Fig.

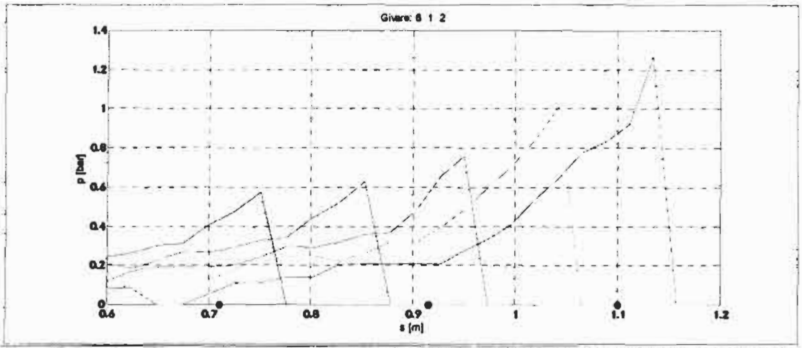

Figure 4: Two-dimensional pressure distributions on the section with three transducers, at a number of time instants.

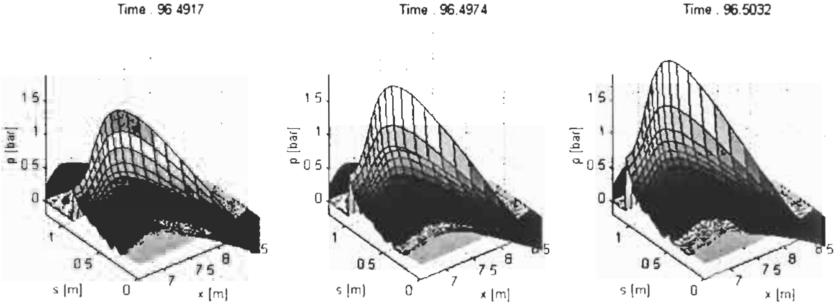

Figure 5: The three-dimensional pressure distribution at three different time instants.

3 FE-CALCUALTIONS

The extension and mesh of the FE model is shown in Fig. This part of the hull is limited by the keel in the bottom edge, the deck in the upper edge, and a transversal bulkhead in fore and aft ends respectively, giving well defined boundary conditions. The shaded part is a panel, limited by a coarse longitudinal stringer in its bottom edge and the stiff chine in its upper edge.

The re-constructed pressure distributions are discretised according to the FE meshing and applied as constant pressures on each element, and the structural response is calculated. Fig shows the sequence of stress distribution propagation with the pressure distribution propagation. In Fig a qualitative comparison is made between measured laminate strain and the calculations in the corresponding locations.

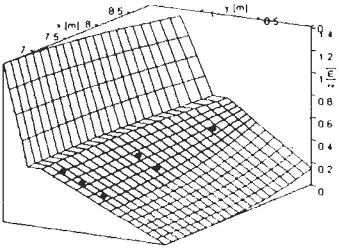

Figure 6: Extension and mesh of the FE-model.

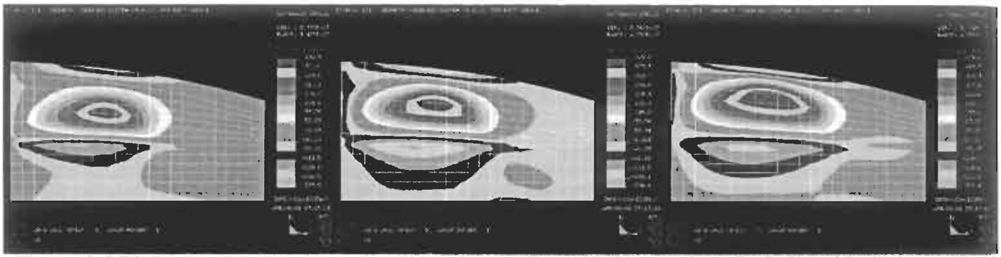

Figure 7: FEA results showing stress distribution propagating with the pressure distribution. Vertical view from above.

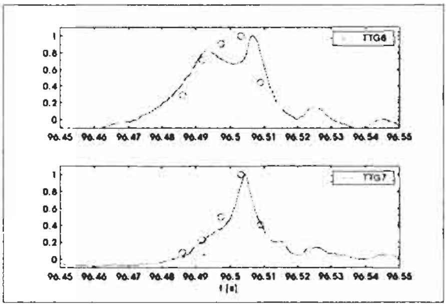

Figure 8: Comparison between laminate strain measured at the full-scale trials and FEA results with the re-constructed pressure distributions. Note that the values given are normalised.

4 CONCLUSIONS AND DISCUSSION

The method for three-dimensional pressure distribution re-construction presented, is simply based on linear interpolation and extrapolation. However, a qualitative comparison between laminate strain measured at full-scale trials and FEA results with loads formulated with the method, indicates that the re-constructed pressure distributions well resembles the actual load. Note that the values given in the comparison are normalised and that the evaluation at this stage is only qualitative.

The method is implemented in MATLAB. In the example given three dimensional pressure distributions were re-constructed for a few instants in one single impact occasion. The distributions where then discretised and transferred to the FE-program where the resulting response was calculated. As long as the FEA is linear, more rational of course, is to calculate the response resulting from a unit pressure applied on one single element, repeat this for unit loads on all elements, and transfer the FE-results for some points of interest for each of the single-element loadcases to MATLAB. Now, the method can be used on a arbitrary time record containing several impacts. At every time step, the discrete value on each element in the momentary re-constructed pressure distribution, is multiplied with corresponding unit load FE-response and superimposed. This gives a time record of FE-results, which enables further quantitative evaluation of the method, which is of course needed.

The method will be used when further analysing the full-scale trials and model tests presented in Rosén & Garme (1999), and Garme & Rosén (2000), and also in the full-scale trials that are going to be performed on the by Kockums newly built corvette Visby which will be equipped with 3x3 pressure transducers.

A non-uniform pressure distribution propagating across a panel in a ship hull, influences the panel boundary conditions. To study this influence in detail is another area were the method might be useful, using as well full-scale as model scale data.

Further, the presented method will be used together with the simulation model presented in Garme (2000). This enables time domain simulation of the structural response and further discussion on design methods based on direct calculations.

References

Allen R.G., Jones J.R. (1978). A Simplified Method for Determining Structural Design Limit Pressures on High Performance Marine Vehicles. *AIAA/SNAME Advanced Marine Vehicle Conference.*
Garme K. (2000). Time-Domain Model for Planing High-Speed Vessels in Head Seas. *Licentiate Thesis TRITA-FKT ISSN 1103-470x, Division of Naval Architecture, KTH*, Stockholm.
Garme K., Rosén A. (2000). Experimental Pressure Investigation on a High-Speed Craft in Waves. *Proc. Hydrodynamics of High Speed Craft, RINA*, UK.
Koelbel J.G. (1995). Comments on the Structural Design of High Speed Craft. *Marine Technology.* **32:2.**
Rosén A. & Garme K. (1999). Slamming Studies on High Speed Planing Craft Through Full-Scale Trials and Simulations. *Proc. FAST'99.* USA.
Savitsky D., Brown P.W. (1976). Procedures for Hydrodynamic Evaluation of Planing Hulls in Smooth and Rough Water. *Marine Technology.*

Practical Design of Ships and Other Floating Structures
You-Sheng Wu, Wei-Cheng Cui and Guo-Jun Zhou (Eds)
© 2001 Elsevier Science Ltd. All rights reserved

ASSESSMENT OF SLOSHING LOADS FOR TANKERS

Pierre C. Sames and Thomas E. Schellin

Germanischer Lloyd AG
Vorsetzen 35, D-20459 Hamburg, Germany

ABSTRACT

A new procedure to assess sloshing loads for tankers is presented and applied to a sample tanker. Starting with computed ship motions and fluid motions inside partially filled tanks, critical fill levels were identified. Simulation of fluid flow was performed with a finite volume method for each critical fill level. Two- as well as three-dimensional flow computations were employed to predict pressure loads for panel sized patches of tank walls. Time traces of pressure were analyzed, and resulting maximum loads were compared for all critical fill levels to determine overall maximum loads. Results generally agreed favorably with current rule based values.

KEYWORDS

Sloshing, tanker, Impact pressure, Finite volume method, Critical fill levels

1 INTRODUCTION

Fluid motion in partially filled tanks can cause large structural loads if the period of tank motion is close to the natural period of fluid inside the tank. This phenomenon, called sloshing, affects structural integrity of seagoing tankers. Bulkheads and tank tops as well as baffles and other internal structures are subject to time dependent pressure loads that can lead to collapse or fatigue failure. As a classification society, Germanischer Lloyd ensure safety of ship structures by means of up-to-date rules and procedures to analyze complex phenomena like sloshing. It has long been recognized that loads due to sloshing can only be accurately predicted if the free surface flow inside the tank is correctly simulated. A comparative study on sloshing loads conducted by the ISSC showed that the majority of contributors used finite difference or finite volume methods to simulate viscous flow inside tanks (Cariou and Casella, 1999). In Germany, the research project Life-Cycle Design, Part B7, was initiated to predict effects of hydrodynamic impact loads. Muzaferija et al. (1998) reported on the development of a new method that accounts for arbitrarily deformed free surfaces, and Sames et al. (1999) successfully applied this method to predict bow flare slamming loads for a container ship. To validate the refined method for sloshing, Sames et al. (2001) predicted fluid flow in several tank configurations and compared results with measurements. Park et al. (1995), implementing a numerical method in their design system to predict sloshing loads, first computed ship motions, checked for possible resonance conditions, and then analyzed fluid motion for different fill levels. They found that excitation amplitude significantly affects sloshing loads. Kim et al. (1995), presenting a three-dimensional coupled analysis of fluid motion and structural response, established a tank motion scenario based on ship motions, and computed fluid motions inside a tank of a VLCC for a selected fill level. After performing an analysis with rigid tank walls to identify highly loaded structural elements, they also accounted for the flexibility of tank walls by computing structural response with a finite element submodel. Here we present a new procedure to assess sloshing loads for tankers. Our method comprises ship motion and fluid motion analyses to identify critical fill levels. The set-up of computations and the analysis of results from sloshing simulations is presented for a sample tanker. Finally, maximum loads are compared with current rule based values.

2 SAMPLE TANKER

For the analysis we selected the modern double hull tanker SEATURBOT, built by Lindenau shipyard in Germany. Principal particulars of this tanker are listed in Table 1. General layout and tank arrangement is shown in Fig. 1. Both ballast draft and design draft data were needed for our analysis. Service speed V was 14.5 knots, and minimum maneuvering speed was assumed to be one third of service speed. Ten cargo tanks of different size are symmetrically arranged on both sides of a central longitudinal bulkhead. Table 2 summarizes main dimensions of the cargo tanks.

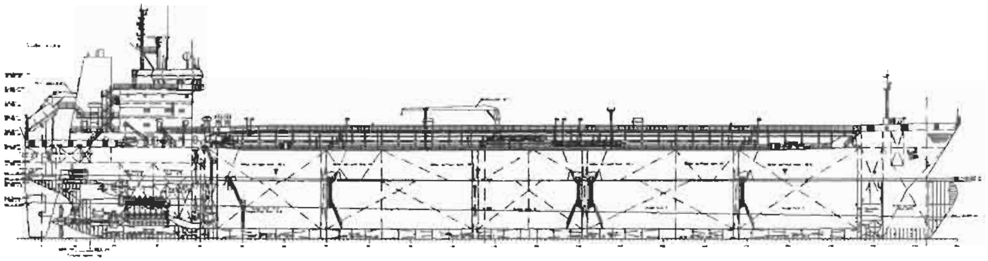

Figure 1: General arrangement of tanker SEATURBOT

TABLE 1

PRINCIPAL PARTICUALRS OF SAMPLE TANKER

Length PP [m] (L_{PP})	168.0
Breadth [m] (B)	28.0
Depth [m] (D)	16.8
Height of double bottom [m] (H_{DB})	1.9

	Ballast	Design
Draft [m] (T)	5.8	11.0
Vertical center of Gravity [m] (VCG)	8.2	11.1

TABLE 2

MAIN DIMENSIONS OF CARGO TANKS

	Tank 1	Tank 2	Tank 3	Tank 4	Tank 5
Max. length [m] (L_T)	22.3	27.6	19.6	27.6	19.6
Max. beam [m] (B_T)	10.8	11.4	11.4	11.4	11.4
Max. height [m] (H_T)	15.4	15.4	15.4	15.4	15.4
Distance from AP to geometric center [m]	132.24	103.44	82.64	56.32	33.04

3 SHIP MOTIONS

The linear seakeeping prediction method GLPANEL was used to compute ship motion characteristics in regular waves for two ship speeds and two drafts (Östergaard and Schellin, 1995). Response amplitude operators (RAO) for roll and pitch were computed for seven headings, ranging from head seas to following seas in 30 deg steps. For each combination of ship speed and draft and for each mode of motion, RAOs were plotted as a function of wave encounter period for all headings, see for example Fig. 2 (only two headings are plotted for clarity). The relevant range of ship motion periods was then determined according to the following 7-step procedure. We then selected the lowest and highest periods from all plots for the two ship speeds and for the two drafts. Table 3 summarizes the resulting lower and upper bounds of periods.

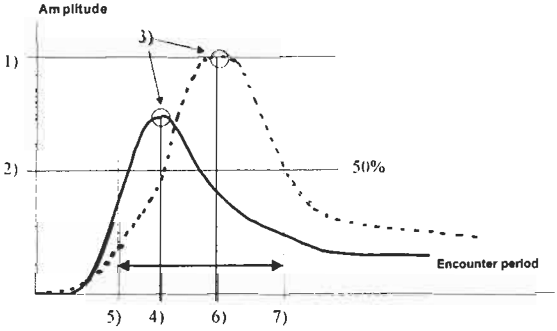

Figure 2: Determination of relevant range of ship motion periods

1. Find maximum value of all RAOs.
2. Take 50 percent of this highest value.
3. Identify all peaks above the 50 percent line.
4. Select peak with lowest period.
5. Determine lower bound of period range by subtracting 30 percent from the period selected in step 4.
6. Select peak with highest period.
7. Determine upper bound of period range by adding 30 percent to the period selected in step 6.

TABLE 3

RELEVANT RANGE OF PERIODS

	Roll period [s]	
	min-	max.
Ballast draft (GL)	8.5	16.3
Design draft (GL)	18.0	38.0

	Pitch period [s]	
	min.	max.
Ballast draft (GL)	5.0	26.9
Design draft (GL)	6.5	18.5

Life-time (maximum) motion amplitudes were required input for our sloshing simulations. We computed these amplitudes with a standard long-term statistical approach using the North-Atlantic wave climate and an exceedence probability of 10^{-8}. Resulting life-time motion amplitudes for heave ζ and pitch θ are summarized in Table 4 for both drafts and speeds. Increasing the draft as well as increasing the speed led to larger motion amplitudes. However, computations generally resulted in unrealistically large values. This was due to a lack of viscous motion damping in our linear seakeeping computations. Therefore, tank motion amplitudes as input for sloshing simulations were determined with approximate formulas given in (1). These approximate values are also listed in Table 4.

4 FLUID MOTIONS INSIDE TANKS

Natural period of fluid, T_F, in partially filled tanks was determined to check for possible resonance with ship motions. We applied a simple formula based on linear wave theory, eqn. (2), for fill heights h corresponding to fill ratios between 10 and 90 percent. All tanks were assumed to be rectangular for this part of the analysis, i.e., maximum dimensions given in Table 2 were used. Either tank beam B_T or tank length L_T were substituted for the free surface length L_F in (4), depending on the mode of motion.

$$\zeta = 7.2 - 0.012 L_{PP}\,, \quad \theta = Arc\tan(1.2\, D / L_{PP}) \qquad (1)$$

$$T_F = 2\pi / \sqrt{g \cdot \frac{\pi}{L_F} \cdot \tanh\left(\frac{h \cdot \pi}{L_F}\right)} \tag{2}$$

TABLE 4
LIFE-TIME SHIP MOTION AMPLITUDES

	Approximate formulas (1)	Long-term statistical values			
		ballast draft		design draft	
		1/3 V	V	1/3 V	V
Heave [m]	5.2	12.6	13.7	13.4	17.7
Pitch [deg]	6.8	14.7	16.9	17.8	17.8

Resulting fluid natural periods for various fill levels were compared with ship motion periods. As an example, we present in Fig. 3 the results for pitch motion. Fluid natural periods varied from 5 s to 12 s depending on fill level. The lower bound of the range of pitch motion (see Table 3) is shown as a dotted line. We accounted for different loading conditions and associated lower fill levels with ballast draft and higher fill levels with design draft conditions. All fill levels having periods larger than the lower bound were then identified as critical fill levels, which were analyzed by flow simulations. We identified 17 critical fill levels that had to be simulated for pitch motion. For tank 1, critical fill levels ranged from 10 to 50 percent; for tanks 2 and 4, from 10 to 80 percent; and for tanks 3 and 5, from 10 to 40 percent. Natural periods of fluid in the transverse direction were not in resonance with ship roll motion periods and, therefore, no sloshing simulations was required.

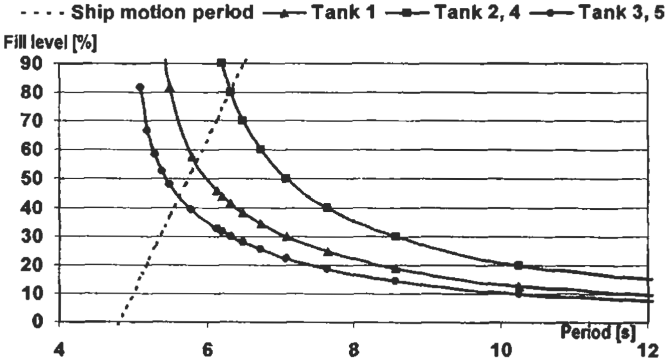

Figure 3: Natural period of fluid inside tanks compared with ship motion period

5 FLUID FLOW SIMULATIONS

Before starting simulations of fluid motion for critical fill levels, amplitude of tank excitation, center of rotation and the duration of the simulation had to be determined. We used the amplitudes given in Table 4 that were calculated with simple formulas. We assumed the center of rotation for all cases to be located amidships, and we fixed the vertical center of gravity to be the mean of the vertical center of gravity for ballast and design draft conditions, and we also accounted for the height of the double bottom. Duration of each simulation was fixed to 20 periods. The finite volume method *Comet* was used for all simulations (Comet, 1998). Discretization of the tanks was a compromise of accuracy and computational effort. Earlier tests indicated that cell sizes of 0.5 m (full scale) offered adequate accuracy. Time step size was then determined, taking into account a Courant criterion and a minimum temporal resolution as follows:

$$\Delta t = \min\left\{\frac{T_F}{100},\ C_{FL\max}\cdot\frac{\Delta Cell}{v_F}\right\} \tag{3}$$

where D_{Cell} is the minimum cell size, $v_F = 2L_F/T_F$ is a measure of the expected fluid velocity inside the tank, and $C_{Flmax} = 0.25$ is the maximum allowable Courant number for the numerical method we used. Cell numbers varied from 800 (2D grid) to 12000 (3D grid) with time step size ranging from 0.01 to 0.05 s, depending on fill level. To reduce data resulting from simulations and to account for typical panel size of ship structures, we subdivided each tank wall into ten segments (panels) and computed characteristic pressures for each panel by summing the pressures of all cells belonging to the particular segment and dividing by the corresponding area. This procedure required more time for preparing the model, but greatly reduced time for analysis of results. We focussed our analysis on tank walls. Panel 1 corresponded to a panel close to the tank bottom, and panel 10 was located close to the tank top.

To demonstrate effects of local pressure peaks versus averaged panel pressures, we compared results computed for tank 2 at a fill level of 20 percent. For panel 1, Fig. 4 compares time traces of panel pressure and point sensor pressure. Peak pressures for the point sensor were only minimally higher than for the panel. This was also observed for other panels and for other fill heights. On the other hand, three-dimensional effects were large in tank 1. This tank narrows towards the forward bulkhead (tank beam aft is about double tank beam forward). Figure 5 shows time traces of pressure at a fill level of 30 percent for panel 3, computed both two-dimensionally and three-dimensionally. Pressures were significantly larger when three-dimensional effects were considered. Fluid motion inside the tank differed for both cases. Figure 6 presents a comparison of the computed free surface for the 2D tank model and the 3D tank model of tank 1. Fluid touched the tank top only in the three-dimensional case. This behavior was caused by the narrowing of the tank beam. Only a three-dimensional model of the tank was able to account for this effect.

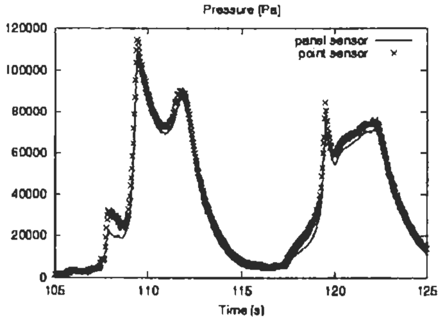

Figure 4: Computed time traces of pressure for a point sensor and for a panel.

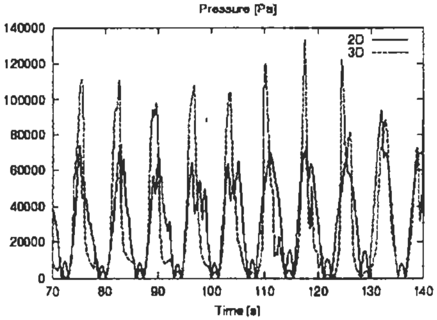

Figure 5: Comparison of time traces of 2D- and 3D-computed pressures.

To identify maximum pressures for each tank and for all fill levels, we extracted maximum pressures from each time trace, taking only the second half of simulations to eliminate transient effects. Resulting pressure peaks were plotted against the corresponding panel number for both bulkheads, the tank bottom and the tank top. In this way, so-called pressure envelopes were constructed. Figure 7 shows an example for the aft bulkhead of tank 2. Maximum pressures from eight fill levels are shown. In general, the highest fill level resulted in the largest pressures. However, highest pressures for panels 2 and 3 were recorded for a fill level of 30 percent, and for panel 10, a fill level of 40 percent resulted in the highest pressure. For tank 1 we recorded higher pressures than for tank 2 despite tank 1 being the smaller tank, see Fig. 8. Fluid motion was large and resulted in high pressures due to 3D effects and due to the tank's location near the bow. For a fill level of 30 percent, three-dimensionally computed pressures were larger than two-dimensionally computed pressures for panels 1, 2, 3, 4 and 5.

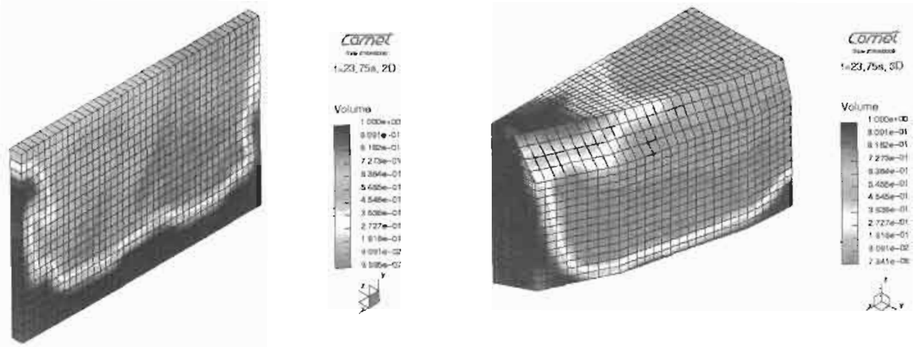
Comet
t=23.75s, 2D
Volume
1.000e+00
9.091e-01
8.182e-01
7.273e-01
6.364e-01
5.455e-01
4.545e-01
3.636e-01
2.727e-01
1.818e-01
9.091e-02
Comet
t=23.75s, 3D
Volume

Figure 6: Comparison of computed free surface deformations for 2D model (left) and 3D model (right).

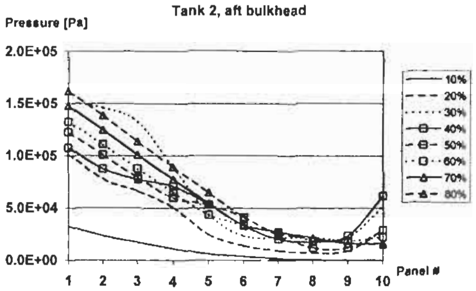

Figure 7: Comparison of computed max. pressures at aft bulkhead of tank 2 for various fill levels.

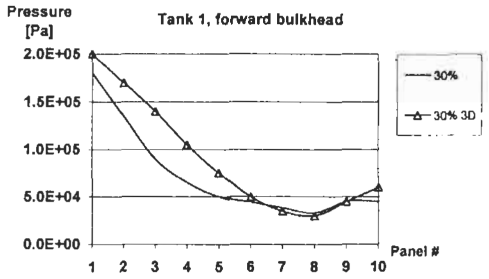

Figure 8: Comparison of 2D and 3D computed max. pressures at forward bulkhead of tank 1.

We compared computed maximum pressures with rule based design pressures (Germanischer Lloyd, 2000). Sample results for the forward bulkheads of tanks 1 and 2 are shown in Fig. 9. Computed maximum pressures display the same trend as rule based design pressures, and absolute levels were also comparable. However, computed maximum pressures were larger than rule based design pressures close to the tank bottom. This effect was caused by breaking wave impact at lower fill levels. On the other hand, computed pressures close to the tank top were smaller than rule based values.

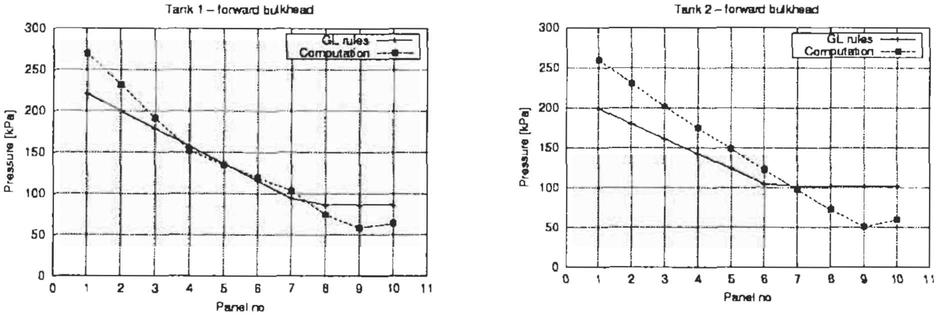

Figure 9: Comparison of computed maximum pressures with rule based design pressures.

6 SUMMARY AND CONCLUSIONS

This investigation is part of an ongoing effort to establish guidelines for the analysis on sloshing in partially filled tanks. We concentrated on a rational method to determine relevant ranges of ship motion periods and to identify critical fill levels. Sloshing simulations were performed for all these critical fill levels, and selected results were presented to illustrate the new approach. Computed pressures were spatially averaged to characterize pressures over ship structural panels. Maximum pressures were extracted from time traces and displayed for all fill levels to identify an envelope of maximum pressure. For the forward tank, three-dimensional computations were necessary to account for the narrowing beam of the tank. For this case, three-dimensionally computed pressures were twice as large a two-dimensionally computed pressures. In general, computed maximum pressures compared favorably with rule based design pressures. However, at the forward tank bulkhead and close to the tank bottom, computed pressures were larger than rule based pressures. Based on our investigations, we recommend to further study tank excitation scenarios to realistically account for motion amplitudes and superposition of relevant modes of ship motion. Also, a systematic investigation of other three-dimensional tank geometries is necessary to assess whether three-dimensional computations are required. In addition, at the tank top we need to reconsider our pressure predictions that were probably affected by fluid spray numerically dissipating into the air.

Acknowledgements

This work was partially supported by the Ministry of Education, Science, Research and Technology (BMBF) of the Federal Republic of Germany under contract MTK 0577 A. The opinions expressed herein are those of the authors. We thank LINDENAU shipyard in Kiel, Germany, for kind permission to use their tanker design as an example for this publication.

References

Cariou, A. and Casella, G. (1999): Liquid Sloshing in Ship Tanks: a Comparative Study of Numerical Simulation, Marine Structures, Vol. 12.
Comet (1998): User Manual, Version 1.03, ICCM GmbH, Hamburg, Germany.
Germanischer Lloyd (2000): Rules for Classification and Construction, I - Ship Technology, Part 1 - Seagoing Ships, Chapter 1 - Hull.
Kim, J.Y., Lee, K.J., Kang, J.M., Yum, D.J., Seol, Y.S., Rashed, S. and Kawahara, A. (1995): Simulation of 3D Sloshing and Structural Response in Ship's Tanks, Trans. SNAME, Vol. 103, pp. 321-342.
Muzaferija, S., Peric, M., Sames, P.C. and Schellin, T.E. (1998): A Two-Fluid Navier-Stokes Solver to Simulate Water Entry, 22nd Symp. on Naval Hydrodynamics, Washington, D.C.
Östergaard, C. and Schellin, T.E. (1995): Development of an Hydrodynamic Panel Method for Practical Analysis of Ships in a Seaway. Trans. STG, Vol. 89, pp. 147-156.
Park, Y.J., Choi, J.K., Kim, Y.S. and Bae, Y.S, (1995): A Practical Prediction Method of Sloshing Loads in Cargo Ship Tanks on Board Ships, 6th PRADS, Seoul, South-Korea.
Sames, P.C., Schellin, T.E., Muzaferija, S. and Peric, M. (1999): Application of a Two-Fluid Finite Volume Method to Ship Slamming, JOMAE, Vol. 121, pp. 47-52.
Sames, P.C., Marcouly, D. and Schellin, T.E. (2001): Sloshing in Rectangular and Cylindrical Tanks, submitted for publication in Journal of Ship Research.

Practical Design of Ships and Other Floating Structures
You-Sheng Wu, Wei-Cheng Cui and Guo-Jun Zhou (Eds)
© 2001 Elsevier Science Ltd. All rights reserved

PREDICTION OF HYDRODYNAMIC FORCES ACTING ON SHIP HULL IN OBLIQUE AND TURNING MOTIONS BY A SIMPLE SURFACE PANEL METHOD

K. Nakatake[1], T. Sekiguchi[2] and J. Ando[1]

[1]Department of Maritime Engineering, Kyushu University,
Hakozaki 6-10-1, Fukuoka, Japan 812-8581
[2]Kouyagi Yard, Mitsubishi Heavy Industries,
Kouyagichou 180, Nagasaki-ken, Japan 850-0310

ABSTRACT

We present a method to calculate the flow field around ship hull in oblique and turning motions, the pressure distributions and the hydrodynamic forces by a simple surface panel method called "SQCM". In this calculation we use the double model and a given shape of trailing vortex sheet. Calculated results are compared with experiments for ship hulls A, B and C, which were performed at SR-221 panel of Japan Ship Research Association. Both results agree fairly well and this simple method is useful for prediction of the hydrodynamic forces in maneuvering problem.

KEYWORDS

Hydrodynamic Forces, Turning Motion, Surface Panel Method, SR-221 Ship Models

1 INTRODUCTION

It is an important problem in the field of maneuverability to estimate the hydrodynamic forces acting on a ship hull in oblique and turning motions. As the theoretical estimation methods, the slender body theory to consider the separated vortices was adopted by Fuwa(1973), Nonaka(1992) and so on. But these methods did not take into consideration accurately the hull shapes and could not calculate the pressure distributions on the hull surface. Recently, Fujino et al (1995) calculated with very long computing time the flow field around ship hulls in maneuvering motion and hydrodynamic forces by CFD calculation using the Navier-Stokes equation taking into account the real hull shape. On the other hand, the panel method (for example, Matsui et al (1994)) based on the potential theory has a merit to be able to obtain with comparatively short computing time the forces acting on the hull.

Recently, we developed a simple surface panel method called SQCM (Source and QCM) (Nakatake et al (1994)) which could calculate easily the flow field around a thick wing and its characteristics, and could satisfy the Kutta condition without iteration even for 3-D wing. Then SQCM has been successfully applied to propeller problem (Ando et al (1995)) and so on.

In this paper, we attempt to apply SQCM to prediction of the hydrodynamic forces acting on the ship hull in oblique and turning motions, using a given shape of trailing vortex sheets. Calculations are performed for the three VLCC hulls (SR221-A, B, C) with different afterbody shapes. We show the usefulness of SQCM by comparing the experimental results with the calculated pressure distributions, the lateral force and the yawing moment acting on the hull.

2 FUNDAMENTAL EQUATIONS

We consider a ship hull (Length L, Breadth B, draft d, Block Coefficient C_b) turning steadily in still water at a constant velocity U with a drift angle β and at a constant angular velocity Ω and then we define the right-handed rectangular coordinate system o-xyz fixed in ship hull (see Figure 1).

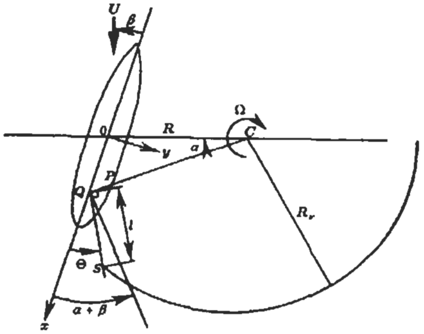

Figure 1 : Coordinate and trailing vortex model

Since the speed is assumed to be small, the free surface is dealt as a solid wall, that is, the flow field around the hull is represented by the double-body flow.

Then the following velocity $\vec{V}_o(u,v,w)$ is flowing on to a point $P(x,y,x)$ on the hull :

$$u = U\cos\beta - y\,\Omega, \quad v = U\sin\beta + x\,\Omega, \quad w = o \tag{1}$$

Denoting the turning radius by R and an angle between $\overline{oC}$ and $\overline{PC}$ in Figure 1 by α, there exist following relations :

$$\tan(\alpha+\beta) = u/v, \qquad R = U/\Omega \tag{2}$$

Since the hull is considered as a lifting body in oblique or turning motions, the hull should be followed by a straight or circular trailing vortex sheets according to the motion type. Matsui et al (1994) used a surface panel method of Morino's model to represent the hull, in which they tested several shapes of trailing vortex sheets.

In our case, we use a simple surface panel method "SQCM ", which was developed at Kyusyu Univ. and successfully applied to propeller problem. Since SQCM uses source distributions on the wing surface and discrete vortex distributions on the camber surface, in case of ship hull we distribute the sources on the hull surface and the vortices on the ship center plane. Then the trailing vortex should start from the keel line and the stern end. By referring Matsui et al's vortex model, we adopt the following given shape of the trailing vortex sheet (see Figure 1).

We assume that the trailing vortex starts from $Q(x,0,-d)$ on the keel with an angle Θ and proceeds on a straight line with length l and after the point S it flows on a circle with radius R_F. After some test calculations, we adopted following Θ and l.

$$\Theta = 0.25(\alpha + \beta), \qquad l = 0.2L \tag{3}$$

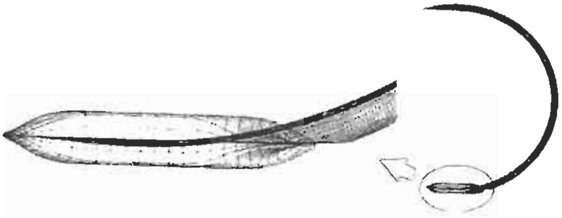

Figure 2 : Panel division and shape of trailing vortex sheet

Figure 2 shows an arrangement of trailing vortex sheet in case of steady turning. We represent the flow field around the hull in oblique or turning motions by SQCM. It uses source distributions on the hull and discrete vortices on the center plane, and we denote the inflow velocity, the velocity induced by the source distributions and the velocity induced by the vortex system by $\vec{V}_0$, $\vec{V}_S$ and $\vec{V}_V$, respectively. Then we have the total velocity $\vec{V}$ as

$$\vec{V} = \vec{V}_0 + \vec{V}_S + \vec{V}_V \tag{4}$$

The source and vortex distributions are determined by the boundary conditions on the hull surface and the center plane.

Defining the ambient static pressure and density by p_0 and δ, respectively, the pressure on the hull surface p and the corresponding pressure coefficient C_p can be expressed as follows.

$$p - p_0 = \frac{\rho}{2}(|\vec{V}_0|)^2 - |\vec{V}|^2 , \qquad C_p = \frac{p - p_o}{\frac{\rho}{2}|\vec{V}_o|^2} \tag{5}$$

Defining the x-, y- components of outward unit normal on the hull surface S by n_x and n_y, we can calculate the lateral force Y and the yawing moment with respect to midship N by the following equations :

$$Y = -\frac{\rho}{2}|\vec{V}|^2 \iint_S C_P \cdot n_y dS , \qquad N = -\frac{\rho}{2}|\vec{V}|^2 \iint_S C_P(n_x \cdot y - n_y \cdot x)dS \tag{6}$$

The nondimensional values Y', N' and Ω' are defined as

$$Y' = \frac{Y}{\frac{1}{2}\rho|V_o|^2 L \cdot d} , \quad N' = \frac{N}{\frac{1}{2}\rho|V_o|^2 L^2 \cdot d} , \quad \Omega' = \frac{\Omega \cdot L}{U} . \tag{7}$$

3 RESULTS AND COMPARISONS

We show in Table 1 the principal particulars of the three ship hulls adopted for calculation. SR221-A,

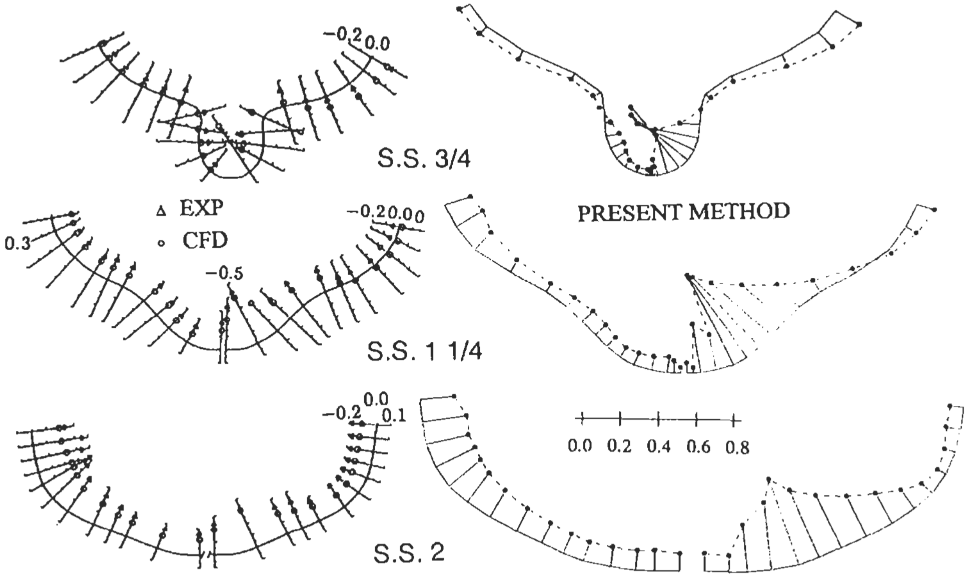

Figure 4 : Comparison of pressure distributions (Ship A)

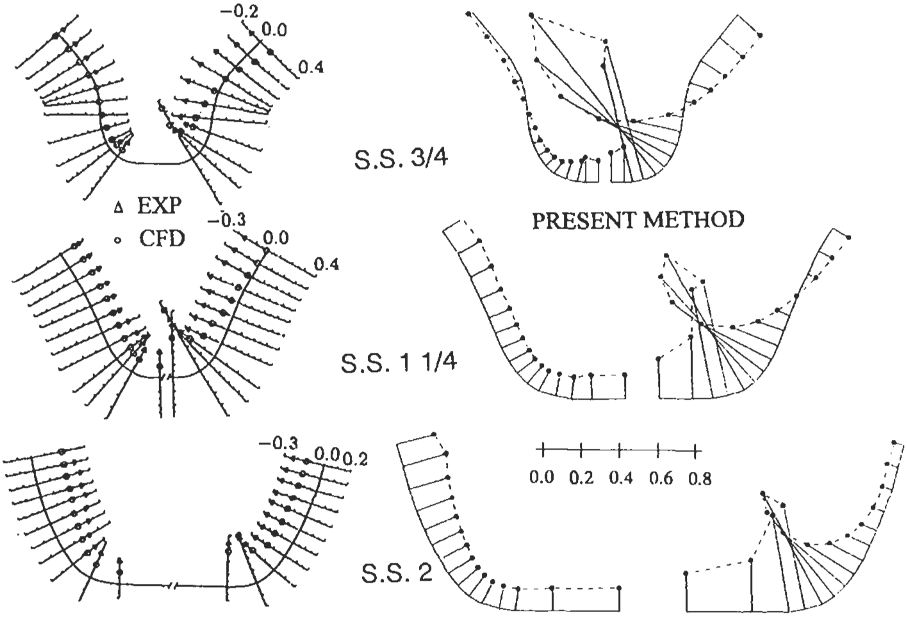

Figure 5 : Comparison of pressure distributions (Ship B)

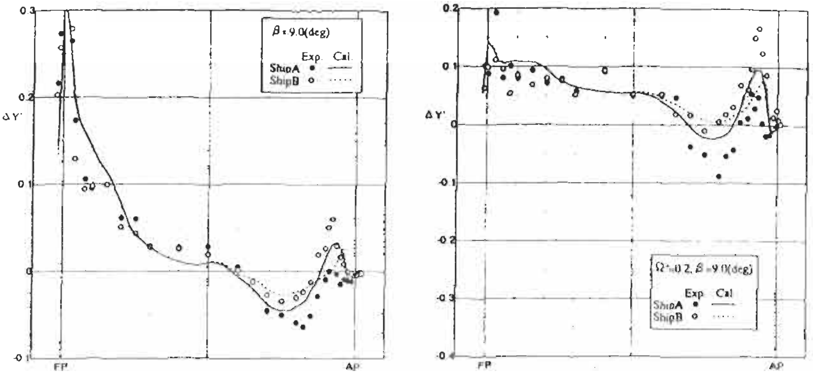

Figure 6 : Longitudinal distribution of lateral force in oblique and turning motions

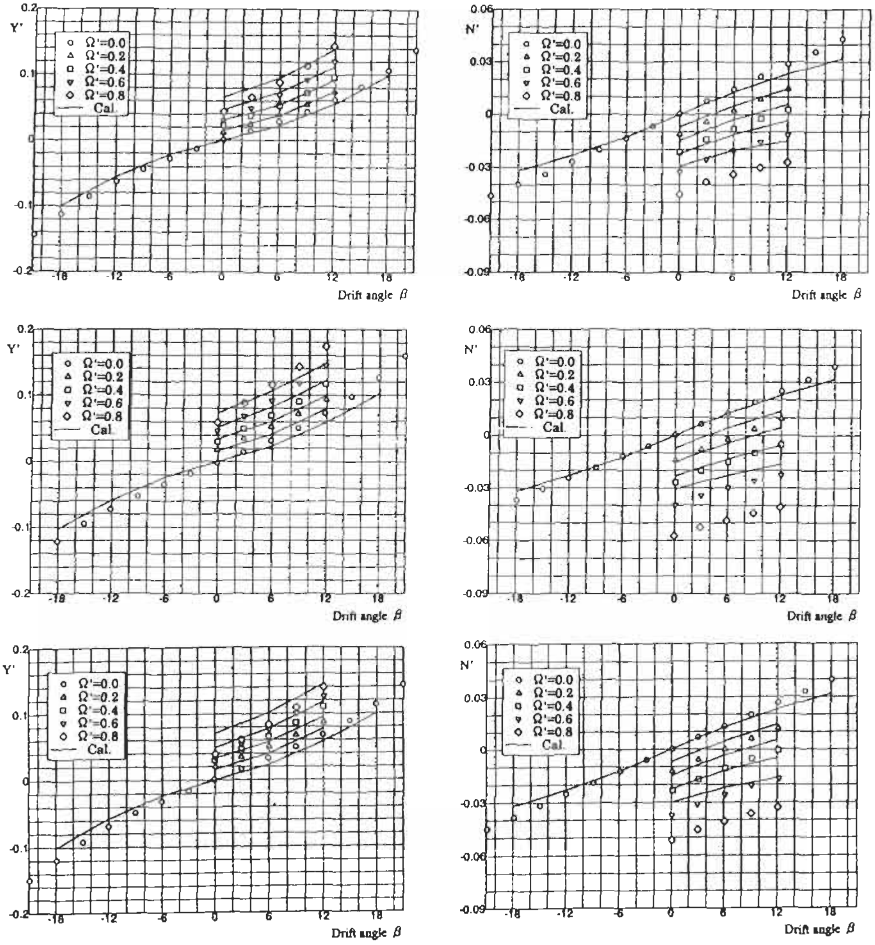

Figure 7 : Comparisons of hydrodynamic forces acting on ship hulls

TABLE 1
PRINCIPAL PARTICULARS OF SHIP HULLS

	SR221-A	SR221-B	SR221-C
L/B	5.520	5.520	5.520
B/d	3.005	3.005	3.005
$2d/L$	0.1205	0.1205	0.1205

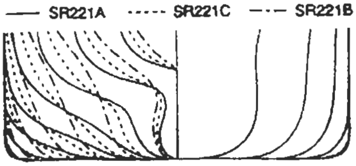

Figure 3 : Body plans of SR221-A,B,C hulls

B, C ship hulls (Japan Ship Research Association (1994~96)) have the same body plans in the forebody and the different body plans in the afterbody as shown in Figure 3. The shapes of frame lines of A, B and C hulls are V-type, U-type and intermediate type, respectively. In the calculation, we divide both sides of the hull surface into 30 divisions in the longitudinal direction and into 15 divisions in the girthwise direction and also divide the center plane into 120 divisions in the longitudinal direction and into 15 divisions in the draftwise direction corresponding to the surface division.

Figures 4 and 5 show pressure distributions at each square station for ship model A and B, respectively. The left side shows experiment (Δ) and CFD $\circ$) (Fujino et al (1995)) and the right side does present calculation. From these Figures, we understand that the three results agree fairly well except at S.S.3/4, where the separation effect is dominant. In the fore and central part of hulls, agreements are better. Figure 6 shows longitudinal distributions of lateral force $\Delta Y'$ in oblique motion at $\beta = 9$ (deg) and in turning motion in the case of $\Omega' = 0.2$ and $\beta = 9$ (deg) for A and B hulls. Calculated $\Delta Y'$ fairly agrees with experimental results. We can say calculated $\Delta Y'$ distribution is similar to experimental one and there appears difference between two hulls. Figure 7 shows comparisons of force coefficients Y', N' of A, B and C hulls for combinations of Ω' and β. The present method can predict fairly well the forces Y and N.

4 CONCLUSIONS

We applied a simple surface panel mothod "SQCM" to oblique towing and steady turning problems of full ship hulls with different afterbody. We confirmed that SQCM can predict the pressure distribution on the hull fairly well and is useful for predicting the lateral force and the yawing moment.

References

Ando J., Maita S., Nakatake K., (1995). A Simple Surface Panel Method to Predict Steady Marine Propeller Performance, *J. of Society of Naval Architects of Japan*, .**178**, 61-69.

Fujino M., Ohmori T., Usami S. and Eguchi S. and Miyata H. (1995). A Study of Flow Field around Full Ship Forms in Maneuvering Motion (2nd Report), *J. of Society of Naval Architect of Japan*, .**177**, 13-28.

Fuwa K. (1973). Hydrodynamic Forces Acting on a Ship in Oblique Towing, *J. of the Society of Naval Architects of Japan*, .**134**, 135-148.

Japan Ship Research Association (1995). A Study on Flow Field around Ship Hulls in Maneuvering Motion, SR-221 Panel, Report of First Year (1994), Report of Second Year.

Matsui S., Yang J., Tamashima M. and Yamazaki R. (1994). Calculation of Flow around a Hull in Turning Motion and Its Hydrodynamic Forces. *T. of the West-Japan Society of Naval Architects*, No.88, 57-72.

Nakatake K., Ando J., Kataoka K. and Yoshitake A. (1994). A Simple Calculation Method for Thick Wing, *T. of the West-Japan Society of Naval Architects*, .**88**, 13-21.

Nonaka K. (1992). Hydrodynamic Forces and Moments Acting on a Moving Body with Separating Thin Vortex Layers. *T. of the West-Japan Society of Naval Architects*, No.84, 131-142.

Practical Design of Ships and Other Floating Structures
You-Sheng Wu, Wei-Cheng Cui and Guo-Jun Zhou (Eds)
© 2001 Elsevier Science Ltd. All rights reserved

A NUMERICAL STUDY ON VISCOUS FLOW ABOUT A SHIP IN MANOEUVRING MOTION*

Xie-Dong Zhang and Xiu-Heng Wu
Wuhan University of Technology, Wuhan, 430063,China

ABSTRACT

In the present paper, the 3D RANS equations were solved on a three-dimensional hull body-fitted coordinate system by using the finite-analytic method and standard $\kappa - \varepsilon$ turbulent model with wall function, and a modilfied new SIMPLER algorithm is proposed as an equal-order pressure-velocity coupling scheme. The three-dimensional viscous flow around a Wigley ship model in oblique motion was computed. Part of the present calculation results is compared with the existing results obtained by experiments and those from other theoretical approaches.

KEYWORDS

Viscous flow, Numerical calculation, Finite-analytic method, Manoeuvring motion

1 INTRODUCTION

Accurate estimation of ship manoeuvrability is required since the IMO adopted the standard for ship manoeuvrability. The accuracy of estimated hydrodynamic forces influences directly the accuracy of the prediction of manoeuvrability. The research on theoretical calculation methods for calculating the hydrodynamic forces acting on ship has been very popular, such as slender body theory and low aspect-ratio wing theory. These sorts of methods are all potential flow theory methods in which the fluid is assumed to be ideal. But in practice, the flow around the ship is viscous flow. So more and more researchers in CFD make efforts on the study of viscous flow around ships.

In the past, the computation of viscous flow past a ship hull was made using mainly the classical boundary-layer equations. This approach has the limitation in the treatment of the viscous-inviscid interaction, especially in the stern region of a hull, where the displacement effect becomes significant. Its severest limitation is that it cannot handle seperation, where it simply breaks down and cannot be computed.

Recently the rapid development of computer hardwares has made large-scale computations feasible in engineering fields. At the same time the research numerical schemes, which take full advantage of the new computer hardwares, has developed to such an extent that the

---

* Supported by the National Natural Science Foundation of China (No:10072044 and No:19672045)

direct computation of the full Navier-Stokes equations has now become a target in the foreseeable future.

Several attempts have been reported, where the computation of the full Navier-Stokes equations has been made. H.Miyata[2], T.Ohmori[3][4], M.Fujino[5]are some researchers on the field. They employed numerical solution method for the Navier-Stokes equations based on the finite-volume approach and studied the viscous flow field around ships.

This paper concerns a numerical method for the solution of complete Reynolds-Adveraged Navier-Stokes equations for three-dimensional flow by using the finite-analytic method and standard κ - ε turbulent model with wall function. The finite-analytic method with the characteristics of natural upwind is employed to solve the Reynolds-averaged Navier-Stokes equations and the κ - ε equation. Under the unstaggered grids, the continuuity equation is replaced with the elliptic different one of the pressure, which is derived by the finite-analytic method, and a modilfied new SIMPLER algorithm is proposed to be used as an equal-order pressure-velocity coupling scheme. A simple procedure is applied to determine the cell-face velocity independent of the under-relaxation factor used in solving the momentum equations. Using the computational model and numerical method, the three-dimensional viscous flow past a Wigley ship model in oblique motion was computed. Part of the present calculation results is compared with the existing results obtained by experiments and those from other theoretical approaches, and they have shown good agreement.

2 COMPUTION METHOD

2.1 Grid Generation

Since the body-fitted coordinate system in the numerical solution of viscous flow has a considerable influence on the results, the grid generation plays an important role in the calculation method. Here, the numerical grid is generated by solving a set of poisson equations.

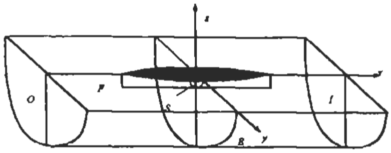

Figure 1: Calculation Domain

The numerical solution of the flow equations is obtained in the computational domain, shown in Fig.1. To generate the body-fitted coordinate system, a two-step Procedure is employed. First, a set of interior node points is obtained by interpolation between points on the boundaries. Then, this approximate grid is smoothed by solving elliptic differential equations in the unknown coordinates x_j.

$$\nabla^2 \xi^i = f^i \qquad (i=1,2,3) \tag{1}$$

where: $\nabla^2 = \frac{1}{h_1 h_2 h_3} \sum_{j=1}^{3} \frac{\partial}{\partial x_j}\left(\frac{h_1 h_2 h_3}{h_j^2} \frac{\partial}{\partial x_j}\right)$; f^i are the control function of the distribution of points in the grid. The moving boundary condition, arc-length inters transformation and linear interpolation method is used to control the density of the grids near the surface of the ship hull and within the computational domain. In this way, the grid points may be clustered in regions where large gradients of flow paramenters are expected, see Fig.2.

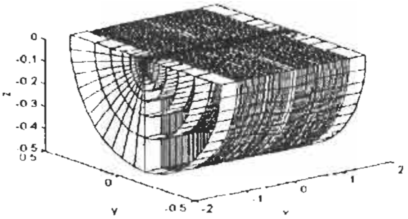

Figure 2: Grid around the Wigley hull

2.2 Governing Equations

The flow equations solved in the present method are the Reynolds-Averaged Navier-Stokes (RANS) equations. They are obtained from the full Navier-Stokes equations by averaging over the largest turbulence scales occuring in the flow. The RANS equations for three-dimensional incompressible flow can be written in Cartesian tensor notation as

$$\frac{\partial (U_i U_j)}{\partial x_j} = -\frac{1}{\rho}\frac{\partial P}{\partial x_i} + \frac{\partial}{\partial x_j}\left[\nu\left(\frac{\partial U_i}{\partial x_j} + \frac{\partial U_j}{\partial x_i}\right)\right] - \frac{\partial (\overline{u_i' u_j'})}{\partial x_j} \tag{2}$$

$$\frac{\partial U_i}{\partial x_i} = 0 \tag{3}$$

where $\overline{u_i' u_j'}$ are the Reynolds stress.

$$\overline{u_i' u_j'} = -\nu_t\left(\frac{\partial U_i}{\partial x_j} + \frac{\partial U_j}{\partial x_i}\right) + \frac{2}{3}\delta_{ij} k \tag{4}$$

where ν_t is the eddy viscosity, its distribution is given by

$$\nu_t = c_\mu \frac{k^2}{\varepsilon} \tag{5}$$

where k is the kinetic energy of the turblence and ε is its rate of dissipation. k and ε are obtained from the transport equations

$$\frac{\partial (k U_j)}{\partial x_j} = \frac{\partial}{\partial x_j}\left[\left(\nu + \frac{\nu_t}{\sigma_k}\right)\frac{\partial k}{\partial x_j}\right] + P_k - \varepsilon \tag{6}$$

$$\frac{\partial (\varepsilon U_j)}{\partial x_j} = \frac{\partial}{\partial x_j}\left[\left(\nu + \frac{\nu_t}{\sigma_\varepsilon}\right)\frac{\partial k}{\partial x_j}\right] + c_{\varepsilon 1} P_k \frac{\varepsilon}{k} - c_{\varepsilon 2}\frac{\varepsilon^2}{k} \tag{7}$$

where σ_k 、σ_ε 、$c_{\varepsilon 1}$ 、$c_{\varepsilon 2}$ are the empirical constants.

2.3 Boundary Condations

Consider a ship fixed in the uniform onset flow U. The calculation domain is shown in Fig.1 The boundary conditions on each of the boundaries are described in the following.

(1) On the inlet plane (I):

$$u = U\cos\alpha,\quad v = U\sin\alpha,\quad w = 0,\quad p = 0 \tag{8}$$

(2) On the exit plane (O):

$$\frac{\partial Q}{\partial \xi} = 0,\quad (\,where\quad Q = u, v, w, p, k, \varepsilon\,) \tag{9}$$

(3) On the free surface (F):

$$w = 0,\ \frac{\partial Q}{\partial n} = 0,\quad (\,where\quad Q = u, v, p, k, \varepsilon\,) \tag{10}$$

(4) On the outer boundary (E):

$$u = 1,\ w = p = 0,\ \frac{\partial k}{\partial \eta} = \frac{\partial \varepsilon}{\partial \eta} = 0 \tag{11}$$

(5) On the ship body surface (S):

A two-point wall-function approach is used to give the boundary condition for *u*, *v*, *w*, *k*, and ε.

3 NUMERICAL METHOD

The governing equations (2),(6) and (7) can be written in the form

$$Q_{\eta\eta} + CQ_{\zeta\zeta} - 2AQ_{\eta} - 2BCQ_{\zeta} = g \qquad (12)$$

where $Q = u, v, w, p, k, \varepsilon$. The transport equation (12) can be discretized by the finite analytic scheme. Evaluation of the analytic solutions at the interior node then provides a eight-point discretization formula of the form of

$$Q_P = \sum_{n=1}^{8} C_n Q_n + C_p g \qquad (13)$$

Under the unstaggered grids, the continuous equation is replaced with the elliptic different one of the pressure, which is also derived by the finite-analytic method, and a modilfied new SIMPLER algorithm is proposed to be used as an equal-order pressure-velocity coupling scheme. A simple procedure is applied to determine the cell-face velocity independent of the under-relaxation factor used in solving the equations.

4 CALCULATION RESULTS

Using the above computational model and numerical method, the three-dimensional viscous flow around a Wigley hull in oblique motion was computed. Some results are presented and discussed. In the presentation of the results, variables are non-dimensionalized using the ship length L, the free-stream speed U and fluid density ρ. The computational conditions are tabulated in Table 1.

After the pressure distributed on the ship body surface is determined, the sway forces Y and yaw moment N can be calculated. Therefor the nondimensional sway force coefficient C_Y and yaw moment coefficient C_N can be expressed as

$$C_Y = Y\Big/\left(\frac{1}{2}\rho U^2 L d\right) \qquad (14)$$

$$C_N = N\Big/\left(\frac{1}{2}\rho U^2 L^2 d\right) \qquad (15)$$

TABLE 1

COMPUTATIONAL CONDITIONS

Ship model	Wigley model
Ship dimensions	L=1.0, B=0.06, D=0.05
Computational domain	2.0×1.0×0.5
Reynolds number	1.0×10^{6}
Grid points	20625 （55×15×25 ）
Minimum spacing of grid	1.0×10^{-3}
Drift angle	5° 、9° 、12°
Time increment	1.0×10^{-3}

Fig.3~Fig.5 show the crossplane-velocity vectors (v-w) for several representative sections when the ship moves obliquely with the angle $\alpha=5^0$、$\alpha=9^0$ and $\alpha=12^0$.

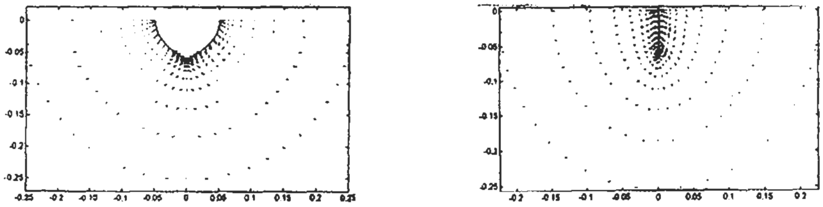

Figure3: Crossplane-velocity vectors ($\alpha=5^0$ x=0 and x=0.75)

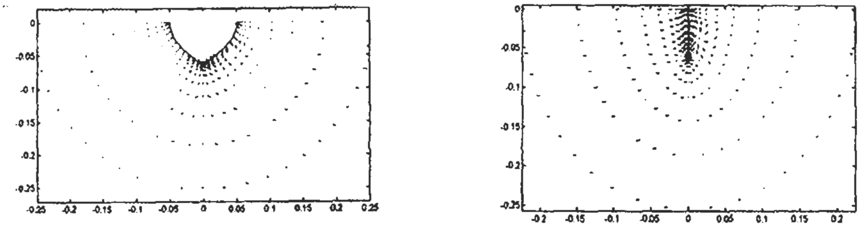

Figure 4: Crossplane-velocity vectors ($\alpha=9^0$ x=0 and x=0.75)

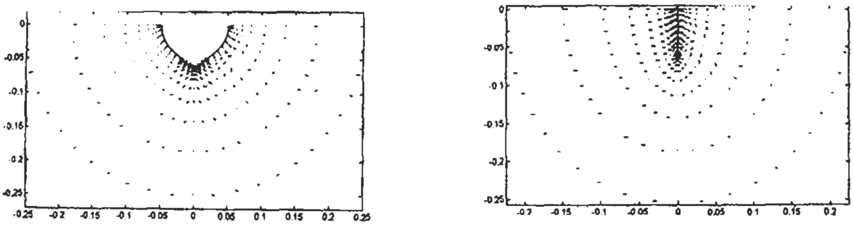

Figure 5: Crossplane-velocity vectors ($\alpha=12^0$ x=0 and x=0.75)

Fig.6~Fig.7 show the nondimensional sway force coefficient C_Y and yaw moment coefficient C_N varied with the different drift angle. The present calculation results are compared with the existing results obtained by experiments[1].

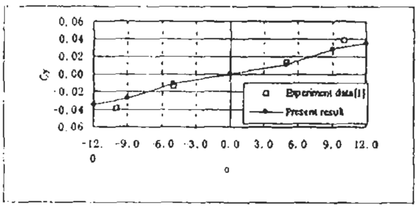

Figure 6: C_Y varied with α

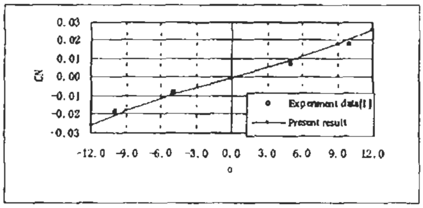

Figure 7: C_N varied with α

5 CONCLUSIONS

A partially parabolic numerical method has been applied to the computation of three-dimensional viscous flow around a Wigley ship model with the drift angle. The method uses a numerically generated body-fitted coordinate system. In general, using this method can reasonably capture the essential feature for the velocity field. From the comparition with the experimental results and other computational results [3][4], the crossplane-velocity vectors (v-w) for several representative sections calculated here have the same tendency. And the present calculational results of the nondimensional sway force coefficient C_Y and yaw moment coefficient C_N have good agreement with the existing results obtained by experiments [1].

Athough the calculation method used here is a useful one for the calculation of the three-dimensional viscous flow past obliquing ship hull, the accuracy of prediction should be improved. Further examinations are necessary for governing equation, grid dependence, numerical method, treatment of boundary condition and so forth.

References

1. K.Nakatake, A.Komura, J.Andu and K.Kataoka. (1990). On the Flow Field and The Hydrodynamic Forces of an Obliquing Ship. *Trans. The West-Japan Soc.Naval Archit* **80**
2. H.Miyata. (1996). Time-Marching CFD Simulation for Moving Boundary Problems. *21st Symposium on Naval Hydrodynamics*, Norway
3. T.Ohmori and H.Miyata. (1993). Oblique Tow Simulation by a Finite-Volume Method. *Journal of the Society of Naval Architects of Japan* **173**
4. T.Ohmori, M.Fujino, H.Miyata and K.Makoto. (1994). A Study on Flow Field Around Full Ship Forms in Maneuvering Motion (1st Report: In Oplique Tow) *Journal of the Society of Naval Architects of Japan* **176**
5. M.Fujino, T.Ohmori, S.Usami, S.Eguchi, and H.Miyata. (1995). A Study on Flow Field Around Full Ship Forms in Maneuvering Motion (2nd Report: Hydrodynamic Forces and Pressure Distribution on Ship's Hull in Steady Turning Condition). *Journal of the Society of Naval Architects of Japan* **177**
6. X.D Zhang. (1999). A Numerical Study on Viscous Problems of Three-dimensional Ship Hull in Manoeuvring Motion. Ph.D. *Thesis of Wuhan Transportation University*, P.R.China
7. L.Xu. (1994). A Numerical Method for Solving 3-D RANS Equations and Modelling the Viscous Flow around the Stern and in the Wake of Ship. *Ph.D. Thesis of Wuhan Transportation University*, P.R.China

Practical Design of Ships and Other Floating Structures
You-Sheng Wu, Wei-Cheng Cui and Guo-Jun Zhou (Eds)

© 2001 Elsevier Science Ltd. All rights reserved

SIMULATION OF THE PROPULSION SYSTEM BEHAVIOUR DURING SHIP STANDARD MANOEUVRES

G. Benvenuto, S. Brizzolara, M. Figari

Dipartimento di Ingegneria Navale e Tecnlogie Marine, University of Genoa,
Genova, Via Montallegro 1, 16145, Italy

ABSTRACT

The paper presents a comprehensive approach to simulate the propulsion system behaviour during ship manoeuvres. The behaviour of the ship systems is simulated by means of a dynamic simulation model that was already validated for the performance prediction of ship propulsion plants with the ship travelling in straight line. Now the dynamic model has been extended to consider the ship manoeuvrability in the horizontal plane.

In order to analyse the different manoeuvres of a ship, the simulation model has been applied to a propulsion system consisting of a twin shaft arrangement with controllable pitch propellers, driven, through reduction gears, by turbocharged medium speed diesel engines.

The accuracy of the simulation procedure is illustrated in the paper through comparison with full scale results for different manoeuvres such as turning circle, zig zag and spiral.

KEYWORDS

Simulation, Propulsion plant, Manoeuvre.

1 INTRODUCTION

The manoeuvring ability of a ship is of great importance from both a technical and an operational point of view. The stopping distance, the turning diameter, are of great interest to ship owners and operators as well as to port and state authorities; these quantities define the manoeuvring ability of a ship that has to comply with the IMO standards for manoeuvrability.

According to the principles assumed by IMO, in order to demonstrate compliance with these standards "scale model tests and/or computer predictions using mathematical models" can be used at the design stage. The ship should then be considered to meet these standards regardless of full-scale trials results. These last trials should be conducted only to validate the mathematical models.

In this context it appears very clear the usefulness of developing mathematical models or simulation tools able to predict the manoeuvring capability of a ship. Indeed, these methods allow to greatly reduce the necessity of conducting costly and time consuming full-scale trials. In the case of a crash stop manoeuvre, for instance, it would be possible to perform the sea-trials starting from a reduced ship speed, while the computer simulation could evaluate the full speed manoeuvre.

The manoeuvring ability of a ship is influenced by parameters of different nature such as those related to her hydrodynamic properties (hull resistance and propulsion coefficients in steady state, added mass and damping coefficients for the motions, rudder and propeller forces, etc.) and those related to her propulsion plant characteristics (like as engine type, governor type, propulsor typology type, etc).

For example the process of stopping a ship is governed by the following key factors: kinetic energy of the travelling ship, kinetic energy of the rotating masses (engines, shaft lines, propulsors), resistance of the hull and of the propulsion unit, reverse thrust produced by the propulsive apparatus, time required by the propulsion control system to modify the thrust.

This paper presents a comprehensive approach to simulate the overall behaviour of the ship and her propulsion system during manoeuvres. The behaviour of the ship systems is simulated by means of a dynamic simulation model, which was already validated for the performance prediction of ship propulsion plants with the ship travelling in straight line, Benvenuto et al. (2000). Now the dynamic model has been extended to consider the ship manoeuvrability in the horizontal plane, Brizzolara (2001).

For each element of the propulsion plant (i.e. engine, governor, propeller, etc.) a library of blocks is already available, representing the elements with different degrees of accuracy (from the highest with emissions predictions to the simplest considering the main dynamic only). To implement the manoeuvre capability, a set of other blocks has been developed and integrated into the main simulator. The ship block with motion responses in 3 degrees of freedom (surge, sway, yaw) and the rudder block have been developed for single screw ships and twin screw ships as well. So, it is possible to use the most suitable blocks for the different application and requested results.

In order to analyse the different manoeuvres of a ship, the simulation model has been applied to a propulsion system consisting of a twin shaft arrangement with controllable pitch propellers, driven, through reduction gears, by turbo charged medium speed diesel engines.

The accuracy of the simulation procedure is illustrated in the paper through the comparison with full scale results of different manoeuvres such as turning circle, zig zag and spiral.

2 SHIP PROPULSION SYSTEM MODEL

The model, developed in a MATLAB®-SIMULINK® environment, represents the various elements of the propulsion system: diesel engine, shaftline, gear, propeller, hull, rudder.

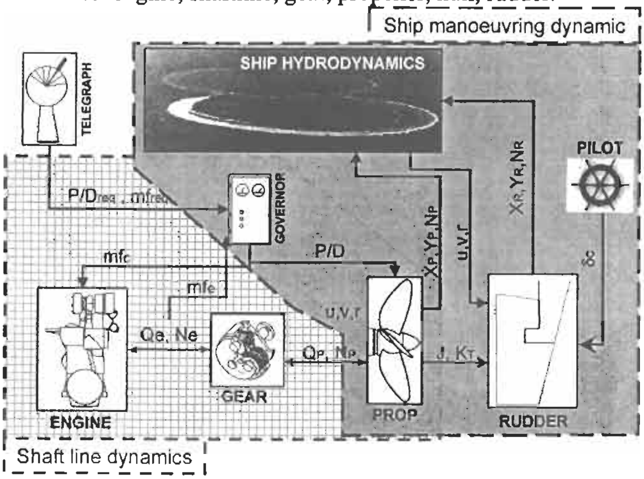

Figure 1: Ship propulsion model functional scheme

The blocks representing the elements are linked together in a proper way, in which the functional relationship between input and output variables are described in terms of tables, functions and differential or algebraic equations.

The modelled propulsion plant consists of a twin shaft arrangement with controllable pitch propellers, driven, through reduction gears, by turbo-charged medium speed diesel engines.

The main elements of the propulsion plant, modelled as separated blocks, are the diesel engine, the governor, the hull, the controllable pitch propeller, the telegraph, and the shaft line. An illustration of the model functional scheme is shown in figure 1.

The mathematical model for the simulation of the dynamics of the propulsion system has already been presented in Benvenuto et al. (2000, 1998, 1994). Here only the new manoeuvring equations are reported.

2.1 Manoeuvring Model

Manoeuvrability mathematical model describes the non linear rigid body dynamics in the horizontal plane. So Newton law for the surge, sway and heave motions are solved in the dynamic model. The equations of motions in a non-inertial right-handed referenced system moving with the ship with the origin at midship and the longitudinal x-axis directed toward the bow, becomes:

$$\begin{cases} m\left(\dot{u} - vr - x_G r^2\right) = X_{\dot{u}}\dot{u} + T(1-t) - R(u) + \left(X_{vr} - Y_{\dot{v}}\right)vr + X_{rr}r^2 + X_R \\ m\left(\dot{v} - ur + x_G\dot{r}\right) = Y_{\dot{r}}\dot{r} + Y_{\dot{v}}\dot{v} + Y_v v + \frac{U}{|U|}Y_{ur}ur + Y_{v|v|}v|v| + \frac{U}{|U|}Y_{r|r|}r|r| + Y_{v|r|}v|r| + Y_R + Y_P \\ I_z\dot{r} + mx_G\left(\dot{v} + ru\right) = N_{\dot{v}}\dot{v} + N_{\dot{r}}\dot{r} + +N_{uv}uv + N_{ur}ur + N_{r|r|}r|r| + N_{rrv}rrv + N_{vvr}vvr + N_P + N_R \end{cases} \qquad (1)$$

where $u, v, r, \dot{u}, \dot{v}, \dot{r}$ are the surge, sway and yaw velocity and acceleration. Roll has not yet been included in the model. Various expression for the non linear right hand side forces and moments can be utilised and a certain number is included in the manoeuvring simulation program (Brizzolara, 2001). The resistance R(u) and the self propulsion coefficients (1-t), (1-w) can be estimated from Holtrop method, if no towing tank tests results are available.

The propeller longitudinal thrust X_P at different pitch and advance ratio has been evaluated by means of the systematic series of Yazaki, opportunely calibrated on the known propeller K_T and K_Q curves at the design pitch.

The mathematical model built in the manoeuvring simulator can use a wide set of non-linear coefficients up to the fifth order when these are known from model tests, that would appear in the right hand sides of eq. (1).

If no experimental derivatives are available, (as for the presented application case) a simple formulation of hull hydrodynamic forces is adopted, like the one used by Wilson and Lewis (1986) that is reported in eq. (1). These equations employ a limited number of non linear terms that can be deduced from published regression formulae. In particular, for the application case presented in the paper, the hydrodynamic derivatives were estimated from the regression formulae proposed by Inoue (1981), while added mass by the regressions proposed by Clark (1983).

The rudder lift and drag forces are usually estimated by simple analytical formulas as function of the aspect ratio and effective angle of attack or other formulas like Whicker and Felner (1958). In the presented application the forces were estimated on the basis of the systematic series of Kerwin et Al. (1972), since the two rudders in the propellers wake were of the flapped type.

The effect of propeller free stream on the rudders and the actual rudder angle of attack as proposed by Ogawa and Kasai (1978) were included in the model. Transversal force of the propeller in inclined flow was estimated by simple axial momentum theory, based on the actual propeller longitudinal thrust coefficient.

The mathematical model has been set up using Simulink®, a dynamic-system oriented toolbox for Matlab®. The differential equation of the ship and shaft lines dynamics are easily solved using a fifth order Runge-Kutta scheme with automatic time step refinement, which grants acceptable calculation times and minimal constant errors on the solution, being well suited for non stiff system like manoeuvring ships.

3 MODEL VALIDATION AND RESULTS

The model has been tested by the simulation of a passenger-car ferry whose main characteristics are reported in Table 1.

TABLE 1

MAIN CHARACTERISTICS OF THE SHIP USED FOR SIMULATIONS

L	176 m	P_b	7240x4 kW
B	28 m	Car	1000
T	6.6 m	Passenger	2250
Speed	24 kn	Trailers	2000 m

The steady state validation has been obtained comparing the simulation results with sea trials data supplied by the ship owner and by the engine manufacturer.
To validate the model in transient conditions the authors have recently performed a campaign of measurements during the normal ship service.

3.1 Coasting Manoeuvre Simulation

The authors have performed a campaign of measurements during last winter in order to collect data for the validation of the model during transient operational conditions of the ship.

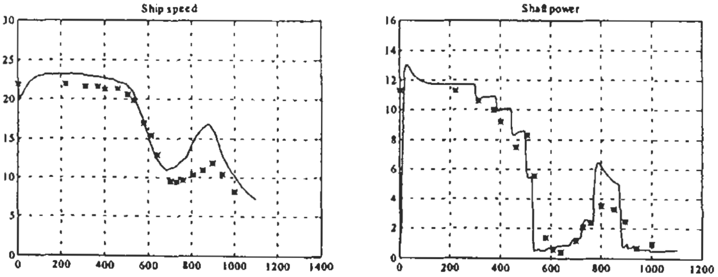

Figure 2: Coasting manoeuvre comparison

For typical manoeuvring situations (i.e. approaching and leaving the port) data have been recorded and compared with the corresponding simulation results.
Figure 2 shows the time histories of some of the recorded parameters, ship speed, shaft power, during a coasting manoeuvre (dots). Simulation results (continuous lines) are superimposed for the sake of comparison. A good agreement is noticed for all of the considered parameters.

3.2 Crash Stop Simulation

In order to verify, for this kind of ship, the possibility of applying the developed simulation code to the prediction of the manoeuvring performance, as required by the IMO standards, the crash-stop manoeuvre has been simulated and the time dependent behaviour of some important variables is reported below.

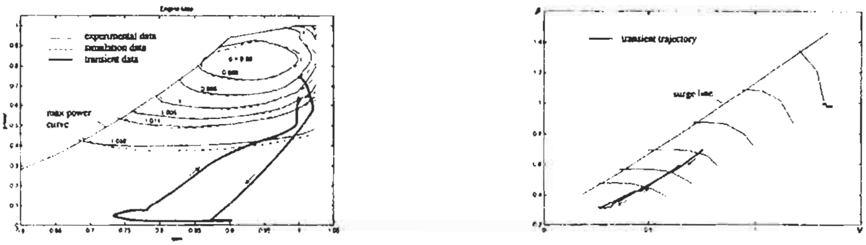

Figure 3: Engine and compressor maps

In figure 3, the calculated transient trajectory of the engine working point during the crash stop manoeuvre is plotted on the engine map. As it may be observed, the engine working trajectory remains on the correct operational area during the entire manoeuvre. Similarly, figure 3 shows, for the same manoeuvre, the working point transient trajectory on the compressor map. Also in this case, a turbocharger good dynamic performance is visualised.

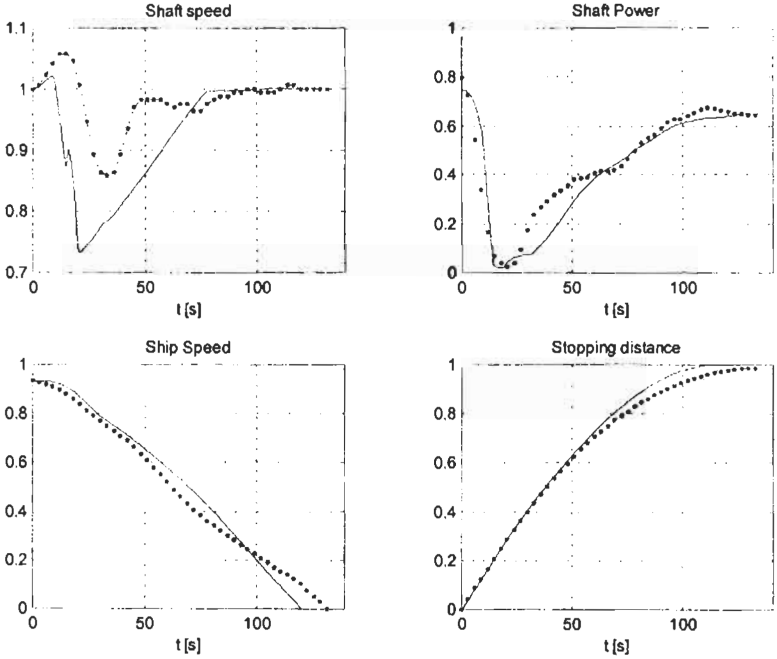

Figure 4: Crash stop comparison

Figures 4 shows the comparison between available data from full scale trials and simulation results. All of the variables show good agreement except the shaft speed that shows a correct behaviour but slightly different values.

3.3 Turning Circle and Zig-zag Manoeuvres

The standard manoeuvres requested by classification societies for obtaining the class were performed in full scale and results were made available by the owner. The more significant manoeuvres, such as turning circle and zig-zag, were also simulated with the mathematical model mentioned in the previous paragraph and in Brizzolara (2001).

A comparison of the main manoeuvring parameters between sea trial measurements and simulation results are presented in Table 2.

The behaviour of the ship in full scale is highly non-linear, nevertheless, the simulated manoeuvres show a very good agreement with full scale values. The simulation predicts sufficiently well the very short turning diameter and the ship response in the zig-zag manoeuvres, as from the comparison presented in Table 1.

TABLE 2

MAIN SIMULATED MANOEUVRES. FULL SCALE RESULTS (PLAIN) VERSUS SIMULATED (BOLD)

Manoeuvre	Init. Speed	Rudder	Advance	Transfer	Tactical Diam.	Final Diam.
	[knots]		[m]	[m]	[m]	[m]
Turning Circle	21.6	35 deg sb	453	118	303	243
Turning Circle	21.6	35 deg ps	434	145	334	265
Simulated Turning Circle	***21.6***	***35 deg***	***470***	***140***	***300***	***210***
Manoeuvre	**Init. Speed**	**Rudder**	**Period**	**1st Overshoot Angle - Time**	**2nd Overshoot Angle - Time**	**3rd Overshoot Angle - Time**
	[knots]		[s]	[deg] - [s]	[deg] - [s]	[deg] - [s]
Zig-Zag 10-10	21.6	10 deg ps	132	14.5 – 20.0	-16.0 – 20.0	24.8 – 28.0
Zig-Zag 10-10	***21.6***	***10 deg***	***135***	***10.0 – 18.0***	***-14.0 – 20.0***	***14.0 - 24.0***

The simulated trajectory for the turning circle and the overshoot angles and times of the zig zag manoeuvres, are plotted in figure 5.

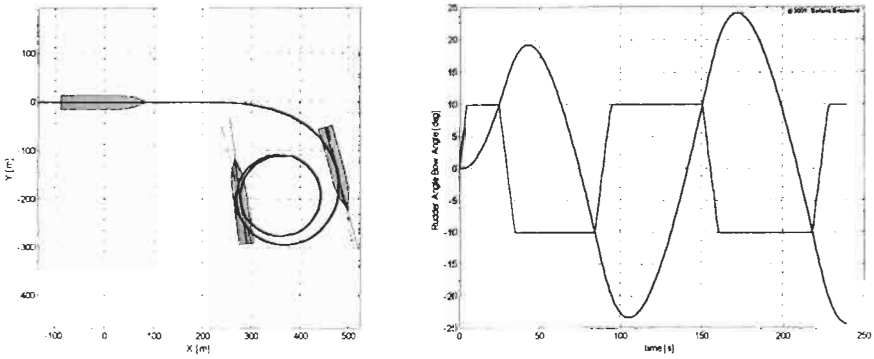

Figure 5: Simulation results
Turning circle at 22 knots, 35 degree rudder angle and Zig-Zag 10-10

During both the manoeuvres, the effect of the automation system that controls the propeller pitch, to maintain the selected rpm of the engine, without overcharging the engine, has been correctly simulated as shown in Figure 6.

In the figure, the time histories of pitch, rpm and propeller torque during the turning circle manoeuvre are presented.

In general, thus, the ship manoeuvring ability predicted with the presented model shows a very good agreement for all the simulated standard manoeuvres; only the unstable behaviour shown by the ship in the zig-zag manoeuvre in the third overshoot angle couldn't be captured by the mathematical model.

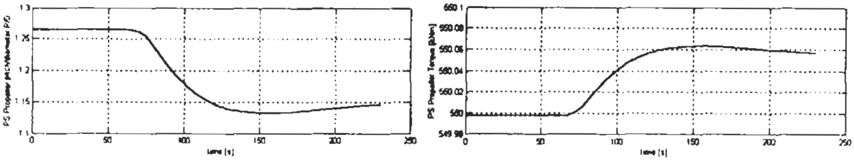

Figure 6: Propeller pitch and torque time histories
during the turning circle manoeuvre with 35 deg rudder

4 CONCLUDING REMARKS

The application of simulation techniques to marine propulsion systems represents a research field developed at the University of Genoa for some years.

We believe that our approach to the performance prediction of a ship in transient conditions can give useful results for what concerns :

- the compliance to IMO manoeuvrability standards avoiding critical sea trials;
- the optimisation of the dynamic behaviour of the ship propulsion system (choice of a suitable pitch/r.p.m. combination law, engine governor calibration, dimensioning of the shaft lines);
- the prevention of engine and other mechanical components overloads during the ship typical manoeuvres.

References

Benvenuto G., Carrera G., Rizzuto E., (1994). Dynamic Simulation of Marine Propulsion Plants. *NAV 94*, Rome, 1994.

Benvenuto G., Campora U., Carrera G., Casoli P., (1998). A Two-Zone Diesel Engine Model for the Simulation of Marine Propulsion Plant Transients. *MARIND 98, Second International Conference on Marine Industry*. Varna, Bulgaria, September 28 – October 2, 1998.

Benvenuto G., Campora U., Carrera G., Figari M., (2000). Ship Stopping Manoeuvre: Simulation of the Propulsion System Behaviour. *NAV 2000*. Venice. Italy.

Brizzolara S., (2001). A Simulation Program for Ship Manoeuvrability Based on Matlab-Simulink®. *DINAV Internal Report SB-02-01* (in Italian).

Clarke D., (1983). The Application of Manoeuvring Criteria in Hull Design using Linear Theory, *Transaction RINA*, Vol.125.

Inoue S., Hirano M., Kijana K., Takashima J., (1981). Hydrodynamic Derivatives in Ship Manoeuvring, *International Shipbuilding Progress*, Vol. 28, No. 321, May.

Inoue S., Hirano M., Kijana K., Takashima J., (1981). A Practical Calculation Method of Ship Manoeuvring Motion, *International Shipbuilding Progress*, Vol. 28, No. 321, September.

Kerwin J.E., Mandel P., Dean Lewis S., (1972). An Experimental Study of a Series of Flapped Rudders. *Journal of Ship Research*, Vol. pp.221-239.

Ogawa A., Kasai H., (1978). On the Mathematical Model of Manoeuvring Motion of Ships. *International Shipbuilding Progress*, Vol.25, pp.306-319.

Whicker L.F., Fehlner L.F. (1958). Free Stream Characteristics of A Family of Low-Aspect Ratio, All Movable Control Surfaces for Application to Ship Design. *DTMB Report 933*, Dec. 1958.

Wilson P.A., Lewis G.D.W., (1986). Predicting Ship Manoeuvring Characteristics for Preliminary Design. *International Conference CADMO '86*, .

Yazaki A., (1966). Further Model Tests of Four Bladed Controllable-Pitch Propellers. *Ship Research Institute* Paper n.16, Tokio, Japan.

Practical Design of Ships and Other Floating Structures
You-Sheng Wu, Wei-Cheng Cui and Guo-Jun Zhou (Eds)
© 2001 Elsevier Science Ltd. All rights reserved

EXPERIMENTAL STUDY ON THE MANEUVERABILITY FOR A WIDE BEAM NEW SUEZMAX CLASS TANKER

Heung-Won Seo, Tae-Il Lee and Seung-Myun Hwangbo

Maritime Research Institute, Hyundai Heavy Industries Co.,Ltd. Ulsan 682-792, Korea

ABSTRACT

In the course of designing and building a wide beam single screw Suezmax tanker with unfavorable main particulars in sense of ship's maneuverability, especially course keeping ability, various kinds of model test techniques such as planar motion mechanism (PMM) test and free running test, from different model basins including Hyundai Maritime Research Institute (HMRI) have been studied to estimate and improve its maneuvering performance and their model test results were compared. Although a special type of high lift rudder with comparatively large area was integrated during the design, it is found that carefully developed hull form, especially in the region of stern profile and section shape, seems to be more important to enhance ship's maneuverability. Through the various model tests, it can be stated that even such a very exceptional dimensioned single screw mono hull is able to maintain sufficient maneuverability by careful design and integration of the hull form and rudder, which will be verified at sea trial that is expected around the end of this year. Furthermore it is believed that this kind of experience is to be very helpful to design another abnormal dimensioned hull form in sense of maneuvering performance. For further investigation, some comparative model tests with conventional rudder and high lift rudder also have been carried out and presented together in this paper.

KEYWORDS

Wide beam, Suezmax, high lift rudder, Conventional rudder, Maneuverability, Stern profile, Hull sections.

1 INTRODUCTION

Recently ship builder and owner are tended to increase the block coefficient and beam and to decrease draft in order to maximize the economic performance of ships. These tendencies of wide breadth and high block coefficient in ship's principal parameters result in inherent poor course stability which have been blamed as one of the main reasons of marine accidents and pollutions. Moreover in case of tanker carrying hurtful material to environment such as oil, chemical product and so on, the possibility becomes more realistic.

There are several international endeavors to prevent the ship from this kind of inherent poor maneuverability. The International Maritime Organization (IMO) have suggested and recommended the regulation and guidelines such as IMO A. 751 concerning maritime safety and the prevention and control of marine pollution from ships and US Coast Guard adopted these rules and requires that all ships entering US or Canadian waters fulfil these IMO criteria. Information on the criteria must be presented with the authorities before permission is granted to enter water [1]. Therefore, the maneuverability of the ships has to be inevitably considered from early initial design stage to verify the criteria.

The main dimension of the vessel is out of range among the similar class ships that we have designed and built before. Because she is intended to carry much more oil and operate even in the shallow depth condition and even more in heavy iceberg floating area. The satisfaction of the requirement of the powering performance and maneuverability is the most important optimization problem during initial design stage. The followings are considered to solve this problem.

- Prediction and evaluation of ship's performance and maneuverability based on data base
- Careful design of the forebody and afterbody including stern profile
- High lift rudder with sufficient movable area

Several model tests have been carried out at the different model basins and using possible model test techniques to confirm the hull form design concept. Furthermore in order to investigate the effect of high lift rudder, the conventional rudder with the same area to that of the special rudder has been applied to the additional model test. The results from model tests are presented and discussed in this paper. Even though the best way to verify the performance of a vessel is to carry out sea trial, it is not available at this time. However, the sea trial results are expected to be in line with the results from the model tests.

2 HULL FORM DESIGN

The Table 1 shows the main dimensions of the vessel. The wave resistance of this kind of slow speed vessel is not generally dominant but the viscous term and flow pattern in the afterbody are much more important. It is the reason why the relatively full forebody is recommended. Consequently, this allows wake distribution of the propeller plane to be homogeneous and provide favorable propeller design environment concerning the cavitations on the propeller blade and enough space for large rudder area.

TABLE 1
MAIN DIMENSIONS OF THE VESSEL

Particulars	Dimensions
Length between perpendiculars	266 m
Breadth, moulded	53 m
Scantling draft	15.6 m
Block coefficient	0.83

2.1 Prediction of Maneuverability

The maneuvering characteristics of the ship are predicted using not only main dimensions but also hull form characteristics such as sections, stem and stern profile and so on which have been accumulated in the database made by HMRI's long experience of sea trial and model tests for many kinds of vessels. However the data and experience for the special high lift rudder is not sufficient. So the prediction for the special rudder is done by the combination and extrapolation from existing a few experimental data for conventional and special rudders [2] [3]. The prediction results given in Table 2 for two types of rudders with 2.3% area indicate that the high lift rudder seems to be sufficient enough to satisfy the criteria and superior to the conventional one.

TABLE 2

PREDICTED MANEUVERING CHARACTERISTICS OF THE VESSEL

Items	Rudder type	High lift Rudder	Conventional Rudder	IMO Interim Standard
Initial turning	Track length (LBP)	1.33	1.80	2.5
Turning	Advance (LBP)	2.35	3.08	4.5
	Tactical dia. (LBP)	2.29	2.97	5.0
10°/10° zig-zag (degree)	1st overshoot angle	8.2	23.5	20
	2nd overshoot angle	12.9	41.5	35
20°/20° zig-zag (degree)	1st overshoot angle	14.9	26.2	25

2.2 Stern Profile and Body Plan

It is well known that the side forces from the complex interaction between the hull, propeller and rudder are deeply related to the maneuverability. The main contributor to this force is rudder. But the effect of the section shapes and stern profile area of hull are not able to be taken aside and should be considered during the hull form design stage. The moderate U-shaped sections and adequately inclined profile of the lower part of the shaft center to increase the area of the stern profile are seen in Figure 1.

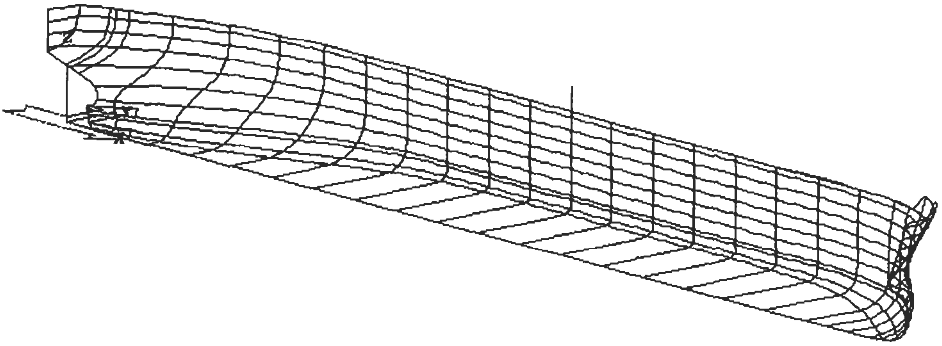

Figure 1: The final hull form

3 RUDDER

The rudder design is based on the movable rudder area of 2.3% of Lbp times scantling draft and the high lift rudder with end plate shown Figure 5 is selected as the applicable to this vessel from estimated results shown in Table 2. The profile of the upper part of the rudder is optimized through the rudder paint test behind the condition. Addition to this rudder, one more rudder with 2.0% area and the same shape to the original one have been designed in order to investigate the effect on the maneuvering performance of rudder area because the rudder with 2.3% area is considered to be sufficiently enough to meet the criteria. The conventional rudder with 2.3% area is also designed to study on the effect of the difference of the rudder section shapes.

4 MODEL TEST RESULTS

To confirm the maneuverability of the designed hull form, model tests carried out at three different model basins with different size of model ship. The PMM tests were done at HMRI and DMI model basin respectively and the free running test in square basin at BSHC. DMI and BSHC used same size of model ship of about 4m and the high lift rudders that have 2.0% and 2.3% of rudder area respectively. HMRI used large model ship of about 7m and the both rudder types that have 2.3% of rudder area. The results of model tests are summarized in Table 3 and Figure 2 ~ Figure. 4 show the comparison results of turning, 10°/10° zig-zag and 20°/20° zig-zag maneuvers for high lift and conventional rudder of 2.3% area. The results in table 3 show that both high lift rudders seem to be successfully applicable to this vessel satisfying the IMO criteria. The result using conventional rudder except for the 2nd overshoot angle is within the criteria, which seems to reflect the positive effect of hull form itself. The deviation among the results from different model basins seems to be thinkable because of the differences of the size of model ships, test methods, the inherent characteristics of model basins itself. The larger high lift rudder doesn't show any remarkable improvement. Regarding the powering performance and maneuverability point of view, it can be stated the smaller high lift rudder is optimum.

TABLE 3

THE RESULT FROM MODEL TESTS FOR THE VESSEL

Items	Rudder type	High lift rudder (2.3%)			High lift rudder (2.0%)		Conventional rudder (2.3%)	IMO Interim Standard
Turning	Advance (LBP)	2.56	3.17	2.97	3.38	2.74	2.99	4.5
	Tactical dia. (LBP)	2.64	2.73	2.93	2.84	2.67	2.90	5.0
10°/10° zig-zag	1st Overshoot angle(degree)	7.1	5.0	7.0	7.0	9.0	14.0	20.0
	2nd Overshoot angle(degree)	14.6	8.5	18.0	13.5	18.5	37.0	35.0
20°/20° zig-zag	1st Overshoot angle(degree)	14.2	11.0	11.0	13.0	10.0	20.5	25.0
Model basin		HMRI	DMI	BSHC	DMI	BSHC	HMRI	
Model size (M)		7	4	4	4	4	7	
Test method		PMM	PMM	Free running	PMM	Free running	PMM	

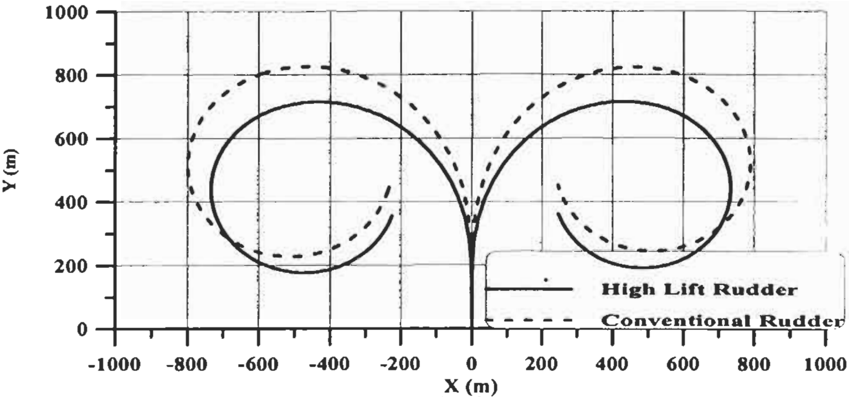

Figure 2: The turning characteristics for two rudders of 2.3% area

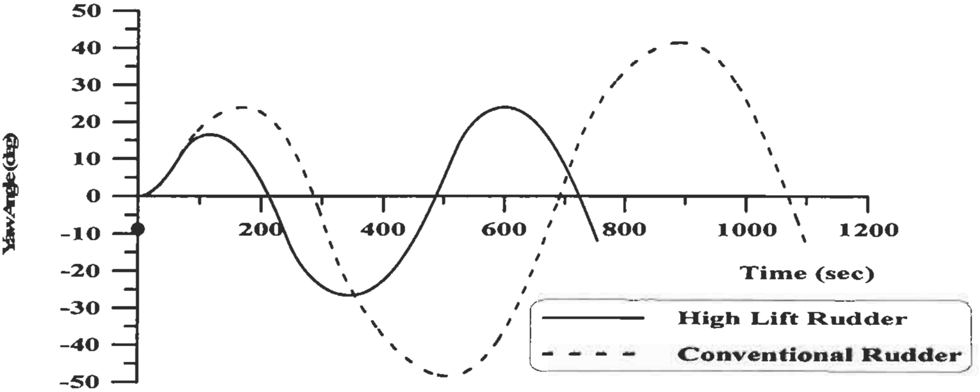

Figure 3: The 10°/10° zig-zag characteristics for two rudders of 2.3% area

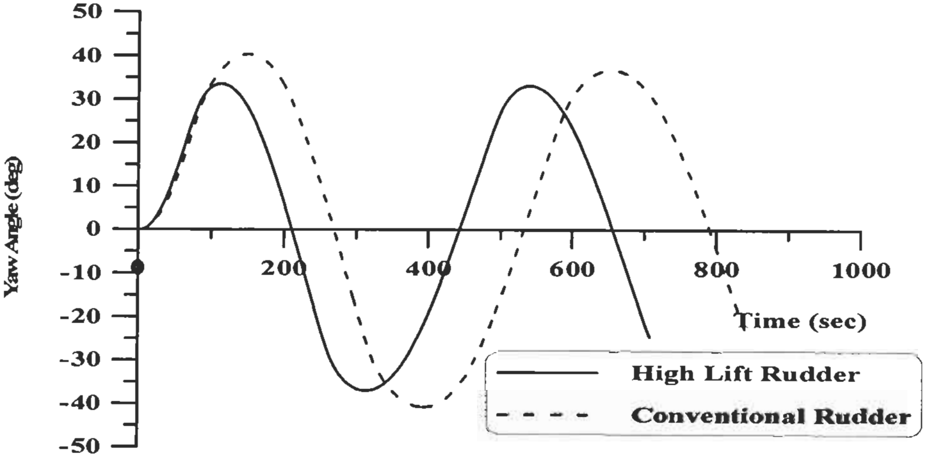

Figure 4: The 20°/20° zig-zag characteristics for two rudders of 2.3% area

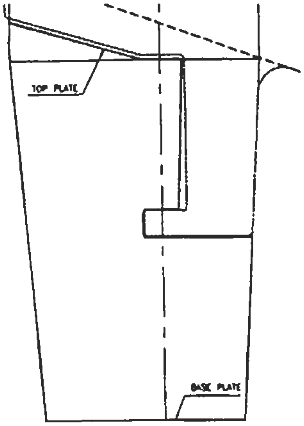

Figure 5: The profile of the high lift rudder

5 CONCLUSIONS

Through various maneuvering study on the hull form and rudder design and also through a series of model tests, the maneuverability of the vessel is cleared to be sufficiently stable and within the IMO criteria. The followings are the results drawn out from the studies.

- Detail and careful hull form design such as the stern profile and section shape seem to be very effective to improve the maneuverability of ship.
- Excessive rudder area in case of using the high lift rudder is not effective and shows only marginal improvement of maneuverability of ship. And so it is the most important that the optimum size and shape of the rudder to satisfy both of the powering performance and maneuverability is appropriately selected in the design stage.
- Even though the maneuvering model tests have been carried out at the different model basins with different test techniques and model sizes, the results are in the reasonable range and consistent.
- It is expected that this kind of experience is to be very helpful to design another abnormal dimensioned hull form in sense of maneuvering performance.

References

[1] MARIN. (2000). Training Course on HYDRODYNAMICS IN SHIP DESIGN, MARIN, The Netherlands

[2] H.Y.Lee and D.J.Yum. (1996). The Theoretical and Experimental Study to Predict Maneuvering Performance. *Internal report of HMRI*

[3] H.Y.Lee, et.al. (1997). Prediction of Maneuverability using PMM Model Tests – Comparative Study of Mathematical Models. *Journal of SNAK* **3:2**

[4] Kuniji KOSE, Hidemitsu YAMADA, Morihisa HOSOKAWA and Kenji AKIFUJI. (1992). A Study on Performance Estimation of Special Rudders. *Transactions of the West Japan of Naval Architects* No.**84**, 49-57

Practical Design of Ships and Other Floating Structures
You-Sheng Wu, Wei-Cheng Cui and Guo-Jun Zhou (Eds)
© 2001 Elsevier Science Ltd. All rights reserved

ON STEADY HORIZONTAL FORCES AND MOMENT DUE TO SHORT WAVES ACTING ON SHIPS IN MANOEUVRING MOTION

M. Ueno[1], T. Nimura[1], H. Miyazaki[1] and K. Nonaka[1]

[1]Ship Research Institute, Ministry of Land, Infrastructure and Transport,
6-38-1 Shinkawa, Mitaka, Tokyo 181-0004 Japan

ABSTRACT

Calculation formula for predicting steady horizontal forces and moment due to short waves acting on ships in manoeuvring motion is presented. Effect of non-uniform flow around ships on deformation of short waves is taken into account and reflection region of short waves around ships' hull is clarified in present method. Calculated results are compared with experimental data for a VLCC model test and the presented method is confirmed to be practically useful to predict steady horizontal forces and moment due to short waves acting on ships in manoeuvring motion. Ship form effects are investigated by comparing calculation for the VLCC and a training ship.

KEYWORDS

Manoeuvrability, Wave drift forces, Turning motion, Added resistance, Non-uniform flow

1 INTRODUCTION

In order to evaluate manoeuvrability of ships effects of steady wave forces and moment must be estimated correctly since it is inevitable that ships suffer those external forces at seas. Moreover, the facts that short waves induce larger steady wave forces and moment than long waves and that short waves exist anytime at seas mean importance of steady horizontal forces and moment due to short waves for safety of ships at seas.

In this report, calculation method for predicting steady horizontal forces and moment due to short waves acting on ships in manoeuvring motion is presented based on Ohkusu(1986)'s method for added resistance. Calculated results are compared with experimental data of a VLCC for evaluation of present calculation method. Ship form effects on steady horizontal forces and moment due to short waves are also investigated by comparing calculation results for the VLCC and a training ship, the former has blunt bow and long parallel part whereas the latter has slender bow and short parallel part.

2 FORMULATION

Let us consider a ship manoeuvring in short waves in unrestricted deep water without current. In order to look into steady wave pressure acting on ships' hull locally, local coordinate system fixed on a ship is shown in Figure 1 where ***s*** and ***n*** denote tangential and inward normal direction to water line of ship surface respectively. Suppose the phenomenon is steady and changes only along ***n*** direction. In far region, there suppose to exist incident wave of wave number vector ***k***, circular frequency ω, amplitude ζ and external flow ***V*** which originates from ship's manoeuvring motion. Direction of wave number vector ***k*** and flow velocity vector ***V*** is represented by γ_w and γ_V, defined clockwise from ***s*** direction. In near region, there suppose to exist tangential flow $\boldsymbol{V_l}$ and refracted wave of wave number vector $\boldsymbol{k_l}$, circular frequency ω_l and amplitude ζ_l. Direction of wave number vector $\boldsymbol{k_l}$ is represented by γ_{wl}. Direction ***s*** coincides with $\boldsymbol{V_l}$ direction.

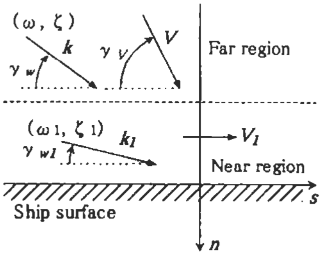

Figure 1: Local coordinate system.

A law of wave crest conservation is written by

$$\omega = \sqrt{gk} + Vk\cos(\gamma_V - \gamma_w) = \omega_l = \sqrt{gk_l} + V_l k_l \cos\gamma_{wl} \tag{1}$$

where g denotes gravitational acceleration. Since wave number is irrotational,

$$k\cos\gamma_w = k_l \cos\gamma_{wl}. \tag{2}$$

Wave number k_l and its direction γ_{wl} in near region are found using Eqn. 1 and Eqn. 2 to be

$$k_l = \frac{(\omega - V_l k\cos\gamma_w)^2}{g} \tag{3}$$

and

$$\gamma_{wl} = \cos^{-1}\left\{\frac{gk\cos\gamma_w}{(\omega - V_l k\cos\gamma_w)^2}\right\}. \tag{4}$$

Based on an assumption of moderate change of wave property propagating from far region into near, a low of wave action conservation can be applied and wave amplitude ζ_l in near region is given by

$$\frac{\zeta_l}{\zeta} = \sqrt{\frac{k_l}{k}\frac{2Vk\sin\gamma_V + \sigma\sin\gamma_w}{\sigma\sin\gamma_{wl}}} \tag{5}$$

where σ that is equal to $(gk)^{1/2}$ represents wave circular frequency in far region in an earth fixed frame.

Let us assume mirror reflection of wave on ship surface. Then steady wave pressure acting on unit length of the ship's waterline F_n is derived by calculating momentum change between n=0 plane and its parallel plane in near region as

$$F_n = \frac{1}{2}\rho g \zeta_1^{\,2} \sin^2 \gamma_{w1} . \tag{6}$$

Eqn. 6 has the same form as the formula derived by Havelock(1940) for steady wave pressure acting on wall. However, differences are that Eqn. 6 takes effects of refraction by tnagential flow in near region into account in ζ_l and γ_{wl}. If we set $\gamma_V = \gamma_w$ equivalent formula obtained by Ohkusu(1986) for local steady wave pressure is derived.

For practical use, we adopt the term representing draft effect given by Fujii and Takahashi (1975) and define steady wave pressure, instead of Eqn. 6, by

$$F_n = \frac{1}{2}\rho g \zeta_1^{\,2} \sin^2 \gamma_{w1} \left\{ \frac{\pi^2 I_1^2(k_1 d)}{\pi^2 I_1^2(k_1 d) + K_1^2(k_1 d)} \right\} \tag{7}$$

where I_1 and K_1 denote modified Bessel functions and d denotes ship draft .

Now we consider relation between manoeuvring motion and properties in local coordinate system. Figure 2 shows coordinate system describing a ship in manoeuvring motion. U, β, r and χ denote ship speed, drift angle, yaw rate and wave encounter angle respectively. X_d, Y_d and N_d denote steady wave forces and moment. $l(x_{wl}, y_{wl})$ of which direction is defined by θ represents coordinate along waterline. Flow velocity vector $\boldsymbol{V}$ and wave number vector $\boldsymbol{k}$ in far region in local coordinate system are written in the form

$$\boldsymbol{V} = \left(U\cos\beta - y_{wl} r, -U\sin\beta + x_{wl} r\right) \tag{8}$$

and

$$\boldsymbol{k} = (k\cos\chi - k\sin\chi) . \tag{9}$$

Direction of $l(x_{wl}, y_{wl})$ is written by

$$\theta = \tan^{-1}\frac{dy_{wl}/dl}{dx_{wl}/dl} . \tag{10}$$

Normal and tangential vector is written, using θ, in the form

$$\boldsymbol{n} = (-\sin\theta, \cos\theta) \tag{11}$$

and

$$\boldsymbol{s} = \left(\cos\theta_s, \sin\theta_s\right),\ \ \theta_s = \theta \ \text{ for } (\boldsymbol{n}\times\boldsymbol{V})_z<0,\ \ \theta_s = \theta - \pi \ \text{ for } (\boldsymbol{n}\times\boldsymbol{V})_z>0 \tag{12}$$

where $(\ )_z$ denotes z-component of a vector in terms of the right-hand rule in coordinate system of Figure 2. Flow direction γ_V and wave number direction γ_w in local far region are then written as

$$\gamma_V = \arg \boldsymbol{V} - \theta_s \tag{13}$$

and

$$\gamma_w = \arg \boldsymbol{k} - \theta_s = -\chi - \theta_s. \tag{14}$$

Following Faltinsen et al. (1980) and Ohkusu (1986), tangential flow velocity $\boldsymbol{V_l}$ is assumed by

$$V_1 = \boldsymbol{s} \cdot \boldsymbol{V}. \tag{15}$$

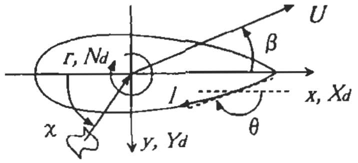

Figure 2: Coordinate system describing ship motion and wave forces and moment

Using all those relations above, steady wave forces and moment X_d, Y_d and N_d are obtained by integrating local steady wave pressure in the form

$$X_d = -\oint F_n \sin\theta \, dl, \;\; Y_d = \oint F_n \cos\theta \, dl, \;\; N_d = \oint F_n (x_{wl}\cos\theta + y_{wl}\sin\theta)\, dl\,. \tag{16}$$

Let us consider about integral region. Since wave must reflect at ship surface, direction of wave in near region must be satisfy,

$$0 < \gamma_{w1} < \pi\,. \tag{17}$$

Moreover, assuming that Eqn. 17 holds, a condition requiring that amplitude in near region can be calculated by Eqn. 5 is written as

$$V \sin\gamma_V + c_g \sin\gamma_w > 0 \tag{18}$$

where c_g represents wave group velocity in far region in an earth fixed frame. Eqn. 18 tells us that normal component of wave energy velocity in far region relative to the ship must direct toward the ship surface locally. Eqn. 18 is a first condition to determine the integral region of Eqn. 16.

The other point to be taken into account is existence of γ_{wl}, direction of wave number $\boldsymbol{k_l}$ in near region. From Eqn. 4 this condition is represented by

$$\left| k\cos\gamma_w \right| \le \frac{(\omega - V_1 k \cos\gamma_w)^2}{g}\,. \tag{19}$$

Since right-hand-side of Eqn.19 is, from Eqn. 3, equal to wave number k_l, Eqn. 19 is understood as requires that wave number k_l must be greater than certain value. When wave number takes minimum value Eqn. 2 tells that direction γ_{wl} is equal to 0 or π, which means wave ray is bended to be parallel to waterline by tangential flow in near region and this disagrees with the assumption of Eqn. 17. In this case wave ray cannot reach ship surface any more. Therefore steady wave pressure cannot be estimated by Eqn. 7. Although this fact does not always mean that waves of which ray is bended to be parallel to ship surface does not have effects on steady wave forces and moment, we assume Eqn. 19 is a second condition to determine the integral region of Eqn. 16.

3 EXPERIMENTAL EVALUATION

Model experiment is carried out using a VLCC model of which length, breadth, draft and block coefficient are 2.97m, 0.5383m, 0.1791m and 0.8033 respectively. Model ship is towed at Froude number 0.069 in oblique motion and in turning motion with and without oblique angle with its periodic motion unconstrained. Steady horizontal forces and moment together with six degrees of periodic motions are measured using a system developed by Ueno et al. (2001). Wavelength ship length ratio λ/L is set to be 0.2 and wave amplitude is set to be 1.1cm. Measured six degrees of motions of wave encounter period are negligible small since wavelength is very short.

For describing experimental data we introduce χ_U as angle between ship speed direction and wave propagating direction as in Figure 3. Wave encounter angle χ and χ_U are related by

$$\chi_U = \chi - \beta . \tag{20}$$

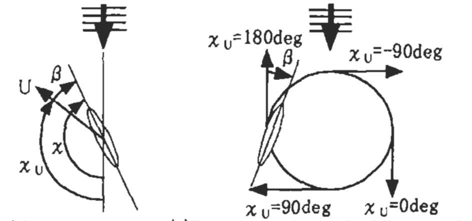

(a)Oblique motion (b)Turning motion with oblique angle

Figure 3: Definition of χ_U in oblique and turning motion

Horizontal forces and moment in oblique motion are shown in Figure 4. X_d, Y_d and N_d are displayed against χ_U for oblique angle +18deg, 0deg and -18deg. Marks show experimental data and corresponding calculations are shown by lines. For steady surge force X_d, although quantitative discrepancy is observed between measured data and calculation, qualitative tendency of calculation explain effects of oblique angle and wave encounter angle. For steady sway force Y_d, measured data show large effect of oblique angle from beam to head seas and calculation well describe these properties. For steady yaw moment N_d, although measured data scatters, calculation explains effect of oblique angle as in steady sway force.

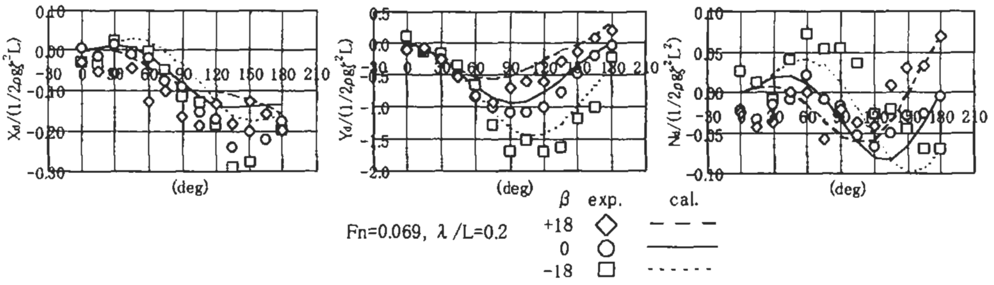

Figure 4: Steady wave forces and moment in oblique motion, experiment and calculation for a VLCC

Horizontal forces and moment in turning motion are shown in Figure 5. Non-dimensional yaw rate, $r'=r(L/U)$, is set to be 0.3 right turning, and oblique angles are 0deg and +18deg. Since wave encounter angle changes gradually during turning, Figure 5 can be regarded as time history for measured forces and moment. Data are obtained by two runs of measurement because water area of model ship basin is not large enough to cover a circle of r'=0.3. On the other hand, calculation is based on an assumption of quasi-steady condition for successive χ_U.

Although measured data scatters because of not high precision, calculation describes effects of turning motion. Effect of oblique angle in turning motion is observed to be small for following wave condition and large for head wave condition for measured data. Calculation explains this coupled effect of oblique angle and turning rate in measured data.

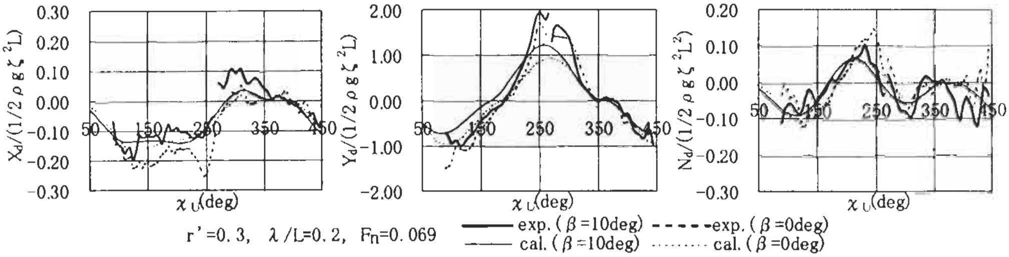

Figure 5: Steady wave forces and moment in turning motion, experiment and calculation for a VLCC

4 EFFECTS OF SHIP FORM

In order to investigate effects of ship form, present calculation method is applied to a training ship of which form is more slender than VLCC. Length, breadth, draft and block coefficient of the training ship are 105m, 17.9m, 5.96m and 0.5075 respectively. Water plane area ratio of the training ship is 0.7141 whereas that of the VLCC is 0.8821. Calculation is carried out under a condition where Froude number is 0.1 and wavelength ship length ratio is 0.2.

Figure 6 shows steady forces and moment due to short waves for the training ship and the VLCC. Oblique angles are set to be +18deg 0deg and −18deg. For 0deg oblique angle, steady surge force X_d shows large difference between the VLCC and the training ship, which is well known as effect of bow shape. It is also remarkable that added resistance of the training ship for β=-18deg around χ_U =130deg is comparable with that of the VLCC for β=0deg in head wave condition. For steady sway force Y_d, ship form effect is negligible for all three oblique angles and for broad range of χ_U. For steady yaw moment N_d, ship form effect is observed largest for β=-18deg and smallest for β=+18deg.

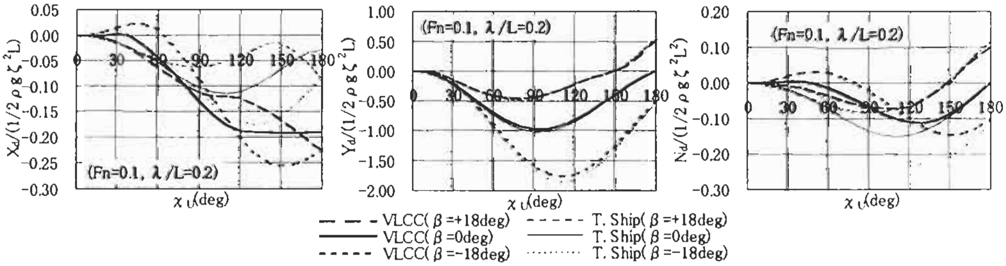

Figure 6: Comparison of steady wave forces for a VLCC and a training ship in oblique motion

Figure 7 shows steady wave forces and moment in turning motion where non-dimensional turning rate

r' is set to be 0.8 and 0.0. For steady surge force X_d, difference remains large in quartering and head seas even in turning motion for both ship forms. For steady sway force Y_d, although ship form effect is small, turning effect is observed larger for the training ship than for the VLCC around χ_U =100deg. The same tendency can be seen for steady yaw moment N_d, around the same χ_U range. This difference between these two ship forms can attribute to difference of magnitude of longitudinal non-symmetry for these two ship forms.

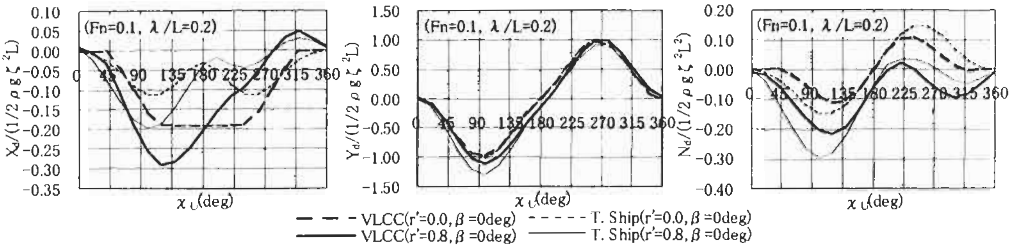

Figure 7: Comparison of steady wave forces for a VLCC and a training ship in turning motion

5 CONCLUDING REMARKS

Calculation method for steady horizontal forces and moment due to short waves acting on ships in manoeuvring motion, presented in this paper, is confirmed to be practically useful by comparison with experimental data. It is also clarified that present method describes effects of ship form on these forces and moment by comparison of calculated results for the VLCC and the training ship.

One of features of present method is that it explains effects of manoeuvring motion on steady horizontal forces and moment due to short waves by regarding them as effects of non-uniform flow around ships in manoeuvring motion on short waves' refraction and reflection. It is also noticeable that integral region to calculate steady horizontal forces and moment due to short waves is defined clearly.

Present calculation method is considered to be applicable to estimate not only steady horizontal forces and moment due to short waves acting on ships in manoeuvring motion but also manoeuvring motion of ships in short waves by time simulation.

References

Faltinsen O. M. et al. (1980). Prediction of Resistance and Propulsion of a Ship in a Seaway. *Proceedings of Thirteenth Symposium on Naval Hydrodynamics*, 505-529

Fujii H. and Takahashi T. (1975). Experimental Study on the Resistance Increase of a Large Full Ship in Regular Oblique Waves. *Journal of The Society of Naval Architects of Japan* **137,** 132-137.

Havelock T. H. (1940). The Pressure of Water Waves upon a Fixed Obstacle. *Proceeding s of Royal Society of London, Series A* **963:175,** 409-420.

Ohkusu M. (1986). Added resistance of Blunt Bow Ships in Very Short Waves. *Journal of The Kansai Society of Naval Architects, Japan* **202,** 39-42.

Ueno M. et al. (2001). Model Experiment on Steady Wave Forces and Moment Acting on A Ship at Rest. *Journal of The Kansai Society of Naval Architects, Japan* **235,** (to be published).

Practical Design of Ships and Other Floating Structures
You-Sheng Wu, Wei-Cheng Cui and Guo-Jun Zhou (Eds)
© 2001 Elsevier Science Ltd. All rights reserved

AN EMPIRICAL FORMULA FOR STEERING GEAR TORQUE OF TANKERS WITH A HORN RUDDER

D. I. Son[1], J. H. Ahn[2] and K. P. Rhee[2]

[1] Hyundai Heavy Industries Co., Ltd., Jeonha-dong, Dong-ku, Ulsan, 682-792, Korea
[2] Dept of Naval Architecture and Ocean Engineering, Seoul National University,
Shillim-dong, Kwanak-ku, Seoul, 151-742, Korea

ABSTRACT

Accurate estimation of rudder capacity is essential at the initial design stage. Horn rudders have been adopted for medium and large-sized ships. There are, however, few experimental or theoretical results for a horn rudder because of its complex geometry and hydrodynamic characteristics. In this paper, an empirical formula was developed to estimate the steering gear torque of a tanker with a horn rudder. The hydrodynamic characteristics of a horn rudder in the free stream condition were obtained using the modified lifting line theory proposed by Molland. Statistical analysis was performed with sea-trial data of 32 tankers, considering interaction effects with hull-form and propeller. It is shown that the formula can be used for predicting the steering gear torque at the initial design stage.

KEYWORDS

Steering Gear Torque, Horn Rudder, Regression Analysis, Modified Lifting Line Theory

1 INTRODUCTION

There are several methods mainly used in the estimation of rudder capacity. One is to calculate the hydrodynamic force and torque of a rudder using the results of Loire plane test performed by Jössel in 1873, which are modified by the empirical values of sea-trial data. Another is to use the equations of each classification's rule calculating the force and torque used in the structure design of a rudder. These methods, however, are not sufficient to consider the hull-form characteristics or the interaction effect of propeller.

Theoretical methods, which agree well with the experimental results, have been developed for an all-movable rudder, but there are few results for a horn rudder because of its complex shape and difficulties in analyzing the flow around it.

In this paper, we suggested an empirical formula for the estimation of steering gear capacity after calculating the hydrodynamic force and torque of a horn rudder in the free-stream on the basis of

Molland's modified lifting line theory and considering the effects of hull-form and propeller by the regression analysis of sea-trial data.

2 CALCULATION OF RUDDER FORCE AND TORQUE

2.1 Force and Torque Acting on a Rudder

The definitions of the lift coefficient, drag coefficient, normal force coefficient and the torque coefficient about the rudder stock described in Figure 1 are as follows.

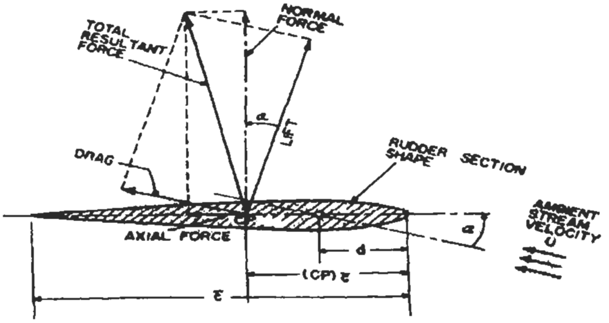

Figure 1: Definitions of rudder forces and its geometry

$$C_L = \frac{L}{\frac{1}{2}\rho A U^2} \tag{1}$$

$$C_D = \frac{D}{\frac{1}{2}\rho A U^2} \tag{2}$$

$$C_N = \frac{F_N}{\frac{1}{2}\rho A U^2} = C_L \cos\alpha + C_D \sin\alpha \tag{3}$$

$$C_{MH} = \frac{Q_H}{\frac{1}{2}\rho A U^2 \bar{c}} = \frac{F_N[d-(CP)_{\bar{c}}]}{\frac{1}{2}\rho A U^2 \bar{c}} \tag{4}$$

where ρ is the fluid density, A is the rudder area, $\bar{c}$ is the mean chord length of rudder, d is the distance between the leading edge of the rudder and the centerline of the rudder stock and Q_H is the hydrodynamic torque experienced by the stock.

2.2 Previous Equations for Calculating Hydrodynamic Force and Torque on the Rudder

In shipyards, the following Beaufoy-Jössel's results reflecting the empirical sea-trial data is generally used to calculate the force and torque acting on the rudder.

$$F_N = 58.8 A U_r^2 \sin\alpha = 15.6 A U^2 \sin\alpha \tag{5}$$

$$(CP)_{\bar{c}} = (0.195 + 0.305 \sin\alpha) \times c \tag{6}$$

$$Q_H = AcV_t^2\left(4.36 - 11.8\frac{d}{c}\right)\times 10^{-3}(ton\cdot m) \tag{7}$$

where α is the angle of attack, $U_r(m/\sec)$ and $U(knots)$ are the flow speeds into the rudder and $V_t(knots)$ is the sea-trial speed. The variables of previous equations are just only the flow speed and angle of attack non-considering the general factors such as aspect ratio, taper ratio.

In the classification (IASC) equations, the normal force on a rudder, its acting point and the torque are decided by using the aspect ratio of rudder, k_R, form factor of rudder area, k_c and the rudder position coefficient in the propeller backflow, k_l.

$$F_N = 0.312k_Rk_ck_lAV^2 \tag{8}$$

$$r = c(a-k) \tag{9}$$

$$Q_R = F_N r \tag{10}$$

where k is the balance ratio of rudder area.

The foregoing both methods are still widely used as the basic equations estimating the rudder torque in spite of the defect that they lack the factors reflecting the influence of hull-form and propeller in detail.

3 CALCULATION OF RUDDER FORCE AND TORQUE IN TERMS OF MODIFIED LIFTING LINE THEORY

Molland provided an appropriate theoretical basis on the characteristics of a horn rudder from wind tunnel test, and also developed a theoretical formula that can reflect the variation of principal specification of rudder such as horn type, aspect ratio, etc.

3.1 Summary of the Lifting Line Analysis

In the basic lifting line theory, rudder is replaced by a lifting line with the length equal to 2*S (span) and each position of the span-wise section from the rudder root is replaced by θ. Then effective angle of attack is as follows.

$$\bar{\alpha}(\theta) = \alpha - f(\theta)\cdot\gamma(\delta,\alpha) \tag{11}$$

where $\gamma(\delta,\alpha)$ is the decrease of incidence angle in the horn part, which can be calculated from the experimental results considering separation.

$$\sum_n\left[A_n \sin n\theta\cdot\left(\mu n + \frac{\sin\theta}{1-k\cos\theta}\right)\right] = \mu\bar{\alpha}\sin\theta,\ \ \mu = \frac{mC_R}{8S} \tag{12}$$

Eqn. 12 should be satisfied at all points ($0 \le \theta \le \pi/2$), so we can get the following equations about the lift and drag forces by calculating A_n.

$$L = \rho V\Gamma = \rho V\left[4SV\sum A_n \sin n\theta\right] = 4\rho SV^2\left[\sum A_n \sin n\theta\right] \tag{13}$$

$$C_L = m(\bar{\alpha} - w/V) \tag{14}$$

$$w = \frac{V\sum nA_n \sin n\theta}{\sin\theta} \tag{15}$$

$$C_{Di} = C_L \cdot \frac{w}{V} \tag{16}$$

There can be the needs of modifying the basic lifting line theory to reflect horn rudder characteristics. The declination of lift force curve is determined from the experimental results (NACA0020: m=5.5) considering thickness of rudder and viscosity effect.

$$C_D = C_{DP} + C_{Di} \tag{17}$$

$$C_{DP} = 0.017 + 0.12C_L^5 \tag{18}$$

$$C_{Di} = C_L \frac{w}{V} \tag{19}$$

where C_{DP} is the rudder profile drag and C_{Di} is the induced drag.

3.2 Calculation of Rudder Force and Torque

The acting points of normal and chord-wise forces of horn rudder actuator is determined by integrating span-wise load distribution using Molland's modified lifting line theory.

$$C_N = C_L \cos\alpha + C_D \sin\alpha \tag{20}$$

$$F_N = C_N \frac{1}{2} \rho A V^2 \tag{21}$$

$$\overline{X} = (CP_c \times \bar{c}) - d \tag{22}$$

$$CP_c = 11.7 + 0.18\alpha^{1.4} + 0.7(AR - 3) \tag{23}$$

$$Q_M = F_N \times \overline{X} \tag{24}$$

where CP_c is the chord-wise pressure center, AR is the rudder aspect ratio and Q_M is the rudder torque calculated by Molland's modified lifting line theory. Figure 2 shows the rudder force, center of pressure and the torque in terms of rudder angle obtained by Molland's formula.

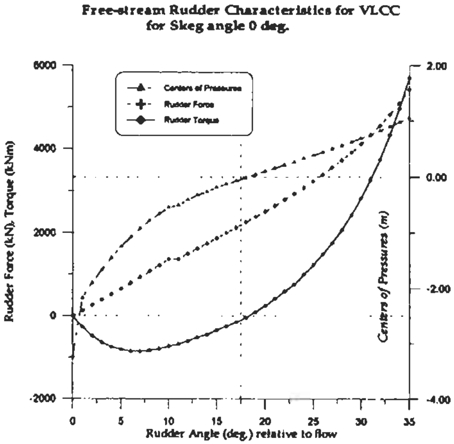

Figure 2: Application of Molland's formula for VLCC

4 DEVELOPMENT OF EMPIRICAL FORMULA

4.1 Basic Assumption of Regression Analysis

Steering gear torque is mainly consisted of the torque by the hydrodynamic force acting on the rudder and the torque loss resulting from the friction of bearing of rudder support. Among the factors influencing the inflow speed and the distribution of angle of attack, excluding mechanical torque loss, we placed more weight on the data usable at initial design stage.

4.2 Factors in Regression Analysis

The regression analysis was performed considering 30 factors related to the characteristics of the rudder, hull-form and the propeller. The underlined items are thought to have significance in the estimation of the rudder torque and used in the final analysis.

1. Distribution of rudder wake	11. Propeller slip ratio	21. Sweep angle of rudder front
2. Reynolds number	12. First overshoot angle of sea-trial	22. Sea-trial condition
3. Maximum thickness of rudder section	13. Change of flow speed in the backflow of propeller	23. Taper ratio of rudder
4. Aspect ratio of rudder	14. Existence of skeg at rudder root	24. Submerged ratio of rudder
5. Propeller thrust	15. Variation of the angle of attack at turning	25. Ratio of difference between the propeller diameter and the breath
6. Ahead speed	16. C_B	26. Froude number
7. Ratio of mean rudder height to propeller diameter	17. LBP/B_m	27. Ratio of section coefficient of horn part
8. Ratio of the distance between boss center of propeller and rudder front to propeller diameter	18. $2 \cdot TL/LBP$	28. Ratio of section coefficient of rudder
9. Distance from the end of rudder root to hull	19. Discrimination of flow velocity due to the wake depending on the relative position of rudder, propeller and hull	29. Friction coefficient of rudder bearing
10. Sectional hull-form ahead of rudder front	20. Ratio of rudder area according to the positions of rudder stock and propeller axis	30. Overlap ratio of horn part and rudder ahead part

4.3 Regression Function Model and Principal Procedure

We have used linear multiple and second regressive model through making the sea-trial torque of steering gear as responding variables and making dimensional factors as explanation variables. However, the results seem to have problems in the significance and covariance of the used variables, so we made another regressive analysis through nondimensionalizing the variables which affect the rudder inflow speed and the inflow angle by the principal data of rudder and propeller. After the model diagnosis which tests the fulfillment of the basic hypothesis of regression analysis is performed, some trends of heteroscedasticity was appeared in our least square model. We overcome this problem by the weighted least square method.

4.4 Empirical Formula by Recurrence Analysis Result

In our analysis the empirical formula of the rudder torque adopting the best matching and meaningful recurrence coefficients are as follows.

$$Q_P = Q_M \times K_{mf} \tag{25}$$

$$\begin{aligned} K_{mf} = {} & 9.857696 - 0.235137 \times \frac{LBP}{B_m} - 2.923753 \times \frac{(B_m - D_p)}{B_m} + 0.757224 \times \frac{G_{ap}}{R_{zm}} \\ & -6.616184 \times C_B - 0.587146 \times \frac{D_p}{R_{zm}} + 0.563221 \times \frac{d_{AP}}{R_{zm}} - 1.348684 \times \frac{D_{rp}}{D_p} \end{aligned} \tag{26}$$

where Q_P is the expected rudder torque. Q_{Mt} is the horn rudder torque. The variables constituting modified factor K_{mt} are the length between the perpendiculars, LBP, molded breadth, B_m, propeller diameter, D_p, sea-trial draft, d_{AP}, the gap between rudder and hull, G_{ap}, mean rudder height, R_{zm}.

5 CONCLUSIONS

As shown in Figure 3 a satisfactory relation corresponding to ship's principal dimensions and rudder characteristics was obtained, along the problems of real ship data were analyzed. This formula can be used at the shipyards with lots of reliability for the following cases.

(1) Horn rudder: NACA 00XX section
(2) The ratio of propeller diameter to rudder height: 0.597 ~ 0.786
(3) The ratio of distance between propeller boss center and rudder front to propeller diameter: 0.239 ~ 0.414
(4) The gap between the hull and the rudder: 0.075 ~ 0.22
(5) C_H : 0.788 ~ 0.842
(6) LBP / B_m : 5.19 ~ 6.8
(7) The submerged ratio of rudder at sea-trial: 1.214 ~ 1.414
(8) The percentage of difference between the propeller diameter and the breadth: 0.783 ~ 0.836

Further studies may be required for the analysis on the turbulent flow in the stern and propeller effect to calculate the rudder force and torque more accurately.

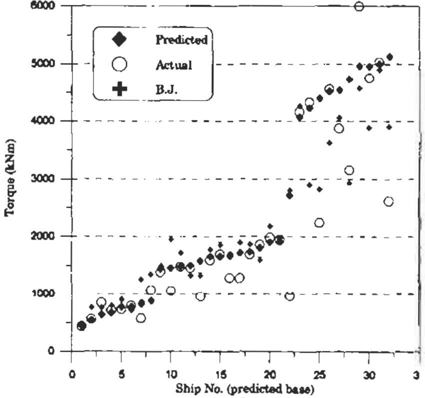

Figure 3: Plot of steering gear torques for regression model, present method and sea-trial results

References

1. Abbott and von Doenhoff. (1959). *Theory of Wing Section*, Dover.
2. Brix J. et al. (1993). *Manoeuvring Technical Manual*, Seehafen Verlag.
3. Draper N.R. and Smith H. (1981). *Applied Regression Analysis*, John Wiley & Sons, Inc.
4. Glauert H. (1948). *The Elements of Aerofoil and airscrew Theory*, Cambridge.
5. IACS Requirements, 1990, v1.1, S10
6. Molland A.F. (1981). The Free-Stream Characteristics of Ship-Skeg Rudders, *Ph.D. Thesis*, University of Southampton.
7. Newman J.N. (1986). *Marine Hydrodynamics*, MIT.
8. SNAME. (1989). *Principles of Naval Architecture* vol.3.

AUTHOR INDEX

Volumes I and II

Abdul Rahim, M. 971
Abt, C. 67
Ahn, Il Jun 113
Ahn, J.H. 679
Andersen, L.F. 403
Anderson, C.D. 517
Ando, J. 645, 719
Arai, M. 331
Arita, M. 221
Atlar, M. 517

Baarholm, G.S. 879
Baarholm, R. 621
Baatrup, J. 261
Bade, S.D. 67
Bai, Y. 175, 1005
Bailey, P.A. 571
Ballard, E.J. 571
Barltrop, N.D.P. 1121
Barry, C.D. 119
Bechepay, G. 1177
Begovic, E. 135
Benvenuto, G. 657
Bereznitski, A. 911
Berge, S. 1071
Berggreen, C. 1323
Bertorello, C. 135, 143
Besnier, F. 1177, 1309
Birk, L. 67, 275
Bjørheim, L.G. 1071
Bjørneboe, N. 349
Brizzolara, S. 657
Bruzzone, D. 143, 547
Buxton, I.L. 293

Candries, M. 517
Cassella, P. 135, 143
Chan, Hoi-Sang 857
Chang, B.-J. 467
Chau, S.W. 777
Chen, Chang-Lung 445
Chen, Rui-Zhang 871
Chen, Shun-Huai 37
Chen, W.C. 777
Chen, Ying-Qiu 245
Chen, You-Fang 865
Cheng, Jing-Yun 373
Cho, C.-H. 685
Cho, Doo-Yeoun 315
Choi, Yoon-Rak 525
Choi, Young-Bok 315
Chou, S.K. 777
Chung, Duk Soo 367
Chung, J.H. 205
Chung, Jung-Hoon 1315
Chung, Kyoon-Yang 1221
Chung, T.Y. 205
Clausen, H.B. 349
Clauss, G.F. 275, 1227
Colbourne, B. 741
Coppola, T. 127
Corr, R.B. 1269
Crossland, P. 563
Cui, W.C. 979

Dahle, E.A. 925
Das, P.K. 1121
de Jager, A. 437
Deng, Yanping 397
Dijkstra, O.D. 1145
Doerk, O. 1137
Dogliani, M. 1243
Dong, Shi-Tang 693
Dong, Wen-Cai 1213
Dong, Zu-Shun 97
Donner, R. 1309
Du, S.X. 847
Du, Shuang-Xing 871
Duffty, B. 119

Egge, E.D. 1293
Egorov, G.V. 1013
Endo, H. 1285
Esposito, P.G. 705
Estefen, S.F. 1037

Faltinsen, O.M. 475, 621
Fang, C.C. 857
Ferry, M. 1177
Figari, M. 657
Fricke, W. 1061
Friesch, J. 749
Frieze, P.A. 1269
Friis-Hansen, A. 349
Fujino, M. 213
Fukasawa, T. 1081

Fukuchi, N. 1253, 1261
Funeno, I. 485

Gao, H.Q. 555
Gao, Xiao-Peng 97
Garme, K. 579
Gu, X.K. 887
Gualeni, P. 547
Guerrero, A. 517
Guo, R.X. 1213

Ha, M.K. 587
Hämäläinen, R. 757
Han, D.G. 451
Harries, S. 67
Hashimoto, K. 389
Hayman, B. 1331
He, Mo-Qin 823
He, Shu-Long 823
Hellan, Ø. 611
Heo, Joo-Ho 323
Herfjord, K. 621
Hess, P.E. 237
Himeno, Y. 719
Hino, T. 699
Hirata, K. 493
Hirayama, T. 187
Hirdaris, S.E. 903
Hishimoto, K. 1081
Hoekstra, M. 437
Hoff, J.R. 611
Hong, S.Y. 205
Hong, Sa-Young 525
Hsin, C.Y. 777
Hu, C. 1253, 1261
Hu, Jia-Jun, 871
Huang, J.Y. 931
Huang, Zhen-Yu 429
Hudson, D.A. 847
Hung, C.F. 1169
Hwangbo, S.M. 791
Hwangbo, Seung-Myun 665

Ikebuchi, T. 485
Ikeda, A. 997
Ikoma, T. 221
Incecik, A. 947
Irisawa, M. 971
Ishida, S. 603
Ishikawa, K. 187

Jang, Chang-Hwan 323
Jang, Jinho 113
Jang, T.S. 699
Janssen, G.T.M. 1145
Jensen, J.J. 261, 839
Ji, Y.J. 205
Ji, Zhuoshang 397
Jiang, T. 509
Jin, Eunseok 459
Johannsen, C. 815
Johansen, A. 1071
Johnson, M.C. 563
Joseph, P.F. 1185

Källstam, T. 253
Kang, Dae Sun 367
Kang, Jeom-Moon 229
Kang, K.J. 151
Kang, S.H. 105
Karlsen, S.I. 593
Kawabe, H. 1089
Kawamura, Y. 341
Kierkegaard, H. 1137
Kim, D.H. 151
Kim, Doe Hyun 1129, 1161
Kim, Eun-Chan 525
Kim, H.T. 301
Kim, Hochung 1045
Kim, Hyochul 133, 367, 799
Kim, Hyoungtae 799
Kim, J.J. 785
Kim, Jaesung 113, 367
Kim, Jungjoong 799
Kim, K. 799
Kim, Keunjae 1045
Kim, Kisung 367
Kim, Kuk Bin 1129
Kim, Moonchan 1045
Kim, O.H. 105, 229
Kim, Sungpyo 1045
Kim, W.S. 1161
Kim, Wha Soo 1129
Kim, Won-Hyun 1221
Kim, Y.J. 587
Kim, Yongsoo 459
Kinoshita, T. 699
Kitamura, O. 997, 1285
Kitazawa, D. 213
Ko, W.J. 1169
Kobayashi, H. 971
Kong, D.S. 785
Konovessis, D. 269
Koushan, K. 501
Kozlyakov, V.V. 1013
Kumakura, Y. 29
Kuratani, F. 485
Kusunoki, Y. 485
Kwon, Jeong-Il 1315

Kwon, Jong Oh 367
Kwon, S.H. 587

Larsen, M.J. 1331
Lauridsen, P.H. 261
Le Sourne, H. 1309
Lee, C.M. 451
Lee, C.-S. 685
Lee, Chun-Ju 151
Lee, H.S. 587
Lee, H.Y. 229
Lee, J.K. 301
Lee, Jae Kyu 367
Lee, Jae Wook 83, 367
Lee, Kyu-Yeul 315
Lee, S.J. 451
Lee, S.S. 301
Lee, Sang Gab 1161, 1315
Lee, Sanghong 367
Lee, Sang-Uk 315
Lee, Seung Hee 113, 367
Lee, Seunghee 799
Lee, S-H. 83
Lee, Soo-Mok 1221
Lee, T.H. 445
Lee, Tae-Il 665
Lee, Yoon Ki 1161
Lee, Young Gill 83, 367
Leer-Andersen, M. 541
Lehmann, E. 1293
Lepeix, R. 767
Levi, C. 421
Lew, J.M. 785
Lew, Jae Moon 367
Li, D.-Q. 541
Li, Jun-Hua 309
Li, Jun-Ming 37
Li, Ke-Jun 1
Li, Ting-Qiu 413
Lim, Choon-Gyu 229
Lin, J. 871
Lin, Shao-Fen 245
Liu, D. 13
Liu, Hao, 197
Liu, P. 741
Liu, Ying-Zhong 1237
Liu, Yujun 397
Löhner, R. 43
Lotsberg, I. 159
Lu, Bei 373
Lu, C.Y. 857
Lu, Jun 309
Lua, Y.J. 237
Ludolphy, J.W.L. 1145
Lundbäck, O. 533
Lützen, M. 349, 1277

Ma, N. 187
Maeda, H. 221
Mandarino, M. 127
Mano, M. 1345
Mansour, A.E. 955
Marquis, G.B. 1113
Masaoka, K. 197
Matsuoka, K. 389
Matter, G.B. 167
Matusiak, J. 413
Mavrakakis, Y. 1177
McGeorge, D. 1331
McGovney, J.E. 955
Miao, Guo-Ping 1237
Mikkola, T.P.J. 1113
Min, K-S. 105
Miwa, I. 493
Miyagi, C.H. 493
Miyazaki, H. 671
Moan, T. 879, 939, 1053
Murawski, L. 1205
Myrhaug, D. 925

Nakatake, K. 645
Nimura, T. 671
Nishimoto, K. 493
Nonaka, K. 671
Noury, P. 1331

Ogawa, Y. 603
Ohtsubo, H. 997, 1301
Okada, H. 197
Osawa, N. 389
Østvold, T.K. 1021
Ottosson, P. 541

Paetzold, H. 1137
Park, J.S. 587
Park, J.W. 785
Park, Jae-Hyung 323
Park, Jinsoo 1129
Park, Kihyun 799
Pasqualino, I.P. 1037
Pedersen, P.T. 1277
Peng, Y.T. 1169
Petinov, S.V. 1153
Postnov, V. 911
Pradillon, J.Y. 1029
Price, W.G. 847, 903
Pu, Y. 947

Qian, G.L. 555
Quesnel, T. 1029

Rajagopalan, K. 965
Rhee, K.P. 679
Rheem, C.K. 221
Rhim, Joong-Hyun 315
Rigo, Ph. 51, 987, 1029
Riola, J.M. 831
Rosén, A. 629
Ryrfeldt, A. 253

Sajit, K.S. 1301
Sakuragi, T. 341
Sales, Jr., J.S. 167
Salvatore, F. 705
Sames, P.C. 637
Sampaio, C.M.P. 493
Sasajima, H. 29
Sasaki, Y. 971
Sawamura, J. 389
Scharrer, M. 1293
Schellin, T.E. 637
Sebastiani, L. 547
Seki, T. 341
Sekiguchi, T. 645
Sen, P. 285
Seo, Heung-Won 665
Shama, M.A. 381
Shen, Hong-Cui 807, 823
Shen, J.W. 887
Shenoi, R.A. 1339
Shi, Li-Juan, 979
Shibazaki, K. 1089
Shimizu, T. 331
Shin, Chin, 741
Shin, H. 229
Shin, H.J. 791
Shin, Yung, 175
Shinkai, N. 389
Sima, C. 895
Simonsen, B.C. 1323
Snell, R.O. 1269
Son, D.I. 679
Song, Museok 113
Soto, O. 43
Spencer, J.S. 955
Sphaier, S.H. 167
Stansberg, C.T. 593, 611
Steen, E. 1021
Stephenson, G.H. 293
Suh, J.-C. 799
Suh, Jung Chun 113, 367
Sumi, Y. 341, 1105
Sun, H.H. 1005
Sun, Li-Ping 1097
Sun, Wei 97
Sun, Yu-Wu 1097
Suzuki, K. 1301

Tabeta, S. 213
Taguchi, H. 603
Tahara, Y. 719
Takeda, Y. 1197
Tam, V.H.Y. 1269
Tan, K.G. 285
Tan, Ting-Shou 713
Tarman, D.D. 955
Temarel, P. 571, 847, 903
Thill, C.H. 75
Toderan, C. 987, 1029
Tomita, Y. 389, 1081
Toxopeus, S.L. 75
Trägårdh, P. 541
Tsubogo, T. 197
Tveitan, B.W. 1053

Ueno, M. 671

Valkhof, H.H. 437
Valle, J. 831
Valsgård, S. 1021
van Heerd, J. 757
van Terwisga, P.F. 75
Vannahme, M. 1227
Vårdal, O.T. 939
Vassalos, D. 269
Vergine, A. 1243

Wanderley, J.B.V. 421
Wang, Cheng-Fang 37
Wang, Dong 397
Wang, G. 919
Wang, G.-Q. 733
Wang, Li-Zheng 91
Wang, W. 1339
Wang, Y.Y. 59
Wang, Z. 839
Watanabe, I. 603
Wei, Jia-Fu 21
Wei, Na Xin 555
Wernicke, R. 1061
Wilckens, H. 359
Wirsching, P.H. 955
Wist, H.T. 925
Wu Nie 1097
Wu, Fan 1213

Wu, Hua-Tung 857
Wu, Xiu-Heng 651
Wu, You-Hua 693
Wu, You-Sheng 871, 895

Xi, Long-Fei 91
Xia, J. 839
Xie, N. 555
Xu, Fa-Yan 865
Xu, L. 59
Xu, Li 865

Yamada, Y. 1285
Yamamoto, N. 997
Yamano, T. 485
Yang, C. 43
Yang, C.-J. 733
Yang, J.M. 931
Yang, Jiman 799
Yang, Qinzheng 475
Yao, Hui-Zhi 807
Yao, T. 987, 997
Ye, Naiquan 1053
Ying, Wen-Ye 309
Yoneda, M. 997
Yoneya, T. 971
Yoon, Hyun Se 525
Yoon, Jaedoon 459
Yoon, Myung-Cheol 229
Yu, Lei 1121
Yu, Zhi-Xing 1237
Yue, Ya-Lin 871

Zhang, Jin-Fei 979
Zhang, L. 1293
Zhang, Sheng-Kun 373
Zhang, W. 1185
Zhang, Wei 37
Zhang, Wei-Xing 865
Zhang, X.D. 651
Zhang, Xiao-Ci 895
Zhao, C.B. 865
Zhao, C.T. 175
Zhao, R. 475, 725
Zhou, Lian-Di 429
Zhou, Q. 1185
Zhou, Wei-Xin 693
Zhu, Y.X. 1213
Zhu, Ying-Fu 309
Zotti, I. 143

KEYWORD INDEX

Volumes I and II

A moving mesh, 413
Accurate manufacturing, 359
Acoustics, 1185
Added mass, 1185, 1197
Added mass effect, 205
Added resistance, 671
Adjustable mould, 367
Advanced second moment method, 931
Aged platform structures, 1097
Aged Ship, 997
Air gap, 621
Air injection, 1213
Air lubrication, 113
Air-liquid two phase mixed boundary layer, 1213
Aluminium, 1053
Analysis, 525, 831
Antifouling, 517
Artificial neural networks, 501
Attained Index A, 261
Axial compression, 1029

Back-propagation, 791
Backward vector auto-regressive model, 1169
Bank effects, 541
Basin, 831
Bayesian network, 349
BEM, 705, 1185
Benchmark test, 413
Bernoulli wave, 541
Body force, 785
Bottom step, 113
Boundary, 1323
Boundary conditions, 1205
Boundary element method, 895, 919
Boundary elements, 547
Boundary layers, 705
Bow height, 603
Bow slamming, 593
Box-stiffener, 1053
Breaking waves, 587
Breath mode, 1197
Brittle and ductile fracture, 1013
Broaching-to, 533
B-spline, 713, 865
Bubbly layer, 1213
Buckling, 965, 1021, 1029
Buckling strength, 971
Buffer bow, 1285
Bulk carriers, 13, 903
Bulk cavitation, 1315
Bulkhead structure, 331

CAD, 301
CAE, 301
Calm water resistance, 493
Cantilever-beam type, 1097
Capsize, 831
Cargo shifting, 253
Cargo ship, 91
Casualties, 13
Catamaran, 83
Cavitation, 733, 749
Cavitation inception, 693
Cavitation tests, 815
CBR, 309
CFD, 459, 467
CFD tools, 43
Circular cylinder, 587
Classification rules, 1331
Coastal ecosystem model, 213
Coatings, 517
Coherence analysis, 587
Collapse, 1037
Collapse analysis, 1029
Collapse mechanism, 1285
Collision analysis, 1301
Collision resistance, 1293
Collisions, 323, 831, 1285, 1277, 1309
Combination of load, 1089
Combined loads, 1021
Compartment fire, 1261
Composite grid, 777
Computational Fluid Dynamics (CFD), 429, 437, 1261
Computational methods, 799, 1105
Condition, 1323
Conical shell, 1285
Construction cost, 51
Container, 467
Container ship, 105, 293
Continuous wavelet transform, 587
Conventional rudder, 665
Correlation coefficient, 1089
Corrosion, 29, 341
Corrosion and fatigue, 1005
Corrosion fatigue diagram, 1045
Coupling effects, 887
Coupling mode between panel and stiffener, 1197
Crack, 341
Crack analysis, 1105
Crack growth, 1129
Crack growth analysis, 1081
Crack initiation, 1129
Critical buckling strength, 979
Critical fill levels, 637
Critical leakage zone, 451
Critical locations, 1153
Cross fairing, 315
Cruciform joint, 1061
Cruise vessel, 767
Crush test, 1285
Curved, 1323
Curved composite laminate, 1339
Cyclic bit pressure, 1097

DAA boundary segments, 1315
Damage, 831
Damages of ship structures, 341
Damping, 831, 1185
Data fitting, 349
Data model, 341
Database, 501, 685

Database technology, 245
Deck wetness, 229, 603
Deckhouse height, 459
Deckhouse vibration, 1221
Deflection, 187
Deflection limits, 1269
Delamination, 1339
Depressor wings, 1227
Design, 29, 127, 269, 293, 359
Design criteria, 275
Design decomposition, 285
Design for environment, 381
Design methodology, 51
Design methods, 629
Design of FPSOs, 947
Design operational condition, 887
Design standards, 1
Design wave condition, 1089
Developable surface, 367
DICAS, 167
Differential numerical approach, 59
Discounted cash flow, 293
Double hull, 237
Draft effect, 221
Drag reduction, 113
Ducted propeller, 725
DYNA3D, 237
Dynamic loading approach, 887
Dynamic loads, 903
Dynamic meshing, 403

Economic and Trade development, 21
Effect of mooring rigidity, 197
Effect of shear rigidity, 197
Effective speed, 509
Effective velocity, 785
Effective wake, 777
Effective width, 965
Elastic response, 221
Empirical method, 501
Energy, 381
Energy operator, 1177
Entire-ship structural analysis, 971
Entrainment failure, 451
Environmental impact assessment, 213
Environmental impacts, 381
Eppler section design, 693
Equivalent body force, 777
Essentially Non-Oscillatory (ENO) schemes, 429
Eulerian-Lagrangian, 445
Exciter test, 1221
Experimental evaluation, 493
Experimental stress analysis, 1071
Experimental test, 1037
Experimental validation, 1227
Explosions, 1269
External mechanics, 1301
Extreme response, 175
Extreme wave loads, 871

Fabrication cost, 29
Fabrication effect, 1061, 1137
Failure strain, 1293
Far field method, 221
Fast Fourier transform (FFT), 1121
Fast marine vehicles, 547
Fatigue, 159, 175, 323, 939, 1053, 1061, 1069, 1145
Fatigue analysis, 1121
Fatigue design, 1071
Fatigue design of hull details, 1153
Fatigue failure, 1045
Fatigue life, 1097
Fatigue properties, 1153
Fatigue strength design, 1081
Fatigue strength, 971, 1071, 1129,
Fatigue testing, 159, 1071
FE idealisation, 903
FEA, 971
FEA simulation, 1285
FEM, 997, 1045, 1169, 1185
Fender systems, 1277
Fiber reinforced plastic, 367
Fibre reinforced polymers, 1331
FINFLO RANS solver, 413
Finite-analytic method, 651
Finite difference, 421
Finite difference method, 919
Finite element analysis, 159, 1071, 1129
Finite element model, 1221
Finite elements, 1309
Finite volume method, 637
Finite water depth, 475
Finite-Volume-Method, 467
Fire, 1243
Fire field model, 1261
Fire safety design, 1253, 1261
Fire simulation, 1243
Fire spread phenomena, 1253
First excursion, 237
First order reliability method, 237
First-principles, 269
Flexible model, 871
Flexural buckling, 979
Floating objects, 1277
Floating production, 611
Flooding, 831
Flow, 467
Flow-induced flutter, 895
Flow passing a tandem fence, 451
Fluid-solid coupling, 919, 1237
Fluid-structure interaction, 911, 1185
Flux splitting, 429
Folding, 1285, 1293
Following sea, 533
Form optimisation, 275
Formal safety assessment, 1243
Forward-oriented wave breaking, 485
Forward speed, 847
Foul release, 517
FPI, 175
FPSO, 159, 167, 175, 593, 611, 1071
Fracture, 159
Fracture mechanics, 1061
Free running, 533
Free surface, 865
Free-surface effect, 451
Frequency domain, 229

Friction, 517
Frictional resistance, 113
FRP ships, 1339
Full scale, 533
Full-scale fatigue test, 1129
Full scale test, 37
Full-scale trials, 555, 629
Fully nonlinear, 445
Fundamental mode, 1197
Funnel height, 459
Funnel position, 459
Fuzzy arithmetic, 931
Fuzzy reliability, 931
Fuzzy set theory, 245

Geometric optimisation, 67
Geometrical non-linearity, 1331
Geometrically similar models, 113
Global loads, 127
Graphic user interface, 685
Green functions, 547
Green sea, 593, 611
Green's function, 847
Ground effect, 97
Guide vane, 807

Heat, 467
Heat transfer, 389
High lift rudder, 665
High performance, 91
High speed, 83
High speed craft, 1331
High speed video recording, 815
High strength steel, 1113
Higher order harmonic component, 887
Higher tensile strength steel, 29
Highly skewed fixed pitch propeller, 1045
High-speed medium size container ship, 301
Hopper knuckle, 323
Horizontally elastic response, 197
Horn rudder, 679
Hot spot stress, 159, 1129, 1137
Hotspot stress analysis, 971
HSC, 135, 579, 629
HSC comparison, 143
Hull fabrication, 397
Hull form, 91
Hull form CAD system, 315
Hull form design, 43, 67, 83
Hull form optimisation, 43, 75
Hull girder, 237, 987, 1029
Hull lines, 767
Hull resistance, 59
Hull sections, 665
Human element, 13
Hybrid approach, 237
Hybrid hydrofoil, 119
Hydrodynamic effects, 1309
Hydrodynamic forces, 645
Hydrodynamic loads, 911
Hydrodynamic pressure, 857
Hydrodynamics, 75, 767, 1345
Hydro-elastic effect, 919
Hydroelasticity, 187, 221, 871, 895, 903, 911
Hydroelastic interaction, 1197
Hydroelastic responses, 205, 229
Hydrofoil, 119, 705, 895
Hydro-ski, 97
HYKAT, 479

Ice-propeller interaction, 741
Impact, 97
Impact load, 97
Impact pressure, 637
Impact pressure distribution, 629
Improved welds, 1113
Impulsive loads, 919
Increase, 525
Infinite dimensional optimization method, 699
Information systems, 341
Initial imperfections, 1013
Integral numerical approach, 59
Integrated fleet, 37
Intelligent, 309
Interaction, 785
Interface design, 685
Intermediate bearing, 1205
Internal mechanics, 1301
International friendship, 1345
International shipping, 21
International symposium, 1345
Inverse heat conducting analysis, 389
Inverted angle stiffener, 1129
Inviscid flows, 705
Irregular frequency, 847
Irregular waves, 229
ISO, 525
Isolated Rankine, sources, 445
ITTC high-speed model, 493

Jack-up platform, 1097
Journal bearing, 1205

Lagrangian particle-tracking method, 451
Lap joint, 1053
Large deflections, 1331
Large eddy simulation, 1261
Large scale fatigue test, 1137
Large-scale welding applications, 403
Large-size foil catamaran, 105
Laser welding product data technology, 359
LDV, 785
LDV technique, 1213
L.I.F., 389
Life cycle analysis, 381
Life cycle cost, 29
Lifting-surface method, 693
Lifting surface theory, 733
Limit states, 51, 1269
Line heat forming, 397
Line heating, 389
Linear FE model, 1293
Load lines, 603
Load transfer, 971
Load-carrying box filler weldment, 1161
Loading/unloading, 301
Local strain approach, 1153
Local stress, 1061

Longitudinal stiffened sub-panel, 979
Longitudinal strength, 323, 925
Longitudinally stiffened panel, 1029
Long term, 879
Long-term distribution, 1089
Long-term prediction, 603, 947
Low Mach number approximation, 1261
LS-DYNA3D/USA code, 1315
LU decomposition, 429

Main engine unbalance moment, 1221
Main particulars, 349
Main-hull, 127
Maintenance cost, 29
Maneuverability, 665
Maneuvring, 167
Manoeuvrability, 671
Manoeuvre, 657
Manoeuvring, 75, 533
Manoeuvring motion, 651
Marine propellers, 705
Marine propulsion, 741
Maritime safety culture, 1
Mean stress, 1113
Mean ultimate stress, 1293
Measurement, 533, 555, 823
Medium frequency, 1177
Mega-float model, 213
Membership function, 931
Memory effect function, 229
Miner's rule, 1089
Minor impacts, 1277
Misalignment, 1061
Mission based design, 75
Mobile agent, 373
Model-based simulation, 301
Model experiment, 113
Model test in tank, 91
Model tests, 37, 83, 205, 555, 593, 629, 725, 871
Model test techniques, 749
Model-ship correlation, 135
Mode superposition, 187
Modified lifting line theory, 679
Momentum theory, 221
Monte Carlo simulation, 237
Moving grid, 421
Multi-criteria analysis, 1029
Multi-hulled vessels, 571
Multi-hulls, 127
Multi-linked compartments, 1253
Multiobjective optimisation, 285
Multi tiers, 1197

Narrow tank, 1197
Natural frequency, 1197
Naval, 127
Naval ship compartment, 309
Near field method, 221
Near field theory, 187
Neural network, 349, 791
New blade section, 693
Newmark β method, 229
NO_2 iso-surface, 459
Noise, 749, 807, 1185
Nominal stress, 1053
Nominal wake, 777
Non-linear, 571
Nonlinear, 879
Nonlinear cable forces, 1227
Nonlinear dynamics, 1227
Nonlinear programming, 719
Nonlinear wave-induced bending moments, 887
Non-manifold data structure, 315
Non-modal method, 1177
Non-uniform flow, 671
Norminal wake, 791
Notch stress, 1053
Numerical analysis, 725, 1037
Numerical calculation, 651
Numerical methods, 1185, 1309
Numerical optimization, 493
Numerical simulation, 83, 187, 213, 1227
Numerical welding simulation, 403

Oblique waves, 857
Offloading, 167
Offshore, 1269
Offshore platforms, 939
Oil fence, 451
Oil leakage, 451
Oil spill, 1285
One week design, 67
Operability, 563
Optimal hull forms, 699
Optimal marine propellers, 699
Optimisation, 269
Optimization, 51, 331, 1323
Optimization procedure, 59
Optimum design, 397
Optimum location, 151
Orbital oscillations, 1227
Oseenlet, 895
Outriggers, 127
Overpressures, 1269

Painting, 29
Panel, 1323
Panel methods, 733, 741
Parametric design, 275
Parametric modelling approach, 67
Parametric study, 459
Partial load and resistance factors, 1269
Partially supported hydrofoil, 119
Partial structural analysis, 971
Particle track, 459
Passenger ferry, 135
Phase vector analysis, 1221
PIV method, 451
Planing, 579
Planing boat, 367
Platform, 611
Plat-ski, 97
Podded drives, 749
Pods, 767
Pollution, 381
Pontoon-type very large floating structure, 205
Portable (wearable) computer, 341
Postbuckling, 1021

Post-collapse, 1037
Powering performance, 151, 807
Practical design, 1345
Pre-fabricated details, 1153
Preliminary design, 51
Preliminary ship design, 349
Pre-load, 1161
Pressure distribution, 713
Pressure measurement, 579
Pressure pulse measurements, 815
Pressure pulses, 749
Probabilistic analysis, 947
Probabilistic damage stability, 261
Probabilities of failure, 1269
Probability density function, 603
Production simulation, 359
Program, 525
Progressive collapse analysis, 987, 997
Propeller, 437, 733, 785, 807
Propeller analysis, 685
Propeller design, 685, 693, 713
Propeller-hull interaction, 777, 799
Propeller loading, 541
Propeller plane, 791
Propulsion, 725, 767, 807
Propulsion plant, 657
Pusher-barge-line, 37

Quantitative risk assessment, 269

Random field generation, 1121
Random process, 237
Random waves, 593
RANS, 785
RANS calculation, 777
RANS equations, 719
Rational constraints, 51
Real time simulation, 213
Rectangular tank, 1197
Re-distribution of residual stress, 1161
Reduced model, 1177
Reduction, 1323
Redundancy, 1021
Reefer, 467
Regression analysis, 679
Regressive analysis, 59
Reliability, 939, 965
Reliability analysis, 947
Reliability based code formulation, 955
Reliability-based design, 947
Reliability design, 925
Remained following waves, 485
Renovation of existing integrated barge, 37
Requalification, 939
Residual resistance, 501
Resistance, 143, 151, 485, 517, 525
Resistance and propulsion prediction, 509
Resistance reduction, 1213
Resistance test, 135
Response surface, 285
Response surface method, 1005
Response surface methodology, 331
Reuse of design data, 285
Reynolds Average Navier-Stokes equations, 59
Reynolds number, 437
Rigid body motions, 571
Rigid body response, 621
Ringing, 587
Risk analysis, 253, 381, 925, 965, 1243
Risk assessment, 245
Risk-based safety standards, 13
River-sea-going ore barge, 37
Roll, 831, 839
Root crack, 1137
Ro-Ro, 831
Rotating ships, 421
Roughness function, 517
Roughness, 517
Run-up, 611

Safety, 1243
Safety index, 965
Sailing model, 1081
Sandwich, 1323
Scale effect, 485
Scale law, 113
SCF, 1053
Sea loads, 865
Sea trials, 563
Seakeeping, 75, 143, 547, 555, 563, 571, 579, 847
Seakeeping criteria, 563
Sectioning method, 1161
Self-propulsion simulator, 719
Self-propulsion test, 777
Semi-displacement hull, 493
Semi planing, 533
Sensitivity analysis, 979, 987
Sensor carrier, 1227
Series 60, 847
Service damages, 1013
Shaft line alignment, 1205
Shaken-down residual stress, 1161
Shallow draft assumption, 221
Shallow water, 83, 509
Sheet cavitation, 705
Ship and Offshore installation, 1
Shipbuilding, 373, 381, 397
Ship design, 59, 261, 1071, 1345
Ship motion, 555
Ship motion prediction, 563
Ship motions, 253
Ship performance, 509
Ship production, 359
Ship resistance, 501
Ship responses, 839
Ship structural design, 955
Ship structures, 919, 965, 971, 1071, 1105, 1169
Shipping system, 37
Shipping water load, 603
Ships, 785, 879, 1145
Ships with a transom, 413
Shock response, 1315
Side longitudinal, 1129
Side-hull, 151
Similar response function method, 1081
Simplified, 879
Simplified method, 1301
Simplified prediction method, 1081

Simulation, 293, 501, 657
Simulation method, 397
Single-skin panels, 1331
Sinkage, 475
Ski, 97
Slamming, 229, 579, 611, 767, 911
Slender ship approximation, 43
Sloshing, 637
Slot type, 1097
Smith's method, 997
Smoke behavior, 459
S-N curve, 1089
S-N data, 159
Society of naval architects, 1345
Soft bow, 1285
Sound, 1185
Spectral analysis, 587
Spectrum fatigue, 1113
Speed, 525
Speed loss, 887
Spread-mooring, 167
SR-221 ship models, 645
Stability, 167, 831
Stability assessment, 301
Statistical analysis, 791
Statistical prediction, 971
Steady drift force, 187
Steel structure, 29
Steering gear torque, 679
Stepped hull, 119
Stern profile, 665
Stern tube bearing, 1205
Stern waves, 485
Stern wedges, 493
Stiffened panels, 987, 1021
Stiffened plates, 965
Stiffened structure, 51
Stiffener tripping, 965, 979
Stiffness, 1323
Stiffness characteristics, 1205
Stochastic finite element method, 237
Storm model, 1081
Strain and stress curve, 987
Strength, 175, 1021, 1331
Stress concentration, 1153
Stress response function, 1081
Strip theory, 839
Structural constraints, 51
Structural design, 331, 1331, 1339
Structural reliability, 237
Structural response, 629, 857
Structural safety, 13
Structural stress, 1053
Structural vibration, 1177
Structures, 127, 1323, 1345
Submarines, 807, 1309
Submersible structure, 1037
Suezmax, 665
Supercavitating propeller, 733
Super-high-speed ships, 105
Supply chain management, 373
Surface model, 315
Surface panel method, 645, 693, 713
Surface parameterization, 43
Surface ship, 1315
Surrounding, 1323
Survivability, 269, 831
Sway force, 541
System identification, 1169

Tankers, 13, 637, 1129
Tanker stern form optimization, 719
Target level, 939
Technical conference, 1345
Temperature, 467
Templates, 403
Tensile mean stress, 1161
Test, 831
Testing technique, 815
Theoretical hydrodynamics, 705
The pseudo-field mathematical model, 1253
Thermal stress, 1197
Thermo-elasto-plastic analysis, 1161
The thickness of heat insulation, 1253
The Yellow Sea, 83
Thickness diminution, 997
Thin ship theory, 475
Three dimensional methods, 547
Three-dimensional source technique, 857
Through life costs, 293
Through-thickness stress, 1339
Thrust, 725
Time domain, 229, 839
Time-domain simulation, 579
Time stepping, 445
Time-variation reliability assessment, 1005
Tokyo Bay, 213
Torque, 725
Total system, 971
Towed underwater vehicle, 1227
Towing test, 823
Transient, 831
Trial, 525
Triangular pulse loading, 1269
Trim, 475
Trimaran, 43, 127, 135, 151
Trimaran model tests, 143
T-type stiffener, 1129
Turbulent diffusion of heat and composed gas, 1253
Turbulent viscosity, 895
Turning motion, 645, 671
Turret, 167
Twenty-first Century, 21
Two-bladed vertical pre-swirl stator vane, 799

Ultimate bending moment, 987, 1029
Ultimate bending strength, 237
Ultimate hull girder strength, 1013
Ultimate longitudinal strength, 997
Ultimate strength, 987, 1005, 1021, 1029
Uncertainty, 979
Uncertainty analysis, 823
Underwater explosion, 1315
Unsteady loading, 741

Unsteady wave pattern, 857
Upgrading, 293

Variable amplitude loading, 1145
Ventilation, 467
Vertical bending moment, 879
Very large floating structure, 187, 221, 229
Vibration, 1169
Vibration reduction, 1213
Virtual reality, 341
Viscous flow, 421, 437, 651
Viscous free-surface flow, 413
Viscous/inviscid coupling, 705
VLCC, 799
VLFS, 197, 213, 221, 229
Vortex-induced vibration, 1237
Vortex ring, 785
Vortex shedding, 1237

Wake, 785
Wake distributions, 437
Wash, 475
Wash wave, 541
Water impact, 911
Watertight subdivision, 261
Waterways with shallow and strong current, 91
Wave cancellation multihull ship, 43
Wave drift forces, 671
Wave excitation, 571
Wave impact, 593, 611
Wave-induced dynamic response, 903
Wave-induced load, 1089
Wave-induced loading, 947
Wave interference, 151
Wave loads, 925, 971, 839
Wave pressure, 1081
Wave resistance, 43, 475
Waves, 525, 533
Weight, 1323
Weight function, 1105
Weld endings, 1153
Welded details, 1145
Welded joint, 1061
Welded structures, 1113, 1137
Wetdeck slamming, 621
Wetted surface, 501
Whipping response, 887
Whirling vibrations, 1205
Wide beam, 665
Wide web frame space, 323
WIG, 97
Wigley hull, 475
Wind, 525
Windows, 685
Wing flow, 1237

Yaw moment, 541
Yoke house, 1097

α-cut, 931

3D-layout, 309
3D Rankine Panel method, 865

4,800 TEU container carrier, 1221

4th Order balancer, 1221

Practical Design of Ships and Other Floating Structures

Proceedings of the Eighth International Symposium on Practical Design of Ships and Other Floating Structures

16-21 September 2001, Shanghai, China

2001
PRADS

CONTENTS

Volume I

Plenary Lectures

1. Design Synthesis for Ships and Floating Systems
2. Production
3. Hydromechanics

Volume II

3. Hydromechanics *(continued)*
4. Structures and Materials

Author Index
Keyword Index

Cover illustration reproduced from paper
by T. Yoneya et al., pp. 971-977

ISBN 0 08 043950 0
9 780080 439501